Majid Hosseini
Abdel Salam Hamdy Makhlouf   *Editors*

Industrial Applications for Intelligent Polymers and Coatings

Springer

Industrial Applications for Intelligent Polymers and Coatings

Majid Hosseini • Abdel Salam Hamdy Makhlouf
Editors

Industrial Applications for Intelligent Polymers and Coatings

Springer

Editors
Majid Hosseini, PhD
Manufacturing and Industrial Engineering
    Department
College of Engineering and Computer Science
The University of Texas – Rio Grande Valley
Edinburg, TX, USA

Abdel Salam Hamdy Makhlouf
RGV STAR Professor, Manufacturing and
    Industrial Engineering Department
College of Engineering and Computer Science
The University of Texas – Rio Grande Valley
Edinburg, TX, USA

Preface

This book is a comprehensive collaboration on intelligent polymers and coatings for industrial applications by world-class researchers and specialists. The authors cover the basic and fundamental aspects of intelligent polymers and coatings, challenges, potential mechanisms and properties, classification and composition, synthesis, characterization, and processing of intelligent polymers and smart coatings, bioactive and electroactive polymers and coatings, and stimuli responses of intelligent polymers and smart coatings. They include recent and emerging industrial applications in medical, smart textile design, oil and gas, electronic, aerospace, and automobile industries as well as other applications including micro-systems, sensors, and actuators, among others. The authors discuss the potential for future research in these areas for improvement and growth of marketable applications, current capability, and scale up of intelligent polymers and smart coatings in order to improve and spread their applications. This book serves as a valuable reference to industries, R&D managers and staff, scientists and engineers (chemical, mechanical, materials, etc.), chemists, academics, and other professionals in polymers and coatings, and manufacturers and designers dealing with intelligent polymers and coatings. It can also be a guide for science and engineering students in universities and research institutes.

Chapter 1 provides a critical discussion and an overview of the stimuli-responsive polymeric based nano-sized hosts and their applications in drug delivery. Furthermore, multi-responsive systems and their forthcoming development as well as the challenges associated with some stimuli-responsive polymeric based systems are discussed. Chapter 2 covers the stimuli responsiveness of smart polymeric coatings in various applications and their future outlooks within the coatings industry, as well as present practical applications and necessities of the stimuli-responsive smart polymeric coatings for industrial applications. Chapter 3 gives a critical review of diverse biomedical systems implementing electroactive polymers and coatings including pharmaceutical and medical industry and highlights their applications, advantages, and possible limitations. The chapter also introduces innovative approaches for enabling EAP and EAC-based systems to attain their full clinical

potential. Chapter 4 highlights some of the recent and novel findings in the development of piezospectroscopic particle reinforced polymers as smart stress and damage sensing coatings. The piezospectroscopic effect for alumina-based particulate composites is outlined and discussed in this chapter for current and future applications in the industry. Chapter 5 provides an overview of the methodologies reported to produce smart polymer surfaces depending on the external stimuli employed to vary reversibly the surface properties. The methodologies to prepare patterned surfaces as a function of their final resolution and some of the applications are highlighted in which smart polymer surfaces have been applied including wettability, biomedical purposes, sensoring, or smart adhesion. Chapter 6 addresses the smart textile transducer elements, textile platforms, application techniques, and construction methods. Multiple applications that have been inspired by the lightweight and compliant characteristics of smart textiles are further discussed in this chapter. Design principles and challenges associated with coating technologies as applied to textiles including surface treatment for strong adhesion, durability and environmental/mechanical constraints, and future trends are also introduced. Chapter 7 highlights new controlled living polymerization methods. Molecule-loading and types of morphologies of self-assembled supramolecular structures derived from smart polymers are also discussed. Chapter 8 discusses functions of bioactive and intelligent natural polymers in the optimization of drug delivery. It provides the contexts of natural bioactive and intelligent polymers and their unique applications in drug delivery that would ultimately benefit drug delivery systems in benchmarking new drug formulations. Chapter 9 looks at the current literature and patents pertaining to aptamer-based smart materials and the applicability of these materials for industrial applications. Aptamer-based smart materials bring together aptamer technology with material science, producing multifunctional, advanced materials with tunable properties that could be applied to many facets of industry. Chapter 10 presents the study of superhydrophobic and water-repellent polymer–nanoparticle composite films. The methods described in this chapter, where nanoparticles are embedded into inherently hydrophobic polymers to achieve the desired hierarchical micro/nanostructure on surface, are easy, low cost, and can be used to treat large surfaces implemented using various nanoparticles and polymers. Chapter 11 deals with the application of conducting polymers in solar water-splitting catalysis. Water splitting assisted by or driven by illumination with sunlight and involving conducting polymers and the properties of conducting polymers that make them favorable for this purpose are also discussed. Comparisons of these properties with those of conventional water-splitting materials are made, and a statement of research and achievements of solar hydrogen production through water splitting using conductive polymers is reported. Chapter 12 provides an in-depth review of the techniques that are typically employed in the preparation and characterization of smart and active biopolymers, films, and microparticles, their potential applications within the food industry, and the challenges that are associated with their use and development. Chapter 13 discusses the use of ATRP and click chemistry for polymerization of various clickable monomers using clickable ATRP initiators along with other post-polymerization modification strategies that can be used to construct macromolecules

with self-healing ability. Chapter 14 comprehensively aims to address a wide overview of polyurethane-based smart polymer and the chemistry behind the shape memory properties. This chapter also summarizes the recent studies on the exploration of SMPU using vegetable oils along with petroleum-based polyol and the potential applications of smart polyurethane. Chapter 15 discusses different polymorphisms of PVDF depending on the chain conformations of trans and gauche linkages. Various methods employed for the investigation of phase transition and strategies for the enhancement of the β-phase such as mechanical stretching, electrical polling, and addition of fillers are also summarized in this chapter. The evaluation components of the piezoelectric efficiency and applications of PVDF polymers are emphasized in the design of piezoelectric sensors, actuators, and energy harvesting devices. Chapter 16 discusses the different types of multifunctional materials used in biotechnology, resuming the opportunities and challenges that are implied by those systems with a focus on the multicomponent systems used for complex needs, with properties derived from interactions between the system constituents. The implementation of multifunctional materials in targeted delivery system that simultaneously perform diagnostics, targeted delivery, and efficient therapy is also summarized. Chapter 17 provides a short classification of the polymer nanocomposites, highlighting the importance of the shape, size, distribution, and origin of the nanofiller. A review of the investigation methods of the microstructure evaluation is performed. Synthesis for the mathematical models developed for their electrical, thermal, and dielectric properties is also presented. The current trends in obtaining intelligent polymer composites (thermo-sensitive, pH responsive, and other responsive stimuli) for various applications are also reviewed. Chapter 18 starts with a brief discussion of the relevant knowledge base, including microstructure of polymer nanocomposites, influence of nanomodification on properties of polymeric coatings, fabrication approaches, and the use of polymeric nanocoating as a carrier for corrosion inhibitors. It also provides a review of technological advances in the use of nanotechnology to produce high-performance polymeric coatings with outstanding corrosion resistance and other relevant properties as well as advanced characterization of nanocomposite coatings for corrosion protection. Chapter 19 introduces amphiphilic invertible polymers as novel smart macromolecules. The amphiphilic invertible polymer macromolecules possess an enhanced flexibility and rapidly respond to changes in an environmental polarity by changing their macromolecular conformation. Chapter 20 discusses functional materials used as reservoirs that enable the controlled delivery of corrosion inhibitors or healing agents and mainly focused on those primary stimuli that cause the release of inhibitive species from the reservoirs: mechanical damage, ion-exchange processes, and local pH changes. Chapter 21 highlights the recent advances and developments in the fabrication of ECPs-based textile supercapacitors, including different types of pure ECPs and their composites with other conducting materials for preparation of hybrid supercapacitors with superior performance for textile supercapacitor applications. Chapter 22 reviews recent advances in preparation and characterization of different self-healing coatings on steel. The main techniques for obtaining self-healing coatings and the challenges for future research are also briefly discussed.

Chapter 23 critically discusses silane resin coatings, their structure, characteristics, and applications. The concepts of the novel silane compound films, the rationale for the research and development, and the application possibilities in many industrial fields are also introduced in this chapter. Chapter 24 provides the principles and fundamentals of various types of smart coatings, materials, design, and processing methods, strategies to heal the mechanical damage, and the microencapsulation approaches to self-healing polymer development. Chapter 25 presents recent results describing sol-gel hybrid optical coating sensors to demonstrate their state-of-the-art industrial applications for gases, pH, solvents, and ionic species monitoring. Chapter 26 is focused on sensory polymers for detecting explosives and chemical warfare agents. Chemical warfare agents, conjugated or conductive polymers, molecularly imprinted polymers, and sensor arrays based on a set of polymers are discussed. The chapter concludes that polymer chemosensors are the best choice when designing and developing chemosensory materials for explosive sensing. Chapter 27 describes the synergistic combination of smart polymeric microencapsulation technology for industrial applications such as coatings and paints, construction, textile industry, food and beverage industry, pharmaceutical formulations, biomedical applications, aerospace, and automobile applications. Chapter 28 provides an overview of the approaches to the destructive and nondestructive characterization of adhesion, from the traditional methods to less common intelligent techniques. The main challenges, strengths, and weaknesses related to the evaluation of adhesion are also communicated in this chapter. Chapter 29 reviews waterborne coatings based on reactive polymer nanoparticles and the first attempts to use smart polymer nanoparticles where the crosslinking is triggered by a stimulus which occurs after the desired extent of interdiffusion. Different types of crosslinking that have the potential to be used in smart waterborne coatings, involving functional groups such as alcoxisilanes, carboxylic acids, carbodiimide, aziridine, isocyanates, and polyols, are also discussed. Chapter 30 introduces a new class of smart UV-curable coatings. Smart coatings such as self-cleaning, self-healing, anti-fog, antibacterial, and synthesizing routes for smart coatings and different types of smart UV-curable coatings for various engineering applications are also discussed. Chapter 31 discusses the use of innovative multifunctional composite silane-zeolite coatings. The method proposed in this chapter is based on the deposition, using a hybrid silane binder, of the adsorbent material based on aluminum zeolite. The characterization of the composite materials in order to evaluate its industrial applicability is also discussed. Chapter 32 gives the approaches for conducting the intercalation of poly [oligo (ethylene glycol)-oxalate] (POEGO) into lithium hectorite. It also discusses the preparation of different nanocomposite materials by varying the molar ratio of the polymer to the lithium hectorite and their characterization using powder XRD, TGA, DSC, and ATR along with the use of AC impedance spectroscopy to measure the ionic resistance of the nanocomposites when complexed with lithium triflate.

Finally, a number of people have helped make this book possible. We hereby acknowledge Ms. Ania Levinson, our editor at Springer Science+Business Media, Mr. Brian Halm and Ms. Lesley Poliner our project coordinators at Springer Science+Business Media, Ms. Abira Sengupta our assistant editor at Springer Science+Business Media, Ms. Megan Rohm, and all authors and reviewers, without whose contributions and support this book would not have been written. We thank you all for all of the excellent work and assistance that has been provided in moving this book project forward.

Spring 2016   Majid Hosseini
                                                          Abdel Salam Hamdy Makhlouf

Contents

Contributors

Mina Abbasipour Department of Textile Engineering, Science and Research Branch, Islamic Azad University, Tehran, Iran

Nedal Y. Abu-Thabit Department of Chemical and Process Engineering Technology, Jubail Industrial College, Jubail Industrial City, Kingdom of Saudi Arabia

Mohammed Alsultan Intelligent Polymer Research Institute, ARC Centre of Excellence for Electromaterial Science (ACES), University of Wollongong, Wollongong, NSW, Australia

Department of Science, College of Basic Education, University of Mosul, Mosul, Iraq

Okezie I. Aruoma School of Pharmacy, American University of Health Sciences, Signal Hill, CA, USA

Sivakumar Balakrishnan Intelligent Polymer Research Institute, ARC Centre of Excellence for Electromaterial Science (ACES), University of Wollongong, Wollongong, NSW, Australia

Carlos Baleizão Centro de Química-Física Molecular, IN-Institute of Nanoscience and Nanotechnology, Instituto Superior Técnico, University of Lisbon, Lisboa, Portugal

Andreea Irina Barzic "Petru Poni" Institute of Macromolecular Chemistry, Iasi, Romania

Saeed Bastani Surface Coating and Corrosion Department, Institute for Color Science and Technology, Tehran, Iran

Center of Excellence for Color Science and Technology, Tehran, Iran

Rose Marie Belardi Universidade Federal de Itajubá, Campus Avançado de Itabira, Minas Gerais, Brazil

Rabin Bissessur Department of Chemistry, University of Prince Edward Island, Charlottetown, PE, Canada

Lucio Bonaccorsi Department of Electronic Engineering, Industrial Chemistry and Engineering, University of Messina, Messina, Italy

Luminita Ioana Buruiana "Petru Poni" Institute of Macromolecular Chemistry, Iasi, Romania

Luigi Calabrese Department of Electronic Engineering, Industrial Chemistry and Engineering, University of Messina, Messina, Italy

Angela Caprì Department of Electronic Engineering, Industrial Chemistry and Engineering, University of Messina, Messina, Italy

Larissa Brentano Capeletti Instituto de Química, UFRGS, Porto Alegre, Brazil

Lina M. Castano Department of Aerospace Engineering, University of Maryland, College Park, MD, USA

Karina da Silva Chaves Universidade Federal de Mato Grosso (UFMT), LEMAT, Campus UFMT Barra do Garças, MT, Brazil

Yahya E. Choonara Wits Advanced Drug Delivery Platform Research Unit, Department of Pharmacy and Pharmacology, School of Therapeutic Sciences, Faculty of Health Sciences, University of the Witwatersrand, Johannesburg, South Africa

Douglas C. Dahn Department of Physics, University of Prince Edward Island, Charlottetown, PE, Canada

V. Dalmoro Institute of Chemistry, Federal University of Rio Grande do Sul, Porto Alegre, RS, Brazil

Dhaneswar Das Department of Chemical Sciences, Tezpur University, Napaam, Assam, India

Maria C. DeRosa Department of Chemistry, Carleton University, Ottawa, ON, Canada

Swapan Kumar Dolui Department of Chemical Sciences, Tezpur University, Napaam, Assam, India

Diego Vinicius do Nascimento Universidade Federal de Mato Grosso (UFMT), LEMAT, Campus UFMT Barra do Garças, MT, Brazil

João Henrique Zimnoch dos Santos Institute of Chemistry, Federal University of Rio Grande do Sul, Porto Alegre, RS, Brazil

Lisa C. du Toit Wits Advanced Drug Delivery Platform Research Unit, Department of Pharmacy and Pharmacology, School of Therapeutic Sciences, Faculty of Health Sciences, University of the Witwatersrand, Johannesburg, South Africa

José Paulo S. Farinha Centro de Química-Física Molecular, IN-Institute of Nanoscience and Nanotechnology, Instituto Superior Técnico, University of Lisbon, Lisboa, Portugal

Fatemeh Farjadian Pharmaceutical Science Research Center, School of Pharmacy, Shiraz University of Medical Sciences, Shiraz, Iran

Alison B. Flatau Department of Aerospace Engineering, University of Maryland, College Park, MD, USA

Gregory Freihofer Department of Mechanical and Aerospace Engineering, University of Central Florida, Orlando, FL, USA

Angelo Freni CNR ITAE, Messina, Italy

Félix C. García Departamento de Química, Facultad de Ciencias, Universidad de Burgos, Burgos, Spain

José M. García Departamento de Química, Facultad de Ciencias, Universidad de Burgos, Burgos, Spain

Pronob Gogoi Department of Chemical Sciences, Tezpur University, Napaam, Assam, India

Chang-Sik Ha Department of Polymer Science and Engineering, Pusan National University, Busan, Korea

Ivan Hevus Department of Coatings and Polymeric Materials, North Dakota State University, Fargo, ND, USA

Majid Hosseini Manufacturing and Industrial Engineering Department, College of Engineering and Computer Science, The University of Texas – Rio Grande Valley, Edinburg, TX, USA

Junhua Huang School of Chemistry, Monash University, Clayton, VIC, Australia

Matthieu Hughes Department of Physics, University of Prince Edward Island, Charlottetown, PE, Canada

Hideyuki Kanematsu Department of Materials Science and Engineering, Suzuka, Mie, Japan

Ioannis Karapanagiotis Department of Management and Conservation of Ecclesiastical Cultural Heritage Objects, University Ecclesiastical Academy of Thessaloniki, Thessaloniki, Greece

Pooneh Kardar Surface Coating and Corrosion Department, Institute for Color Science and Technology, Tehran, Iran

Ramin Khajavi Nanotechnology Research Center, Islamic Azad University, South Tehran Branch, Tehran, Iran

Ananiy Kohut Department of Organic Chemistry, Lviv Polytechnic National University, Lviv, Ukraine

Pradeep Kumar Wits Advanced Drug Delivery Platform Research Unit, Department of Pharmacy and Pharmacology, School of Therapeutic Sciences, Faculty of Health Sciences, University of the Witwatersrand, Johannesburg, South Africa

Mohammad Mahdavian Department of Surface Coatings and Corrosion, Institute for Color Science and Technology, Tehran, Iran

Abdel Salam Hamdy Makhlouf Manufacturing and Industrial Engineering Department, College of Engineering and Computer Science, The University of Texas – Rio Grande Valley, Edinburg, TX, USA

Panagiotis Manoudis Department of Management and Conservation of Ecclesiastical Cultural Heritage Objects, University Ecclesiastical Academy of Thessaloniki, Thessaloniki, Greece

J.M.G. Martinho Centro de Química-Física Molecular, IN-Institute of Nanoscience and Nanotechnology, Instituto Superior Técnico, University of Lisbon, Lisboa, Portugal

Emily Mastronardi Department of Chemistry, Carleton University, Ottawa, ON, Canada

Madhappan Santha Moorthy Department of Polymer Science and Engineering, Pusan National University, Busan, Korea

Liana Maria Muresan Faculty of Chemistry and Chemical Engineering, Babes-Bolyai University, Cluj-Napoca, Romania

Saravanan Nagappan Department of Polymer Science and Engineering, Pusan National University, Busan, Korea

Mehdi Honarvar Nazari Department of Civil and Environmental Engineering, Washington State University, Pullman, WA, USA

Ndidi C. Ngwuluka Faculty of Pharmaceutical Sciences, University of Jos, Jos, Nigeria

Nelson A. Ochekpe Faculty of Pharmaceutical Sciences, University of Jos, Jos, Nigeria

Jesús L. Pablos Departamento de Química, Facultad de Ciencias, Universidad de Burgos, Burgos, Spain

Polymer Photochemistry Group, Instituto de Ciencia y Tecnología de Polímeros, C.S.I.C., Madrid, Spain

Mayra Cristina Silva Pereira Universidade Federal de Mato Grosso (UFMT), LEMAT, Campus UFMT Barra do Garças, MT, Brazil

Paula Becker Pertuzatti Laboratorio de Analise de Alimentos, UFMT Campus UFMT Barra do Garças, MT, Brazil

Susana Piçarra Escola Superior de Tecnologia de Setúbal, Instituto Politécnico de Setúbal, Setúbal, Portugal

Viness Pillay Wits Advanced Drug Delivery Platform Research Unit, Department of Pharmacy and Pharmacology, School of Therapeutic Sciences, Faculty of Health Sciences, University of the Witwatersrand, Johannesburg, South Africa

Fernanda S. Poletto Departamento de Química Orgânica, Instituto de Química, Universidade Federal do Rio Grande do Sul, Porto Alegre, RS, Brazil

Edoardo Proverbio Department of Electronic Engineering, Industrial Chemistry and Engineering, University of Messina, Messina, Italy

Seetha Raghavan Department of Mechanical and Aerospace Engineering, University of Central Florida, Orlando, FL, USA

Bahram Ramezanzadeh Department of Surface Coatings and Corrosion, Institute for Color Science and Technology, Tehran, Iran

Abbas Ranjbar Intelligent Polymer Research Institute, ARC Centre of Excellence for Electromaterial Science (ACES), University of Wollongong, Wollongong, NSW, Australia

Kummara Madhusudana Rao Department of Polymer Science and Engineering, Pusan National University, Busan, Korea

Felisa Reyes-Ortega Tecnologías Avanzadas Inspiralia, S.L., Parque Científico de Madrid, Madrid, Spain

Juan Rodríguez-Hernández Institute of Polymer Science and Technology (ICTP-CSIC), Madrid, Spain

Iskandar Saada Department of Chemistry, University of Prince Edward Island, Charlottetown, PE, Canada

Bhaskar Jyoti Saikia Department of Chemical Sciences, Tezpur University, Napaam, Assam, India

Katsuhiko Sano R&D Section, Sakura, Yokkaichi, Mie, Japan

C. Santos Institute of Chemistry, Federal University of Rio Grande do Sul, Porto Alegre, RS, Brazil

Felipe Serna Departamento de Química, Facultad de Ciencias, Universidad de Burgos, Burgos, Spain

Xianming Shi Department of Civil and Environmental Engineering, Washington State University, Pullman, WA, USA

Ricardo Stefani Universidade Federal de Mato Grosso (UFMT), LEMAT, Campus UFMT Barra do Garças, MT, Brazil

Gerhard F. Swiegers Intelligent Polymer Research Institute, ARC Centre of Excellence for Electromaterial Science (ACES), University of Wollongong, Wollongong, NSW, Australia

Toshihiro Tanaka Department of Materials Science and Engineering, Osaka, Japan

Marli Luiza Tebaldi Universidade Federal de Itajubá, Campus Avançado de Itabira, Minas Gerais, Brazil

Victoria Trenton Department of Physics, University of Prince Edward Island, Charlottetown, PE, Canada

Gabrielle L.R.R.B. Vinhal Universidade Federal de Mato Grosso (UFMT), LEMAT, Campus UFMT Barra do Garças, MT, Brazil

Andriy Voronov Department of Coatings and Polymeric Materials, North Dakota State University, Fargo, ND, USA

Stanislav Voronov Department of Organic Chemistry, Lviv Polytechnic National University, Lviv, Ukraine

Gordon G. Wallace Intelligent Polymer Research Institute, ARC Centre of Excellence for Electromaterial Science (ACES), University of Wollongong, Wollongong, NSW, Australia

Hossein Yari Department of Surface Coatings and Corrosion, Institute for Color Science and Technology, Tehran, Iran

Norazwani Muhammad Zain Fabrication and Joining Section, Universiti Kuala Lumpur Malaysia France Institute, Selangor, Malaysia

Syazana Ahmad Zubir School of Materials and Mineral Resources Engineering, Universiti Sains Malaysia, Pulau Pinang, Malaysia

Irina J. Zvonkina University of Akron, Akron, OH, USA

About Authors
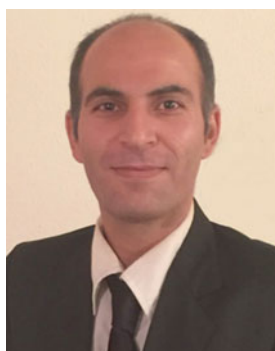
Majid Hosseini has earned both his Ph.D. and M.S. degrees in Chemical Engineering from *The University of Akron* in Ohio, United States. He has also completed his Bachelors degree in Chemical Engineering at *Sharif University of Technology* in Tehran, Iran. Dr. Hosseini's research interests, expertise, and experiences are very diverse, ranging from intelligent polymers and coatings to micro/encapsulation, nanoparticles for biomedical applications, industrial biotechnology, renewable energies, bioprocess engineering and developement, and biofuels. Dr. Hosseini has been actively engaged in various fields of polymers, bio/nanotechnology, sustainability, biofuels, and related technology development both in industry and academia. He is a persistent reviewer of leading international journals, has published high caliber research articles, and coinvented US and international patent application technologies. Dr. Hosseini has been a member of several professional bodies in the USA including *The New York Academy of Sciences, American Institute of Chemical Engineers (AICHE), AICHE-Institute for Sustainability, AICHE-SBE (Society of Biological Engineering), New Design Institute for Emergency Relief Systems (DIERS), International Society for Pharmaceutical Engineering (ISPE), AICHE-Pharmaceutical Discovery, Development and Manufacturing Forum, and The National Society of Collegiate Scholars.*

Abdel Salam Hamdy Makhlouf Dr. Makhlouf is RGV STAR Professor in the Department of Manufacturing & Industrial Engineering, UTRGV. He is the Founder of Surface Engineering Laboratory and a leading faculty of the Rapid Response Manufacturing Center.

Prof. Makhlouf is a multiple-award winner for his academic excellence: He received several prestigious awards in Germany (Humboldt Research Award for Experienced Scientists at Max Planck Institute); USA (Fulbright Visiting Scholar, NSF Fellow, and Dept. of Energy Fellow); Belgium (Belgian Federal Science Research Fellowship); Arab League (Arab Youth Excellence Award in Innovation 2013); Jordan (Abdul Hameed Shoman Award in Engineering Science 2012); Egypt (National Prize of Egypt in Advanced Science and Technology 2006, Egyptian Prize of Excellence in Surface Technology and Corrosion 2006, and Egyptian Prize of Excellence and Innovation in Materials Science and their Applications 2009); and Palestine (An-Najah Prize for Research 2014). Makhlouf's biography was selected to be included in *Who's Who in the World*® 2015, 2007, and 2006.

Prof. Makhlouf was able to make breakthroughs in several highly important areas of materials science and engineering. His publication list (+170) includes studies and review papers authored in journals from top publishers. He is the editor of 11 books and 20 book chapters. One of his articles has been ranked the second among the Top 25 Hottest Articles in Materials Science, Elsevier, 2006. He has made significant contributions to the field of materials science and manufacturing engineering, all of which place him among the top scientists working in his field. In fact, when performing a Google Scholar database search using the keywords "silica conversion coatings aluminum"; "corrosion aluminum composites"; "corrosion niobium stainless steels"; "smart coatings materials protection"; "Electroless Ni–P alloy coatings"; "self-healing coatings magnesium"; or "nano-particle aluminum coating", his articles on these subjects appear among the top 1st–7th out of >100,000 scholarly articles on these highly specialized research topics. Thus, his publications are among the most important and influential articles. Dr. Makhlouf's book "Handbook of Nanoelectrochemistry: Electrochemical Synthesis Methods, Properties, and Characterization Techniques", published by Springer, 2016 has been featured in the website of the International Society of Electrochemistry.

Prof. Makhlouf has gained invaluable experience by working in coatings and corrosion laboratories in USA, Italy, and Germany and by collaborating on a multitude of international projects with American, French, Romanian, Saudi, and Korean institutions among others. His career has spanned appointments and invitations to work with other scientists in the top 1 % of material engineering across the globe, and he has been called upon exhaustively to report his expert opinion on scientific panels, conference keynote addresses, and to government and industry committees. He is a Consultant for Innosquared GmbH, and for Covestro, Germany. He has organized and served as a head speaker at numerous highly prestigious international symposiums and conferences over 30 times. His work as a professor has also brought him acclaim, with numerous appointments at outstanding institutions and universities in the USA, Germany, Italy, Egypt, and Asia and a record of having supervised and graduated 11 PhD and Master's students and 5 postdoctoral fellows.

Prof. Makhlouf is a persistent journal reviewer, advisor, and judge of the work of his peers. He is a referee for over 30 international journals of a high caliber and a continued board member of over 22 journals. He is also an experienced Editor with board titles at journals published by Springer and Elsevier, an Expert Evaluator for the EU's FP7, with an estimated budget of over €50.521 billion, expert for the German Ministry of Education and Research, reviewer for the German Academic Exchange Service, and expert for the German Aerospace Center. He is a reviewer/panelist for the NSF programs: MME, MEP, and CREST; with an estimated budget of over $7.6 billion. He is a reviewer for the US Fulbright Commission, the Qatar National Research Fund, and the Kuwait Foundation for the Advancement of Sciences.

Chapter 1
Smart Stimuli-Responsive Nano-sized Hosts for Drug Delivery

Majid Hosseini, Fatemeh Farjadian, and Abdel Salam Hamdy Makhlouf

Abstract The evolution in the synthesis of smart polymers broadens new horizons for their potent application in medicine, especially in drug delivery. Many synthetic polymers that exhibit environmentally responsive behavior are potential smart carrier candidates that allow for controlled therapeutic delivery. These materials can be loaded with specific drugs for therapeutic applications, releasing treatment in response to a stimulus. This stimuli-responsive capability has enabled smart polymeric materials to distribute drugs in response to commonly known exogenous and/ or endogenous stimuli. Examples of these various stimuli include pH, enzyme concentration, temperature, ultrasound intensity, as well as light, magnetic field, redox gradients and a multitude of other potential stimuli. This chapter provides a detailed critical discussion and an overview of the stimuli-responsive polymers which have found applications in targeted drug delivery. Furthermore, multiresponsive systems and their forthcoming development as well as challenges associated with some stimuli-responsive systems are discussed. Finally, the most recent and emerging trends along with a look toward expected future breakthroughs using these types of nanocarriers are discussed.

Keywords Smart polymers • Stimuli-responsive polymers • Nanocarriers • Drug delivery

M. Hosseini (✉)
Manufacturing and Industrial Engineering Department, College of Engineering and Computer Science, The University of Texas – Rio Grande Valley, Edinburg, TX, USA
e-mail: majid.hosseini01@utrgv.edu

F. Farjadian (✉)
Pharmaceutical Sciences Research Center, School of Pharmacy, Shiraz University of Medical Sciences, P.O. Box 71345-1583, Shiraz, Iran
e-mail: farjadian_f@sums.ac.ir

A.S.H. Makhlouf (✉)
Manufacturing and Industrial Engineering Department, College of Engineering and Computer Science, The University of Texas – Rio Grande Valley, Edinburg, TX, USA
e-mail: abdel.makhlouf@utrgv.edu

1.1   Introduction

The developments in pharmaceutical sciences have made improvements in the drug administration fields including design, action, toxicity, and delivery. The research being done in this field has resulted in reducing the drug's side effects and consequently has improved the treatment, and in some cases prevention, of a vast array of diseases. The most significant approaches are in controlled and targeted drug delivery. Delivering an existing drug to cure the affected diseased area, while leaving healthy organs unscathed, is the key concept in this field. For this purpose, scientists have taken advantage of the wide breadth of knowledge offered through the cooperation of multidisciplinary fields, including nanotechnology and material sciences. Nanotechnology is as an emerging field in medicine which has revolutionized the traditional and unsuccessful methods of drug delivery involving the application of high drug dosages, especially in terminal diseases like cancer. Indeed, nanocarriers that are engineered from sustainable materials could be synthesized and used as efficient hosts for therapeutic agents. One of the emerging contributions from the collaboration between nanotechnology and material chemistry is the design of smart nanocarriers. Materials that are capable of responding to external stimuli are commonly referred to as "intelligent" and/or "smart" materials [1]. Intelligent polymers (IPs) are a significant class of polymers with broad applications. Polymers which respond not only to environmental changes but to small external stimuli as well are sometimes called soluble/insoluble stimuli-responsive polymers [2]. IPs show great promise and are already widely used in drug delivery, cell culture, gene carriers, tissue engineering, drug and gene delivery, cancer therapy, dental and medical devices, and protein purification [3].

   Generally, three main groups of stimuli are known to influence structural changes of IPs: physical, biological, and chemical. The first group of physical stimuli includes light, mechanical forces and/or stress, temperature, ultrasound wavelengths, etc. Of the chemical stimuli group, ionic strength and changes in pH can be mentioned. The group of stimuli, referred to as biological stimuli, can include enzymes and biomolecules [4]. Recent developments and further improvements of smart nanocarriers have made them suitable candidates as vehicles for the deliberate release of drug. Versatile, controllable, sensitive, and stimuli-responsive macromolecules play a crucial role in smart nanoparticle's formation [4, 5]. Thus, such carriers have the ability to adapt their physicochemical properties and as such have the ability to react to a plethora of stimuli in multiple fashions. They can also respond to naturally promoted internal stimuli of certain pathophysiological conditions, including those aforementioned responses to external stimuli. Several monomers are stimuli-sensitive specific and have the ability to be customized with either a single stimuli-responsive homopolymer or with copolymers responding to multiple stimuli. The sensitivity of IPs can potentially be fine-tuned in order for them to respond to a selected stimulus within a narrow range. These benefits of intelligent nanocarriers systems must be considered to accurately and efficiently program drug delivery [5]. This chapter covers an introduction to intelligent nano-sized hosts which have found applications in drug delivery, their future outlook; and presents practical applications and necessities

of the intelligent/smart nanocarriers for drug delivery applications. Broadly speaking the nanocarriers are generally categorized as polymer-based, lipid-based, and metal-and/or inorganic-based nanocarriers. In the following sections, intelligent nano-polymeric micelles, nanogels, magnetic nanoparticles, mesoporous silica, and gold nano-sized structures capable of responding to different stimulus with an emphasis on pH, temperature, and dual-responsive systems will be discussed.

1.2   Stimuli-Responsive Nano-polymeric Micelles Drug Delivery System

Polymeric micelles are typical aggregates of di- or triblock copolymers which consist of hydrophobic and hydrophilic blocks [6, 7]. Functional polymers of block construction allow for drug entrapment within these structures and make versatile delivery systems [6]. The development of reversible addition–fragmentation chain transfer (RAFT) as well as atom transfer radical polymerization (ATRP) (i.e., controlled living polymerization techniques) allows for molecular weight as well as dispersion control of block copolymers, which favors micelle formation while controlling chain sizes [8, 9]. Nano-sized micelles are appropriate vehicles for targeted drug delivery systems [10]. Smart micelles, composed of hydrophilic blocks, are able to respond to a plethora of stimuli including: optic changes, medium, temperature, and, etc. [11]. Smart micelles can also potentially self-assemble in response to stimulus [12, 13]. During these conformational changes, the therapeutic agents which could be entrapped in these structures would be released in response to stimulus [11, 13]. A schematic illustration of a block copolymer capable of micellization in response to stimulus is shown in Fig. 1.1.

In drug delivery systems, the research community has placed a great deal of focus on sensitivity to temperature [14, 15]. Block copolymers, composed of thermoresponsive segments, are potent pre-micelle structures which can self-assemble when they undergo changes in temperature [14, 16]. The changes of such structures are highly dependent on their lower critical solution temperature (LCST) [17]. It should be noted that temperature variation can cause changes in solubility and would consequently influence the effective control of the drug release rate while maintaining physicochemical stability and biological activity within the human
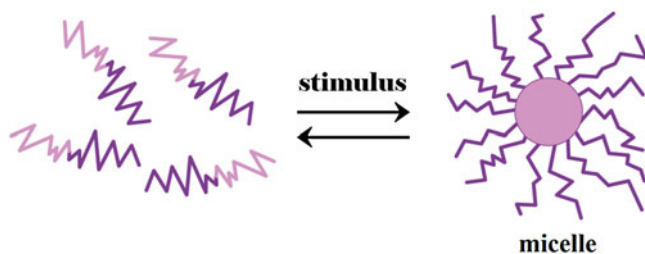

Fig. 1.1 Micellization in response to external stimuli

body [15]. This solubility transformation can potentially be associated to the presence of hydrophobic (alkyl) groups which are significant in establishing either LCST or upper critical solution temperatures (UCST). N-alkyl acrylamides are the most widely studied precursor in the synthesis of thermoresponsive macromolecules [15, 18]. Meanwhile, poly(N-isopropyl acrylamide) (PNIPAAm) is mostly incorporated in synthesis of thermoresponsive micelles for delivery systems [19]. The overwhelming applications of PNIPAAm in biological systems are related to a specific LCST (i.e., 32 °C), which is near the temperature profiles exhibited in the human body. However, when surfactants and additives are added, the LCST can be increased to a temperature that is more comparable to that of the human biological system. Furthermore, comonomers, be they hydrophobic or hydrophilic in nature, can be utilized in the copolymerization required for the arrangement of LCST [19]. This is illustrated by the polymer's hydrophilic properties that, when enhanced, higher transition temperatures can be obtained through the subsequent increase of the macromolecules' hydrogen-bonding ability. Conformational change of the polymer, exacerbating insolubility, and hydrophobic tendencies occur when temperatures are above the LCST [20]. In an aqueous environment, solubility of the polymeric system increases at sub-LCSTs. LCST systems are also dependent on pressure, and rely upon not only temperature, but the entropy of mixing as well [20].

By disrupting the water assembly that surrounds the polymer structure, the inclusion of moieties (i.e., hydrophobic moieties) was found to result in the decrease of the LCST. Micelle formation in copolymers with thermosensitive PNIPAAm can take place in two different circumstances: shell formation will occur when below the LCST and as a corona when above the LCST [21, 22]. It is possible to create micelles with core–shell characteristics by utilizing copolymer systems that contain both PNIPAAm and hydrophobic segments, where the hydrated PNIPAAm-segmented outer shell is hydrophilic and the inner core is hydrophobic below the PNIPAAm's LCST [22]. Drugs which are hydrophobic can be loaded in the inner core, while aqueous solubilization and responsiveness to temperature is managed by PNIPAAm's outermost shell. The interior's core is prevented from interacting with the biocomponents by the hydrophilic PNIPAAm outer shell, also acting as a micelle stabilizer. However, hydrophobicity can be induced through localized heating of the outer PNIPAAm shell [23]. It is possible to increase the selective, localized micelle amassing through improving their cell adsorption which is dictated through those hydrophobic interactions from the cells and polymeric micelles [24]. Therapeutics can be delivered by thermoresponsive micelles by means of a stimuli-responsive targeting process; for example, a solid tumor could be treated by site-specific heating. In conjunction with their enhanced permeability and retention (EPR) effects, thermally sensitive micelles are predicted to display their dual-targeting functionality with the capability of being induced through both thermal and passive means. Micelle destabilization can also occur at temperature exceeding the LCST, causing the site-specific drug release to be increased [25].

Pioneering research in regards to block copolymer micelles that responded to thermal changes were comprised of PNIPAAm and polystyrene (PSt) segments [23]. Preparation of a series of polymers that were PNIPAAm-based was accomplished in later studies through the use of free radical polymerizations while utilizing either
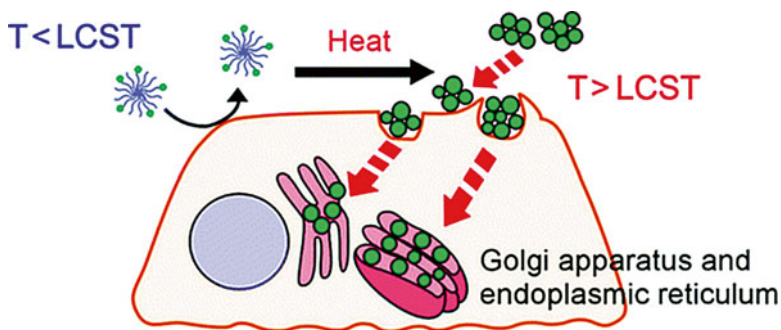
Fig. 1.2 An illustration of thermoresponsive drug-loaded nanoparticle uptake into the cells (Reprinted with permission from [29], Copyright American Chemical Society)

polycondensations, chain transfer agents, or polymerizations with ring openers, with the following products being created: "alkyl-terminated PNIPAAm" [26], PNIPAAm that had been altered to be hydrophobic [27], "PNIPAAm-*b*-poly(butyl methacrylate) (PNIPAAm-*b*-PBMA)" [25], and "PNIPAAm-*b*-poly(D,L-lactide) (PNIPAAm-*b*-PLA)" [22]. Sluggish drug delivery was found to occur in micelles of PNIPAAm-*b*-PBMA carrying doxorubicin (DOX) [25]. However, rapid DOX release may potentially be coaxed through purposeful micelle structure deformation at conditions higher than the LCST. Furthermore, structural changes of temperature-responsive micelles were stimulated by LCST temperature cycling, thus regulating the DOX release behavior [25]. In contrast, due to their stiff core of PSt ($Tg \sim 100$ °C) being unaffected by expansion then contraction of the PNIPAAm coronas' conformational transition, no significant DOX release above the LCST for PNIPAAm-*b*-PSt micelles was observed. It was reported that the stability and the thermosensitive drug release properties of polymeric micelles were dependent upon the hydrophobic segment construction of the inner core [23].

As in vivo application was impractical due to the LCST of "PNIPAAm, P(NIPAAm-*co*-N, N-dimethylacrylamide)-*b*-poly(caprolactone)" [28] and degradable "P(NIPAAm-*co*-N, N-dimethylacrylamide)-*b*-poly(D,L-lactide) (P(NIPAAm–DMAAm)-*b*-PLA)" [29] copolymers consisting of LCST greater than physiological conditions (40 °C) were created. Further, P(NIPAAm–DMAAm)-*b*-PLA's mechanism allowing for intracellular uptake when exposed to a thermal stimulus was examined within carotid endothelial cells [29]. Each of the following factors had a considerable effect on the micelles' internalization: thermal conditions, the viability of the cells, time, and the concentration of the micelles. Internal lysosome observation could not take place for the "P(NIPAAm–DMAAm)-*b*-PLA" micelles that surrounded the "Golgi apparatus/endoplasmic reticulum." Figure 1.2 is a schematic illustration of this phenomenon adapted from Okano et al.'s report [29].

The data gathered from Okano et al.'s study reveals that micelles with thermally responsive properties may find application as intracellular drug delivery systems for either drugs that are sensitive to pH and certain enzymes or for biomolecules such as DNS, proteins, and peptides; each of which can be activated via heat at the desired delivery site [29].

The evaluation of micelle cores consisting of thermally sensitive "PNIPAAm, PMNP [poly(N-acryloyl-5-methoxy-2-pyrrolidone)]", or "PBNP [poly(N-acryloyl-5-butoxy-2-pyrrolidone)]" were performed in order to determine their DOX-loading efficiency (DLE) [30]. Micelles loaded with DOX displayed the following DLE trend: "PNIPAAm–PNP < PNIPAAm–PMNP < PNIPAAm–PBNP." This is associated with the relationship between the core's increasing desire to be hydrophobic and the enhanced cohesive forces displayed between it and the drug [30]. When temperatures are greater than the LCST, the release of the drug is as follows, which implies that the cohesive forces that allow for excellent encapsulation also hinder release: "PNIPAAm–PNP > PNIPAAm–PMNP > PNIPAAm–PBNP" [30]. pH-responsive micelles are copolymers containing pH-sensitive segments which are capable of varying their dimensions when responding to pH variations of their surrounding medium [31, 32]. Herein, two kinds of pH-sensitive micelles are to be considered and discussed: anionic amphiphilic polymers which have a block of functional group containing an acidic group and when immersed in basic pH swell, while others consist of groups that are basic and when exposed to acidic pH, swell. The nano-sized micelles of IPs can be designed for delivery systems of anticancer drugs where changes and/or manipulation of pH can potentially influence the drug's release. Due to acidic medium of most tumors' cells (pH of 5.8–7.2), which is different from that of healthy organs, pH triggering could be successful in releasing the entrapped drug in pH-responsive micelles [33].

It was shown that the solubilization of the membranes of lipids by hydrophobic polyelectrolyte poly(2-ethylacrylic acid) is highly dependent upon pH [34]. When such drug-loaded pH-responsive particles passes through the *"extracellular space"*, encountering *"early"* and *"late endosomes"* along with *"lysosomes"*, a drug is exposed to pHs ranging from 7.4 to 5 [34].

Pharmaceutical scientists take advantage of cell membrane pH gradient so as to stimulate and activate carriers, (i.e., lipids, colloids, polymers, and particles) causing disruption while permitting drug escape from the endosomal compartments. Due to their low toxicity and high efficacy, acidic membrane-disruptive polymers, that are inert at an above neutral pH (7.4) and are relevant to endolysosomal trafficking (pH of 5–7), have been exploited in intracellular delivery applications [35, 36]. A vast array of anionic and cationic polymers, able to trigger a stimulus response based upon the pH-reliant protonation states driving the transitions that are physicochemical, are able to provide precise membranolytic activity within these limits [34, 37].

pH-sensitive polymers with anionic groups are copolymers and can contain many different segments with examples being that of acrylic acid and alkyl acrylates, hydrophobic monomers and alkyl acrylic acids [38], or the poly(styrene-*alt*-maleic anhydride) altered with alkyl amide [39]. The polymers become protonated when exposed to an acidic environment, encouraging aggregation with their newly hydrophobic backbones along with their acquired membrane-partitioning behavior. At a high or even neutral pH, these polymers are deprotonated and become hydrophilic. Thus, self-aggregation performance becomes more precise by means of these structures [39].

With simple preparation methods, established polymeric materials, minimal toxicity, and particle sizes between 10–1000 nm, polymeric nanospheres are able to perform as pH-sensitive oral drug delivery vessels [40]. Hoping to improve upon the peptidic and peptidomimetic drugs' bioavailability, these pH-sensitive polymeric nanospheres were initially developed that ultimately led to the creation of the gastro-resistant coating agent Eudragit® (L100–55, L100, and S100) family of MAA copolymers [41, 42]. Cationic amphiphilic micelles are another type of pH-responsive polymeric systems. Several nanomicellar systems for drug delivery have been introduced based on polyethyleneimine (PEI) including PEG–*b*-PEI [43], PLGA–*b*-PEI [44], and MPEG–PCL-*g*–PEI [45]. Although there are many polymers that present desirable cytotoxicity and transfection efficiency properties (i.e., PAMAM, poly(N, N-dimethyl aminoethyl methacrylate) (PDMAEMA), poly(L-lysine) (PLL), and modified chitosan), researchers continue to use polyethyleneimine (PEI) as a baseline that all novel polymeric systems are evaluated [31]. Nanospheres synthesized from mixtures of chitosan and pH-sensitive polyanions (Eudragit®) were applied for oral delivery of insulin [46]. Rat oral studies displayed increased plasmatic drug levels for the systems when evaluated against encapsulated insulin [46].

Anionic polymers with PAA, PMAA, PEAA, PPAA, PBAA, NIPAM, PGA, or other carboxylic groups are some of the most frequently utilized polymers that respond to changes in pH [31]. The quick phase transition and tight conformation that is characteristic of PAA is caused by the carboxylic acid groups due to the promotion of aggregation via their induced hydrophobic interactions [31]. These multipurpose polymer classes are suitable vehicles for macromolecular intracellular deliveries such as that of DNA, siRNA, drugs, peptides, and proteins while maintaining their affability for creation via controlled polymerization techniques (i.e., RAFT) [47].

As an example of all stemming from a polyphosphoester block copolymer system that is biodegradable in nature, variation of nanoparticles' surface charge/functionality will quickly and simply yield pH-sensitive block copolymers [48]. Micelle formation (i.e., positive, negative, neutral, zwitterionic) occurred rapidly when various amphiphilic diblock polyphosphoesters were separately suspended in water [48]. Figure 1.3 represents an illustration of different types of micelles, adapted from Wooley et al.'s report [48]. These micelles showed high biocompatibility and low cytotoxicity and are attractive for drug delivery purposes [48].

Researchers have used all of the resources at their disposal so as to determine the best way to modify carrier's structure so as they are able to respond to a plethora of stimuli (e.g., pH, oxidation–reduction, photons, electrons, enzymes, temperature, as well as magnetic fields) while increasing the drug's effectiveness and retaining its targeting mechanism [49]. Among all of the dual-responsive nanosystems, those nanoparticles that act upon pH and temperature changes are among those that are most studied. Figure 1.4 is a schematic illustration representing pH and temperature response, adapted from Schilli et al.'s report [50]. Thermal, pH, and solvent variation, as well as the length of the block, were all key factors in distinct micelle formation from PNIPAAm-b-PAA copolymers [50].
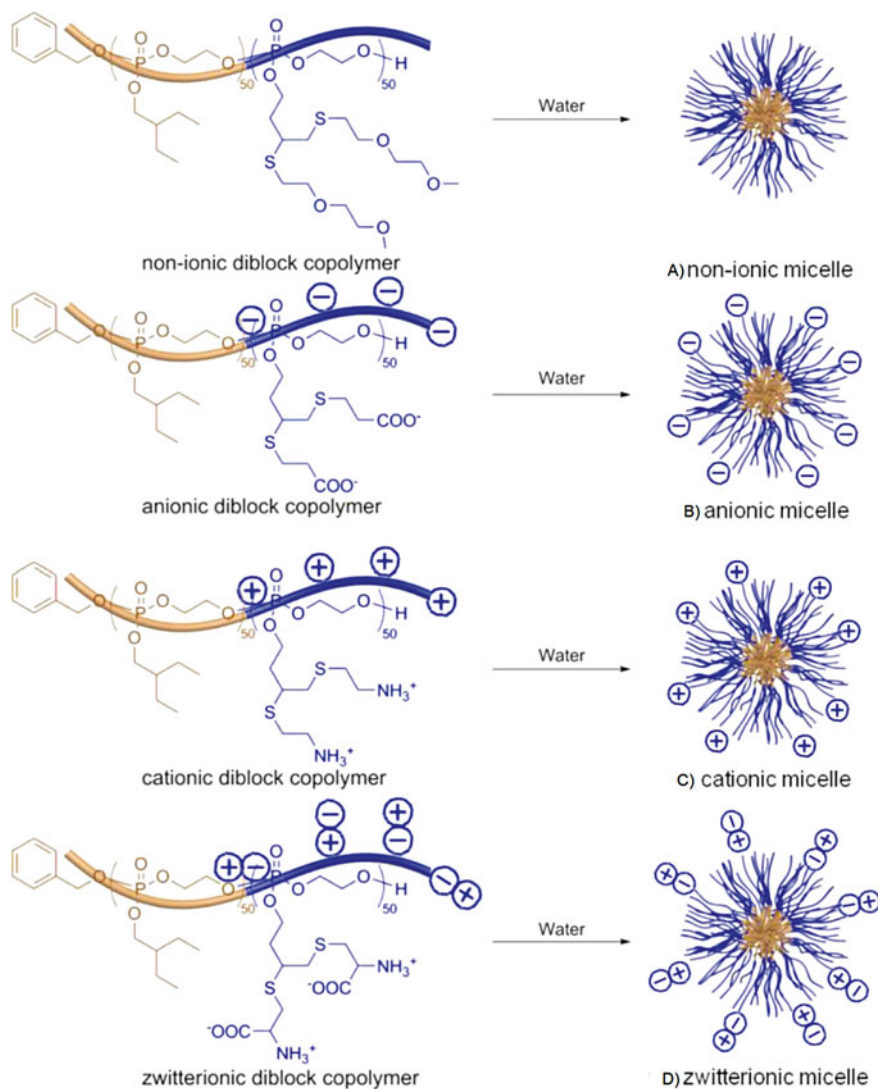
Fig. 1.3 An illustration of different type of micelles; (**a**) nonionic, (**b**) anionic, (**c**) cationic, (**d**) zwitterionic (Reprinted with permission from [48], Copyright American Chemical Society)

In designing these dual-responsive systems, many researchers have included weak acids, which in and of themselves are pH sensitive, into thermosensitive PNIPAAm, granting with the network a pH-dependent LCST. The precise phase transition is activated by slight changes in pH and thus creates tumor-fighting drug delivery systems that rely upon pH activation [50].

Self-assembled, thermal/pH-sensitive core–shell nanoparticles composed of poly(NIPAAm-*co*-N, N-dimethylarylamide-*co*-10-undecenoic acid) were found to

Fig. 1.4 pH and temperature response from PNIPAAm-*b*-PAA (Reprinted with permission from [50], Copyright American Chemical Society)
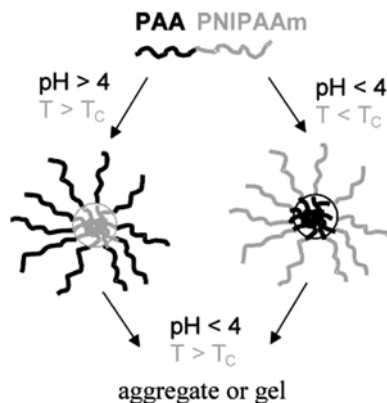
be stable in simulated physiological conditions (pH of 7.4, 37 °C); deforming/ precipitating in an acidic environment [51]. In an in vitro study, rapid DOX release was achieved in a simulated tumor environment (pH of 6.6) when compared to the same study conducted in a typical physiological environment (pH of 7.4) [51, 52].

Thermal/pH-responsive nanoparticles synthesized were formed from a poly(NIPAAm-*co*-AA) block as well as a hydrophobic polycaprolactone block [53]. Interestingly, the nanoparticles were encapsulated up to 30 % (weight) by the polymeric systems and aggregated in the following conditions (pH 6.9; 37 °C) with higher temperatures and an acidic environment encouraging expedited drug release [53]. Many other interesting examples include "poly(D, L-lactide)-*g*-poly(NIPAAm-*co*-MAA)" for 5-fluorouracil's controlled delivery [54], methoxy-PEG-*b*-P(N-(2-hydroxypropyl) methacrylamide dilactate-*co*-(N-(2-hydroxy propyl) methacrylamide-*co*-histidine) for controlled delivery of DOX [55], and poly(NIPAAm-*b*-poly(histidine) for the delivery of DOX [56].

Macromolecular chimeras are a fascinating group of block copolymers that consist of synthetic polymers that have been conjugated with polypeptides. Within these systems, lysine and glutamic acid are frequently used and "poly(N, N-diethylacrylamide)-*b*-poly-(L-lysine)", with its thermal/pH-sensitive characteristics, was recently studied [57]. However, with desirable characteristics including non-toxicity, biocompatibility, increased efficiency, nutritional functionality, and poignant pH sensitivity, poly(L-histidine) [p (His)] stands out against other amino acids as a promising contender [56]. Effective drug release may be accomplished through the implementation of a core or corona of p (His) in polymeric micelles [56].

1.3 Stimuli-Responsive Nanogels in Drug Delivery Systems

Nanogels can be defined as cross-linked colloidal particles swelling through large solvent absorption, unable to dissolve due to the polymeric network's structure, be it chemically or physically cross-linked [58]. The behavior of these micro-/nanogels encompasses that from the swollen form (polymeric solution) to their collapsed

form (hard particles). Responses to stimuli vary depending on whether they are chemical, physical, or biochemical. The interactions between nanogels, whether between themselves or drugs, can be reversibly tuned depending upon the particle's swelling degree, opening the door to a vast array of opportunities [59]. The key component of nanogels, also commonly known as nano-hydrogels or hydrogel nanoparticles (NPs), varies in size (10–1000 nm) is three-dimensional hydrophilic networks. Typical nanogel characteristics are that of stability, high specific surface area, high water content, and biocompatibility. Nanogels are classified as nanogels that respond to stimuli or as nanogels that are sensitive to their environment [59]. The potential use in drug delivery applications has allowed nanogels to be in the spotlight of research in nanomedicine [60–63]. Although they already are capable of biological barrier crossing, provide drug degradation protection in physiological conditions, and provide ample surface area for conjugating targeting ligands, several other properties of stimulus-responsive nanogels make them truly unique and desirable. Such properties are as follows: hydrophilic interior network provides both protection for hydrophilic small molecules/biomacromolecule drugs and loading capabilities; their chemically cross-linked structure and the hydrophilic surface polymer chains allow for increased stability and prolonged exposure within the circulatory system; external stimuli can dictate the loading and release profile of a drug, reducing side effects while improving loading efficiency and enhance bioavailability; targeting external stimuli are site-specific; and increased retention in the diseased site [64]. The RAFT process can yield nanogels consisting of a well-defined structure and functionality by one of two approaches: either by the pre-formed polymer approach or the direct polymerization approach [65, 66]. It should be noted that while some micelle nanostructures synthesized by cross-linked, block copolymer assemblies are comparable to nanogels, the focus of the following discussion lies outside of the self-assembling block copolymer process.

Temperature-induced changes of a nanogel's polymer size, though rapid in nature, take place at the volume phase transition temperature (VPTT) [67]. These thermal-responding nanogels can be segregated into two groups depending upon their volume phase transition profile: positively or negatively temperature responsive [68]. Accelerated increase in particle size occurs when approaching the VPTT in positively temperature-responsive nanogels, while shrinkage is hastened above the VPTT in nanogels that are negatively temperature-responsive [68]. Although they are formed from PNIPAAm, possess a desirable LCST in aqueous solutions, and are at the center of more studies [69], negatively temperature-responsive nanogels are not efficient drug delivery carriers. Preference has been given to positively temperature-responsive nanogels, as their swelling behavior is induced by localized temperature fluctuations; this, along with their UCST, provides predictable and stable release of the encapsulated drug [69]. Conversely, negatively temperature-responsive nanogels release their drug payload through the collapse of their structure, which is less efficient and has the increased potential to release the drug prematurely. Regrettably, advancement in the use of positively temperature-responsive nanogels as delivery vehicles for therapeutics has stalled in the research stage.

So as not to inhibit drug release, nanogels that are to be used as drug delivery systems must possess a VPTT that is slightly greater than that of normal tissue, as the

area that requires treatment is typically inflamed or local hyperthermia can be easily induced. Attempting to increase the VPTT of a PNIPAAm chain proved successful through the incorporation of hydrophilic monomers; however this rendered the structure unusable for thermosensitive drug release systems, as it diminished the sharpness of their volume phase transition and extended the phase transition temperature range [70]. Good examples of such systems are hydrogels including PNIPAAm. An "ON/OFF release" mechanism activating in response to stepwise temperature changes was achieved by synthesizing cross-linked NIPAAm and BMA copolymers, providing desirable mechanical properties and swelling behavior that is thermally dependent. The release profile of the drug named indomethacin was observed and documented as "OFF" at elevated temperatures and "ON" at reduced temperatures [71].

Positive thermosensitive hydrogels expand at elevated temperatures and collapse at reduced temperatures. Those hydrogels that include PAA interpenetrating polymer network (IPN) and "PAAm or P(AAm–*co*-BMA)" exhibited a positive reliance on temperature during their expansion and the transition temperature, increasing with additional BMA [69]. Hydrogels respond to abrupt thermal changes, with their reversible swelling behavior allowing the drug's release rate, in this case ketoprofen, to be reversible from said monolithic device [69].

Pluronics and Tetronics are among the most frequently used thermoreversible gels, some of which have passed approval cycles for both the EPA (United States Environmental Protection Agency) and FDA (Food and Drug Administration) so as to be used in food, pharmaceutical, and also agricultural products [72]. Thermoreversible gels administration for parenteral application biodegradability is desirable, therefore a biodegradable poly(L-lactic acid) segment is typically used in lieu of the PPO portion of the PEO–PPO–PEO structure [73].

A potential approach for site-specific therapeutic delivery is by implementing pH reactive nanogels that are designed to change shape and/or their structure when exposed to a predetermined critical pH value. The critical pH that the nanogels respond to is determined by the weakly acidic groups' pK_a or the weakly basic groups' pK_b present on their polyelectrolyte structure, thus enabling the identification of two different system classifications: cationic or anionic [72]. Anionic pH-responsive nanogels swell when exposed to a pH environment greater than the pK_b value while the inverse cationic systems, where swelling occurs at a pH value lower than the pK of the weakly basic group [72]. Additional alkyl residues that are hydrophobic incorporated into the polyelectrolyte backbone of the nanogel will shift the pH.

The changing pH found within the human gastrointestinal tract provides a perfect environment for the application of orally delivered pH-responsive microgels and nanogels, where the conditions within the stomach are acidic (pH 2) and then become basic within the intestines (pH 5–8) [74]. An in vitro study reporting on the pH-sensitive glutaraldehyde cross-linked pectin-based nanogels used as drug delivery vehicles was conducted in several simulated physiological fluids: colonic, gastric, and intestinal [74]. Upon completion, data gathered indicated that the nanogels appeared to be well suited as drug delivery vessels, specifically for delivery to the colon, as release speed was increased by a higher pH environment and the pectinolytic enzyme resent within the colon [74].

The pH-responsive nanogels have been utilized in chemotherapy treatments, releasing the treatment to the diseased area an initiated via local pH gradients [64]. Nanogels can be customized, based on application and the response desired, to release the loaded drug either extracellulary or intercellulary. The positive or negative charges found on the amphoteric polyelectrolyte polymeric chains also influence the response behavior of the nanogels. The isoelectric point (IEP) feature of these polymeric structures has also piqued the interest of researchers, as it can significantly influence both the equilibrium swelling ratio and loading/releasing profiles. Interior loading of nanogels with large oppositely charged biomacromolecules as the polyelectrolyte chains can handle their electrostatic interactions. This type of pH-responsive nanogel loading is very efficient and can become effective gene delivery systems as immobilized polynucleotides are now loadable [75].

Researchers have proven that external stimulus-responsive systems are capable of responding, both independently and simultaneously, to multiple stimuli (i.e., pH, temperature). These systems have been formed using various techniques and a wide array of materials. A simple solution is through the copolymerization of two different stimuli-responsive units (i.e., one pH sensitive, the other temperature) as is seen with PNIPAAm-*co*-PAA [76]. Multiple evaluations have been undertaken to assess the potential for hydrogel systems of PNIPAAm construction to be used as drug carrier vehicles that respond to various types of stimuli [62]. At reduced temperatures, PAA and polymers with an amide moiety PAAm create hydrogen bonds, dissociating at another thermal value; the behavior is known as the "zipper effect" [77]. Also, the interaction induced by hydrogen bonds for IPN or mixture solutions of linear PAAm and linear PAA has been reported [77].

Another very apparent solution to the researchers was the RAFT copolymerization of poly(NIPAAm-*co*-propylacrylic acid) which, when considered alongside their low polydispersities, presents a severe response to minute changes in stimuli (i.e., temperature, pH) [78]. Furthermore, the utilization of ATRP creates acrylic-based hydrogels, potentially used as drug carrying vehicles or in tissue engineering, where thermal and pH changes dictate the swelling ratios and kinetics [79]. By grafting or blending, polymers that respond to thermal cues can be incorporated with pH-responsive polysaccharides, thus being able to be used in a dual-responsive system [79].

1.4   Stimuli-Responsive Magnetic Nanoparticles

Biomedical, coating, microfluidic, and microelectronic fields are some of the many disciplines that may benefit from the development of research in magnetic-responsive nanoparticles. These systems can be achieved through the combination of magnetic and polymeric components, while subsequently yielding magnetic-responsive composites that possess noninvasive control methods. In summation, magnetic-responsive composite materials can be categorized by the following three key attributes: deformation exhibited when exposed to a magnetic field, magnetic guidance ability, and viability as a thermoresponsive system activator [80]. Within

the biomedical field, magnetic nanoparticles have been increasingly studied and used as effective delivery systems as seen in their utilization as MRI contrast agents, hyperthermia cancer treatment intermediary, as well as in other site-specific treatments [81, 82]. Found as either hybrid materials or iron oxide composites, magnetic nanoparticles (MNPs) described as core–shell systems highlight some of the most interesting properties of hybrid organic/inorganic nanocomposites and may hold promise in a vast array of applications within the biomedical field [83, 84]. Researchers have experienced great difficulty in determining the optimal design for stimuli-responsive systems that are to be used in various applications since structurally significant changes are restricted kinetically (expansion/shrinking profiles). This can be accomplished through the application of magnetic and or electric fields and the use of appropriately sensitive systems (MNPs) that respond to such signal quickly and through non-contact agitation [82].

Magnetothermally responsive materials are the integration of thermally responsive materials along with MNPs and, with their activation able to be triggered remotely via *ac* magnetic field generation, are able drug delivery systems, delivering the payload through macromolecular conformational alterations (open pore) [82]. It was reported that surfactant-free emulsion polymerization of NIPAAm and N-acryloxysuccinimide (NAS) yielded magnetothermally responsive core–shell latex particles that could be used in in vivo applications [85]. Inclusion of thermoresponsive NIPAAm within the latex particle resulted in flocculation that could be inducing thermally [85]. Additionally, this behavior, via the covalent bonding of NAS's reactive ester groups, could be utilized so as to immobilize chymotrypsin [85].

The remote-controlled release of multiple pulsatile drugs along with varying "ON/OFF" magnetic field oscillation periods was developed from the integration of super magnetic iron oxide nanoparticle (SPIONs) and PNIPAAm thermosensitive hydrogels that exhibited both "ON/OFF" and remote-controlled drug release functionality [86]. Chitosan-based polymeric coatings were applied to magnetic nanoparticles loaded with drugs (LCST 38 °C) and showed accelerated release over a period of multiple hours when in an environment above the polymer's LCST [87]. This newly discovered nanodelivery system is distinguished by the following identifiers: a core comprised of functionalized black iron oxide (Fe_3O_4); drug-core conjugation occurs via an *"acid-labile hydrazone bond"*; and a thermally responsive polymer (chitosan-*g*-poly(NIPAAm-*co*-DMAAm)) was used for encapsulation [87]. The polymer used for encapsulation allows for the "ON/OFF" triggering of drug release due to its LCST (38 °C). At conditions below the LCST, slow release of drug was observed and accelerated when conditions exceeded the LCST [87]. The profile exhibited an initial burst of release which then tapered off into a more controlled state with this stability exaggerated when exposed to a pH value of 5.3 (i.e., slightly acidic environment). It was concluded that when the thermally responsive polymer's structure collapses and the *"acid-labile hydrazone bond"* cleaves, the release of the system's payload occurs [87].

One of the main points of contention in using MNPs as *ac* magnetic field (AMF) heat inductors in vivo is the possibility of irreversible healthy tissue damage due to the heat generation caused by magnetic field exposure [88]. There are two potential solutions to this problem, the first being in vivo thermal monitoring via thermometry,
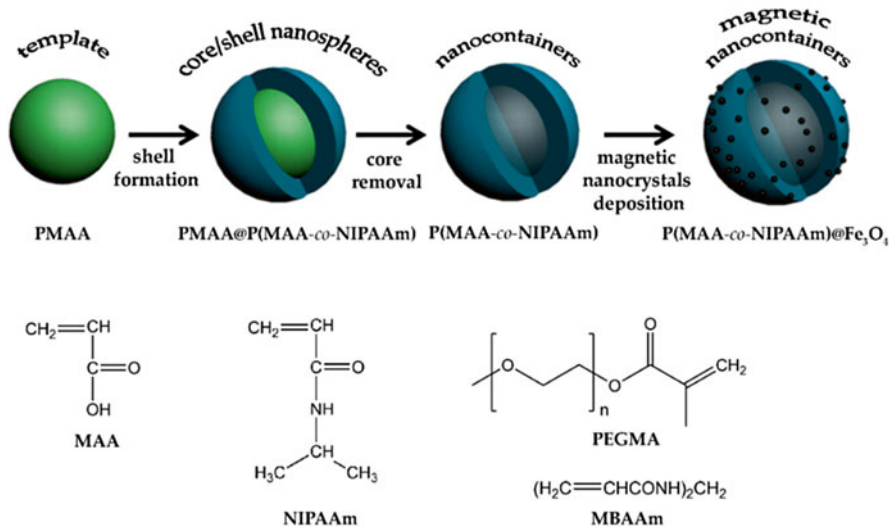
Fig. 1.5 Schematic illustration of the synthesis procedure for the preparation of magnetic nano-containers (Reprinted with permission from [94], Copyright John Wiley & Sons)

which is invasive [88]. The second is to utilize the MNP's reliance upon thermal conditions; specifically, choosing materials possessing Curie temperatures that can mimic physiological conditions (i.e., lanthanum strontium manganese oxide MNPs) [89].

Nanoparticles that are sensitive to fluctuations in pH are typically synthesized with components capable of responding to changes in pH with physicochemical alterations (i.e., swelling, hydrolysis, charge conversion, etc.). Several functional groups can potentially be incorporated into the structural components that make up pH-responsive systems such as but not limited to carboxyl [90], amine [91], and Schiff base [92].

The release profiles of iron oxide nanoparticles with a grafted pH-responsive polymer shell loaded with cancer-treating drugs were observed and plotted for its relationship with pH [90]. PMAA present within this shell allowed for neutral pH loading while enhancing delivery at a lower pH environment (sub 5.5) with the protonated carboxylate groups of PMAA [90].

While literature provides ample information on dual stimuli-responsive nanospheres used as drug delivery systems, there is little data available on microspheres that exhibit ternary stimuli-responsive behavior. A study has been undertaken recently on multisensitive PNIPAAm-*co*-PAA-Fe$_3$O$_4$ hydrogel nanospheres intended for site-specific drug delivery, in this case DOX. The researchers analyzed the DOX-loaded and unloaded magnetic hydrogel nanospheres' physiochemical properties of nanosphere including size, morphology, magnetism, and release profile [93]. On the other hand, magnetic nanodevices based on PNIPAAm-*co*-PAA were prepared and used for delivery of daunorubicin (DNR). This multiresponsive system was able to respond to temperature, pH, as well as magnetic stimulus [94]. Figure 1.5 is a schematic representation showing the synthesis procedure for the said magnetic nanodevice based on PNIPAAm-*co*-PAA [94]. It was concluded that

the nanocontainers loaded with DNR showed comparable *"antitumor effect"* to that of the free drugs. These observations can potentially provide crucial information for the delivery of the drug, as well as the release systems [94].

1.5 Stimuli-Responsive Mesoporous Silica

Among all of the different highly dispersed and porous material varieties available, those that are considered ordered mesoporous were defined by IUPAC as uniform with adjustable pore sizes (2–50 nm). Specifically, mesoporous silica (MS) production generally occurs in the presence of a specific organic template, such as one that is a surfactant type. The template acts as a directing agent, encouraging inorganic structure growth only on its sides. A *"soft template"*, such as a surfactant or block polymer (i.e., amphiphilic molecules), is the most common foundation used when synthesizing ordered MS structures [95].

SBA15, HMS, MCM-41, TUD-1, HMM-33, and FSM-16 are some of the well-known classifications of MS materials. With advances in production come newly viable applications, this case being uses in sensors and separations [96], catalysis [97], novel functional materials [98], selective adsorption [99], guest molecular hosts [100], and a newly proposed application as drug adsorber [101]. MS materials, defined by their excellent chemical/thermal stability, morphology control, and surface functionalization, may prove to be suitable candidates in notable biological applications including sequestration, controlled pharmaceutical active agent's delivery, drug delivery, and imaging [102, 103].

Owing to their potential for revolutionary innovation within nanomedicine, mesoporous silica nanoparticles (MSNPs) are currently under the spotlight of many eager researchers. The voids in the mesopores of the nanoparticles can be loaded with large quantities of deliverable material which can be secured with different nanogates; uncapping the entrances to the pores, thus releasing the payload, is accomplished via a wide array of external or internal stimuli.

Customizable and advanced smart nanosystems that address the user's unique needs, can be made through the combination of MSNPs and magnetic nanoparticles (MNPs), retaining the desirable properties, multiple functionality, and diverse applicability of both [104]. Hurdles that must be overcome so as to deliver systems that possess the best possible combination of MSNPs, MNPs, and stimuli-responsive nanosystems required by the end user are described herein.

By planting internally or externally stimulated nanogates at pore entrances, MSNPs can be potentially converted into advanced smart carrier systems loaded with drugs and mitigate the chance of premature or undesirable release. The nanogates or *"gatekeepers"* can release their payload in reaction to a specific stimuli or a combination of multiple stimuli (dual or multiresponsive); examples of external stimuli include temperature, pH, and oxidation potential while internal stimuli examples include ultraviolet light or a magnetic field. A good example of such systems is that of protein-gated carbohydrate-functionalized MSNPs [105].

Fig. 1.6 Illustrative image representing gatekeepers in mesoporous silica
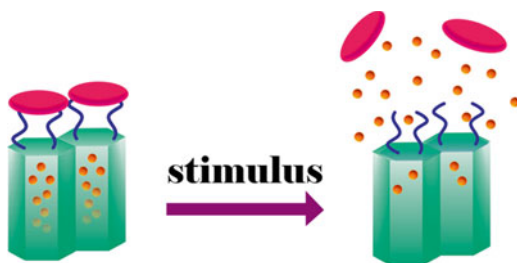
Comprehensive reviews of the utilization of MSNPs in designing nanodevices to be used in smart delivery have been reported [106]. Figure 1.6 is an illustrative image describing MSNP as a smart carrier system loaded with drug-containing gatekeepers capable of realizing in response to stimulus.

Currently, cancer patients undergo chemotherapy as a treatment option which, while effective, is unable to differentiate between tissue type (affected vs non), ultimately causing extreme cytotoxicity along with other adverse consequences. As such, smart *"zero release"* drug delivery nanosystems could carry their payload directly to a designated site, for instance, a tumor. In order to carry out this directive, the MSNPs that are to be utilized in this endeavor must have multipurpose functionality along with an easily modifiable external surface for use of targeting agents like antibodies or peptides. Furthermore, these particles can also be given *"stealth"* capabilities through the integration of biopolymers (i.e., polyethylene glycol) to the particles' surface, thus reducing opsonization [107]. In addition to their use as drug delivery vehicles, nanosystems may also find utility as a bioimaging indication in conjunction with florescent dyes or MRI complexes [108, 109].

These drug carrier devices can be designed to be site-explicit, *"zero release"*, and stimuli-responsive, thereby alleviating many of these ill effects. MS-based carrier devices were developed to react to two specific types of stimuli: exogenous which includes examples like exposure to light or a magnetic field; and endogenous with examples including pH and enzyme presence [106].

MSNPs are able to deliver their payloads in response to an internal stimulus, in this case temperature, by the surface attachment through a thermally sensitive polymer, such as PNIPAAm. A thermosensitive drug delivery system was designed with mesostructured cellular foam (MCF) encasing PNIPAAm by ATRP and was evaluated with an appropriate control drug (ibuprofen) [110]. Its design was such that is incorporated three desirable characteristics into one system: a black iron oxide MNP core, a thermally responsive shell composed of P(NIPAM-*co*-NHMA), and an MS layer between the other two [110]. Both the thermally responsive ibuprofen release and the VPTT were influenced by the presence of the comonomer with hydrophilic properties [110]. Octadecyltrimethoxysilane-functionalized thermoresponsive MSNPs were loaded with fluorescent model drug [111]. In this system, the MSNP is surrounded by a hydrophobic layer formed by alkyl-paraffin interactions and release is accomplished by melting of the paraffin with a thermally appropriate/desirable profile [111].

Early attempts in the creation of effective pH-responsive gated MS particles released their loaded drugs when the surface anchor ligand experienced macromolecular dissociation. Design of a therapeutic delivery carrier, sensitive to changes in pH and comprised of MSN that were coated with chitosan, was undertaken by researchers [112]. The MSNs' surface phosphonate moieties allowed for phosphoramidate covalent bonding with the cationic amino groups of the chitosan, thus effectively coating the system [112]. A drug release profile was obtained for ibuprofen by altering the pH of the environment (4.0–7.4) so as to induce the pH responsiveness displayed by chitosan's cationic shell structure [112]. When exposed to elevated pH conditions (7.4), ibuprofen was contained within the structure as the change to a gel-like structure of the chitosan prevented its release. At pH < 6.3, chitosan's amino moieties become protonated, thus allowing for release of its payload. It was concluded that the effective drug delivery systems can potentially be created from pH-sensitive MSNs coated with chitosan [112]. Other examples include the calcein-loaded PEI-modified MSNPs were blocked with cyclodextrin [113].

Systems that act in response to more than one stimuli (independently or synergistically) are defined as multiresponsive-controlled or dual-controlled delivery systems. A controllable drug delivery system based upon a dual-responsive (pH, thermal) composite structure was synthesized that composed of the following parts: a MSN core capable of holding the desired payload, a shell of copolymer–lipid bilayer composed of phospholipids (soy phosphatidylcholine, SPC) that are natural, and poly(NIPAAM-*co*-octadecyl acrylate) copolymer, which acts as a gate shell that is dual responding to stimuli [114]. As such, the structure's MSN core enables the user to load a large quantity of drug while providing a stable, sustained release period for the patient; the copolymer–lipid bilayer could additionally allow for customizable release functionality (i.e., pH or thermal responsiveness) [115].

By varying the pH and anion content of the release medium, pH-sensitive and anion-controllable gatekeepers by affixing polyamines to the MSNP surface were synthesized, resulting in the controlled $(Ru(bipy)_3^{2+})$ dye release from a mesoporous matrix [115]. Thermo-/pH-coupling-sensitive core–shell MSNPs are among the latest, where the outer shell consisted of cross-linked poly(NIPAAm-*co*-MAA) polymer and possessed a magnetic MSNP core [116]. The system exhibited thermo-/pH-responsive controlled drug release behavior when subjected to changes in the VPTT; small amounts of drug were released at sub-VPTT conditions and increased above said value.

1.6 Stimuli-Responsive Gold Nanoparticles

With low toxicity, customizable surface properties, excellent chemical stability, and possessing optical features dictated by size and shape, a large amount of focus has been placed on gold nanoparticles (GNPs) and their potential contributions to the biomedical field [117]. However, prior to use in clinical trials, GNPs must undergo surface modification so as to stabilize their properties within serums and colloidal

systems. Chemical or physical means that have been employed as GNPs stabilizers for use in stimuli-responsive macromolecules in the following applications: phototherapy, light-activated drug release systems, and photoacoustic imaging agents [118, 119].

Specifically, the thermal responsiveness of the macromolecules that are N-vinylcaprolactam (NVCL)-based [120] and NIPAAm-based [121], along with their LCST value in an aqueous solution, has garnered much attention from the research community. The environmental conditions dictate the interaction between water and the macromolecules. Water is considered as an excellent solvent (at sub-LCST) for coiled chains that are hydrated. When above the LCST, the opposite is true, with water acting as a poor solvent with the chains dehydrating and are globular in form. Tumor treatment could potentially benefit from the use of GNPs with a thermally responsive coating since the diseased environment observed increased temperature with higher blood flow to the peripheral region, allowing for the implementation of carrier systems which are thermoresponsive and deliver their payload only to the desired area [117]. Furthermore, due to the thermosensitive-coated GNPs' nanodimensions, improved site specificity and release efficacy of the drug can be accomplished through accumulation alone [117]. Successful nanoparticle fabrication while in the company of stabilizers can be completed through in situ preparation, yielding innovative hybrid nanoparticles from the selective molecular bonding on the particle's surface [119].

Incorporating macromolecules having biocompatible properties with nanoparticles that are inorganic may increase the likelihood of use in the biomedical field due to their preferable structural integrity. Carrying out the in situ methodology, preparation of Au-PVOH-*b*-PNVCL nanoparticles was completed with the assistance of the stabilizer poly(vinyl alcohol)-*b*-poly(N-vinylcaprolactam) (PVOH-*b*-PNVCL), a thermally responsive copolymer that was synthesized per the *"cobalt-mediated radical polymerization (CMRP)"* strategy [122]. The model drug chosen for the release study conducted at varying temperatures was nadolol, a β-blocker (hydrophilic, nonselective) used in the patients that exhibit pain in the chest area as well as those with high blood pressure [122]. Figure 1.7 shows the synthesis of gold@PVOH-b-PNVCL NPs as well as different conformations of both PVOH (black) and PNVCL (red) segments [122].

Research has already established that production via postmodification or physisorption for stabilized GNPs is possible. However, more recently, the "graft-from" and "graft-to" methods have also proven to be successful [123]. The "graft-from" technique is described as the GNPs experiencing chain initiation which is then anchored to active surface sites, proving desirable as both the molecular weight and distribution can be controlled through such methodology [123]. The "graft-to" technique can then be described as the stabilization of GNPs via the addition of gatekeepers; examples of this during the production of GNPs are the incorporation of thiol group used as end caps and the stabilization of disulfide-containing polymers instead of the more typical addition of alkanethiol ligands approach [124].

Development of GNPs/polymersome formulations were investigated as hydrophilic, multimodal therapeutic carrier vehicles with innovation stemming from prior success seen through the integration of GNPs with polymer vesicles that were both
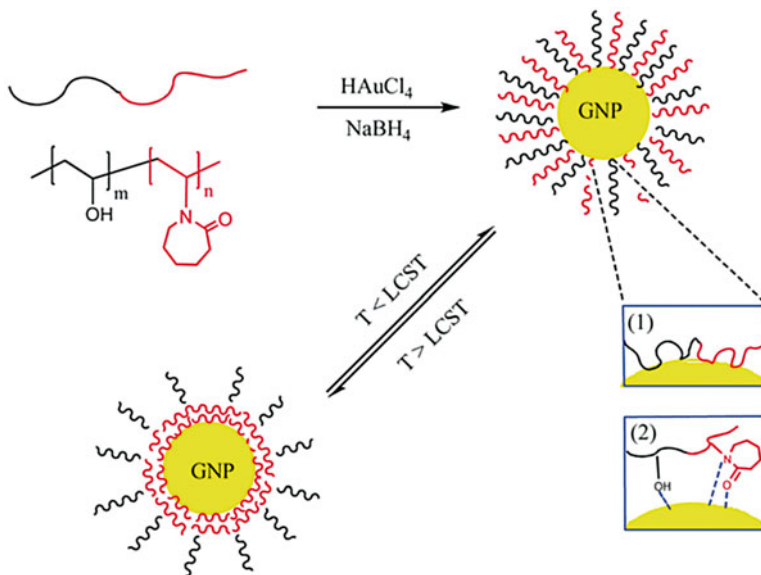
Fig. 1.7 Schematic illustration synthesis of gold@PVOH-b-PNVCL NPs and different conformations of both PVOH (*black*) and PNVCL (*red*) segments (Reprinted with permission from [122], Copyright the Royal Society of Chemistry)

biocompatible and responded to changes in pH [125]. Poly(ε-caprolactone)-*b*-poly(ethylene oxide)-*b*-poly(2-vinylpyridine)-*b*-poly(ethylene oxide)-b-poly(ε-caprolactone), an amphiphilic pentablock terpolymer (PCL-PEO-P2VP-PEO-PCL), was chosen to synthesize the polymer vesicles, as it has a P2VP/PCL membrane that responds to changes in pH while maintaining biodegradability with PEO looping chains (both neutral and hydrophilic) surrounding it [126]. The introduction of cationic groups was accomplished by the partial quaternization of the P2VP block [125]. Release studies were performed in a couple of different pH-simulated environments (physiological = 7.4, tumor = 5.5) for the vesicles' hydrophilic aqueous lumen encapsulating the GNPs hydrophobic molecule carrier systems (dispersible in water) [125]. Possessing an easily modifiable LCST (32–50 °C) with thermally sensitive properties, poly(NIPAAm-*co*-AAm) was applied as a coating to gold nanocages (Au NCs); as a whole, the system was effective in treating breast cancer cells through the NIR-induced DOX release [126].

1.7   Conclusion

Highlighted within this chapter are the principles driving intelligent and stimuli-responsive nanocarriers' usage in targeted and triggered treatment of patients. A considerable amount of advancement has taken place in bionanotechnology and nanoscale drug delivery systems has, in the not-so-distant past, aided in the

progression of these vehicles for therapeutic delivery. Implementation of these pioneering devices creates a pathway from therapeutic need to distribution, emphasizing the focus be placed on the emerging field of smart drug delivery applications. Research has shown that smart materials can adapt their architecture and functionality as a reactionary measure to environmental cues, thus melding into the delivery systems themselves. These centric systems allow for high biocompatibility, increased half-life, and increased area specificity and can potentially overcome membrane barriers. pH and temperature prompts were studied extensively and employed as crucial signals for the therapeutic delivery, the key limitation being the slow response time to the cue from the device itself. Although smart polymeric drug delivery systems could potentially be utilized in many applications and show future promise, with a number of potential opportunities, however, there are several challenges facing this field.

1.8 Future Outlook

New nanofabrication technologies have allowed for the precise control (shape and size) of the nanocarrier delivery system. Their design can be such that they are sensitive to exogenous or endogenous stimuli, representing a viable alternative to site-specific delivery. The multitude of stimuli able to trigger the discharge of a drug at the correct place and time, and the diversity of responsive materials and structures capable of being assembled in vast arrays of configurations, provides for flexible design of systems that are sensitive to these cues. However, although several in vitro trials were documented, a limited number of systems have been studied in in vivo preclinical models, and even fewer (i.e., thermoresponsive liposomes and iron oxide nanoparticles) have attained clinical evaluation. For most of these systems, their complex structure and obstacles found in production scale-up are likely to hinder their transition from the bench to the bedside. From a compositional viewpoint, the devices' delivery mechanism performs as desired in in vitro studies but fails in in vivo trials. By this logic, a simple, straightforward, efficient, and decently precise preparation with broadly applicable strategies must be found in order to widely distribute these intelligent systems. The next generation of intelligent nanocarrier-based therapeutic delivery systems must also enhance the efficiency and mitigate the undesirable side effects. Sensitivity to discrete variations of redox potential, temperature, or pH is not easily achievable, and problems concerning the externally applied stimulus' penetration depth would eventually need to be rectified. Identifying which stimuli-responsive nanosystems are most likely to succeed is challenging; typically, the least complicated system has the better chance of reaching the clinical trial phase. Scientists are focusing on expanding systems that are capable of detecting disparities in the physicochemistry or biology between targeted and non-targeted areas. Future breakthroughs using these types of carriers are expected to mainly be focused toward those systems that are clinically acceptable and capable of being sensitive to those discrete variations in particular stimuli.

References

1. Schwartz M (2008) Smart materials. CRC Press, Boca Raton, FL
2. Aguilar MR, Roman J (2014) Smart polymers and their applications. Elsevier, Cambridge
3. Galaev I, Mattiasson B (2007) Smart polymers: applications in biotechnology and biomedicine. CRC Press, Boca Raton, FL
4. Hu J, Zhang G, Liu S (2012) Enzyme-responsive polymeric assemblies, nanoparticles and hydrogels. Chem Soc Rev 41(18):5933–5949
5. Mura S, Nicolas J, Couvreur P (2013) Stimuli-responsive nanocarriers for drug delivery. Nat Mater 12(11):991–1003
6. Jhaveri AM, Torchilin VP (2014) Multifunctional polymeric micelles for delivery of drugs and siRNA. Front Pharmacol 5:77, 10.3389/fphar.2014.00077
7. Riess G (2003) Micellization of block copolymers. Prog Polym Sci 28(7):1107–1170
8. Braunecker WA, Matyjaszewski K (2007) Controlled/living radical polymerization: features, developments, and perspectives. Prog Polym Sci 32(1):93–146
9. Smith AE, Xu X, McCormick CL (2010) Stimuli-responsive amphiphilic (co) polymers via RAFT polymerization. Prog Polym Sci 35(1):45–93
10. Yokoyama M (2005) Drug targeting with nano-sized carrier systems. J Artif Organs 8(2):77–84
11. Miyata K, Christie RJ, Kataoka K (2011) Polymeric micelles for nano-scale drug delivery. React Funct Polym 71(3):227–234
12. Rodriguez-Hernandez J, Chécot F, Gnanou Y, Lecommandoux S (2005) Toward 'smart' nano-objects by self-assembly of block copolymers in solution. Prog Polym Sci 30(7):691–724
13. Mohamed S, Parayath NN, Taurin S, Greish K (2014) Polymeric nano-micelles: versatile platform for targeted delivery in cancer. Ther Delivery 5(10):1101–1121
14. Akimoto J, Nakayama M, Okano T (2014) Temperature-responsive polymeric micelles for optimizing drug targeting to solid tumors. J Control Release 193:2–8
15. Roy D, Brooks WL, Sumerlin BS (2013) New directions in thermoresponsive polymers. Chem Soc Rev 42(17):7214–7243
16. Strandman S, Zhu X (2015) Thermo-responsive block copolymers with multiple phase transition temperatures in aqueous solutions. Prog Polym Sci 42:154–176
17. Bernstein R, Cruz C, Paul D, Barlow J (1977) Behavior in polymer blends. Macromolecules 10(3):681–686
18. Hocine S, Li M-H (2013) Thermoresponsive self-assembled polymer colloids in water. Soft Matter 9(25):5839–5861
19. Wei H, Cheng S-X, Zhang X-Z, Zhuo R-X (2009) Thermo-sensitive polymeric micelles based on poly (N-isopropylacrylamide) as drug carriers. Prog Polym Sci 34(9):893–910
20. James HP, John R, Alex A, Anoop K (2014) Smart polymers for the controlled delivery of drugs–a concise overview. Acta Pharm Sin B 4(2):120–127
21. Xu J, Liu S (2008) Polymeric nanocarriers possessing thermoresponsive coronas. Soft Matter 4(9):1745–1749
22. Hales M, Barner-Kowollik C, Davis TP, Stenzel MH (2004) Shell-cross-linked vesicles synthesized from block copolymers of poly (D, L-lactide) and poly (N-isopropyl acrylamide) as thermoresponsive nanocontainers. Langmuir 20(25):10809–10817
23. Cammas S, Suzuki K, Sone C, Sakurai Y, Kataoka K, Okano T (1997) Thermo-responsive polymer nanoparticles with a core-shell micelle structure as site-specific drug carriers. J Control Release 48(2):157–164

24. Nishiyama N, Kataoka K (2006) Current state, achievements, and future prospects of polymeric micelles as nanocarriers for drug and gene delivery. Pharmacol Ther 112(3):630–648
25. Chung J, Yokoyama M, Yamato M, Aoyagi T, Sakurai Y, Okano T (1999) Thermo-responsive drug delivery from polymeric micelles constructed using block copolymers of poly (N-isopropylacrylamide) and poly (butylmethacrylate). J Control Release 62(1):115–127
26. Chung J, Yokoyama M, Suzuki K, Aoyagi T, Sakurai Y, Okano T (1997) Reversibly thermo-responsive alkyl-terminated poly (N-isopropylacrylamide) core-shell micellar structures. Colloids Surf B 9(1):37–48
27. Chung J, Yokoyama M, Aoyagi T, Sakurai Y, Okano T (1998) Effect of molecular architecture of hydrophobically modified poly (N-isopropylacrylamide) on the formation of thermo-responsive core-shell micellar drug carriers. J Control Release 53(1):119–130
28. Nakayama M, Okano T, Miyazaki T, Kohori F, Sakai K, Yokoyama M (2006) Molecular design of biodegradable polymeric micelles for temperature-responsive drug release. J Control Release 115(1):46–56
29. Akimoto J, Nakayama M, Sakai K, Okano T (2010) Thermally controlled intracellular uptake system of polymeric micelles possessing poly (N-isopropylacrylamide)-based outer coronas. Mol Pharm 7(4):926–935
30. Sun X-L, Tsai P-C, Bhat R, Bonder E, Michniak-Kohn B, Pietrangelo A (2015) Thermoresponsive block copolymer micelles with tunable pyrrolidone-based polymer cores: structure/property correlations and application as drug carriers. J Mater Chem B 3(5):814–823
31. Liu J, Huang Y, Kumar A, Tan A, Jin S, Mozhi A, Liang X-J (2014) pH-sensitive nano-systems for drug delivery in cancer therapy. Biotechnol Adv 32(4):693–710
32. Dai S, Ravi P, Tam KC (2008) pH-responsive polymers: synthesis, properties and applications. Soft Matter 4(3):435–449
33. Liu Y, Wang W, Yang J, Zhou C, Sun J (2013) pH-sensitive polymeric micelles triggered drug release for extracellular and intracellular drug targeting delivery. Asian J Pharm Sci 8(3):159–167
34. Thomas JL, Barton SW, Tirrell DA (1994) Membrane solubilization by a hydrophobic polyelectrolyte: surface activity and membrane binding. Biophys J 67(3):1101
35. Mellman I, Fuchs R, Helenius A (1986) Acidification of the endocytic and exocytic pathways. Annu Rev Biochem 55(1):663–700
36. Iversen T-G, Skotland T, Sandvig K (2011) Endocytosis and intracellular transport of nanoparticles: present knowledge and need for future studies. Nano Today 6(2):176–185
37. Fattal E, Couvreur P, Dubernet C (2004) "Smart" delivery of antisense oligonucleotides by anionic pH-sensitive liposomes. Adv Drug Deliv Rev 56(7):931–946
38. Chen T, Mcintosh D, He Y, Kim J, Tirrell DA, Scherrer P, Fenske DB, Sandhu AP, Cullis PR (2004) Alkylated derivatives of poly (ethylacrylic acid) can be inserted into preformed liposomes and trigger pH-dependent intracellular delivery of liposomal contents. Mol Membr Biol 21(6):385–393
39. Henry SM, El-Sayed ME, Pirie CM, Hoffman AS, Stayton PS (2006) pH-responsive poly (styrene-alt-maleic anhydride) alkylamide copolymers for intracellular drug deliver. Biomacromolecules 7(8):2407–2414
40. Gaucher G, Satturwar P, Jones M-C, Furtos A, Leroux J-C (2010) Polymeric micelles for oral drug delivery. Eur J Pharm Biopharm 76(2):147–158
41. Leroux J-C, Cozens RM, Roesel JL, Galli B, Doelker E, Gurny R (1996) pH-sensitive nanoparticles: an effective means to improve the oral delivery of HIV-1 protease inhibitors in dogs. Pharm Res 13(3):485–487
42. De Jaeghere F, Allémann E, Kubel F, Galli B, Cozens R, Doelker E, Gurny R (2000) Oral bioavailability of a poorly water soluble HIV-1 protease inhibitor incorporated into pH-sensitive particles: effect of the particle size and nutritional state. J Control Release 68(2):291–298
43. Vinogradov S, Batrakova E, Kabanov A (1999) Poly (ethylene glycol)–polyethyleneimine NanoGel™ particles: novel drug delivery systems for antisense oligonucleotides. Colloids Surf B 16(1):291–304

44. Sutton D, Durand R, Shuai X, Gao J (2006) Poly (D, L-lactide-co-glycolide)/poly (ethyleni-mine) blend matrix system for pH sensitive drug delivery. J Appl Polym Sci 100(1):89–96

45. Shi S, Shi K, Tan L, Qu Y, Shen G, Chu B, Zhang S, Su X, Li X, Wei Y (2014) The use of cationic MPEG-PCL-g-PEI micelles for co-delivery of Msurvivin T34A gene and doxorubi-cin. Biomaterials 35(15):4536–4547

46. Sonaje K, Lin Y-H, Juang J-H, Wey S-P, Chen C-T, Sung H-W (2009) In vivo evaluation of safety and efficacy of self-assembled nanoparticles for oral insulin delivery. Biomaterials 30(12):2329–2339

47. Boyer C, Bulmus V, Davis TP, Ladmiral V, Liu J, Perrier SB (2009) Bioapplications of RAFT polymerization. Chem Rev 109(11):5402–5436

48. Zhang S, Zou J, Zhang F, Elsabahy M, Felder SE, Zhu J, Pochan DJ, Wooley KL (2012) Rapid and versatile construction of diverse and functional nanostructures derived from a polyphosphoester-based biomimetic block copolymer system. J Am Chem Soc 134(44): 18467–18474

49. Cheng R, Meng F, Deng C, Klok H-A, Zhong Z (2013) Dual and multi-stimuli responsive polymeric nanoparticles for programmed site-specific drug delivery. Biomaterials 34(14): 3647–3657

50. Schilli CM, Zhang M, Rizzardo E, Thang SH, Chong Y, Edwards K, Karlsson G, Müller AH (2004) A new double-responsive block copolymer synthesized via RAFT polymerization: poly (N-isopropylacrylamide)-block-poly (acrylic acid). Macromolecules 37(21):7861–7866

51. Wei H, Zhang X-Z, Cheng H, Chen W-Q, Cheng S-X, Zhuo R-X (2006) Self-assembled thermo-and pH responsive micelles of poly (10-undecenoic acid-b-N-isopropylacrylamide) for drug delivery. J Control Release 116(3):266–274

52. Soppimath KS, Liu LH, Seow WY, Liu SQ, Powell R, Chan P, Yang YY (2007) Multifunctional core/shell nanoparticles self-assembled from pH-induced thermosensitive polymers for tar-geted intracellular anticancer drug delivery. Adv Funct Mater 17(3):355–362

53. Zhang L, Guo R, Yang M, Jiang X, Liu B (2007) Thermo and pH dual-responsive nanopar-ticles for anti-cancer drug delivery. Adv Mater 19(19):2988–2992

54. Lo C-L, Lin K-M, Hsiue G-H (2005) Preparation and characterization of intelligent core-shell nanoparticles based on poly (D, L-lactide)-g-poly (N-isopropyl acrylamide-co-meth-acrylic acid). J Control Release 104(3):477–488

55. Chen Y-C, Liao L-C, Lu P-L, Lo C-L, Tsai H-C, Huang C-Y, Wei K-C, Yen T-C, Hsiue G-H (2012) The accumulation of dual pH and temperature responsive micelles in tumors. Biomaterials 33(18):4576–4588

56. Johnson RP, Jeong YI, John JV, Chung C-W, Kang DH, Selvaraj M, Suh H, Kim I (2013) Dual stimuli-responsive poly (N-isopropylacrylamide)-b-poly (L-histidine) chimeric materi-als for the controlled delivery of doxorubicin into liver carcinoma. Biomacromolecules 14(5):1434–1443

57. Zhang X, Monge S, In M, Giani O, Robin J-J (2013) Thermo-and pH-sensitive aggregation behavior of PDEAm-b-P (l-lysine) double hydrophilic block copolymers in aqueous solution. Soft Matter 9(4):1301–1309

58. Ahmed EM (2015) Hydrogel: preparation, characterization, and applications. A review. J Adv Res 6(2):105–121

59. Lim HL, Hwang Y, Kar M, Varghese S (2014) Smart hydrogels as functional biomimetic systems. Biomater Sci 2(5):603–618

60. Hamidi M, Azadi A, Rafiei P (2008) Hydrogel nanoparticles in drug delivery. Adv Drug Deliv Rev 60(15):1638–1649

61. de las Heras Alarcón C, Pennadam S, Alexander C (2005) Stimuli responsive polymers for biomedical applications. Chem Soc Rev 34(3):276–285

62. Qiu Y, Park K (2012) Environment-sensitive hydrogels for drug delivery. Adv Drug Deliv Rev 64:49–60

63. Zha L, Banik B, Alexis F (2011) Stimulus responsive nanogels for drug delivery. Soft Matter 7(13):5908–5916

64. Eckmann D, Composto R, Tsourkas A, Muzykantov V (2014) Nanogel carrier design for targeted drug delivery. J Mater Chem B 2(46):8085–8097

65. An Z, Qiu Q, Liu G (2011) Synthesis of architecturally well-defined nanogels via RAFT polymerization for potential bioapplications. Chem Commun 47(46):12424–12440

66. Oh JK, Drumright R, Siegwart DJ, Matyjaszewski K (2008) The development of microgels/nanogels for drug delivery applications. Prog Polym Sci 33(4):448–477

67. Keerl M, Smirnovas V, Winter R, Richtering W (2008) Interplay between hydrogen bonding and macromolecular architecture leading to unusual phase behavior in thermosensitive microgels. Angew Chem 120(2):344–347

68. Pelton R (2000) Temperature-sensitive aqueous microgels. Adv Colloid Interface Sci 85(1):1–33

69. Katono H, Maruyama A, Sanui K, Ogata N, Okano T, Sakurai Y (1991) Thermo-responsive swelling and drug release switching of interpenetrating polymer networks composed of poly (acrylamide-co-butyl methacrylate) and poly (acrylic acid). J Control Release 16(1):215–227

70. Zha L, Hu J, Wang C, Fu S, Elaissari A, Zhang Y (2002) Preparation and characterization of poly (N-isopropylacrylamide-co-dimethylaminoethyl methacrylate) microgel latexes. Colloid Polym Sci 280(1):1–6

71. Bae YH, Okano T, Hsu R, Kim SW (1987) Thermo-sensitive polymers as on-off switches for drug release. Makromol Chem Rapid Commun 8(10):481–485

72. Bromberg LE, Ron ES (1998) Temperature-responsive gels and thermogelling polymer matrices for protein and peptide delivery. Adv Drug Deliv Rev 31(3):197–221

73. Jeong B, Bae YH, Lee DS, Kim SW (1997) Biodegradable block copolymers as injectable drug-delivery systems. Nature 388(6645):860–862

74. Chang C, Wang Z-C, Quan C-Y, Cheng H, Cheng S-X, Zhang X-Z, Zhuo R-X (2007) Fabrication of a novel pH-sensitive glutaraldehyde cross-linked pectin nanogel for drug delivery. J Biomater Sci Polym Ed 18(12):1591–1599

75. Sethuraman VA, Na K, Bae YH (2006) pH-responsive sulfonamide/PEI system for tumor specific gene delivery: an in vitro study. Biomacromolecules 7(1):64–70

76. Chen Y, Chen Y, Nan J, Wang C, Chu F (2012) Hollow poly (N-isopropylacrylamide)-co-poly (acrylic acid) microgels with high loading capacity for drugs. J Appl Polym Sci 124(6):4678–4685

77. Dai H, Chen Q, Qin H, Guan Y, Shen D, Hua Y, Tang Y, Xu J (2006) A temperature-responsive copolymer hydrogel in controlled drug delivery. Macromolecules 39(19):6584–6589

78. Yin X, Hoffman AS, Stayton PS (2006) Poly (N-isopropylacrylamide-co-propylacrylic acid) copolymers that respond sharply to temperature and pH. Biomacromolecules 7(5):1381–1385

79. Bao H, Li L, Gan LH, Ping Y, Li J, Ravi P (2010) Thermo-and pH-responsive association behavior of dual hydrophilic graft chitosan terpolymer synthesized via ATRP and click chemistry. Macromolecules 43(13):5679–5687

80. Thévenot J, Oliveira H, Sandre O, Lecommandoux S (2013) Magnetic responsive polymer composite materials. Chem Soc Rev 42(17):7099–7116

81. Kumar CS, Mohammad F (2011) Magnetic nanomaterials for hyperthermia-based therapy and controlled drug delivery. Adv Drug Deliv Rev 63(9):789–808

82. Xie J, Liu G, Eden HS, Ai H, Chen X (2011) Surface-engineered magnetic nanoparticle platforms for cancer imaging and therapy. Acc Chem Res 44(10):883–892

83. Liu T-Y, Hu S-H, Liu D-M, Chen S-Y, Chen I-W (2009) Biomedical nanoparticle carriers with combined thermal and magnetic responses. Nano Today 4(1):52–65

84. Medeiros S, Santos A, Fessi H, Elaissari A (2011) Stimuli-responsive magnetic particles for biomedical applications. Int J Pharm 403(1):139–161

85. Chen J-P, Su D-R (2001) Latex particles with thermo-flocculation and magnetic properties for immobilization of α-chymotrypsin. Biotechnol Prog 17(2):369–375

86. Satarkar NS, Hilt JZ (2008) Magnetic hydrogel nanocomposites for remote controlled pulsatile drug release. J Control Release 130(3):246–251

87. Yuan Q, Venkatasubramanian R, Hein S, Misra R (2008) A stimulus-responsive magnetic nanoparticle drug carrier: magnetite encapsulated by chitosan-grafted-copolymer. Acta Biomater 4(4):1024–1037

88. Jordan A, Wust P, Fähling H, John W, Hinz A, Felix R (2009) Inductive heating of ferrimagnetic particles and magnetic fluids: physical evaluation of their potential for hyperthermia. Int J Hyperthermia 25(7):499–511

89. Louguet S, Rousseau B, Epherre R, Guidolin N, Goglio G, Mornet S, Duguet E, Lecommandoux S, Schatz C (2012) Thermoresponsive polymer brush-functionalized magnetic manganite nanoparticles for remotely triggered drug release. Polym Chem 3(6):1408–1417

90. Guo M, Yan Y, Zhang H, Yan H, Cao Y, Liu K, Wan S, Huang J, Yue W (2008) Magnetic and pH-responsive nanocarriers with multilayer core–shell architecture for anticancer drug delivery. J Mater Chem 18(42):5104–5112

91. Kohler N, Sun C, Wang J, Zhang M (2005) Methotrexate-modified superparamagnetic nanoparticles and their intracellular uptake into human cancer cells. Langmuir 21(19):8858–8864

92. Pourjavadi A, Hosseini SH, Alizadeh M, Bennett C (2014) Magnetic pH-responsive nanocarrier with long spacer length and high colloidal stability for controlled delivery of doxorubicin. Colloids Surf B 116:49–54

93. Fan T, Li M, Wu X, Li M, Wu Y (2011) Preparation of thermoresponsive and pH-sensitivity polymer magnetic hydrogel nanospheres as anticancer drug carriers. Colloids Surf B 88(2):593–600

94. Tziveleka LA, Bilalis P, Chatzipavlidis A, Boukos N, Kordas G (2014) Development of multiple stimuli responsive magnetic polymer nanocontainers as efficient drug delivery systems. Macromol Biosci 14(1):131–141

95. Hoffmann F, Cornelius M, Morell J, Fröba M (2006) Silica-based mesoporous organic–inorganic hybrid materials. Angew Chem Int Ed 45(20):3216–3251

96. Unger K, Kumar D, Grün M, Büchel G, Lüdtke S, Adam T, Schumacher K, Renker S (2000) Synthesis of spherical porous silicas in the micron and submicron size range: challenges and opportunities for miniaturized high-resolution chromatographic and electrokinetic separations. J Chromatogr A 892(1):47–55

97. Grün M, Lauer I, Unger KK (1997) The synthesis of micrometer-and submicrometer-size spheres of ordered mesoporous oxide MCM-41. Adv Mater 9(3):254–257

98. Alothman ZA (2012) A review: fundamental aspects of silicate mesoporous materials. Materials 5(12):2874–2902

99. Sierra I, Pérez-Quintanilla D (2013) Heavy metal complexation on hybrid mesoporous silicas: an approach to analytical applications. Chem Soc Rev 42(9):3792–3807

100. Knezevic N, Durand J-O (2014) Large pore mesoporous silica nanomaterials for application in delivery of biomolecules. Nanoscale 7(6):2199–2209

101. Farjadian F, Ahmadpour P, Samani SM, Hosseini M (2015) Controlled size synthesis and application of nanosphere MCM-41 as potent adsorber of drugs: a novel approach to new antidote agent for intoxication. Microporous Mesoporous Mater 213:30–39

102. Popat A, Hartono SB, Stahr F, Liu J, Qiao SZ, Lu GQM (2011) Mesoporous silica nanoparticles for bioadsorption, enzyme immobilisation, and delivery carriers. Nanoscale 3(7):2801–2818

103. Wang L, Zhao W, Tan W (2008) Bioconjugated silica nanoparticles: development and applications. Nano Res 1(2):99–115

104. Knežević NŽ, Ruiz-Hernández E, Hennink WE, Vallet-Regí M (2013) Magnetic mesoporous silica-based core/shell nanoparticles for biomedical applications. RSC Adv 3(25):9584–9593

105. Park C, Oh K, Lee SC, Kim C (2007) Controlled release of guest molecules from mesoporous silica particles based on a pH-responsive polypseudorotaxane motif. Angew Chem Int Ed 46(9):1455–1457

106. Colilla M, González B, Vallet-Regí M (2013) Mesoporous silica nanoparticles for the design of smart delivery nanodevices. Biomater Sci 1(2):114–134

107. Owens DE, Peppas NA (2006) Opsonization, biodistribution, and pharmacokinetics of polymeric nanoparticles. Int J Pharm 307(1):93–102

108. Lin Y-S, Hung Y, Su J-K, Lee R, Chang C, Lin M-L, Mou C-Y (2004) Gadolinium (III)-incorporated nanosized mesoporous silica as potential magnetic resonance imaging contrast agents. J Phys Chem B 108(40):15608–15611

109. Hsiao JK, Tsai CP, Chung TH, Hung Y, Yao M, Liu HM, Mou CY, Yang CS, Chen YC, Huang DM (2008) Mesoporous silica nanoparticles as a delivery system of gadolinium for effective human stem cell tracking. Small 4(9):1445–1452

110. Zhou Z, Zhu S, Zhang D (2007) Grafting of thermo-responsive polymer inside mesoporous silica with large pore size using ATRP and investigation of its use in drug release. J Mater Chem 17(23):2428–2433

111. Aznar E, Mondragón L, Ros-Lis JV, Sancenón F, Marcos MD, Martínez-Máñez R, Soto J, Pérez-Payá E, Amorós P (2011) Finely tuned temperature-controlled cargo release using paraffin-capped mesoporous silica nanoparticles. Angew Chem 123(47):11368–11371

112. Popat A, Liu J, Lu GQM, Qiao SZ (2012) A pH-responsive drug delivery system based on chitosan coated mesoporous silica nanoparticles. J Mater Chem 22(22):11173–11178

113. You Y-Z, Kalebaila KK, Brock SL (2008) Temperature-controlled uptake and release in PNIPAM-modified porous silica nanoparticles. Chem Mater 20(10):3354–3359

114. Wu X, Wang Z, Zhu D, Zong S, Yang L, Zhong Y, Cui Y (2013) pH and thermo dual-stimuli-responsive drug carrier based on mesoporous silica nanoparticles encapsulated in a copolymer–lipid bilayer. ACS Appl Mater Interfaces 5(21):10895–10903

115. Casasús R, Climent E, Marcos MD, Martínez-Máñez R, Sancenón F, Soto J, Amorós P, Cano J, Ruiz E (2008) Dual aperture control on pH-and anion-driven supramolecular nanoscopic hybrid gate-like ensembles. J Am Chem Soc 130(6):1903–1917

116. Chang B, Sha X, Guo J, Jiao Y, Wang C, Yang W (2011) Thermo and pH dual responsive, polymer shell coated, magnetic mesoporous silica nanoparticles for controlled drug release. J Mater Chem 21(25):9239–9247

117. Dykman L, Khlebtsov N (2012) Gold nanoparticles in biomedical applications: recent advances and perspectives. Chem Soc Rev 41(6):2256–2282

118. Zhang L, Li Y, Jimmy CY (2014) Chemical modification of inorganic nanostructures for targeted and controlled drug delivery in cancer treatment. J Mater Chem B 2(5):452–470

119. Zeng S, Yong K-T, Roy I, Dinh X-Q, Yu X, Luan F (2011) A review on functionalized gold nanoparticles for biosensing applications. Plasmonics 6(3):491–506

120. Beija M, Marty J-D, Destarac M (2011) Thermoresponsive poly (N-vinyl caprolactam)-coated gold nanoparticles: sharp reversible response and easy tunability. Chem Commun 47(10):2826–2828

121. Contreras-Cáceres R, Sánchez-Iglesias A, Karg M, Pastoriza-Santos I, Pérez-Juste J, Pacifico J, Hellweg T, Fernández-Barbero A, Liz-Marzán LM (2008) Encapsulation and growth of gold nanoparticles in thermoresponsive microgels. Adv Mater 20(9):1666–1670

122. Liu J, Detrembleur C, Hurtgen M, Debuigne A, De Pauw-Gillet M-C, Mornet S, Duguet E, Jérôme C (2014) Thermo-responsive gold/poly (vinyl alcohol)-b-poly (N-vinylcaprolactam) core–corona nanoparticles as a drug delivery system. Polym Chem 5(18):5289–5299

123. Li D, Cui Y, Wang K, He Q, Yan X, Li J (2007) Thermosensitive nanostructures comprising gold nanoparticles grafted with block copolymers. Adv Funct Mater 17(16):3134–3140

124. Genson KL, Holzmueller J, Jiang C, Xu J, Gibson JD, Zubarev ER, Tsukruk VV (2006) Langmuir-Blodgett monolayers of gold nanoparticles with amphiphilic shells from V-shaped binary polymer arms. Langmuir 22(16):7011–7015

125. Popescu M-T, Tsitsilianis C (2013) Controlled delivery of functionalized gold nanoparticles by pH-sensitive polymersomes. ACS Macro Lett 2(3):222–225

126. Yavuz MS, Cheng Y, Chen J, Cobley CM, Zhang Q, Rycenga M, Xie J, Kim C, Song KH, Schwartz AG (2009) Gold nanocages covered by smart polymers for controlled release with near-infrared light. Nat Mater 8(12):935–939

Chapter 2
Stimuli-Responsive Smart Polymeric Coatings: An Overview

Saravanan Nagappan, Madhappan Santha Moorthy, Kummara Madhusudana Rao, and Chang-Sik Ha

Abstract Coatings are an important topic within the scientific community, spanning from the ancient to the modern world. Coatings are not only used for decorative purposes but also for functionality, for example, coatings that are resistant to the effects of weathering (i.e., rain, UV light, etc.). Up until present, several coating materials were developed using various types of natural and synthetic materials. The scientific improvements of the modern era have made it easy to create novel coating formulations by mimicking ancient pathways. Recently nonstick, self-cleaning, self-healing, and stimuli-responsive surfaces have attracted special interest in the formulation of smart coating materials. Several attempts were made to synthesize and develop highly efficient smart polymeric coatings from the practical point of view due to the increasing need for smart coatings in modern technologies and industrial applications. Stimuli-responsive smart coatings are also very useful in extending the life of final products, which is also a reason to develop a variety of new coating formulations for industrial purpose. On the other hand, the synthesis of stimuli-responsive smart coatings and maintaining the stability of the coated surfaces under major environmental changes were quite difficult, which necessitated careful selection and synthesis of the coating materials. The applicability of stable stimuli-responsive smart polymeric coating can be extended into various industrial and commercial applications. This chapter covers the stimuli responsiveness of smart polymeric coatings in various applications and their future outlooks within the coating industry as well as present practical applications and necessities of the stimuli-responsive smart polymeric coatings for other industrial applications.

Keywords Stimuli responsiveness • Smart polymers • Self-cleaning • Antireflection • Industrial applications

S. Nagappan • M.S. Moorthy • K.M. Rao • C.-S. Ha (✉)
Department of Polymer Science and Engineering, Pusan National University,
Busan 609-735, Korea
e-mail: csha@pnu.edu

2.1 Introduction

Polymeric materials have widespread applications due to their versatile characteristics, cost effectiveness, and ease of availability. Surface interactions of polymer substrates are an essential area of study in many fields such as medical, military, textile, transport, construction, electronics, and other industries for protection against corrosion and abrasion, as well as other surface protection purposes. For all applications, the surface characteristics of polymeric materials play a key role in determining its utility and reliability. For example, in biomedical applications, the biocompatibility and bodily response to foreign material depended on the surface characteristics of the polymeric materials. In addition, surface science is an integral part of the formulation, manufacturing, and ultimate application of coatings. Until now several coating materials were developed by using various types of natural and synthetic materials. The scientific improvements of modern society have made it easy to create novel coating formulations by mimicking ancient pathways.

2.1.1 Smart Polymeric Coatings

Recently, nonstick, self-cleaning, self-healing, and stimuli-responsive surfaces have attracted special interest in the formulation of smart coating materials [1–5]. Several attempts were made to synthesize and develop highly efficient smart polymeric coatings from a practical point of view due to the increasing need for smart coatings in modern technologies and industrial applications. Life extension of the final products is also a reason to develop a variety of new coating formulations for industrial purposes. On the other hand, the synthesis of stimuli-responsive smart coatings and maintaining the stability of the coated surfaces under major environmental changes were quite difficult, which necessitated careful selection and synthesis of the coating materials. Designing functional materials with smart coating allows for the usual functions of coatings, such as protection and decoration, as well as provides the functionality that environmental stimulus-based coatings offer. Smart coatings are designed to remain passive unless prompted to perform a stimuli-based function and are able to repeat the process over and over, up to thousands of cycles or more, spanning over several years. The surface modifications of stimuli-responsive polymers are sensitive to magnetic properties, pH, light, and temperature [6–10]. The surface property is directly dependent on the nature of the polymers, grafting density, and surface roughness [11]. The polymeric materials can be easily functionalized on the surfaces using post- or prepolymerization methods. However, these surfaces produced with the polymers via spin coating or layer-by-layer (LbL) methods are sensitive, and the coated polymers can be removed easily by a simple chemical or physical change of their environment. In this case, however, the generation of a regular micro-order roughness on a flat surface is difficult because of their flexible and sprawled properties. It is necessary to produce materials with good surface properties such as surface roughness in order to enhance the properties of the material.

2.1.2   Stimuli-Responsive Smart Polymers

The most unique characteristic property of smart polymers is their ability to show reversible changes from hydrophilicity to hydrophobicity because of swelling and shrinkage of polymeric chains in the presence of external stimuli [5]. It is possible to construct materials with responsive properties by incorporating some stimuli-responsive polymers into the backbone of the materials. These responsive polymers possess the ability to swell, shrink, bend, or even degrade in response to a signal. They reversibly swell and shrink with small changes in environmental conditions. The most common environmental factors that cause an abrupt volume changes in such smart polymeric materials are pH, temperature, electric field, light, atmosphere, and solvent exposure. Table 2.1 summarizes some examples of smart polymers and their responsive properties for various applications.

Table 2.1   Stimuli-responsive smart polymers and their applications

Smart polymer	Properties	Applications	Ref.
Poly(N-isopropylacrylamide) (PNIPAM)	pH and temperature responsive, hydrophilicity to hydrophobicity	Drug delivery	[10]
Cross-linked polyurethane network	Atmosphere responsive	Self-healing coatings	[12]
Poly(methyl methacrylate) (PMMA)/silica composite	Highly durable, enhanced moduli, scratch resistance	Scratch resistance coatings	[13]
Poly(styrene) (PS)/polydimethylsiloxane (PDMS)	Solvent responsive	Photonic paper	[14]
PS-block-PMMA copolymer	Antireflection	Broadband and solar cells	[15]
PS-block-poly(4-vinylpyridine) (P4VP)	Solvent responsive, antireflection	Antireflective coatings	[16]
Polyimide (PI)/inorganic hybrid	Light responsive	Aerospace and antireflective coatings	[17–19]
Poly(3-cyanomethyl-1-vinylimidazolium) bis(trifluoromethanesulfonyl)imide	Porous polymer, solvent responsive	Actuators	[20]
Poly(acrylic acid) (PAA)	pH responsive	Drug delivery and medical devices	[21, 22]
Poly(2-(diethylamino)ethyl methacrylate) (PDMAEMA)	pH and temperature responsive	Drug and gene delivery	[23, 24]
Poly(N-vinylcaprolactam) (PNVCL)	pH and temperature responsive	Drug delivery	[25]
Poly(vinylpyridine)	pH-sensitive barrier	Controlled drug delivery	[26]
Poly(ethyleneimine)	pH responsive	Drug and gene delivery	[27]
Covalently grafted fluorinated polymer on end PEG polymer	Solvent responsive, self-cleaning and antifogging	Oil-repellant antifog coating	[28]

2.2 Applications of Smart Coatings

The applications of smart polymeric coatings are not limited to a particular field due to the switchable property of the polymeric materials. Smart polymers are used widely in several applications such as in the following examples: fabrication of transparent substrate; nonstick, self-cleaning, and self-healing coatings in anti-stain and scratch-resistant coatings; antireflective and anticorrosion coatings; electronic displays and actuators; smart textiles; biomedical applications such as drug and gene delivery, cancer therapy, and dental and medical devices; and other potential applications such as environmental applications, automobiles and aerospace, and houseware appliances (Fig. 2.1) [1–5]. A desirable property of these polymeric coatings is their ability to switch the surface property of the material under external stimuli and form stable bonding with the substrate. Moreover, the smart polymeric coatings also have excellent thermal stability and durability.

2.2.1 Smart Nonstick and Self-Cleaning Coatings

Nonstick- and self-cleaning-based surface coatings are potentially useful in several application areas due to the resistance capacity of the coating substrate against water and dust particles. The continuous development and growth of chemical and
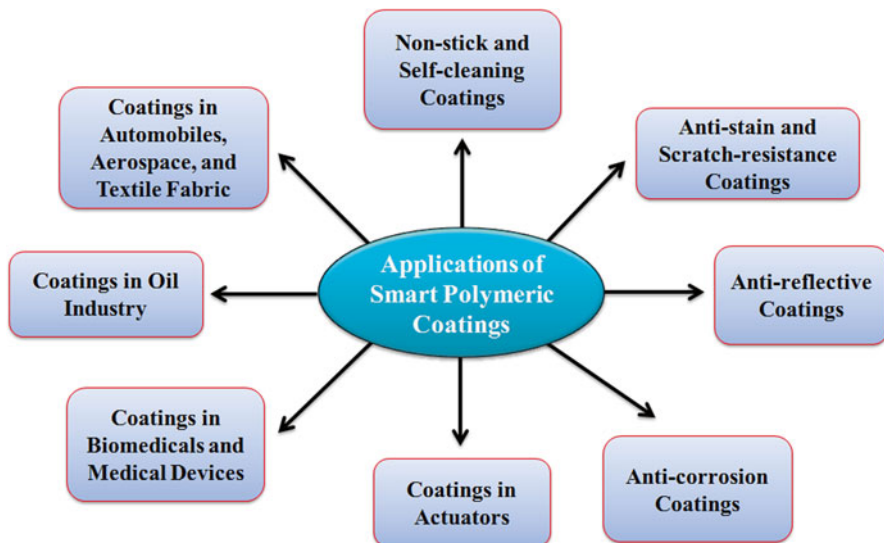

Fig. 2.1 Schematic representation for the smart polymeric coatings in various applications

various other industries may lead to the creation of various types of environmental pollution. In particular, dust pollutants create severe health effects to humans and other mammalians. Dust pollution is considered to be hazardous; dust particles are inhaled via the nose, mouth, or particles transported by the hand to other bodily areas. An exceeding level of dust particles in our body can create problems such as breathing difficulty, vomiting, diarrhea, and other similar diseases. Various commercial products such as protective gloves, masks, and eyeglasses can be used to protect one's health from severe environmental pollutants caused by dust particles. On the other hand, dust particles on the range of nano- or micro-sizes are difficult to identify through the naked eye alone. There are several means available for the uptake of these dust particles into human bodies, many through substances used in daily life. This is due to the easy adhesion of the dust particles on the hydrophilic surface of these substrates, and their complete removal of those accumulated dust particles from the substrate surfaces is difficult. To overcome this problem, superhydrophobic coating substrates have recently attracted considerable attention in self-cleaning coating applications [1] because of the nonstick and the easy dust removable properties of the superhydrophobic coating substrates. Superhydrophobic surfaces with stimuli-responsive properties are also attractive, owing to their excellent applicability in several industrial applications. In addition, these stimuli-responsive surfaces are also used for several other applications due to the responsiveness of the substrates under physicochemical as well as other environmental conditions such as UV, laser, plasma lights, pH, solvent, and temperature.

Superhydrophobic and self-cleaning coatings are considered to be promising candidates for protecting our health from dust pollution because of the easy removal of dust particles from the substrate. In most cases, the dust particles are easily removed from the superhydrophobic substrate by gravitational force with the help of water droplets. The surfaces with contact angle (CA) over 150° are termed as superhydrophobic surfaces [1, 2]. On the other hand, the surfaces with CA below 10°, 10–90°, and 90–150° are termed as superhydrophilic, hydrophilic, and hydrophobic surfaces, respectively. Superhydrophobic surfaces are generally mimicked from natural surfaces such as lotus leaves, rice leaves, butterfly wings, and water striders [29].These natural surfaces have dual micro-nanohierarchical surfaces which repel water droplets on the surface. Inspired by nature, several researchers mimicked the dual surface properties that have been previously described. Superhydrophobic properties can be developed in various substrates by simple techniques such as dip coating, spraying, and lay-up techniques. The superhydrophobic material-coated textile substrates can be used as a protective mask, easily cleaned by simple washing. Recently, a novel superhydrophobic hybrid micro-nanocomposite suspension using leaf powder, polymethylsiloxane, and alkyl-substituted silica ormosil aerogels was developed [1]. The suspension possessed superhydrophobic properties via the coating on various substrates followed by evaporation of the solvents at room temperature (Fig. 2.2) [1].

The superhydrophobic surface also showed excellent nonstick and self-cleaning properties on various substrates. The superhydrophobic surface can easily remove the dust particles deposited on the coated substrate surface by simply dripping water
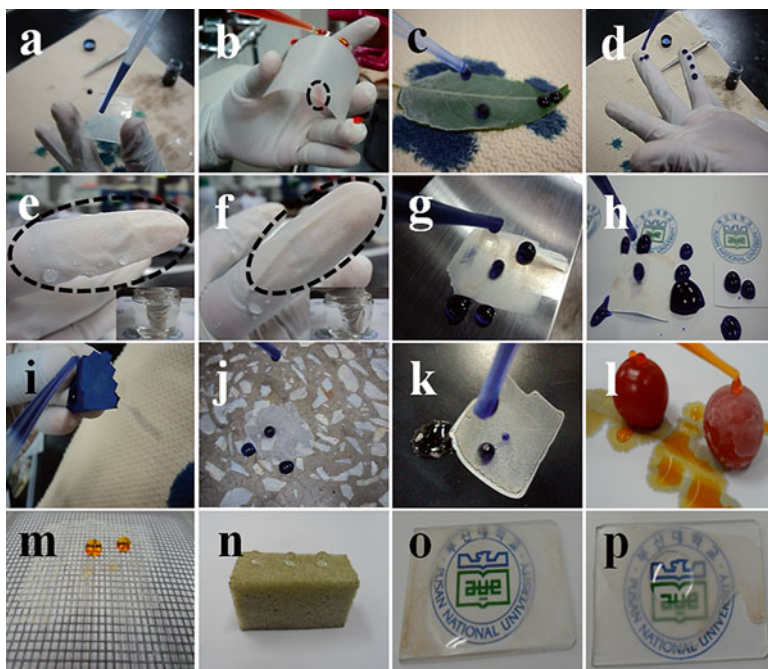
Fig. 2.2 Instant superhydrophobic properties of the hybrids on various substrates, such as (**a**) glass, (**b**) flexible laminating film, (**c**) tree leaf, and (**d**) glove. (**e** and **f**) Glove immersed in water before and after casting (attraction and reflection of uncasted and casted finger in water). (**g**) Stainless steel plate, (**h**) paper, (**i**) cotton cloth, (**j**) cement floor, (**k**) wooden board, (**l**) cherry tomato, and (**m**) fiber glass mesh (pore diameter, 1.5 mm). (**n**) Superhydrophobicity of the dip-coated hybrid/PDMS sponge dried at room temperature. (**o** and **p**) Superoleophilicity of the hybrid casted glass substrate for dodecane and soybean oil (Reproduced from Ha et al. [1])

droplets on the substrate surface. Owing to the excellent nonstick property of the superhydrophobic surface, water droplets are repelled on the substrate surface, where dust particles are collected, and then roll away by gravitation force. Moreover, the hybrid superhydrophobic surface also showed stimuli responsiveness to some low-density oils (e.g., dodecane). The superhydrophobic surface is wetted completely by the contact of dodecane droplet and reforms its original properties after evaporation. This switchable property may be useful in capturing volatile organic compounds (VOCs). Several researchers focused on this surface property due to its excellent applicability of the prepared materials for various applications. In most cases, nonstick and self-cleaning properties are considered to be the primary requirement for various industrial products. This coating is very useful in electronic gadgets; mirrors and wall construction; automobiles; as well as the aerospace, textile, and biomedical industries.

2.2.2   Smart Anti-stain and Scratch Resistance Coatings

Self-healable and responsive materials have been considered for use as smart surface coatings. This is due to the self-healing property of the materials when exposed to external stress, pressure, and mechanical abrasions. In most cases, scratches created by external stress reduced the lifetime of the product. The durability of the final product under stress is considered to be an important parameter for industrial applications. It was quite difficult to achieve scratch-resistant products until the introduction of self-healable materials. Self-healable materials have the ability to reform its original shape and structure by adjusting and reforming the broken chemical chains, thus proving useful in industrial products. The scratch-free products with anti-stain properties along with the ability to switch surface properties under external stimuli are all considered to be important parameters in industrial applications. This durable surface property has the ability to resist stains such as fingerprints and some viscous liquids (i.e., coffee stains). Fingerprinting on a substrate reduces product visibility and could be solved through surface treatment with anti-stain coatings. Self-healable materials with very high transparency could also solve this problem. The durability or stability of the coated materials is practically important. Materials with good transparency, durability under external stress, and self-healing behavior are the most promising for industrial applications. Recently, supramolecular polymers and some other polymer hybrid nanocomposites showed high durability property and were able to self-repair the scratched areas by sunlight or other stimuli.

Yang and Urban [12] studied these properties more deeply using various stimuli-responsive polymers and supramolecular polymers. They found highly durable and scratch-resistant coating materials from polyurethane networks containing a cross-linked sugar moiety (Fig. 2.3) [12]. The polymer showed a self-repairing property on the scratched substrate when exposed to atmospheric carbon dioxide (CO_2) and water. Sugar moieties in the cross-linked PU network played a vital role reacting with CO_2 and water in the self-repairing mechanism [12]. The broken chains were reformed through strong covalent bonding. The mechanical properties of the polymer networks were regained during this stage. This simple approach played a vital role for self-repairing and scratch-free substrate preparation. Moreover, the material did not require any additional process initiating the self-repairing mechanism, allowing for the wider usage of the smart polymer for various applications.

Van Vliet et al. [13] also developed highly durable, enhanced moduli, and scratch resistance coatings using polymethyl methacrylate (PMMA)/silica-based nanocomposites. The brittle nature of PMMA can be mechanically tailored using functional silica nanoparticles which can help to enhance mechanical strength and durability. Based on these approaches, the authors used two different functionalized silica nanoparticles with methyl and amino functional groups that were mechanically embedded on the PMMA films and heated the surface up to the glass transition (*T*g) temperature of the polymer. This way, the mechanical and scratch resistance properties of the PMMA/silica hybrid films were improved significantly in comparison with the pristine PMMA film. These approaches are practically reliable in
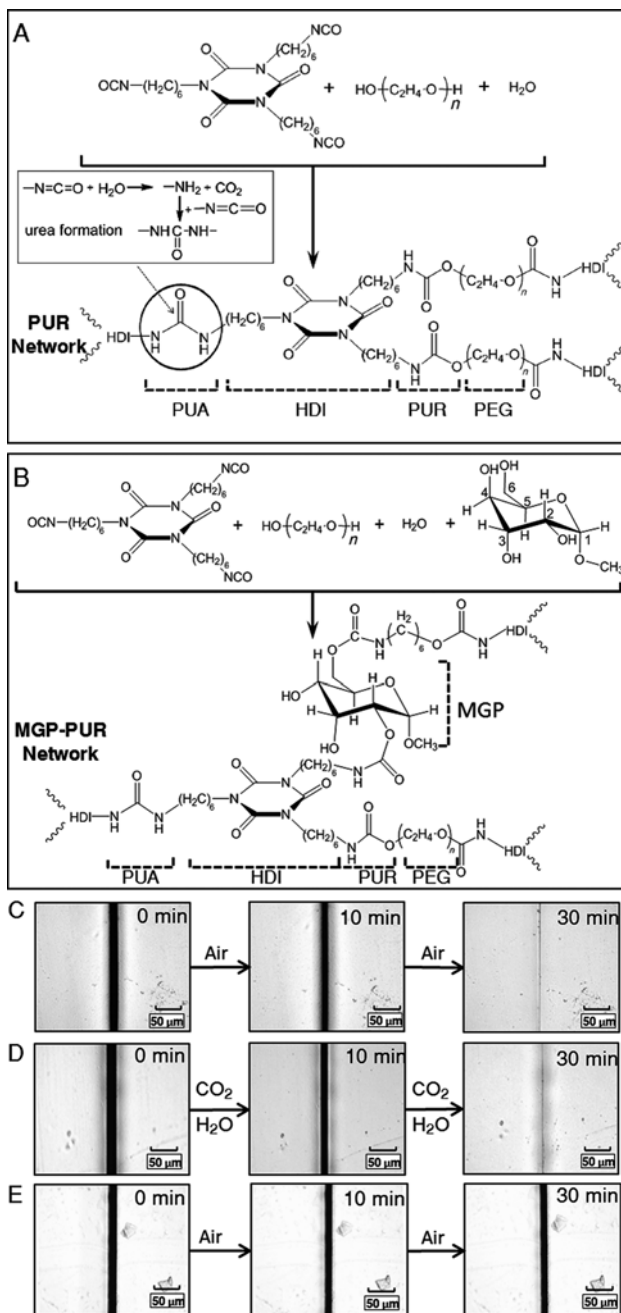
Fig. 2.3 (**a**) Reactions of isocyanate (NCO) groups of HDI and OH of PEG in the presence of H_2O generate CO_2 during PUR formation; (**b**) Reactions of NCO groups of HDI and OH of PEG and MPG in the presence of H_2O result in MGP-PUR network formation. Each network linkage and/or component is identified as follows: *PUA* polyurea, *HDI* hexamethylene diisocyanate trimmer, *PUR* polyurethane, *PEG* polyethylene glycol, *MGP* methyl-a-D-glucopyranoside. Self-repair of MGP-PUR network exposed to (**c**) air at 258 °C; (**d**) self-repair of MGP-PUR network exposed to the CO_2/H_2O mixture; (**e**) self-repair is not observed for PUR itself exposed to air (Reproduced from Yang and Urban [12])

forming highly durable surface coatings. Several works were also carried for the enhancement of scratch resistance of the coating materials. Functionalized nanoparticle additions, the use of low Tg-coating materials, and the use of high cross-linking density (XLD) materials attracted considerable attention for the improvement of scratch resistance of the substrate [30]. The use of these materials in a stimuli-responsive polymer also exhibited the improved properties of the material.

2.2.3   Smart Antireflective Polymeric Coatings

Antireflective (AR) coatings are an important application in the coating industry when producing safe mirrors for automobiles. The refractive index of the coated materials is a very important parameter for antireflective coating applications. The low refractive index of the material will improve performance, and as such, research in said materials is ongoing, using various types of metal alkoxides by sol–gel method, polymers, and polymer-based hybrid materials as well as stimuli-responsive polymers. The SiO_2 and TiO_2 mixture-based sol compositions of the final product could have refractive index values between 1.458 and 2.22 (for 500 nm) [31, 32]. Liu and Yeh [33] also developed sol–gel-based silica colloidal particles with lower refractive index.

Similarly, Beobide et al. [34] prepared SiO_2/TiO_2 porous hybrid nanoparticles with multifunctional and self-cleaning properties. The porous hybrid material also showed lower refractive index value. They compared porous hybrid materials and their refractive index values with dense SiO_2 and TiO_2. The authors found that porous hybrid materials have a lower refractive index with multifunctional applications such as self-cleaning and photocatalytic behaviors [34]. The optimum refractive index value of a sample can vary based on the materials' physical and chemical properties. The light-responsive polymers will play a key role in the antireflective coatings. This is due to the switchable properties of the polymers under light which can control the transmittance of the light's wavelength. Automobiles, aerospace, building mirrors, light-responsive fabrics, and other fields require antireflective coatings. Fudouzi and Xia [14] developed a novel solvent-responsible photonic paper using stimuli-responsive polymer [polystyrene (PS) beads and polydimethylsiloxane (PDMS)] coatings on a paper substrate. The coated substrates were selectively responsible for the particular solvents, emitting different colors on the pre-patterned commercial stamps placed on the substrate (Fig. 2.4). Schenning et al. [35] reviewed this work, placing more emphasis on the various stimuli-responsive polymers used for antireflective coating and their photonic applications. The photonic stimuli polymers are responsible for the surface property switching from hydrophilic to hydrophobic or hydrophobic to hydrophilic based on the *on* and *off* mechanism of the light stimuli. Kim et al. [15] synthesized a novel PS-block-PMMA block copolymer that was spin coated on a glass substrate. The block copolymer showed broadband antireflection property on the coated glass substrate. Increasing the layers of block copolymer film on the glass substrate by spin coating
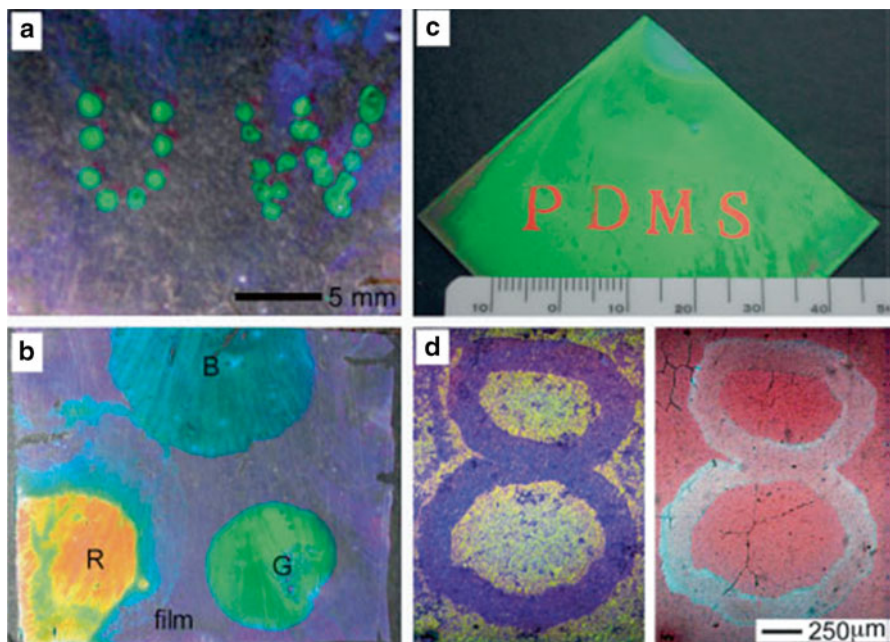
Fig. 2.4 (**a**, **b**) Photographs of test patterns written on photonic papers by delivering ink droplets to their surface using a Pilot pen. (**a**) Two *dotted letters* written with octane. (**b**) *Dots* of three different colors written on the same colloidal crystal using silicone liquid of various molecular weights: *blue dot* (with T15, Mw = 3780), *green dot* (with T05, Mw = 770), and *red dot* (with T00, Mw = 1620). (**c**, **d**) Photographs of the test patterns formed on the surfaces of photonic papers by stamping with silicone fluid (T11, Mw = 1250). (**c**) Two letters generated using a commercial rubber stamp. (**d**) The number "eight" generated using a microfabricated PDMS stamp: reflection image (*left*) and transmission image (*right*) (Reproduced from Fudouzi and Xia [14]).

increased the antireflection property of the material which is useful for the broadband as well as for solar cell applications. Han et al. [16] developed an antireflective coating using a solvent-responsible stimuli porous block copolymer [PS-block-poly(4-vinylpyridine) (P4VP)].

In a similar way, the photonic stimuli polymers are also responsive to solvents, pH, humidity, and temperature [15]. Recently polyimide (PI)-based coating materials are also used for antireflective coating applications. The extreme stability, flexibility, and durability of the PI-based thin film are very useful in aerospace and other industrial applications. Wang and Chen [17, 18] prepared highly transparent and photo-responsive PI/inorganic hybrid materials for antireflective coating applications. The materials showed good transparency and light-responsive properties with a low refractive index. Similarly, Yu et al. [19] also prepared PI/inorganic hybrid materials for antireflective coating applications. The PI/hybrid coating film also showed excellent stability and allows refractive index value.

2.2.4   Smart Anticorrosion Polymeric Coatings

Corrosion formation on aluminum, steel, iron, wood, and other substrates can cause serious damage to the substrate. Sometimes, the rupture of the substrate can cause accidents within the industry, creating problems for the surrounding area and people. Similarly, marine biofouling can also damage ships, boats, and oil refinery substrates under the seawater. This biofouling can directly affect the fishing and refinery industries. To avoid the corrosion and biofouling, the substrate should be protected by coating it with the proper corrosion resistance materials. Several metal nanoparticle-based corrosion resistance coatings have been developed which showed improved performance in corrosion resistance as well as in their biofouling properties. In most cases, chromium (VI)-based materials were used for the corrosion resistance coating. This is due to the self-reforming property of the Cr (VI) on the corroded substrate. Meanwhile, Cr (VI) is considered to be highly toxic as well as a cancer-creating metal ion. Thus, the use of Cr (VI) was banned from use in anticorrosion and other applications. As an alternative to Cr (VI), other less volatile metal ions were used in anticorrosion coatings. Recently, functionalized silica, hollow and mesoporous silicas, and stimuli-responsive polymer coatings were used for the corrosion resistance and antifouling coatings (Fig. 2.5) [36, 37]. The technical advantage of using stimuli-responsive polymer coatings for anticorrosion is their responsiveness to acidic and basic conditions, temperature, and chemical exposure. The responsiveness of the coating substrate will protect the substrate from corrosion.

Recently, superhydrophobic coatings have also been used for anticorrosion and antifouling applications. The advantage of the extreme water resistance properties of superhydrophobic coatings could help to protect surfaces from corrosion. There has also been additional development in stimuli-responsive superhydrophobic coatings for anticorrosion and antifouling applications. Coated substrates showed excellent stability, durability, and stimuli responsiveness under acidic and basic conditions, temperature, and chemical exposure and had better performance in anticorrosion and antifouling applications [38]. Based on the excellent properties of the stimuli-responsive superhydrophobic coatings, the applications of the coated materials can be used in various other applications. The research on their surface properties has increased in recent years using various types of stimuli-responsive smart polymer hybrid coatings.

2.2.5   Smart Polymeric Coatings in Actuators

An actuator is a device which is responsible for the mechanical movement of any object from one place to another. Actuator devices can respond to changes in solvents, pH, applied electric fields, and humidity. Actuating devices are used widely in all types of industries. These devices have attracted considerable attention recently due to easy responsible nature of the smart polymer under some physical or
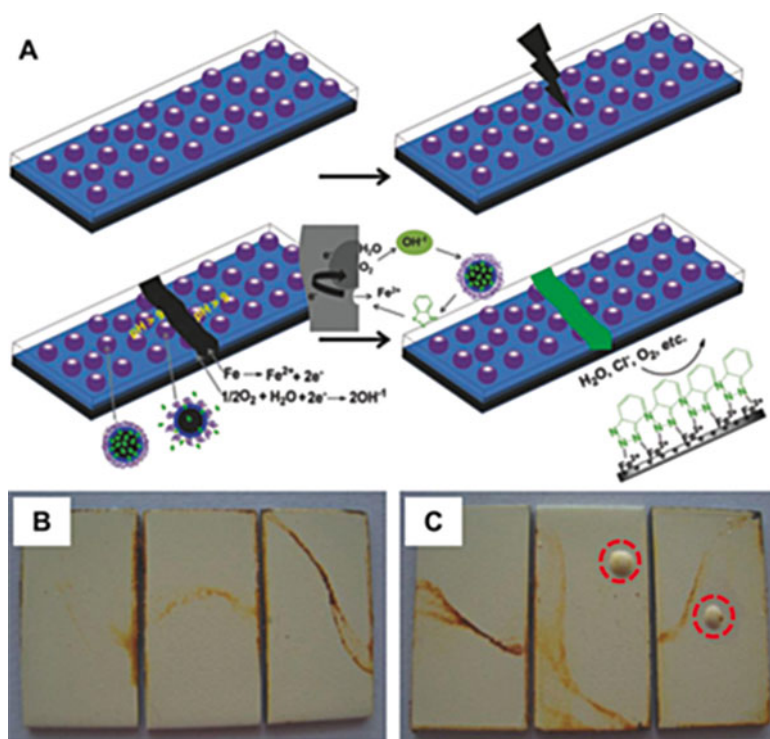
Fig. 2.5 (**a**) The self-healing mechanism of polymeric nanocontainer-doped epoxy organic coatings on metal surfaces for corrosion protection. (**b**) Epoxy coating doped with 3 wt% PS-benzotriazole (BTA)/polyethyleneimine (PEI)-3 nanocontainers (the three substrates are with the same coatings after the same corrosion time); (**c**) commercial epoxy coating with zinc phosphate as inhibiting pigment (the three substrates are with the same coatings after the same corrosion time). *Red circles* indicate pitting corrosions (blistering) (Reproduced from Li et al. [36])

chemical environments. Yuan et al. [20] developed a novel multi-responsive and free-standing porous smart polymer actuator film using cationic polyionic liquid (poly(3-cyanomethyl-1-vinylimidazolium) bis(trifluoromethanesulfonyl)imide). The prepared film showed selective responsiveness to acetone vapor, folding inside itself when in contact with the vapor. Meanwhile, the folded polymer film returns to its original form after drying the acetone vapor from the film surface. The self-foldable, switchable, and free-standing properties are also emphasizing the higher flexibility of the film, particularly useful for industrial applications [20]. The porous actuator film also showed similar properties for other solvents such as tetrahydrofuran (THF), piperidine, and pyridine. On the other hand, the porous polymer film was much less responsive in its adsorption behavior for dioxane, methanol, ethanol, and isopropanol. The excellent responsibility of the film for the solvents comes from the solubility of polymer and interactions with other molecules in the system that triggers the actuation behavior. Several works were carried out using responsive polymers for actuator applications. Recently, solvent-, humidity-, optical-, thermo-, and magneto-responsive actuators were fabricated for the easy movement of a system
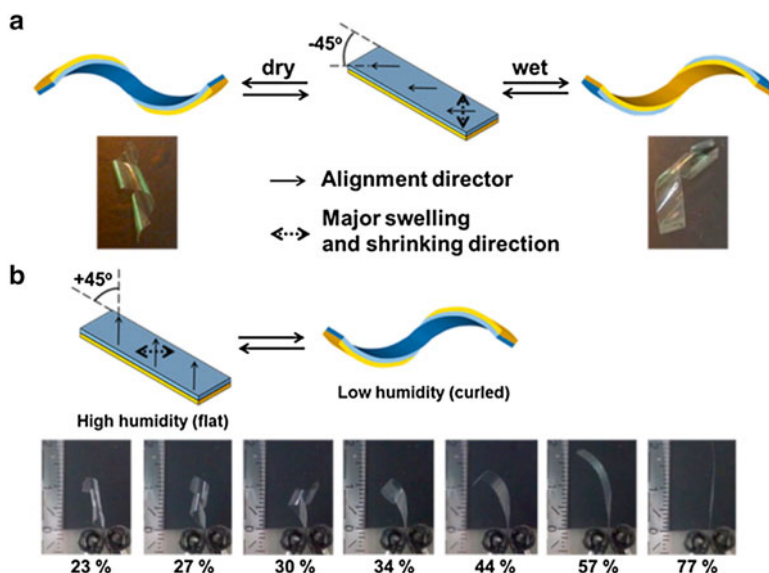
Fig. 2.6 Curling actuators prepared by one-side base exposure of liquid crystalline (LC) films (*blue* area). (**a**) Ribbon with the molecular director at a −45° angle with respect to the long axis of the film and the resulting curling behavior after activation in KOH solution, both in the wet and dry state. (**b**) Curling and uncurling of the +45° actuator at high and low humidity, respectively. The behavior of this actuator is also shown in the humidity chamber with increasing humidity (Reproduced from Broer et al. [39])

(Fig. 2.6) [39–47]. The solvent- and humidity-responsive actuators are also quite cheap to use in industrial applications.

2.2.6 Smart Coatings in Drug and Gene Delivery and Medical Devices

Recently, significant advances have been achieved in the synthesis and further modification of inorganic nanoparticles for biomedical applications. Among them, mesoporous silica materials offer a robust framework which is suitable for modification of various organic functional units on their surfaces. In addition, mesoporous silica materials possess many advantages such as high surface areas, pore volumes, thermal and chemical stability, and excellent biocompatibility [48].

2.2.6.1 Smart Polymer-Coated Mesoporous Silica Materials for Drug Delivery

Mesoporous silica materials provide excellent drug loading capacity due to their large mesopore volume and ability to load and release of drug molecules by the mesoporous silica nanoparticles [49]. Moreover, mesoporous silica nanocarrier is
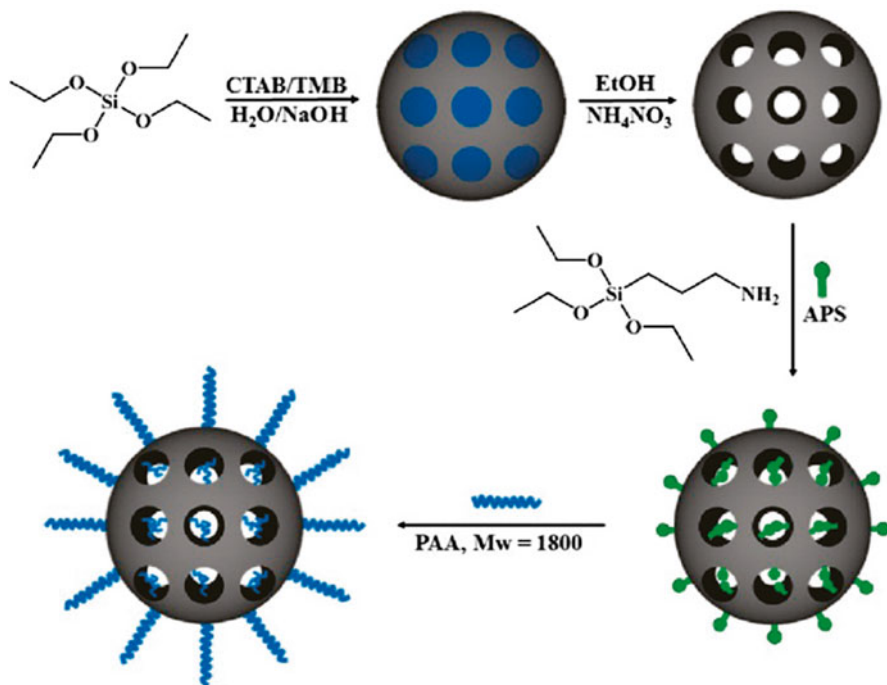
Fig. 2.7 Schematic preparation process of PAA-MSN (Reproduced from Yu et al. [19])

also used for controlled delivery of the drug molecules for particular applications. The great diversity in surface functionalization of mesoporous silica nanoparticles offers a unique advantage in the construction of nanogates that respond to different stimuli. Various types of nanoparticles, organic molecules, and biomolecules have been used as capping agents to block molecule transport from a silica mesopore and to unlock the entrance for triggered release under specific external stimuli [50, 51]. A combination of mesoporous silica and functional smart polymers generates a novel type of hybrid nanoswitch that takes advantage of the unique features of polymers and porous materials. For example, mesoporous silica coated with thermosensitive poly(N-isopropylacrylamide) could control the molecule release at different temperatures [10]. Hong et al. [21] developed a novel pH-sensitive mesoporous silica smart nanovalve by surface grafting onto the exterior surface by RAFT polymerization of acrylic acid (AA) for the biomedical application. Similarly, mesoporous silica surface was modified by grafting or atom transfer radical polymerization (ATRP) by using poly(4-vinylpyridine) or poly(2-(diethylamino)ethyl methacrylate) [23, 24]. Yu et al. [22] prepared PAA-grafted mesoporous silica nanoparticles (PAA-MSNs) by a facile graft onto strategy (i.e., the amidation between PAA homopolymer and amino group functionalized MSNs) (Fig. 2.7). Due to the presence of covalent graft of hydrophilic and pH-responsive PAA, the PAA-MSNs were well dispersed in aqueous solution, which is favorable when utilized as drug carriers in a pH-responsive controlled drug delivery system [22].

Hollow mesoporous silica materials were modified with the long-chain hydrocarbon octadecyltrimethoxysilane (C18) and the fluorescent agent rhodamine B isothiocyanate (RITC) on the surface of the silica. After loading with drug molecules, the material was encapsulated by a photodegradable amphiphilic copolymer. The drug release occurred while irradiating with visible light [52]. Most anticancer drugs have severe adverse effects on healthy tissues while in transit to the tumor target [53]. Therefore, the construction of smart drug delivery systems should prevent the premature release of their payload when en route to the target tissues. This requires the combination of drug carriers and smart polymers that facilitate the target drug release without premature release.

It is important that when selecting a polymer to be used as a coating on mesoporous silica drug carriers, the polymer should decompose under external stimulus such as pH, temperature, light, enzyme, or ionization that will facilitate the drug release process. Yang et al. [25] prepared a reductive-responsible disulfide, namely, poly(N-vinylcaprolactam-s-s-methacrylic acid) cross-linked polymer-coated mesoporous silica carrier, which provided pH/thermal stimuli-responsive drug release. Pan et al. [54] prepared reversibly cross-linked polymer-coated mesoporous silica nanoparticles via surface reversible addition–fragmentation chain transfer (RAFT) polymerization using the reactive monomer oligo(ethylene glycol) acrylate (OEGA) and the more reactive cross-linker N, N′-cystaminebismethacrylamide (CBMA). Owing to the reversible cleavage and restoration of disulfide bonds via reduction/oxidation reactions, the polymer shells can control the on/off switching of the nanopores and regulate the drug loading and release.

2.2.6.2 Smart Polymer-Coated Mesoporous Silica Materials for Gene Delivery

Gene delivery is another major application of mesoporous silica carriers besides the delivery of small molecules and proteins. The use of mesoporous silica for gene delivery has been extensively explored because their surfaces can be easily modified with cationic molecules, allowing for not only the stable condensation with nucleotides that are highly negatively charged but also protecting them from nuclease in physiological conditions. A significant amount of progress toward the understanding and utilization of mesoporous silica materials for controlled gene release has occurred in recent years. Mesoporous silicas have been explored in biomedical applications, drug delivery, and DNA delivery for gene therapy [49]. Mesoporous silicas contain a porous structure with hundreds of channels referred to as mesopores, which are able to absorb bioactive molecules. Additionally, the efficient cellular uptake of mesoporous silica particles is size dependent, with optimal uptake occurring at the submicron scale with potential for controlled DNA release [55]. Yu et al. [26] developed a novel biocompatible poly(2-dimethylaminoethyl acrylate) (PDMAEA)-functionalized mesoporous nanocarrier for gene delivery application. The designed cationic polymer unit binds to genetic molecules and undergoes a self-catalyzed hydrolysis in water to form a nontoxic anionic poly(acrylic acid) allowing the controlled release of siRNA in the cells.

Nel et al. [27] prepared a polyethylenimine-coated mesoporous silica material by surface functionalization approaches. The resulting system enhanced cellular uptake and allowed for nucleic acid delivery in addition to drug delivery. Noncovalent attachment of polyethylenimine (PEI) polymers that functionalized on the silica surfaces not only increased cellular uptake of silica materials but also generated a cationic surface which DNA and siRNA constructs could be attached. Cho et al. [56] studied the effect of mesoporous silica nanoparticles (MSN) coupled with mannosylated polyethylenimine (MP). The modified MSN has been shown to be an effective method in lowering the cytotoxicity while enhancing the transfection efficiency through receptor-mediated endocytosis. The results showed enhanced transfection efficiency through receptor-mediated endocytosis via mannose receptors [56]. Lin et al. [57] reported a novel gene transfection system by covalently attaching a polyamidoamine dendrimer onto mesoporous silica MCM-41 nanospheres. This system was used to complex with a plasmid DNA (pEGFPC1) that codes for an enhanced green fluorescence protein-based gene transfection reagent (Fig. 2.8) [57].
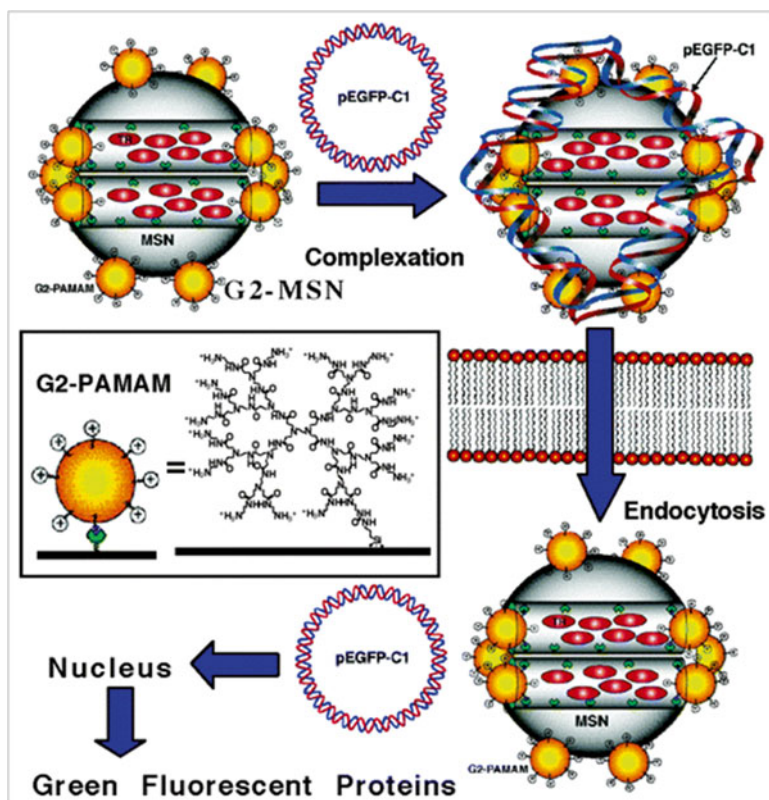

Fig. 2.8 Schematic representation of a nonviral gene transfection system based on a Texas Red (TR)-loaded, G2-PAMAM dendrimer-capped MSN material complexed with an enhanced green fluorescence protein (*Aequorea victoria*) plasmid DNA (pEGFP-C1) (Reproduced from Lin et al. [57])

2.2.6.3 Smart Polymer-Coated Mesoporous Silica Materials for the Preparation of Medical Devices

Biomedical engineers have recently recognized that medical implants require well-defined and controlled interfaces. One of the major obstacles preventing the clinical application of active devices that perform biologically is that of functionality. Biosensors and drug delivery implants are active medical devices that must be capable of function during use over a period of months, years, or possibly decades. These devices must exhibit functional stability under a wide range of biological conditions [58]. Silica-based ceramics have received a great deal of interest for the development of stimuli-responsive nanocarrier for biomedical field applications [59]. However, the scope of the silica materials with clinical applications has considerably changed in the last few years. For instance, it is worth mentioning the research effort carried out in mesoporous materials for designing biomedical devices has resulted in two main uses: drug delivery systems and bone tissue regeneration. Tissue engineering is an emerging area directed toward the design of materials that can help an organism to improve its ability of regeneration by recovering both the structure and its function. For this purpose, biocompatible and bioresorbable scaffolds are desirable as they enhance tissue growth and increase the cellular function (i.e., aid the development of cells into a functioning tissue in preparation for implantation). Recently, these materials have been proposed to be applied in biomaterial science [60]. Owing to their textural properties of surface and porosity, ordered mesoporous materials have shown to be excellent candidates for bone tissue regeneration. Vallet–Regi et al. [61] have prepared an ordered mesoporous materials in the system SiO_2–CaO–P_2O_5, with different CaO contents. By changing the CaO content, the bioactive behavior can be modified due to the different network connectivity and the textural properties. The mesoporous silica bioactive glasses can be used for bone tissue regeneration applications [61]. The same group has also prepared a MCM-41-based mesoporous materials at alkaline pH which contain phosphorous atoms linked to silicon atoms of the framework through oxygen bonds. This new material displayed the capability of phosphorous-doped MCM-41 to act as a bioactive material [62]. Zhao et al. [63] prepared a highly ordered mesoporous bioactive glasses, synthesized with superior bone-forming bioactivity, in vitro. These mesoporous silica-based bioactive materials showed superior bone-forming bioactivity when compared to normal BGs derived from sol–gels [63].

2.2.7 Smart Coatings in Oil Industry

Oil industries are considered to be the driving factor for the automobile, aerospace, and another energy generation applications. Oil industries are also changing the economy and life styles of people by increasing or decreasing the price of fuel. In the past few decades, several accidents have happened in the oil industry or in oil transport ships where many tons of oil were spilled on the seawater

surface. Oil spills on the ocean surface can cause serious health problems to the native creatures in the sea as well as to surrounding people near the affected area. In order to selectively capture the spilled oils from the seawater surface, several absorbents or adsorbents have been developed so far using natural or synthetic materials. In that, superhydrophobic surfaces such as sponges, foams, aerogels, membranes, and wire meshes attracted much attention for their selective oil spill capture capability and for other oil/water separation applications. This is due to the easy capture of spilled oils as well as an improved recyclable capacity by using the superhydrophobic surfaces. Moreover, the captured oils can be recovered at higher level, which can be purified and reused for various applications. These smart approaches are also considered to be more effective in the selective oil sorption and oil/water separation from the oil spills than other methods used before. Functionalized superhydrophobic surfaces are also promising for the oil industry due to the selective sorption and separation of oils from water as well as the responsive nature of the substrate. Several new techniques were developed recently by using various types of superhydrophobic surfaces for oil/water separation applications. On the other hand, hydrophilic surfaces are also used sometimes for oil/water separation. Recently, Howarter and Youngblood [28] developed novel stimuli-responsive polymer brushes for self-cleaning coating applications. The prepared surface also showed an antifogging property which is useful for dual-purpose applications. A surface with advancing contact angle (CA) lower than 40° can show better antifogging property than advancing the CA higher than 40° [64].

Meanwhile, in most cases, superhydrophilic surfaces are exhibiting better performance in antifogging applications than other substrates [65]. Owing to the complete wettable property of the superhydrophilic substrate, the substrate can be transparent due to formation of thin films of water vapors on the substrate. In contrast, superhydrophilic surfaces lack this self-cleaning property. Based on this concept, Howarter and Youngblood [28] developed a hydrophilic stimuli-responsive surface by surface functionalization and grafting of polyethylene glycol with short perfluorinated end caps (f-PEG) and isocyanate-functionalized silane. The material-coated glass substrate showed solvent-selective stimuli-responsive behavior. They discovered the self-cleaning behavior of the hydrophilic substrate and found that the real mechanism of the property was based on the water and oil CAs on the substrate. The substrate with receding CA of oil (hexadecane) is higher than the advancing CA of water, thus causing the hydrophilic surface to thermodynamically self-clean the oil droplets on the surface (Fig. 2.9). This is due to the higher energy gain of water-substrate contact than the energy losing oil-substrate contact [28]. This solvent-selective, self-cleaning, and antifogging coating substrate may prove to be useful in water and oil removal in industrial applications.
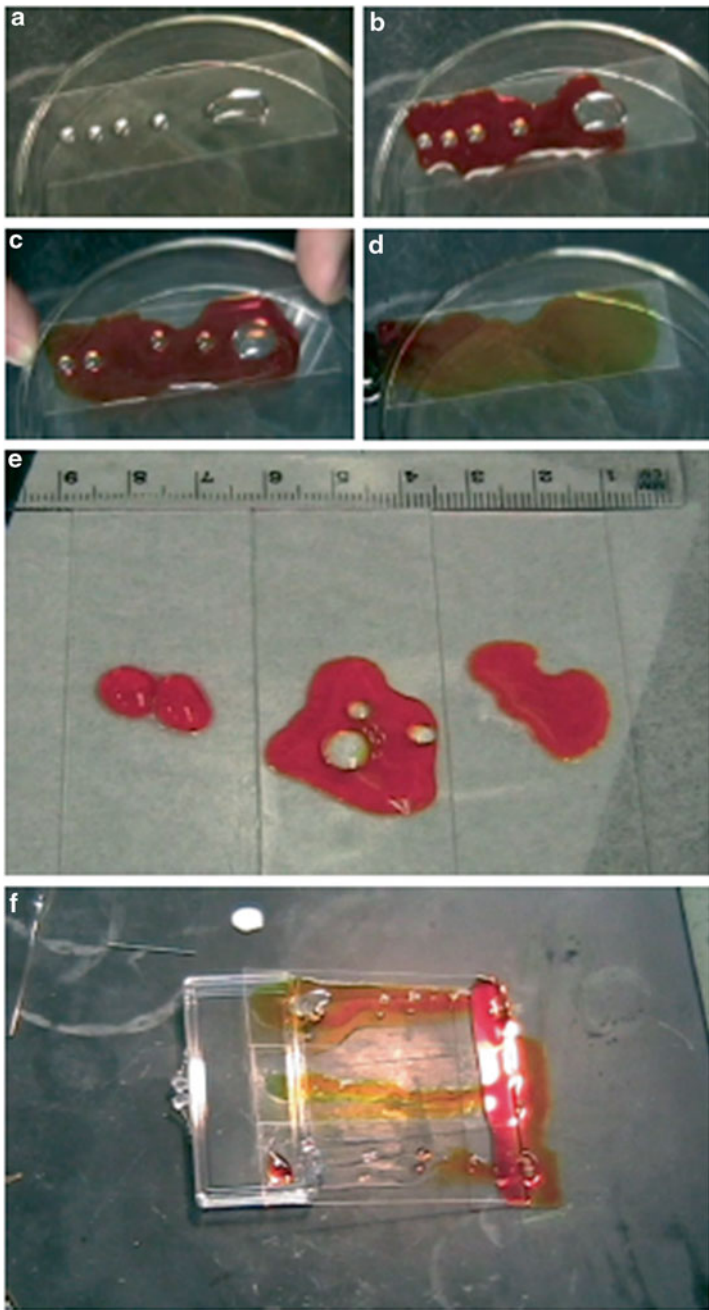
Fig. 2.9 Self-cleaning response of f-PEG: (**a–d**) Oil droplets are placed on the f-PEG surface (**a**) followed by water (*reddish-orange*). (**b**) With minimal mechanical agitation, water displaced the oil (**c**) on the surface. Upon tilting the sample, the oil floats off and is removed from the slide (**d**). (**e**) When oil is placed in contact with water on hydrophobized glass (*left*), f-PEG-modified glass (*middle*), and clean glass (*right*), the surfaces show differing behavior. (**f**) Oil on hydrophobized glass (*bottom*), f-PEG-modified glass (*middle*), and clean glass (*top*) exposed to gently flowing water (Reproduced from Howarter and Youngblood [28])

2.2.8   Smart Polymeric Coatings in Automobiles, Aerospace, and Textile Fabrics

Smart polymers have wide usages in automobiles, aerospace, and textile fabric applications. Several metal nanoparticle- and metal alloy-based coatings were used for automobile and aerospace applications in order to protect the surface properties from scratches and corrosions. Superhydrophobic and self-cleaning, stimuli-responsive self-healing, scratch resistance, and anticorrosion coatings have attracted more attention from the automobiles and aerospace industries. This is because the use of these surface properties can protect the automobile and aerospace products from dust, corrosion, and scratches. These properties can also extend the lifetime of the surface-treated products, which is desirable when utilizing these materials in industrial applications. Recently, Shi et al. [66] developed a novel robotic chemical-responsive superhydrophobic miniature boat. The developed boat showed sensitivity to solvent and accelerated from one place to another place by itself with the internal energy created by the solvent system. This self-robotic acceleration of the superhydrophobic coating by the solvent could prove to be useful when applying this system in the practical transportation applications. Similarly, the stimuli-responsive smart polymer coatings are also used widely in the preparation of various types of textile fabrics such as shape-memory foams, fibers, fabrics, etc. [67]. Hu et al. [67] briefly reviewed the stimuli responsiveness of various polymers used for the development of smart textiles. The smart polymeric textile fabrics were also developed by using various types of responsive polymer coatings such as thermal-, pH-, moisture-, water-, solvent-, and light-responsive coatings for a variety of applications in textile industries such as transportation, thermal wears, protective gloves and masks, and biomedical applications.

2.3   Conclusion and Future Outlook

Surface coatings are the most important parameter for almost all kinds of products that are used in daily life. The look of the finished product depends on the performance, durability, and ability to resist harsh conditions such as temperatures, pHs, chemicals, environment, and external stresses. In order to improve the quality and capability of the finished products in industrial applications, smart coatings are widely used to protect the surface or switch the surface properties so as to protect them from the external stress. These switchable surface properties are important for increasing the durability, mechanical strength, and resistance against corrosion and scratches. Several smart polymers and polymer hybrid materials have been developed so far to enhance the quality of the product. Recently, superhydrophobic and self-cleaning coatings and self-healable, scratch resistance, and anticorrosion coatings are considered to be an attractive properties for materials used for several industrial applications. The technical usages of these coatings in industrial

applications are not limited to any one particular application due to the excellent properties of smart coatings. In this book chapter, the various surface properties, stimuli-responsive polymers, and their uses in various applications were briefly discussed. The applications of smart coatings are emerging in various fields and also can be developed in different types of coating methodologies in the future. Recently, multifunctional smart coatings have also been developed to treat various surface coatings. The proper selection of materials is necessary in order to develop smart surface coatings with multifunctional groups for various applications.

References

1. Nagappan S, Park JJ, Park SS, Lee WK, Ha CS (2013) J Mater Chem A 1:6761–6769
2. Stuart MAC, Huck WTS, Genzer J, Muller M, Ober C, Stamm M, Sukhorukov GB (2010) Nat Mater 9:101–113
3. Chen JK, Chang CJ (2014) Materials 7:805–875
4. Mano JF (2008) Adv Eng Mater 10:515–527
5. Uhlmann P, Lonov L, Houbenov N, Nitschke M, Grundke K, Motornov M, Minko S, Stamm M (2006) Prog Org Coat 55:168–174
6. Nagappan S, Ha CS (2015) J Mater Chem A 3:3224–3251
7. Motornov M, Roiter Y, Tokarev I, Minko S (2010) Prog Polym Sci 35:174–211
8. Hoare T, Pelton R (2008) Biomacromolecules 9:733–740
9. Lapeyre V, Ancla C, Catargi B, Ravaine V (2008) J Colloid Interface Sci 327:316–323
10. Fu Q, Rao GVR, Ista LK, Wu Y, Andrzejewski BP, Sklar LA, Ward TL, López GP (2003) Adv Mater 15:1262–1266
11. Minko S (2006) J Macromol Sci Part C Polym Rev 46:397–420
12. Yang Y, Urban MW (2014) Angew Chem Int Ed 53:12142–12147
13. Qu M, Meth JS, Blackman GS, Cohen GM, Sharp KG, Van Vliet KJ (2011) Soft Matter 7:8401–8408
14. Fudouzi H, Xia Y (2003) Adv Mater 15:892–896
15. Joo W, Kim HJ, Kim JK (2010) Langmuir 26:5110–5114
16. Li X, Yu X, Han Y (2012) Langmuir 28:10584–10591
17. Wang YW, Chen WC (2010) Compos Sci Technol 70:769–775
18. Wang YW, Chen WC (2011) Mater Chem Phys 126:24–30
19. Yu YY, Chien WC, Lin JM, Yu HH (2011) Thin Solid Films 519:4731–4736
20. Zhao Q, Dunlop JWC, Qiu X, Huang F, Zhang Z, Heyda J, Dzubiella J, Antonietti M, Yuan J (2014) Nat Commun 5:4293. doi:10.1038/ncomms5293
21. Hong CY, Li X, Pan CY (2009) J Mater Chem 19:5155–5160
22. Yuan L, Tang QQ, Yang D, Zhang JZ, Zhang FY, Hu JH (2011) J Phys Chem C 115:9926–9932
23. Liu R, Liao P, Liu J, Feng P (2011) Langmuir 27:3095–3099
24. Sun JT, Hong CY, Pan CY (2010) J Phys Chem C 114:1481–1486
25. Chang B, Chen D, Wang Y, Chen Y, Jiao Y, Sha X, Yang W (2013) Chem Mater 25:574–585
26. Hartono SB, Phuoc NT, Yu M, Jia Z, Monteiro MJ, Qiao S, Yu C (2014) J Mater Chem B 2:718–726

27. Xia T, Kovochich M, Liong M, Meng H, Kabehie S, George S, Zink JI, Nel AE (2009) ACS Nano 3:3273–3286
28. Howarter JA, Youngblood JP (2007) Adv Mater 19:3838–3843
29. Nagappan S, Park SS, Ha CS (2014) J Nanosci Nanotechnol 14:1441–1462
30. Groenewolt M (2008) Prog Org Coat 61:106–109
31. Hussmann EK (1998) Key Eng Mater 150:49–66
32. Chen D (2001) Sol Energy Mater Sol Cells 68:313–336
33. Liu BT, Yeh WD (2010) Colloids Surf A Physicochem Eng Aspects 356:145–149
34. Prado R, Beobide G, Marcaide A, Goikoetxea J, Aranzabe A (2010) Sol Energy Mater Sol Cells 94:1081–1088
35. Stumpel JE, Broerab DJ, Schenning APHJ (2014) Chem Commun 50:15839–15848
36. Li GL, Schenderlein M, Men Y, Möhwald H, Shchukin DG (2014) Adv Mater Interfaces 1:1300019
37. Fu JJ, Chen T, Wang MD, Yang NW, Li SN, Wang Y, Liu XD (2013) ACS Nano 7:11397–11408
38. Chen T, Fu JJ (2012) Nanotechnology 23:505705
39. de Haan LT, Verjans JMN, Broer DJ, Bastiaansen CWM, Schenning APHJ (2014) J Am Chem Soc 136:10585–10588
40. Dai M, Picot OT, Verjans JMN, de Haan LT, Schenning APHJ, Peijs T, Bastiaansen CWM (2013) ACS Appl Mater Interfaces 5:4945–44950
41. Zhang X, Pint CL, Lee MH, Schubert BE, Jamshidi A, Takei K, Ko H, Gillies A, Bardhan R, Urban JJ, Wu M, Fearing R, Javey A (2011) Nano Lett 11:3239–3244
42. Du D, Wen H, Hu Z, Weng Y, Zhang WD (2014) Nanotechnology 25:195503
43. Nakahata M, Takashima Y, Hashidzume A, Harada A (2013) Angew Chem Int Ed 52:5731–5735
44. Huck WTS (2008) Mater Today 11:24–32
45. Behl M, Kratz K, Noechel U, Sauter T, Lendlein A (2013) Proc Natl Acad Sci U S A 110:12555–12559
46. Woodward RT, Olariu CI, Hasan EA, Yiu HHP, Rosseinsky MJ, Weaver JVM (2011) Soft Matter 7:4335–4340
47. Kim H, Kwon S (2013) Science 339:150–151
48. Liong M, Lu J, Kovochich M, Xia T, Ruehm SG, Nel AE, Tamanoi F, Zink JI (2008) ACS Nano 2:889–896
49. Slowing II, Vivero-Escoto JL, Wu CW, Lin VSY (2008) Adv Drug Deliv Rev 60:1278–1288
50. Hernandez R, Tseng HR, Wong JW (2004) J Am Chem Soc 126:3370–3371
51. Schlossbauer A, Kecht J, Bein T (2009) Angew Chem Int Ed 48:3092–3095
52. Yang S, Li N, Chen D, Qi X, Xu Y, Yu Q, Li H, Lu J (2013) J Mater Chem B 1:4628–4636
53. Vivero-Escoto JL, Slowing II, Trewyn BG, Lin VSY (2010) Small 6:1952–1967
54. Sun JT, Piao JG, Wang LH, Javed M, Hong CY, Pan CY (2013) Macromol Rapid Commun 34:1387–1394
55. Morille M, Passirani C, Vonarbourg A, Clavreul A, Benoit JP (2008) Biomaterials 29:3477–3496
56. Park IY, Kim IY, Yoo MK, Choi YJ, Cho MH, Cho CS (2008) Int J Pharm 359:280–287
57. Radu DR, Lai CY, Jeftinija K, Rowe EW, Jeftinija S, Lin VSY (2004) J Am Chem Soc 126:13216–13217
58. Anglin EJ, Cheng L, Freeman WR, Sailor MJ (2008) Adv Drug Deliv Rev 60:1266–1277
59. Cheng Q, Miyaji F, Kokubo T, Nakamura T (1999) Biomaterials 20:1127–1134
60. Vallet-Regi M, Ruiz-Gonzalez L, Izquierdo-Barba I, González-calbet JM (2006) J Mater Chem 16:26–31
61. Lopez-Noriega A, Arcos D, Izquierdo-Barba I, Sakamoto Y, Terasaki O, Vallet-Regi M (2006) Chem Mater 18:3137–3144
62. Vallet-Regi M, Izquierdo-Barba I, Rámila A, Pariente JP, Babonneau F, González-calbet JM (2005) Solid State Sci 7:233–237

63. Yan X, Yu C, Zhou X, Tang J, Zhao D (2004) Angew Chem Int Ed 43:5980–5984
64. Grosu G, Andrzejewski L, Veilleux G, Ross GG (2004) J Phys D Appl Phys 37:3350–3355
65. Lai Y, Tang Y, Gong J, Chi L, Lin C, Chen Z (2012) J Mater Chem 22:7420–7426
66. Xiao M, Guo X, Cheng M, Ju G, Zhang Y, Shi F (2014) Small 10:859–865
67. Hu J, Meng H, Li G, Ibekwe SI (2012) Smart Mater Struct 21:053001

Chapter 3
Electroactive Polymers and Coatings

Lisa C. du Toit, Pradeep Kumar, Yahya E. Choonara, and Viness Pillay

Abstract Electroactive polymers (EAPs) and coatings (EACs) provide an expanding and progressive frontier for responsive drug delivery and the design of biomedical devices. EAPs possess the distinctive propensity to undergo a change in shape and/or size following electrical current activation. Current interest in EAPs and EACs extends to use in controlled drug delivery applications, where an "on-off" mechanism for drug releases would be optimal, as well as application in a biomedical devices and implants. This chapter explores and molecularly characterizes various EAPs such as polyaniline, polypyrrole, polythiophene, and polyethylene, which can ultimately be incorporated into responsive hydrogels in conjunction with, for example, a desired bioactive, to obtain a stimulus-controlled bioactive release system, which can be actuated by the patient, for enhanced specificity. The institution of hybrids of conducting polymers and hydrogels has also been subjected to increasing investigation as soft EACs, which have been applied, for example, in the improvement of the mechanical and electrical performance of metallic implant electrodes. The various interconnected aspects of EAP-based systems, including their synthesis, proposed *modus operandi*, physical properties, as well as functionalization approaches for enhancing the performance of these systems, are delineated. The use and comparison of these EAPs and EACs alone, and in conjunction with hydrogels, is further elaborated, together with strategies for integrating electroactive components and hydrogels. Approaches for modeling and explaining the proposed *modus operandi* of these systems are delineated. A critical review of diverse biomedical systems implementing EAPs and EACs having application in the pharmaceutical and medical industry, specifically, is provided, highlighting their applications, potential advantages, and possible limitations. Ultimately, this chapter illuminates innovative approaches for enabling EAP- and EAC-based systems to attain their full clinical potential.

L.C. du Toit • P. Kumar • Y.E. Choonara • V. Pillay (✉)
Wits Advanced Drug Delivery Platform Research Unit, Department of Pharmacy and Pharmacology, School of Therapeutic Sciences, Faculty of Health Sciences, University of the Witwatersrand, Johannesburg, 7 York Road, Parktown 2193, South Africa
e-mail: viness.pillay@wits.ac.za

Keywords Electroactive polymers • Electroactive coatings • Hydrogels • Poly-electrolytes • Dopant • Drug delivery systems • Biomedical devices • Stimulus responsive

3.1   Introduction

Electroactive polymers (EAPs) have been ushered in as a novel generation of intelligent biomaterials enabling direct delivery of electrical, electrochemical, and electromechanical stimulation to cells [1]. EAPs, in some definitions, have been referred to as artificial muscles due to the similarity in functional response, as well as potential to mimic the mechanical performance, of biological muscles. Essentially, they are polymeric materials with the intrinsic ability to change their shape or size following electrical current activation. Actuation via the use of electrical energy is an attractive activation method for causing elastic deformation in polymers, and it offers great convenience and practicality.

More and more, nature provides biologically inspired adaptations in designed biomedical devices and delivery systems. There is a diversity of polymers that have the potential to undergo a change in size or shape in the presence of stimuli, including temperature, light, chemical, magnetic, pneumatic, magnetic, and electrical. The attraction of electrical activation for causing polymeric deformation lies in its convenience and practicality [2, 3].

The reported history of polymers possessing electrically stimulated behavior has extended over more than 100 years, but this fact has received little attention possibly due to the comparatively small response to the stimulus, until recently. In the passing two decades, polymer scientists have achieved the synthesis of EAPs and electroactive coatings (EACs) that have demonstrated more notable elastic deformations and ultimately shape and size changes. These materials have attracted multidisciplinary interests and have had exciting applications as, for example, robotic fish, artificial eyelids, and catheter steering elements [3]. EAPs and EACs provide an expanding and progressive frontier for responsive, controlled drug delivery, where an "on-off" mechanism for drug releases would be optimal, as well as application in biomedical devices and implants.

Encompassed within the family of EAPs are conductive polymers, electrets, and piezoelectric and photovoltaic materials [3]. Electrets and piezoelectric materials enable electrical stimulus delivery in the absence of an external power source; however, stimulus control is limited. Conversely, conductive polymers enable good electrical stimulus control, good electrical and optical properties, and a favorable conductivity/weight ratio and can be rendered biocompatible, biodegradable, and porous [4]. Specific modification of the chemical, physical, and electrical properties of conductive polymers is also possible via incorporation of enzymes, antibodies, or other biological moieties, for particular applications, which are also alterable following exposure to stimuli [1, 5].

Table 3.1 Diverse electroactive polymer systems and abbreviations [1, 9, 10]

EAP system	Abbreviation
Polypyrrole	PPy
Polyaniline	PANI
Poly(3,4-ethylenedioxythiophene)	PEDT, PEDOT
Polythiophene	PTh
Polythiophene-vinylene	PTh-V
Poly(2,5-thienylenevinylene)	PTV
Poly(3-alkylthiophene)	PAT
Poly(*p*-phenylene)	PPP
Poly(*p*-phenylene sulfide)	PPS
Poly(*p*-phenylenevinylene)	PPV
Poly(*p*-phenylene-terephthalamide)	PPTA
Polyacetylene	PAc
Poly(isothianaphthene)	PITN
Poly(α-naphthylamine)	PNA
Polyazulene	PAZ
Polyfuran	PFu
Polyisoprene	PIP
Polybutadiene	PBD
Poly(3-octylthiophene-3-methylthiophene)	POTMT
Poly(*p*-phenylene-terephthalamide)	PPTA

Since their inception, more than 25 EAP systems have been reported (Table 3.1), possessing the combined attributes of metals (charge conduction, good electrical and optical properties) and polymers (processing flexibility and ease of synthesis) [6]. The initial "discovery" of conductive polymers was with the observation that the conductivity of polyacetylene (a fairly semiconducting polymer) could have its conductivity increased 10 millionfold upon oxidation via iodine vapor [7]. This also introduced the phenomenon of "doping," the process through which conductivity is introduced to polymers. It ignited the search for more EAPs, such as the polyhetero-cycles, which include polypyrrole, polyaniline, and polythiophenes. These examples possess an enhanced stability compared to polyacetylene and good conductance as well [8].

This chapter provides an in-depth discussion on the principles and applications of EAPs, EACs, and their composites while building on concepts introduced in the review of Pillay and co-workers [11]. The use and comparison of these EAPs and EACs alone, and in conjunction with hydrogels, is further elaborated, together with strategies for integrating electroactive components and hydrogels. The various interconnected aspects of EAP-based systems, depicted in Fig. 3.1, including their synthesis, proposed mechanism of operation, physical properties, as well as functionalization approaches for enhancing the performance of these systems, are delineated. A critical review of diverse biomedical systems implementing EAPs and EACs while having application in the pharmaceutical and medical industry, specifically, is provided, highlighting their applications, potential advantages, and possible limitations. Ultimately, this chapter illuminates innovative approaches for enabling EAP- and EAC-based systems to attain their full clinical potential.
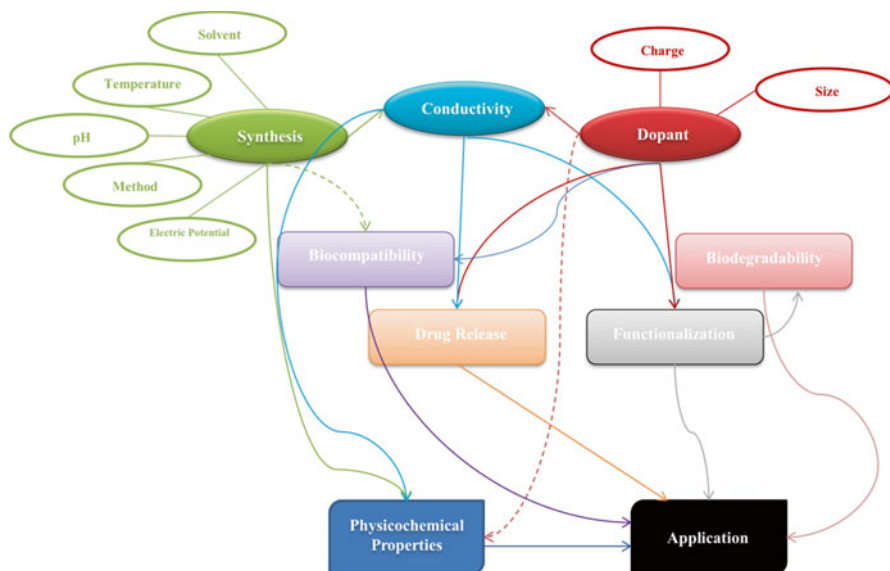
Fig 3.1 Schematic demonstrating the interconnectivity of the various aspects of EAPs. Adapted from Balint et al. [1]

3.2 Classification of Electroactive Polymers

Roentgen essentially made the seminal report of EAP materials in 1880 [12]. This was by subjecting a rubber band (having a fixed end and a mass attached to the free end) to an electric field. This was followed by Eguchi's discovery and description of electrets in 1925. These are dielectric materials possessing a quasi-permanent electric charge or dipole polarization. In 1969, Kawai described the piezoelectricity of polyvinylidene fluoride (PVDF). EAPs and coatings can be categorized as ionic and electronic (or field activated) [3]:

(a) Ionic EAPs

These include conjugated polymers. Actuators are comprised of an electrolytic polymer film with a 2-electrode coating with activation implicating ion mobility due to electrical excitation [13]. Their advantages include generation of large bending displacement following low-voltage activation; however, there is the maintenance requirement of electrolyte wetness, low efficiency of energy conversion, and limited ability to sustain constant displacement via direct current (DC) voltage activation (except for conducting polymers) [14]. Examples of ionic EAP materials include the ionomeric polymer-metal composites (IPMCs), conducting polymers, carbon nanotubes, and ionic polymer gels. IPMCs are the most widely investigated EAPs in this group, with the base polymer enabling movement of positive ions through its channels of interconnected clusters of fixed network negative ions [13]. Pertinently, IPMCs undergo significant bending in response to a fairly low electrical voltage (1 V); however, the response frequency is slow (<10 Hz) [3].

(b) Electronic (field-activated) EAPs

These include piezoelectric polymers, electrorestrictive polymers, nonionic gels, and dielectric elastomers. Activation is via Coulomb force instigating an alteration in dimension, which may be a result of either direct thickness reduction, seen, for example, in dielectric elastomers, or internal polarization with molecular alignment noted in ferroelectric EAP [15]. A high electric field (>10-V/μm) is commonly required, which can approach the electric breakdown level due to the low dielectric constant. The voltage required can be reduced by employing thin multilayers as a stack and creating a composite incorporating high dielectric constant filler material. This group of EAPs possess a fast response time, maintaining the generated displacement under DC voltage, as well as greater mechanical energy density. The requirement of a high activation field potentially close to electric breakdown level is their main disadvantage [3].

Compared to conducting polymers, redox polymers possess redox sites, with electrostatic or covalent bonds to the polymer, and electronic and spatial localization [16], whereas conducting polymers exhibit delocalization of electronic states [17]. Depending on the synthetic reaction for the polymerization process, the EAP may be an addition or condensation polymer, and this reaction is implicit in defining the electrical properties of the synthesized EAP [18]. A more recently arising novel technique is for the formation of modified EAPs, where the polymer possesses distinct properties from the monomers, is electropolymerization, undertaken on the surface of electrodes [19]. Herein, however, lies its drawback, as the yield from the electropolymerization at the electrode surface is too low for industrial application [20–23].

3.3 The Mechanism of Operation and Conductivity Source of Electroactive Polymers

When an electric charge is applied to an EAP with sufficient mobility, there is charge redistribution within the polymer, with the response either being a change in dielectric properties (either (a) dielectric properties which represent polarization or (b) tangent of dielectric loss angle representing relaxation phenomena) or bulk conductive properties (either (a) dielectric strength representing breakdown phenomena or (b) conductivity representing electric conduction). Additional distinct EAP properties encompass piezoelectric, pyroelectric, ferroelectric, triboelectric, photovoltaic, and photoconductive properties [24].

Charge conduction in EAPs is due to the ease of electron jumping between the polymeric chains on oxidation or reduction of the EAP. This is due to a combination of factors. Within the conjugated polymer backbone, the series of alternating single and double bonds provides both localized σ-bonds, which are chemically strong, and less strongly localized π-bonds, respectively [25, 26] (Fig. 3.2). Overlapping of the p-orbitals of consecutive π-bonds enables easy delocalization and thus free movement of electrons between atoms. As the polymer must be synthesized in its conducting form (i.e., oxidized), a dopant molecule, generally an anion, is essential
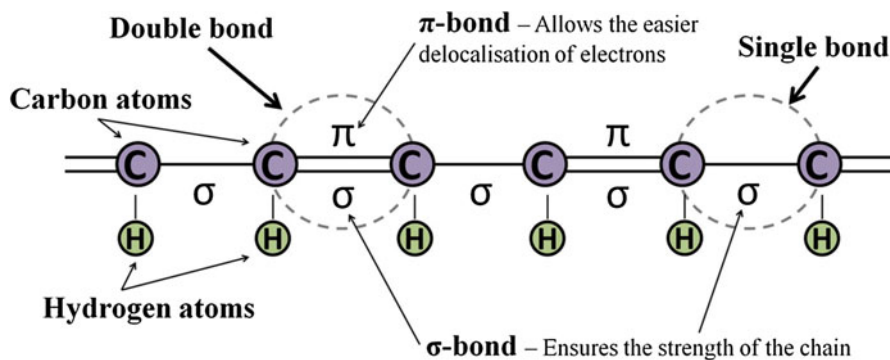
Fig 3.2 Depiction of a conjugated backbone indicating alternating single and double bonds.
Source: Balint et al. [1]
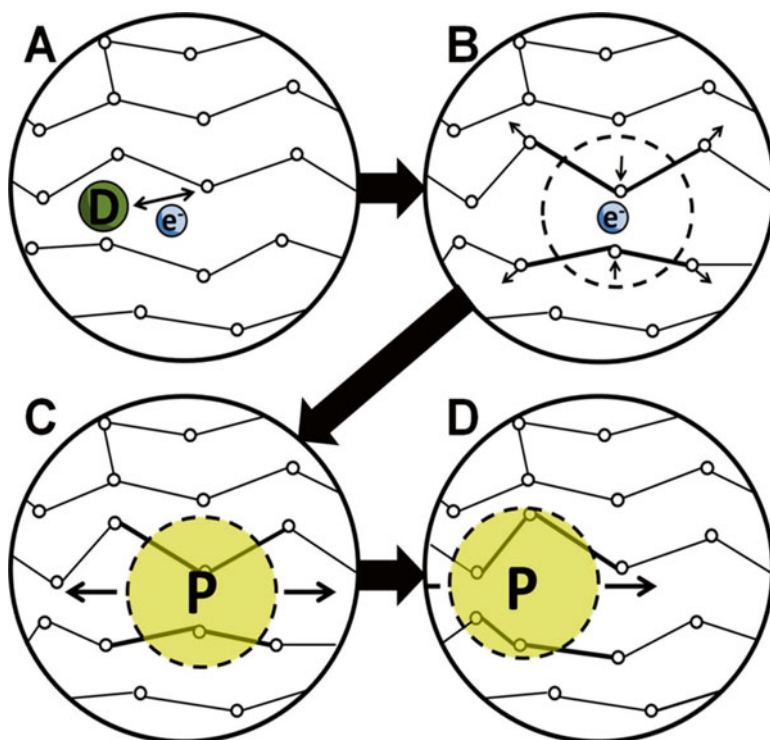
Fig 3.3 Schematic illustrating the electrical conductivity of conducting polymers. (**a**) The dopant removes or adds an electron from/to the polymer chain, creating a delocalized charge. (**b**) Charge localization is energetically favorable and the charge is surrounded by a local distortion of the crystal lattice. (**c**) This distortion-engulfed charge is a polaron (a radical ion and the associated lattice distortion). (**d**) Conduction of electricity is due to the polaron movement along the polymer chain. Source: Balint et al. [1]

for charge neutralization and backbone stabilization. Simultaneously, the dopant brings a charge carrier into the system through introduction or removal of electrons into or from the polymer chains, causing their relocalization as polarons or bipolarons (loosely held yet localized electrons enclosed within a crystal lattice distortion) (Fig. 3.3). The application of an electrical potential causes movement of dopant into or out of the EAP, causing polymer backbone disruption, thus enabling the charge to pass through the polymer as the polarons or bipolarons [1, 25, 26].

In polypyrrole (PPy), the bipolaron (*p*-type) conduction creates conductivity, with electron hopping and anion and cation movement [6]. The overall conductivity of the EAP depends on the polaron, charge transfer to adjacent molecules, and length of conjugation, which can be varied in accordance with the dopant type and quantity. Conductivity may be limited by defect sites in the EAP backbone, potentially due to exposure to water or oxygen or redox switching [27].

The diffusion coefficient is employed to describe this rate of oxidation or reduction within the EAP and is an indication of the charge percolation efficiency through the polymer, as measured via cyclic voltammetry (CV) or chronoamperometry (CA) [28]. In addition, the type of EAP used also affects the response time. A rapid response time of milliseconds is demonstrated by electronic-based EAPs, but with the requirement of a high actuation voltage. On the other hand, ionic-based EAPs respond more slowly, but at a lower actuation voltage [29].

3.4   Creating an Electroactive Polymer: The Process and Considerations

Certain EAPs have been the focus of intensive investigation as responsive platforms including PANi [30], polythiophene (PTh), and PPy [31]. The advantages, limitations, and various modifications for potential improvement of these commonly employed EAPs are provided in Table 3.2. The versatility of PANi and its derivatives is due to their potential for processing into various redox states and possession of tunable conductivity and stability. The applications of PANi include dental uses (maxillofacial surgery and dental implants), antistatic applications, gas sensors, and artificial muscle design [32–37].

The behavior of EAPs can be tailored via doping with various counterions. This has enabled, for example, the mimicry of basic insect and animal movements by investigators in the field of biomimetics. There has been a shift in focus on EAPs as their actuation ability improves, as well as the availability of a wider selection of biomaterials [11]. However, this brings concerns with regard to the biocompatibility of these new materials [57]. A study specifically assessing the biocompatibility of PANi conjugates investigated the subcutaneous implantation of ethylene vinyl acetate (EVA) copolymer (PE) and PANi (emeraldine, nigraniline, and leucoemeraldine states) in Sprague-Dawley rats over a period of 19–90 weeks with subsequent histological evaluation. No carcinogenic effects were observed on rat tissues, even after the extended periods of time, highlighting adequate biocompatibility [58, 59]. The

Table 3.2 Summary of the advantages and limitations of leading EAPs. Adapted from Pillay et al. [11]

EAP	Differentiating properties and advantages	Challenges	Strategies to improve EAP	References
Polyaniline	Good air and moisture stability High electrical conductivity Unique redox properties	Harsh synthetic conditions Not easily processed Limited organic solvent solubility	Combine with other monomers during polymerization—PANi copolymer Synthesis of water solubility through normal or electropolymerization with a water-soluble analogue or aniline monomer—increase processability Synthesis as a film via casting or composite polymer preparation to improve mechanical properties Employment of newer oxidation agents (e.g., benzoyl peroxide) enables better temperature control during polymerization	[31, 38–47]
Polypyrrole	Similar structure therefore similar advantages to PANi Three oxidation states (two oxidized, one unoxidized) High conductivity with polarons and bipolarons playing a pertinent role Dopant has notable effect on conductivity Multivalent anions increase cross-linking intensity High conductivity and high thermal and environmental stability PPy with enhanced processability can be applied in drug delivery system design, biomimetics, and robotics	Processing is difficult—poor solubility in most solvents	Methods researched for improving solubility: – Dissolution of PPy in an organic solvent in the presence of surfactant (however solubility still limited in polar solvents) – Synthesis of PPy from modified monomers of pyrrole obtaining PPy via counterion processability, e.g., oxidative polymerization in the presence of polyacrylic acid or polyvinyl pyrrolidone – Synthesis of PPy as a self-doped copolymer containing a high level of sulfonic moieties acting as a PPy dopant Improving solubility enhances processability of PPy	[48–52]

Polythiophene	Considerable conductivity Synthesized from thiophene monomer (sulfur heterocyclic structure) vs. imine groups in PANi or PPy Doping forms bipolarons on backbone—act as charge carriers for electrical conduction Unique optical properties and electroactivity application in light-emitting diodes, electrochromic devices, field-effect transistors, recording materials Good environmental and thermal stability Easy to fabricate with good processability and mechanical strength Broad applications and can be tailored to individual requirements	Alkyl-substituted PTh lack flexibility—rigid backbone	Solubility in common organic solvent improved by further modification with alkyl or alkoxy chains—alkyl side chain furnishes solubility in most organic solvents in both doped and undoped form	[53–56]

biocompatibility of the EAP PPy has also been demonstrated in humans, as well as its controllable physicomechanical behavior and chemically or electrochemically enabled synthesis.

The mechanism of polymerization of PPy is followed by most EAPs, with the polymerization commencing via oxidation of the pyrrole monomer (Fig. 3.4). The counterion employed in its synthesis is C-, with its negative charge enabling incorporation into the polymer, which is in equilibrium with the polymer backbone's positive charge [60]. As highlighted in Fig. 3.4a, incorporation of diverse counterions during the polymerization process is enabled, allowing for alteration of the overall physicomechanical properties. The use of a combination of counterions is also possible for achieving the desired degree of conductivity and physical attributes [61].

Zhao and co-workers [62] indicated that the transport mechanism within the EAP is controlled by the counterions, most notably, the anions. Following the application of sufficient negative potential, outward anion diffusion occurs and the reaction is reduced. Application of a repetitive pulsed potential waveform to the membrane maintains transport through it. Incorporation of counterions into a polymeric membrane can be achieved through electropolymerization; however, if they are trapped during this process, immobility is a potential concern. Sulfonated aromatic groups have proved suitable [62]. Following expulsion of an anion from the polymeric system, reincorporation is achieved via repetitive pulsed potential waveform; furthermore, if the anion-loaded polymer is placed in a cationic electrolyte solution, these may also be assimilated into the polymeric system. Three criteria must be satisfied for efficacy of this electroactive transport mechanism: (1) a transport system with a rapid on-off switching mechanism, (2) controllable flux and sustainable transport within the polymeric system, and (3) controlled selectivity.

3.4.1   The Electropolymerization Process

Electropolymerization is a specific method originated for the formation of EAPs. Being a more stable approach than chemical synthesis of an EAP, it also yields EAPs with less variation in molecular mass as a result of the exothermic reaction during chemical oxidation of the monomer, with temperature fluctuations impacting the polymer chain length [63]. The process implicates dissolution of the monomer in an appropriate solvent together with a selected anionic doping salt; this is followed by oxidation of the monomer at the anode. Oxidation furnishes free cationic radicals of the monomer, which interact to form oligomers and subsequently the EAP [64]. Factors influencing the elaborate electropolymerization process include the degree of monomeric substitution, choice of electrolyte and solvent, solvent and aqueous medium pH, and the electrochemical method employed [65]. Bearing these factors in mind, there lies the potential for synthesis of a novel synthetic approach or polymer with desirable attributes. Current intensity is influenced by the electrolyte employed, which ultimately affects the EAP quantity formed [65]. Solvents possess
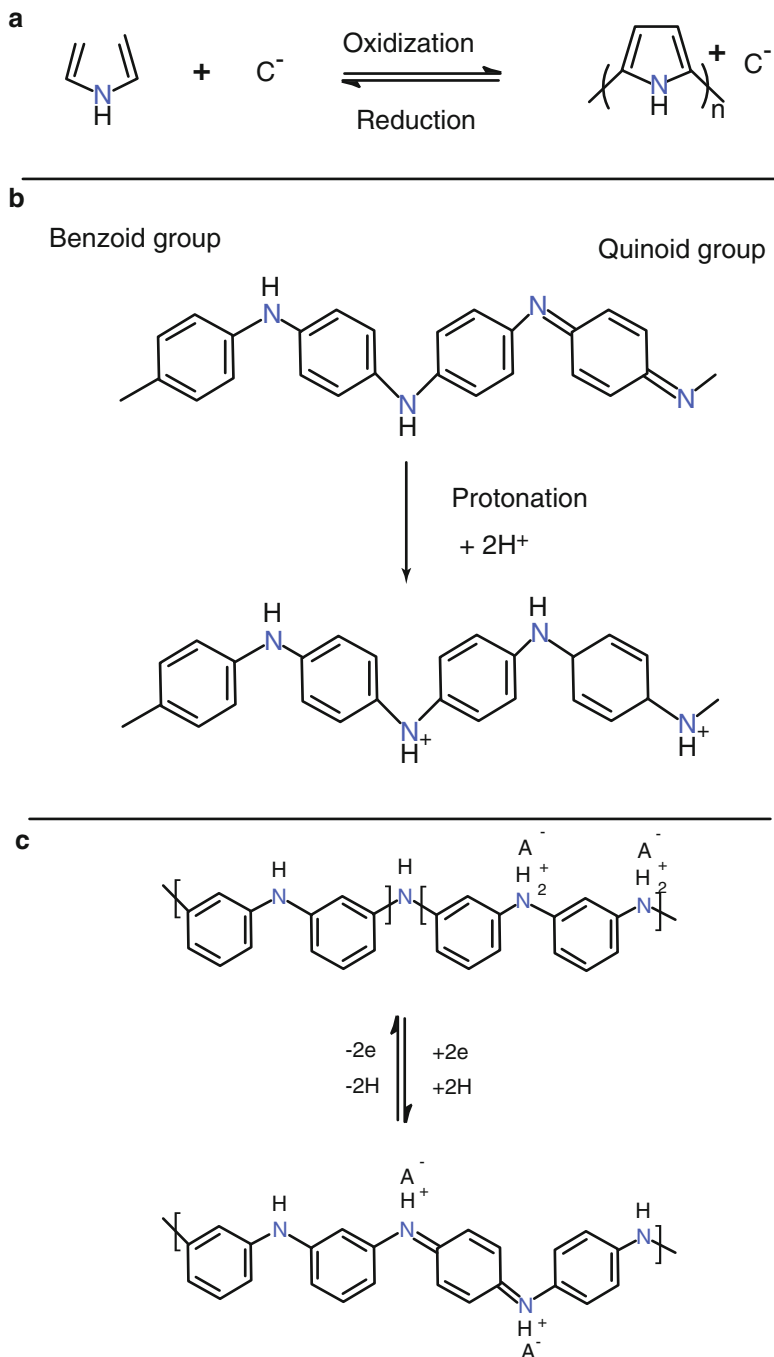
Fig 3.4 Schematic depicting: (**a**) Polypyrrole (PPy) chemical synthesis. (**b**) Polymer protonation via protonic acid (acid counterions are not illustrated). (**c**) Mechanism of an oxidation reaction of PANi (downward arrow represents the oxidation reaction). Source: Pillay et al. [11]

various donor numbers influencing cationic monomer radical deprotonation, as well as possessing varying dielectric constants, influencing chain propagation [66]. Solvent choice further depends on it providing a medium with ionic conductivity and on its stability at the monomer's oxidation potential [64]. Solvent pH is important due to its effect on monomer solubility (via chemical reaction) and on the polymer's physical attributes [e.g., aniline undergoes polymerization under acidic conditions as a result of PANi protonation, resulting in enhanced conductivity (doping effect)] [67, 68]. Monomers need to dissolve in the solvent for electropolymerization to ensue. Inert materials (e.g., gold, platinum, or glass-like carbon) commonly comprise the anode employed for the polymerization reaction; partially reactive materials may dissolve with polarization of the anode [69, 70]. The physicochemical properties of the synthesized EAP are implicitly based on the electropolymerization method instituted, but generally this approach imparts EAPs with comparable conductivity, for application in research and system design [11].

3.4.2   The Doping Process

The overall goal in EAP synthesis is attainment of the required conductive, mechanical, and sometimes optical properties. Doping implicates introduction of a chemical agent for direct interaction with the polymer chain and has a pertinent impact of the physicomechanical attributes of the EAP. Figure 3.1b demonstrates this; there is protonization of nitrogen atom of the quinoid group in PANi by protonic acid [71]. Commonly, doping is performed with EAP in the base form which is then combined with an acid; the protonated EAP has increased conductivity, due to the protonated imine nitrogen emanating in increased polarons in EAPs (i.e., PANi and PPy) [72]. The preferential synthesis of PANi is thus in an acidic environment, as discussed previously [72]. However, these conditions may be considered harsh and undesirable, possibly necessitating the addition of other solutions to the acid. Mirmohseni and Wallace [73] synthesized PANi films adding doping agents to an acetone: 1M HCl solution, with immersion of the PANi in this solution for 24 h enabling sufficient doping, followed by vacuum drying. Transition metals (e.g., $NiCl_2$, $EuCl_3$, and $ZnCl_2$) represent more progressive doping agents compared to conventional protonic acids where only a dopant change is induced on the polymer, whereas transition metals also elicit a dual effect causing a change in morphology as well [71].

The preparation of EAPs via emulsion polymerization enables the generation of a conducting salt in the absence of a postdoping processing step with acid [74], as investigated by Kinlen and co-workers [75]. They demonstrated the polymerization of PANi salts of hydrophobic acids (e.g., dinonylnaphthalene) in an organic solvent (2-butoxyethanol).

3.5 Redox Reactions in Electroactive Polymers

3.5.1 Conductivity of EAPs via Redox Reactions

The responsiveness of EAPs is intrinsic to their potential for undergoing oxidation and reduction reversibly. The transport of ions through the EAP and subsequent controlled movement of ions from the EAP conducting film is described via redox reactions. Examining PANi as an example of a conducting polymer, the amine groups serve as its redox centers, undergoing oxidation to imine groups; subsequent to oxidative, there is some level of conductivity. PT and PPy may be similarly classified [76]. The site of occurrence of the redox reaction is commonly at the interface of the film and solution, as here there is the potential for the reaction of dissolved ions with the conducting polymer. The steps implicit to the redox switching of an EAP are (noted in Fig. 3.4c for PANi):

1. Change in conformation
2. Solvent molecule entry or exit, potentially altering the swelling state
3. Conformational change of EAP-bound ions
4. EAP electroneutrality balance via ion ejection or injection

3.5.2 Evaluation of Redox Reactions in EAPs

An EAP's redox potential has pertinent influence on the extent of swelling/deswelling and electroactivity of the polymer. Assessment of the redox reaction of the EAP via the following techniques enables prediction of EAP electroactivity:

1. Linear sweep voltammetry (LSV)—measurement of the current at the working electrode relative to a potential range (i.e., EAP voltammetric response). Peaks and troughs in the generated voltammogram represent oxidation or reduction within the EAP. LSV is also employed for quantification of ions in a sample [77, 78]. Cyclic voltammetry has largely replaced this technique as it provides more data.
2. Cyclic voltammetry (CV)—an extension of LSV where there is an inversion of the working electrode potential on attainment of the end potential and provides a potentiodynamic electrochemical measurement [79]. It enables determination of an analyte in solution [79], as well as the surveillance of oxidation and reduction behavior of the EAP. A cyclic voltammogram plot is generated of the current accumulated at the working probe versus the applied potential difference. The potential is linearly increased in CV, and as it approaches the oxidation potential of the analyte, there is an increase in the current, which ultimately falls as the analyte concentration at the electrode decreases on oxidation. The shortcomings of CV are its low structural resolution; however, it is still a popular redox reaction-determining tool.

3. Impedance spectroscopy (IS)—a nondestructive approach importantly employed for the characterization of the intrinsic electrical properties of a polymer, such as conductivity, dielectric coefficient, static properties (at the interface), and dynamic changes resulting from charge transfer. Its application even extends to the assessment of body makeup, specifically in overweight individuals [80]. IS is employed for gaining information on the kinetics and electrochemical reactions of EAPs and confirmation of a model for diffusion of ions in and out of an EAP in solvent or diffusion of counterions or electrons at the EAP/solvent interface [81, 82]. Disadvantages of this technique are difficulty of data interpretation and that it is essentially a complementary approach.

4. Chronoamperometry (CA)—in this technique, there is maintenance of the potential for a period, followed by stepping up, thus creating a faradic process with the resultant current (resulting from oxidation or reduction) recorded. For analysis, the EAP is applied as a thin-film coating to the electrode. A limitation is that the alternating current can affect the results recorded. The employment of CA is important where determination of the migration flux of charged particles in EAPs is required through analysis in a constant electric field of the concentration distribution and current-time plots of a polymer film [11]. With regard to conductive EAPs, they can be applied in CA as sensors enabling detection of simple and complex electroactive or nonactive substances [83].

3.6 Creating Composites of Smart Hydrogels and Electroactive Polymers

The composition of hydrogels as three-dimensional interconnected hydrophilic networks is well known. They absorb water and swell, retaining their structure due to the presence of cross-links, entanglement, or crystallinity [84]. In their native form, they lack an inherently electroresponsive nature; however, the incorporation of EAPs enables their responsivity in the presence of electrical stimuli [85, 86]. The application of electroresponsive hydrogels is diverse as actuators, separation devices, and responsive, sometimes miniaturized, delivery systems [87–90]. Such hydrogels may also be classified as "intelligent" or "smart" where responsivity to more than one stimulus, including electrical, is present [91–95]. The limitations of EAPs have been discussed, when used in isolation (e.g., the poor solubility and mechanical properties of PANi and PPy). Approaches to addressing these challenges and enhancing the physicomechanical and physicochemical attributes of the EAP include creating an EAP-biomaterial blend with an insulating biomaterial, electrochemical, or chemical oxidative polymerization of the EAP into a polymeric matrix or formulation via codeposition of a composite EAP-insulating polymer [96]. Hydrogels commonly exhibit stimulus-responsive behavior as a conformational change, which could be catalysis, actuation, signaling, movement, or an interaction [97]. The stimuli in question are diverse and include temperature, pH, electric fields, light/UV, chemicals, magnetic fields antigens, etc. [98].

Drug delivery approaches have been developed employing an EAP which has been integrated within the polymeric membrane [99]. As indicated, there is inward and outward movement of counterions when an electrical current is initiated. In certain EAPs (PPy and PANi), a high cation flux occurs upon oxidation. This has been applied, for example, to glutamate and ATP, which have been electrostatically charged to attain their controlled release [100, 101].

As indicated, transport of ions is also enabled during redox reaction switching via changes in conformation, which includes swelling, deswelling, or shape change (i.e., a shape-memory effect, thus embodying the action of an artificial muscle) [102]. This slow relaxation with shape change is exhibited by EAPs such as PANi and those falling within its group. This relaxation effect is absent in certain EAPs [e.g., poly(o-aminophenol), poly(o-phenylenediamine), and poly(benzidine)] [103]. In studies by Silk and Tamm [104] on halogenide-doped PPy films, they reported the effect of cations on this redox switching process in terms of relaxation times.

Hydrogel performance can be enhanced through the inclusion of acidic or basic groups into the structure to create a polyelectrolyte (the solid matrix network, ionic species, and fluid component). Popular polyelectrolyte hydrogels employed include polyacrylic acid (PAA) as sodium and potassium salts [105–108]. Investigators have employed the sodium salt of hyaluronic acid hydrogels, demonstrating its reduction in volume at the anode with consequent drug release [109]. It follows that drug release from hydrogel networks is affected by the monomeric composition, swelling degree, and cross-linking density, which ultimately impact the porosity and network structure. The presence of ionizable groups in the hydrogel elicits chemical and physical changes in the structure, thus enabling drug release [110]. Electrical stimulation of a responsive polyelectrolyte causes drug migration to the oppositely charged electrode, and contraction of the hydrogel, emanating in drug expulsion [111]. This drug movement is represented in Fig. 3.5.

3.6.1 Responsive Hydrogels: Electrocompatible Preparation Approaches

The versatility of hydrogels and their potential application in an electroresponsive system has been introduced [112]. An increase in the degree of cross-linking of the hydrogel enhances the architectural integrity, lowering the amount of water imbibed and thus decreasing the degree of swelling [113, 114]. Hydrogel synthesis may be via blending, copolymerization, grafting, or formation of an interpenetrating polymer network or composite. Blending implicates interaction between two or more agents, for example, through esterification between hydroxyl group of polyvinyl alcohol (PVA) and the carboxyl group of gelatin [115]. Copolymerization occurs via reaction of two monomers. Grafting is similar to copolymerization, except that the polymer employed for hydrogel formation is a graft copolymer (a branched polymer where the main chain and side chain differ) possessing the combined properties of both polymers [111, 116].
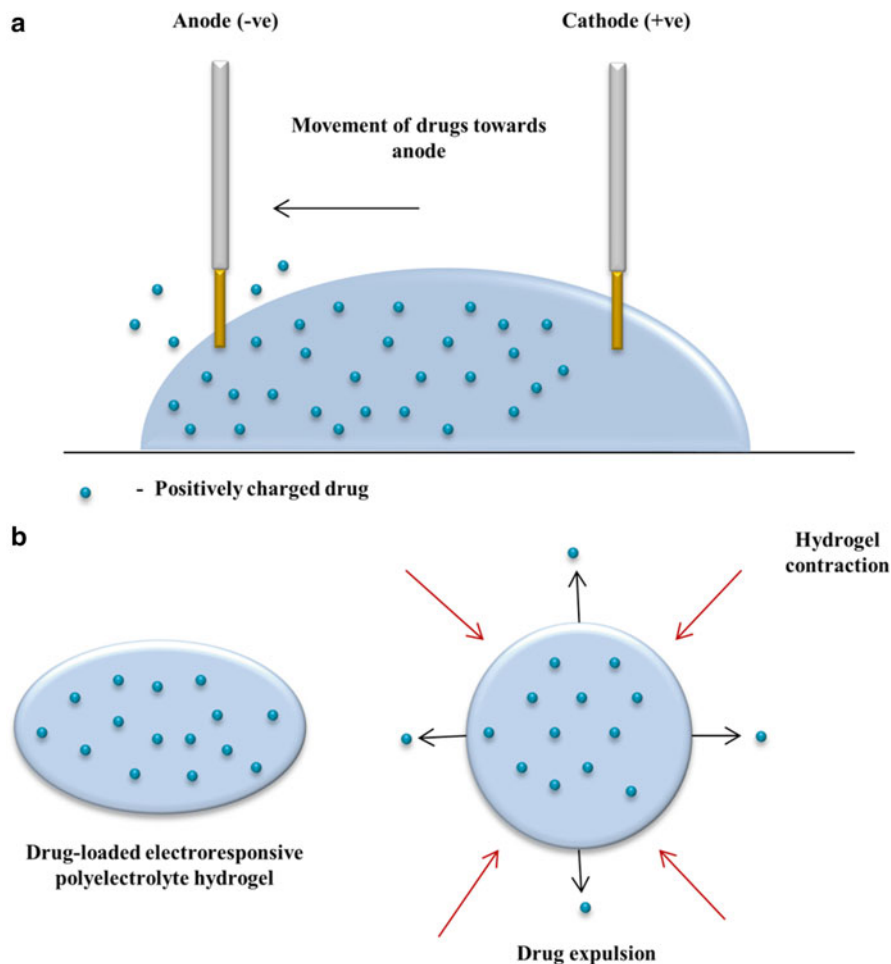
Fig 3.5 Schematic depicting: (**a**) Positively charged drug particle migration toward the negatively charged anode. (**b**) Contraction of the hydrogel with forced drug exudation from the system. Adapted from Pillay et al. [11]

With regard to interpenetrating polymer networks (IPNs), the hydrogel network incorporates a network of a component, where there is polymerization or cross-linking of at least one component in the presence of another. Thus, there can be incorporation of an EAP into a hydrogel to create an IPN, thereby potentially increasing the electrical stimulation conductivity into the hydrogel and the ultimate electroresponsiveness [117, 118].

Formation of a composite hydrogel occurs by embedding a particle into a hydrogel network, where the particle does not interact directly with the hydrogel [119]. All these approaches may be instituted in the synthesis of an electroresponsive hydrogel system, with selection based on swellability, structural integrity, and response required.

3.7   Electroactive Polymer Functionalization for Specific Applications

Various approaches exist for the functionalization of EAPs for the binding of bioactives and optimization of the properties of the device or delivery system (i.e., porosity, hydrophobicity, degradability, conductivity), as represented in Fig. 3.6. This ultimately enhances their potential for numerous biomedical applications. Entrapment and absorption techniques do not involve chemical reactions that could affect bioactive activity and are thus commonly employed for biosensor applications [120].

1. Absorption—The EAP is introduced to a solution of the functionalizing agent, enabling its physical adsorption to the polymer matrix via static interactions between the molecule's charge and the polymer matrix. This is a simple approach; however, it exhibits sensitivity to pH, and outward leaching of the bioactive can occur [121]. Examples include the physical adsorption binding of calf thymus DNA to PPy as a toxicant biosensor [122].
2. Entrapment—The functionalizing molecule, the monomer of the polymer, the dopant, and the solvent are mixed prior to synthesis. Incorporation of the functionalizing agent molecules close to the electrode into the polymeric chain occurs
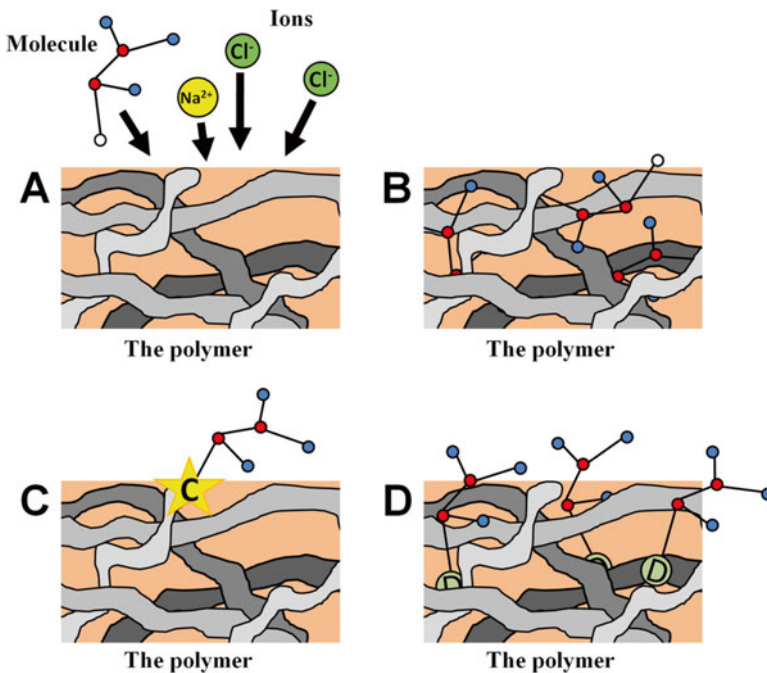

Fig 3.6 Approaches to functionalizing EAPs: (**a**) physical absorption, (**b**) entrapping, (**c**) covalent bonding, and (**d**) exploiting the doping mechanism. Source: Balint et al. [1]

during electrochemical polymerization. Application of this method to the binding of large molecules, such as DNA and enzymes, is common, as their size generally inhibits their escape upon entrapment [120]. Entrapment has been employed, for example, for the binding of glucose oxidase for formation of glucose sensors [123]. DNA has been bound for the detection of aromatic amines, cDNA, and Hep C virus [124].

3. Covalent bonding—The molecule is covalently bound strongly to the monomer of the polymer the long-term stability of the polymer is enhanced. There is the possibility of a reduction in the EAP's conductivity. An example is the covalent binding of cysteines via sulfide bonds to the beta-positions of PPy. Additional bioactive molecules can be anchored to the cysteines [125].
4. Exploitation of the doping process—Enables bonding of a wide range of bioactives with the prerequisite that they are charged. The binding of biomolecules such as collagen, growth factors, heparin, and chitosan has been achieved through doping; however, this is limited by the small amount of molecules that can be bound, as well as a notable reduction in the conductivity [25, 126, 127].

Diverse biological molecules of interest have also been employed to functionalize EAPs, thus enhancing their bioactivity. The following have been applied, for example, to PPy [128, 129]:

1. Dermatan sulfate to enhance keratinocyte viability
2. Heparin to promote endothelial cell proliferation
3. Laminin-derived peptide doping to improve neuron and astrocyte adhesion
4. Neural growth factor and poly-L-glutamic acid to enhance neuronal growth
5. Hyaluronic acid and chitosan to promote skeletal myoblast growth and differentiation [130]

3.8 The Diverse Applications of Electroactive Polymers and Coatings to the Pharmaceutical and Biomedical Industry: Controlled Delivery Applications

Application of responsive polymers is divided by application areas, including cardiovascular devices, ophthalmic devices, surgical devices, dental and orthopedic devices, respiratory devices, gastrointestinal devices, urogenital devices, drug delivery devices, and implantable biosensors [131].

3.8.1 EAPs in Controlled Drug Release Applications

The need for the controlled delivery of chemical compounds is a prerequisite for a number of industries, specifically the medical and pharmaceutical disciplines [5]. The institution of EAPs is an exciting avenue for overcoming the challenges in the

design of effective controllable delivery devices. The great potential of EAPs lies in the fact that upon application of a negative (reducing) potential, controlled expulsion of molecules bound through doping into EAPs is enabled [5, 132, 133]. EAP devices can be rendered porous, with delocalization of charge carriers facilitating bound molecule diffusion. Successful release of numerous therapeutic agents from EAP-based systems has been demonstrated and reported for 2-ethylhexyl phosphate, dopamine, naproxen, heparin, neural growth factor (NGF), and dexamethasone [132–137]. These and further examples are elaborated on in Fig. 3.7.

The attainment of intelligence in drug release, where the appropriate amount of drug is released at the required site at the correct time, is the main goal of pharmaceutical researchers. The design of such systems is ultimately beneficial to the patient for enhancing compliance and reducing side effects [92]. This is where EAPs as electroresponsive systems have pertinent application. EAP-based hydrogels achieve controlled release as a result of the inward and outward movement of charged particles. Models explicating the mechanism of release are minimal. Murdan [92] described three different scenarios:

1. Gel deswelling resulting in forced drug convection
2. Drug migration due to charged electrodes (drug electrophoresis)
3. EAP hydrogel erosion on electrical stimulation with the consequent release of drug

Fig 3.7 EAP- and EAC-based controlled drug delivery systems

The limitations of employing EAP-based hydrogels for drug release are that:

1. The drug must be charged to enable electrochemical movement control into and from the hydrogel [138].
2. There is difficulty in the absorption (thus resulting in relatively low drug loading), as well as release of large volumes of drug by the hydrogel [137–139].
3. There is a decreased control over drug release with continued ion exchange between the surrounding medium and drug [138].
4. Rapid drug expulsion (this could also be an advantage in some instances) [137, 139].
5. Diffusional leaching of drug with replacement by other molecules in the EAP's environment [137, 139].
6. EAP fatigue on repeated electrical stimulation due to irreversible polymeric oxidation, thus limiting EAP lifetime. Swelling and deswelling due to continual doping agent movement cause consequent polymeric degradation [5, 7].

Drug loading can be enhanced through the application of biotin-streptavidin coupling, with biotin acting as a dopant, covalently binding the bioactive, and ultimately providing release kinetics that are more uniform [139].

Zinger and Miller [100] investigated the controlled release of charged particles (the anionic neurotransmitter, glutamate) covalently bound to the polymer backbone of PPy which was coated onto a glass-like carbon electrode. Ferrocyanide was incorporated to enhance PPy conductivity. Controlled release of the drug was successfully achieved [100]. With regard to cationic drug release, Zhou et al. [140] demonstrated the anodic release of protonated dimethyl dopamine from a cationic poly(N-methyl-pyrrole)/polyanion composite. Drug release from bilayered polymers as a dual layer transport system has also been verified by Pyo and Reynolds [141]. A low redox potential inner layer (PPy and polystyrene sulfonate) was separated via insulating film from a high redox potential outer layer [either poly(N-methyl pyrrole) or poly(vinyl ferrocene) (PVFc)]. This intelligent design enabled both the release of charged particles and the reuptake of specified charged particles present in the surrounding medium.

Determination of the behavior of the EAP-based hydrogel requires the correct application of the current. There should be immersion of the hydrogel in the conducting medium, with embedding or contact of one or both electrodes with the hydrogel. Alternatively there can be direct contact of the hydrogel with the electrode in the absence of conducting media, which will ultimately result in a varied release profile compared to institution of the first method, which should be considered on selection of the optimal approach [92]. Investigation of release mechanisms has been undertaken by Kanokpom and co-workers [142], employing a cross-linked PVA hydrogel doped with sulfosalicylic acid. It was demonstrated that release of drug varied linearly with the square root of time. There was dependence of the diffusion coefficient of the hydrogel on the applied electric current and the degree of cross-linking. Institution of polyelectrolytes (water-soluble electrically charged polymers) as the main component of the hydrogel also influences drug release, potentially creating electrical, temperature, and pH-responsive hydrogels, as elaborated in the ensuing section.

3.8.2   EAP-Based Polyelectrolyte Hydrogels in the Delivery of Biologics

The movement and shape of these electrically charged water-soluble polymers are controlled by their charge, as well as by Brownian motion, resulting in either coiling or stretching. Depending on the ionizable groups present such as those that are acidic (e.g., carboxylic, phosphoric, sulfonic) or basic (amino groups), a polyelectrolyte can be classified as a polyacid, polybase, or polyampholyte [143]. The application of polyelectrolytes in the field of EAP-based bioactive delivery is of pertinence based on their structural response to pH, temperature, and electrical current alterations [144]. DNA is a polyelectrolyte, thus indicating the potential for synthesizing biocompatible polyelectrolytes [11].

The incorporation of a polyelectrolyte into a hydrogel creates the potential for swelling, collapse, or even shape change of the system when exposed to solutions of varying pH or charge [145]. Examples of electrically responsive polyelectrolytes include PAA and PVA copolymer membranes, sulfonated cross-linked polystyrene gel, acrylamide/acrylic acid copolymer with PPy/carbon black, and chitosan/carboxymethylcellulose hydrogels [146], which can display good electrical responses at various pH values. As indicated, with electrical stimulation, the kinetic motion is one of hydrogel collapse/contraction of the cationic or anionic polymer at either the anode or cathode, respectively, occurring in two areas. This is due to electrochemical processes following Faraday's law and is evident first in the area of high gel response. Thereafter there is a possibility for electro-osmotic water release in an area having a low response [145]. In addition to drug release applications, and owing to their biocompatibility and stimulus sensitivity, these EAP-based polyelectrolyte hydrogels also have shown potential as biosensors, microsurgical tools, miniature bioreactors, and for use in DNA hybridization. Polyelectrolyte multilayers may also be employed as fibers or coatings for bioactive and diagnostic agent release [147, 148]. Inoue et al. [149] evaluated the pH-responsive drug release from hydrophobic or cationic polyelectrolyte hydrogels. There were notable variances in the rate of swelling and drug release at different pHs.

Certain hydrogels and EAPs may function as stimulus-actuated systems, which are biodegradable and, when implanted at a target site, begin eroding with release of incorporated drug upon actuation [150]. Natural polymers possessing this potential include gelatin and dextran. Biodegradable EAPs may also achieve controlled release in this manner including multiblock polylactide and aniline pentamer copolymers [45], which were evaluated in rat models. Guimard and co-workers [150] fabricated 5, 5′″-bis (hydroxymethyl)-3,3′″-dimethyl-2,2′:5′,2″:5″,2′″-quaterthiophene-*co*-adipic acid polyester via incorporation of alternating electroactive quaterthiophene units and biodegradable ester units to create a macromolecular framework. Nanoscale applications of EAPs have also been investigated, with sizes of even 100 nm demonstrating electroactivity [151, 152]. A summative account of EAP-based delivery systems is provided in Fig. 3.7, highlighting the progressive potential of this field for drug delivery. Future investigations could see the application of drug-loaded EAP

systems as injectable nanorobots or nanobiosensors, with subsequent activation via electrical and other stimuli, ultimately leading to a more patient-specific treatment approach.

3.8.3 Application of EAPs in Medical Devices

Tanaka et al. [161] developed a stop valve on a microchip. First, a novel stop valve structure was conceptualized with fabrication, and subsequent measurement, of the displacement of the diaphragm in the absence of fluid. Second, the functionality of the stop valve installed on a glass microchip was demonstrated. Figure 3.8 depicts the structure and actuation principles of the stop valve. There is thinning and elongation of the EAP horizontally upon voltage application (Fig. 3.8a). The EAP is held between soft electrodes and mounted on a silicon rubber diaphragm. Elongation in the horizontal direction is inhibited in this structure; thus diagonal elongation occurs upon voltage application in order to close the penetrating hole in a chamber within a microchip (Fig. 3.8b). For valve function demonstration, a linear microchannel with a valve structure in the center of the channel was designed (Fig. 3.8c).

3.8.4 The Application of EAPs as Biomimetic Sensors: Electroactive Polymeric Sensors in Hand Prostheses

Biddiss and Chau [162] took on the task of creating a prosthetic hand incorporating EAPs, a daunting undertaking, considering the complexity of the natural human hand (17,000 tactile receptors all of which can access the sensory information generated). EAPs are a suitable choice for such prosthetics as they are diverse, lightweight, shatterproof, and pliable, with adjustable electrochemical properties, and find dual application as an actuator and as a sensor. This has allowed EAPs to be used in numerous sensory applications such as neural and haptic interfaces as well as artificial noses [163], chemical sensing systems [164], and devices for measurement of blood pressure and pulse rates [165]. Table 3.3 summarizes some of the EAPs successfully applied as biomimetic sensors [162].

For their experimental setup (Fig. 3.9), Biddiss and Chau [162] employed a gold-coated IPMC film, having an appropriate geometric fit for the metacarpophalangeal joint of a typical hand prosthesis. Their goal was characterization of the material response to quasistatic and dynamic bending embodied by the prosthetic hand. They ascertained the performance of a calibrated IPMC sensor with regard to prediction errors for various bending rates and angles. Bending was achieved by loading of the sample as a cantilever beam from angles of 0 to 90°. Fixing one end of the IPMC sample was achieved via a stationary clamp fitted with isolated electrodes for measurement of the voltage potential across the polymer, while the opposite end was fixed to a rotating platform. This was operated by a computer-controlled stepper
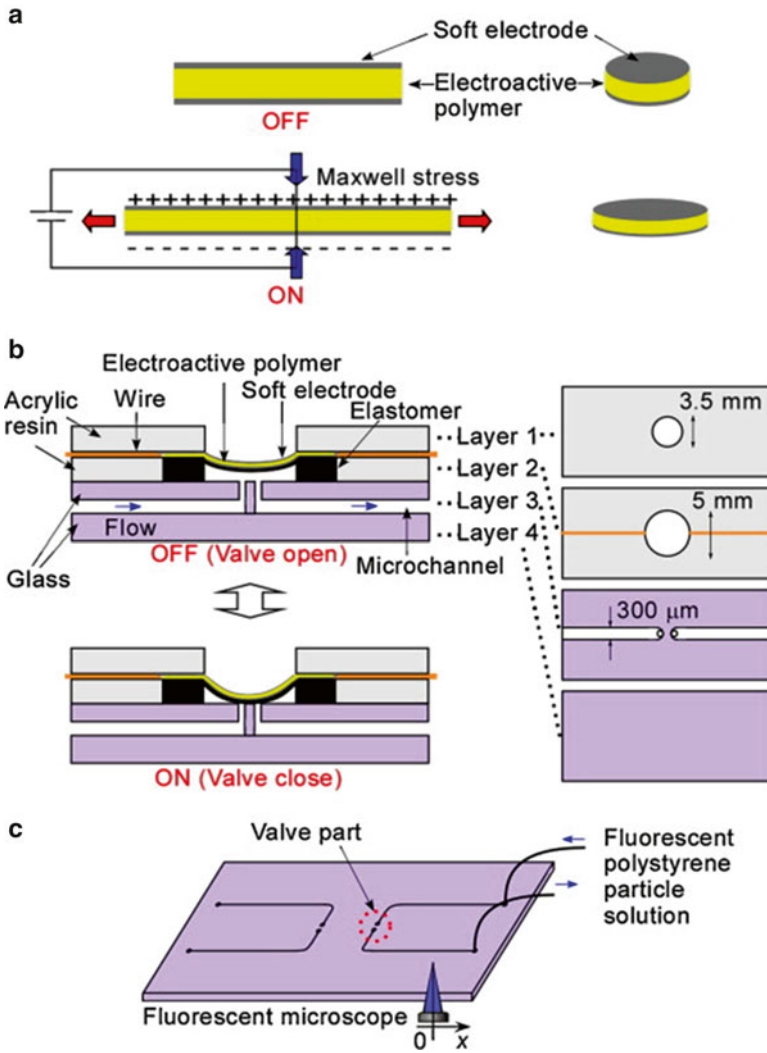
Fig 3.8 Design and mechanism of operation of a microchip with a stop valve. (**a**) Deformation of an EAP by an applied voltage. (**b**) Schematic of the stop valve. (**c**) Microchip design and observation method of the microchannel fluid flow. Source: Tanaka et al. [161]

motor working in increments of 0.9°, for reliable variation of bending angles and rates. The angle of rotation of the stepper motor shaft (bending angle) and the shaft angular velocity (bending rate) was the input. The output voltage was amplified 100 times, which was converted by a data acquisition board to a digital signal.

Biddiss and Chau [162] indicated that the application of EAP technology to biomimetic sensors is at various stages, with established systems such as conduc-

Table 3.3 EAPs as biomimetic sensors. Adapted from Biddiss and Chau [162]

Sensor	Principle of operation	Advantages	Related applications
Polypyrrole	Redox reactions instigate material property changes (e.g., volume, resistance)	Biocompatible Multiformable (into sheets, fibers, or films) Good manufacturability Electrically, mechanically, thermally, and chemically responsive	Strain gauges and sensing fabrics Sensory gloves for rehabilitation (movement monitoring and assistance) Tactile sensors
PVDF(polyvinylidene fluoride)	Bidirectional piezoelectric effect (electrical response to mechanical deformation)		Vibration and contact sensors in robotic and prosthetic applications (tactile discrimination, slip detection)
IPMC (ionic polymeric metal composites) A thin polymeric material inserted between two plated metal electrodes	Deformation causes shift of mobile charges = charge imbalance	Sensitivity to vibrations and large deformation bends Biomimetic response Moisture and metal content and distribution sensitivity	Tactile sensors New advancements

tive rubber pressure sensors, to exceedingly innovative IPMC systems. Through their studies, they found that IPMS sensor errors (3–5° amplitude errors) were in line with those of the natural proprioceptive system in the metacarpophalangeal joints. There is high resolution and accuracy with conventional sensors (e.g., fiber optics, strain gauges, etc.) but lack durability, flexibility, or of sufficiently small size, rendering them with minimal clinical acceptability for prosthetic devices. There is no need for auxiliary mechanisms or an external power source when IPMCs are employed, significantly reducing bulk. The favorable response through enhanced functional and sensory capacity demonstrated by the IPMC sensor in this study renders them as a necessitated alternative for proprioceptive sensory feedback in prosthetics.

3.8.5 *EAPs as Nanocomposites*

Organic-inorganic material hybrids have gained increasing amounts of recognition, with hybrid nanocomposites furnishing materials with unique physical properties, greatly exceeding the performance of the individual components alone [166]. These hybrid nanocomposites possess diverse applications; hybrids of nanoparticles and conducting polymers (e.g., Pt, Au, Pd, $Zr(HPO_4)_2$, MoO_3, MnO_2, Mo_3Se_3, γ-Fe_2O_3, Fe_3O_4, and IrO_2) have been applied to the fields of electrocatalysis, energy storage
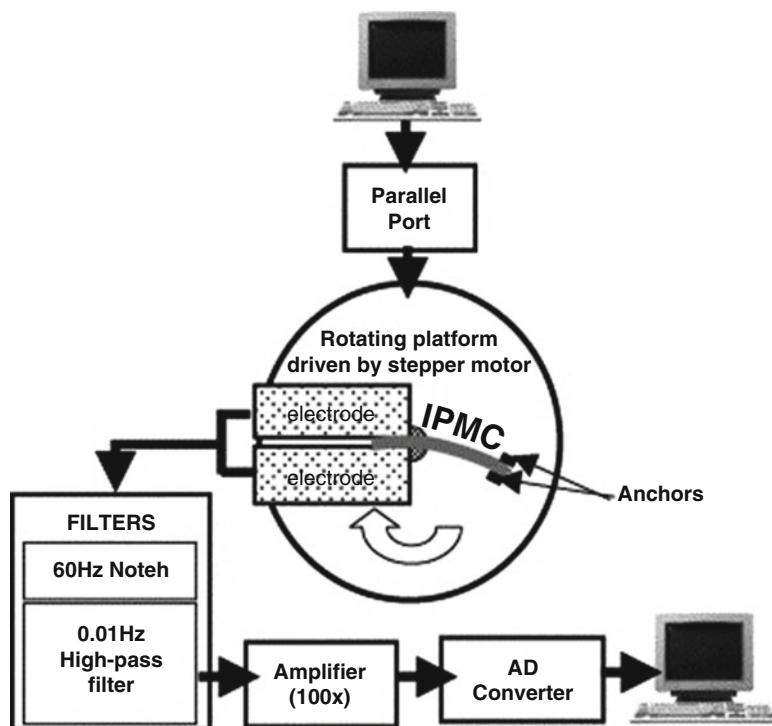
Fig 3.9 Schematic of experimental setup with rigid mounting of polymer on one end, with anchoring on the opposite end to a stepper motor-driven rotating platform. There is subsequent filtering, amplification, and digitization of the polymer response for signal processing. Source: Biddiss and Chau [162]

devices (e.g., supercapacitors), sensors, battery cathodes, microelectronics, magnetic materials, and electrochemical devices [167–175]. As most of the aforementioned hybrids incorporate metals or their oxides, moisture sensitivity may be an issue if not entrapped within an organic material matrix, thus forming a core/shell nanostructure [176].

The biomedical field could also reap rewards from the application of these hybrid structures with application as electrodes in soft tissue implants. Composites of PPy and carbon nanotubes have been employed in chronic implantable neural probes as electrodes for neural interfaces. The application of iridium oxide (IrO_2) as the inorganic component of hybrid materials has been used in numerous applications as a substrate for culture, growth, and neural cell electrical stimulation, as well as a medical electrostimulation electrode and sensor coatings [177–179]. The organic component could be comprised of conducting polymers such as PEDOT and PPy. This combination was predicted by Moral-Vico et al. [176] to be suitable for biomedical electrode applications, with the addition of the EAP providing the required flexibility and biocompatibility for implantation in a living organism [176]. Together with potentially enhanced electrochemical intensive properties,
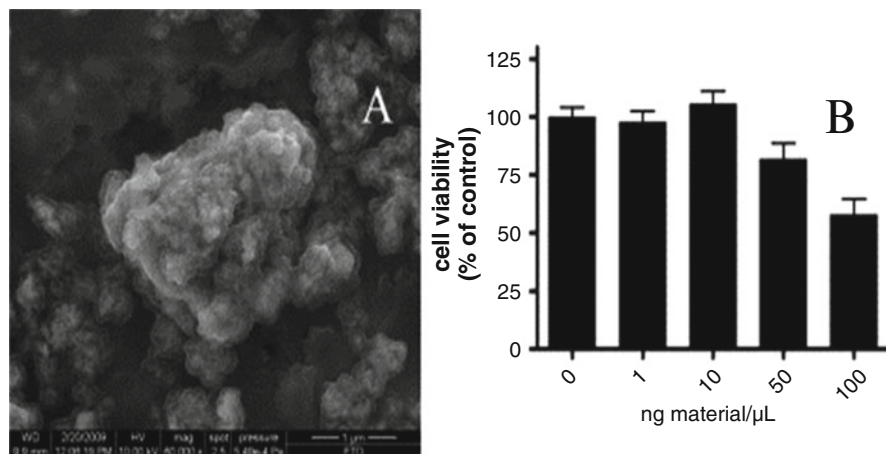
Fig 3.10 (**a**) SEM image of hybrid nanocomposite of polypyrrole and iridium oxide (IrO_2), (**b**) corresponding results of a cytotoxic assay. Source: Moral-Vico et al. [176]

they also anticipated a significant increase in charge capacity due to the Faradic properties of both components.

Other industries have also realized the potential of these novel hybrid phases, for example, as coatings or powders, as PEDOT, PPy, and IrO_2 all have applications in energy devices (e.g., solar and fuel cells), electrochromic devices, and sensors [179–181].

In the investigation performed by Moral-Vico and co-workers [176], two novel organic-inorganic nanocomposites comprised either of PPy or PEDOT encapsulating IrO_2 (i.e., PPy-IrO_x and PEDOT-IrO_x) were formulated via a facile hydrothermal reaction in various oxidation states employing a suspension of the IrO_2 and the monomer as precursor. Their biocompatibility was ascertained in the presence of cortical neuron cells and compared with IrO_2 and PPy-ClO_4 single phase toxicity, with a view of potential applications in the neural system [176] (Fig. 3.10). There was encapsulation and entrapment of IrO_2 by the polymer film in all instances. Conductivity and electrochemical activity were evident in varying degrees for the resultant material, with dependence on the initial oxidation state and the relative amount of each component. Biocompatibility was demonstrated by the hybrid materials for neuronal growth and differentiation. In terms of the suspension, a limited amount of material could be employed prior to the observance of toxicity, thus indicating that the nanocomposite maintains the biocompatibility in comparison with the non-hybrid-conducting polymers. The composite thus has potential for application as electroactive phases in biological media, when employed as a coating for bioelectrodes or for nanoparticulate delivery [176].

3.8.6 EAPs in Shape-Memory Applications

Shape-memory polymers (SMPs) possess the unique potential of deformation and fixing into a temporary shape, with recovery of their initial permanent shape following application of an external stimulus, which includes thermal, light, electrical, and magnetic stimuli to name a few [182]. SMPs have advantages over shape-memory alloys (SMAs), such as nickel titanium, including lightness, flexibility, processability, high shape recovery ratio, and low cost, in addition to high elastic deformation and low recovery temperature [183]. Their industrial applications are vast ranging from clothing manufacture, space structures, morphing aircraft, and biomedical treatments [184, 185]. There are certain limitations to SMPs limiting wider application including the following: low rubbery moduli lead to small recovery; poor thermal conductivity leads to low recovery speed; and the electrical insulation of most polymeric materials renders them inert to electromagnetic stimuli (compared to SMAs). Various investigations have been undertaken to overcome these challenges; specifically, approaches have been developed to enable electrical actuation of SMPs, resulting in the induction of the recovery of SMP composites via electrically resistant joule heating. This is achieved through combination of SMPs with conductive fillers such as carbon black, carbon fibers, nickel, and PPy, which generate heat in accordance with Joule's law to enable heat transfer for triggering the shape recovery of the SMP matrix [185–188]. This, however, requires high loading amounts of the conductive filler. Lower loading with notable enhancement of shape recovery can be implemented through institution of nanofillers (e.g., surface-functionalized carbon nanotubes) [185, 189].

Most investigations to date have focused on thermoplastic SMP resins such as polyurethane SMP as an electroactive SMP composite. Its invention was basically the inception of biodegradable SMPs as intelligent polymeric materials for biomedical applications [190]. Thermoplastic SMPs, however, possess poor thermal and mechanical attributes. Investigators then looked toward polylactide (PLA) and its copolymers, but its use was limited by brittleness. Hiljanen-Vaino and co-workers [191] then improved the mechanical properties of PLA via polycondensation with ε-caprolactam, ensued by introduction of urethane linkages for chain extension to poly(ester-urethane). Raja and co-workers [185] then proceeded to delve into an investigation on the shape-memory capabilities of polyurethane-polylactide (PU/PLA) blends, which saw the introduction of pristine and modified carbon nanotubes (CNTs) via a melt mixing process. The electroactive and shape-memory properties of the composite were investigated. Modified CNTs loaded into the PU/PLA blend furnished a significant improvement in the mechanical properties (tensile strength, dynamic storage modulus) and glass transition temperature compared to the pristine CNT-loaded system, as enhanced polymer-CNT interactions were enabled. The fine dispersion of the modified CNT in the matrix emanated in the formation of PU/PLA CNT nanocomposites with good electrical and thermal conductivity, which in turn enhanced the electroactive shape-memory behavior of the resultant composite (Fig. 3.11).

Fig 3.11 Shape-memory
effect of pristine and
modified CNT-filled PU/
PLA nanocomposites.
Source: Raja et al. [185]

PU/PLA/Pristine CNT composites (ULA-NT$_P$10)

PU/PLA/modified CNT composites (ULA-NT$_S$10)
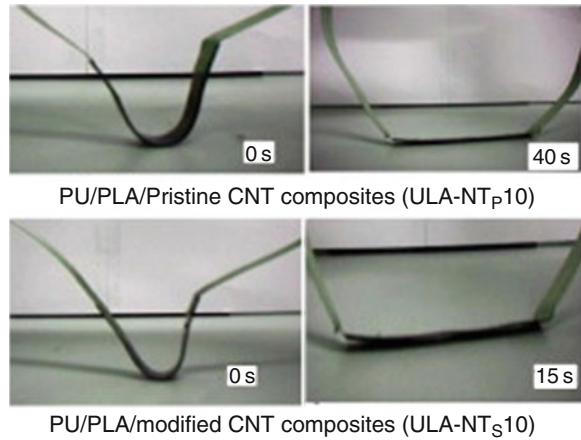
3.8.7   EAPs as Artificial Muscles

Polymeric actuators can exceed the performance of natural muscle in a number of aspects; hence, their suitability for biomedical devices, medical prostheses, biomimetic robots, and micro-/nano-electromechanical systems. As mentioned, the sandwiched structure of the ionic exchangeable polymeric core and platinum electrode face sheets of IPMCs are the favored EAPs for electrically driven bending actuators. Wang and co-workers [192] developed a novel biomimetic artificial muscle based on a cross-linked ionic networking membrane of sulfonated poly(arylenethioethersulfone) copolymer (SPTES) and PVA. This muscle was designed to demonstrate electrically actuated bending deformation. Synthesis of the SPTES copolymer was via direct copolymerization of the sulfonated monomers. This was followed by cross-linking with PVA via the dehydration approach with the cross-linking mechanism between the polymeric backbones highlighted in Fig. 3.12. There is transformation of the hydrophilic (–OH) and (–SO$_3$H) groups into the less hydrophilic (–OSO$_2$–) sulfonic ester groups during dehydration. The cross-linking of PVA and SPTES molecules' membranes minimizes swelling, in addition to altering the hydrophilic-hydrophobic balance inside the membranes. Ion-exchange processes and electroless plating achieved the final electroactive PVA/SPTES actuator. Application of an electric field to the IPMC caused cations within the membrane to carry solvent molecules in the direction of the cathode, with the ion movement instigating bending deformation and thus the actuation force. The cross-linked PVA/SPTES membrane demonstrated significantly enhanced proton conductivity and ionic exchangeable capacity compared to a Nafion membrane (a sulfonated tetrafluoroethylene-based fluoropolymer-copolymer with conductive properties). The bending deformation of the PVA/SPTES actuator is larger, in the absence of straightening-back relaxation and harmonic responses under sinusoidal excitations in a wide frequency band [192].
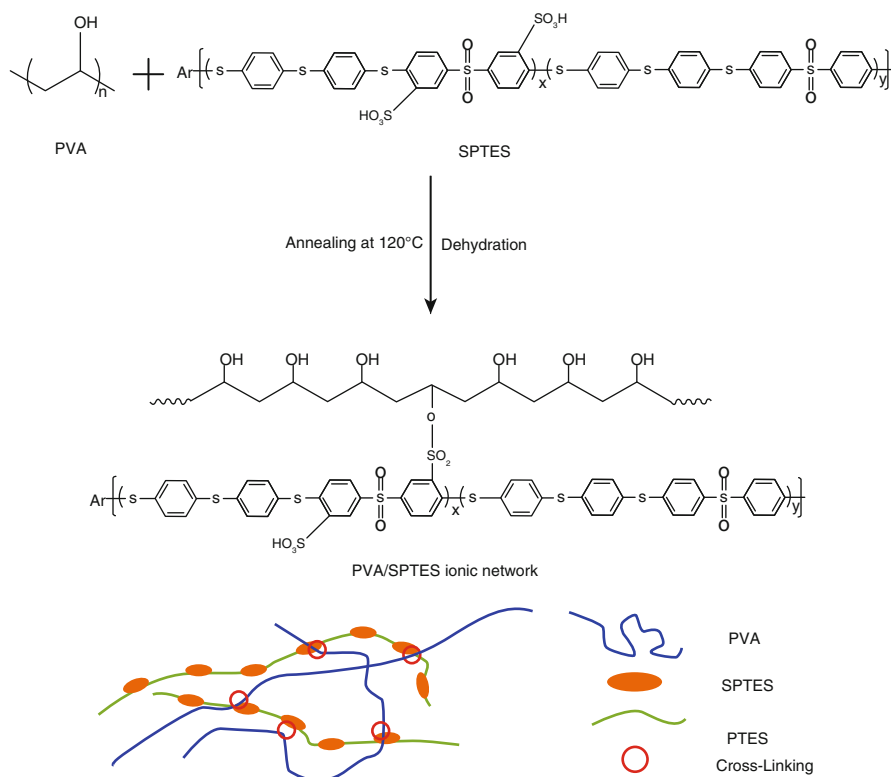
Fig 3.12 Chemical structure and cross-linking mechanism of PVA/SPTES. Source: Wang et al. [192]

3.8.8   Advances in Electroactive Coatings

Investigations have focused on the formation of hybrids of conducting EAPs and hydrogels as soft electroactive coatings for enhancing the mechanical and electrical performance of metallic implant electrodes. These soft electroactive materials mediate the mechanical mismatch between stiff metals and soft tissues. A challenge encountered is that it is difficult to achieve submicron coatings, using hydrogel fabrication approaches, which results in bulky implants, displacing excessive tissue volumes. Baek et al. [193] addressed this concern by covalently bonding polymer brushes of poly(2-hydroxyethyl methacrylate) (pHEMA) to a gold electrode via surface-initiated atom transfer radical polymerization (SI-ATRP). Electropolymerization, through the brush layer, of the CP poly(3,4-ethylene dioxythiophene) (PEDOT), formed a thin hydrophilic coating (Fig. 3.13). The electrical properties of the hybrid were shown to be superior to homogenous conducting EAPs. The material formed had potential as a hybrid coating for bioelectrode applications and supported the attachment and differentiation of model neural cells.
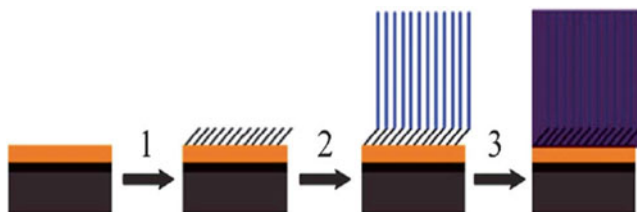
Fig 3.13 Schematic of the fabrication of the CP-brush hybrid. *1* Surface initiator self-assembly. *2* Surface-initiated atom transfer radical polymerization of pHEMA. *3* PEDOT/pTS electrodeposition through pHEMA. Source: Baek et al. [193]

3.9 Conclusion

EAPs encompass a novel technology platform that holds pertinent potential with diverse industrial applications. This chapter highlighted their specific impact in the medical and pharmaceutical industries. The key to their success is their extensive versatility, with the choice of dopant being important for definition of the overall properties. In this chapter, an overview has been provided of all the factors implicit to the successful operation of an EAP-based delivery system or device. Stemming from this, a panoply of drug delivery systems and biomedical devices has been developed, demonstrating the intelligence of design inherent in these systems, which can ultimately enable patient-controlled electroresponsive bioactive release for the tailored control of the clinical response. This being said, these developments are not without their limitations. Developments, specifically in the design of hybrid nanocomposites, could see these hurdles overcome. It is clear that the future will bring further examples of EAP-based systems in nanorobotics, nanobiosensors, prosthetics, and responsive miniaturized delivery systems where "smart" capabilities will be the name of the game.

References

1. Balint R, Cassidy NJ, Cartmell SH (2014) Conductive polymers: towards a smart biomaterial for tissue engineering. Acta Biomater 10:2341–2353
2. Bar-Cohen Y (2004) Electroactive polymer (EAP) actuators as artificial muscles – reality, potential and challenges, vol PM136, 2nd edn. SPIE Press, Bellingham, WA, pp 1–176
3. Bar-Cohen Y (2012) Biomimetic muscles and actuators using electroactive polymers (EAP). In: Bhushan B (ed) Encyclopedia of nanotechnology. Springer, Dordrecht, pp 285–290
4. Lakard B, Ploux L, Anselme K, Lallemand F, Lakard S, Nardin M et al (2009) Effect of ultrasounds on the electrochemical synthesis of polypyrrole, application to the adhesion and growth of biological cells. Bioelectrochemistry 75:148–157
5. Guiseppi-Elie A (2010) Electroconductive hydrogels: synthesis, characterization and biomedical applications. Biomaterials 31:2701–2716
6. Ateh DD, Navsaria HA, Vadgama P (2006) Polypyrrole-based conducting polymers and interactions with biological tissues. J R Soc Interface 3:741–752

7. Zhou DD, Cui XT, Hines A, Greenberg RJ (2010) Conducting polymers in neural stimulation applications. In: Zhou DD, Greenbaum E (eds) Implantable neural prostheses, vol 2. Springer, Berlin, pp 217–252

8. Guimard NK, Gomez N, Schmidt CE (2007) Conducting polymers in biomedical engineering. Prog Polym Sci 32:876–921

9. Kirchmeyer S, Reuter K (2005) Scientific importance, properties and growing applications of poly(3,4-ethylenedioxythiophene). J Mater Chem 15:2077–2088

10. Wan M (2008) Introduction of conducting polymers. In: Wan M (ed) Conducting polymers with micro or nanometer structure. Springer, Berlin, pp 1–15

11. Pillay V, Tsai T-S, Choonara YE, du Toit LC, Modi G, Naidoo D, Tomar LK, Tyagi C, Kumar P, Ndesendo VMK (2014) A review of integrating electroactive polymers as responsive systems for specialized drug delivery applications. J Biomat Res A 102:2039–2054

12. Roentgen WC (1880) About the changes in shape and volume of dielectrics caused by electricity, section III. In: Wiedemann G (ed) Annual physics and chemistry series, vol 11, John Ambrosius Barth Publisher. Leipzig, German, pp 771–786 (In German)

13. Park IS, Jung K, Kim DSM, Kim KJ (2008) Physical principles of ionic polymer-metal composites as electroactive actuators and sensors, special issue dedicated to EAP. Mater Res Soc MRS Bull 33:190–195

14. Madden JDW, Madden PG, Hunter IW (2002) Conducting polymer actuators as engineering materials. In: Bar-Cohen Y (ed) Proceeding of the SPIE smart structures and materials 2002: electroactive polymer actuators and devices (EAPAD). SPIE Press, Bellingham, WA, pp 176–190. doi:10.1117/12.475163

15. Cheng Z, Zhang Q (2008) Field-activated electroactive polymers, special issue dedicated to EAP. Mater Res Soc MRS Bull 33:190–195

16. Inzelt G, Szabo L (1986) The effect of the nature and the concentration of the counter-ions on the electrochemistry of poly (vinylferrocene) polymer film electrodes. Electrochim Acta 31:1381–1387

17. Bott AW (2001) Electrochemical techniques for the characterization of redox polymers. Curr Sep 19:71–77

18. History of polymer and plastics for students. American Chemistry Council. http://plastics.americanchemistry.com/Education-Resources/Hands-on-Plastics/Introduction-to-Plastics-Science-Teaching-Resources/History-of-Polymer-and-Plastics-for-Students.html. Accessed on April 7, 2015.

19. Karyakin AA, Karyakina EE, Schmidt H (1998) Electropolymerized azines: a new group of electroactive polymers. Electroanalysis 11:149–155

20. Asami R, Atobe M, Fuchigami T (2005) Electropolymerization of an immiscible monomer in aqueous electrolytes using acoustic emulsification. J Am Chem Soc 127:13160–13161

21. Ali E, Mahmood K, Mansoor K (2006) Electropolymerization of aniline on plastically deformed Pd surface: structure at micro- and nano-scale. Polym J 38:329–334

22. Wang Z, Kang J, Liu X, Ma Y (2007) Capacitive detection of theophylline based on electropolymerized molecularly imprinted polymer. Int J Polym Anal Charact 12:131–142

23. Walter MG, Wamser CC (2010) Synthesis and characterization of electropolymerized nanostructured aminophenylporphyrin films. J Phys Chem C 114:7563–7574

24. Ku CC, Liepins R (1987) Dielectric breakdown in polymers. In: Ku CC, Liepins R (eds) Electrical properties of polymers—chemical principles. Hanser Publishers, Munich, Germany, pp 102–199

25. Ghasemi-Mobarakeh L et al (2011) Application of conductive polymers, scaffolds and electrical stimulation for nerve tissue engineering. J Tissue Eng Regen Med 5:e17–e35

26. Ravichandran R, Sundarrajan S, Venugopal JR, Mukherjee S, Ramakrishna S (2010) Applications of conducting polymers and their issues in biomedical engineering. J R Soc Interface 7:S559–S579

27. Pelto J et al (2010) Electroactivity and biocompatibility of polypyrrolehyaluronic acid multiwalled carbon nanotube composite. J Biomed Mater Res 93A:1056–1067

28. Lyons MEG, Fay HG, McCabe T, Corish J, Vos JG, Kelly AJ (1990) Charge percolation in electroactive polymer films. J Chem Soc Faraday Trans 86:2905–2910
29. Bar-Cohen Y (2007) Focus issues on biomimetics using electroactive polymers as artificial muscles. Bioinsp Biomim 2:E01
30. Bidez PR, Li S, Macdiarmid AG, Venancio EC, Wei Y, Lelkes PI (2006) Polyaniline, an electroactive polymer, supports adhesion and proliferation of cardiac myoblasts. J Biomater Sci Polym Ed 17:199–212
31. Wang LX, Soczka-Guth T, Havinga E, Mullen K (2003) Poly(phenylenesulfidephenylenamine) (PPSA)—the "compound" of polyphenylenesulfide with polyaniline. Angew Chem 35:1495–1497
32. Otero TF, Rodriguez J, Angulo E, Santamaria C (1993) Artificial muscles from bilayer structures. Synth Met 55–57:3713–3717
33. Della Santa A, De Rossi D, Mazzoldi A (1997) Performance and work capacity of a polypyrrole conducting polymer linear actuator. Synth Met 90:93–100
34. Kincal D, Kumar A, Child A, Reynolds J (1998) Conductivity switching in polypyrrole-coated textile fabric as gas sensors. Synth Met 92:53–56
35. Lekpittaya P, Yanumet N, Grady BP (2004) Resistivity of conductive polymer-coated fabric. J Appl Polym Sci 92:2629–2636
36. Lopes A, Martin S, Moraö A, Magrinho M, Gonçalves I (2004) Degradation of a textile dye, C.I. Direct Red 80 by electrochemical processes. Portug Electrochim Acta 22:79–94
37. Moschou EA, Peteu SF, Bacha LG, Madou MJ, Daunert S (2004) Artificial muscle material with fast electroactuation under neutral pH conditions. Chem Mater 16:2499–2502
38. Kenji M, Shunzo S, Makoto U, Katsuhiko N (2000) Synthesis of a novel soluble polyaniline using imide super-acid. Nippon Kagakkai Koen Yokoshu 78:114–119
39. Lindström H, Holmberg A, Magnusson E, Lindquist S, Malmqvist L, Hagfeldt A (2001) A new method for manufacturing nanostructured electrodes on plastic substrates. Nano Lett 1:97–100
40. McCarthy PA, Juang J, Yang S, Wang H (2002) Synthesis and characterization of water-soluble chiral conducting polymer nanocomposites. Langmuir 18:259–263
41. Chao D, Lu X, Chen J, Liu X, Zhang W, Wei Y (2006) Synthesis and characterization of electroactive polyamide with amine-capped aniline pentamer and ferrocene in the main chain by oxidative coupling polymerization. Polymer 47:2643–2648
42. Palaniappan S, Devi SL (2006) Thermal stability and structure of electroactive polyaniline-fluoroboric acid-dodecylhydrogensulfate salt. Polym Degrad Stab 91:2415–2422
43. Zhang H, Li HX, Cheng HM (2006) Water-soluble multi-walled carbon nanotubes functionalized with sulphonated polyaniline. J Phys Chem B 110:9095–9099
44. Huang Y, Yu H, Xiao C (2007) pH-sensitive cationic guar gum/poly (acrylic acid) polyelectrolyte hydrogels: swelling and in vitro drug release. Carbohydr Polym 69:774–783
45. Huang L, Hu J, Lang L, Wang X, Zhang P, Jing X, Wang X, Chen X, Lelkes PI, Macdiarmid AG, Wei Y (2007) Synthesis and characterization of electroactive and biodegradgble ABA block copolymer of polylactide and aniline pentamer. Biomaterials 28:1741–1751
46. Guo B, Finne-Wistrand A, Albertsson A (2011) Versatile functionalization of polyester hydrogels with electroactive aniline oligomers. J Polym Sci Polym Chem 49:2097–2105
47. Tsai T, Pillay V, Choonara YE, du Toit LC, Modi G, Naidoo D, Kumar P (2011) A polyvinyl alcohol polyaniline based electro-conductive hydrogel for controlled stimuli-actuable release of indomethacin. Polymers 3:150–172
48. Yin W, Ruckenstein E (2001) A water-soluble self-doped conducting polypyrrole-based copolymer. J Appl Polym Sci 79:86–89
49. Bae WJ, Kim KH, Jo WH (2005) A water-soluble and self-doping conducting polypyrrole graft copolymer. Macromolecules 38:1044–1047
50. Ansari R (2006) Polypyrrole conducting electroactive polymers: synthesis and stability studies. E J Chem 3:186–201
51. Kim J, Deshpande SD, Yun S, Li Q (2006) A comparative study of conductive polypyrrole and polyaniline coatings on electro-active papers. Polym J 38:659–668

52. Sutar D, Aswal DK, Gupta SK, Yakhmi JV (2007) Electrochemical actuator from conductive electroactive polymer polypyrrole deposited on gold. Indian J Pure Appl Phys 45:354–357

53. Fichou D, Ziegler C (1999) Single crystals and thin films. In: Fichou D (ed) Handbook of oligo- and polythiophenes. Wiley-VCH, Weinheim, Germany, pp 185–282

54. Granstrom M, Harrison MG, Friend RH (1999) Electrooptical polythiophene devices. In: Fichou D (ed) Handbook of oligo- and polythiophenes. Wiley-VCH, Weinheim, Germany, pp 54–58

55. Gnanakan SRP, Rajasekhar M, Subramania A (2009) Synthesis of polythiophene nanparticles by surfactant-assissted dilute polymerization method for high performance redox supercapacitors. Int J Electrochem Sci 4:1289–1301

56. Heeger AJ (2001) Semiconducting and metallic polymers: the fourth generation of polymeric materials. J Phys Chem B 105:8475–8491

57. Bar-Cohen Y, Kwang J, Kim KJ, Choi HR, Madden JDW (2007) Electroactive polymer materials. Smart Mater Struct 16, E01

58. Kinoshita Y, Kuzuhara T, Kobayashi M, Ikada Y (1995) Reduction in tumor formation on polyethylene by collagen immobilization. J Long Term Eff Med Implants 5:275–284

59. Sengothi K, Tan P, Wang J, Lee T, Kang ET, Wang HC (1999) Biocompatibility of polyaniline polymers in tissue: Biomaterial surface interactions. In: AIChE annual meetings, Dallas, TX

60. Zhao H, Price WE, Too CO, Wallace GG, Zhou D (1996) Parameter influencing transport across conducting electroactive polymer membranes. J Membr Sci 119:199–212

61. Zhao H, Price WE, Wallace GG (1998) Synthesis, characterization and transport properties of layered conducting electroactive polypyrrole membrane. J Membr Sci 148:161–172

62. Zhao H, Prince WE, Wallace GG (1994) Effect of counter-ions employed during synthesis on the properties of polypyrrole membranes. J Membr Sci 87:47–56

63. Cirić-Marjanović G, Dragićević L, Milojević M, Mojović M, Mentus S, Dojćinović B, Marjanović B, Stejskal J (2009) Synthesis and characterization of self-assembled polyaniline nanotubes/silica nanocomposite. J Phys Chem B 113:7116–7127

64. Sadki S, Schottland P, Brodie N, Sabourand G (2000) The mechanisms of polypyrrole electropolymerization. Chem Soc Rev 29:283–293

65. Pistoia G, Bagnarelli O, Maiocco M (1978) Evaluation of factors affecting the radical electropolymerization of methylmethacrylate in the presence of HNO3. J Appl Electrochem 9:343–349

66. Yamada K, Tenshima K, Kobayashi N, Hirohashi R (1997) Electropolymerization of aniline derivatives in non-aqueous solution without a proton donor. J Electroanal Chem 394:71–79

67. Roeder J, Zucolotto V, Shishatskiy S, Bertolino JR, Nunes SP, Pires ATN (2006) Mixed conductive membrane: Aniline polymerization in an acid SPEEK matrix. J Membr Sci 279:70–75

68. Hatchett DW, Josowicz M, Janata J (1999) Acid doping of polyaniline: spectroscopic and electrochemical studies. J Phys Chem B 103:10992–10998

69. Kowalski D, Ueda M, Ohtsuka T (2008) The effect of ultrasonic irradiation during electropolymerization of polypyrrole on corrosive prevention of the coated steel. Corros Sci 50:286–291

70. Shabani-Nooshabadi M, Ghoreishi SM, Behpour M (2009) Electropolymerized polyaniline coatings on aluminum alloy 3004 and their corrosion protection performance. Electrochim Acta 54:6989–6995

71. Dimitriev OP (2003) Doping of polyaniline by transition metals: effect of metal cation on film morphology. Synth Mater 142:299–303

72. Taka T, Laakso J, Levon K (1994) Conductivity and structure of DBSA-protonated polyaniline. Solid State Commun 92:393–396

73. Mirmohseni A, Wallace GG (2003) Preparation and characterization of processable electroactive polyaniline–poly vinyl alcohol composites. Polymer 44:3523–3528

74. Palaniappan S, Saravanan C, John A (2005) Emulsion polymerization for preparation of polyaniline-sulfate salt, using non-ionic surfactant. J Macromol Sci Part A 42:891–900

75. Kinlen PJ, Frushour BG, Ding Y, Menon V (1999) Synthesis and characterization of organically soluble polyaniline and polyaniline block copolymers. Synth Mater 101:758–761

76. Posadas D, Florit MI (2004) The redox switching of electroactive polymers. J Phys Chem 108:15470–15476

77. Scampicchio M, Lawrence NS, Arecchi A, Mannino S (2007) Determination of sulphite in wine by linear sweep voltammetry. Electroanalysis 20:444–447

78. Pathiratne KAS, Skandaraja SS, Jayasena EMCM (2008) Linear sweep voltammetric determination of free chlorines in waters using graphite working electrodes. J Nat Sci Found Sri Lanka 36:25–31

79. Heinze J (2003) Cyclic voltammetry—"electrochemical spectroscopy": new analytical method. Angew Chem 23:831–847

80. Fortunato R, Branco LC, Afonso CAM, Benavente J, Crespo JG (2006) Electrical impedance spectroscopy characterization of supported ionic liquid membranes. J Membr Sci 270:42–49

81. Gabrielli C, Keddam M, Nadi N, Perrot H (2000) Ion and solvent transport across conducting polymers investigated by AC electrogravimetry. Application to polyaniline. J Electroanal Chem 485:101–113

82. Lyons MEG (1996) Transport and kinetics in electroactive polymers. In: Prigogine I, Rice SA (eds) Advances in chemical physics: polymeric systems, vol 94. Wiley, Hoboken, NJ, Chapter 5

83. Nguyen TA, Kobot S, Ongarato DM, Wallace GG (1999) The use of chronoamperometry and chemometrics for optimization of conducting polymer sensor arrays. Electroanalysis 11:1327–1332

84. Peppas NA, Bures CD (2006) Glucose-responsive hydrogels. In: Wnek GE, Bowlin GL (eds) Encyclopedia biomaterials and biomedical engineering. Dekker, New York, NY

85. Deng K, Zhang P, Ren X, Zhong H, Gou Y, Dong L, Li Q (2009) Synthesis and characterization of a pH/temperature responsive glycine-mediated hydrogel for drug release. Front Mater Sci China 3:374–379

86. Wang Q, Mynar JL, Yoshida M, Lee E, Lee M, Okuro K, Kinbara K, Aida T (2010) High-water-content mouldable hydrogels by mixing clay and a dendritic molecular binder. Nature 463:339–343

87. Bikram M, Gobin AM, Whitmire RE, West JL (2007) Temperature sensitive-hydrogel with SiO2–Au nanoshells for controlled drug delivery. J Control Release 123:219–227

88. Westbrook KK, Qi HJ (2008) Actuator designs using environmentally responsive hydrogels. J Intell Mater Syst Struct 19:597–607

89. Park C, Orozco-Avila I (2008) Concentrating cellulose from fermented broth using a temperature sensitive hydrogel. Biotechnol Prog 8:521–526

90. You J, Auguste DT (2010) Conductive, physiologically responsive hydrogels. Langmuir 26:4607–4612

91. Qui Y, Park K (2001) Environment-sensitive hydrogels for drug delivery. Adv Drug Deliv Rev 53:321–329

92. Murdan S (2003) Electro-responsive drug delivery from hydrogel. J Control Release 93:1–17

93. Li H, Yuan Z, Lam KY, Lee HP, Chen J, Hanes J, Fu J (2004) Model development and numerical simulation of electric-stimulus-responsive hydrogels subject to an externally applied electric field. Biosens Bioelectron 19:1097–1107

94. Li L, Huang C (2007) Electrochemical/electrospray mass spectrometric studies of electrochemically stimulated ATP release from PP/ATP films. J Am Mass Spectrom 18:919–926

95. Luo R, Li H, Birgersson E, Lam KY (2008) Modeling of electric-stimulus responsive hydrogels immersed in different bathing solutions. J Biomed Mater Res 85A:248–257

96. Brahim S, Guiseppi-Elie A (2004) Electroconductive hydrogels: electrical and electrochemical properties of polypyrrole-poly (HEMA) composite. Electroanalysis 17:556–570

97. Ehrick JD, Deo SK, Browning TW, Bachas LG, Madou MJ, Daunert S (2005) Genetically engineered protein in hydrogels tailors stimuli-responsive characters. Nat Mater 4:298–302

98. Miyata T, Asami N, Uragami T (1999) A reversibly antigen-responsive hydrogel. Nature 399:766–769
99. Pernaut J, Reynolds JR (2000) Use of conducting electroactive polymers for drug delivery and sensing of a bioactive molecular. A redox chemistry approach. J Phys Chem B 104:4080–4090
100. Zinger B, Miller LL (1984) Timed release of chemicals from polypyrrole films. J Am Chem Soc 106:6861–6863
101. Pyo M, Reynolds JR (1994) Electrochemically stimulated adenosine 5′-triphosphate (ATP) release through redox switching of conducting polypyrrole films and bilayers. Chem Mater 8:128–133
102. Otero TF, Padilla J (2004) Anodic shrinking and compaction of polypyrrole blend: electrochemical reduction under conformational relaxation kinetic control. J Electroanal Chem 561:167–171
103. Moina YG, Andrade C, Molina EM, Florit FV, Rodríguez Presa MI, Posada MJ (2003) Conformational changes during the redox switching of electroactive polymers. J Argentine Chem Soc 91:119–134
104. Silk T, Tamm J (1996) Voltammetric study of the influence of cations on the redox switching process of halogenide-doped polypyrrole. Electrochim Acta 41:1883–1885
105. Li L, Hsieh Y (2005) Ultra-fine polyelectrolyte hydrogel fibres from poly (acrylic acid)/poly (vinyl alcohol). Nanotechnology 16:2852–2860
106. Wang Y, Shen Y, Zhang Y, Yue B, Wu C (2006) pH-sensitive poly acrylic acid (PAA) hydrogels trapped with polysodium-p-styrenesulfonate (PSS). J Macromol Sci Part B 45:563–571
107. Adnadjevic B, Jovanovic J (2007) Novel approach in investigation of the poly (acrylic acid) hydrogel swelling kinetics in water. J Appl Polym Sci 107:3579–3587
108. Chansai P, Sirivat A (2008) Electrical field responsive polypyrrole in poly(acrylic acid) hydrogel for transdermal drug delivery. Adv Sci Technol 57:170–175
109. Sutani K, Kaetsu I, Uchida K (2001) The synthesis and the electric-responsiveness of hydrogel entrapping natural polyelectrolyte. Radiat Phys Chem 61:49–54
110. Gao F, Reitz FB, Pollack GH (2003) Potentials in anionic polyelectrolyte hydrogel. J Appl Polym Sci 89:1319–1321
111. Kulkarni RV, Sa B (2009) Electroresponsive polyacrylamide-grafted-xanthan hydrogels for drug delivery. J Bioact Compat Polym 24:368–384
112. Hoffman AS (2002) Hydrogels for biomedical applications. Adv Drug Deliv Rev 43:3–12
113. Francis S, Kumar M, Varshney L (2004) Radiation synthesis of superabsorbent poly (acrylic-acid)-carrageenan hydrogels. Radiat Phys Chem 69:481–486
114. Rokhade AP, Patil SA, Aminabhavi TB (2007) Synthesis and characterization of semi-interpenetrating polymer network microsphere of acrylamide grafted dextran and chitosan for controlled release of acyclovir. Carbohydr Polym 6:605–613
115. Pawde SM, Deshmukh K (2008) Characterization of poly vinyl alcohol/gelatin blend hydrogel films for biomedical applications. J Appl Polym Sci 109:3431–3437
116. Sui K, Gao S, Wu W, Xia Y (2010) Injectable supermolecular hybrid hydrogels formed by MWNT-grafted-poly ethylene glycol and α-cyclodextrin. J Polym Sci 48:3145–3151
117. Prashantha KV (2001) IPNs based on polyol modified castor oil polyurethane and poly (HEMA): synthesis, chemical, mechanical and thermal properties. Bull Mater Sci 24:535–538
118. Lü S, Liu M, Ni B, Gao C (2010) A novel pH- and thermo-sensitive PVP/CMC semi-IPN hydrogel: swelling, phase behavior, and drug release study. J Polym Sci B Polym Phys 48:1749–1756
119. You J, Almeda D, Ye GJC, Auguste DT (2010) Bioresponsive matrices in drug delivery. J Biol Eng 4:15
120. Cosnier S (1999) Biomolecule immobilization on electrode surfaces by entrapment or attachment to electrochemically polymerized films. A review. Biosens Bioelectron 14:443–456
121. Ahuja T, Mir IA, Kumar D, Rajesh (2007) Biomolecular immobilization on conducting polymers for biosensing applications. Biomaterials 28:791–805

122. Arora K et al (2006) Application of electrochemically prepared polypyrrole–polyvinyl sulphonate films to DNA biosensor. Biosens Bioelectron 21:1777–1783
123. Nien PC, Tung TS, Hoa KC (2006) Amperometric glucose biosensor based on entrapment of glucose oxidase in a poly(3,4-ethylenedioxythiophene) film. Electroanalysis 18:1408–1415
124. Prabhakar N, Arora K, Singh SP, Singh H, Malhotra BD (2007) DNA entrapped polypyrrole–polyvinyl sulfonate film for application to electrochemical biosensor. Anal Biochem 366:71–79
125. De Giglio E, Sabbatini L, Zambonin PG (1999) Development and analytical characterization of cysteine-grafted polypyrrole films electrosynthesized on Pt and Ti-substrates as precursors of bioactive interfaces. Biomater Sci Polym 10:845–858
126. Cortés MT, Moreno JC (2003) Artificial muscles based on conducting polymers. e-Polymers 4:1–42
127. Ghasemi-Mobarakeh L et al (2011) Application of conductive polymers, scaffolds and electrical stimulation for nerve tissue engineering. J Tissue Eng Regen Med 5:e17–e35
128. Stauffer WR, Cui XT (2006) Polypyrrole doped with 2 peptide sequences from laminin. Biomaterials 27:2405–2413
129. Zhang L, Stauffer WR, Jane EP, Sammak PJ, Cui XT (2010) Enhanced differentiation of embryonic and neural stem cells to neuronal fates on laminin peptides doped polypyrrole. Macromol Biosci 10:1456–1464
130. Gomez N, Lee JY, Nickels JD, Schmidt CE (2007) Micropatterned polypyrrole: a combination of electrical and topographical characteristics for the dtimulation of cells. Adv Funct Mater 17:1645–1653
131. Li J, Stachowski M, Zhang Z (2015) Application of responsive polymers in implantable medical devices and biosensors. In: Zhang Z (ed) Switchable and responsive surfaces and materials for biomedical applications, Chapter 11. Elsevier, eBook, pp 259–298
132. Li Y, Neoh NG, Kang ET (2005) Controlled release of heparin from polypyrrole–poly(vinyl alcohol) assembly by electrical stimulation. J Biomed Mater Res 73A:171–181
133. Wadhwa R, Lagenaur CF, Cui XT (2006) Electrochemically controlled release of dexamethasone from conducting polymer polypyrrole coated electrode. J Control Release 110:531–541
134. Miller LL, Zhou XU (1987) Poly(N-methylpyrrolylium) poly(styrenesu1fonate). A conductive, electrically switchable cation exchanger that cathodically binds and anodically releases dopamine. Macromolecules 20:1594–1597
135. Kontturi K, Pentti P, Sundholm G (1998) Polypyrrole as a model membrane for drug delivery. J Electroanal Chem 453:231–238
136. Massoumi B, Entezami AA (2002) Electrochemically stimulated 2-ethylhexyl phosphate (EHP) release through redox switching of conducting polypyrrole film and polypyrrole/poly(N-methylpyrrole) or self-doped polyaniline bilayers. Polym Int 51:555–560
137. Gomez N, Schmidt CE (2007) Nerve growth factor-immobilized polypyrrole: bioactive electrically conducting polymer for enhanced neurite extension. J Biomed Mater Res A 81:135–149
138. Lira LM, Cordoba de Torresi SI (2005) Conducting polymer-hydrogel composites for electrochemical release device: synthesis and characterization of semi-interpenetrating polyaniline-polyacrylamide network. Electrochem Commun 7:717–723
139. George PM, LaVan DA, Burdick JA, Chen CY, Liang E, Langer R (2006) Electrically controlled drug delivery from biotin-doped conductive polypyrrole. Adv Mater 18:577–581
140. Zhou Q, Miller LL, Valentine JR (1989) Electrochemically controlled binding and release of protonated dimethyldopamine and other cations from poly(N-methyl-pyrrole)/polyanion composite redox polymer. J Electroanal Chem 261:147–167
141. Pyo M, Reynolds JR (1995) Poly(pyrrole adenosine 5-triphosphate) (PP-ATP) and conducting polymer bilayers for transport of biologically active ions. Synth Mater 71:2233–2236
142. Kanokpom J, Sumonman N, Ratanaa R, Anuvat S (2008) Electrically controlled release of sulfosalicyclic acid from crosslinked poly (vinyl alcohol) hydrogel. Int J Pharm 356:1–11

143. Katchalsky A (1964) Polyelectrolytes and their biological interactions. Biophys J 4:9–41
144. Sorenson MH, Samoshina Y, Claesson P, Alberius P (2009) Sustained release of ibuprofen from polyelectrolyte encapsulated mesoporous carrier. J Disper Sci Technol 30:892–902
145. Budtova T, Suleimenov I, Frenkel S (1995) Electrokinetics of the contraction of a polyelectrolyte hydrogel under the influence of constant electric current. Polym Gels Netw 3:387–393
146. Shang J, Shao Z, Chen X (2008) Electrical behavior of a natural polyelectrolyte hydrogel: Chitosan/carboxymethylcellulose hydrogel. Biomacromolecules 9:1208–1213
147. Grieshaber D, Vörös J, Zambelli T, Ball V, Schaaf P, Voegel JC, Boulmedais F (2008) Swelling and contraction of ferrocyanide-containing polyelectrolyte multilayers upon application of an electric potential. Langmuir 24:13668–13676
148. Schreyer HB, Gebhart N, Kim KJ, Shahinpoor M (2000) Electrical activation of artificial muscles containing polyacrylonitrile gel fibers. Biomacromolecules 1:642–647
149. Inoue T, Chen G, Nakamae K, Hoffman AS (1997) A hydrophobically-modified bioadhesive polyelectrolyte gel for drug delivery. J Control Release 49:167–176
150. Guimard NKE, Sessler JL, Schmidt CE (2009) Toward a biocompatible and biodegradable copolymer incorporating electroactive oligothiophene units. Macromolecules 42:502–511
151. Sohn K, Shih SR, Park SJ, Kim SJ, Yi B, Han SY, Kim SI (2007) Hysteresis in a carbon nanotube based electroactive polymer microfiber actuator: numerical modeling. J Nanosci Nanotechnol 7:3974–3979
152. Kornbluh R, Sommer-Larsen P, De Rossi D, Alici G (2011) Guest editorial introduction to the focused section on electroactive polymer mechatronics. IEEE/ASME Trans Mechatron 16:1–8
153. Thompson BC, Moulton SE, Ding J, Richardson R, Cameron A, O'Leary S, Wallace GG, Clark GM (2006) Optimising the incorporation and release of a neurotrophic factor using conducting polypyrrole. J Control Release 116:285–294
154. Wadhwa R, Lagenaur CF, Cui XT (2006) Electrochemically controlled release of dexamethasone from conducting polymer polypyrrole coated electrode. J Control Release 110:531–541
155. Thompson BC, Richardson RT, Moulton SE, Evans AJ, O'Leary S, Clark GM, Wallace GG (2010) Conducting polymers, dual neurotrophins and pulsed electrical stimulation—dramatic effects on neurite outgrowth. J Control Release 141:161–167
156. Sharma M, Waterhouse GI, Loader SW, Garg S, Svirskis D (2013) High surface area polypyrrole scaffolds for tunable drug delivery. Int J Pharm 443:163–168
157. Chansai P, Sirivat A, Niamlang S, Chotpattananont D, Viravaidya-Pasuwat K (2009) Controlled transdermal iontophoresis of sulfosalicylic acid from polypyrrole/poly(acrylic acid) hydrogel. Int J Pharm 381:25–33
158. Esrafilzadeh D, Razal JM, Moulton SE, Stewart EM, Wallace GG (2013) Multifunctional conducting fibres with electrically controlled release of ciprofloxacin. J Control Release 169:313–320
159. Niamlang S, Sirivat A (2009) Electrically controlled release of salicylic acid from poly(p-phenylene vinylene)/polyacrylamide hydrogels. Int J Pharm 371:126–133
160. Spizzirri UG, Hampel S, Cirillo G, Nicoletta FP, Hassan A, Vittorio O, Picci N, Iemma F (2013) Spherical gelatin/CNTs hybrid microgels as electro-responsive drug delivery systems. Int J Pharm 448:115–122
161. Tanaka Y, Fujikawa T, Kazoe Y, Kitamori T (2013) An active valve incorporated into a microchip using a high strain electroactive polymer. Sens Actuators B Chem 84:163–169
162. Biddiss E, Chau T (2006) Electroactive polymeric sensors in hand prostheses: bending response of an ionic polymer metal composite. Medical Eng Phys 28:568–578
163. Bar-Cohen Y (2001) EAP applications, potential, and challenges. In: Bar-Cohen Y (ed) Electroactive polymer (EAP) actuators as artificial muscles. SPIE Press, Bellingham, WA, pp 616–655
164. Riley PJ, Wallace GG (1991) Intelligent chemical systems based on conductive electroactive polymers. J Intell Mater Syst Struct 2:228–238

165. Keshavarzi A, Shahinpoor M, Kim KJ, Lantz J (1999) Blood pressure, pulse rate, and rhythm measurement using ionic polymer–metal composites sensors. In: Bar-Cohen Y (ed) Proceedings of SPIE—The International Society for Optical Engineering, vol 3669., pp 369–376

166. Gómez-Romero P (2001) Hybrid organic–inorganic materials. In search of synergic activity. Adv Mater 13:3

167. Gangopadhyay R, De A (2000) Conducting polymer nanocomposites: a brief overview. Chem Mater 12:608–622

168. Rajesh B, Thampi KR, Bonard JM, Mathieu HJ, Xanthopoulos M, Viswanathan B (2005) Electronically conducting hybrid material as high performance catalyst support for electro-catalytic application. J Power Sources 141:35–38

169. Xia H, Cheng D, Xiao C, Chan HSO (2005) Controlled synthesis of polyaniline nanostructures with junctions using in situ self-assembly of magnetic nanoparticles. J Mater Chem 15:4161–4166

170. Leroux Y, Eang E, Fave C, Trippe G, Lacroix JC (2007) Conducting polymer/gold nanoparticle hybrid materials: a step toward electroactive plasmonic devices. Electrochem Commun 9:1258–1262

171. Rajesh, Ahuja T, Kumar D (2009) Recent progress in the development of nano-structured conducting polymers/nanocomposites for sensor applications. Sens Actuators B 136:275–286

172. Chen L, Sun LJ, Luan F, Li Y, Liu X (2010) Synthesis and pseudocapacitive studies of composite films of polyaniline and manganese oxide nanoparticles. J Power Sources 195:3742–3747

173. Fu Y, Manthiram A (2012) Core–shell structured sulfur–polypyrrole composite cathodes for lithium–sulfur batteries. RSC Adv 2:5927–5929

174. Khosla A (2012) Nanoparticle-doped electrically-conducting polymers for flexible nano-micro systems. Electrochem Soc Int (Fall-Winter): 67–70

175. Chen H, Dong W, Ge J, Wang C, Wu H, Lu W et al (2013) Ultrafine sulfur nanoparticles in conducting polymer shell as cathode materials for high performance lithium/sulfur batteries. Sci Rep 3:1910

176. Moral-Vicoa J, Sánchez-Redondo S, Lichtenstein MP, Suñol C, Casañ-Pastor N (2014) Nanocomposites of iridium oxide and conducting polymers as electroactive phases in biological media. Acta Biomater 10:2177–2186

177. Göbbels K, Kuenzel T, Van Ooyen A, Baumgartner W, Schnakenberg U, Bräunig P (2010) Neuronal cell growth on iridium oxide. Biomaterials 31:1055–1067

178. Cruz AM, Casañ-Pastor N (2013) Graded conducting titanium–iridium oxide coatings for bioelectrodes in neural systems. Thin Solid Films 534:316–324

179. Prats-Alfonso E, Abad L, Casañ-Pastor N, Gonzalo-Ruiz J, Baldrich E (2013) Iridium oxide pH sensor for biomedical applications. Case urea-urease in real urine samples. Biosens Bioelectron 39:163–169

180. Cai W, Gong X, Cao Y (2010) Polymer solar cells: recent development and possible routes for improvement in the performance. Sol Energy Mater Sol Cells 94:114–127

181. Makris T, Dracopoulos V, Stergiopoulos T, Lianos T (2011) A quasi solid-state dye-sensitized solar cell made of polypyrrole counter electrodes. Electrochim Acta 56:2004–2008

182. Dietsch B, Tong T (2007) A review—features and benefits of shape memory polymers (SMPs). J Adv Mater 39:3–12

183. Ratna D, Karger-Kocsis J (2008) Recent advances in shape memory polymers and composites: a review. J Mater Sci 43:254–269

184. Liu YJ, Lv HB, Lan X, Leng JS, Du SY (2009) Review of electro-active shape-memory polymer composite. Compos Sci Technol 209(69):2064–2068

185. Raja M, Ryu SH, Shanmugharaj AM (2013) Thermal, mechanical and electroactive shape memory properties of polyurethane (PU)/poly (lactic acid) (PLA)/CNT nanocomposites. Eur Polym J 49:3492–3500

186. Leng JS, Lv HB, Liu YJ, Du SY (2008) Synergistic effect of carbon black and short carbon fiber on shape memory polymer actuation by electricity. J Appl Phys 104:104917
187. Leng JS, Lan X, Liu YJ, Du SY, Huang WM, Liu N et al (2008) Electrical conductivity of thermoresponsive shape-memory polymer embedded micron sized Ni powder chains. Appl Phys Lett 92:014104
188. Gunes IS, Jimenez GA, Jana SC (2009) Carbonaceous fillers for shape memory actuation of polyurethane composites by resistive heating. Carbon 47:981–997
189. Koerner H, Price G, Pearce NA (2004) Remotely actuated polymer nanocomposites-stress-recovery of carbon-nanotube-filled thermoplastic elastomers. Nat Mater 3:115–120
190. Lendlein A, Langer R (2002) Biodegradable, elastic shape-memory polymers for potential biomedical applications. Science 296:1673–1676
191. Hiljanen-Vainio M, Kylma J, Hiltunen K, Seppala JV (1997) Rubber toughening of poly(lactide) by blending and block copolymerization. J Appl Polym Sci 63:1335–1343
192. Wang X-L, Oh I-K, Lee S (2010) Electroactive artificial muscle based on crosslinked PVA/SPTES. Sens Actuators B Chem 150:57–64
193. Baek S, Green R, Granville A, Martensa P, Poole-Warrena L (2013) Thin film hydrophilic electroactive polymer coatings for bioelectrodes. J Mater Chem B 1:3803

Chapter 4
Characterization and Performance of Stress- and Damage-Sensing Smart Coatings

Gregory Freihofer and Seetha Raghavan

Abstract Mechanical enhancement of polymers with high modulus reinforcements, such as ceramic particles, has facilitated the development of structural composites with applications in the aerospace industry where strength to efficiency ratio is of significance. These modifiers have untapped multifunctional sensing capabilities that can be enabled by deploying these particles innovatively in polymer composites and as coatings. This chapter highlights some of the recent and novel findings in the development of piezospectroscopic particle-reinforced polymers as smart stress- and damage-sensing coatings. The sections in this chapter describe the piezospectroscopic effect for alumina-based particulate composites, show the derivation of multiscale mechanics to quantify substrate stresses with piezospectroscopy, and demonstrate their performance in stress and damage sensing applied to a composite material. The noninvasive instrumentation is outlined and discussed for current and future applications in the industry ranging from manufacturing quality control to in-service damage inspections.

Keywords Smart coatings • Piezospectroscopy • Multiscale mechanics

4.1 Introduction

Modern industry is advancing towards multifunctional composites to meet concurrently demanding needs. The concept of "materials as sensors" is presented here in line with this multifunctional approach of monitoring structures while reinforcing and protecting them through a novel combination of inherent and unique material properties. Piezo-optical properties of luminescent particles deployed on structural materials as smart polymer coatings are used to engineer a high spatial resolution stress- and damage-sensing capability. This presents the potential for a novel, non-contact monitoring technique to support advanced damage models for tracking

G. Freihofer • S. Raghavan (✉)

Department of Mechanical and Aerospace Engineering, University of Central Florida, Orlando, FL 32816-2450, USA
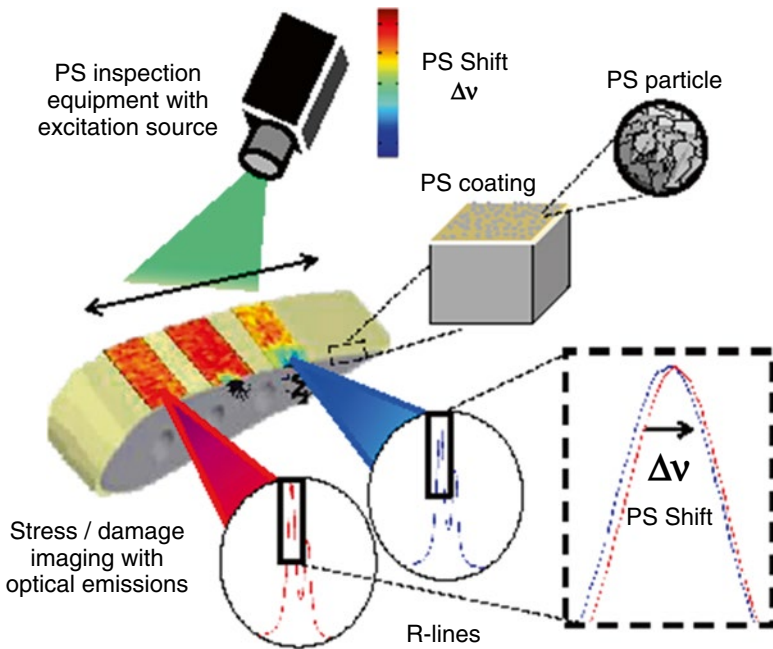e-mail: seetha.raghavan@ucf.edu

Fig. 4.1 An illustration of a stress- and damage-sensing concept for application on aerospace structures using a smart piezospectroscopic coating

degradation leading to outcomes in accelerating composite development and structural health monitoring as illustrated in Fig. 4.1.

Piezospectroscopy (PS) is a material phenomenon which correlates optical emissions with a material's state of stress [1]. It involves excitation of a material with a laser source and recording of the optical emissions. The technique is generally applicable to a surface measurement with some depth penetration depending on the transparency of the matrix and optics used to record the shifts of the emission spectra with stress, known as the PS effect. Observation of the PS effect is noninvasive and can be done with high spatial resolution over a large field of view. The PS constituents could either be deployed as a surface coating or a ply on a composite. Some common fillers used to enhance mechanical properties in structures, such as carbon fibers [2] and alumina [3], have inherent piezospectroscopic (PS) properties. When these constituents are used within a composite, the resulting composite will retain and potentially enhance the sensitivity of the PS properties [4]. This presents a new and attractive concept for developing smart polymer composites and coatings for structures with inherent sensing capabilities.

The piezospectroscopic effect has been investigated extensively to support pressure- and stress-sensing applications over the last few decades. The phenomenon was first widely used as a pressure sensor in diamond anvil cells [5] and for measuring residual stresses in ceramic oxides [6]. Later, it was developed for an industrial nondestructive evaluation (NDE) application to monitor stresses in a thermally

grown oxide (TGO) within thermal barrier coating (TBC) systems [7]. The stresses in this naturally occurring TGO layer relax during the lifetime of the TBC and can be used as a method to predict the remaining life and quantify damage. The aforementioned examples pertain to chromium-doped alumina, a material with very well-established PS properties [8]. However, the method is similarly applicable to other PS materials such as silicon and carbon fiber, utilized in the electronics [9] and aerospace [10] industry, respectively, to monitor residual stresses that arise during manufacturing. Work has also been done to observe the micromechanics of embedded PS constituents [11], to assist in verification of analytical and finite element models [12, 13], and to investigate edge effects of standard compression tests [14, 15]. Here, the application of smart polymer composites and coatings based on piezospectroscopy is explored for industrial applications as a next-generation NDE technique which is compliant and adaptable to a wide variety of structures and for structural health monitoring.

4.2 Alumina as Particulate Sensors in a Polymer Matrix

Alumina is a material of focus for piezospectroscopic sensing because of its strong photoluminescence (PL) signal [16] from trace amounts of chromium leading to well-defined PS properties [8]. In addition, this material presents multifunctionality in its mechanical properties when deployed as particulates in a polymer matrix [17]. Other PS materials such as carbon nanotubes have been adapted as strain-sensing coatings [18]. The same mechanics and concepts presented in this chapter for alumina could be modified for various PS constituents. However, due to the wide variety of optical phenomena and PS materials, the scope of the work presented is to outline the methods to convert PS properties into useful engineering quantities for damage diagnosis using alumina as a leading example.

Alumina-based particulate composites have emerged as materials with exceptional mechanical properties to meet structural applications. They combine the dissimilar mechanical properties between the polymer matrix and the ceramic to provide a unique and desirable mechanical response to external loading and allow for tailoring of these properties with volume fraction, particle sizes, and morphology. Alumina is often introduced in coatings for tribological properties because of its extremely high hardness, wear/corrosion resistance, and thermal/electrical insulation abilities. Here, alumina-based composite coatings are studied for their stress-sensing ability creating multifunctionality with mechanical property improvements. This section begins with a brief background into the role of alumina in enhancing mechanical properties of polymer composites and provides a vision for these structural coatings to be highly valued for their noninvasive stress-sensing abilities.

Reinforced composites with constituents of particulates, such as alumina, present high strength-weight ratio properties that are ideal for applications in aerospace and defense. Some examples of these applications include lightweight armors requiring superior load bearing capability under external impact of blast as well as energetic

materials that require high amount of energy release with reduced sensitivity to impact [19–25]. In general, the addition of particles improves compressive strength [26] as seen in mechanical tests with applications such as elements for shock depoling and lightweight armors [27]. Introduction of alumina nanoparticles has varying effects on fracture toughness [28] with general trends showing increases in the fracture toughness. In addition, alumina composites have been observed to greatly increase wear resistance when made in compression molds [17] and more modestly increase wear resistance when casted [29]. The wear resistance for alumina composites increased 600 % when compared to unfilled samples [30]. Further increases in wear resistance by 3000 % were observed when the nanoparticles had irregular shapes [17]. Effects of surface treatment and smaller particles were also observed to increase wear resistance [29, 31]. The dynamic response of alumina-based particulate composites has been heavily investigated through experiments ranging from quasi-static or low strain rate tests to split Hopkinson pressure bar (SHPB) tests at high strain rates. In these tests, shock profiles are used to develop response models, while recovered alumina fragments subjected to detailed characterization are the basis for damage models representing failure initiation and propagation [32].

The general outcomes of improved moduli and strength under loads are largely dependent on the material configuration. There are many related factors to consider when evaluating the mechanical performance improvements including: size [28, 33–35], particle shape [36], surface treatment [33, 35, 36], and dispersion [33]. To hasten the optimization of these many factors, piezospectroscopy is becoming a valuable characterization technique to monitor particle dispersion [37] and can also be used to quantify load transfer across the particle-matrix interface [11, 38]. Here it can be seen that piezospectroscopy not only adds value to these polymer composites while they are in service but also in their development. Experimental characterization that enables the understanding of the microstructural response is key in these studies since microcracking and microplasticity play a role in the deformation and failure of these materials under various loading conditions [39–41]. An important aspect of creating a smart coating is to correlate the particle stress-induced shifts to the overall stress state of the substrate through the development of the relevant multiscale mechanics relations.

4.3 Multiscale Mechanics of Smart Piezospectroscopic Composites and Coatings

This section briefly addresses the mechanics associated with converting a photoluminescence signal from particulate sensors within a polymer into a usable stress measurement representing the substrate's stress state. This starts with a background of well-known PS properties of polycrystalline materials, followed by more recently derived PS properties of nanocomposite materials. These different properties are combined with analytical multiscale mechanics to produce a straightforward interpretation of the PS effect necessary to enable stress and damage sensing.

The photo-stimulated luminescence of alumina comes from the interstitial Cr^{3+} ion embedded within the alumina lattice. When excited, typically with a visible laser, it emits characteristic peaks known as R-lines. When the alumina lattice is under strain, it changes the energy levels of the ligand field surrounding the Cr^{3+} impurity and causes a frequency shift in the spectral peaks [1]. In a polymer composite, these alumina particles (p) which are embedded within the matrix are polycrystalline and can have a grain size on the order of tens of nanometers. The PS properties for each individual grain are anisotropic, but the measurement volume (i.e., laser dot size) is typically greater than one micron. This creates an averaging effect within the probed volume which simplifies the PS relationship to be a measurement of the first stress invariant (σ_{jj}^{p}). The PS coefficient ($\Pi_{ii}^{p} = 7.6$ (GPa/cm^{-1})) relates the mean frequency shift ($\Delta\nu$) to σ_{jj}^{p} with a first order relationship. Sometimes it is more convenient to represent this relationship with strain. This conversion uses the relationship between the first invariant of stress and strain for isotropic materials ($\sigma_{ii} = 3K\varepsilon_{ii}$), where K is the bulk modulus.

$$\Delta\nu = \frac{1}{3}\Pi_{jj}^{p}\sigma_{jj}^{p} = K^{p}\Pi_{jj}^{p}\varepsilon_{jj}^{p} \tag{4.1}$$

While the stress sensitivity has been historically limited in range for uniaxial loads to approximately 2.5 (cm^{-1}/GPa) under uniform applied stress, recent efforts have demonstrated tailorability when the luminescing material, alpha alumina, is distributed in a nanoparticulate form within a matrix, yielding enhanced PS sensitivity increases of up to 130 % [4, 11]. To represent the enhancement, Eq. (4.1) is rewritten for an experiment which observes a nanocomposite's PS coefficient (Π^{c}) which relates $\Delta\nu$ to a uniaxial stress imposed on the composite (σ_{1}^{c}). For enhanced PS properties, $\Pi_{ii}^{c} > \Pi_{ii}^{p}$, and under uniaxial stress, $\sigma_{1}^{c} = \sigma_{ii}^{c}$.

$$\Delta\nu = \frac{1}{3}\Pi_{jj}^{c}\sigma_{jj}^{c} \tag{4.2}$$

To relate the enhancement in PS properties to particulate mechanics, Eqs. (4.1) and (4.2) are set equal to each other. This is possible because $\Delta\nu$ is originating from the same type of alumina constituent.

$$\frac{\Pi_{ii}^{c}}{\Pi_{ii}^{p}} = \frac{\sigma_{ii}^{p}}{\sigma_{ii}^{c}} \tag{4.3}$$

The result in Eq. (4.3) signifies that an experimental measure of Π_{ii}^{c} can quantify the partitioning of stress from the composite into the particle. The load transfer from particle to matrix has been well described by analytical methods of Eshelby [42] and its derivative theories [43]. These particle load transfer theories are capable of calculating σ_{ii}^{p} when an arbitrary σ_{ii}^{c} is applied. Using a modification to the Eshelby mechanics, which assumes that the matrix can be more accurately represented as the effective composite properties, the partitioning of the first stress invariant can be

derived [11, 44]. In some applications, as will be shown in Sect. 4.4, it is more convenient to represent the PS properties in terms of strain.

$$\frac{\sigma_{ii}^p}{\sigma_{ii}^c} = \frac{-3E^p\left(v^c-1\right)}{2E^c+E^p-4E^cv^p+E^pv^c} \tag{4.4}$$

$$\frac{\varepsilon_{ii}^p}{\varepsilon_{ii}^c} = \frac{-3E^c\left(2v^p-1\right)\left(v^c-1\right)}{\left(2v^c-1\right)\left(2E^c+E^p-4E^cv^p+E^pv^c\right)} \tag{4.5}$$

Now, the first order relationship between Δv and the composite's state of stress/strain can be physically quantified by the elastic mismatch (E and v) between the effective composite properties (c) and the embedded particle (p). Therefore, the observation of Π_{ii}^c can quantify the composite's elastic properties and can provide a measure of elastic degradation as illustrated in Fig. 4.2.

The multiscale mechanics needed to interpret the PS properties of a composite have been defined. This needs only to be taken one step further for a PS composite coating. A coating mechanics term has been derived [11, 44] which relates interfacial strains between an isotropic coating and substrate system under plane stress.

$$\frac{\varepsilon_{ii}^c}{\varepsilon_{ii}^s} = \frac{\left(1-v^s-v^{s2}\right)\left(1-v^s\right)\left(1+v^s\right)\left(1-2v^s\right)}{\left(1-v^c-v^{c2}\right)\left(1-v^c\right)\left(1+v^c\right)\left(1-2v^c\right)} \tag{4.6}$$

With relations representing the multiscale mechanics of the coating defined, validation of the piezospectroscopic coating's stress-sensing capability was achieved for
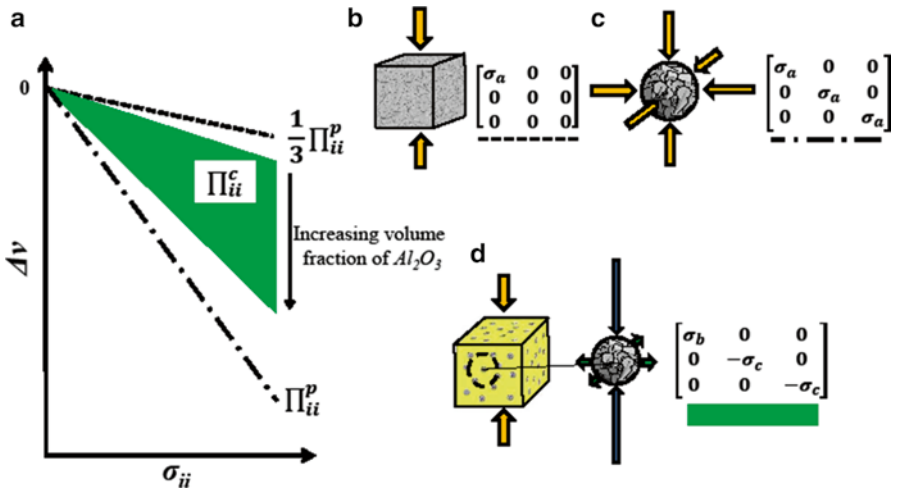
Fig. 4.2 The piezospectroscopic relationships for different loading conditions of a PS constituent [11]

a standard composite coupon test through concurrent measurements with a technique of comparable spatial resolution, digital image correlation. This served as a technology demonstration of the applicability and benefits of the smart coatings.

4.4 Technology Demonstration of a Smart Piezospectroscopic Coating

Open-hole tension testing for strength of aerospace structural composites is an important indicator of allowable stresses and sometimes is the limiting factor that drives design. Combining the unavoidable geometrical interaction with material properties, this test often serves as an early indicator of a material's structural performance [45]. Stress- and damage-sensing capabilities have an increased significance in these tests with the greatest need being to capture the onset of damage and the evolution of material properties as the damage progresses. This test served as an excellent means to assess and validate the damage-sensing capabilities of the smart polymer-based alumina coating.

The coating, manufactured by Elantas PDG, was loaded with 20 % volume fraction alumina nanoparticles in an EPON 828 matrix and applied to the open-hole tension (OHT) composite substrate consisting of laminated IM7-8552 unidirectional tape manufactured and tested in accordance with ASTM standards [46]. The sample was loaded using displacement control during holds to maintain constant substrate strain. During each hold, piezospectroscopic data was collected with a prototype portable spectrometer system. Digital image correlation (DIC) measurements were taken concurrently on the opposing face of the composite coupon for correlation (Fig. 4.3). The photo-stimulated luminescence spectra, over a measurement area of 25.4 (mm^2), was collected using a synchronized translation stage in a 60×60 grid snake scan corresponding to a spatial resolution of 0.4 (mm). This spatial resolution can be adjusted to micrometer scales for specific applications.

The stress-sensing coating detected the onset of composite failure at 77 % failure load, earlier than standard DIC measurements, and subsequently tracked the distribution of stresses within the coating in the immediate vicinity of the crack as it progressed. The early detection is indicative of how the technique is capable of sensing internal ply damage initiation from the stress relief of the particles attached to the surface as a coating, and this is a breakthrough that cannot be achieved with current techniques [46, 47].

Multiscale mechanics, developed in the previous section (i.e., 4.3), were applied to diagnose the damage. Unique to this experiment, spatial data was collected simultaneously for biaxial strain ($\boldsymbol{\varepsilon}_b$), where ($\boldsymbol{\varepsilon}_b = \boldsymbol{\varepsilon}_1 + \boldsymbol{\varepsilon}_2$) and PS shift ($\Delta\nu$). These were correlated to each other to map a PS coefficient ($\boldsymbol{\Pi}^c$) during in-situ mechanical loading over a field of view as illustrated in Fig. 4.4. Interpreting this combination of collected data with multiscale mechanics is essential to adding value to the smart coatings. A series of ratios transform the physics and length scales into conventional engineering terms for structural engineers and is represented by $\boldsymbol{\Pi}^c$.
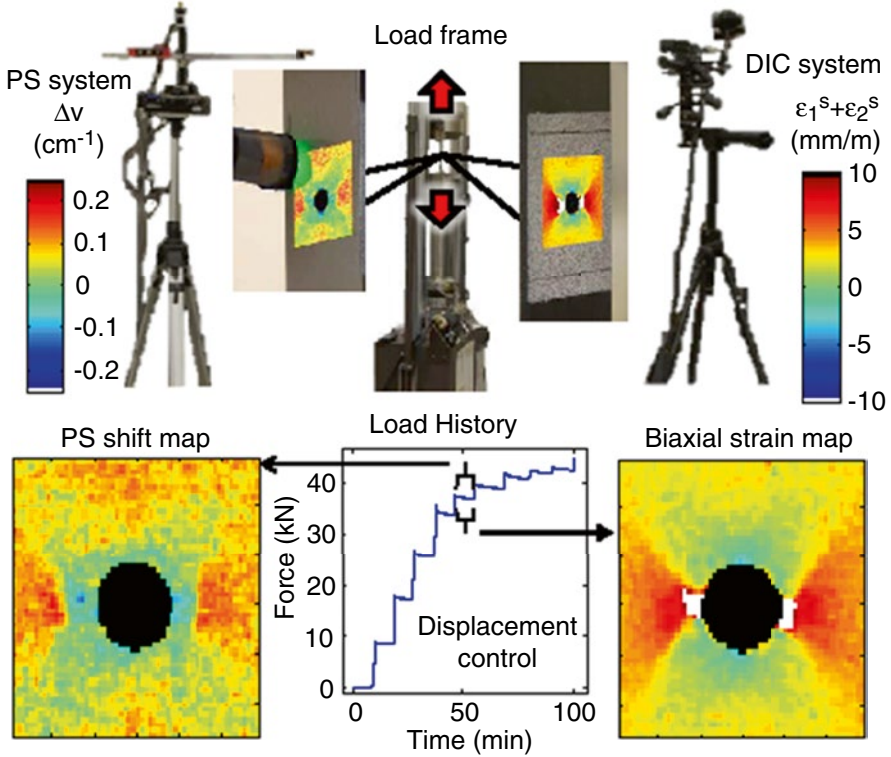
Fig. 4.3 Experimental configuration of the PS and digital image correlation (DIC) systems about a hydraulic load frame. Front side PL peak shift contours collected at discrete loads and DIC data collected on the back side of the composite substrate are shown
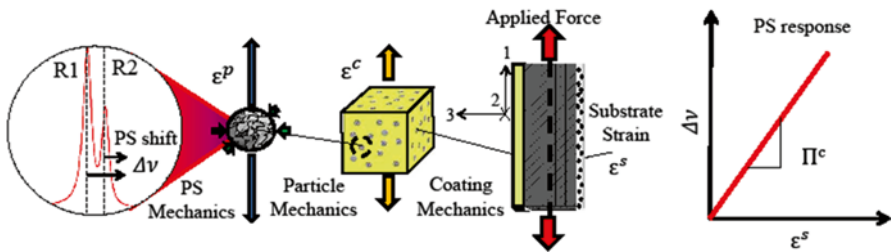

Fig. 4.4 The multiscale mechanics used to describe the relationship between piezospectroscopic shift and substrate strain

$$\Delta v = \frac{\Delta v}{\varepsilon_{ii}^{p}} \frac{\varepsilon_{ii}^{p}}{\varepsilon_{ii}^{c}} \frac{\varepsilon_{ii}^{c}}{\varepsilon_{ii}^{s}} \frac{\varepsilon_{ii}^{s}}{\left(\varepsilon_{1}^{s} + \varepsilon_{2}^{s}\right)} \tag{4.7}$$

Unloading curves are simulated in order to apply an elastic degradation damage model. The unloading curves simulate no elastic degradation and purely plastic deformation up until the point of the maximum PS shift. Continued loading records

a "PS drop" that is analogous to a load drop in a conventional mechanical test due to the loss of load-carrying capacity of the material. The unloading curves past this PS shift maximum are modeled with no plastic deformation and purely elastic degradation. These damage mechanics, applied over a field of view, create a damage map comprising the substrate's degrading elastic modulus. This was evaluated from the experimental measurements in an innovative way as shown in Fig. 4.5 [47, 48]. Here, the unique capability of detecting local damage through the piezospectroscopic measurements is highlighted.

This novel mapping technique, which was conducted in conjunction with DIC and piezospectroscopy, quantified the damage for intrinsic patterns for the composite coupon. This includes initial fiber failure [49], transverse cracking [50], and intralaminar cracking [51] as illustrated in Fig. 4.6. This demonstration successfully showed these alumina-polymer nanocomposite coatings along with the appropriate instrumentation have immense potential as a comprehensive NDE damage mapping technology.

The degraded elastic modulus can be quantified with an uncertainty of 10 GPa with the current experimental setup and multiscale mechanics. The intrinsic damage patterns, listed here, are anticipated to locally degrade the elastic modulus greater than this uncertainty. The dominating contribution to this uncertainty is the ability to resolve the PS shift and can be improved by increasing the equipment's spectral resolution and signal quality. Further development of the instrumentation will lead to an uncertainty in the degraded elastic modulus which is low enough to detect initial matrix microcracking of the composite.
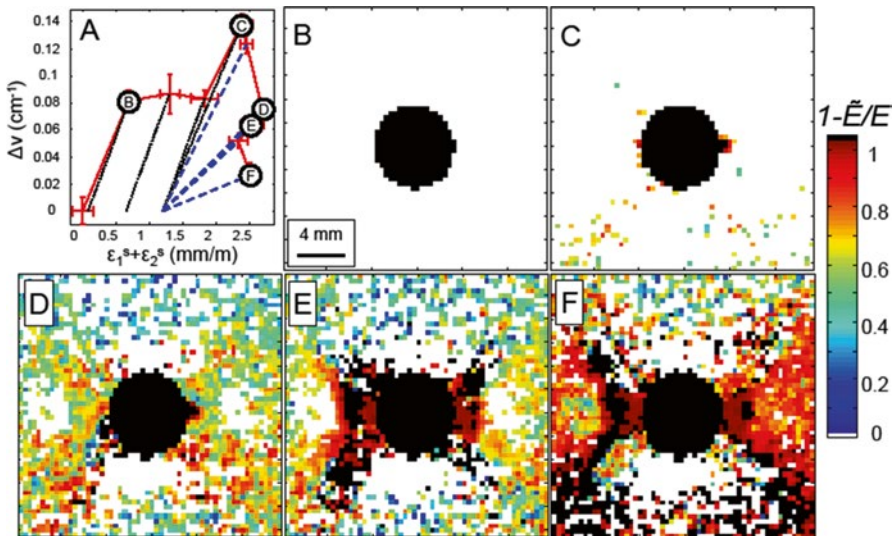

Fig. 4.5 (**a**) The simulation of the unloading curves for a PS response using plastic deformation until the max PS shift, after which purely elastic degradation is initiated. (**b–f**) Failure loads which exhibited significant progressions of damage are shown [47]
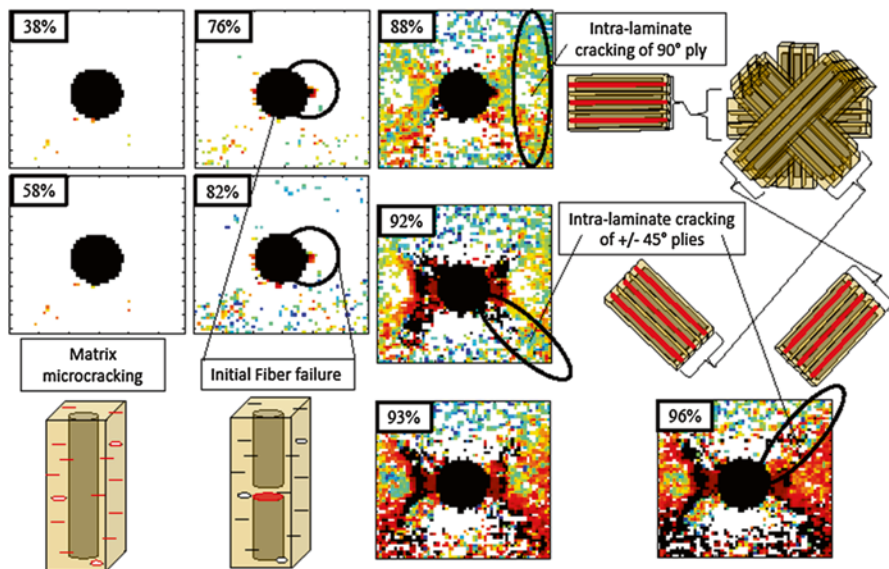
Fig. 4.6 Quantifying and correlating damage for the composite with progressive modes of failure such as matrix microcracking, initial fiber failure, and intralaminate cracking of the various plies

4.5 Measurement Instrumentation for Piezospectroscopic Sensing

Along with the development of smart coatings, accessibility to piezospectroscopic measurements plays an important role in the successful transition to industrial applications where remote access and portability are key requirements. Fiber optics provides a remote capability to spectroscopy measurements. Laser excitation and the corresponding emission transmitted by optical fibers are the basis for recent efforts in the integration of a portable system for in situ spectroscopy [52] shown in Fig. 4.7. The portable spectrometer allows for the extension of the laser excitation and collection to be achieved outside of this, through fiber optic probes that enable coupling with mechanical testing instrumentation. This step forward has allowed for initial successful outcomes with the results presented herein that demonstrate the viability of the technique to join the ranks of noninvasive structural integrity monitoring methods existing today. The prototype system houses a number of components that were strategically chosen to optimize its performance while maintaining its portability. The overall system can be split into two major categories, the hardware and software. The hardware consists of seven main components: a spectrograph, charge-coupled device (CCD), X–Y–Z stage, laser, fiber optics, computer, and support equipment. Software programs are mainly used for data gathering from the CCD, controlling and commanding the X–Y–Z stage, and data post-processing.

Data collection of the photoluminescent spectra, from laser excitation of a sample over an area, can be configured using the synchronized translation stage in a grid
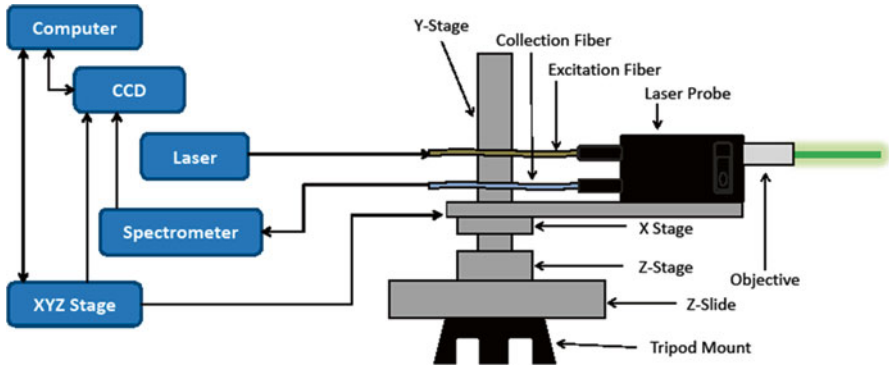
Fig. 4.7 Prototype portable spectrometer system instrumentation enables in situ measurements [52]

snake scan with high spatial resolution. Once a map is complete, the raw hyperspectral data undergoes four major post-processing steps, which are exporting, filtering, curve fitting, and plotting, before achieving a complete piezospectroscopic map. A combination of instrumentation and technique development will support the transition of smart piezospectroscopic coatings to meet a variety of industrial applications.

4.6 Conclusion and Future Outlook

An immediate application for these smart piezospectroscopic coatings is using them for enhanced damage diagnosis during coupon level testing. Monitoring the piezospectroscopic properties of a coated coupon with in situ mechanical loading gives a higher level of understanding into the progressive damage mechanisms associated with advanced composites [46]. Many NDE techniques have been utilized during coupon testing in an attempt to gather more information on the mechanical properties of the materials. However, piezospectroscopy offers something unique in the fact that it can map degradation of material properties by using the multiscale mechanics derived in Sect. 1.3. This laboratory application offers an excellent stepping stone for understanding the fundamentals of these smart PS composites and coatings, before widespread utilization of multifunctional PS composites for structural applications.

In the future, the smart piezospectroscopic coatings can serve as quality control and add value to the composites before they are even deployed into an application. This includes the measurement and determination of residual stresses and sensing of stress concentrations during curing or sintering processes associated with advanced manufacturing. Once deployed, value can be added to its capability of noninvasive measurements of stress through the utilization of a multifunctional property that is inherent to the material. These coatings can be strategically located

in regions within a structure which are prone to various types of damage. The stress can be monitored in either real time with a fixed measurement device or for regular inspections using portable instrumentation.

Challenges to further extend the applications of these coatings towards a commercially viable solution for stress and damage detection lie in two areas of technological needs. The first material gap in technology is in achieving advances in manufacturing methods for particle-polymer combinations that ensure more homogeneous dispersion of particles within the polymer and excellent adhesion between particle and the polymer matrix. This plays a major role of the sensing behavior both to achieve sensing to the maximum range of the substrate strength before failure and to demonstrate repeatable sensing behavior over several cycles. The second optics gap in technology lies in the speed of data collection through point-by-point detection that is achievable from the current prototype measurement. The benefits of high spatial resolution and multiscale sensing enabled through this novel approach can be retained while implementing an area sensing configuration to envision this innovation meeting needs of structural sensing for large-scale aerospace or civil engineering applications.

Stress- and damage-sensing smart coatings utilizing an alumina-polymer nanocomposite have been demonstrated to be useful for the diagnosis of intrinsic progressive failure in composite coupons. The applications for these coatings and composites to be deployed into structural applications for damage sensing were discussed and could be adapted to a variety of industries. The added value these composites retain with the implementation of their inherent PS properties is not only limited to in-service damage sensing but also for manufacturing quality control. The calibration and testing of these coatings were shown in the technology demonstration to go hand in hand with the development of new composite materials.

References

 1. Kaplyanskii AA, Przhevuskii AK (1962) Sov Phys Dokaldy 7(1):313
 2. Frank O, Tsoukleri G, Riaz I, Papagelis K, Parthenios J, Ferrari AC, Geim AK, Novoselov KS, Galiotis C (2011) Nat Commun 2(255):1
 3. He J, Clarke DR (1997) J Am Ceram Soc 80:69–78
 4. Stevenson A, Jones A, Raghavan S (2011) Nano Lett 11:3274
 5. Barnett JD, Block S, Piermarini GJ (1973) Rev Sci Instrum 44:1
 6. Grabner L (1978) J Appl Phys 49(5):580
 7. Christensen R, Lipkin D, Clarke D (1996) Appl Phys Lett 69:3754
 8. Ma Q, Clarke DR (1993) J Am Ceram Soc 76(6):1433
 9. Porporati AA, Miyatake T, Schilcher K, Zhu W, Pezzotti G (2011) J Eur Ceram Soc 31:2031
10. Liu H, Wang Q, Wu J, Zhang C, Wang J, Tang Y (2008) Seventh international conference on photonics and imaging in biology and medicine

11. Freihofer G, Schulzgen A, Raghavan S (2014) Acta Mater 81:211
12. Munisso MC, Yano S, Zhu W, Pezzotti G (2008) Continuum Mech Thermodyn 20:123
13. Pezzotti G (1999) J Raman Spectrosc 30:867
14. Raghavan S, Imbrie PK (2009) Am Ceram Soc 11(11):1
15. Raghavan S, Imbrie P (2008) Proceedings of the materials science and technology 2008 conference, Pittsburgh, PA
16. Lipkin D, Clarke D (1996) Oxid Met 45:267
17. Burris DL, Sawyer WG (2006) Wear 260(7):915
18. Withey PA, Vemuru VSM, Bachilo SM, Nagarajaiah S, Weisman RB (2012) Nano Lett 12(7):34970
19. Lee MY, Ahn SK, Montgomery ST (2006) Statistical analysis of compositional factors affecting the compressive strength of alumina-loaded epoxy. Technical report, SANDIA National laboratories
20. Setchell RE, Anderson MU, Montgomery ST (2007) J Appl Phys 101:083527
21. Millett JCF, Deas D, Bourne NK, Montgomery ST (2007) J Appl Phys 102:063518
22. Song B, Chen W, Montgomery S, Forrestal M (2009) J Compos Mater 43:1519
23. Siegel R, Chang S, Ash B, Stone J, Ajayan P, Doremus R, Schadler L (2001) Scripta Mater 44:2061–2064
24. Derby B (1998) Curr Opinion Solid State Mater Sci 3:490
25. Suraj RPS, Zunjarrao C (2006) Compos Sci Technol 66:2296–2305
26. Vaia RA, Maguire JF (2007) Chem Mater 19:2736–2751
27. Millett JCF, Bourne NK, Deas D (2005) J Phys D Appl Phys 38:930
28. Marur P, Batra R, Garcia G, Loos A (2004) J Mater Sci 39(4):1437
29. Ji QL, Zhang MQ, Rong MZ, Wetzel B, Friedrich K (2004) J Mater Sci 39(21):6487
30. Sawyer WG, Freudenberg KD, Bhimaraj P, Schadler LS (2003) Wear 254:573
31. Shao X, Xue Q, Liu W, Teng M, Liu H, Tao X (2005) J Appl Polym Sci 95(5):993
32. Chen B (2004) Encyclopedia of nanoscience and nanotechnology. Dekker, New York
33. Zunjarrao SC, Singh RP (2006) Compos Sci Technol 66(13):2296
34. Cho J, Joshi M, Sun C (2006) Compos Sci Technol 66:1941
35. Douce J, Boilot JP, Biteau J, Scodellaro L, Jimenez A (2004) Thin Solid Films 466(1):114
36. Lim S, Zeng K, He C (2010) Mater Sci Eng A 527(21):5670
37. Stevenson A, Jones A, Raghavan S (2011) Polymer 43:923
38. Beyerlein IJ, Amer MS, Schadler LS, Phoenix SL (2011) Sci Eng Compos Mater 7(1–2):151
39. Ravichandran G, Subhash G (1995) lnt J Solids Struct 32:2627
40. Lankford J (1977) J Mater Sci 12:791
41. Lankford J, Predebon W, Staehler J, Subhash G, Pletka B, Anderson C (1998) Mech Mater 29:205
42. Eshelby R (1957) Proc R Soc Lond A241:376
43. Mori T, Tanaka K (1973) Acta Metall 21(5):571
44. Freihofer G (2014) Nanocomposite coating mechanics via piezospectroscopy. PhD thesis, University of Central Florida
45. Hallett SR, Green BG, Jiang WG, Cheung KH, Wisnom MR (2009) Int J Fract 158:169
46. Freihofer G, Dustin J, Tat H, Schlzgen A, Raghavan S (2015) AIP Adv 5:037139
47. Freihofer G, Schülzgen A, Raghavan S (2015) Damage mapping with a degrading elastic modulus using piezospectroscopic coatings. NDT E Int 75:65–71
48. Freihofer G, Bullock A, Vaughn F, Tat H, Dustin J, Schülzgen A, Raghavan S (2014) Proceeding of the society for the advancement of material and process engineering 2014 conference, Seattle, WA
49. Camanho PP, Maimí P, Davila C (2007) Compos Sci Technol 67(13):2715
50. Vinogradov V, Hashin Z (2005) Int J Solids Struct 42:365
51. Mollenhauer D, Iarve E, Kim R, Langley B (2006) Compos A Appl Sci Manuf 37:282
52. Hanhan I, Durnberg E, Freihofer G, Akin P, Raghavan S (2014) J Instrum 9, P11005

Chapter 5
Smart Polymer Surfaces

Juan Rodríguez-Hernández

Abstract The preparation of smart surfaces (i.e., surfaces exhibiting switchable and a priori contradictory properties) has been extensively pursued during the last decade. Their unique adaptability by property variation as a function of environmental changes has found multiple industrial applications in fields including sensing and diagnosis or in the biomedical field to promote, for instance, cell and tissue engineering. This chapter will provide an overview of the main strategies reported to produce adaptive surfaces depending on the external stimuli employed to vary reversibly the surface properties. The variation of the surface topography at the micro- and nanopatterned interfaces will be described as an additional tool to significantly alter the final surface properties. Differentiation will be provided between the methodologies to prepare patterned surfaces as a function of their final resolution. Finally, some of the applications will be highlighted in which smart polymer surfaces have been applied including wettability, biomedical purposes, sensing, or smart adhesion.

Keywords Polymer surfaces • Smart interfaces • Micro-/nanopatterned surfaces • Stimulus responsive

5.1   Introduction to Smart Polymer Surfaces

Smart polymer surfaces, also recognized under different names including stimulus-responsive surfaces and adaptive or intelligent surfaces, refer to those interfaces capable of undergoing reversible switchable transitions [1, 2]. The reversible transitions observed in these interfaces are associated to environmental changes such as pH, temperature, or conductivity. Surfaces with a priori antagonistic behaviors that can be changed in an accurate and predictable fashion have increasingly received attention due to the novel requirements to advanced materials. In particular, such

J. Rodríguez-Hernández (✉)
Institute of Polymer Science and Technology (ICTP-CSIC), C/ Juan de la Cierva n3, Madrid 28006, Spain
e-mail: jrodriguez@ictp.csic.es

interfaces may find potential application in the fabrication of micro- and nanofluidic devices, self-cleaning, and antifog surfaces along with sensor devices [3, 4]. In addition, stimulus-responsive surfaces have been employed to "mimic," at least to some extent, biologically occurring processes. More precise examples include the modulation of biological activity, protein immobilization or the control over cell adhesion, and migration processes [1].

5.2   Stimulus-Responsive Polymers

Stimulus-responsive surfaces are created by the immobilization of stimulus-responsive polymers. Stimulus-responsive polymers exhibit fast and large changes on their conformation, charge, or solubility among others as a function of environmental variations such as temperature [5, 6], ionic strength [7], pH [8], electric field [4, 9, 10], light [11–16], or solvent exposure [2, 17, 18]. It is outside of the scope of this chapter to thoroughly revise the existing stimulus-responsive polymers but rather highlight those more extensively employed. Here below a general overview will be provided of the most extended responsive polymers that can be grouped into four different classes: pH-responsive, temperature-responsive, photo-responsive, and bio-responsive polymers. In addition, more complex systems will be presented in which the polymers can respond to more than one stimulus.

pH-sensitive polymers are typically polyelectrolytes that accept or release protons in response to changes in environmental pH. Their side chain acidic or basic groups undergo reversible ionization and as a consequence they can be in a neutral or in a charged state. More importantly, changes between charged and uncharged sate significantly varied the hydrodynamic radius. The positively or negatively charged functional groups along the polymer backbone provoke electrostatic repulsions that result in an increase in the hydrodynamic volume of the polymer.

Thermosensitive polymers exhibit reversible solubility as a result of changes in hydrophobic–hydrophilic balance induced by increasing temperature. Thermoresponsive polymers are typically uncharged polymers capable of forming hydrogen bonds with water molecules. However, upon increasing the temperature, the efficiency of hydrogen bonding between the polymer and water is significantly reduced. In this situation, a phase transition is observed in which the polymer changes from a hydrophilic state to a hydrophobic sate. In fact, above this critical temperature, referred to as lower critical solution temperature (LCST), the polymer dehydrates and aggregates. The phase separation is completely reversible and the smart polymer dissolves in water when the temperature is reduced below the transition temperature. Three families of thermosensitive smart polymers are widely studied and used. First of all, poly(N-alkyl-substituted acrylamides) and the most well known of them, poly(N-isopropyl acrylamide), have a transition temperature of 32 °C (depending on the polymer's molecular weight) [19–24]. The second example of these polymers is oligo(ethylene glycol) methacrylate (OEGMA) derivatives [25–29]. Finally, elastin-like polypeptides (ELP) are also among the most studied

thermoresponsive systems [30, 31]. These linear polypeptides are composed of repeating units of the pentapeptide valine-proline-glycine-X-glycine (with X corresponding to any amino acid, except proline).

More recently other polymers with an upper critical solution temperature (UCST) have been equally described. For instance, poly[2-(methacryloyloxy)ethyl]-dimethyl(3-sulfopropyl) ammonium hydroxide (PMEDSAH) has been reported by Azzaroni et al. [32]. This polymer forms zwitterionic PMEDSAH brushes with a particular complex temperature behavior that depends, among others, on PMEDSAH's molecular weight and various inter- and intra-chain-associated states.

"Photochemical stimuli" are potentially very useful in generating responsive systems. Photosensitive polymers react to light in different ways such as isomerization, elimination, photosensitization, and local heating [3]. An illustrative example of the complexity and degree of sophistication of multiresponsive systems has been reported by Sumaru et al. [33] where polymers possessing switchable properties via photochemical stimulation were prepared. These said materials were developed from the derivation of the thermally responsive *N*-isopropyl acrylamide copolymer alongside a spirobenzopyran that was functionalized with acrylamide as can be seen in Fig. 5.1. The resulting system merged to form a thermo/photo-responsive polymer that, when irradiated or exposed to changes in temperature and pH, interconverted between two forms (neutral and zwitterionic).
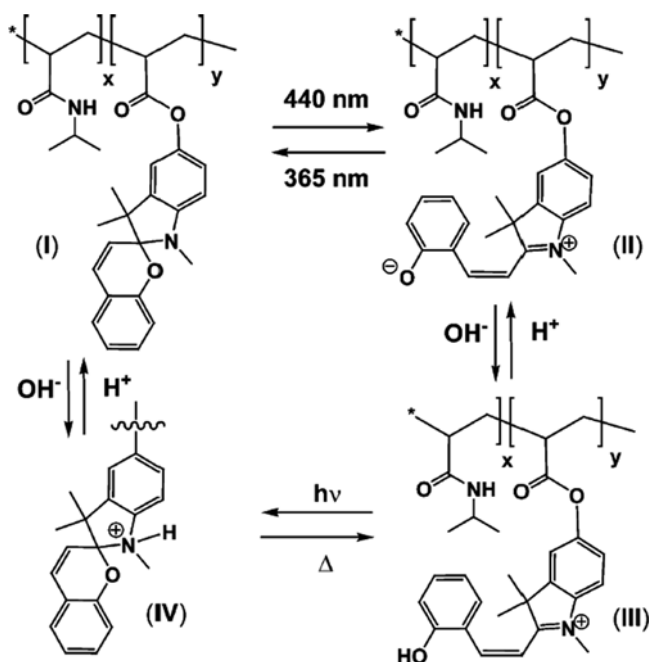
Fig. 5.1 Photochemically switchable polymers as prepared by Sumaru et al. [33], with proposed neutral, zwitterionic, and ionic states (I–IV)

Some polymers are able to respond to static *electric field*s. In general, the wettability of different polymer films in water increases by increasing the voltage between the water and an electrode placed below the polymer film. One of the pioneering studies was carried out by Berge et al. who used poly(ethylene terephthalate) and observed a decrease on the contact angle up to 30° by applying high voltages [34]. More sophisticated systems reported translocation of molecules upon reduction/oxidation resulting in the control of the reversible hydrophilic and hydrophobic properties of the surface [10].

5.3 Modified Polymer Surfaces: Smart Interfaces

A large variety of synthetic strategies have been developed for the fabrication of smart polymer surfaces. Examples of these procedures include the use of physisorption of copolymers either on an inorganic support or produced by surface segregation/surface rearrangement at polymer surfaces or by using grafting approaches [35].

As a function of the type of polymer immobilized, surfaces with variable surface responsiveness can be fabricated. Herein, the main types of responsive surfaces as a function of the stimulus will be summarized.

5.3.1 pH- and Temperature-Responsive Surfaces

pH-responsive surfaces have typically been prepared by surface immobilization of polyacids or polybases. Examples of these include poly(acrylic acid) or poly(methacrylic acid) for polyacids [36] and poly(N,N′-dimethylaminoethyl methacrylate) (PDMAEMA), poly(N,N′-diethylaminoethyl methacrylate) (PDEAEMA), or poly(4- or 2-vinylpyridine) (P4VP or P2VP) as polybases. A recent example of pH-responsive surfaces has been reported by Chen and coworkers [37]. They immobilized poly(2-dimethylaminoethyl methacrylate) (PDMAEMA) brushes and gold nanoparticles (AuNPs) and evaluated the potential use of these surfaces as pH nanosensors. Based on the pH-induced swelling–deswelling of polymer brushes, they reported the variation of the optical properties of PDMAEMA–AuNP nanoassemblies (Fig. 5.2).

Equally, temperature-responsive surfaces have been typically fabricated using polymer brushes either with LCST or UCST properties. A large number of examples have been reported in the literature in this area. Selected examples include the work of Fu et al. [38] who fabricated a dynamic superhydrophobic/superhydrophilic surface. For this purpose, they synthesized a PNIPAAm brush on a nanoporous anodic aluminum oxide surface. In a similar context of control over the surface wettability, Sun et al. [39] grafted thermally responsive PNIPAAm brushes on both a flat and a rough silicon substrate. In this case a reversible, thermoresponsive system switching between superhydrophilic and superhydrophobic states was accomplished, supported by the microscopic roughness of the substrate. Similarly, the immobilization of thermoresponsive polymers on surfaces has been employed by Yamato et al. [40] to facilitate patterned cell seeding and coculture.
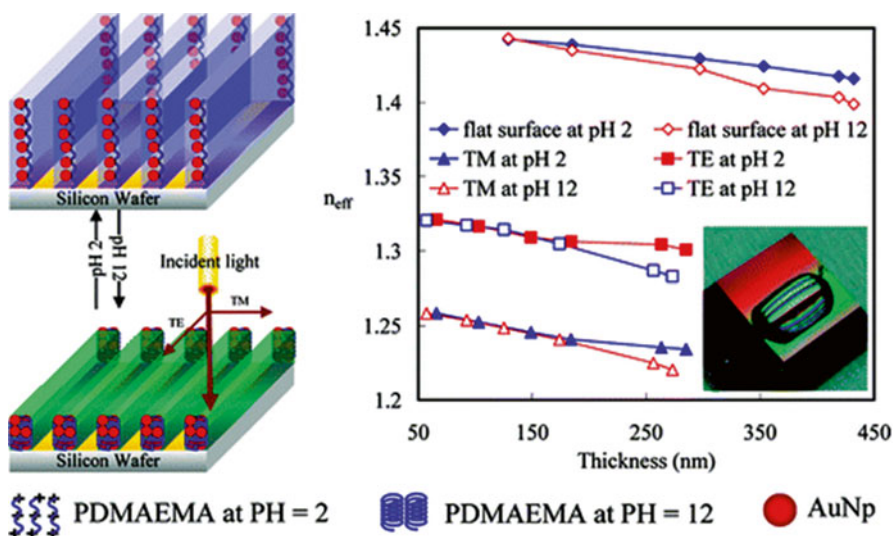
Fig. 5.2 pH dependence of the flat PDMAEMA–AuNP nanoassemblies and its OPRG in terms of refractive indices for TM and TE polarization with various thicknesses. Inserted is the photographic image of WCA along with TM and TE directions on OPRG of the PDMAEMA brushes with 284 nm thickness after aqueous solution treatment at pH 2. Reproduced with permission from [37]

5.3.2 Photo-responsive Surfaces

Azobenzenes [41] and spiropyrans [42] are among the most extended molecules incorporated onto polymers to induce light responsiveness. Photo-responsive polymers react to light in different ways following photoisomerization, photoreaction, reversible ionic dissociation, or the addition–fragmentation processes. These, in turn, have associated different chain movements such as twisting, rotation, or oscillations. As a result, macroscopic properties can be modulated depending on the exposure or lack thereof to light. As an example of this behavior, Athanassiou et al. [43] investigated the wettability of photochromic spiropyran-doped polymeric surfaces. In the study, the team witnessed that irradiation via UV lasers augmented the hydrophilic properties as conversion to polar merocyanine isomers from nonpolar spiropyran molecules took place. It was also found that the process is completely reversible with irradiation provided from a green laser.

5.3.3 Electroactive Interfaces

In some cases environmental changes such as pH or temperature could inflict undesired consequences on the morphology of the material. An interesting approach to induce dynamic changes on polymeric surfaces concerns the use of electroactive polymers. In this case, the environment remains unaltered (e.g., solvent, electrolyte
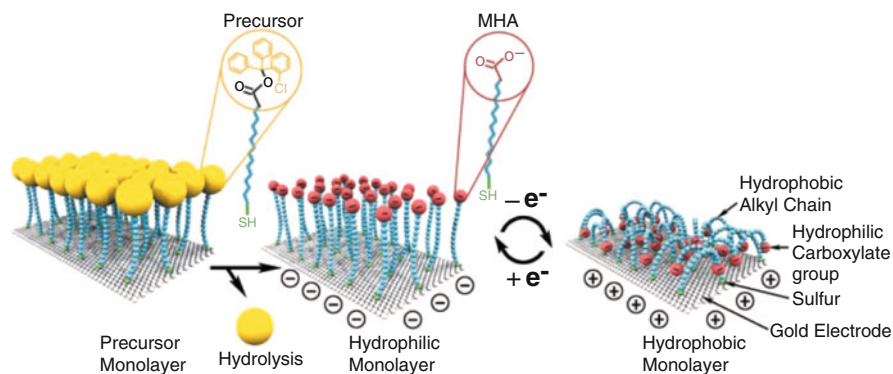
Fig. 5.3 Schematic representation of the transition between *straight* (hydrophilic) and *bent* (hydrophobic) molecular conformations. The precursor molecule MHAE, characterized by a bulky end group and a thiol head group, was synthesized from MHA by introducing the (2-chlorophenyl) diphenylmethyl ester group [9]

content, pH, temperature, and pressure). Reversible changes of electric potential have been employed by Lahann et al. [9] to produce dynamic changes on the surface wettability. For that purpose, the authors prepared a single layer of (16-mercapto) hexadecanoic acid (MHA). This molecule self-assembled as a single layer on gold with a carboxylate group (hydrophilic) capping the chain (hydrophobic), enabling the possibility for total system surface property alteration. Further, the molecules in question morphed from a hydrophobic to a hydrophilic state via the conformational transitions that took place (Fig. 5.3).

5.3.4 Solvent- and Environment-Responsive Interfaces

Switching of the conformation of surface-grafted polymer chains, essentially the surface properties can be accomplished by varying the solvent employed or the environment of exposure. An interesting example was reported by Chen et al. [44, 45]. This group described a methodology for generating multiple patterns of polymeric brushes via an immersion in a graft polymerization/solvent bath. Specifically, PMMA brushes were utilized with their pattern variations observed when treated with both poor and excellent solvents. Solvent quality was found to be the determining factor in the conformational transitions of the polymeric system due in part to their solvent responsiveness. The use of self-assembled block copolymers [17] may additionally produce not only variations on the thickness of the polymer layer but drastically modify the surface structure observed as depicted in Fig. 5.4.

Surface reorganization occurs when the environment of exposure is modified [38, 39, 46, 47]. This phenomenon can be observed not only in functional and block copolymers but also in polymer blends and is driven by the difference in the surface energies of the components. When in contact with air, the low surface energy groups are
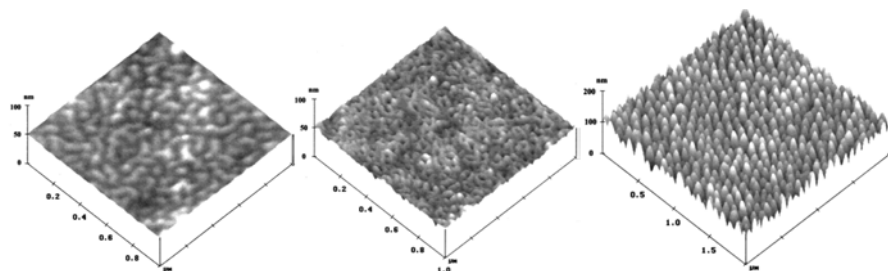
Fig. 5.4 AFM image of the tethered PS-*b*-PMMA brushes with 23 nm-thick PS layer and 14 nm-thick PMMA layer after. *Left*: treatment with CH₂Cl₂ at room temperature for 30 min and drying with a clean air stream. *Center*: after treatment with cyclohexane at 35 °C for 1 h and drying with a clean air stream. *Right*: after treatment with mixture of CH₂Cl₂ and cyclohexane and % of cyclohexane gradually increased [17]

located at the surface. For instance, in the case of block copolymers, microphase separation into alternating lamellae of the blocks may occur [47]. Substitution of the air with water vapor significantly alters the hydrophilicity of the environment and favors the surface reconstruction, placing the hydrophilic groups in contact with the surface.

5.3.5 *Multiresponsive Interfaces*

The examples mentioned above can produce reversible changes but are responsive exclusively to one kind of stimuli. More recent efforts have been focused on the design of interfaces able to simultaneously respond to more than one stimulus [35, 48, 49]. One of the first examples of multiresponsive surfaces was reported by Jiang and coworkers[50]. This group reported the preparation of a dual stimulus-responsive surface (temperature and pH) with tunable wettability along with reversible switching between superhydrophilicity and superhydrophobicity (Fig. 5.5). Such surfaces were obtained by fabricating a microstructured poly(N-isopropyl acrylamide-co-acrylic acid) [P(NIPAAm-co-AAc)] copolymer thin film.

Other combinations of stimuli to produce multi-stimulus-responsive surfaces have been also reported including the work of Stayton and coworkers [51] using temperature- and photochemically responsive polymers or the work of Xia et al. [52] who used a block copolymer comprised of a pH-/glucose- and a temperature-sensitive block. For instance, Stayton et al. [51] synthesized via conjugation a switchable (thermal/photochemical) azopolymer (poly(*N*,*N*′-dimethylacrylamide)-*co*-4-phenylazophenyl acrylate) to an engineered cysteine-containing endoglucanase enzyme. The resulting system exhibited opposing responses depending on the stimulus used to activate the "switch" (thermal versus UV–vis). The polymer–endoglucanase conjugate was active in glycoside hydrolase activity against *o*-nitrophenyl-D-cellobioside (ONPC) under UV irradiation at 350 nm but inactive for glycoside hydrolysis at higher wavelengths (420 nm). A related azopolymer–enzyme conjugate, poly((*N*,*N*′-dimethylacrylamide)-
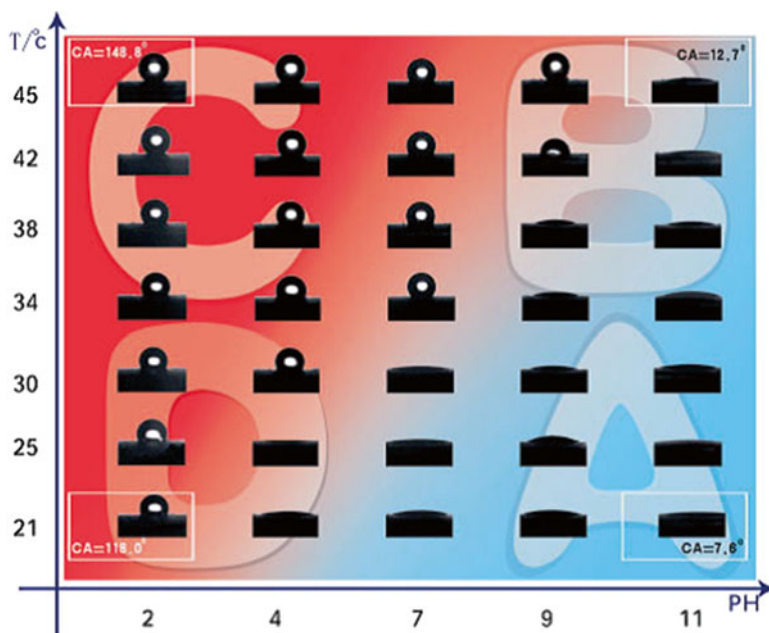
Fig. 5.5 The contact angle varies reversibly, as depicted in the four different regions A to D, depending both on the pH and temperature

co-4-phenylazophenyl acrylamide)-graft-endoglucanase, was active under longer wavelength light but inactive under irradiation at 350 nm. The variation in the responses is due in part to the changing polarity/dipole moments preceding the photo-induced trans–cis azobenzene isomerization.

5.4 Patterned Responsive Surfaces: Micro- and Nanometer-Scale Topography

Micro- and nanostructuring of polymer surfaces has been developed in parallel to surface functionalization strategies and provides together new tools to researches for the preparation of surfaces with more sophisticated features. As an example, cell proliferation, differentiation, migration, or apoptosis is governed by chemical surface cues placed in precise positions [53]. Moreover, the response of surfaces to external stimuli may be enhanced by surface structuring [50]. Many different patterning alternatives are available nowadays to prepare structured interfaces with micro- to nanometer-scale moieties. The most extended methodologies include soft lithography (including microcontact printing), photolithography, ink-jet printing, or more sophisticated and higher resolution techniques such as laser-guided writing, block copolymer self-assembly, or scanning probe lithography [53, 54].
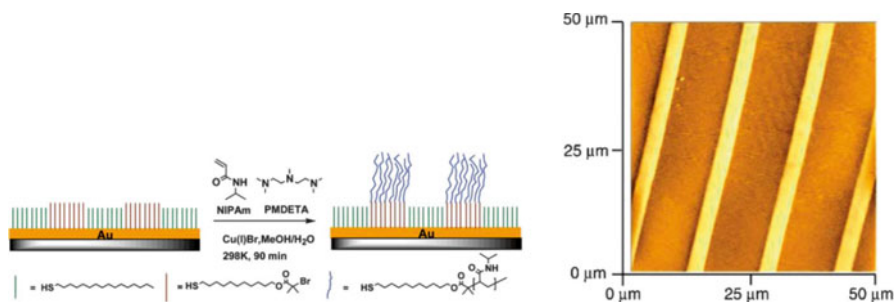
Fig. 5.6 Microcontact printing of gold surfaces and surface-initiated ATRP of N-isopropyl acrylamide [20]

Microcontact printing has been extensively employed to precisely place stimulus-responsive polymers on surfaces. An illustrative example is depicted in Fig. 5.6 where the immobilization of poly(N-isopropyl acrylamide) within micropatterned domains is shown. Their strategy involves two steps in which the 3-aminopropyltriethoxysilane (APTES) is immobilized onto silica surfaces and then the thermoresponsive polymer is grafted to APTES-functionalized surfaces by carbodiimide-mediated coupling. More importantly, according to this study, the changes on the surface properties, driven by temperature, play a key role on the adhesion of model proteins as well as bacteria [20].

Patterns of higher resolution, down to their nanometer-size features, can be obtained by using other techniques such as scanning probe lithography (SPL) [21] or block copolymer self-assembly [36]. Stimulus-responsive, surface-confined poly(*N*-isopropyl acrylamide) (PNIPAAm) brush nanopatterns were prepared on gold-coated silicon substrates in a "grafting-from" approach that combines "nanoshaving," a scanning probe lithography method, with surface-initiated polymerization using atom transfer radical polymerization (ATRP). The reversible, stimulus-responsive conformational height change of these nanopatterned polymer brushes was demonstrated by inverse transition cycling in water and water/methanol mixtures (1:1, v:v). The study's findings are consistent with the behavior of laterally confined and covalently attached polymer chains, where chain mobility is restricted largely to the out-of-plane direction. This nanofabrication approach is generic and can likely be extended to a wide range of vinyl monomers [21].

As an alternative to the use of sophisticated patterning techniques, several groups have employed self-assembling block copolymers to produce nanostructured surfaces [55, 56]. Within this context, Bousquet et al. [36] reported the preparation of stimulus-responsive surfaces produced by surface segregation of block copolymer micelles. The design is based on homopolymer/block copolymer blends. The block copolymer employed, PS-b-PAA, migrates toward the interface upon water vapor annealing and produced two different nanometer-size structures (hills or holes) depending on the pH (Fig. 5.7).
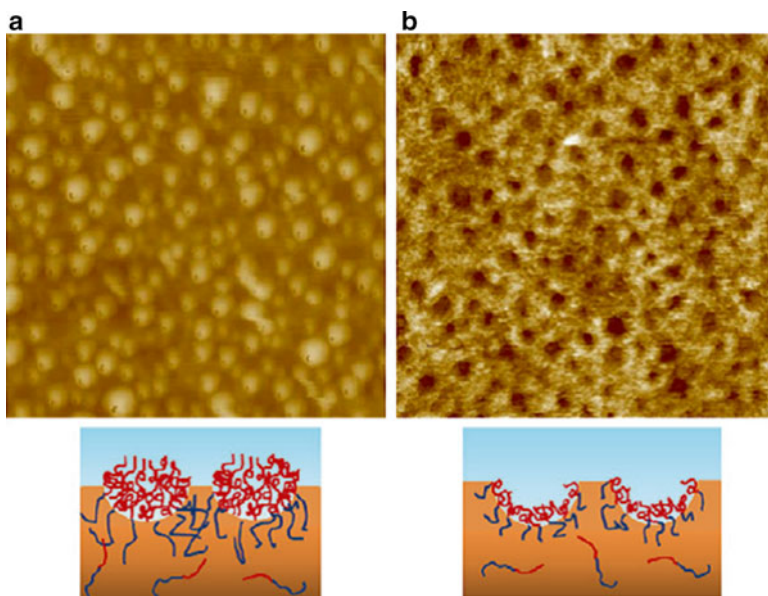
Fig. 5.7 AFM images of polymer blends having 20 % of a diblock copolymer and 80 % of polystyrene taken at (**a**) basic pH and (**b**) acid pH. The diblock copolymer employed was asymmetric PS_{49}-b-PAA_{17} [36]

5.5 Applications of Smart Polymer Surfaces

Smart polymer surfaces have found potential applications in many different fields. Herein, this discussion will be limited to some of the following selected examples.

5.5.1 Controlled Wettability

Surface wettability control is among the most sought after applications of polymer surfaces. Light-responsive [11, 12] or pH- and thermally responsive [6] polymers have been largely investigated for this purpose. Sun et al. [6] explored the role of the roughness-enhanced thermally responsive wettability of a poly(N-isopropyl acrylamide) (PNIPAAm)-modified surface. Most notably, reversible switching between superhydrophilicity and superhydrophobicity in a system is possible within a tight thermal span of approximately 10 °C, due to the surface chemical composition's synergistic effect as well as its roughness (Fig. 5.8).

Light can be equally employed to induce changes on the surface wettability and can even direct the movement of water droplets. A totally synthetic molecular system was created by Berna et al. [15] in which external energy (light) is converted into biased Brownian motion, capable of moving macroscopic loads and completing
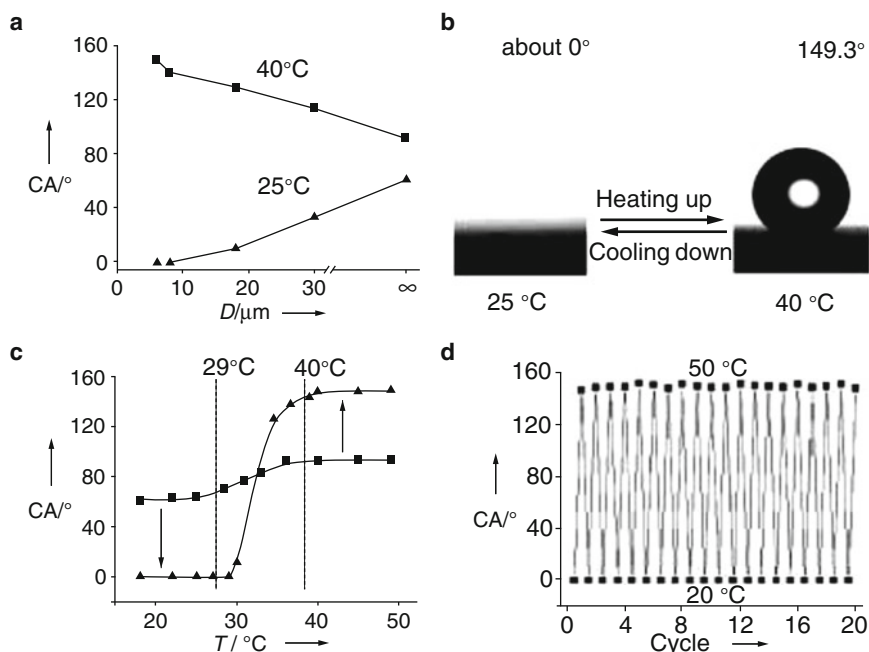
Fig. 5.8 Surface roughness-enhanced wettability of a PNIPAAm-modified surface. (**a**) The relationships between groove spacing (D) of rough surfaces and the water CAs at low temperature (*triangles*, 25 °C) and at high temperature (*squares*, 40 °C). The groove spacing of ¥ represents flat substrate. (**b**) Water drop profile for thermally responsive switching between superhydrophilicity and superhydrophobicity of a PNIPAAm-modified rough surface with groove spacing of about 6 mm, at 25 °C and 40 °C. The water CAs are about 0° and 149.3±2.5°, respectively. (**c**) Temperature (T) dependences of water CAs for PNIPAAm thin films on a rough substrate with groove spacing of about 6 μm (*triangles*) and on flat substrate (*squares*). (**d**) Water CA at two different temperatures for a PNIPAAm-modified rough substrate with groove spacing of 6 μm. Half cycles, 20 °C, and integral cycles, 50 °C [6]

quantifiable work. The millimeter-scale surface movement of a liquid is achieved through biased Brownian motion of stimulus-responsive rotaxanes ("molecular shuttles") that either reveal or hide fluoroalkane residues, thereby modifying its surface tension. The collaborative working of a molecular shuttle monolayer is enough to fuel a diiodomethane microliter droplet's travel up an incline of 12°.

5.5.2 Bio-related Applications

Surface modifications incorporating temperature-responsive polymers have been carried out in order to immobilize specific molecules or to manipulate cell sheets in tissue engineering processes [1]. In this sense, the application of temperature-responsive polymers to modified surfaces exploits the fact that most proteins show

significantly greater adsorption on hydrophobic surfaces than in hydrophilic ones. Above the LCST, the polymer will adsorb peptides and proteins from a solution, and these biomolecules can be desorbed by decreasing the temperature as has been done in chromatographic supports incorporating PNIPAAm while using water as an eluent [49].

Tissue engineering applications have also been explored mainly using thermoresponsive polymers [57–59]. Typically, mammalian cells are cultivated on hydrophobic solid culture dishes and are usually detached from it by protease treatment. This treatment is inefficient since it causes damage of the cells. However, the change in surface properties of the thermoresponsive polymers, from hydrophobicity displayed above the critical temperature to hydrophilicity shown below it, has been used in tissue culture applications. The surface of tissue cultured with polystyrene grafted with PNIPAAm allows cells to adhere and proliferate above the LCST of the polymer whereas cell detachment was detected at temperatures below LCST [40]. Indeed, at temperatures above the LCST [around 37 °C, for a substrate surface coated with grafted poly(N-isopropyl acrylamide)], the surface is hydrophobic because this temperature is above the critical temperature of the polymer and the cells grow well. However, when the temperature is decreased to 20 °C, this results in the surface becoming hydrophilic, allowing the cells to be easily detached without any damage while maintaining the cell–cell junction. Similar strategies have been proposed to control the adhesion of microorganisms to synthetic surfaces [48].

5.5.3 Sensors

The surface changes associated to external stimulus can also be employed for the design of biosensors. Particularly interesting are those systems sensitive to important biomolecules. Among the pioneering studies [60, 61] was the immobilization of glucose oxidase onto a porous polycarbonate membrane with a grafted pH-responsive poly(acrylic acid) (PAA) layer. Densely charged PAA polymer chains were observed in a neutral pH environment and displayed an extended conformation. In this situation, the pores of the membrane are blocked, preventing insulin transport. Upon exposure to glucose, the pH decreases and the polymer chains become protonated and adopt a more compact conformation. Further, pore blockage is reduced and insulin is transported through the membranes.

Optical sensors have been also developed using similar strategies [62]. For instance, Chen et al. [37] synthesized silicon wafers containing well-defined PDMAEMA and described PDMAEMA chains immobilizing AuNPs onto macroscopic surfaces through pH-responsive polymer brush exploitation. Control of the mean refractive index (RI) of the PDMAEMA–AuNP nanoassemblies is possible via the one-dimensional periodic relief grating (OPRG) structure's filling factors, thus creating the desired stimulus-induced RI distribution for the polymer brush–gold OPRG. Such were used for the fabrication of pH nanosensors which were composed of PDMAEMA–AuNP nanoassemblies and its binary gratings through the

exploitation of the swelling–deswelling capabilities of the pH-responsive polymer brushes alongside PDMAEMA–AuNP nanoassemblies' tunable optical properties.

5.5.4   Smart Adhesives

Reversible adhesives have been developed for industrial, consumer, and military settings. These systems have been studied based on spreading velocity of liquids on a liquid crystalline polymeric surface's liquid spreading velocity, which is extremely sensitive to minute thermal variations. Crevoisier et al. [5] detected a sharp change in rigidity (stiff to soft) as well as tackiness of the liquid crystalline polymer when observing its bulk transition between a highly ordered smectic and an isotropic phase. Today, light-switchable adhesives are commercially available and have been demonstrated their practicality within the paper, graphical, and electronic industries. Furthermore, they can find uses as tapes within industry, as adhesive foils that de-bond when required, or for products that require skin friendly removal [63].

5.6   Conclusion and Future Outlook

This chapter provides, through selected examples, a general overview over stimulus-responsive polymers and their use to prepare smart interfaces. This chapter reviewed the most extended strategies employed to prepare surfaces so as to modify their properties as a function of a particular external stimulus. Moreover, the control over their surface distribution can additionally enhance the variations of the surface properties. The main strategies to produce micro- and nanostructured interfaces have been equally introduced. Finally, this chapter concludes with the main areas in which stimulus-responsive surfaces have introduced significant advantages over previous polymeric systems.

References

1. Mendes PM (2008) Stimuli-responsive surfaces for bio-applications. Chem Soc Rev 37(11):2512–2529
2. Motornov M, Minko S, Eichhorn KJ, Nitsche M, Simon F, Stamm M (2003) Reversible tuning of wetting behavior of polymer surface with responsive polymer brushes. Langmuir 19(19):8077–8085
3. Alexander C, Shakesheff KM (2006) Responsive polymers at the biology/materials science interface. Adv Mater 18(24):3321–3328
4. Gras SL, Mahmud T, Rosengarten G, Mitchell A, Kalantar-Zadeh K (2007) Intelligent control of surface hydrophobicity. Chem Phys Chem 8(14):2036–2050
5. Crevoisier GB, Fabre P, Corpart JM, Leibler L (1999) Switchable tackiness and wettability of a liquid crystalline polymer. Science 285(5431):1246–1249

6. Sun TL, Wang G, Feng L, Liu B, Ma Y, Jiang L, Zhu D (2004) Reversible switching between superhydrophilicity and superhydrophobicity. Angew Chem Int Ed 43(3):357–360

7. Kontturi K, Mafé S, Manzanares JA, Svarfvar BL, Viinikka P (1996) Modeling of the salt and pH effects on the permeability of grafted porous membranes. Macromolecules 29(17):5740–5746

8. Wilson MD, Whitesides GM (1988) The anthranilate amide of polyethylene carboxylic-acid shows an exceptionally large change with ph in its wettability by water. J Am Chem Soc 110(26):8718–8719

9. Lahann J, Mitragotri S, Tran TN, Kaido H, Sundaram J, Choi IS, Hoffer S, Somorjai GA, Langer R (2003) A reversibly switching surface. Science 299:371–374

10. Katz E, Lioubashevsky O, Willner I (2004) Electromechanics of a redox-active rotaxane in a monolayer assembly on an electrode. J Am Chem Soc 126(47):15520–15532

11. Ichimura K, Oh SK, Nakagawa M (2000) Light-driven motion of liquids on a photoresponsive surface. Science 288:1624–1626

12. Feng CL, Jin J, Zhang YJ, Song YL, Xie L, Qu GR, Xu Y, Jiang L (2001) Reversible light-induced wettability of fluorine-containing azobenzene-derived Langmuir-Blodgett films. Surf Interface Anal 32(1):121–124

13. Raduge C, Papastavrou G, Kurth DG, Motschmann H (2003) Controlling wettability by light: illuminating the molecular mechanism. Eur Phys J E 10(2):103–114

14. Cooper CG, MacDonald JC, Soto E, McGimpsey WG (2004) Noncovalent assembly of a photoswitchable surface. J Am Chem Soc 126(4):1032–1033

15. Berna J, Leigh DA, Lubomska M, Mendoza SM, Pérez EM, Rudolf P, Teobaldi G, Zerbetto F (2005) Macroscopic transport by synthetic molecular machines. Nat Mater 4(9):704–710

16. Jiang WH, Wang G, He Y, Wang X, An Y, Songa Y, Jiang L (2005) Photoswitched wettability on an electrostatic self-assembly azobenzene monolayer. Chem Commun 28:3550–3552

17. Zhao B, Brittain WJ, Zhou W, Cheng SZD (2000) Nanopattern formation from tethered PS-b-PMMA brushes upon treatment with selective solvents. J Am Chem Soc 122(10):2407–2408

18. Julthongpiput D, Lin YH, Teng J, Zubarev ER, Tsukruk VV (2003) Yshaped amphiphilic brushes with switchable micellar surface structures. J Am Chem Soc 125(51):15912–15921

19. Berndt E, Ulbricht M (2009) Synthesis of block copolymers for surface functionalization with stimuli-responsive macromolecules. Polymer 50(22):5181–5191

20. Alarcon CDH, Farhan T, Osborne L, Huck WTS, Alexander C (2005) Bioadhesion at micro-patterned stimuli-responsive polymer brushes. J Mater Chem 15(21):2089–2094

21. Kaholek M, Lee W-K, LaMattina B, Caster KC, Zauscher S (2004) Fabrication of stimulus-responsive nanopatterned polymer brushes by scanning-probe lithography. Nano Lett 4(2):373–376

22. Matsuda N, Yamato M, Okano T (2007) Tissue engineering based on cell sheet technology. Adv Mater 19(20):3089–3099

23. Mizutani A, Kikuchi A, Yamato M, Kanazawaa H, Okano T (2008) Preparation of thermoresponsive polymer brush surfaces and their interaction with cells. Biomaterials 29(13):2073–2081

24. Ernst O, Lieske A, Holländer A, Lankenau A, Duschl C (2008) Tuning of thermo-responsive self-assembly monolayers on gold for cell-type-specific control of adhesion. Langmuir 24(18):10259–10264

25. Yamamoto S, Pietrasik J, Matyjaszewski K (2007) ATRP synthesis of thermally responsive molecular brushes from oligo(ethylene oxide) methacrylates. Macromolecules 40(26):9348–9353

26. Lutz J-F, Andrieu J, Üzgün S, Rudolph C, Agarwal S (2007) Biocompatible, thermoresponsive, and biodegradable: simple preparation of "all-in-one" biorelevant polymers. Macromolecules 40(24):8540–8543

27. Lutz J-F, Weichenhan K, Akdemir Ö, Hoth A (2007) About the phase transitions in aqueous solutions of thermoresponsive copolymers and hydrogels based on 2-(2-methoxyethoxy)ethyl methacrylate and oligo(ethylene glycol) methacrylate. Macromolecules 40(7):2503–2508

28. Becer CR, Hahn S, Fijten MWM, Thijs HML, Hoogenboom R, Schubert US (2008) Libraries of methacrylic acid and oligo(ethylene glycol) methacrylate copolymers with LCST behavior. J Polym Sci Part A PolymChem 46(21):7138–7147

29. Holder SJ, Durand G, Yeoh C-T, Illi E, Hardy NJ, Richardson TH (2008) The synthesis and self-assembly of aba amphiphilic block copolymers containing styrene and oligo(ethylene glycol) methy ether methacrylate in dilute aqueous solutions: elevated cloud point temperatures for thermoresponsive micelles. J Polym Sci Part A Polym Chem 46(23):7739–7756

30. Meyer DE, Chilkoti A (2004) Quantification of the effects of chain length and concentration on the thermal behavior of elastin-like polypeptides. Biomacromolecules 5(3):846–851

31. Fernandez-Trillo F, van Hest JCM, Thies JC, Michon T, Weberskirch R, Cameron NR (2009) Reversible immobilization onto peg-based emulsion-templated porous polymers by co-assembly of stimuli responsive polymers. Adv Mater 21(1):55–59

32. Azzaroni O, Brown AA, Huck WTS (2006) Wetting transitions of polyzwitterionic brushes driven by self-association. Angew Chem Int Ed 45(11):1770–1774

33. Sumaru K, Kameda M, Kanamori T, Shinbo T (2004) Reversible and efficient proton dissociation of spirobenzopyran-functionalized poly(N-isopropylacrylamide) in aqueous solution triggered by light irradiation and temporary temperature rise. Macromolecules 37(21):7854–7856

34. Vallet M, Berge B, Vovelle L (1996) Electrowetting of water and aqueous solutions on poly(ethylene terephthalate) insulating films. Polymer 37(12):2465–2470

35. Wischerhoff E, Badi N, Laschewsky A, Lutz J-F (2011) Smart polymer surfaces: concepts and applications inbiosciences. In: Börner HG, Lutz J-F (eds) Bioactive surfaces. Springer, Berlin, pp 1–33

36. Rodriguez-Hernandez J, Ibarboure E, Papon E (2011) Surface segregation of polypeptide-based block copolymer micelles: an approach to engineer nanostructured and stimuli responsive surfaces. Eur Polym J 47(11):2063–2068

37. Chen J-K, Pai P-C, Chang J-Y, Fan S-K (2012) pH-responsive one- dimensional periodic relief grating of polymer brush–gold nanoassemblies on silicon surface. ACS Appl Mater Inter 4(4):1935–1947

38. Luzinov I, Minko S, Tsukruk VV (2004) Adaptive and responsive surfaces through controlled reorganization of interfacial polymer layers. Prog Polym Sci 29(7):635–698

39. Bousquet A, Pannier G, Ibarboure E, Papon E, Rodríguez-Hernández J (2007) Control of the surface properties in polymer blends. J Adhes 83(4):335–349

40. Yamato M, Konno C, Utsumi M, Kikuchi A, Okano T (2002) Thermally responsive polymer-grafted surfaces facilitate patterned cell seeding and co-culture. Biomaterials 23(2):561–567

41. Behrendt R, Renner C, Schenk M, Wang F, Wachtveitl J, Oesterhelt D, Moroder L (1999) Photomodulation of the conformation of cyclic peptides with azobenzene moieties in the peptide backbone. Angew Chem Int Ed 38(18):2771–2774

42. Bunker BC, Kim BI, Houston JE, Rosario R, Garcia AA, Hayes M, Gust D, Picraux ST (2003) Direct observation of photo switching in tethered spiropyrans using the interfacial force microscope. Nano Lett 3(12):1723–1727

43. Athanassiou A, Lygeraki MI, Pisignano D, Lakiotaki K, Varda M, Mele E, Fotakis C, Cingolani R, Anastasiadis SH (2006) Photocontrolled variations in the wetting capability of photochromic polymers enhanced by surface nanostructuring. Langmuir 22(5):2329–2333

44. Chen J-K, Hsieh C-Y, Huang C-F, Li P-M, Kuo S-W, Chang F-C (2008) Using solvent immersion to fabricate variably patterned poly(methyl methacrylate) brushes on silicon surfaces. Macromolecules 41(22):8729–8736

45. Chen J-K, Hsieh C-Y, Huang C-F, Li P-M (2009) Characterization of patterned poly(methyl methacrylate) brushes under various structures upon solvent immersion. J Colloid Interface Sci 338(2):428–434

46. Stuart MAC, Huck WTS, Genzer J, Müller M, Ober C, Stamm M, Sukhorukov GB, Szleifer I, Tsukruk VV, Urban M, Winnik F, Zauscher S, Luzinov I, Minko S (2010) Emerging applications of stimuli responsive polymer materials. Nat Mater 9(2):101–113

47. Russell TP (2002) Surface-responsive materials. Science 297(5583):964–967
48. Alarcón CDLH, Twaites B, Cunliffe D, Smith JR, Alexander C (2005) Grafted thermo- and pH responsive co-polymers: surface-properties and bacterial adsorption. Int J Pharm 295(1–2):77–91
49. Nath N, Chilkoti A (2002) Creating "smart" surfaces using stimuli responsive polymers. Adv Mater 14(17):1243–124
50. Xia F, Feng L, Wang S, Sun T, Song W, Jiang W, Jiang L (2006) Dual-responsive surfaces that switch between superhydrophilicity and superhydrophobicity. Adv Mater 18(4):432–436
51. Shimoboji T, Larenas E, Fowler T, Kulkarni S, Hoffman AS, Stayton PS (2002) Photoresponsive polymer-enzyme switches. Proc Natl Acad Sci USA 99(26):16592–16596
52. Xia F, Ge H, Hou Y, Sun T, Chen L, Zhang G, Jiang L (2007) Multiresponsive surfaces change between superhydrophilicity and superhydrophobicity. Adv Mater 19(18):2520–2524
53. Falconnet D, Csucs G, Grandin HM, Textor M (2006) Surface engineering approaches to micropattern surfaces for cell-based assays. Biomaterials 27(16):3044–3063
54. Lupitskyy R, Roiter Y, Tsitsilianis C, Minko S (2005) From smart polymermolecules to responsive nanostructured surfaces. Langmuir 21(19):8591–8593
55. Kim H-C, Hinsberg WD (2008) Surface patterns from block copolymer self-assembly. J Vac Sci Technol A 26(6):1369–1382
56. Park C, Yoon J, Thomas EL (2003) Enabling nanotechnology with self assembled block copolymer patterns. Polymer 44(22):6725–6760
57. Kim YS, Lim JY, Donahue HJ, Lowe TL (2005) Thermoresponsive terpolymeric films applicable for osteoblastic cell growth and noninvasive cell sheet harvesting. Tissue Eng 11(1–2):30–40
58. da Silva RMP, López-Pérez PM, Elvira C, Mano JF, San Román J, Reis RL (2008) Poly(N-Isopropylacrylamide) surface-grafted chitosan membranes as a new substrate for cell sheet engineering and manipulation. Biotechnol Bioeng 101(6):1321–1331
59. An YH, Webb D, Gutowska A, Mironov VA, Friedman RJ (2001) Regaining chondrocyte phenotype in thermosensitive gel culture. Anat Rec 263(4):336–341
60. Casolaro M, Barbucci R (1991) An insulin-releasing system responsive to glucose: thermodynamic evaluation of permeability properties. Int J Artif Organs 14(11):732–738
61. Imanishi Y, Ito Y (1995) Glucose-sensitive insulin-releasing molecular systems. Pure Appl Chem 67(12):2015–2021
62. Ye G, Wang X (2010) Polymer diffraction gratings on stimuli-responsive hydrogel surfaces: soft-lithographic fabrication and optical sensing properties. Sens Actuators B 147(2):707–713
63. http://www.lumina.se/ (Last accessed: May 2015)

Chapter 6
Smart Textile Transducers: Design, Techniques, and Applications

Lina M. Castano and Alison B. Flatau

Abstract Smart textiles are emerging technologies with numerous applications and technical advantages. These are textiles which have undergone alteration in order to be utilized as sensors, actuators, and/or other types of transducers. Sensing and actuation features can be imparted to fabric substrates by applying intelligent coatings such that they will be sensitive and/or reactive to more than one type of stimulus, (e.g., chemical or physical). Smart coating polymers applied to fabrics include inherently conductive, semiconductive, and particle-doped polymers. These coatings can be piezoresistive, magnetoresistive, piezoelectric, photochromic, and sensitive to chemicals, gases, changes in humidity, and temperature, among others. In this chapter, an overview of the smart textile transducer elements, textile platforms, application techniques, and construction methods will be presented. Multiple applications have been inspired by the lightweight and compliant characteristics of smart textiles: industrial (i.e., uniforms), aerospace (i.e., space suit liners), military (i.e., soldier gear), and medical (i.e., patient garments), among others. These applications will define the current development of smart textile technologies and will be further discussed in this chapter. Furthermore, design principles and challenges associated to coating technologies as applied to textiles including surface treatment for strong adhesion, durability, and environmental/mechanical constraints are introduced. Future trends will arise from the integration of novel technologies into portable platforms with intelligent polymer coatings, alongside development of wearable technologies for fast input/data processing and streamlined user interfaces.

Keywords Textile transducers • Polymer transducers • Smart textiles • E-textiles

L.M. Castano (✉) • A.B. Flatau (✉)
Department of Aerospace Engineering, University of Maryland,
College Park, MD 20742, USA
e-mail: linacs@umd.edu; linacastano1@gmail.com; aflatau@umd.edu

6.1 Introduction: Overview of Polymer-Based Textile Transducers

In the era of personalized electronics, textiles have become the perfect platform to integrate new technologies into everyday life. These materials have advantages over conventional electronics and have introduced an entire genre of applications. These range from interfaces with personal electronics to stand-alone soft circuits and are found to be useful in different sectors such as the military, medical, and civilian fields. Seamless integration into daily life is made possible with platforms that can blend into ubiquitous items such as clothing, furniture, and other textile-based articles. This inherent nearness to the subject opens a unique functionality for fabric-based transducers (SFTs). These may be sensors, actuators, batteries, and energy generators, among others.

Textile transducers consist of fabrics which have been modified, altered, or crafted to have transducer capabilities. Sensors, actuators, and other types of transducers can be fully or partially based on textile structures and platforms. Several techniques and materials can be used to bestow transducer qualities onto textiles. Polymers are some of the most useful materials which allow for this functionalization. Textiles can either be coated with or made out of polymers with different types of transducer qualities. For instance, polymers which are sensitive to changes in temperature, humidity, pressure, light, and more can be used to coat fabric substrates of interest or can be extruded into fibers and yarns which can later be used to construct textiles. Textile substrates and structures are the underlying foundation of polymer-based transducers as they determine the mechanical and electrical properties of the resulting transducer, among others [1].

Fabrics are structured fibrous materials which are typically ordered hierarchically in that smaller units make larger units [2]. Fibers, which typically have a high aspect ratio, form larger units which can be yarn or thread. These in turn are interlocked to form fabric surfaces by means of techniques such as knitting or weaving. These larger surfaces can also be compounded to form composite fabrics. Transducer qualities can be introduced at any point of this construction and are not limited to the larger structures but can also be used at lower hierarchical levels. For instance, a polymer-based textile gas sensor would benefit more from coated tufted fibers which have a larger sensing surface as compared to a coated knitted surface. Fabric substrates are typically knitted, woven, nonwoven, tufted, and nets, among others. Each construction has different mechanical properties and therefore different applications. For instance, knits are inherently elastic, whereas weaves are not. Nonwovens may contain additional chemicals and have less available surface for coatings, as they are typically compressed and chemically modified materials. Composite substrates may be useful when forming local electronic components such as fabric capacitors, as well as other types of macro-electronic sensing devices such as tactile sensors.

In addition to the platform considerations at all levels of the fabric construction, composition properties are also a determining factor. Properties of textile fibers may be divided into three groups: geometrical, physical, and chemical. Length, cross-sectional area, and crimp are the three geometrical factors that describe the fiber dimension and

form [3]. The chemical properties of fibers entail resistance to acidic and alkaline environments, reducers, and oxidizers, among others. The polymer chain's organization (i.e., domains that are crystalline or noncrystalline) will dictate the fibers' physical properties [3]. The interactions displayed by interface of the polymer and the surface of the fabric at a molecular level will determine the final properties of a coated transducer [4] as well as one made from the polymer material alone [5]. Chemical as well as physical bonds may be established between polymers and fabrics, depending on the surface chemistry of each. Interactions of textile molecules with the polymer can occur by means of hydrogen bonding, van der Waals forces, or covalent interaction, among others. Natural fibers are made of organic compounds and have different behavior from synthetic fibers. Synthetic fibers are mostly hydrophobic and therefore more mechanically stable; natural fibers however are hydrophilic and therefore less mechanically stable [6]. These factors are very important when considering that most of the polymer-based textile transducers are to be interfaced with telemetry devices or personal electronic devices as well as power sources. Buildup of static charge may also be a concern when dealing not only with electronic devices but also human users. All these factors require consideration when building the textile polymer transducer.

Polymer-based textile sensors can either consist of sensing coatings applied to fabric surfaces or textile structures made out of sensing polymer materials. They can also consist of miniaturized conventional electronics elements (i.e., MEMS), where the sensing polymer has been encapsulated or mounted on textile substrates by e-textile techniques (Fig. 6.1). In particular for sensor applications, the polymers may have different physical or chemical sensing mechanisms. Polymers may be able to sense changes in mechanical pressure, temperature, electric charge, magnetic fields, amount of chemical compounds, and intensity of visible light. The mechanisms for energy transduction and therefore sensing of these parameters may stem from changes in polymer electrical resistance, shape, chemical composition, and color. The sensing mechanisms can be inherent or enabled through chemical and molecular modifications.

Polymer-based textile sensors have many advantages over conventional electronic sensors. Compliant substrates make them adaptable to any shape and surface and make them portable, if some short-range telemetry is used [10]. They can also become a less expensive and ubiquitous alternative. The disadvantages include environmental stability, wear and tear, washability, and encapsulation, as well as data acquisition interfacing.

6.2   Design Principles, Intelligent Polymer/Coating Materials, and Construction Methods

6.2.1   Design Principles

The design of textile transducers needs to start from the end product, application, or goal and then track the necessary elements to make that application possible and realizable. The set of constraints will start from heuristic evaluations and become
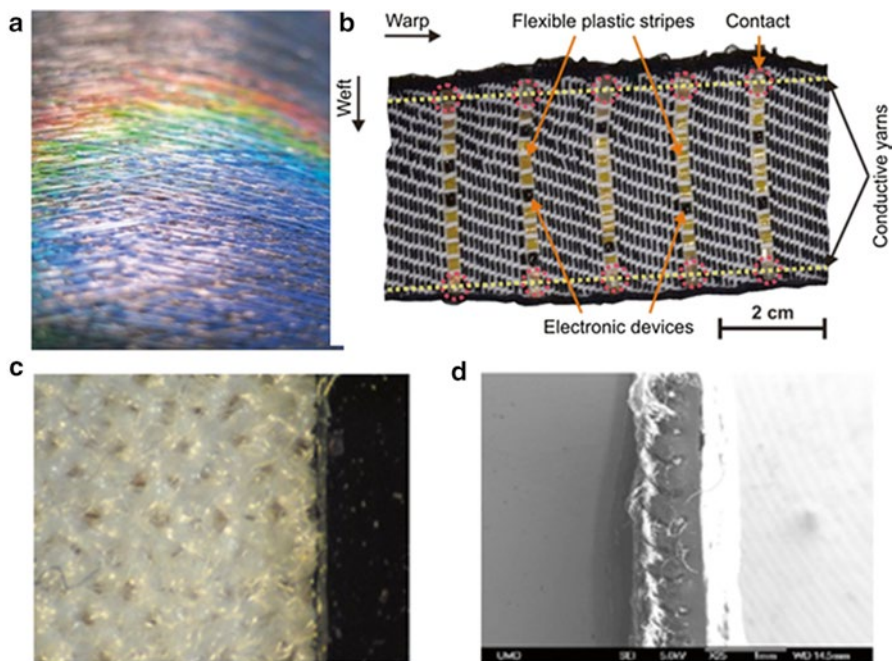
Fig. 6.1 Textile sensors: (**a**) thermochromic sensing fibers, with permission from [7]; (**b**) e-textile sensor, plastic strips host LED sensors, with permission from [8]; (**c**) carbon black-coated knitted fabric [9]; and (**d**) SEM of cross section of an ECP-coated polymer and fabric substrate [9]

more deterministic as the design process moves forward. This approach is rather different from conventional sensor and PCB (printed circuit board) design in that the elements needed depend on an initial deterministic design and are not determined a priori. This is due to the nature of the textile platforms and compatible elements, which are all application dependent. Application requirements stem from wearable to semi-wearable platforms to completely static ones. These will determine platform characteristics such as substrate flexibility, stability, environmental constraints, level of user input, and interaction, as well as sensor characteristics such as sensor type, polymer sensing materials, sensitivity, and robustness, among others. The choice of textile substrate, textile structures, and sensor materials will also determine the necessary connections, connectors, bonding agents, sealing or encapsulating mechanisms, and any additional elements necessary to fulfill the mechanical and environmental requirements. The application constraints will also determine whether the textile transducer needs to have a stand-alone electronic system for data acquisition and processing or if it needs to communicate to a personal network via Wi-Fi or Bluetooth, in order to make good use of the sensory information coming from the textile transducer. A flowchart of the textile sensor design process can be seen in Fig. 6.2.

A polymer textile transducer, in particular a polymer-based textile sensor, can be constructed by either coating textile substrates with specific types of polymers
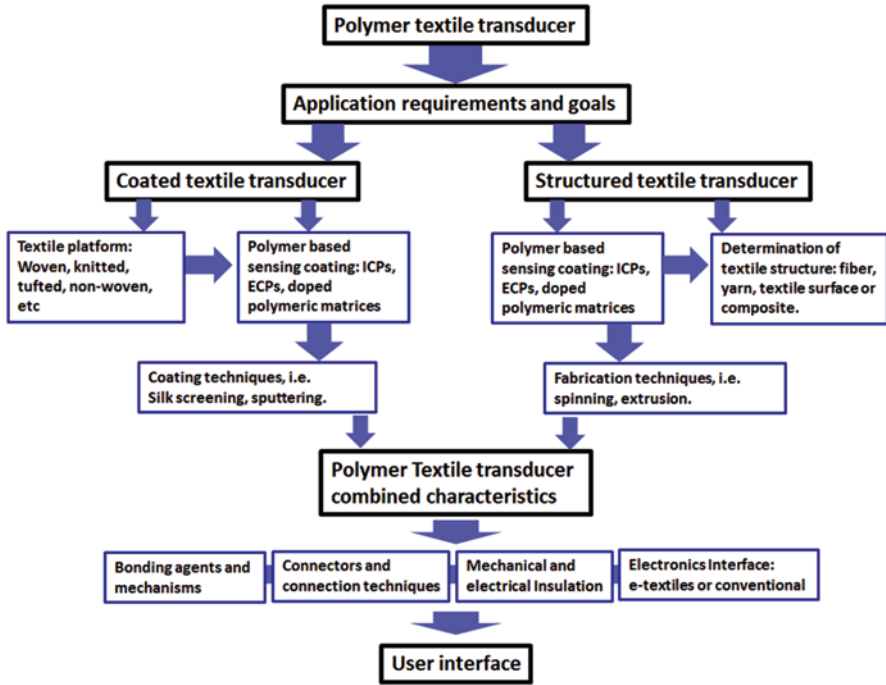
Fig. 6.2 Polymer-based textile sensor design process

responsive to different types of stimuli or by fabricating fibers, yarns, or other textile structures out of polymers with sensing properties [1]. Polymer-based textile sensors may also consist of miniature rigid electronics with encased or encapsulated polymers which may have openings in order to be able to react to light, gases, or other stimuli. This is an adaptation of conventional sensors to textiles or e-textiles. Coatings are typically composed of polymers which are responsive to different inputs such as strain, humidity, and pressure. The textile substrate usually serves as mechanical platform or is part of the sensing mechanism. For instance, strain sensors require for the textile substrate to allow for in-plane stress to produce variations in the coated sensor. Pressure sensors made of textile materials require that the material be responsive to out-of-plane stress.

Cover factor, C, which provides a quantifiable value for fabric openness, air permeability, and resistance to moisture, should be considered prior to coating a fabric substrate. This factor indicates the degree to which the coating can go through the fabric, having an impact on how well the coating will adhere to the substrate [11]. Consider a woven fabric composed of a warp fiber and a filling yarn. The cover factor is then given by Eq. (6.1) [4]:

$$C = \left(w * d_w + f * d_f - w * f * d_w * d_f \right) \tag{6.1}$$

where w is the number of warp threads per inch, f is the filling threads per inch, d_w is the diameter of warp yarn in inches, and d_f is the diameter of the filling yarn in inches. Another measure of the fabric permeability to a coating is given by the packing factor, PF, given by Eq. (6.2) [11]:

$$PF = \frac{fabric\ density}{fiber\ density} = \frac{W * V_{fabric}}{W * V_{fiber}} = \frac{V_{fiber}}{V_{fabric}} \tag{6.2}$$

where W is the total combined weight. The porosity, P, is complementary to the packing factor PF. In order to ascertain the flow parameter through porous mediums, Darcy's law can be utilized in modeling the penetration of the coating, where the porous media's average velocity is proportional to the fabric substrate's vertical pressure gradient. Rheology and surface chemistry will also dictate the uniformity and smoothness of the coating. Furthermore, other material parameters to be considered when applying this technique are viscosity, specific gravity, surface tension, and shear. This is all in reference to the critical step necessary to achieve a uniform coating. So as to balance the properties, leveling must be undertaken when high surface tension causes coating craters and very low viscosity causes sagging. This relationship is defined as put forth in Eq. (6.3) where the leveling half time $T^{1/2}$ of the striation marks created in process is used [4]:

$$T^{1/2} \propto \frac{\eta L}{\gamma} \frac{\lambda^4}{h_m^3} \tag{6.3}$$

where γ is the surface tension, ηL is the viscosity, λ is the striation wavelength, and h_m is the mid-coating penetration distance. Thixotropic effects need to be considered when the viscosity of the coating is not constant in time. Microcracks will also appear in the coating for other reasons, such as when the difference between the elastic modulus of the coating layer and of the substrate is too large [12], the coating suffers a deformation over its maximum elongation or when the coating is brittle or loses its natural moisture causing a decrease in its elastic behavior.

A sensor that has gone through the coating process is dependent on the following variables: the yarn/fabric substrate's internal geometry and mechanics, composition, elasticity, the coating's consistency, and sensing characteristics as well as the method employed. Coating permeation of the substrate will determine the sensor's properties and how well one adheres to the other, conforming to the application-dependent specifications. For instance, coatings which are activated upon stress inputs need to be well bonded to the textile surface to produce the desired strain sensitivity. Techniques used to improve adhesion of fibers in fiber-reinforced composites can be applied to improvement of adhesion of sensor coatings. The alteration of the surface layer's chemical and physical structures, tailoring the fiber matrix bond strength, or interfacial strength is known as surface modification. This type of material modification can be categorized into multiple different methodologies including mechanical, chemical, combustion, and plasma [3].

6.2.2 Intelligent Polymer Coating Materials and Construction Methods

6.2.2.1 Materials

Polymer-based textile sensors can be constructed from a wide range of materials which are mainly responsive to chemical or physical inputs. Polymers can be inherently reactive or can be doped with particles to allow for sensitivity to different stimuli such as temperature, pH, mechanical forces, electric currents, magnetic fields, light intensity, analytes, ions, gases, temperature, and so on. They can be organic compounds with modified functional groups or with particulate inclusions which have been dispersed within a matrix. These particulates range from micro- and nanoparticles to nanotubes and other nanostructured materials. Polymers used in textile sensors can be found in a variety of forms including solutions, pastes, gels, self-assembled nanoparticles, multilayer films, and bulk solids [13]. The methods by which these polymers are coated onto textile structures will also determine the final sensor characteristics. Reversible as well as nonreversible sensing properties are found among the different sensing techniques.

Fabric textile sensors resemble mechanisms used in conventional electronics but have also expanded these conventional transducing mechanisms to a variety of direct and indirect measurements of physical quantities. Table 6.1 illustrates the many types of transduction mechanisms which are possible with polymer textile sensors.

Physical sensing mechanisms used in textile polymer sensing can be of resistive, capacitive, electromagnetic, or optical origin. For instance, fabric pressure sensors based on capacitive mechanisms resemble conventional mechanisms in that textile surfaces acting as plates are coated with conductive polymers, and a textile spacer is used as a dielectric. However, pressure can also be sensed by distinguishing resonant frequency variations of fabric-based antennas, which is not a conventional method. Chemical sensors which use gas, pH, and analyte sensing polymers are made by exploring molecular reactivity disparities as well as lock-and-key molecular recognition and binding [35], as would be conventional. However, novel sensing properties can be given to the polymer by manipulating its solubility, hydrodynamic volume, chain configuration, and conformation. Sensing polymer systems can be made from semiconductor, semiconducting metal oxides, electrolyte solids, insulating materials, metals, and catalytic components, as well as organic semiconductors and membranes [36]. Most of the solid state sensing mechanisms are based on catalytic reactions produced by catalysts present in the base polymer or added catalysts. Ion exchanges, and oxidation reactions, are also possible sensing mechanisms of sensing polymers [i.e., ion exchange in solid electrolytes, Nafion, and stabilized zirconia (ZrO_2)]. Other solid state mechanisms entail changes in percolation networks and contact resistance. Many more examples of sensing polymer coatings are found in the literature for detection of humidity [37], gases [31], chemicals [38], analytes [36], pressure, strain [1], and polymer optical fibers with multiple sensing features [39].

Table 6.1 Polymer-based textile sensor types

Characteristics and sensor type		Sensing element	Substrate	Sensing mechanism
Pressure, force, switches, tension, compression, torsion	Capacitive	Electrodes: woven[a], knitted[b] plates, inks[c], paints	Synthetic foams, fabric spacers, soft polymers	Reduction of capacitor spacing
	Resistive, piezoresistive	Conductive ICP[d] and ECP[e] polymers, pressure-sensitive polymers[f]	Soft elastomers, polyester, polyurethane	Resistance changes upon elongation of sensing element
	Electromagnetic	Resonant frequency of antennas[g], light intensity in fiber optics	Soft polymer, fabric spacers	Changes in inductance, magnetization, etc... among other parameters
	Piezoelectric	Piezoelectric elements, i.e., PZT[h], PVDF	Cotton, soft polymers	Changes in voltage of piezoelectric element.
	Optical and piezochromic	Optical fiber[i] chromic polymer[j]	Fabric substrate	Changes in fiber-optic wavelength, transmittance, geometry, etc. polymer chromatic properties
Strain	Piezoresistive	Metal fibers, conductive thread[k], carbon fibers[l], ICP and ECP conductive polymers	No spacer needed in some cases, stretchable fabric, stretchable yarn	Increased number of conductive contacts, elongation of sensing element
	Optical	Fiber optics[m]	Fibrous textile substrate	Strain produces changes in fiber wavelength
Humidity	Resistive	ICPs[n]	Polyimide, lycra	Changes in humidity will produce changes in electrical resistance
	Capacitive	PES, PSF, and fabric dielectrics[o]	Fabric dielectric	Water absorption generates capacitive effects

Gases and chemicals	Chemoresistors	Inherently conductive polymers[p]	PET substrates, fabric substrates	Changes in particle absorption will produce changes in resistance
	Amperometric	Electrode oxidation[q]	Fabric substrate	Oxidation produces changes in electric current
	Optical/luminescent	Optical fiber based on ICPs[r]	Optical fiber substrate	Changes in light absorption when exposed to chemicals
Temperature	Resistive	ICPs[s]	Fabric substrate	Resistance changes with increased or decreased temperatures
	Optical	Fiber Bragg grating[t]	Light intensity	Temperature changes induce changes in the fiber wavelength
	Shape memory	Shape memory polymer[u]	Fabric substrate	Temperature causes polymer to go back to "memorized" shape
	Pyroelectric/ferroelectric	Pyroelectric polymer[v]	Fibers, yarns, and fabrics	Temperature changes cause polymer to generate a voltage

a[14], b[15], c[16], d[17], e[18], f[19], g[20], h[21], i[22], j[23], k[24], l[25], m[26], n[27], o[28], p[29], q[30], r[31], s[27], t[32], u[33], v[34]

Among the different sensing polymers, polymers that are electrically conductive can be employed in a vast array of applications because electrical resistance oscillation correlates well to variations in mechanical pressure, strain, light, analytes, and humidity. Conductive polymers can be inherently conductive, ICP, or extrinsically conductive, ECP. These polymers also possess active properties and therefore are also classified as electroactive polymers or EAPs. These organic materials are capable of changing shape or dimensions in response to an applied stimulus. Literature provides multiple instances of where EAPs have been used in fabric sensing applications [40]. EAPs can be identified by their activation mechanism as it is either ionic or electronic. Ionic or molecular induction is the hallmark of ionic EAP activation, while electronic EAPs require an external field or Coulomb forces for activation [41]. Ionic EAP examples include polyelectrolyte gels, ionic polymer-metal composites, and carbon nanotubes. Electronic EAP examples include piezoelectric, electrostrictive, electrostatic, ferroelectric, and dielectric elastomers. Examples of EAPs with active and passive properties are shown in Table 6.2.

Some of the most important ICPs used in textile sensors include polypyrrole, polyaniline, polythiophenes, and all their derivatives, as they are sensitive to a large number of chemical and physical inputs. Polypyrrole is an inherently conductive polymer with elevated conductivity and excellent environmental stability. It is easily produced, has good adhesion, and is nontoxic. Generally, they are synthesized via chemical polymerization or oxidative coupling of the monomer, pyrrole, or aniline [42]. Polypyrrole can sense biological compounds such as glucose and fructose as well as many different gases such as CO_2, N_2, H_2O_2, and CH_4, and humidity levels. As a piezoresistive sensor, it can be coated on many different fibers and textile substrates such as nylon, lycra, PET/Spandex, cotton, and so on. It is sensitive to environmental changes and needs to be blended with other polymers to make it less brittle. Polyaniline is another important ICP with numerous sensing features and textile coating possibilities. Through electrochemical deposition and spinning techniques, this material can be created on the surface of a fabric. Polyaniline can sense levels of biological compounds such as glucose and triglycerides, as well as many chemical vapors including aliphatic alcohols, ammonia, methanol, ethanol, propanol, and butanol. It can sense changes in humidity and temperature. Polyester, nylon, wool, acrylics, cotton, silica, and glass are some of the materials that have been coated with polyaniline. Polythiophenes are also an important class of ICPs. It has electrical conductivity properties, good solubility, outstanding electrochemical and thermal stability, and additional optical properties [32]. Microelectronic strain gauges can be fashioned from PEDOT-based piezoresistive sensors [43] and can coat hard surfaces like fibers, fabrics, and other media (i.e., foams). Nanotubes and nanofibers are the result of PEDOT microfabrication [44]. Other polymers which can be coated and possess sensing qualities are PVC membranes, Nafion, epoxy resins, acetates, polyisoprene, polypropylene, and PVA.

Extrinsically conductive polymers can also have many sensing features, with the added mechanical resilience of elastic nonconducting matrices. Such materials are composed of semiconductive or metallic filler along with a nonconductive insulating matrix. The particle inclusions can be of any size and morphology such as nanotubes,

Table 6.2 EAP materials with sensing and actuation properties[a]

Passive			Active	
Physical effects	Sensor devices	EAPs	Physical effects	Sensing devices
Piezoresistivity	Strain gauges	CCPs, e.g., CNTs, SWNT, MWNTs ICPs, e.g., polypyrrole (PPy), polyaniline (PANI), polythiophene (PT), polyacetylene (PA), pyrolyzed polyacrylonitrile (PAN) (PEDOT)	Piezoelectricity	Piezoelectric sensors
Thermoresistivity	Bolometers	Poly-(p-phenylene vinylene) (PPV)	Thermoelectricity	Thermocouples
Magnetoresistivity	Magnetoresistive sensors	Polyacetylene (PA) Pyrolyzed polyvinyl acetate (PVAc)	Pyroelectricity	Pyroelectric sensors
Chemoresistivity	Chemoresistive sensors	Polypyrrole (PPy) Polythiophene (PT) Ionic conducting polymers Charge transfer complexes	Chemoelectricity	Galvanic cells
Photoresistivity	Photoresistive sensors	Copper phthalocyanines Polythiophene complexes	Photoelectricity	Photoelectric cells

[a]Chart based on [41]

nanowires, and nanorods. Nanocomposites are known to have special sensing properties due to conduction effects present at the nanoscale such as electron tunneling. Fillers, such as carbon black [45], carbon fibers, graphite, and single-walled (SWNT) and multiwalled nanotubes (MWNT) [46], can be immersed in matrices such as epoxies, gels, styrene-butadiene copolymers, and siloxanes which can then be applied to fabric substrates to construct the textile sensor.

6.2.2.2 Construction Methods

Polymer textile sensors can be coated on a substrate, fabricated into a textile structure, or adapted from miniaturized electronic components. A sensor unit will then have been developed, and integration elements such as connectors and interfaces need to be chosen accordingly. These steps are outlined in Fig. 6.3.

Table 6.3 describes some of the most common methods for polymer coating onto different substrates. The technique to be chosen is dictated by the applied polymer's characteristics (chemical or physical). For instance, less viscous polymers can be applied using techniques such as sputtering or electrodeposition. The fabric application of liquid polymers can be accomplished by metal plating methods (Cu, Sn, Ag), electroplating, electrochemical deposition [56], sputtering (Au, Cu) [40], electrospinning, printing, ink printing [57], micro-contact printing [58], spraying [59], wet spinning [11], or by silk [60] and screen printing. More viscous polymers (i.e., thicker coatings) like pastes that are carbon loaded or other organically doped polymers can be "hand applied" [25], by masking methodologies along with screening, dip coating [11], soft lithography [48], embossing, or imprinting. Other fabric coating applications include magnetorheological, electrorheological, visible light sensitive/photoresponsive, self-oscillating, electrostrictive, pH sensitive, humidity sensitive, and electrochromic [61]. Application techniques will also depend on substrate characteristics such as mechanical tension, porosity, moisture resistance, and fabric permeability.
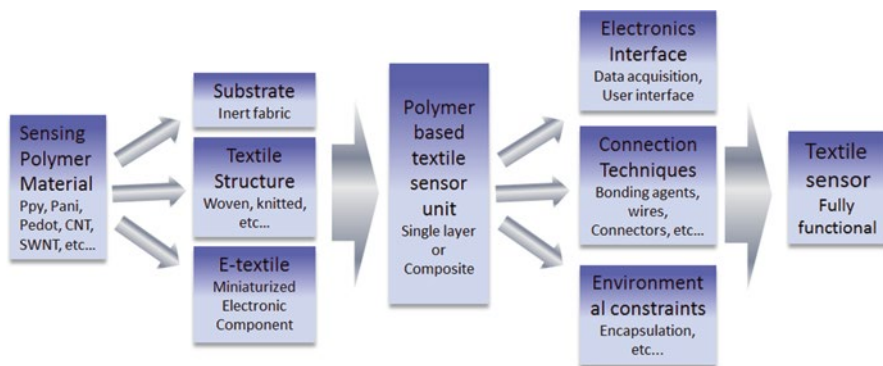
Fig. 6.3 Fully functional textile sensor construction process

Table 6.3 Coating and fabrication techniques for sensing polymers and fabrication

Techniques and description	Description	Polymer examples
Dip coating	Insertion and removal of substrate from a coating bath	PEDOT[a]
Inkjet printing	Precise generation of free-flying fluid droplets and impingement on substrate	PEDOT-PSS[b]
Chemical polymerization	Typically in situ oxidation of monomer solution produces polymerization	PPy/PET[c]
Spin coating	High-speed centripetal distribution of fluid coating onto substrate surface	PEDOT[d]
Electrospinning	Spinning technique which uses electrostatic forces to produce fine fibers from polymer solutions	Polyaniline[e]
Screen printing	Coating is transferred by means of a flexible blade, onto a porous printing plate through a stencil	Carbon black[f]
Solution casting	Thin-film formation around a mold when immersed in polymer solution	MWCNT[g]
Chemical vapor deposition	Deposition of layers of polymer compound through chemical reactions in a gaseous medium surrounding the component at an elevated temperature	PPy[h]
Electrochemical deposition	Coating deposited by simple electrolysis on substrate	Polyaniline[i]
Electroless plating	Metallic coatings are formed as a result of a chemical reaction between the reducing agent present in the solution and metal ions	PEDOT[j]
Sputtering	Ion momentum transfer process between anode and cathode from plasma	Polyaniline-HCl[k]
Sol-gel coating	Coating which undergoes a transition from colloid with suspended particles to solid when coated	Sol-gel phase polymers[l]

[a][27], [b][47], [c][28], [d][48], [e][49], [f][50], [g][46], [h][51], [i][52], [j][53], [k][54], [l][55]

6.3   Applications: Industrial, Aerospace, Military, and Medical

Smart fabric transducers have applications in many different fields. The advantage of lightweight components, compliant characteristics, and nearness to the wearer allows for numerous application possibilities. The following sections provide an overview of applications in the industrial, aerospace, military, and medical fields.

6.3.1 Military and Aerospace

In the race for better battle equipment, sensorized garments can be used to improve soldier performance. Although there are many examples of the use of functionalized textiles for military applications (e.g., chemical and biological protective suits, masks, gloves, tents, ballistic blankets, solar array blankets, flame retardant suits, etc. [60]), the incorporation of sensors and a means for transmission of the sensed information is a relatively new trend made possible by smart fabrics. The expectation is that sensorized fabrics will further increase soldier security and survivability by transmitting information about the soldier and his/her environment. Winterhalter et al. [62] describe the use of fabric-based sensors to create a personal area network (PAN) to provide a fast reaction mechanism for the monitoring of a soldier's vital signs and psychological condition. Their concept employs the battlefield dress uniform as an electronic network that is able to transmit data back and forth to the soldier's computer, all of which are worn. The PAN would be able to evaluate a situation but would also report in cases when external help is required. Wireless networking of the PAN would enable medics to monitor the health status of the soldier, reporting on injuries and transmitting data automatically for a safe and rapid response [63]. Future warrior systems [64] will feature a heads-up display, wireless weaponry, GPS applications, threat detection for chemical/biological weapon's use, harvested energy battery power, personal physiological status sensors, and combat ID sensors. All of these will be linked to the soldier's personal computer to assist in situational awareness and understanding of strategies and deployment. Some of these soldier aids may be realizable with e-textiles, for instance, textile antennas for communications and novel textile conductive cables (Fig. 6.4) for reduced overall weight. A textile-based antenna incorporated into modular lightweight load-carrying equipment (MOLLE) may prove beneficial when compared to the standard 30-in antenna in use by conforming to the body without compromising the soldier's camouflage. An adapted fabric USB port was developed by the US Army Soldier Systems Center (Natick), which is a first step on developing a PAN [48]. Energy can be harvested from soldier kinetics and photovoltaics by means of textile sensors and could be used to power the soldier's electronic devices.

In the next generation of army uniforms and equipment, nanotechnology is sure to be incorporated. Garments that are chemically protective and self-decontaminating overgarments can be produced with the aid of nanotechnology, e.g. (Institute for soldier nanotechnologies) ISN [63], shielding the soldier from deadly microorganisms or deadly chemicals. It has been shown that many inherently conductive polymers (ICPs) have chemical and gas reactivity, making them suitable for these types of applications [66]. Some of the toxic gases which can be detected include ammonia, nitrogen dioxide, and DMMP, a chemical warfare simulant [63]. Modified cladding materials can also be used to detect changing environmental conditions by changing the refractive index of inserted optical fibers. Electromagnetic interference (EMI) shielding fabrics can be used as camouflage by absorption rather than reflection of electromagnetic waves. BAE's Broadsword uses e-textiles for power and data management. All the technologies aimed at establishing PANs may also be applied to military shelters, such that they can blend in with the environment, change
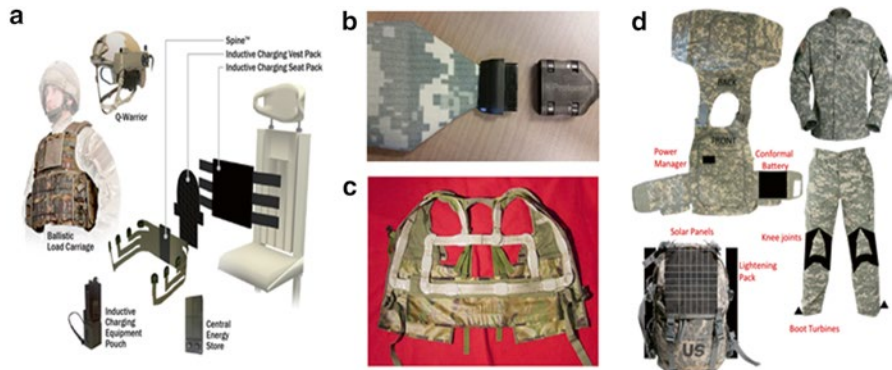
Fig. 6.4 (**a**) BAE Broadsword, with permission from [64]; (**b**) fabric data connector, with permission from [65]; US Army (**c**) double loop antenna integrated into MOLLE vest, with permission from [62]; and US Army (**d**) e-textile network for power harvesting, with permission from US Army. Images of the US Army are courtesy of Dr. Carole Winterhalter, from the US Army Natick Soldier Research, Development and Engineering Center

shape, repel chemicals, and provide protection from heat sensors or electromagnetic detectors [67].

Smart fabric transducers also have promising aerospace applications that could possibly improve crew safety and reduce mass, power, and volume requirements of existing support hardware. Extravehicular activity (EVA) suits can have push buttons and sliders made out of fabric switches. Fabric sensors can be used in robotic augmentation of a space suit to reduce astronaut workload during EVA [68]. Fabric sensors for electromyography (EMG) measurements could also be integrated into the astronaut's inner garments that would sense contractions within the muscles. The astronaut would only need to slightly move their hand/arm to carry out commands instead of the need to reach for external controls. Health monitoring to prevent muscle loss in space is also needed. ESA (European Space Agency) and Ohmatex [69] are working on building intelligent socks to monitor electrical and metabolic activity in leg muscles. Inflatable habitats targeted for space exploration could also greatly benefit from integrated fabric sensors [68].

6.3.2   Medical

Smart fabric transducers are being used for short term as well as long-term monitoring of patients. In general, patients want to be treated at home and with as little discomfort/inconvenience as possible. Many ambulatory medical devices can achieve such goals by means of wireless communications and friendly graphical user interfaces [70]. Wearable wireless devices can be connected to storage devices for off-line medical analysis, or they can stream sensor data for real-time medical monitoring and guidance [71]. However, long-term monitoring is challenging due to the requirements that the sensors must have. These requirements include portability, lightweight, softness, and

robustness. Fabric-based systems fulfill these requirements as they can be worn comfortably for long periods of time. They are particularly useful when monitoring chronic diseases, the handicapped, the elderly, or a heart condition. Multiple investigations have reported that detecting changes in heart rate over a 24-h period is critical when monitoring disease evolution and progression [72]. Systemic blood pressure monitoring can detect essential hypertension and can be a predictor of peripheral-organ damage. Safety monitoring and software-assisted physical therapy also benefit from textile sensor platforms [73]. Given the impact that continuous monitoring has on healthcare, prevention, therapy, and assistance, a number of smart fabric-based initiatives have been explored. For instance, a cluster of seven projects including MyHeart [24], BIOTEX [74], PROeTEX [75], STELLA [76], OFSETH [77], CONTEXT [78], and MERMOTH [79] addressed smart fabrics and interactive textiles for wearable systems. These projects had the goal of providing integrated health monitoring, such as electrocardiograms (ECGs), plethysmographic data, oximetry, fall sensors, temperature, and chemical sensors. Heart rate and respiration patterns can also be measured [80], for instance, with PPy polymerized foam. Unfortunately, over time the resistance drift and hysteresis after compression remain to be a huge downside to foam. Several other textile-based ECGs have been performed using different types of fabric electrodes. Knitted conductive yarn, embroidered stainless steel yarn [81], metal-coated fabric, Cu sputtering, and Cu/Ni [40] electroless plating are some of the materials used. Fabric electrodes can also measure Galvanic Skin Response (GSR) which indicates gland activity usually associated with psychophysiological activity [82].

Likewise, other sensorized devices aim to provide wearability without disrupting normal activities (Fig. 6.5). Examples of these types of applications include pressure insoles for shoes [86], arm and elbow angle sensors [40], knee joint motion sensors [87], and electrical conductivity armband sensors [88]. These are all sensors that are affixed to a person's garments (Table 6.4). Another example of in situ devices entails a smart fabric jacket for neonatal monitoring [117]. However, there are also sensors which can be placed in the environment with which the patient interacts as exosensors. These can be integrated for instance into a mattress pad or a sheet liner used on hospital beds to record body motion or posture. Complete body posture monitoring on hospital beds has been achieved using force-sensitive resistor (FSR) distributed sensors [89]. Sitting postures can be characterized with silver-coated fabric sensor arrays [14]. Other exosensors can be used to monitor the quality of the air and environmental monitoring. Fabric sensors can be constructed to detect the presence of harmful or carcinogen substances [56]. The development of better and healthier garments is also a possibility [118].

6.3.3   Civil and Industrial

Smart fabrics are being used to redefine human-machine interaction [119]. Levi Strauss and Phillips [120] developed the first commercially offered smart fabric-based jackets, one of them being the Mooring. An integrated textile keypad that can

Fig. 6.5 Health and sports applications of textile sensors: (**a**) NuMetrex heart rate monitoring shirt and chest strap, with permission from [83]; (**b**) Sensing Tex textile system for measuring pressure distribution, with permission from [84]; (**c**) ESA muscle monitoring suit for astronauts, by Ohmatex, with permission from [69]; and (**d**) Sensoria smart sock for foot pressure measurements, with permission from [85]

Table 6.4 Some fabric-based medical sensors and systems for body monitoring

	Application	Compliant and fabric sensing	Ref
Body posture, gesture, joint motion	Hospital beds	FSR distributed sensors	[89]
	Sitting postures	Capacitive fabric sensor arrays	[14]
	Elbow, arm angles	Tubular knitted coils	[90]
		Knitted piezoresistive	[40]
		Printed piezoresistive	[91]
	Knee, leg, torso	Printed piezoresistive sensors	[47, 87]
	Hand, fingers	Printed piezoresistive sensors	[92, 93]
Heart rate—ECG, plethysmography, and EMG	Electrodes and sensors	Knitted and woven stainless steel coil	[94]
		Embroidered stainless steel yarn	[40]
		Printed piezoresistive sensors	[24]
		Hydrogel membrane	[24]
		Coated pressure sensing foam	[80]
		PVDF/silicon strip	[95]

(continued)

Table 6.4 (continued)

	Application	Compliant and fabric sensing	Ref
Personal monitoring sensorized garments	Shirts, vests	MyHeart—ECG, EMG, pleth.	[24]
		SmartShirt (Sensatex)—ECG, EMG, pleth.	[96]
		LifeShirt (Vivometrics)—ECG, EEG, EMG	[97]
		BIOTEX—chemical sensing	[74]
		VTAMN—ECG, pleth., accels, temp.	[98]
		OFSETH—ECG, pleth., temp.	[77]
		SmartLife HealthVest	[99]
		SMASH shirt	[100]
	Chest straps	Textronics NuMetrex—ECG	[101]
		Zephyr BioHarness—ECG, pleth.	[102]
	Gloves	MARSIAN, temperature, conductance	[70]
		CyberGlove	[103]
		5DT Data Glove Ultra	[104]
		AcceleGlove	[105]
	Arm band	SenseWear Body Armband—skin electrical/thermal conductivity	[88]
	Outer garments, bedsheets, jackets	PROeTEX, biochemical sensing	[76]
		PASTA, integrating platform	[106]
		Scottevest jacket	[107]
		Infineon O'neill jacket	[108]
		Philips Lumalive	[109]
	Shoes (insoles)	Adidas FootScan	[110]
		Nike—capacitive/piezoresistive sensing	[111]
		Tekscan—piezoresistive ink	[112]
		Pedar insoles	[113]
		Pressure profile systems (PPS)	[114]
	Socks	Texisense smart sock	[115]
		Sensoria smart sock	[85]
		Alpha-Fit smart sock	[116]

be integrated into any garment has been developed [121]. Touchpad interfaces [122] can be incorporated into jackets for increased access to MP3 player functions. These smart fabric interfaces consist of washable piezoresistive conductive fabrics. Such is the case for a snowboarding jacket with MP3 and Bluetooth functionality [108]. In this device, the microphone and cell phone are integrated into the jacket; the cell phone is controlled via Bluetooth to enable hands-free operation. Bags are also being functionalized by building iPod remotes into the straps, incorporating built-in speakers and built-in Bluetooth capabilities to synchronize the electronic devices the

person is carrying. Smart backpacks such as those with embedded voltaic flexible solar cells [123] allow the consumer to recharge their handheld electronics at any time using solar cell energy. Solar panels can also be attached to over garments and clothes [123]. The panels charge a small battery which powers the device nearly instantaneously once the solar panels are engaged. When charging is complete, removal of the panels is completed, and portable electronic devices can be connected to use the stored power [107]. Other power possibilities include textile-based coils which allow the wireless charging of fabric-based transducers [94]. Fabric energy storage elements can potentially be incorporated into any flexible substrate [123].

Electroluminescent fabrics have commercial applications for use in many areas including upholstery, protective garments, safety garments, and potentially any fabric surface. LED-based electroluminescent fabrics which can change color and act as a programmable display have been developed [109]. These textiles can carry dynamic messages, graphics, or multicolored images and are designed to enhance the observer's mood and behavior [87]. Other safety equipment where smart fabrics are applied is a waterproof antenna that can be sewn into life vests [124]. Upon activation, the antenna can transmit its coordinates, allowing a fast and successful rescue effort. Fire suits with built-in heat sensors can display an alert when under risky conditions. Fishermen can also be protected by using smart garments. The Safe at Sea project [125] is developing protective clothing with many features including an alert of overboard falling. Similar types of garments can be implemented in the workplace to avoid situations where the worker's safety is compromised. Heating vests can be entirely based on textile materials [126]. Durable and washable, textile heating technologies are being currently incorporated in commercial products such as blankets and upholstery. Other specialized fabrics include garments which can react to cold or warm environments to maintain a comfortable temperature for the wearer such as smart suits impregnated with microparticles of paraffin wax which melt when cooling is needed [127]. Stimulating garments are being explored as well. Such is the case of the sports uniforms [128] which consist of ionized fabrics that maximize blood flow and cool and calm the wearer to maximize power output and decrease recovery times. Fabric surfaces can be designed with specific purposes. Super hydrophobic self-cleaning surfaces are designed to resist spills, repel stains, and resist static [87]. Smart carpets can be used to sense the location of individuals in a room, finding applications in monitoring age groups such as toddlers and the elderly [129]. Geotextiles can be very useful in protection of infrastructure [130] and structural health monitoring using different types of fabric sensors [131].

Health and sports applications for smart fabric sensor technologies include heat blankets [132], heart sensing cardio shirts [83], foot scanning shoe insoles [110], and portable pedometers [111]. Commercial chest straps [102] are another one of the advanced products that emerged from smart textile developments. They measure the heart rate and rhythm and can monitor the expansion and contraction of the chest. With a series of solid state sensors, three accelerometers, and a thermometer, these devices can transmit data wirelessly through an ISM (industrial, scientific, and medical band) link, being GPRS (general packet radio service) enabled as well. It can

provide readings such as ECG, respiration trends, posture, activity, and skin temperature. Other health-related commercial fabric transducers include shoe insoles for pressure monitoring. These can aid diabetics to detect the early symptoms of diabetic peripheral neuropathy (DPN) which is preceded by calluses and inflammation [133]. FSR (force-sensitive resistor) tactile and plantar sensors are also used for the pressure sensing task [114]. Smart textile technologies for everyday life applications such as household and apparel products have also been developed.

Disappearing electronics will facilitate new methods of accessing knowledge and communication. Sooner or later this phenomenon will redefine the human computer interaction standards shifting technology design toward "experiential design" [134]. That is, a method which takes the user's experience and makes it part of the design process. This is different from conventional product development, where the user is typically offered a finished product. Society will be impacted as technology continues to address every basic aspect of life. Interpersonal communication will change as a result of possible new fabric-enabled forms of communication (i.e., electroluminescent fabrics [109]), which may feature individual wearable screens. It will also be a new tool for creativity, gaming, and, very importantly, education. Mobile computing has already brought innovation to modern education, but a major impact would be seen if electronics were to find their way into student culture at an early age, for example, through the use of wearable e-textile applications [135]. Figure 6.6 shows different types of functionalized garments that use smart fabric transducers.

6.4 Conclusion

Polymer-based textile sensors have a wide variety of possibilities both in sensing mechanisms and applications. Polymer coatings applicable to fabrics have many sensing possibilities such as temperature, pH, humidity, chemicals, analytes, strain, pressure, and light, among others. These polymers can be inherently reactive to such inputs or can be modified both intrinsically and extrinsically to become reactive. Inherently conductive polymers are sensitive not only to several different chemicals but also to mechanical stress and temperature. Extrinsically conductive polymers can also have many sensing applications, especially those with nano-inclusions due to their special physical and chemical qualities. All these polymers will have different properties depending on the coating method, or fabrication methods, if they are made into fabric structures. A wide range of fabrics and fibrous materials can be used as substrates for the sensing coatings. These range from natural fibers (i.e., cotton) to synthetics (i.e., polyester) and include knitted, woven and nonwoven (i.e., felt) fabrics, as well as foams (i.e., polyurethane foam). Design of polymer-based textile sensors begins with the scope of the application and then choosing the sensing materials as well as the substrates and the connection methods. A complete sensing textile requires an interface to data acquisition electronics and user interface.

Although the many sensing possibilities are promising, features such as mechanical stability, environmental resilience, cost, lack of readily available materials and

Fig. 6.6 Functionalized smart jackets: (**a**) Philips Lumalive LED-based jacket, with permission from [109]; (**b**) Scottevest Solar Jacket with added functionality, with permission from [107]; and (**c**) Visijax commuter jacket with turn signals, uses Eleksen's conductive textile technology, with permission from [136]

components, as well as ease of manufacturability are challenges that need to be overcome in order to have further commercialization of these types of sensors. The plethora of applications should drive these developments. Civilian applications will allow the human to interact with technology in a more natural way. Military and aerospace applications can greatly benefit with added soldier or astronaut monitoring and assistance features. Medical applications greatly benefit the wearer in monitoring health and vital signals. Research opportunities are also expanded with textile sensors, as these open possibilities which were not reachable with conventional sensors.

6.5 Future Outlook

Future work is required toward the standardization of textile sensing components and materials, e-textiles, as well as polymer-based transducers. New techniques to enhance repeatability, sensor stability, environmental robustness, and resilience

to wear and tear will need to be developed in order to have widespread usage of these devices. Portable data acquisition and telemetry need to be seamless both at the electronic circuitry level as well as the user interaction level. Standardized interfaces would aid in connections of conventional sensors, cell phones, and computers with e-textiles and polymer-based textile sensors.

Application trends will be catalyzed by wearable technologies and new portable electronic devices such as smart watches. Clothes will become much more functional and useful for nonconventional tasks. Places will also become interactive; live environments will create more communication paths for interpersonal interactions as well as for research and development. Overall, these sensors will continue to evolve and be more integrated in many more aspects of society.

References

1. Castano LM, Flatau AB (2014) IOP Smart Mater Structures 23:053001
2. Schwartz P (2008) Structure and mechanics of textile fibre assemblies. Elsevier, Boca Raton, FL
3. Shijian L, Van Ooij WJ (2002) J Adhes Sci Technol 16:1715–1735
4. Tracton A (2006) Coatings technology handbook, 3rd edn. CRC Press, Boca Raton, FL
5. Niu C et al (1997) Appl Phys Lett 70:1480–1482
6. Célino A, Fréour S, Jacquemin F, Casari P (2013) Front Chem 1:43
7. Thermochromic sensing fibers, Commonwealth Scientific and Industrial Research Organization (CSIRO). Available from http://www.csiro.au/en/Research/MF/Areas/Chemicals-and-fibres/Advanced-fibres/Smart-clothing-and-textiles/Smart-bandages-reveal-healing. Accessed 20 Dec 2015
8. Zysset C et al (2013) Opt Express 21:3213–3224
9. Castano LM (2010) Smart fabric sensors for foot motion monitoring. Thesis, University of Maryland, College Park
10. Gao Y, Zheng Y, Diao S, Toh WD, Ang CW, Je M, Heng CH (2011) IEEE Trans Biomed Eng 58:768–772
11. Adanur S (1995) Wellington sears handbook of industrial textiles. Lancaster, Philadelphia
12. Chen Z, Cottrell B, Wong W (2002) Eng Fract Mech 69:597–603
13. Jinming H, Liu S (2010) Macromolecules 43:8315–8330
14. Meyer J, Arnrich B, Schumm J, Troster G (2010) IEEE Sens J 10:1391–1398
15. Post ER, Orth M, Russo PR, Gershenfeld N (2000) IBM Syst J 39:840–860
16. Sergio M, Manaresi N, Campi F, Canegallo R, Tartagni M, Guerrieri R (2003) IEEE J Solid-State Circuits 38:966–975
17. Hui Z, Ming TX, Xi YT, Sheng LX (2006) Pressure sensing fabric. Materials Research Society, Symposium Proceedings, Smart Nanotextiles, 920:113–119
18. Shimojo M, Namiki A, Ishikawa M, Makino R, Mabuchi K (2004) IEEE Sens J 4:589–596
19. Bloor D, Graham A, Williams EJ, Laughlin PJ, Lussey D (2006) Appl Phys Lett 88:102103
20. Mohammad I, Huang H (2012) Pressure and shear sensing based on microstrip antennas. Proceedings of the SPIE sensors and smart structures technologies for civil, mechanical, and aerospace systems, San Diego, CA
21. Yang W, Torah R, Yang K, Beeby S, Tudor J (2012) A novel fabrication process to realize piezoelectric cantilever structures for smart fabric sensor applications. IEEE Sensors Conference, Taipei, Taiwan
22. Rothmaier M, Luong M, Clemens F (2008) Sensors 8:4318–4329
23. Dashti M, Mokhtari J, Nouri M, Shirini F (2012) J Appl Polym Sci 124:3007–3012

24. Pacelli M, Caldani L, Paradiso R (2006) Textile piezoresistive sensors for biomechanical variables monitoring. 28th Annual international conference of the IEEE engineering in medicine and biology society EMBS, New York City, NY
25. Huang CT, Shen CL, Tang CF, Chang SH (2008) Sens Actuators A Phys 141:396–403
26. Witt J et al (2012) IEEE Sens J 12:246–254
27. Daoud WA, Xin JH, Szeto YS (2005) Sens Actuators B Chem 109:329–333
28. Kim H, Kim Y, Kwon Y, Yoo H (2008) A 1.12mW continuous healthcare monitor chip integrated on a planar-fashionable circuit board. Digest of Technical Papers. IEEE International Solid-State Circuits Conference (ISSCC), Philadelphia, PA
29. Kwon OS, Park E, Kweon OY, Park SJ, Jang J (2010) Talanta 82:1338–1343
30. Yang YL et al (2010) Analyst 135:1230–1234
31. Bai H, Shi G (2007) Sensors 7:267–307
32. Samsonidze G, Ribeiro FJ, Cohen ML, Louie SG (2014) Phys Rev B 90:035123
33. Liu C, Qin H, Mather PT (2007) J Mater Chem 17:1543–1558
34. Hammes PCA, Regtien PPL (1992) Sens Actuators A Phys 32:396–402
35. Jefferson C, Dodani SC, Chang CJ (2012) Nat Chem 4:973–984
36. Basudam A, Majumdar S (2004) Prog Polym Sci 29:699–766
37. Sakai Y, Sadaoka Y, Matsuguchi M (1996) Sens Actuators B Chem 35:85–90
38. Persaud KC (2005) Mater Today 8:38–44
39. Peters K (2011) IOP Smart Mater Structures 20:013002
40. Cho G, Jeong K, Paik MJ, Kwun Y, Sung M (2011) IEEE Sens J 11:3183–3193
41. Carpi F, De Rossi D (2005) IEEE Trans Inf Technol Biomed 9:574
42. Kim HK et al (2003) Mol Crystals Liquid Crystals 405:161–169
43. Lang U, Rust P, Schoberle B, Dual J (2009) Microelectron Eng 86:330–334
44. Martinez O, Bravos AG, Pinto N (2009) Macromolecules 42:7924–7929
45. Cochrane C, Koncar V, Lewandowski M, Dufour C (2007) Sensors 7:473–492
46. Oliva-Avilés AI, Avilés F, Sosa V (2011) Carbon 49:2989–2997
47. Calvert P, Patra P, Sawhney A, Agrawal A, Duggal D (2007) Printed conducting polymer strain sensors for textiles. 23rd International conference on digital printing technologies, Anchorage, AK
48. Wang X, Ostblom M, Johansson T, Inganas O (2004) Thin Solid Films 449:125–132
49. Okuzaki H, Harashina Y, Yan H (2009) Eur Polym J 45:256–261
50. Lorussi F, Scilingo EP, Tesconi M, Tognetti A, De Rossi D (2005) IEEE Trans Inf Technol Biomed 9:372–381
51. Li Y, Leung MY, Tao XM, Cheng XY, Tsang J, Yuen MCW (2005) J Mater Sci 40:4093–4095
52. Wu J (2004) Synthesis, characterization and applications of conducting polymer coated textiles. Dissertation, University of Wollolong
53. Sawhney A, Agrawal A, Patra P, Calvert P (2006) Proc Mat Res Soc Symp Smart Nanotextiles 920:103–111
54. Menegazzo N et al (2012) Anal Chem 84:5770–5777
55. Mujahid A, Lieberzeit PA, Dickert FL (2010) Materials 3:2196–2217
56. Jin G, Norrish J, Too C, Wallace G (2004) Curr Appl Phys 4:366–369
57. Yoshioka Y, Jabbour G (2006) Synth Met 156:779–783
58. Boltau M, Walheim S, Mlynek J, Krausch G, Steiner U (1998) Nature 391:877–879
59. Sen AK (2001) Coated textiles: principles and applications, 2nd edn. CRC Press, Boca Raton, FL
60. Kim H, Kim Y, Kim B, Yoo HJ (2009) A wearable fabric computer by planar-fashionable circuit board technique. Sixth international workshop on wearable and implantable body sensor networks, Berkeley, CA
61. Bhowmick AK (2008) Current topics in elastomers research. CRC Press, Boca Raton, FL
62. Winterhalter CA, Teverovsky J, Wilson P, Slade J, Horowitz W, Tierney E, Sharma V (2005) IEEE Trans Inf Technol Biomed 9:402–406

63. Institute for soldier nanotechnologies. Massachusetts Institute of Technology. Available from http://www.web.mit.edu/isn/. Accessed 20 Dec 2015
64. BAE Broadsword soldier suite. BAE Systems. Available from http://www.baesystems.com. Accessed 20 Dec 2015
65. Winterhalter CA, Teverovsky J, Horowitz W, Sharma V, Lee K (2004) Wearable electro-textiles for battlefield awareness. Army Natick Soldier Center MA Report ADA431955
66. Collins GE, Buckley LJ (1996) Synth Met 78:93–101
67. Sahin O, Kayacan O, Bulgun Y (2005) Def Sci J 55:195–205
68. Simon C, Potter E, McCabe M, Baggerman C (2010) Smart Fabrics Technology Development, NASA Innovation Fund Project, NASA Johnson Space Center Report
69. Ohmatex-Smart Textile Technology. Available from http://www.ohmatex.dk. Accessed 20 Dec 2015
70. Axisa F, Schmitt PM, Gehin C, Delhomme G, McAdams E, Dittmar A (2005) IEEE Trans Inf Technol Biomed 9:325–336
71. Carlos R, Coyle S, Corcoran B, Diamond D, Tomas W, Aaron M, Stroiescu F, Daly K (2011) Web-based sensor streaming wearable for respiratory monitoring applications. IEEE Sensors Conference, Limerick, Ireland
72. Engin M, Demirel A, Engin EZ, Fedakar M (2005) Measurement: J Int Measurement Confederation 37:173–188
73. Patel S et al (2012) J Neuroeng Rehabil 9:21
74. Coyle S et al (2010) IEEE Trans Inf Technol Biomed 14:364–370
75. Magenes G, Curone D, Caldani L, Secco EL (2010) Fire fighters and rescuers monitoring through wearable sensors: The ProeTEX project. 32nd Annual International Conference of the IEEE Engineering in Medicine and Biology Society EMBC, Buenos Aires, Argentina
76. Loher T, Manessis D, Heinrich R, Schmied B, Vanfleteren J, DeBaets J, Ostmann A, Reichl H (2006) Stretchable electronic systems. 8th Electronics packaging technology conference EPTC '06, Singapore
77. Grillet A, Kinet D, Witt J, Schukar M, Krebber K, Pirotte F, Depre A (2008) IEEE Sens J 8:1215–1222
78. Langereis G, De Voogd-Claessen L, Spaepen A, Siplia A, Rotsch C, Linz T (2007) ConText: contactless sensors for body monitoring incorporated in textiles. IEEE international conference on portable information devices, Orlando, FL
79. Custodio V, Herrera FJ, Lopez G, Moreno JI (2012) Sensors 12:13907–13946
80. Brady S, Diamond D, Lau KT (2005) Sens Actuators A 119:398–404
81. Scilingo EP, Gemignani A, Paradiso R, Taccini N, Ghelarducci B, De Rossi D (2005) IEEE Trans Inf Technol Biomed 9:345–352
82. Healey J (2011) GSR sock: a new e-textile sensor prototype 2011. 15th Annual international symposium on wearable computers ISWC, San Francisco, CA
83. Numetrex heart rate monitoring. Available from http://www.numetrex.com. Accessed 20 Dec 2015
84. Sensingtex Pressure Textile Sensor. Available from http://www.sensingtex.com. Accessed 20 Dec 2015
85. Sensoria fitness smart sock. Copyright Sensoria Inc. 2015. All rights reserved. Images and products protected by US and international intellectual property legislations. Available from http://www.sensoriafitness.com. Accessed 20 Dec 2015
86. Shu L, Hua T, Wang Y, Li Q, Feng DD, Tao X (2010) IEEE Trans Inf Technol Biomed 14:767–775
87. Coyle S, Wu Y, Lau KT, De Rossi D, Wallace G, Diamond D (2007) MRS Bull 32:434–442
88. Hill K, Dolmage TE, Woon L, Goldstein R, Brooks D (2010) Thorax 65:486–491
89. Harada T, Mori T, Nishida Y, Yoshimi T, Sato T (1999) Body parts positions and posture estimation system based on pressure distribution image. Proceedings of the IEEE international conference on robotics and automation, Detroit, MI
90. Wijesiriwardana R (2006) IEEE Sens J 6:571–579

91. Calvert P, Duggal D, Patra P, Agrawal A, Sawhney A (2008) Mol Crystals Liquid Crystals 484:291–302
92. Scilingo EP, Lorussi F, Mazzoldi A, De Rossi D (2003) IEEE Sens J 3:460–467
93. Liu N, Fang G, Wan J, Hai Z, Long H, Zhao X (2011) J Mater Chem 21:18962–18966
94. Catrysse M, Puers R, Hertleer C, Langenhove LV, Van Egmondc H, Matthys D (2004) Sens Actuators A Phys 114:302–311
95. Kim KJ, Chang YM, Yoon SK, Hyun J (2009) Integrated Ferroelectrics 107:53–68
96. Pantelopoulos A, Bourbakis N (2008) A survey on wearable biosensor systems for health monitoring. 30th Annual international conference of the IEEE engineering in medicine and biology society EMBS, Vancouver, Canada
97. Heilman KJ, Porges SW (2007) Biol Psychol 75:300–305
98. Noury N et al (2004) VTAMN – a smart clothe for ambulatory remote monitoring of physiological parameters and activity. 30th Annual international conference of the IEEE engineering in medicine and biology society EMBS, San Francisco, CA
99. McCarthy B, Varakliotis S, Edwards C, Roedig U (2010) Real-world wireless sensor networks. Lecture Notes in Computer Science 6511:37–48
100. Harms H, Amft O, Tröster G, Roggen D (2008) SMASH: a distributed sensing and processing garment for the classification of upper body postures. Proceedings of the ICST 3rd international conference on body area networks BodyNets '08. ICST Institute for Computer Sciences, Social-Informatics and Telecommunications Engineering, Brussels, Belgium
101. Textronics-Energy activated fabrics. Available from http://www.textronicsinc.com/textiles. Accessed 20 Dec 2015
102. Zephyr bioharness. Available from http://www.zephyr-technology.nl/en/product/71/zephyr-bioharness.html. Accessed 20 Dec 2015
103. Xu D (2006) A neural network approach for hand gesture recognition in virtual reality driving training system of SPG. 18th international conference on pattern recognition ICPR, Hong Kong, China
104. Kamel NS, Sayeed S, Ellis GA (2008) IEEE Trans Pattern Anal Mach Intell 30:1109–1113
105. Hernandez-Rebollar JL, Kyriakopoulos N, Lindeman RW (2002) The AcceleGlove: a whole-hand input device for virtual reality. ACM SIGGRAPH conference abstracts and applications, San Antonio, TX
106. Kallmayer C, Simon E (2012) Large area sensor integration in textiles. International multi-conference on systems, signals and devices SSD, Chemnitz, Germany
107. Scottevest Smart Jacket. Available from http://www.scottevest.com. Accessed 20 Dec 2015
108. Yanfen L, Pu H (2011) Smart sportswear. International conference on future computer science and education (ICFCSE), Xi'an, China
109. Koninklijke Philips Electronics N.V. © 2006 Reprinted, with permission, from Password, Philips Research technology magazine, issue 28, October 2006
110. Strickland P, Reid G, Burrows B (1997) Thermal profiles in footwear design: an in-sole measurement system. Proceedings of the 4th annual conference mechatronics and machine vision in practice, Toowoomba, Australia
111. McClusky M (2009) Wired 17:07
112. Boyd BS et al (2007) J Neurosci Res 85:2272–2283
113. Hurkmans LP, Bussmann JBJ, Benda E, Verhaar JAN (2006) Gait Posture 23:118–125
114. PPS digitacts human tactile system. Available from http://www.pressureprofile.com/. Accessed 20 Dec 2015
115. Texisense smart sock. Available from http://www.texisense.com/. Accessed 20 Dec 2015
116. Textile Sensoric Alphafit- Smart Sock and Alphamat. Available from http://www.alpha-fit.de. Accessed 20 Dec 2015
117. Chen W, Nguyen ST, Bouwstra S, Coops R, Brown L, Oetomo SB, Feijs L (2011) Design of wireless sensor system for neonatal monitoring. 4th IFIP international conference on new technologies, mobility and security NTMS, Paris, France

118. Campbell T, Munro B, Wallace G, Steele J (2007) J Biomech 40:3056–3059
119. Quinn B (2002) Techno Fashion. Berg, Oxford
120. Farringdon J (2001) Tech Textiles Int 10:22–24
121. Meoli D, May-Plumlee T (2002) JTATM 2:2
122. Sandbach DL (2002) Detector constructed from fabric having non-uniform conductivity. US Patent No 6,369,804, 9 April 2002.
123. Schubert MB, Werner JH (2006) Mater Today 9:42–50
124. Serra AA, Nepa P, Manara G (2012) IEEE Trans Antennas Propag 60:1035–1042
125. Wiggen ON, Storholmen TCB, Naesgaard OP, Faerevik H (2012) Safe@Sea- Improved protective clothing for fishermen in the high north. 3rd Barents occupational health workshop, Oulu, Finland
126. Rantanen J et al (2000) Smart clothing for the arctic environment. The fourth international symposium on wearable computers. IEEE
127. Eidsmo RR, Hilde F, Kristine H, Kare RJ (2008) SINTEF Smart helicopter survival suit. Innovations Report SINTEF S6971
128. Short DC et al (2011) Ionized performance fabric composition. United States Patent 7896928
129. Takamatsu S, Kobayashi T, Shibayama N, Miyake K, Itoh T (2011) Meter-scale surface capacitive type of touch sensors fabricated by weaving conductive-polymer-coated fibres. Symposium on design, test, integration and packaging of MEMS/MOEMS DTIP, Bernin, France
130. Zheng N, Wu Z, Lin M, Yang LT, Pan G (2010) IEEE Trans Syst Man Cybernetics 40:36–51
131. Liehr S et al (2008) Distributed strain measurement with polymer optical fibers integrated into multifunctional geotextiles. Proceedings of the SPIE optical sensors, Strasbourg, France
132. Heat blanket by Eeonyx. Available from http://www.eeonyx.com/. Accessed 20 Dec 2015
133. Yip M, He DD, Winokur E, Balderrama AG, Sheridan R, Hongshen Ma (2009) A flexible pressure monitoring system for pressure ulcer prevention. Annual international conference of the IEEE engineering in medicine and biology society EMBC, Minneapolis, MN
134. Baurley Pers S (2004) Ubiquit 8:274–281
135. Buechley L (2006) A construction kit for electronic textiles. 10th IEEE international symposium wearable computers, Montreux, Switzerland
136. Visijax Commuter Jacket with turn signals. Available from: http://www.visijax.com. Accessed 20 Dec 2015

Chapter 7
Smart Polymers: Synthetic Strategies, Supramolecular Morphologies, and Drug Loading

Marli Luiza Tebaldi, Rose Marie Belardi, and Fernanda S. Poletto

Abstract Smart polymers are a relatively new type of material that is attracting attention from considerable attention from polymer scientists due to their promising applications in several high-tech industry fields. The properties of the smart polymers can change in various ways due to the action of a number of triggers such as temperature, pH, enzymes, ionic strength, and light intensity. The design of the polymer architecture is a key factor to obtain structures with the desired properties. The advent of controlled radical polymerization techniques has led to the development of a variety of polymers with controlled characteristics. Functionalization of these polymers has been successfully used to synthesize numerous structures with desired architectures creating unprecedented opportunities for the design of advanced materials with stimuli-responsive properties. In this chapter, recent advances in this fascinating research field will be presented highlighting new controlled living polymerization methods. Some concepts will also be introduced regarding drug loading and types of morphologies of self-assembled supramolecular structures derived from smart polymers.

M.L. Tebaldi (✉) • R.M. Belardi
Universidade Federal de Itajubá, Campus Avançado de Itabira,
Minas Gerais 35903-087, Brazil
e-mail: marlitebaldi@unifei.edu.br; rosebelardi@unifei.edu.br

F.S. Poletto (✉)
Departamento de Química Orgânica, Instituto de Química, Universidade Federal do Rio Grande do Sul, Av. Bento Gonçalves 9500, Porto Alegre, RS 91501-970, Brazil
e-mail: fernanda.poletto@ufrgs.br

7.1 Introduction

Over the last few decades, remarkable advancements have been made in science and technology to obtain materials with new exciting properties. A multidisciplinary approach was fundamental for scientists to gain a better understanding of the relationship among the structures, properties, processing, performance, and functions of new materials in engineering. These advances are a result from a huge breakthrough in polymer science, which involves the comprehensive understanding of organic and physical chemistry, biochemistry, biology, and engineering fields. The wide variety of current polymer structures makes them a class of materials with numerous potential uses [1]. Recently great attention has been paid on the study of the so-called smart polymers, which may respond to several stimuli from the environment. The properties of the smart polymers can change in various ways due to the action of a number of triggers such as temperature, pH, enzymes, ionic strength, and light [2].

Various natural macromolecules such as proteins, carbohydrates, and nucleic acids are examples of systems with inherently responsive properties. The advance in polymer science has led to the development of diverse synthetic polymeric mimics of these biopolymers [2, 3] or new approaches to modifying the chemical structure of the macromolecules using covalently bonded synthetic oligomers/polymers [4, 5]. The ways to change the polymeric material structure to achieve the desired properties are enormous. With the advent of the controlled radical polymerization (CRP) techniques, also known as living polymerizations, it became possible to synthesize polymers with a predetermined molar mass, very narrow polydispersity, and planned chain-end functionality. The functionalized chains may be part of the strategy used to design different molecular architectures such as graft and block copolymers [6] and several supramolecular structures such as polymer aggregates, polymer gels, and polymeric micelles [7].

The narrow polydispersity and well-controlled molar mass of polymers and copolymers obtained by living polymerization techniques are related to the mechanism of this class of reactions. As a general rule, chain transfer and chain termination reactions are virtually absent, while the rate of chain initiation is usually fast compared to the rate of chain propagation. As a result, the number of kinetic-chain carriers is essentially constant throughout the polymerization.

Over several decades, copolymers were obtained only via living anionic polymerization [8]. However, this technique is limited to nonpolar monomers such as styrene, isoprene, or butadiene, and the reaction conditions must be highly controlled. As a result, impressive costs are involved in this process, making large-scale production less feasible. Living carbocationic polymerization was also used, but the commercial application of this strategy is still limited despite some progress had been made with the discovery of new catalysts [9]. Other living ionic techniques such as cationic ring-opening polymerization (CROP) have been developed providing several industrially important polymers [10, 11]. During this time period,

synthetic chemists dreamed of living polymerization reactions with a broader scope for monomers and more flexible reaction conditions than those from ionic polymerization reactions. Nowadays this dream is a reality and almost all monomers containing a carbon–carbon double bond can be polymerized by living radical polymerization [12–14]. The possibilities to accommodate different functional groups and the great of possible monomers that can be used provide numerous architectures that otherwise could not be prepared without complex reaction conditions [15]. The modern polymer chemistry approaches include controlled radical polymerization (CRP) with different mechanisms as nitroxide-mediated polymerization (NMP) [13, 16], atom transfer radical polymerization (ATRP) [17–19], and reversible addition–fragmentation transfer (RAFT) [20, 21]. These mechanisms have revolutionized the field of synthetic polymer chemistry over the last 20 years and have shown unprecedented opportunities to prepare tailored polymeric architectures such as block copolymers, polymer gels, and polymer surface brushes. Low radical concentrations provided by CRP prevent side reactions, which is extremely important for designing of polymeric structures with specific properties. The combination of CRP methods with strategies such as *"click chemistry"* to modify functional groups is a key to obtaining a series of tailored advanced polymeric materials with novel compositions [22, 23].

Smart polymers can be obtained from synthetic and natural sources. Polymeric systems from renewable sources have received special attention due to their sustainability, biocompatibility, and natural abundance [22, 23]. Cellulose is the most abundant biopolymer on earth with a great range of worldwide industrial applications [24–29]. Chitosan is another natural polymer that has been attracting attention due to its adequate biocompatibility, lack of toxicity, and mucoadhesive properties [30, 31]. Polylactide (PLA) is a thermoplastic polyester obtained from renewable sources that has been extensively investigated due to its mechanical properties which are similar to those from petroleum-based polymers. The most attractive aspect of PLA is the high biocompatibility, which opens up wide range of applications in the biomedical field. Despite this, PLA has drawbacks such as increased hydrophobicity, poor toughness, and slow degradation rate that limit its use for certain applications. Several studies have been carried out to improve the PLA properties by functionalization and copolymerization [32]. The functionalization on the surfaces of natural polymers has been extensively investigated to obtain smart systems [27]. This modification can be carried out using the natural polymer as a macro-initiator (or macro-chain transfer agent, MCTA) of living radical polymerizations, which can start new polymerizations with a wide range of monomers and reaction conditions.

In this chapter, recent advances concerning the synthesis techniques of smart polymers will be presented highlighting new controlled living polymerization methods as well as synthetic post-modification procedures. Supramolecular morphologies of smart polymeric systems and drug loading will also be discussed.

7.2   Stimuli-Responsive Polymer Architectures

Smart polymers respond to small changes from their environment with major changes in their structure and properties [2]. The polymer chains can be planned to respond to particular external stimuli using different strategies. For instance, pH-sensitive polymers can be obtained by incorporating acid or basic moieties into the chain [33, 34]. The responsive functional moieties can be located in several positions on the polymer backbone. These positions include side chains on one of the blocks from copolymers, chain-end groups, or junctions between blocks. Considering the polymer architecture, smart polymers may be classified as [2] (1) linear free chains in solution which undergo extension/collapse in response to the trigger, (2) covalently cross-linked gels that shrink or swell in the presence of the trigger, and (3) chain-adsorbed or surface-grafted forms where extension/collapse of the chains occurs on the surface in response to the trigger (Fig. 7.1).

The response may be reversible or not, depending on the nature of the process triggered on the polymer chain at a microscopic level. In this way, the first step for
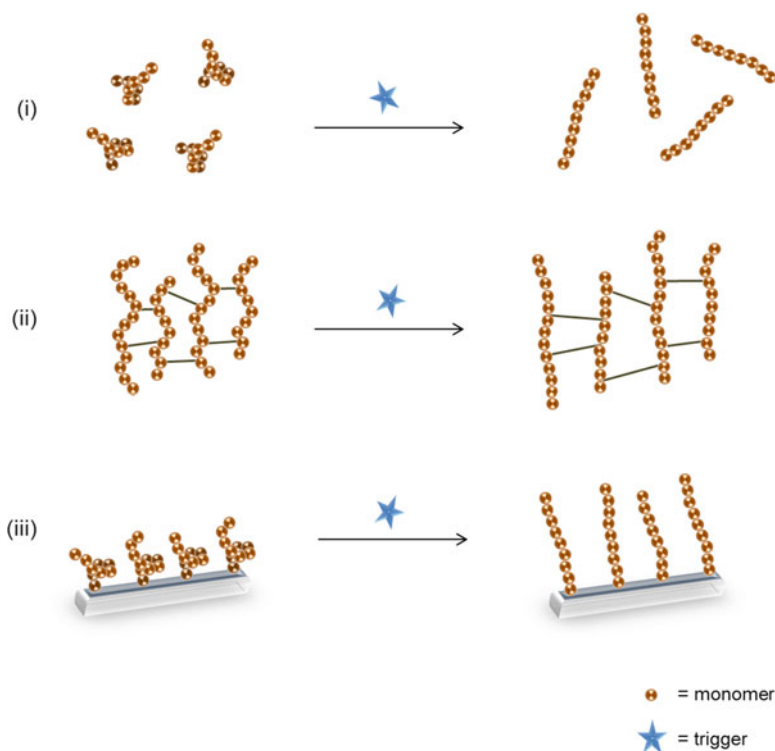
Fig. 7.1 Schematic illustration of (i) linear free chains in solution, (ii) covalently cross-linked gels, and (iii) surface-grafted polymer chains, and the extension/swelling of the chains in response to the trigger

designing smart polymers is the choice of the trigger, which may be placed into one of the following categories: physical, chemical, or biological. The former category of trigger modifies the polymer chain dynamics, whereas the second may affect interactions between the polymer and solvent molecules or between the polymer chains. Biological stimuli involve the action of physiological molecules on the on the polymer chains, which may induce different effects such as chemical bond cleavage and conformational changes [35].

7.2.1   Polymers Responsive to Physical Triggers

The most common physical triggers are temperature, light, and electric field stimuli. Thermoresponsive polymer solutions present a critical temperature in which hydrophobic and hydrophilic interactions between the polymeric chains and the solvent abruptly change, inducing chain collapse or expansion. This response can occur at upper critical solution temperature (UCST) and/or lower critical solution temperature (LCST). Phase separation displayed by monophasic solutions from thermoresponsive polymers below the UCST is driven by attractive enthalpic considerations. On the other hand, the polymer solutions may become biphasic above LCST due to an entropically driven mechanism related to strong interactions such as hydrogen bonding between the polymer chain and water [36]. The LCST and UCST values can be changed by incorporating hydrophilic or hydrophobic segments into the chain [37]. In this way, adequate balance between hydrophilic and hydrophobic segments in amphiphilic block copolymers may suit the phase transition temperature (e.g., to body temperature) [38]. Thermoresponsive polymers reported in the literature include poly(N-alkyl-substituted acrylamides), poly(N-vinylalkylamides), and copolymers such as poly(ethylene oxide)–poly(propylene oxide)–poly(ethylene oxide) (PEO–PPO–PEO) [39, 40].

Photo-responsive polymers, another important class of polymers responsive to physical triggers, may capture optical signals by light-sensitive chromophores such as azobenzene, spiropyran, or nitrobenzyl groups in the polymer chain, converting them to chemical signals [41]. This process typically results in isomerization, cleavage, or dimerization. On the other hand, electrically responsive polymers are conducting molecules that can show swelling, shrinking, or bending in response to an external field [42]. In these structures, electrons are delocalized along the conjugated backbones. Typical examples are polythiophene (PT) and sulfonated polystyrene (PSS). This class of polymers has been excitingly investigated as artificial muscles and sensors in microfluidic platforms [43].

7.2.2   Polymers Responsive to Chemical Triggers

Ionic strength, pH, and redox conditions are the most common chemical stimuli reported to trigger responses from smart polymers. The key factor for pH-responsive polymers is the existence of weak acidic or basic moieties covalently attached to a

hydrophobic chain. The ionization of these moieties causes electrostatic repulsion of the charges and extension of the coiled chains. The critical pH value required to induce the changes can be tuned according to the pK_a of the pendant acidic or basic groups [44]. Polymers with pH-responsive properties include chitosan and poly(acrylic acid) derivatives [45]. Polymers containing ionizable groups can also respond to ionic strength. Attractive interactions between oppositely charged species may affect the polymer solubility in media with different salt concentrations. As a consequence, some relevant properties such as rheological behavior can be considerably altered [46].

Redox-responsive polymers can be obtained whether the polymer chain presents acid labile moieties, as observed in polyanhydrides, polymers synthesized from α-hydroxy acids, and poly(β-amino esters) (PβAEs) [47]. Cleavable disulfide groups have also been displayed by redox-responsive polymers because they are unstable in a reducing environment in which the corresponding thiol groups are formed. The redox reaction can be induced by reductive molecules such as cysteine and glutathione [48].

7.2.3 Polymers Responsive to Biological Triggers

Smart polymers can be engineered for responsiveness to enzymes, receptors, metabolites, small biomolecules like glucose, and other relevant biological compounds as triggers with great potential for in vivo applications. In most systems, enzymes degrade the polymer backbone under mild conditions exhibiting high selectivity [49]. For instance, ester bonds in the polymer chain may be cleaved by hydrolytic enzymes, such as lipases. As a consequence, lipases can trigger degradation of drug-loaded supramolecular structures based on polymers presenting ester bonds releasing the drug to the external medium [50]. Enzymes can also form new covalent bonds that may change the macroscopic properties of the polymers. An illustration of this concept comprises the action of transglutaminase, which promotes cross-linking between the side chains of lysine and glutamine residues in peptide chains [51].

Development of stimuli-responsive strategies involving small biomolecules and metabolites as triggers is a promising strategy. In general, these systems attempt to mimic physiological self-regulating mechanisms in order to control the release kinetics of loaded drugs. For example, reactive oxygen metabolites generated from inflammatory processes have been used as triggers for drug release by the controlled degradation of cross-linked hyaluronic acid gels [52]. Glucose-responsive polymer bearing a phenyl borate derivative as a glucose-sensing moiety [53] is another biological approach with promising results. A major development related to research and the technological application of biological responsive polymer materials is expected for the next years.

7.3 Synthetic Strategies Using Controlled Radical Polymerization

As mentioned earlier, controlled radical polymerization is the preferred technique to synthesize smart polymers. The key feature of all CRP mechanisms involves a dynamic equilibrium between propagating radicals [P•] and dormant species that may be reversibly trapped in a deactivation or activation process. In addition, the propagating radicals are present in much smaller concentrations than the dormant species and this is the most important characteristic of CRP. In other words, the activation rate (K_{act}) must be considerably smaller than the deactivation rate (K_{deact}) of the propagating species to ensure a low termination rate (Fig. 7.2). This is central to all CRP systems and fundamental to control the molar mass and its distribution. The details of the CRP mechanisms are very well described in recent reviews from literature [13, 15, 21]. The most well-established methods include atom transfer radical polymerization (ATRP), reversible addition–fragmentation transfer (RAFT), and nitroxide-mediated polymerization (NMP). A brief description of each synthetic method as well as their limitations and some important examples of the applications from literature are presented below.
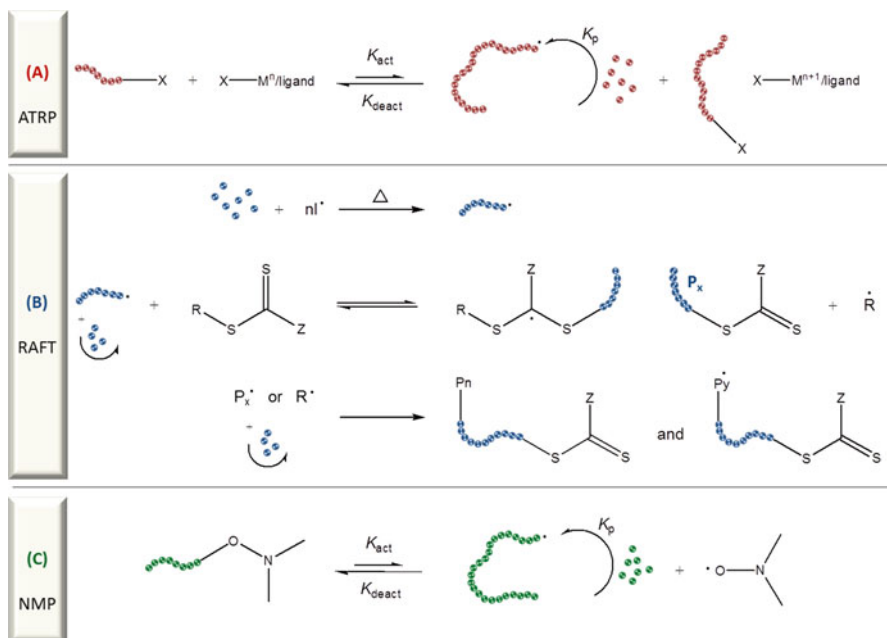
Fig. 7.2 Schematic representation of various CRP mechanisms (**a**) ATRP, (**b**) RAFT, and (**c**) NMP

7.3.1   ATRP Reaction

ATRP is one of the most versatile techniques used to synthesize polymers with well-defined structures, various architectures/functionalities, and controlled dispersity [54–57]. Conventional ATRP reactions include the monomer, an initiator with a transferable halogen (generally alkyl bromide or alkyl chloride) and a catalyst system that presents a transition metal with a suitable ligand. The dynamic equilibrium between dormant and active species is achieved by a reversible redox process in which the transition metal from the catalyst system activates an alkyl halide to generate the corresponding radical and transition metal complex in its higher oxidation state (see Fig. 7.2a). This strategy can be illustrated by the preparation of graft copolymers of cellulose, which was discussed in the excellent review by Cameron and coworkers [56], is where the preparation of graft copolymers of cellulose and its derivatives under homogeneous conditions by the ATRP technique is described in detail. Generally, for cellulose the "grafting-from" strategy is more common, and it involves two steps: (1) macroinitiator (MI) preparation via chemical modification of hydroxyl group from cellulose to bromide and (2) using MI to initiate the ATRP reaction in the presence of monomers from the backbone generating graft copolymers.

The concentration of transition metal species in the conventional ATRP reaction cannot be lower than that of the chains involved in radical–radical termination reactions to sustain an adequate rate of polymerization. Stoichiometric or slightly sub-stoichiometric ratios of the transition metal catalyst to the initiator may be used leading to a higher catalyst concentration in the polymeric material [58]. It is important to note that reactions with monomers containing strongly coordinating groups such as acid groups cannot be performed by ATRP because there is a loss of catalytic activity due to complexation between the monomer and the metallic catalyst. Although ATRP proved to be a remarkable technique in controlling polymer architecture, some reasons have limited its use for industrial scale production: (1) the catalyst is sensitive to air and other oxidants, which may adversely affect the control of polymerization, and (2) purification after polymerization is necessary to remove the mildly toxic transition metals composing the catalyzers. To overcome these drawbacks, new initiation processes for ATRP have been developed, employing a significantly lower concentration of catalyst and oxidative stable complexes. An example of this strategy is comprised of a catalyst containing Cu (II) that is activated in the presence of reducing agents (RAs) such as tin (II) 2-ethylhexanoate ($Sn(EH)_2$), glucose, ascorbic acid, and others. In this process, RA regenerates the activator species Cu (I) (Fig. 7.3). This new approach is particularly attractive to synthesize materials for biomedical applications because the polymers obtained from these reactions are nearly free of metal contamination.

It is well known that high proportion of living chains and low catalyst concentration are required for the preparation of well-defined polymeric architectures by ATRP. High catalyst concentrations may lead polymers to drop the halide chain-
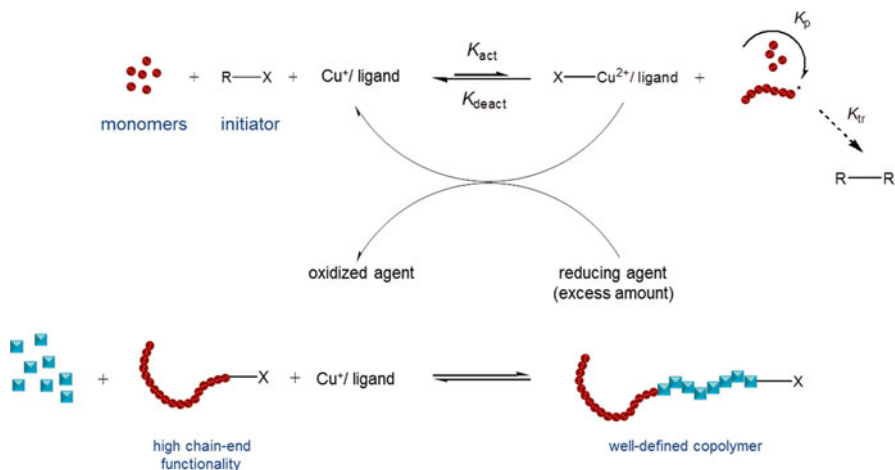
Fig. 7.3 General mechanism of ATRP with excess of reducing agent and very low amount of copper-based catalyst. High proportion of chain-end functionality and well-defined copolymers. *R–R (radical–radical bond

end functionality due to terminations or other side reactions [59]. Matyjaszewski's group [60] developed a simultaneous reverse and normal initiation (SR&NI) process but it was not suitable for block copolymer synthesis because polymer chains were initiated by the free radical initiator added to the reaction medium. Another strategy called activators generated by electron transfer (AGET) partially solved the problem because the addition of a free radical initiator, which could initiate new chains, was not involved. Instead, reducing agents that can react with transition metals in a higher oxidation state were used to generate the reduced activator. Consequently, the formation of homopolymers as side products was avoided during the copolymerization. However, it is difficult to estimate the exact amount of RA needed for the reaction [61]. In the process based on continuous activator regeneration (ICAR) [19], a source of organic free radicals is employed in a small amount with the aim to continuously regenerate the metal activator. As a result, the catalyst concentration can be significantly decreased without affecting the controlled polymerization. A simple and versatile technique via activators regenerated by electron transfer atom transfer radical polymerization (ARGET-ATRP) [18] proved to be one of the most relevant techniques to produce a high proportion of living chains and consequently pure block copolymers with controlled functionalities, compositions, and smart properties [55, 59]. There are several variables associated to the new ATRP strategies that must be optimized in each case, but all of these strategies show similar advantages: the environmental impact is reduced, the reactions can be performed in aqueous medium under room temperature, and they may be adapted in order to be carried out under biological conditions [62].

7.3.2 RAFT Polymerization

RAFT is among the most powerful polymerization techniques, in particular due to a wide range of monomers that cannot be polymerized by ATRP. The mechanistic process is very well described in excellent reviews [15, 20, 21]. The basic principle of RAFT is similar to that of conventional free radical polymerization, but incorporates a chain transfer agent (CTA) that contains a labile bond as thiocarbonylthio moiety. The CTA is added to the monomeric radical species forming labile intermediates (dormant species) that can fragment releasing R* (free radicals) or P$_x$*(polymeric radicals) (see Fig. 7.2b). These radicals are added to the monomer reinitiating the polymerization and creating another thiocarbonylthio moiety. Equilibrium is reached between the propagating polymeric radical and the dormant species resulting in uniform chain growth and excellent control over the molar mass. The final polymer is a macro-CTA, which can be isolated, and subsequently the chain can be extended attaching a second monomer on the macro-CTA. The RAFT agent retained in the polymer chain-end may induce toxicity when the polymer is planned to be used for biomedical purposes. There are some methods available to replace the RAFT end group including aminolysis, radical-induced reduction, and thermal elimination [63]. Tailoring the end groups to obtain the desired polymer architectures is an important advantage of functionalization by RAFT agent due to lability of the thiocarbonylthio group, which allows prompt post-polymerization modification. The ability to remove and subsequently tailor the end group is widely applicable as reported by O'Reilly and coauthors [64], who described the advances and main advantages regarding chain-end group modifications from polymers synthesized by RAFT.

7.3.3 NMP Reaction

Nitroxide-mediated polymerization (NMP) (or aminoxyl-mediated radical polymerization (AMRP) as proposed by IUPAC) is one of the three most important CRP methods. The key factor in the mechanism of NMP is the reversible thermal deactivation (C–O bond cleavage) of a polymeric alkoxyamine such as 2,2,6,6-tetramethyl -1-piperidinyloxyl (TEMPO) to generate the polymeric radical and a dormant alkoxyamine. The subsequent monomer insertion and nitroxide trapping lead to the chain-extended polymer. The advantages of NMP are high purity of the polymer and wide scope of functional monomers, including those with unsaturated hydrocarbon structure as polyisoprene and polybutadiene, which cannot be polymerized by ATRP due to chelation of the copper catalyst [13, 14]. In addition, NMP can be optimized for large-scale production. The disadvantages of the NMP method are related to high temperatures and lengthy polymerization times required by the reaction to occur with a reasonable rate. A new generation of nitroxides consisting of acyclic β-phosphorylated nitroxide [N-tert-butyl-N-(1-(diethoxyphosphoryl)-2,2-dimethylpropyl-N-oxyl nitroxide] also

known as SG1 or BlocBuilder showed high efficiency in the synthesis of well-defined polymers and copolymers with predictable molecular weight [65]. However, these molecules were not efficient in controlling the polymerization of methacrylic monomers due to the formation of irreversible termination reactions among unstable propagating macroradicals.

Recently, some strategies for optimizing the NMP method, such as polymerization-induced self-assembly (PISA), have led to the in situ formation of pH-responsive amphiphilic block copolymers. Darabi and coworkers [66] synthesized poly(DEAEMA-co-S)-SG1 and poly(DMAEMA-co-S)-SG1 macroalkoxyamines and used them in their protonated form as stabilizers and macroinitiators for the nitroxide-mediated surfactant-free emulsion polymerization of MMA and styrene. One of the main advantages of this strategy was the absence of surfactants that can alter the properties of the final product.

It is evident that each strategy has its own advantages and limitations. ATRP may be best suited to produce low molecular weight polymers with special functionalities but it is inadequate if the monomers contain strongly coordinating groups. RAFT is the most efficient system for these monomers and higher molecular weights may be obtained. On the other hand, there is no need to use metal or sulfur-containing controlling agents in the NMP process, which is the best option when the absolute absence of these elements in the polymer is imperative.

7.3.4 Combining CRP and Click Reactions

Although the click chemistry strategy is not new (proposed by Huisgen in 1963), it received little attention over decades due to technical difficulties related to the synthetic protocol. Sharpless and coworkers [67] reintroduced this reaction in 2001 using Cu (I) as a catalyst. This new mechanism is based on high-efficiency reactions between two functional groups (e.g., azides and alkynes) that are readily reactive together. The click reactions are performed with high yields producing harmless by-products that can be removed by non-chromatographic methods. Furthermore, the starting materials and reagents are readily accessible, and the reactions are performed in mild conditions and nontoxic solvents, such as water. In addition, the functional groups related to click reactions are compatible with enzymes under physiological conditions and may be easily incorporated into various macromolecules [68]. A schematic representation of click chemistry reactions is shown in Fig. 7.4.

The combination of both CRP and click chemistry strategies offers the possibility to obtain well-defined and tailored functionalized macromolecular structures with smart properties. The optimization of the reaction conditions involving the monomer, initiator, solvent, and/or catalyst is always required in order to reach absolute control over the macromolecule structures. The post-polymerization of functional macromolecules with small organic molecules or other macromolecules is considered a powerful tool to obtain block copolymers or star-shaped polymers with interesting applications in biomedical and nanotechnology research fields.
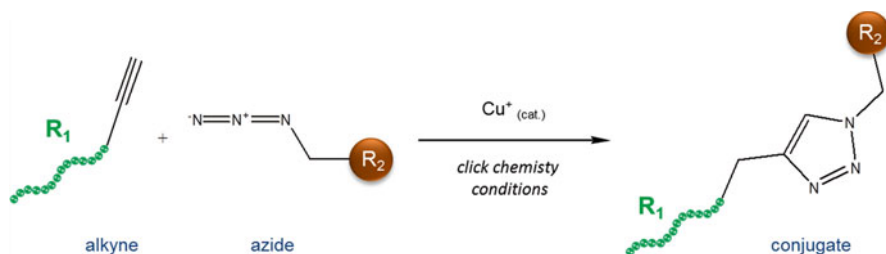
Fig. 7.4 Schematic representation of the click reaction using azide and alkyne as functional groups

The reactive chain-end groups from macroinitiators can be successfully used for structure modification by click chemistry. This idea is illustrated by a previous report from Wang and coworkers [69]. In this work, NaN_3 and an amphiphilic tri-block copolymer obtained via ATRP were reacted in order to modify the polymer chain-end groups into azide groups. Subsequently, the azide groups reacted with alkynated biotin forming a functional interface between the hydrophilic shell and the hydrophobic core of self-assembled polymeric micelles. The recent study from Chen and coworkers [23] presents another approach to controlling complex macro-molecular architectures. In this study, smart tetrablock polymers with dual stimulus response were obtained by combination of ATRP, RAFT, and click chemistry. The combination of two or more techniques is a clever strategy when a unique method is not suitable to synthesize the polymer.

7.4   Self-Assembled Supramolecular Structures and Drug Loading

A number of self-assembled supramolecular morphologies can be designed for smart polymer-based systems depending on the desired application [35, 70, 71] such as nanoparticles, dendrimers, vesicles, micelles, hydrogels, and polymer brushes. It should be noted that this is not a wide-ranging list. Nowadays, more and more smart polymeric structures with new morphologies and remarkable properties are arising from the efforts and creativity of researchers working in several fields. Drug delivery [71], tissue engineering [72], food products [73], cosmetics [74], biosensor devices [75], smart textiles [76], smart coatings [77], and thermal energy storage [78] may be cited among the industrial activities where smart supramolecular polymer structures promise to make the greatest impact.

Polymer vesicles, also called polymersomes, are spherical structures in which an aqueous compartment is enclosed by a bilayer membrane made of amphiphilic block copolymers. There are reports mentioning polymersomes responsive to a redox environment, pH, temperature, and others [79], in particular for drug delivery. Hydrophilic molecules can be loaded into the inner aqueous compartment, whereas

more hydrophobic compounds can be accommodated within the polymeric shell. Stimuli-triggered disassembly of the vesicles can induce drug release in specific environments. The responsiveness is related to the architecture of the polymer chain and its functional moieties. Recently, self-immolative polymersomes (SIPsomes) based on hydrophobic blocks terminally modified with capping moieties responsive to different triggers were reported as an alternative approach for triggered drug co-release [80]. These moieties comprised perylen-3-yl, 2-nitrobenzyl, or disulfide bond, which may respond to visible light, UV light, and reductive milieu as stimuli, respectively. Upon deprotection by the corresponding trigger, the vesicle disintegrated due to a cascading depolymerization reaction. This study exemplifies the concept of polymersomes with modular responsive modes sensitive to different types of stimuli. The advances, challenges, and potential applications of smart polymersomes were recently discussed in detail by Du and O'Reilly [81].

Polymer micelles are usually formed by the spontaneous self-assembly of amphiphilic block copolymers in a solvent. They can be described as core–shell structures with spherical shape and sizes varying around 10–100 nm. Poly(ethylene glycol)-based block copolymers are commonly used to prepare self-assembled micelles for biocompatible environments [82]. In an aqueous medium, the micelle core is composed of the hydrophobic blocks from the copolymer, whereas the hydrophilic blocks constitute the micelle corona. In this way, lipophilic drugs are expected to be solubilized into the hydrophobic micelle core, significantly increasing drug concentration in aqueous solution. On the other hand, some hydrophilic molecules can be adsorbed on the outer shell of micelles due to strong interactions by Coulombic forces or hydrogen bonding according to the nature of the micelle surface. Smart polymer-based micelles offer multiple possible approaches to trigger drug release. Strategies reported in literature involve degradation, cleavage, swelling, self-assembly/disassembly, and others [83, 84].

Polymer-based systems include hydrogels, which are defined as three-dimensional polymeric networks that have the tendency to absorb large amount of water while their dimensional stability is maintained due to physical or chemical crosslinking. Smart hydrogels may respond to varied stimuli, such as pH, biological triggers, and temperature [85]. Fast-response hydrogels translate external stimuli into local alteration of mechanical or physical properties to promote drug release. In the most widespread strategy used to achieve rapid kinetics, the size of the smart hydrogel is reduced in the presence of the trigger.

Temperature is probably the most common trigger for smart polymer-based hydrogels. Hydrogels composed of polymers with a UCST may shrink when cooled below this critical temperature value. On the contrary, hydrogels with LCST may shrink upon heating above their LCST. A classic example of thermoresponsive hydrogel is made from poly(*N*-isopropylacrylamide) (PNIPAAm), which exhibits a phase transition temperature around 32–34 °C in water [86]. Other common smart polymers used to prepare hydrogels responsive to different types of stimuli include polylactide (PLA) and polysaccharides [87].

A polymer brush consists of end-tethered polymer chains stretched away from the substrate due to the excluded volume effect. Interaction forces between the

brush and the external medium may be switched due to the action of the trigger in the polymer chain. In mixed brushes, in which two or more different polymers are grafted to the same substrate, the chains may preferentially segregate to the top of the brush or on the substrate surface according to the nature of each type of chain and the stimuli from the external medium. Some key strategies for preparing polymer brushes and current and future challenges related to these systems are discussed in an excellent review written by Peng and Bhushan [88].

7.5 Conclusion

The opportunities are growing fast for high-tech industry in creating and consuming polymeric systems with stimuli-responsive characteristics. Research and innovation involving smart polymers are relatively new. Precise synthetic approaches leading to exact polymeric architectures have always been a challenge, and recent advances in CRP polymerizations have created unprecedented opportunities for the design and synthesis of innovative smart polymers with well-defined structures. Furthermore, development of strategies involving CRP combined with click chemistry opened up the opportunity for new technological advances in which smart polymers can be planned to incorporate new functionalities and self-assemble into several supramolecular structures that potentially have a great impact on relevant fields for industry.

References

1. Ebewele RO (2000) Polymer science and technology. CRC Press, Boca Raton, FL
2. Kumar A, Srivastava A, Galaev IY, Mattiasson B (2007) Smart polymers: physical forms and bioengineering applications. Prog Polym Sci 32(10):1205–1237
3. Na K, Jung J, Kim O, Lee J, Lee TG, Park YH, Hyun J (2008) "Smart" biopolymer for a reversible stimuli-responsive platform in cell-based biochips. Langmuir 24(9):4917–4923
4. Gandini A (2011) The irruption of polymers from renewable resources on the scene of macromolecular science and technology. Green Chem 13:1061–1083
5. Lindqvist J, Malmström E (2006) Surface modification of natural substrates by atom transfer radical polymerization. J Appl Polym Sci 100:4155–4162
6. Joglekar M, Trewyn BG (2013) Polymer-based stimuli-responsive nanosystems for biomedical applications. Biotechnol J 8(8):931–945
7. Hu J, Zhang G, Liu S (2012) Enzyme-responsive polymeric assemblies, nanoparticles and hydrogels. Chem Soc 41(18):5933–5949
8. Baskarana D, Müller AHE (2007) Anionic vinyl polymerization—50 years after Michael Szwarc. Prog Polym Sci 32:173–219
9. Kostjuk SV (2015) Recent progress in the Lewis acid co-initiated cationic polymerization of isobutylene and 1,3-dienes. RSC Adv 5:13125–13144
10. Penczek S (2000) Cationic ring-opening polymerization (CROP) major mechanistic phenomena. J Polym Sci A Polym Chem 38:1919–1933
11. Nuyken O, Pask SD (2013) Ring-opening polymerization—An introductory review. Polymers 5:361–403

12. Matyjaszewski K, Davis TP (2002) Handbook of radical polymerization. Wiley-Interscience, Hoboken, NJ
13. Nicolas J, Guillaneuf Y, Lefay C, Bertin D, Didier G, Charleux B (2013) Nitroxide-mediated polymerization. Prog Polym Sci 38:63–235
14. Savelyeva X, Maric M (2014) Pyrrolidone-functional smart polymers via nitroxide-mediated polymerization. J Polym Sci A Polym Chem 52:2011–2024
15. Matyjaszewski K (2005) Macromolecular engineering: From rational design through precise macromolecular synthesis and processing to targeted macroscopic material properties. Prog Polym Sci 30:858–875
16. Harrisson S, Nicolas J, Maksimenko A, Bui DT, Mougin J, Couvreur P (2013) Nanoparticles with in vivo anticancer activity from polymer prodrug amphiphiles prepared by living radical polymerization. Angew Chem Int Ed 52:1678–1682
17. Miao J, He W, Zhang L, Wang Y, Cheng Z, Zhu X (2012) AGET ATRP of water-soluble PEGMA: fast living radical polymerization mediated by iron catalyst. J Polym Sci A Polym Chem 50:2194–2200
18. Kwak Y, Magenau AJD, Matyjaszewski K (2011) ARGET ATRP of methyl acrylate with inexpensive ligands and ppm concentrations of catalyst. Macromolecules 44:811–819
19. Konkolewicz D, Magenau AJD, Averick SE, Simakova A, He H, Matyjaszewski K (2012) ICAR ATRP with ppm Cu catalyst in water. Macromolecules 45:4461–4468
20. Sun JT, Hong CY, Pan CY (2013) Recent advances in RAFT dispersion polymerization for preparation of block copolymer aggregates. Polym Chem 4:873–881
21. Barner-Kowollik C, Perrier S (2008) The future of reversible addition fragmentation chain transfer polymerization. J Polym Sci A Polym Chem 46:5715–5723
22. Nasrullah MJ, Vora A, Webster CD (2011) Block copolymer synthesis via a combination of ATRP and RAFT using click chemistry. Macromol Chem Phys 212:539–549
23. Chen J, Liu M, Gong H, Cui G, Lü S, Gao C, Huang F, Chen T, Zhang X, Zhen L (2013) Synthesis of linear amphiphilic tetrablock quaterpolymers with dual stimulus response through the combination of ATRP and RAFT by a click chemistry site transformation approach. Polym Chem 4:1815–1825
24. Meng T, Gao X, Zhang J, Yuan J, Zhang Y, He J (2009) Graft copolymers prepared by atom transfer radical polymerization (ATRP) from cellulose. Polymer 50:447–454
25. Lindqvist J, Nyström D, Östmark E, Antoni P, Carlmark A, Johansson M, Hult A, Malmström E (2008) Intelligent dual-responsive cellulose surfaces via surface-initiated ATRP. Biomacromolecules 9:2139–2145
26. Roy D, Guthrie JT, Perrier S (2005) Graft polymerization: Grafting poly(styrene) from cellulose via reversible addition–fragmentation chain transfer (RAFT) polymerization. Macromolecules 38:10363–10372
27. Hufendiek A, Trouillet V, Meier MAR, Barner-Kowollik C (2014) Temperature responsive cellulose-graft-copolymers via cellulose functionalization in an ionic liquid and RAFT polymerization. Biomacromolecules 15:2563–2572
28. Semsarilar M, Ladmiral V, Perrier S (2010) Synthesis of a cellulose supported chain transfer agent and its application to RAFT polymerization. J Polym Sci A Polym Chem 48:4361–4365
29. Negishi K, Mashiko Y, Yamashita E, Otsuka A, Hasegawa T (2011) Cellulose chemistry meets click chemistry: syntheses and properties of cellulose-based glycoclusters with high structural homogeneity. Polymers 3:489–508
30. Andersen T, Bleher S, Flaten GE, Tho I, Mattsson S, Škalko-Basnet N (2015) Chitosan in mucoadhesive drug delivery: focus on local vaginal therapy. Mar Drugs 13:222–236
31. Luo Y, Teng Z, Li Y, Wang Q (2015) Solid lipid nanoparticles for oral drug delivery: chitosan coating improves stability, controlled delivery, mucoadhesion and cellular uptake. Carbohydr Polym 122:221–229
32. Cunningham A, Ko NR, Oh JK (2014) Synthesis and reduction-responsive disassembly of PLA-based mono-cleavable micelles. Colloids Surf B 122:693–700

33. Wang Z, Rutjes FP, Hest JCV (2014) pH responsive polymersome Pickering emulsion for simple and efficient Janus polymersome fabrication. Chem Commun 50(93):14550–14553

34. Chen YH, Chung YC, Wang IJ, Young TH (2012) Control of cell attachment on pH-responsive chitosan surface by precise adjustment of medium pH. Biomaterials 33(5):1336–1342

35. Raghupathi KR, Guo J, Munkhbat O, Rangadurai P, Thayumanavan S (2014) Supramolecular disassembly of facially amphiphilic dendrimer assemblies in response to physical, chemical, and biological stimuli. Acc Chem Res 47(7):2200–2211

36. Taylor LD, Cerankowski LD (1975) Preparation of films exhibiting a balanced temperature dependence to permeation by aqueous solutions - a study of lower consolute behavior. J Polym Sci Polym Chem 13:2551–2570

37. Tebaldi MLS, Chaparro TC, Santos AM (2010) Tri-block copolymers obtained by RAFT polymerization: a promising material for drug-delivery systems. Mater Sci Forum 636–637: 76–81

38. Gu L, Gao Y, Qin Y, Chen X, Wang X, Wang F (2013) Biodegradable poly(carbonate-ether)s with thermoresponsive feature at body temperature. J Polym Sci A Polym Chem 51:282–289

39. Yıldız B, Işık B, Kış M (2001) Synthesis of thermoresponsive N-isopropylacrylamide–N-hydroxymethyl acrylamide hydrogels by redox polymerization. Polymer 42(6):2521–2529

40. Suwa K, Morishita K, Kishida A, Akashi M (1997) Synthesis and functionalities of poly(N-vinylalkylamide). J Polym Sci A Polym Chem 35:3087–3309

41. Wagner N, Theato P (2014) Light-induced wettability changes on polymer surfaces. Polymer 55(16):3436–3453

42. Roncali J (1992) Conjugated poly(thiophenes): synthesis, functionalization, and applications. Chem Rev 92(4):711–738

43. Wallace RA (1973) Electrical conduction in sulfonated polystyrene films. J Appl Polym Sci 17(1):231–238

44. Qiu Y, Park K (2012) Environment-sensitive hydrogels for drug delivery. Adv Drug Deliv Rev 64:49–60

45. Shi L, Yang L, Chen J, Pei Y, Chen M, Hui B, Li J (2004) Preparation and characterization of pH-sensitive hydrogel of chitosan/poly(acrylic acid) co-polymer. J Biomater Sci Polym 15(4):465–474

46. Marques NN, Curti PS, Maia AMS, Balaban RC (2013) Temperature and pH effects on the stability and rheological behavior of the aqueous suspensions of smart polymers based on N-isopropylacrylamide, chitosan, and acrylic acid. J Appl Polym Sci 129(1):334–345

47. Lallana E, Tirelli N (2013) Oxidation-responsive polymers: which groups to use, how to make them, what to expect from them (biomedical applications). Macromol Chem Phys 214:143–158

48. Nagahara N (2011) Intermolecular disulfide bond to modulate protein function as a redox-sensing switch. Amino Acids 41:59–72

49. Ganesh VA, Baji A, Ramakrishna S (2014) Smart functional polymers—A new route towards creating a sustainable environment. RSC Adv 4:53352–53364

50. Arouri A, Hansen AH, Rasmussen TE, Mouritsen OG (2013) Lipases, liposomes and lipid-prodrugs. Curr Opin Colloid Interface Sci 18:419–431

51. Hu BH, Messersmith PB (2003) Rational design of transglutaminase substrate peptides for rapid enzymatic formation of hydrogels. J Am Chem Soc 125(47):14298–14299

52. Burdick JA, Chung C, Jia X, Randolph MA, Langer R (2005) Controlled degradation and mechanical behavior of photopolymerized hyaluronic acid networks. Biomacromolecules 6:386–391

53. Matsumoto A, Yoshida R, Kataoka K (2004) Glucose-responsive polymer gel bearing phenylborate derivative as a glucose-sensing moiety operating at the physiological pH. Biomacromolecules 5:1038–1045

54. Ran J, Wu L, Zhang Z, Xu T (2014) Atom transfer radical polymerization (ATRP): a versatile and forceful tool for functional membranes. Prog Polym Sci 39:124–144

55. Król P, Chmielarz P (2014) Recent advances in ATRP methods in relation to the synthesis of copolymer coating materials. Prog Org Coat 77:913–948

56. Joubert F, Musa OM, Hodgson DRW, Cameron NR (2014) The preparation of graft copolymers of cellulose and cellulose derivatives using ATRP under homogeneous reaction conditions. Chem Soc Rev 43:7217–7235
57. Braunecker WA, Matyjaszewski K (2007) Controlled/living radical polymerization: features, developments and perspectives. Prog Polym Sci 32:93–146
58. Chan N, Cunningham MF, Hutchinson RA (2008) ARGET ATRP of methacrylates and acrylates with stoichiometric ratios of ligand to copper. Macromol Chem Phys 209:1797–1805
59. Jakubowski W, Kirci-Denizli B, Gil RR, Matyjaszewski K (2008) Polystyrene with improved chain-end functionality and higher molecular weight by ARGET ATRP. Macromol Chem Phys 209:32–39
60. Li M, Jahed NM, Min K, Matyjaszewski K (2004) Preparation of linear and star-shaped block copolymers by ATRP using simultaneous reverse and normal initiation process in bulk and miniemulsion. Macromolecules 37:2434–2441
61. Jakubowski W, Matyjaszewski K (2005) Activator generated by electron transfer for atom transfer radical polymerization. Macromolecules 38:4139–4146
62. Averick S, Simakova A, Park S, Konkolewicz D, Magenau AJD, Mehl RA, Matyjaszewski K (2012) ATRP under biologically relevant conditions: grafting from a protein. ACS Macro Lett 1:6–10
63. Roth PJ, Kessler D, Zentel R, Theato P (2008) A method for obtaining defined end groups of polymethacrylates prepared by the RAFT process during aminolysis. Macromolecules 41:8316–8319
64. Willcock H, O'Reilly RK (2010) End group removal and modification of RAFT polymers. Polym Chem 1:149–157
65. Grimaldi S, Finet JP, Moigne FL, Zeghdaoui A, Tordo P, Benoit D, Fontanille M, Gnanou Y (2000) Acyclic β-phosphonylated nitroxides: a new series of counter-radicals for "living"/controlled free radical polymerization. Macromolecules 33:1141–1147
66. Darabi A, Shirin-Abadi AR, Pinaud J, Jessop PG, Cunningham MF (2014) Nitroxide-mediated surfactant-free emulsion copolymerization of methyl methacrylate and styrene using poly(2-(diethyl)aminoethyl methacrylate-co-styrene) as a stimuli-responsive macroalkoxyamine. Polym Chem 5:6163–6170
67. Kolb HC, Finn MG, Sharpless KB (2001) Click chemistry: diverse chemical function from a few good reactions. Angew Chem Int Ed 40:2004–2021
68. Nwe K, Brechbiel MW (2009) Growing applications of "click chemistry" for bioconjugation in contemporary biomedical research. Cancer Biother Radiopharm 24(3):289–302
69. Wang X, Liu L, Luo Y, Zhao H (2009) Bioconjugation of biotin to the interfaces of polymeric micelles via in situ click chemistry. Langmuir 25:744–750
70. Schattling P, Jochum FD, Theato P (2014) Multi-stimuli responsive polymers—the all-in-one talents. Polym Chem 5:25–36
71. Bajpai AK, Shukla SK, Bhanu S, Kankane S (2008) Responsive polymers in controlled drug delivery. Prog Polym Sci 33(11):1088–1118
72. Bendrea A, Cianga L, Cianga I (2011) Review paper: progress in the field of conducting polymers for tissue engineering applications. J Biomater Appl 26:3–84
73. Chaudhry Q, Castle L (2011) Food applications of nanotechnologies: an overview of opportunities and challenges for developing countries. Trends Food Sci Technol 22:595–603
74. Mihranyan A, Ferraz N, Strømme M (2012) Current status and future prospects of nanotechnology in cosmetics. Prog Mater Sci 57:875–910
75. Wang Y, Papadimitrakopoulos F, Burgess DJ (2013) Polymeric "smart" coatings to prevent foreign body response to implantable biosensors. J Control Release 169:341–347
76. Cherenack K, Pieterson L (2012) Smart textiles: challenges and opportunities. J Appl Phys 112:091301
77. Montemor MF (2014) Functional and smart coatings for corrosion protection: a review of recent advances. Surf Coat Technol 258:17–37

78. Sinha-Ray S, Sahua RP, Yarin AL (2011) Nano-encapsulated smart tunable phase change materials. Soft Matter 7:8823–8827
79. Feng A, Yuan J (2014) Smart nanocontainers: progress on novel stimuli-responsive polymer vesicles. Macromol Rapid Commun 35(8):767–779
80. Liu G, Wang X, Hu J, Zhang G, Liu S (2014) Self-immolative polymersomes for high-efficiency triggered release and programmed enzymatic reactions. J Am Chem Soc 136:7492–7497
81. Du J, O'Reilly RK (2009) Advances and challenges in smart and functional polymer vesicl. Soft Matter 5:3544–3561
82. Li Y, Gao GH, Lee DS (2013) pH-sensitive polymeric micelles based on amphiphilic polypeptide as smart drug carriers. J Polym Sci A Polym Chem 51:4175–4182
83. Nishiyama N, Bae Y, Miyata K, Fukushima S, Kataoka K (2005) Smart polymeric micelles for gene and drug delivery. Drug Discov Today Technol 2(1):21–26
84. Harnoy AJ, Rosenbaum I, Tirosh E, Ebenstein Y, Shaharabani R, Beck R, Amir RJ (2014) Enzyme-responsive amphiphilic PEG-dendron hybrids and their assembly into smart micellar nanocarriers. J Am Chem Soc 136(21):7531–7534
85. White EM, Yatvin J, Grubbs JB, Bilbrey JA, Locklin J (2013) Advances in smart materials: stimuli-responsive hydrogel thin films. J Polym Sci Part B Polym Phys 51:1084–1099
86. Heskins M, Guillet JE (1968) Solution properties of poly(N-isopropylacrylamide). J Macromol Sci Chem A2:1441–1455
87. Zhu J, Marchant RE (2011) Design properties of hydrogel tissue-engineering scaffolds. Expert Rev Med Devices 8(5):607–626
88. Peng S, Bhushan B (2012) Smart polymer brushes and their emerging applications. RSC Adv 2:8557–8578

Chapter 8
Functions of Bioactive and Intelligent Natural Polymers in the Optimization of Drug Delivery

Ndidi C. Ngwuluka, Nelson A. Ochekpe, and Okezie I. Aruoma

Abstract Bioactive polymers, by their structural configuration and conformation, possess the ability to exert biological activities and consequently elicit responses from cells and tissues. Intelligent polymers are smart polymers which respond to internal and external stimuli in order to propel the release or modify the release of drugs. Natural polymers are biogenic, biocompatible, biodegradable, and safe for consumption. Consequently, they present as suitable materials that the human body can identify with and not treat as foreign bodies, thereby reducing the complications encountered when dealing with synthetic polymers. Natural polymers have been shown to be bioactive, exhibiting biological activities such as antitumor, anticoagulant, antioxidant, antimicrobial, antiulcer, anti-inflammatory, and antirheumatic. In addition, natural polymers are meritorious materials for the fabrication of self-regulated or externally regulated drug delivery systems. These systems respond to the state of the environment for efficacious therapy. Drug delivery technology is shifting from the controlled release of drugs over time to the release of drugs when and where needed, especially for chronic diseases. Indeed, intelligent polymers are choice polymers for such delivery systems. Their synthetic counterparts were actually synthesized to mimic these natural polymers which further buttress the need to revert to nature for intelligent and bioactive polymers. The contexts of natural bioactive and intelligent polymers have unique applications in drug delivery, embracing nanobiotechnology. This would ultimately benefit drug delivery systems in benchmarking new drug formulations.

Keywords Bioactive • Biogenic • Drug delivery • Intelligent polymers • Nanobiotechnology • Natural polymers

N.C. Ngwuluka (✉) • N.A. Ochekpe
Faculty of Pharmaceutical Sciences, University of Jos, Jos 930001, Nigeria
e-mail: Ndidi.Ngwuluka@biodrudel.com; Nelson.Ochekpe@biodrudel.com

O.I. Aruoma
School of Pharmacy, American University of Health Sciences, Signal Hill, CA, USA
e-mail: oaruoma@auhs.edu

8.1 Introduction

Before civilization and manufacturing industries were widespread, men who were faced with ailments treated them with herbs. They had rudimentary technology such as using stones to grind the herbs or fashioning knives from stone to cut the herbs. The plants growing in their midst were experimentally used for various ailments including injuries they encountered as they executed their day's work.

However, as civilization advanced, there was a shift from nature to synthesized materials and petroleum-based resources. This shift became even more attractive as manufacturing provided a high yield of materials compared to nature. Consequently, the use of petroleum resources for drug carriers and synthesized active ingredients has persisted for years. However, as petroleum resources dwindle and synthesized materials continued to produce unpleasant adverse effects, there has been a reversal of this trend. Scientists are reverting to nature for solutions in prevention, treatment, and management of diseases. Even more appropriate is the use of the natural materials that make up a human body for drug delivery. These natural materials are identified as physiologically compatible and cooperation is enhanced. Polymers are macromolecules made of many small parts of the same or different molecules. Natural polymers are polymers found in nature within living organisms and outside. Polymers found within human body are proteins, polysaccharides, and lipids. These natural polymers perform complex functions that facilitate the growth, development, and well-being of the body. Some of these polymers are edible and are known to be functional and intelligent, making them vital materials in the delivery of drugs. Consequently, the use of these polymers in drug delivery may enhance the efficacy of therapy through additive or synergistic effects. The biogenicity of natural polymers and their biotic characteristics including identifying and cooperation with cells, ability to degrade enzymes, extracellular network likeness, as well as their chemical flexibility solidify them as the ideal components for drug delivery [1]. One significant advantage natural polymers have over synthetic polymers is their low toxicity. Other advantages include biocompatibility, biodegradability, flexibility, renewability, as well as being human and environmentally friendly [2].

Natural polymers have progressively been commercialized for utilization in drug delivery systems. However, before a natural polymer obtains approval to be used, it has to undergo extensive characterization. Excipients used in drug products are approved as part of new drug applications as there is currently no independent process for excipient approval. However, natural polymers stand a better chance of not causing regulatory issues than synthetic polymers. Most natural polymers, especially those from plants, could be regarded as safe since they are edible. Although novel excipient applications are submitted as part of new drug application, details of manufacture, characterization, clinical, and nonclinical safety data are submitted. The process of producing approvable natural polymers for drug delivery systems is referred to as naturapolyceutics [1]. This involves the processes of producing pharmaceutical grade natural polymers from extraction and purification to modification, characterization, application, and safety studies.

Most natural polymers are not inert and so would not be regarded as an inert excipient. Natural polymers are multifunctional. While they may help to improve the absorption, permeability, or targeting of drugs, a host of them are biologically active and intelligent.

8.2 Bioactive Polymers for Treatment and Management of Diseases

Bioactive polymers, potentially excipients, are functional polymers which exert biological or pharmacological effects. For effectiveness and application, a bioactive polymer has to be liberated from its carrier (if encapsulated or compressed), absorbed, distributed, metabolized, and excreted. In certain cases, it may be localized or targeted and may not necessarily need to get into systemic circulation. In addition, bioactive polymers that are able to exert pharmacological effects with little or no adverse effects thereby improving the quality of life of patient will be of significance. Consequently, natural bioactive polymers are the polymers of choice.

Basically, natural polymers are able to function as bioactives against diseases due to their immunomodulation. Most natural polymers, such as the polysaccharides, potentiate the immune system. It is suggested that they function by potentiating the host's standard and acquired immune responses, thus triggering immune cells like cytotoxic macrophages, monocytes, neutrophils, and dendritic cells that are crucial in maintaining homeostasis [3]. In addition, potentiation stimulates the release of chemical messengers (cytokines such as interleukins, interferons, and colony-stimulating factors) that trigger complementary and acute phase responses [3]. Natural polymers can be used to prevent, treat, and manage diseases. Figure 8.1 highlights some of the pharmacological effects of natural polymers.

8.2.1 Natural Polymers with Antitumor Activity

Cancer is one of the most prevalent diseases globally. It is also one of the most challenging diseases to treat and manage. Cancer therapy is fraught with adverse effects due to the nonspecific cytotoxic activity of the chemotherapeutic agents. Consequently, patients require hospital visits and palliative care. Antitumor agents functioning by mechanisms other than nonspecific cytotoxic activity will be of significance in cancer therapy. Some natural polymers known to be safe and less toxic elicit antitumor activity. Polysaccharides from mushrooms have shown antitumor activity both in vitro and in animal models. These polysaccharides, β-D-glucans and proteoglycans from mushrooms, include lentinan, schizophyllan, active hexose correlated compound (AHCC), maitake D-fraction, polysaccharide-K, and polysaccharide-P. Lentinan has been studied in humans and has gone through phase III clinical
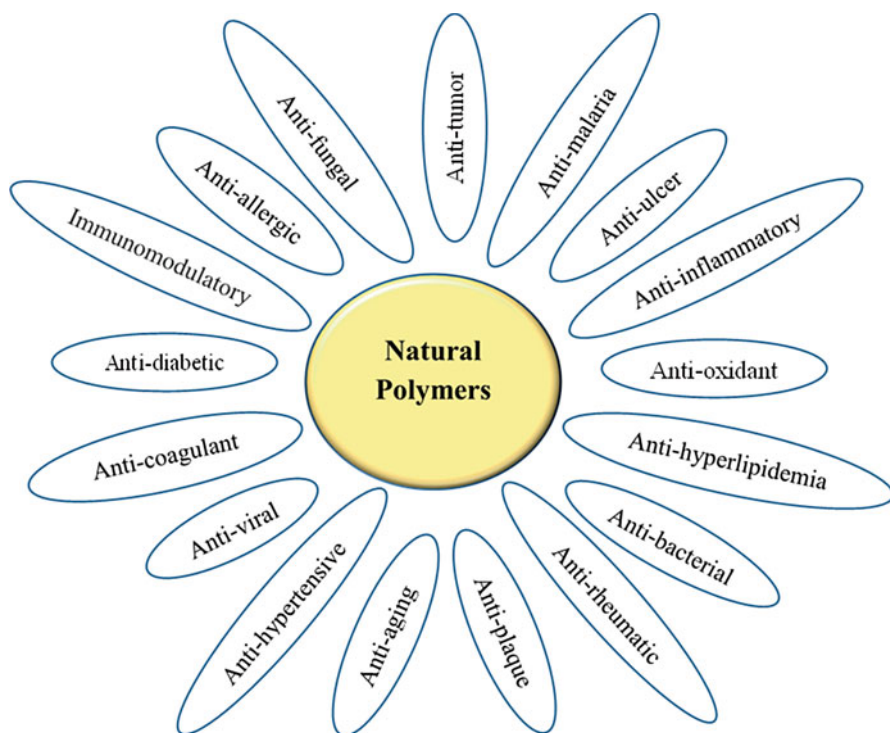
Fig. 8.1 Schematic depicting some of the pharmacological effects exerted by natural polymers

trials. A randomized controlled study of lentinan alongside chemotherapeutic agents, 5FU+mitomycin C or tegafur, on subjects with late stage or recurring gastric and colorectal cancers indicated lentinan significantly prolonged the life span of the patients [4]. Survival rates were 12.97 % at 2 years, 9.51 % and 3.81 % at 3 and 4 years, respectively, for gastric cancer patients, and then 9.10 % and 4.55 % at 2 and 3 years, respectively, for colorectal patients. However, lentinan and schizophyllan have limited oral bioavailability [5]. Consequently, lentinan was given intravenously. While lentinan showed extended survival in patients with gastric and colorectal cancers, schizophyllan showed prolonged survival in patients with head and neck cancers [6, 7]. However, polysaccharide-K (PSK) and polysaccharide peptide (PSP) showed the most promise as possible antitumor agents that can be given as immunoceuticals as they are orally bioavailable. They are proteoglycans, named for the peptide moieties bound to the polysaccharides. PSK has been shown to be active against stomach [8, 9], esophagus [10, 11], nasopharynx [12], colorectal [13, 14], and lung cancers [15]. PSK extended survival of the patients from 5 to 15 years. However, it was utilized as an immunotherapeutic agent which was only efficient in cases with some degree of immunity. The phase III clinical trials in which PSP was utilized exhibited significant benefits in stomach, esophagus, and lung cancers [5]. Studies such as the phase II double-blind trials in various Shanghai hospitals (China)

accentuated the benefits of PSP, consisting of 274 patients with various forms of cancer including lung, stomach, and esophageal [16]. The PSP-treated group, in combination with chemo-/radiotherapies (82 %), experienced mitigated symptoms common to those suffering from cancer, including fatigue, anorexia, nausea, thirst, cold sweat, and pain [16]. In addition, there was a marked reduction of the incidence of adverse effects of chemotherapy and radiotherapy regimens when treated with PSP [17]. The potency of these polysaccharides as antitumor agents is suggested to be related to their molecular weight, degree of branching, and solubility in water [3]. In these studies, the polysaccharides were given to cancer patients to boost their immune system, thereby protecting them against immunosuppression that is usually precipitated by long-term chemotherapy. Other natural polymers with antitumor activity include glucans [18, 19], proteoglycans [20], laminarin [21], and angelan [22]. Zong and co-workers reviewed antitumor polysaccharides obtained from microorganisms, algae, plants, and animals [23]. These polysaccharides prevented tumor growth by direct cytotoxicity, prevention of the multistep process of tumor development, immunopotentiation when given with chemotherapy, and prevention of tumor metastasis.

8.2.2   Natural Polymers with Anticoagulant Activity

Fucoidans, polysaccharides known as sulfated fucans comprised mainly of fucose and sulfate with small fractions of galactose, xylose, mannose, and uronic acids, are extracted from brown seaweed cell walls. Low molecular weight fucans obtained from fucoidans by acid hydrolysis or radical cleavage were studied for their antico-agulant activity [24]. Anticoagulant activity was examined using activated partial thromboplastin time (APTT), thrombin time (TT), and antifactor Xa and antifactor IIa [24–26]. The sulfated fucans were found to possess anticoagulant activity. The degree of anticoagulation varied based on a number of factors such as source of the sulfated fucans, fractionation, molecular weight, proportion of sulfate, and sugar content. It was observed that anticoagulant activity increased with sulfate content and molecular weight, fucose being the only sugar needed for the anticoagulant effect. While heparin is of animal origin and has adverse effects, sulfated fucans are extracted from various species of algae. The sulfated fucans present an inexpensive and easy source of anticoagulants with little or no adverse effect. Among other natural polymers, carrageenan has also been shown to exhibit an anticoagulant effect [27].

8.2.3   Natural Polymers with Antioxidant Activity

Fucoidan, lambda-, kappa-, iota-carrageenans, and two heterogenous fucans from *Padina gymnospora* were subjected to antioxidant assays such as the scavenging activities of superoxide anion and hydroxyl radical as well as liver microsomal lipid

peroxidation [28]. Inhibition of superoxide radicals was found to be more effective at lower concentration with fucoidan and lambda-carrageenan, while fucoidan and iota-carrageenan were better hydroxyl radical scavengers than lambda- and kappa-carrageenans. Iota- and lambda-carrageenans were better hydrogen peroxide scavengers than fucoidan and others. This study suggests that to obtain encompassing antioxidants and free radical-scavenging activities, lambda-carrageenan can be given alone or in combination with fucoidan to produce an additive or synergistic effect.

In order to produce efficient pulmonary drug delivery and to circumvent oxygen radical-mediated pulmonary toxicity and other inflammatory responses produced by nanoparticles and synthetic materials, chitosan/fucoidan nanoparticles were produced as carriers for gentamicin delivery [29]. Chitosan and fucoidan, which are both antioxidant agents, effectively displayed both scavenging and antioxidant activities against induced 1,1-diphenyl-2-picrylhydrazyl (DPPH), reactive oxygen species (ROS), superoxide anion (O_2^-), and inflammatory mediators such as nitric oxide (NO) and interleukin-6 (IL-6). However, the antioxidant efficacy (90 %) was enhanced when fucoidan concentration was greater than 0.31 mg/mL. Along with the other properties of chitosan such as mucoadhesion, permeability, good entrapment, and controlled release, there was a biphasic release of gentamicin over 72 h with an initial burst release over 10 h followed by a sustained release. This study allays the concerns of using nanoparticles for pulmonary delivery and suggests that natural bioactive polymers can be utilized in fabrication of nanoparticles to minimize the inflammatory responses and other adverse effects elicited by nanoparticles. In addition, these polymers apart from being bioactive are biocompatible and biodegradable and possess other drug delivery properties needed to optimize therapy.

Alginates and laminarin were also studied for their antioxidant properties [30]. However, while they exhibited antioxidant properties, they were not as effective as fucoidan. Fucoidan had higher sulfate content. In addition, the antioxidant and scavenging activities of crude fucoidan from *Laminaria japonica* and its fractions were compared with ulvan from *Ulva pertusa* Kjellman, porphyran from *Porphyra haitanensis*, and vitamin C [31]. Fucoidan and its fractions had greater scavenging activity against superoxide radicals than ulvan, porphyran, and vitamin C. Comparing crude fucoidan with its fractions, the fractions had greater scavenging activity against hydroxyl radicals and a better ferrous ion-chelating effect. In another study, the fucoidan from *Sargassum fulvellum* was compared with commercial fucoidan from *Fucus vesiculosus*, galacto-fucoidan from *Undaria pinnatifida*, butylated hydroxytoluene (BHT), and α-tocopherol among others [32]. However, it was observed that their activities against the various radicals varied. In summary, the antioxidant activity of the sulfated polysaccharides is determined by their structural properties such as sulfate content, molecular weight, major sugar component, and glycosidic branching [33]. Low molecular weight sulfated polysaccharides are more potent antioxidants due to their ability to be engulfed into the cells and donate protons more actively than the high molecular weight sulfated polysaccharides. Indeed, natural antioxidants can be employed in the food, cosmetic, and pharmaceutical

industries, individually or in combination producing an antioxidant effect with little or no toxicity. Quite a number of the sulfated polysaccharides are extracted from edible seaweeds.

8.2.4   Natural Polymers with Anti-inflammatory Activity

Chondroitin sulfate (CS), a polymeric carbohydrate sourced from pork, chicken, fish, and shark tissues, has been shown to exhibit anti-inflammatory activity [34]. A study in which 11 patients with long-standing psoriasis were administered oral chondroitin sulfate (800 mg daily) for 2 months showed significant improvement in 91 % of the cases, displaying reduced swelling, redness, flaking, and itching and increase in skin hydration, skin softening, and scale amelioration [35]. In another study, the effect of oral CS against dextran sulfate sodium-induced rat colitis was investigated in comparison with 5-aminosalicylic acid (5-ASA) [36]. CS (in the same dose as 5-ASA) showed more improvement of colitis symptoms such as bloody stool, erosion, and increase in white blood cells than 5-ASA.

8.2.5   Natural Polymers with Antidiabetic Activity

Carrageenan has been shown to decrease postprandial glycemia [37]. This is suggested to be due to carrageenan increasing the volume and viscosity of the intestinal content, thereby slowing the enzymatic diffusion as well as substrate and nutrient diffusion to the intestine's absorptive surface. However, Li and co-workers suggested that the hypoglycemic activity of natural macromolecules is linked to their antioxidant activity [20]. A study of a polysaccharide-protein complex, from which a fraction LB-1b was tested in (tetraoxypyrimidine)-induced mice, using a (+) control of butylated hydroxyanisole (BHA) and a (–) control of 0.9 % NaCl, indicated that LB-1b decreased the glucose level by 16.6 %. BHA decreased glucose levels by 8.32 %, while NaCl increased levels by 1.35 % [20]. The pathologies of diabetes are related to the toxicity of reactive oxygen species [20, 38]. Hence, on extrapolation of this mechanism, antioxidant agents such as LB-1b may prevent the attack of β-cells and increase insulin secretion.

8.2.6   Natural Polymers with Antimicrobial Activity

Some sulfated polysaccharides such as dextran sulfate, chrondroitin sulfate, heparin, carrageenan, curdlan sulfate, fucoidan, galactan, spirulan, xylomannan, and heteroglycan have exhibited antiviral activities in most in vitro studies [39]. The sulfated polysaccharides have exhibited activity over a range of viruses including herpes (herpes simplex type 1 [HSV-1], thymidine kinase-deficient [TK⁻] HSV-1,

herpes simplex type 2 [HSV-2], cytomegalovirus [CMV]), toga (Sindbis, Semliki Forest), arena (Junin, Tacaribe), rhabdo (vesicular stomatitis [VSV]), orthomyxo (influenza A), and paramyxoviruses (respiratory syncytial virus [RSV]) [40, 41]. Competitive inhibition is used to block viral attachment [41]. The mechanism of antiviral activity of carrageenan is suggested to prevent the attachment of the virus to the host cell by impeding viral glycoprotein gC's initial binding to the cellular heparin sulfate proteoglycans [27].

Sulfated konjac glucomannan displayed its antiviral activity by exhibiting high anti-HIV capabilities [42]. The mechanism of anti-HIV activity is suggested to be by the interaction of the negatively charged sulfate groups alongside positively charged glycoprotein gp120 on HIV's surface, thereby changing the complex's configuration thus preventing the HIV from infecting the T cells [43]. In addition, chitosan oligosaccharides have been shown to exhibit antifungal [44] and antibacterial [45] activities.

8.2.7   Natural Polymers with Antiulcer Activity

Chitosan (C) and carrageenan (CG) are gastroprotective. However, a study in which a complex of chitosan and carrageenan was explored for gastroprotective/antiulcer activity in Wistar female rats presented an interesting outcome [46]. C:CG at a ratio of 10:1 (w/w) exhibited significantly higher gastroprotection than C:CG at ratio of 1:10 (w/w), chitosan only and the reference drug Phosphalugel. Indeed the C:CG complex [10:1 (w/w)] provided synergistic gastroprotection. The researchers attributed the synergistic effect to structural modification facilitated by the complexation at 10:1 (w/w). The supramolecular structure of C:CG complex [10:1 (w/w)] was different from that of C:CG complex [1:10 (w/w)].

Other natural polymers known to exhibit gastroprotection include fucoidan from *Cladosiphon okamuranus* [47]. *Cladosiphon* fucoidan acts as an antiulcer agent by inhibiting the adhesion of *Helicobacter pylori* to gastric epithelium by attaching to the bacterial surface proteins [47]. In addition, *Cladosiphon* fucoidan inhibits peptic activity, binds to proteins, and prevents the instability of basic fibroblast growth factor (bFGF).

8.2.8   Natural Polymers with Other Biological Activities

Panlasigui and co-workers suggested that carrageenan may modulate cholesterol content in food by its ability to simulate the texture and sensory qualities of fat, thereby reducing the quantity of fat in foods [48]. Consequently, they undertook a randomized crossover study in human volunteers to assess the antihyperlipidemic activity of carrageenan. The volunteers served as their control. The report indicated

that carrageenan reduced cholesterol and triglycerides levels by 33 % and 32 %, respectively. While high-density lipoprotein (HDL) cholesterol was increased by 32 %, there was no significant difference in low-density lipoprotein (LDL) cholesterol in the presence of carrageenan. Other natural polymers possessing antihyperlipidemic include porphyran [49] and ulvan [50].

Tooth decay occurs when there is an imbalance between demineralization and remineralization, leading to the loss of dental enamel. Dental enamel loss is prevented by enhancing the remineralization phase [51]. Gum arabic from *Acacia senegal* has been shown to prevent tooth decay by enhancing the remineralization phase [51]. In addition, gum arabic consists of cyanogenic glycosides as well as various enzymes such as oxidases, peroxidases, and pectinases which have displayed antimicrobial activity against dental organisms such as *Porphyromonas gingivalis* and *Prevotella intermedia* [52, 53]. Although not stated by the author [52], these components of acacia may also be responsible for the delay in plaque deposition.

Moon and co-workers suggested in their study that fucoidan can be used to prevent and possibly treat skin photoaging caused by ultraviolet B irradiation-induced matrix metalloproteinase-1 (MMP-1) expression [54]. Agar has been shown to have antirheumatic activity [55], while angiotensin-converting enzyme (ACE) inhibitory peptides from soy protein have antihypertensive activity [56]. Table 8.1 provides some of the polymers and their sources and biological activities.

8.3   Intelligent Polymers for Treatment and Management of Diseases

Intelligent polymers are polymers that are able to adapt their behavior in response to an external stimulus so as to elicit an effect or a change (Fig. 8.2). In drug delivery, they are polymers that, by reason of their response to external stimuli, modulate drug release and consequently, therapeutic or pharmacological effects. Intelligent polymers are also known as smart polymers, stimuli-responsive polymers, or environmental-responsive polymers. Intelligent polymers respond to physiological changes such as pH, ions, enzymes, antigens, biochemical, temperature, magnetic, and electric fields [2]. Intelligent polymers can be used to fabricate delivery systems that can maintain extracellular stability and achieve intracellular release of an active ingredient. Nature and materials in nature respond to one stimuli or another. Consequently, natural polymers are more inherently disposed to respond to environmental changes than their synthetic analogues. Synthetic polymers are actually designed to mimic these natural polymers which further buttress the need to revert to nature for intelligent and bioactive polymers. Natural polymers are meritorious materials for the fabrication of self-regulated or externally regulated drug delivery systems. A drug delivery system can be formulated to sense a physiological change with regard to a particular disease, trigger drug release, and, when the physiological condition is normal, cut off drug release.

Table 8.1 Natural polymers, sources, and their biological activities

Polymers	Sources	Bioactivities	References
Carrageenans	Red seaweeds (Rhodophyta) *Chondrus crispus* *Gigartina stellata* *Eucheuma spinosum* *Eucheuma cottonii*	Anticoagulant Antioxidant Antidiabetic Antiviral Antiulcer Antihyperlipidemic	[27] [28] [37] [46]
Lentinan	Mushroom—*Lentinus edodes*	Antitumor	[4]
Hyaluronic acid	Animals and microorganisms	Antioxidant Antifungal Antibacterial Antiviral	[57]
Polysaccharide-P	Mushrooms—*Coriolus versicolor*	Antitumor	[16]
Polysaccharide-K	Mushrooms—*Coriolus versicolor*	Antitumor	[8, 9]
Laminarin	Brown algae *Laminaria longicruris*	Antitumor Antioxidant	[21] [30]
Angelan	Plant—*Angelica gigas* Nakai	Antitumor	[22]
Fucoidans	Brown algae *Fucus vesiculosus* *Sargassum fulvellum*	Anticoagulant Antioxidant Antiviral Antiulcer Anti-photoaging	[24] [28] [32] [47] [54]
Chitosan	Shrimps and other crustacean shells	Antioxidant Antifungal Antibacterial Antiulcer	[29] [44] [45] [46]
Alginates	Brown seaweed (Phaeophyceae)	Antioxidant Antiulcer	[30] [21]
Ulvan	Green algae *Ulva pertusa* Kjellman	Antioxidant Antihyperlipidemic	[31] [50]
Porphyran	Red algae *Porphyra haitanensis*	Antioxidant Antihyperlipidemic	[31] [49]
Galacto-fucoidan	Algae—*Undaria pinnatifida*	Antioxidant	[32]
Chondroitin sulfate	Porcine, chicken, fish, and shark tissues	Anti-inflammatory Antiviral	[34]
Astragalus polysaccharide	Plant *Astragalus membranaceus*	Antidiabetic Anti-inflammatory Antimicrobial Immunostimulator Antihyperlipidemic Anti-hypertrophic	[58] [59] [60] [61]
Costus glucans	Plant—*Costus spicatus* Swartz	Anti-inflammatory Immunomodulatory	[62]

(continued)

Table 8.1 (continued)

Polymers	Sources	Bioactivities	References
Dextran sulfate	Microorganisms—*Leuconostoc*, *Lactobacillus*, and *Streptococcus* genera	Antiviral	[63]
Heparin	Endothelial cells	Anticoagulant Antiviral	[64]
Curdlan sulfate	Microbial—*Agrobacterium* sp.	Antiviral	[65]
Galactan	Microorganisms, plants, and animals	Antiviral Anti-inflammatory	[66]
Spirulan	Blue-green algae—*Spirulina platensis*	Antiviral	[67]
Xylomannan	Red algae—*Nothogenia fastigiata*	Antiviral	[68]
Heteroglycan	Mushrooms—*Lentinus edodes Pleurotus florida*	Antioxidant Immunomodulator	[69]
Konjac glucomannan	Tubers of *Amorphophallus konjac*	Antiviral	[42]
Agar	Red algae—*Gelidium*, *Pterocladia, Pterocladiella species*	Antirheumatic	[55]
Soy peptides	Soy protein	Antihypertensive	[56]
Levans	Microorganisms *Microbacterium laevaniformans Zymomonas mobilis Paenibacillus polymyxa* EJS-3	Antitumor Antihyperlipidemic Immunomodulator Anti-inflammatory	[70] [71]
Schizophyllan	Mushroom *Schizophyllum commune*	Antitumor Immunomodulator	[72]
Pullulan sulfate	Microorganism— *Aureobasidium pullulans*	Anticoagulant	[73]
Longan polysaccharide	Plant *Dimocarpus longan* Lour.	Antitumor Immunomodulator Antioxidant	[74]
Gellan sulfate	Microorganism *Pseudomonas elodea*	Anticoagulant Antimalaria	[75]
Emulsan	Microorganism—*Acinetobacter calcoaceticus*	Immunomodulator	[76]
Arabinogalactan	Plant—*Stevia rebaudiana*	Antiviral	[77]
Albumin	Animal, soybean, grains	Antioxidant Anti-inflammatory Anticoagulant Antithrombotic	[78]
Lectin	Microorganisms, plants, and animals	Antibacterial Immunomodulator Antiviral Antitumor	[79] [80]
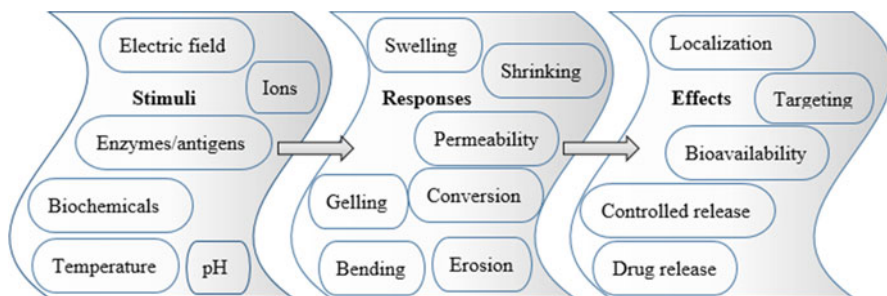
Fig. 8.2 Schematic diagram depicting potential stimuli, responses, and resultant effects of the responses

8.3.1 Natural Polymers with Response to pH

The response to pH plays a key role in the delivery of drugs, especially through the oral route as the gastrointestinal tract presents wide variations in pH value. pH is being employed to deliver drugs to the colon. As a colon-specific carrier is administered, the release of the drug is controlled or prevented until the carrier is transported to the colon. Control of drug is made possible by the use of polymer which responds to higher pH. As the carrier passes through the gastric region (stomach), the drug is entrapped within the polymer matrix. However, as it arrives to the colon, the higher pH in the colon will facilitate the ingress of the physiological medium into the matrix, engineering the diffusion and release of the drug from the matrix. The polymer may respond to pH by swelling or de-swelling and the drug is released in the pH that facilitates swelling. Consider the mechanism by which chitosan responds to pH; at higher pH, the amino groups are neutralized breaking down the electrostatic linkages between the amino groups and the negatively charged sulfonate groups [81]. Electrostatic repulsion ensues between the sulfonate groups thereby enhancing swelling. Modification of chitosan further ensures release of drug at higher pH values than in acidic conditions. Matrices formed from chitosan phthalate and chitosan succinate resisted hydration and subsequent release of incorporated drugs at gastric pH conditions [82]. However, the matrices hydrated and there was subsequent release at higher pH, with moderate release at pH 6.4 and high levels of release at pH 7.4, making chitosan phthalate and chitosan succinate good drug carriers for colon-specific delivery. For chitosan-fucoidan nanoparticulate systems, interaction at a ratio of 1:1 was found to be pH sensitive [83]. The nanoparticles, fabricated via the interaction that formed polyelectrolyte complexes, were subjected to pH values ranging from 1.2 to 7.4. The sizes increased from nano- to micro size, the zeta potential changed from positive to negative, and the drug was significantly released at pH 7.4. These findings suggest that the particulate system can migrate from the gastric region to the intestinal region with limited drug released in the stomach. Consequently, chitosan-fucoidan particulate system can be used for

colon-specific drug delivery. An interpolymeric blend comprised of an IPEC (carboxymethylcellulose and Eudragit E100) and locust bean gum produced a pH-sensitive system in which the hydrogel swelled and retained its three-dimensional shape at pH 1.2, producing a first-order release pattern while it underwent surface erosion at pH 4.5 and 6.8 producing a zero-order release pattern [84].

8.3.2 Natural Polymers with Response to Biochemicals

The functionalities of the human body are facilitated by natural polymers, making them good candidates for self-regulated drug delivery systems. Self-regulated drug delivery systems respond to physiological changes in order to elicit their therapeutic effects. Such changes are due to the presence of biochemicals such as enzymes, antigens, and glucose. The presence and concentration levels of the biochemicals will facilitate the release of the therapeutic agent from the drug delivery system. Such regulation will enhance the management of chronic diseases whereby the therapeutic agent is released only when needed.

Various studies have been undertaken to deliver insulin for the management of diabetes. Insulin can be delivered such as it is only released from the matrix when the glucose levels in the cells are low. pH sensitive hydrogels have been used to deliver insulin as a change of pH occurs when glucose is converted to gluconic acid by glucose oxidase (in the cells) [2]. Consequently, insulin is released to promote the uptake of glucose from the blood into the cells. However, there are also glucose-sensitive delivery systems. Concanavalin A (Con A), a glucose-binding plant protein, has been used to regulate insulin delivery [85–87]. Glucose-sensitive hydrogel systems are fabricated by mixing Con A with polysaccharides or oligosaccharides leading to the formation of a gel which changes in viscosity or gel strength (sol-gel phase reversible systems) depending on the concentration of glucose, thereby acting as insulin regulator. The release of insulin becomes a function of the concentration of glucose [86].

8.3.3 Natural Polymers with Response to Temperature

A number of natural polymers such as gelatin, agarose, amylase, amylopectin, cellulose derivatives, carrageenans, and gellan display thermo-reversible gelation behavior [88] whereby the solutions of the polymers form gels at lower temperatures. However, some cellulose derivatives form gels at higher temperatures. Formulation of drug delivery systems that respond to temperature can be used for localization, targeting, and sustained release of drugs. The sol-gel transition leading to gelation at body temperature is utilized to prepare injectables. These formulations can serve as a depot releasing the active ingredient over time. Methylcellulose,

a cellulose derivative which forms a solution at room temperature, is able to gel at body temperature by changing concentration or addition of additives [89]. The localization and release of lysozymes were modified when lysozyme-loaded microspheres were incorporated into thermosensitive methylcellulose-based hydrogels [90]. Lysozyme-loaded microspheres had a 50 % burst release and lysozyme was released within 10 days. Lysozyme incorporated directly into the hydrogel had a 30 % burst release which completed in 15 days. However, lysozyme-loaded microspheres dispersed in thermosensitive methylcellulose-based sol gelled at body temperature; there was no burst release and lysozyme released over 30 days.

Grafting of polyethylene glycol (PEG) to chitosan produced a thermosensitive hydrogel for the sustained delivery of bovine serum albumin (BSA) [88]. The hydrogel formed a gel at body temperature; however, 70 % of BSA was released in 5 h. When PEG-g-chitosan solution was cross-linked with genipin, a gel was formed at 37 °C but the gel formation was not reversible. However, the release of BSA was sustained; 12–15 % released the first day and another 25–30 % in 1 week. The non-reversibility of cross-linked PEG-g-chitosan is not a challenge, as once the solution is injected, it becomes a depot and releases over time. The gel can dissolve or erode over time. Other graftings which are thermosensitive include chitosan-g-poloxamer [91], chitosan-g-poly(*N*-isopropylacrylamide), hyaluronic acid-g-chitosan-g-poly(*N*-isopropylacrylamide) [92], and pullulan-g-poly(*N*-isopropylacrylamide-*co*-acrylamide) [93]. Xyloglucan was utilized for sustained ocular delivery of pilocarpine hydrochloride due to its gelling ability at the temperature (34 °C) of the eye surface [94].

8.3.4   Natural Polymers with Response to Electric Field

The ability for a polymer to respond to an electric field is based on the polymer's electric potential. Typically such polymers are polyelectrolytes where the response to an electric field will require the presence of ions. Usually the response to electric fields is a mechanical response. A semi-interpenetrating polymer network (semi-IPN) hydrogel of chitosan and polyacrylonitrile (PAN) was prepared at a ratio of 1:1 and thereafter cross-linked with glutaraldehyde [95]. The film that was formed was immersed in a NaCl solution equipped with two parallel carbon electrodes. The hydrogel bent toward the anode (Fig. 8.3) and reverted to its original state when the electric field was deactivated. Such a mechanical response to an electric field promotes the use of natural polymers and their derivatives in the fabrication of artificial organ components such as sensors, actuators, and artificial muscles. Electric fields can also be used to modulate drug release as the electric field can produce the concomitant swelling of one side of the drug carrier and shrinkage of the other side of the drug carrier (or the hemisphere as shown in Fig. 8.3). Cross-linked chitosan/poly(ethylene glycol) hydrogel fibers also displayed a reversible bending in response to an electric field [96].
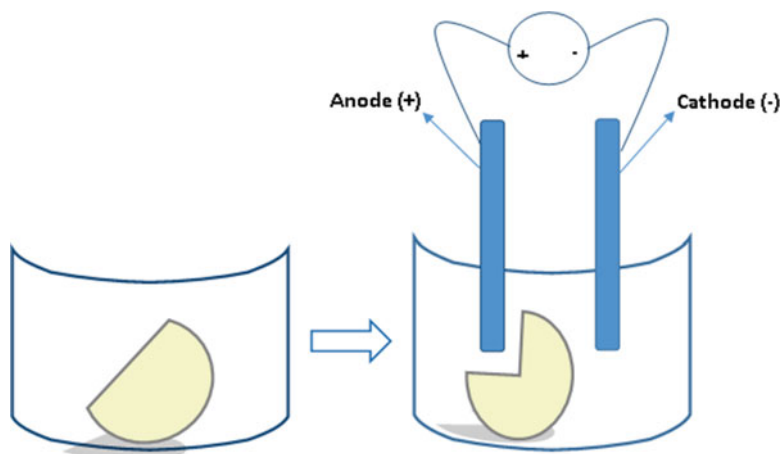
Fig. 8.3 Schematic diagram depicting the response of a hydrogel to electric field

8.3.5 Natural Polymers with Response to Ions

The response of a semi-interpenetrating polymer network (semi-IPN) hydrogel of chitosan and polyacrylonitrile (PAN) in the presence of ions was determined [95]. The hydrogel swelled rapidly in a NaCl solution and reached equilibrium (swelling range: 151–206 %) in 2 h. However, as the concentration of NaCl is increased, swelling of the hydrogel decreased.

Gellan gum has been used in the formulation of ophthalmic carriers which are liquids but become gels when administered in the presence of tear fluid cations, thereby sustaining the rate of drug release and increasing ocular bioavailability [97, 98].

8.3.6 Natural Polymers with Response to Other Stimuli

Modification of natural polymers by blending, cross-linking, derivative formation, and grafting has produced polymers exhibiting dual responses. Blending two natural polymers, xyloglucan and pectin, resulted in a system that exhibited dual responsiveness to variations in temperature and ions [99]. A blend of 1.5 or 2.0 % (w/w) xyloglucan/0.75 % (w/w) pectin produced a stronger gel once in contact with gastric fluid, reducing gel erosion and consequently sustaining drug release.

8.4   Bionanotechnological Applications of Bioactive and Intelligent Polymers

Bionanotechnology is the concept of using biological fundamentals for the creation of materials and devices at a nanoscale. It is the concept of using biological materials as building blocks for the fabrication of nanodevices for biological and non-biological applications. Some of the biological principles explored for nanotechnological applications are smart recognition and self-assembly. A robust, practical, and affordable principle of self-assembly that prevails for nanoscale building blocks in devices comes from their various desirable pros including repeatability, grandiose scale of production, monodispersity, and simple experimental techniques [100]. Peptide monomers can self-assemble to form nanotubes while maintaining their smart functions such as molecular recognition and biomineralization. Furthermore, nanotubes without such abilities can be functionalized with an antigen or antibody for biomolecular recognition in new applications. Peptide nanotubes with smart recognition can be incorporated into a membrane (Fig. 8.4) and the resultant system can be used as biosensor [101] for the detection of biological events or changes. Peptide nanotubes are biocompatible making them valuable devices for biomolecular filters as well [100]. Cyclic peptides stack up to form hollow, β-sheet-like tubular structures that are open-ended and have been shown to exert antibacterial effects by enhancing the membrane permeability [102]. A bioactive polymer, which is also intelligent or incorporated into an intelligent polymer, fabricated or self-assembled into a nanodevice and used in prevention, treatment/management, and diagnosis of a disease, is a formidable device. In addition to enhancing therapeutic efficacy, toxicity is minimized and quality of life enhanced. Patients would not have to be subjected to several devices when one device can accomplish prevention, treatment, and diagnosis.

Peptide
Nanotubes

Membranes
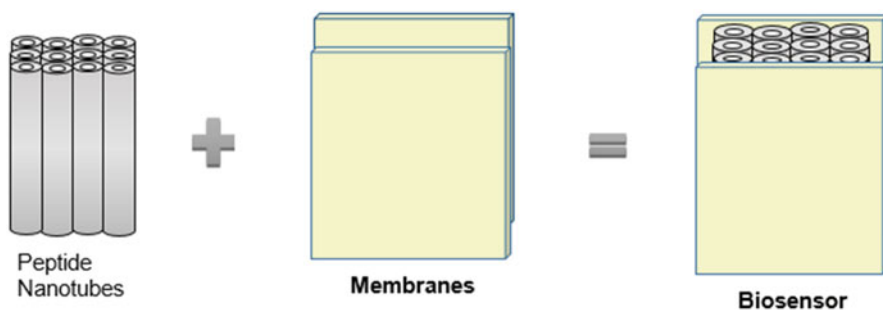
Biosensor

Fig. 8.4 Schematic diagram depicting the production of a biosensor using peptide nanotubes and membranes

8.5 Commercialized Bioactive and Intelligent Drug Delivery Systems

Lentinan is currently being produced and sold in Japan as an antitumor agent. Mushrooms and polysaccharides from mushrooms are currently being grown, purified, standardized, produced, and sold by a number of companies including: Zhejiang Fangge Pharmaceutical & Healthcare Products Co. Ltd, China; FineCo Ltd, Korea; and Aloha Medicinals Inc. and Mushroom Wisdom, USA. These polysaccharides are produced under good manufacturing practices (GMPs), research, and development using state-of-the-art technology. Timoptic XE® (Timoptol LP® or Timoptol LA® in Europe) is given once daily as opposed to the regular Timoptol given twice daily. This is made possible by the presence of low-acetyl gellan gum in the formula. Astragalus polysaccharide is commercially available from China Shineway Pharmaceutical Group, a supplier of traditional Chinese medicine injectable, soft gels, and particles. Some of these polysaccharides such as carrageenan are being explored as microbicides.

8.6 Conclusion and Future Outlook

As naturapolyceutics continues to advance, the use of natural polymers for biological functions and drug delivery will continue to evolve and progress. As the quest for active ingredients with little or no toxicity increases, so will research and possible commercialization of natural bioactive polymers. Natural polymers, being compatible with the body, biogenic and biodegradable, give them an edge over their synthetic analogues. As currently available drugs, such as antimicrobials, fail, natural bioactive polymers will be increasingly sought after. Presently, considering the prevalence of cancer, the use of bioactive natural polymers is being advocated for chemoprevention. Self-regulated drug delivery systems are the solution to the management of chronic diseases and personalized medicines. For prolonged depot of the delivery system, natural intelligent polymers are preferred thereby limiting adverse effects. Due to the multifunctionality of natural polymers, they can be used to fabricate formidable devices. Bioactive intelligent natural polymers are the polymers for the fabrication of "all-in-one" devices which are able to prevent, diagnose, and manage chronic diseases. Natural polymers are the materials of our times. However, extensive research, characterization, and regulatory approvals are required before more of these polymers become available.

References

1. Ngwuluka NC, Ochekpe NA, Aruoma OI (2014) Polymers 6:1312–1332
2. Ngwuluka NC, Ochekpe N (2015) In: Mishra M (ed) Encyclopedia of biomedical polymers and polymeric biomaterials. Taylor & Francis, New York, NY, 11 volume set

3. Sullivan R, Smith JE, Rowan NJ (2006) Perspect Biol Med 49:159–170
4. Taguchi T, Furue H, Kimura T, Kondo T, Hattori T, Itoh I et al (1985) Gan To Kagaku Ryoho 12:366–378
5. Kidd PM (2000) Altern Med Rev 5:4–27
6. Borchers AT, Stern JS, Hackman RM, Keen CL, Gershwin ME (1999) Proc Soc Exp Biol Med 221:281–293
7. Kimura Y, Tojima H, Fukase S, Takeda K (1994) Acta Otolaryngol 114:192–195
8. Niimoto M, Hattori T, Tamada R, Sugimachi K, Inokuchi K, Ogawa N (1988) Jpn J Surg 18:681–686
9. Nakazato H, Koike A, Saji S, Ogawa N, Sakamoto J, Nakazato H et al (1994) The Lancet 343:1122–1126
10. Okudaira Y, Sugimachi K, Inokuchi K, Kai H, Kuwano H, Matsuura H (1982) Jpn J Surg 12:249–256
11. Ogoshi K, Satou H, Isono K, Mitomi T, Endoh M, Sugita M (1995) Cancer Invest 13:363–369
12. Go P, Chung C (1989) J Int Med Res 17:141–149
13. Torisu M, Hayashi Y, Ishimitsu T, Fujimura T, Iwasaki K, Katano M et al (1990) Cancer immunology. Immunotherapy 31:261–268
14. Mitomi T, Tsuchiya S, Iijima N, Aso K, Suzuki K, Nishiyama K et al (1992) Dis Colon Rectum 35:123–130
15. Si-Iiojima SKK, Furuta M, Niibe H (1993) Anticancer Res 13:1815–1820
16. Liu J, Zhou J (1993) Anonymous PSP international symposium, Fudan University Press, Hong Kong, pp 183
17. Sun Z, Yang Q, Fei H (1999) In: Yang, Q. (ed), Advanced Research in PSP. Hong Kong Association for Health Care Ltd., Hong Kong, pp. 304–307.
18. Gonzaga MLC, Bezerra DP, Alves APNN, de Alencar NMN, de Oliveira Mesquita R, Lima MW et al (2009) J Nat Med 63:32–40
19. Yan J, Wang W, Li L, Wu J (2011) Carbohydr Polym 85:753–758
20. Li N, Li L, Fang JC, Wong JH, Ng TB, Jiang Y et al (2012) Biosci Rep 32:221–228
21. Nagaoka M, Shibata H, Kimura-Takagi I, Hashimoto S, Aiyama R, Ueyama S et al (2000) Biofactors 12:267
22. Han S, Lee CW, Kang MR, Yoon YD, Kang JS, Lee KH et al (2006) Cancer Lett 243:264–273
23. Zong A, Cao H, Wang F (2012) Carbohydr Polym 90:1395–1410
24. Chevolot L, Foucault A, Chaubet F, Kervarec N, Sinquin C, Fisher A et al (1999) Carbohydr Res 319:154–165
25. Dobashi K, Nishino T, Fujihara M, Nagumo T (1989) Carbohydr Res 194:315–320
26. Colliec S, Fischer A, Tapon-Bretaudiere J, Boisson C, Durand P, Jozefonvicz J (1991) Thromb Res 64:143–154
27. Cáceres PJ, Carlucci MJ, Damonte EB, Matsuhiro B, Zúñiga EA (2000) Phytochemistry 53:81–86
28. de Souza MCR, Marques CT, Dore CMG, da Silva FRF, Rocha HAO, Leite EL (2007) J Appl Phycol 19:153–160
29. Huang Y, Li R (2014) Mar Drugs 12:4379–4398
30. Rupérez P, Ahrazem O, Leal JA (2002) J Agric Food Chem 50:840–845
31. Wang J, Zhang Q, Zhang Z, Li Z (2008) Int J Biol Macromol 42:127–132
32. Kim S, Choi D, Athukorala Y, Jeon Y, Senevirathne M, Rha CK (2007) J Food Sci Nutr 12:65–73
33. Wijesekara I, Pangestuti R, Kim S (2011) Carbohydr Polym 84:14–21
34. Lauder RM (2009) Complement Ther Med 17:56–62
35. Vergés J, Montell E, Herrero M, Perna C, Cuevas J, Dalmau J et al (2005) Dermatol Online J 11:31
36. Hori Y, Hoshino J, Yamazaki C, Sekiguchi T, Miyauchi S, Horie K (2001) Jpn J Pharmacol 85:155–160

37. Dumelod BD, Ramirez RPB (1999) Int J Food Sci Nutr 50:283
38. Jang JS, Lee JS, Lee JH, Kwon DS, Lee KE, Lee SY et al (2010) Arch Pharm Res 33:853–861
39. Smit AJ (2004) J Appl Phycol 16:245–262
40. Witvrouw M, De Clercq E (1997) Gen Pharmacol Vascular Syst 29:497–511
41. Ghosh T, Chattopadhyay K, Marschall M, Karmakar P, Mandal P, Ray B (2009) Glycobiology 19:2–15
42. Bo S, Muschin T, Kanamoto T, Nakashima H, Yoshida T (2013) Carbohydr Polym 94(2):899–903
43. Jeon K, Katsuraya K, Inazu T, Kaneko Y, Mimura T, Uryu T (2000) J Am Chem Soc 122:12536–12541
44. Hirano S, Nagao N (1989) Agric Biol Chem 53:3065–3066
45. Jeon Y, Park P, Kim S (2001) Carbohydr Polym 44:71–76
46. Volod'ko AV, Davydova VN, Chusovitin E, Sorokina IV, Dolgikh MP, Tolstikova TG et al (2014) Carbohydr Polym 101:1087–1093
47. Shibata H, Kimura-Takagi I, Aiyama R, Nagaoka M, Ueyama S, Yokokura T et al (2000) Biofactors 11:235
48. Panlasigui LN, Baello OQ, Dimatangal JM, Dumelod BD (2003) Asia Pac J Clin Nutr 12:209–214
49. Tsuge K, Okabe M, Yoshimura T, Sumi T, Tachibana H, Yamada K (2004) Food Sci Technol Res 10:147–151
50. Pengzhan Y, Quanbin Z, Ning L, Zuhong X, Yanmei W, Zhi'en L (2003) J Appl Phycol 15:21–27
51. Onishi T, Umemura S, Yanagawa M, Matsumura M, Sasaki Y, Ogasawara T et al (2008) Arch Oral Biol 53:257–260
52. Gazi MI (1991) J Clin Periodontol 18:75–77
53. Clark DT, Gazl MI, Cox SW, Eley BM, Tinsley GF (1993) J Clin Periodontol 20:238–243
54. Moon HJ, Lee SR, Shim SN, Jeong SH, Stonik VA, Rasskazov VA et al (2008) Biol Pharm Bull 31:284–289
55. Armisen R, Galatas F (1987) In: McHugh DJ (ed) Production and utilization of products from commercial seaweeds, vol 288., pp 1–57
56. Wu J, Ding X (2001) J Agric Food Chem 49:501–506
57. Ardizzoni A, Neglia R, Baschieri M, Cermelli C, Caratozzolo M, Righi E et al (2011) J Mater Sci Mater Med 22:2329–2338
58. Liu M, Wu K, Mao X, Wu Y, Ouyang J (2010) J Ethnopharmacol 127:32–37
59. Lu J, Chen X, Zhang Y, Xu J, Zhang L, Li Z et al (2013) Int J Mol Med 31:1463–1470
60. Cheng Y, Tang K, Wu S, Liu L, Qiang C, Lin X et al (2011) PLoS One 6, e27437
61. Dai H, Jia G, Liu X, Liu Z, Wang H (2014) Environ Toxicol Pharmacol 38:263–271
62. da Silva BP, Parente JP (2003) Carbohydr Polym 51:239–242
63. Nakashima H, Yoshida O, Baba M, De Clercq E, Yamamoto N (1989) Antiviral Res 11:233–246
64. Coombe DR, Harrop HA, Watton J, Mulloy B, Barrowcliffe TW, Rider CC (1995) AIDS Res Hum Retroviruses 11:1393–1396
65. Guzdek A, Rokita H (1997) Mediators Inflamm 6:58–63
66. Delattre C, Fenoradosoa TA, Michaud P (2011) Braz Arch Biol Technol 54:1075–1092
67. Hayashi T, Hayashi K, Maeda M, Kojima I (1996) J Nat Prod 59:83–87
68. Pujol C, Matulewicz M, Cerezo A, Damonte E (1998) Phytomedicine 5:205–208
69. Maji PK, Sen IK, Devi KSP, Maiti TK, Sikdar SR, Islam SS (2013) Carbohydr Res 368:22–28
70. Yoo S, Yoon EJ, Cha J, Lee HG (2004) Int J Biol Macromol 34:37–41
71. Liu J, Luo J, Ye H, Zeng X (2012) Food Chem Toxicol 50:767–772
72. Giavasis I (2014) Curr Opin Biotechnol 26:162–173
73. Shingel KI (2004) Carbohydr Res 339:447–460

74. Zhong K, Wang Q, He Y, He X (2010) Int J Biol Macromol 47:356–360
75. Recuenco FC, Kobayashi K, Ishiwa A, Enomoto-Rogers Y, Fundador NGV, Sugi T et al (2014) Scientific Rep 4:4723
76. Panilaitis B, Johri A, Blank W, Kaplan D, Fuhrman J (2002) Clin Diagn Lab Immunol 9:1240–1247
77. de Oliveira AJB, Cordeiro LM, Gonçalves RAC, Ceole LF, Ueda-Nakamura T, Iacomini M (2013) Carbohydr Polym 94:179–184
78. Evans T (2002) Aliment Pharmacol Ther 16:6–11
79. Liao W-R, Lin J-Y, Shieh W-Y, Jeng W-L, Huang R (2003) J Ind Microbiol Biotechnol 30:433
80. Teixeira EH, Arruda FVS, do Nascimento KS, Carneiro VA, Nagano CS, da Silva BR et al (2012) In: Chang C-F (ed) Carbohydrates – comprehensive studies on glycobiology and glycotechnology. InTech, Croatia, pp 533–558
81. Mitsumata T, Suemitsu Y, Fujii K, Fujii T, Taniguchi T, Koyama K (2003) Polymer 44:7103–7111
82. Aiedeh K, Taha MO (1999) Arch Pharm (Weinheim) 332:103–107
83. Huang Y, Lam U (2011) J Chin Chem Soc 58:779–785
84. Ngwuluka NC, Choonara YE, Modi G, du Toit LC, Kumar P, Ndesendo VM et al (2013) AAPS PharmSciTech 14:605–619
85. Lee SJ, Park K (1996) J Mol Recognit 9:549–557
86. Brownlee M, Cerami A (1979) Science 206:1190–1191
87. Jeong SY, Kim SW, Holmberg DL, McRea JC (1985) J Control Release 2:143–152
88. Bhattarai N, Ramay HR, Gunn J, Matsen FA, Zhang M (2005) J Control Release 103:609–624
89. Zhang Y, Gao C, Li X, Xu C, Zhang Y, Sun Z et al (2014) Carbohydr Polym 101:171–178
90. Ying L, Jiali S, Jiang G, Jia Z, Fuxin D (2007) Chin J Chem Eng 15:566–572
91. Bhattarai N, Gunn J, Zhang M (2010) Adv Drug Deliv Rev 62:83–99
92. Chen J, Cheng T (2009) Polymer 50:107–116
93. Fundueanu G, Constantin M, Ascenzi P (2008) Biomaterials 29:2767–2775
94. Miyazaki S, Suzuki S, Kawasaki N, Endo K, Takahashi A, Attwood D (2001) Int J Pharm 229:29–36
95. Kim SJ, Shin SR, Lee JH, Lee SH, Kim SI (2003) J Appl Polym Sci 90:91–96
96. Sun S, Mak AF (2001) J Polym Sci B 39:236–246
97. Rozier A, Mazuel C, Grove J, Plazonnet B (1997) Int J Pharm 153:191–198
98. Rozier A, Mazuel C, Grove J, Plazonnet B (1989) Int J Pharm 57:163–168
99. Itoh K, Yahaba M, Takahashi A, Tsuruya R, Miyazaki S, Dairaku M et al (2008) Int J Pharm 356:95–101
100. Gao X, Matsui H (2005) Adv Mater 17:2037–2050
101. Bong DT, Clark TD, Granja JR, Ghadiri MR (2001) Angew Chem Int Ed 40:988–1011
102. Fernandez-Lopez S (2001) Nature 412:452

Chapter 9
Outlook of Aptamer-Based Smart Materials for Industrial Applications

Emily Mastronardi and Maria C. DeRosa

Abstract "Smart" materials are advanced materials that are able to change their physical or chemical properties in response to external stimuli in their environment, and they are finding uses in industry such as in drug delivery, for example. By adding a molecular recognition probe to the material that is specific to a target of interest, these smart materials can become responsive to specific molecules or biomolecules. Aptamers are single-stranded oligonucleotides that fold into complex structures and bind their targets with high affinity and selectivity. Due to their stability and facile method of synthesis and labeling, DNA aptamers are well suited to incorporation in smart materials. The addition of aptamers into these advanced materials allows the material to gain functionality from target recognition, altering the properties of the material upon target binding. Aptamer-based smart materials bring together aptamer technology with materials science, producing multifunctional, advanced materials with tunable properties that could be applied to many facets of industry. This chapter will discuss current literature and patents pertaining to aptamer-based smart materials and discuss the applicability of these materials for industrial applications.

Keywords Aptamers • Biosensors • Molecular recognition • Targeted delivery

9.1 Aptamer Smart Materials

Materials science is a growing field, often combining engineering with physical science to yield multifunctional materials. "Smart" materials are a result of this marriage, comprising materials which are able to alter their physical properties as a result of sensing a change in their environment such as pH, temperature, and electric or magnetic fields [1]. These materials can do more than sense changes in their

E. Mastronardi • M.C. DeRosa (✉)
Department of Chemistry, Carleton University,
1125 Colonel By Drive, Ottawa, ON K1S5B6, Canada
e-mail: emilymastronardi@gmail.com; maria.derosa@carleton.ca

environment; they can adapt to and report on the changes occurring. Shape memory materials can change their shape in response to stress, temperature, or changes in magnetic field and are being explored for less invasive medical implants such as stents and heart valves [2, 3]. Thermochromic, electrochromic, and photochromic materials have been developed, which change color in response to temperature, applied voltage, and light, respectively [4–10]. Piezoelectric materials can convert applied strain energy into electric energy and are being studied for self-powered devices and power harvesting [11–13]. The demand for such materials exists in the aerospace, automotive, and packaging industries, with piezoelectric actuators, self-dimming mirrors, and smart labels as examples [14]. As demand for multifunctional materials increases, smart materials are gaining popularity in sensing, molecular electronics, and controlled release applications.

This area of research has extended into biological applications, creating materials that are responsive to biomolecular stimuli. By incorporating a molecular recognition probe, such as an antibody, molecularly imprinted polymer (MIP), or an aptamer into the material structure, they become responsive to specific targets of interest. Aptamers are particularly well suited to incorporation into smart material systems [15, 16]. Aptamers are single-stranded oligonucleotides that fold into three-dimensional structures that can bind targets with high affinity and selectivity [17, 18]. They are made synthetically with a relatively low cost of production and labeling and little batch-to-batch variation, which makes them ideal for industrial applications. Many aptamers have already been developed for a wide range of targets, from small molecules to entire cells and organs which could be adapted to serve as triggers for bioresponsive smart materials [19–21]. DNA aptamers provide an extra layer of regulation to these systems as they can be inactivated by hybridization of their complement DNA strands.

This chapter will discuss the current developments in aptamer smart materials and how they can be utilized in industry to generate multifunctional, bioresponsive materials with tunable properties. The aptamer smart materials discussed will include materials whose properties are altered by the aptamer-target binding event. These materials do more than sense and report the target molecule, but undergo a physical change in response to the target, such as degradation of the material or the release of a cargo molecule. The incorporation of aptamers into hydrogels, gated pores, and polyelectrolyte films will be examined. As the focus of the chapter is on industrial applications, examples will be drawn from both patents and journal articles. Furthermore, an assessment of the future outlook of this area in terms of commercial applications will be provided.

9.2 Aptamer-Based Hydrogels

Hydrogels are composed of cross-linked hydrophilic polymers that can readily absorb water, causing them to swell. They have been engineered to become responsive, by allowing the amount of swelling to be influenced by environmental factors such as pH, ionic strength, temperature, electric field, light, and exposure to

solvents [22]. Hydrogels are used in the production of hygiene products, contact lenses, wound dressings, as well as in tissue engineering applications [23]. In order for a hydrogel to be considered bioresponsive, its cross-linking density must change as a result of a biological stimulus [24]. Many examples where the binding of DNA aptamers to their targets to control the phase transition of hydrogels have been described in patents and papers (select patents are shown in Table 9.1).

Tan and coworkers [24] were among the first to describe such a system, employing DNA aptamers to cross-link polyacrylamide monomers. Each monomer was conjugated to a short piece of single-stranded DNA and could be brought together through a rationally designed DNA linker strand. The linker strand contained an aptamer specific to ATP, as well as an extended region complementary to the DNA on each monomer. Adding the linker strand caused hydrogel cross-linking, while adding the target (ATP) preferentially removed the linker strand due to aptamer-target complex formation which led to the disassembly of the hydrogel network [24]. Tan and coworkers patented this technology [36]. This bioresponsive hydrogel could be used for controlled delivery applications, which Tan's group demonstrated with the ATP-dependent delivery of gold nanoparticles (AuNPs) that had been sequestered in the hydrogel. They also showed the generality of this approach, by applying it to the thrombin aptamer and successfully achieving target-derived hydrogel dissolution. With thrombin, the dissolution kinetics were slightly slowed, demonstrating the tunability of the bioresponsive hydrogels depending on the combination of aptamer and target used. Wei et al. [40] describe a similar DNA-mediated sol-gel hydrogel system. Two short DNA probes were grafted to polyacrylamide, and a linker DNA strand, which contained the α-thrombin aptamer, was complementary to these probes causing a hydrogel to form. When prepared in the presence of the aptamer's target, α-thrombin, the aptamer bound the protein and held it in the hydrogel. Addition of a DNA strand complementary to the linker strand caused hydrogel disassembly and the release of α-thrombin.

Rather than using the aptamers to control the cross-linking of their hydrogels, Liu and coworkers [41] used them to create target-specific release of cargo, while the hydrogel remained intact. Gold nanoparticles were attached to the hydrogel surface using the ATP aptamer. When ATP was introduced, the aptamer preferentially bound its target, releasing the gold nanoparticles from the hydrogel. This cargo release was shown to be specific, not responding to structural analogs, and was able to be generalized, giving the same target-specific release of rhodamine-labeled liposomes. The authors could dry and rehydrate the hydrogel, resulting in better target binding and slower release properties. This system also worked effectively in physiological conditions, showing its potential as a controlled release system for therapeutics.

The ability to deliver multiple cargo molecules from one material could be beneficial and was investigated by Wang's group [42, 43]. The authors designed aptamer-functionalized hydrogels capable of releasing multiple protein targets on demand, utilizing the aptamers' predictable hybridization to their complementary strands (Fig. 9.1). The authors functionalized streptavidin-coated polystyrene microparticles with both the VEGF and PDGF-BB aptamers and incorporated these microparticles into a hydrogel. The aptamers were shown to bind their respective protein targets and hold them within the hydrogel. Each protein could be released

Table 9.1 A selection of patents developed using aptamer-responsive hydrogel materials

Patent title	Claims	Ref
Biomedical device implantable in bone and/or cartilaginous tissue, and corresponding method to manufacture said biomedical device	A biomaterial to be implanted is coated with aptamers to facilitate cell adhesion to the biomaterial	[25] WO 2014128289 A1
Hybrid target analyte responsive polymer sensor with optical amplification	A target-responsive polymer matrix containing receptors (e.g., aptamers) and high refractive index nanoparticles is on the surface of an optical sensor. Target binding causes a detectable change in refractive index	[26] US 8841137 B2
Affinity hydrogels for controlled protein release	Controlled release of proteins from porous matrices. Affinity sites in the matrix are functionalized with aptamers. The release rate is tuned by aptamer affinity or by complement	[27] US 20130196915 A1, WO 2011091307 A8, WO2011091307A1
Device, system, and method for controllably reducing inflammatory mediators in a subject	Controlling inflammatory responses in a patient through specific devices, systems, and methods are described. One method includes an aptamer-target interaction changing properties of a hydrogel to promote delivery of a substance	[28] US 8430831 B2
Colloidal crystal gel label-free visual detection method with aptamer as identification unit	Hydrogel containing colloidal nanocrystals linked with aptamers is described; target binding causes conformational change causing a change in volume and color of the film	[29] CN 102590185 B
Affinity-based materials for the nondestructive separation and recovery of cells	Aptamers in a hydrogel can bind a target of interest and release it using the complement, separating the target from a mixture	[30] WO 2013056090 A1
Polynucleotide aptamer-based cross-linked materials and uses thereof	Using multivalent aptamers and conjugates including two or more affinity ligands, a target competes for binding resulting in the release of conjugate that is target concentration dependent	[31] US 86 03529 B2
Self-regulating chemo-mechano-chemical systems	A chemo-mechano-chemical system that includes an environmentally responsive gel (can contain an aptamer) that changes volume in response to a stimulus and interacts with another layer, producing a chemical or physical response	[32] WO 2013067525 A2

Photo-cross-linked nucleic acid hydrogels	Methods for producing hydrogel nucleic acid (including aptamer) structures using photo-cross-linking are described. Uses include the encapsulation and delivery of compounds	[33] US 20120040397 A1, EP 2324045 A2, CN 102171234 A, WO 2010017264 A2
Triggered drug release via physiologically responsive polymers	Associative polymers (e.g., cross-linked with aptamers) can release a pharmaceutical agent, optical signal, or change its physical properties upon target binding. Polymers that break apart, dissolve, or swell in the presence of a stimulus are also described	[34] US 20100209516 A1
Systems and methods using photoluminescent nanostructure based hydrogels	Responsive hydrogels (e.g., cross-linked with aptamers) including photoluminescent nanostructures can undergo a change in physical, chemical, dielectric, or other property when in contact with an altering stimulus	[35] WO 20100099446 A1, US20100279421, US 8377700 B2
Target-responsive hydrogels	DNA aptamers act as cross-linkers; target binding causes dissolution of the hydrogels	[36] WO 2009146147 A2
Apparatus comprising a protein integrated hydrogel polymer which undergoes conformation transition in the presence of a target molecule	A biopolymer (such as an aptamer) is incorporated into a hydrogel network. Target binding induces reversible swelling and the release of a biomolecule, for use as an actuator or biosensor	[37] US 7625951 B2
Drug delivery system and method	A hydrogel is cross-linked by conjugating an aptamer and its target within the gel for example. A preloaded active drug can be controllably released by competitive binding of the aptamer's target	[38] WO 2008060575 A2, WO2008060575A3, US 20080138408 A1
Multimeric biopolymers as structural elements, sensors, and actuators in microsystems	Multimeric biopolymers (e.g., DNA) undergo a conformational change in response to a target, which can be used to sense and/or actuate a response	[39] US 20020068295 A1, CA2419156A1, EP1301585A2, WO2002006789A2, WO2002006789A3
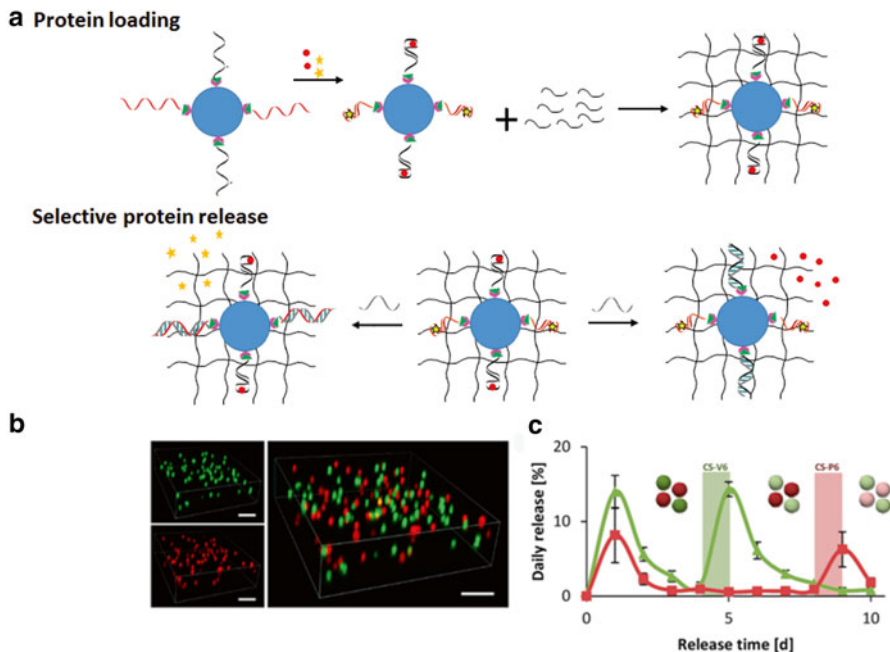
Fig. 9.1 Aptamer-functionalized hydrogels for multiple protein release. (**a**) (top) Streptavidin (fuchsia)-coated polystyrene microparticles (*blue*) were decorated with two different aptamers (*red*, *black*). Two targets were added (*yellow*, *red*) and bound their respective aptamers. The microparticles were incorporated into a hydrogel (*black*) and (bottom) could release either target with the addition of each aptamer's complement strand [42, 43]. (**b**) A laser confocal micrograph showing two different aptamer-functionalized microparticles in a hydrogel. (**c**) Daily release profiles of VEGF (*green*) and PDGF-BB (*red*) from a hydrogel, mediated by the addition of sequence-specific complementary sequences (CS). CS-V6 and CS-P6 were introduced for an hour on days 4 and 8, respectively, triggering the release of VEGF and PDGF-BB, respectively. Modified with permission from [43], Copyright 2012 American Chemical Society

only when its aptamer's complement was added. The authors achieved a daily release rate of 14 % (up from 1 %) for VEGF and around 6 % (up from 0.5 %) for PDGF when their complement strands were introduced. Importantly, the addition of one aptamer's complement strand was not found to affect the release of the other protein. The authors suggest that many aptamer-protein targets could be included in one hydrogel, serving as a promising therapeutic tool for complex illnesses requiring more than one drug for treatment. The same group acquired a patent for this multi-aptamer-hydrogel composite system [27]. The release rates of the protein cargo could be tuned with the aptamer's dissociation constant (K_d) or by the addition of the aptamer's complement strand. This responsive hydrogel system could lead to promising new drug formulations.

Mi and coworkers [44] were able to achieve the recognition and separation of a target molecule in a complex mixture, creating a "catch and release" aptamer-hydrogel system. A DNA linker strand was designed containing an aptamer sequence, DNA

segments complementary to the hydrogel monomers, as well as a toehold sequence. This strand was incubated with target molecules in a mixture, and the aptamer sequence recognized and bound the specific target. After adding the hydrogel monomers, the complementary sequences on the linker strand caused the hydrogel formation, with target molecules sequestered inside it. The hydrogel was washed to keep only the target of interest, and the target was subsequently released on demand by adding a DNA strand complementary to the full linker strand. The authors demonstrated the utility of this method, successfully separating ATP from a mixture of ATP and GTP, as well as α-thrombin from a mixture of α-thrombin and bovine serum albumin. This specific "catch and release" system could be promising in many applications such as molecular separation and environmental monitoring. Wang et al. [30] used this affinity hydrogel separation strategy in a patent they obtained in 2013. By functionalizing a hydrogel substrate with aptamers, the authors can bind target mammalian cells in physiological conditions, wash and separate the aptamer-target complex, and release the target cells using the complement DNA strand. The authors suggest separating cancer cells from healthy cells in a physiological fluid for example.

Smart aptamer-based materials with applications as alternatives to traditional computing have been investigated, including rationally designed molecular systems which are capable of Boolean logic operations. Because of its predictable three-dimensional shape and capacity to store information, DNA has been used in such logic operations [45]. Aptamer-based logic gates capable of responding to multiple targets have been described in multiple papers [46–51] and patents [52–55]. Tan's group created a bioresponsive logic gate using aptamer hydrogels with gold nanoparticles as a visual output, where specific target binding led to hydrogel disassembly and dispersal of red AuNPs [56]. In this system, the confined state of the AuNPs in the hydrogel was equated to "FALSE," while the AuNPs dispersed in solution indicated "TRUE." The authors used the ATP and cocaine aptamers to create an "AND" and "OR" logic gate. For the "AND" gate, the hydrogel was formed using three DNA sequences that were designed to form a Y-shaped structure, where each strand was half complementary to each other strand. When both ATP and cocaine targets were added, they each bound their respective aptamer and disassembled the hydrogel. When only one target was added, two of the three-strand complex remained hybridized, leaving the hydrogel assembled. Similarly, an "OR" gate was created where the addition of either target could trigger hydrogel disassembly. The specificity of this logic gate was also demonstrated, as structural analogs GTP and benzoylecgonine were unable to initiate the disassembly of the hydrogel.

9.3 Gated Pores

Mimicking biological pores and channels, such as the gated ion channels found in cells, is of great interest to facilitate transport and to create molecular actuators and transducers [57]. Using nanoscale porous materials with stimuli-responsive polymers has led to controlled transport responsive to pH, ionic strength, and

temperature [58]. Applying aptamer-target binding to these systems in order to control transport could create bioresponsive materials for delivery and sensing and has been investigated by a number of groups. Schafer and Ozalp [59] created an anodized aluminum oxide membrane that was responsive to ATP. The membrane contained 20 nm sized pores and was functionalized with amino groups and avidin to allow the biotinylated-ATP aptamer to be immobilized on the surface. By adding seven nucleotides to the 3′ end, the group was able to create a DNA hairpin with exaggerated structure-switching in response to its ATP target. Without an ATP target, the hairpin structure allowed the passage of fluorescein sodium salt through the membrane. In the presence of ATP, the structure of the aptamer changed and no longer allowed the fluorescein to permeate the membrane. The authors found this target-derived permeability change to be dependent on the ATP concentration, to be specific to ATP, as GTP generated a much smaller response and was reversible.

Zhu et al. [60] created gated nanochannels using a porous anodic aluminum oxide membrane containing a regular arrangement of 25 nm channels, gated with ATP aptamers and graphene oxide (Fig. 9.2). The membrane contained a thin film of gold allowing the thiol-modified ATP aptamers to be functionalized to its surface. These single-stranded aptamers are able to interact with graphene oxide through π-π stacking, keeping the rigid graphene oxide sheet close enough to block the flow through the channel. Upon introduction of ATP, the aptamer binds its target, letting go of the graphene oxide sheet and allowing the channel to open. The authors successfully impeded the flow of glucose, bovine serum albumin, and gold nanoparticles. The specificity of this responsive gate was also confirmed as structural analogs CTP, GTP, and TTP were unable to restore flow through the channels. The use of such a responsive gate can be imagined in controlled release and molecular separation applications.

Applying this gated pore technology to sensing applications, Wang et al. [61] used a bio-nanogate to develop a sensitive, label-free detection system for AIV H5N1 virus (Fig. 9.3). The enzyme lactate dehydrogenase (LDH) uses the substrate L-lactate and NAD⁺ to generate pyruvate, NADH, and protons, while amperometric measurements can be used to detect the increase in current when this reaction occurs. The authors immobilized LDH on a glassy carbon electrode. To this enzyme-electrode, the authors attached a porous gold membrane onto which thiolated single-stranded DNA probes, complementary to an aptamer, were immobilized. Adding the aptamer the group developed for AIV H5N1 virus would close the 20 nm pores present in the gold membrane through aptamer-probe hybridization, thus blocking access to the enzyme-electrode through the pores. The increase in current obtained by the LDH reaction was blocked 52 % when the aptamer blocked the pores. When target was added, the aptamer preferentially formed a virus-aptamer complex, dehybridizing from the single-stranded probes and opening the pores. This allowed substrate and coenzyme to flow freely to the immobilized enzymes, and an increase in current could be detected. The authors were able to use this aptamer-nanogate to get electrochemical signals proportional to the concentration of target, with a limit of detection of 2–9 HAU. Testing with similar viruses H1N1, H2N2, H4N8, and H7N2 yielded very little current, suggesting the aptamer-nanogate developed was specific
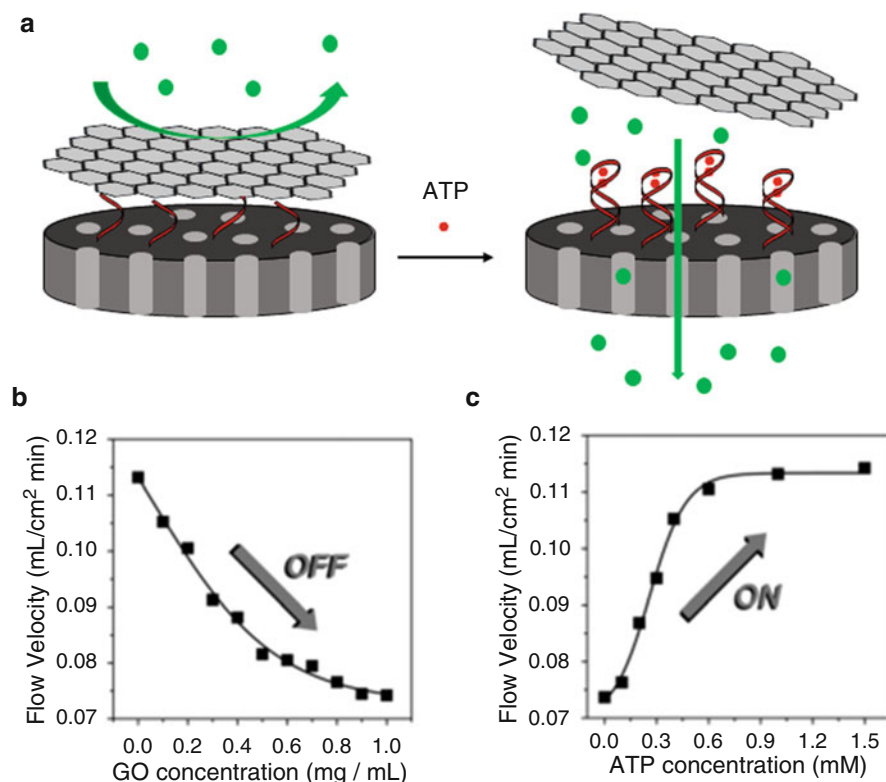
Fig. 9.2 Aptamer and graphene oxide-gated nanochannels. (**a**) Aptamers (*red*) were functionalized to a porous aluminum oxide membrane (*dark gray*). The aptamers interacted with a graphene sheet (*light gray*) blocking flow (*green*) through the channels. Addition of target (*red*) caused the aptamers to let go of the graphene sheet binding target instead, and restoring flow through the channels. (**b**) Graphene oxide reduces the flow velocity through the nanochannels (no target is present). (**c**) Target (ATP)-binding restores the flow velocity. Modified with permission from [62], Copyright 2014 Royal Society of Chemistry

to the AIV H5N1 virus. Such a detection system could be applied using the many aptamers for biomarkers, toxins, and viruses.

Porous nanoparticles can serve as delivery vehicles and can be made bioresponsive by gating these pores using DNA aptamers, resulting in target-derived payload delivery. The Wang group [62] demonstrated an aptamer-gated mesoporous silica particle, capable of selectively delivering their fluorescein payload. The mesoporous silica particle had ATP derivative molecules immobilized on its surface, allowing the AuNP-functionalized ATP aptamers to bind. The bulky AuNPs blocked the pores, allowing the fluorescein payload to remain inside the nanoparticle. When ATP was added, it competed for aptamer binding, removing the blockage and allowing the fluorescein to be released. The payload release rate could be altered with ATP concentration and was unaffected by structural analogs GTP, CTP, and UTP.
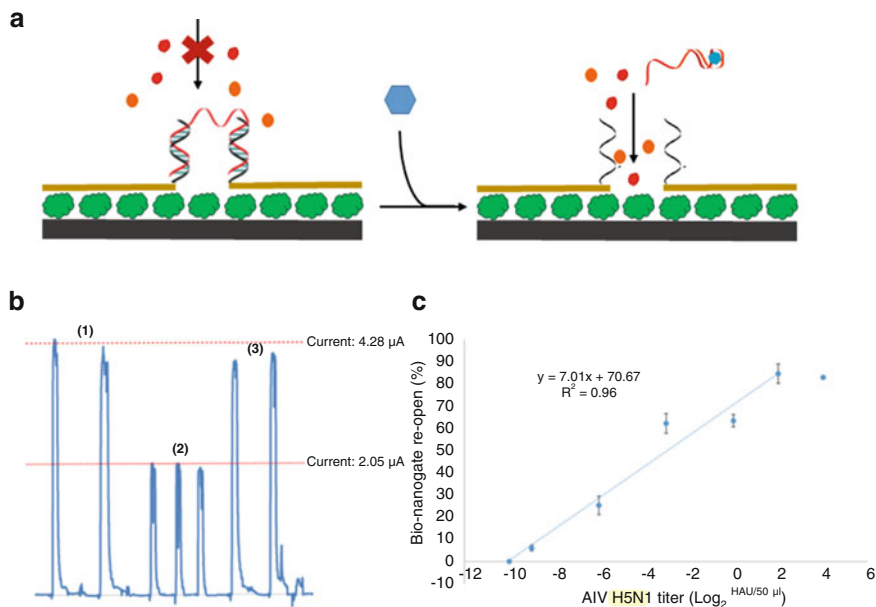
Fig. 9.3 Aptamer-functionalized bio-nanogate virus detection system. (**a**) Lactate dehydrogenase (*green*) was immobilized on a glassy carbon electrode (*gray*). A porous gold layer (*dark yellow*) was added, allowing single-stranded DNA probes (*gray*) to be attached. An aptamer (*red*) bound the probes, closing the pore and blocking substrate (*orange*) and cofactor (*red*) from the electrode. Addition of virus (*blue*) removed the aptamer, opening the pore and allowing substrates and cofactors to reach the electrode. (**b**) The peak currents of the bio-nanogate system: (1) Before aptamer was added, (2) after aptamer was added and pores were blocked, (3) after the target virus was added, restoring current through the gate. (**c**) Detection of H5N1 using the bio-nanogate system. A linear relationship was observed between 2^{-10} and 2^2 HAU. Modified with permission from [61], Copyright 2015 from Elsevier

An aptamer-gated nanoparticle system was also developed by Ozalp and Shafer [59], this time exploiting the aptamer's structural change upon target binding to create a reversibly gated nanoparticle. Without the target present, the ATP aptamer formed a bulky hairpin structure. This hairpin was immobilized on the surface of mesoporous silica nanoparticles which were preloaded with a fluorescein payload. The bulky nature of the aptamer hairpin blocked the pores, confining the cargo inside the nanoparticle. In the presence of ATP, the aptamer bound its target which altered the aptamer's shape. The new, less sterically hindered aptamer no longer blocked the pores, allowing the fluorescent cargo to be released. Removal of the ATP target caused the aptamer to revert to its bulky hairpin structure, blocking the pores once again. This reversible aptamer-gated nanoparticle is a promising step toward controlled and sustained release pharmaceuticals.

Using exclusively DNA, Douglas et al. [64, 65] reported and patented a DNA nanorobot controlled by an aptamer gate, which can change its shape in response to a stimulus molecule and release a payload. The hexagonal robot was created using

DNA origami, having two domains held together with single-stranded DNA hinges. The robot was closed with two aptamer-complement locks, which consisted of aptamer strands on one domain hybridizing to partially complementary strands on the other domain. When specific target molecules bound both aptamers, the aptamers dehybridized from their complement strands allowing the DNA robot to open and sequestered cargo to be released. The authors demonstrated the specificity of their system using combinations of an aptamer derived for platelet-derived growth factor (PDGF) and two aptamers developed for T-cell acute lymphoblastic leukemia cells (CCRF-CEM). The DNA robot was loaded with fluorescently labeled antibody fragments specific to human leukocyte antigen and was incubated with different cell types. Using flow cytometry to measure fluorescence, the authors found labeled cells only when the correct combination of aptamer targets corresponding to the aptamer locks were present on the cells, allowing the DNA robot to open and expose the cells to its fluorescent cargo. Since two aptamer locks were present on the robot, using different aptamer locks created an "AND" gate, allowing the robot to distinguish between different cell types. The authors also demonstrated the DNA robot's ability to affect cell behavior, using antibodies to human CD33 and human CDw328 as cargo. These targets have been shown to arrest growth of leukemic cells, and when specifically delivered by the DNA robot, cell growth was arrested in NKL cells. More recently, the authors expanded their DNA nanorobot system creating logic gates, by using the key for one robot as cargo in another, for example, such that the opening of the first robot from an external stimulus released the key for the second, allowing the robots to open in succession [66] (Fig. 9.4). This was successfully completed in a cockroach model, creating "AND," "OR," "XOR," "NAND," "NOT," "CNOT," and half adder logic gates in vivo. The authors demonstrated biological computing, and work in this area could provide computational control of therapeutic delivery.

9.4   Aptamer-Polyelectrolyte Films and Microcapsules

There are many applications of thin films in industry, requiring films with consistent composition and thickness. The layer-by-layer technique is one way to achieve films with controllable properties and involves the repeated layering of oppositely charged polyelectrolytes. This process can be easily automated and scaled up [67] and is well suited to aptamer incorporation, as DNA is a negatively charged polymer [68, 69]. Polyelectrolyte films have already found their way into commercial applications, such as coatings for contact lenses and flexible conducting films known as metal rubber [70, 71]. The first report of a multilayered aptamer-polyelectrolyte thin film was in 2009 and showed that aptamers embedded in films were still able to bind their targets, retaining their specificity with only a slight decrease in their affinity [72]. This showed that aptamers were able to confer their target-binding ability to the polyelectrolyte thin films, opening the door for sensing and controlled release applications.
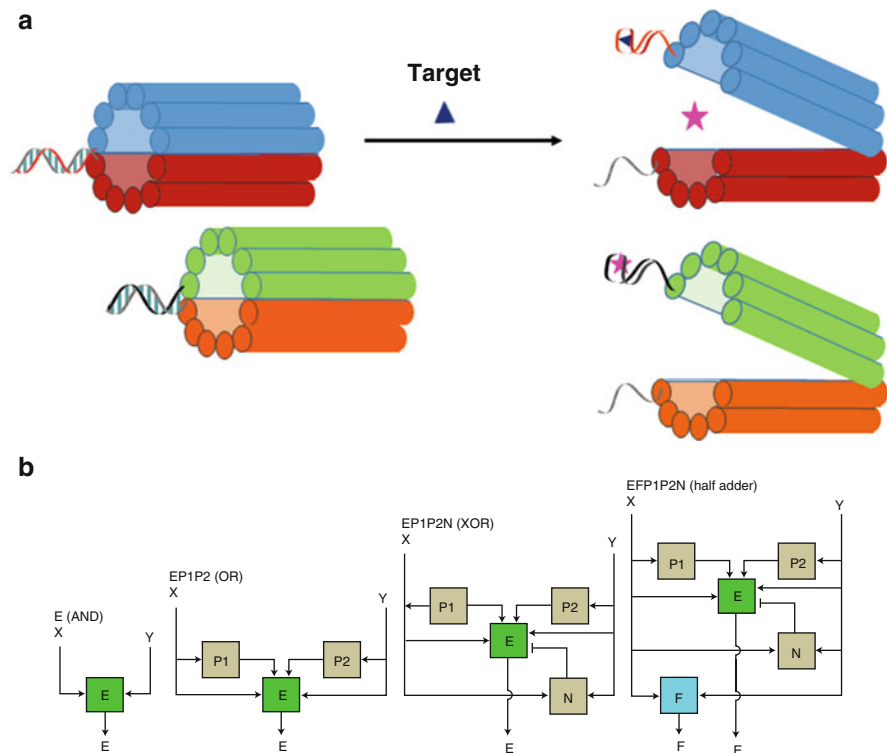
Fig. 9.4 Aptamer-gated DNA nanorobot. (**a**) Hexagonal DNA "robots" were created using DNA origami with two domains held together by DNA aptamer locks. When a target (navy) was added, aptamer-target binding caused the domains to open, releasing a second target (fuchsia). The second target acted as the key for another robot, causing successive opening. (**b**) Design of various logic gates by mixing P (positive regulator robot, loaded with a key for subsequent robot) and N (negative regulator robot, loaded with clasps forcing subsequent robot to close) robots with effector (E) robots at different ratios. "AND" gate: E robot opened if both X and Y cues were present. "OR" gate: Two robots were added, P1 (opened in response to X and carried the key to Y gate of E) and P2 (opened in response to Y and carried the key to X gate of E) such that robot E could open with either X or Y. "XOR" gate: N robots were added, such that X and Y together activate N which closed E, creating a "XOR" gate which opened in response to X or Y, but not both. Half Adder: F robot was added which did not respond to P1 or P2, nor was negated by N. Robot E was activated by either X or Y while XY together activates F (E was closed by N). Modified with permission from [66], Copyright 2014 MacMillan Publishers Ltd

Toward this goal, target-responsive polyelectrolyte films were made into micro-capsules, incorporating the aptamer into the walls, and the effect on permeability was studied [73]. The diffusion of sulforhodamine B dye through the microcapsule walls was investigated using fluorescence recovery after photobleaching (FRAP). The microcapsules containing aptamers embedded in their walls showed an increase in dye diffusion almost an order of magnitude higher than microcapsules containing a random DNA strand, or containing no DNA. This was suspected to be caused by the aptamer changing its shape upon target binding, altering the permeability of the film.

Chen et al. [74] describe an electrochemiluminescent (ECL) sensor platform that utilizes the target-derived permeability change of aptamer layer-by-layer films. A glassy carbon electrode was modified with an efficient ECL nano-emitter, Au-g-C_3N_4. On top of this layer, the authors added thin films containing DNA aptamers for BPA which acted as a gate. The diffusion of $S_2O_8^{2-}$ to the ECL sensor was needed to generate an ECL response, and its diffusion through the film was dependent on aptamer-target binding. Without BPA, the $S_2O_8^{2-}$ was less able to reach the sensor. When BPA was added, it could bind its aptamer in the polyelectrolyte film causing a conformational change and increased diffusion through the film. When BPA was present, the ECL intensity increased 64 times, indicating a target-responsive permeability change in the film. The authors achieved a limit of detection of 0.05 ng/mL of BPA and were able to regenerate their sensor by unfolding the aptamer with 1.0 M imidazole. This study shows the promise of developing sensitive and specific detection platforms using aptamer-based target-responsive films.

Zhang et al. [75] were able to achieve target-molecule-triggered rupture of layer-by-layer polyelectrolyte microcapsules containing aptamers as a scaffold. The polyelectrolyte films were deposited on a $CaCO_3$ core that had been doped with polystyrene sulfonate and sulforhodamine B dye-specific aptamers. The aptamers acted as a scaffold that supported the outer polyelectrolyte layers. When the target dye was incubated with the microcapsules, almost all the microcapsules collapsed after 24 h and after 6 days of incubation, 60 % of the microcapsules had collapsed and burst. This suggested that target dye could permeate the layer-by-layer microcapsules, and aptamer-target complex formation resulted in collapse of the microcapsules. This same bursting phenomenon of the microcapsules was not seen when using a structural analog, showing the specificity of the aptamer-target complex. This system could have applications for controlled delivery in response to specific targets (Fig. 9.5).

9.5 Future Outlook

While recent efforts to date have confirmed that aptamer-based smart materials hold a great deal of promise, the question remains whether these multifunctional materials can make the transition from research curiosity to commercial applications. Practical limitations, such as cost, could be a major obstacle to the industrial and commercial application of these materials. While the synthesis of nucleic acid aptamers is relatively inexpensive when compared to other molecular recognition elements, such as antibodies, it would still make up the major fraction of the cost of smart material production. However, given the rapid advances in technologies associated with the synthetic production of DNA, it is reasonable to expect that the cost of aptamer production will continue to decrease [76]. Another potential drawback of this technology is that its generality has not been extensively tested. Many of the
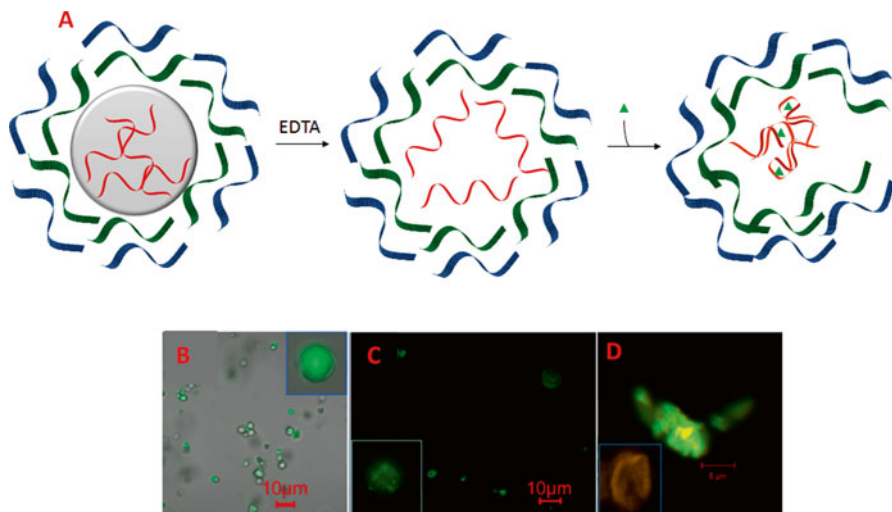
Fig. 9.5 Aptamer-responsive polyelectrolyte microcapsules. (**a**) Aptamers (*red ribbons*) were doped into a CaCO₃ core (*gray circle*), onto which polyelectrolytes (*blue* and *green ribbons*) were deposited. Removing the CaCO₃ left an aptamer scaffold supporting the polyelectrolyte film. Target (*green triangles*) bound the aptamers, removing the scaffold and causing the microcapsules to collapse and burst. (**b**) Confocal laser scanning microscopy (CLSM) image of sulforhodamine B aptamer (SA): polystyrene sulfonate (PSS)-CaCO₃ microcapsules prepared with fluorescein-labeled aptamers. (**c**) CLSM image of SA: PSS-(Polydiallyldimethylammonium chloride (PDDA)/PSS)₅ microcapsules prepared from fluorescein-labeled aptamers. (**d**) Colocalization experiment showing aptamer-target binding caused microcapsule rupture after 6 days. Sulforhodamine B target at 1 mM and 0.1 KCl was used. Inset image shows ruptured nonfluorescent aptamer microcapsule. Modified with permission from [75], Copyright 2013 American Chemical Society

studies reporting aptamer smart materials involve proof-of-concept aptamer-target systems such as for ATP, sulforhodamine B dye, or thrombin. Numerous aptamers have been developed for a wide range of pertinent biological targets and could be utilized in these systems to produce novel smart materials. An unlimited number of aptamer smart material systems could be accessed by selecting new aptamers for important targets such as small molecules and proteins implicated in disease, and inserting them into these reported systems. With many proof-of-concept studies completed, researchers can now move into building useful tools for immediate use. New materials should also be developed to maximize the utility of aptamer smart materials for controlled delivery for example. Introducing biodegradable polymers could facilitate the use of these systems. Recently, the sulforhodamine B DNA aptamer was incorporated into layer-by-layer films of chitosan and hyaluronan and the aptamers were shown to retain their binding function [77]. The success of this biodegradable film system shows that aptamers can easily be applied to many combinations of films, tailored to the desired function. It also shows that aptamers can be applied to the biodegradable and biocompatible systems that would be required

in pharmaceutical and biomedical applications. Incorporating aptamers into new polymer materials, beyond polyelectrolytes, to make them bioresponsive will also expand the capabilities of aptamer smart materials.

Beyond widening the scope of targets and polymer systems, new applications for smart materials should be investigated. Active targeting of therapeutics using DNA aptamers has been found to decrease off-site toxicity in the delivery of drugs, such as chemotherapeutics for example [21]. Using smart materials in these formulations could add an extra layer of control, in addition to simply targeting. Using aptamer materials could regulate the dose of drug delivered once the target site is reached, tailoring the dose to the level of disease in each individual. This type of dual labeling could be applied to porous nanoparticles, with an aptamer for targeting and another for gating, or to hydrogels, with an aptamer for targeting and another for controlling cross-linking, creating many new targeted responsive materials. Aptamer-gated pores could also find utility in selective microbial and/or cell culture applications. Porous aluminum oxide substrates have attracted a lot of attention of late in biomedical applications [78]. Aptamers could be employed for both the selective attachment through cell surface biomarkers, as well as the triggered delivery of nutrients, differentiation factors, and others. Similarly, aptamer-functionalized surfaces could facilitate the adhesion of multiple cell types in predetermined patterns for the fabrication of micro-organs and tissues [79]. For the creation of "organs-on-chips," the position and orientation of cells are particularly important and have been investigated by seeding cells in confined microfluidic devices. The incorporation of aptamers to these devices could facilitate cell-specific adhesion, nutrient delivery, as well as the specific delivery of differentiation factors to individual cell types. These micro-organs and tissues built using aptamer-functionalized materials could facilitate drug development and accelerate regenerative medicine.

9.6 Conclusion

Using DNA aptamers in advanced materials generates bioresponsive systems with tunable properties, with uses in sensing, molecular electronics, and controlled delivery. The feasibility of aptamer smart materials was demonstrated through the successful development of smart hydrogels, gated pores and nanomaterials, and aptamer-responsive polyelectrolyte films, while their industrial and commercial promise was demonstrated through the many patents obtained for aptamer hydrogels and logic gates. Applying these systems to biologically-relevant targets and creating new materials could generate innovative sensors, controlled release formulations, and molecular separation devices for novel pharmaceutical and environmental products.

References

1. Roy I, Gupta MN (2003) Smart polymeric materials: emerging biochemical applications. Chem Biol 10:1161–1171. doi:10.1016/j

2. Sun L, Huang WM, Ding Z, Zhao Y, Wang CC, Purnawali H, Tang C (2012) Stimulus-responsive shape memory materials: a review. Mater Des 33:577–640. doi:10.1016/j.matdes.2011.04.065

3. Yu Z, Zhang Q, Li L, Chen Q, Niu X, Liu J, Pei Q (2011) Highly flexible silver nanowire electrodes for shape-memory polymer light-emitting diodes. Adv Mater 23:664–668. doi:10.1002/adma.201003398

4. Pardo R, Zayat M, Levy D (2011) Photochromic organic-inorganic hybrid materials. Chem Soc Rev 40:672–687. doi:10.1039/c0cs00065e

5. Seeboth A, Ruhmann R, Mühling O (2010) Thermotropic and thermochromic polymer based materials for adaptive solar control. Materials (Basel) 3:5143–5168. doi:10.3390/ma3125143

6. Mortimer RJ (2011) Electrochromic materials. Annu Rev Mater Sci 41:241–268. doi:10.1146/annurev.ms.16.080186.001153

7. Scherer MRJ, Steiner U (2013) Efficient electrochromic devices made from 3D nanotubular gyroid networks. Nano Lett 13:3005–3010. doi:10.1021/nl303833h

8. Seeboth A, Lötzsch D, Ruhmann R, Muehling O (2014) Thermochromic polymers–function by design. Chem Rev 114:3037–3068. doi:10.1021/cr400462e

9. Kline WM, Lorenzini G, Sotzing GA (2014) A review of organic electrochromic fabric devices. Coloration Technol 130(2):73–80. doi:10.1111/cote.12079

10. Zhang J, Zou Q, Tian H (2013) Photochromic materials: more than meets the eye. Adv Mater 25:378–399. doi:10.1002/adma.201201521

11. Anton SR, Sodano HA (2007) A review of power harvesting using piezoelectric materials (2003–2006). Smart Mater Struct 16:R1–R21. doi:10.1088/0964-1726/16/3/R01

12. Pan C, Li Z, Guo W, Zhu J, Wang ZL (2011) Fiber-based hybrid nanogenerators for/as self-powered systems in biological liquid. Angew Chem Int Ed 50:11192–11196. doi:10.1002/anie.201104197

13. Chi Z, Xu Q (2014) Recent advances in the control of piezoelectric actuators. Int J Adv Robot Syst 11:1–11. doi:10.5772/59099

14. The Institute of Materials MAM Materials Foresight – Smart materials for the 21st century (http://www.iom3.org/smart-materials-systems-committee/smart-materials-systems-foresight) Accessed March 2015.

15. Ruigrok VJB, Levisson M, Eppink MHM, Smidt H, van der Oost J (2011) Alternative affinity tools: more attractive than antibodies? Biochem J 436:1–13. doi:10.1042/BJ20101860

16. Iliuk AB, Hu L, Tao WA (2011) Aptamer in bioanalytical applications. Anal Chem 83:4440–4452. doi:10.1021/ac201057w

17. Tuerk C, Gold L (1990) Systematic evolution of ligands by exponential enrichment: RNA ligands to bacteriophage T4 DNA polymerase. Science 249:505–510

18. Ellington AD, Szostak JW (1990) In vitro selection of RNA molecules that bind specific ligands. Nature 346:818–822. doi:10.1038/346183a0

19. Cibiel A, Dupont DM, Ducongé F (2011) Methods to identify aptamers against cell surface biomarkers. Pharmaceuticals 4:1216–1235. doi:10.3390/ph4091216

20. Duan N, Wu S, Chen X, Huang Y, Xia Y, Ma X, Wang Z (2013) Selection and characterization of aptamers against salmonella typhimurium using whole-bacterium systemic evolution of Ligands by exponential enrichment (SELEX). J Agric Food Chem 61:3229–3234. doi:10.1021/jf400767d

21. Xiang D, Shigdar S, Qiao G, Wang T, Kouzani AZ, Zhou S (2015) Nucleic acid aptamer-guided cancer therapeutics and diagnostics: the next generation of cancer medicine. Theranostics. doi:10.7150/thno.10202

22. Yoshida R, Okano T (2010) Stimuli-responsive hydrogels and their application to functional materials. In: Biomedical applications of hydrogels handbook. pp 19–43. doi:10.1007/978-1-4419-5919-5

23. Caló E, Khutoryanskiy VV (2014) Biomedical applications of hydrogels: a review of patents and commercial products. Eur Polym J 65:252–267. doi:10.1016/j.eurpolymj.2014.11.024
24. Yang H, Liu H, Kang H, Tan W (2008) Engineering target-responsive hydrogels based on aptamer-target interactions. J Am Chem Soc 130:6320–6321. doi:10.1021/ja801339w
25. Galli C, Macaluso GM (2014) Biomedical device implantable in bone and/or cartilaginous tissue, and corresponding method to manufacture said biomedical device
26. DeLouise L, Bonanno L. Hybrid target analyte responsive polymer sensor with optical amplification
27. Wang Y, Soontornworajit B, Chen N (2013) Affinity hydrogels for controlled protein release
28. Hyde RA, Ishikawa MY, Jung EKY, Langer R, Leuthardt EC, Myhrvold NP, Sweeney EA, Wood LL Jr (2013) Device, system, and method for controllably reducing inflammatory mediators in a subject
29. (2013) Colloidal crystal gel label-free visual detection method with aptamer as identification unit
30. Wang Y, Zhang Z, Chen N, Li S (2013) Affinity-based materials for the non-destructive separation and recovery of cells
31. Zion TC, Lancaster TM (2013) Polynucleotide aptamer-based cross-linked materials and uses thereof
32. Aizenberg J, He X, Aizenberg M (2013) Self-regulating chemo-mechano-chemical systems
33. Luo D, Roh YH (2012) Photo-crosslinked nucleic acid hydrogels
34. Benkoski JJ, Mason AF, Baird LM, Sample JL (2010) Triggered drug release via physiologically responsive polymers
35. Strano MS, Barone PW (2010) Systems and methods using photoluminescent nanostructure based hydrogels
36. Tan W, Huanghao Y, Liu H (2009) Target-responsive hydrogels
37. Daunert S, Deo SK, Ehrick JD, Browning TW, Bachas LG (2009) Apparatus comprising a protein integrated hydrogel polymer which undergoes conformational transition in the presence of a target molecule
38. Mark B, Siddarth V, Jacek W (2008) Drug delivery system and method
39. Madou M, Bachas L, Daunert S (2002) Microarray for use in the detection of preferential particles in solution
40. Wei B, Cheng I, Luo KQ, Mi Y (2008) Capture and release of protein by a reversible DNA-induced sol-gel transition system. Angew Chem Int Ed 47:331–333. doi:10.1002/anie.200704143
41. El-Hamed F, Dave N, Liu J (2011) Stimuli-responsive releasing of gold nanoparticles and liposomes from aptamer-functionalized hydrogels. Nanotechnology 22:494011. doi:10.1088/0957-4484/22/49/494011
42. Soontornworajit B, Zhou J, Wang Y (2010) A hybrid particle–hydrogel composite for oligonucleotide-mediated pulsatile protein release. Soft Matter 6:4255. doi:10.1039/c0sm00206b
43. Battig MR, Soontornworajit B, Wang Y (2012) Programmable release of multiple protein drugs from aptamer-functionalized hydrogels via nucleic acid hybridization. J Am Chem Soc 134:12410–12413. doi:10.1021/ja305238a
44. He X, Wei B, Mi Y (2010) Aptamer based reversible DNA induced hydrogel system for molecular recognition and separation. Chem Commun (Camb) 46:6308–6310. doi:10.1039/c0cc01392g
45. Wu C, Wan S, Hou W, Zhang L, Xu J, Cui C, Wang Y, Hu J, Tan W (2015) A survey of advancements in nucleic acid-based logic gates and computing for applications in biotechnology and biomedicine. Chem Commun 51:3723–3734. doi:10.1039/C4CC10047F
46. Yoshida W, Yokobayashi Y (2007) Photonic Boolean logic gates based on DNA aptamers. Chem Commun (Camb) 9:195–197. doi:10.1039/b613201d
47. Liu Y, Ren J, Qin Y, Li J, Liu J, Wang E (2012) An aptamer-based keypad lock system. Chem Commun 48:802. doi:10.1039/c1cc15979h
48. Xu X, Zhang J, Yang F, Yang X (2011) Colorimetric logic gates for small molecules using split/integrated aptamers and unmodified gold nanoparticles. Chem Commun (Camb) 47: 9435–9437. doi:10.1039/c1cc13459k

49. You M, Zhu G, Chen T, Donovan MJ, Tan W (2015) Programmable and multiparameter DNA-based logic platform for cancer recognition and targeted therapy

50. Zhu C-L, Song X-Y, Zhou W-H, Yang H-H, Wen Y-H, Wang X-R (2009) An efficient cell-targeting and intracellular controlled-release drug delivery system based on MSN-PEM-aptamer conjugates. J Mater Chem 19:7765. doi:10.1039/b907978e

51. Wang J, Lu J, Su S, Gao J, Huang Q, Wang L, Huang W, Zuo X (2015) Binding-induced collapse of DNA nano-assembly for naked-eye detection of ATP with plasmonic gold nanoparticles. Biosens Bioelectron 65:171–175. doi:10.1016/j.bios.2014.10.031

52. (2014) Electroluminescence logic gate adopting adenosine monophosphate and adenosine deaminase as excimers

53. Seelig G, Lutz B (2013) Systems and methods for detecting biomarkers of interest

54. Stojanovic MN (2003) Oligonucleotide-based logic gates and molecular networks

55. Sen D, Fahlman RP (2011) DNA conformational switches as sensitive electronic sensors of analytes

56. Yin B-C, Ye B-C, Wang H, Zhu Z, Tan W (2012) Colorimetric logic gates based on aptamer-crosslinked hydrogels. Chem Commun 48:1248. doi:10.1039/c1cc15639j

57. Jiang Y, Liu N, Guo W, Xia F, Jiang L (2012) Highly-efficient gating of solid-state nanochannels by DNA supersandwich structure containing ATP aptamers: a nanofluidic IMPLICATION logic device. J Am Chem Soc 134:15395–15401. doi:10.1021/ja3053333

58. Abelow AE, Schepelina O, White RJ, Vallée-Bélisle A, Plaxco KW, Zharov I (2010) Biomimetic glass nanopores employing aptamer gates responsive to a small molecule. Chem Commun (Camb) 46:7984–7986. doi:10.1039/c0cc02649b

59. Schäfer T, Özalp VC (2015) DNA-aptamer gating membranes. Chem Commun. doi:10.1039/C4CC09660F

60. Zhu X, Zhang B, Ye Z, Shi H, Shen Y, Li G (2015) An ATP-responsive smart gate fabricated with a graphene oxide–aptamer–nanochannel architecture. Chem Commun 51:640–643. doi:10.1039/C4CC07990F

61. Wang R, Xu L, Li Y (2015) Bio-nanogate controlled enzymatic reaction for virus sensing. Biosens Bioelectron 67:400–407. doi:10.1016/j.bios.2014.08.071

62. Zhu CL, Lu CH, Song XY, Yang HH, Wang XR (2011) Bioresponsive controlled release using mesoporous silica nanoparticles capped with aptamer-based molecular gate. J Am Chem Soc 133:1278–1281. doi:10.1021/ja110094g

63. Ozalp VC, Eyidogan F, Oktem HA (2011) Aptamer-gated nanoparticles for smart drug delivery. Pharmaceuticals 4:1137–1157. doi:10.3390/ph4081137

64. Douglas SM, Bachelet I, Church GM (2012) A logic-gated nanorobot for targeted transport of molecular payloads. Science 335:831–834

65. Bachelet I, Church G, Douglas S (2012) DNA origami devices

66. Amir Y, Ben-Ishay E, Levner D, Ittah S, Abu-Horowitz A, Bachelet I (2014) Universal computing by DNA origami robots in a living animal. Nat Nanotechnoli 9:353–357. doi:10.1038/nnano.2014.58

67. Izquierdo A, Ono SS, Voegel JC, Schaaf P, Decher G (2005) Dipping versus spraying: exploring the deposition conditions for speeding up layer-by-layer assembly. Langmuir 21:7558–7567. doi:10.1021/la047407s

68. Jansen JA, Nolte RJM, Sommerdijk NAJ, Walboomers XF, Van DBJJ, Vos MR-J (2006) DNA-based coatings for implants

69. Borbely J, Bodnar M, Hajdu I, Hartman JF, Keresztessy Z, Nagy L, Vamosii G (2009) Polymeric nanoparticles by ion-ion interactions

70. Winterton LC, Vogt J, Lally JM, Stockinger F (1999) Coating of Polymers.

71. Claus RO, Liu Y (2001) Transparent abrasion-resistant coatings, magnetic coatings, and UV absorbing coatings on solid substrates

72. Sultan Y, Walsh R, Monreal C, DeRosa MC (2009) Preparation of functional aptamer films using layer-by-layer self-assembly. Biomacromolecules 10:1149–1154. doi:10.1021/bm8014126

73. Sultan Y, DeRosa MC (2011) Target binding influences permeability in aptamer-polyelectrolyte microcapsules. Small 7:1219–1226. doi:10.1002/smll.201001186
74. Chen L, Zeng X, Ferhan AR, Chi Y, Kim D-H, Chen G (2015) Signal-on electrochemiluminescent aptasensors based on target controlled permeable films. Chem Commun 51:1035–1038. doi:10.1039/C4CC07699K
75. Zhang X, Chabot D, Sultan Y, Monreal C, Derosa MC (2013) Target-molecule-triggered rupture of aptamer-encapsulated polyelectrolyte microcapsules. ACS Appl Mater Interfaces 5:5500–5507. doi:10.1021/am400668q
76. Kosuri S, Church GM (2014) Large-scale de novo DNA synthesis: technologies and applications. Nat Methods 11:499–507. doi:10.1038/nmeth.2918
77. Foster A, DeRosa MC (2014) Development of a biocompatible layer-by-layer film system using aptamer technology for smart material applications. Polymers (Basel) 6:1631–1654. doi:10.3390/polym6051631
78. Brüggemann D (2013) Nanoporous aluminium oxide membranes as cell interfaces. J Nanomater. doi:10.1155/2013/460870
79. Verhulsel M, Vignes M, Descroix S, Malaquin L, Vignjevic DM, Viovy JL (2014) A review of microfabrication and hydrogel engineering for micro-organs on chips. Biomaterials 35: 1816–1832. doi:10.1016/j.biomaterials.2013.11.021

Chapter 10
Superhydrophobic and Water-Repellent Polymer-Nanoparticle Composite Films

Ioannis Karapanagiotis and Panagiotis Manoudis

Abstract The wetting properties of the surfaces of polymer films changed dramatically from the usual inherent hydrophobicity (or slight hydrophilicity) to superhydrophobicity (contact angle, CA > 150°) by embedding oxide nanoparticles into the polymer matrices. The desired hierarchical roughness at the micrometer and nanometer scale was induced in poly(methyl methacrylate), polystyrene, and four poly(alkyl siloxane) films enriched with silica, tin oxide, alumina, and zinc oxide nanoparticles, ranging from 7 to 70 nm in mean diameter. Particles were added in the polymer solutions which were afterward sprayed on various substrates, such as glass, silicon, concrete, aluminum, silk, paper, wood, marble (white), sandstone, and mortar. It is stressed that superhydrophobicity was accompanied by water repellency, as evidenced by the low contact angle hysteresis (CAH < 10°). Consequently, it is demonstrated that the simple suggested method for transforming the wetting properties of polymer films to achieve extreme nonwetting is flexible as it can be effectively applied using different materials, including polymers and nanoparticles of low cost. Moreover, the method can be easily used for the surface treatment of large and various substrates. The effects of the (1) concentration and size of the nanoparticles, (2) chemical nature of the polymer matrix, and (3) treated substrate on the wetting properties of the films were investigated and interpreted using scanning electron microscopy (SEM). Finally, it is shown that depending on the color of the underlying substrate, the superhydrophobic water-repellent polymer-nanoparticle films may have a negligible effect on the aesthetic appearance of the treated substrate.

Keywords Superhydrophobic • Water repellent • Polymer nanoparticle • Lotus

I. Karapanagiotis (✉) • P. Manoudis
Department of Management and Conservation of Ecclesiastical Cultural Heritage Objects, University Ecclesiastical Academy of Thessaloniki, Thessaloniki 54250, Greece
e-mail: y.karapanagiotis@aeath.gr; pan.manoudis@gmail.com

10.1 Introduction

Nanoparticles and nanofillers are often embedded into polymer matrices to produce nanocomposites with improved mechanical, thermal, electronic, or optical properties [1, 2]. With the increased interest on superhydrophobic and water-repellent surfaces, the wetting properties of the surfaces of these nanocomposites have recently attracted considerable attention [3–29]. Nanoparticles, used as additives, can modify the surface structure enhancing, for instance, surface roughness. The latter is a key parameter to achieve superhydrophobicity and water repellency, which was first displayed on hierarchical structured biosurfaces.

Two biological surfaces that have been extensively used as model surfaces to fabricate biomimetics materials of special and controlled wettabilities are that of the lotus leaf and rose petal [30, 31]. Both plant surfaces exhibit superhydrophobic properties, implying that the static contact angle (CA) of a resting water droplet is large, CA > 150°. However, the two plant surfaces show different dynamic wetting which is directly related to water repellency/adhesion. That is, water droplets can effortlessly roll off the surface of a lotus leaf ("lotus effect") [30] whereas they stay pinned to the surface of a red rose petal ("petal effect") [31], thus corresponding to low and high contact angle hysteresis (CAH), respectively. Hence, industrial materials with lotus leaf-like surfaces are useful for applications relevant to water repellency, self-cleaning, and friction reduction. Artificial surfaces with rose petal properties show water adhesion and therefore have potential for applications such as the controlled transport of small volumes of liquid in open microfluidic devices [32]. Potential applications of biomimetics materials with special wetting properties are discussed at the end of the article.

Several parameters of a binary polymer-nanoparticle film may affect its surface wettability: the roles of the (1) concentration and size of the nanoparticles, (2) polymer matrices, and (3) substrates, used to support the composite films, are investigated herein. Oxide nanoparticles, with sizes ranging from 7 to 70 nm, are dispersed in polymer solutions at various concentrations. Dispersions are afterward sprayed on several substrates, and the wettabilities of the resulting composite polymer-nanoparticle films are investigated with contact angle measurements (CA and CAH) of water drops and interpreted using scanning electron microscopy (SEM). It is shown that the deposited films can have superhydrophobic and water-repellent properties, provided that the key parameters described above have been selected appropriately. Consequently, the studied method can be used to tune the wetting properties of polymer-nanoparticle films and achieve nonwetting.

The method has some important advantages: (1) it is an easy, one-step method; (2) it is of low cost, as it does not include the use of any sophisticated instrumentation or expensive materials; (3) the method can be easily used for the surface treatment of large and various substrates; and finally (4), superhydrophobicity and water repellency are achieved using various oxide nanoparticles and polymers, thus providing a lot of flexibility to engineers who would like to adapt the method using materials, polymers, and nanoparticles according to their needs.

On the other side, a drawback of the suggested method is that it may have an impact on the aesthetic appearance of the treated substrates because the oxide particles are white and therefore not transparent in visible light. As coloring alterations induced by protective coatings are usually undesirable, colorimetric measurements were carried out and discussed in detail.

10.2   Experimental

For most studies described in the following, Rhodorsil was used, which is a poly(methyl siloxane) dissolved in white spirit (mixture of aliphatic and alicyclic hydrocarbons) at a concentration of 7 % wt. Silica nanoparticles, 14 nm in mean diameter, were dispersed in the Rhodorsil solution in various concentrations. The Rhodorsil-silica dispersions were stirred mechanically and sprayed on silicon wafers, used as substrates to support the Rhodorsil-silica nanocomposites. The surfaces of the produced composite films were used for extensive studies. However, other nanoparticles, polymers and substrates, summarized in Table 10.1, were included for further investigations.

Dispersions were applied using an airbrush system with a nozzle of 733 μm in diameter. After drying, the wettabilities of the surfaces of the films were investigated by the sessile drop method using a Krüss DSA 100 apparatus and distilled water. Water droplets were carefully placed on the surfaces and the images of the

Table 10.1 Materials used in the study

Nanoparticle			Polymer solution		
Material	Mean particle size (nm)	Mean particle SSA (m²/g)	Polymer	Solvent	Substrate
Silica (SiO₂)	7	390	Rhodorsil, poly(methyl siloxane)	White spirit	Glass, silicon, concrete, aluminum, silk, paper, wood, marble (white), sandstone, mortar
Silica (SiO₂)	14	200	PMMA, poly(methyl methacrylate)	Toluene	
Tin oxide (SnO₂)	32.5	30	PS, polystyrene	Toluene	
Alumina (Al₂O₃)	45	36	Silres BS 290, poly(alkyl siloxane)	White spirit	
Zinc oxide (ZnO)	70	17.5	Porosil VV plus, poly(alkyl siloxane)	White spirit	
			Silres BS 4004, poly(alkyl siloxane)	Water	

Nanoparticles of different sizes and specific surface areas (SSAs) were dispersed in various polymer solutions. Dispersions were sprayed on various substrates, described in the table. It is noteworthy that a water-soluble resin (Silres BS 4004) was included in the study

Table 10.2 CA of water droplets on smooth polymer surfaces, which were prepared by spin coating onto silicon wafers

Polymer	CA (°)
PMMA	72
PS	90
Silres BS 290	97
Rhodorsil	102
Porosil	104
Silres BS 4004	111

droplets were captured immediately to measure the static contact angle (CA). The contact angle hysteresis (CAH) was calculated by the dynamic sessile drop method. The advancing/receding contact angle was the maximum/minimum angle measured, while the volume of the droplet was increased/decreased without increasing/decreasing the solid-liquid interfacial area. The reported CA and CAH are averages of several measurements which varied within ±2°.

The morphologies of the film surfaces were investigated using scanning electron microscopy (SEM, Jeol JSM-840A). Colorimetric measurements were carried out with a MiniScan EZ (HunterLab) instrument, and the results were evaluated using the L* a* b* coordinates of the CIE 1976 scale. L*, a*, and b* are the brightness (0 for black and 100 for white), the red-green component (positive for red and negative for green), and the yellow-blue component (positive for yellow and negative for blue), respectively.

Finally, solutions of pure polymers (without particles) were spin coated onto silicon wafers to produce smooth surfaces and to evaluate the inherent degree of hydrophobicity of the organic materials. CA measurements of water droplets on these very smooth polymer surfaces are summarized in Table 10.2.

10.3 Results and Discussion

10.3.1 Effect of the Particle Concentration on the Wettability of the Composite Films

Figure 10.1a shows the variations of the static contact angle (CA) and the contact angle hysteresis (CAH) with particle concentration, for water droplets placed on Rhodorsil-silica (14 nm) films. The CA initially increases with particle concentration from 105°, for pure Rhodorsil without particles, to 163° for 1 % w/v or higher particle concentrations. Further increase in particle concentration (>1 % w/v) does not have any significant effect on the CA which is (1) stable, corresponding to the plateau of the curve in Fig. 10.1a, and (2) extremely high, (>150°) corresponding to superhydrophobicity. As silica is a hydrophilic material, it is safe to conclude that the nanoparticles only contribute to surface roughness, while it is the siloxane polymer that is in the topmost layer all over the surface [6, 21, 33].
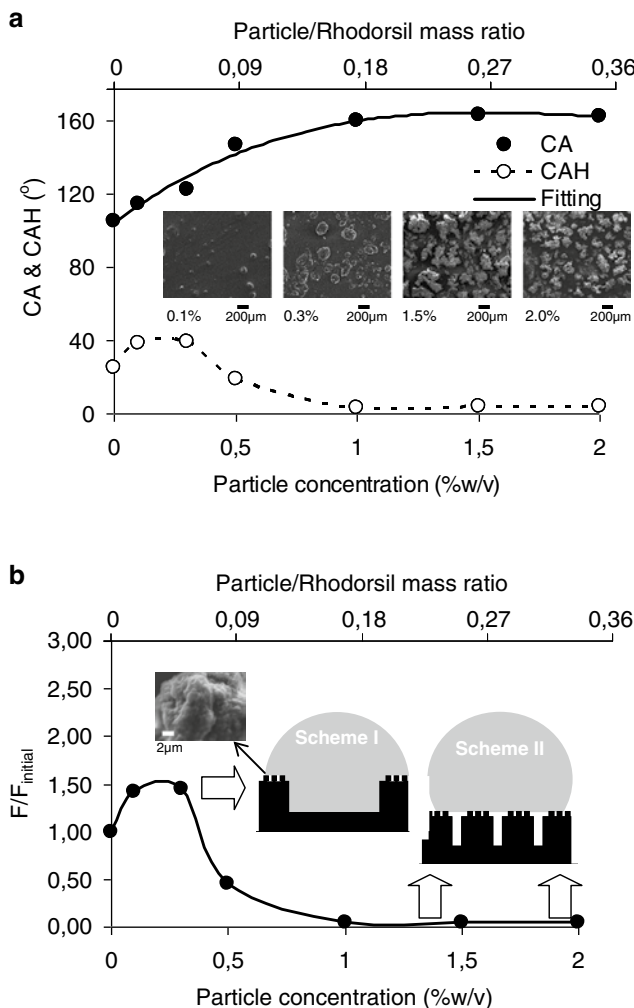
Fig. 10.1 (**a**) Static contact angle (CA) and contact angle hysteresis (CAH) versus the concentration of silica particles (14 nm) embedded in Rhodorsil. Films were deposited on silicon wafers. The data of CA is fitted with a three-order polynomial function to guide the eye. SEM images revealing the evolution of surface structure are included. (**b**) Force needed to start a drop moving over the Rhodorsil-silica film surface (F) normalized to its initial value ($F_{initial}$), which corresponds to pure Rhodorsil, versus the particle concentration. Schemes I and II show the wetting scenarios for films prepared using low and high particle concentration, respectively. The nanocrevices existing on the protruded clusters are revealed by the SEM image

The results of the CA in Fig. 10.1a are in agreement with previously published studies which described the effect of nanoparticles on the surface of polymer-nanoparticle composite films [6, 13, 19, 21]. Nanoparticles form microscale clusters which enhance the roughness of the surface at the micrometer/nanometer scale. Initially, the clusters are randomly distributed and are separated by smooth areas of continuous polymer film, as shown in the SEM images of Fig. 10.1a, captured for films prepared using dispersions of 0.1 and 0.3 % w/v nanoparticles. Larger (coalesced) clusters are formed at elevated particle concentrations, resulting in a continuous rough surface according to the SEM images corresponding to 1.5 and 2 % w/v particle concentration. This dense rough surface structure is responsible for the observed superhydrophobicity, as it was first evidenced on the surfaces of various plants, including that of the lotus leaf [30].

The variation of the CAH with particle concentration is more complicated compared to the behavior of CA, described above. According to the results of Fig. 10.1a, as the particle concentration increases, an increase in CAH is first recorded, which reaches a maximum value and then decreases. At the particle concentration of around 1 % w/v, CAH is minimized (<5°) and becomes constant. The variation of CAH with particle concentration is interpreted by the SEM images included in the same Fig. 10.1a. Water may fill the large, smooth interspaces that exist, among the clusters, in films prepared using low particle concentration. Therefore, the clusters may act as pinning sites resulting in an increase of CAH. As the particle concentration increases, a continuous rough structure is formed eliminating the pinning sites, thus decreasing droplet adhesion and enhancing repellency. Therefore this change of the surface morphology is accompanied by a drop of CAH which reaches a very small value. As the surface structure of the Rhodorsil-silica film becomes saturated, both CA and CAH become constant, corresponding to very high and low values, respectively. Consequently, both superhydrophobicity and water repellency occur at the surfaces of the films which correspond to particle concentration >1 % w/v.

According to the SEM images of Fig. 10.1a, surface roughness increases with particle concentration. This was observed in previous studies on polymer-nanoparticle composites [6, 7, 13, 14, 19, 21]. Consequently, it can be argued that the horizontal axis of the plot in Fig. 10.1a corresponds qualitatively to surface roughness. Therefore, it is concluded that the variation of CAH in Fig. 10.1a is in agreement with the results reported by (1) Johnson and Dettre who measured the advancing and receding contact angles of water drops on wax [34], (2) Tserepi et al. who carried out CAH measurements on plasma-treated PDMS surfaces [35], and (3) Morra et al. who reported advancing and receding contact angles on plasma-treated PTFE surfaces [36]. Finally, the CAH variation reported in Fig. 10.1a for composites prepared using 14 nm silica particles is in excellent agreement with a previous investigation where the effect of 7 nm silica nanoparticles on the wettability of a siloxane-silica composite was reported [6].

As described previously, superhydrophobicity is assessed by the large CA. However, water repellency or adhesion is evaluated through CAH, which is directly related to the force needed to start a drop moving over a solid surface [37]:

$$F = \gamma_{lv} \left(\cos RCA - \cos ACA \right) \tag{10.1}$$

where F is the critical force per unit length, γ_{lv} the liquid-vapor interfacial surface tension, and RCA and ACA are the receding and advancing contact angles, respectively. According to Eq. (10.1), F must vary according to CAH which is the difference between ACA and RCA (CAH = ACA−RCA). This is shown in the plot of Fig. 10.1b where the force F normalized to its initial value, $F_{initial}$, is shown as a function of the particle concentration. The curve in Fig. 10.1b follows the behavior of CAH reported in Fig. 10.1a. Two schemes illustrating water droplets on the rough surfaces are provided. As argued previously, in scheme I (low particle concentration), water fills the large, smooth areas that exist among the clusters. In this case, clusters act as pinning sites resulting in an increase of F. However, it is quite possible that water does not penetrate the nanocrevices (SEM image in Fig. 10.1b) that exist on the surface of the protruding clusters because of the Laplace pressure. Apparently, scheme I cannot be rationalized by the Cassie-Baxter model [38] which can be applied to interpret the scenario of scheme II (high particle concentration), where a dense rough structure exists inducing non-sticking properties. In the Cassie-Baxter state of scheme II, the force F is extremely small, as evidenced by the results of Fig. 10.1b. In particular, for particle concentration ≥1 % w/v, $F/F_{initial}$ equals 0.05, implying that it takes 20 times as less force to move a drop on Rhodorsil-silica than on a pure Rhodorsil film. On the contrary, a higher F than $F_{initial}$ must be applied when the scenario of scheme I is realized.

10.3.2   Effect of the Particle Size on the Wettability of the Composite Films

Figure 10.2 shows the CA and CAH measurements of water droplets on Rhodorsil-nanoparticle composites which were prepared using five different nanoparticles: silica (of two sizes), tin oxide, alumina, and zinc oxide. The particles are described in Table 10.1. For comparison, the CA and CAH measured on pure Rhodorsil (without nanoparticles) are included in the graph. It is stressed that the Rhodorsil-silica composites were prepared using 2 % w/v particle concentration. Higher concentrations (10 % w/v) of tin oxide, alumina, and zinc oxide nanoparticles were embedded in the Rhodorsil matrix to achieve the results reported in Fig. 10.2. The cross-influence effect of particle size and concentration on the wettability of the composite film is discussed later. The goal of Fig. 10.2 is to prove that superhydrophobicity (CA > 150°) and water repellency (CAH < 10°) can be achieved using various nanoparticles ranging from a few, up to several tenths of nanometers. This result is important because it provides the flexibility to select appropriate nanoparticles depending on the desired application. Karapanagiotis et al. [39] and Ogihara et al. [16] showed that superhydrophobicity can be induced using nanoparticles that are up to 150 and 200 nm in mean diameter, respectively (i.e., particles bigger
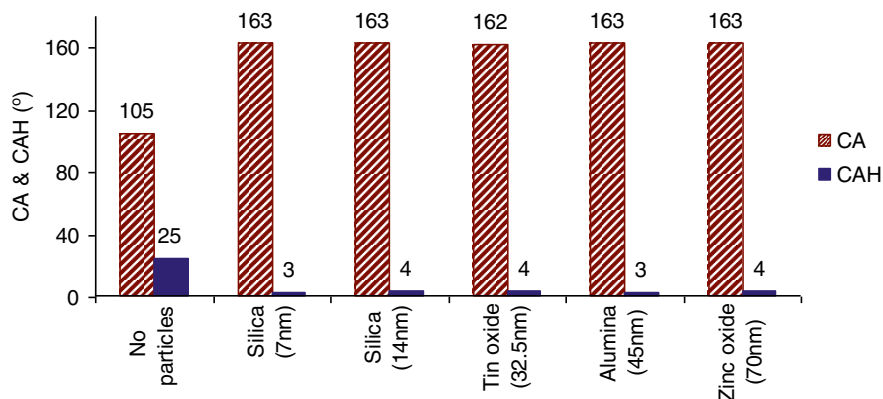
Fig. 10.2 CA and CAH on Rhodorsil-nanoparticle composites which were prepared using the particles of Table 10.1. Particle concentrations used to prepare the films were as follows: 2 % w/v silica (of two sizes) and 10 % w/v tin oxide, alumina, and zinc oxide. For comparison, CA and CAH on pure Rhodorsil (no particles) are included. CA and CAH are independent of the particle used; as for the five composite films, the angles range within only 162–163° and 3–4°, respectively. Consequently, the wettabilities of the five composite films are similar and clearly different than the hydrophobic character of the pure Rhodorsil (no particles) which is described by a low CA (105°) and high CAH (25°)

than the 70 nm zinc oxide particles included in Fig. 10.2). Ogihara et al. [16] indicated that superhydrophobicity is not achieved when particles of 500 nm in mean diameter (or higher) are embedded in the polymer matrix. Consequently, the high CA values reported in Fig. 10.2 are in agreement with the two previously published reports [16, 39]. Furthermore, Fig. 10.2 shows that the superhydrophobic and water-repellent characteristics of the composite films are not affected by the size and chemical nature of the nanoparticles. For the five nanoparticles included in Fig. 10.2, CA varies only between 162 and 163°, whereas CAH falls within 3–4°. Consequently, the wetting properties of the five composite films are similar. This result offers support to the argument provided previously that nanoparticles only contribute to surface roughness, while it is the polymer that is in the topmost layer all over the surface.

Figure 10.3 shows the variation of CA with particle concentration for Rhodorsil-silica (7 nm) and Rhodorsil-zinc oxide films, which are the composites prepared using the smallest and biggest nanoparticles of the study (Table 10.1). The two curves in Fig. 10.3 follow the tendency explained in Fig. 10.1a. In both sets of data of Fig. 10.3, the same maximum CA is achieved (163°) corresponding to the plateaus of the two curves. This maximum CA was reported in Fig. 10.2 and it is independent of the particle size. However, Fig. 10.3 clearly shows that in order to achieve the maximum CA, different particle concentrations must be used for nanoparticles of different sizes. More/less nanoparticles must be embedded in the polymer matrix when big/small nanoparticles are used to achieve the maximum superhydrophobicity.
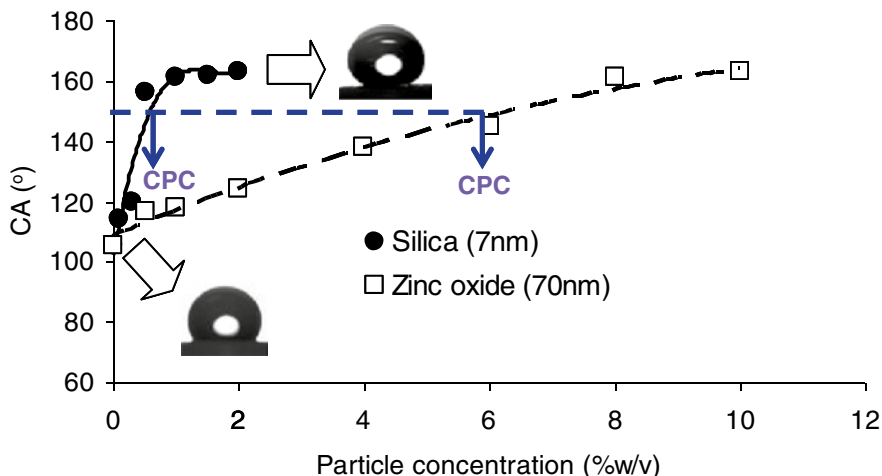
Fig. 10.3 CA versus the concentration of silica (7 nm) and zinc oxide (70 nm) particles embedded in Rhodorsil. The two sets of data are fitted with three-order polynomial functions. Photographs of water drops on hydrophobic, pure Rhodorsil and superhydrophobic composite films are included. The calculation of the critical particle concentrations (CPCs) corresponding to CA = 150° is illustrated for the two curves

Figure 10.4 provides a better understanding of the cross-influence effects of particle size and concentration on the wettability of the composite films. The vertical axis of the plot corresponds to the critical particle concentration (CPC), defined as the minimum particle concentration that must be used to achieve superhydrophobicity [39], that is, the particle concentration which corresponds to CA = 150°. CPCs corresponding to the Rhodorsil-silica (7 nm) and Rhodorsil-zinc oxide composite films were illustrated in Fig. 10.3. The horizontal axis of the plot in Fig. 10.4 corresponds to the particle specific surface area (SSA) and not to the particle size. SSA values for the five nanoparticles included in the study are given in Table 10.1. The SSA is the fundamental property of the particles which is responsible for the creation of the "new surface" and the increase of surface roughness, occurring with the addition of the particles into the polymer matrix. Because surface roughness directly affects the wetting properties of a surface, it is concluded that SSA must be included in the study's considerations. In principle, SSA is related to the particle size; the smaller the particle, the higher the SSA. However, this rough rule is not always correct, as evidenced by the data of tin oxide and alumina particles in Table 10.1. Consequently, the variation of CPC for different composites should be studied with respect to the SSA and not to the actual particle size. For this reason SSA is used in the plot of Fig. 10.4.

Figure 10.4 shows that when particles of high SSA are used for the preparation of the polymer-particle composite, low CPC is required to achieve superhydrophobicity. Two regimes are defined in Fig. 10.4: (1) a superhydrophobic regime that falls above the CPC curve and (2) a hydrophobic regime that falls below the fit of the data. The tendency of the curve shown in Fig. 10.4 is similar to the behavior reported
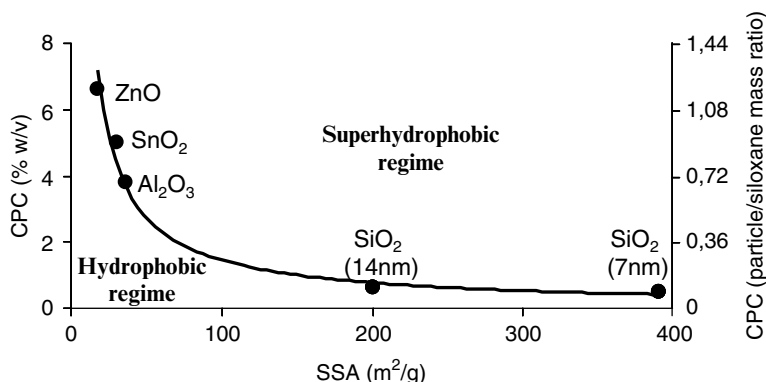
Fig. 10.4 Critical particle concentration (CPC) corresponding to CA = 150° versus the particle specific surface area (SSA). The results are fitted with a smooth *line*, which reveals the tendency of the data and is useful to guide the eye

previously for polymer-nanoparticle composite films which were prepared using three alumina nanoparticles of different sizes [39]. Furthermore, the plot of Fig. 10.4 shows that decreasing the SSA from 390 to 200 m^2/g does not have any significant effect on the CPC and that the two silica nanoparticles used herein had comparable effects on the wettability of the composite films. However, decreasing the SSA from 200 to 36 m^2/g (SSA of the alumina particle) results in a considerable increase of the measured CPC which becomes very sensitive to any further decrease of the SSA.

10.3.3 Effect of the Polymer on the Wettability of the Composite Films

In the last section, the same polymer (Rhodorsil) was blended with different nanoparticles. Here, the same type of particles, that is, silica (7 nm), at a concentration of 2 % w/v, is dispersed in solutions of six polymers including PMMA, PS, Silres BS 290, Porosil, Silres 4004, and Rhodorsil. Solvents used to prepare the solutions are described in Table 10.1. According to Table 10.2, CAs measured on smooth surfaces of the aforementioned polymers range from 72 to 111°. Consequently, the inherent wetting properties of the tested polymers are very different.

Figure 10.5 shows the CA and CAH results, obtained for the polymer-silica composites which were prepared using the six polymers. It can be seen that superhydrophobicity (CA > 150°) and water repellency (CAH < 10 °) were achieved on any of the tested polymer-silica surfaces. Interestingly, a considerable variation is observed on the reported CAs ranging from 153° (PMMA-silica) to 166 ° (Silres 4004-silica). The origin of this variation is discussed next.

The wettabilities of the six surfaces included in Fig. 10.5 correspond to the non-sticking, Cassie-Baxter state. The Cassie-Baxter equation correlates the elevated
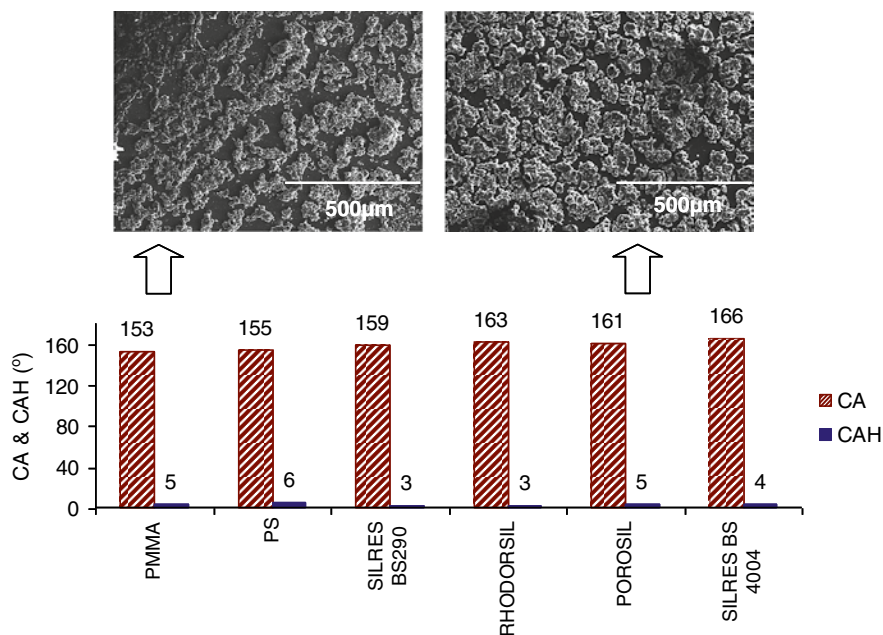
Fig. 10.5 CA and CAH on polymer-silica composites which were prepared using 2 % w/v silica nanoparticles (7 nm) and six different polymers which are labeled in the horizontal axis of the plot. SEM images revealing the surfaces of PMMA-silica and Porosil-silica films are included

apparent contact angle (θ^*) observed on a surface with augmented roughness and the contact angle (θ) measured on a smooth surface [38]:

$$\cos\theta^* = -1 + f_s\left(\cos\theta + 1\right) \tag{10.2}$$

where f_s is the surface porosity factor, that is, the fraction of the rough surface which is in direct contact with water. The f_s factors of the six superhydrophobic composite films included in Fig. 10.5 can be calculated, using Eq. (10.2). The angles θ and θ^* correspond to the CAs on pure (smooth) polymers and on composite (rough) films, respectively. The former (θ) are provided in Table 10.2 and the latter (θ^*) are shown in Fig. 10.5. It is reported that the calculated f_s factors varied within a very narrow range, from 0.05 to 0.09, thus implying that the surfaces of the six composite films should exhibit similar structures. Indeed, the SEM images of the PMMA-silica and Porosil-silica films, shown in Fig. 10.5, look very similar.

Because the surface structures of the six composite films are similar, it can be argued that the variation in the CAs of the composite films (Fig. 10.5) originated exclusively from the different chemical natures of the polymers used to prepare the composites. This argument is supported by the results of Fig. 10.6, which shows the plot of the CAs of the rough (superhydrophobic) composites versus the CAs of the smooth, pure polymers. Angles are plotted in terms of their cosines. It is shown that a
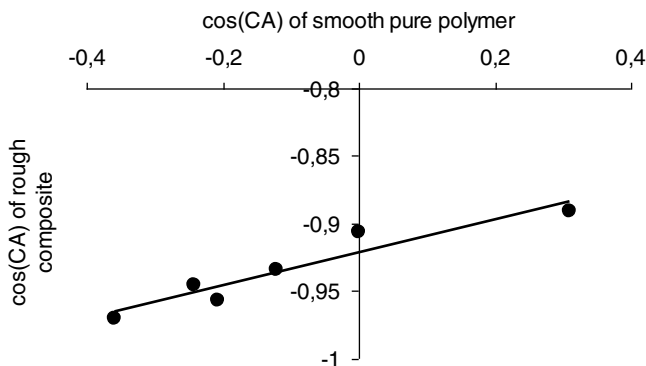
Fig. 10.6 CA on rough polymer-silica (superhydrophobic) composites versus CA on smooth, pure polymer. Angles are plotted in terms of their cosines. A linear function is used to fit the data

linear function provides a good fit for the results, thus implying that the application of the Cassie-Baxter equation (Eq. 10.2) using a single value for f_s is possible to describe the wettabilities of the six different composites. Consequently, the variation of the CAs of the six superhydrophobic composite films reported in Fig. 10.5 originated from the variation of the CAs of the pure polymers (Table 10.2), that is, the different chemical characteristics of the pure polymers. Using the linear fit of the data in Fig. 10.6, it can be calculated that θ^* obtains the critical value of 150° when $\theta = 63°$. Consequently, superhydrophobicity can be achieved in a composite polymer-silica film only if the contact angle of the smooth polymer used is equal or higher than 63°.

10.3.4 Effect of the Underlying Substrate on the Wettability of the Composite Films

Figure 10.7 shows CA and CAH measurements of water droplets on Rhodorsil-silica (7 nm and 2 % w/v) composites which were deposited on various substrates. It is seen that superhydrophobicity (CA > 150°) and water repellency (CAH < 10°) were achieved on any of the tested surfaces. This result shows that the spray method can be used to induce nonwetting properties to various inherently hydrophilic materials, by applying polymer-nanoparticle films. This is an important finding as it enhances the versatility of the suggested method which can be easily applied to treat large and different surfaces. Films included in Fig. 10.7 were prepared using 2 % w/v silica (7 nm) nanoparticles and Rhodorsil. At this relatively high level of particle concentration, the surface structure is extremely rough, inducing wetting properties which are practically unaffected by the underlying substrate. Both CA and CAH reported in Fig. 10.7 for various treated substrates show narrow ranges of variations.

Figure 10.8 shows the variation of CA with particle concentration for Rhodorsil-silica (7 nm) films deposited on glass and sandstone. The two substrates exhibit different surface morphologies, as glass is atomically smooth whereas sandstone is
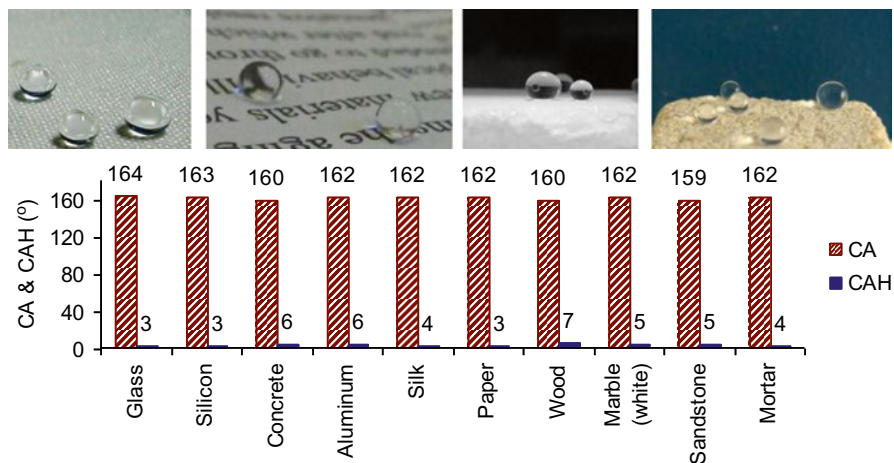
Fig. 10.7 CA and CAH on Rhodorsil-silica composites which were prepared using 2 % w/v silica nanoparticles (7 nm). Composite films were deposited on different substrates as indicated in the horizontal axis of the plot. Photographs showing water drops on silk, paper, marble, and sandstone are included
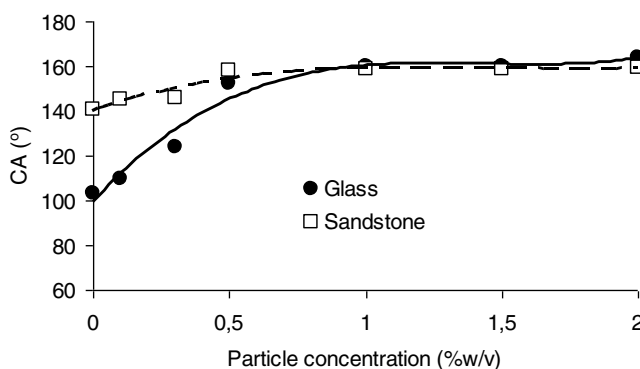
Fig. 10.8 CA versus the concentration of silica nanoparticles (7 nm) embedded in Rhodorsil. The composite films were deposited on glass and sandstone. The two sets of data are fitted with three-order polynomial functions to guide the eye

rough, corresponding to a surface porosity on the order of 8 % [10]. This difference between glass and sandstone does not affect the maximum CA obtained in Fig. 10.8 for the two sets of data. The maximum CA is achieved using high particle concentration (≥ 1 % w/v) and is practically unaffected by the underlying substrate. This result is in agreement with the CA measurements presented in Fig. 10.7, which corresponds to a 2 % w/v particle concentration.

However, according to Fig. 10.8, the role of the substrate roughness becomes important for films prepared using low particle concentration (<1 % w/v). The CA for a smooth Rhodorsil film (no particles) on glass is only 103°. However, the

Rhodorsil film on sandstone exhibits a roughness which originated from the roughness of the underlying substrate. Consequently, the CA measured on pure Rhodorsil (no particles) deposited on sandstone is 141°, which is substantially higher than the CA = 103°, measured on glass, covered by pure Rhodorsil. Embedding nanoparticles in the polymer matrix results in an increase of CA, which is more dramatic when the film is deposited on glass than on sandstone. At a concentration of approximately 1 % w/v, the film morphologies become saturated and the effect of the substrate roughness is diminishing.

10.3.5   Effect of the Superhydrophobic Composite Films on the Aesthetic Appearance of Substrates

In several applications, any effect on the aesthetic appearance of the substrate raised by the application of a protective coating is not acceptable. For example, water-repellent coatings designed to produce self-cleaning window glasses should be transparent in visible light [40]. Therefore, the polymer-nanoparticle composites, discussed herein, are not appropriate for glass protection because the white oxide nanoparticles clearly affect glass transparency. However, the effect of the suggested coatings on the aesthetic appearance of colored substrates can be within acceptable limits, especially when the color of the underlying substrate is close to the color coordinates of the white nanoparticles. This is demonstrated next.

   Colorimetric measurements were first carried out on bare, untreated white marble, sandstone, and wood. The results for the L*, a*, and b* coordinates are summarized in Table 10.3 and show that the three selected materials correspond to a broad range of the coloring palette, that is, from the bright white marble to the dark brown wood, with sandstone placed in between. Moreover, colorimetric measurements were carried out on the three aforementioned specimens covered by pure (hydrophobic) Silres BS 4004 and (superhydrophobic) Silres BS 4004-silica (7 nm and 2 % w/v) films. As described in Table 10.1, Silres BS 4004 is a waterborne siloxane product which makes it very attractive for practical applications, avoiding the use of volatile

Table 10.3 Results of colorimetric measurements, carried out on white marble, sandstone, and wood specimens which were (1) bare, untreated, and used as received, (2) covered by pure Silres BS 4004 films, and (3) covered by Silres BS 4004-silica composite films, prepared using silica particles (7 nm) at the concentration of 2 % w/v

| Substrate | Color coordinates for untreated substrates | | | ΔE^* after film deposition | |
	L*	a*	b*	Pure Silres BS 4004	Silres BS 4004-silica composite
Marble	90.0	0.2	4.5	0.37	0.09
Sandstone	77.1	3.8	14.0	0.73	2.72
Wood	72.2	8.1	21.7	2.07	9.45

The surfaces of the films in (2) and (3) had hydrophobic and superhydrophobic properties, respectively

organic solvents. The global color differences (ΔE^*) occurring because of the film depositions were calculated as follows:

$$\Delta E^* = \sqrt{\Delta L^{*2} + \Delta a^{*2} + \Delta b^{*2}} \qquad (10.3)$$

The calculated ΔE^* are summarized in Table 10.3. The use of nanoparticles to treat white marble had a positive effect on the aesthetic appearance of the specimen. When pure polymer was deposited, ΔE^* was 0.37. ΔE^* was reduced to 0.09 when the protective polymer film was blended with silica nanoparticles (composite film). Consequently, in the case of marble, the superhydrophobic composite coating induces less color change to marble than the pure hydrophobic polymer. This result is explained if it is considered that the white color of the silica nanoparticles is close to that of marble. In particular, the L*, a*, and b* coordinates for the silica nanoparticles are 88.0, −2.5, and −7.0, respectively, which are close to the corresponding coordinates of white marble, reported in Table 10.3.

The use of silica nanoparticles had a negative effect on the aesthetic appearance of the brown sandstone. The application of the pure polymer on sandstone resulted in $\Delta E^* = 0.73$ which increased to 2.72 when the polymer was enriched with silica nanoparticles. However, it is important to note that color changes corresponding to $\Delta E^* < 3$ are typically not visible with naked eye. Consequently, the effect of the composite film on the aesthetic appearance of sandstone should be considered as being within the acceptable limit perceived by the human eye.

The color coordinates of silica, described above, are very different from the corresponding coordinates of the dark brown wood (Table 10.3). Consequently, the application of the composite film on wood resulted in a high ΔE^* (9.45) which is substantially higher than the $\Delta E^* = 2.07$ (<3) result obtained when pure polymer was applied on wood. Therefore, silica nanoparticles had a major impact on the color of the wood specimen.

In summary, the results of Table 10.3 show that the method, described in the present report to impart superhydrophobicity to various substrates, is not necessarily accompanied by a severe penalty on the aesthetic appearance of the treated material. If the color coordinates of the substrate are comparable with the corresponding coordinates of the used nanoparticles, then the application of polymer-nanoparticle coatings can be acceptable from an aesthetic point of view, gaining simultaneously the beneficial superhydrophobic and water-repellent properties induced by these composite coatings.

10.4 Industrial Applications

Inspired by the hierarchical micro-/nanostructures found extensively in nature (e.g., lotus leaf, rose petal, mosquito eye, spider silks, butterfly wings, gecko feet, desert beetle, and water strider) [41], several strategies have been designed to produce surfaces of special wetting properties including superhydrophobicity and

water repellency which can be used in several applications such as self-cleaning coatings on outdoor surfaces (automobiles, buildings, etc.); anti-biofouling paints for boats; antisticking of snow for antennas, windows, and airplanes; microfluidics; lab-on-a-chip devices; metal refining; stain-resistant textiles; clotting preventive coatings in artificial blood vessels; and so on [41–43].

The method described in this article, where nanoparticles are embedded into polymers to achieve the desired hierarchical micro-/nanostructure, is a rapid, low cost method, which can be used to treat large surfaces, and can be implemented using various nanoparticles and polymers. Consequently, the method might be useful for some of the aforementioned applications of superhydrophobic coatings.

10.5   Conclusion

Various oxide nanoparticles (7–70 nm) were added in various polymer solutions, described in Table 10.1. Dispersions were sprayed on silicon. It was shown that the surfaces of the resulting composite polymer-nanoparticle films exhibit superhydrophobic and water-repellent properties (Figs. 10.2, 10.3, 10.4, and 10.5) which can be interpreted using the Cassie-Baxter model (Fig. 10.6), provided that an appropriate, elevated particle concentration was added in the polymer solution (Fig. 10.1). The extreme nonwetting properties are induced because the nanoparticles enhance the surface roughness at the micrometer and nanometer scale, as revealed by SEM images (e.g., Fig. 10.1). Furthermore, the spray method was applied to treat various substrates, achieving high and low contact angle and contact angle hysteresis, respectively, as shown in Figs. 10.7 and 10.8. Consequently, it is concluded that the simple suggested method for transforming the wetting properties of polymer films achieving extreme nonwetting is flexible, as it can be effectively applied to treat various substrates using common polymers and nanoparticles. Finally, it was shown that depending on the color of the underlying substrate, the superhydrophobic, water-repellent polymer-nanoparticle films may have negligible effect on the aesthetic appearance of the treated substrate.

References

1. Rozenberg BA, Tenne R (2008) Prog Polym Sci 33:40–112
2. Li S, Lin MM, Toprak MS, Kim DK, Muhammed M (2010) Nano Rev 1:5214. doi:10.3402/nano.v1i0.5214
3. Hsieh C-T, Chen J-M, Kuo R-R, Lin T-S, Wu C-F (2005) Appl Surf Sci 240:318–326
4. Chibowski E, Hołysz L, Terpilowski K, Jurak M (2006) Colloids Surf A 291:181–190
5. Yüce MY, Demirel AL (2008) Eur Phys J B 64:493–497
6. Manoudis PN, Karapanagiotis I, Tsakalof A, Zuburtikudis I, Panayiotou C (2008) Langmuir 24:11225–11232
7. Ramaratnam K, Iyer SK, Kinnan MK, Chumanov G, Brown PJ, Luzinov I (2008) J Engineered Fibers Fabric 3:1–14

8. Cao L, Jones AK, Sikka VK, Wu J, Gao D (2009) Langmuir 25:12444–12448
9. Manca M, Cannavale A, De Marco L, Aricò AS, Cingolani R, Gigli G (2009) Langmuir 25:6357–6362
10. Manoudis PN, Karapanagiotis I, Tsakalof A, Zuburtikudis I, Kolinkeov B, Panayiotou C (2009) Appl Phys A 97:351–360
11. Du X, Li X, He J (2010) ACS Appl Mater Interfaces 2:2365–2372
12. Ke Q, Fu W, Wang S, Tang T, Zhang J (2010) ACS Appl Mater Interfaces 2:2393–2398
13. Tiwari MK, Bayer IS, Jursich GM, Schutzius TM, Megaridis CM (2010) ACS Appl Mater Interfaces 2:1114–1119
14. Karmouch R, Ross GG (2010) Appl Surf Sci 257:665–669
15. Gao N, Yan YY, Chen XY, Zheng XF (2010) J Bionic Eng 7:S59–S66
16. Ogihara H, Okagaki J, Saji T (2011) Langmuir 27:9069–9072
17. Men X, Zhang Z, Yang J, Zhu X, Wang K, Jiang W (2011) New J Chem 35:881–886
18. Ogihara H, Katayama T, Saji T (2011) J Colloid Interface Sci 362:560–566
19. Basu BJ, Kumar VD (2011) ISRN Nanotechnol Article ID 803910
20. de Ferri L, Lottici PP, Lorenzi A, Montenero A, Salvioli-Mariani E (2011) J Cult Her 12:356–363
21. Schutzius TM, Bayer IS, Jursich GM, Das A, Megaridis CM (2012) Nanoscale 4:5378–5385
22. Yilgor I, Bilgin S, Isik M, Yilgor E (2012) Polymer 53:1180–1188
23. Flores-Vivian I, Hejazi V, Kozhukhova MI, Nosonovsky M, Sobolev K (2013) ACS Appl Mater Interfaces 5:13284–13294
24. Li K, Zeng X, Li H, Lai X, Ye C, Xie H (2013) Appl Surf Sci 279:458–463
25. Lin J, Chen H, Fei T, Zhang J (2013) Colloids Surf A 421:51–62
26. Xue C-H, Ji P-T, Zhang P, Li Y-R, Jia S-T (2013) Appl Surf Sci 284:464–471
27. Seyedmehdi SA, Zhang H, Zhu J (2013) J Appl Polym Sci 128:4136–4140
28. Manoudis PN, Karapanagiotis I (2014) Prog Org Coat 77:331–338
29. D'Amato R, Caneve L, Giancristofaro C, Persia F, Pilloni L, Rinaldi A (2014) J Nanoeng Nanosyst 228:19–26
30. Barthlott W, Neinhuis C (1997) Planta 202:1–8
31. Feng L, Zhang Y, Xi J, Zhu Y, Wang N, Xia F, Jiang L (2008) Langmuir 24:4114–4119
32. Ebert D, Bhushan A (2012) J Colloid Interface Sci 384:182–188
33. Kulinich SA, Farzaneh M (2009) Langmuir 25:8854–8856
34. Johnson RE, Dettre RH (1964) Adv Chem Ser 43:112–135
35. Tserepi AD, Vlachopoulou M-E, Gogolides W (2006) Nanotechnology 17:3977–3983
36. Morra M, Occhiello E, Garbassi F (1989) Langmuir 5:872–876
37. Furmidge CGL (1962) J Colloid Sci 17:309–324
38. Cassie ABD, Baxter S (1944) Trans Faraday Soc 40:546–551
39. Karapanagiotis I, Manoudis PN, Savva A, Panayiotou C (2012) Surf Interface Anal 44:870–875
40. Karapanagiotis I, Manoudis PN, Zurba A, Lampakis D (2014) Langmuir 30:13235–13243
41. Lai Y-K, Chen Z, Lin C-J (2011) J Nanoeng Nanomanuf 1:18–34
42. Latthe SS, Gurav AB, Maruti CS, Vhatkar RS (2012) J Surf Eng Mater Adv Technol 2:76–94
43. Karapanagiotis I, Manoudis P (2012) J Mech Behav Mater 21:21–32

Chapter 11
Application of Conducting Polymers in Solar Water-Splitting Catalysis

**Mohammed Alsultan, Abbas Ranjbar, Gerhard F. Swiegers,
Gordon G. Wallace, Sivakumar Balakrishnan, and Junhua Huang**

Abstract Water splitting is the general term for a chemical reaction in which water is separated into its constituent materials, oxygen and hydrogen. Hydrogen is widely considered to be an ideal fuel of the future due to its potential to replace fossil fuels. The key to an energy-efficient water-splitting process lies in catalysts that can carry out the water oxidation and reduction reactions with minimal energy losses. Conducting polymers are attractive materials for this technology and application because they may combine several desirable properties, including electronic conduction, ionic conduction, sensor functionality, and electrochromism. In this chapter, water splitting assisted by or driven by illumination with sunlight and involving conducting polymers is reviewed. The properties of conducting polymers that make them favorable for this purpose are also discussed. Comparisons of these properties with those of conventional water-splitting materials are made. Finally, a statement of research and achievements of solar hydrogen production through water splitting using conductive polymers will be reported.

Keywords Water splitting • Conducting polymers • Water-splitting catalysis • Properties of conducting polymers

M. Alsultan
Intelligent Polymer Research Institute, ARC Centre of Excellence for Electromaterial Science (ACES), University of Wollongong, Wollongong, NSW 2522, Australia

Department of Science, College of Basic Education, University of Mosul, Mosul, Iraq

A. Ranjbar (✉) • G.F. Swiegers (✉) • G.G. Wallace • S. Balakrishnan
Intelligent Polymer Research Institute, ARC Centre of Excellence for Electromaterial Science (ACES), University of Wollongong, Wollongong, NSW 2522, Australia
e-mail: ar143@uow.edu.au; Swiegers@uow.edu.au

J. Huang
School of Chemistry, Monash University, Clayton, VIC 3800, Australia

Abbreviations

AAO	Anodized aluminum oxide
APS	3-(Aminopropyl)triethoxysilane
BHJ	Bulk heterojunction
BI-VPP	Base-inhibited vapor-phase polymerization
CB	Conduction band
CP	Conducting polymer
CV	Cyclic voltammogram
CTAB	Cetyltrimethyl ammonium bromide
DBSNa or SDBS	Sodium dodecylbenzene sulfonate
DSC	Dye-sensitized solar cell
ESR	Electron spin resonance
FESEM	Field emission scanning electron microscopy
FTIR	Fourier transform infrared spectroscopy
FTO	Fluorine-doped tin oxide
h^+	Hole (in the valence band)
GC	Glassy carbon
HER	Hydrogen evolution reaction
HOMO	Highest occupied molecular orbital
IPCE	Incident photon-to-current conversion efficiency
ITO	Indium tin oxide
LM2	Poly(2-ethynyl-N-aminopropylpyridiniumbromide)
LM3	Poly(2-ethynyl-N-carboxypropylpyridiniumbromide)
LSV	Linear sweep voltammogram
LUMO	Lowest unoccupied molecular orbital
OER	Oxygen evolution reaction
OPE-O electrode	Organic photoelectrode (oxidation) electrode
OPE-R electrode	Organic photoelectrode (reduction) electrode
ORR	Oxygen reduction reaction
OSC	Organic thin-film solar cells
PANI	Polyaniline
PCBM	Phenyl-C_{61}-butyric acid methyl ester
PDTT	Poly(dithieno[3,2-b:2′,3′-d]thiophene)
PEC	Photoelectrochemical (cell)
PEDOT	Poly(3,4-ethylenedioxythiophene)
PEDOT-PEG	Poly(3,4-ethylenedioxythiophene)–poly(ethylene glycol)
PEDOT-**1**	Poly(3,4-ethylenedioxythiophene)–Mn-porphyrin
PEG	Poly(ethylene glycol)
PET	Poly(ethylene terephthalate)
PPy	Polypyrrole
PRR	Proton reduction reaction
PTh	Polythiophene
PTT	Poly(thieno[3,2-b]thiophene)

PTTh   Polyterthiophene
p-TS   *p*-toluenesulfonate
P3HT   Poly(3-hexylthiophene)
SHE   Standard hydrogen electrode
TSNa   Sodium *p*-toluenesulfonate
VB   Valence band
VPP   Vapor-phase polymerization
WOR   Water oxidation reaction

11.1 Introduction

In 1978, Shirakawa and colleagues demonstrated that polyacetylene becomes electrically conductive after being treated with electron-accepting (*p*-doped) or electron-donating dopants (*n*-doped) [1, 2]. Since that time, an entire class of polymeric conductors have been developed, including polypyrroles (PPys), poly(3,4-ethylenedioxythiophenes) (PEDOTs), polythiophenes, and polyanilines; Fig. 11.1 shows the parent forms of these polymers [3]. Conducting polymers (CPs) have two broad potential application areas [4]. The first utilizes the conductivity of CPs in, for example, electrostatic materials, conducting adhesives, electromagnetic shielding, printed circuit boards, artificial nerves, and electronics (diodes, transistors). The second makes use of their electroactivity in, for example, molecular electronics,
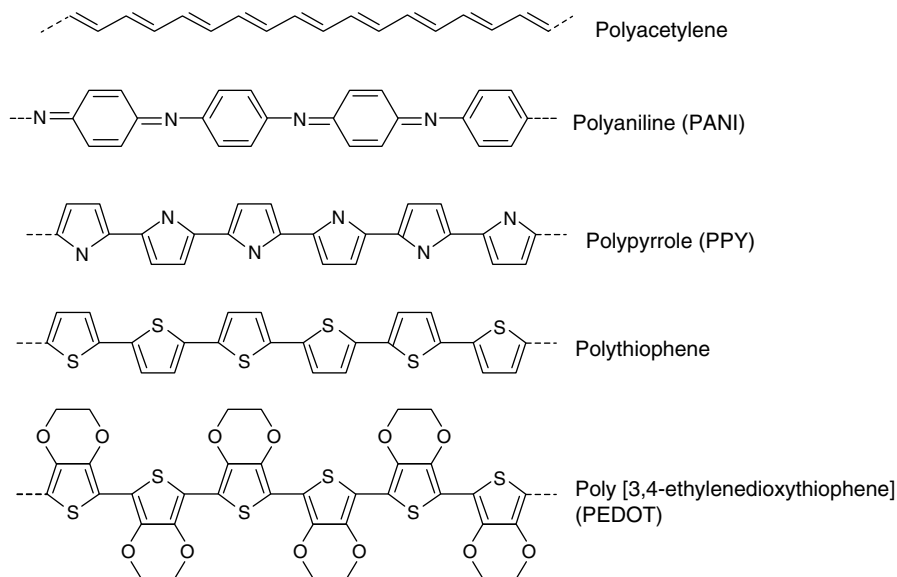
Fig. 11.1 Common conducting polymers

biochemical and thermal sensors, optical computers, rechargeable batteries and solid electrolytes, drug release systems, and ion-exchange membranes. CPs are extensively conjugated molecules that have backbones of π-electrons due to C=C conjugated bonds that are able to interconvert between single and double bonds. In these molecules, electrons are able to move from one end of the polymer to the other, through the extended π-orbital system. This feature imparts CPs with interesting properties, including low ionization potential, low-energy optically transitions, and high electron affinity, which allow the polymer to be oxidized and reduced relatively easily [5]. Conducting polymers are typically insulators in their pure state, but when they are doped with other materials, their behavior changes to the conducting state [6]. Doping of conducting polymers can be viewed as a charge transfer reaction, which results in oxidation or reduction of sites along the polymer chains. This induces upward shifts in the energy of the "*highest occupied molecular orbital* (HOMO)" of the *"valence band"* (VB) and downward shifts in the energy of the "*lowest unoccupied molecular orbital* (LUMO)" of the "*conducting band* (CB)", decreasing the bandgap in the process [7]. By contrast, the doping reaction in solid-state semiconductors creates either electron-rich or electron-deficient sites with no charge transfer between these sites. The general doping reaction process of CPs follows the equations [8]:

$$\mathbf{Polymer} + \mathbf{X} \rightleftarrows \left(\mathbf{Polymer}\right)^{\mathbf{n+}} + \mathbf{X^{n-}}\, p - \text{doping reaction}\left(X = \text{oxidizing agent}\right).$$

$$\mathbf{Polymer} + \mathbf{M} \rightleftarrows \left(\mathbf{Polymer}\right)^{\mathbf{n-}} + \mathbf{M^{n+}}\, n - \text{doping reaction}\left(M = \text{reducing agent}\right)$$
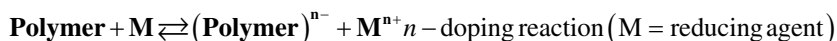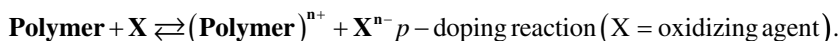
(X includes I, Br, and AsF, while M includes Na and Li.)

The conductivity of a polymer depends on the level of doping, the relative alignment of the polymer chains, the conjugated chain length, and the sample purity, among others [8]. The conductivity can be measured using the equation:

$$\sigma = 1/\mathbf{R} = \mathbf{n}\,\mathbf{e}\,\mu \tag{11.1}$$

where σ = conductivity (Ω^{-1} m^{-1} or Sm^{-1}, typically reported as S cm^{-1}), n = number of charge carriers (electrons or holes [e, h$^+$]), e = electron charge, and μ = charge carrier mobility. CPs can be controlled if the nature of the process that regulates them can be understood [6].

CPs have other unique properties such as tunable conductivity between insulating and metallic regions and adjustable permeability, are relatively low cost, have readily available processing capacities, and have controllable microwave absorption properties which make them significant for industrial applications [9].

Solar cell applications involving CPs have attracted broad research interest due to their potential in the fabrication of low-cost, flexible, and large-area electrochemical devices. The conversion efficiency of such "polymer" solar cells is, however, still low when compared with inorganic semiconductors. A key challenge is therefore to find polymers that display the properties needed for high conversion effi-

ciency, such as broad/intense absorptions, and high charge carrier mobility at appropriate energy levels [10]. One possible way to increase the conversion efficiency involves utilizing two or more chemical materials with different spectral responses to achieve a higher overall utilization of solar energy [11]. This principle has been applied to modify, for example, photoelectrochemical (PEC) anodes with conducting polymers to thereby render them capable of splitting water when illuminated with sunlight. In this work, the properties of the major classes of CPs are reviewed and their application in solar water-splitting catalysis is considered.

11.2 Solar Water Splitting Using Polypyrrole

Polypyrrole (PPy) is commercially inexpensive and processable (conductivity approximately 10–50 S cm^{-1}). It is thermodynamically stable and can be readily prepared by polymerization of its monomer, using a chemical oxidant such as $FeCl_3$, or via its electrochemical synthesis, with the incorporation of counterions into the polymer matrix. PPy has high conductivity due to its charge carrier mechanism [12–14].

PPy was studied as a nanoparticle coating for water oxidation catalysis by Arthur and Honda more than 30 years ago [15]. They reported that when CdS nanoparticles were modified with a PPy layer, the PEC performance in the oxidation of water to O_2 gas was improved. They also reported that the presence of the PPy stabilized the semiconductor surface against photodegradation. By contrast, when polystyrene was used as a coating instead of PPy, it reduced the ΔG for solvation of the CdS lattice, resulting in photocorrosion of the CdS semiconductor surface.

Recently, Tan and colleagues [16] fabricated a new PEC design for hydrogen (H_2) evolution under visible light using TiO_2 modified with PPy. PPy/TiO_2 nanoparticles (NPs) were prepared with two different morphologies: particles and film. PPy was combined with TiO_2 nanoparticles through in situ polymerization using water–trihexyl(tetradecyl)phosphonium dicyanamide in ionic liquid/water or toluene/water. The film generated from toluene displayed a higher H_2 generation rate compared to the particle morphology, which yielded lower H_2 production but higher thermal stability. As PPy coats the surface of TiO_2 nanoparticles, the PPy/TiO_2 NPs have a core–shell structure. The low bandgap of PPy (2.6 eV) allowed the absorption of visible light and the transfer of an excited electron into the conduction band of TiO_2 (3.2 eV), resulting in an electron–hole pair, which was able to split water into H_2 at the TiO_2 interface and O_2 at the PPy interface. The transfer of the excited electrons into the conduction band (CB) of first PPy and then TiO_2, which has a lower energy than the excited state of PPy, diminished the rate of electron–hole recombination in PPy. The electrons on the surface of TiO_2 are sufficiently energetic that they are able to reduce water to produce hydrogen. The holes that remain on the PPy are able to oxidize water. The mechanism is shown schematically in Fig. 11.2.

In addition, the PPy/TiO_2 photoelectrode, which generated 0.04 mmol min^{-1} of hydrogen, was nontoxic and inexpensive when compared with other inorganic
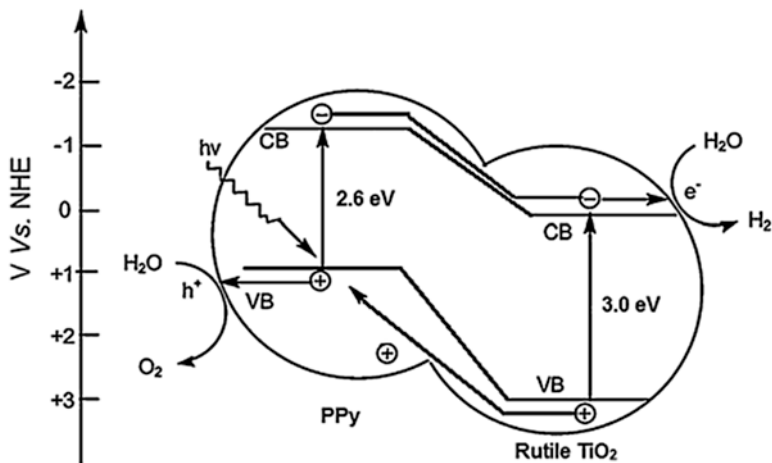
Fig. 11.2 The mechanism of electron transfer to the CB of TiO_2, which assisted H_2 and O_2 evolution in PPy/TiO_2 nanoparticles. It should be noted that the CB in the PPy component is actually an excited electronic state (LUMO). Reproduced with permission from Ref. [16]

materials such as in TaO_4 (bandgap 2.25 eV) and $YBiWO_6$ (bandgap 2.71 eV), which produce similar rates of H_2 (0.05 mmol min^{-1} and 0.07 mmol min^{-1}, respectively, under light of wavelength >420 nm). Furthermore, the combined PPy/TiO_2 appeared to be better than other systems based on Pt or shuttle redox mediators such as IO^{3-}/I^{-1} and Fe^{3+}/$^{2+}$ [17–19]. Other similar core–shell systems have been described elsewhere [20]. Perhaps the best known polymerization technique for semiconductor modification is in situ polymerization, which includes sol–gel, blending, and vapor-phase polymerization methods. Simple operation and mild reaction conditions are required. Wang and co-workers [21] used in situ polymerization to modify TiO_2 with PPy. The resulting TiO_2/PPy (core/shell) had higher photoactivity under irradiation than TiO_2 modified with methyl orange. Moreover, higher conductivity and better absorption of visible light could be achieved by treating the PPy with dopants such as anthraquinone-2-sulfonic acid, sulfonic acid ferric sulfonate, and para-toluene-2-sulfonic acid.

The chemical structure and the doping method played a significant role in determining the properties of PPy in such fabricated photoanodes [22]. A core–shell system employing CdS modified with PPy, was prepared by in situ polymerization. CdS is, in theory, an excellent semiconductor for water splitting since it has a near-ideal bandgap (2.4 eV) with the energy of the conduction band (CB) well placed for water oxidation [23]. Zhang et al. [24] used in situ polymerization to improve the conductivity and the absorbance of PPy on CdS. Sodium dodecylbenzene sulfonate (DBSNa), hexadecyltrimethyl ammonium bromide (CTAB), and sodium *p*-toluenesulfonate (TSNa) were employed as dopants. Na_2S and Na_2SO_3 acted as sac-
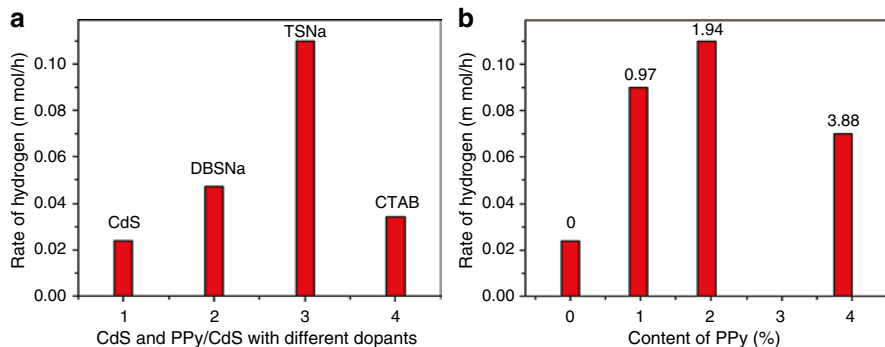
Fig. 11.3 Hydrogen evolution rates of (**a**) CdS and PPy/CdS with different dopants: DBNa, TSNa, and CTAB, and (**b**) PPy/CdS doped by TSNa having different levels of PPy. Reproduced with permission from Ref. [24]

rificial reagents to diminish recombination. The results revealed that PPy/CdS displayed higher performance than CdS alone, with larger H_2 generation rates observed. The use of TSNa as dopant yielded the best photoactivity for H_2 generation, while samples doped by CTAB displayed lower photoactivity (Fig. 11.3).

PPy is a promising conductive polymer that generates excited electrons in direct response to visible light. Nanoparticles modified with PPy may display amplified photocurrents and improved conversion efficiencies when used as a photoelectrode in a PEC application [25]. PPy is also stable in acidic and neutral solutions, helping to prevent electron–hole recombination reactions (backward reactions). These properties encouraged Wang et al. [26] to combine PPy with the semiconductor ZnO, which is a promising photoanode for PEC water splitting. ZnO is also commercially inexpensive, and its bandgap is more suitable than other semiconductors such as TiO_2 [27]. PPy/ZnO core–shell nanoparticles were synthesized on indium tin oxide (ITO) by a chemical oxidation method, which included using boric acid as a buffer solution containing potassium chloride and sodium dodecylsulfate. $FeCl_3$ was used as oxidant. Figure 11.4 schematically shows the structure of the combined PPy/ZnO NPs [26].

Wang's work highlighted three important features of PPy which make it useful for catalytic water-splitting applications when combined with a conventional semiconductor, namely: (1) PPy has a bandgap that enhances PEC performance under visible light, (2) the conductivity of PPy accelerates the transfer of electrons during the creation of holes, and (3) the stability of PPy in water suppresses photocorrosion of the solid-state semiconductor and thereby enhances the stability of the PEC system toward water oxidation. Figure 11.5 illustrates the mechanistic steps for PEC performance as described in Wang's work. The holes are generated at the PPy film by light excitation of electrons to the CB of the PPy. The excited electrons are then injected into the CB of ZnO. The holes in the VB of PPy oxidize water. The PEC was improved by increasing the gap in the Fermi levels to facilitate electron transfer
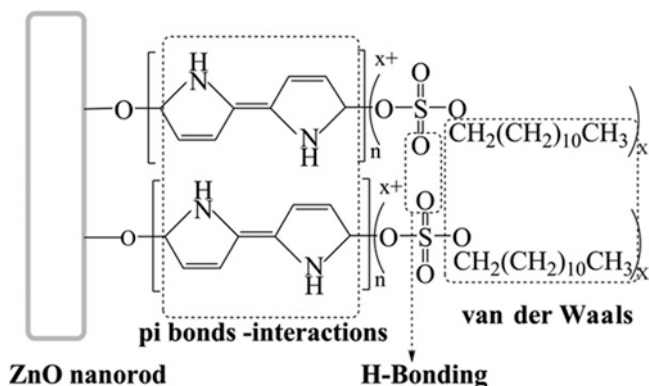
Fig. 11.4 Schematic of the structure of PPy/ZnO on the surface of ZnO nanorods (NRs) [26]

Fig. 11.5 Illustration of PPy/ZnO NP mechanism as PEC catalyst for water splitting under visible light. Reproduced with permission from Ref. [26]
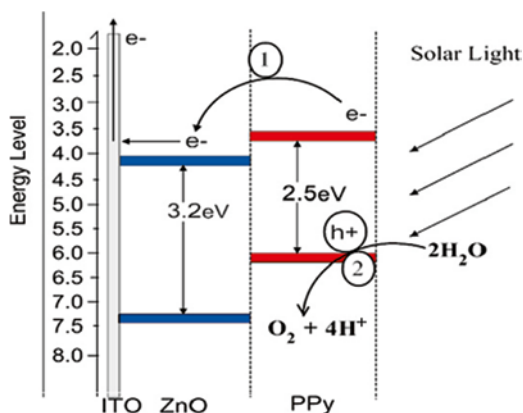
from PPy to ZnO. Polypyrrole oligomers and molecular materials have also been investigated in water splitting [28, 29].

11.3 Solar Water Splitting Using Poly(3,4-ethylenedioxythiophene)

While PEDOT is formally a functionalized thiophene, it will be addressed separately in this work because PEDOT is widely considered to be the best available CP in terms of conductivity, processability, transparency to visible light, stability, and fast electrochemical switching [30–32]. Solar water-splitting catalysis by the other polythiophenes is described in further detail in Sect. 11.5. PEDOT can be combined
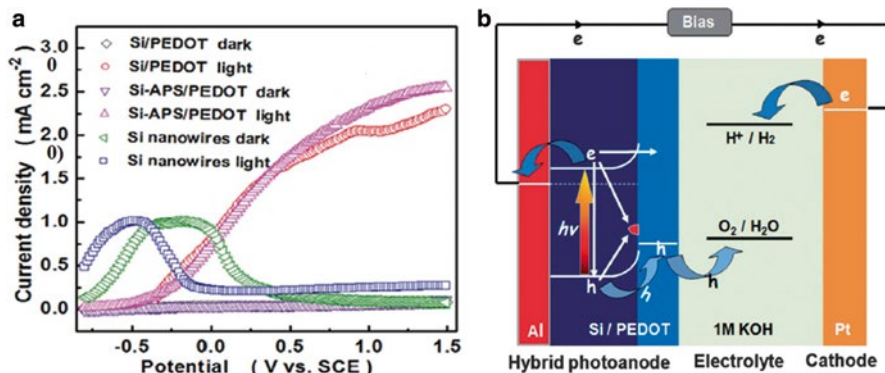
Fig. 11.6 (**a**) Current density of hybrid Si-APS/PEDOT compared to Si/PEDOT or Si nanowire as control. (**b**) The proposed mechanism of water oxidation using Si-APS/PEDOT as photoanode. Reproduced with permission from Ref. [37]

with dispersions which act as counterions, such as poly(styrene sulfonic acid). The presence of a counterion enhances the positive charge in oxidized PEDOT, increasing its solubility and yielding PEDOT/PSS [33]. The properties of PEDOT encouraged researchers to use it to enhance the performance of PECs for both the oxygen evolution reaction (OER) and the hydrogen evolution reaction (HER) from water.

Thin films of PEDOT and poly(ethylene glycol) (PEG) have been synthesized on gold (Au), glassy carbon (GC), and titanium foil (Ti) substrates [34, 35]. Li and colleagues have also fabricated a hybrid Si-APS/PEDOT core–shell nanowire system by vapor-phase polymerization (VPP) [APS = 3-(aminopropyl)triethoxysilane] [36]. APS was used as the initial monolayer coating on the Si nanowire surface because PEDOT grows homogeneously on an APS surface. Subsequent vapor-phase polymerization of the monomer EDOT produced a strong, mechanically adhered PEDOT coating on the Si nanowire. PEDOT has a high selectivity for this application and could be finely patterned onto the nanoparticles due to the strong interaction between the N-H group on APS and PEDOT. The use of $FeCl_3$ as oxidant also dramatically improved the adhesion between the PEDOT film and the combined substrate [37]. The resulting hybrid photoelectrode Si-APS/PEDOT exhibited notable catalytic performance in water splitting, generating high relative current densities (as shown in Fig. 11.6a). It also displayed improved corrosion stability.

The mechanism of H_2 generation in this system was investigated. The Si nanowire absorbed visible light through the thin, overlying layer of PEDOT, which is highly transparent. Electron–hole pairs form at the Si. These pairs become separated at the Schottky heterojunction. As depicted in Fig. 11.6b, thanks to the external bias, the electrons moved toward the aluminum (Al) circuit contact and then, via the external circuit, onto the Pt cathode, where they reduced water to form hydrogen. The holes (h^+) transferred to the PEDOT film, facilitating water oxidation on the surface to generate oxygen gas. Short nanowires suppressed the recombination of the generated electron–hole pairs but yielded lower activity toward hydrogen

reduction. Long nanowires were better from an activity point of view, but resulted in increased recombination reactions.

PEDOT can also be combined with sensitizers and with other conducting polymers, such as poly(ethylene glycol) (PEG) and polythiophene (PTh), to exhibit significant electrocatalytic properties. For example, PEDOT-PEG has been reported to catalyze water reduction to hydrogen at rates higher than classical catalysts like Pt [38]. The PEG was believed to facilitate ion diffusion in the interior of the polymer materials. The VPP method was said to enhance the incorporation of PEG to thereby ensure that the polymer structure has an open morphology which allowed electrolyte access. Thus, the main role of the conductive polymer in water reduction was to provide a source of electrons [38].

Studies have also examined PEDOT combined with other polymers in such PEC systems. For example, Kolodziejczyk and co-workers [39] studied a new heterojunction design involving alloys of two conjugated polymers, PEDOT and polyterthiophene (PTTh), as a light-assisted catalyst of (1) oxygen reduction (to form water) and (2) water oxidation (to form oxygen). In acting as an oxygen reduction photocatalyst, the mixed polymers, deposited using the VPP method on either bulk gold or on Goretex sputter coated with gold, exhibited excellent performance, with stability lasting up to 98 h. However, this photocatalyst did not display a notable water oxidation effect, likely due to the recombination reactions.

Gustafson et al. [40] investigated the performance of conjugated polymers for water oxidation under illumination by UV light. Four sets of mixtures were prepared by VPP, namely, PEDOT/PTT, PEDOT/PDTT, PEDOT/PEG/PTT, and PEDOT/PEG/PDTT, with different ratios. It was observed that PEDOT/PEG/PDTT in the ratio of 1:2:2 achieved the highest current density under illumination followed by PEDOT/PEG (1:1) and PEDOT/PDTT (1:2), respectively (Fig. 11.7). The reasons for this behavior were not explored in detail. However, it was suggested that the behavior may arise from a higher degree of order or alignment in the PEDOT. The interesting thing that was observed was that the active junction could potentially be enhanced to achieve a relative photovoltage and photocurrent increase under illumination.

As noted earlier, PEDOT may display anticorrosion properties in water due to the Schottky junction between the PEDOT layer and its substrate. The junction facilitates the transfer of holes to the solution [41, 42]. These properties encouraged Duan et al. [43] to select PEDOT as the coating for Ag nanoparticles (AgNPs) modified with core–shell Si nanowires (SiNW). Water/methanol was used as the electrolyte. The PEDOT film was deposited on the surface of the SiNWs by electropolymerization. The resulting AgNPs modified with SiNWs/PEDOT displayed stronger light absorbance than unmodified PEDOT/SiNWs, AgNP/SiNWs, or SiNWs (Fig. 11.8a). In addition, the PEDOT facilitated a lattice mismatch between the AgNPs and SiNWs, which (1) encouraged the charge carriers to diffuse with higher efficiency, (2) improved the photocatalysis in aqueous solution, (3) increased stability, and (4) reduced the onset potential (Fig. 11.8b). The conversion efficiency for this system reached 2.86 %. Similar designs made by Jeong et al. used Si nanocones with poly(styrene sulfonate) (PEDOT/PSS) [44].
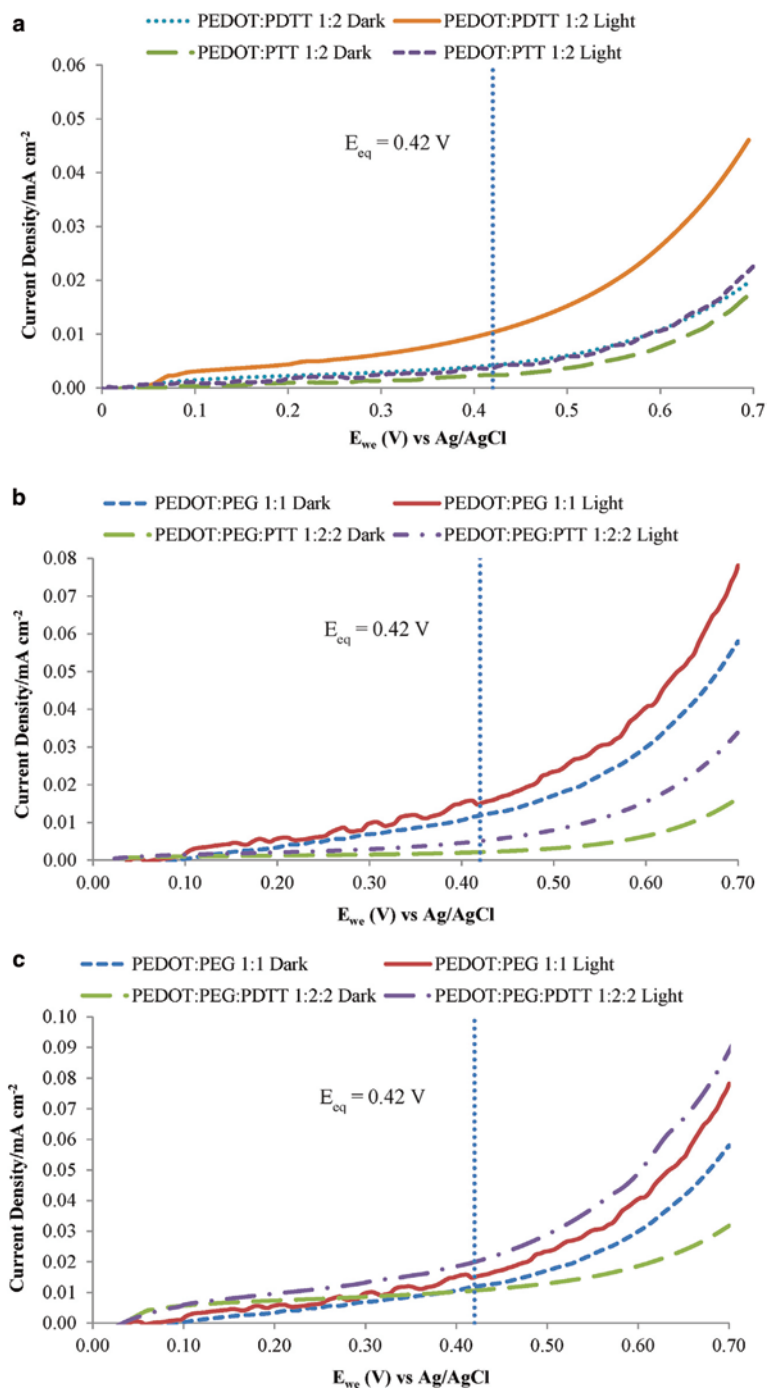
Fig. 11.7 Comparison of photocurrent densities for conjugated PEDOT with PEG, PDTT, and PTT in different ratios in dark and light. Scan rate: 1 mV s^{-1} at pH 11 vs. Ag/AgCl (E$_{eq}$ 0.42 V). Reproduced with permission from Ref. [40]
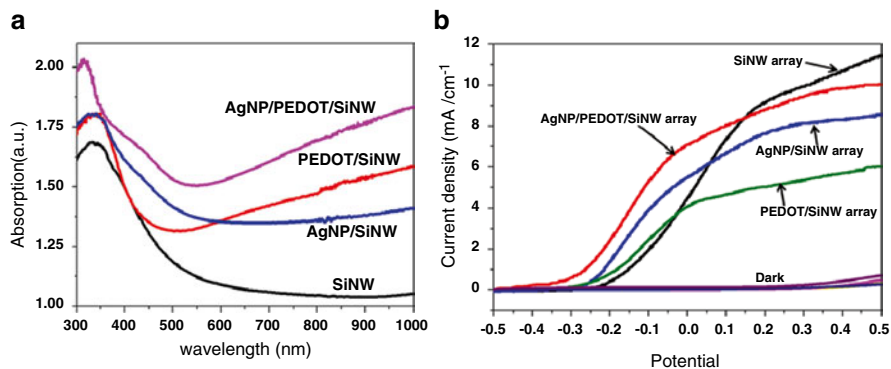
Fig. 11.8 (**a**) UV–visible absorption spectra of AgNPs/PEDOT/SiNW arrays, PEDOT/SiNW arrays, AgNP/SiNW arrays, and AgNPs/SiNW arrays. (**b**) Current–potential characteristics of the different photoanodes in the dark and under illumination, collected at a scan rate of 50 mV/s from −0.5 to +0.5 V (vs. SCE). Reproduced with permission from Ref. [43]

In order to be useful in solar water splitting, CP coatings need to display notable electrocatalytic properties. Several studies have examined the electrocatalytic capabilities of PEDOT-based coatings and their application in, for example, gas diffusion electrodes.

Chowdhury and co-workers [45] fabricated highly active catalysts that were inexpensive relative to Pt/C and bifunctional electrocatalysts for oxygen reduction (ORR) and the oxygen evolution reactions (OER). Their PEDOT–CoMnO$_4$ nanocomposites were prepared by polymerization of the aqueous micellar dispersion consisting of dodecylbenzene sulfonic acid (DBSA) as the surfactant, EDOT as the monomer, and CoMn$_2$O$_4$ nanoparticles. The resulting dark blue-colored nanocomposites were dropcast directly from alcoholic slurries onto a rotating disk glassy carbon electrode (GCE), which was air-dried to allow solvent evaporation. The GCE/PEDOT–CoMn$_2$O$_4$ nanocomposites catalyzed H$_2$ evolution in the higher potential range. The electrode was immersed in a KOH solution saturated with O$_2$. For LSV measurements, the nonconducting α-MnO$_2$ and CoMn$_2$O$_4$ spinel was mixed with acetylene black and Teflon binder to create a well-mixed paste. The results revealed that PEDOT-based CoMn$_2$O$_4$ had better ORR catalytic activity compared to the spinel itself. The catalytic activity of the CoMn$_2$O$_4$ spinel was reduced when it was mixed mechanically with the acetylene powder. However, it displayed better performance in the form of nanocomposites with the conducting PEDOT polymer (Fig. 11.9a). The activity for the OER reaction, which can be viewed as a reverse process of the ORR, is shown in Fig. 11.9b. In 0.1 M KOH, the CoMn$_2$O$_4$–PEDOT nanocomposites displayed higher OER currents than either free α-MnO$_2$ nanorod or CoMn$_2$O$_4$ nanocrystals. The α-MnO$_2$ nanorod did not show any OER/ORR activity.

Inherently conducting polymers (ICPs) such as PEDOT have also been used to fabricate electrodes that contain three-phase gas–solid–liquid interfaces. Goretex
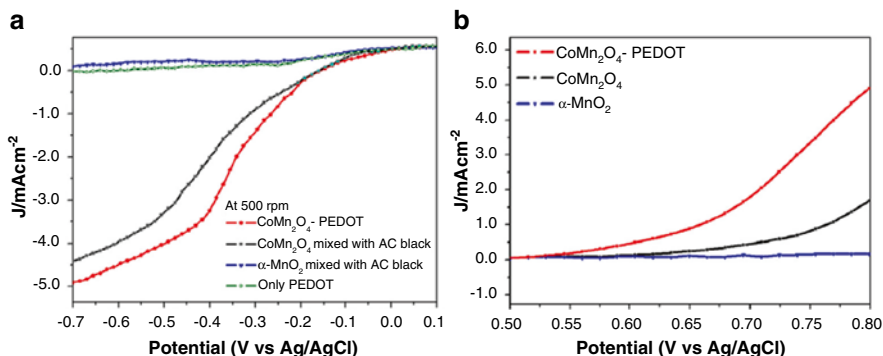
Fig. 11.9 Voltammetry curves of the OER measured at different rotation rates in the potential window of 0.5–0.8 V. Electrochemical comparison of $CoMn_2O_4$–PEDOT nanocomposites with $CoMn_2O_4$, PEDOT, and π-MnO_2 as (**a**) ORR and (**b**) OER electrocatalysts. Reproduced with permission from Ref. [45]

membranes are well-known porous, hydrophobic materials that prevent aqueous electrolytes from passing through it. Its porous structure is however highly permeable to gas. When Goretex is coated with Au and then with PEDOT/PTS (by VPP), a high surface area gas diffusion electrode is created. The layer of PEDOT/PTS then lies at the interface of the gas and the liquid electrolyte phases, where it may catalyze water splitting as shown in Fig. 11.10. At negative potentials, electrons are injected into the oxidized PEDOT/PTS, generating an intermediate reduced PEDOT/PTS. The reduced PEDOT/PTS is not stable in the presence of H^+ and therefore readily reoxidizes by reducing $2H^+$ to H_2 [46, 47].

A significant study wherein PEDOT was used as a "stand-alone," light-assisted water oxidation catalyst has been carried out by Chen and co-workers [48]. In their investigation, PEDOT films were deposited on ITO-PET sheets by VPP, with and without the incorporation of the anionic sulfonated Mn-porphyrin **1** (Fig. 11.11). PEDOT without **1** exhibited a blue–white color, while PEDOT-**1** displayed a green color. PEDOT-**1** also exhibited large absorption peaks between 350 and 450 nm corresponding to the porphyrin. Energy-dispersive X-ray spectroscopy (EDX) revealed that the porphyrin in the PEDOT films was uniformly distributed in a ratio of 1:3 (1 Mn-porphyrin/3 EDOT monomer). Linear sweep voltammograms (LSV) were carried out at a slow scan rate (5 mVs^{-1}) to study their performance as water oxidation catalysts, of photoanodes based on PEDOT and PEDOT-**1** films in aqueous solutions, with and without light illumination. The results showed a clear photocurrent associated with O_2 formation from water, starting from ca. 0.32 V vs. Ag/AgCl (0.55 V vs. NHE) (Fig. 11.12). This was substantially below the onset potential for poly(terthiophene)-**1** (0.91 V vs. NHE). It was also negative of the theoretical minimum.

Further work investigated light illumination of PEDOT-**1**/ITO glass electrode at a constant potential of 0.70 V vs. Ag/AgCl (0.93 V vs. NHE) in aq. 0.1 M Na_2SO_4. The results indicated an immediate photocurrent under visible light. When the light
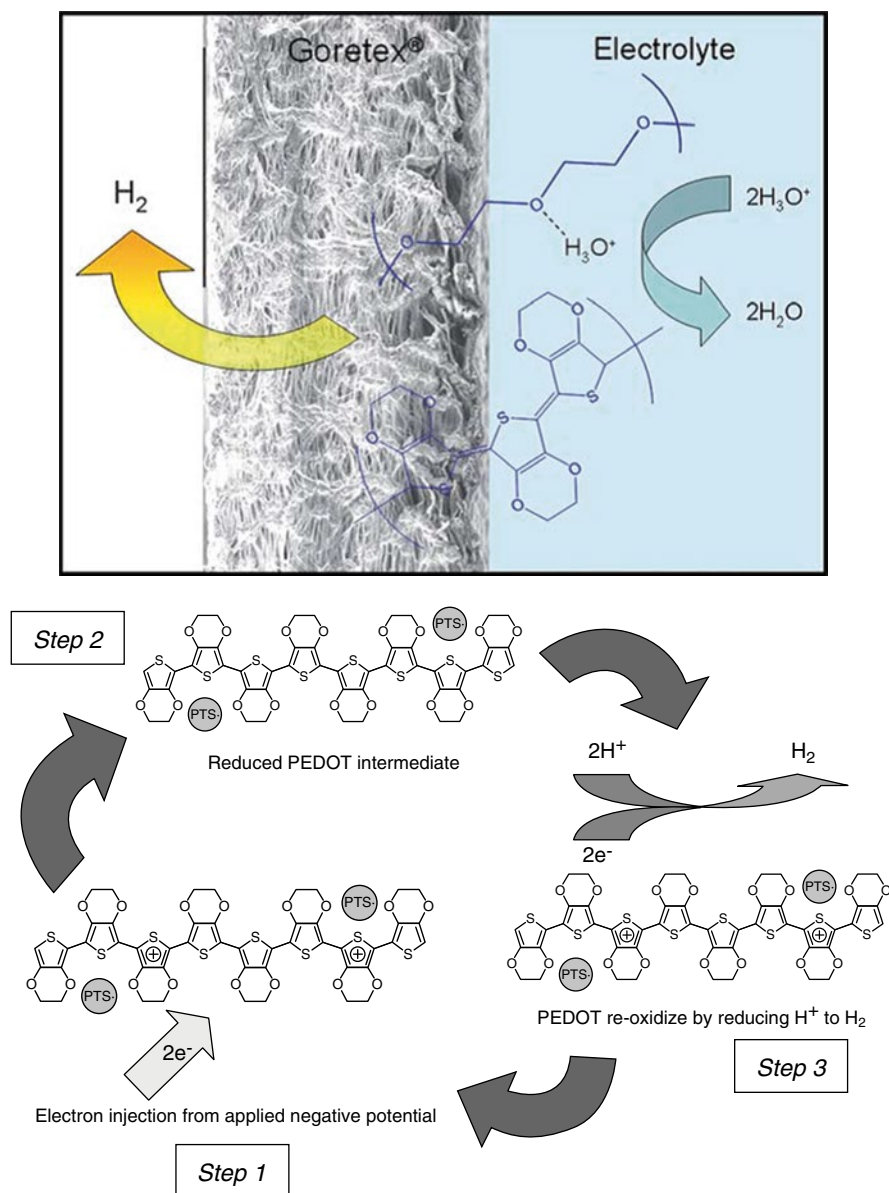
Fig. 11.10 *Left diagram*: The synthesis of PEDOT/PTS-coated Goretex Au for water splitting. *Right diagram*: The proposed mechanism for hydrogen production by the PEDOT. Reproduced with permission from Ref. [46]

Fig. 11.11 PEDOT-**1**
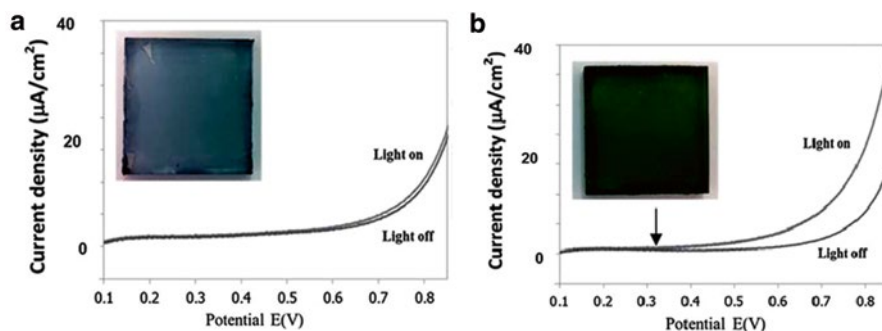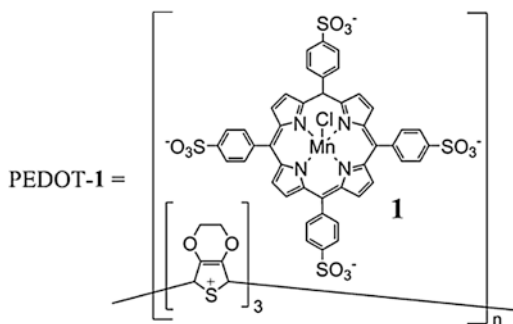
Fig. 11.12 Current density plot as a function of applied voltage with and without light illumination (vs. Ag/AgCl) (scan rate, 5 mV s^{-1} using aqueous 0.1 M Na$_2$SO$_4$ and pH 7) of (**a**) PEDOT and (**b**) PEDOT-**1**. The arrow in (**b**) shows the earlier onset potential for light-assisted water oxidation catalysis. Reproduced with permission from Ref. [48]

was switched off, the photocurrent reduced rapidly (Fig. 11.13). The mechanism for this system was investigated and proposed to involve light being absorbed by Mn-porphyrin (**1**) with the excited electrons injected into the PEDOT, which was reduced from the oxidized to the neutral form. The neutral form was then immediately reoxidized, where afterward the hole in the remaining **1**$^+$ interacted with an adjacent, cofacial *face-to-face* Mn-porphyrin in its clusters, leading to the extraction of electrons from two water molecules to create O$_2$.

11.4 Solar Water Splitting Using Polyaniline

Polyaniline (PANI), known as *"aniline black"*, was discovered in 1834 by Runge [49]. PANI has three distinct oxidation states, the *"leucoemeraldine"* state, the *"pernigraniline"* state, and the *"emeraldine base* (EB)" state, which is its most
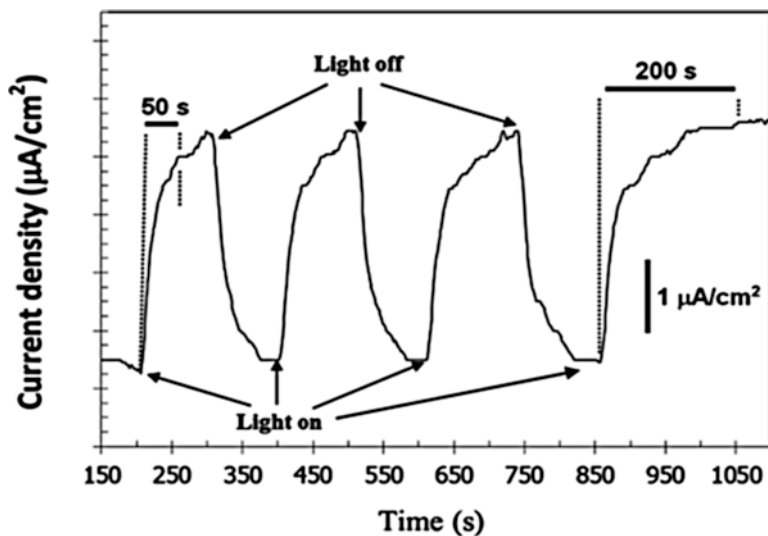
Fig. 11.13 Photocurrent densities of PEDOT-**1**/ITO glass with and without illumination at a constant potential of 0.7 V vs. Ag/AgCl in 0.1 M Na_2SO_4 solution. The points marked "light on" and "light off" indicate when the illumination was switched on and switched off, respectively. Reproduced with permission from Ref. [48]
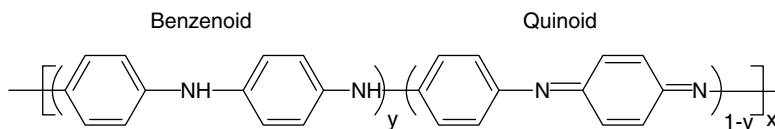
Fig. 11.14 Different forms of polyaniline: $y = 1$ (leucoemeraldine), 0.5 (emeraldine), and 0 (pernigraniline) [49]

important form (Fig. 11.14) [49, 50]. It can be prepared by chemical/electrochemical polymerization of aniline monomer, photochemically initiated polymerization or enzyme-catalyzed polymerization [50–52]. Polyaniline derivatives can be prepared by doping the EB state with organic and inorganic dopants that improve processability and compatibility [53]. PANI has wide applications [54, 55]. Consequently, PANI is a candidate for use in organic–inorganic, hybrid water-splitting photocatalysts that operate under illumination by visible light. Combining PANI with semiconductors leads to an increase in the absorption of incident light at the active surface. A semiconductor that has been widely used in this respect is titanium dioxide (TiO_2) [56].

Belabed and co-workers [57] modified TiO_2 with an emeraldine salt PANI coating in the ratio of 1:1 of PANI–TiO_2 catalyst for investigation of H_2 production from water under illumination with light (29 mW cm^{-2}). The results demonstrated H_2 evolution at a higher rate for PANI–TiO_2 than for PANI alone in a control (Fig. 11.15).

Fig. 11.15 Hydrogen evolution using PANI and PANI/TiO$_2$ photocatalysts under visible light in a neutral solution of Na$_2$SO$_3$. Reproduced with permission from Ref. [57]
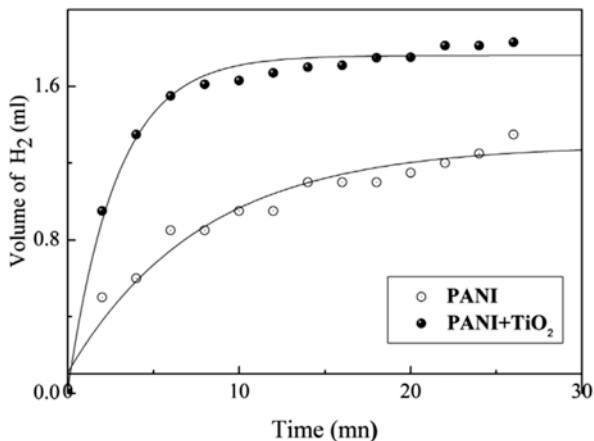
The proposed mechanism is explained as follows. When PANI was exposed to external light, the excited photoelectrons transferred to the CB of the TiO$_2$, which then facilitated hydrogen production at the surface of the TiO$_2$. The reactions that occur at the photoelectrode were proposed to be the following:

$$PANI + 2\,hv \rightarrow PANI\ \ CB(2e^-) + PANI\ \ VB(2h^+) \tag{11.2}$$

$$PANI\ \ CB(2e^-) + 2\,H_2O \rightarrow 2\,H_2 + 2\,OH^- \tag{11.3}$$

$$PANI\ \ VB(2h^+) + SO_3^{-2} + 2\,OH^- \rightarrow SO_4^{2-} + H_2O \tag{11.4}$$

$$PANI\ \ VB(2h^+) + 2\,SO_3^{-2} \rightarrow S_2O_6^{2-} \tag{11.5}$$
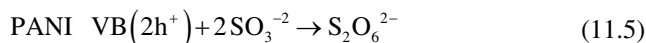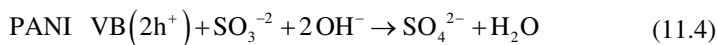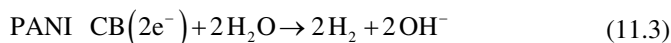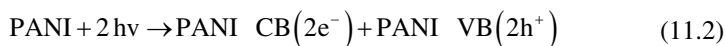
While at the cathode, the following reaction is proposed:

$$2\,H_2O + 2e^- \rightarrow H_2 + 2\,OH^- \tag{11.6}$$
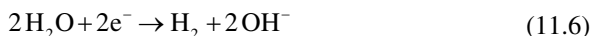
Studies have also examined PANI as a sensitizer for PEC-based water oxidation. To illustrate how PANI may be applied, the fabrication of a uniform nanocomposite film of TiO$_2$/PANI will be described [58]. Firstly, a PANI solution was synthesized by oxidative polymerization starting from the aniline dimer. The synthesis was performed in the aqueous phase using poly(styrene sulfonate) (PSS) as doping agent to generate PANI in the emeraldine conductive form. A TiO$_2$ mesoporous film was then deposited onto fluorine-doped tin oxide (FTO) glass by spin-coating TiO$_2$ nanoparticles and a nonionic surfactant (Tween 20); the coating was subsequently annealed in air at 500 °C. The TiO$_2$ film was then dipped into the PANI solution for 10 min and dried at 80 °C under vacuum for 24 h. A uniform and continuous PANI/TiO$_2$ nanocomposite film was obtained. FESEM, FTIR, and UV–Vis all confirmed the surface

sensitization of the TiO_2 film with PANI and indicated an increase in the optical absorption of TiO_2 in the visible region. The PEC activity of both TiO_2 and PANI/TiO_2 composite films was studied by linear sweep voltammetry (LSV) and electrochemical impedance spectroscopy (EIS). PANI/TiO_2 was used as the anode for the water photo-electrolysis reaction, with a Pt wire as the cathode and a Ag/AgCl reference electrode. LSVs were run in the dark and under simulated solar light (using a 450 W Xe lamp, AM 1.5 filter), in a 0.1 M aqueous NaOH electrolyte solution. Under these conditions, the PANI/TiO_2 composite film produced more than double the solar-to-hydrogen efficiency than the original TiO_2 film. It also demonstrated stability over periods up to 1 h. Such results suggest possible applications for PANI as a sensitizer for PEC water-splitting [58].

Several other studies have also demonstrated that coupling PANI to TiO_2 can improve its performance in photoelectrochemical water splitting. The delocalized conjugated structures of PANI promote charge separation and slow charge recombination [59]. For example, Palmas et al. [60] reported that modifying nanotubes (NTs) of TiO_2 with PANI improved their performance both in water splitting and as an energy storage device. The TiO_2 NTs were first treated in an organic solution with fluorides, followed by electro-polymerization of monomer aniline by cyclic voltammetry. The result confirms that PANI may play an important role in facilitating water splitting.

Several other conventional photocatalysts modified with PANI have been investigated, including $BiVO_4$, SnO_2, and MoO_3, among others. Zhang et al. [61] prepared a new stable, nontoxic, PdS–CdS photocatalyst using a sonochemical approach. PANI was dissolved in an appropriate concentration in THF and added to different mixtures of PdS–CdS nanocrystals which were previously prepared by a coprecipitation method. The suspension was then sonicated and stirred for a time, after which it was filtered. The final PANI/PdS–CdS photocatalyst was then washed with water and dried in an oven. The resulting PdS–CdS NPs yielded an increase in hydrogen evolution from water under illumination when modified with PANI. The PdS had an important influence on the activity of the composite photocatalyst; 1 wt% PdS–CdS gave the highest hydrogen evolution rate, while 1 wt% PANI/1 % PdS–CdS ratio PANI yielded the greatest hydrogen evolution rate (Fig. 11.16).

Further investigation revealed that the PANI formed a conductive network on the surface of the PdS–CdS NPs, promoting the formation of photogenerated electrons and holes, accelerating the transfer of the holes from the VB of CdS to the CB of PdS with accompanying suppression of the recombination reaction [62].

As noted in the introduction, when conventional semiconductors are modified with CPs, the bandgap between the VB and CB may be diminished, resulting in an improved performance in water splitting under visible light. This effect is illustrated in work by Nsib and co-workers [62], who fabricated Ni-doped ZnO coated with PANI. The Ni-doped ZnO was formed by homogeneous precipitation using different levels of Ni, followed by drying at temperatures up to 400 °C. The Ni-ZnO was then modified with PANI by oxidative polymerization of aniline monomer using ammonium persulfate (ApS) in acidic solution of H_2SO_4 at a pH of less than 3. The resulting photocatalyst demonstrated clear and amplified H_2 production from water
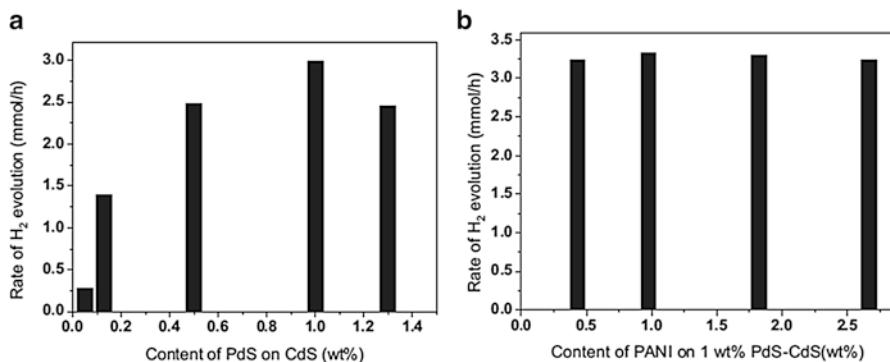
Fig. 11.16 The hydrogen evolution rate for (**a**) CdS photocatalysts with different contents of PdS and (**b**) PdS–CdS photocatalysts with different contents of PANI. Reproduced with permission from Ref. [61]

under visible light. The rate of hydrogen generation increased with an increase in the ratio of PANI in $Ni_{0.1}Zn_{0.9}O/PANI_y$, where $y = 3 > 6 > 10$. The H_2 production rate in Ni-ZnO/PANI also depended on the nature of the sacrificial electron donors used, in the following order: thiosulfate > sulfide > propanol.

Nsib et al. also proposed a mechanism for the water-splitting photocatalysis. When the Ni-ZnO/PANI photoelectrode was exposed to visible light, photons were absorbed at the interfacial region between the Ni-ZnO and the PANI layer. In that region, the lowest unoccupied molecular orbital (LUMO) level of PANI was higher in energy than the CB of ZnO. Photogenerated electrons of PANI therefore transferred into the CB of ZnO, which was capable of reducing protons to hydrogen. The remaining holes reacted with the sacrificial electron donors (carbonate species) to form carbonate radicals (HCO_3^-) and possibly CO_2, which prevented the generation of O_2 at the photocatalyst surface, thereby also minimizing the reverse recombination reaction.

Mao et al. [63] reported that PANI may improve photocatalytic water splitting by enhancing the morphology of a PEC. Their design employed *n*-type hematite (α-Fe_2O_3), which has a bandgap of 2.0–2.2 eV, allowing 40 % of incident light to be absorbed with improved photochemical stability at pH < 3. Gold (Au) was also used. Au has lower Fermi levels than semiconductors so that photoexcited electrons can easily transfer from semiconductors to the metal, reducing the possibility of a recombination reaction. An anodized aluminum oxide (AAO) template coated with a thin layer of Au was used as an electrode. Vertically aligned hematite nanorods and nanotube arrays were prepared by two different methods. In one route, PANI was electrodeposited into the pores of the AAO template by potentiostatic cycling, where α-Fe_2O_3 nanotubes were later electrodeposited between the PANI-NRs and the walls of the AAO pores. In the second route, electrodeposition using an aqueous solution of $KAu(CN)_2$ and KH_2PO_4 allowed Au to be electrodeposited into the AAO pores, where α-Fe_2O_3 was deposited later as nanorods. Both the nanotubes and
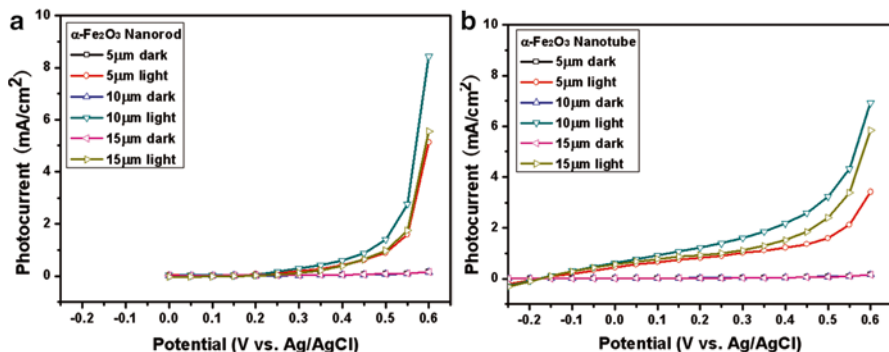
Fig. 11.17 Photocurrent density–voltage behavior of different lengths (in μm) of (**a**) PANI/α--Fe$_2$O$_3$ nanorods and (**b**) PANI/α-Fe$_2$O$_3$ nanotubes under visible light in 1 M NaOH electrolyte. Reproduced with permission from Ref. [63]
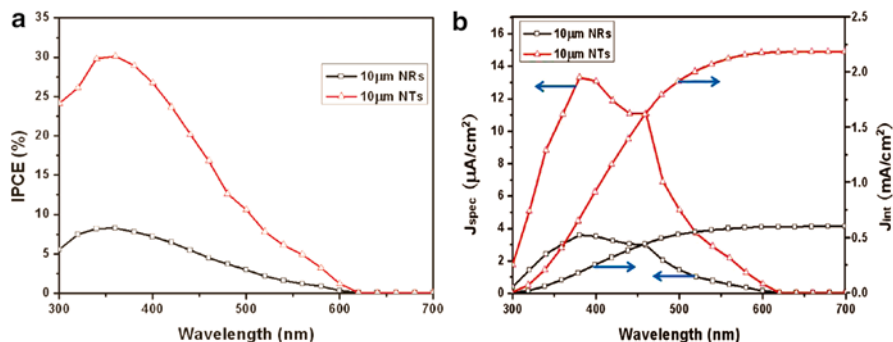
Fig. 11.18 Spectral photo response of 10 μm-long R-Fe$_2$O$_3$ nanorods and R-Fe$_2$O$_3$ nanotubes at 0.43 V vs. Ag/AgCl under illumination by AM 1.5 light in 1 M NaOH electrolyte: (**a**) incident photon-to-current conversion efficiency (IPCE); (**b**) solar photocurrent spectral (Jspect) and integrated solar photocurrent (Jint). Reproduced with permission from Ref. [63]

nanorods were tested as photoanodes for water oxidation. The hematite nanotubes displayed greater photoelectrochemical activity than the hematite nanorods. They had larger photocurrent densities, more negative onset potentials, better photon harvesting, and a better ability to transfer photogenerated electrons–holes. It was also observed that long nanorods or nanotubes reduced the photocurrent density due to an increase in the recombination reactions, as shown in Figs. 11.17 and 11.18.

PANI may also be used as a simple electrocatalyst for water splitting. Damian and Omanovic [64] used PANI as a support/matrix/template for the construction of Ni and NiMo hydrogen evolution catalyst layers on an inert electrode substrate [glassy carbon (GC)]. PANI was chosen for this study because of its (1) insulating properties at voltages suitable for H$_2$ evolution, (2) patterned morphology, (3) stability in a low-pH environment, and (4) simple electrochemical polymerization method. The resulting

electrode demonstrated three features that are important in HER catalysis, namely, an actual intrinsic electrocatalytic effect of the material, a large active surface area per unit volume, and catalytic stability. Alloying elements (such as Ni) together with other transition metals (like W, Mo, and Fe) yielded increased electroactivity for the HER compared to the corresponding pure elements due to the electronic structure of the metals and the effects of synergy in these heterogeneous catalysts.

Damian and Omanovic also investigated HER electroactivity by pure Ni on GC, Ni/PANI deposited on GC, and NiMo/PANI deposited on GC. Scanning electron microscopy (SEM) revealed that NiMo/PANI had the highest surface coverage, which was greater than the Ni/PANI layer and pure Ni. The presence of the PANI clearly increased the roughness of the surface. Alloying Ni with Mo increased the electrocatalytic activity. NiMo/PANI displayed higher electroactivity than Ni/PANI or Ni alone. Although this system did not investigate the effect of visible light on these systems, it showed that PANI, which incorporated transition metals, displayed a water-splitting effect when exposed to light.

11.5   Solar Water Splitting Using Polythiophene

Polythiophene (PTh) may exist at room temperature in both neutral and conductive states [65, 66]. PTh can be prepared by chemical and electrochemical oxidation of its monomer. The chemical polymerization of PTh can be brought about by an appropriate chemical oxidant such as $FeCl_3$, $MoCl_5$, and $RuCl_3$. Electrochemical polymerization occurs by the application of a suitable potential [67, 68]. It should be noted that thiophene is difficult to oxidize, so direct preparation is generally avoided. It is usually necessary to start with bithiophene or terthiophene for electrochemical preparation. Other approaches to prepare polythiophene include ultrasonically assisted electrochemical, photochemical, and template synthesis [69]. The removal of π-electrons from the polymer backbone creates a moving radical cation (polaron) that can be detected by electron spin resonance (ESR) [70]. PTh's useful features include (1) high charge carrier mobility, (2) environmental stability, and (3) higher wavelength absorption compared to other conductive polymers. The incorporation of substituents on PTh may improve its physical properties [71, 72] and make it easier to polymerize. These features allow PTh to be used in many applications or potential applications, including the use in transistors, solar cells, sensors, electrochromic devices, supercapacitors, and light-emitting diodes. For example, Tsekouras and Wallace [73] showed that PTh could be used to fabricate a photovoltaic solar cell that employed light-harvesting dyes (porphyrins). While many studies have examined PTh as an electrocatalyst, relatively few of those have been directed to its use in water splitting under illumination with visible light.

Porphyrin dyes are widely used as photosensitizers for DSSCs. The porphyrins and their derivatives are able to harvest visible light energy via their highly developed π-conjugation system [74]. The addition of porphyrin dyes to materials as diverse as GaN/ZnO, TiO_2, and FTO has been shown to produce photocatalysts for water splitting [75].

Fig. 11.19 Sulfonated monomeric Mn-porphyrin complex **2** used in water splitting by polyterthiophene (PTTh) [76]
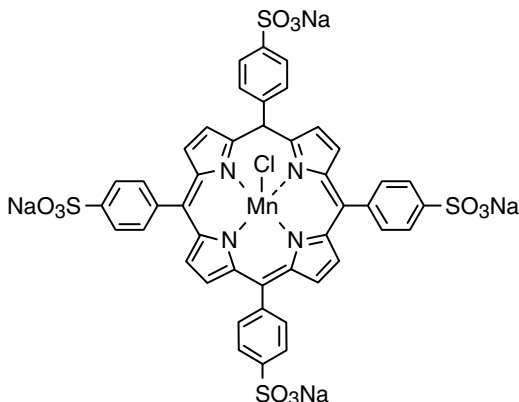
Chen and co-workers [76] reported that whereas the sulfonated, monomeric Mn-porphyrin complex **2** shown in Fig. 11.19 is normally catalytically inactive, when it is incorporated within a thin layer of poly(terthiophene) (PTTh), it produced a remarkable light-assisted catalyst with a low overpotential for water splitting at pH 7. Under light illumination in seawater, it generated only O_2 and not the toxic gas Cl_2, which is produced by essentially all other known electrocatalysts.

The sulfonated Mn-porphyrin monomer was uniformly incorporated into a thin PTTh film by electrochemical polymerization of monomer in ethanol/dichloromethane (1:1 volume). The PTTh–Mn-porphyrin was deposited as a composite film onto indium tin oxide (ITO) glass or a flexible ITO-coated poly(ethylene terephthalate) (PET) sheet. X-ray mapping using EDX indicated a uniform distribution of the Mn-porphyrin in the coating. The ratio of Mn-porphyrin to PTTh was 1:3. Cyclic voltammograms (CVs) with and without light were used to examine the performance of PTTh–Mn-porphyrin/ITO in an aqueous solution using 0.1 Na_2SO_4 under an external light. The results indicated a large current commencing at the onset potential of 0.68 V (Fig. 11.20).

Peak A in Fig. 11.20 was studied by linear sweep voltammetry (LSV) after the electrode was preconditioned for 1 h by maintaining it at potentials of 0.8 V (I), 0.9 V (II), and 1.0 V(III). It was found that peak A separated into peaks A' and A", which are indicative of adsorbed dioxygen (O_2) and peroxide (O_2^{2-}), respectively. As shown in Fig. 11.20, the oxygen peak (A') increases with increasing conditioning potential, thereby confirming the formation of dioxygen.

Photocurrent measurements also examined the performance of PTTh–Mn-porphyrin/ITO in an aqueous solution at 0.8 and 0.9 V. A photocurrent of ca. 9 μA at 0.8 V and 23 μA at 0.9 V was obtained under illumination. This photocurrent disappeared when the light was turned off. It reappeared when the light was turned on (Fig. 11.21).

The standard potential for water oxidation at pH 0 is 1.23 V versus the standard hydrogen electrode (SHE). The minimum theoretical potential to drive water oxidation falls to 0.82 V versus SHE at pH 7. However, the PTTh–Mn-porphyrin/ITO
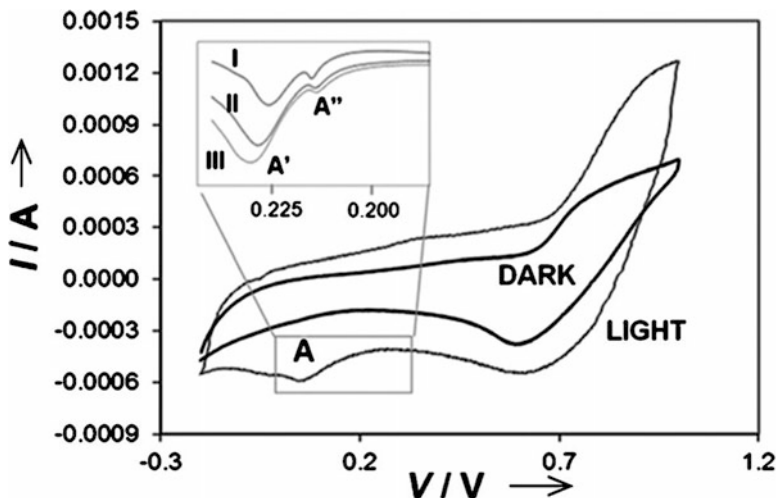
Fig. 11.20 Cyclic voltammograms (vs. Ag/AgCl) of PTTh–Mn-porphyrin **2**/ITO glass in aqueous 0.1 M Na$_2$SO$_4$ (pH 7) with ("light") and without ("dark") illumination using a halogen light bulb (12 V, 50 W). The inset displays linear sweep voltammograms of peak A taken immediately after the electrode was preconditioned for 1 h by maintaining it at potentials of 0.8 V (I), 0.9 V (II), and 1.0 V(III). Scan rate, 50 mVs^{-1}. Reproduced with permission from Ref. [76]
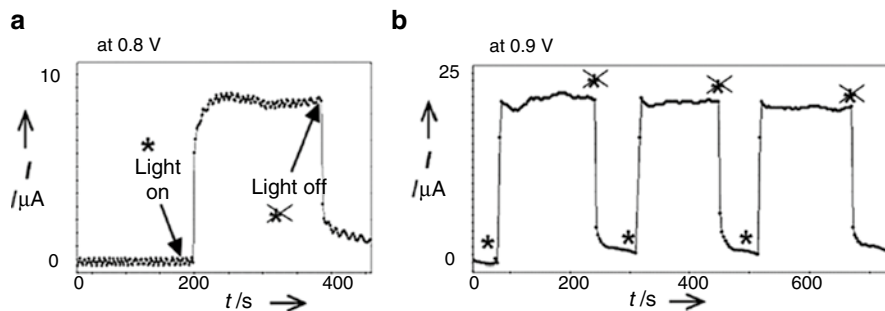
Fig. 11.21 Photocurrent with and without illumination, by PTTh–Mn-porphyrin **2**/ITO glass in 0.1 m Na$_2$SO$_4$ (aq) at (**a**) 0.8 V and (**b**) 0.9 V vs. Ag/AgCl. Asterisks signify "light on." Asterisks with crosses through them indicate "light off." Reproduced with permission from Ref. [76]

facilitated water oxidation under illumination with visible light at potentials above 0.68 V versus that of Ag/AgCl. The additional energy of the light illumination explains the ability of this system to operate at values less than the minimum theoretical potential.

Perhaps the most significant result with PTTh–Mn-porphyrin was its electrocatalytic reaction in seawater. The photocurrent measurement under illumination in seawater was carried out using PTTh–Mn-porphyrin on conductive, ITO-coated PET (Fig. 11.22). A comparison was made with the control PTTh-pTS/ITO-PET (where
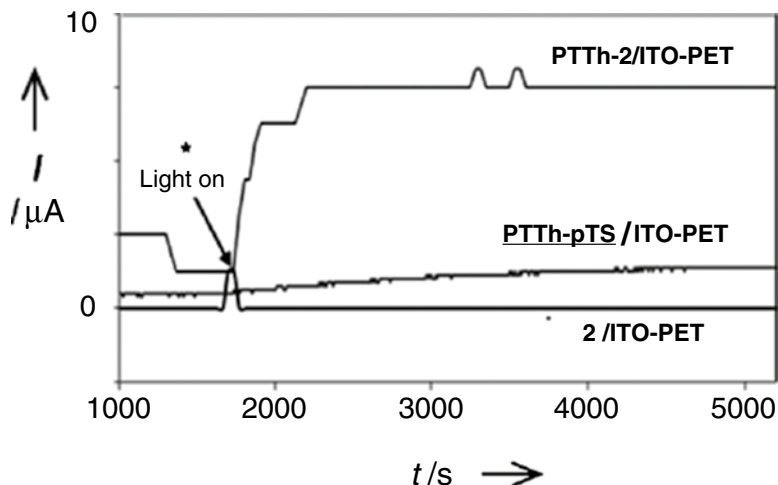
Fig. 11.22 Photocurrent measurement under illumination, using seawater as electrolyte at a potential of 0.9 V for PTTh–Mn-porphyrin **2** on ITO-PET, PTTh-pTS on ITO-PET, and ITO-PET in a solution containing 0.1 M Mn-porphyrin **2**. Reproduced with permission from Ref. [76]

p-TS = p-toluenesulfonate). This work demonstrated that polythiophene yields a high photocurrent [76], with the sole product generated being dioxygen with no measurable production of chlorine, Cl_2. By contrast, all other known man-made photoelectrocatalysts generate chlorine when immersed in aqueous solutions containing chloride ions [76]. While oxygen formation (E^o 1.23 V) is thermodynamically favored over chlorine formation (E^o 1.36 V), the overpotential for oxygen formation is substantially higher than that for chlorine formation.

It was suggested that the mechanism involved the Mn-porphyrin dopant absorbing photons and then the transfer of the excited electrons to PTTh which, at the applied potential, would be immediately reoxidized by the electrode, returning to its conductive form. The remaining holes then facilitate water oxidation by extracting electrons from water.

Gustafson et al. [77] fabricated an organic, bulk heterojunction (BHJ) solar cell capable of facilitating light-assisted electrocatalysis of water splitting. The design employed a charge-separation layer comprised of poly(hexylthiophene) (PHT) and a C_{60}-fullerene, laminated to an ITO-PET electrode using a PEDOT/PSS or a ZnO layer. A thin Pt layer was sputter coated on the outer, electrolyte-facing side of the electrode. The two electrode structures were an ITO-PET/PEDOT/PSS/P3HT/PCBM (OPE-R) electrode for the proton reduction reaction and an ITO-PET/ZnO/P3HT/PCBM (OPE-O) electrode for the water oxidation reaction (OPE = organic photoelectrode, PET = poly(ethylene terephthalate), PSS = poly(styrene sulfonate), P3HT = poly(3-hexylthiophene), and PCBM = phenyl-C_{61}-butyric acid methyl ester). Figure 11.23 shows the electron–hole pathways in (a) the OPE-R electrode and (b) the OPE-O electrode. The 1:1 mixture of P3HT/PCBM is known to offer a successful platform for BHJ [77].
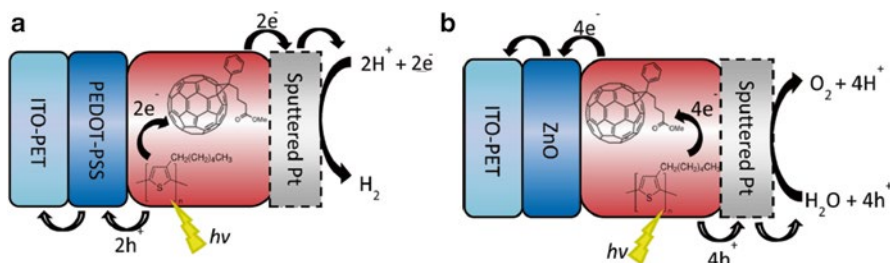
Fig. 11.23 Photoelectrodes in a bulk heterojunction (BHJ) solar cell developed by Gustafson et al. that facilitated (**a**) proton reduction (OPE-R) and (**b**) water oxidation (OPE-O). Reproduced with permission from Ref. [77]
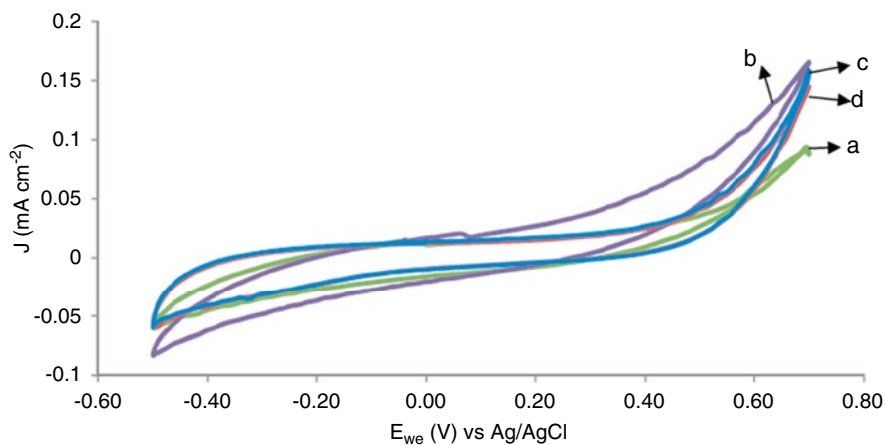
Fig. 11.24 Cyclic voltammograms of the OPE-O in the *dark* (*a*) (*green*) and under light illumination (*b*) (*purple*); the comparable curves for the ITO-PET/Pt control are also shown as in the *dark* (*c*) (*blue*) and under light illumination (*d*) (*red*). Scan rate, 10 mV/s in 0.1 M phosphate buffer in aqueous vs. Ag/AgCl at pH 7. Reproduced with permission from Ref. [77]

The OPE-O electrode demonstrated enhanced water oxidation upon illumination. As shown in Fig. 11.24, the OPE-O electrode displayed an onset potential of ca. 0.1 V versus that of Ag/AgCl at a pH of 7, which was substantially more negative than the onset potential of an ITO-PET/Pt control electrode, which was 0.45 V. The OPE-O produced a photocurrent of 0.15 mA/cm^2 at 0.7 V.

The OPE-O was more stable than the OPE-R after immersion in water. This was due to the ZnO layer blocking out more water than the PEDOT/PSS layer, which also appeared to allow PSS migration in the OPE-R samples. The BHJ exhibited charge separation at the P3HT/PCBM interface [77].

Aoki et al. [78] also fabricated a bulk heterojunction (BHJ) organic thin-film PEC consisting of poly(3-hexylthiophene) as an electron donor combined with
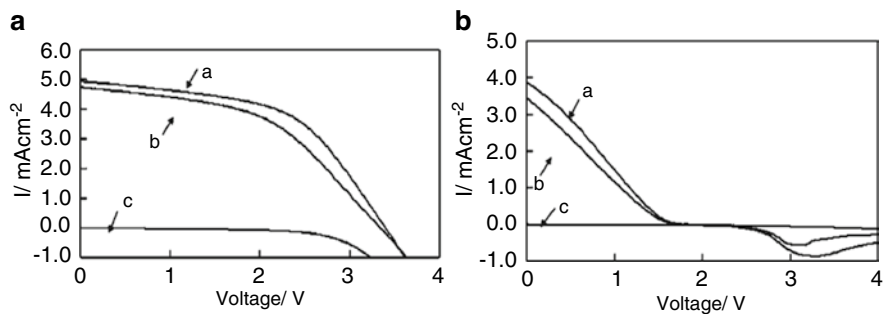
Fig. 11.25 Photocurrent vs. potential plots for the series circuit of six organic *thin-film* solar cells (OSCs) (**a**) and for the combination of the series circuit of six OSCs with an electrolysis cell using Pt electrodes (**b**); (*a*) as irradiated, (*b*) after 1 h of irradiation, and (*c*) under *dark* conditions. Reproduced with permission from Ref. [78]
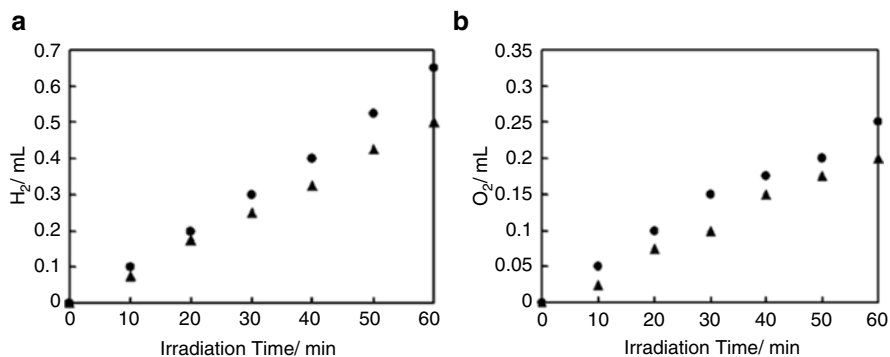
Fig. 11.26 (**a**) H_2 generation and (**b**) O_2 generation volumes against irradiation time: (*filled circle*) obtained at the electrolysis cell using two Pt electrodes with an electrolyzing current of 1.47 mA and (*filled triangle*) at the electrolysis cell using a PtC cathode and a Ni anode with an electrolyzing current of 1.09 mA. Reproduced with permission from Ref. [78]

[6,6]-phenyl C_{61}-butyric acid methyl ester as an electron acceptor. The cell was composed of six series of these units in order to supply enough potential to convert water to hydrogen and oxygen gases at optimum power conversion efficiency under visible light. The six series units were then connected to an electrolysis cell using Pt electrodes. As shown in Figs. 11.25 and 11.26, the results clearly demonstrated an increase in photocurrent density under radiation. This cell was able to produce 1.09 mA and 2.3 V under simulated solar irradiation (100 $mWcm^{-2}$, AM 1.5G); 0.65 mL of H_2 and 0.27 mL of O_2 were generated in 1 h.

11.6 Conclusion

The unique properties of CPs make them suitable for solar water-splitting applications. These properties include conductivity, permeability to water, low cost, environmental nontoxicity, electrochemical stability, useful light absorption, combining readily with other materials, excellent electron transfer properties, and uncomplicated preparative methods. This diversity and utility impart CPs with great promise in the catalytic generation of hydrogen and/or oxygen from water under illumination by sunlight.

References

1. Chiang CK, Druy MA, Gau SC, Heeger AJ, Louis EJ, MacDiarmid AG, Park YW, Shirakawa H (1978) J Am Chem Soc 100:1013
2. Baseescu N, Liu ZX, Moses D, Heeger AJ, Naarmann H, Theophilou N (1987) Nature 327:403
3. Yahyaie I, Ardo S, Oliver DR, Thomson DJ, Freund MS, Lewis NS (2012) Energy Environ Sci 5:9789
4. Pratt C (2015) Applications of conducting polymers. http://homepage.ntlworld.com/colin.pratt/applcp.pdf. Accessed 14 May 2015.
5. Molapo KM, Ndangili PM, Ajayi RF, Mbambisa G, Mailu SM, Njomo N, Masikini M, Baker P, Iwuoha EI (2012) Int J Electrochem Sci 7:11859
6. Ziadan K (2012) Conducting polymers application. In: Souza Gomes AD (ed) New polymers for special applications. InTech, Rijeka, pp 1–22
7. Chandrasekhar P (1999) Conducting polymers, fundamentals and applications: a practical approach. Kluwer, Boston
8. Bachhshi AK, Bahalla G (2004) J Sci Ind Res 63:715
9. Saini P, Arora M (2012) Microwave absorption and EMI shielding behavior of nanocomposites based on intrinsically conducting polymers, graphene and carbon nanotubes. In: Souza Gomes AD (ed) New polymers for special applications. InTech, Rijeka, pp 72–112
10. Almeida LC, Ebrary I (2013) Conducting polymers: synthesis, properties and applications. Nova Science, New York
11. Tributsch H (2008) Int J Hydrogen Energy 33:5911
12. Vernitskaya TV, Efimov ON (1997) Russ Chem Rev 66:443
13. Ilicheva NS, Kitaeva NK, Duflot VR, Kabanova VI (2012) ISRN Polym Sci 2012:1
14. Kassim A, Basar ZB, Mahmud HN (2002) J Chem Sci 114:155
15. Arthur J, Honda K (1985) J Photochem 29:195
16. Tan Y, Chen Y, Mahimwalla Z, Johnson MB, Sharma T, Brüning R, Ghandi K (2014) Synth Met 189:77
17. Zou Z, Ye J, Sayama K, Arakawa H (2001) Nature 414:625
18. Liu H, Yuan J, Shangguan W, Teraoka Y (2008) J Phys Chem 112:8521
19. Abe R, Takata T, Sugihara H, Domen K (2005) Chem Commun 14:3829–3831
20. Gu S, Li B, Zhao C, Xu Y, Qian X, Chen G (2011) J Alloys Compd 509:5677
21. Wang D, Wang Y, Li X, Luo Q, An J, Yue J (2008) Catal Commun 9:1162
22. Håkansson E, Lin T, Wang H, Kaynak A (2006) Synth Met 156:1194
23. Zhang S, Chen Q, Jing D, Wang Y, Guo L (2011) Int J Hydrogen Energy 37:791
24. Zhang S, Chen Q, Wang Y, Guo L (2012) Int J Hydrogen Energy 37:13030
25. Zhang Z, Yuan Y, Liang L, Cheng Y, Xu H, Shi G, Jin L (2008) Thin Solid Films 516:8663
26. Wang Z, Xiao P, Qiao L, Meng X, Zhang Y, Li X, Yang F (2013) Phys B 419:51
27. Mingzhao L, Chang-Yong N, Charles T, Jovan K, Lihua Z (2013) J Phys Chem C 117:13396

28. Mola J, Mas-Marza E, Sala X, Romero I, Rodríguez M, Viñas C, Parella T, Llobet A (2008) Angew Chem Int Ed 47:5830
29. Brimblecombe R, Dismukes GC, Swiegers GF, Spiccia L (2009) Dalton Trans 43:9374
30. Pyshkina O, Kubarkov A, Sergeyev V (2010) Sci J Riga Tech Univ 21:51
31. Kros A, Sommerdijk NAJM, Nolte RJM (2005) Sens Actuators 106:289
32. Carlberg C, Chen X, Inganäs O (1996) Solid State Ionics 85:73
33. Wei W, Wang H, Hu YH (2014) Int J Energy Res 38:1099
34. Chaokang G, Brent C, Norris F, Christopher W, Bielawski C, Allen J (2012) ACS Catal 2:746
35. Metsik J, Saal K, Mäeorg U, Lõhmus R, Leinberg S, Mändar H, Kodu M, Timusk M (2014) J Polym Sci B Polym Phys 52:561
36. Li X, Lu W, Dong W, Chen Q, Wu D, Zhou W, Chen L (2013) Nanoscale 5:5257
37. Kim S, Pang I, Lee J (2007) Macromol Rapid Commun 28:1574
38. Swiegers GF, Smith PF, Spiccia L, Wagner P, Wallace GG, Winther-Jensen B, Winther-Jensen O, MacFarlane DR, Officer DL, Ballantyne A, Boskovic D, Chen J, Dismukes GC, Gardner GP, Hocking RK (2012) Aust J Chem 65:577
39. Kolodziejczyk B, Winther-Jensen O, MacFarlane D, Winther-Jensen B (2012) J Mater Chem 22:1821
40. Gustafson MP, Matsumoto K, MacFarlane DR, Winther-Jensen B (2014) Electrochim Acta 122:166
41. Winther-Jensen B, Fraser K, Ong C, Forsyth M, MacFarlane DR (2010) Adv Mater 22:1727
42. Yang T, Wang H, Ou X, Lee C, Zhang X (2012) Adv Mater 24:6199
43. Duan C, Wang H, Ou X, Li F, Zhang X (2014) ACS Appl Mater Interfaces 6:9742
44. Jeong S, Garnett EC, Wang S, Yu Z, Fan S, Brongersma ML, McGehee MD, Cui Y (2012) Nano Lett 12:2971
45. Chowdhury AD, Agnihotria N, Senb P, De A (2014) Electrochim Acta 118:81
46. Winther-Jensen B, MacFarlane DR (2011) Energy Environ Sci 4:2790
47. Winther-Jensen O, Winther-Jensen B, Forsyth M, MacFarlane DR (2008) Science 321:671
48. Chen J, Wagner PW, Tong L, Boskovic D, Zhang W, Officer DL, Wallace GG, Swiegers GF (2013) Chem Sci 4:2797
49. Masdarolomoor F (2007) Novel nanostructured conducting polymer systems based on sulfonated polyaniline. Ph.D thesis, University of Wollongong, Wollongong, NSW.
50. Liu W, Cholli AL, Nagarajan R, Kumar J, Tripathy S, Bruno FF, Samuelson L (1999) J Am Chem Soc 121:11345
51. Wallace GG, Spinks GM, Teasdale PR (2002) Conductive electroactive polymers. CRC Press, London
52. Pron A, Rannou P (2002) Prog Polym Sci 27:135
53. McCall RP, Ginder JM, Leng JM, Ye HJ, Epstein AJ (1990) Phys Rev B 41:5202
54. Song E, Choi J-W (2013) Nanomaterials 3:498
55. Skotheim TA, Reynolds JR (2007) Handbook of conducting polymers. CRC Press, Boca Raton
56. Wen Z, Ci S, Mao S, Cui S, Lu G, Yu K, Luo S, He Z, Chen J (2013) J Power Sources 234:100
57. Belabed C, Abdi A, Benabdelghani Z, Rekhila G, Etxeberria A, Trari M (2013) Int J Hydrogen Energy 38:6593
58. Hidalgo DH, Hernandez SP, Bocchini S, Fontana G, Pirri CF (2013) Deposition of polyaniline in TiO_2 mesoporous film and its use as sensitizer for photocatalytic water splitting. In: International congress on materials and renewable energy. Athens, Greece, 1–3 July 2013. http://porto.polito.it/2519080/. Accessed 14 May 2015.
59. Zhao Z, Zhou Y, Wan W, Wang F, Zhang Q, Lin Y (2014) Mater Lett 130:150
60. Palmas S, Masciaa M, Vaccaa A, Llanosb J, Menab E, Rodrigo MA, Ampudia P (2014) Chem Eng Trans 41:337
61. Zhang S, Chen Q, Jing D, Wang Y, Guo L (2012) Int J Hydrogen Energy 37:791
62. Nsib MF, Saafia S, Rayes A, Houas A (2014) Sci Techol A—N°39. 107.

63. Mao A, Shin K, Kim JK, Wang DH, Han GY, Park JH (2011) ACS Appl Mater Interfaces 3:1852
64. Damian A, Omanovic S (2006) J Power Sources 158:464
65. Cutler C (2000) Electrochemical and photoelectrochemical studies of functionalised polythiophene. PhD thesis, University of Wollongong, Wollongong, NSW.
66. Bertho D, Jouanin C (1987) Phys Rev B 35:626
67. Koeckelberghs G, De Cremer L, Persoons A, Verbiest T (2007) Macromolecules 40:4173
68. Senthilkumar B, Thenamirtham P, KalaiSelvan R (2011) Appl Surf Sci 257:9063
69. Kim J, Sharma AK, Lee Y (2006) Mater Lett 60:1697
70. Brédas JL, Wudl F, Heeger AJ (1987) Solid State Commun 63:577
71. Valaski R, Moreira LM, Micaroni L, Hümmelgen A (2003) Braz J Phys 33:392
72. Hajian A, Rafati AA, Afraz A, Najafi M (2014) J Electrochem Soc 161:B196
73. Tsekouras G, Too CO, Wallace GG (2007) Synth Met 157:441
74. Moore GF, Blakemore JD, Milot RL, Hull JF, Song H, Cai L, Schmuttenmaer CA, Crabtree RH, Brudvig GW (2011) Energy Environ Sci 4:2389
75. Hagiwara H, Watanabe M, Daio T, Ida S, Ishihara T (2014) Chem Commun 50:12515
76. Chen J, Wagner P, Tong L, Wallace GG, Officer DL, Swiegers GF (2012) Angew Chem 124:1943
77. Gustafson MP, Clark N, Winther-Jensen B, MacFarlane DR (2014) Electrochim Acta 140:309
78. Aoki A, Naruse M, Abe T (2013) ChemPhysChem 14:2317

Chapter 12
Smart Biopolymers in Food Industry

Ricardo Stefani, Gabrielle L.R.R.B. Vinhal, Diego Vinicius do Nascimento, Mayra Cristina Silva Pereira, Paula Becker Pertuzatti, and Karina da Silva Chaves

Abstract Over the course of the last decade, significant interest in the use of biopolymers within the food industry as smart and active polymer systems has emerged. Such polymers have been successfully utilized to entrap micronutrients within microparticles and antioxidant packaging and have also been employed within food quality monitoring systems, such as active and intelligent packaging systems. The technologies that are associated with smart and active biopolymers have the potential to drive the development of a new generation of intelligent/active packaging systems that integrate food quality monitoring systems and microparticles in a manner that extends the shelf life of food products and their nutritional value. This chapter provides an in-depth review of the techniques that are typically employed in the preparation and characterization of smart and active biopolymers, films and microparticles, their potential applications within the food industry, and the challenges that are associated with their use and development.

Keywords Smart packaging • Microparticles • Biopolymers • Food safety • Antioxidants

12.1 Introduction

The food industry plays an important role in modern society, and manufacturing organizations have important responsibilities that extend far beyond the production and distribution of food products alone. This industry is also responsible for controlling the quality and safety of the products it manufactures and meeting consumer

R. Stefani (✉) • G.L.R.R.B. Vinhal • D.V. do Nascimento • M.C.S. Pereira
K. da Silva Chaves
Universidade Federal de Mato Grosso (UFMT), LEMAT, Av. Senador Valdon
Varjao 6390, Campus UFMT Barra do Garças, MT 78600-000, Brazil
e-mail: rstefani@ufmt.br

P.B. Pertuzatti
Laboratorio de Analise de Alimentos, UFMT
Campus UFMT Barra do Garças, MT 78600-000, Brazil

demand for nutritional food. It is critical that the industry produces foods that are of a sufficient quality and that this quality [1] can be assured from production line all the way through to the consumer's home. This places manufacturers under pressure to produce foods that have longer shelf lives. As such, a growing interest in the development of active and smart polymers that can prolong the amount of time a commodity can be stored has emerged. These polymers, which include biopolymers, can serve two primary uses. First, they can be used in the development of active films or in the microencapsulation of bioactive compounds that form part of an active packaging system that possesses antimicrobial and/or antioxidant properties [2]. Second, they can also be used to create chemical sensors that are capable of monitoring and indicating food spoilage.

Many studies have attempted to evaluate the antioxidant capacity and colorimetric properties of biopolymer films with the intention of developing technologies that can improve the effectiveness and efficiency of food packaging. For example, research in this area has focused on antioxidant packaging [3–8] colorimetric indicators [9–14], photochromic films [15], bacterial growth indicators [16], intelligent inks [17], oxidation indicators [18, 19], and the microencapsulation, stabilization, and release of bioactive compounds and nutrients [20–22]. Undoubtedly, biopolymer films and microparticles represent technologies that have numerous potential applications within the food industry. This chapter examines some of these applications and assesses the challenges associated with the development and use of smart polymers in the food industry.

12.2   Preparation of Smart Biopolymers

12.2.1   Preparation of Active and Smart Films for Food Packaging

The active and smart films that are used for food packaging are typically prepared using a casting technique that can produce films efficiently at a low cost. Briefly, hydrocolloid suspensions are prepared by suspending the required amount of biopolymer in distilled or deionized water. The suspension is then poured onto acrylic or glass plates and dried until weight is constant, at which point the films can be obtained. The casting technique has been successfully applied in the development of smart films that incorporate polyaniline [23], cassava starch/glycerol [24, 25], chitosan [13], chitosan/PVA [11, 26], and chitosan/starch [27]. Among the diverse biopolymers that have been successfully utilized in smart and active packaging, biopolymers, such as starches, gums, pectin, gelatin, and chitosan, are those that have demonstrated the greatest stability because they have the ability to form networks of structured and thermally stable copolymers. Furthermore, these polymers can form stable hydrocolloid suspensions. Casting, therefore, represents a versatile, inexpensive, rapid, and simple method of preparing films, and the effectiveness and

efficiency of this approach have been extensively covered in existing literature. Although other techniques, such as nanocomposites [28], layer by layer [29], and polymeric matrix [30], are also used to develop smart polymer films, the simple casting technique represents the method of choice for the production of new and improved smart polymer films because it does not require the use of complicated laboratory instruments. Another advantage of the casting technique is that it provides a method by which micromolecules can be readily incorporated into the polymeric film, simply by adding molecules, such as natural pigments that act as sensors, into the film-forming solution. Several forms of pigments, both natural [11, 26, 31] and artificial [32, 33], are currently used for the purpose of sensing dyes, and a large amount of research in this area has focused on the application of such pigments in alternative thin-film sensors [11, 26, 34, 35]. These pigments are usually solubilized in water, ethanol, or a mixture of both, and then added to the film-forming solution in an amount that varies, from 2 to 25 %, to form very sensitive final films.

Although active films are commonly manufactured through the use of a casting procedure, this approach does not represent a standard production method for antioxidant films [36]. However, as some studies have demonstrated, casting processes can produce materials that exhibit a reduced loss of antioxidant compounds in the film with respect to the nominal content. This is due to the fact that the manufacturing approach that is employed is less aggressive than that used in other techniques [37]. For example, the thermomechanical processes involved with alternative approaches, such as extrusion and co-extrusion multilayer films and laminates, cut off their material structure, consequently potentiating the degradation of the antioxidant compounds that are present in the system.

According to Rauwendaal [38], "to extrude" means to push or force out. Material is extruded when it is pushed through an opening. The part of the machine that contains the opening through which the material is forced is referred to as the extruder die. As material passes through the die, it acquires the shape of the die opening, although this shape does generally change to some extent as the material exits the die. There are two basic types of extruders: continuous and discontinuous or batch type.

Polymers are commonly processed using extrusion, which is also referred to as hot-melt extrusion in the industry, because this approach provides a continuous, quick, simple, and versatile operation by which raw materials can be transformed into finished products [39]. When the co-extrusion process is utilized, different polymers are pushed through the same die in order to produce a multilayer product that combines the properties (mechanical, optical, adhesion, barrier) of the different layers [40]. The film extrusion technique is currently used for the purposes of producing packaging because it lends itself well to large-scale manufacturing. Extrusion can be implemented as a continuous unit operation that allows producers to control temperature, size, shape, and moisture [41]. Furthermore, various processing parameters, such as screw speed, temperature, feeding rate, and screw configuration, can also be carefully controlled. However, even the smallest variations during processing can result in the production of very different products [42].

12.2.2   Microparticle Preparation

Many techniques are currently in use to produce microparticles. Encapsulation techniques can be divided into physical (spray drying, spray chilling, spray cooling, fluid bed coating, extrusion, freeze drying, and co-crystallization), chemical (interfacial polymerization), and physicochemical (simple and complex coacervation, ionotropic gelation, and liposomes) methods. To ensure that the most appropriate method is selected, manufacturers need to take into account processing and storage conditions, the type of the desired microcapsule (size and shape), properties of the carrier material, triggers and mechanisms of release, and cost and scale of production [43–45]. Of the factors described above, the properties of the carrier materials or wall materials represent very important parameters because they affect the stability of the microparticle and the efficiency of the microencapsulation. Spray drying, spray cooling, spray chilling, extrusion, emulsion, freeze drying, simple and complex coacervation, and liposomes are the techniques that are most commonly used to encapsulate food ingredients. Spray drying is one of the oldest of these encapsulation techniques and it is very popular in the food industry because it is economical, flexible, makes use of equipment that is readily available, and produces morphologically homogeneous microparticles. This technique uses a solution in a hot air stream to evaporate the solvent, which in the case of food applications is the water, before the dried particles are separated [44, 46, 47]. The parameter selection, such as types of atomizers (single-fluid, high-pressure spray nozzle or spinning disk), concentration and viscosity of the feed, and feed flow rate, can be used to control the particle size, which ranges from 5 to 80 μm [45–48]. This technique is most widely used to encapsulate flavors [49, 50], lipids [51], vitamins [52], bacteria [53], phenolic compounds [54], aroma [55], and heat-sensitive compounds because the particle is only exposed to hot air for a very short period of time.

Alternative encapsulation techniques that are similar to spray drying but involve slightly different processes include spray cooling and spray chilling. Both of these also involve dispersing encapsulating material in a liquid and then spray coating the material from a nozzle in a controlled environment to produce small droplets. The difference between these techniques and spray drying is that the wall material is dried using cold air, which enables the solidification of the particle [44, 47]. These techniques typically use lipids as carrier materials to encapsulate key ingredients, vitamins [56], and some flavors [57]. The extrusion technique is the most popular method of encapsulating probiotic bacteria because particle production is simple, it can be performed at relatively low temperatures, and it does not require the use of organic solvents. The extrusion technique involves adding food ingredients or probiotics to a hydrocolloid solution and then dripping this through a syringe needle or nozzle into a solution that promotes gelation. The size of the particles is influenced by the diameter of the needle or nozzle, flow rate and viscosity of the solution, and the properties of the gelling environment [44, 48].

Another common technique is emulsion. The food ingredient (discontinuous phase) is added to oil (continuous phase) and the mixture is homogenized to form two combinations of emulsion: water/oil or oil/water and water/oil/water. Once the emulsion has formed, this is then dispersed by adding $CaCl_2$ to form the particles within the oil phase [48, 58]. The particles are collected via centrifugation or filtration. As the speed of agitation controls the size of the beads, the particles can vary from 25 to 2 mm [44].

The freeze drying method is based on sublimation and involves a simple dehydration process that is completed under low temperature and low pressure. This technique has been used to encapsulate heat-sensitive compounds, as well as phenolic compounds [59], anthocyanins [60], flavor [61], and probiotics [62, 63]. The major disadvantages associated with this method are that it involves a long processing time and offers poor protection for the encapsulated substance due to the porous wall of the microparticle. Coacervation is a physicochemical method that is also referred to as phase separation. This technique involves the fluid-fluid phase separation of an aqueous polymeric solution, via which changes in the characteristics of the medium (temperature, ionic strength, pH, and polarity) result in a precipitation of wall material and a continuous coating of wall polymer around the core droplets. There are two types of coacervation: simple and complex. Simple coacervation involves only one polymer, and the separation phase occurs as a result of the addition of salt or through changes in the pH and/or temperature. Complex coacervation involves two polymers and phase separation occurs as a result of anion-cation interaction. This encapsulation process is very efficient, relatively simple, low cost, and can be used to encapsulate a range of different ingredients such as flavors [64], lipids [65], and others.

Liposome is an encapsulation technique that involves different methods of preparation to load the entrapped agents before or during the production of liposomes. During the manufacturing procedure, a mixture of the lipid/ingredient is dispersed in an organic solvent. The organic solvent is then removed via evaporation, and the dry lipidic film that is deposited on the flask wall is redisposed in aqueous media under agitation at a higher temperature than that of the lipid transition. The methods that are typically described in the literature for liposome preparation include thin-film hydration, or the Bangham method, detergent dialysis, solvent injection techniques, and reversed phase evaporation. Novel technologies that can be implemented on an industrial scale have been employed to prepare liposomes. These include supercritical fluid technology, dual asymmetric centrifugation, membrane contactor technology, cross-flow filtration technology, and freeze drying technology [66].

The major advantage of the use of liposome methods in the food industry is that liposome can be formed from natural ingredients such as egg, soy, dairy, or sunflower lecithin. Due to variations in the composition and structural properties of liposomes, they are extremely versatile and can be used to encapsulate enzymes [67], carotenoids [68], micronutrients [69], and other food ingredients.

12.3   General Characterization of Smart Biopolymers

Films and microparticles can be prepared using many types of biopolymers. The selection of the biopolymer or combination of biopolymers employed will determinate the physical, chemical, physicochemical, and functional properties of the films and microparticles. The spectroscopical, optical, thermal, and mechanical features are deemed to be the most important properties in the production of effective packaging polymers and microparticles [70]. A good biopolymer for packaging applications should have chemical and physical features that are comparable with those of commercially available packaging polymers; for example, they should offer thermal stability, water vapor permeability, and mechanical resistance. The size and charge of the microparticles are also of importance when considering the functional properties that impact the stability of the particle.

12.3.1   Spectroscopy Characterization

As the physical and chemical properties of a polymeric film depend on its chemical structure, spectroscopic characterization of the films and microparticles is important to determine their composition. The chemical structure of the polymeric films is often characterized through the use of UV-visible spectroscopy, X-ray photoelectron spectroscopy, fast Fourier transform infrared spectroscopy, and Raman spectroscopy. These techniques provide a picture of the functional groups that are present in the chemical structure and offer useful insights into the way they interact; for example, the presence of hydrogen bonds and cross-linking groups can predict some blend properties, such as mechanical resistance.

12.3.2   Morphology Characterization

Polymeric film morphological characterization is useful because it can identify defects in the microstructure of polymeric matrix that can affect the film properties. Four techniques that are commonly used in polymeric film morphological characterization are optical, atomic force microscopy (AFM), scanning electronic microscopy (SEM), and X-ray diffraction (XRD). Microscopy analysis provides useful composition and topology information about the microstructure and surface characteristics (e.g., porosity, presence of cracks, homogeneity, and smoothness). As such, microscopy can be useful in studies that aim to examine the structural integrity of the polymeric matrix.

12.3.3   Thermal Characterization

Differential scanning calorimetry (DSC) and thermogravimetric analysis (TG) are both thermoanalytical techniques that provide clear insights into the thermal stability of biopolymeric compounds and the way in which the microparticles and biopolymer blend components that are present in the films and microparticles interact, since these interactions can result in changes to the melting point of each component.

12.3.4   Mechanical Properties

In order to be used effectively in food packaging, it is important that thin polymeric films demonstrate good mechanical properties. The mechanical properties of these films can be determined through a variety of measurements including tensile strength, elongation at break, and Young's modulus. A biopolymer film that is suitable for food packaging applications will typically demonstrate mechanical properties that are comparable to the polymers that are in commercial use. These mechanical properties are measured using the method described in ASTM D1708-10 [71], which is suitable for determining the mechanical properties of plastics or the traction of films with thicknesses ranging from 0.0025 to 2.5 mm, which is sufficient for use in food packaging. The mechanical properties of the microparticles can be assessed using micropipette aspiration, particle poking, optical tweezers, nano-indention, and atomic force microscopy [72].

12.3.5   Characterization of Interaction with Water
and Humidity

The way in which the polymeric matrix interacts with water and humidity can be measured using water vapor permeability (WVP), which assesses how fast the polymeric matrix absorbs humidity and thus swells or reduces in size [13]. The WVP provides a good indication of how the polymeric matrix will behave when it interacts with pure water. That is, how fast the polymeric matrix will absorb the water. Both WVP and the swelling index, which is a measure of the mass of water swelled by the polymeric matrix, are often gravimetrically determined. The standard test method that is most commonly applied to measure WVP is the ASTM E96M-14 [73]. When this approach is employed, the samples are maintained in an environment in which the humidity and temperature are carefully controlled and during assay the samples are weighed at a specific time interval, until the weight becomes constant, and the changes in weight are plotted as a function of time. The final WVP is calculated according to Eq. 12.1:

$$WVP = \frac{w}{\theta} \cdot \frac{24t}{A\Delta p}$$

(12.1)

where w is the weight gain, θ is the time during which w occurred (hours), t is the sample thickness (mm), A is the test area (m^2), and Δp is the vapor pressure difference (kPa). For the swelling index (SI) assay, the samples are cut into slices and then stored in a desiccator with silica gel until constant weight is achieved. Following this procedure, the samples are weighed and then immersed in distilled water in beakers for different time intervals at room temperature. At each time interval, the samples are removed, dried, and weighed. The swelling index (SI %) is calculated according to Eq. 12.2:

$$SI = \frac{FinalWeight - IntialWeight}{FinalWeight} \cdot 100$$

(12.2)

12.3.6 Microparticle Size

Microparticle size is typically measured using the dynamic light scattering, static light scattering laser diffraction, and microscopy methods, which provide information about the release rate of the ingredients and insights into the microparticles that are present in the food matrix.

12.3.7 Microparticle Charge

Zeta potential (ζ-potential) analysis is often used to predict the stability of microparticles in suspension and its feasibility to aggregation and to study the interaction between oppositely charged biopolymers' wall on the microparticle, thus providing an indication of the electrostatic forces that act between the microparticles.

12.4 Antioxidant Carbohydrate Films

According to data published by the Food and Agriculture Organization of the United Nations [74], a third of all food produced worldwide was wasted in 2013. Their report estimated that 46 % of waste occurred at the processing, distribution, and consumption stages and claimed that this "downstream" wastage resulted in significant damage to the environment. As a direct result of consumers purchasing more

food than they need, a great deal of food is wasted in developed countries, and food that is perfectly edible and safe to eat is often thrown away.

Active packaging represents one method by which downstream food waste can be reduced [75]. Of the various active packaging technologies that are available, films that incorporate antioxidant compounds stand out. Many studies have aimed to evaluate the antioxidant capacity of films with the intention of developing these technologies for use in active packaging. It is generally recognized that incorporating antioxidant extracts in films can improve the shelf life of products and decrease oxidation in food that is rich in unsaturated fatty acids [65].

Extensive scientific research has been performed on the use of synthetic antioxidants, such as BHT, BHA, polyphenols, thioesters, and organophosphate in food packaging. There is a current lack of understanding in the use of natural antioxidants in food packaging. This is predominantly because some synthetic antioxidants have demonstrated physiological effects. As such, a large number of studies have examined the application of natural antioxidants as films (Table 12.1). The findings of much of this research indicate that many of these films exhibit beneficial effects when used in food packaging. These effects vary according to the type of food to which film is applied. For example, research that analyzed the peroxide value and hexanal levels revealed that when used with foods that contain high amounts of unsaturated fatty acids, such as nuts, a decrease in oxidation can be observed [86], while a further study that assessed thiobarbituric acid reactive substances (TBARS) and sensory evaluation in turkey meat also showed the positive effect of the film's application [5].

In addition to examining lipid oxidation, researchers have evaluated myoglobin oxidation in meat and fish products [5, 86, 87]. Furthermore, scientists have assessed how the enzymatic browning that is caused by the enzyme polyphenol oxidase present in oxygen converts phenolic compounds into dark-colored pigments that appear on the surface of fruits and vegetables [86].

Despite the large amount of scientific work on antioxidant films that has been produced in recent years, Cooksey [70] affirmed that much of the work on active packaging has remained at the research stage, although some developments have been commercialized. Among the antioxidant active packaging that has been commercialized, packaging that incorporates independent devices, such as a sachet that contains an oxygen scavenger, stands out. The most common oxygen scavenger in use incorporates iron or ferrous oxide in a fine powder, although other compounds can be used [36]. However, research in this area is lacking, and it is clear that further research on antioxidant films is necessary before they can be used commercially.

12.4.1 Characterization of Antioxidant Films

Antioxidants can be characterized in many different ways. Some authors [88] consider a broad definition of antioxidants to be as follows: "…any substance that when present at low concentrations compared with those of an oxidizable substrate

Table 12.1 Examples of antioxidant films

Antioxidant compound	Material	Preparation technique	Application	Reference
Oregano essential oil and green tea extract components	Ethylene vinyl alcohol	Casting	–	[76]
Sodium metabisulfite combined with citric acid, green tea extract, cinnamon essential oil, and purple carrot extract	Polyethylene terephthalate	Artibal S.A. (Sabiñánigo, Spain)	Fresh mushrooms (*Agaricus bisporus*)	[77]
Polyvinylpolypyrrolidone washing solution extract/rosemary extract	Low-density polyethylene	–	Beef	[3]
Curcuma ethanol extract	Pig skin gelatin type A	Casting	–	[4]
Grape pomace extract	Chitosan	Casting	–	[78]
Tocopherol	Low-density polyethylene	Extrusion	Salmon (*Salmo salar*)	[79]
Green tea extract, grape seed extract (proanthocyanidins), grape seed extract (polyphenols), ginger extract, gingko leaf extract	Fish skin (silver carp)	Casting	–	[80]
Oregano essential oil and green tea extract	Polyethylene terephthalate/polyethylene/ ethylene vinyl alcohol/polyethylene	Artibal S.A. (Sabiñánigo, Spain)	Foal meat	[81]
Marigold flower extract	Poly(lactic acid)	Extrusion	–	[82]
Essential oils (garlic, clove, and oregano)	Fish protein	Casting	–	[83]
Rosemary extract	Low-density polyethylene		Chicken meat	[84]
Barley husk extract	Low-density polyethylene	–	Frozen blue shark	[85]

significantly delays or inhibits oxidation of that substrate…" [89]. Thus, when applied to films, antioxidants function to delay the auto-oxidation of fats and/or inhibit oxidation of pigments. The extent to which an antioxidant will be effective when used in a packaging system depends not only on its chemical reactivity toward free radicals but also on additional factors such as the compatibility between the antioxidant compound and the packaging material, as well as the compatibility of the antioxidant and the food. Thus, it is crucial that the polymer that is used in the antioxidant film takes into consideration key characteristics such as polarity, viscosity, pH, and other barrier properties. Once antioxidants are released into the food, the solubility of the antioxidant can determine its effectiveness. As such, the selection of the most appropriate antioxidant should take into consideration the type of food to be packaged [36].

Many methods that are based on mechanisms, free radicals, or different reactive species can be used to determine and quantify the extent to which a film, or material incorporated in a film, has antioxidant capacity. Furthermore, it is important to take into consideration the fact that when a plant extract is incorporated into a film, the extract itself may have several compounds, each of which may present different antioxidant mechanisms. It is, therefore, necessary to use different analytical methods to evaluate the antioxidant capacity of a given film.

Moon and Shibamoto [90] identified two types of methods that can be used to classify antioxidant capacity: chemical and biological. Chemical methods involve the use of analytical instruments, such as a spectrophotometer, chromatographer, and chromatography/mass spectrometer, and the other involves the use of biological assay, such as enzyme-linked immunosorbent assay (ELISA). Of the various methods that are available, chemical approaches, in particular spectrophotometric methods, are most commonly used in determining the antioxidant capacity of films. Roginsky and Lissi [59] further divided these methods into two subdivisions: indirect and direct. Indirect approaches focus on examining the extent to which the antioxidant can scavenge free radicals, something that is not associated with oxidative degradation or the effects of transient metals. However, H-donating capacity does correlate with antioxidant capacity. Examples of some of the indirect methods that are used to determine the antioxidant capacity of films are: ABTS, 2, 2-diphenyl-1-picrylhydrazyl (DPPH) radical scavenging capacity assay, and ferric reducing antioxidant power (FRAP). Direct methods, such as the β-carotene/linoleic acid model system and oxygen radical absorbance capacity (ORAC) assays, are typically associated with studies on chain peroxidation [75].

Among the indirect and direct methods mentioned above, there is a chemical differentiation on the principle of the method. As a result, major antioxidant capacity assays can be roughly divided into two categories: single electron transfer (ET) reaction-based assays, where some of the most useful methods are the FRAP assay and the ABTS assay, also known as the trolox equivalent antioxidant capacity assay (TEAC method); and hydrogen atom transfer (HAT) reaction-based assays, examples of which are ORAC and the β-carotene/linoleic acid model system [36, 91, 92]. The difference between both categories involves the chemical reaction that is utilized.

The ET-based assays involve one redox reaction with the oxidant as an indicator of the reaction endpoint. In other words, to perform these assays it is necessary that two components are present in the reaction mixture: antioxidants and oxidants (also the probe). When the oxidant extracts an electron from the antioxidant, the probe changes color. The HAT-based assays, on the other hand, normally occur between antioxidants and peroxyl radicals and the hydrogen atom donating capacity is quantified [91]. Furthermore, some antioxidant capacity methods utilize both HAT and ET mechanisms, an example of one such method is 2, 2-diphenyl-1-picrylhydrazyl (DPPH) assay [36].

12.5 Colorimetric Time-Temperature Indicator Films for Food Packaging Systems

Time-temperature indicator (TTI) films are among the most promising intelligent packaging systems that are currently available for use in the food industry. TTI films can safely provide the manufacturer or consumer with a real-time indication of the conditions of the food throughout processing, transportation, and storage. Furthermore, these films are promising because they are low cost and provide a visual indication of the condition of the food. The basic concept behind TTIs takes into consideration the fact that many food products deteriorate due to changes in temperature, which cause chemical reactions and microbial growth. These changes in temperature can be detected through the use of a TTI film. Several types of TTI, such as colorimetric [9, 12, 13, 16], radio frequency [93], photochromic [15], bacterial growth kinetic sensor [16], intelligent inks [17], oxygen indicators [18, 19], and nanotechnology sensor systems, have been developed and successfully tested both in academia and in the industry. Of these systems, colorimetric TTI systems, which can provide a response via a change in color in accordance with the pH changes of the product, provide information about the conservation and actual quality of a food in a visual and intuitive way. These systems have grown in importance and diversity because of their low cost, simplicity, and reliability. In addition to offering a simple solution, the common features of such systems is that they are based on biodegradable polymeric films and pH indicator dyes; thus, they do not rely on expensive analytical instruments. These types of smart biopolymer sensors have been successfully utilized in many food packaging applications. Wu et al. [12] developed a TTI system that was based on urease. This device can indicate temperature changes from 5 to 30 °C through color changes [12]. Existing literature also describes the use of colorimetric TTI to provide an indication of the quality of meat and fish products [14, 24, 26, 88]. Freshness indicators that measure the volatile compounds produced by microorganisms, such as carbon dioxide [94] and volatile nitrogen bases [9], have also been successfully employed.

There is a distinct need in the food industry for environmentally friendly packaging systems that can provide accurate real-time indicators of the quality of food. Colorimetric TTIs that are based on the use of carbohydrate polymers as a supporting

matrix with indicator dyes have been developed and are well established in literature. The following section will report on the preparation and characterization techniques that are typically involved in such systems.

12.5.1 Film Characterization

In order to evaluate the potential use of biopolymer and copolymer blends in food packaging applications, it is necessary to physically and chemically characterize them. Although biopolymers are nontoxic and biodegradable, which makes them potentially environmentally friendly, they have high water vapor permeability and low mechanical/thermal resistance. This limits the extent to which they can be used in smart food packaging. In order to overcome these limitations, biopolymers are often combined as blends that offer better features than pure biopolymers in order to ensure that the film is suitable for use in food packaging. Colorimetric TTI films are characterized according to the features discussed in Sect. 12.3. As the color change dynamic is also an important parameter, the dynamic parameters of color should also be evaluated because this parameter indicates how the film color changes and assesses the extent to which these changes can be detected by the naked eye.

12.5.1.1 Dynamic Parameters of Color

The color parameters of the film are determined using a UV-Vis color measurement spectrophotometer. Tests are performed in triplicate, and the total color values of L* (lightness), a* (red–green) and b* (yellow–blue) are registered. The color differences are obtained according to Eq. 12.3:

$$\Delta \mathbf{E} = \left(\left(\Delta L^* \right)^2 + \left(\Delta a^* \right)^2 + \left(\Delta b^* \right)^2 \right)^2 \tag{12.3}$$

where $\Delta L^* = L^* - L_0*$, $\Delta a^* = a^* - a_{0*}$ and $\Delta b^* = b^* - b_0* L0*$, and $a0_*$ and $b0_*$ are the initial color values of the sensing films.

12.6 Microencapsulation

Microencapsulation has been widely used to protect encapsulated materials from the adverse conditions of processing and storage of food. In packaging applications, this technology consists of active substances that use a thin polymer coating as a protective film that is applied to the liquid, solid, or gaseous material [95, 96]. In food science, this technology has been seen as a promising method of overcoming the limitations associated with the instability of several of the substances that are typically incorporated into food, such as micronutrients [97, 98], enzymes [99], flavor [98], probiotics [53, 96, 100], antioxidants, and antimicrobial agents [101, 102].

Research indicates that microencapsulation has the potential to reduce the effect of the interaction between bioactive compounds and the product and increases the product's bioavailability after ingestion. Microencapsulation is well established in the modern-day food industry, and many different methods and biopolymers can be used to microencapsulate food items. Several studies have demonstrated how the microencapsulation of ingredients can improve stability in final products as well as during processing. For example, probiotic *Lactobacillus acidophilus* has been successfully encapsulated in the microparticles of pectin and whey protein via a combination of ionotropic gelation and complex coacervation [103]. In one study, the probiotic encapsulated in stirred yogurt demonstrated lower post-acidification and higher survival rates than those stored as free cells after 35 days of refrigerated storage. The encapsulated product also demonstrated higher survival during simulated gastrointestinal conditions and no significant difference in the sensory characteristics (appearance, aroma, flavor, and overall impression) was observed for both samples. Only the attribute of texture for the yogurt containing probiotic encapsulated exhibited less than acceptable feedback when compared to the yogurt containing free cells, and this may be due to the size of the microparticle (253.3 μm). The acceptability of biopolymer microparticles in food products is influenced by their perception within the mouth, and this can be influenced by the size, morphology, or hardness of the microparticles [72, 102]. In one study, pomegranate peel phenolics were successfully encapsulated using spray drying before being added as a functional ingredient to ice cream [104]. The results of this study indicated that processing had no effect on the antioxidant activity of the encapsulated extract. Furthermore, sensory evaluation showed more than 75 % of the panelists accepted the phenolic-enriched ice creams. Another example of the application of encapsulated ingredients in food demonstrated the protective effect of microparticles and indicated that the compounds were more stable during processing and storage when different methods and wall materials were used [69, 96, 99, 105–107].

There is an increasing demand for nutritious and healthy foods as key players in the food industry have invested significant amounts of money researching and developing microparticles that can add value to their final product. A wide range of encapsulated products have been developed, manufactured, and marketed, and these include dairy products, breads, chewing gum, chocolate, juices, and meat products.

12.7 Conclusion

The food industry has been searching for new technologies in order to produce high-quality products. Smart and active packaging and microencapsulation are technologies that have been extensively applied with the aim of supporting the growing demand for high-quality products. In this manner, the development of new technologies and the concern with cost reduction can drive the application of new smart materials for the conservation and monitoring of food products, from the production to the final consumer.

References

1. Jokerst JC, Adkins JA, Bisha B, Mentele MM, Goodridge LD, Henry CS (2012) Anal Chem 84:2900–2907
2. Bhattarai J, Sharma A, Fujikawa K, Demchenko AV, Stine KJ (2015) Carbohydr Res 405:55–65
3. Barbosa-Pereira L, Cruz JM, Sendón R, Quirós ARB, Ares A, Castro-López M, Abad MJ, Maroto J, Paseiro-Losada P (2014) Food Control 31:236–246
4. Bitencourt CM, Fávaro-Trindade CS, Sobral PJA, Carvalho RA (2014) Food Hydrocoll 40:145–152
5. Contini C, Allvarez R, Sullivan MO, Dowling DP, Gargan SO, Monahan FJ (2014) Meat Sci 96:1171–1176
6. Ramos M, Beltrán A, Peltzer M, Valente AJ, Garrigós MDC (2014) LWT Food Sci Technol 58:470–477
7. Sies H, Stahl W (1995) Am J Clin Nutr 62:1315S–1321S
8. Tongnuanchan P, Benjakul S, Prodpran T (2013) J Food Eng 117:350–360
9. Pacquit A, Frisby J, Diamond D, Lau K, Farrell A, Quilty B (2007) Food Chem 102:466–470
10. Pacquit A, Lau KT, McLaughlin H, Frisby J, Quilty B, Diamond D (2006) Talanta 69:515–520
11. Pereira VA, de Arruda INQ, Stefani R (2015) Food Hydrocoll 43:180–188
12. Wu D, Wang Y, Chen J, Ye X, Wu Q, Liu D, Ding T (2013) Food Control 34:230–234
13. Yoshida CM, Maciel VBV, Mendonça MED, Franco TT (2014) LWT Food Sci Technol 55:83–89
14. Zhang X, Lu S, Chen X (2014) Sens Actuators B Chem 198:268–273
15. Kreyenschmidt J, Christiansen H, Hübner A, Raab V, Petersen B (2010) Int J Food Sci Technol 45:208–215
16. Zhang C, Yin A-X, Jiang R, Rong J, Dong L, Zhao T, Sun L-D, Wang J, Chen X, Yan CH (2013) ACS Nano 7:4561–4568
17. Mills A (2005) Chem Soc Rev 34:1003–1011
18. Eaton K (2002) Sens Actuators B Chem 85:42–51
19. Vu CHT, Won K (2013) Food Chem 140:52–56
20. Lam P, Gambari R (2014) J Control Release 178:25–45
21. Madene A, Jacquot M, Scher J, Desobry S (2006) Int J Food Sci Technol 41:1–21
22. Rutz JK, Zambiazi RC, Borges CD, Krumreich FD, da Luz SR, Hartwig N, da Rosa CG (2013) Carbohydr Polym 98:1256–1265
23. Garcia M, Pinotti A, Martino M, Zaritzky N (2004) Carbohydr Polym 56:339–345
24. Golasz LB, da Silva J, da Silva SB (2013) Ciênc Tecnol Aliment 33:155–162
25. Kuswandi B, Jayus A, Restyana A, Abdullah A, Heng LY, Ahmad M (2012) Food Control 25:184–189
26. Silva-Pereira MC, Teixeira JA, Pereira-Júnior VA, Stefani R (2015) LWT Food Sci Technol 61:258–262
27. Vásconez MB, Flores SK, Campos CA, Alvarado J, Gerschenson LN (2009) Food Res Int 42:762–769
28. Qureshi UK, Karthikeyan MA, Karthikeyan SP, Ahmed KP, Sudhir U, Pakistan M (2012) J Food Sci 22:23–31
29. Brasil I, Gomes C, Puerta-Gomez A, Castell-Perez M, Moreira R (2012) LWT Food Sci Technol 47:39–45
30. Marek P, Velasco-Veléz JJ, Haas T, Doll T, Sadowski G (2013) Sens Actuators B Chem 178:254–262
31. Chigurupati N, Saiki L, Gayser C, Dash AK (2002) Int J Pharm 241:293–299
32. Kim MJ, Jung SW, Park HR, Lee SJ (2012) J Food Eng 113:471–478
33. Salinas Y, Ros-Lis JV, Vivancos J-L, Martínez-Máñez R, Marcos MD, Aucejo S, Herranz N, Lorente I (2012) Analyst 137:3635–3643

34. Shahid M, ul-Islam S, Mohammad F (2013) J Clean Prod 53:310–331
35. Veiga-Santos P, Ditchfield C, Tadini CC (2010) J Appl Polym Sci 120:1069–1079
36. Gómez-Estaca J, de Dicastillo CL, Hernández-Muñoz P, Catalá R, Gavara R (2014) Trends Food Sci Technol 35:42–51
37. de Dicastillo CL, Alonso JM, Catala R, Gavara R, Hernandez-Munoz P (2010) J Agric Food Chem 58:10958–10964
38. Rauwendaal C (2014) Polymer extrusion, 5th edn. Carl Hanser Verlag, Munich
39. Sauceau M, Fages J, Common A, Nikitine C, Rodier E (2011) Prog Polym Sci 36:749–766
40. Mahdaoui O, Laure P, Agassant J-F (2013) J Nonnewton Fluid Mech 195:67–76
41. Gómez-Guillén M, Pérez-Mateos M, Gómez-Estaca J, López-Caballero E, Giménez B, Montero P (2009) Trends Food Sci Technol 20:3–16
42. Hanani ZN, O'Mahony JA, Roos YH, Oliveira PM, Kerry J (2014) Food Packag Shelf Life 2:91–101
43. Levi S, Rac V, Manojlovi V, Raki V, Bugarski B, Flock T, Krzyczmonik KE, Nedovi V (2011) Procedia Food Sci 1:1816–1820
44. Martín MJ, Lara-Villoslada F, Ruiz MA, Morales ME (2015) Innov Food Sci Emerg Technol 27:15–25
45. Shahidi F, Han X (1993) Crit Rev Food Sci Nutr 33:501–547
46. Gharsallaoui A, Roudaut G, Chambin O, Voilley A, Saurel R (2007) Food Res Int 40:1107–1121
47. Shewan HM, Stokes JR (2013) J Food Eng 119:781–792
48. Nazzaro F, Orlando P, Fratianni F, Coppola R (2012) Curr Opin Biotechnol 23:182–186
49. de Barros Fernandes RV, Marques GR, Borges SV, Botrel DA (2014) Ind Crop Prod 58:173–181
50. Krishnan S, Kshirsagar A, Singhal R (2005) Carbohydr Polym 62:309–315
51. Aghbashlo M, Mobli H, Madadlou A, Rafiee S (2012) Food Res Int 49:379–388
52. Donhowe EG, Flores FP, Kerr WL, Wicker L, Kong F (2014) LWT Food Sci Technol 57:42–48
53. Maciel G, Chaves K, Grosso C, Gigante M (2014) J Dairy Sci 97(4):1991–1998
54. Fang Z, Bhandari B (2012) Food Res Int 48:478–483
55. da Costa JMG, Silva EK, Hijo AACT, Azevedo VM, Malta MR, Alves JGLF, Borges SV (2015) Powder Technol 274:296–304
56. Gamboa OD, Gonçalves LG, Grosso CF (2011) Procedia Food Sci 1:1732–1739
57. Sillick M, Gregson CM (2012) LWT Food Sci Technol 48(1):107–113
58. Heidebach T, Först P, Kulozik U (2012) Crit Rev Food Sci 52:291–311
59. Roginsky V, Lissi E (2005) Food Chem 92:235–254
60. Khazaei KM, Jafari S, Ghorbani M, Kakhki AH (2014) Carbohydr Polym 105:57–62
61. Kaushik V, Roos YH (2007) LWT Food Sci Technol 40:1381–1391
62. Dianawati D, Mishra V, Shah NP (2013) Food Res Int 51:503–509
63. Martin-Dejardin F, Ebel B, Lemetais G, Minh HNT, Gervais P, Cachon R, Chambin O (2013) Eur J Pharm Sci 49:166–174
64. Jun-xia X, Hai-yan Y, Jian Y (2011) Food Chem 125:1267–1272
65. Wang B, Adhikari B, Barrow CJ (2014) Food Chem 158:358–365
66. Huang Z, Li X, Zhang T, Song Y, She Z, Li J, Deng Y (2014) Asian J Pharm Sci 9:176–182
67. Kheadr EE, Vuillemard J, El-Deeb S (2003) Food Res Int 36:241–252
68. Xia S, Tan C, Zhang Y, Abbas S, Feng B, Zhang X, Qin F (2015) Colloids Surface B Biointerfaces 128:172–180
69. Abbasi S, Azari S (2011) Int J Food Sci Technol 46:1927–1933
70. Cooksey K (2010) In: Robertson GL (ed) Food packaging and shelf life: a practical guide. Taylor & Francis, London, pp 367–381
71. ASTM Standard D1708-13 (2013) Standard test method for tensile properties of plastics by use of microtensile specimens. In: ASTM International, West Conshohocken, PA. doi: 10.1520/D1708, www.astm.org. (Last Accessed: May 2015)
72. Joye IJ, McClements DJ (2014) Curr Opin Colloid Interface Sci 19:417–427

73. ASTM E96/E96M-14 (2014) Standard test methods for water vapor transmission of materials. In: ASTM International, West Conshohocken, PA. doi: 10.1520/E0096_E0096M-14, www.astm.org. (Last Accessed: May 2015)

74. FAO (2013) OCDE-FAO El desperdicio de alimentos daña al clima, el agua, la tierra y la biodiversidad.

75. Robertson GL (2006) Food packaging and shelf life, 2nd edn. CRC Press, London

76. Muriel-Galet V, Cran MJ, Bigger SW, Hernández-Muñoz P, Gavara R (2015) J Food Eng 149:9–16

77. Wrona M, Bentayeb K, Nerín C (2015) Food Control 54:200–207

78. Ferreira AS, Nunes C, Castro A, Ferreira P, Coimbra MA (2014) Carbohydr Polym 113:490–499

79. Barbosa-Pereira L, Cruz JM, Sendon R, de Quiros ARB, Ares A, Castro-Lopez M, Abad MJ, Maroto J, Paseiro-Losada P (2013) Food Control 31:236–243

80. Li J-H, Miao J, Wu J-L, Chen S-F, Zhang Q-Q (2014) Food Hydrocoll 37:166–173

81. Lorenzo JM, Batlle R, Gomez M (2014) LWT Food Sci Technol 59:181–188

82. Samsudin H, Soto-Valdez H, Auras R (2014) Food Control 46:55–66

83. Teixeira B, Marques A, Pires C, Ramos C, Batista I, Saraiva JA, Nunes ML (2014) LWT Food Sci Technol 59:533–539

84. Bolumar T, Andersen ML, Orlien V (2011) Food Chem 129:1406–1412

85. de Abreu DAP, Losada PP, Maroto J, Cruz JM (2011) Innov Food Sci Emerg Technol 12(1):50–55

86. Bonilla J, Atarés L, Vargas M, Chiralt A (2012) J Food Eng 110:208–213

87. López-Caballero M, Gómez-Guillén M, Pérez-Mateos M, Montero P (2005) Food Hydrocoll 19:303–311

88. Shukla V, Kandeepan G, Vishnuraj MR (2015) Food Anal Methods. doi:10.1007/s12161-014-0066-6

89. Halliwell B, Gutteridge J (1989) Free radicals in biology and medicine, 2nd edn. Oxford University Press, Oxford

90. Moon J-K, Shibamoto T (2009) J Agric Food Chem 57(5):1655–1666

91. Huang D, Ou B, Prior RL (2005) J Agric Food Chem 53:1841–1856

92. Pertuzatti PB, Barcia MT, Rodrigues D, da Cruz PN, Hermosín-Gutiérrez I, Smith R, Godoy HT (2014) Food Chem 164:81–88

93. Wang T, Zhang J, Zang X (2010) Afr J Biotechnol 9:6146–6151

94. Nopwinyuwong A, Trevanich S, Suppakul P (2010) Talanta 81(3):1126–1132

95. Anal AK, Singh H (2007) Trends Food Sci Technol 18:240–251

96. Shoji A, Oliveira A, Balieiro J, Freitas O, Thomazini M, Heinemann R, Okuro P, Favaro-Trindade C (2013) Food Bioprod Process 91:83–88

97. Nesterenko A, Alric I, Silvestre F, Durrieu V (2014) Food Hydrocoll 38:172–179

98. Wang J, Cao Y, Sun B, Wang C (2011) Food Chem 127:1680–1685

99. Anjani K, Kailasapathy K, Phillips M (2007) Int Dairy J 17:79–86

100. Gebara C, Chaves KS, Ribeiro MCE, Souza FN, Grosso CR, Gigante ML (2013) Food Res Int 51:872–878

101. Betz M, Kulozik U (2011) Procedia Food Sci 1:2047–2056

102. Betz M, Steiner B, Schantz M, Oidtmann J, Mäder K, Richling E, Kulozik U (2012) Food Res Int 47:51–57

103. Ribeiro MCE, Chaves KS, Gebara C, Infante FN, Grosso CR, Gigante ML (2014) Food Res Int 66:424–431

104. Çam M, Içyer NC, Erdoğan F (2014) LWT Food Sci Technol 55:117–123

105. Estrada J, Boeneke C, Bechtel P, Sathivel S (2011) J Dairy Sci 94:5760–5769

106. Ezhilarasi P, Indrani D, Jena B, Anandharamakrishnan C (2013) J Food Eng 117:513–520

107. Gupta C, Chawla P, Arora S, Tomar S, Singh A (2015) Food Hydrocoll 43:622–628

Chapter 13
Designing Self-Healing Polymers by Atom Transfer Radical Polymerization and Click Chemistry

Bhaskar Jyoti Saikia, Dhaneswar Das, Pronob Gogoi, and Swapan Kumar Dolui

Abstract The development of smart self-healing polymeric materials and composites has been the subject of a tremendous amount of research over last few years. When self-healing materials are mechanically damaged, either internally (via crack formation) or externally (by scratching), they have the ability of restoring their original strength and recovering their inherent properties. For polymers to exhibit such a healing ability, they must contain some functionality which will either rebound among themselves or have the ability of coupling with other functionalities. Preparation of such multifunctional and well-defined macromolecules requires a smart selection of a controlled polymerization technique in combination with appropriate coupling reactions. Among all the polymerization techniques introduced so far, atom transfer radical polymerization (ATRP) is the most versatile owing to its exceptional properties like preparation of polymer with predetermined molecular weight, narrow polydispersity index, predetermined chain-end functionality, and tunable architecture. Click chemistry is an extremely powerful coupling approach which in combination with ATRP can be used for generation of polymers with almost all of the desired properties. In this chapter, an overview on the use of ATRP and click chemistry for polymerization of various "clickable" monomers using "clickable" ATRP initiators is provided along with other post-polymerization modification strategies that can be used to construct macromolecules with self-healing ability.

Keywords Self-healing polymers • ATRP • Click chemistry

B.J. Saikia • D. Das • P. Gogoi • S.K. Dolui (✉)
Department of Chemical Sciences, Tezpur University, Napaam, Assam, India
e-mail: swapandolui@gmail.com

13.1 Introduction

Inspired by nature's most remarkable features of self-repairing, the development of self-healing polymeric materials has been a subject on the frontier of research over the last decade [1–3]. Presently humanity is in an age of plastic. Polymers and their composites are used in almost every material used by modern society. However, these materials are susceptible to damage which is induced by chemical, mechanical, UV radiation, thermal, or a combination of these factors [4]. Whenever these polymeric materials become damaged, only a few methods are available to extend their service life. Manual repairing methods are insufficient in restoring the original properties of the material and require continuous monitoring when implementing. However, it is believed that a vast majority of structural failure results from the propagation of initial microcracks. Eventually if repairs can be made at the micro-level, the lifetime of the materials can be significantly enhanced. Currently, development of automatic or self-healing materials is of prime importance where it can self-repair itself immediately after even invisible microcracks are formed. Self-healing materials when damaged mechanically, either externally or internally, have the ability of healing the damage automatically, restoring its original strength. These smart polymers are gaining wide appeal in various applications such as biomedicine, electronics, paints and surface coatings, robotics, etc. Encapsulation of monomers/catalysts to polymer matrix, dynamic covalent bond formation, and supramolecular self-assembly are the prevailing adopted strategies for preparing self-healing polymers [3, 5–11]. Among various approaches investigated, in order to attain polymers exhibiting such behavior, ATRP and click chemistry are the most versatile means for tailoring the functionality of a polymer toward effective self-healing [12–15]. This chapter is based on the progress made in the methods of synthesis for self-healing polymers by ATRP and click chemistry while also providing a comprehensive discussion of click chemistry approaches to generate self-healing polymers.

13.2 Application of ATRP for Designing Self-Healing Polymers

At present, functional polymers with complex architecture are of considerable interest due to their wide range of applications, beginning with structural all the way to electronic applications. ATRP is the most versatile controlled radical polymerization technique, as it furnishes the simplest route in the design and synthesis of a large variety of well-defined polymers with predetermined molecular weight, narrow molecular weight distribution, and high degree of chain-end functionalities [16–19]. The role of ATRP in the synthesis of functional polymers makes it an exceptionally useful polymerization technique compared to ionic polymerization techniques. It has been effectively applied in the preparation of polymers with precisely controlled

functionalities, topologies, and compositions [20]. This broadens the range of monomers that can be polymerized or copolymerized via ATRP and provides the ability for the straightforward introduction of various functionalities into a polymer structure. In general, there are four major strategies for the synthesis of telechelic polymers with functional groups via ATRP:

1. By using functional initiators
2. Substitution of the terminal halogen atom with nucleophile
3. Polymerization of functional monomers
4. Polymerization of "protected" monomers, followed by post-polymerization chemical transformations

While using the first two approaches, chain-end-functionalized polymers can be harvested as the last two methods yield polymers with multiple functionalities along their backbone. Therefore, it is very convenient to apply ATRP when designing self-healing polymers as healing requires special functionalities within the polymers; typically it is nearly impossible to introduce a moiety into the polymer's backbone or chain end via other polymerization techniques.

Although numerous methods are currently available for the design of self-healing polymers and polymer composites, focus will be placed upon the strategies set forth by ATRP and click chemistry. There are three major categories of self-healing polymers or composites which can be prepared by ATRP [21]:

1. Automatic one-component self-healing polymers
2. Self-healing by semi-encapsulation methods
3. Self-healing by encapsulation method

An illustration of all the above processes is shown in Fig. 13.1.
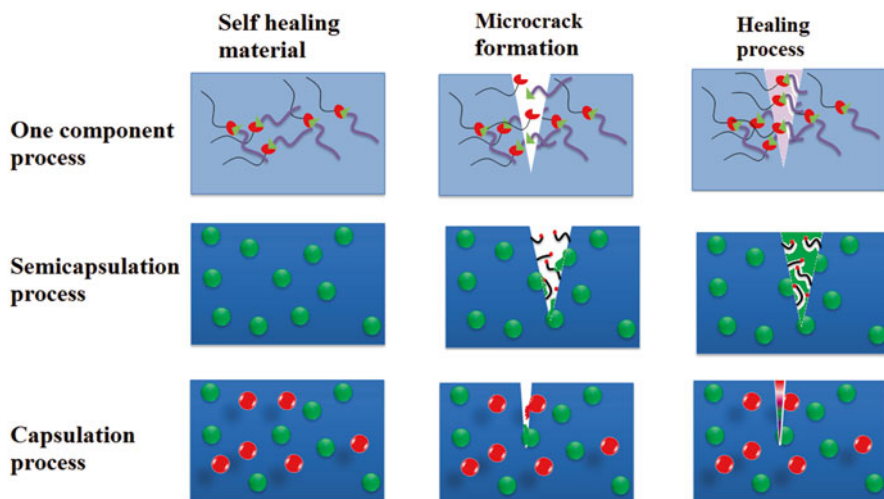
Fig. 13.1 Various approaches for synthesis of self-healing polymers

13.2.1 Automatic One-Component Self-Healing Polymers

The development of polymeric materials that automatically repair themselves after mechanical damage would significantly improve the safety, lifetime, energy efficiency, and environmental impact of these materials [22–24]. Most approaches to activating self-healing materials require an external stimulus like energy, solvent, healing agents, or plasticizers. Intrinsic self-healing materials utilize reversible chemical bonds (non-covalent and covalent) which allows for the design of single-component self-healing materials. Intrinsic self-healing mechanisms can be classified into the following two categories [21]:

1. Self-healing by reversible non-covalent bond formation
2. Self-healing by covalent bond formation

ATRP can be successfully applied in the design of all of the above categories of intrinsic self-healing polymers, as it is the most flexible polymerization method in regard to functionality and architecture.

13.2.2 ATRP for Designing Reversible Non-covalent Bond-Forming Material

The main advantage of self-healing polymers based on non-covalent bond formation is that they are reversible which allows them to heal themselves repeatedly in the same place; therefore, the recovery of the material's properties is inherent to the material's abilities. This type of polymer employs various non-covalent bonds such as hydrogen bonding, ionomers, π–π stacking, and others [25–27] to form a supramolecular network. While weak when singled out, the collaborative effort put forth by a group of these bonds creates a dynamic load-bearing structure at ambient temperature, thus enabling autonomic damage healing to take place. However, the molecular dynamics of these networks need a great deal of plasticization, as well as the single-phase dynamic assembly of small oligomers. As such, this technique can only be utilized in low-modulus rubber purposes. A balance between dynamic healing and mechanical stiffness properties is necessary when designing supramolecular systems. Intense relationships between the two produce an unyielding but less dynamic network while a weak relationship produces a soft yet dynamically healing system [28]. ATRP can be successfully applied to design a single-phase dynamic polymer chain that contains both stiff and flexible moieties in the same molecule (Fig. 13.2).

Thus a useful method for developing self-healing polymers is by incorporating reversible non-covalent hydrogen-bonding moieties into the polymer structure. Yulin Chen and his coworkers [28] have demonstrated a novel multiphase design methodology for an autonomic responsive healing system that can impart crucial mechanical properties (e.g., high modulus, high elasticity, and toughness) via
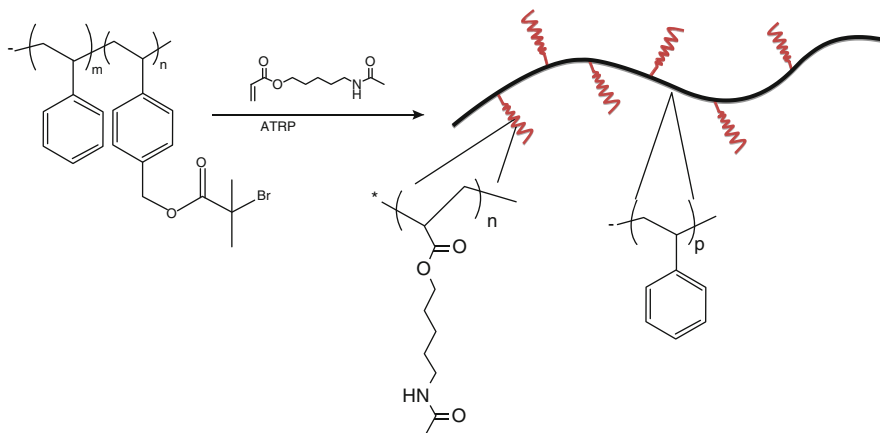
Fig. 13.2 An intrinsic self-healing polymer with a stiff backbone of polystyrene along with flexible side chain [28]

hydrogen bonding and ATRP. The research team was able to repair, on demand and without any external intervention, a single-component solid material.

π–π interactions are associated with the interaction between the π-orbitals of a molecular system. Self-healing materials based on aromatic π–π stacking interactions can be synthesized combining π-electron-rich (e.g., pyrenyl) and π-electron-poor (e.g., diimide) moieties in the same polymer chain [29]. π–π stacking interactions can also be achieved by preparing end-capped π-electron-deficient groups with other π-electron-rich aromatic backbones [30]. Since end-capped polymers can be achieved by using relevant initiators via ATRP, it is a useful method in the preparation of self-healing polymers with π–π stacking. Post-polymerization modification of polymer chains prepared by ATRP or the preparation of various shapes of polymers such as heteroarmed stars or brushes can also fulfill these requirements. Heteroarmed star polymers designed by ATRP are especially advantageous when designing a self-healing polymer with substantial π–π interactions. The use of dynamic bonds in self-healing polymeric systems allows for the restoration of the chemical structure and mechanical properties multiple times. In this respect, the use of ionomers represents a promising approach. Ionomeric copolymers are a class of polymer which contains ionic segments (normally not more than 20 %) that can form clusters that act as reversible cross-links [30]. These clusters can be activated by external stimuli such as temperature or ultraviolet (UV) irradiation. Since the formation of the clusters is reversible, multiple local healing events are possible. The heat generated during projectile damage can act as the trigger for a self-healing event when using this type of polymer. Direct ATRP is less applicable when synthesizing this type of polymer, but post-polymerization modification methods can be employed. For example N. Hohlbein et al. [31] reported a model system based on the copolymers of n-butyl acrylate and a varying fraction of t-butyl acrylate which was prepared by ATRP with adjustable molecular weight and a
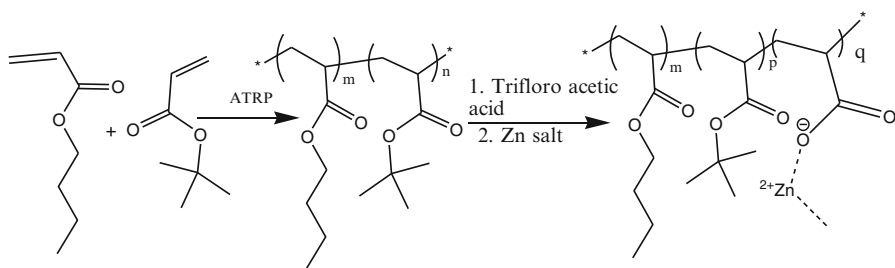
Scheme 13.1 Schematic representation of formation of ionomers by ATRP

narrow molecular weight distribution. Carboxylic acid moieties were formed by hydrolysis of the t-butyl acrylate moiety that was subsequently neutralized with basic sodium, zinc, or cobalt salts to produce the corresponding ionomer (Scheme 13.1). Carboxylated NBR was transferred to these ionomeric elastomers. For synthesis of composites that are activated via localized heating, cobalt, magnetite, and cobalt ferrite nanoparticles were incorporated in different contents into the model copolymer and NBR matrices, respectively, resulting in highly efficient stimulated self-healing material.

13.2.3 Self-Healing by Covalent Bond Formation

Covalent bond formation is undoubtedly an efficient healing technique. Numerous methods are available under this category and can be subdivided into reversible and irreversible methods. Reversible methods, like the Diels–Alder/retro-Diels–Alder (DA/r-DA) reactions or polycondensations provide the opportunity for multiple healing cycles, while irreversible methods, like the microcapsule-based concept, epoxides, or various click approaches cannot heal once an area is damaged a second time. Single-component intrinsic self-healing polymers with reversible bond formation can be easily synthesized by ATRP. DA healing reactions are the most popular for this purpose [32]. Acrylic-based one-component polymer systems can be easily synthesized, containing both binding units for the DA reaction (i.e., maleimide and the furan moiety) along with relevant comonomers to tune the mechanical and thermal properties (Scheme 13.2). The ATRP of maleimide methacrylate (MIMA) and furfuryl methacrylate (FMA) along with different acrylic polymers can be utilized to synthesize well-defined functional terpolymers, which could be cross-linked via subsequent thermal treatments [33].

Similarly, ATRP can be used for copolymerization of functional monomers either directly or by post-polymerization modification, yielding one-component, reversible, covalent bond-forming polymers. It is however generally not possible to synthesize one-component self-healing polymers with *irreversible covalent* bond formation by ATRP as most ATRP processes require elevated temperatures where cross-linking reactions are most likely to occur.
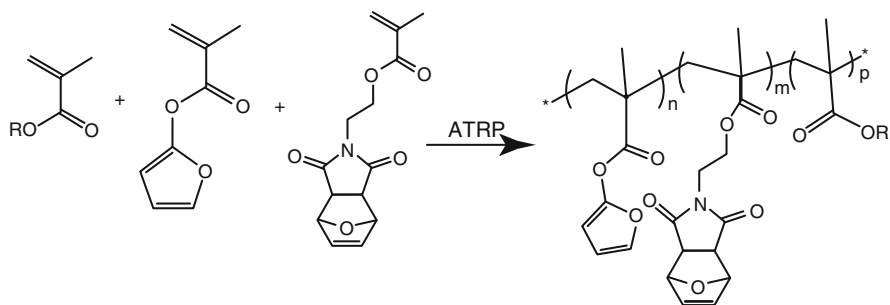
Scheme 13.2 Schematic representation of synthesis of intrinsic DA/r-DA self-healing polymer by ATRP

13.2.4 *Self-Healing by Semi-encapsulation Methods*

Semi-encapsulation methods are those in which healing agents are encapsulated in nano- or microcapsules which are homogenously dispersed in the polymer matrix. Most of these methods are intrinsic healing methods as they do not require external stimuli. Presently microcapsules have been widely used for the fabrication of self-healing polymers and polymeric composites [34–37].

The mechanism is based on the fact that microcapsules containing a healing agent are pre-embedded in the polymer matrix. When these microcapsules are ruptured upon cracking, they release the reparative substance into the cracked planes, which is then polymerized and re-bond the damaged portions. Development within this methodology offers considerable potential toward extending the service life of structural materials and saving on maintenance costs. Poly(urea–formaldehyde)-walled microcapsules containing dicyclopentadiene [38], poly(urea–formaldehyde)-walled microcapsules containing epoxy [39], melamine–formaldehyde resin-walled microcapsules containing dicyclopentadiene [40], and many others are most extensively used for this purpose. The healing agent may be a monomer, cross-linker, or oligomer where the polymer matrix may be reactive toward the encapsulated agents.

Formation of microcracks in the polymers also breaks these capsules, leaching out the healing agents to the cracks. ATRP can be extensively used for the preparation of a reactive thermoplastic matrix. Since polymers prepared by ATRP retain their "living" characteristics, this property alone can provide the self-healing nature required. Living polymerization is a polymerization process in which the chain transfer and termination process is removed [41]. Because the resultant polymer carries living ends, chain growth is always allowed as long as reactive monomers are available. It is therefore a popular method for synthesizing block copolymers since the polymer can be prepared in stages, each of which contains a different monomer. Due to this interesting characteristic of living polymerization, a self-healing polymer can be prepared with a microencapsulated monomer (healing agent) with a living polymer matrix.

Owing to the infinitely long lives of the molecule chain ends of the matrix, as soon as the monomer is released from the spheres as a result of crack initiation or propagation, the polymerization process of the healing agent (monomers) will begin at ambient temperature wherever the monomer meets the matrix. Formation of covalent bonds as a result of copolymerization through the healing process restores the original strength (sometimes better depending upon the type of encapsulated monomer) back to the polymer. The newly formed macromolecules, which are covalently attached to the interface, fill the interstitial space of cracks and fuse with the matrix. This is a very good way to achieve multiple healing events.

13.2.5 Self-Healing by Encapsulation Method

The encapsulation method is a dual capsule self-healing system in which two different reactive components are encapsulated separately and dispersed in the thermoset or thermoplastic polymer matrix that will require healing [23].The two components must have sufficient stability in the service life of the base polymer or composite and high reactivity when exposed to one another. It is the oldest and most widely used method for designing self-healing polymers. In regard to mass production and application popularity, the synthesis approach based upon binary microcapsules containing liquid healing agent is fairly promising. The ATRP-based encapsulation method utilizes two low-molecular-weight polymers having reactive functionalities as healing agents. Azide–alkyne cycloaddition, Diels–Alder reaction, thiol–ene reaction, thiol–yne reaction, and so forth can be utilized in the healing reaction (to be discussed later) if one microcapsule contains the first functionality and the other microcapsule contains the second functionality. Low-molecular-weight star-shaped polymers are especially beneficial in this capacity as they have low viscosity and very high density functionality.

13.3 Click Chemistry

Thought of as an environmentally friendly alternative, click chemistry deals with the instantaneous nearly 100 % efficient creations of molecules without by-product all while utilizing mild reaction conditions.

Sharpless and coworkers [42] defined the reaction as being large in ability, being simple to complete, having no exotic reagents required, and being unaffected by oxygen and water. There are even multiple circumstances where water acts as the ideal reaction solvent, producing at the highest amounts and fastest times. With purification and analysis avoiding harsh solvents and chromatographs, click chemistry, though not as easily definable as a reaction, describes a methodology in the creation of products in such a way that mimics nature while creating materials through the combination of tinier building blocks.

In summary, desirable click chemistry reaction would have the following key characteristics [42]: modular, large scope, high yielding, has inconsequential by-product production, stereospecific, physiologically stable, has high atom economy, and exhibits a large thermodynamic driving force (>84 kJ/mol) in order to favor a reaction with a single reaction product. Furthermore, the process would preferably have the following restrictions: possesses simple reaction conditions, requires no exotic materials or reagents, uses only benign or easily removable solvents, and provides simple product isolation via non-chromatographic methods.

The potential of click chemistry for material synthesis has been increasingly recognized and has already resulted in the growth of a wide range of smart materials. Owing to their high selectivity, high yields, and tolerance toward a wide range of functional groups and reaction conditions, click reactions have recently attracted increased attention in polymer synthesis in addition to polymer modification [43–48]. Owing to their many promising benefits, click chemistry has been exclusively used as a cross-linking reaction in the design of self-healing polymers, providing highly efficient healing. Among various click reactions, DA/r-DA, azide–alkyne cycloaddition, and thiol–ene/yne click reactions are broadly applicable in the field of polymer chemistry as well as in the design of self-healing polymers. An overview of these click reactions used for designing self-healing polymers is discussed below.

13.3.1 Diels–Alder (and Retro-Diels–Alder) Click Reaction
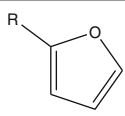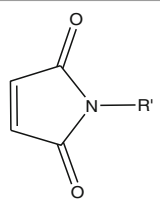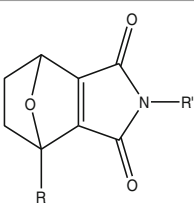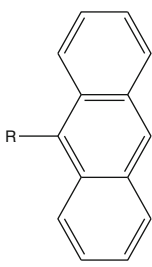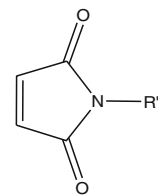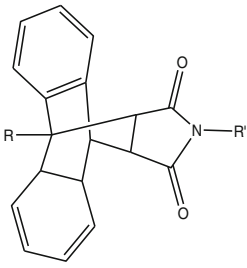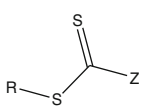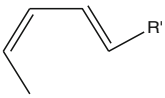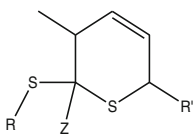
The most known reaction employed in the creation of intrinsic self-healing materials is the Diels–Alder (DA) reaction. DA reaction meets most of the requirements needed to be a click reaction. A stable cyclohexene adduct is formed from the $4+2$ cycloaddition reaction between electron-rich dienes (furan and its derivatives, 1,3-cyclopentadiene and its derivatives, etc.) and electron-poor dienophiles (maleic acid and its derivatives, vinyl ketone, etc.) (Table 13.1). This reaction has become one of the most frequently used reactions in polymer science as it has extremely low energy requirements to form a cyclohexene ring while simultaneously allowing the formation and functionalization of numerous molecules. The general mechanism of DA/r-DA reaction is given in Scheme 13.3.

DA click reaction can be utilized for self-healing materials in the following ways:

(a) Using telechelic polymers with DA functionality

The DA click reaction can be applied in the synthesis of telechelic polymers. Telechelic polymers are those macromolecules which contain reactive end groups that have the capacity to enter into further polymerizations or other reactions. A simple matrix of telechelic polymers with DA functionality or a mixture of two compatible polymers with DA functionality can act as a thermally triggered self-healing polymer (Fig. 13.3).

Table 13.1 Selected DA reaction for synthesis of self-healing polymers

Reagent A	Reagent B	Mechanism	Adduct
		[4+2] r-DA [4+2] DA [4+2] hetero-DA	

Scheme 13.3 General mechanism of DA/r-DA reaction
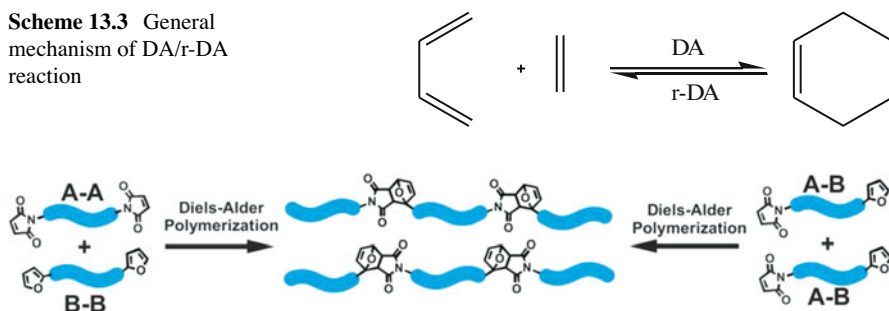
Fig. 13.3 Coupling process of a telechelic polymer with DA functionality (reprinted with permission from [31])

(b) Using bifunctional polymers

In this approach, two monomers, one carrying a diene and another carrying a dienophile group, are reacted to yield a cross-linked copolymer (reaction scheme same as Scheme 13.1). Healing of any crack formation can be achieved by heating the polymer above the temperature required for a reversible DA reaction to occur. The heat causes a partial disconnection of the polymer chains and increases the mobility of individual chains. Upon cooling, new DA bonds are formed and the chains become cross-linked again, thus healing the crack (Fig. 13.4).
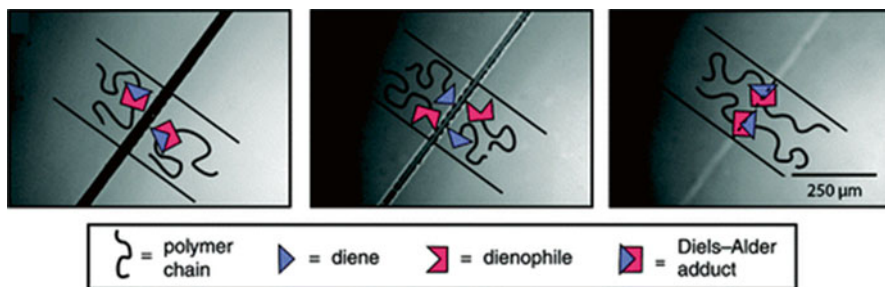
Fig. 13.4 Thermally reversible self-healing process via DA/r-DA clicks (reprinted with permission from [47])

(c) Encapsulation method

When employing the encapsulation method, both thermoplastic and thermosetting plastics as well as their composites can be fashioned into self-healable materials using the binary capsule system via DA/r-DA. This approach requires one capsule having a multifunctional diene and another capsule having a multifunctional dienophile. The primary requirement is that the reagents must crosslink so as to generate a solid mass so that upon crack formation, they can act as internal glue. Some examples of such diene and dienophile reagent systems are given below:

Multifunctional dienes	Multifunctional dienophiles
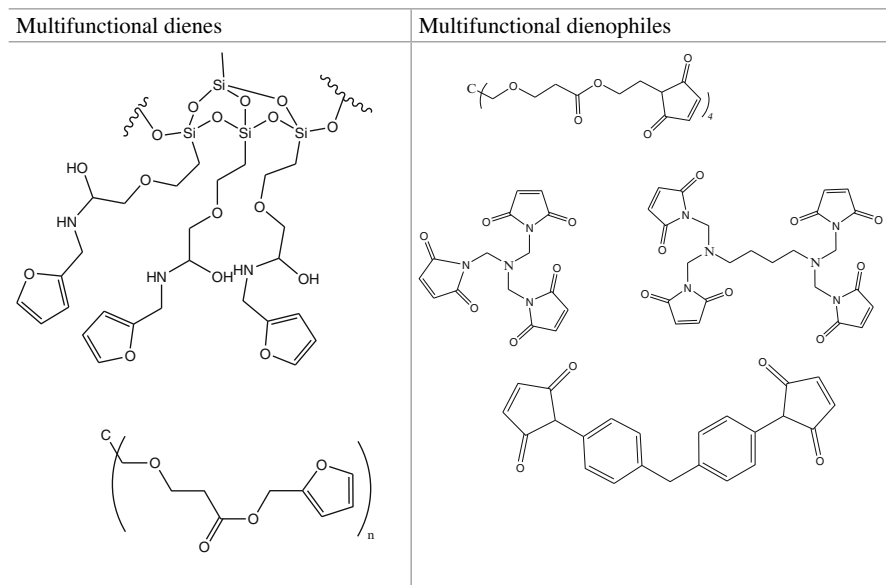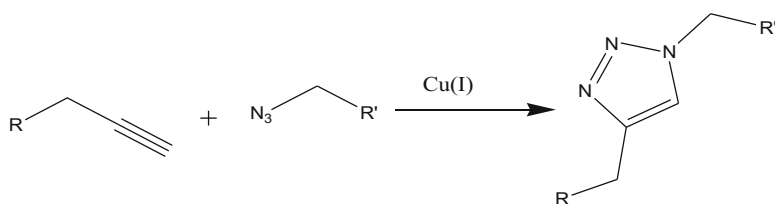
Scheme 13.4 General mechanism of CuAAC

13.3.2 Cu (I)-Catalyzed Azide–Alkyne Cycloaddition (CuAAC)

Although the DA/r-DA reaction discussed above is a valuable tool for tailoring self-healing materials, in most of these cases, the underlying DA reactions require temperatures significantly higher than room temperature, often at 80−100 °C, resulting in cross-linked materials such as hydrogels, shape memory materials, adhesives, or coatings [49]. These problems can be completely eliminated by catalyzed azide–alkyne cycloaddition introduced by Rolf Huisgen [50]. A 1,3-dipolar cycloaddition between an azide and a terminal or internal alkyne yields a 1,2,3-triazole which can be carried out at room temperature while in the presence of a copper catalyst (Scheme 13.4). This reaction, though capable of being completed with Cu (I) (e.g., CuBr, CuI), performs best when a mixture of Cu (II) (e.g., Cu_2SO_4) is utilized alongside a reducing agent (e.g., sodium ascorbate), thus producing Cu (I) in situ. Owing to the versatility of CuAAC's cross-linking ability, it can be applied as a powerful self-healing mechanism. Semi-encapsulation and encapsulation approaches are applicable for this purpose. A one-component healing mechanism is not possible by using this tool since a cross-linked mass would be the final product because CuAAC proceeds even in the absence of catalyst, albeit slowly:

(a) Semi-capsulation method for CuAAC
   The main strategy employed by the semi-capsulation method is that a thermoplastic matrix is prepared with either azide or alkyne functionality with an embedded copper catalyst (preferably CuBr $(PPh_3)_3$) and microcapsules containing the complementary functionality. As soon as the damaging event occurs, the liquid cross-linker will dissolve the embedded catalyst from the matrix, initiating the cross-linking reaction between the azide and alkyne, thus healing the cracks.

(b) Capsulation methods for CuAAC
   As previously mentioned, this method utilizes binary capsules. Some of the capsule contents are listed below. This healing method can be utilized for both thermoplastic and thermosetting plastics. A schematic representation of the method is shown in Scheme 13.5. Star-shaped or hyperbranched azides/alkynes containing reagents with sufficient room temperature fluidity are beneficial for this purpose (Fig. 13.5). Examples of some alkynes and azides are given below:

Multifunctional alkynes

Multifunctional azides
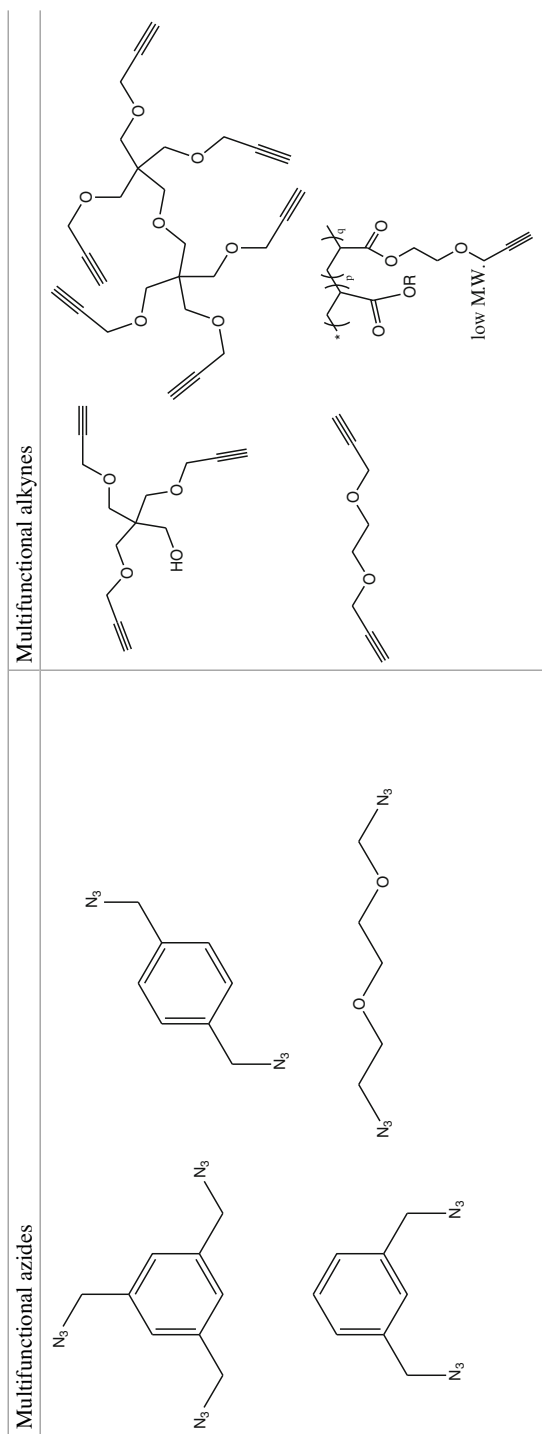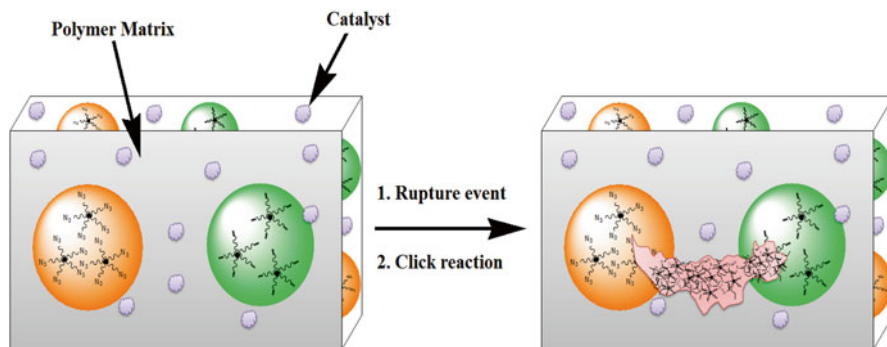
Fig. 13.5 Representation of CuAAC-based self-healing process via microcapsulation method [11]
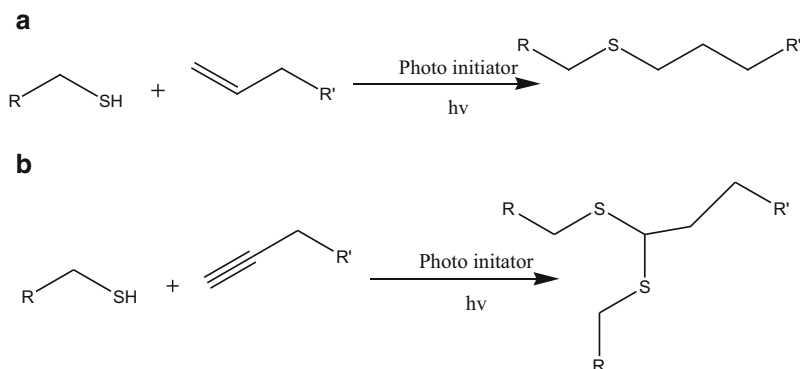
Scheme 13.5 General mechanism of thiol–ene reaction (**a**) and thiol–yne reaction (**b**)

13.3.3 Thiol–ene/yne Click Reaction

Even though the azide–alkyne cycloaddition reaction eliminates the requirement of high temperature, it lacks in the purity of material due to the presence of biotoxic copper salts. This problem can be overcome by photochemically triggering thiol–ene and thiol–yne click reactions (Scheme 13.5). Moreover, these click reactions attract the considerable attention of scientists due to their ability in combining all the advantages of click chemistry and the potential of light-triggered reactions, thus permitting a spatially and temporally controlled self-healing process. Although both of these click reactions are similar, thiol–yne polymerization reactions complement the more well-known thiol–ene polymerization processes, with the added advantage of increased functionality. The application of these two reactions in self-healing material synthesis is mechanistically similar to the azide–alkyne cycloaddition reaction mentioned above (i.e., semi-capsulation and capsulation methods). The only difference is that instead of a copper catalyst, it requires a photoinitiator (e.g., 2,2-dimethoxy-2-phenylacetophenone) to be embedded in the matrix. The major drawback in designing self-healing materials by these two methods is that the matrix must be transparent, which limits its applicability considerably. Examples of some typical multifunctional enes and thiols are given below:

Multifunctional thiols

Multifunctional enes
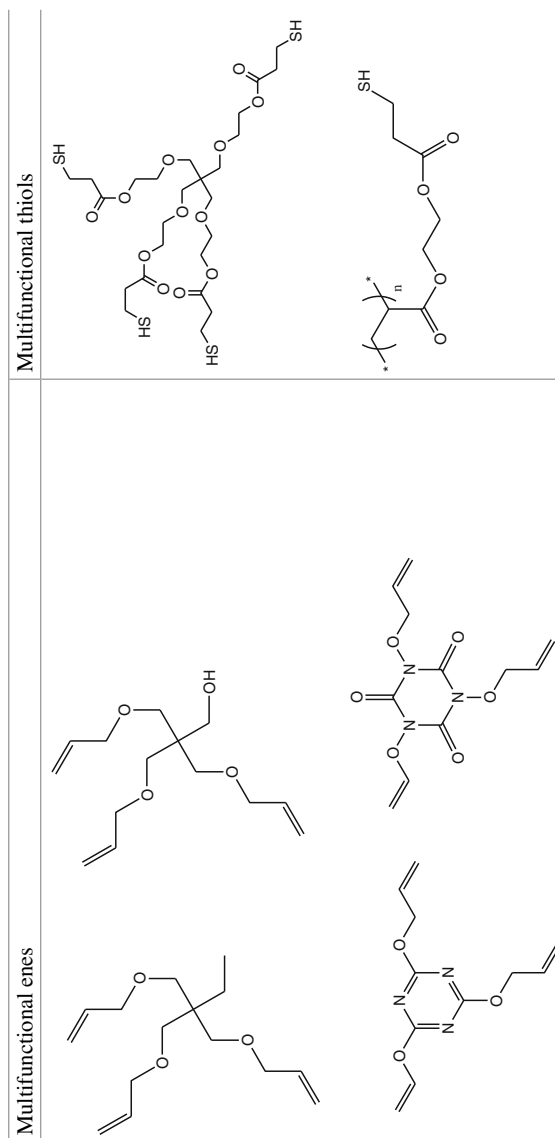
13.4   Combination of ATRP and Click Chemistry to Synthesize Self-Healing Material

As already mentioned, ATRP is the most versatile controlled radical polymerization technique available, while click chemistry is the most promising coupling technique currently known in the field of polymer chemistry. There are a range of possibilities where ATRP can be further broadened by the integration of click chemistry. A combination of these two techniques can provide numerous ways of designing self-healing polymers. Some of these methods are listed below. The monomers and initiators that are used are for representative purpose only. Multifunctional products can be obtained by using a corresponding multifunctional initiator.

13.4.1   ATRP Used for Synthesis of Azide End-Functionalized Polymers
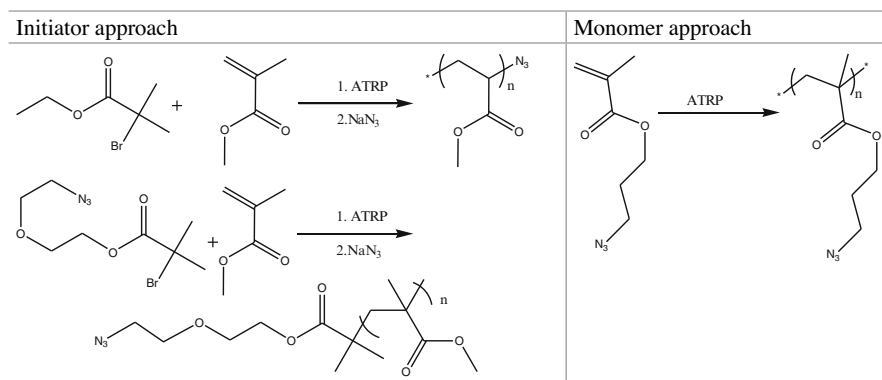
13.4.2   ATRP Used for Synthesis of Alkyne End-Functionalized Polymers

Initiator approach	Monomer and post-polymerization modification approach
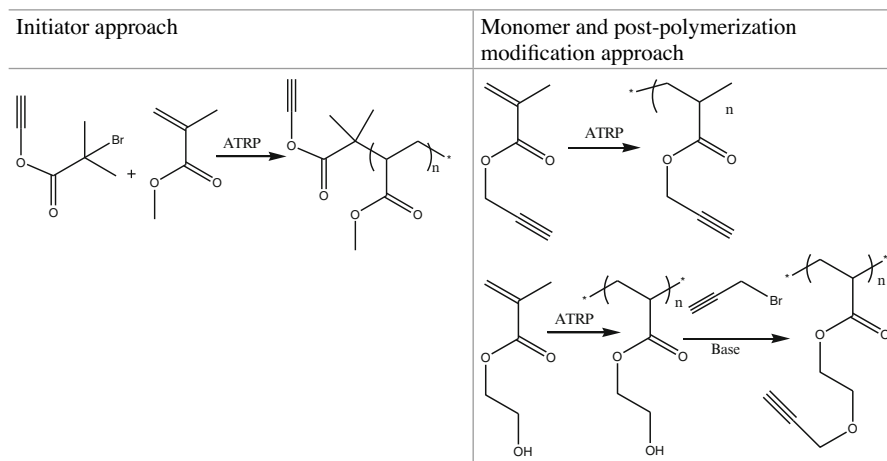
13.4.3   ATRP Used for Synthesis of Diene-/Dienophile- Functionalized Polymers

(a) Initiator approach

Dienophile	Diene

(b) Monomer approach

Diene-containing polymer	Dienophile-containing polymers	Both diene- and dienophile-containing polymer
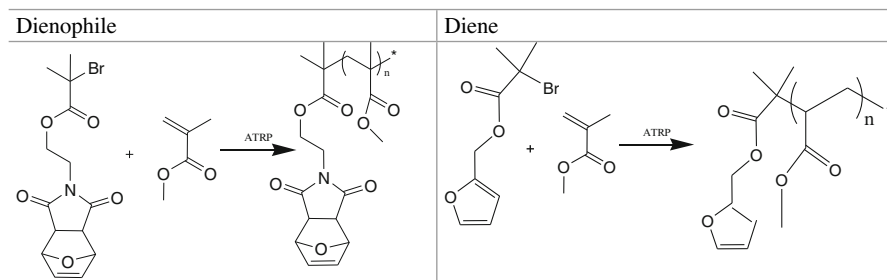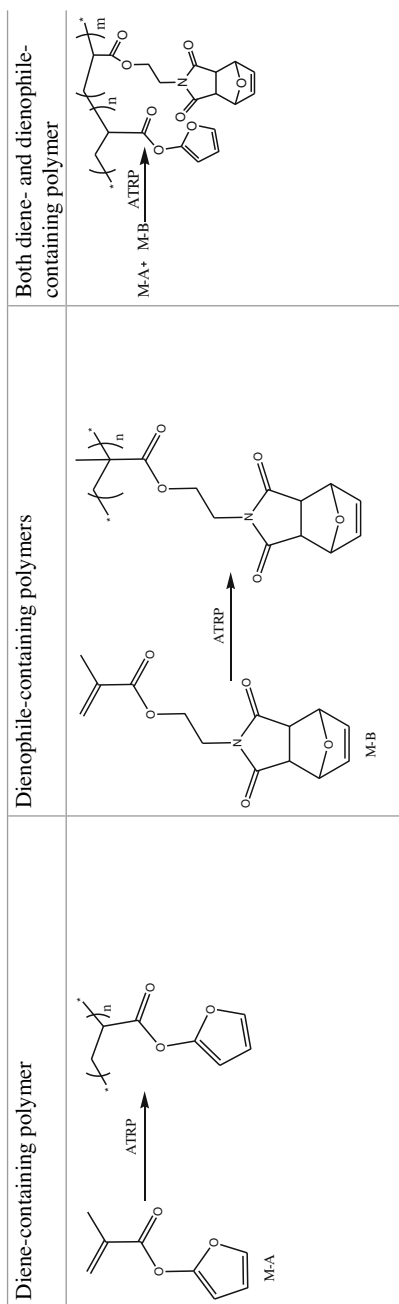
13.4.4   ATRP Used for Synthesis of Thiol-Containing Polymers

Initiator approach	Post-polymerization modification
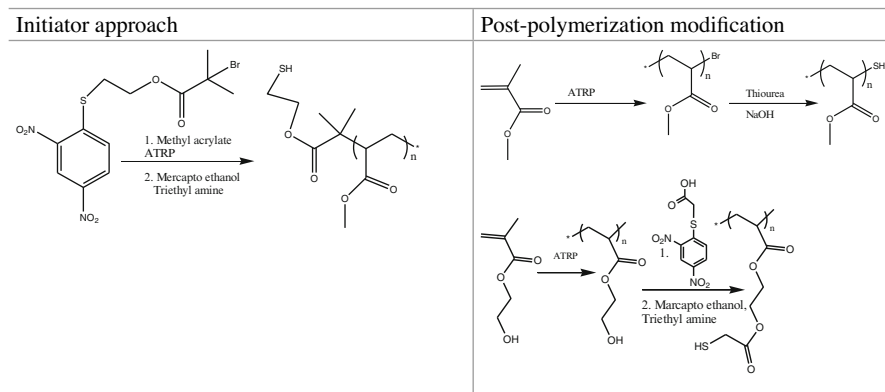
13.4.5   ATRP Used for Synthesis of Ene-Containing Polymers

Initiator approach	Monomer approach
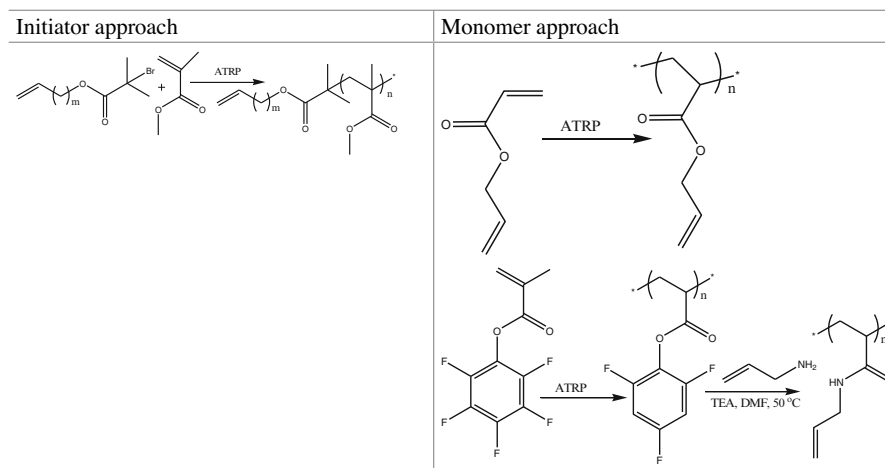
13.5   Conclusion

To summarize, the combination of ATRP and click chemistry is an inexorable route for preparing highly efficient, easy-to-implement, and highly functional tailor-made polymers that chemists find highly desirable. This combination has been tremendously advanced since the introduction of the click chemistry concept by the cumulative efforts of a large number of research groups all over the world. These developments on the preparation of new well-defined clickable polymers by ATRP enabled straightforward access to a large variety of self-healing polymers and polymeric composites. This chapter demonstrated both individual and numerous combinations of ATRP and click chemistry to aid in the design of efficient intrinsic as well as extrinsic self-healing polymeric materials. Finally it can be concluded that the combination of ATRP and click chemistry methods will continue to thrive in the near future and in advancing the tailoring of new functional polymeric materials with more effective healing properties.

References

1. Chen X, Dam M, Ono A, Mal K, Shen A, Nutt H, Sheran SR, Wudl K (2002) Science 295:1698
2. Chen X, Wudl F, Mal A, Shen H, Nutt SR, Sheran K (2003) Macromolecules 36:1802
3. White SR, Sottos NR, Guebelle PH, Moore JS, Kessler MR, Sriram SR, Brown EN, Viswanathan S (2001) Nature 409:794
4. Nathalie K, Guimard K, Kim O, Jiawen Z, Stefan H, Friedrich GS, Christopher BK (2012) Macromol Chem Phys 213:131
5. Brown EN, Sottos NR, White SR (2002) Exp Mech 42:372
6. Keller MW, White SR, Sottos NR (2007) Adv Funct Mater 17:2399
7. Guan Z, Roland JT, Bai JZ, Ma SX, McIntire TM, Nguyen M (2004) J Am Chem Soc 126:2058
8. Varley RJ, Zwaag VD (2008) Polym Test 27:11
9. Tadano K, Hirasawa E, Yamamoto H, Yano S (1989) Macromolecules 22:226
10. Zare P, Mahrova M, Tojo E, Stojanovic A, Binder WH (2013) J Polym Sci A Polym Chem 51:190
11. Gragert M, Schunack M, Binder WH (2011) Macromol Rapid Commun 32:419
12. Saiki BJ, Gogoi P, Sharmah S, Dolui SK (2015) Polym Int 64:437
13. Matyjaszewski K (2012) Macromolecules 45:4015
14. Quirk P, Kim J (1991) Rubber Chem Technol 64:450
15. Zhang L, Liu W, Lin L, Chen D, Stenzel MH (2008) Biomacromolecules 9:3321
16. Laurent BA, Grayson SM (2006) J Am Chem Soc 128:4238
17. Van Camp W, Germonpre V, Mespouille L, Dubois P, Goethals EJ, Du Prez FE (2007) React Funct Polym 67:1168
18. Durmaz H, Karatas F, Tunca U, Hizal G (2006) J Polym Sci A Polym Chem 44:3947
19. Mantovani G, Lecolley F, Tao L, Haddleton DM, Clerx J, Cornelissen JJLM, Velonia K (2005) J Am Chem Soc 127:2966
20. Gao H, Matyjaszewski K (2006) Macromolecules 39:4960
21. White SR, Blaiszik BJ, Kramer SLB, Olugebefola SC, Moore JS, Sottos NR (2011) Am Sci 99:392
22. Murphy EB, Wudl F (2010) Prog Polym Sci 35:223

23. Blaiszik BJ, Kramer SLB, Olugebefola SC, Moore JS, Sottos NR, White SR (2010) Annu Rev Mater Res 40:179
24. Zhang MQ, Rong MZ (2012) Sci China Chem 55:648
25. Müller M, Dardin A, Seidel U, Balsamo V, Iván B, Spiess HW, Stadler R (1996) Macromolecules 29:2577
26. Greenland BW, Burattini S, Hayes W, Colquhoun HM (2008) Tetrahedron Lett 64:8346
27. Kalista SJ, Ward TC, Oyetunji Z (2007) Mech Adv Mater Struct 14:391
28. Chen Y, Kushner AM, Williams GA, Guan Z (2012) Nat Chem 4:467
29. Rahman MdA, Penco M, Spagnoli G, Peroni I, Ramorino G (2012) AIP Conf Proc 163:1459
30. Hart LR, Nguyen NA, Harries JL, Mackay ME, Colquhoun HM, Hayes W. doi:10.1016/j.polymer.2015.03.028
31. Hohlbein N, Pelzer T, Nothacker J, von Tapavicza M, Nellesen A, Datta H, Schmidt AM (2013) 'Self-healing processes in ionomeric elastomers', ICSHM, 680.
32. Tasdelen MA (2011) Polym Chem 2:2133
33. Kötteritzsch J, Hager MD, Schubert US (2013) One-component intrinsic self-healing polymer for coatings based on reversible crosslinking by Diels-Alder-cycloadditions, ICSHM, 624
34. Yang J, Keller MW, Moore JS, White SR, Sottos NR (2008) Macromolecules 41:9650
35. Ghosh D, Sharman R, Rao HR, Upadhyaya S (2007) Decis Support Syst 42:2164
36. Kessler MR, Sottos NR, White SR (2003) Compos A 34:743
37. Hayes SA, Jones FR, Marshiya K, Zhang W (2007) Compos A 38:1116
38. Kirkby EL, Michaud VJ, Månson JAE, Sottos NR, White SR (2009) Polymer 50:5533
39. Noh HH et al (2013) Express Polym Lett 7:88
40. Hua J, Chenb HQ, Zhanga Z (2009) Mater Chem Phys 118:63
41. Halasa AF (1981) Rubber Chem Technol 54:627
42. Kolb HC, Finn MG, Sharpless KB (2001) Angew Chem Int Ed 40:2004
43. Rostovtsev VV, Green LG, Fokin VV, Sharpless KB (2002) Angew Chem Int Ed 41:2596
44. Tornoe CW, Christensen C, Meldal M (2002) J Org Chem 67:3057
45. Kumaraswamy G, Ankamma K, Pitchaiah A (2007) J Org Chem 72:9822
46. Schunack M, Gragert M, Döhler D, Michael P, Binder WH (2012) Macromol Chem Phys 213:205
47. Evans RA (2007) Aust J Chem 60:384
48. Weizman H, Nielsen C, Weizman OS, Nasser SN (2011) J Chem Educ 88:1137
49. Döhler D, Michael P, Wolfgang HB (2012) Macromolecules 45:3335
50. Huisgen R (1961) Proc Chem Soc 357

Chapter 14
Polyurethane-Based Smart Polymers

Norazwani Muhammad Zain and Syazana Ahmad Zubir

Abstract Polyurethane is a highly versatile polymer that may be used in various types of applications with a wide range of properties. The combination of different types and ratios of isocyanate and polyol allows for the control of the desired end properties. Due to its unique properties, it has found applications in the fields of medical, military, automobile, and aerospace industries. Recently, there has been a prodigious interest in producing polyurethane-based smart polymers, especially shape memory polyurethane (SMPU). This is due to its excellent ability to change shape upon the application of external stimuli such as heat, electric field, magnetic field, and light. The existence of phase-separated structure known as soft- and hard-segment domains contributes toward the shape memory properties of polyurethane. The soft-segment domains are responsible for maintaining the temporary shape, while hard segments fix the permanent shape. This chapter comprehensively aims to address a wide overview of polyurethane-based smart polymer and the chemistry behind the shape memory properties. In addition, this chapter also summarizes the recent studies on the exploration of SMPU using vegetable oils along with petroleum-based polyol and the potential applications of smart polyurethane.

Keywords Smart polymers • Polyurethane • Vegetable oil based • Shape memory

N.M. Zain (✉)
Fabrication and Joining Section, Universiti Kuala Lumpur Malaysia France Institute,
Jalan Teras Jernang, 43650 Bandar Baru Bangi, Selangor, Malaysia
e-mail: norazwani@unikl.edu.my

S.A. Zubir
School of Materials and Mineral Resources Engineering, Universiti Sains Malaysia,
Engineering Campus, Nibong Tebal, 14300 Seberang Perai Selatan, Pulau Pinang, Malaysia
e-mail: syazanazubir@usm.my

14.1   Introduction

Polyurethane-based smart polymers are defined as polyurethane (PU) that responds to different stimuli or changes in the environment. This chapter reviews the chemistry of smart PUs including their basic components. The main focus of this chapter is on smart PU that has shape memory functionalities. Shape memory refers to the ability of materials to remember the shape of the demand even after a rather severe deformation. The structure of shape memory polyurethane (SMPU) and shape memory effect are also highlighted. Furthermore, this chapter highlights current scenarios involving SMPU elastomers based on petroleum and vegetable oil. The applications of smart PU particularly in textile, biomedical, and engineering purposes are also reviewed.

14.2   Chemistry of Smart Polyurethane

Smart polyurethane is similar to conventional polyurethane (PU). It is produced by a combination of a diisocyanate or polymeric isocyanate with a diol or polyol in the presence of suitable catalysts and additives. It possesses segmented structures, and a wide range of glass transition temperature make it different from conventional PU. The synthesis of smart PU involves polymerization reactions that contain features of both addition and condensation polymerization either via the one-step or multistep process. This preparation may require solvents (solution polymerization) or is solvent-free (bulk polymerization).

One-step process involves a simultaneous reaction between the polyol, diisocyanate, and chain extender in the presence of a catalyst. A higher order of crystallinity can be obtained in one-step polymers. The process is faster and easier and can be used to its best advantage where the reaction rates of the diols and isocyanates are comparable. However, this method does not have the control required to yield regular block sequences [1–3]. The factors such as different reactivities of isocyanate groups and different types and amounts of a chain extender and a hydroxyl group (polyol) may affect the distribution of the hard segments in the chain.

The most common technique for the synthesis of smart PU, particularly SMPU, consists of two steps that are known as the prepolymer method. The first step involves the reaction between a diisocyanate with polyol and produces a prepolymer in excess of diisocyanate that has a low molecular weight (Fig. 14.1). In the second step, the prepolymer reacts with a chain extender in the presence of a catalyst to produce a high-molecular-weight PU. This provides a more typical hard-soft-hard-soft sequence compared to the one-step synthesis route. This method is more popular than the one-step process because it is easier to control the chemistry of the reaction while imparting greater structure and physical properties to the PU. As the prepolymer method is more controlled, it produces linear PU chains and fewer side reactions.

$$2 \; O=C=N-R-N=C=O \;\; + \;\; HO-R'-OH$$

$$NCO-R-\overset{H}{\underset{|}{N}}-\overset{O}{\underset{||}{C}}-O-R'-O-\overset{O}{\underset{||}{C}}-\overset{H}{\underset{|}{N}}-R-NCO$$

prepolymer

reaction with diol   reaction with diamine
HO−R"-OH $H_2N-R"-NH_2$

$$-O-R"-O-\overset{O}{\underset{||}{C}}-\overset{H}{\underset{|}{N}} \cdots \overset{H}{\underset{|}{N}}-\overset{O}{\underset{||}{C}}-O-R"-O-$$

polyurethane

$$N-R"-\overset{H}{\underset{|}{N}}-\overset{O}{\underset{||}{C}}-\overset{H}{\underset{|}{N}} \cdots \overset{H}{\underset{|}{N}}-\overset{O}{\underset{||}{C}}-\overset{H}{\underset{|}{N}}-R"-N$$
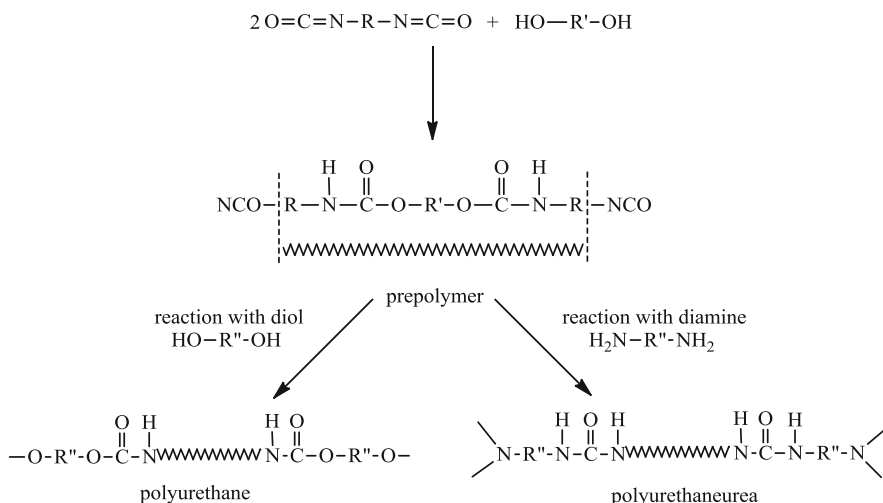
polyurethaneurea

Fig. 14.1 Two-step polyurethane syntheses (reprinted from [4], with permission from CRC Press)

14.2.1   Basic Component of Smart Polyurethane

The chemistry of smart PU can be varied through the chemistry of diisocyanate, polyol, chain extender, and the ratios in which they are reacted. The chemistry ultimately affects the mechanical and biological properties of the finished material.

A. Polyol

The polyols that are commonly used in smart PU production are polyether and polyester compounds that have a molecular weight of 1000–6500 g/mol and low functionality. The soft segments are comprised of long flexible polyol chains and act as the backbone for the structure of the PU elastomer. Polypropylene glycol (PPG) and polytetramethylene ether glycol (PTMG) are examples of commonly used polyether polyols used to produce PU elastomers. PPG and PTMG are produced by addition polymerization of the epoxide [5]. Other polyether polyols used are polyethylene glycol (PEG) and polytetramethylene oxide (PTMO). Polyether-based PU possesses high hydrolysis stability as compared to polyester-based PU, more efficiently designed when the polarity of the backbone is essential [6].

Meanwhile, polyester polyols used among researchers include polycaprolactone diol (PCL), polycarbonate (PC), polyethylene adipate (PEA) diol, and poly(butylene adipate) (PBA) diol. Polyester polyol has a greater oil and heat resistance than polyether making it an attractive choice as a soft segment of PU. Furthermore, crystalline structures attributed to the existence of secondary bonding forces link to the polyester chain resulting in a stronger PU network compared to polyether-based PU [7]. Thus, PU synthesized from polyesters possesses relatively good physical and mechanical properties; however, they are susceptible to hydrolytic cleavage of the ester linkage.

PCL is one of the most attractive polyester diols among the researchers. The presence of long and repetitive hydrophobic segments ($-(CH_2)_5-$) in its chemical structure contributes to good hydrolysis [7] and weather stability [8]. PCL has a partially crystalline structure with a melting point (T_m) ranging from 45 to 64 °C and a glass transition temperature (T_g) of −60 °C. The range of molecular weight, M_n, between 1000 and 90,000 g/mol and its crystallization structure decrease as the molecular weight increases [9]. In addition, PCL possesses excellent biodegradability and mechanical properties. It is also compatible with a large number of other polymers, lignin, and starch. These advantages make PCL crucial in polymer blends and within the composites industry [10].

In addition, the PU industry has also placed intensive interest to the production of bio-based polyols, mainly synthesized from vegetable oils such as castor, soybean, palm, sunflower, and rapeseed oil. These vegetable oil polyols may be produced using several methods that include transesterification [11], epoxidation [12], and/or transamidation processes [13]. Most of the vegetable oils contain mainly triglyceride molecules where the three hydroxyl functions of glycerol are esterified with fatty acids. These renewable bio-based polyols are very interesting since various reactions could be performed from their different groups with diisocyanates in order to produce PU. In addition, vegetable-based PU offers similar or greater properties as petroleum-based PU.

B. Isocyanate

Diisocyanate forms hard segments in the PU chains when reacted with a short-chain diol or diamine. Hard segments have low molecular weight and able to establish an interaction between networks via hydrogen bonds and form a hard-segment domain. There are two types of diisocyanate: aliphatic and aromatic. Aromatic diisocyanate is more reactive than aliphatic diisocyanate. However, aliphatic diisocyanate has excellent properties that enable it to be used exclusively in the production of high-performance materials. For example, isophorone diisocyanate (IPDI) has a high resistance to degradation by light, specifically UV radiation, thus preventing the polymer from turning yellow in color when exposed to UV light [14]. In addition, aliphatic diisocyanate is also able to increase the phase separation between soft and hard segments when compared with aromatic diisocyanate [15].

Diisocyanates that are commonly used in the PU elastomer industry are aromatic diisocyanate such as "4,4′-methylenediphenyl diisocyanate (MDI) and toluene diisocyanate (TDI). MDI is formed by the condensation of aniline and formaldehyde while in the presence of hydrochloric acid. The resulting polyamine is subsequently treated using phosgene to produce MDI. TDI is produced from toluene by the nitration process, converted to a diamine, and treated with phosgene [5].

C. Chain Extender

In the production of PU, chain extenders serve to produce polymers with a high molecular weight when reacted with a prepolymer. Selection of a chain extender depends on the final properties of a polymer material that is needed. Short chains such as diamine and diol are typically used as chain extenders in the PU network.
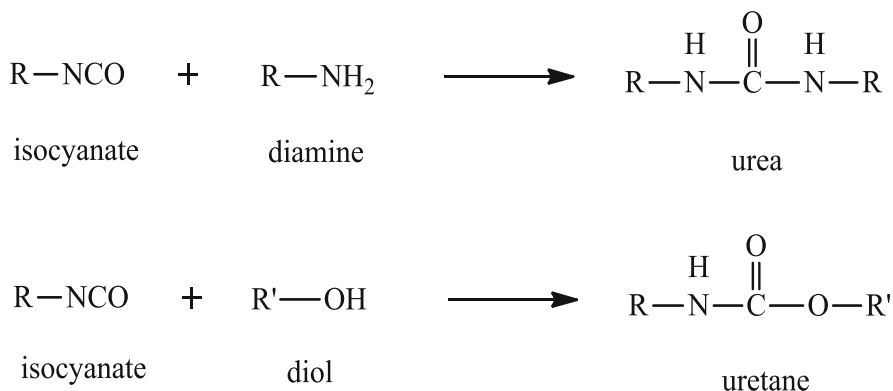
Fig. 14.2 Reaction of diamine and diol with isocyanate

Meanwhile, triol is used if chemical cross-linking is necessary for the polymer while the linear polyols are often used as a plasticizer for reducing the hardness of the polymer [14].

The reaction between a diisocyanate with a diamine and diol produces urea and urethane networks (Fig. 14.2). The existence of strong hydrogen bonding between the urea networks results in better final properties of the polymer when diamine is used as a chain extender when compared to a diol. The number of carbon atoms in the chain extender also affects the strength of hydrogen bonding. Chain extenders that possess an even number of carbon atoms exhibit better physical and thermal properties than one with an odd number of carbon atoms [15]. This is due to the steric hindrance that makes it difficult in the interactions of hydrogen bonding when the molecules containing an odd number of carbon atoms forming the hard segments.

14.2.2 Structure and Shape Memory Effect

PU elastomers tend to form phase separations due to a thermal mismatch between the soft and hard segments. This is because of the strong polar interactions in PU copolymer block, leading to the formation of aggregate structures. The soft segment phase contributes to the elastic properties of the materials because of molecular motion in a rubbery state and affects performance such as modulus, rigidity, and strength at low temperatures. Meanwhile, the hard segments form physical cross-links between urethane networks due to hydrogen bonding, polar interaction, or crystallization in the hard domains [16]. Formation of phase separation is dependent on hydrogen bonding between urethane networks, processing, molecular weight, and types of polyol used.

Final properties of PU are influenced by the degree of phase separation and morphological characteristics of soft- and hard-segment domains that have been formed. According to Prisacariu [17], the formation of phase separation between soft and hard segments is preferred in order to achieve the desired elastomeric performance.

Segmented PU consists of mostly the soft segments with the hard segments (approximately 30–40 %) being uniformly distributed between the soft segments. These phases are known to have a microphase-separated structure that highly impacts the mechanical properties. Figure 14.3 shows the structure of PU with the formation of a separated and mixed phase.

In addition, there are several factors that influence the final properties of PU, namely, the molecular weight of the polyol, intermolecular forces, backbone rigidity, and crystallinity. The molecular weight of polyols affects the tensile strength, elongation, flexibility, transition temperatures (glass transition temperature and melting point), and modulus of the resulting polymer. This is due to the molecular weight or long-chain polyols affecting the frequency of hard segments present in the PU [10]. The longer the chain of polyols results in a more flexible polymer. In thermoplastic SMPU, intermolecular forces that are present between the urethane networks play an important role in producing physical cross-links that are responsible for maintaining the original shape.

The physical cross-links also affect the mechanical properties of materials at high temperatures due to high thermal stability. The rigidity of the backbone chain of a polymer depends on the type of polyol used in the production of said polymers. Ether linkage is more flexible than ester linkage, allowing rotation of chemical bonds along the chain, hence increasing the flexibility of the polymer molecules and in turn affecting the softness and the transition temperature [7]. In general, the incorporation of groups such as –O–, –O–O–, and –CO–O– in the backbone increases the flexibility and drops the T_m and T_g [18]. Conversely, the presence of a phenyl group in the backbone increases the stiffness and transition temperature. The formation of crystalline structures in PU restricts the movement of polymer chains thereby increasing the rigidity, tensile strength, and melting point. At the same time, it lowers the solubility, elongation, and flexibility of the polymer [7]. In SMPU, crystallinity plays an important role in the behavior of shape memory as it is responsible for maintaining the temporary shape.

Fig. 14.3 PU structure (**a**) separated phase and (**b**) mixed phase (reprinted from [17], with permission from Springer)
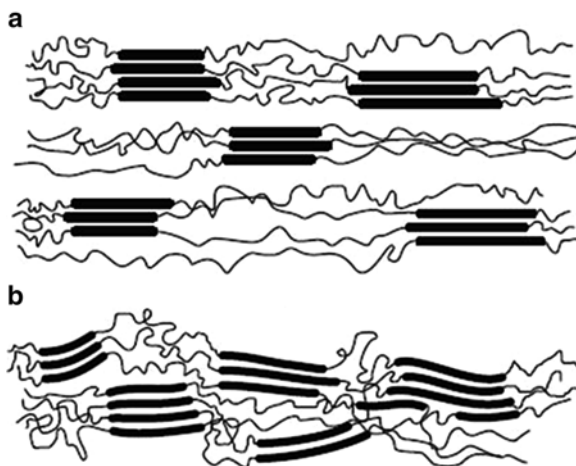
The shape memory effect refers to the following interesting phenomenon: after being severely and quasi-plastically distorted, a material can recover its original shape in the presence of the right stimulus. The shape memory effect that occurs in the polymer does not depend on the specific properties of the polymer; rather it depends on a combination of polymer structure and morphology together with the processing technology used [19].

Almost all existing shape memory polymers (SMPs) fall into three major categories according to the types of stimulus applied to induce the shape memory effect. The first category is thermo-responsive SMP, which is normally induced by means of heating, including inductive, joule, mechanical, light, etc. The second category is photo-responsive SMP that are induced by light with different wavelengths but without any heat involved. Meanwhile, the third category is chemo-responsive SMP, which involves chemicals, such as water, ethanol, etc. [20–22]. In fact, shape recovery specifically in an SMP may be generated by a few different stimuli or inducements. For example, heat, water, and ethanol are all possible stimuli for polyurethanes (PUs) and their composites.

Elastomer exhibits shape memory functionality if the material can be stabilized in the deformed state while in a range of temperature that is relevant for the particular application [19]. This can be reached by using the network chains as a kind of molecular switch. For this reason, the flexibility of the segments should be a function of the temperature. One possibility for a switch function is a transition temperature (T_{trans}) of the network chains in the interest range of temperature for the particular application. At temperatures above T_{trans}, the chain segments are flexible, whereas the flexibility of the chains below the thermal transition is at least partly limited.

Selection of the T_{trans} for the polymer is broad and depends on the application of the polymer produced. T_{trans} can be either a T_m or a T_g and depends on a network of polymer chains that are either crystalline or amorphous. If T_m is chosen for the fixation of the temporary shape, the strain-induced crystallization of the switching segment can be instigated by cooling materials that have been stretched at temperatures above the T_{trans}. However, the crystallization is always incomplete since there is a certain amount that remains amorphous, which generates the retractive force when the stress is relieved after cooling that leads to shrinkage. In addition, the crystallite structure formed restricts the movement of the chain, thus preventing the segments from reforming their coil-like structure [19].

The hard segments of SMPU can be either chemical or physical cross-links, also known as SMPU thermosets or SMPU thermoplastics, respectively [22]. The chemical cross-links that are responsible for maintaining the permanent shape of SMPU may be formed via reactions between isocyanate and triol cross-linker or may arise from the chemical cross-links of the polyol chains itself. The presence of chemical cross-links hinders the polymer from softening and reshaping upon heating. On the other hand, thermoplastic SMPU consists of hard-segment domains that are bonded by physical cross-links via intermolecular interactions such as hydrogen bonding, dipole interaction, and induced dipole moment. Besides, the entanglement of long polymer chains could also develop physical cross-links forming hard-segment domains. The hard-segment domains have the highest thermal transition tempera-
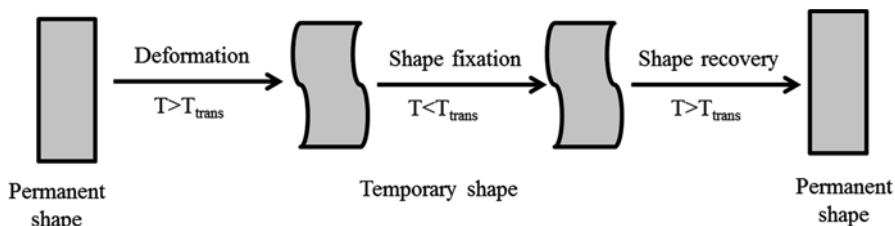
Fig. 14.4 Thermally induced shape memory effect

ture (T_{perm}) which is responsible in fixing the permanent shape. Heating above T_{perm} will cause melting of the polymer chains and destroys the physical cross-links among the hard-segment domains.

Figure 14.4 shows the thermally induced shape memory effect in polymers. Heating the SMP above the T_{trans} of the hard segment enables its deformation. The original shape can be memorized by cooling the material below the T_{trans} of the hard phase. Cooling the SMP below the T_{trans} of the soft segment while the shape is deformed allows a temporary shape to be fixed, often measures as shape fixity. The permanent (original) shape of the SMP is recovered by heating it above the T_{trans} of the soft phase [23]. In SMPU, cooling below the highest thermal transition temperature (T_{perm}) while still above T_{trans} of its soft segments allows it to become relatively soft, but the physical cross-links prevent it from flowing. Thus, it can be easily deformed to a temporary shape by stretching or compression. Reheating the SMPU above the T_{trans} of its soft segments but below T_{perm} relieves the stresses and strains, thus inducing shape recovery [24] and causing the material to return to its original shape [23]. Heating the SMPU above than T_{perm} destroys the physical cross-links between the hard segments, and the SMPU can be processed to a permanent shape just like a thermoplastic material.

14.3 Current Scenario on Shape Memory Polyurethane

Polyurethane with smart functions has already been used in our daily lives at high capacity as it is found in electronic devices, engine parts, sportswear, packaging, piping, and many more products. Its usage is expanding and is gaining more attention, especially in the biomedical and structural fields where a vast amount of research is currently being undertaken. Commercial products based on SMPU had been used in surgical devices and are still undergoing numerous studies in order to enhance their properties while simultaneously determining new applications.

More recently, there are increasing trends in producing segmented SMPU using bio-based materials as an effort to reduce the consumption of petrochemical-based raw materials for polymer production [25]. The triggered response was due to environmental awareness regarding the depletion of petroleum resources and has urged industries to produce materials with sustainability and environ-

ment-friendly means in mind. Consequently, the demand for renewable resources as an alternative to currently available raw materials in producing polymers has increased abruptly.

Bio-based PU may be synthesized using different kinds of renewable resources such as cellulose, sucrose, lignin, agricultural by-products (furfural), vegetable oil, and starch [7]. Vegetable oils are the most promising raw materials due to their abundance and are readily available and inexpensive [26], and there are few attempts by several research groups in developing SMPU based on vegetable oils. Therefore, this subtopic will highlight recent developments involving segmented SMPU elastomers based on vegetable oil as well as the conventional petrochemical-based SMPU in the following section.

14.3.1   *Petrochemical-Based Shape Memory Polyurethane*

The technology of petrochemical-based PU with excellent finished product properties has been thoroughly developed, thus making them popular choices as raw materials for SMPU elastomers. PEG, PPG, PCL, PTMG, PBA, and PEA are among the most commonly used petrochemical-based polyols for SMPU production, whereas MDI, IPDI, 1,6-hexamethylene diisocyanate (HDI), and TDI are used as isocyanates. The type of chain extender is chosen depending on the type of cross-linking and final properties desired. The NCO:OH ratio is fixed at 1:1 on the basis of equivalent isocyanate (NCO) and hydroxyl (OH) groups of isocyanate, polyol, and chain extenders.

The selection of soft and hard segments depends on the application requirements. It is based on the intended design of molecular structure, such as the transition temperature of the soft segment (either melting or glass transition), mechanical properties of segmented PU, light fastness, and other required properties [24]. According to the nature of the switching segment, the SMPU can be classified into two categories based on the transition temperature, T_g and T_m, denoting the amorphous and crystalline nature of soft segment, respectively.

SMPU synthesized using a shorter length of soft-segment chains tends to exhibit an amorphous switching segment, whereas the longer one would demonstrate the semicrystalline nature of the molecular switch [27]. However, the value and range of T_g may be adjusted by using an appropriate chain extender [28], varying hard-segment content [29–31], or the type of isocyanate used [32].

On the other hand, the melting transition of the crystalline soft segment is much sharper as compared to the T_g, enabling easier selection of switching temperature for fixation of temporary shape and recovery of permanent shape. The degree of crystallinity of the soft segment plays an important role affecting the ability of the polymer to maintain its temporary shape, measured as shape fixity (S_f). Several factors including the chemical structure of polyol, type and ratio of the hard segment, and processing conditions influence the degree of crystallinity of the soft segment [23, 30].

In spite of its switching segment nature, extensive studies have been undertaken to investigate the effects of varying the length and type of polyols [33, 34], isocyanates [35], and chain extender [27, 28] on the shape memory performance of SMPU elastomers. As for thermoset SMPU, the cross-linking agent is normally introduced during synthesis in order to form chemical cross-linking between soft-hard segments and is responsible for maintaining the permanent shape. Trimethylolpropane (TMP) is the most commonly employed cross-linker in producing a thermoset SMPU [34, 36–39]. There are also other types of the cross-linking agents that can be utilized in SMPU production. Chung and coworkers conducted systematic studies examining the effect of different types of cross-linker, namely, celite, glucose, dextrin, and PEG, on shape memory properties of SMPU based on PTMG, MDI, and BD [40–43].

Besides the conventional SMPU with linear and cross-linked architecture, SMPU with a hyperbranched structure was also explored [44]. Sivakumar and Nasar [45] prepared hyperbranched SMPU via a A_2 (oligomer)$+B_3$ (monomer) approach using PCL as switching segment and TMP, glycerol, and triethanolamine (TEA) as B_3 monomers. They reported that the shape recovery rate of the resulting hyperbranched polymer was twice as much as those obtained by linear SMPU. In other works, Karak and coworkers [46, 47] have done substantial work on hyperbranched SMPU via the same approach, using monoglyceride from different types of vegetable oil (castor, sunflower, and *Mesua ferrea* L. seed oils) as bio-based chain extenders. They also used TEA as multifunctional moiety, PCL as soft segment, and TDI as the hard segments. The produced hyperbranched SMPU using long, flexible macroglycol coupled with long, flexible hydrocarbon chain of castor oil showed enhanced toughness with good shape memory effect as compared to other hyperbranched SMPU.

The majority of the reported studies on SMPU typically focus on its potential applications in the biomedical field. Since it involves the insertion into a living organism, great care in the selection of raw materials must be considered. Aside from being biocompatible, the degraded products must also be nontoxic and able to be metabolized or eliminated by the living organism [48]. Biodegradable and biocompatible segmented SMPUs are normally based on PCL owing to its thermal transition of the switching segment in the range of 46–64 °C which is suitable for application in minimally invasive surgery [19]. Many studies have been done attesting that SMPU based on PCL are biocompatible and non-cytotoxic [31, 49, 50], thus placing them as promising candidates for biomedical application.

Most of the synthesized segmented SMPU utilize a single type of polyol as soft segment as it is much easier to predict the final range of the switching temperature. Nevertheless, there were also studies on multiblock segmented SMPU using multiple blocks of polyol as the soft segments [51]. Gu and Mather synthesized thermoplastic SMPU using PCL, PEG, and lysine methyl-ester diisocyanate (LDI) via the one-step method [52]. They reported that both PCL and PEG can be regarded as soft blocks since they share very similar melting temperatures. The resulting SMPU possessed a high degree of entanglements which acted as physical cross-linkages and demonstrated outstanding properties specifically high recoverable strains (>800 %) at high recovery rate.

In summary, the previous sections mentioned several factors, specifically the types and amounts of polyol, isocyanate, chain extender, and cross-linking agent that affect the nature of switching segment and final properties of segmented SMPU elastomers. Moreover, vegetable oil has been used in the production of polyurethane since 2000 by the Dow Chemical Company in producing soy-based polyol for PU production [53]. The main components of vegetable oils are triglycerides of fatty acids, both saturated and unsaturated (Table 14.1). The rapid development of conventional SMPU using various parameters, hyperbranched, both biocompatible and biodegradable, and multiblock SMPU has also been recently developed. Some of the selected studies are summarized in Table 14.2.

14.3.2   Vegetable Oil-Based Shape Memory Polyurethane

Castor oil is the only ideal vegetable oil that can be used directly in producing PU without the need to go through a modification process first. The fatty acid of castor oil is composed of 87.5 % ricinoleic acid which allows its hydroxyl groups to react with isocyanate, forming PU [7]. In spite of having naturally occurring hydroxyl groups in the fatty acids, castor oil has become one of the most exploited vegetable oils in the chemical industry with various attempts at modification so as to produce castor oil-based polyols for PU preparation. Meanwhile, other vegetable oils such as soybean, palm, linseed, rapeseed, and sunflower oils must undergo a modification process to increase the hydroxyl functional groups in order to enhance its reactivity.

In recent years, the development of PU elastomers using vegetable oil-based polyols as soft segments had gained special interest among researchers worldwide due to environmental concerns [56–59]. Since then, a number of studies are devoted by several research groups on the modification of vegetable oils for SMPU preparation [60]. Zhang and coworkers [26] developed a novel method to produce vegetable oil-based polyols using a solvent/catalyst-free pathway as an effort to produce 100 % bio-based polyols for SMPU preparation. They studied the effect of different vegetable oil (olive, canola, castor, grape seed, and linseed oils)-derived polyols as a soft segment in SMPU. The vegetable oil-based polyols were prepared through a ring-opening reaction between epoxidized vegetable oils and castor oil fatty acid. The resulting bio-

Table 14.1 The most common and important natural fatty acids [7, 25, 55]

Fatty acid	C atoms/number of double bonds	Formula
Stearic acid	$C_{18}:0$	$C_{18}H_{36}O_2$
Oleic acid	$C_{18}:1$	$C_{18}H_{34}O_2$
Linoleic acid	$C_{18}:2$	$C_{18}H_{32}O_2$
Linolenic acid	$C_{18}:3$	$C_{18}H_{30}O_2$
Palmitic acid	$C_{16}:0$	$C_{16}H_{32}O_2$
Ricinoleic acid	$C_{18}:1:hydroxyl$	$C_{18}H_{34}O_3$
Licanic acid	$C_{18}:3:carbonyl$	$C_{18}H_{28}O_3$

Table 14.2 Petrochemical-based SMPU

Hard segment	Soft segment	T_{switch} (°C)	Synthesis	Parameter studied	Comment	Ref.
MDI/TMP	PBAG (M_n 1000, 2000, 2800)	T_g; −6.8 to 57	SMPU; bulk polymer	Effect of different amount of TMP and length of PBAG chains on transition temperature and shape memory effect	The higher amount of TMP caused an increase of T_g and a broader range of the glass transition. The longer length of PBAG had lowered the T_g but broadened the range of T_g. Utilizing TMP as cross-linker had shown excellent shape recovery	[34]
IPDI/hybrid diol(HD)	PEO (M_w 400)	T_g; 19–53	SMPU; solution polymer	Effect of the different molar ratio of PEO:HD on T_g and shape memory effect. HD was synthesized using 2-hydroxyethylacrylate and 3-aminopropyl triethoxysilane containing Si-O-Si network	Decreased HD amount had decreased the T_g value as the Si-O-Si restricted the mobility of PU chains. Increase amount of HD had enhanced the shape recovery rate but lowered the shape fixity	[54]
MDI/BD, TDI/BD, and IPDI/BD	PLLA (M_n 3200)	T_g; 48–63	SMPU; solution polymer	Effect of different isocyanate on SMPU based on PLA as soft segment and BD as a chain extender	MDI-based SMPU has the highest T_g followed by IPDI and TDI. All samples showed excellent shape recovery 93–100 % and able to retain their temporary form at RT easily	[32]

MDI/BD	PCL (M_n 10,000)	T_m: 36–46	SMPU; bulk polymer	Effect of hard-segment content on thermal, mechanical, and shape memory properties and comparison with commercially available orthotic material	The SMPU samples prepared exhibit shape recovery, whereas the commercial splint had a negative response. Increasing hard-segment content decreased shape fixity. The cytotoxicity test indicated that the samples are non-cytotoxic	[31]
MDI/BD	PCL (M_w 4000)	T_m: 37–49	SMPU; solution polymer	Effect of different hard-segment content (10–50 %)	T_m decrease with increasing HSC. S_f decrease with an increase of HSC due to lower strain-induced crystallization of SS. Shape recovery was enhanced to nearly 100 % by applying predeformation above T_m on SMPU samples before shape memory test	[30]
MDI/BD/ ethylenediamine (ED)	PTMG (M_w 2000)	T_g(BD-PU); −18 to −10 T_g (ED-PU); 15–25	SMPU; bulk polymer	Effect of different chain extenders on shape memory properties of resulting SMPU	T_{trans} of ED-based SMPU increased by 30 °C as compared to BD-SMPU. Enhanced mechanical and shape memory properties obtained by ED-SMPU as compared to BD-SMPU	[28]

Table 14.2 (continued)

Hard segment	Soft segment	T_{switch} (°C)	Synthesis	Parameter studied	Comment	Ref.
MDI/BD, MDI/BPE, MDI/BES, and MDI/ND	PTMG (M_w 1000 and 2000)	T_g; −51 to 61 (PTMG1000) T_m; 14–24 (PTMG2000)	SMPU; bulk polymer	Effect of different chain extenders; BD, 4,4-bis(4-hydroxyhexoxy)-isopropylene (BPE), bis(2-phenoxyethanol)-sulfone (BES), napathoxy diethanol (ND), and length of PTMG (M_w 1000 and 2000)	SMPUs with PTMG-1000 exhibit amorphous soft segment, whereas SMPUs with PTMG-2000 have both amorphous and crystalline soft segments. Benzoyl and naphthalate group of chain extender showed improved shape memory effect as compared to aliphatic 1,4-BD	[27]
MDI/BD	PTMG (M_w 2000)	T_m; 1–30	SMPU; solution polymer	Effect of different types of cross-linker – glycerol (G), 1,2,6-trihydroxyhexane (H), and 2,4,6-trihydroxybenzaldehyde (B)	The higher range of T_m obtained using G and H owing to their aliphatic nature, whereas B-SMPU had the lowest T_m due to its rigid aromatic structure. The higher content of cross-linker did not further improve the shape recovery. Thus, minimal amount is sufficient. All the three cross-linker showed excellent shape memory effect. However, the impact of cross-linker structure on SME was minimal	[41]

based polyol was reacted with IPDI in the presence of dibutyltin dilaurate (DBTDL) as a catalyst in order to produce SMPU. The OH number of the vegetable oil-based polyols obtained increased from olive oil polyol < canola oil polyol < grape seed oil polyol < linseed oil polyol < castor oil polyol. Therefore, an increase in the degree of cross-link density of the thermoset SMPU prepared was observed. Consequently, castor oil-based polyol SMPU showed the highest in the value of T_g (54.6 °C), Young's modulus (495.3 MPa), tensile strength (29.1 MPa), and shape recovery (98.19 %).

Another research group, Corcuera and coworkers, prepared segmented SMPU by employing either a semicrystalline or amorphous castor oil-based polyol as the soft segment with HDI or MDI and BD as the hard segment [61]. It was reported that the soft-segment transition temperature of the SMPU for the amorphous system was in the range of 37–54 °C, whereas SMPUs with semicrystalline soft segment were between 56 and 65 °C. Shape fixity of the SMPU with a semicrystalline soft segment was higher than those with the amorphous soft segment, and the shape recovery decreased with increasing hard-segment content. On the other hand, the SMPU system with HDI showed lower shape fixity and higher shape recovery as compared to SMPU based on MDI. Later on, the same research group developed a SMPU using castor oil-based polyols as the soft segment, HDI, and corn-sugar-based 1,3-propanediol (PDO) as chain extenders via in situ polymerization method with 17 % hard-segment content and two different fillers, namely, cellulose and chitin nanocrystals [62, 63]. Both fillers showed improvement in shape memory properties while increasing filler loading.

Several other studies focused on vegetable oil-based polyol SMPU are tabulated in Table 14.3. These polymers are prepared via the two-step prepolymer method, in either solution or bulk, and the resulting mechanical and shape memory properties of the SMPUs are highlighted. Albeit only a few studies on SMPUs based on vegetable oil were found, there are many other research works in progress concerning vegetable oil-based segmented PU that could be potential candidates for shape memory polymers [57, 67–73]. As most of the works concentrate on producing SMPU with vegetable oils as the soft segment while still using petrochemical-based diisocyanate as the hard segment, Hojabri and coworkers [74] devoted a study on preparing segmented PU using fatty acid-derived diisocyanate and vegetable oil-based polyol in an effort to produce a fully bio-based PU. The value of soft segment's T_g was 27.5 °C and was suitable to be used as a smart PU.

14.4 Potential Application of Smart Polyurethane

Smart PUs are widely used in textile, engineering, and medical applications. In the textile area, SMPU is applied in fiber spinning and fabric and garment finishing. It can offer a temperature dependence on water vapor permeability for a SMPU-coated fabric. There is also potential to coat SMPU on a fabric such that its permeability changes as the wearer's environment and body temperature change, forming an ideal combination of thermal insulation and vapor permeability for military clothing. When the body temperature is low, the fabric is less permeable and retains body

Table 14.3 Vegetable oil-based SMPU

Hard segment	Soft segment	T_{switch} (°C)	Synthesis	Parameter studied	Comment	Ref.
MDI	Castor oil polyol (COP)	T_g: 8–28	COP; ADMET polymer. SMPU; solution polymer	Study of the different molar ratio of 10-undecenol in formulations of polyols. The mechanical and shape memory properties of the resulting SMPU were investigated	SMPUs derived from polyols with high amount of 10-undecenol (5 % molar ratio) exhibit semicrystalline nature and possessed shape memory properties while with the lower amount of 10-undecenol yield amorphous nature and do not exhibit shape memory effect	[64]
HDI/1,3-PDO	Soybean oil polyol (SOP)	T_g: 2–5	SOP; mild chemo-enzymatic route. SMPU; bulk polymer	Investigation of the effect of different molar ratio of SOP: PDO:HDI	Improved mechanical properties and excellent shape recovery obtained by increasing the molar ratio of PDO	[65]
HDI	Soybean oil polyol (SOP)	T_g: 3–32	SOP; chemo-enzymatic route. SMPU; Bulk polymer	Investigation of SMPU from soybean oil polyols having different structures (ring opening of epoxidized soybean oil using lactic acid, water, and isopropanolamine)	All SMPUs can recover their permanent shape at body temperature. Tensile strength varies between 3.9 and 18 MPa, whereas elongation at break in the range of 48–141 %	[66]

| HDI/corn-sugar-based 1,3-propanediol (PDO) | Castor oil polyol (semicrystalline, $M_n = 1900$) | T_m; 59–62 | SMPU; in situ solution polymer | The effect of chitin nanocrystal as reinforcing agent on mechanical and shape memory behavior | The YM and yield strength increased with increasing amount of filler (0.25–2 wt%) due to nucleation effect promoted by chitin nanocrystals, hence increased the hard-segment crystallinity. The thermomechanical cyclic test showed the constant value of Sf between 97 and 98 % while Sr increased from 52 % to 74 % with the addition of chitin nanocrystals at first cycle | [57] |

heat. When the body is sweating, it allows water vapor to escape into the air because its moisture permeability becomes very high with increasing body temperature. SMPU also can be laminated, filmed, foamed, and even converted directly into fibers. SMPU-laminated fabric produces a smart fabric with excellent properties (waterproof, windproof, and breathable) [75, 76].

Smart PU combines excellent mechanical properties with good blood compatibility, which favors their use and development as biomaterials, particularly as components for implanted devices [4]. SMPUs also have tremendous applications in other biomedical devices such as smart sutures, vascular stents, and micro-actuator for blood vessel clots and cardiovascular dent applications [77]. In surgical suture applications, the shape memory property of SMPU enables wound closure and supports both healing and tissue regeneration [78].

In technical and engineering applications, a combination of functionalities such as self-healing, antifouling, and superhydrophobic in PU smart coating make it preferable as a corrosion protection for steel. It is essential to mitigate corrosion problems in assets that are exposed to marine environments. Polyurea capsules functionalized with amino silanes were used to encapsulate hydrophobic linseed oil. The capsules were embedded in a polyurethane coating applied to steel and tested in 5 % NaCl solution. The final system shows an improvement in corrosion resistance due to the release of linseed oil into the micro cracks [79]. In addition, smart PU can also be used in food industry. The ox-CNT/PU nanocomposite has potential applications for controlling tags or proof marks in the area of frozen food due to a higher shape recovery ratio for the first cycle along with faster recovery [80].

14.5   Conclusion

In conclusion, smart polyurethanes are prospective materials in numerous different applications as their end properties may be tailored accordingly by the proper selection of raw materials. This chapter also presented the current trends in the development of conventional SMPU along with vegetable oil-based SMPU in response to environmental awareness. Though the idea of vegetable oil-based SMPU has evolved for some time now and several significant advances have been made in the novel route of producing vegetable oil-based polyols and the resulting SMPU, further efforts are still necessary in developing a practical synthesis method for bulk production.

References

1. Hepburn C (1982) Polyurethane elastomers. Applied Science, London
2. Oertel G (1985) Polyurethane handbook. Hanser Publishers, Munich
3. Petrovic ZS (2005) Polyurethanes. In: Kricheldorf HR, Nuyken O, Swift G (eds) Handbook of polymer synthesis, 2nd edn. Marcel Dekker, New York, NY

4. Lamba NMK, Cooper SL, Woodhouse KA (1998) Polyurethanes in biomedical applications. CRC Press, New York, NY
5. Wright P, Cumming APC (1969) Solid polyurethane elastomers. Maclaren and Sons, London
6. Thomson T (2005) Polyurethanes as specialty chemicals; principles and applications. CRC Press, Boca Raton, FL
7. Ionescu M (2005) Chemistry and technology of polyols for polyurethanes. Rapra Technology Limited, Shropshire
8. Schneberger GL (1983) Adhesives in manufacturing. Marcel Dekker, New York, NY
9. Jenkins MJ, Harrison KL (2006) Polym Adv Technol 17:474–478
10. Labet M, Thielemans W (2009) Chem Soc Rev 38:3484–3504
11. Tanaka R, Hirose S, Hatakeyama H (2008) Bioresour Technol 99:3810–3816
12. Lee CS, Lee SC (2010) Am J Pharmacol Toxicol 5:133–138
13. Badri KH, Ahmad SH, Zakaria S (2001) J Appl Polym Sci 81:384–389
14. Clemitson IR (2008) Castable polyurethane elastomers. CRC Press, New York, NY
15. Hepburn C (1992) Polyurethane elastomers. Elsevier, New York, NY
16. Cho JW, Goo NS, Jung YC, Kim JW (2005) Macromol Rapid Commun 26:412–416
17. Prisacariu C (2011) Polyurethane elastomers: from morphology to mechanical aspects. Springer, New York, NY
18. Meng KC, Young RJ (1989) Pengantar polimer. Dewan Bahasa & Pustaka, Kuala Lumpur
19. Lendlein A, Kelch S (2002) Reviews: Shape memory polymers. Angew Chem Int Ed 41:2034–2057
20. Lendlein A (2010) Shape-memory polymers. Springer, Berlin
21. Liu C, Mather PT, Qin H (2007) J Mater Chem 17:1543–1558
22. Pretsch T (2010) Polymer 2:120–158
23. Leng J, Du S (2010) Shape-memory polymers and multifunctional composites. CRC Press, New York, NY
24. Hu J (2007) Shape memory polymers and textiles. Woodhead Publishing Limited, Cambridge
25. Zhang L, Huang M, Yu R, Huang J, Dong X, Zhang R, Zhu J (2014) J Mater Chem A 2:11490–11498
26. Zhang C, Madbouly SA, Kessler MR (2015) ACS Appl Mater Interfaces 7:1226–1233
27. Wang HH, Yuen UE (2006) J Appl Polym Sci 102:607–615
28. Chun BC, Cho TK, Chung YC (2006) Eur Polym J 42:3367–3373
29. Jeong HM, Lee SY, Kim BK (2000) J Mater Sci 35:1579–1583
30. Ji FL, Hu JL, Li TC, Wong YW (2007) Polymer 48:5133–5145
31. Meng Q, Hu J, Zhu Y (2008) J Biomater Sci Polym Ed 19(11):1437–1454
32. Wang W, Ping P, Chen X, Jing X (2007) Polym Inter 56:840–846
33. Ahmad M, Luo J, Xu B, Purnawali H, King PJ, Chalker PR, Fu Y, Huang W, Miraftab M (2011) Macromol Chem Phys 212:592–602
34. Lin JR, Chen LW (1999) J Appl Polym Sci 73:1305–1319
35. Chung YC, Kim WS, Cho TK, Chun BC (2008) Fibers Polym 9(4):388–392
36. Lee SH, Kim JW, Kim BK (2004) Smart Mater Struct 13:1345–1350
37. Buckley CP, Prisacariu C, Caraculacu A (2007) Polymer 48:1388–1396
38. Feng Y, Xue Y, Guo J, Cheng L, Jiao L, Zhang Y, Yue J (2009) J Appl Polym Sci 112:473–478
39. Azra C, Ding Y, Plummer CJG, Månson JAE (2013) Eur Polym J 49:184–193
40. Chung YC, Choi JH, Chun BC (2008) J Mater Sci 43:6366–6373
41. Chung YC, Choi JW, Moon S, Chun BC (2009) Fibers Polym 10(4):430–436
42. Chung YC, Chun BC, Lee SD, Park JS (2010) J Appl Polym Sci 115:3568–3575
43. Chung YC, Nguyen DK, Choi JW, Chun BC (2010) Fibers Polym 11(7):952–959
44. Cao Q, Liu P (2006) Polym Bull 57:889–899
45. Sivakumar C, Nasar AS (2009) Eur Polym J 45:2329–2337
46. Kalita H, Karak N (2014) J Appl Polym Sci 131. doi:10.1002/app.39579
47. Kalita H, Karak N (2012) Polym Eng Sci 52:2454–2461
48. Fernandez AM, Abraham GA, Valentin JL, Roman JS (2005) Polymer 47:785–798

49. Ajili SH, Ebrahimi NG, Soleimani M (2009) Acta Biomater 5:1519–1530
50. Deka H, Karak N, Kalita RD, Buragohain AK (2010) Carbon 48:2013–2022
51. D'hollander S, Assche GV, Mele BV, Preza FD (2009) Polymer 50:4447–4454
52. Gu X, Mather PT (2012) Polymer 53:5924–5934
53. Dow launches soy-based polyol, joining a growing field. Plastics Today. http://www.plasticsto-day.com/articles/dow-launches-soy-based-polyol-joining-growing-field (Last Accessed: May 2015)
54. Xu J, Shi W, Pang W (2006) Polymer 47:457–465
55. Guner FS, Yagci Y, Erciyes AT (2006) Prog Polym Sci 31:633–670
56. Sonnenschein MF, Ginzburg VV, Schiller KS, Wendt BL (2013) Polymer 54:1350–1360
57. Zlatanic A, Lava C, Zhang W, Petrovic ZS (2004) J Polym Sci B Polym Phys 42:809–819
58. Bueno-Ferrer C, Hablot E, Garrigós MC, Bocchini S, Averous L, Jiménez A (2012) Polym Deg Stab 97:1964–1969
59. Ferrer MCC, Babb D, Ryan AJ (2008) Polymer 49:3279–3287
60. Li F, Larock RC (2002) J Appl Polym Sci 84:1533–1543
61. Corcuera MA, Saralegi A, Fernandez-d'Arlas B, Mondragon I, Eceiza A (2012) Macromol Symp 321–322:197–201
62. Saralegi A, Fernandes SCM, Alonso-Varona A, Palomares T, Foster EJ, Weder C, Eceiza A, Corcuera MA (2013) Biomacromolecules 14:4475–4482
63. Saralegi A, Gonzalez ML, Valea A, Eceiza A, Corcuera MA (2014) Composites Sci Technol 92:27–33
64. Rio ED, Lligadas G, Ronda JC, Galia M, Meier MAR, Cadiz V (2010) J Polym Sci A Polym Chem 49:518–525
65. Miao S, Wang P, Su Z, Liu Y, Zhang S (2012) Eur J Lipid Sci Technol 114:1345–1351
66. Miao S, Callow N, Wang P, Liu Y, Su Z, Zhang S (2013) J Am Oil Chem Soc 90:1415–1421
67. Petrovic ZS (2008) Polym Rev 48(5):109–155
68. Zhang C, Li Y, Chen R, Kessler MR (2014) ACS Sustain Chem Eng 2:2465–2476
69. Miao S, Sun L, Wang P, Liu R, Su Z, Zhang S (2012) Eur J Lipid Sci Technol 114:1165–1174
70. Das B, Konwar U, Mandal M, Karak N (2013) Ind Crops Prod 44:396–404
71. Miao S, Zhang S, Su Z, Wang P (2013) J Appl Polym Sci 127:1929–1936
72. Saralegi A, Rueda L, Fernandez-d'Arlas B, Mondragon I, Eceiza A, Corcuera MA (2013) Polym Int 62:106–115
73. Yaganeh H, Talemi PH (2007) Polym Deg Stab 92:480–489
74. Hojabri L, Kong X, Narine SS (2009) Biomacromolecules 10:884–891
75. Wirpsza Z (1993) Polyurethanes: chemistry, technology and applications. Ellis Horwood, New York, NY
76. Mondal S, Hu JL, Liu Y, Szeto YS, Yang Z (2002) Res J Textile Apparel 6:75–83
77. Yakacki CM, Eckstein A, Gall K, Lanning C, Rech B, Shandas R (2007) Biomaterials 28:2255–2263
78. Lendlein A, Langer R (2002) Science 296:1673–1675
79. Montemor MF (2014) Surf Coat Technol 258:17–37
80. Gu S, Liu L, Ren J, Yan B (2013) Eur Polym J 49:3867–3877

Chapter 15
Piezoelectric PVDF Polymeric Films and Fibers: Polymorphisms, Measurements, and Applications

Ramin Khajavi and Mina Abbasipour

Abstract The development of piezoelectric materials has surged forward due to their ability to convert mechanical energy into electrical energy and conversely. A wide range of materials have so far been introduced in the field, among which lead zirconate titanate (PZT) and polyvinylidene fluoride (PVDF) are the highlighted products because of their higher conversion efficiency, especially the high flexibility of the latter. PVDF is a semicrystalline polymer whose molecular structure is composed of a repeating monomer unit of $(-CH_2CF_2-)_n$. In this chapter, different polymorphisms of PVDF depending on the chain conformations of trans (T) and gauche (G) linkages are presented. Also, various methods such as Fourier transform infrared spectroscopy (FTIR), X-ray powder diffraction (XRD) analysis, and differential scanning calorimetry (DSC) employed for the investigation of phase transition are summarized. Strategies for the enhancement of the $\boldsymbol{\beta}$-phase such as mechanical stretching, electrical polling, and addition of fillers are discussed. Moreover, the evaluation components of the piezoelectric efficiency including piezoelectric coefficients, responding voltage, polarization-electric field (P-E) hysteresis loops, electric displacement field (charge per unit area), permittivity (also known as dielectric constant), and dielectric loss factor (tan $\boldsymbol{\delta}$) are emphasized. Finally, the applications of PVDF polymers were discussed in the design of piezoelectric sensors, actuators, and energy harvesting devices.

Keywords Piezoelectric materials • Fiber and film • Polymorphism • $\boldsymbol{\beta}$-Phase • Sensors • Actuators • Energy harvesting

R. Khajavi (✉)
Nanotechnology Research Center, Islamic Azad University,
South Tehran Branch, Tehran, Iran
e-mail: khajavi@azad.ac.ir; rkhajavi@gmail.com

M. Abbasipour
Department of Textile Engineering, Science and Research Branch,
Islamic Azad University, Tehran, Iran
e-mail: mina.abbasipour@gmail.com

15.1   Introduction

Medical devices that incorporate wireless technologies and are to be used in applications for the replacement of vital human organs have to be small and drive active functioning. Micro-electromechanical (MEM) and nano-electromechanical (NEM) devices are new possibilities that can be used to meet the energy requirements of such devices. Outstanding in the field, piezoelectric materials have been used widely. It is due to "their wide bandwidth, fast electromechanical response," and "relatively low power requirements." Piezoelectricity means the "generation of electrical polarization" for materials in response to a mechanical stress (direct effect), and vice versa [1]. Different materials exhibit piezoelectric properties, such as "zinc oxide, lead zirconate titanate (PZT), cadmium sulfide, barium titanate and gallium nitride" [1–5].

Piezoelectric polymers have received great attention in literature. Polyvinylidene fluoride (PVDF) is one example of such polymers that exhibit piezoelectric properties. Kawai [6] was the first to discuss PVDF's piezoelectric properties in 1969, highlighting its incredible flexibility and processability, thus enabling the creation of an entirely novel category of electroactive polymers (EAPs). Unfortunately, restraints such as reduced voltages and their ability for force generation have hindered the widespread adoption of EAPs [7–10]. In an attempt to triumph over these known EAP restrictions, various inorganic, high dielectric constant fillers such as ceramic powders, "barium titanate ($BaTiO_3$), lead titanate ($PbTiO_3$), lead zirconate titanate (PZT)," and lead magnesium niobate–lead titanate (PMN–PT) have been integrated into the matrix of PVDF [11].

This chapter discusses the different polymorphisms of a PVDF polymer depending on its chain conformation of trans (T) and gauche (G) linkages. Various methods to investigate its **β**-phase are presented, including Fourier transform infrared (FTIR), X-ray diffraction method (XRD), and differential scanning calorimeter (DSC). Some techniques are also presented for the enhancement of the **β**-phase such as stretching, electrical polling, and filler addition. Different methods are introduced for the evaluation of piezoelectric efficiency, including piezoelectric coefficients, voltage response, polarization-electric field (P-E) hysteresis loop, electric displacement (charge per unit mass), permittivity (dielectric constant), and loss in dielectric materials (tan **δ**). Finally, its applications as sensors, actuators, and energy harvesting are discussed.

15.2   Polymorphisms of PVDF

PVDF refers to a semicrystalline polymer with superior piezoelectric properties, having a repeated monomer unit of ($-CH_2CF_2-$)$_n$ [12]. The PVDF polymer has five distinct crystallite polymorphs, which are dependent upon the trans (T) and gauche (G) linkages in the overall chain conformation. PVDF's dominant **α-**phase polymorph

is composed of a monoclinic unit cell and is distinguished by its chain conformation of TGTG′ ("T=trans, G=gauche+, G′=gauche−"). PVDF's **β**-phase is of the most interest as it is the conformation [all-trans (TTTT)] that exhibits the piezoelectric crystallization polymorph alongside an orthorhombic unit cell. The other phases of interest are the **γ** (orthorhombic unit cell, TTTGTTTG′ conformation), **δ** (polar version of **α**), and **ε** (anti-polar version of **γ**). From all of these PVDF conformations, the most influential and typical are those of the **α**- and **β**-phases. The segment of **α**-PVDF's network is comprised of two chains that have a TGTG′ conformation, where the axis of the chain and the dipole components are antiparallel, thus neutralizing each other. As such, the **α**-phase is classified as being nonpolar and non-piezoelectric. In contrast, the **β**-phase's chain's axis and the dipole components are parallel. Therefore, its crystal formation creates the greatest spontaneous polarization while displaying pronounced ferroelectric and piezoelectric characteristics [12–15].

15.3   β-Phase Measurements

A wide range of strategies have been developed to measure the electroactive phases of PVDF, such as FTIR, XRD, and DSC [13]. FTIR spectra and XRD patterns are usually used for the identification of the phases. The **α-** and **β**-phases of PVDF are simply identified by FTIR spectroscopy and X-ray diffraction. However, the **γ**-phase has been incorrectly identified as the **β**-phase. It is difficult to identify and quantify both **γ-** and **β**-phases due to the similarity of specific conformations of their phases and their characteristics [15–23].

15.3.1   Fourier Transformed Infrared Spectroscopy

FTIR is used to explain differences in the crystalline forms of PVDF, where there are some common bands in the **α**- and **β**-phases. In addition, the sample can possess more than one crystal structure based on the preparation conditions. The **α**-phase of PVDF is easily detected by the FTIR absorption and is characterized by absorption bands at 489, 614, 766, 795, 855, and 976 cm^{-1}. Characteristic band patterns of the **β**-phase have been identified at 845, 745, 510, 445, and 1279 cm^{-1}.

As previously mentioned, the **β**- and **γ**-phases show a similar number of bands and waves due to the same polymer chain conformations. For example, the band at 512 cm^{-1} for the **γ**-phase is very close to the band at 510 cm^{-1} for the **β**-phase [16]. On the other hand, the band at 840 cm^{-1} is common to both **β**- and **γ**-phases; it is, however, a strong band just for the **β**-phase while demonstrating a shoulder on the 833 cm^{-1} band for the **γ**-phase (Fig. 15.1b). The bands at 431, 776, 812, 833, and 1233 cm^{-1} are attributed to the **γ**-phase [17, 18].

The FTIR results are also commonly used for the quantification of the electroactive phase content of PVDF; however, there is no single, uniform way to perform
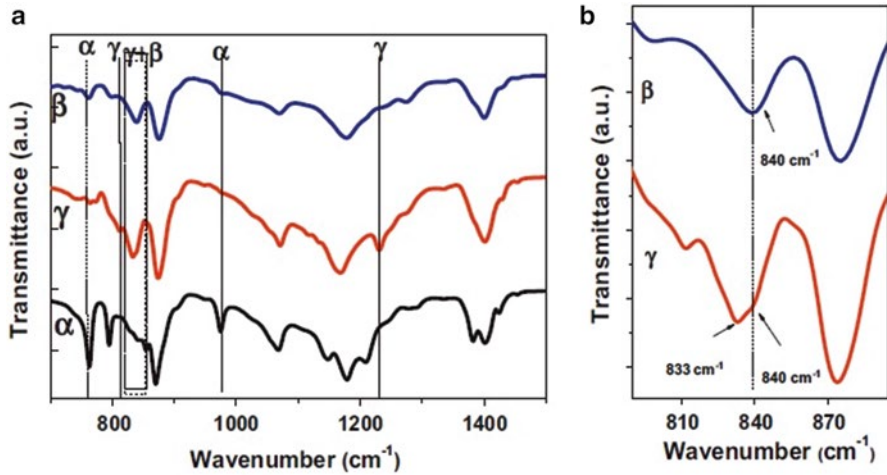
Fig. 15.1 FTIR–ATR spectra of **α**-, **γ**-, and **β**-PVDF with identification of the **α**-, **β**-, and **γ**-phase characteristics bands (**a**) and a detail of the **β**- and **γ**-characteristic region commonly used in the literature for the identification of the phases (**b**) (reprinted with permission from [24], copyright Elsevier)

this analysis. The calculation of β-phase content is determined by a band at 766 and 840 cm^{-1}, where K_α and K_β are the absorption coefficients at these wave numbers. Therefore, the relative fraction of the **β**-phase is calculated by using Eq. (15.1) [20]:

$$f(\beta) = \frac{A\beta}{\left(\dfrac{K\beta}{K\alpha}\right)A\alpha + A\beta}$$

(15.1)

15.3.2   X-Ray Diffraction

XRD is another method that can be utilized to identify the PVDF's phases. Until recently, the preparation of a sample with the **γ**-phase has been limited, and therefore, few diffraction diagram characteristics have been obtained from this phase [25, 26]. However, the comparative analysis of the diffraction peaks of the **α**- and **γ**-phase samples allows the identification of diffraction peaks belonging to the **γ**-phase [16]. Lopes et al. prepared a PVDF/clay and showed the characteristics peaks of **γ**-phase in XRD patterns [27]. All the **α**-, **β**-, and **γ**-phases show an intense peak around 2θ=20°, but only **α**- and **γ**-phases demonstrate different peaks close to 2θ=18°. Therefore, it is easy to distinguish the **β**-phase [26]. The **β**-phase shows a defined peak at 2θ=20.26° attributed to the 110 and 200 plane diffractions [26, 27]. The **α**-phase presents characteristic peaks at 2θ=17.66° and 18.30° corresponding

to 100, 020, and 110 planes, respectively. In addition, the **α**-phase also presents a
peak at $2\theta = 26.56°$ corresponding to the 021 diffraction plane [26, 28, 29]. Finally,
the **γ**-phase provides peaks at $2\theta = 18.5°$ and $2\theta = 19.2°$ related to the 020 and 002
planes, respectively. Also, a more intense peak can be detected at $2\theta = 20.04°$ associ-
ated to the 110 crystalline plane. Similar to the **α**-phase, the **γ**-phase presents a
weaker peak at the region of 26.8° associated with the (022) plane. Figure 15.2
shows the diffraction for crystal plane and angle for different phases of PVDF.

15.3.3   Differential Scanning Calorimetry

DSC is a widely used method that can be utilized to determine the PVDF's crystal-
line phases. Different melting peaks appear in the DSC thermogram according to
the crystalline phase of PVDF. Prest and Luca recorded the **α**-phase in the endother-
mal peak at 172 °C [15], while Gregorio and Cestarini obtained a peak at 167 °C
[25]. In other words, the **β**-crystallites exhibit a melting temperature which is simi-
lar to that of **α**-PVDF [16, 18, 25]. Thus, DSC was not applied to differentiate these
two phases [27, 28]. The melting temperature was about 8 °C, greater than that of
the **α**-phase (between 179 and 180 °C). The **γ**-phase acquired by the crystallization
of the melt (from the **α**→**γ**-transformation; represented as **γ**′) showed the melting
temperature was about 18 °C, greater than the melting temperature of the **α**-phase
(189–190 °C) [16, 18].

15.4 Enhanced β-Phase Formation in PVDF Polymer

Multiple techniques have been utilized during the production process so as to achieve dipole alignment in the crystalline structures in an attempt to fabricate **β**-phase PVDF, including uniaxial or biaxial stretching [26, 30–34], high electric field [35], thermal annealing [36–40], and fillers [41–45]. Polymer chains are aligned into the all-trans planar zigzag (TTT) conformations when stress is applied in the film. The stretching process caused the normal alignment of the polymer chain's dipoles in the direction of the applied stress [30]. It was reported that the stretching speed had little effect on F (β), whereas the drawing ratio had a significant influence on F (β) value. Li et al. found that the characteristic peak of the **β**-phase was increased with increases in stretching temperatures [29]. As reported, the highest **β**-phase content was observed at 80 °C, the temperature required reaching maximum β-phase content along with a stretch ratio (R) of 5. Via the mechanical stretching methodology, PVDF's **α**- to **β**-crystal transformation was illustrated by 3D-DM photos upon completion of in situ investigation under an optical tensile stress microscopy tester (Fig. 15.3). Post-stretching, transversal belt creation can be seen in the middle of the deformed spherulites.

Apart from mechanical stretching and electrical poling on phase changes, various fillers, such as graphene [46–60], carbon nanotubes (CNT) [61–67], and clay [28, 68, 69], have been introduced to improve the **β-**phase content. For example, in a reported study, nanoclay materials were added in order to enhance the formation of the

Fig. 15.3 The polarized photo of stretched samples observed by polarized module of 3D digital microscope (reprinted with permission from [41], copyright RSC)

β-phase [69]. Different studies have proven the effect of CNT (such as single-wall carbon nanotube (SWCNT), multi-wall carbon nanotube (MWCNT), and modified MCNT with NH$_2$) on the β-phase formation [61–67]. The β-phase was found to increase by increasing the CNT content in the matrix. For example, the intensity of β-phase peak increased as the SWCNT content increased. The β-phase content was elevated up to 14 % through the addition of 3 wt% SWCNT. However, the β-phase content was increased to 39 % by adding a 3 wt% MWCNT [62]. The MWCNTs was reported to act as nuclei which could lead to higher crystallization in the β-phase [70]. Further, the interactions between the functional groups on the MWCNTs and the CF$_2$ dipole of PVDF chains result in the establishment of local orientation of the β-phase, significantly affected by the increased crystallization rate that occurs because of the McCants's presence. A PVDF/Ag nanowire (AgNW) nanofibers by using the electrospinning method was prepared by Li et al. [71]. It was observed that the AgNW increased the content of β-phase [71]. The produced electrospun PVDF/clay nanofibers by Liu et al. [72] revealed the α-phase, whereas the α-phase was completely removed in the electrospun PVDF/clay nanofibers.

15.5 Piezoelectric Measurements

15.5.1 Piezoelectric Charge Constant (d)

When mechanical stress (1 N/m^2) is applied to a film's surface, the *piezoelectric charge constant* (C/N) is identical to the charge density (Coulomb/m^2). Conversely, a piezoelectric material receives mechanical deformation (m/m) per unit of the electric field (V/m). In the following equation, d's first subscript refers to the polarization direction generated in the material, when the electric field (E) is 0 or, conversely, displays the applied field strength's direction. d_{3j} shows the film's piezo-activity, relating to the electrical charges supplied by 1 m^2 when a pressure of 1 Pa is exerted along the "j" axis (Eq. 15.2) [73]:

$$\mathbf{dij} = \text{electrical charge density / applied stress} = \frac{Qi}{Ai} / \frac{Fj}{Aj} \tag{15.2}$$

(A_x = area according to axis x, F = force, Q = charge)

Generally, mechanical stretching is identified as positive while compression is identified as negative. Furthermore, the positive electric field's direction is related to the dipoles' orientation. As such, d_{33} is negative, while both d_{31} and d_{32} are identified as positive. These films exhibit a positive side mark. This side will measure positive voltage (the other grounded), when the film is compressed along axis three or stretched along the axes one or two. It should be noted that the voltage reading from the film's opposing side results in a reversed value. d_{33} is obtained by using Eq. (15.3) [73]:

$$Q = d_{33}.F \tag{15.3}$$

A polarized PVDF film was found to exhibit $d_{31} = 17$, $d_{32} = 5$–6, and $d_{33} = 21$ pC/N [74]. Fillers can enhance dielectric constants. A reported study concluded that d_{33} of a PVDF film was increased by adding a MWCNT [75]. The value of d_{33} was found to be dependent on the amount of β-phase, showing the same behavior as the β-phase. An average piezoelectric coefficient ($d_{33} = -57.6$ pm/V) for electrospun PVDF nanofibers through a near-field electrospinning technique were obtained [76]. The electrospun PVDF nanofibers exhibited various piezoelectric coefficients by changing fiber diameters. Various studies have reported different piezoelectric coefficients due to different thicknesses. For example, the piezoelectric activity of a PVDF/nanoclay/MWCNT nanocomposite was reported to be zero [77]. The possible reason for this is strong interactions between nanomaterials and PVDF chains which limit the mobility of PVDF chains, thereby shifting the stretching force on the chains toward the crystal front.

15.5.2   Voltage Response

The *piezoelectric voltage constant* (g) is defined as the generation of an electric field via piezoelectric material per unit of applied mechanical stress applied to said material, or in other words, it is the mechanical strain exerted upon a piezoelectric material per unit of electric applied displacement [73]. The term **g**'s initial subscript designates the material's generated electric field direction or the applied electric displacement directionality. The subsequent subscript is the applied stress' direction or the induced strain's direction. The product of the applied stress and **g** values yields the piezoelectric material's generated electric field strength as a response to an applied physical stress; thus, the assessment of a material's applicability for sensing (sensor) applications relies heavily upon the value of **g**. Generation of an electric field (E) via an external stress (σ) in piezoelectric materials and the magnitude of said electric field are believed to be theoretically "proportional to the piezoelectric voltage coefficient [g_{33} (Eq. 15.4)] [78]:

$$E = g_{33}.\sigma \tag{15.4}$$

The equation can be simplified to **E=V/L** and **σ =εY**, where the length of the material is represented by **L** and **Y** stands for the material's Young modulus. The output voltage is denoted as **V** which can be obtained by Eq. (15.5) [78]:

$$V = g_{33}\varepsilon YL \tag{15.5}$$

Chang et al. produced a PVDF nanogenerator by using the near-field electrospinning technique [79]. While undergoing mechanical stretching, generation of positive voltage (5–30 mV) and current (0.5–3 nA) took place. As the nanogenerator

released strain, observation of corresponding negative peaks was witnessed in output voltage and current readings. However, poly ethylene oxide (PEO) nanofibers were noisy, although no visible peaks were shown. It means that PEO nanofibers demonstrated some piezoelectric behavior unlike PVDF nanofibers. Chang et al. found that piezoelectricity enhanced by incorporating CNT [79]. The PVDF/CNT nanofiber generated 6.2 mV under 0.076 % strain.

15.5.3   Polarization-Electric Field (P-E) Hysteresis Loop

Data gathered from the comparison between field and polarization studies provide addition insight into the material's properties including losses, charge storage, and impedance characteristics, all of which are crucial in the design of driving electronics. Minimum coercive energy and remnant polarization (P_r) are exhibited by neat PVDF films. While similar coercive energy is displayed at certain electric fields by PVDFs that are rolled and poled, differences can be seen in the P_r and the area under the peak. Piezoelectric behavior is observed when preferential orientation is achieved in the dipoles (electric field parallel to the plane), which is achieved via rolling [80]. In a reported study, the effects of the addition of MWCNT on the P-E [70] have been investigated. The authors obtained a larger remnant polarization (**P_r**) for the drawn and poled PVDF/MWCNT nanofiber composite films when compared to drawn and poled nano-fibrous pure PVDF films [70]. PVDF/MWCNT composite films resulted in a much higher value of **P_r** than neat PVDF films, which was due to an increase in the amount of the **β**-phase at the presence of MWCNT [75].

15.5.4   Electric Displacement (Charge per Unit Mass)

Precise actuator strain versus field characteristic measurements are needed so that the piezoelectric or electro-strictive actuators in smart structure systems are effective. As most often seen in electro-strictive materials, non-linearities are exhibited by these properties along with fluctuations in hysteresis, temperature, frequency, and aging effects. For quality control, design, and optimization purposes, these actuator control systems require precise characterization [80]. The central deformations of PVDF fibers using a finite element analysis software and digital microscope with a charge-coupled device (CCD) were measured [76]. It was found that the existence of the piezoelectric effect led to larger downward displacements (−0.418 μm) under a negative electric field (−1.2 V/μm), as compared to the displacements (0.425 μm) under a positive electric field (1.2 V/μm) [76]. Similarity, center displacements of 5 μm for PVDF/MWCNT fibers were obtained [75]. Central displacements were produced when an external electric field (+E) was applied along the fiber length. There was a linear relationship between fiber central deformations and applied electric fields. Cauda et al. obtained butterfly displacement-field loops

in PVDF and poly(vinylidene–fluoride–trifluoroethylene) [P(VDF–TrFE)] NWs [81]. It was found that the displacement of PVDF/MWCNT enhanced as the **β**-phase increased [70]. Energy densities can be calculated though the electric displacement–electric field (D–E) loops obtained from the P–E loops by using the relationship as follows (Eq. 15.6):

$$\bar{D} = \varepsilon \bar{E} + \bar{P} \tag{15.6}$$

(where P is the polarization, E is the applied electric field, and D is the electric displacement field).

15.5.5 Permittivity (Dielectric Constant)

Generally speaking, two parameters dictate the dielectric constant: the dipole orientation found in the polymer's amorphous segments and formation of crystal defects inflicted by the chain folding and free chain ends. In this regard, dielectric polarization is affected by the orientation of the crystals and close packing. There is speculation that reorientation of dipoles can be prevented by the intense chain attractions that come from the close packing of the crystals. The processing effects imposed upon the PVDF's dielectric properties have been studied and reported [80]. The dielectric constants in a specific frequency range (10^2–10^6 Hz) were found to be similar for neat, poled, and rolled PVDFs. This behavior is due to the fact that for ambient temperature, the orientation of the dipole within the amorphous regions is unaffected by the poling process. Since the rolled samples display and electric field perpendicular to the chain, neat PVDF has a lower "dielectric permittivity" than those that are rolled. It seems that two possible reasons contribute in decreasing of permittivity. First, the crystal created in the rolling process limits the free movement of the electric dipoles. Secondly, the presence of crystal–amorphous interfaces leads to decreased "dielectric permittivity." As reported, the "dielectric permittivity" of annealed PVDF films is less than that of the neat PVDF due to de-poling effects. In addition, simultaneously poling and mechanical rolling processes lead to a decrease in the "dielectric permittivity." This can be attributed to a negative effect of poling at 100 °C and destruction of the structure due to mechanical rolling. It can be concluded that a mixed process resulted in decreased "dielectric permittivity."

Gregorio and Ueno studied the effects of the crystalline phase, uniaxial drawing, and temperature on real (ε') and imaginary parts (ε'') of complex relative permittivity of PVDFs at a frequency range of 10^2 and 10^6 Hz [82]. It was found that the crystalline phase induced strong influences on the values of ε' and ε''. An increase in ε'' at high-frequency regions can be attributed to the α_a relaxation process (or **β**-relaxation), associated with the glass transition of PVDF. In addition, the molecular orientation led to increased values of ε' for both PVDF phases and also modified its dependency to the temperature over the whole frequency range. Phase transformations and crystal structure changes resulted from nanofillers that could further influence

the electric/dielectric properties of a nanocomposite. For instance, the crystalline phase exerted a strong impact on both real (ε') and imaginary parts (ε'') of complex relative permittivity, indicating that the ε' increased along with amounts of **β**-phase and molecular orders.

It was found by that the dielectric constant could be expressed as a function of annealing time and temperature [83]. Decreases in dielectric and piezoelectric responses were observed in the initial 4 h at a specific temperature (specifically, above 80 °C), with stability increasing over extended annealing periods. PVDFs' dielectric properties and the influence that carbon nanofibers (CNFs) exert upon them were studied by Tang et al. [84]. The authors evaluated the dielectric constant of different pure, stretched, and recrystallized samples at a frequency range of 10^3–10^6 Hz at ambient temperature. An increase in the dielectric constant was observed as the CNF content increased. Furthermore, the impact of CNTs on the "dielectric permittivity" of PVDF nanofibers [85] demonstrated that composites with higher content of CNTs had higher permittivity values [86]. For example, the permittivity values measured for the PVDF fibers with 0, 1, 2, and 3 wt% CNT at 100 Hz were 9, 12, 14.6, and 16.6, respectively. Moreover, the dielectric properties of PVDF/MWCNT nanocomposites have been investigated [87]. It was shown that the dielectric constant values increased with increased MWNT loading levels [86]. Also, the dielectric constant of a composite with higher content of MWCNT was greater than that of low loaded content. In a separate work, the dielectric constant of a PVDF/clay composite with different contents of clay [42] was reported to be increased with the addition of clay content and that the sample with a higher content of clay had a higher dielectric constant. The dielectric behavior of electrospun PVDF/ZnO nanocomposites has also been studied [87]. When compared to composite's (bulk-ZnO/PVDF) and constituent materials' (both bulk-ZnO and PVDF) dielectric constants, the dielectric constant was found to significantly enhance at lower frequencies [87]. A 0.1 wt% graphene oxide (GO) nanocomposite was found to exhibit higher relative dielectric constants than the pure copolymer sample [88]. The reason was that the pure Poly(vinylidene fluoride-hexafluoropropylene) sample had less polar phases (**β**- and **γ**-phase) than the PVDF–HFP/GO. The relative dielectric constants for the pure copolymer and the 0.1 wt% PVDF–HFP/GO at 1 kHz were 11.5 and 13.9, respectively. When characterizing the dielectric constant of a PVDF/functionalized GO [89], it was observed that the dielectric constant began to increase due to the addition of functionalized GO.

15.5.6 Loss in Dielectric Materials (tan δ)

The term tan **δ** (or loss tangent) is typically utilized to explain the loss in dielectric materials and it is shown by Eq. (15.7) [81]:

$$\tan\delta = \frac{\varepsilon''}{\varepsilon'} \tag{15.7}$$

where the imaginary and real parts of permittivity are expressed as ε' and ε'', respectively. This behavior may be due to the "high packing density and crystallographic texture" imparted by the mechanical rolling process, where a lower tan δ places limitations on chain mobility. These investigations have determined that, with minimal losses, materials with decently large dielectric constants can be synthesized industrially via the mechanical rolling process [81]. The dielectric loss can be potentially increased with the addition of clay at lower frequencies [42], while it was remained constant for different samples at 10^2 Hz to 1 MHz. The dielectric loss of PVDF–HFP and PVDF–HFP/GO films by using dielectric spectroscopy has also been evaluated and reported [88]. The results showed that the dielectric loss was due to the dipolar relaxation mechanism of a polymer above 10 kHz and the conduction loss of GO below 10 Hz. Moreover, the dielectric loss of both materials was similar in the range of 0.04 at 1 kHz to 0.11 at 1 MHz. It is worth mentioning that with an increase in the functionalized GO into PVDF, the dielectric loss can be increased [89].

15.6 Piezoelectric PVDF Application

PVDF is attractive for many energy converting applications between the electric and mechanical forms as it has an inexpensive structure, high flexibility, and biocompatibility. PVDF's piezoelectric properties have been utilized in the production of multiple products including "strain sensors, mechanical actuators, energy harvesters and artificial muscles" [90–94].

15.6.1 Sensors

Piezoelectric materials can be directly used as sensors in structures that cannot generate their own power and require little external circuitry. Such piezoelectric sensors can measure vibration signals in the structure as to indicate the onset of damage (i.e., acoustic emission). PVDF and its copolymers such as P(VDF–TrFE) are used in sensing applications. The sensitivity of PVDF sensors is related with the content of β-phase [90]. Lee et al. investigated effects of different substrates [e.g., slide glass, poly(ethylene terephthalate), and poly(ethylene naphthalate)] and the effect of paper thickness on the piezoelectricity of PVDF nanofibers [91]. The study revealed that the thinnest paper substrate led to the highest voltage output. Development of a new acoustic sensor was achieved via the dual-electrode sandwiching of microsized PVDF pillars [92]. Individual PVDF transducers (single units or with a curved configuration) could be used to build ultrasonic range sensors, transmitters, or receivers [93]. Characterization and comparison was completed for a large-area PVDF film with another PZT so as to evaluate their ultrasonic performance [94]. Due to their proclivity for robotic applications [95], the proposal of a new PVDF touching sensor called "piezoelectric oxide semiconductor field effect transistor (POSFET)" [96] was

applied for human skin condition monitoring [97]. While taking into consideration a conventional PVDF touch sensor, one of multilayered film construction was procured for pain sensor production [98], and peak monitoring within the PVDF sensors output enables material identification after contacting its target [99, 100]. The detection of the incident slippage and static friction was completed via PVDF-based tactile sensors with structured electrodes [101].

In study of a piezoelectric sensor based on PVDF nanofibers [102], the sensitivity of the sensor was investigated with different applied forces. Moreover, a pressure sensor utilizing PVDF/AgNW nanofibers was developed [90], where the sensitivity was found to enhance with increasing the content of AgNW. This study obtained a sensitivity close to 30 pC/N for the nanofiber webs with 1.5 wt% Ag NWs, near to that of poly(vinylidene–fluoride–trifluoroethylene) [i.e., (P(VDF–TrFE)], 77/23 (wt/wt). Through the production of c fibers, it was found that the electrical sensitivity was improved with increasing PPy [103]. The explanation for the improvement was that the relative conductivity was enhanced by increasing the contact between PVDF/PPy fibers. According to a reported study, a greater voltage response (i.e., 96.62 V/J) could be achieved by the sponge-supported sensor, compared to the rubber-supported sensor (82.26 V/J) [74]. When using a developed PVDF/CNT nanocomposite for the application of strain sensors, the sensitivity of the sensor was evaluated with a gauge factor [104], and an impact sensor was produced by a PVDF film sandwiched. Sharma et al. [105] provided aligned core-shell PVDF–TrFE nanofibers (PVDF–TrFE used as the shell and PVP/PEDOT: PSS as the core) for pressure sensors of endovascular repair [106]. The authors tested the sensor's response in vitro under simulated physiological conditions. It has been reported that the core-shell fiber-based sensor exhibited 40-fold higher sensitivity than thin film structure.

15.6.2 Actuators

Given their converse piezoelectric properties, piezoelectric materials can be used as actuator systems. They have unique properties because they provide mechanical excitations to a structure (e.g., guided waves) when driven by a tuned AC electrical signal. Under an applied electric field, the piezoelectric effect will generate a mechanical strain of a magnitude (ε_p) along the fiber axis as described in Eq. (15.8) (without considering external forces applied to the fiber) [76]:

$$\varepsilon_p = d_{33}E \tag{15.8}$$

where $\mathbf{E}$ is the applied electric field vector and $\mathbf{d_{33}}$ is the piezoelectric coefficient.

Compression and stretching in the fiber, respectively, was due in part by the positive (same direction of fiber polarity) and negative (opposite direction to polarity) electric fields form the negative $\mathbf{d_{33}}$ value of PVDF [76]. PVDF fibers were synthesized by via the implementation of near-field electrospinning methods [76]. Many applications for these fiber-based actuators have been found including artificial

muscles and switches. Sulfonated poly(ether ether ketone) (i.e., SPEEK) and PVDF were combined to form a novel electroactive polymer based upon blended polymer membrane, created as a cost-saving, high-performance, controllable rigid/ionic networked polymer actuator [106]. The SPEEK/PVDF actuator was found to generate much larger tip displacements (approximately 1.2 in 0.1 Hz and 2.5 in 3 V) than the SPEEK actuator [106]. In a recent study, a hybrid electroactive polymer actuator using PVDF/bacterial cellulose nanowhiskers via an electrospinning method was developed [107]. The actuator caused a significant performance as 3.4 mm and 4.5 mm for the sinusoidal and step inputs. The development of a micro-cantilever actuator based on a PVDF film using a spin-coating technique has also been reported [108]. Two cantilevers were fabricated having different thickness and width (20 μm and 500 μm) and length (2 mm and 3 mm) values. The result was maximum actuations of 100 μm for 2 mm length and 170 μm for 3 mm length at 300 V. Fu et al. used piezoelectric PVDF/nickel iron for the design of piezoelectric cantilever actuator [109]. The cantilever generated a deflection of 70 μm. A poly(styrene-alt-maleimide) (PMS) incorporated PVDF composite by using electroless-plating technique was prepared by Lu et al. [110]. The authors measured resonant frequency, tip displacement, current, and blocking force so as to compare the composite actuator to the traditional Nafion actuator. The displacement of PDF/PMSI actuator was larger than that of the Nafion-based actuator.

A piezoelectric sensor can also be used for simultaneous actuation and sensing of the vibration. Of such utilizations, the use of a PZT wafer as a structural actuator and/or sensor and the PVDF film as a sensor [111], as well as a new double PVDF actuator/sensor pair arrangement for vibration control in a cantilever tip [112], can be mentioned. Furthermore, in order to provide both actuator and sensing capabilities, the optimization between $\mathbf{d}_{31}$ and $\mathbf{g}_{31}$ has been performed and reported [113].

15.6.3 Energy Harvesters and Nanogenerators

Power generation devices based on piezoelectricity have been investigated in small mechanical energy harvesting applications. Mateu and Moll designed a piezoelectric generator to harvest energy from human activities during walking (Fig. 15.4) [114]. In another study, a piezoelectric PVDF generator was fabricated to harvest energy from walking [115]. Instead of alumina foil, the collector was covered by a nickel-copper-coated PET to produce nanostructures and, consequently, to increase the output performance. The maximum output voltage, power, and output current obtained were 210 V, 2.1 mW, and 45 μA, respectively. Through the utilization of backpack device, a new energy harvesting device has been created with PVDF that could produce electricity via the differential forces found between the user and the device used (Fig. 15.5) [116].

Evaluating the energy scavenging abilities of carbon black-filled poly(vinylidene–fluoride–trifluoroethylene–chlorofluoroethylene) [P(VDF–TrFE–CFE)] composite, Lallart et al. [117] found that the P(VDF–TrFE–CFE)/carbon had an electric energy

Fig. 15.4 A piezoelectric film-based power generator (reprinted with permission from [4], copyright Springer Ltd)

Fig. 15.5 Schematic of the backpack with piezoelectric straps (reprinted with permission from [4], copyright Springer Ltd)

density 2000 times higher than pure polyurethane. The voltage responses of both PZT composite structures and PVDF strips under various wind speeds and water droplets for the generation of electricity have been investigated [118]. In this study, the influence of material dimensions, drop mass, drop release height, and speed of the wind was examined for voltage output. Greater voltage/power generation could be achieved through the use of PVDF over other PZT materials. The energy harvesting capacity of piezoelectric PVDF was determined for simulated blood pressures via FEM analysis so as to theoretically evaluate both square and circular configurations

[119]. Fang et al. [120] fabricated randomly oriented PVDF nanofibers by a needless electrospinning technique. The authors found that the higher **β**-phase resulted in higher energy conversion efficiency and that the generation of pulse voltages was observed when the nanofibers' membrane subjected to compression [121]. Through a design of a self-charging power cell, hybridizing energy generation and storage with a piezoelectric PVDF film and lithium-ion battery were studied [122]. This harvester allows conversion of mechanical energy to electricity and further stores electric energy in the form of chemical energy. In a produced $BaTiO_3$ nanoparticle/piezoelectric PVDF film [123], it was observed that the voltage reached 150 V, capable to turn on three light emitting diodes. An output voltage of 16.7 V and a current density of 0.2 $\mu A\ cm^{-2}$ were obtained for 800 mN of stretching power of a piezoelectric film device consisting of a PEDOT/PVDF/PODET layer used in harvesting systems to convert mechanical energy to electrical power [124]. Moreover, the design of a triboelectric–pyroelectric–piezoelectric hybrid cell for high-efficient energy harvesting and self-powered sensing has recently been reported [125].

Using a polarized PVDF film, a flexible hybrid energy cell was fabricated to harvest thermal and mechanical energies [126]. The usage of Li batteries as energy storage devices can drive four red LEDs. Of the most recently developed energy harvesting devices is a novel energy harvesting device from human motion at low frequencies and low forces [127], in which the pendulum is used to convert the energy of walking and jogging into electricity. It was found that a maximum of 300 μm was produced at the frequency of 2 Hz. Electrical outputs of approximately 0.1 V and 10 nA cm^{-2} at an angle 90° were achieved using an energy harvester based on PVDF/ZnO NW fibers to convert low-frequency motions (<1 Hz) of the human arm into electricity [128]. Spin-coating method has been utilized to fabricate a flexible nanogenerator made of a P(VDF–TrFE) film [129], in which the nanogenerator exhibited an open-circuit voltage up to 7 V and short-circuit current of 58 nA. In another research, the usage of piezoelectric PVDF micro-belts to convert the energy of low-speed airflow to electricity was reported [130]. With the harvester fixed in the corrugation direction at two edges and free on the others, a bimorph power harvester composed of corrugated PVDF has been postulated [131].

So as to maintain the harvester optimal running conditions, adjustments were made to its resonant frequency by altering its geometrical configuration. By utilizing its switch-mode power electronics as a control mechanism, a piezoelectric device's voltage/charge relative to the mechanical input was optimized for energy conversion in an active energy harvesting scheme put forth by Liu [132]. The amount of energy harvested increased by a factor of 5 for the same mechanical displacement was achieved by this methodology in comparison to an optimized diode rectifier-based circuit. Through using near-field electrospinning to produce piezoelectric PVDF nanofibers, under mechanical stretching, repeatable electrical outputs with efficient energy conversion were reported [79]. Made up of a piezoelectric PVDF nanofiber generator, a hybrid energy scavenging device that gathers biomechanical and biochemical energy was developed by Hansen et al. [133]. Medical micro-robots intended for use within blood vessels were thought to benefit from the minute energy harvesting devices [134]. These devices were synthesized via conversion of efficient
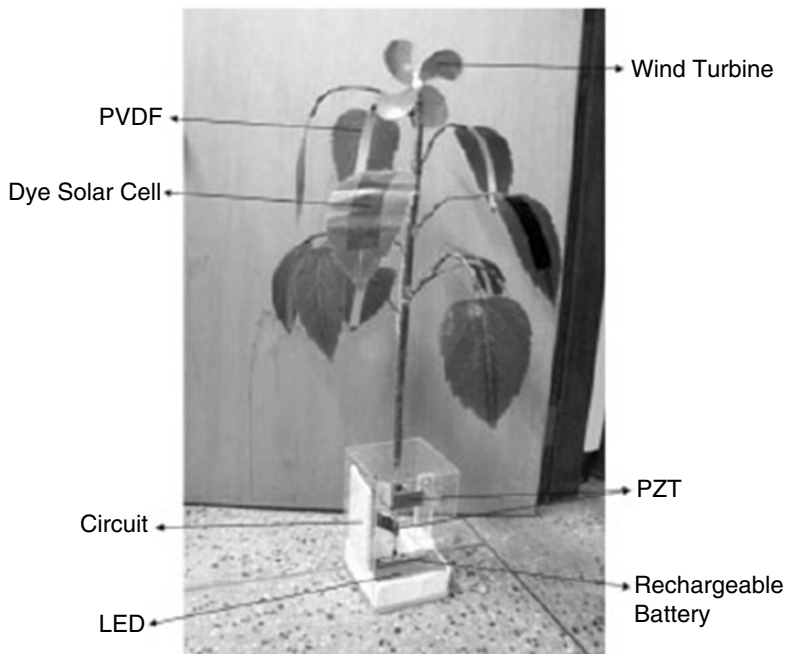
Fig. 15.6 A prototype tree-shaped wind power system (reprinted with permission from [4], copyright Springer Ltd)

piezoelectric PVDF components so as to yield coaxial nanofibers (polyaniline core, PVDF shell). Piezoelectric materials have also been utilized in the design of a tree-shaped wind-powered system for energy scavenging [135]. The system was driven by PVDF (as the leaf element) and PZT (trunk portion) as to generate power (Fig. 15.6). The production of a pressure nanogenerator by using the far-field electrospinning method for P(VDF–TrFE) has been the focus of a study in which an output voltage of about 400 mV under different compression tests was reported [136].

15.7 Conclusion

Recently, a great deal of attention has been paid to the piezoelectric materials because of their capability in converting mechanical energy into electricity. The application of piezoelectric materials has been investigated in MEM and NEM devices; however, piezoelectric PVDF polymers have been widely studied due to their flexibility. A wide range of strategies are employed for the dipolar alignment in crystalline PVDF structures to obtain the **β**-phase of PVDF, including uniaxial or biaxial stretching, high electric field, thermal annealing, and filler addition. Different methods such as FTIR, XRD, and DSC are applied for the identification and

quantification of the **β**-phase. Piezoelectric PVDF has been used for varieties of technologies including but not limited to sensors, actuators, energy harvesters, and nanogenerators. Measurements of voltage response, polarization-electric field hysteresis loop, displacement, permittivity, and piezoelectric constant are usually performed when investigating the piezoelectric properties of PVDF polymers.

References

1. Nechibvute A, Chawanda A, Luhanga P (2012) Piezoelectric energy harvesting devices: an alternative energy source for wireless sensors. Smart Mater Res 2012:1–13
2. Dakua I, Afzulpurkar N (2013) Piezoelectric energy generation and harvesting at nano-scale: materials and device. Nanomater Nanotechnol 3:1–16
3. Fang X-Q, Liu J-X, Gupta V (2013) Fundamental formulations and recent achievements in piezoelectric nano-structures: orientation. Nanoscale 5:1716–1726
4. Kim HS, Kim J-H, Kim J (2011) A review of piezoelectric energy harvesting based on vibration. Int J Precis Eng Manuf 12:1129–1141
5. Bowen C, Kim A, Dunn S, Weaver P (2013) Piezoelectric and ferroelectric materials and structures for energy harvesting application. Energy Environ Sci. doi:10.1039/C3EE42454E
6. Kawai H (1969) The piezoelectricity of poly(vinylidene fluoride). Jpn J Appl Phys 8:975–976
7. Bar-Cohen Y, Zhang Q (2008) Electroactive polymer actuators and sensors. MRS Bull 33:173–181
8. Lovinger AJ (1983) Ferroelectric polymers. Science 220:1115–1121
9. Fukada E (2000) History and recent progress in piezoelectric polymers. IEEE Trans Ultrason Ferroelectr Freq Control 47:1277–1290
10. Kepler RG, Anderson RA (1978) Piezoelectricity and pyroelectricity in polyvinylidene fluoride. J Appl Phys 49:4490–4494
11. Chang J, Dommer M, Chang C, Lin L (2012) Piezoelectric nanofibers for energy scavenging applications. Nano Energy 1:356–371
12. Lovinger AJ (1982) Annealing of poly(vinylidene fluoride) and formation of a fifth phase. Macromolecules 15:40–44
13. Correia HMG, Ramos MMD (2005) Quantum modeling of poly(vinylidene fluoride). Comput Mater Sci 33:224–229
14. Bachmann MA, Gordon WL, Koenig JL, Lando JB (1979) An infrared study of phase-III poly(vinylidene fluoride). J Appl Phys 50:6106–6112
15. Prest WM, Luca DJ (1978) Formation of gamma-phase from alpha-polymorphs and beta-polymorphs of polyvinylidene fluoride. J Appl Phys 49:5042–5047
16. Gregorio R (2006) Determination of the alpha, beta, and gamma crystalline phases of poly(vinylidene fluoride) films prepared at different conditions. J Appl Polym Sci 100: 3272–3279
17. Boccaccio T, Bottino A, Capannelli G, Piaggio P (2002) Characterization of PVDF membranes by vibrational spectroscopy. J Membr Sci 210:315–329
18. Imamura R, Silva AB, Gregorio R Jr (2008) Gamma→beta phase transformation induced in poly(vinylidene fluoride) by stretching. J Appl Polym Sci 110:3242–3246
19. Bormashenko Y, Pogreb R, Stanevsky O, Bormashenko E (2004) Vibrational spectrum of PVDF and its interpretation. Polym Test 23:791–796
20. Esterly DM, Love BJ (2004) Phase transformation to beta-poly(vinylidene fluoride) by milling. J Polym Sci B 42:91–97
21. Lanceros-Méndez S, Mano JF, Costa AM, Schmidt VH (2001) FTIR and DSC studies of mechanically deformed beta-PVDF films. J Macromol Sci, Phys B40:517–527

22. Gregorio R, Capitao RC (2000) Morphology and phase transition of high melt temperature crystallized poly(vinylidene fluoride). J Mater Sci 35:299–306

23. Benz M, Euler WB (2003) Determination of the crystalline phases of poly(vinylidene fluoride) under different preparation conditions using differential scanning calorimetry and infrared spectroscopy. J Appl Polym Sci 89:1093–1100

24. Martines P, Lopes AC, L-Mendez S (2014) Electroactive phases of poly(vinylidene fluoride): determination, processing and applications. Prog Polym Sci 39:683–706

25. Gregorio R, Cestari M (1994) Effect of crystallization temperature on the crystalline phase content and morphology of poly(vinylidene fluoride). J Polym Sci B 32:859–870

26. Sencadas V, Moreira VM, Lanceros-Méndez S, Pouzada AS, Gregorio R (2006) Alpha-to-beta transformation on PVDF films obtained by uniaxial stretch. Mater Sci Forum 514:872–876

27. Lopes AC, Costa CM, Tavares CJ, Neves IC, Lanceros-Méndez S (2011) Nucleation of the electroactive β phase and enhancement of the optical transparency in low filler content poly(vinylidene)/clay nanocomposites. J Phys Chem C 115:18076–18082

28. Martins P, Costa CM, Lanceros-Méndez S (2011) Nucleation of electroactive beta-phase poly(vinilidene fluoride) with CoFe2O4 and NiFe2O4 nanofillers: a new method for the preparation of multiferroic nanocomposites. Appl Phys A 103:233–237

29. Li L, Zhang M, Rong M, Ruan W (2014) Studies on the transformation process of PVDF from a to b phase by stretching. RSC Adv 4:3938–3943

30. Salimi A, Yousefi AA (2003) FTIR studies of beta-phase crystal formation in stretched PVDF films. Polym Test 22:699–704

31. Ribeiro C, Sencadas V, Gomez Ribelles JL, Lanceros-Méndez S (2010) Influence of processing conditions on polymorphism and nanofiber morphology of electroactive poly(vinylidene fluoride) electrospun membranes. Soft Mater 8:274–287

32. Sencadas V, Gregorio R Jr, Lanceros-Méndez S (2009) Alpha to beta phase transformation and microstructural changes of PVDF films induced by uniaxial stretch. J Macromol Sci, Part B: Phys 48:514–525

33. Ferreira A, Costa P, Carvalho H, Nobrega JM, Sencadas V, Lanceros- Méndez S (2011) Extrusion of poly(vinylidene fluoride) filaments: effect of the processing conditions and conductive inner core on the electroactive phase content and mechanical properties. J Polym Res 18:1653–1658

34. Sajkiewicz P, Wasiak A, Goclowski Z (1999) Phase transitions during stretching of poly(vinylidene fluoride). Eur Polym J 35:423–429

35. El Mohajir BE, Heymans N (2001) Changes in structural and mechanical behaviour of PVDF with processing and thermomechanical treatments. 1. Change in structure. Polymer 42:5661–5667

36. Pan H, Na B, Lv R, Li C, Zhu J, Yu Z (2012) Polar phase formation in poly(vinylidene fluoride) induced by melt annealing. J Polym Sci B 50:1433–1437

37. Ince-Gunduz BS, Alpern R, Amare D, Crawford J, Dolan B, Jones S, Kobylarz R, Reveley M (2010) Impact of nanosilicates on poly(vinylidene fluoride) crystal polymorphism: part 1. Melt-crystallization at high supercooling. Polymer 51:1485–1493

38. Yang DC, Chen Y (1987) Beta-phase formation of poly(vinylidene fluoride) from the melt induced by quenching. J Mater Sci Lett 6:599–603

39. Gradys A, Sajkiewicz P, Adamovsky S, Minakov A, Schick C (2007) Crystallization of poly(vinylidene fluoride) during ultra-fast cooling. Thermochim Acta 461:153–157

40. Martins P, Caparros C, Gonçalves R, Martins PM, Benelmekki M, Botelho G, Lanceros-Mendez S (2012) Role of nanoparticle surface charge on the nucleation of the electroactive β-poly(vinylidene fluoride) nanocomposites for sensor and actuator applications. J Phys Chem C 116:15790–15794

41. Buckley J, Cebe P, Cherdack D, Crawford J, Ince BS, Jenkins M, Pan NN, Reveley M, Washington N, Wolchover N (2006) Nanocomposites of poly(vinylidene fluoride) with organically modified silicate. Polymer 47:2411–2422

42. Patro TU, Mhalgi MV, Khakhar DV, Misra A (2008) Studies on poly(vinylidene fluoride)-clay nanocomposites: effect of different clay modifiers. Polymer 49:3486–3499

43. He L, Sun J, Wang X, Wang C, Song R, Hao Y (2013) Facile and effective promotion of crystalline phase in poly(vinylidene fluoride) via the incorporation of imidazolium ionic liquids. Polym Int 62:638–646

44. Henkel K, Lazareva I, Mandal D, Paloumpa I, Mueller K, Koval Y, Muller P, Schmeisser D (2009) Electrical investigations on metal/ferroelectric/insulator/semiconductor structures using poly vinylidene fluoride trifluoroethylene as ferroelectric layer for organic nonvolatile memory applications. J Vac Sci Technol B 27:504–507

45. Wu Y, Hsu SL, Honeker C, Bravet DJ, Williams DS (2012) The role of surface charge of nucleation agents on the crystallization behavior of poly(vinylidene fluoride). J Phys Chem B 116:7379–7388

46. Eswaraiah V, Balasubramaniam K, Ramaprabhu S (2012) One-pot synthesis of conducting graphene–polymer composites and their strain sensing application. Nanoscale 4:1258–1262

47. Layek RK, Samanta S, Chatterjee DP, Nandi AK (2010) Physical and mechanical properties of poly(methyl methacrylate)-functionalized graphene/poly(vinylidine fluoride) nanocomposites: piezoelectric b polymorph formation. Polymer 51:5846–5856

48. Kim HJ, Noor-A-Alam M, Son JY, Shin Y-H (2014) Origin of piezoelectricity in monolayer halogenated graphane piezoelectrics. Chem Phys Lett 603:62–66

49. Shang J, Zhang Y, Yu L, Shen B, Lv F, Chu PK (2012) Fabrication and dielectric properties of oriented polyvinylidene fluoride nanocomposites incorporated with graphene nanosheets. Mater Chem Phys 134:867–874

50. El Achaby M, Arrakhiz FZ, Vaudreuil S, Essassi EM, Qaiss A (2012) Piezoelectric β-polymorph formation and properties enhancement in graphene oxide—PVDF nanocomposite films. Appl Surf Sci 258:7668–7677

51. Rahman MA, Lee B-C, Phan D-T, Chung G-S (2013) Fabrication and characterization of highly efficient flexible energy harvesters using PVDF–graphene nanocomposites. Smart Mater Struct 22:1–10

52. Yu J, Jiang P, Wu C, Wang L, Wu X (2011) Graphene nanocomposites based on poly(vinylidene fluoride): structure and properties. Polym Compos 32:1483–1491. doi:10.1002/pc.21106

53. Mohamadi S, Sharifi-Sanjani N (2011) Investigation of the crystalline structure of PVDF in PVDF/PMMA/graphene polymer blend nanocomposites. Polym Compos 32:1451–1460. doi:10.1002/pc.21175

54. Ansari S, Giannelis EP (2009) Functionalized graphene sheet—poly(vinylidene fluoride) conductive nanocomposites. J Polym Sci B 47:888–897

55. Wang D, Bao Y, Zha J-W, Zhao J, Dang Z-M, Hu G-H (2012) Improved dielectric properties of nanocomposites based on poly(vinylidene fluoride) and poly(vinyl alcohol)-functionalized graphene. ACS Appl Mater Interfaces 4:6273–6279

56. Shang J, Zhang Y, Yu L, Luan X, Shen B, Zhang Z, Lv F, Chu PK (2013) Fabrication and enhanced dielectric properties of graphene–polyvinylidene fluoride functional hybrid films with a polyaniline interlayer. J Mater Chem A 1:884–890

57. Kwon J, Sharma BK, Ahn J-H (2013) Graphene based nanogenerator for energy harvesting. Jpn J Appl Phys 52:1–9

58. Wu L, Alamusi, Xue J, Itoi T, Hu N, Li Y, Yan C, Qiu J, Ning H, Yuan W, Gu B (2014) Improved energy harvesting capability of poly(vinylidene fluoride) films modified by reduced graphene oxide. J Intell Mater Syst Struct 25(14):1813–1824

59. Li Y, Xu J-Z, Zhu L, Zhong G-J, Li Z-M (2012) Role of ion−dipole interactions in nucleation of gamma poly(vinylidene fluoride) in the presence of graphene oxide during melt crystallization. J Phys Chem B 116:14951–14960

60. Alamusi, Xue JM, Wu LK, Hu N, Qiu J, Chang C, Atobe S, Fukunaga H, Watanabe T, Liu YL, Ning HM, Li JH, Li Y, Zhao Y (2012) Evaluation of piezoelectric property of reduced graphene oxide (rGO)–poly(vinylidene fluoride) nanocomposites. Nanoscale 4:7250–7255

61. Liu ZH, Pan CT, Lin LW, Lai HW (2013) Piezoelectric properties of PVDF/MWCNT nanofiber using near-field electrospinning. Sensors Actuators A 193:13–24

62. Lund A, Gustafsson C, Bertilsson H, Rychwalski RW (2011) Enhancement of b phase crystals formation with the use of nanofillers in PVDF films and fibres. Compos Sci Technol 71:222–229
63. Yu S, Zheng W, Yu W, Zhang Y, Jiang Q, Zhao Z (2009) Formation mechanism of β-phase in PVDF/CNT composite prepared by the sonication method. Macromolecules 42:8870–8874
64. Glau B, Steinmann W, Walter S, Beckers M, Seide G, Gries T, Roth G (2013) Spinnability and characteristics of polyvinylidene fluoride (PVDF)-based bicomponent fibers with a carbon nanotube (CNT) modified polypropylene core for piezoelectric applications. Materials 6:2642–2661
65. Qu ZY, Liu ZH, Pan CT, Lin LW, Chen YJ, Lai HW. Study on piezoelectric properties of near-field electrospinning PVDF/MWCNT nano-fiber, NEMS 2012, Kyoto, Japan, 5–8 March 2012, pp 125–128
66. Dror Y, Salalha W, Khalfin R, Cohen Y, Yarin AL, Zussman E (2003) Carbon nanotubes embedded in oriented polymer nanofibers by electrospinning. Langmuir 19:7012–7020
67. Ge JJ, Hou H, Li Q, Graham MJ, Greiner A, Reneker DH, Harris FW, Cheng SZD (2004) Assembly of well-aligned multiwalled carbon nanotubes in confined polyacrylonitrile environments: electrospun composite nanofiber sheets. J Am Chem Soc 126:15754–15761
68. Shah D, Maiti P, Gunn E, Schmidt DF, Jiang DD, Batt CA, Giannelis ER (2004) Dramatic enhancements in toughness of polyvinylidene fluoride nanocomposites via nanoclay-directed crystal structure and morphology. Adv Mater 16:1173–1177
69. Priya L, Jog JP (2002) Poly(vinylidene fluoride)/clay nanocomposites prepared by melt intercalation: crystallization and dynamic mechanical behavior studies. J Polym Sci B 40:1682–1689
70. Ahn Y, Lim J, Hong SM, Lee J, Ha J, Choi HJ, Seo Y (2013) Enhanced piezoelectric properties of electrospun PVDF/MWCNT composites due to high β phase formation in PVDF. J Phys Chem C 117:11791–11799
71. Li B, Zheng J, Xu C. Silver nanowire dopant enhancing piezoelectricity of electrospun PVDF nanofiber web, Electro active polymers, Proc. SPIE 8793, Fourth International Conference on Smart Materials and Nanotechnology in Engineering, 879314 (9 August 2013). doi:10.1117/12.2026758
72. Liu YL, Ying Li Y, Xu J-T, Fan Z-Q (2010) Cooperative effect of electrospinning and nanoclay on formation of polar crystalline phases in poly(vinylidene fluoride). ACS Appl Mater Interfaces 2:1759–1768
73. Piezoelectric ceramics: principles and applications. APC International Ltd
74. Jia Y, Chen X, Ni Q, Li L, Ju C (2013) Dependence of the impact response of polyvinylidene fluoride sensors on their supporting materials' elasticity. Sensors 13:8669–8678
75. Kim GH, Hong SM, Seo Y (2009) Piezoelectric properties of poly(vinylidene fluoride) and carbon nanotube blends: β-phase development. Phys Chem Chem Phys 11:10506–10512
76. Pu J, Yan X, Jiang Y, Chang C, Lin L (2010) Piezoelectric actuation of direct-write electrospun fibers. Sensors Actuators A 164:131–136
77. Yousefi AA (2011) Hybrid polyvinylidene fluoride/nanoclay/MWCNT nanocomposites: PVDF crystalline transformation. Iran Polym J 29:725–733
78. Chang C, Fuh Y-K, Lin LW (2010) Direct-write piezoelectric polymeric nanogenerator with high energy conversion efficiency. Nano Lett 10:726–731
79. Chang C, Tran VH, Wang J, Fuh Y-K, Lin L (2010) Direct-write piezoelectric polymeric nanogenerator with high energy conversion efficiency. Nano Lett 10:726–731
80. Sharma M, Madras G, Bose S (2014) Process induced electroactive b-polymorph in PVDF: effect on dielectric and ferroelectric properties. Phys Chem Chem Phys 16:14792–14799
81. Cauda V, Stassi S, Bejtka K, Canavese G (2013) Nanoconfinement: an effective way to enhance PVDF piezoelectric properties. ACS Appl Mater Interfaces 5:6430–6437
82. Gregorio R, Ueno EM (1999) Effect of crystalline phase, orientation and temperature on the dielectric properties of poly (vinylidene fluoride) (PVDF). J Mater Sci 34:4489–44500
83. Silva MP, Costa CM, Sencadas V, Paleo AJ, Lanceros-Méndez S (2011) Degradation of the dielectric and piezoelectric response of poly(vinylidene fluoride) after temperature annealing. J Polym Res 18:1451–1457

84. Tang C-T, Li B, Sun L, Lively B, Zhong W-H (2012) The effects of nanofillers, stretching and recrystallization on microstructure, phase transformation and dielectric properties in PVDF nanocomposites. Eur Polym J 48:1062–1072

85. Baji A, Mai Y-W, Abtahi M, Wong S-C, Liu Y, Li Q (2013) Microstructure development in electrospun carbon nanotube reinforced polyvinylidene fluoride fibers and its influence on tensile strength and dielectric permittivity. Compos Sci Technol 88:1–8

86. Huang X, Jiang P, Kim C, Liu F, Yin Y (2009) Influence of aspect ratio of carbon nanotubes on crystalline phases and dielectric properties of poly(vinylidene fluoride). Eur Polym J 45:377–386

87. Dagdeviren C, Papila M (2010) Dielectric behavior of fibrous-ZnO/PVDF nanocomposite. Polym Compos 31:1003–1010

88. Li Y, Hu J, He J, Gao L. The graphene oxide polymer composites with high breakdown field strength and energy storage ability. In: Oral AY et al (eds) International Congress on Energy Efficiency and Energy Related Materials (ENEFM2013), Springer Proceedings in Physics 155, pp 431–438. doi:10.1007/978-3-319-05521-3_55

89. Wang J, Wu J, Xu W, Zhang Q, Fu Q (2014) Preparation of poly(vinylidene fluoride) films with excellent electric property, improved dielectric property and dominant polar crystalline forms by adding a quaternary phosphorus salt functionalized graphene. Compos Sci Technol 91:1–7

90. Li B, Xu C, Zheng J, Xu C (2014) Sensitivity of pressure sensors enhanced by doping silver nanowires. Sensors 14:9889–9899

91. Lee B-S, Park B, Yang H-S, Han JW, Choong C, Bae J, Lee K, Yu W-R, Jeong U, Chung U-I, Park J-J, Kim O (2014) Effects of substrate on piezoelectricity of electrospun poly(vinylidene fluoride)-nanofiber-based energy generators. ACS Appl Mater Interfaces 6:3520–3527

92. Xu J, Dapinoa MJ, Gallego Perez D, Hansford D (2009) Microphone based on polyvinylidene mahapatrafluoride (PVDF) micro-pillars and patterned electrodes. Sensors Actuators A Phys 153:24–32

93. Toda M, Dahl J (2007) PVDF corrugated transducer for ultrasonic ranging sensor. Sensors Actuators A Phys 134:427–435

94. Rathod VT, Mahapatra DR, Jain A, Gayathri A (2010) Characterization of a large-area PVDF thin film for electromechanical and ultrasonic sensing applications. Sensors Actuators A Phys 163:164–171

95. Seminara L, Capurro M, Cirillo P, Cannata G, Valle M (2011) Electromechanical characterization of piezoelectric PVDF polymer films for tactile sensors in robotics applications. Sensors Actuators A Phys 169:49–58

96. Dahiya RS, Valle M, Metta G, Lorenzelli L, Adami A. Design and fabrication of posfet devices for tactile sensing. In: Proceedings of the International Solid-State Sensors, Actuators and Microsystems Conference (TRANSDUCERS), Denver, CO, 21–25 June 2009, 1881–1884

97. Tsuchimi D, Okuyama T, Tanaka M. Development of a haptic sensor system for monitoring human skin conditions. In: Proceedings of the 13th International Conference on Biomedical Engineering, Singapore, 3–6 December 2008, pp 2219–2222

98. Matsunaga N, Zengin AT, Kawaji S. Evaluation of multilayered pain sensor model of human skin. In: Proceedings of the ICROS-SICE International Joint Conference, Fukuoka, Japan, 18–21 August 2009, pp 3840–3845

99. Gao G, Wang Z, Gao R (1990) A PVDF film sensor for material identification. Sensors Actuators A Phys 23:886–889

100. Kimoto A, Sugitani N (2010) A new sensing method based on PVDF film for material identification. Meas Sci Technol. doi:10.1088/0957-0233/21/7/075202

101. Chuang CH, Liou YR, Chen CW (2012) Detection system of incident slippage and friction coefficient based on a flexible tactile sensor with structural electrodes. Sensors Actuators A Phys 188:48–55

102. Wang YR, Zheng JM, Ren GY, Zhang PH, Xu C (2011) A flexible piezoelectric force sensor based on PVDF fabrics. Smart Mater Struct 20:045009 (1–7)

103. Merlini C, Almeida RS, D'Ávila MA, Schreiner WH, Barra GMO (2014) Development of a novel pressure sensing material based on polypyrrole-coated electrospun poly(vinylidene fluoride) fibers. Mater Sci Eng B 179:52–59

104. Ferreira A, Rocha JG, Ansón-Casaos A, Martínez MT, Vaz F, Lanceros-Mendez S (2012) Electromechanical performance of poly(vinylidene fluoride)/carbon nanotube composites for strain sensor applications. Sensors Actuators A 178:10–16

105. Sharma T, Naik S, Langevine J, Gill B, Zhang JX (2015) Aligned PVDF-TrFE nanofibers with high-density PVDF nanofibers and PVDF core–shell structures for endovascular pressure sensing. IEEE Trans Biomed Eng 62:188–195

106. Jeon JH, Kang SP, Lee S, Oh I-K (2009) Novel biomimetic actuator based on SPEEK and PVDF. Sensors Actuators B 143:357–364

107. Kim S-S, Kee C-D (2014) Electro-active polymer actuator based on PVDF with bacterial cellulose nano-whiskers (BCNW) via electrospinning method. Int J Precis Eng Manuf 15:315–321

108. Mahale BP, Gangal SA, Bodas DS. PVDF based micro actuator, Physics and Technology of Sensors (ISPTS), 2012 1st International Symposium on 2012, pp 59–62

109. Fu Y, Harvey EC, Ghantasala MK, Spinks GM (2006) Design, fabrication and testing of piezoelectric polymer PVDF microactuators, Smart Mater Struct 15. doi:10.1088/0964-1726/15/1/023

110. Lu J, Kim S-G, Lee S, Oh Il-K (2008) Fabrication and actuation of electro-active polymer actuator based on PSMI-incorporated PVDF. Smart Mater Struct 17. doi:10.1088/0964-1726/17/4/045002

111. Pascal RJ (1999) Actuator and sensor design and modeling for structural acoustic control. PhD Dissertation, Department of Aeronautics and Astronautics, Massachusettes Institute of Technology

112. Lee JS, Shin KY, Kim C, Jang J (2013) Enhanced frequency response of a highly transparent PVDF–graphene based thin film acoustic actuator. Chem Commun 49:11047–11049

113. Kowbel W, Xia X, Withers JC, Crocker MJ, Wada BK. PZT/PVDF flexible composites for actuator and sensor applications. In: Proc. SPIE 3324, Smart Structures and Materials 1998: Smart Materials Technologies 1998, 106. doi:10.1117/12.316853

114. Mateu L, Moll F (2005) Optimum piezoelectric bending beam structures for energy harvesting using shoe inserts. J Intell Mater Syst Struct 16:835–845

115. Huang T, Wang C, Yu H, Wang H, Zhang Q, Zhu M. Human walking-driven wearable all-fiber triboelectric nanogenerator containing electrospun polyvinylidene fluoride piezoelectric nanofibers, Nano Energy. http://dx.doi.org/10.1016/j.nanoen.2015.01.038

116. Granstrom J, Feenstra J, Sodano HA, Farinholt K (2007) Energy harvesting from a backpack instrumented with piezoelectric shoulder straps. Smart Mater Struct 16:1810–1820

117. Lallart M, Cottinet PJ, Lebrun L, Guiffard B, Guyomar D (2010) Evaluation of energy harvesting performance of electrostrictive polymer and carbon-filled terpolymer composites. J Appl Phys 108:034901

118. Vatansever D, Hadimani RL, Shah T, Siores E (2011) An investigation of energy harvesting from renewable sources with PVDF and PZT. Smart Mater Struct 20:055019

119. Sohn JW, Choi SB, Lee DY (2003) An investigation on piezoelectric energy harvesting for MEMS power sources. J Mech Eng Sci 219:429–436

120. Fang J, Niu H, Wang H, Wang X, Lin T (2013) Enhanced mechanical energy harvesting using needleless electrospun poly(vinylidene fluoride) nanofibre webs. Energy Environ Sci 6:2196–2202

121. Fang J, Wang X, Lin T (2011) Electrical power generator from randomly oriented electrospun poly(vinylidene fluoride) nanofibre membranes. J Mater Chem 21:11088–11091

122. Xue X, Wang S, Guo W, Zhang Y, Wang ZL (2012) Hybridizing energy conversion and storage in a mechanical-to-electrochemical process for self-charging power cell. Nano Lett 12:5048–5054

123. Zhao Y, Liao Q, Zhang G, Zhang Z, Liang Q, Liao X, Zhang Y (2015) High output piezoelectric nanocomposite generators composed of oriented BaTiO3 NPs@PVDF. Nano Energy 11:719–727

124. Park T, Kim B, Kim Y, Kim E (2014) Highly conductive PEDOT electrodes for harvesting dynamic energy through piezoelectric conversion. J Mater Chem A 2:5462–5469

125. Zi Y, Lin L, Wang J, Wang S, Chen J, Fan X, Yang PK, Yi F, Wang ZL (2015) Triboelectric–pyroelectric–piezoelectric hybrid cell for high-efficiency energy-harvesting and self-powered sensing. Adv Mater 27:2340–2347

126. Yang Y, Zhang H, Zhu G, Lee S, Lin Z-H, Wang ZL (2013) Flexible hybrid energy cell for simultaneously harvesting thermal, mechanical, and solar energies. ACS Nano 7:785–790

127. Shukla R, Bell AJ (2015) PENDEXE: a novel energy harvesting concept for low frequency human waistline. Sensors Actuators A 222:39–47

128. Lee M, Chen C-Y, Wang S, Cha SN, Park YJ, Kim JM, Chou L-J, Wang ZL (2012) A hybrid piezoelectric structure for wearable nanogenerators. Adv Mater 24:1759–1764

129. Pi Z, Zhang J, Wen C, Zhang Z-B, Wu D (2014) Flexible piezoelectric nanogenerator made of poly (vinylidenefluoride-co-trifluoroethylene) (PVDF-TrFE) thin film. Nano Energy 7:33–41

130. Sun C, Shi J, Bayerl DJ, Wang X (2011) PVDF microbelts for harvesting energy from respiration. Energy Environ Sci 4:4508–4512

131. Hu HP, Zhao C, Feng SY, Hu YT, Chen CY (2008) Adjusting the resonant frequency of a PVDF bimorph power harvester through a corrugation-shaped harvesting structure. IEEE Trans Ultrason Ferroelectr Freq Control 55:668–674

132. Liu YM, Tian G, Wang Y, Lin JH, Zhang QM, Hofmann HF (2009) Active piezoelectric energy harvesting: general principle and experimental demonstration. J Intell Mater Syst Struct 20:575–585

133. Hansen BJ, Liu Y, Yang R, Wang ZL (2010) Hybrid nanogenerator for concurrently harvesting biomechanical and biochemical energy. Am Chem Soc 4:3647–3652

134. Liu WT, Cheng XY, Fu X, Stefanini C, Dario P (2011) Preliminary study on development of PVDF nanofiber based energy harvesting device for an artery microrobot. Microelectron Eng 88:2251–2254

135. Oh SJ, Han HJ, Han SB, Lee JY, Chun WG (2010) Development of a tree-shaped wind power system using piezoelectric materials. Int J Energy Res 34:431–437

136. Mandal D, Yoon S, Kim KJ (2011) Origin of piezoelectricity in an electrospun poly(vinylidene fluoride-trifluoroethylene) nanofiber web-based nanogenerator and nano-pressure sensor. Macromol Rapid Commun 32:831–837

Chapter 16
Multifunctional Materials for Biotechnology: Opportunities and Challenges

Luminita Ioana Buruiana

Abstract The use of multifunctional materials in different biomedical applications has attracted much attention in recent years. Desire for biocompatible devices has paved the way for highly degradable and biocompatible materials that are specifically designed for targeted drug delivery and imaging contrast agents. Cellular and molecular interactions as well as those for engineered materials (atoms, molecules, and molecular fragments) are the foundation of biotechnology, where smart multifunctional materials can serve as targeted drug delivery carriers, able to release therapeutic agents or genes in large doses into malignant cells without harming healthy cells. Simultaneously, these systems have the potential to radically change oncology, allowing for easy detection followed by effective targeted treatment at the onset of the disease. In this context, given the exhaustive possibilities available to polymeric particle chemistry, research has been directed at multifunctional materials that combine tumor targeting, tumor therapy, and tumor imaging in an all-in-one system, providing a useful multimodal approach in the battle against cancer. In this context, a wide range of multifunctional systems, formed by liposomes, polymeric-coated magnetic particles, nanoemulsions, micelles, and hydrogels, have shown tremendous progress in biotechnology applications. These engineered multifunctional materials have evolved to possess interesting properties such as prolonged life cycling while circulating in blood, target specificity, and increased cell penetration of the therapeutic drugs and molecules. Current research is focused on understanding and taking advantage of the features of a tumor's microenvironment, including pH and temperature changes.

Keywords Multifunctional materials • Polymers • Biotechnology • Drug delivery

L.I. Buruiana (✉)
"Petru Poni" Institute of Macromolecular Chemistry,
41A Grigore Ghica Voda Alley, 700487 Iasi, Romania
e-mail: luminitab25@yahoo.com

16.1   Multifunctional Materials as Targeted Drug Delivery Vesicles

Multifunctional materials have gained increasing interest in many bio-related subjects, including vehicles for drug delivery or tissue engineering applications and biosensors and as bioseparation materials. They are typically a composite or hybrid of several distinct materials, in which each one performs a different but necessary function, such as structure, transport, or energy storage. Because each phase of the material accomplishes an essential function, multifunctional materials ensure a more flexible weight-efficient and volume-efficient performance than that of a classic multicomponent system. Multifunctional materials are designed to improve the general performances of the system [1]. Thus, a multifunctional material requires a new design methodology in which system performance is underlined over the optimization of individual functions that are not usually used in material science. On the other hand, biological systems have perfected multifunction on a small scale. The complexity of these systems will require a comprehensive understanding of how the basic physical mechanisms can be handled to create a new, potentially favorable, procedure of achieving function and multivariable optimization tools.

The usage of technology by the society is an indirect measure of advancement and development of the said society. The period where we stand today is the manifestation of the increased knowledge coupled with the incoming of many novel technologies, such as nanotechnology, biotechnology, and information that may make the most profound impact [2]. Nanotechnology and biotechnology are expected to influence almost all sectors of daily life. The global research on these technologies is going to make the world more competitive in terms of the knowledge and its use. There are various engineering devices, assemblies, or architectures studied as platforms in biotechnological applications. These include polymeric micelles, dendrimers, polymeric capsules, liposomes, and magnetic particles [3, 4].

Drug and diagnostic agents are able to be incorporated into the said systems via encapsulation, covalent attachment, or surface adsorption. Activation of the release mechanism can be accomplished through pH, chemical, magnetic field, or heat stimuli. As such, the multifunctional design of these systems illustrates the combination of targeted tissue delivery and imaging. Within a biological microenvironment, this behavior is not identical for multifunctional particles as their stability and cellular distribution are dependent upon their morphology and size [5].

These biodegradable systems are ideal for drug delivery applications just from their basic properties alone, allowing for site-specific drug accumulation due in part by their small size, penetrating capabilities into blood vessels (capillaries), and ability to collect within cells. Furthermore, preparation of the system allows for targeted drug release over a period of days or weeks after the initial dosing, thus establishing the basic concepts of utilization of the system.

The main objective of this chapter is to discuss the different types of multifunctional materials used in biotechnology, resuming the opportunities and challenges that are implied by those systems.

16.1.1   Polymeric Micelles

Over the past several years, literature has presented many studies regarding the development of nanomedicine in drug delivery and molecular imaging applications [6, 7]. These therapeutic systems that incorporate therapeutic agents are under development as the next generation of multifunctional materials, to improve the therapeutic result of drug therapy. Therefore, *polymeric micelle* utilization has proven effective in hydrophobic molecule delivery.

When hydrophilic and hydrophobic segments within an amphiphilic block copolymer are subjected to an aqueous environment, the large difference between the two segments' solubility fuel is polymeric micelle formation. They exhibit a unique architecture, core-shell type, in which the hydrophobic core fulfills its role as a natural carrier environment for hydrophobic drugs, while the hydrophilic shell permits particle stabilization in liquid solution (Fig. 16.1) [8].

In the case of tumor tissues, it has been observed that a significant uptake of micelles occurs in reticuloendothelial systems (the liver, spleen), although the leaky vasculature of solid tumor increases micelle accumulation in tumor tissues. To improve drug efficiency and cancer specificity, the evolution of multifunctional polymeric micelles systems can target tumors by molecular recognition of cancer-specific markers.

An example of multifunctional polymeric micelles contains three significant components, namely:

- A chemotherapeutic agent, doxorubicin, released from the system through a pH-dependent mechanism
- A ligand that can target integrin on endothelial cells and then induce receptor-mediated endocytosis for cellular uptake
- A cluster of superparamagnetic iron oxide nanoparticles loaded inside the hydrophobic core of a micelle for magnetic resonance imaging [9]

These systems were evolved to provide effective targeting for integrin receptors and growth inhibition in tumor cells. The future of research in this domain will open important opportunities for the targeted delivery of anticancer agents to tumors and also for using MRI as a noninvasive strategy to efficiently target tumors for improved therapeutic results of drug therapy.
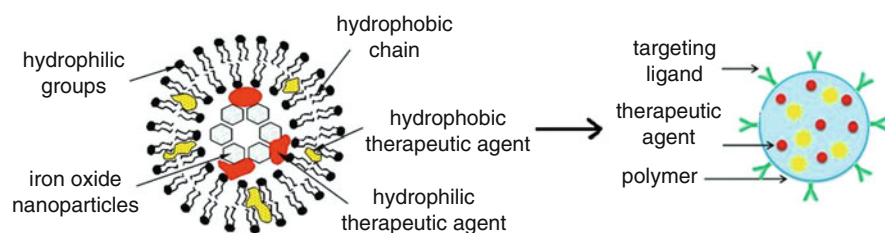
Fig. 16.1 Polymeric micelles used in the delivery of drugs

Another type of polymeric micelles is composed of poly(L-histidine)/polyethylene glycol and poly(L-lactic acid) block copolymers, with folate conjugation [10]. The samples were investigated for pH-dependent drug release, showing drug release as the pH decreased from 8.0. When the micelles were conjugated with folic acid, the results obtained in vitro established that the micelles were more effective in destroying tumor cells due to accelerated drug release and folate receptor-mediated tumor uptake. This type of multifunctional polymeric micelles is expected to be useful for treatment of solid tumors in vivo.

To improve tumor specificity, exposure of multifunctional polymeric micelles composed of a tumor targeting ligand, biotin, to the slightly acidic conditions of solid tumors (6.5<pH<7.0) has been investigated. The core-shell-type micelle may dissociate at more acidic conditions (6.5<pH), causing the increased release of anticancer drug in early endosomal membrane disruption. This approach was made to overcome the limitation of intracellular release of anticancer drugs, their non-specificity becoming a main concern in tumor targeting and delivery. Although systems based on biotin transport in cells have not been fully investigated until now, literature mentions that all cells have a biotin transport system [11]. For that reason, biotin was selected as a nonspecific ligand that can be representative of endogenous ligands, like folic acid or vitamin B_{12}. Thus, the studied smart micelles present four features when exposed to pH variation: ligand exposure at pH 7.0, micelle instability below pH 6.8, increased doxorubicin release, and endosomal membrane disruption. The first feature is expected to improve tumor pH specificity to nonspecific ligands, while the other three features may help in treating solid tumors that are difficult to treat by conventional chemotherapy (resistant tumors).

16.1.2 Polymeric Microcapsules

Nano- and microparticles functionalized with different molecules are of great interest in many scientific domains, like cell biology, biotechnology, diagnostics, and pharmaceutics [12, 13]. Functionalized particles can be utilized as sensing and diagnostic tools on the cellular level within the biomedical field. The benefits that could be gained from a controlled microenvironment through the use of nano-/micro-size containers are hardly mentioned in currently available literature. Beyond use as delivery systems, new applications have been found for multifunctional nanocontainers such as controlled release, enzymatic catalysis, and directed drug delivery. The system's ability to be multipurpose is described by the following characteristics:

– Luminescent semiconductor nanocrystals, or quantum dots, assist in both imaging and the identification of various capsules.
– Superparamagnetic nanoparticles provide suitable capsule handling within a magnetic field.
– Surface coatings aid in providing targeting for the capsules to the desired cells.
– Capsule wall-entrapped metallic nanoparticles serve as aggregates for electromagnetic fields while also providing heat for the controlled release.
– Reactions are uniquely available for specific pharmaceutical agents (i.e., enzymes).

The advantage of polymeric microcapsules comparatively with other systems is they can be functionalized at the same time with the components mentioned above, permitting the combination of their characteristics into a single item. A schematic representation of a hollow microcapsule is shown in Fig. 16.2.

These capsules are able to investigate the intracellular environments and release the encapsulated content under an external trigger. Also, they can protect proteins, enzymes, peptides, drugs, or hormones against chemical and biological degradation and can be released subsequently in a controlled manner [14].

Hollow nanocapsules based on polyelectrolytes are permeable for water-soluble molecules, while liposomes are nearly impermeable for ions. Combination of the systems was undertaken so as to release the tiny ionic molecules into the localized area [14]. Studies have shown that permeation for minute hydrophilic solutes decreases when polyelectrolyte beads are coated with a lipid membrane; improved permeation is thus accomplished by coating liposomes with a polyelectrolyte layer (Fig. 16.3). Liposome used as a template is useful for increasing biocompatibility. Also, one can say that permeability for small molecules, soluble in water, can be dictated through the rebuilding of the membrane channels. Novel hybrid materials have been produced with specific properties by employing this methodology, choosing either natural or modified proteins. Isolating free materials from those that are encapsulated, researchers have used of magneto-liposomes, synthesized via the

Fig. 16.2 Schematic representation of a hollow microcapsule

- Hollow microcapsule -
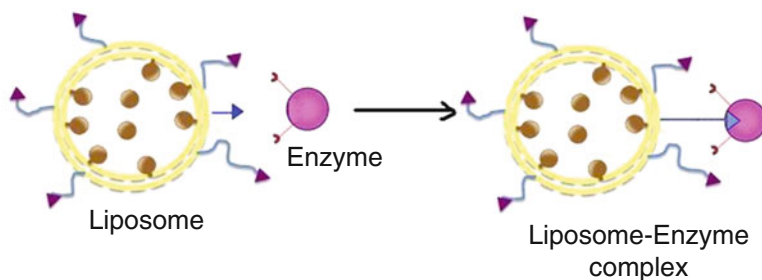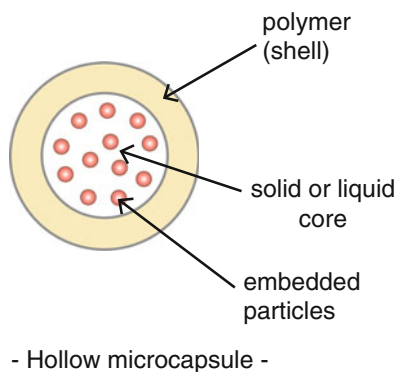
Fig. 16.3 Liposome–enzyme complex

rehydration of a dried rhodamine-B-labeled fluorescent lipid film with a superpara-magnetic fluid (iron oxide nanoparticles acquired via the coprecipitation method) [15]. After the separation procedure, the magneto-liposomes were concentrated using a permanent magnetic. Subsequently, liposomes may be functionalized by coating with a polyelectrolyte layer that assures mechanical and biological stability.

Also, magnetic nanoparticles (Fe_3O_4) were entrapped into capsule shells, useful for specifically trapping polymer capsules, functionalized Cu magnetic nanoparticles, and luminescent nanocrystals. The application is illustrated by using a model system for bloodstream flow and by creating a magnetic field at the desired place with a permanent magnet [14, 16]. Here, increased cellular uptake of the capsules can be seen via a fluorescence microscope as the capsule shells have the nanocrystals embedded within them. Research has shown that polymer capsules functionalized with magnetic nanoparticles can aggregate in an area with a magnetic field and can effectively accumulate in breast cancer cells because of the high site-specific capsule concentration. As such, this behavior is well suited for the site-specific delivery of therapeutically loaded magnetic polymer capsules.

16.1.3 Gold Nanostructures for Biomedical Applications

Metal nanoparticles, especially those of gold, are considered to be versatile materials for various applications, such as electronic and optical detection systems, therapeutics, diagnostics, photovoltaics, and catalysis [17–19]. Suitable properties of these structures determine their tailoring for special applications and while the chemical composition of a nanoparticle is important; even more important are the morphological aspect (size and shape) and its surface-colloidal properties.

The main property that calls for the use of gold structures in biomedical application is represented by surface chemistry of gold, especially their nonreactive and bio-inert nature that increases its capacity to been used for in vitro and in vivo applications [20] (Fig. 16.4). Low cytotoxicity and clinical biocompatibility are two additional important characteristics that nurture the employment of these structures in biotechnology and in medical uses [21]. Gold colloids were applied in cancer research as radiotracers for lymph nodes and, in recent years, as drug carriers based on gold nanospheres were all tested with minimal side effects observed despite the high doses of drug. Latest research underlines the importance of several factors that

gold nanoparticle   +   **polymer**   ⟶   **gold nanoparticle functionalized with polymer**
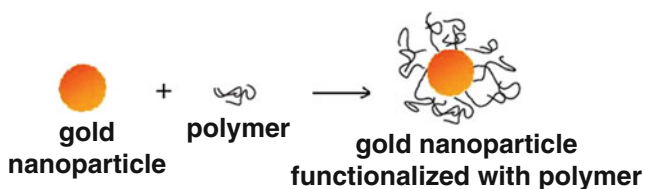
Fig. 16.4 Gold nanoparticle complex

decide the suitability of these materials, especially the size and the shape of the particles, the surface coatings, and the method of administration [22].

Synthesizing metal nanoparticles in solution represents the most commonly used method of chemical reduction of metal ions, involving organic solvents and ligands. In comparison with this synthesis method, another process based on the use of water as a solvent should provide an environmentally friendly route for the production of gold nanoparticles; the product formed can be easily incorporated into diverse products (from composites to cells). A strategy based on the physical adsorption of ligands on the nanoparticle surface is preferred in order to maintain the specific properties of the nanomaterial. Although some progress in this process has been made, there are still concerns regarding the preparation of metal nanoparticles, like the by-products from the reducing agent, the multiple steps of the reaction, and the high concentration of the protective agents. The future utilization of nontoxic chemicals, eco-friendly solvents, and renewable materials are upcoming issues where greater attention must be paid when developing synthetic strategies [23].

In recent years, the challenges and opportunities pointed out above have been under consideration by many researchers. In this context, poly(ethylene oxide)–poly(propylene oxide) can be used as a copolymer block that acts as stabilizers in the synthesis method; the preparation of gold nanoparticles takes place in an air-saturated aqueous solution, at environmental temperature [24], using nontoxic polymers (Pluronic, Poloxamers). This synthesis method is very fast (less than 2 h) and has favorable cost and low impact to the environment. As a result, the polymer's chemical composition, architecture, molecular weight, and concentration permit the fine-tuning of the size and shape of the resulting nanoparticles. This functional polymer-based method [25] presents advantageous environmental conditions and small number of reactants, the resulting gold nanostructures obtained being applied in biological and biomedical applications. The advantage of having a single functional polymer that may serve as structure-directing agent and colloidal stabilizer for metal nanoparticles (as in example presented above) can be extended to other polymers as well. Recent trends in macromolecular synthesis, together with the latest knowledge in the domain of metal nanoparticle, offer great opportunities for connecting polymer science with nanotechnology toward the design and development of new nanomaterials, which can be integrated into various devices and processes [26, 27].

16.1.4 Polymer–Polyelectrolyte Complex Used in Delivery of a Therapeutic Agent

Modern technologies based on polymeric nanoconstructs are used as targeted carriers in diagnostics, drug and gene delivery, and are considered a research priority in nanomedicine. This leads to a strategy between disciplines to converge upon a solution whereas they typically work independently of one another, with such fields including engineering and molecular biology, chemistry, and virology physics and surgery. Nanostructure complexes are considered, in this context, to be formed by

macromolecular compounds. These structures were initially meant to be vaccine and cancer treating drug vehicles so as to reduce the toxicity incurred by conventional methods. The nanoparticle complex can be prepared from different materials, synthetic polymers, or biopolymers (polysaccharides or proteins) [28, 29].

The active component that can be embedded in the complex at the molecular level offers important advantages by improving their physicochemical characters like stability and dissolution. There are several ways for active substances to be encapsulated in a polymer-polyelectrolyte complex:

– Entrapped via the solution during precipitation of the complex.
– Absorbed from the solution and incorporated into previously formed complex.
– Chemically bound to at least one complex partner and precipitates during complexation.
– The active compound itself may act as a polyion and forms a polyelectrolyte complex.

In all of those cases, the active substance from the complex will be released by solution equilibration, by ion exchange mechanism, by charge interaction, by slow decomplexation, or by breakdown and dissolution of the complex.

Drug delivery carrier can be enhanced by the implementation of peptide segments, proteins, or other small molecules along with the targeting and therapeutic properties of the nanoparticulate polymer matrices. Some of the possible advantages include the drug's controlled release as well as prolonged cycle time within the circulatory system. These drug delivering vehicles can be created with varying constructs, structures, and patterns such as dendrimers, liposomes, polymeric micelles, or virus-derived capsid nanoparticles [30–33]. Acquisition of the said systems can be accomplished through different many means, some requiring the use of potentially toxic solvents or other materials such as dispersion, emulsion, or inverse microemulsion polymerization of biodegradable and non-biodegradable monomers. Furthermore, chemical reactions may require the use of mineral oils and strong organic solvents to stabilize the polymer stability as well as to enhance reaction efficiency, thus compromising the final products' biocompatibility via the initiators, surfactants, or unreacted products [34]. These issues bring up multiple limitations for potential biomedical application. As such, development of biodegradable, water-soluble polymer–polyelectrolyte complexes was undertaken to solve the said issues. Polymeric polyelectrolytes used as drug delivery systems present the following advantageous properties: there is slow rate of degradation, water can be used as a solvent, and normal cell function will remain unchanged. Intense electrostatic interactions between charged microdomains of two oppositely charged polyelectrolytes yield a unique, complex architecture [35]. The complex can be acquired by the control of several factors such as rigidness of the polymeric chain, temperature, pH, as well as ionic strength and site location. Beyond their gene delivery applications and cell/tissue microencapsulation [36, 37], polymer–polyelectrolyte complexes are capable of functionalization with therapeutic, targeting, or imaging agents and may have different applications like in vitro cellular uptake, neovascular targeting, or controlled in vivo distribution.

Some studies found in literature present the development and characterization of drug–polyelectrolyte matrices using different drugs like lidocaine or metoclopramide [38]. These drugs proved that they can be loaded in high proportions into the polymer matrix; at the same time, the complex containing lidocaine presented better delivery properties in regard to the proportions of the loaded drug. On the other hand, dexamethasone, another active component encapsulated in a drug-loaded chitosan–alginate fiber (prepared by interfacial polyelectrolyte complexation method), was completely released within 2 h [39]. Meanwhile, some charged components like bovine serum albumin or avidin showed sustained release for 3 weeks. Per the data gather from this study, fibers loaded with therapeutics could be potentially synthesized via interfacial polyelectrolyte complexation and had the following desirable properties: improved encapsulation, sustained release kinetics, and retention of the encapsulants' bioactivity.

Research concerning chitosan/poly(acrylic acid) polyionic complexes has been conducted for a vast array of copolymer compositions while utilizing two different drugs (i.e., amoxicillin trihydrate and amoxicillin sodium) [40]. Polymer/drug and polymer/polymer interactions were evaluated based on the resulting solute transport and swelling behaviors exhibited. It was found that the polyionic complexes' swelling ration determined amoxicillin trihydrate's diffusion, with electrostatic polymer/polymer interactions being found between chitosan's cationic groups and poly(acrylic acid)'s anionic groups. One can observe and conclude that limitations of amoxicillin sodium diffusion could be remedied by interactions between polymer and ionized drug delaying the drug release.

It can be concluded that future advances in polymeric drug and gene delivery demand the development of nontoxic multicomponent materials to be used in both targeting and imaging applications. Polymer–polyelectrolyte complexes into a biocompatible and flexible system are an alternative to currently available delivery mechanisms that employ organic solvents as a reaction medium. Producing the ideal polymer complexes for in vivo and in vitro applications is no small feat. Therefore, issues concerning stability and site-specific targeting (i.e., the liver, lungs, and spleen) have to be resolved prior to clinical consideration.

16.1.5   Magnetic Particles in Biotechnology

One important nanotechnological pathway that has shown great promise in current state-of-the-art studies includes nanostructured magnetic materials. The synthesis and investigation of magnetic properties of these materials present interest from both a fundamental and technological point of view. The use of magnetic nanoparticles in a wide range of fields from biology to data storage has been explored. For example, control over the particle size, shape, composition, and surface chemistry is crucial in achieving the desired properties for biomedical applications. Furthermore, utilizing particles with ambient temperature superparamagnetic behavior (no remanence, fast changing magnetic state) is preferential. These nanosystems can apply heat,

thus giving them potential uses as hyperthermia agents, as delivery vessels for toxic level of thermal energy to tumors, or as enhancing agents for cancer therapeutics (e.g., chemotherapy, radiotherapy) where moderate heat application results in better cell destruction [41, 42]. Moreover, interesting properties abound in magnetic nanomaterials with examples being huge magnetoresistance or an extremely large magneto-caloric effect. Then, there are an obvious interest and a permanent effort placed on studying magnetic nanoparticles with improved properties and their applications in many fields of activity, especially in biomedical domain, the highest priority field. Superparamagnetic iron oxide nanoparticles, sized between 10 and 100 nm, were used in a wide range of preclinical and clinical therapies, especially due to their biodegradable and biocompatible nature [43, 44]. Iron oxide is usually prepared by the coprecipitation of Fe^{2+} and Fe^{3+} salts in an aqueous solution (the effect is less toxic), resulting in a magnetic core of magnetite (Fe_3O_4), maghemite (γ-Fe_2O_3), or a mixture of the two. The nanosize of the obtained particles is determined by the anionic salt content, the Fe^{2+} and Fe^{3+} ratio, pH, and the ionic strength in the aqueous solution. In the preparation process, it is important to prevent the oxidation of the nanoparticles and protect their magnetic properties by carrying on the reaction under inert gas, either nitrogen or argon [45]. The materials used for coating the magnetic core are added during the coprecipitation method in order to prevent the agglomeration of the formed nanoparticles into microparticles [46]. From the coating materials that use stabilizing iron oxide nanoparticles, the most employed are polyethylene glycol, dextran, polyvinylpyrrolidone, polypeptides, and gelatin [44, 47]. The choice of the coatings is very important for controlling material size and for making them suitable for clinical applications. Superparamagnetism, the special property of these particles, is characterized by the special feature of each particle to be small enough to not have a measurable permanent dipole moment in the absence of external magnetic field. At the same time, a suspension of nanoparticles presents magnetic susceptibility higher than paramagnetic materials, being magnetized by an external magnetic field. As a conclusion, superparamagnetic behavior of magnetic nanoparticles is not only due to core size effect; it can also depend on surface modification; nanoparticles should be properly coated to reduce magnetic dipole–dipole interactions.

Literature has reported several methods that suggest a way that therapy can be combined with diagnosis [48–50]:

– Incorporating the therapeutic agents into the polymer coating by covalent or noncovalent chemical binding
– Hydrophobic or electrostatic interaction
– Encapsulating the drug molecules

The therapeutic agent could be a genetic material such as a small interfering RNA or a drug with small molecule (doxorubicin or paclitaxel). Drug molecules bound to magnetic nanoparticles were activated specifically in cancer cells by taking advantage of the pH differences between the intracellular conditions of malignant and nonmalignant cells. Thus, magnetic particles loaded with doxorubicin targeted cancerous tumors (especially breast cancer) and were activated in the tumor environment, accomplishing a more specific treatment for some types of tumors

Fig. 16.5 Magnetic particles for magnetic-induced hyperthermia
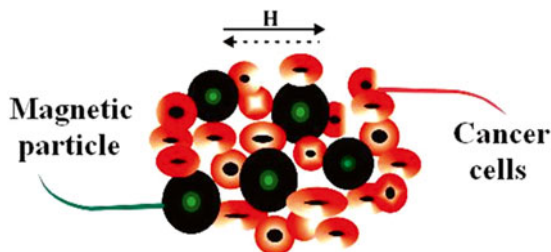
[51]. Upon uptake of the nanoparticles by the cancer cells, the nanoparticles released the drug molecules and killed the tumor cells (Fig. 16.5).

Although these nanoparticles have great potential, there are still some issues that need to be resolved before clinical applications begin. First, there is need to have a better control over the size and magnetization of the nanoparticles. Second, it is imperative to remove any toxicity associated with administration of iron oxide nanoparticles where inflammation, chromosomal damage or condensations, and deficiency in mitochondrial function are some of the common effects reported in literature [52, 53]. The biocompatibility and biosafety concerns associated with the particle usage should be resolved for potential clinical applications. Also, the bio-availability, as evidenced by maximizing the interaction of the nanoparticles with the target tissues and eliminating or minimizing the uptake by other organs, represents another effect that may have to be studied more detailed. Although the majority of the current studies regarding the application of magnetic nanoparticles in cancer biology are at the research stage, finding the solutions for the above issues will increase the chances for their clinical uses in the near future.

Rapid identification of the detection threshold of some targeted biomolecules (DNA, antibodies, metabolites) constitutes a crucial biomedical requirement. Classical methods of detection, although improved over the years, still are time-consuming and exhibit a high detection threshold. In this context, magnetic methods show some benefits in comparison with the classical ones, such as multi-analyte detection which is low cost and rapid results. Thus, in recent years, biosensors based on giant magneto-resistance (GMI) were developed using magnetic particles and magnetic fields for biomolecule detection [54, 55]. The major advantage of this sensor is represented by its ability to process only electronic signals while being extremely sensitive; at the same time, the magnetic particles used as markers exhibit superior characteristics toward other molecules like radioisotopes, enzymes, or fluorescent molecules.

Magnetic particles are stable and easy t o manipulate and have the ability to be used with a large spectrum of molecules; usually, biological samples include no magnetic background that could interfere with them. On the other hand, the biosensor sensitivity constitutes an important condition in the detection of the low concentration of some biomolecules (i.e., RNA). In this context, new magnetic biosensors based on the GMI effect were studied in the magnetic amorphous wire applications [55] (Fig. 16.6). Results obtained have shown a very high sensitivity, good thermal stability, and a high detection surface of this biosensor, due to its three-dimensional
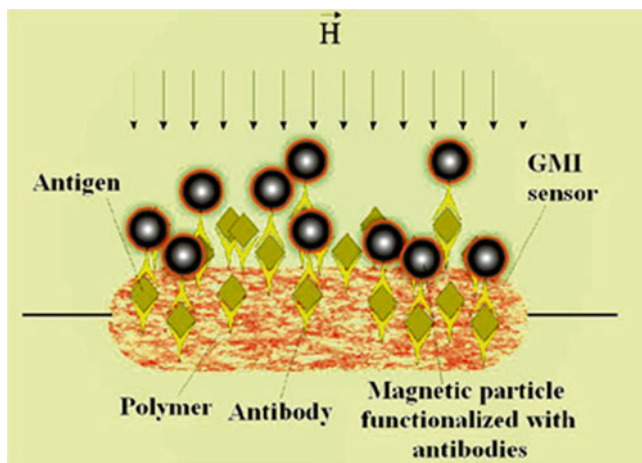
Fig. 16.6 Representation of a GMI-based magnetic biosensor

representation. One important condition that makes the GMI-based sensor work as biosensor is represented by its functionalization with specific bioreceptors. For that, the glass-coated amorphous microwire was covered with a polymer, obtaining a new giant magnetoimpedance biosensor prototype [56]. The results obtained emphasize the optimal measurement conditions and the influence of a liquid suspension of commercially available polymer-based magnetic microparticles on the magnetoimpedance response of the array. The study also highlights the excellent magnetic detection characteristics of glass-coated microwires array comparatively with a single microwire. All of these properties recommend these microwires, ordered in an array, to be used as sensing elements in a magnetoimpedance-based biosensor for biomolecule detection.

16.1.6 Metallopolymers as New Multifunctional Materials

Development of synthetic polymers in the last century had changed fundamentally as the materials are available in daily life. As materials with advanced properties, polymeric materials based on carbon continue to extend their specific synthesis methods and fast scientific evolution at the interfaces with physics, supramolecular chemistry, and biology. Metal centers play a major role in solids with 2D and 3D structures and in biological macromolecules, providing access to key properties and functions. Some examples include magnetic materials used in data storage, superconductors, luminescent materials, or biological catalysts like metalloenzymes [57]. Recent studies have focused on the recent developments and current trends in this area in terms of their properties and applications as multifunctional materials [58–61].

Macromolecular materials that show a response to external stimuli have been studied intensely, the presence of metal centers offering special opportunities in this domain. In this context, one can mention sensory materials based on conductivity changes or stimuli-responsive materials like thin films, capsules, and microspheres with a wide variety of potential applications. Structures that permit the release of encapsulated drugs at a specific location by an external stimulus represent a crucial parameter in nanotechnology, bioengineering, and medicine [62]. Highly metallized polymers that contain high concentrations of metal centers offer potential as precursors to compact arrangements of metal nanoparticles [63]. Furthermore, obtaining synthetic biometallopolymers and metallopolymer-biopolymer conjugates that incorporate biological molecules like peptides exhibit access to metal-functionalized structures is of great importance.

In conclusion, metallopolymers constitute a developing field that exhibit new opportunities for exploratory and application research. Thus, the metallopolymer field offers many exciting future challenges as well as opportunities, and the scientific community can look forward to further developments.

16.1.7 Biodegradable Polymer Composite Used as Three-Dimensional Polymeric Scaffolds

Biomaterials have been used intensively in personal care, medicine, and food applications, with polymers designed as scaffolds for use in tissue engineering and regenerative medicine being extensively studied. The areas of active research in tissue engineering contain:

– Biomaterials design
– Incorporation of the desired chemical or physical agents and structural properties, necessary to guide cell and tissue organization
– Integration of the cell/scaffold
– Enclosing of the cell for transplantation or biomolecules into the biomaterial scaffold from the host to promote integration with the tissue after implantation
– Biomolecule delivery
– Inclusion of growth factors, small molecules, or peptides which develop cell survival and tissue regeneration

The concept of a polymeric scaffold includes a three-dimensional structure and a newer injectable material that provides a controlled microenvironment for the cells. This microenvironment is composed of cell interactions with other cells, soluble or matrix-bound growth factors, and adhesion molecules, as well as the biomaterial itself through mechanical and chemical stimuli [64]. The future perspective is highlighted on the understanding of tissue enough to design a polymeric biomaterial with proper properties for in vitro or in vivo applications. Finding the suitable combination of factors and timing is really difficult due to the fact that some of those are not yet known. Nevertheless, scaffolds are being designed with growth factors,

adhesive peptides, and proteins entrapped in the polymeric scaffolds for guiding cells. These scaffolds present great potential for in vitro screening, providing important data on cell and tissue response in the future [65].

To conclude, understanding the cellular microenvironment and incorporating this into biomaterials design strategies represent an important aim of future research. At the same time, science and engineering must cooperate to define the cellular microenvironment and subsequently to use this information to engineer the tissue scaffolds. Certainly, the vastness and complexity of this field require a multidisciplinary collaboration in order to achieve the desired goals.

16.2   Conclusion

Most strategies for conjugating particle surfaces with different agents produce efficient biomedical diagnosis agents and platforms for engineering of multifunctional materials devices. The chapter focused on the multicomponent systems used for complex needs, with special properties derived from interactions between the system constituents. The implementation of multifunctional materials in targeted delivery system that simultaneously perform diagnostics, targeted delivery, and efficient therapy is also summarized. Multifunctional materials are functionalized with amphiphilic polymer or silica to transform particles soluble in water suitable with biomedical applications. In this context, bioconjugated particles (particles conjugated with antibody, protein or peptide) exhibit properties for using as functional probes for imaging and also as anticancer drug delivery vehicle under an external magnetic field. However, there are technological and scientific challenges that still have to be overcome so as to better fulfill the demands necessary to more accurately mimic the in vivo environment. By optimizing the complex parameters discussed above, drug delivery systems and tissue engineering based on multifunctional biomaterials will act as future therapeutic alternatives to the classical medical methods. Future directions of study should exploit the latest discoveries recorded in biomedical fields.

References

1. Thomas JP, Qidwai MA (2004) Mechanical design and performance of composite multifunctional materials. Acta Mater 52:2155–2164
2. Rennie J (2000) Science 282:8–10
3. Haag R, Vogtle F (2004) Highly branched macromolecules at the interface of chemistry, biology, physics, and medicine. Angew Chem Int Ed 43:272–273
4. Moghimi SM, Hunter AC, Murray JC (2001) Long-circulating and target-specific nanoparticles: theory to practice. Pharmacol Rev 53:283–318
5. Drummond DC, Zignani M, Leroux JC (2000) Current status of pH-sensitive liposomes in drug delivery. Prog Lipid Res 39:409–460
6. Li KC, Pandit SD, Guccione S, Bednarski MD (2004) Molecular imaging applications in nanomedicine. Biomed Microdevices 6:113–116

7. Nasongkla N, Bey E, Ren J, Ai H, Khemtong C, Guthi JS, Chin SF, Sherry AD, Boothman DA, Gao J (2006) Multifunctional polymeric micelles as cancer-targeted, MRI-ultrasensitive drug delivery systems. Nano Lett 6:2427–2430

8. Otsuka H, Nagasaki Y, Kataoka K (2003) PEGylated nanoparticles for biological and pharmaceutical applications. Adv Drug Deliv Rev 55:403–419

9. Lee ES, Na K, Bae YH (2003) Poly(L-histidine)-PEG block copolymer micelles and pH-induced destabilization. J Control Release 91:103–113

10. Lee ES, Na K, Bae YH (2005) Super pH-sensitive multifunctional polymeric micelle. Nano Lett 5:325–329

11. Hymes J, Wolf B (1999) Human biotinidase isn't just for recycling biotin. J Nutr 129:S485–S489

12. Buck SM (2004) Optochemical nanosensor PEBBLEs: photonic explorers for bioanalysis with biologically localized embedding. Curr Opin Chem Biol 8:540–546

13. Sukhorukov GB, Rogach AL, Zebli B, Liedl T, Skirtach AG, Kçhler K, Antipov AA, Gaponik N, Susha AS, Winterhalter M, Parak WJ (2005) Nanoengineered polymercapsules: toolsfordetection, controlleddelivery, and site-specific manipulation. Small 1:194–200

14. Sukhorukov GB, Rogach AL, Garstka M, Springer S, Parak WJ, Munoz-Javier A, Kreft O, Skirtach AG, Susha AS, Ramaye Y, Palankar R, Winterhalter M (2007) Multifunctionalized polymer microcapsules: novel tools for biological and pharmacological applications. Small 3:944–955

15. Martina MS, Fortin JP, Fournier L, Menager C, Gazeau F, Clement O, Lesieu S (2007) Magnetic targeting of rhodamine-labeled superparamagnetic liposomes to solid tumors: in vivo tracking by fibered confocal fluorescence microscopy. Mol Imaging 6:140–146

16. Zebli B, Susha AS, Sukhorukov GB, Rogach AL, Parak WJ (2005) Magnetic targeting and cellular uptake of polymer microcapsules simultaneously functionalized with magnetic and luminescent nanocrystals. Langmuir 21:4262–4265

17. Sau TK, Rogach AL, Jackel F, Klar TA, Feldmann J (2010) Properties and applications of colloidal nonspherical noble metal nanoparticles. Adv Mater 22:1805–1825

18. Zhou JF, Ralston J, Sedev R, Beattie DA (2009) Functionalized gold nanoparticles: synthesis, structure and colloid stability. J Colloid Interface Sci 331:251–262

19. Giljohann DA, Seferos DS, Daniel WL, Massich MD, Patel PC, Mirkin CA (2010) Gold nanoparticles for biology and medicine. Angew Chem Int Ed 49:3280–3294

20. Lewinski N, Colvin V, Drezek R (2008) Cytotoxicity of nanoparticles. Small 4:26–49

21. Paciotti GF, Myer L, Weinreich D, Goia D, Pavel N, McLaughlin RE, Tamarkin L (2004) Colloidal gold: a novel nanoparticle vector for tumor directed drug delivery. Drug Deliv 11:169–183

22. Murphy CJ, Gole AM, Stone JW, Sisco PN, Alkilany AM, Goldsmith EC, Baxter SC (2008) Gold nanoparticles in biology: beyond toxicity to cellular imaging. Acc Chem Res 41:1721–1730

23. Reijnders L (2008) Hazard reduction in nanotechnology. J Ind Ecol 12:297–306

24. Sakai T, Alexandridis P (2004) Single-step synthesis and stabilization of metal nanoparticles in aqueous pluronic block copolymer solutions at ambient temperature. Langmuir 20:8426–8430

25. Alexandridis P (2011) Gold nanoparticle synthesis, morphology control, and stabilization facilitated by functional polymers. Chem Eng Technol 34:15–28

26. Rozenberg BA, Tenne R (2008) Polymer-assisted fabrication of nanoparticles and nanocomposites. Prog Polym Sci 33:40–112

27. Ofir Y, Samanta B, Rotello VM (2008) Polymer and biopolymer mediated self-assembly of gold nanoparticles. Chem Soc Rev 37:1814–1825

28. Taylor S, Qu LW, Kitaygorodskiy A, Teske J, Latour RA, Sun YP (2004) Synthesis and characterization of peptide–functionalized polymeric nanoparticles. Biomacromolecules 5:245–248

29. Vinogradov SV, Bronich TK, Kabanov AV (2002) Nanosized cationic hydrogels for drug delivery preparation, properties and interactions with cells. Adv Drug Deliv Rev 54:135–147

30. Kramer M, Stumbe JF, Grimm G, Kaufmann B, Kruger U, Weber M, Haag R (2004) Dendritic polyamines: a simple access to new materials with defined tree-like structures for application in non-viral gene delivery. Chem Biochem 5:1081–1087

31. Yu FQ, Liu YP, Zhu RX (2004) A novel method for the preparation of core-shell nanoparticles and hollow polymer nanospheres. J Appl Polym Sci 91:2594–2600

32. Talsma SS, Babensee JE, Murthy N, Williams IR (2006) Development and in vitro validation of a targeted delivery vehicle for DNA vaccines. J Control Release 112:271–279

33. Thomas TP, Majoros IJ, Kotlyar A, Kukowska-Latallo JF, Bielinska A, Myc A, Baker JR (2005) Targeting and inhibition of cell growth by an engineered dendritic nanodevice. J Med Chem 48:3729–3735

34. Hartig SM, Greene RR, Dikov MM, Prokop A, Davidson JM (2007) Multifunctional nanoparticulate polyelectrolyte complexes. Pharm Res 24:2353–2369

35. Schatz C, Lucas JM, Viton C, Domard A, Pichot C, Delair T (2004) Formation and properties of positively charged colloids based on polyelectrolyte complexes of biopolymers. Langmuir 20:7766–7778

36. Carlesso G, Kozlov E, Prokop A, Unutmaz D, Davidson JM (2005) Nanoparticulate system for efficient gene transfer into refractory cell targets. Biomacromolecules 6:1185–1192

37. Fisher KD, Ulbrich K, Subr V, Ward CM, Mautner V, Blakey D, Seymour W (2000) A versatile system for receptor-mediated gene delivery permits increased entry of DNA into target cells, enhanced delivery to the nucleus and elevated rates of transgene expression. Gene Ther 7:1337–1343

38. Jimenez-Kairuz AF, Llabot JM, Allemandi DA, Manzo RH (2005) Swellable drug-polyelectrolyte matrices (SDPM): characterization and delivery properties. Int J Pharm 288:87–99

39. Liao IC, Wan ACA, Yim EK, Leong KW (2005) Controlled release from fibers of polyelectrolyte complexes. J Control Release 104:347–358

40. de la Torre MP, Enobakhare Y, Torrado G, Torrado S (2003) Release of amoxicillin from polyionic complexes of chitosan and poly(acrylic acid) Study of polymer/polymer and polymer/drug interactions within the network structure. Biomaterials 24:1499–1506

41. Herea DD, Chiriac H, Lupu N (2011) Preparation and characterization of magnetic nanoparticles with controlled magnetization. J Nanopart Res 13:4357–4369

42. Alexiou C, Tietze R, Schreiber E, Jurgons R, Richter H, Trahms L, Rahn H, Odenbach S, Lyer S (2011) Cancer therapy with drug loaded magnetic nanoparticles-magnetic drug targeting. J Magn Magn Mater 323:1404–1407

43. Kievit FM, Zhang M (2011) Surface engineering of iron oxide nanoparticles for targeted cancer therapy. Acc Chem Res 44:853–862

44. Gupta AK, Wells S (2004) Surface-modified superparamagnetic nanoparticles for drug delivery: preparation, characterization, and cytotoxicity studies. IEEE Trans NanoBiosci 3:66–73

45. Kim DK, Zhang Y, Voit W, Rao KV, Muhammed M (2001) Synthesis and characterization of surfactant-coated superparamagnetic monodispersed iron oxide nanoparticles. J Magn Magn Mater 225:30–36

46. Gupta AK, Gupta M (2005) Synthesis and surface engineering of iron oxide nanoparticles for biomedical applications. Biomaterials 26:3995–4021

47. Portet D, Denizot B, Rump E, Lejeune JJ, Jallet P (2001) Nonpolymeric coatings of iron oxide colloids for biological use as magnetic resonance imaging contrast agents. J Colloid Interface Sci 238:37–42

48. Kievit FM, Wang FY, Fang C, Mok H, Wang K, Silber JR, Ellenbogen RG, Zhang M (2011) Doxorubicin loaded iron oxide nanoparticles overcome multidrug resistance in cancer in vitro. J Control Release 152:76–83

49. Kumar M, Yigit M, Dai G, Moore A, Medarova Z (2010) Image-guided breast tumor therapy using a small interfering RNA nanodrug. Cancer Res 70:7553–7561

50. Sun C, Lee JS, Zhang M (2008) Magnetic nanoparticles in MR imaging and drug delivery. Adv Drug Deliv Rev 60:1252–1265

51. Lim EK, Huh YM, Yang J, Lee K, Suh JS, Haam S (2011) pH-triggered drug-releasing magnetic nanoparticles for cancer therapy guided by molecular imaging by MRI. Adv Mater 23:2436–2442

52. Singh N, Jenkins GJ, Asadi R (2010) Doak SH Potential toxicity of superparamagnetic iron oxide nanoparticles (SPION). Nano Rev 1:5358–5373
53. Yigit MV, Moore A, Medarova Z (2012) Magnetic nanoparticles for cancer diagnosis and therapy. Pharm Res 29:1180–1188
54. Chiriac H, Tibu M, Dobrea V, Murgulescu I (2004) Thin magnetic amorphous wires for GMI sensor. J Optoelectron Adv Mater 6:647–650
55. Chiriac H, Tibu M, Moga AE, Herea DD (2005) Magnetic GMI sensor for detection of biomolecules. J Magn Magn Mater 293:671–676
56. Chiriac H, Herea DD, Corodeanu S (2007) Microwire array for giant magneto-impedance detection of magnetic particles for biosensor prototype. J Magn Magn Mater 311:425–428
57. Ward TR (2005) Artificial metalloenzymes for enantioselective catalysis based on the noncovalent incorporation of organometallic moieties in a host protein. Chem Eur J 11:3798–3804
58. Abd-El-Aziz AS, Todd EK, Okash RM, Afifi TH (2003) Organo-iron polymers containing azo dyes. Macromol Symp 196:89–99
59. Andres PR, Schubert US (2004) New functional polymers and materials based on 2, 2': 6', 2"-terpyridine metal complexes. Adv Mater 16:1043–1068
60. Holliday BJ, Swager TM (2005) Conducting metallopolymers: the roles of molecular architecture and redox matching. Chem Commun 23–36
61. Westgate T (2006) Chem World 3:64
62. Whittell GR, Manners I (2007) Metallopolymers: New multifunctional materials. Adv Mater 19:3439–3468
63. Chan WY, Clendenning SB, Berenbaum A, Lough AJ, Aouba S, Ruda HE, Manners I (2005) Highly metallized polymers: synthesis, characterization, and lithographic patterning of polyferrocenylsilanes with pendant cobalt, molybdenum, and nickel cluster substituents. J Am Chem Soc 127:1765–1772
64. Shoichet MS (2010) Polymer scaffolds for biomaterials applications. Macromolecules 43:581–591
65. Causa F, Netti PA, Ambrosio L (2007) A multi-functional scaffold for tissue regeneration: the need to engineer a tissue analogue. Biomaterials 28:5093–5099

Chapter 17
Nanocomposite Polymeric-Based Coatings: From Mathematical Modeling to Experimental Insights for Adapting Microstructure to High-Tech Requirements

Andreea Irina Barzic

Abstract Nanocomposite polymeric-based coatings have been widely investigated owing to their high performance and physical properties that can be easily controlled through various factors. The performance of such systems is determined not only by the characteristics of the polymers or nanofiller but also by the interactions occurring between them. For understanding the improvement routes of their properties, a short classification of the polymer nanocomposites highlighting the importance of the shape, size, distribution, and origin of the nanofiller is presented. A review of the investigation methods of the microstructure evaluation, starting from solution phase to solid coatings, is performed. These techniques include rheology, UV-VIS spectroscopy, microscopic techniques, electron tomography, X-ray diffraction, mechanical tests, permeability measurements, and advanced thermal analysis. In addition to experimental evaluation tools, synthesis for the mathematical models developed for their electrical, thermal, and dielectric properties is presented. The current trends in obtaining intelligent polymer composites (thermo-sensitive, pH-responsive, and other responsive stimuli) for various applications are also reviewed.

Keywords Polymer nanocomposites • Microstructure • Intelligent materials

17.1 Introduction

Nanocomposite polymeric-based coatings represent an alternative to current polymer materials owing to their ease of processing and their tunable physical properties [1]. Recent trends in industrial sectors or in biomedical fields are focused in enhancing the current performance of the nanocomposites and to render upon them an intelligent behavior [2]. In this context, it seems that aside from choosing the proper

A.I. Barzic (✉)
"Petru Poni" Institute of Macromolecular Chemistry,
Grigore Ghica Voda Alley 41A, 700487 Iasi, Romania
e-mail: irina_cosutchi@yahoo.com

system components, one should carefully examine the microstructure, which determines the interactions between the phases [3]. The nanofiller's properties and level of dispersion dictate the performance of the composite. For example, in some instances, controlled particle aggregation is needed to produce a percolating system while other circumstances may need a dispersion that is totally homogeneous [4]. The formation of a pseudo-solid-like network of nanoparticles inside the macromolecular chains enhances the interactions between the phases. This leads to a significant increase of some important physical properties by creating additional conduction paths in the nanocomposite. Other approaches are directed to various functionalization routes [5] of the nanoparticles inserted into the polymer matrix in order to reduce thermal barriers or the loss of the polarization.

There have been multiple methodologies used to ascertain the variation in the microstructure of a nanocomposite when it is exposed to many different types of solvent [6,7]. Rheology is a type of analysis that is sensitive to the polymer matrix's filler dispersity [8]. These characterization techniques are critical in determining the viscoelastic behavior of nanocomposites and are relevant for both processing and research purposes when investigating the materials' dynamic properties and architecture. However, in many cases the theoretical assessment of the materials' properties must be performed prior to their preparation and processing since it would provide a deeper understanding of the nanocomposite modeling [9]. This motivates scientists to focus on the development of several mathematical approaches that describe the electric or thermal behavior of the nanocomposite [9–11]. Unfortunately, there are few of them that take into consideration the state of dispersion and/or the shape of the nanofiller.

Taking into consideration the actual state of research in the field of reinforced materials, a short classification of the polymer nanocomposites highlighting the importance of the shape, size, distribution, and origin of the nanofiller is constructed, followed by a review of mathematical approaches used for predetermination of the physical properties. The main methods used in analysis of the reinforced polymer microstructure changes are described. The current state of affairs regarding intelligent polymer composites is also presented.

17.2   Classification of Polymer Nanocomposites

A polymer nanocomposite is constituted from a continuous phase, namely, the polymer matrix, in which it is introduced the disperse phase [12]. The reinforcement phase is represented by nanoscale compounds with properties dependent on their shape and size. Considering these aspects, these materials can be classified by several criteria:

- Based on the origin of both phases, one can distinguish natural and synthetic polymer nanocomposites. Starting from the matrix properties, polymer composites can be divided into thermoplastic, thermo-resistant, and elastomeric. They

can be also divided on the basis of matrix, that is, a non-biodegradable matrix and biodegradable matrix. Bio-based composites made from natural/biofiber and biodegradable polymers are known as green composites.

- The classifications according to the shape of the nanofiller are particulate composites (composed of particles that have sphericity factor ≤ 1), fibrous composites (composed of fibers), and tubular composites (composed of tubes).
- The manner in which the nanofiller is distributed inside the continuous phase leads to layered and dispersed nanocomposites. In case of nanotubes or nanofibers, the distribution of such fillers can be isotropic or anisotropic.
- Depending on the chemical nature of the reinforcement agent, the polymer nanocomposites can be classified into metallic, ceramic, and carbon-based categories. The reinforcement of a polymer with metallic particles (like gold, silver, copper, aluminum) leads to the enhancement of the electric and thermal conductivity. This also generates an increase in material density that limits the requirements related to the low weight. Ceramic nanopowders, such as aluminum nitride, boron nitride, silicon carbide, or beryllium oxide, are widely inserted into polymers in order to increase their thermal conduction ability. In addition, some ceramic nanoparticles, like barium titanate, lead to the increase of the dielectric constant. Carbon-based polymer nanocomposites are the most promising owing to their high conduction characteristics and their low weight. Carbon fibers, black carbon, fullerene, graphene, and carbon nanotubes are widely used as reinforcement agents.

The classification criteria of polymer nanocomposites are displayed in Fig. 17.1.
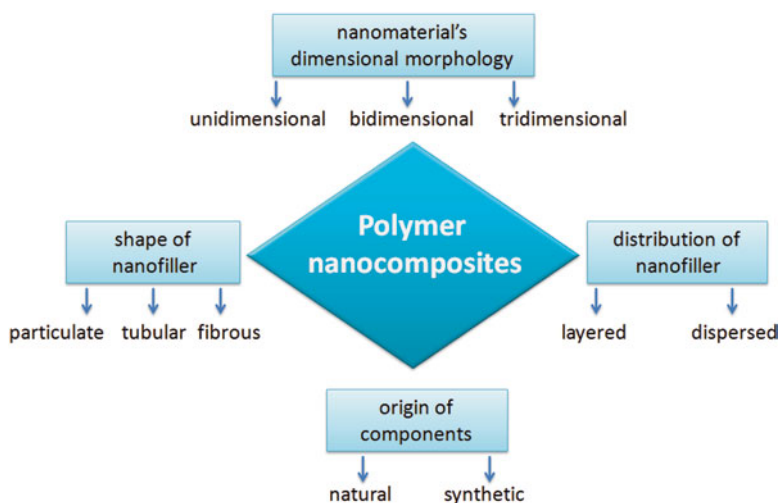
Fig. 17.1 General classification of polymer nanocomposites

17.3   Mathematical Models for Prediction of Nanocomposite Properties

The properties of the composite material can be determined in the incipient stage with mathematical models. Newly developed models have proved to be very helpful, leading to results close to the experimental data. Various approaches have been proposed for the evaluation of electrical, thermal, and dielectric properties. Few models take into consideration the filler geometry, distribution, and the contact between the filler and matrix.

17.3.1   Models for Thermal Conductivity

The *Maxwell–Eucken model* [13] is made for spherical nanoparticles that are randomly distributed in the homogenous matrix and it presumes no interactions among the reinforcement agent:

$$k_c = k_m \frac{2k_m + k_p + 2\varphi_p \left(k_p - k_m\right)}{2k_m + k_p - 2\varphi_p \left(k_p - k_m\right)} \tag{17.1}$$

where k_m, k_p, and k_c are the thermal conductivity of the matrix, nanoparticle, and composites, respectively, and Φ_p is the volume fraction of the filler.

The *Fricke model* [14] proposes a relation for thermal conductivity for the case where the nanofillers have an ellipsoidal shape and are randomly distributed in the polymer:

$$k_c = k_m + \left\{ \frac{1 + \varphi_p \left[F \left(k_p / k_m - 1\right) \right]}{1 + \varphi_p \left(F - 1\right)} \right\} \tag{17.2}$$

where F is the ratio between the temperature gradients of phases.

The *Lewis–Nielsen model* [15] combines the effect of filler shape and orientation:

$$k_c = k_m \left[\frac{1 + AB\varphi_p}{1 - B\psi\varphi_p} \right] \tag{17.3}$$

where the constant $A = K_E - 1$ reflects the effect of the particle shape and orientation, K_E is Einstein coefficient, $B = \left(k_p / k_m - 1\right) / \left(k_p / k_m + A\right)$, and $\psi = 1 + \varphi \cdot \left[\left(1 - \varphi_m\right) / \varphi_m^2 \right]$.

The *Springer–Tsai* model [16] assumes a quadratic distribution of cylindrical particles in the matrix:

$$k_c = k_m \left[1 - 2\sqrt{\frac{\varphi_p}{\pi}} + \frac{1}{B} \left(\pi - \frac{4}{\sqrt{1 - \left(B^2 \varphi_p / \pi\right)}} \tan^{-1} \left(\frac{\sqrt{1 - \left(B^2 \varphi_p / \pi\right)}}{1 + B\sqrt{\varphi_p / \pi}} \right) \right) \right] \quad (17.4)$$

where $B = 2\left(\left(k_m / k_p\right) - 1\right)$.

The *Nan model* [17] introduces the Kapitza resistance (a_k) for polymers containing particles with random shape. This approach is used for determining the effect of filler shape, size, orientation, and interfacial thermal resistance of polymer nanocomposites:

$$k_c = k_m \frac{3 + \varphi_p \left(\beta_x + \beta_z\right)}{3 - \varphi_p \beta_x} \quad (17.5)$$

where $\beta_x = \frac{2\left(k_{11} - k_m\right)}{k_{11} + k_m}$, $\beta_z = \frac{k_{33}}{k_m} - 1$, $k_{11} = \frac{k_p}{1 + \frac{2a_k}{d} \frac{2k_p}{k_m}}$, $k_{33} = \frac{k_p}{1 + \frac{2a_k}{l} \frac{2k_p}{k_m}}$,

while d and l are the diameter and length of the nanofiller.

The *Vysotsky model* [18] starts with the observation that reinforced polymers present a percolation network. Thus, the critical volume fraction corresponding to the occurrence of the percolation processes was introduced in calculation of thermal conductivity:

$$k_c = k_p \left(k_{percol} / k_p\right)^{\left(1 - \varphi_p / 1 - \varphi_{percol}\right)^n} \quad (17.6)$$

where n is the percolation network exponent that depends on several factors including shape size and distribution of nanoparticles and k_{percol} and Φ_{percol} are the thermal conductivity and filler volume fraction at the percolation threshold.

The *Barzic model* [10] modifies the Vysotsky approach by considering the thermal properties of the matrix, the shape of the filler, and the percolation effect:

$$\lambda = \varphi_{AlN} \cdot \lambda_{AlN} \left(\frac{\lambda_{percol}}{\lambda_{AlN}}\right)^{\frac{1}{f}\left(\frac{1 - \varphi_{AlN}}{1 - \varphi_{percol}}\right)^n} + \varphi_{P4VP} \cdot \lambda_{P4VP} \left(\frac{\lambda_{percol}}{\lambda_{P4VP}}\right)^{\left(\frac{1 - \varphi_{P4VP}}{1 - \varphi_{percol}}\right)^n} \quad (17.7)$$

where f is the factor of the particle shape, defined as $f = 3 / \psi$ (the sphericity is $\psi \leq 1$).

17.3.2   Models for Dielectric Constant

The *Bottcher model* [19] approximates the binary system as being composed of repetitive unitary cells composed of a matrix with spherical inclusions placed in the center:

$$\varphi_p \frac{\varepsilon_p - \varepsilon_c}{\varepsilon_p + 2\varepsilon_c} + \left(1 - \varphi_p\right)\frac{\varepsilon_m - \varepsilon_c}{\varepsilon_m + 2\varepsilon_c} = 0 \tag{17.8}$$

where ε_c, ε_p, and ε_m represent the dielectric constants of the nanocomposite, nanofiller, and matrix, respectively.

The *Lichtenecker model* [20] removes the inconvenience that is related to the particle shape and defines the dielectric constant of the nanocomposite as being a power law expression:

$$\varepsilon_c^{\beta} = \varphi_p \varepsilon_p^{\beta} + \left(1 - \varphi_p\right)\varepsilon_m^{\beta} \tag{17.9}$$

where β is a non-dimensional parameter related to the shape and orientation of nanofiller:

$$\beta = 1 - 2\left[\frac{1}{1 + 1.6\left(a/b\right) + 0.4\left(a/b\right)^2)}\right] \tag{17.10}$$

where a and b are the axial dimensions of the nanoparticles; when a=b the filler presents spherical shape and $\beta = 1/3$.

The *Giordano model* [21] is fitted for fillers with ellipsoidal shape that are aligned or randomly dispersed in the matrix:

$$1 - \varphi_p = \frac{\varepsilon_p - \varepsilon_c}{\varepsilon_p - \varepsilon_m}\left(\frac{\varepsilon_p + 5\varepsilon_m}{\varepsilon_p + 5\varepsilon_c}\right)^{2/5} \tag{17.11}$$

The *Yamada model* [22] contains parameters that reflect the filler's morphology:

$$\varepsilon_c = \varepsilon_m\left[1 + \frac{\varphi_p\left(\varepsilon_p - \varepsilon_m\right)}{\varepsilon_m + n\left(\varepsilon_p - \varepsilon_m\right)\left(1 - \varphi_p\right)}\right] \tag{17.12}$$

where n is the morphological fitting constant corresponding to the ellipsoidal shape of the particle and its orientation in regard to the nanocomposite film surface.

17.3.3 Models for Electrical Conductivity

The *Kirkpatrick model* [23] allows the evaluation of electrical conductivity in direct current starting from the assumption that the nanoparticles are in contact with one another inside the polymer:

$$\sigma_c = \sigma_p\left(\varphi_p - \varphi_{p,percol}\right)^b \tag{17.13}$$

where σ_c and σ_p are electrical conductivities of nanocomposite and nanofiller, $\varphi_{p,percol}$ is the volume fraction of the percolation threshold, and b is an exponent reflecting the type of spatial dimension.

The *Mamunya model* [24] includes the surface energy of the polymer and filler (and its aspect ratio, AR) but also the percolation effect:

$$\sigma_c = \sigma_{c,percol} + \left(\sigma_{c,max} - \sigma_{c,percol}\right)\left[\left(\varphi_p - \varphi_{p,percol}\right)/\left(F - \varphi_{p,percol}\right)\right]^d \quad (17.14)$$

where $d = \dfrac{K\varphi_{p,percol}}{\left(\varphi_p - \varphi_{p,percol}\right)^{0.75}}$ is an exponent with values ranging between 1.6 and

1.9, $K = A - B\gamma_{mp}$ and $F = \dfrac{5}{75/\left(10 + AR\right) + AR} = \dfrac{\varphi_p}{\varphi_p + \varphi_m}$, A and B are constants,

whereas γ_{mp} is the interfacial tension of polymer filler and F is packing factor.

The *Maxwell–Wagner model* [25] assumes that the composite microstructure is composed of conducting spheres covered with a dielectric component leading to two arcs in the plot of complex impedance:

$$\frac{\sigma_c - \sigma_m}{\sigma_c + 2\sigma_m} - \varphi_p \frac{\sigma_p - \sigma_m}{\sigma_p + 2\sigma_m} = 0 \quad (17.15)$$

17.4 Methods for Microstructure Evaluation

The manner in which the nanofillers are distributed into the polymer matrix affects the nanocomposite properties. For this reason many characterization methods have been used for evaluation of the microstructure changes of the polymer upon adding nanoparticles. Estimation of the nanofiller dispersion degree is usually done by microscopic or analytical means but cannot provide a detailed, in-depth morphological and structural characterization. By incorporating many laboratory analyses, the data that is generated makes up for the shortcomings of any one analysis on its own.

17.4.1 Rheology

This method is very efficient for nanocomposite solutions that are very sensitive to the filler dispersion in the matrix. Kotsilkova [8] developed a complex rheological approach for optimization of nanocomposite technology by rapid control of the three most important effects: nanofiller dispersion, formation of the 3D structure of nanoparticles, and polymer–filler interactions. This approach relies on routine rheological

experiments and modeling, and it is focused on the control of both technology and formulation of nanocomposites with either thermoset or thermoplastic polymers.

The proposed rheological approach [8] is based on three methods for the characterization of polymer nanocomposites: method I that compares the degree of nanofiller dispersion, method II that quantifies the nanofiller superstructure of nanocomposites, and method III that assesses the polymer–nanofiller interactions. Figure 17.2 displays the main rheological approaches used for polymer nanocomposite characterization. These characterization techniques are critical in determining the viscoelastic behavior of nanocomposites and are relevant for both processing and research purposes when investigating the materials' dynamic properties and architecture. Viscosity gains are observed when there is an intense interaction between the polymer and the particles, leading to the creation of a pseudo-solid-like network. The "rheological percolation" transition is the abrupt alteration of rheological properties, which has been investigated for multiple kinds of nanofiller suspensions based on low viscous solvents.

It is easy to control the degree of nanofiller dispersion in polymer matrices by using experimental data from low-amplitude oscillatory shear and steady-state shear flow. It is assumed that, if the reinforcement degree and other variables are maintained constant, the primary factor determining the rheological response of nanocomposites at low deformation rates will be nanoparticle dispersion. The method determines two rheological parameters, which are essential to quantify the dispersion quality of nanocomposites [8,10]: terminal zone slopes of the dynamic storage and loss moduli (m and n) and the shear thinning exponent (n, flow index). However, in order to achieve meaningful data, the comparison samples need to be comprised of a constant nanofiller concentration, because both shear thinning and terminal regime behavior are functions of the volume fraction of nanofiller. Moreover, the flow behavior of the pristine polymer must be investigated to be used as a reference.
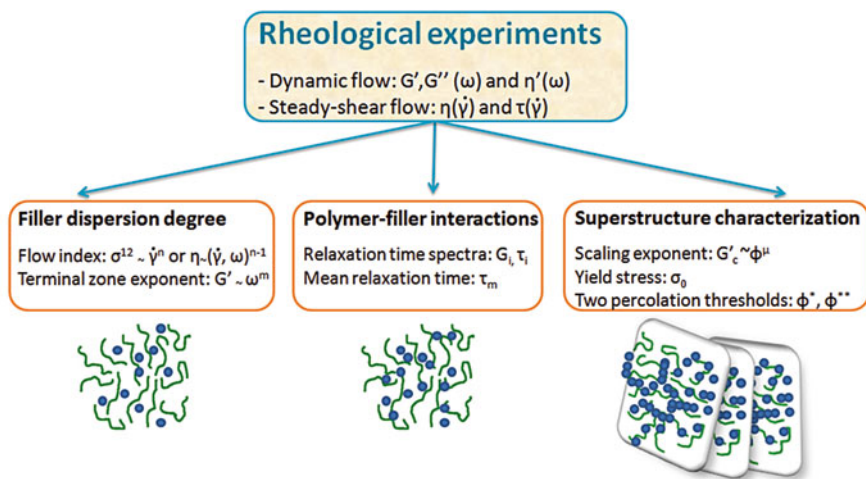
Fig. 17.2 Scheme of the three rheological approaches for polymer nanocomposite characterization

17.4.2 UV-VIS Spectroscopy

UV-VIS spectrometry is an efficient tool for the characterization of polymer nanocomposites [7,26,27]. This method is particularly useful for polymers reinforced with metal nanoparticles. The formation of a nano-metal from its precursor can be monitored by UV-VIS spectroscopy experiments in a good solvent. Metal nanoparticles present a unique characteristic spectrum of individual metals. For instance, the occurrence of silver nanoparticles in a polymer is noticed in UV-VIS absorption data. There is no absorption peak in UV-VIS spectrum for Ag^+ solution in a polymer prior to reduction. The lack of an Ag^+ peak might be due to its d^{10} configuration. The absorption spectra of Ag/polymer nanocomposite at various reinforcement percents are generally represented in Fig. 17.3, with a peak at around 400–410 nm that is characteristic to silver surface plasmon resonance.

   The plasmon absorption peak shifts to higher wavelengths with the increase of filler aggregation (as the reinforcement amount is higher). The sharpness of the peaks is a good indication of the narrow size distribution of the metal nanofiller.

17.4.3 Microscopic Techniques

Microscopy techniques like scanning electron microscopy (SEM) and transmission electron microscopy (TEM) are widely used to evaluate the dispersion state in polymer nanocomposites. SEM allows for the study of the nanocomposite's topography and sometimes provides information on crystallography and composition. The cross-sectional analysis with SEM is useful for the evaluation of nanoparticle dispersion, as well as to examine the surface for filler pullout, possibly giving insight into the strength of interfacial adhesion [28]. However, SEM generally cannot resolve the degree of exfoliation of the platelets and is therefore best utilized as a
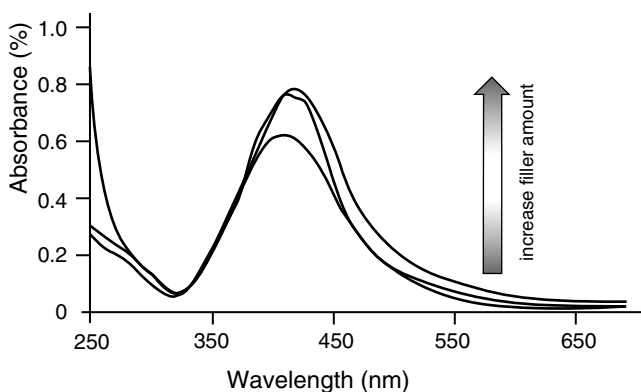
Fig. 17.3 General UV-VIS spectra of Ag/polymer nanocomposites

complementary technique. TEM is useful in the analysis of the internal structure of reinforced polymers providing data about the size, shape, and distribution of the system components at the atomic scale [6]. TEM allows a qualitative understanding of the changes in the internal structure of the polymer during reinforcement. The recording of TEM images of a nanocomposite containing various percent's of nanoparticles is useful in explaining their distribution in the matrix under fixed processing conditions.

17.4.4   Electron Tomography

In order to obtain a comprehensive 3-D structure map of subcellular macromolecular systems, scientists employ electron tomography (ET). By utilizing a transmission electron microscope, ET collects data and acts as an extension to conventional TEM. In the process, a beam of electrons is passed through the polymer nanocomposite medium at incremental degrees of rotation around the center of the target sample. This information is collected and used to construct a 3-D image of the target. Current resolutions of ET systems are in the 5–20 nm range, suitable for examining polymers that are reinforced with nanometric particles [7].

17.4.5   X-Ray-Based Methods

X-ray diffraction (XRD) can only provide the distribution of basal spacing (layer-layer distances within parallel stacked clusters) [29,30]. In case of polymer/layered nanofiller composites, XRD will not show a peak in the overall diffraction diagram if the layers are exfoliated. Conversely, a small and a broad peak can be distinguished at a lower angle compared to the pure nanofiller for intercalated or partially exfoliated nanocomposites. For immiscible composites the original peaks of filler layers are retained completely in the composite. There are two types of X-ray diffraction depending on the angle scanned by the diffracted ray: wide-angle X-ray scattering (WAXS) [31], for which $0° < 2\theta < 90°$, and small-angle X-ray scattering (SAXS) [29] for which the experiments are performed at an angle up to 2 or 5°. The first technique gives information on the degree of crystallinity, orientation/perfection of crystalline region, and nature of the ordering. SAXS reveals data about the dimensions of the tiny crystalline region. SAXS can give additional parameters, such as mean number of layers per stack and "projected" lateral dimension of layers. WAXS can more rapidly give insight into the state of dispersion over a larger volume of composite. Given the fact that the scattering intensity varies with the concentration of the scattering feature, some morphological information might be missed. Immiscibility of the phases and/or insufficient exfoliation of the filler prior to mixing with the polymer can result in large agglomerates consisting of stacked

platelets leading to a diffraction peak corresponding to the interlayer spacing of the filler. An exfoliated morphology of reinforcement agent is desired as it provides higher aspect ratio platelets relative to stacked or intercalated platelets. This state of dispersion is reflected by a scattering profile corresponding to that of the neat matrix polymer. Even so the multilayer intercalated platelets could actually be dispersed (as observed by TEM) despite the absence of a diffraction peak. Recently, high spatial resolution X-ray ultramicroscopy was developed [32] to provide 2-D and 3-D information on filler distribution in polymer composites.

17.4.6 Mechanical Tests

The flexural modulus' dependence on reinforcement amount can give valuable information on the dispersion degree of the inserted particles in the polymer. In most cases the flexural modulus of nanocomposites is enhanced relative to the matrix and the modulus increases by decreasing the processing temperature. Corcione and coworkers [33] correlated the flexural modulus to the degree of nanofiller dispersion by interlacing the equation for the isotropic composites' modulus with the Halpin–Tsai equation. An increased efficiency of nanofiller dispersion in the polymer matrix can be achieved when the processing temperature decreases in response to an increase in the mechanically analyzed calculated values for the AR.

17.4.7 Permeability Measurements

Macroscopic evaluation of nanofiller dispersion can also be performed by permeability measurements as shown by Corcione and coworkers [33,34]. They considered the preparation of a poly(ethylene terephthalate) (PETg) amorphous matrix and organically modified montmorillonite clay (omMMT, 8 % by volume) to create model nanocomposite. The resulting systems were gathered via melt mixing (batch mixer, 60 min, at 150, 180, and 210 °C). The mathematical models were evaluated again the obtained experimental data in an attempt to correlate process parameter with dispersion degree, characterized as the average AR lamellar nanofiller stacks. After being processed at 150 °C, the PETg and the nanocomposite's water vapor permeabilities were determined. The AR (i.e., between lamellar stacks, thickness and width) obtained from permeability data was compared against data gathered from randomly oriented nanoparticles with the Bharadwaj equation [35]. The shape and content of the reinforcing particles affect the permeability of nanocomposites with gases and vapors. Upon addition of the nanofiller, the permeability of the matrix decreases. Permeability measurements lead to an AR in good agreement with the values determined from mechanical and rheological properties.

17.4.8   Thermal Analysis

A newly developed thermal analysis methodology that can be applied for quantifying the degree of nanofiller dispersion throughout the polymeric matrix was developed by Miltner and coworkers [36]. They applied this approach to poly(3-caprolactone) (PCL) nanocomposites containing layered silicates or polyhedral oligomeric silsesquioxane (POSS) nano-cages. During quasi-isothermal crystallization experiments, an excess heat capacity (Cp) was noticed for all nanocomposites owing to reversible melting and crystallization on the timescale of the imposed temperature modulation. The Cp's excess magnitude further increases in the presence of well-dispersed nanofillers (particularly when they display a high aspect ratio). This effect was ascribed to the occurrence of morphological modifications generated by the incorporation of the reinforcement particles, promoting the growth of subsidiary PCL crystals and significantly affecting the amount and the nature of the crystalline/amorphous contact surface within the matrix. It was furthermore revealed that this method can also be used for estimating the degree of filler dispersion within the PCL matrix, the modification of the crystalline morphology being a direct consequence of the amount of matrix/filler interface.

17.5   Current Trends in Intelligent Polymer Composites

17.5.1   Thermosensitive Nanocomposites

Introduction of superparamagnetic Fe_3O_4 particles in negative temperature-sensitive poly(N-isopropylacrylamide) leads to the creation of intelligent hydrogels composites. The systems were characterized for temperature-responsive swelling, remote heating in the presence of an alternating magnetic field, and remote-controlled drug delivery applications. The rise in temperature from an external alternating magnetic field depends on the Fe_3O_4 filler loading. The remote-controlled drug release revealed reduced release in the presence of an alternating magnetic field [37].

Thermally responsive polymer-metal nanocomposites are composed of a gold nanoparticle core and thermally responsive interpenetrating polymer network (IPN) shell, with functionalized surface [38]. Gold nanoparticles were encapsulated inside of a polyacrylamide (PAAm)/poly (acrylic acid) (PAA) IPN shell by in situ inverse emulsion polymerization. The surface of the nanocomposite was modified via covalent grafting of a linear methoxy-poly(ethylene glycol)-hydroxysuccinimide to the primary amine groups of the PAAm network. Dynamic light scattering was used to prove that these IPN nanospheres exhibit a positive and sharp sigmoidal swelling response with increases in temperature. Thus, the swelling and the therapeutic release of the nanocomposites can be controlled externally using noninvasive laser heating of the gold nanoparticles of these systems, making them an externally triggered intelligent therapeutic system [38].

Shape memory polymers (SMPs) have the ability to recover large strains when pre-deformed at high temperatures, cooled to lower ones, and reheated. The thermo-mechanical behavior of SMPs can be tailored through molecular structure of the polymer or by inserting nanofillers. Addition of SiC filler in the thermoset SMP epoxy matrix leads to thermomechanical behavior in three-point flexure [39]. These SMP nanocomposites have higher elastic modulus, being capable of generating higher recovery forces as compared to the matrix. Pre-deformation above the glass transition temperature, Tg, the stress–strain response at the pre-deformation temperature governs the relationship between the recovery stress/strain and the corresponding constraining strain/stress, while below Tg, the opposite process occurs. Rather, a peak recovery stress, that is, smaller than the pre-deformation stress, is formed at a temperature close to the Tg [39].

17.5.2   pH-Responsive Nanocomposites

The pH-responsive nanocomposites based on poly(4-vinylpyridine) (PVP) brush grafted gold nanoparticles were proven to have two-stage change in their hydrodynamic size. The surface plasmon resonance (SPR) response revealed that the gold/PVP nanocomposites have a two-stage response to the pH change that is ascribed to the polymer collapse and to the particle agglomeration. This type of intelligent polymer shell/inorganic core nanocomposites can be considered as building blocks for the fabrication of 2-D/3-D smart nanomaterials, which could be useful for the construction of biosensors [40].

The poly(2-(dimethylamino)ethyl methacrylate) (PDMA)/gold nanocomposites were used to obtain a pH-responsive, colloidal stable, and hydrophilic PDMA nanocapsule after cross-linking the polymer brushes and etching out the gold cores, as well as the similarly obtained nanocapsules of PDMA's copolymer with poly(2-(diethylamino)ethyl methacrylate) and poly(methoxyl oligo(ethylene glycol) methacrylate). This type of uniform capsule resulted from gold nanoparticle templates having high pH sensitivity. The capsule hydrodynamic radius (Rh) can alter their size as the environmental pH changes [41–43].

17.5.3   Other Stimuli-Responsive Polymer Nanocomposites

Photosensitive polymers are widely used for the preparation of intelligent nanocomposites. Photodeformability of such materials relies on the following mechanisms: photoisomerizable molecules, photoreactive molecules, and reversible photoinduced ionic dissociation. Light-active reinforced polymers can be used in bioseparation [44,45], morphing skins of aircrafts [46], and remotely triggered drug delivery systems [44].

Magnetic-active reinforced polymers respond to variation of the localized magnetic field via the magnetic-active effect. Gels and elastomers are loaded with magnetic particle, known as magnetoelastic or magnetostrictive polymeric composites, in order to create these systems [47]. These systems can be categorized as either magnetic-active elastomers or polymeric gels, depending mainly upon their origins (i.e., polymer matrix). Magnetic actuation of polymer nanocomposites using a range of iron, iron–cobalt, and iron–manganese nanoparticles is widely studied. Remote actuation occurs by applying electromagnetic or magnetostatic fields. Burke et al. [48] reported nanocomposites with a metallic iron core and the particle shells derived from the polymeric dispersant bonded to the core. The nanocomposites display room-temperature magnetic behavior ranging from superparamagnetic to ferromagnetic. The saturation magnetization and coercivity were found to depend on the diameter of the iron core.

Electrical active systems refer to actuator-hybrid materials that deform when electric voltage is applied. Many studies were devoted to the production, shaping, and implementation of ionic polymer–metal composites. These composites are typically made up of an ion exchange polymer that has had a conductive medium (platinum or gold) implanted at a depth of several microns within the matrix's surface. Ion exchange polymers that are most frequently used are perfluorinated alkenes and styrene–divinylbenzene copolymers since they have the ability to exchange environmental ions with their own [49–51]. The side chains are terminated by specific groups that allow cation exchange (sulfonate or carboxylate) or anion exchange (ammonium cations). Thus, these systems can interact with specific solvents producing the electro-active effect. The cations that can be utilized to accomplish this task are alkali-metal cations, Li^+, Na^+, K^+, Rb^+, and Cs^+ in addition to alkyl-ammonium cations, tetramethyl and tetrabutyl ammonium. From this viewpoint, an investigation into the triggering properties of single-walled carbon nanotubes (CNTs), CNT sheets, and CNT bundling is undertaken [52,53]. These electrostatics actuators made of CNT have the potential to be used in the following applications: random-access memory (RAM), force measuring tools, nano-motors, bearings, and servo motors and on/off switches [54–56].

17.6   Conclusion

Rendering an intelligent behavior to polymer nanocomposites requires a deep understanding of the fundamental concepts regarding the preparation and processing routes. It is also important to elucidate the microstructure changes upon reinforcement by using complementary characterization techniques. In most cases, after selection of the system components, it is useful to apply mathematical models for predetermination of their physical properties. The performance of polymer nanocomposites can be enhanced if they can respond in a specific manner to external stimuli.

References

1. Davim JP, Charitidis CA (2013) Nanocomposites: materials, manufacturing and engineering (advanced composites). Wer De Gruyter, Berlin
2. Lim EK, Sajomsang W, Choi Y, Jang E, Lee H, Kang B, Kim E, Haam S, Suh JS, Chung SJ, Huh YM (2013) Chitosan-based intelligent theragnosis nanocomposites enable pH-sensitive drug release with MR-guided imaging for cancer therapy. Nanoscale Res Lett 8:467
3. Mittal V (2010) Polymer nanocomposites: synthesis, microstructure, and properties. In: Optimization of polymer nanocomposite properties. Wiley, Weinheim
4. Mutlay İ, Tudoran LB (2014) Percolation behavior of electrically conductive graphene nano-platelets/polymer nanocomposites: theory and experiment. Nanotube Carbon Nanostruct 22:413
5. Zhang X, Servos MR, Liu J (2012) Instantaneous and quantitative functionalization of gold nanoparticles with thiolated DNA using a pH-assisted and surfactant-free route. J Am Chem Soc 134:7266
6. Sumfleth J, Buschhorn ST, Schulte K (2011) Comparison of rheological and electrical percolation phenomena in carbon black and carbon nanotube filled epoxy polymers. J Mater Sci 46:659
7. Yu J, Lu K, Sourty E, Grossiord N, Koning CE, Loos J (2007) Characterization of conductive multiwall carbon nanotube/polystyrene composites prepared by latex technology. Carbon 45:2897
8. Kotsilkova R (2007) Thermoset nanocomposites for engineering applications. Smithers RapraTechnology Limited, Shawbury
9. Mittal V (2012) Modeling and prediction of polymer nanocomposite properties. Wiley, Weinheim
10. Barzic RF, Barzic AI, Dumitrascu G (2014) Percolation network formation in poly(4-vinylpyridine)/aluminum nitride nanocomposites: rheological, dielectric, and thermal investigations. Polym Compos 35:1543
11. Barzic RF, Barzic AI, Dumitrascu G (2014) Percolation effects on dielectric properties of polystyrene/batio3 nanocomposites. UPB Sci Bull Ser A 76:225
12. Thomas S, Joseph K, Malhotra SK, Goda K, Sreekala MS (2012) Polymer composites, vol 1. Wiley, Weinheim
13. Eucken A (1940) Allgemeine gesetzmassigkeiten fur das warmeleitvermfigen verschiedener stoffarten und aggregatzustande. Forsch Gebiete Ingenieur 11:6
14. Fricke H (1924) A mathematical treatment of the electric conductivity and capacity of disperse systems i. the electric conductivity of a suspension of homogeneous spheroids. Phys Rev 24:575
15. Nielsen E, Landel RF (1994) Mechanical properties of polymers and composites, 2nd edn. Marcel Dekker, New York, NY
16. Springer GS, Tsai SW (1967) Thermal conductivities of unidirectional materials. J Compos Mater 1:166
17. Nan CW, Birringer R, Clarke DR, Gleiter H (1997) Effective thermal conductivity of particulate composites with interfacial thermal resistance. J Appl Phys 10:6692
18. Vysotsky VV, Roldughin VI (1999) Aggregate structure and percolation properties of metal-filled polymer films. Colloid Surf A 160:171
19. Böttcher CF (1973) Theory of electric polarisation. Elsevier, Amsterdam
20. Karkkainen KK, Sihvola AH, Nikoskinen KI (2000) Effective permittivity of mixtures: numerical validation by the FDTD method. IEEE Trans Geosci Remote Sens 38:1303
21. Giordano S (2003) Effective medium theory for dispersions of dielectric ellipsoids. J Electrostatics 58:59
22. Yamada T, Ueda T, Kitayama T (1982) Piezoelectricity of a high-content lead zirconate titanate/polymer composite. J Appl Phys 53:4328
23. Kirkpatrick S (1973) Percolation and conduction. Rev Mod Phys 45:574

24. Mamunya YP, Davydenko VV, Pissis P, Lebedev EV (2002) Electrical and thermal conductivity of polymers filled with metal powders. Eur Polym J 38:1887
25. Balberg I, Anderson CH, Alexander S, Wagner N (1984) Excluded volume and its relation to the onset of percolation. Phys Rev B 30:3933
26. Bhat RR, Genzer J (2006) Combinatorial study of nanoparticle dispersion in surface-grafted macromolecular gradients. Appl Surf Sci 252:2549
27. Karak N (2009) Fundamentals of polymers: raw materials to finish products. PHI Learning, New Delhi
28. Rafiee MA, Rafiee J, Wang Z, Song H, Yu ZZ, Koratkar N (2009) Enhanced mechanical properties of nanocomposites at low graphene content. ACS Nano 3:3884
29. Jenkins R (2000) X-ray techniques: overview. In: Meyers RA (ed) Encyclopedia of analytical chemistry. Wiley, Chichester
30. Žukas T, Jankauskaitė V, Žukienė K, Baltušnikas A (2012) The influence of nanofillers on the mechanical properties of carbon fibre reinforced methyl methacrylate composite. Mater Sci (Medžiagotyra) 18:250
31. Potts JR, Dreyer DR, Bielawski CW, Ruoff RS (2011) Graphene-based polymer nanocompositess. Polymer 52:5
32. Šupová M, Martynková GS, Barabaszová K (2011) Effect of nanofillers dispersion in polymer matrices: a review. Sci Adv Mater 3:1
33. Corcione CE, Cavallo A, Pesce E, Greco A, Maffezzoli A (2011) Evaluation of the degree of dispersion of nanofillers by mechanical, rheological, and permeability analysis. Polym Eng Sci 51:1280
34. Greco A, Cavallo A, Corcione CE, Maffezzoli A (2011) Macroscopic evaluation of nanofiller dispersion. SPE Plast Res Online. doi:10.1002/spepro003641
35. Bharadwaj RK (2001) Modeling the barrier properties of polymer-layered silicate nanocomposites. Macromolecules 34:9189
36. Miltner HE, Watzeels N, Goffin AL, Duquesne E, Benali S, Dubois P, Rahier H, Van Mele B (2010) Quantifying the degree of nanofiller dispersion by advanced thermal analysis: application to polyester nanocomposites prepared by various elaboration methods. J Mater Chem 20:9531
37. Satarkar NS, Hilt JZ (2008) Hydrogel nanocomposites as remote controlled biomaterials. Acta Biomater 4:11
38. Owens DE III, Eby JK, Jian Y, Peppas NA (2007) Temperature responsive polymer-gold nanocomposites as intelligent therapeutic systems. J Biomed Mater Res A 83:692
39. Liu Y, Gall K, Dunn ML, McCluskey P (2003) Thermomechanical recovery couplings of shape memory polymers in flexure. Smart Mater Struct 12:947
40. Li D, He Q, Yang Y, Mohwald H, Li J (2008) Two-stage pH response of poly(4-vinylpyridine) grafted gold nanoparticles. Macromolecules 41:7254
41. Li D, He Q, Li J (2009) Smart core/shell nanocomposites: intelligent polymers modified gold nanoparticles. Adv Colloid Interface Sci 149:28
42. Duan HW, Kuang M, Wang DY, Kurth DG, Möhwald H (2005) Colloidally stable amphibious nanocrystals derived from poly{[2-(dimethylamino)ethyl] methacrylate} capping. Angew Chem Int Ed 44:1717
43. Duan HW, Kuang M, Zhang G, Wang DY, Kurth DG, Möhwald H (2005) pH-responsive polymeric nanocapsules by templating nanocrystals. Langmuir 21:11495
44. Meng H, Hu J (2010) A brief review of stimulus-active polymers responsive to thermal, light, magnetic, electric, and water/solvent stimuli. J Intell Mater Syst Struct 21:859
45. Wang W, Wan J, Ning B, Xia J, Cao X (2008) Preparation of a novel light-sensitive copolymer and its application in recycling aqueous two-phase systems. J Chromatogr A 1205:171
46. Snyder EA, Tong TH (2005) Towards novel light-activated shape memory polymer: thermomechanical properties of photo-responsive polymers. Mater Res Soc Symp Proc 872:353
47. Hogea CS, Armstrong WD (2002) The time-dependent magneto-visco-elastic behavior of a magnetostrictive fiber actuated viscoelastic polymer matrix composite. J Acoust Soc Am 112:1928

48. Burke NAD, Stover HDH, Dawson FP (2002) Magnetic nanocomposites: preparation a and characterization of polymer- coated iron particles. Chem Mater 14:4752
49. Kottke EA, Partridge LD, Shahinpoor M (2007) Bio-potential neural activation of artificial muscles journal of intelligent material systems and structures. J Intell Mater Syst Struct 18:103
50. Shahinpoor M, Kim KJ (2005) Ionic polymer–metal composites: IV Industrial and medical applications. Smart Mater Struct 14:197
51. Shahinpoor M, Kim KJ, Leo DJ (2003) Ionic polymer-metal composites as multifunctional materials. Polym Compos 24:24
52. Fraysse J, Minett AI, Jaschinski O, Duesberg GS, Roth S (2002) Carbon nanotubes acting like actuators. Carbon 40:1735
53. Qu L, Peng Q, Dai L, Spinks GM, Wallace GG, Baughman RH (2008) Carbon nanotube electroactive polymer materials: opportunities and challenges. MRS Bull 33:215
54. Fennimore AM, Yuzvinsky TD, Han WQ, Fuhrer MS, Cumings J, Zettl A (2003) Rotational actuators based on carbon nanotubes. Nature 424:408
55. Lefevre R, Goffman MF, Derycke V, Miko C, Forro L, Bourgoin JP, Hesto P (2005) Scaling law in carbon nanotube electromechanical devices. Phys Rev Lett 95:185504
56. Cumings J, Zettl A (2000) Low-friction nanoscale linear bearing realized from multiwall carbon nanotubes. Science 28:60

Chapter 18
Polymer-Based Nanocomposite Coatings for Anticorrosion Applications

Mehdi Honarvar Nazari and Xianming Shi

Abstract The successful use of polymeric coatings for corrosion prevention or mitigation is often hindered by their inherently porous microstructure that fails to resist the ingress of detrimental species and/or by their vulnerability to damage by surface abrasion, wear, or scratches. Incorporation of nanomaterials in polymeric coatings can greatly improve their barrier performance. While the last decade has seen a substantial amount of research on polymeric nanocomposite coatings, the knowledge underlying the critical roles nanomaterials play remains scattered. This chapter discusses the utilization of nanotechnology to greatly enhance the properties of polymer-based coatings for anticorrosion applications, by modifying the microstructure of the coating bulk or endowing it with additional functionality. It starts with a brief discussion of the relevant knowledge base, including: microstructure of polymer nanocomposites, influence of nanomodification on properties of polymeric coatings, fabrication approaches, and the use of polymeric nanocoating as a carrier for corrosion inhibitors. It also provides a review of technological advances in the use of nanotechnology to produce high-performance polymeric coatings with outstanding corrosion resistance and other relevant properties. The chapter concludes with a snapshot review of the advanced characterization of nanocomposite coatings for corrosion protection.

Keywords Nanocomposite coating • Anticorrosion application • Self-healing • Active protection • Encapsulation • Nanoidentification

M. Honarvar Nazari
Department of Civil and Environmental Engineering, Washington State University, 642910, Pullman, WA 99164-2910, USA
e-mail: m.honarvarnazari@wsu.edu

X. Shi (✉)
Department of Civil and Environmental Engineering, Washington State University, Dana 221, 642910, Pullman, WA 99164-2910, USA
e-mail: Xianming.Shi@wsu.edu

18.1   Introduction

Nanotechnology is one of the best approaches to addressing the technological challenges in the twenty-first century [1], especially those related to materials science and engineering. Achieving the fundamental understanding of processes and behaviors of materials at the nanometer and submicron scales has enabled substantial advances in the fields of materials design and fabrication. It is also known that decreasing the dimensions of materials to the nanometer scale can greatly improve their properties. The term "nanomaterials" is attributed to materials that have at least one dimension below 100 nm [2], where their structural defects diminish and aspect ratio increases significantly. The increases in aspect ratio (Fig. 18.1) and specific surface area lead to enhanced molecular-level interactions at the phase interfaces. The synergistic effects of these phenomena may be employed to induce significant improvements in physical and mechanical properties of nanocomposite materials, even if the nanoparticles are added at a very low volume fraction [2, 4, 5].

Currently there is an urgent need to establish innovative designs for protective coating systems that feature both excellent performance and environmental
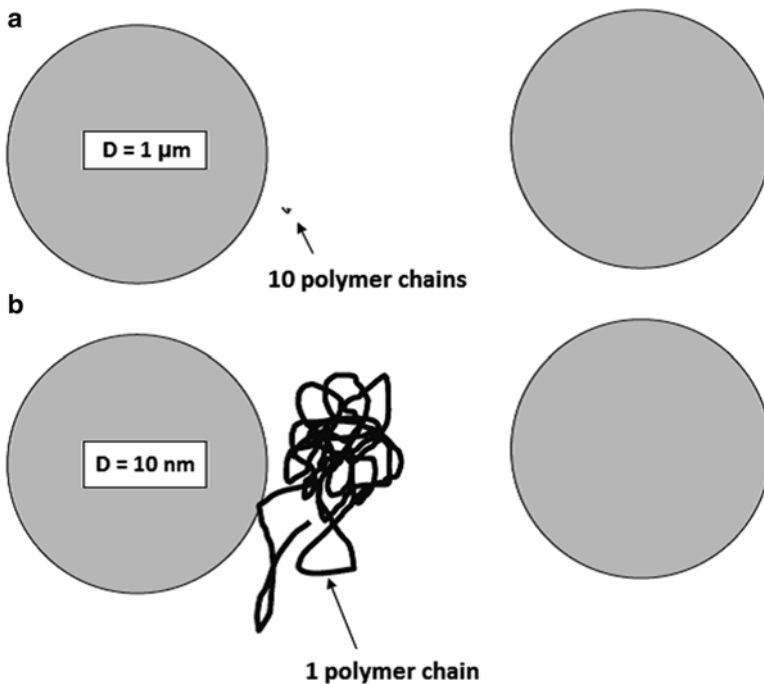
Fig. 18.1 Schematic illustration of the relative size of polymer chains in a composite coating with (**a**) micron-size materials and (**b**) nanomaterials, which shows a significantly larger chain-particle interface area for the polymer-based nanocomposites relative to microcomposites (adapted with permission from [3], Copyright © 2010 Elsevier Inc.)

stewardship. Polymer-based coatings are good candidates as the polymers are chromate-free and can have outstanding processability, excellent chemical resistance, and strong adhesion to various metallic substrates. A typical function of polymeric coatings is to serve as a physical barrier layer for a metallic substrate and block or limit the access of active species from an aggressive environment, thus decreasing the corrosion rate of the metal [6]. Yet, the successful use of polymeric coatings for corrosion prevention or mitigation is often hindered by their inherently porous microstructure that fails to resist the ingress of detrimental species and/or by their vulnerability to damage by surface abrasion, wear, or scratches.

Incorporation of nanomaterials in polymeric coatings can greatly improve their barrier performance by decreasing the porosity and zigzagging the diffusion path for corrosive species such as oxygen and chloride anions (Cl^-) [7]. The nanosize effect enables the use of a much lower volume of nanomaterials for modifying the microstructure of polymeric coatings to achieve the same level of protection properties, relative to the case of using micro-sized or larger particles as fillers [8, 9]. The fabrication of polymer-based nanocomposites is feasible for nearly all polymer types, including: thermoplastics which are rigid and meltable (e.g., polyethylene), thermosets which are rigid and not meltable (e.g., epoxy), and elastomers which are stretchable (e.g., rubber) [2, 10]. Both nonconducting and conducting polymers can be employed as a matrix for polymeric nanocomposite coatings.

It is cautioned, however, that nanomaterials often serve more than just the role of a nanofiller. While the last decade has seen a substantial amount of research on polymeric nanocomposite coatings, the knowledge underlying the critical roles nanomaterials play remains scattered. Often, there is a lack of consensus or fundamental understanding of the interactions between the incorporated nanomaterials and the polymer matrix. Furthermore, how these interactions in both liquid and solid phases affect the anticorrosion properties of polymeric coatings needs clarification. Further complicating this issue is the recent introduction of intelligent nanocomposite coatings with self-healing properties, featuring the incorporation of corrosion-inhibitor-loaded nanocontainers into the polymer matrix.

In this context, this chapter aims to synthesize the available information in the published domain on polymer-based nanocomposite coatings for anticorrosion applications, with a focus on recent advances published in the period of 2005–2015. This state-of-the-art review will assist materials scientists, corrosion scientists, engineers, and other stakeholders in the design, fabrication, evaluation, and research of polymer-based nanocoatings. The following sections will start with a discussion of the microstructure of polymer nanocomposites, influence of nanomodification on the properties of polymeric coatings, and fabrication approaches, followed by a high-level overview of the polymeric nanocoatings as carriers for corrosion inhibitors and advanced characterization of nanocomposite coatings for corrosion protection. The focus of this work will be given to polymer-based coatings loaded with nanoparticles as a physical barrier against corrosive species ("*passive protection*") and also intelligent polymer-based coatings incorporated with nanocontainers as reservoirs for corrosion inhibitors ("*active protection*").

18.2   Microstructure of Polymer-Based Nanocomposites

Nanomaterials with a wide range of shapes and sizes have been employed for fabrication of polymer nanocomposites. The nanomaterials can be divided into four main categories, including: zero-dimensional particles which include atomic clusters such as silica, one-dimensional particles such as nanotubes, two-dimensional nanolayer-structured materials such as clay platelets, and three-dimensional hybrid nanomaterials [11].

The nanocomposite microstructure can be categorized according to the interaction between the polymer matrix and the added nanomaterial (i.e., phase-separated, hybrid-phase, intercalated, and exfoliated composites) [12]. For instance, when the inorganic particles remain as inert fillers inside the organic polymer bulk, the microstructure would be described as phase-separated. This is the typical type of microstructure in conventional polymer composites and can also be seen in polymer composites with the nanomaterial(s) poorly dispersed. If the nanomaterial is dispersed well in the polymer matrix and physically or chemically interacts with the polymer chains, the microstructure would be described as a hybrid-phase (organic/inorganic nanocomposite in some cases). For nanomaterials with platelet structure (e.g., nanoclays), once the electrostatic forces of interaction between platelets partially dissipate, a single or sometimes more than one extended polymer chain penetrates between them. This increases the spacing between platelets without changing the regular gallery structure, and the microstructure is described as intercalated [13, 14]. The microstructure is described as exfoliated, when the individual platelets are homogenously dispersed in the polymer matrix such that the periodicity of their platelet arrangement is completely lost. This phenomenon occurs when the electrostatic forces between the platelets are totally dissolved [12, 14]. Under this condition, the aspect ratio of the nanomaterial can reach as high as 1000 with a specific surface area up to 750 m^2/g [15].

The morphology of various forms of layered silicate/polymer nanocomposites has been obtained by transmission electron microscopy (TEM), as shown in Fig. 18.2, in which the dark lines correspond to the cross section of aluminosilicate platelets. Figure 18.2a displays a phase-separated microstructure for a clay/polymer composite, in which the two phases of silicate platelets (filler) and polymer matrix are not intermixed at all. As such, the performance of this composite would not be as desirable as the nanocomposite with better microstructures shown in Fig. 18.2b or 18.2c. Figure 18.2b illustrates the intercalated morphology, where the periodic order of the silicate platelets remains intact despite the increase in their spacing caused by interlayer diffusion of polymer chains. Figure 18.2c illustrates an exfoliated morphology of silicate platelets in the polymer matrix, with a uniform distribution of platelets caused by the complete diffusion of polymer chains. Based on first-principles physical approach, there is an energy match between the polymer molecules and the surface of the filler material in order to receive the required free energy for exfoliation [16]. It is noteworthy that a fully intercalated or exfoliated microstructure has been rarely seen and most of the time a mixture of these morphologies has been observed [11].
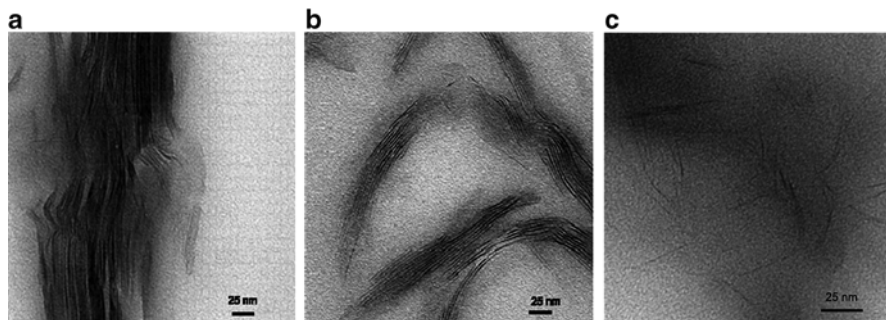
Fig. 18.2 TEM pictures of the polymer-clay composites showing the three main possible morphologies as a function of platelets distribution: (**a**) phase-separated, (**b**) intercalated, and (**c**) exfoliated (reprinted with permission from [11], Copyright © 2010 John Wiley and Sons Inc.)

Fig. 18.3 Zigzagging the diffusion path of corrosive media due to incorporation of nanoplatelets (reprinted with permission from [20], Copyright © 2008 Springer Inc.)
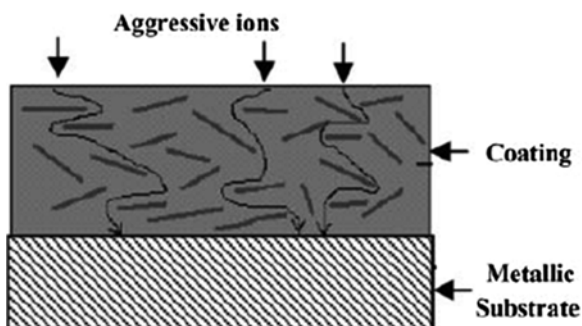
18.3   Influence of Nanomodification on the Properties of Polymer Coatings

The successful use of polymeric coatings is often hindered by their vulnerability to damage by surface abrasion and wear [17, 18]. They may also have poor resistance against the initiation and growth of cracks [19] which can induce localized defects in the coating and thus compromise their appearance, mechanical properties, performance, and durability. These defects have a detrimental influence on the barrier properties of the coatings as they can act as pathways facilitating the access of aggressive species onto the metallic substrate, resulting in its localized corrosion.

The physical barrier performance of polymer coatings can be improved by the incorporation of a second phase that is miscible with the polymer, by decreasing the porosity and zigzagging the diffusion path for deleterious species, as shown in Fig. 18.3. The incorporation of nanomaterials (polyaniline/ferrite, Fe_2O_3, halloysite clay, etc.) into conventional polymer coatings significantly enhanced the anticorrosive performance of such coatings on steel substrates, as shown in Table 18.1. This table presents a variety of polymer nanocomposite barrier coatings and their anticorrosion performance for various metallic substrates, along with other characteristics.

Table 18.1 Some recently developed polymer-based nanocomposite coatings and a comparison between their properties and their counterpart coatings without nanomodification

Metal substrate	Polymer	Nanomaterial (NM)	Calculated corrosion inhibition efficiency for nanocomposite coating compared to polymer coating without NM	Properties other than corrosion resistance and mechanisms of protection in addition to physical barrier	Ref
Mild steel	Alkyd polymer	Polyaniline/ferrite	48.6 %, 28.1 %, 50 % for 1.5 % NM in 5 % HCl, 5 % NaOH, 3.5 % NaCl solution, respectively, after 960 h immersion	The nanostructured coating was dense and nonporous with continuous network-like structure	[21]
Mild steel	Alkyd-based waterborne polymer	Fe_2O_3, ZnO	n.d.	UV resistance, scratch resistance, and abrasion resistance were improved	[22, 23]
Steel	Epoxy resin	SiO_2, Zn, Fe_2O_3, and halloysite clay	96.9 %, 90.9 %, 99.9 %, 99.8 % for SiO_2, Zn, Fe_2O_3, halloysite clay (at 1 % NM), respectively, in 3 % NaCl solution after 28 days immersion	SiO_2 and Zn enhanced the Young's modulus while halloysite clay and Fe_2O_3 decreased it	[6]
Iron	Polyaniline	Clinoptilolite (Clino)	74.9 %, 95.8 %, −38.7 % for 3 % NM in 1 M H_2SO_4, 1 M HCl, 3.5 % NaCl solution, respectively	The alignment of polyaniline chains was improved	[24]
Carbon steel	Polyurethane	Organoclay	88.2 %, 98.7 %, 99.7 % for 1 %, 2 %, 3 % NM, respectively, in 5 % NaCl solution after 30 days immersion	Adhesion of coating decreased with increasing weight percent of NM	[25]
Galvanized steel	Epoxy-polyamide	ZnO	n.d.	The nanocomposite coating had less decrease in cross-linking density, indentation hardness, and adhesion after immersion than control	[26]
Carbon steel	Epoxy resin	Waterborne polyaniline	95.5 % for 1 % NM in 5 % NaCl solution after 720 h immersion	Better physico-mechanical properties. Formation of passive oxide layer on metal	[27]
Carbon steel	Epoxy resin	Al	67.6 % for 40 %[a] NM in 0.1 M NaCl solution after 16 days immersion	Nanoscale complex oxides containing Al and Fe increased the corrosion resistance	[28]
Carbon steel	Epoxy resin	Si	76.2 % for 40 %[a] NM in 0.1 M NaCl solution after 8 h immersion	Si particles have sacrificial effect against the substrate corrosion	[29]

Metal substrate	Polymer	Nanomaterial (NM)	Calculated corrosion inhibition efficiency for nanocomposite coating compared to polymer coating without NM	Properties other than corrosion resistance and mechanisms of protection in addition to physical barrier	Ref
Steel	Polyurethane	Silica (SiO$_2$)	n.d.	The water absorption was reduced; the curing temperature and abrasion resistance were increased	[30]
Carbon steel	Epoxy resin	Urea-modified montmorillonite clay	30.3 %, 34.5 %, 77.7 % for 1 %, 2 %, 3 % NM, respectively, in 3.5 % NaCl solution	The protectiveness of coating decreased with increasing temperature	[31]
Carbon steel	Epoxy resin	Hybrid nanozinc dust and halloysite	n.d.	Thermal stability of epoxy coating was improved. Nanozinc dust served as sacrificial anode	[32]
Aluminum grade 2024-T3	Polyurea/siloxanes/epoxy ester	Montmorillonite clay	n.d.	The presence of clay nanoparticles decreased diffusivity	[33]
Magnesium grade AZ31	Polyetherimide/diethylenetriamine	Hydroxyapatite	n.d.	Biocompatibility, adhesion, and uniformity were enhanced	[34]
Steel	Polystyrene	Organo-functionalized graphene oxide	91.4 %, 96.4 %, 99.2 % for 1 %, 1.5 %, 2 % NM, respectively, in 3.5 % NaCl solution after 30 days immersion	The exfoliated dispersion of the graphene oxide reduced gas permeability and improved mechanical strength	[35]
Steel	Epoxy resin	Clay	n.d.	The microstructure has been modified to a homogeneous exfoliated structure. The mechanical properties have been improved. The thermal properties were improved	[36]
Steel	Waterborne epoxy resin	Polyaniline-mesoporous silica MCM-41	n.d.	The cross-linking density became higher. Polyaniline acts as an electronic and chemical diffusion barrier	[37]

Table 18.1 (continued)

Metal substrate	Polymer	Nanomaterial (NM)	Calculated corrosion inhibition efficiency for nanocomposite coating compared to polymer coating without NM	Properties other than corrosion resistance and mechanisms of protection in addition to physical barrier	Ref
Aluminum bipolar	Polyaniline	Carbon nanotube	71.5 %, 87.7 %, 92.9 % for 0.4 %, 0.6 %, 0.8 % NM, respectively, in 0.1 M H_2SO_4	The electrical conductivity of coating was increased. Increased the adhesion strength of coating and decreased the oxygen and water permeability	[38]
Mild steel	Polyaniline	Functionalized multi-walled carbon nanotube	91.9 %, 96.9 %, 99.2 % for 1 %, 2 %, 3 % NM, respectively, in 3.5 % NaCl solution	The hardness was increased significantly and the surface became more hydrophobic	[39]
Mild steel	Epoxy resin	Polyaniline–camphorsulfonate	n.d.	Durable bond strength between coated rebar and concrete after 1 year. Presence of a protective passive layer on the steel surface	[40]
Mild steel	Epoxy resin	Polyesteramide-clay	n.d.	No significant improvement in thermal stability	[41]
Mild steel	Epoxy resin	Zirconia (ZrO_2)	n.d.	The tensile and hardness properties of the coatings were improved	[42]
Aluminum grade 1050	Polyaniline	TiO_2, Ag, Zn	5.7 %, 71.3 %, 12.9 % for TiO_2, Ag, Zn (1 % NM), respectively, in 3.5 % NaCl solution	Polyaniline/Ag film was the most homogeneous coating	[43]

The values for NM and NaCl solution are in wt%

[a] Adding nanomaterials at 40 wt% into a polymeric coating is an unusual and questionable practice, which leads to concerns over the dispersion of the nanomaterials and their cost-effectiveness
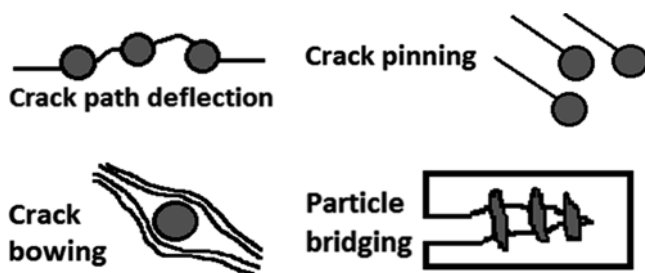
Fig. 18.4 Scheme of toughening mechanisms in polymer-based nanocomposite coatings (reproduced with permission from [47], Copyright © 2014 Society of Plastic Engineers)

In order to calculate the corrosion inhibition efficiency (*IE%*), the corrosion rate (*CR*) or the current density (i_{corr}) was typically derived from potentiodynamic polarization curves or from charge transfer resistance (R_{ct}) obtained by electrochemical impedance spectroscopy.

Incorporation of nanomaterials into polymer matrix offers environmentally benign solutions for enhancing the integrity and durability of coating systems, since the nanomaterials dispersed in coatings can fill cavities [44–46] and lead to particle bridging, crack path deflection, crack bowing, and crack pining [47, 48], as shown schematically in Fig. 18.4. Nanomaterials can also prevent polymer disaggregation during curing, resulting in a more homogenous coating. With their nanosize and high surface area, nanomaterials can occupy small pinhole defects formed from local shrinkage during the polymer curing and act as a bridge interconnecting more molecules. This results in a reduced total free volume as well as an increase in the cross-linking density [49, 50]. In general, polymer coatings containing a small amount of nanomaterials (typically no more than 4 % by weight of polymer) offer significant barrier properties for corrosion protection and reduce the likelihood for the coating to blister or delaminate [18, 25].

The mechanisms by which nanomaterials affect the molecular dynamics of polymer-based composites have been the interest of many researchers [51–53]. Ramanathan et al. [51] studied the mechanical properties and the fracture surfaces of poly(methyl methacrylate)-based nanocomposites. These nanocomposites contained either expanded graphite or functionalized graphene sheets with the smallest measured thickness of about 0.8 nm by the atomic force microscopy (AFM). The nanoscale graphene sheets had a wrinkled topology which could be attributed to their extremely small thickness. The fracture surface featured an extensive plastic deformation around the graphene sheets, which suggests strong interfaces between polymer matrix and graphene sheets. In contrast, there were relatively little plastic deformation and low energy absorption before fracture for the samples with expanded graphite. Relative to expanded graphite, graphene sheets have better interaction with the polymer matrix, which translates to higher Young's modulus and higher tensile strength of graphene/polymer composites. It was concluded that the nanoscale size of graphene sheets and their surface roughness played an important

role for the improved mechanical interlocking of nanographene sheets with the polymer chains and altered the polymer mobility around them.

The interfacial region has an important role in the characteristics of polymer-based nanocomposites. By defining the thickness of the interface between nanomaterials and polymer matrix as 1 nm, the volume percent of the interfacial region can reach up to 30 % [54]. Due to their high surface activity, nanomaterials may serve as template to guide the curing of monomers and oligomers in close proximity to them and lead to formation of better cured polymeric networks in the interfacial region. This beneficial effect could translate to significant improvements in barrier and mechanical properties of nanocomposite coatings.

Schwenke et al. [55] simulated the particle–particle interactions of polymer-coated nanoparticles at a liquid–liquid interface, using a molecular dynamics model considering two immiscible liquids with a diffuse interface between them, and nanoparticles with a core–shell configuration. By comparing the simulated adsorption energy values with the measured values, the authors suggested that the polymer shell around the nanoparticles had a lens shape with the chains extended in the interface plane, as shown in Fig. 18.5. It was found that the interfacial region around the core–shell nanoparticles is strongly affected by the swelling of the polymers, which is dependent on the type of solvent used.

Rolldughin et al. [56] modeled the glass transition temperature (T_g) of polystyrene-based nanocomposites incorporating silicasol nanoparticles. Each silicasol particle consisted of a silica core and an ethyl phenyl shell. The experimental
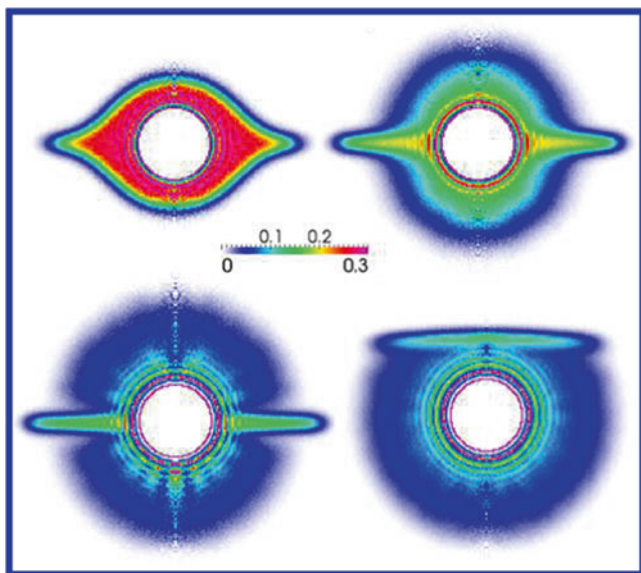
Fig. 18.5 The profiles of the monomers density around the spherical nanoparticles for different monomer–solvent interaction strengths (reprinted with permission from [55], Copyright © 2014 American Chemical Society)

results indicated both an increase and a decrease in T_g after loading silicasol particles into the polystyrene matrix. The authors introduced two competing mechanisms in which the size of hybrid nanoparticles affects T_g. First, the organic shell of nanoparticles increases the degrees of freedom and the entropy of the system and thus induces a decrease in T_g. Second, the presence of the silicasol nanoparticles in the polymer matrix limits the configuration states of macromolecules. This leads to a decrease in the disorientation entropy and thus induces an increase in T_g.

18.4 Fabrication Approaches

The most common methods for fabrication of polymer-based nanocomposite coatings include in situ polymerization, solution exfoliation, and melt intercalation. In the in situ *polymerization* method, the nanomaterials are swollen in monomer liquid or monomer solution. Low molecular weight of the monomer allows it to effectively diffuse between nanomaterial galleries and then polymerize. The polymerization can be initiated and controlled by heat, radiation, diffused initiator, pre-intercalated organic initiator, etc. The growth of polymer chains between nanomaterials can lead to an exfoliated microstructure with a uniform distribution of the nanomaterials. The level of nanomaterial swelling and the diffusion rate of monomers are the main factors influencing the exfoliation procedure [57]. An incomplete polymerization may lead to a heterogeneous polymer microstructure due to localized distribution of oligomers. To achieve a high level of nanomaterial exfoliation, precise control of the polymerization parameters is required [13]. In situ polymerization is suitable for the preparation of polymer-based nanocomposites containing polymers with limited or little solubility, such as nylon 6, epoxy, polyethylene oxide, polystyrene, polyurethane, unsaturated polyesters, and polyethylene terephthalate [58].

In the *"solution exfoliation"* method, the polymer or prepolymer and the nanomaterials are dissolved in the solvents with same composition. The solvent may be water, toluene, chloroform, etc. After swelling the nanomaterials in the solvent, the polymer solution is then mixed with the nanomaterial suspension. In this process, the polymer chains are absorbed to the nanomaterials by intercalating and displacing the solvent between them. Finally, the remaining solvent is removed through vaporization or precipitation. The produced material would be a nanocomposite with an exfoliated or intercalated structure depending on the type of organically modified nanomaterial [59, 60]. This is a typical method for processing water-soluble polymers such as epoxy, polyimide, polyethylene, and polymethylmethacrylate [58, 61]. Often, this method is not considered environmentally friendly considering the use of large amounts of solvent and therefore cannot be readily implemented by industry [15].

In the *"melt intercalation"* method, nanoparticles are directly mixed with the polymer matrix in their molten state at temperatures above the polymer's softening point. The mixing process can be performed under shear or statically. The rate-limiting step of the process is the diffusion of polymer chains into the nanomaterial

galleries, which may be accelerated by any tool that can overcome the electrostatic forces holding the nanomaterials together. Usually high temperatures and surface modification of nanomaterials are the most promising approaches to accelerating the process. The use of high temperatures needs to be closely monitored to avoid potential thermal degradation of the polymer or undesirable modification on the surface of the nanomaterials. It is known that low temperatures can cause slow diffusion of polymer molecules into the galleries [13, 60]. As such, it is crucial to choose an optimum temperature in the melt intercalation method in order to produce a uniformly exfoliated structure. This method is environmentally friendly, as it does not require the use of solvent in the fabrication process. In addition, conventional industrial processes such as plastic extrusion and injection molding are compatible with this method [15]. This method is suitable for the fabrication of thermoplastic-based nanocomposites containing polymers such as nylon 6, polystyrene, and polyethylene [12, 61].

Surface modification of nanomaterials is often achieved by the use of strong acids or alkalis or by using surfactants [62–64]. These are designed to address the polarity difference between the nanomaterials and the majority of polymers. To facilitate the adsorption of surfactant onto the surface of nanomaterials, sonication is a commonly employed technique. The procedure consisted of adding the nanomaterial and surfactant into a solvent and then sonicating the mixture [65]. There is some complexity in the process of sonication for nanomaterials with a multilayer structure such as multi-walled carbon nanotubes (MWNTs). It has been seen that the outermost tubes in a bundle of MWNTs are treated more than the innermost tubes, and as a result, the tubes have tendency to be exfoliated from the bundle ends. To isolate the carbon nanotubes from the bundles, they must be mechanically exfoliated (e.g., using an ultrasonic treatment) in addition to the use of surfactant. It should be mentioned that high-power sonication may destroy the carbon nanotubes, and this risk can be mitigated by using low power sonication (<10 W). Another parameter which has a considerable effect on the dispersion of nanomaterials is the sonication time. The duration of the sonication process should be sufficient to ensure good dispersion of nanomaterials [65]. In reality, it is difficult to obtain a solution with a completely distributed orientation of single nanotubes even after tens of hours of sonication. Most of the time the produced solution consisted of a solution with dispersed single nanotubes and some tube bundles. Gravity sedimentation and ultracentrifugation are recommended for removal of large and small tube bundles, respectively [65].

18.5 Polymeric Nanocoating as Carrier for Corrosion Inhibitors

The design and synthesis of nanostructured materials extend the possibility of engineering intelligent coatings that can be used to release repairing or protective agents in a regulated manner, mainly to the corrosion defects and/or damaged zones of the

coating once triggered by external stimuli. This design provides an active and long-term corrosion protection for the coated metal [66]. There are two main approaches for the implementation of intelligent coatings with self-healing properties used for anticorrosion applications. The first method features localized repair of the damaged coating by controlled release of polymerizable agents, whereas the second method entails electrochemical protection of the exposed metallic substrate using the corrosion inhibitors stored in the nanocontainers [9]. The first method needs a high volume of monomer(s) reserved, typically within the microcapsules, which makes for a serious challenge in ensuring its uniform distribution throughout the thickness of the polymer coating [67]. In comparison, for anticorrosion applications, the second method has been reported to be easy-to-implement and cost-effective, as the nanoscale reservoirs provide uniform and extended release of corrosion inhibitors [68], as schematically shown in Fig. 18.6.

The main philosophy behind reserving corrosion inhibitor in nanocontainers instead of directly loading it inside the polymer coating is that the former approach minimizes the risk of early leaching of inhibitor and delivers the inhibitor when and where it is needed. In addition, the latter approach runs the risk of having undesirable interactions between the corrosion inhibitor and the polymer matrix that negatively affect the coating's performance [70, 71]. The nanomaterials that serve as reservoirs for corrosion inhibitors should have certain characteristics, such as good mechanical and chemical stability, high compatibility with the polymer
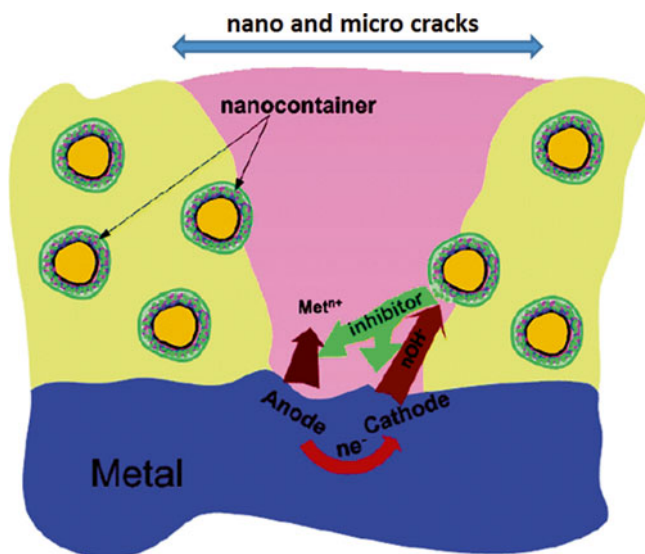
Fig. 18.6 A schematic representation of the self-healing effect of nanocontainers loaded with corrosion inhibitor (adapted with permission from [69], Copyright © 2007 American Chemical Society)
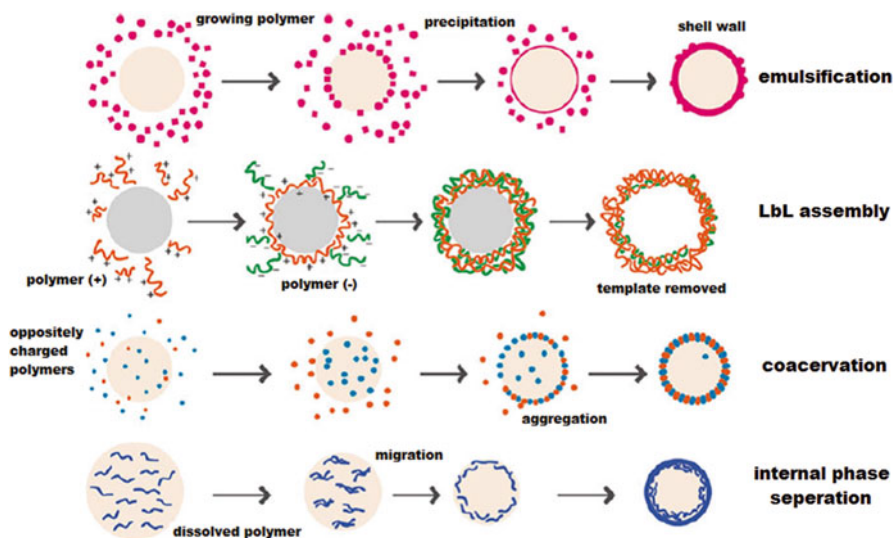
Fig. 18.7 Schematics of preparation methods for nanocapsules by using polymeric shells (adapted with permission from [72], Copyright © 2013 Springer Inc.)

matrix, and impermeable yet sensitive shell wall which releases the inhibitor only on demand [67].

Generally, three main approaches have been employed for encapsulating corrosion inhibitors inside nanocontainers. The first approach is encapsulation using polymeric layers or shells through methods such as the layer-by-layer (LbL) assembly, coacervation, internal phase separation, and emulsification [72], as shown schematically in Fig. 18.7. The second approach is encapsulation using inorganic shells (e.g., SiO_2) via a sol–gel route [73]. The third approach entails the use of nanovalves engineered in the opening of nanochannels. The nanovalve (a metal-inhibitor complex) is formed by a reaction between the loaded inhibitor and transition-metal ions [74, 75]. For instance, the nanochanneled structures such as halloysite nanoclays and mesoporous silica nanoparticles have been employed as containers for corrosion inhibitors in polymer-based anticorrosion coatings. The extended controllable release of corrosion inhibitors is achieved by either LbL assembly of polyelectrolytes (Fig. 18.8) or by application of stoppers at the opening of the channels (Fig. 18.9). The latter route entails the diffusion of transition-metal ions into the opening of the channels to form insoluble metal-inhibitor complexes, which act as stoppers for the trapped inhibitor [74–78].

A variety of other methods have been used for filling nanocapsules, such as: stirring the suspension of capsules and corrosion inhibitors, soaking the nanomaterial in inhibitor solution, using vacuum, and LbL deposition [72]. Furthermore,
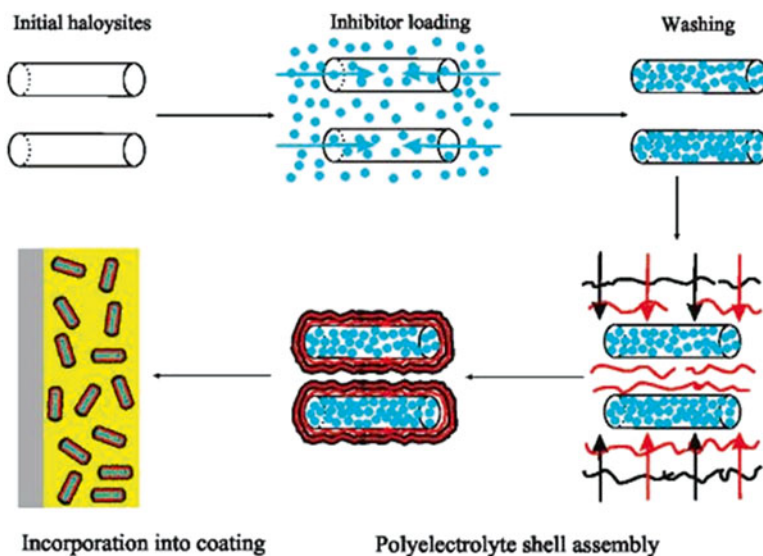
Fig. 18.8 Schematics of the LbL assembly for halloysite nanocontainers (reprinted with permission from [76], Copyright © 2008 American Chemical Society)
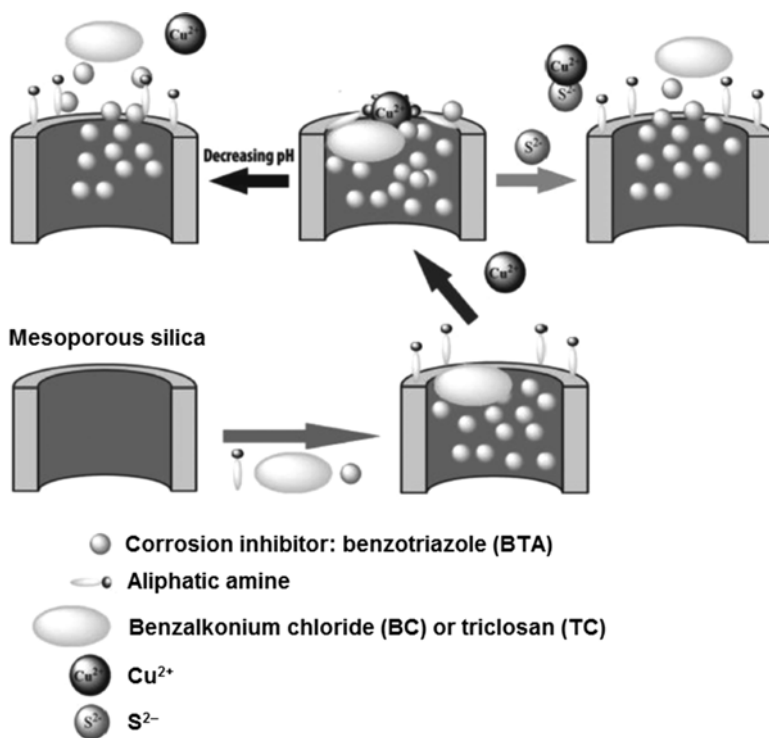
Fig. 18.9 Schematics of the preparation procedure and the release mechanism in mesoporous silica nanoreservoirs using a metal-inhibitor complex as nanovalve with a pH/sulfide ion triggering mechanism (adapted with permission from [75], Copyright © 2013 John Wiley and Sons Inc.)

surface-modified nanocontainers such as mesoporous silica and halloysite nanotubes have been employed by some researchers for loading corrosion inhibitors [78–80]. The triggering mechanisms for the release of the reserved corrosion inhibitors range from desorption-controlled release, pH-controlled release, ion-exchange control of release, release under mechanical rupture [81], to temperature-controlled release [78].

Layered double hydroxide (LDH) is another emerging method for reserving the corrosion inhibitors, which cannot be considered as an encapsulating method. The LDH nanocontainers prepared by this method offer a good corrosion protection at the early stages of corrosion because of their fast ion-exchange nature. In comparison, the encapsulated nanoreservoirs offer good protection only when the corrosion is about to start or has already started, in light of their pH-controlled slow release [9, 79]. LDH can be used for the storage and release of anionic corrosion inhibitors, as well as entrapment for the corrosive species such as chloride ions [81].

Table 18.2 presents a variety of polymer nanocomposite intelligent coatings loaded with corrosion inhibitors and their corrosion performance for various metallic substrates, along with other characteristics. The methods for calculating the corrosion inhibition efficiency are the same as those used for Table 18.1.

18.6   Advanced Characterization of Nanocomposite Coatings for Corrosion Protection

This section will provide a high-level overview of some of the advanced characterization tools employed to study the microstructure, behavior, and properties of nanocomposite coatings for corrosion protection. For instance, surface analysis methods are often employed for nanoidentification of composite microstructures. Among them, TEM is the best one that provides a clear view of the microstructure. For instance, TEM images from halloysite nanotubes prior to loading with inhibitor (Fig. 18.10) demonstrated that they have an outer diameter of 50 ± 5 nm and an inner lumen diameter of 15–20 nm with a constant thickness throughout the cut sample. The length size of halloysite particles has been reported within 1–15 μm [77]. Scanning electron microscopy (SEM) is another technique used by many researchers [44, 48] for studying the morphology and thickness of polymer-based nanocomposite coatings. SEM can be coupled with energy X-ray dispersion spectroscopy (EDS) for determining the elemental distribution in the heterogeneous coating matrix. Figure 18.11 presents the morphology and elemental analysis of nanoscale CeMO containers prior to loading with inhibitor. The SEM results illustrate that the synthesized CeMO nanoparticles have a spherical shape and the EDS results reveal that they consist of cerium, molybdenum, and oxygen which confirm the formation of CeMO layer on the organic core. The observed carbon peak in the EDS data could be attributed to the organic core. Kartsonakis et al. [85] doped these

Table 18.2 Some recently developed polymer-based intelligent coatings incorporating inhibitor-loaded nanomaterials and their properties and other characteristics

Metal substrate	Coating	Nanomaterial	Active agent	Triggering mechanism	Calculated corrosion inhibition efficiency	Properties other than corrosion resistance and mechanisms of protection in addition to physical barrier and corrosion inhibitor	Ref
Steel	Acrylic resin	Ag/SiO_2 with a core–shell structure	Ag	n.d.	n.d.	This coating is antibacterial and is able to offer long-term protection in marine environment	[73]
Galvanized steel	Epoxy resin	Layered double hydroxides and cerium molybdate	2-Mercaptobenzothiazole	n.d.	n.d.	Cerium molybdate reduced the barrier properties. Early and long-term corrosion inhibition	[82]
Steel	Polyester	Mesoporous silica	Benzotriazole and benzalkonium chloride	pH/sulfide ion	n.d.	Benzalkonium chloride is a biocide, and the coating thus provides an antifouling effect	[75]
Steel	Polyurethane	Polymeric	5-Amino-1-pentanol, diethanolamine and triethanolamine	pH	n.d.	n.d.	[83]
Carbon steel grade ST37	Epoxy/polyaniline	ZnO	Zn^{2+} cation ion	Cl$^-$ and pH (OH$^-$ anion ion)	n.d.	Coating is crack free, uniform, and compact with less water permeability	[84]

(continued)

Table 18.2 (continued)

Metal substrate	Coating	Nanomaterial	Active agent	Triggering mechanism	Calculated corrosion inhibition efficiency	Properties other than corrosion resistance and mechanisms of protection in addition to physical barrier and corrosion inhibitor	Ref
Aluminum grade 2024-T3	Epoxy resin	CeMo	8-HQ	n.d.	n.d.	Water traps and chloride traps were used for more corrosion protection	[85]
Carbon steel	Epoxy resin	Cellulose	Calcium nitrite	Scratch	n.d.	n.d.	[86]
Mild steel	Polypyrrole	Mesoporous silica	Molybdate ion	Cl⁻ and pH	n.d.	n.d.	[79]
Aluminum grade 5083 and galvanneal	Waterborne epoxy	n.d.	2-Mercaptobenzothiazole	pH	n.d.	Nanocapsules do not have any negative effect on the barrier properties of the coatings	[87]
Steel	Epoxy	Polyaniline	Cardanol-based phenalkamine	n.d.	46.8 % for 3 % NM in 12 % NaCl solution after 60 days	Water repellency and adhesion strength were improved	[88]
Mg	Alkyd	Mesoporous silica	NaF	n.d.	70 % for 1 % NM in 2 g dm^{-3} NaCl solution after 1 week immersion	n.d.	[80]
Aluminum grade 2024	Epoxy resin	Surfactant-modified halloysite	Benzotriazole	pH and temperature	n.d.	n.d.	[78]
Aluminum grade 2024-T3	Waterborne epoxy	Poly-electrolyte	2-Methylbenzothiazole and 2-mercaptobenzothiazole	Scratch	n.d.	n.d.	[89]

The values for NM and NaCl solution are in wt%

Fig. 18.10 TEM images of halloysite nanotubes (reprinted with permission from [77], Copyright © 2010 Elsevier Inc.)
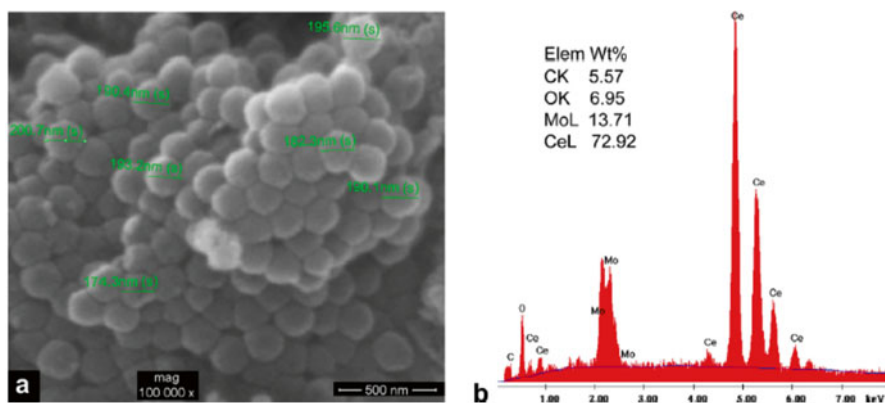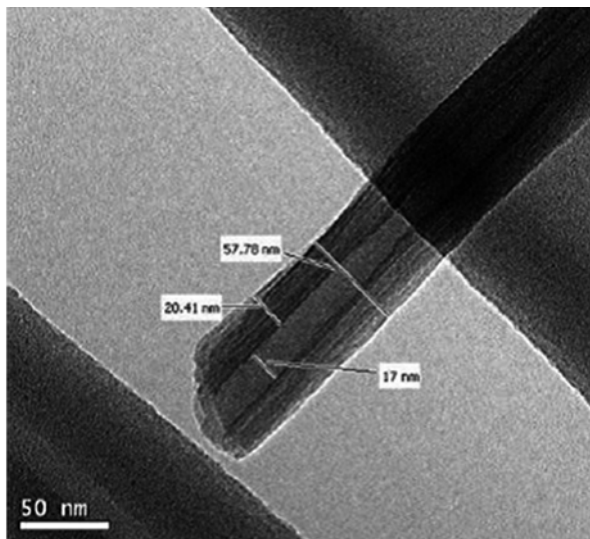
Fig. 18.11 (**a**) SEM image of unloaded CeMO nanocontainers and (**b**) EDS results (reprinted with permission from [85], Copyright © 2014 Elsevier Inc.)

nanocontainers in an epoxy coating, which produced a nanocomposite coating with superior corrosion protection properties.

AFM is another high-tech method which reveals the topography of the ultrathin top surface (or interface), with a vertical resolution of less than 0.1 nm and X–Y resolution of around 1 nm. AFM can be run at atmospheric pressure which is an advantage over TEM and SEM [90]. Dhoke and Khanna [23] employed AFM to study the surface topography of alkyd-based coatings with and without nano-Fe_2O_3 particles, after a salt spray test. Figure 18.12a shows the topographic height image of the neat (non-modified) sample, in which its surface exhibited roughness with
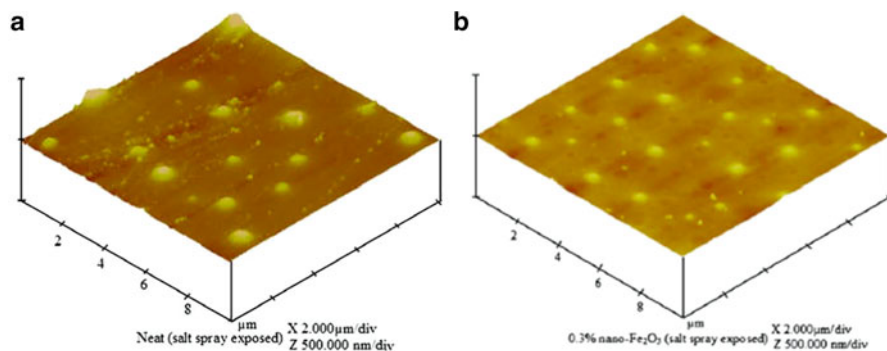
Fig. 18.12 AFM topographic images of alkyd-based waterborne coatings (**a**) without any incorporated particles and (**b**) with 0.3 % nano-Fe$_2$O$_3$ particles after 720 h salt spray test (adapted with permission from [23], Copyright © 2009 Elsevier Inc.)

some distorted microstructures due to coating blistering caused by the salt spray. The coating modified with nano-Fe$_2$O$_3$ (Fig. 18.12b) exhibited a smoother surface texture, corresponding to its improved corrosion resistance.

AFM has also been used for measuring the nano-/micromechanical properties of nanocomposite epoxy coatings, following the nanoindentation method. Shi et al. [6] observed a hysteresis between the loading and unloading curves indicating a plastic deformation of the epoxy coatings upon the indentation. The nearly linear slope of the unloading curves indicated that the tip indentation resulted in very little elastic deformation and thus the loading curve was fitted to obtain the mechanical properties of the coating. The authors assumed that all the coatings had uniform mechanical properties across the entire thickness and the Young's modulus was then obtained by fitting only the initial part of the loading indentation process to the Hertzian model. The epoxy coating modified with 1 wt% nano-SiO$_2$ or nano-Zn showed a substantial increase in their Young's moduli at the submicron scales, whereas the nanoclay- and nano-FeO-modified samples showed, respectively, ~30 % and ~25 % decreases relative to the non-modified epoxy coating.

Advanced tools are also available to help obtain an in-depth insight about what is going on at the interface of nanomaterials and host polymers. For instance, in situ analysis methods such as surface-sensitive helium ion microscopy (He-IM) can shed light on relevant processes and interactions. He-IM has been successfully used by Campo et al. [91] to investigate the interaction of carbon nanotubes (CNTs) and a poly(methyl methacrylate) (PMMA) matrix in an electrospun polymer-based nanocomposite.

Electrochemical techniques can help illustrate the role of coating components in the processes of general protection and local protection [92]. A variety of electrochemical techniques have been employed for studying the polymer-based nanocomposite coatings. Among them, electrochemical impedance spectroscopy (EIS) is the most common method used for studying both physical barrier coatings and intelligent coatings. EIS measurements have been aided by potentiodynamic polarization
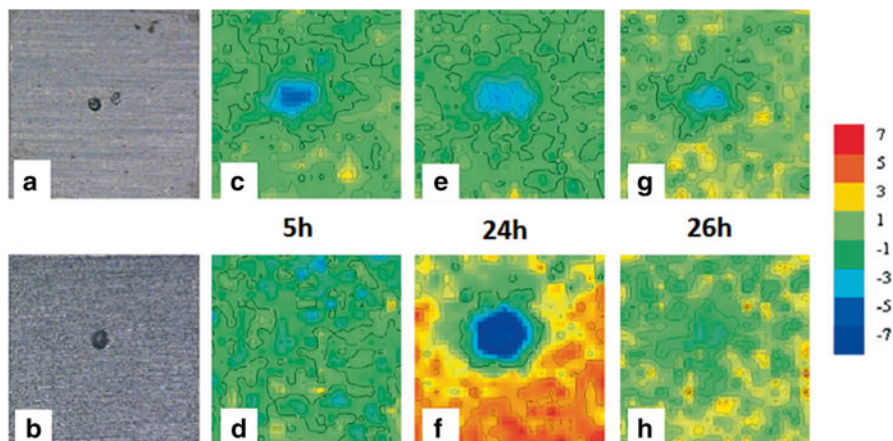
Fig. 18.13 Artificially defected aluminum grade 2024 (**a** and **b**) and SVET maps above the defected area protected by a physical barrier polymer coating (**c**, **e**, and **g**) or a self-healing polymer coating with inhibitor-loaded nanocontainers (**d**, **f**, and **h**). Scale units: µA cm^{-2} and scanned area: 2 mm×2 mm (adapted with permission from [94], Copyright © 2006 John Wiley and Sons Inc.)

curves in investigating the corrosion rates and corrosion mechanisms of metals protected by physical barrier coatings [31, 33, 39] and sometimes by intelligent coatings [86, 93]. In addition, scanning vibrating electrode technique (SVET, Fig. 18.13) and localized EIS are among the emerging spatially resolved electrochemical techniques used to investigate the self-repairing process enabled by controlled release of corrosion inhibitors [9, 83, 87, 95]. These techniques can detect the self-healing mechanisms in the microscale defects in the coating layer [9].

18.7 Conclusion

Nanotechnology has brought fundamental changes to the methods of mitigating corrosion risk at the metal/electrolyte interface. Incorporation of nanomaterials in polymeric coatings can greatly improve their barrier performance by decreasing the porosity and zigzagging the diffusion path for corrosive species such as oxygen and chloride anions. It is cautioned, however, that nanomaterials often serve more than just the role of a nanofiller. Nanomaterials with a wide range of shapes and sizes have been employed for the fabrication of polymer nanocomposites, through a variety of approaches (e.g., in situ polymerization, solution exfoliation, and melt intercalation). The nanocomposite microstructure can be categorized according to the interaction between the polymer matrix and the added nanomaterial (i.e., phase-separated, hybrid-phase, intercalated, and exfoliated composites). The cost-effective use of nanomaterials to enhance the anticorrosion performance of polymeric coatings hinges on their dispersion in the host polymer. Incorporation of

nanomaterials into polymer matrix offers environmentally benign solutions for enhancing the integrity and durability of coating systems. In general, polymer coatings containing a small amount of nanomaterials (typically no more than 4 % by weight of polymer) offer significant barrier properties for corrosion protection and reduce the tendency for the coating to blister or delaminate. Due to their high surface activity, nanomaterials may serve as a template to guide the curing of monomers and oligomers near them and lead to formation of better cured polymeric networks in the interfacial region. The main philosophy behind reserving corrosion inhibitors in nanocontainers instead of directly loading them inside the polymer coating is that the former approach minimizes the risk of early leaching of the inhibitor and delivers the inhibitor when and where it is needed. TEM, SEM, AFM, He-IM, EIS, and SVET are among some of the advanced characterization tools employed to study the microstructure, behavior, and properties of nanocomposite coatings for corrosion protection.

References

1. Gacitua WE, Ballerini AA, Zhang J (2005) Polymer nanocomposites: synthetic and natural fillers a review. Maderas, Ciencia y tecnología 7:159–178
2. Anandhan S, Bandyopadhyay S (2011) Polymer nanocomposites: from synthesis to applications. In: Cuppoletti J (ed) Nanocomposites and polymers with analytical methods. InTech, Rijeka, Croatia, pp 3–26
3. Jancar J, Douglas JF, Starr FW, Kumar SK, Cassagnau P, Lesser AJ, Sternstein SS, Buehler MJ (2010) Current issues in research on structure–property relationships in polymer nanocomposites. Polymer 51:3321–3343
4. Bréchet Y, Cavaillé J-Y, Chabert E, Chazeau L, Dendievel R, Flandin L, Gauthier C (2001) "Polymer Based Nanocomposites: Effect of Filler-Filler and Filler-Matrix Interactions," Adv Eng Mater 3:571–577
5. Fu Q, Tang C, Deng H, Zhang Q (2010) "Polymer Nanotube Nanocomposites," In: Mittal V (ed) Polymer nanotube nanocomposites: synthesis, properties, and applications. Wiley, New York, NY, pp 83–112
6. Shi X, Nguyen TA, Suo Z, Liu Y, Avci R (2009) "Effect of nanoparticles on the anticorrosion and mechanical properties of epoxy coating," Surf Coat Technol 204:237–245
7. Shi X, Xiao Z, Wu J (2013) "The use of nanotechnology to improve the bulk and surface properties of steel for structural applications," In: Pacheco-Torgal F, Diamanti MV, Nazari A, Granqvist C-G (eds) Nanotechnology in eco-efficient construction. Woodhead Publishing, Cambridge, pp 75–107
8. Fang FF, Choi HJ, Joo J (2008) "Conducting polymer/clay nanocomposites and their applications," J Nanosci Nanotechnol 8:1559–1581
9. Montemor MF (2014) "Functional and smart coatings for corrosion protection: A review of recent advances," Surf Coat Technol 258:17–37
10. Klosterman D, Wang CS, Rice B, Lafdi K (2003) Conductive polymer nanocomposites. www.readco.com/files/pdfs/UniversityofDayton.ppt. Accessed 6 Mar 2015
11. Mittal V (2010) "Polymer Nanocomposites: Synthesis, Microstructure, and Properties," In: Mittal V (ed) Optimization of polymer nanocomposite properties. Wiley-VCH Verlag GmbH & Co. KGaA, Weinheim, pp 1–19
12. Alexandre M, Dubois P (2000) "Polymer-layered silicate nanocomposites: preparation, properties and uses of a new class of materials," Mater Sci Eng R Rep 28:1–63

13. Mittal V (2009) "Polymer/layered silicate nanocomposites: a review from preparation to processing," Materials 2:992–1057
14. Xu W-B, Bao S-P, He P-S (2002) "Intercalation and exfoliation behavior of epoxy resin/curing agent/montmorillonite nanocomposite," J Appl Polym Sci 84:42–849
15. Olad A (2011) "Polymer/Clay Nanocomposites," In: Reddy B (ed) Advances in diverse industrial applications of nanocomposites. InTech, Rijeka, Croatia, pp 113–138
16. Brent JR, Savjani N, Lewis EA, Haigh SJ, Lewis DJ, O'Brien P (2014) "Production of few-layer phosphorene by liquid exfoliation of black phosphorus," Chem Commun 50:13338–13341
17. Wetzel B, Haupert F, Qiu Zhang M (2003) "Epoxy nanocomposites with high mechanical and tribological performance," Compos Sci Technol 63:2055–2067
18. Zhang MQ, Rong MZ, Yu SL, Wetzel B, Friedrich K (2002) "Improvement of Tribological Performance of Epoxy by the Addition of Irradiation Grafted Nano-Inorganic Particles," Macromol Mater Eng 287:111–115
19. Yamini S, Young RJ (1977) "Stability of crack propagation in epoxy resins," Polymer 18:1075–1080
20. Zaarei D, Sarabi AA, Sharif F, Kassiriha SM (2008) "Structure, properties and corrosion resistivity of polymeric nanocomposite coatings based on layered silicates," J Coat Technol Res 5:241–249
21. Alam J, Riaz U, Ashraf SM, Ahmad S (2007) "Corrosion-protective performance of nano polyaniline/ferrite dispersed alkyd coatings," J Coat Technol Res 5:123–128
22. Dhoke SK, Khanna AS, Sinha TJM (2009) "Effect of nano-ZnO particles on the corrosion behavior of alkyd-based waterborne coatings," Prog Org Coat 64:371–382
23. Dhoke SK, Khanna AS (2009) "Effect of nano-Fe_2O_3 particles on the corrosion behavior of alkyd based waterborne coatings," Corros Sci 51:6–20
24. Olad A, Naseri B (2010) "Preparation, characterization and anticorrosive properties of a novel polyaniline/clinoptilolite nanocomposite," Prog Org Coat 67:233–238
25. Heidarian M, Shishesaz MR, Kassiriha SM, Nematollahi M (2010) "Characterization of structure and corrosion resistivity of polyurethane/organoclay nanocomposite coatings prepared through an ultrasonication assisted process," Prog Org Coat 68:180–188
26. Ramezanzadeh B, Attar MM (2011) "Studying the effects of micro and nano sized ZnO particles on the corrosion resistance and deterioration behavior of an epoxy-polyamide coating on hot-dip galvanized steel," Prog Org Coat 71:314–328
27. Jadhav RS, Patil KJ, Hundiwale DG, Mahulikar PP (2011) "Synthesis of waterborne nanopolyanilne latexes and application of nanopolyaniline particles in epoxy paint formulation for smart corrosion resistivity of carbon steel," Polym Adv Technol 22:1620–1627
28. Madhankumar A, Nagarajan S, Rajendran N, Nishimura T (2011) "EIS evaluation of protective performance and surface characterization of epoxy coating with aluminum nanoparticles after wet and dry corrosion test," J Solid State Electrochem 16:2085–2093
29. Madhankumar A, Rajendran N, Nishimura T (2012) "Influence of Si nanoparticles on the electrochemical behavior of organic coatings on carbon steel in chloride environment," J Coat Technol Res 9:609–620
30. Mills DJ, Jamali SS, Paprocka K (2012) "Investigation into the effect of nano-silica on the protective properties of polyurethane coatings," Surf Coat Technol 209:137–142
31. Toloei A, Atashin S, Bahrololoom ME (2013) "A New Approach in Modifying Polymeric Coatings to Increase Corrosion Resistance Properties," Int Sch Res Not 2013, e648246
32. Moazeni N, Mohamad Z, Faisal NLI, Tehrani MA, Dehbari N (2013) "Anticorrosion epoxy coating enriched with hybrid nanozinc dust and halloysite nanotubes," J Appl Polym Sci 130:955–960
33. Singh-Beemat J, Iroh JO, Feng L (2013) "Mechanism of corrosion protection of aluminum alloy substrate by hybrid polymer nanocomposite coatings," Prog Org Coat 76:1576–1580
34. Zomorodian A, Garcia MP, Moura e Silva T, Fernandes JCS, Fernandes MH, Montemor MF (2013) "Corrosion resistance of a composite polymeric coating applied on biodegradable AZ31 magnesium alloy," Acta Biomater 9:8660–8670

35. Yu Y-H, Lin Y-Y, Lin C-H, Chan C-C, Huang Y-C (2013) "High-performance polystyrene/graphene-based nanocomposites with excellent anti-corrosion properties," Polym Chem 5:535–550

36. Tomić MD, Dunjić B, Likić V, Bajat J, Rogan J, Djonlagić J (2014) "The use of nanoclay in preparation of epoxy anticorrosive coatings," Prog Org Coat 77:518–527

37. Wang N, Wu YH, Cheng KQ, Zhang J (2014) "Investigation on anticorrosion performance of polyaniline-mesoporous MCM-41 composites in new water-based epoxy coating," Mater Corros 65:968–976

38. Deyab MA (2014) "Corrosion protection of aluminum bipolar plates with polyaniline coating containing carbon nanotubes in acidic medium inside the polymer electrolyte membrane fuel cell," J Power Sources 268:50–55

39. Madhan Kumar A, Gasem ZM (2015) "In situ electrochemical synthesis of polyaniline/f-MWCNT nanocomposite coatings on mild steel for corrosion protection in 3.5 % NaCl solution," Prog Org Coat 78:387–394

40. Pour-Ali S, Dehghanian C, Kosari A (2015) "Corrosion protection of the reinforcing steels in chloride-laden concrete environment through epoxy/polyaniline–camphorsulfonate nanocomposite coating," Corros Sci 90:239–247

41. Ganjaee Sari M, Ramezanzadeh B, Shahbazi M, Pakdel AS (2015) "Influence of nanoclay particles modification by polyester-amide hyperbranched polymer on the corrosion protective performance of the epoxy nanocomposite," Corros Sci 92:162–172

42. Haddadi SA, Mahdavian M, Karimi E (2015) "Evaluation of the corrosion protection properties of an epoxy coating containing sol–gel surface modified nano-zirconia on mild steel," RSC Adv 5:28769–28777

43. Ates M, Topkaya E (2015) "Review study of electrochemical impedance spectroscopy and equivalent electrical circuits of conducting polymers on carbon surfaces," Prog Org Coat 82:33–40

44. Lam CK, Lau KT (2006) "Localized elastic modulus distribution of nanoclay/epoxy composites by using nanoindentation," Compos Struct 75:553–558

45. Hartwig A, Sebald M, Pütz D, Aberle L (2005) "Preparation, Characterisation and Properties of Nanocomposites Based on Epoxy Resins – An Overview," Macromol Symp 221:127–136

46. Shi G, Zhang MQ, Rong MZ, Wetzel B, Friedrich K (2003) "Friction and wear of low nanometer Si_3N_4 filled epoxy composites," Wear 254:784–796

47. Chaudhary S, Parthasarathy S, Kumar D, Rajagopal C, Roy P (2014) "Simple toughening of epoxy thermosets by preformed thermoplastics," SPE plastic research online. doi:10.2417/spepro.005409. Available: www.4spe.org (Last Accessed: May 2015)

48. Dietsche F, Thomann Y, Thomann R, Mülhaupt R (2000) "Translucent acrylic nanocomposites containing anisotropic laminated nanoparticles derived from intercalated layered silicates," J Appl Polym Sci 75:396–405

49. Becker O, Varley R, Simon G (2002) "Morphology, thermal relaxations and mechanical properties of layered silicate nanocomposites based upon high-functionality epoxy resins," Polymer 43:4365–4373

50. Crosky A, Kelly D, Li R, Legrand X, Huong N, Ujjin R (2006) "Improvement of bearing strength of laminated composites," Compos Struct 76:260–271

51. Ramanathan T, Abdala AA, Stankovich S, Dikin DA, Herrera-Alonso M, Piner RD, Adamson DH, Schniepp HC, Chen X, Ruoff RS, Nguyen ST, Aksay IA, Prud'Homme RK, Brinson LC (2008) "Functionalized graphene sheets for polymer nanocomposites," Nat Nanotechnol 3:327–331

52. Ramanathan T, Liu H, Brinson LC (2005) "Functionalized SWNT/polymer nanocomposites for dramatic property improvement," J Polym Sci B Polym Phys 43:2269–2279

53. Rao Y, Pochan JM (2007) "Mechanics of Polymer−Clay Nanocomposites," Macromolecules 40:290–296

54. Dennis RV, Patil V, Andrews JL, Aldinger JP, Yadav GD, Banerjee S (2015) "Hybrid nano-structured coatings for corrosion protection of base metals: a sustainability perspective," Mater Res Express 2:032001

55. Schwenke K, Isa L, Cheung DL, Del Gado E (2014) "Conformations and Effective Interactions of Polymer-Coated Nanoparticles at Liquid Interfaces," Langmuir 30:12578–12586

56. Roldughin VI, Serenko OA, Getmanova EV, Novozhilova NA, Nikifirova GG, Buzin MI, Chvalun SN, Ozerin AN, Muzafarov AM (2015) "Effect of hybrid nanoparticles on glass transition temperature of polymer nanocomposites," Polym Compos. doi:10.1002/pc.23376

57. Santos L, Montiel A, Alvarado M (2008) Reactive block copolymers as additives for the preparation of silicate-polymer composites. US20080033092 A1

58. Zeng QH, Yu AB, Lu GQ, Paul DR (2005) "Clay-based polymer nanocomposites: research and commercial development," J Nanosci Nanotechnol 5:1574–1592

59. Lim SK, Kim JW, Chin I, Kwon YK, Choi HJ (2002) "Preparation and Interaction Characteristics of Organically Modified Montmorillonite Nanocomposite with Miscible Polymer Blend of Poly(Ethylene Oxide) and Poly(Methyl Methacrylate)," Chem Mater 14:1989–1994

60. Weng C-J, Chang C-H, Yeh J-M (2012) "Polymer nanocomposites in corrosion control," In: Saji VS, Cook R (eds) Corrosion protection and control using nanomaterials. Woodhead Publishing, Cambridge, pp 330–356

61. Kornmann X, Lindberg H, Berglund LA (2001) "Synthesis of epoxy–clay nanocomposites. Influence of the nature of the curing agent on structure," Polymer 42:4493–4499

62. Rao JP, Geckeler KE (2011) "Polymer nanoparticles: Preparation techniques and size-control parameters," Prog Polym Sci 36:887–913

63. Vivekchand SRC, Govindaraj A, Rao CNR (2007) "Nanotubes and Nanowires: Recent Developments," In: Rao CNR, Müller A, Cheetham AK (eds) Nanomaterials chemistry. Wiley-VCH Verlag GmbH & Co. KGaA, Weinheim, pp 45–118

64. Arrakhiz FZ, Elachaby M, Bouhfid R, Vaudreuil S, Essassi M, Qaiss A (2012) "Mechanical and thermal properties of polypropylene reinforced with Alfa fiber under different chemical treatment," Mater Des 35:318–322

65. Xin X, Xu G, Li H (2013) "Dispersion and Property Manipulation of Carbon Nanotubes by Self-Assembles of Amphiphilic Molecules," In: Suzuki S (ed) Physical and chemical properties of carbon nanotubes. InTech, Rijeka, Croatia

66. Samadzadeh M, Boura SH, Peikari M, Kasiriha SM, Ashrafi A (2010) "A review on self-healing coatings based on micro/nanocapsules," Prog Org Coat 68:159–164

67. Wei H, Wang Y, Guo J, Shen NZ, Jiang D, Zhang X, Yan X, Zhu J, Wang Q, Shao L, Lin H, Wei S, Guo Z (2014) "Advanced micro/nanocapsules for self-healing smart anticorrosion coatings," J Mater Chem A 3:469–480

68. Shi X (2010) "On the Use of Nanotechnology to Manage Steel Corrosion," Recent Pat Eng 4:44–50

69. Zheludkevich ML, Shchukin DG, Yasakau KA, Möhwald H, Ferreira MGS (2007) "Anticorrosion Coatings with Self-Healing Effect Based on Nanocontainers Impregnated with Corrosion Inhibitor," Chem Mater 19:402–411

70. Snihirova D, Lamaka SV, Montemor MF (2012) "SMART" protective ability of water based epoxy coatings loaded with $CaCO_3$ microbeads impregnated with corrosion inhibitors applied on AA2024 substrates," Electrochim Acta 83:439–447

71. Borisova D, Möhwald H, Shchukin DG (2013) "Influence of Embedded Nanocontainers on the Efficiency of Active Anticorrosive Coatings for Aluminum Alloys Part II: Influence of Nanocontainer Position," ACS Appl Mater Interfaces 5:80–87

72. Stankiewicz A, Szczygieł I, Szczygieł B (2013) "Self-healing coatings in anti-corrosion applications," J Mater Sci 48:8041–8051

73. Le Y, Hou P, Wang J, Chen J-F (2010) "Controlled release active antimicrobial corrosion coatings with Ag/SiO_2 core–shell nanoparticles," Mater Chem Phys 120:351–355

74. Abdullayev E, Price R, Shchukin D, Lvov Y (2009) "Halloysite Tubes as Nanocontainers for Anticorrosion Coating with Benzotriazole," ACS Appl Mater Interfaces 1:1437–1443

75. Zheng Z, Huang X, Schenderlein M, Borisova D, Cao R, Möhwald H, Shchukin D (2013) "Self-Healing and Antifouling Multifunctional Coatings Based on pH and Sulfide Ion Sensitive Nanocontainers," Adv Funct Mater 23:3307–3314

76. Shchukin DG, Lamaka SV, Yasakau KA, Zheludkevich ML, Ferreira MGS, Möhwald H (2008) "Active Anticorrosion Coatings with Halloysite Nanocontainers," J Phys Chem C 112:958–964

77. Jafari AH, Hosseini SMA, Jamalizadeh E (2010) "Investigation of Smart Nanocapsules Containing Inhibitors for Corrosion Protection of Copper," Electrochim Acta 55:9004–9009

78. Khajouei A, Jamalizadeh E, Hosseini SMA (2015) "Corrosion protection of coatings doped with inhibitor-loaded nanocapsules," Anti-Corros Methods Mater 62:88–94

79. Yeganeh M, Saremi M, Rezaeyan H (2014) "Corrosion inhibition of steel using mesoporous silica nanocontainers incorporated in the polypyrrole," Prog Org Coat 77:1428–1435

80. Yeganeh M, Saremi M (2015) "Corrosion inhibition of magnesium using biocompatible Alkyd coatings incorporated by mesoporous silica nanocontainers," Prog Org Coat 79:25–30

81. Zheludkevich ML, Tedim J, Ferreira MGS (2012) "Smart" coatings for active corrosion protection based on multi-functional micro and nanocontainers," Electrochim Acta 82:314–323

82. Montemor MF, Snihirova DV, Taryba MG, Lamaka SV, Kartsonakis IA, Balaskas AC, Kordas GC, Tedim J, Kuznetsova A, Zheludkevich ML, Ferreira MGS (2012) "Evaluation of self-healing ability in protective coatings modified with combinations of layered double hydroxides and cerium molibdate nanocontainers filled with corrosion inhibitors," Electrochim Acta 60:31–40

83. Choi H, Kim KY, Park JM (2013) "Encapsulation of aliphatic amines into nanoparticles for self-healing corrosion protection of steel sheets," Prog Org Coat 76:1316–1324

84. Mostafaei A, Nasirpouri F (2014) "Epoxy/polyaniline–ZnO nanorods hybrid nanocomposite coatings: Synthesis, characterization and corrosion protection performance of conducting paints," Prog Org Coat 77:146–159

85. Kartsonakis IA, Athanasopoulou E, Snihirova D, Martins B, Koklioti MA, Montemor MF, Kordas G, Charitidis CA (2014) "Multifunctional epoxy coatings combining a mixture of traps and inhibitor loaded nanocontainers for corrosion protection of AA2024-T3," Corros Sci 85:147–159

86. Yabuki A, Kawashima A, Fathona IW (2014) "Self-healing polymer coatings with cellulose nanofibers served as pathways for the release of a corrosion inhibitor," Corros Sci 85:141–146

87. Plawecka M, Snihirova D, Martins B, Szczepanowicz K, Warszynski P, Montemor MF (2014) "Self healing ability of inhibitor-containing nanocapsules loaded in epoxy coatings applied on aluminium 5083 and galvanneal substrates," Electrochim Acta 140:282–293

88. Chu D, Wang J, Han Y, Ma Q, Wang Z (2015) "High performance epoxy protective coatings incorporated with polyaniline nanowires using cardanol-based phenalkamine as the curing agent," RSC Adv 5:11378–11384

89. Kopeć M, Szczepanowicz K, Mordarski G, Podgórna K, Socha RP, Nowak P, Warszyński P, Hack T (2015) "Self-healing epoxy coatings loaded with inhibitor-containing polyelectrolyte nanocapsules," Prog Org Coat 84:97–106

90. Dhawan A, Sharma V (2010) "Toxicity assessment of nanomaterials: methods and challenges," Anal Bioanal Chem 398:589–605

91. Campo EM, Larios E, Huynh C, Ananth M (2015) "Helium ion microscopy of electrospun CNT–polymer composites," J Mater Res 30:130–140

92. Fayyad EM, Almaadeed MA, Jones A, Abdullah AM (2014) "Evaluation Techniques for the Corrosion Resistance of Self-Healing Coatings," Int J Electrochem Sci 9:4989–5011

93. Hamdy AS, Doench I, Möhwald H (2011) "Smart self-healing anti-corrosion vanadia coating for magnesium alloys," Prog Org Coat 72:387–393

94. Shchukin DG, Zheludkevich M, Yasakau K, Lamaka S, Ferreira MGS, Möhwald H (2006) "Layer-by-Layer Assembled Nanocontainers for Self-Healing Corrosion Protection," Adv Mater 18:1672–1678

95. Snihirova D, Liphardt L, Grundmeier G, Montemor F (2013) "Electrochemical study of the corrosion inhibition ability of "smart" coatings applied on AA2024," J Solid State Electrochem 17:2183–2192

Chapter 19
Amphiphilic Invertible Polymers and Their Applications

Ananiy Kohut, Ivan Hevus, Stanislav Voronov, and Andriy Voronov

Abstract Amphiphilic invertible polymers (AIPs) are novel smart macromolecules. Synthesized from short lipophilic and hydrophilic constituents that are alternately or randomly distributed along the polymer backbone, the AIP macromolecules possess an enhanced flexibility and rapidly respond to changes in an environmental polarity by changing their macromolecular conformation. By increasing a solution concentration, the AIP macromolecules self-organize into micellar assemblies that can change their physicochemical properties in response to changes in a medium polarity. The micellar assemblies from AIPs can be applied for the development of smart nanoreactors for the synthesis of metal and semiconductor nanoparticles of a controlled shape and size, as well as for the growth of fibrillar carbon nanostructures and the formation of smart nanocontainers for drug delivery. Synthetic routes to (1) amphiphilic invertible polyurethanes based on poly(ethylene glycol), polytetrahydrofuran, and 2,4-tolylene diisocyanate and (2) amphiphilic invertible polyesters based on poly(ethylene glycol) and aliphatic dicarboxylic acids were elaborated, and the corresponding polymers were successfully synthesized. The effect of reaction conditions on the reaction course and the macromolecular configuration of the resulting polymers were revealed. It was demonstrated that the chemical nature and structure of the macromolecules of the amphiphilic invertible polyurethanes and polyesters determine the self-assembly of the AIP macromolecules, both in an aqueous and organic media, resulting in a formation of micellar assemblies, which can serve as nanoreactors, nanocontainers, and nanocarriers.

Keywords Amphiphilic polymers • Invertibility • Self-assembly • Nanoreactors • Nanoparticles

A. Kohut • S. Voronov
Department of Organic Chemistry, Lviv Polytechnic National University,
vul. S. Bandery, 12, Lviv 79013, Ukraine
e-mail: ananiy.kohut@gmail.com; stanislav.voronov@gmail.com

I. Hevus • A. Voronov (✉)
Department of Coatings and Polymeric Materials, North Dakota State University,
NDSU Dept. 2760, 6050, Fargo, ND 58108-6050, USA
e-mail: ivan.hevus@ndsu.edu; andriy.voronov@ndsu.edu

19.1 Introduction

Advances in the field of contemporary nanotechnologies require the development of fundamental science: chemistry, physics, biochemistry, and, in particular, polymer chemistry. Recently, numerous studies on the preparation of polymeric materials with novel properties for applications in medicine, biology, catalysis, electronics, and optics have been carried out. The synthesis of new polymers for developing polymeric nanoreactors, which aid in conducting chemical reactions, and the preparation of metal and semiconductor nanoparticles are of growing interest [1]. In addition, such synthesis can allow for designing nanocontainers and developing new polymer-based systems that deliver lipophilic drugs to pathologic cells and, simultaneously, protecting the drug from side reactions and effects [2]. In this regard, much attention is paid to polymers, the macromolecules of which are capable of self-organizing and forming self-assembled structures that change their physicochemical properties in response to changes in the environmental parameters [3]. Such polymers are considered smart materials.

Among numerous studies on smart polymers (e.g., sensitive to changes in temperature, moisture, pH, light, electric and magnetic field), only a small number of publications report on the polymers capable of responding to changes in a medium polarity [4, 5]. Nevertheless, such polymers can be considered as prospective candidates in different applications as nanoreactors and nanocontainers [5]. In this regard, the synthesis of new amphiphilic invertible polymers, the macromolecules, which contain short lipophilic and hydrophilic fragments in the backbone, linked by oxygen atoms, can be of great interest. The presence of oxygen atoms in the polymer backbone is known to significantly enhance the macromolecular flexibility. Varying the fragments' chemical structure enables an efficient control over the self-assembly of the macromolecules in the solution and the formation of hierarchical micellar assemblies with a well-defined structure. It was assumed that such polymers with either an alternating or a random distribution of different fragments in the macromolecules would undergo phase separation in selective solvents and would self-assemble into the micellar assemblies. Besides, due to the low molecular weight of the macromolecular lipophilic and hydrophilic fragments, they will be capable of rapidly responding to changes in medium polarity by changing the conformation of the macromolecular backbone and, hence, exhibiting invertible properties.

Over the last few decades, metal nanoparticles have attracted broad attention from researchers worldwide because of their increasing applications in various fields of science and industry. However, a strong need for elaborating new methods for the controlled synthesis of nanoparticles is still an ongoing challenge for many of these researchers. Developing nanoreactors from the new AIPs can be expected to become a promising approach to the synthesis of metal nanoparticles of controlled size, shape, and structure, which could broaden their potential applications.

Amphiphilic invertible polymers with PEG fragments in their macromolecular backbone have been shown to be able to reduce metal ions and produce high-purity metal nanoparticles. These particles can be easily dispersed in both polar and

nonpolar solvents and form stable colloidal solutions due to the invertibility of the macromolecules, which act as steric stabilizers for nanoparticles. The AIPs can also be applied for the development of nanocontainers in order to solubilize poorly water-soluble drugs, control the interaction with cell membranes, and deliver the drugs into pathologic cells. The presence of short hydrophilic and lipophilic constituents in the backbone enables the chain flexibility to rapidly respond to changes in a medium polarity by changing macromolecular conformation. To this end, AIPs can be considered prospective candidates for the development of smart nanocarriers capable of penetrating through cell membranes. Upon the interaction with cytoplasmic membranes, the AIP macromolecules can change their conformation and, thus, facilitate the delivery of the drug into the cells' membranes.

Hybrid sorbents formed from silica nanoparticles and the AIPs are able to adsolubilize hydrophobic substances in an adsorbed polymer layer. The hybrid sorbents could have potential applications in the development of various industrial products such as pharmaceuticals, cosmetics, and health-care products, the preparation of polymer thin films, and wastewater treatment in order to remove different organic pollutants.

19.2 Synthesis and Properties of Amphiphilic Invertible Polymers

Amphiphilic invertible polymers are new smart polymers. The AIPs invertibility is considered to be a fast conformational change of the macromolecules in response to change in the solvents' nature.

19.2.1 Synthesis of Amphiphilic Invertible Polyurethanes

Amphiphilic invertible polyurethanes (AIPUs) with a random distribution of hydrophilic poly(ethylene glycol) and lipophilic polytetrahydrofuran fragments were synthesized by the reaction of 2,4-tolylene diisocyanate (2,4-TDI) with a mixture of PEG (mol. weight 600 or 1000, PEG_{600} and PEG_{1000}) and PTHF (mol. weight 650 or 1000, $PTHF_{650}$ and $PTHF_{1000}$) as shown in Fig. 19.1. The molar ratio of the reactants was 2:1:1, respectively [6].

By varying the length of hydrophilic PEG and lipophilic PTHF chains, four different random AIPUs were synthesized (Table 19.1). Hydrophilic–lipophilic balance calculated via the Griffin method varied from 7 to 11.

The structure of the synthesized random AIPUs was confirmed by FTIR and ^{1}H NMR spectroscopy [6].

AIPUs with an alternating distribution of hydrophilic PEG and lipophilic PTHF fragments were synthesized using a two-step procedure (Fig. 19.2) [6].
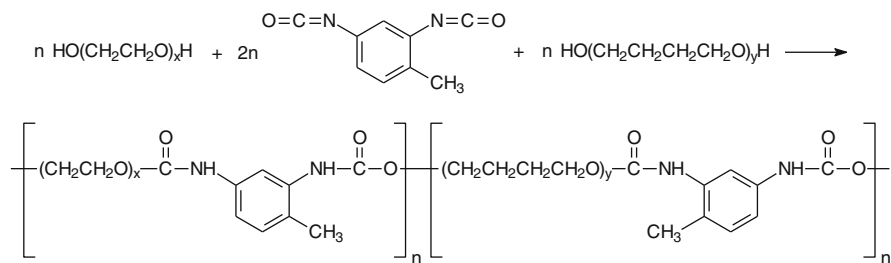
Fig. 19.1 Reaction of the synthesis of random AIPUs

Table 19.1 Characteristics of random AIPUs

#	Polymer	x	y	$M_w \cdot 10^{-3}$	$M_n \cdot 10^{-3}$	PDI	DP	HLB
1	PEG$_{1000}$-co-PTHF$_{650}$	22.3	8.8	14.9	11.9	1.26	29.8	10.9
2	PEG$_{1000}$-co-PTHF$_{1000}$	22.3	13.6	15.0	11.2	1.35	25.6	9.2
3	PEG$_{600}$-co-PTHF$_{650}$	13.2	8.8	15.3	11.7	1.30	38.3	8.6
4	PEG$_{600}$-co-PTHF$_{1000}$	13.2	13.6	15.8	10.0	1.58	32.4	7.0

DP polymerization degree
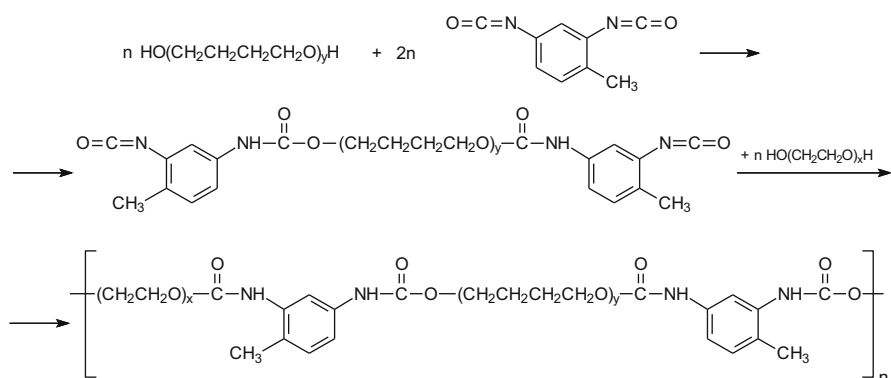
Fig. 19.2 Reaction of the synthesis of alternating AIPUs

To synthesize the prepolymer needed to create AIPUs, the reaction between PTHF$_{650}$ or PTHF$_{1000}$ and 2,4-TDI in molar excess (two times) is required to yield PTHF that is isocyanate terminated. Preferably, the isocyanate group in position 4 reacted with PTHF's OH functionality due to its higher reactivity in comparison with that of the isocyanate group in position 2. This is followed by a reaction with the prepolymer and an equimolar amount of hydroxy-terminated PEG$_{600}$ or PEG$_{1000}$ that yields polyurethanes with alternating hydrophilic and hydrophobic fragments. By implementing this strategy, four alternating AIPUs (Table 19.2) that vary in length of hydrophilic and lipophilic fragment, along with their HLB values, were created.

Table 19.2 Characteristics of alternating AIPUs

#	Polymer	x	y	$M_w \cdot 10^{-3}$	$M_n \cdot 10^{-3}$	PDI	DP	HLB
1	PEG$_{1000}$-*alt*-PTHF$_{650}$	22.3	8.8	18.2	13.2	1.37	36.4	10.9
2	PEG$_{1000}$-*alt*-PTHF$_{1000}$	22.3	13.6	17.5	13.0	1.35	29.8	9.2
3	PEG$_{600}$-*alt*-PTHF$_{650}$	13.2	8.8	16.3	11.4	1.42	40.8	8.6
4	PEG$_{600}$-*alt*-PTHF$_{1000}$	13.2	13.6	15.1	10.3	1.46	31.0	7.0

DP polymerization degree

$$n \; HO(CH_2CH_2O)_xH \; + \; n \; \overset{O}{\underset{HO}{C}}-(CH_2)_y-\overset{O}{\underset{OH}{C}} \quad \xrightarrow[\; - (2n - 1)\, H_2O \;]{H^+} \quad HO\left[(CH_2CH_2O)_x-\overset{O}{C}-(CH_2)_y-\overset{O}{C}-O\right]_n H$$
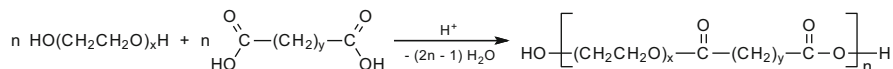
Fig. 19.3 Reaction for the synthesis of AIPEs

Table 19.3 Characteristics of alternating AIPEs

#	Polymer	x	y	$M_w \cdot 10^{-3}$	$M_n \cdot 10^{-3}$	PDI	DP	HLB
1	PEG$_{300}$S	6.4	8	9.5	6.7	1.42	28.8	10.1
2	PEG$_{300}$D	6.4	10	7.9	5.5	1.44	22.3	9.2
3	PEG$_{600}$S	13.2	8	9.3	6.4	1.45	16.7	12.4
4	PEG$_{600}$D	13.2	10	32.0	17.7	1.81	44.6	11.4
5	PEG$_{1000}$S	22.3	8	11.7	6.0	1.95	10.3	15.4
6	PEG$_{1000}$D	22.3	10	7.6	5.0	1.53	8.4	14.4

DP polymerization degree

19.2.2   Synthesis of Amphiphilic Invertible Polyesters

Amphiphilic invertible polyesters (AIPEs) were synthesized via the polycondensation of PEG$_{300}$, PEG$_{600}$, or PEG$_{1000}$ with aliphatic dicarboxylic acids, decanedioic (sebacic) and dodecanedioic (Fig. 19.3).

Six different AIPEs (Table 19.3) with alternately distributed lipophilic and hydrophilic fragments along the macromolecular backbone were synthesized. The HLB values of the polyesters, calculated via the Davies method, varied from 9.2 to 15.4.

Thus, synthetic routes to (1) amphiphilic invertible polyurethanes based on polyethylene glycol, polytetrahydrofuran, and 2,4-tolylene diisocyanate and (2) amphiphilic invertible polyesters based on polyethylene glycol and aliphatic dicarboxylic acids were elaborated, and the corresponding polymers were successfully synthesized. The effect of reaction conditions on the reaction course and the macromolecular configuration of the resulting polymers were revealed [6].

It was demonstrated that by changing the AIP macromolecular structure and physicochemical properties, the micellar assemblies of different morphologies can be prepared, from monomolecular micelles to polymolecular associates, depending on the polymer concentration in the solution [7].
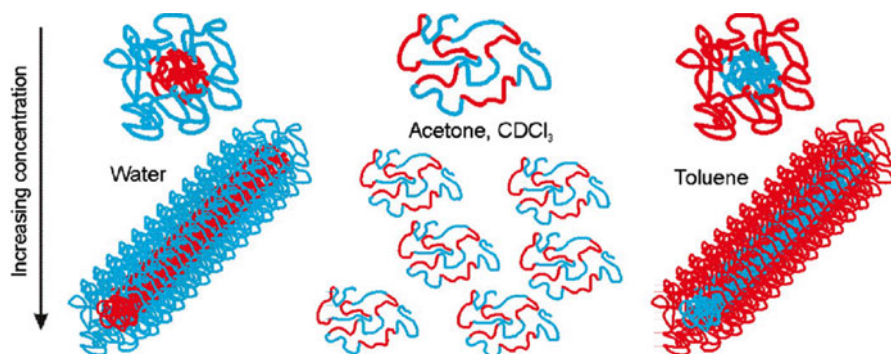
Fig. 19.4 Formation of micelles and hierarchical micellar assemblies (nanoreactors) depending on a medium polarity and AIP concentration (with permission from A. Kohut, A. Voronov, Langmuir 2009, 25 4356–4360)

In a nonpolar organic solvent, the AIP macromolecules form micellar structures with a hydrophilic interior and a lipophilic exterior (Fig. 19.4), which could serve as nanoreactors for conducting chemical reactions in the interior and for the synthesis of metal and semiconductor nanoparticles. In an aqueous environment, micellar structures with a lipophilic interior and a hydrophilic exterior are formed (Fig. 19.4). These assemblies can be applied as nanocontainers of lipophilic substances in water. The formation of the micellar structures both in aqueous and organic media was confirmed using small-angle neutron scattering, ^{1}H NMR spectroscopy, and the solubilization of a fluorescent probe of pyrene and solvatochromic dyes [7]. The study on the formation of micellar structures from the amphiphilic invertible polymers, their colloidal properties, and solubilization ability allowed for the development of micellar nanoreactors and the synthesis of metal (Ag, Au, Pd), semiconductor (CdSe, Si) nanoparticles, as well as polymer–metal complexes as catalysts for the growth of carbon nanostructures.

19.3 Amphiphilic Invertible Polymers as Nanoreactors for the Synthesis of Metal (Ag, Au, Pd) and Semiconductor (CdSe, Si) Nanoparticles

Metal and semiconductor nanoparticles have attracted significant attention from researchers worldwide because of their unique chemical and physical, in particular, optical, electrical, magnetic, and thermal, properties [1, 8] and their broad variety of applications in contemporary nanotechnologies [9, 10].

19.3.1 Synthesis of Metal Nanoparticles

Micellar assemblies formed by the AIP macromolecules in nonpolar organic solvents have a lipophilic exterior comprised of PTHF chains (AIPU), or aliphatic dicarboxylic acid moieties (AIPE), and a hydrophilic interior built from PEG chains [6]. Such assemblies can be used as nanoreactors for conducting chemical reactions in their interior and for the synthesis of various metal nanomaterials and semiconductor nanoparticles as depicted in Fig. 19.5.

Silver nanoparticles were synthesized in polymeric nanoreactors by adding a [Ag (NH$_3$)$_2$] OH precursor to a concentrated AIPU solution in benzene (at polymer concentration 20 and 30 % w/w) where micellar structures were formed (Fig. 19.5). The precursor was solubilized within the micellar structures, localized in the hydrophilic PEG domains, and Ag$^+$ was reduced to Ag^0. Silver nanoparticles were formed in the polymeric nanoreactors prepared from the AIPE, based on PEG$_{1000}$, as well as PEG$_{600}$-co-PTHF$_{650}$. By increasing the length of PEG's hydrophilic constituents while maintaining a steady precursor/polymer concentration, this aided in the creation of nanoparticles while simultaneously reducing the [Ag (NH$_3$)$_2$] OH precursor. Cavities or pseudo-crown ether structures are formed by the PEG chains, and because they are able to bind metal ions, they can then be reduced to metal nanoparticles. PEG$_{1000}$-based AIPUs of high efficiency are thought to be produced due to longer PEG fragments imparting a greater loading capacity and metal ion-reducing activity [11].

A pseudo-crown ether cavity's methylene group (PEG chain in the AIP macromolecule) interacting with Ag$^+$ will cause proton separation, Ag$^+$ reduction, and poly(ethylene oxide) (PEO) macroradical's production [12]. The formation of PEO is via the one-electron reduction mechanism. The reaction is detailed in the following steps: Ag$^+$ interacts with mobile H from the PEG chains, yielding macroradicals; protons are generated; and Ag$^+$ is reduced to Ag^0 [12].

At first, the Ag$^+$ (oxidation agent) interacts with a mobile H of the PEG fragment (reducing agent) while in the company of "bare" anions, OH$^-$. Thus, Ag^0, PEG macroradicals, and H$_2$O are created:

$$\left(CH_2-CH_2-O\right)_n + Ag^+ + OH^- \longrightarrow \left(CH_2-\overset{\bullet}{C}H-O\right)_n + Ag^0 + H_2O$$
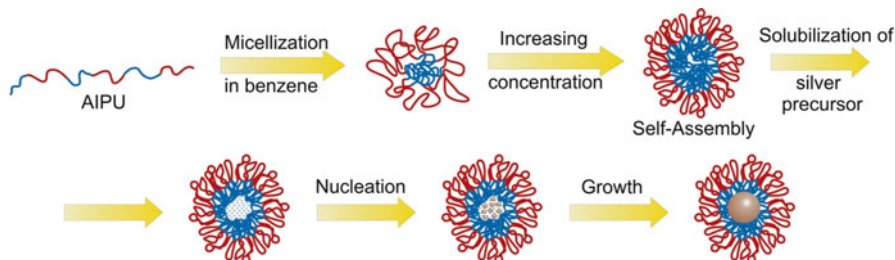
Fig. 19.5 Development of silver nanoparticles in polyurethane micellar structures formed by the AIPU macromolecules in benzene (with permission from [11])

This is followed by Ag^+ receiving an electron via the PEG macroradical, thus reducing to Ag^0. As such, the macroradical is transformed into a carbocation. The anion OH^- interacts with the newly formed carbocation and forms PEO fragments that contain hydroxyl moieties.

$$\left(\!\!-CH_2\!\!-\overset{\bullet}{C}H\!\!-O\!-\!\right)_n \; + \; Ag^+ \; + \; OH^- \longrightarrow \; \left(\!\!-CH_2\!\!-\overset{\overset{\displaystyle OH}{|}}{C}H\!\!-O\!-\!\right)_n \; + \; Ag^0$$
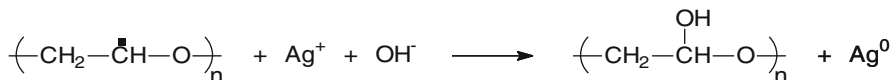
The subsequent interaction is between the Ag^+ and the mobile H of the PEG fragments' polarized carbon. The electron combines with the Ag^+, yielding Ag^0 and a new macroradical.

$$\left(\!\!-CH_2\!\!-\overset{\overset{\displaystyle OH}{|}}{C}H\!\!-O\!-\!\right)_n \; + \; Ag^+ \; + \; OH^- \longrightarrow \; \left(\!\!-CH_2\!\!-\overset{\overset{\displaystyle OH}{|}}{\overset{\bullet}{C}}\!\!-O\!-\!\right)_n \; + \; Ag^0 \; + \; H_2O$$
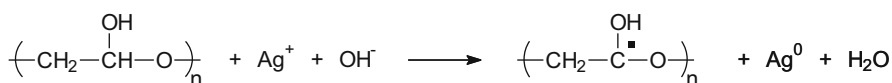
Finally, the macroradical's hydroxyl moiety generates H^+. Two electrons from the oxygen then create a double bond (carbonyl compound) and Ag^0.

$$\left(\!\!-CH_2\!\!-\overset{\overset{\displaystyle OH}{|}}{\overset{\bullet}{C}}\!\!-O\!-\!\right)_n \; + \; Ag^+ \; + \; OH^- \longrightarrow \; \left(\!\!-CH_2\!\!-\overset{\overset{\displaystyle O}{\parallel}}{C}\!\!-O\!-\!\right)_n \; + \; Ag^0 \; + \; H_2O$$
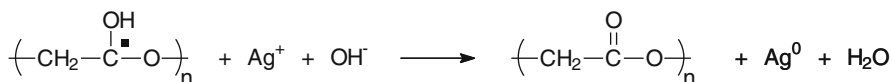
It is suggested that the key reason for silver nanoparticle formation within PEG_{600}-*co*-$PTHF_{650}$ polymeric nanoreactors is because of the presence of macromolecular sequences that consist of multiple PEG units connected with TDI groups in random polyurethane macromolecules. The greater the amount of PEG units present effectively increases the hydrophilic fragments' length in macromolecules and thus allows for reduction to be possible. The AIPU macromolecules' composition and configuration as well as the polymer's concentration appear to dictate the size of the silver nanoparticles, from 6 to 14 nm (Fig. 19.6). Monodispersed spherical silver nanoparticles in polymeric nanoreactors' formation, based on PEG_{1000}-*co*-$PTHF_{650}$ (plot 3 in Fig. 19.6b), are confirmed as seen in the synthesized nanosilver's TEM micrograph (Fig. 19.7). Data gathered by DLS measurements confirms the average nanoparticle diameter of approximately 7 nm.

Reactive mixtures were further analyzed using the XRD technique. A pattern recorded on the dried silver–PEG_{1000}-alt-$PTHF_{650}$ nanocomposites is shown in Fig. 19.8. The diffraction maxima at $2\theta = 38.2$, 44.3, 64.5, and 77.5° correspond to the (111), (200), (220), and (311) planes of the face-centered cubic silver, respectively, [13, 14] and confirm the presence of Ag in the nanoparticles.

Because of the presence of hydrophilic PEG and lipophilic PTHF chains, and the invertible properties of the AIPUs, the synthesized silver nanoparticles can be
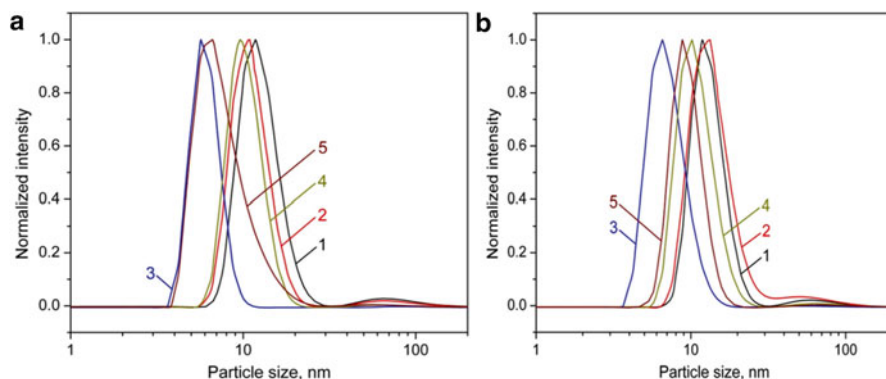
Fig. 19.6 Size distribution of a silver nanoparticle synthesized in nanoreactors prepared in 20 % w/w (**a**) and 30 % w/w (**b**) AIPU solutions in benzene: *1* PEG$_{1000}$-*alt*-PTHF$_{650}$, *2* PEG$_{1000}$-*alt*-PTHF$_{1000}$, *3* PEG$_{1000}$-*co*-PTHF$_{650}$, *4* PEG$_{1000}$-*co*-PTHF$_{1000}$, *5* PEG$_{600}$-*co*-PTHF$_{650}$ (with permission from [11])

Fig. 19.7 TEM micrograph of silver nanoparticles developed in nanoreactors from PEG$_{1000}$-*co*-PTHF$_{650}$ (at concentration 30 % w/w)
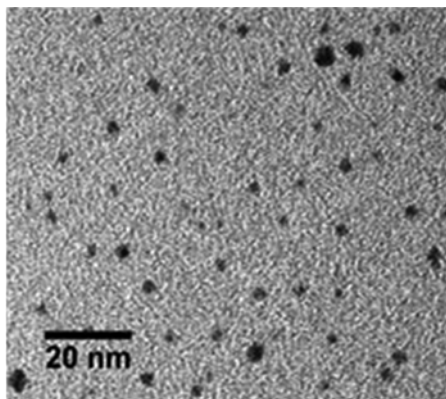
Fig. 19.8 X-ray diffraction pattern of silver nanoparticles synthesized in nanoreactors from PEG$_{1000}$-*alt*-PTHF$_{650}$ (at concentration 30 % w/w)
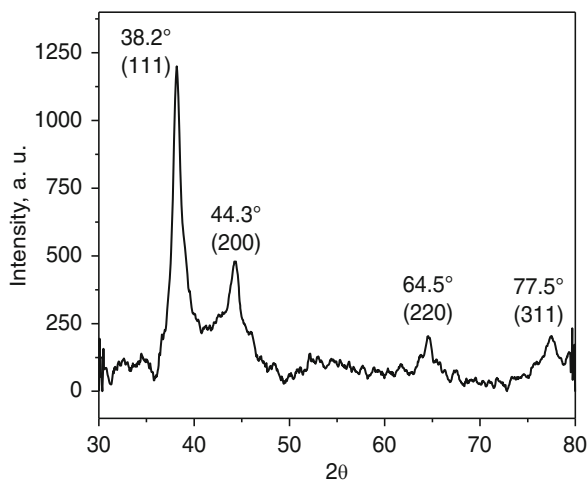
Fig. 19.9 Size distribution of silver nanoparticles synthesized in nanoreactors prepared in 50 % w/w AIPE solutions in benzene: *1* PEG$_{300}$S, *2* PEG$_{600}$S, *3* PEG$_{300}$D, *4* PEG$_{600}$D (with permission from A. Voronov, A. Kohut, W. Peukert, Langmuir 2007, 23, 360–363)
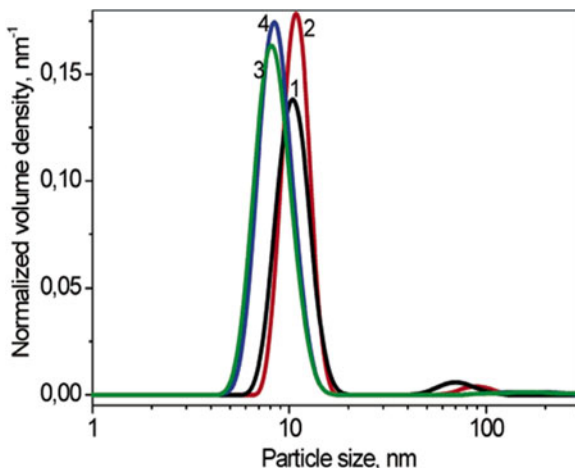
Fig. 19.10 SEM micrograph of silver nanoparticles developed in nanoreactors from PEG$_{600}$S (at concentration 50 % w/w)
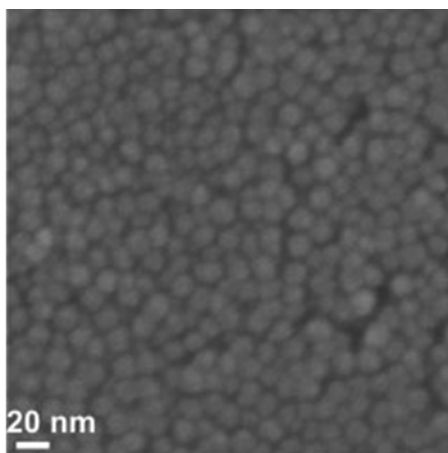
successfully dispersed in either polar or nonpolar media, where they form stable colloidal solutions.

For the synthesis of silver nanoparticles in polymeric nanoreactors based on the AIPEs, the [Ag (NH$_3$)$_2$] OH precursor was added to a concentrated AIPE solution in benzene (at polymer concentration 25 and 50 % w/w), where micellar structures were formed. Regardless of polymer composition, concentration, and HLB, no significant variation of the silver nanoparticles' size was observed. Conducting the synthesis within the polymeric nanoreactors based on the AIPEs with different lengths of the lipophilic dicarboxylic acid moieties and hydrophilic PEG chains resulted in the formation of spherical silver nanoparticles with the average diameter of about 10 nm (Figs. 19.9 and 19.10).

For the synthesis of gold nanoparticles in polymeric nanoreactors based on the AIPEs, HAuCl$_4$ precursor was added to concentrated PEG$_{300}$S and PEG$_{600}$S solu-
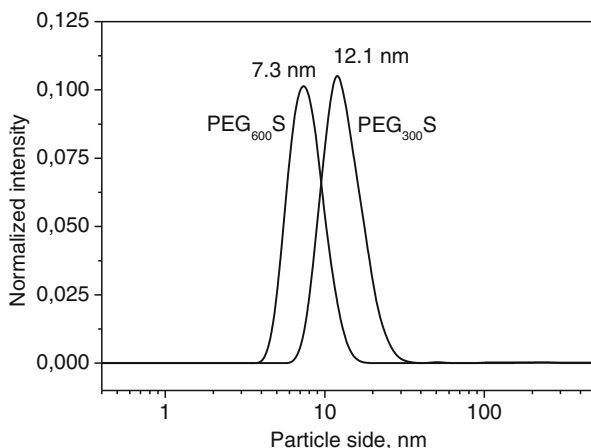
Fig. 19.11 Size distribution of gold nanoparticles synthesized in AIPE nanoreactors from 50 % w/w solutions in benzene

Fig. 19.12 SEM micrograph of gold nanoparticles developed in nanoreactors from PEG$_{600}$S (at concentration 50 % w/w)
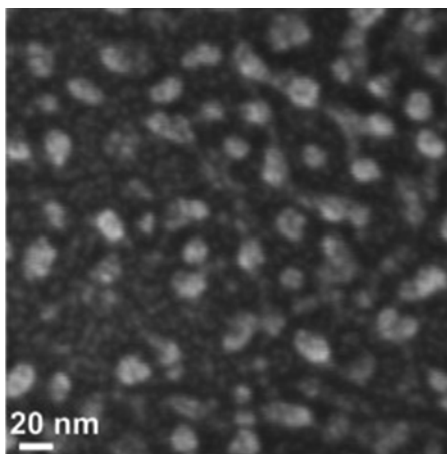
tions in benzene (at polymer concentration 50 % w/w), where micellar structures were formed. The particle size distribution plots (Fig. 19.11) show the maximum at about 7.3 nm and 12.1 nm for the syntheses of gold nanoparticles in the polymeric nanoreactors from PEG$_{600}$S and PEG$_{300}$S, respectively. This result is in agreement with the scanning electron microscopy data (Fig. 19.12).

For the synthesis of palladium nanoparticles in polymeric nanoreactors based on the AIPEs, the H$_2$PdCl$_4$ precursor was added to a concentrated PEG$_{600}$S solution in benzene (at polymer concentration 50 % w/w), where micellar structures were formed. The reduction process was carried out at 80 °C. According to the DLS analysis (Fig. 19.13) and SEM data (Fig. 19.14), the average diameter of the synthesized palladium nanoparticles was about 8 nm.
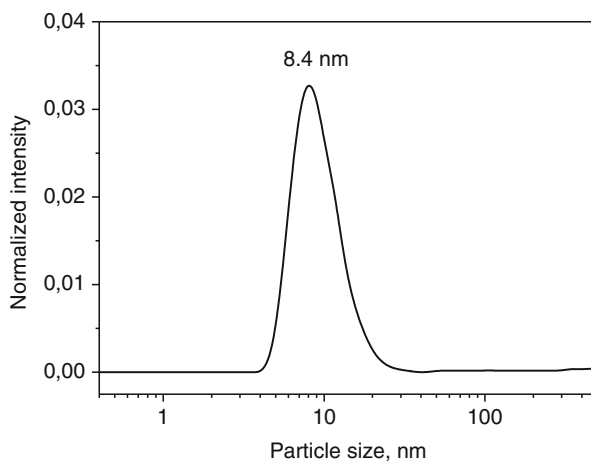
Fig. 19.13 Size distribution of palladium nanoparticles synthesized in PEG$_{600}$S nanoreactors from 50 % w/w solutions in benzene

Fig. 19.14 SEM micrograph of palladium nanoparticles developed in nanoreactors from PEG$_{600}$S (50 % w/w)
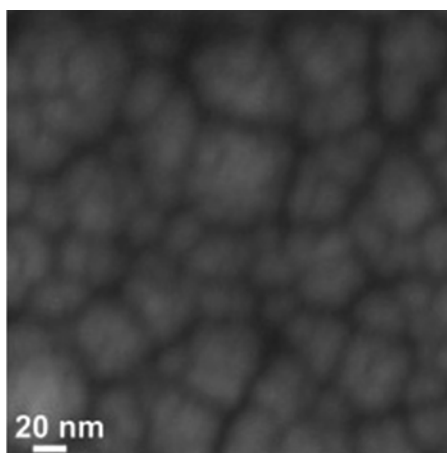
The self-assembled micellar assemblies formed by the AIP macromolecules in nonpolar organic media serve simultaneously as nanoreactors (i.e., provide a micro-environment for conducting chemical reactions), reducing agents of metal ions, and steric stabilizers of the developed metal (silver, palladium, gold) nanoparticles. The nature to the polymer, its composition, chain configuration, and concentration apparently dictate the synthesized particles' size, changing from 6 nm and 14 nm respectively. PTHF utilized as a lipophilic constituent in amphiphilic invertible polymers is advantageous in terms of changing polyurethane HLB to a larger extent in contrast to polyesters and, as such, the final nanoparticles' size.

19.3.2   Synthesis of Semiconductor Nanoparticles

To synthesize nonspherical CdSe nanoparticles, a solution–liquid–solid method using silver nanoparticles, formed in the AIPU nanoreactors, as seeds to promote anisotropic crystal growth was developed (Fig. 19.15).

According to this method, the reaction mixture in a high-boiling nonpolar solvent, diphenyl ether, is heated to 220 °C, a temperature at which a quasi-molten surface layer is formed on the nanoparticle surface. Cadmium oxide precursor dissolves in the quasi-molten surface layer, and CdSe crystal growth starts from the silver surface after injecting trioctylphosphine selenide, a second precursor, into the reaction mixture. During the process, the AIPU macromolecules provide stabilization for both silver nanoparticle seeds and cadmium selenide crystals. After the reaction, CdSe nanocrystals were separated from the reactive mixture, including nanosilver seeds, by hexane extraction. Particle size distribution of the synthesized CdSe nanocrystals measured by DLS (Fig. 19.16a) indicates an average size of
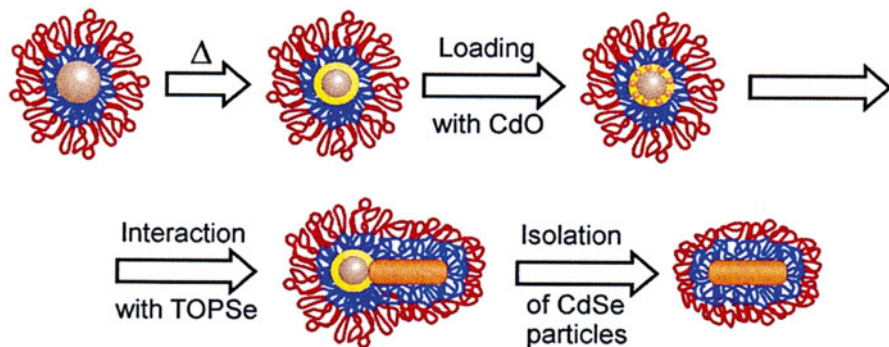
Fig. 19.15 Synthesis of cadmium selenide nanoparticles using silver nanoparticle seeds formed in the AIPU nanoreactors
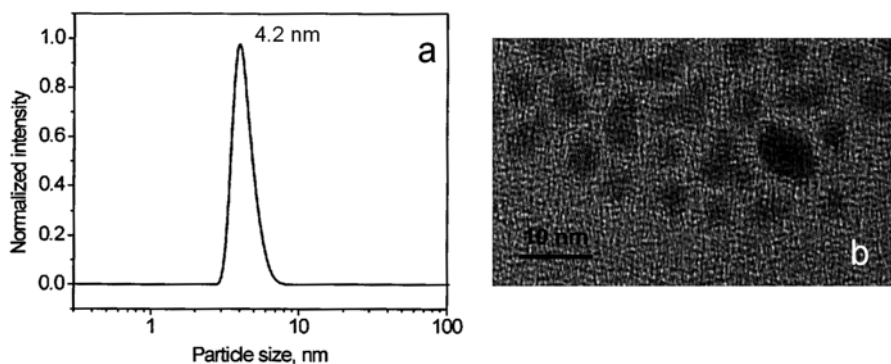
Fig. 19.16 Size distribution (**a**) and TEM micrograph (**b**) of the cadmium selenide nanoparticles synthesized in polymeric nanoreactors from AIPU, using nanosilver seeds

4.2 ± 0.6 nm. A representative TEM micrograph of the synthesized cadmium selenide (Fig. 19.16b) confirms the presence of elongated nanoparticles with the average size of ca. 5 nm.

Micellar structures developed from $PEG_{600}S$ macromolecules in benzene were also applied as polymeric nanoreactors for the synthesis of silicon nanoparticles, which is another semiconductor material.

For this purpose, a liquid cyclohexasilane precursor, Si_6H_{12}, was applied. A ^{1}H NMR study on model low-molecular-weight substances, diethyl sebacate, and poly(ethylene glycol) dimethyl ether, which resemble repeating units in $PEG_{600}S$ macromolecules, revealed Lewis acid–base interactions between the oxygen-based functional groups of the $PEG_{600}S$ macromolecules and the Si_6H_{12} rings to give "inverse sandwich" complexes (Fig. 19.17) [15].

The ^{1}H NMR study has shown that by solubilizing precursor molecules in polymeric nanoreactors, initially, Lewis acid–base interaction occurs between Si_6H_{12} and the ester functional groups of $PEG_{600}S$. Higher concentrations of Si_6H_{12} result in a second type of physical interactions between the precursor and $PEG_{600}S$ ether groups. Hence, the $PEG_{600}S$ micellar structures serve as nanocontainers for cyclohexasilane molecules by facilitating the "host–guest" interactions. Silicon nanoparticles were synthesized by the photopolymerization of Si_6H_{12} solubilized within the $PEG_{600}S$ micellar assemblies formed in benzene, according to the scheme depicted in Fig. 19.18.
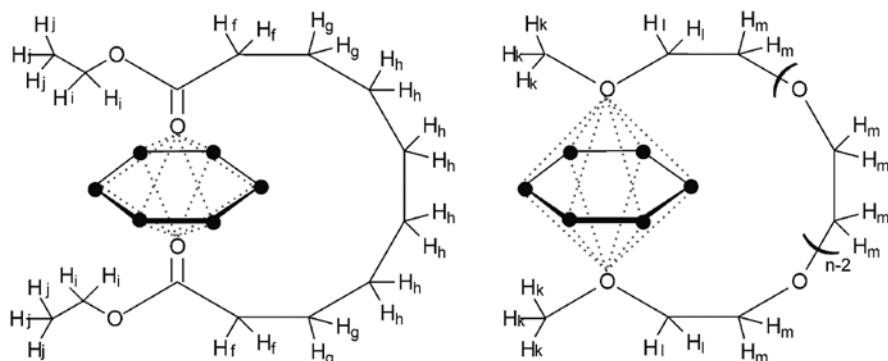
Fig. 19.17 Schematic illustration of two possible molecular orientations for Si_6H_{12}–diethyl sebacate (*left*) and Si_6H_{12}–PEGDM (*right*) complexes (with permission from [15])
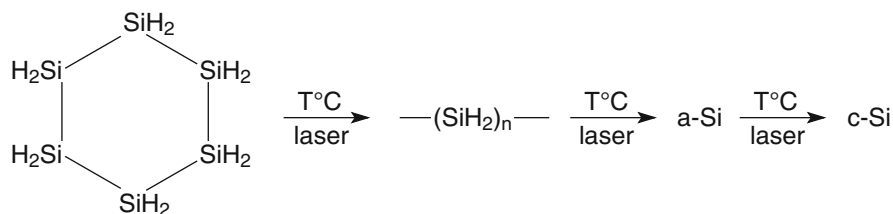
Fig. 19.18 Reaction of cyclohexasilane polymerization and crystalline silicon synthesis
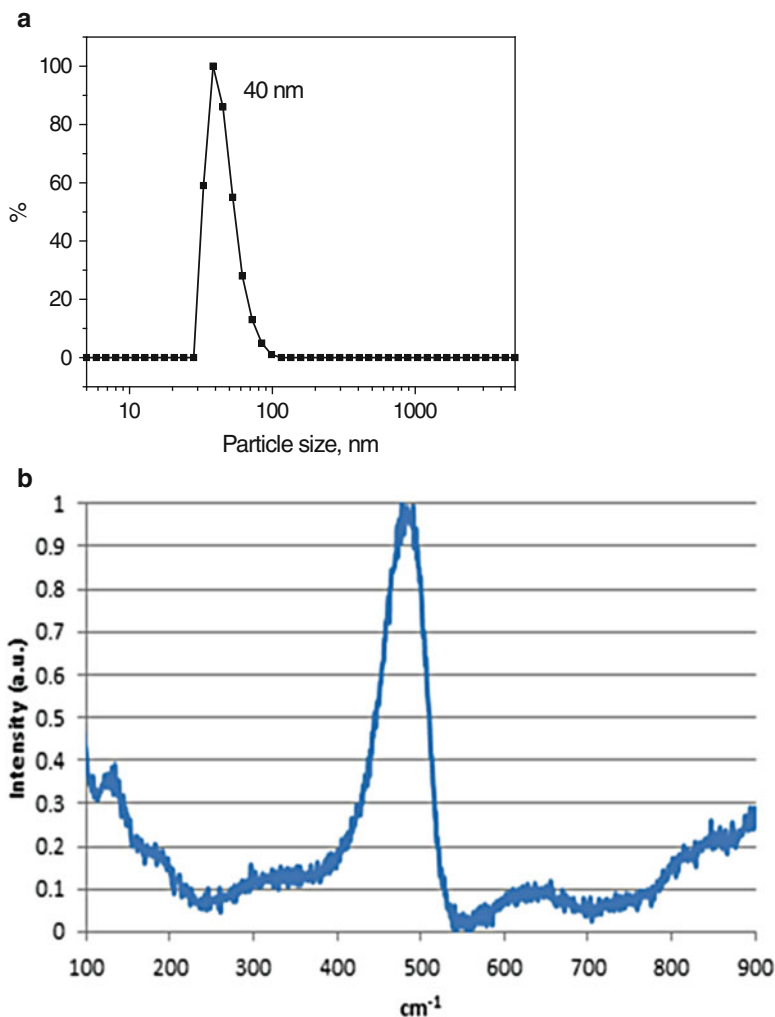
Fig. 19.19 Size distribution (**a**) and Raman spectrum (**b**) of the silicon nanoparticles synthesized via cyclohexasilane photopolymerization in polymeric nanoreactors from $PEG_{600}S$ prepared in benzene (at concentration 20 g/100 mL)

As determined by dynamic light scattering, the average size of the synthesized silicon nanoparticles is about 40 nm (Fig. 19.19a). The adsorption band at 480 cm^{-1} in the Raman spectrum (Fig. 19.19b) confirms the formation of elemental silicon in the sample.
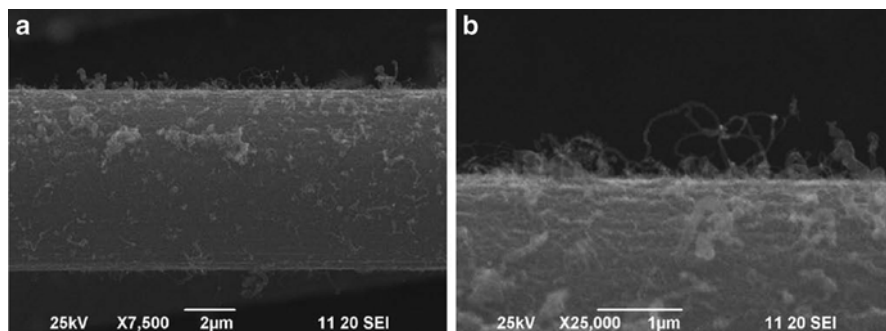
Fig. 19.20 SEM images showing the catalytic growth of carbon nanostructures on the surface of carbon microfibers loaded with AIP–metal complex in benzene (with permission from [16])

19.3.3 Synthesis of Fibrillar Carbon Nanostructures

For the synthesis of fibrillar carbon nanostructures on the surface of carbon microfibers, the micellar structures formed from the $PEG_{600}S$ macromolecules in benzene were applied. Formation of the micellar assemblies in benzene, a nonpolar organic solvent, allowed ferric nitrate [Fe $(NO_3)_3 \cdot 9H_2O$], a catalyst for the growth of carbon nanostructures in micellar interior, to be solubilized. The colloidal solution of Fe $(NO_3)_3$ was used to form a uniform layer of the catalyst on the surface of carbon microfibers [16].

Afterward, the growth of carbon nanostructures was performed at 750 °C by means of the thermal CVD technique, using C_2H_4/CH_4 mixture (1:1) to provide fibrillar carbon nanostructures with the ability to cover the surface of carbon microfibers (Fig. 19.20).

In summary, the application of the AIP micellar structures as nanoreactors for conducting chemical reactions in an organic medium allows the facile synthesis of metal (Ag, Au, Pd) and semiconductor (CdSe, Si) nanoparticles. The size of the synthesized particles can be easily controlled by the polymer's chemical nature and concentration. In addition, using the polymeric micellar assemblies formed in benzene for the solubilization of Fe $(NO_3)_3$ catalysts resulted in the uniform distribution of the grown fibrillar carbon nanostructures on the carbon microfiber substrate surface.

19.4 Conclusion

New amphiphilic "smart" polymers were developed, the macromolecules of which are capable of quickly changing their conformation in response to changes in the solvent's nature (medium polarity). Amphiphilic invertible polyurethanes with an

alternating or random distribution of hydrophilic and lipophilic fragments, as well as amphiphilic invertible polyesters, were synthesized. The amphiphilic invertible polymers are prospective candidates for application as nanoreactors for the controlled synthesis of metal and semiconductor nanoparticles and the growth of fibrillar carbon nanostructures in organic solvents of lower polarity. Besides, in an aqueous medium, the amphiphilic invertible polymers show promise as nanocarriers for the solubilization of poorly water-soluble drugs and their delivery to pathologic cells as well as substrate surface modification.

References

1. Zhang A-Q, Cai L-J, Sui L, Qian D-J, Chen M, Reducing properties of polymers in the synthesis of noble metal nanoparticles (2013) Polym Rev 53:240–276
2. Torchilin VP, Micellar nanocarriers: pharmaceutical perspectives (2007) Pharm Res 24:1–16
3. Luzinov I, Minko S, Tsukruk VV, Adaptive and responsive surfaces through controlled reorganization of interfacial polymer layers (2004) Prog Polym Sci 29:635–698
4. Basu S, Vutukuri DR, Shyamroy S, Sandanaraj BS, Thayumanavan S, Invertible amphiphilic homopolymers (2004) J Am Chem Soc 126:9890–9891
5. Arumugam S, Vutukuri DR, Thayumanavan S, Ramamurthy V, Amphiphilic homopolymer as a reaction medium in water: product selectivity within polymeric nanopockets (2005) J Am Chem Soc 127:13200–13206
6. Hevus I, Kohut A, Voronov A, Amphiphilic invertible polyurethanes: synthesis and properties (2010) Macromolecules 43:7488–7494
7. Kudina O, Kohut A, Tarnavchyk I, Hevus I, Voronov A, Solvent-responsive self-assembly of amphiphilic invertible polymers determined with SANS (2014) Langmuir 30:3310–3318
8. Beecroft LL, Ober CK, Nanocomposite materials for optical applications (1997) Chem Mat 9:1302–1317
9. Cortie M, New uses for gold in the emerging field of nanotechnology (2003) Gold Bull 36:74
10. Shan J, Tenhu H, Recent advances in polymer protected gold nanoparticles: synthesis, properties and applications (2007) Chem Commun 4580–4598
11. Hevus I, Kohut A, Voronov A, Micellar assemblies from amphiphilic polyurethanes for size-controlled synthesis of silver nanoparticles dispersible both in polar and nonpolar media (2012) J Nanopart Res 14:820/1–820/11
12. Berlin AA, Kislenko VN, Kinetics and mechanism of radical graft polymerization of monomers onto polysaccharides (1992) Prog Polym Sci 17:765–825
13. Bajpai SK, Johnson S, Superabsorbent hydrogels for removal of divalent toxic ions. Part I: synthesis and swelling characterization (2005) React Funct Polym 62:271–283
14. Thomas V, Murali Mohan Y, Sreedhar B, Bajpai SK, A versatile strategy to fabricate hydrogel–silver nanocomposites and investigation of their antimicrobial activity (2007) J Colloid Interface Sci 315:389–395
15. Kohut A, Dai X, Pinnick D, Schulz DL, Voronov A, "Host–guest" interaction between cyclohexasilane and amphiphilic invertible macromolecules (2011) Soft Mater 7:3717–3720
16. Shafranska O, Voronov A, Kohut A, Wu X-F, Akhatov IS (2009) Carbon 47:3137–3139

Chapter 20
Smart Coatings for Corrosion Protection

V. Dalmoro, C. Santos, and João Henrique Zimnoch dos Santos

Abstract The investigation of coatings that can be used to reduce corrosion rates is mandatory because the degradation of metallic structures engenders severe economic, environmental, and social consequences. The primary action of most typical corrosion protection coatings occurs as a result of barrier properties or inhibitive process that is carried out by a corrosion inhibitor incorporated into the coating. Nevertheless, these coatings offer protection over a limited time. Thus, smart coatings have been investigated in the recent years, which possess an active component that releases with an environmental stimulus, for example, corrosion inhibitors to compensate the coating damage. This technology extends the lifetime of coatings. Different attempts have been made to produce coatings with self-healing properties, which allow the inhibitor or healing agent to be released on demand at the coating/metal surface. The most important triggers reported for releasing these agents are local pH gradients, mechanical damage, and ion-exchange processes, all of which are reviewed in the present chapter. Despite numerous researches in this field, the production of smart coatings for corrosion protection on an industrial scale remains a challenge.

Keywords Self-healing • Corrosion inhibitors • Local action

20.1   Introduction

Metallic materials are extensively used in many technological and industrial applications such as pumps, oil platforms, ships, cars, and aeronautical components. The properties of these materials are unique, and the combination of metals to form metal alloys can lead to improved mechanical and physicochemical properties. Nevertheless, the metals and metal alloys typically employed in industry are susceptible to the corrosion process. The corrosion phenomenon encompasses the charge transfer reactions and electron transfer resulting in metal oxidation with progressive

V. Dalmoro • C. Santos • J.H.Z. dos Santos (✉)
Institute of Chemistry, Federal University of Rio Grande do Sul,
Av. Bento Gonçalves 9500 – CEP 91501-970, Porto Alegre, RS, Brazil
e-mail: vidalmoro@gmail.com; cristiane.engbio@gmail.com; jhzds@iq.ufrgs.br

degradation of the material when exposed to an aggressive environment [1, 2]. From a thermodynamic point of view, this process is spontaneous and irreversible. Moreover, corrosion mechanisms depend significantly on the local environment [2].

The addition of alloy elements can result in galvanic corrosion and an increase of localized corrosion. For example, the aluminum alloy 2024 employed in the aeronautical industry has a complex distribution and composition of intermetallic particles. It is well known that the corrosion process begins at the intermetallic particles, specifically those in the S-phase with preferential dissolution of Al and Mg [3–5]. The localized corrosion constitutes the main degradation pathway of this alloy and involves a cooperative mechanism [6] that results in corrosion of the grain boundary network, which in turn leads to mechanical failure [7].

According to the *World Corrosion Organization* [8], the annual cost due to corrosion is equivalent to over 3 % of the world's GDP. Because of the enormous economic damage that corrosion can cause, it continues to be a subject of broad interest, with efforts particularly aimed at minimizing expenses to an acceptable economic and environmental level [2].

Corrosion protection has been improved by cathodic protection [1], organic coatings [9], conversion layers [10], corrosion inhibitors [11], and conductive polymer layers [12], with organic coatings being the most widely employed. A key determinant for the lifetime of organic coatings is their adhesion to the metal surface when exposed to a corrosive medium. The physicochemical properties of the metal–coating interface are usually improved by a pretreatment. For example, chromatization was a pretreatment widely used for lightweight metals such as aluminum and its alloys, especially in the aerospace industry [1]. This is due to the fact that chromatization served as both an anchor for the organic coating and a corrosion-inhibiting system. However, environmental legislation has prohibited the utilization of this type of pretreatment.

In recent decades, films produced by sol–gel technology using silica precursors have been proposed as an environmentally friendly alternative to the chromate pretreatment [13–19]. Such systems are capable of forming bonds with both the metal substrate and a reactive organic group of the paint.

The fundamental strategy of coating protection is passive action based on a physical barrier [20–22]. Nevertheless, coatings contain small pores through which water, oxygen, and aggressive ions may penetrate to the metal surface. Therefore, an active protecting coating is necessary for extending the lifetime of the metallic substrate. A simple example of active protection is the use of cerium ions incorporated within a sol–gel matrix. In such systems, cerium ions react with hydroxide in the cathodic zone to form cerium oxide/hydroxide, which in turn is deposited on metallic surface, reducing the corrosion rate [23, 24]. However, the direct addition of corrosion inhibitors into a coating matrix may lead to coating degradation, inhibitor deactivation, and a rapid release of inhibitor (and consequently its depletion if the inhibitor is soluble) [20, 25].

In recent years, the concept of smart coatings has been emerged as a method of active protection. Smart coatings are functional systems whose properties or characteristics may be altered in a controlled way in response to a stimulus gener-

ated by an intrinsic or extrinsic event [26, 27]. Smart coatings usually exhibit a self-healing effect (i.e., self-recovery of the initial properties of the coating following the corrosion process) [28–30]. The term self-repairing is sometimes used in the context of smart coatings and has the same meaning as self-healing.

Several methodologies have been employed to obtain coatings with the ability to self-heal upon being triggered by stimuli such as local pH changes, capsule rupture induced by mechanical stress, ion-exchange reactions, water trapping, electrochemical potential changes, light irradiation, and thermal variations [26]. In the following sections, functional materials used as reservoirs that enable the controlled delivery of corrosion inhibitors or healing agents will be discussed. More specifically, this chapter is focused on those primary stimuli that cause the release of inhibitive species from the reservoirs: mechanical damage, ion-exchange processes, and local pH changes.

20.2 Mechanical Damage as a Releasing Stimulus

The development of smart coatings for corrosion protection began with studies of polymer-based coatings with micrometer-scale containers, filled with monomers or appropriate catalysts that were released by mechanical rupture [31]. Mechanical damage is an important external stimulus with negative consequences on the barrier properties of coatings [32]. Examples of mechanical damage include various types of impact, scratches, thermal cycles, and fatigue associated with wear of the structure [28]. Such events produce contact between the catalyst and monomer, which initiates the polymerization process that seals the defected area. In such approach, the catalyst may be dispersed in the matrix coating or can be released from another container [33, 34].

The first nanocontainer proposed in the development of self-healing coatings was urea–formaldehyde capsules filled with polymerizable agents [35]. In the investigation reported by White et al. [35], the self-healing process was triggered by the crack-induced rupture of the incorporated poly(urea–formaldehyde) capsules. The core material, dicyclopentadiene (DCPD), was released, and ring-opening metathesis polymerization (ROMP) occurred in the presence of a Grubbs' catalyst.

The presence of a catalyst within the coating matrix can produce a major discontinuity [30, 36]. Therefore, an alternative approach is the use of healing agents that are active in the absence of a catalyst. In such systems, the healing agent may be activated by moisture/water from its environment [34, 37] and by the oxidation of oils such as tung [38] or linseed oil [36, 39, 40]. For instance, steel-coated epoxy paint containing tung oil encapsulated in poly(urea–formaldehyde) capsules exhibits a self-healing ability, as revealed by electrochemical impedance spectroscopy (EIS) and scanning electronic microscopy (SEM) [38]. The corrosion resistance of epoxy-coated panels was drastically decreased after suffering a mechanical scratch, whereas samples containing the capsules exhibited very little reduction in corrosion resistance. The self-healing is produced by release of tung oil from incorporated capsules, and the polymerization occurs in contact with air. SEM images (Fig. 20.1)
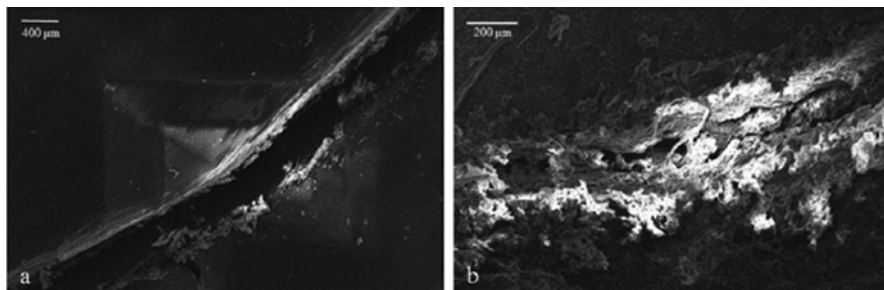
Fig. 20.1 (**a**) SEM image of an artificial scratch on epoxy coating; (**b**) SEM image of a healed scratch on epoxy coating containing microcapsules filled with tung oil. Reprinted with permission from [38]

obtained 24 h after the scratch confirm the healing and corrosion protection of the substrate for epoxy panels containing the incorporated capsules.

Several parameters (e.g., the encapsulation method or shell thickness) need to be adjusted so that the carried capsules behave as an effective self-healing material [27, 41]. For example, if the wall thickness of the microcapsule is too large, the rupture is very difficult and healing may not occur, whereas if the shell wall is too thin, the microcapsules can rupture the coating or the healing agent could leak or diffuse into the matrix over time [27]. Furthermore, the embedded capsules within the coating matrix negatively can impact the physical properties of the coating [30]. In the research of Boura et al. [36], the adhesion strength of epoxy coatings on steel was reduced with the incorporation of poly(urea–formaldehyde) capsules containing linseed oil. However, this weakening of the adhesion could be compensated by decreasing the capsule size. Poly(urea–formaldehyde) capsules of a smaller size were synthesized by employing low temperatures and a high stirring rate [39] or ultrasonic energy [36] during the encapsulation process.

The uptake of aggressive agents in the coating can induce the corrosion phenomena. Therefore, when mechanical damage occurs, the corrosion can already be in an advanced stage so that release of the healing agent from the ruptured capsule is inefficient for mitigating the corrosion of the metallic surface.

20.3   Inhibitor Nanocontainers: Release Controlled by an Ion-Exchange Reaction

The use of ion-exchange clays and zeolites as reservoirs of corrosion inhibitors has also been extensively investigated [18, 42–70]. Anionic and cationic inhibitors have been immobilized in anion-exchange and cation-exchange pigments, respectively. The release of the inhibitor is stimulated by an ion-exchange reaction with the corrosive medium (e.g., exchange with aggressive chloride ions in the case of anion-exchange pigments).

20.3.1   Anionic Materials

Layered double hydroxides (LDHs), also known as anionic clays, have aroused interest as corrosion protection systems due to their anion-exchange properties. The general formula of an LDH is $[M(II)_{1-x}M(III)_x(OH)_2][A_{x/n}{}^{n-}].mH_2O$, where M(II) and M(III) are divalent and trivalent cations, respectively, occupying octahedral holes in a brucite-like layer. The A^{n-} in the formula corresponds to interlayer anions that counterbalance the excessive positive charge caused by partial substitution of the divalent cation by a trivalent in the brucite layer [42–44]. The positive hydroxide sheets and anions are stacked together and spatially organized with rhombohedral or hexagonal symmetry [45].

These materials are also called hydrotalcite-like compounds due to their structural analogies with the natural mineral hydrotalcite, which contain Mg(II) and Al(III) in a 3/1 molar ratio [20]. LDH compounds exhibit advantageous properties such as versatile intercalation chemistry, good stability, and low toxicity, and their synthetic preparation is simple and cheap [46].

The distance between hydroxide layers enables a wide variety of corrosion inhibitor anions to be inserted. Of such inhibitors, ethylenediaminetetraacetic acid (EDTA) [47], vanadate species [44, 48], carbonate/nitrate [45], 2-benzothiazolylthio-succinic acid (BTSA) [43], 4- or 3-aminobenzenesulfonic acid (4- or 3-ABSA), 3,4-dihydroxybenzoic acid (3,4-HHBA) [49], and molybdate [50] can be mentioned. These intercalated anionic inhibitors can be released and substituted through an anion-exchange reaction by aggressive species such as chloride anions from the environment.

Positive results in terms of coating stability have been achieved by chloride entrapment in layered double hydroxide intercalated with nitrate anions [51] and tungstate [52]. A comprehensive model for inhibitor release and the capture of chloride ions by hydrotalcite/vanadate in epoxy coating for AA2024 was reported by Wang et al. [53]. Using computational modeling, they found that the most important parameter for the performance of this system was the pH dependence of the steady-state inhibitor release rate [53]. Additionally, the inhibitor release rate was also influenced by the scratch size. For smaller scratches, the inhibition may be complete, whereas increasing the scratch size makes the transportation of vanadate ions to the entire scratched area more difficult. The change of inhibitor ions by aggressive ions can reduce the chloride concentration in the bulk solution from 100 to 40 mM after 16.7 h [53].

In general, the chloride concentration determines the rate of inhibitor release from the LDH structure. This indicates that it is a chemical process based on an exchange reaction between the anionic inhibitor and chloride ions governed by a dynamic equilibrium and exchange isotherm [20, 43, 48]. For BTSA that was intercalated in magnesium–aluminum-layered double hydroxides using the coprecipitation method, it was verified that the release percentage of BTSA was 20 %, 50 %, 53 %, and 61 % after 72 h of immersion in an ethanol/water mixture containing 0 %, 0.5 %, 1 %, and 3 wt% NaCl, respectively [43]. This finding was very promising because
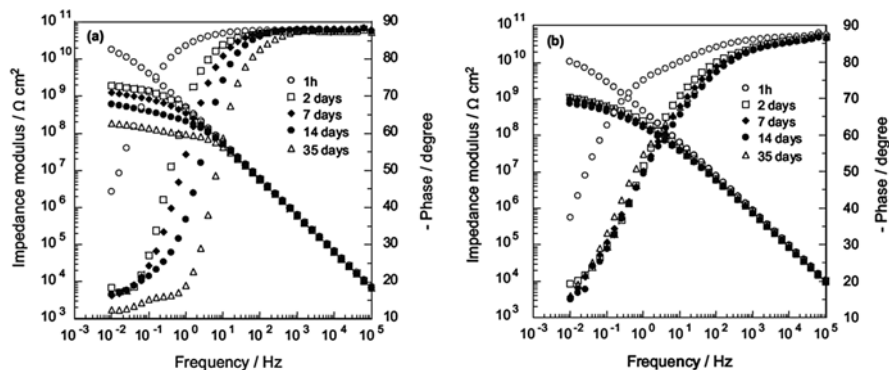
Fig. 20.2 Bode diagrams obtained after different exposure times to 0.5 M NaCl solution for carbon steel coated with (**a**) pure epoxy and (**b**) epoxy containing LDH–BTSA. Reprinted with permission from [43]

the corrosion rate increases with the chloride concentration. EIS measurements (Fig. 20.2) of carbon steel panels coated with epoxy containing BTSA intercalated within LDH revealed that the impedance modulus values after a decrease from 1 h to 2 days of immersion in 0.5 mol L^{-1} NaCl remain stable in the order of $10^9 \Omega$ cm^2, whereas neat epoxy samples underwent a continuous reduction.

In the study of Ferreira et al. [48], the composition of the LDH pigments influenced the anticorrosive behavior. The AA2024 samples in chloride solution containing Mg–Al–NO$_3$ exhibited lower impedance modulus in comparison to those observed in panels in Zn–Al–NO$_3$, due to additional protection of the aluminum alloy by Zn^{2+} cations that are released from LDHs into the solution [20]. Moreover, the ratio between the metal cations [M(II)/M(III)] determines the specific charge of the host layer and consequently the fraction of adsorbed anionic inhibitors [44].

The inhibitive power also depends on the structure of the organic anion intercalated in LDH [49, 54]. The inhibition efficiency for filiform corrosion of epoxy-coated AA2024 with different inhibitors (anion-exchange hydrotalcite pigments) increased in the following order: ethyl xanthate < oxalate < benzotriazolate [54]. An improvement in the barrier properties of the epoxy primer was achieved in the presence of LDH pigments modified with 3- and 4-aminobenzenesulfonic acid by coprecipitation, whereas a deleterious effect in the protection of AA2024 was observed with 3,4-dihydroxybenzoic (3,4-HHBA) intercalated into LDH [49]. The authors assumed that Zn^{2+} from anodic dissolution of LDH/3,4-HHBA and Cu^{2+} compete for chelation to 3,4-HHBA leading to acceleration of the copper dissolution and the corrosion process [49].

The corrosion mechanism of LDHs with quinaldate and 2-mercaptobenzothiazolate prepared by an anion-exchange reaction has also been investigated [20]. It was verified that the corrosion inhibition activity of nanocontainers dispersed in aqueous solution was highly dependent on the solution pH, with the best anticorrosive performance achieved in neutral solution for AA2024 [20]. Another research group evaluated the addition of 2-mercaptobenzothiazole (MBT)-intercalated

Zn–Al-layered double hydroxides into epoxy resin [55]. The overall impedance modulus remained almost constant for Q345 steel panels coated with this system after 20 days of exposure in 3.5 wt% NaCl solution. Results of this study revealed that the MBT anions were released from the LDH to the damaged area and may form an inhibitor film on it. This result confirmed the self-healing ability of the MBT/LDH epoxy coating.

Two approaches have been proposed in the literature for modifying LDH: the coprecipitation method [43, 49] and the ion-exchange reaction method following LDH synthesis [20]. The direct synthesis of LHD, whose charge is compensated by a negatively charged inhibitor, is carried out in the former. EIS data and visual observation showed that Zn–Al–VO_3 LDH prepared by anion exchange was more effective at protecting against the corrosion of AA2024 when compared to that prepared by direct synthesis [48].

Another interesting feature of LHD compounds is their structural memory effect, as demonstrated by Buccheit et al. [56] for a calcined LDH embedded in epoxy coatings applied on the AA2024. According to an X-ray diffraction (XRD) analysis, when the panels were exposed to 0.5 mol L^{-1} NaCl aqueous solutions, it took 5 days for LDH reconstruction. Thus, calcinated LDH can retard the uptake of water and thus serve as a material suitable for sensing early-stage coating degradation.

Another strategy for the preparation of a smart coating from LHD is the direct synthesis of a lamellar structure onto a metallic substrate [57–59]. With modification by phytic acid, in situ prepared Mg–Al hydrotalcite conversion coatings on AZ91 magnesium alloy showed to provide efficient protection under alkaline conditions due to self-healing [58]. Using coprecipitation followed by a hydrothermal process, Chang-Zheng et al. [57] prepared a molybdate-intercalated hydrotalcite on AZ31 Mg, which led to the improvement of corrosion performance. Based on the experimental results, the authors proposed a corrosion mechanism model that is illustrated in Fig. 20.3. The first step is the release of anodic inhibitor MoO_4^{2-} and the adsorption and retention of Cl^- ions. The MoO_4^{2-} ions can then react with the dissolved Mg^{2+} to form a protective deposition film, which reduces pitting corrosion. The
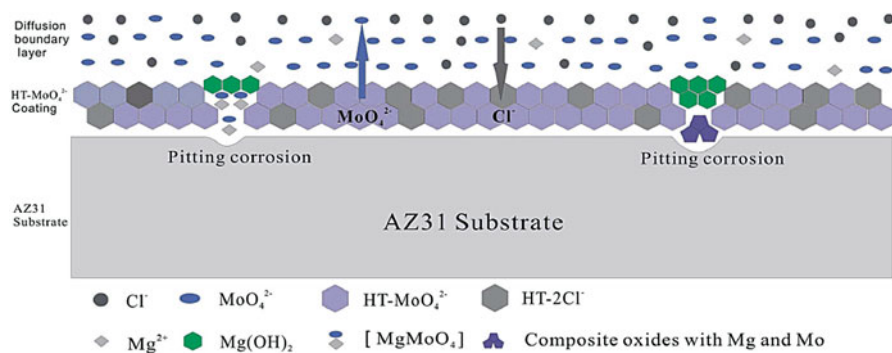
Fig. 20.3 Schematic representation of the corrosion protection mechanism associated with the hydrotalcite-MoO_4^{2-} coating. Reprinted with permission from [57]

HT-MoO$_4{}^{2-}$ and HT-2Cl$^-$ form an effective barrier for the uptake of aggressive species, and the pitting corrosion can be healed by an anodic inhibitor and a magnesium hydroxide layer, the latter of which is generated by a redox process.

In addition to releasing inhibitor molecules by trapping aggressive species (such as chloride anions) and OH$^-$ ions from a cathodic process through an anion-exchange reaction, LDH containers may also be activated/stimulated by changes in pH. The LDH framework is unstable in an acidic medium; therefore, the anodic corrosion phenomenon can dissolve the host structure and release the guest anticorrosive agent [47, 49].

The drawbacks of the synthesis of LDH are that it must be performed under a nitrogen or argon atmosphere and boiled distilled water must be used to prepare the solutions in order to exclude CO$_2$, which would otherwise cause the incorporation of carbonate into the LDH.

20.3.2 Cationic Materials

Cationic clays and zeolites have also been employed as nanocontainers for organic and inorganic inhibitors [18, 60–70].

Cation-exchange properties have been observed in natural clays such as bentonite or montmorillonite independently of pH [60]. Ce^{3+} ions exhibited fast release kinetics for cerium-modified montmorillonite. When these particles were incorporated into hybrid sol–gel films deposited onto galvanized steel [61], the corrosion rates were reduced only for a short immersion time (1 h), and the healing effect was not clearly observed. However, the strategy of adding neat montmorillonite and cerium ions into sol–gel films affords superior corrosion resistance of aluminum samples in comparison with films containing only montmorillonite [18].

Advances in the corrosion protection of steel include the addition of montmorillonite clay-modified amino trimethylene phosphonic acid [62] and indole-3-butyric acid (IBA) [25] into epoxy resin. Local electrochemical impedance measurements performed on scratched panels revealed the inhibitive action of amino trimethylene phosphonic acid at the carbon steel/coating interface [62]. Nevertheless, superior adherence was achieved only for epoxy coatings with IBA-modified clay [25]. According to the authors, the inhibitors can be released with water from montmorillonite or migrate during the drying of the epoxy. Considering that the pKa of IBA is 4.9, in a subsequent study, these researchers [63] explained that the IBA release is increased from pH 5 because the nitrogen functional group is no longer charged. Thus, the interactions between clay and the inhibitor were reduced.

In the search for environmentally friendly pigments for paints, Bohm et al. [64] compared the performance of bentonite pigments prepared by cation exchange in aqueous solutions of cerium (III) chloride and calcium (II) chloride with commercial calcium (II)-exchanged silica pigment (Shieldex). The pigments were dispersed in polyester resin-based primer and applied to galvanized steel. In a salt spray test, the calcium (II) and cerium (III) bentonite pigments exhibited superior efficiency compared with the commercial pigment for the same pigment volume concentration

[64]. The aqueous solution with Shieldex pigments had a pH of 9.1; therefore, such pigments induced alkali-catalyzed hydrolysis of the carboxylic ester functions of the polyester resin (i.e., degradation of the resin). Conversely, the calcium (II) bentonite pigment had a pH of 6.5, and their intrinsic cation-exchange properties are independent of pH, being more effective at carrying the corrosion inhibitor [64].

Ion-exchanged zeolites have been employed as reservoirs in several coatings, such as alkyl [66, 67], polyurethane [68], and sol–gel films [69, 70]. The structure of zeolites consists of a network of SiO_4^{4-} and AlO_4^{5-} tetrahedra that form channels and cages with large specific surface areas and are neutralized by exchangeable cations [69, 71, 72].

Deyá et al. [66] evaluated modified zeolites as an anticorrosive pigment for paint. The zeolites were modified by ionic exchange in a molybdenyl cation solution. From salt spray and electrochemical assays of steel coated with alkyl paint containing zinc phosphate and modified zeolites, a synergic effect between both pigments was observed. As a result, this new pigment allows that the concentration of zinc phosphate pigments normally used in paint formulations to be reduced by around a factor of 3. According to the researchers, when the electrolyte ($NaClO_4$) and water permeate into the paint, sodium cations are exchanged for molybdenyl cations, which react with water to produce molybdate anions. The latter species is a good inhibitor for steel, due to their formation of a ferrous molybdate layer. After immersion in an electrolyte solution containing modified zeolite, the surface of the steel exhibited a cracked film with small spheres containing a high concentration of molybdenum, as observed by energy-dispersive X-ray spectroscopy (EDX), thus confirming the proposed mechanism.

Sol–gel films with zeolites bearing nanocontainers for Ce (III) ions have also been studied [69, 70]. The extent of release of cerium ions from the zeolite structure in 3 % NaCl solution was dependent on the pH. In an acid medium (pH 2.6), the release was 69 ± 1 %, whereas at pH value of 8.8, no Ce ions were detected [69]. The corrosion behavior of aluminum alloy AA2024, which is employed in the aerospace industry, coated with the zeolite microparticles incorporated in the sol–gel films was investigated. As a result of the corrosion process, the pH decreases at anodic areas, causing the release of inhibitor due to the exchange mechanism of Ce (III) by Na^+ and K^+ ions of the electrolyte solution and the Cu^{2+} ions produced by the corrosion process [70]. Subsequently, the Ce (III) ions react with the hydroxide ions formed by water reduction, producing a precipitate in the cathodic areas that decreases the corrosion rate. Moreover, the authors of that study verified that cerium-modified zeolite adsorbs Cl^- ions, which was explained by the formation of an ionic bond between Cl^- ions and encapsulated cerium ions and by the trapping of chloride ions inside the zeolite structure [70]. A schematic representation of the corrosion inhibition propitiated by Ce-enriched zeolite proposed by the authors is displayed in Fig. 20.4. Unfortunately, zeolites increase the pH of the coating, which has detrimental effects on the barrier properties [70].

The intrinsic characteristics of ion-exchange materials allow a small amount of cationic or anionic inhibitor to be incorporated in their structure. Nevertheless, the availability of a great number of inhibitive species is required to ensure prolonged corrosion protection, so that the release occurs during the entire time of exposure to
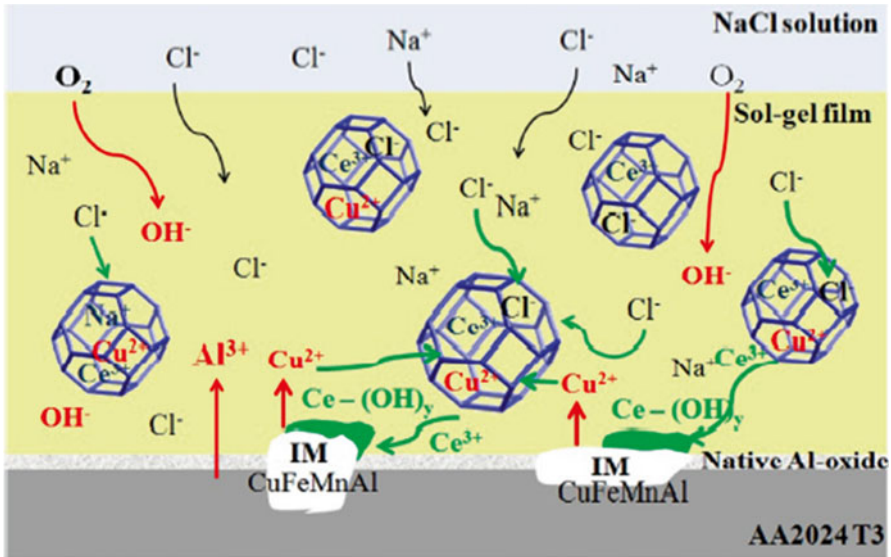
Fig. 20.4 Schematic representation of the ion-exchange process on Ce–Na zeolite. Reprinted with permission from [70]

an aggressive environment. Therefore, to compensate for the lower content of inhibitor, a large amount of these materials needs to be incorporated into the coatings. However, this sometimes leads to impaired physical properties and therefore a reduction in the corrosion protection.

During the production of the coating, the cationic and anionic clays can suffer exfoliation, thereby losing their ion-exchange properties. Moreover, the size of these reservoirs is of fundamental importance because their addition into thin films such sol–gel films can, despite their nanometer size, drastically affect the barrier properties of the coating. The ion-exchange materials exhibit good compatibility with the sol–gel matrix but not always with the organic coating. Therefore, its surface can be treated by introducing new chemical groups to increase the compatibility.

In summary, ion-exchange materials have demonstrated great potential in the area of smart coatings; however, some improvements are still required before they can be applied commercially in different coatings and metals.

20.4 Response Based on pH Changes Due to Corrosion Processes

The local pH change in the corrosive area is one of the most important aspects of the corrosion phenomenon. The primary reactions involved in corrosion processes are metallic oxidation at anodic areas and water or oxygen reduction at cathodic areas

generating hydroxyl ions, causing a local alkalization. In contrast, depending on the metal, the hydrolysis of metallic cations can occur, producing an acidic pH in the anodic region [1]. Materials that suffer dissolution or momentary distortion at acid and alkaline pH have been incorporated in coatings to produce smart coatings. Among them, polyelectrolytes have shown interesting results. Such systems are characterized by macromolecules carrying functional groups that are either charged or, under appropriate conditions, can become charged [31]. The polyelectrolyte molecules may be polycations, polyanions, or both, depending on the functional groups present [31, 73].

The permeability of the polyelectrolyte shell depends on pH. Thus, the local pH change on the metallic surface due to the corrosion process induces the opening of nanocontainers in the local area. Consequently, the inhibitor is released and suppresses the corrosion activity, resulting in the healing of the corroded area [74, 75]. When the pH is returned to its initial value, the shell closes and the release of the inhibitor stops [75].

The requirements for the incorporation of polyelectrolyte reservoirs in coatings are compatibility with the material of the protective film to prevent film distortion and a nanometer-scale size to ensure uniform distribution in the coating [75, 76].

In recent years, the layer-by-layer (LbL) technique has been used to regulate the storage/release of the inhibitor in the nanocontainers. The traditional processing method is the deposition of polyelectrolytes of opposite charge from their aqueous or nonaqueous solutions onto the surface of the template [75, 77]. The permeability of the polyelectrolyte multilayers depends on the nature of the polyelectrolytes [78].

The LbL technique has been employed to produce silica containers loaded with corrosion inhibitors. In the initial step [76], a layer of positive polyelectrolyte poly(ethylene imine) (PEI) was deposited on negatively charged silica nanoparticles, followed by a polystyrene sulfonate (PSS) layer, resulting in a negative zeta potential (ξ-potential). In the next step, the adsorption of benzotriazole was accompanied by a positive shift in the ξ-potential. Finally, the PSS/benzotriazole deposition was repeated to increase the inhibitor loading in the final LbL structure. This system (SiO$_2$/PEI/PSS/benzotriazole/PSS) was incorporated into a silica/zirconia sol–gel film and evaluated as a corrosion protection system for AA2024. The scanning vibrating electrode technique (SVET) analyses that were carried out proved the self-healing effect. SVET provided a mapping of the anodic and cathodic current along the metal surface. The authors observed that the cathodic current density induced by the formed defect continuously increases for the sol–gel film without nanocontainers. The behavior of sol–gel film with silica nanocontainers was distinct being that the cathodic activity appears only after 24 h of immersion in chloride solution and in the following 2 h, a decrease in the local current density occurs (Fig. 20.5). This effect was due to the release of benzotriazole and its deposition on the damaged areas, which decreased the corrosion activity. The panels with silica nanocontainers on the hybrid matrix, in which was a previously formed defect, exhibited a recovery of oxide-film resistance after 60 h of immersion. Such behavior was not verified for undoped system; thus, the EIS data reinforced the concept of self-healing.
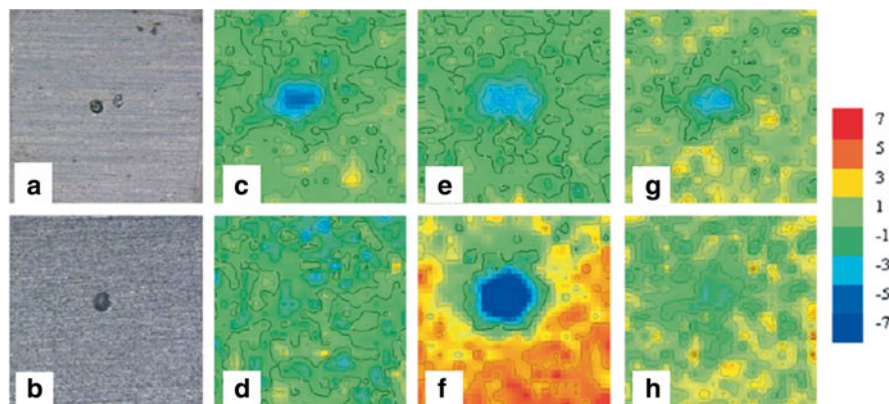
Fig. 20.5 SVET maps of the ionic currents measured above the surface of the artificially defected AA2024, coated with an undoped sol–gel pretreatment film (**a**, **c**, **e**, and **g**) and sol–gel film with SiO$_2$/PEI/PSS/benzotriazole/PSS (**b**, **d**, **f**, and **h**). The maps were obtained 5 (**c** and **d**), 24 (**e** and **f**), and 26 h (**g** and **h**) after defect formation. Scale units: l A cm^{-2}. Scanned area: 2 mm×2 mm. Reprinted with permission from [76]

Another inhibitor, 2-(benzothiazol-2-ylsulfanyl)-succinic acid, was incorporated into SiO$_2$ nanoparticles covered by a PEI/PSS/PEI/PSS layer [74]. The authors verified that the release of the entrapped inhibitor was triggered at pH value of 10.1, which was close to the cathodic zone pH value during the corrosion process of the aluminum alloy [74]. The alkaline pH led to a distortion of the polyelectrolyte layer structure, which generated the release of inhibitor from the nanocontainers. The inhibitor adsorbed on the damaged metallic surface hindered the cathodic and anodic processes. Thus, the pH was returned to a neutral value, which closes the polyelectrolyte shell until another corrosion attack occurs [74–76].

In another study, halloysite was embedded in a polyelectrolyte layer and evaluated as a nanocontainer. Halloysite (Al$_2$Si$_2$O$_5$(OH)$_4$×nH$_2$O) is a two-layer aluminosilicate with a predominant hollow tubular structure [79, 80] that allows for loading with cationic compounds [31]. Shchukin et al. [80] produced sol–gel films with halloysite nanotubes loaded with 2-mercaptobenzotriazole to investigate their effect on the corrosion behavior of AA2024. Approximately 32 % of the inhibitor was released from halloysite nanotubes without a polyelectrolyte shell after 10 days of storage in neutral water. For the halloysite containing 2-mercaptobenzotriazole modified by the LbL deposition of polystyrene sulfonate/polyallylamine hydrochloride bilayers, the release was triggered at pH 10, similar to the pH value that occurs in the localized corrosion process. Using EIS measurements, the authors have shown that the coatings with modified halloysites afford better barrier properties of the sol–gel matrix and higher low-frequency impedance compared with the undoped coating.

The loading capacity for silica and halloysite nanocontainers is approximately 5 wt% (i.e., not high enough to ensure long-term protection against corrosion) [81, 82]. To increase the loading capacity, coatings were formed by the consecutive

deposition of polyelectrolyte and inhibitor layers [82, 83]. Delamination was observed with direct deposition of polyelectrolyte (PEI and PSS) layers with entrapped 8-hydroxyquinoline on an AA2024 surface. When that system was applied on top of a sol–gel coating, good adherence was achieved. Furthermore, the resistances associated with sol–gel films, oxide layer, and charge transfer processes were enhanced compared with sol–gel samples and sol–gel films containing 8-hydroxyquinoline [82].

Another approach for the production of a feedback coating is inhibitor encapsulation via oil-in-water emulsification [81, 84]. Polymers based on acrylate derivatives have been proposed for encapsulating triethanolamine [84] and 8-hydroxyquinoline [81] using this approach. Nanometric polymer capsules loaded with triethanolamine obtained by sequential emulsion polymerization were added to polyurethane resin. The release of triethanolamine from these capsules was faster in both low and high pH media than in a neutral environment, which enabled the corrosion inhibition of steel [84]. On the other hand, the encapsulation of 8-hydroxyquinoline with a cationic polymer based on dimethylaminoethyl methacrylate and other neutral methacrylic acid esters generated pH-sensitive particles whose release was more pronounced in acidic media [81]. The healing effect of an epoxy coating loaded with the pH-sensitive particles modified on AA2024 was confirmed by localized EIS (Fig. 20.6). The normalized average admittance at the center of the defects formed on the coatings increased with the immersion time for AA2024 coated with a water-based epoxy coating. However, the behavior of the same coating with the encapsulated 8-hydroxyquinoline was the opposite due to the release of the inhibitor as a consequence of pH acidification [81].

In addition to polyelectrolytes, other materials may be stimulated by changes in pH, namely, hydroxyapatite [85], halloysite [86], hollow mesoporous zirconia nanospheres [87], hollow mesoporous silica particles combined with supramolecular complexes [88], TiO_2–casein [89], and $CaCO_3$ microbeads [90].

The storage/release of the inhibitor employing the LbL deposition approach is an attractive method for the production of smart self-healing anticorrosion coatings. The early stages of corrosion are combatted by release of the corrosion inhibitor, which in turn is regulated by the permeability of polyelectrolyte assemblies based on local pH changes due to the initial cathodic and anodic corrosion processes. Nevertheless, this method encompasses complex technologies whose industrial implementation would be highly demanding and is therefore still restricted to the lab scale.

20.5 Other Trigger Mechanisms

In recent years, studies exploring the concept of self-repairing with other materials have also been reported.

In conductive polymer coatings, the galvanic coupling between the metal and the coating is the driving force for releasing the dopant, which acts as an inhibitor [91, 92]. For instance, Kendig et al. [92] verified that anion-doped polyaniline films inhibited
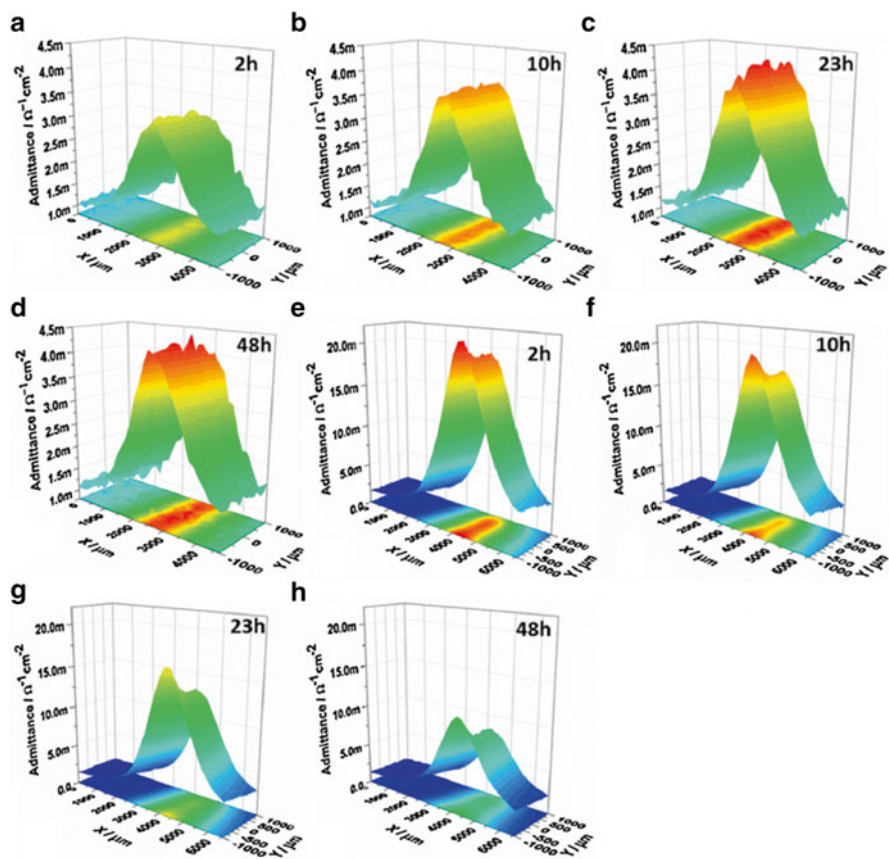
Fig. 20.6 LEIS maps of AA2024 coated with reference coating (**a–d**) and coating containing encapsulated 8-hydroxyquinoline using a cationic polymer (**e–h**). The maps were obtained over an artificial defect. Reprinted with permission from [81]

the corrosion of AA2024 at a scratch due to the release of the dopant. According to the authors, when the coating was fractured, the oxidized PANI film containing inhibiting anions (the dopant) became a cathode and the metal scratch an anode. The anodic corrosion reaction drives the reduction of the film and consequently the release of the inhibiting anions.

A new mechanism based on the laser-driven release of inhibitors from loaded materials was reported in 2009 for AA2024 coated with zirconia–organosilica films [93]. A polyelectrolyte shell with noble metal particles was applied on mesoporous titania and silica particles loaded with benzotriazole via LbL assembly and added into a zirconia–organosilica matrix. The polyelectrolyte multilayer shell was modified with silver nanoparticles, which act as absorption centers for energy supplied by the laser beam. These absorption centers cause local heating that locally disrupts the polymer shells, inducing the release of benzotriazole stored in the container.
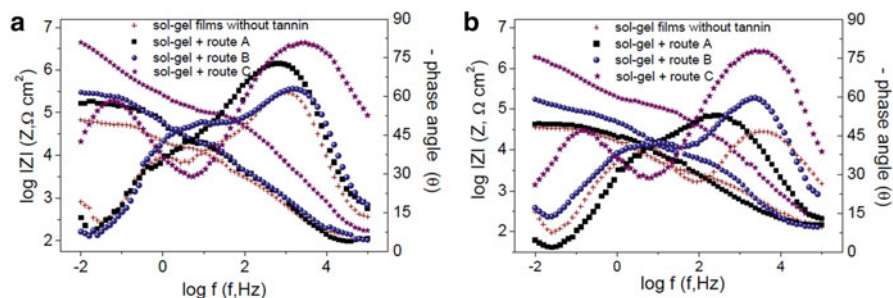
Fig. 20.7 Bode diagrams of AA2024 coated with undoped MTMS/TEOS and MTMS/TEOS doped with tannin encapsulated via acid and alkaline sol–gel routes after 24 h and 168 h of immersion in 0.05 mol L⁻¹ NaCl

Oxide nanoparticles [94–96], nanostructured porous oxide layer [97], and β-cyclodextrin-inhibitor complexes [98, 99] have been explored as prospective reservoirs for corrosion inhibitors. The general mechanism can be explained as slow release of the inhibitor from containers and the self-healing of corrosion defects.

The development of spectroscopic sensors based on color changes and fluorescence has been reported in several works, the aim of which is to indicate the early stage of the corrosion process [100–103]. In these attempts, pH-sensitive compounds such as bromothymol blue [100] and phenolphthalein [100, 101] were incorporated into the coatings. Due to pH increase at cathodic areas during the corrosion process, such compounds change color. Another corrosion-sensing approach utilizes the interaction between a smart indicator and metal ions produced by metal oxidation, leading to fluorescence in these areas [103].

Evaluation of the corrosion behavior of AA2024 coated with methyltrimethoxysilane (MTMS) and tetraethyl orthosilicate (TEOS) sol–gel films containing or not containing encapsulated tannin was completed. The results showed that, with the direct incorporation of tannin in the sol–gel films, the lixiviation occurs, leading to similar corrosion behavior to that which was observed for panels coated only with sol–gel matrix. The EIS data of aluminum alloy coated with sol–gel films containing tannin encapsulated by different sol–gel routes after 24 h and 168 h of immersion in 0.05 mol L⁻¹ are depicted in Fig. 20.7. The Bode diagrams are characterized by the presence of two time constants of approximately $10^{3.5}$ and $10^{0.5}$ Hz, which are related to the silica layer on the metallic surface and the interfacial layer composed of aluminum oxide and metalosiloxane bonds, respectively. The results indicated that the sol–gel route employed to encapsulate the tannin compounds had a fundamental role in the corrosion behavior of samples. The overall impedances for films containing encapsulated tannin were higher than those of samples coated only with MTMS/TEOS films. Nevertheless, route C provided the best corrosion protection performance due to the more controlled release of tannin. The obtained results are very promising, and this system may constitute a new approach for providing long-term corrosion protection.

20.6   Conclusion

Intense academic research concerning smart coatings for corrosion protection has been developed with a primary focus on self-healing coatings, which enable the release of a corrosion inhibitor or healing agent in a controlled manner. A variety of stimuli can induce the release of active agents, such as corrosion, which cause local pH changes, characteristics of the medium that lead to ion-exchange reactions, and the formation of cracks in degraded coatings due to UV exposure, temperature, or mechanical stress. Smart coatings undoubtedly possess interesting benefits for prolonging the lifetime of coatings. Nevertheless, its limitations are clear and dependent on the characteristics of the nanocontainer, namely, a small loading capacity, release kinetics that are not completely understood, reduction of the coating's physical properties, and effective cost/performance. Due to these drawbacks, further research and improvement of smart coatings is still required and remains a technological gap that must be closed prior to wide industrial implementation. The performance of smart coatings depends on the coating matrix, employed metal, and type of nanocontainers (i.e., its mechanism of action). Perhaps, the combination of nanocontainers with different mechanisms of action will emerge as a more effective device for decreasing the corrosion rates of metals.

References

1. Bard AJ, Stratmann M, Frankel GS (2006) Encyclopedia of electrochemistry: corrosion and oxide films, 5th edn. Wiley VCH, Weinheim
2. Brett CMA, Breet AMO (1993) Electrochemistry principles, methods and applications, 1st edn. Oxford University Press, New York, NY
3. Buchheit RG, Grant RP, Hlava PF, Mckenzie B, Zender GL (1997) J Electrochem Soc 144:2621–2628
4. Ilevbare GO, Schneider O, Kelly RG, Scully JR (2004) J Electrochem Soc 151:B453–B464
5. Schmutz P, Frankel GS (1998) J Electrochem Soc 145:2296–2306
6. Hughes AE, Boag A, Glenn AM, McCulloch D, Muster TH, Ryan C, Luo C, Zhou X, Thompson GE (2011) Corros Sci 53:27–39
7. Glenn AM, Muster TH, Luo C, Zhou X, Thompson GE (2011) Corros Sci 53:40–50
8. Hays GF (2013) Now is the time. World Corrosion Organisation. http://www.corrosion.org/. Accessed 2 Apr 2015
9. Bierwagen G (2008) J Coat Technol Res 5:133–155
10. Campestrini P, Terryn H, Hovestad A, de Wit JHW (2004) Surf Coat Technol 176:365–381
11. Maege I, Jaehne E, Henke A, Adler H-JP, Bram C, Jung C, Stratmann M (1998) Prog Org Coat 34:1–12
12. Rizzi M, Trueba M, Trasatti SP (2011) Synth Met 161:23–31
13. Dalmoro V, dos Santos JHZ, Alemán C, Azambuja DS (2015) Corros Sci 92:200–208
14. Van Schaftinghen T, Le Pen C, Terryn H, Hörzenberger F (2004) Electrochim Acta 49:2997–3004
15. Wang D, Bierwagen GP (2009) Prog Org Coat 64:327–338
16. Dalmoro V, dos Santos JHZ, Armelin E, Alemán C, Azambuja DS (2014) J Colloid Interface Sci 426:308–313

17. Zhu D, van Ooij WJ (2004) Electrochim Acta 49:1113–1125
18. Naderi R, Fedel M, Deflorian F, Poelman M, Olivier M (2013) Surf Coat Technol 224:93–100
19. Dalmoro V, dos Santos JHZ, Armelin E, Aleman C, Azambuja DS (2012) Corros Sci 60:173–180
20. Poznyak SK, Tedim J, Rodrigues LM, Salak AN, Zheludkevich ML, Dick LFP, Ferreira MGS (2009) ACS Appl Mater Interfaces 1:2353–2362
21. Zheludkevich ML, Tedim J, Ferreira MGS (2012) Electrochim Acta 82:314–323
22. Wei H, Wang Y, Guo J, Shen NZ, Jiang D, Zhang X, Yan X, Zhu J, Wang Q, Shao L, Lin H, Wei S, Guo Z (2015) J Mater Chem A 3:469–480
23. Tamborim SM, Maisonnave APZ, Azambuja DS, Englert GE (2008) Surf Coat Technol 202:5991–6001
24. Zheludkevich ML, Serra R, Montemor MF, Yasakau KA, Salvado IMM, Ferreira MGS (2005) Electrochim Acta 51:208–217
25. Truc TA, Hang TTX, Oanh VK, Dantras E, Lacabanne C, Oquab D, Pébère N (2008) Surf Coat Technol 202:4945–4951
26. Montemor MF (2014) Surf Coat Technol 258:17–37
27. Murphy EB, Wudl F (2010) Prog Polym Sci 35:223–251
28. García SJ, Fischer HR, van der Zwaag S (2011) Prog Org Coat 72:211–221
29. Luo X, Mather PT (2013) ACS Macro Lett 2:152–156
30. Samadzadeh M, Hatami Boura S, Peikari M, Kasiriha SM, Ashrafi A (2010) Prog Org Coat 68:159–164
31. Andreeva DV, Shchukin DG (2008) Mater Today 11:24–30
32. Shchukin DG (2013) Polym Chem 4:4871–4877
33. Yang Z, Wei Z, Le-Ping L, Si-Jie W, Wu-Jun L (2012) Appl Surf Sci 258:1915–1918
34. Zhang Z, Hu Y, Liu Z, Guo T (2012) Polymer 53:2979–2990
35. White SR, Sottos NR, Geubelle PH, Moore JS, Kessler MR, Sriram SR, Brown EN, Viswanathan S (2001) Nature 409:794–797
36. Hatami Boura S, Peikari M, Ashrafi A, Samadzadeh M (2012) Prog Org Coat 75:292–300
37. García SJ, Fischer HR, White PA, Mardeld J, González-García Y, Mole JMC, Hughes AE (2011) Prog Org Coat 70:142–149
38. Samadzadeh M, Hatami Boura S, Peikari M, Ashrafi A, Kasiriha M (2011) Prog Org Coat 70:383–387
39. Nesterova T, Dam-Johansen K, Pedersen LT, Kiil S (2012) Prog Org Coat 75:309–318
40. Selvakumar N, Jeyasubramanian K, Sharmila R (2012) Prog Org Coat 74:461–469
41. Nesterova T, Dam-Johansen K, Kiil S (2011) Prog Org Coat 70:342–352
42. Liu J, Zhang Y, Yu M, Li S, Xue B, Yin X (2015) Prog Org Coat 81:93–100
43. Xuan Hang TT, Truc TA, Duong NT, Pébère N, Olivier M-G (2012) Prog Org Coat 74:343–348
44. Salak AN, Tedim J, Kuznetsova AI, Vieira LG, Ribeiro JL, Zheludkevich ML, Ferreira MGS (2013) J Phys Chem C 117:4152–4157
45. Williams G, McMurray HN (2003) Electrochem Solid State Lett 6:B9–B11
46. Posati T, Costantino F, Latterini L, Nocchetti M, Paolantoni M, Tarpani L (2012) Inorg Chem 51:13229–13236
47. Stimpfling T, Leroux F, Hintze-Bruening H (2013) Appl Clay Sci 83–84:32–41
48. Zheludkevich ML, Poznyak SK, Rodrigues LM, Raps D, Hack T, Dick LF, Nunes T, Ferreira MGS (2010) Corros Sci 52:602–611
49. Stimpfling T, Leroux F, Hintze-Bruenin H (2014) Colloids Surf A 458:147–154
50. Yu X, Wang J, Zhang M, Yang L, Li J, Yang P, Cao D (2008) Surf Coat Technol 203:250–255
51. Tedim J, Kuznetsova A, Salak AN, Montemor F, Snihirova D, Pilz M, Zheludkevich ML, Ferreira MGS (2012) Corros Sci 55:1–4
52. Li D, Wang F, Yu X, Wang J, Liu Q, Yang P, He Y, Wang Y, Zhang M (2011) Prog Org Coat 71:302–309

53. Wang H, Presuel F, Kelly RG (2004) Electrochim Acta 49:239–255
54. Williams G, McMurray HN (2004) Electrochem Solid State Lett 7:B13–B15
55. Dong Y, Wang F, Zhou Q (2014) J Coat Technol Res 11:793–803
56. Wong F, Buchheit RG (2004) Prog Org Coat 51:91–102
57. Zeng R-C, Liu Z-G, Zhang F, Li S-Q, Cui H-Z, Han E-H (2014) J Mater Chem A 2:13049–13057
58. Chen J, Song Y, Shan D, Han E-H (2013) Corros Sci 74:130–138
59. Chen J, Song Y, Shan D, Han E-H (2012) Corros Sci 65:268–277
60. Williams G, McMurray HN, Loveridge MJ (2010) Electrochim Acta 55:1740–1748
61. Motte C, Poelman M, Roobroeck A, Fedel M, Deflorian F (2012) Prog Org Coat 74:326–333
62. Hang TTX, Truc TA, Nam TH, Oanh VK, Jorcin J-B, Pébère N (2007) Surf Coat Technol 201:7408–7415
63. Hang TTX, Truc TA, Olivier M-G, Vandermiers C, Guerit N, Pebere Prog N (2010) Org Coat 69:410–416
64. Bohm S, McMurray HN, Powell SM, Worsley DA (2001) Mater Corros 52:896–903
65. McMurray HN, Williams D, Williams G, Worsley D (2003) Corros Eng Sci Technol 38:112–118
66. Deyá C, Romagnoli R, del Amo B (2007) J Coat Technol Res 4:167–175
67. Deyá MC, del Amo B, Spinelli E, Romagnoli R (2013) Prog Org Coat 6:525–532
68. Pokhmurskii VI, Zin IM, Bily LM, Vynar VA, Zin YI (2013) Surf Interface Anal 45:1474–1478
69. Dias SAS, Lamaka SV, Nogueira CA, Diamantino TC, Ferreira MGS (2012) Corros Sci 62:153–162
70. Dias SAS, Marques A, Lamaka SV, Simões A, Diamantino TC, Ferreira MGS (2013) Electrochim Acta 112:549–556
71. Schoonheydt RA, Geerlings P, Pidko EA, van Santen RA (2012) J Mater Chem 22:18705–18717
72. Kang Y, Emdadi L, Lee MJ, Liu D, Mi B (2014) Environ Sci Technol Lett 1:504–509
73. Shiratori SS, Rubner MF (2000) Macromolecules 33:4213–4219
74. Skorb EV, Fix D, Andreeva DV, Möhwald H, Shchukin DG (2009) Adv Funct Mater 19:2373–2379
75. Zheludkevich ML, Shchukin DG, Yasakau KA, Möhwald H, Ferreira MGS (2007) Chem Mater 19:402–411
76. Shchukin DG, Zheludkevich M, Yasakau K, Lamaka S, Ferreira MGS, Möhwald H (2006) Adv Mater 18:1672–1678
77. DeLongchamp DM, Hammond PT (2003) Chem Mater 15:1165–1173
78. Shchukin DG, Möhwald H (2007) Adv Funct Mater 17:1451–1458
79. Lvov YM, Shchukin DG, Möhwald H, Price RR (2008) ACS Nano 2:814–820
80. Shchukin DG, Lamaka SV, Yasakau KA, Zheludkevich ML, Ferreira MGS, Möhwald H (2008) J Phys Chem C 112:958–964
81. Snihirova D, Lamaka SV, Cardoso MM, Condeço JAD, Ferreira HECS, Montemor MF (2014) Electrochim Acta 145:123–131
82. Lamaka SV, Shchukin DG, Andreeva DV, Zheludkevich ML, Möhwald H, Ferreira MGS (2008) Adv Funct Mater 18:3137–3147
83. Andreeva DV, Skorb EV, Shchukin DG (2010) ACS Appl Mater Interfaces 2:1954–1962
84. Choi H, Song YK, Kim KY, Park JM (2012) Surf Coat Technol 206:2354–2362
85. Snihirova D, Lamaka SV, Taryba M, Salak AN, Kallip S, Zheludkevich ML, Ferreira MGS, Montemor MF (2010) ACS Appl Mater Interfaces 2:3011–3022
86. Fix D, Andreeva DV, Lvov YM, Shchukin DG, Möhwald H (2009) Adv Funct Mater 19:1720–1727
87. Wang MD, Liu MY, Fu JJ (2015) J Mater Chem A 3:6423–6431
88. Fu JJ, Chen T, Wang MD, Yang NW, Li SN, Wang Y, Liu XD (2013) ACS Nano 7:11397–11408

89. Yabuki A, Sakai M (2011) Corros Sci 53:829–833
90. Snihirova D, Lamaka SV, Montemor MF (2012) Electrochim Acta 83:439–447
91. Arefinia R, Shojaei A, Shariatpanahi H, Neshati J (2012) Prog Org Coat 75:502–508
92. Kendig M, Hon M, Warren L (2003) Prog Org Coat 47:183–189
93. Skorb EV, Skirtach AG, Sviridov DV, Shchukin DG, Möhwald H (2009) ACS Nano 3:1753–1760
94. Kartsonakis I, Daniilidis I, Kordas G (2008) J Sol-Gel Sci Technol 48:24–31
95. Mekeridis ED, Kartsonakis IA, Pappas GS, Kordas GC (2011) J Nanopart Res 13:541–554
96. Kartsonakis IA, Kordas G (2010) J Am Ceram Soc 93:65–73
97. Lamaka SV, Zheludkevich ML, Yasakau KA, Serra R, Poznyak SK, Ferreira MGS (2007) Prog Org Coat 58:127–135
98. Khramov AN, Voevodin NN, Balbyshev VN, Donley MS (2004) Thin Solid Films 447–448:549–557
99. Khramov AN, Voevodin NN, Balbyshev VN, Mantz RA (2005) Thin Solid Films 483:191–196
100. Zhang J, Frankel GS (1999) Corrosion 55:957–967
101. Maia F, Tedim J, Bastos AC, Ferreira MGS, Zheludkevich ML (2014) RSC Adv 4:17780–17786
102. Augustyniak A, Ming W (2011) Prog Org Coat 71:406–412
103. Augustyniak A, Tsavalas J, Ming W (2009) ACS Appl Mater Interfaces 1:2618–2623

Chapter 21
Smart Textile Supercapacitors Coated with Conducting Polymers for Energy Storage Applications

Nedal Y. Abu-Thabit and Abdel Salam Hamdy Makhlouf

Abstract Over the last few years, the development of nanotechnology has resulted in generation of new materials and innovation for a wide range of applications and products. Among these applications, textile industry is expected to hold a considerable potential for the development of advanced nano-based materials. For example, nanotechnology enabled the production of novel smart "multifunctional" textiles with combined properties in one fabric. Conductive textiles represent a key class of smart textiles with promising future's applications in areas such as electronic textiles, display devices, health monitoring devices, thermal and moisture management, flexible energy storage, and power generation devices. Recently, a remarkable attention has been devoted to the development of textile supercapacitor for energy storage and wearable electronics applications. Supercapacitor textiles offer advantages such as lightweight, flexibility, stretchability, and ease of integration with electronic textiles. Different approaches have been investigated for fabrication of smart conductive textiles for supercapacitor applications. Among these approaches, textiles coated with electrically conducting polymers (ECPs) are one of the most promising and facile approaches for fabrication of textile supercapacitors. ECP-coated textiles are characterized with high specific capacitance through fast redox reaction ease of integration into planar, flexible, and stretchable textile substrates with various shapes and large areas, thin film fabrication with controlled nanostructured morphology, and applicability for fabrication of composite and asymmetric textile supercapacitors. This chapter highlights the recent advances and developments in the fabrication of ECP-based textile supercapacitors, including different

N.Y. Abu-Thabit
Department of Chemical and Process Engineering Technology, Jubail Industrial College,
PO Box 10099, Jubail Industrial City 31961, Kingdom of Saudi Arabia

A.S.H. Makhlouf (✉)
Manufacturing and Industrial Engineering Department, College of Engineering and Computer Science, The University of Texas – Rio Grande Valley, 1201 West University Drive, Edinburg, TX 78539-2999, USA
e-mail: abdel.makhlouf@utrgv.edu

types of pure ECPs and their composites with other conducting materials for preparation of hybrid supercapacitors with superior performance for textile supercapacitor applications.

Keywords Supercapacitor textiles • Supercapacitor fibers • Smart textile • Conducting polymers • Conductive textiles

21.1 Introduction

21.1.1 Smart Textiles

Smart textiles are defined as textile products such as fibers, filaments, and yarns together with woven, knitted, or nonwoven structures, which can interact with the environment/user [1]. Smart textiles are attracting a great interest due to their versatile functionalities and capabilities of sensing, actuating, responding to external stimuli, communicating, power generation, and storage, whereby health monitoring, safety, and protection can be endorsed. Indeed, increasing competition in the textile industry has been observed after the introduction of the concepts "smart textiles" and "ultrasmart textiles." During the period between 1995 and 2011, the global growth of technical textiles market was estimated to be 133 billion USD [2]. This extraordinary growth is attributed to the recent development and integrated expertise on nanotechnologies, material science, electronics, and manufacturing processes. As depicted in Fig. 21.1, smart textiles have been utilized for a wide range of applications including stimuli-responsive textiles [3, 4], antibacterial textiles [5, 6], flame retardant textiles [7–10], shape-memory textiles [11–13], textiles for engineered membranes [14], personal thermal management textiles [15], moisture management textiles [16–18], self-cleaning textiles [19–22], and smart conductive textiles [23, 24].

21.1.2 Smart Conductive Textiles

As can be inferred from Fig. 21.1, smart conductive textiles represent an important class of smart functional textiles due to their wide range of possible applications and technologies including luminescent textiles [25–27], photovoltaic devices and dye-sensitized solar cells [28–31], Li-ion batteries [32–37], supercapacitors [38–45], transistors [46–49], sensors [50–53], biosensor [54–56], display devices [57–59], water purification [60–65], and personal thermal management [66, 67]. The key requirement for successful use of smart conductive textiles in each of the above-listed applications depends on their electrical conductivity.
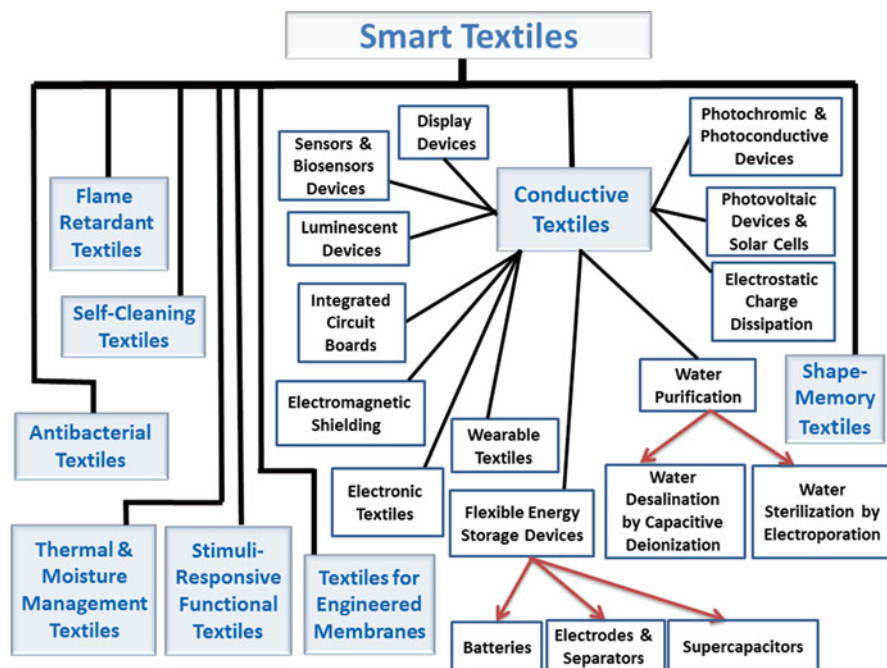
Fig. 21.1 Applications of smart textiles

According to their electrical conductivity, textiles can be classified into conductive and nonconductive categories. Conductive textiles are those textiles which exhibit inherent electrical conductivity such as metal-based textiles (mainly knitted wire meshes) and carbon-based textiles, whereas the nonconductive textiles include natural and synthetic polymeric fibers and textiles. Metal textiles have high electrical conductivities and lack important features such as flexibility, stretchability, lightweight per unit area, and resistance to atmospheric oxidation. The aforementioned missing features are inconsistent with the materials and geometries that are required for conductive textiles, because the incorporation of metal wires within textiles increases stiffness and reduces elasticity [1]. Therefore, metal-based textiles are expected to have limited applications and uses in areas such as wearable electronic textiles ("e-textiles") and flexible textiles for energy and environmental applications.

The most used and commercialized carbon-based textiles are made from graphitic carbon and are known as carbon cloth (CC) [68, 69]. Compared to metals, carbon-based conductive textiles offer features such as flexibility and stability with respect to atmospheric oxidation.

Textiles made from natural or synthetic polymer fibers are prepared by using different technologies such as gel spinning, melt spinning, wet spinning, dry spinning, and electrospinning techniques. Natural and synthetic polymeric fibers offer

advantages such as a wide range of selection, low cost, flexibility, stretchability, durability, lightweight, porosity, good tensile and elastic properties, good moisture management, and thermal management properties. However, natural and synthetic fibers/textiles are nonconductive and do not allow for the flow of electricity through their structure. The insulation feature of these textiles can be recognized from the electrical properties of the corresponding neat polymers that exhibit high electrical resistivity values and low dielectric constants [70, 71]. The inability of nonconductive textiles to transport electrical current is accompanied by their ability to generate static electricity that allows electrical charges to remain fixed on the textiles' surface. The stored static electricity can cause problems during textile processing and end-user applications due to the electrostatic discharge. The introduction of conductive textile materials provides a solution to the aforementioned problem through transport and dissipation of the electrical charges.

Conductive textile can be made directly by converting a nonconductive woven/nonwoven textile into a conductive one or indirectly by using different conductive fibers and converting them into conductive textiles through a knitting or weaving process. A general overview for various direct and indirect techniques used for preparation of conductive textiles will be highlighted in Sect. 21.2.

21.1.3 Smart Conductive Textiles for Energy Applications

Recently, the interest in smart electronic textiles for medical, sports, military, and energy applications has increased markedly [1, 72]. Electronic textiles offer advantages such as low cost, lightweight, stretchability, and flexibility to be integrated into variously shaped structures that would otherwise be impossible with traditional electronics technology. Currently, most wearable e-textiles are made by the attachment of electronic devices onto the textile surface [1]. However, such detachable devices still need to be flexible. This limitation can be overcome by the direct fabrication of devices into the textile/fabric. The rough surface of textiles makes this task extremely challenging for fabrication of many electronic devices [73]. Regardless, the large surface roughness property of textiles is preferred by other energy devices such as supercapacitors and Li-ion batteries [73]. In such devices, the surface roughness and porosity of the conductive textile electrodes provide an ideal situation for manipulation of ion movements between two sides of the fabricated device.

This chapter provides a brief description of various methods for preparation of conductive textiles (Sect. 21.2), including the use of metals, carbons, electrically conducting polymers (ECPs), and other recent proposed technologies for preparation of functional conductive textiles. Section 21.3 provides a general background on electrochemical supercapacitors as an emerging technology for energy storage devices. Section 21.4 highlights the recent advances in the utilization of ECPs for preparation and fabrication of flexible supercapacitor textiles for various applications.

21.2 Preparation of Conductive Textiles

21.2.1 Coated Conductive Fibers and Textiles

Electrically conductive fibers and textiles can be produced by coating the fibers with conductive materials such as metals, metallic salts, metal oxides, or ECPs. Coatings can be applied to the surface of fibers, yarns, or even fabrics to create electrically conductive textiles. The main textile coating methods include electroless plating, chemical vapor deposition (CVD), atomic layer deposition (ALD), and sputtering as well as coating with ECPs and conductive inks.

21.2.1.1 Sputtering

Sputtering is an established technique that enables the use of a variety of metals, polymers, metal oxides, or mixtures thereof. However, the sputtering process for functionalization of textiles is expensive and usually performed on the side facing the target which prevents the deposition of the functional coating onto the inner layers of thick textile materials [74]. In sputtering process, a good adhesion between the sputter-coated layer and the fibers can be obtained by increasing the thickness of the deposited layers which may be critical for the final use and application in cases such as that of wearable electronic textiles [74].

21.2.1.2 Evaporative Deposition Techniques

Evaporative deposition techniques, such as CVD and ALD, offer a practical way for preparation of textiles with conductive functionality [74]. However, these techniques are expensive when scaling-up the technology and require the use of relatively high temperatures which may not be suitable for the commodity textiles used in daily life applications [74]. The thickness of the deposited film is very critical for the adhesion of the deposited conductive film. Higher thicknesses are susceptible to cracking and lower thicknesses may not provide uniform conductivity [75]. One of the challenges in case of the ALD technique is the chemistry and requirements of the employed precursors. For example, the precursors must chemisorb onto the substrate to be coated, and they must have a reasonably high vapor pressure to allow saturation of the chamber volume upon dosing [76]. The precursors must have a good thermal stability so as to avoid decomposition in the subsequent steps [76].

21.2.1.3 Electroless Plating Technique

Electroless plating technique is the simplest one and does not require electrical energy. However, the electroless plating process is carried out under high- or low-pH conditions which impose a deterioration effect on the treated fibers and textiles [74].

The presence of impurities during the electroless plating process can cause pitting and reduced ductility, adhesion, and roughness [74]. The adhesion of the metal particles exhibits a moderate strength on the surface of the fabric which may be peeled off when the plated metal is exposed to the air. The whole process of electroless plating is a multistage process which requires the use of complex chemicals and generates a lot of chemical waste.

21.2.1.4 Electrically Conducting Polymer Coatings

Coatings offer advantages such as their suitability for different synthetic and natural fibers as well as good electrical conductivity without significantly altering existing key substrate properties such as density, flexibility, and handling. However, in case of metal coatings discussed above, the adhesion between the metal and the coated fibers/textiles as well as corrosion resistance are challenging for the final use and application.

ECPs offer an alternative approach for coating various types of textiles, fibers, and fabrics. The coating process is simple and fast and does not require complicated or long procedures. The coating of ECPs is cost-effective; does not have restrictions related to substrate shape, type, surface chemistry (i.e., hydrophobic/hydrophilic), and fiber type (i.e., woven/nonwoven); and can be done at temperatures less than or equal to room temperature. Compared to the evaporative deposition techniques, the coating process of ECPs covers all the internal microfibrils of the coated fibers/textile. This advantage ensures the homogeneity of the whole coating and provides a more uniform coating which is critical for its performance during the end-use applications. The mechanical properties and physical appearance of the ECP-coated fibers and textiles are not affected, and they are not susceptible to cracking like metal and metal oxide coatings. Hence, the flexibility and integrity of the coated fibers and textiles are not affected by physical forces such as bending and stretching. Although the conductivity of the ECP coatings is much less than that of metal coatings, the conductivity of the ECP-coated textiles can be controlled and tailored by controlling parameters such as concentrations of monomers, temperature, doping agents, and the nanostructured morphology of the ECPs (e.g., arrays of nanowires) [77]. All the abovementioned advantages of ECP coatings make them suitable candidates for the preparation of functional smart conductive textiles for various applications and device fabrication.

ECPs can be prepared mainly by two methods, electrochemical polymerization and oxidative chemical polymerization (OCP) [78]. However, electrochemical polymerization can be used only for coating conductive substrates such as carbon-based materials and metals [79, 80]. Also, electrochemical polymerization is not suitable for the bulk production of conductive polymers and is not suitable for controlled preparation of films with thicknesses above 100 μm. However, the electrochemical polymerization methodology can be employed using different scan rates for obtaining ECPs with different nanostructured morphologies [81, 82]. On the other hand, the OCP, which is often called redox polymerization, is more versatile and can be used for both conductive and nonconductive substrates, which makes it a good choice for the preparation of a wide range of conductive textiles. OCP offers

the advantage of controlling the morphology of the nanostructured conductive coating by adjusting the nucleation and growth chemistry during the chemical polymerization process [77, 83]. Since the ECPs are polyelectrolytes, textiles can be coated with ECP polyelectrolytes through the layer-by-layer coating methodology [84, 85]. In addition, ECPs can be prepared by using an interfacial polymerization technique which is very useful for deposition of thin film coatings with controlled nanofiber morphology [86–88]. ECPs with a nanofiber morphology can be obtained by approaches such as the use of template polymerization [82, 89–92], templateless polymerization [93], seeding polymerization [94], oligomer-assisted polymerization [95], dilute polymerization [96, 97], and surfactant-assisted polymerization [98] and using different oxidants such as vanadic acid [99] and silver nitrate [61]. Similarly, ECPs with nanowire morphology can be obtained by using template or templateless polymerization methods [77]. In addition to chemical and electrochemical polymerization, ECPs can be incorporated into various textiles by the vapor phase polymerization (VPP) technique [40, 100–102].

21.2.2 Conductive Ink Coatings

Compared to metal coatings, the use of conductive Nanoink, such as carbon nanotubes and graphene, allows for retaining the porous structure of the textile without blocking the external surface of treated textiles [73]. Conductive inks can be used for preparation of conductive textiles and fibers by one the following methods.

21.2.2.1 Dip-Dry Coating

Dip-dry coating is a very simple and quick method that can be applied to different types of textiles and fibers. The target textile must possess a good porosity to absorb the maximum amount of the ink solution. Cotton-based conductive textiles, which are highly porous and hydrophobic, are easily prepared by the dipping-drying procedure. The ink is prepared from a dispersion containing the conductive ingredient (e.g., carbon nanotubes, graphene oxide, graphene, graphite, or carbon black) with dispersing agent or surfactant and the usual solvent used is water. The conductivity of the textile substrate depends on the number of dipping cycles. The final step requires washing out the employed dispersing surfactant to maintain the maximum conductivity and to clean up the coated substrate.

21.2.2.2 Inkjet Printing

Direct printing with an inkjet printer is a material-saving, high-speed, and low-cost process. The inkjet printing process is more challenging than simple conformal coating with dispersible ink. Different types of conductive inks can be used including colloidal suspensions of nanoparticles [103], organometallic compounds in solution

[104], conductive polymer dispersions [105–107], carbon nanotube dispersions [108–110], graphene [107, 111–113], and graphene oxide [114] dispersions. Regardless of the type of ink employed, the inks should satisfy the following requirements to be used for conductive inkjet printing [1, 113, 115, 116]:

- High electrical conductivity.
- Stability toward oxidation in air (e.g., silver and gold are stable; copper and nickel are easily oxidized in air).
- Dry out without clogging the nozzle during printing.
- Good adhesion to the substrate.
- Ink shall not agglomerate and clog the nozzles (stable dispersion).
- Solvent properties (nontoxic solvent, solvent with reasonable viscosity at room temperature).
- Solvent must readily evaporate once deposited but not so fast that it dries out at the nozzle when idle, causing nozzle clogging.
- Fluid properties of the formulated ink such as viscosity, density, and surface tension.

21.2.2.3 Reactive Inkjet Printing

An alternative way to fabricate conductive textiles and fibers using inkjet printing involves the deposition of two inks, which react to form the conductive material [115]. The main advantage of this reactive inkjet printing technique is that it allows different materials to be selectively produced or removed [115]. For example, Li et al. [117] have utilized the reactive inkjet printing methodology for the preparation of copper conductive ink. The reactive ink solution was prepared from a copper citrate solution acting as a metal precursor and a sodium borohydride solution acting as a reducing agent. Recently, Walker and Lewis employed the reactive ink technique for the preparation of silver ink with high conductivity similar to that of bulk silver [116]. The preparation procedure was simple and based on the modified Tollens' process [116].

21.2.2.4 Screen Printing

Screen printing is useful for fabricating electrics and electronics due to its ability to produce patterned, thick layers from paste-like conducting materials. The screen printing technique, a stencil process, includes the printing of a viscous paste through a patterned fabric screen which is then followed by a drying step. However, screen printing using thick conductive ink pastes for the production of conductive textiles has not been thoroughly investigated or employed due to it being both labor and capital intensive and may cause production delays when designs are modified or changed over [118]. Recently, Kazani et al. [119] employed silver ink paste for screen printing on different conductive woven textile substrates including cotton, polyester, polyamide, and viscose. It was found that the square resistance of the

printed samples remained high enough even after the washing process. After 20 washes, the printed conductive layer that was covered by a protective polyurethane (PU) thin layer was stable compared with the uncovered samples which showed cracks and peeling of the printed conductive layer.

21.2.3   Conductive Textiles from Conductive Fibers

An alternative approach for preparation of conductive textiles is by the knitting and weaving of conductive fibers. Various conductive fibers can be used such as carbon-based conductive fibers, ECP-based conductive fibers, and metal fibers. The main factor that limits the applicability of certain conductive fibers for the fabrication of conductive textiles is their ability to withstand the weaving/knitting processes without being broken apart. This means that the conductive fibers should have enough tensile strength without being brittle when contorted through the knitting machine.

21.2.3.1   Carbon-Based Conductive Fibers

Due to the recent advances in nanotechnologies, different types of carbon-based fibers have been fabricated such as carbon nanotube fibers (CNFs) [120–122], graphene fibers (GFs) [123, 124], graphene oxide fibers (GOFs) [125], graphene-carbon nanotube composite fibers [126, 127], and silver-doped graphene fibers [128]. The former processes are expensive, complicated, and not yet scaled up to a commercial level. A detailed description and discussion for the preparation of carbon-based conductive fibers can be found in literature [129].

21.2.3.2   ECP-Based Conductive Fibers

ECPs are a class of polymers with a fully conjugated aromatic backbone structure. The full delocalization of π electrons provides the unique feature of electrical conductivity for this class of polymers. However, due to the high aromaticity of ECPs, they possess a rigid backbone structure, which makes them available in relatively low molecular weight forms, so much so that the elasticity of their solutions is generally insufficient for the direct spinning or electrospinning of their fibers. However, there are some reports describing the preparation of ECP fibers by spinning, coaxial spinning, and electrospinning [130–136].

21.2.3.3   Twisted Conductive Fibers

Conductive textiles can be made by the integration of conductive yarns in a textile structure [1]. This was achieved by twisting metal wires into a fabric textile. However, the integration of conductive yarns in a fabric structure is a complex

process, and the resulting conductive fabrics were hard, rigid, and uncomfortable for electronic textiles and wearing applications [1].

21.2.3.4 Biscrolled Conductive Fibers

A new technology was recently developed for preparation of smart functional fibers based on the biscrolling technique by incorporating functional guests into yarns [137, 138]. The fabrication process of biscrolled yarns involves the twist-based spinning of CNT sheets (the host) that are overlaid with a layer of up to 99 wt% of one or other functional materials (the guest). The guest-host bilayers were scrolled into biscrolled yarn in such a way that the minor CNT sheet concentration confined guest powders down to nanometer-scale proximity in the scroll galleries. The guest material can be deposited into the host CNT sheets by electron beam evaporation, sputtering, exposure to an aerosol formed by gas-phase reaction, or simple filtration-based guest deposition. The main advantage of this technology relies on its ability to incorporation versatile functional guest materials in different applications [137]. The biscrolled yarns can be knotted and sewn with potential applications in various smart textiles.

21.2.3.5 Welded Conductive Fibers

Recently, Jost et al. [139] employed a technology called "natural fiber welding" [140] (NFW) for the preparation of conductive yarns in knittable textile supercapacitor applications. As illustrated in Fig. 21.2, the NFW process employs activated carbon as the conductive material embedded into cellulose yarns (cotton, linen, bamboo, or viscose) being swelled in an ionic liquid (IL) solution. This step is followed by removal of the IL by washing it in water as anti-solvent and, finally, twisting the activated carbon-NWFs with a highly conductive stainless steel yarn. The prepared conductive cotton yarns were too brittle and broke apart during the knitting process. In contrast, conductive yarns made from linen, bamboo, and viscose were knitted successfully into fabric textiles and utilized for making a knitted stretchable supercapacitor device as shown in Fig. 21.3.

21.3 Capacitors for Energy Storage Devices

21.3.1 Conventional Capacitors

Conventional capacitors consist of two conducting electrodes separated by an insulating dielectric material. When a voltage is applied to a capacitor, opposite charges accumulate separately on the surfaces of each electrode, which results in the
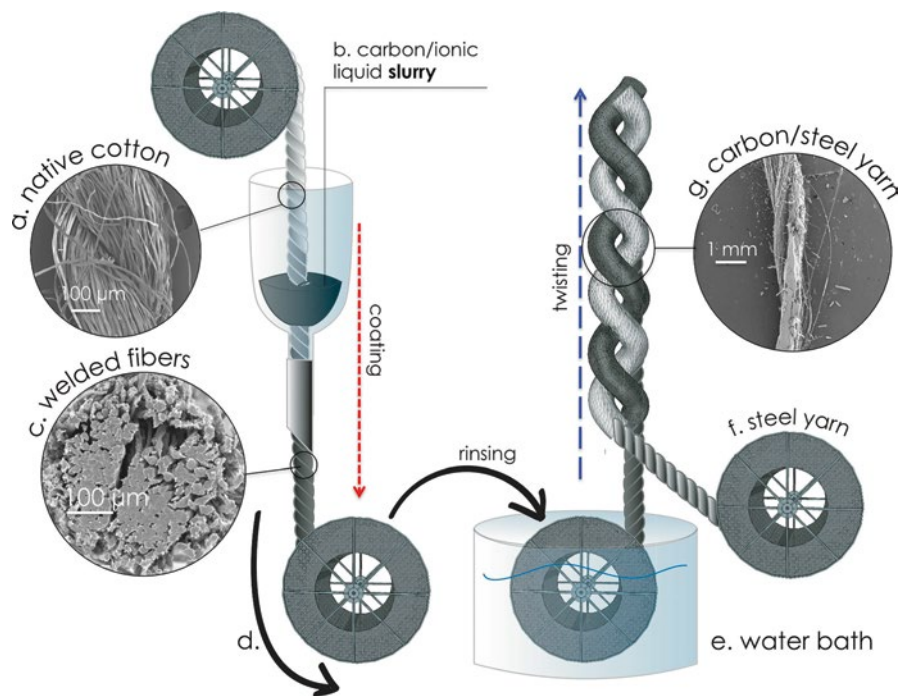
Fig. 21.2 Schematic illustration of the natural fiber welding process for preparation of conductive fibers. Reproduced with permission from [139]
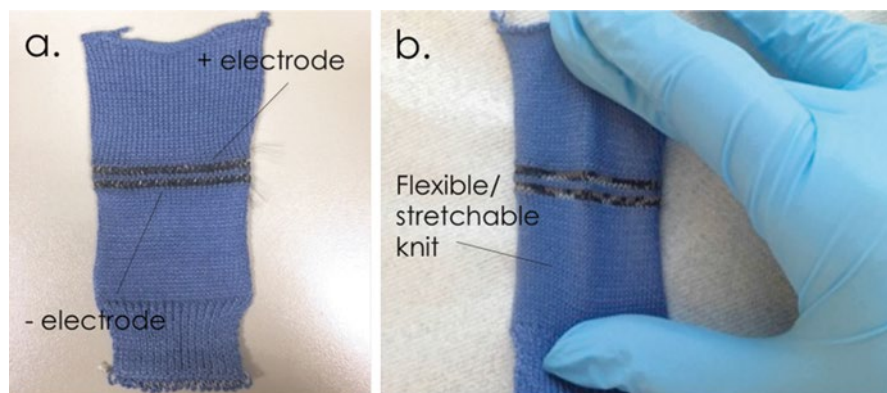
Fig. 21.3 Photographs of knitted samples: (**a**) photograph of a flat knitted supercapacitor, (**b**) photograph of knitted supercapacitor while stretched. Reproduced with permission from [139]

generation an electric field that allows the capacitor to store energy. The ratio of the stored (positive) charge (Q) to the applied voltage (V) is called capacitance (C):

$$C = \frac{\mathbf{Q}}{V} \tag{21.1}$$

For conventional capacitors, C is directly proportional to the surface area (A) of the electrodes and inversely proportional to the distance (D) between the electrodes:

$$C = \varepsilon_0 \varepsilon_r \frac{\mathbf{A}}{D} \tag{21.2}$$

where

ε_0 = dielectric constant "permittivity" of the space and

ε_r = dielectric constant of the separating "dielectric" material.

The main attributes of the capacitor are "energy density (E)" and "power density (P)." For both (E) and (P), the density can be calculated as quantity per unit mass or unit volume. The stored energy (E) is defined as:

$$E = \frac{1}{2} C V^2 \tag{21.3}$$

where P is the energy consumed per unit time. In order to determine the power, one has to consider that the capacitor is represented as a circuit in series, with an external load/resistance (R). Also, there is a contribution from the internal components of the capacitor (e.g., current collectors, electrodes, and dielectric materials), which is measured in aggregate by a quantity known as the equivalent series resistance (ESR). The voltage during discharge is determined by these resistances. When measured at matched impedance (R = ESR), the maximum power for the capacitor P_{max} is

$$P_{\max} = \frac{V^2}{4\,xESR} \tag{21.4}$$

From Eq. (21.4), it is clear that as resistance increases, the capacitor becomes less efficient providing lower power densities.

Compared with electrochemical batteries and fuel cells, conventional electrostatic capacitors exhibit relatively high power densities but relatively low energy densities (Fig. 21.4). Hence, a battery can store more total energy than a capacitor, but it cannot deliver it very quickly, which means its power density is low. On the other hand, capacitors store relatively less energy per unit mass or volume, but the
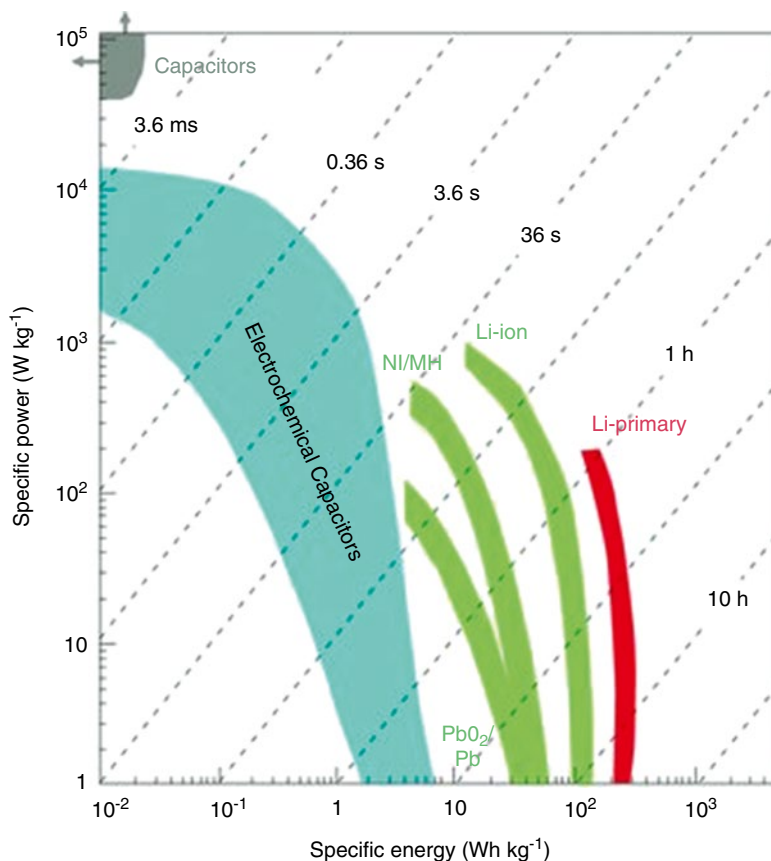
Fig. 21.4 Ragone plots showing the specific power against specific energy for various electrical energy storage systems [141], copyright 2008, Nature Publishing Group

stored energy can be discharged rapidly to produce a lot of power, so their power density is usually high.

21.3.2   Supercapacitors

Supercapacitors, often called electrochemical capacitors (ECs), are governed by the same basic principles as conventional electrostatic capacitors. However, they incorporate electrodes with much higher surface areas (A) and much thinner dielectrics that decrease the distance (D) between the electrodes. Thus, from Eqs. (21.2) and (21.3), it can be inferred that supercapacitors are able to reach higher values for both

capacitance and energy. In addition, supercapacitors can reach comparable power densities to those of the conventional capacitors by maintaining low values of ESR. Supercapacitors have several advantages over electrochemical batteries and fuel cells, including higher power density, shorter charging times, and longer cycle and shelf lives [142].

The electrochemical performance of supercapacitors can be described by specific capacitance, which can be considered the most important characteristic of a supercapacitor indicating its capability of storing charges. The specific capacitance (C_{sp}) is calculated from the charge–discharge curve according to the following equation:

$$C_{sp} = \frac{2i}{m\Delta V / \Delta t} \tag{21.5}$$

where m is the mass, which is usually specified to active materials, one electrode or entire device; i is the charge and discharge current and usually fixed during the tests; and ΔV is the applied voltage window during tests. The upper limit of voltage depends on the type of the employed electrolyte. Generally, a water-based electrolyte has a voltage maximum of 1.2 V (and usually charged to 1.0 V) which is the decomposition voltage of water. However, organic electrolytes allow for higher charge voltages. The capacitance is impervious to voltage window but dictated by the scanning rate, $\Delta V/\Delta t$, which is the slope of the charge–discharge curve.

21.3.3   Electrochemical Capacitors

Different than conventional electrostatic capacitors (sometimes called film capacitors or film dielectric capacitors) which store charges in an electric field imposed across a thin layer of dielectric material, ECs store charges at the electrochemical interfaces between the high surface area, porous electrode material, and the electrolyte. The effective capacitance of ECs is typically a few orders of magnitude higher than those resulting from electrostatic capacitors which is attributed to the large specific surface area of the porous electrodes ($\approx$500–2000 m^2 g^{-1} for ECs) and the shorter path length between the electrode and the electrolyte ions (in order of nanometer) [143]. According to the used energy storage mechanism, ECs can be classified into the following three categories.

21.3.3.1   Electrochemical Double-Layer Capacitors

In case of electrochemical double-layer capacitors (EDLCs), charges are stored electrostatically via ion absorption at the electrode/electrolyte interface. Carbon-based materials with high surface areas are the most commonly used electrode

materials for EDLCs [73, 144–146]. Due to their fast and near-surface electrochemical process, EDLCs have the ability to provide very high power and possess an excellent cycle life. However, the energy stored in EDLCs is often limited by the finite electrical charge separation at the interface of electrode/electrolyte and by the working voltages that is primarily determined by the stable potential window of the used electrolyte.

21.3.3.2   Pseudocapacitors

In contrast to EDLC, pseudocapacitors employ fast and reversible faradic processes (redox reactions) at the surface of electroactive materials for charge storage. Faradic electrodes provide higher specific pseudocapacitance values ($\approx$300–1000 F g^{-1}) that exceed the specific capacitance of double-layer charge storage devices using carbon-based materials (100–259 F g^{-1}). Typical active pseudocapacitive materials are transition metal oxides [147–150] and ECPs such as polyaniline (PANI), polypyrrole (PPY), and polythiophene (PTH) [77, 151, 152].

21.3.3.3   Hybrid Capacitors

Hybrid capacitors try to exploit the advantages and mitigate the disadvantages of EDCs and pseudocapacitors to achieve better performance characteristics. Utilizing both Faradaic and non-Faradaic processes for charge storage, hybrid capacitors have achieved greater energy and power densities than EDCs without affecting the cycling stability and affordability that have limited the success of pseudocapacitors. Depending on the used electrode configuration, three different types of hybrid capacitors can be recognized which are composite, asymmetric, and battery type, respectively.

Composite ECs

Composite electrodes utilize a combination of two or more different materials of the following main categories: ECPs, metal oxides, and carbon-based materials. The hybrid composite materials integrate both physical and chemical charge storage mechanisms in a single electrode. The carbon-based materials provide a capacitive double layer of charge with an accessible high surface area that increases the contact between the deposited pseudocapacitive materials and electrolyte. The pseudocapacitive materials provide increases in the capacitance through Faradaic reactions.

Asymmetric ECs

Asymmetric hybrids combine Faradaic and non-Faradaic processes by coupling an EDC electrode with a pseudocapacitor electrode. In this case, the negative electrode will use carbon-based materials and the second positive electrode will use ECPs or metal oxides. The lack of an efficient, negatively charged, conducting polymer material has limited the success of conductive polymer pseudocapacitors. The implementation of a negatively charged, activated carbon electrode attempts to avoid this problem. Asymmetric hybrid capacitors that couple these two electrodes are expected to achieve higher energy and power densities than comparable EDCs along with better cycling stability than comparable pseudocapacitors.

Battery-Type ECs

Battery-type hybrids couple two different electrodes, a supercapacitor electrode with a battery electrode. This specialized configuration addresses the need for higher-energy supercapacitors and higher-power batteries, combining the energy characteristics of batteries with the power, cycle life, and recharging times of supercapacitors.

21.4 Materials for Textile Supercapacitors

As discussed previously (Sect. 21.3.3), the research efforts for making supercapacitors were directed into utilizing three categories of materials: highly conductive carbon-based materials with a large surface area, transition metal oxides, and ECPs. Various methods for preparation of conductive textiles utilizing different carbon-based material and ECPs were also discussed earlier (Sect. 21.2). The use of nanomaterials, such as CNTs and graphene, is expected to improve energy storage devices because the size reduction of materials will increase the contact surface area between the electrode and the electrolyte and decrease the length of the transport path for both electrons and ions [77]. Recently, several smart conductive textiles based on carbon materials have been investigated as flexible supercapacitors including spun carbon nanotube (CNT) yarns [44], CNT-based smart textiles [73, 153], CNF-based flexible supercapacitors [154], and CNT-based composite textile supercapacitors [155–157]. However, the performance of these ECs is limited by their inherently low specific capacitance [158]. On the other hand, pseudocapacitors based on transition metal oxides and ECPs showed very high capacitance behavior (Fig. 21.5). This section discusses the recent advances in utilizing ECP-based textiles for the preparation of flexible and lightweight high-performance supercapacitors.
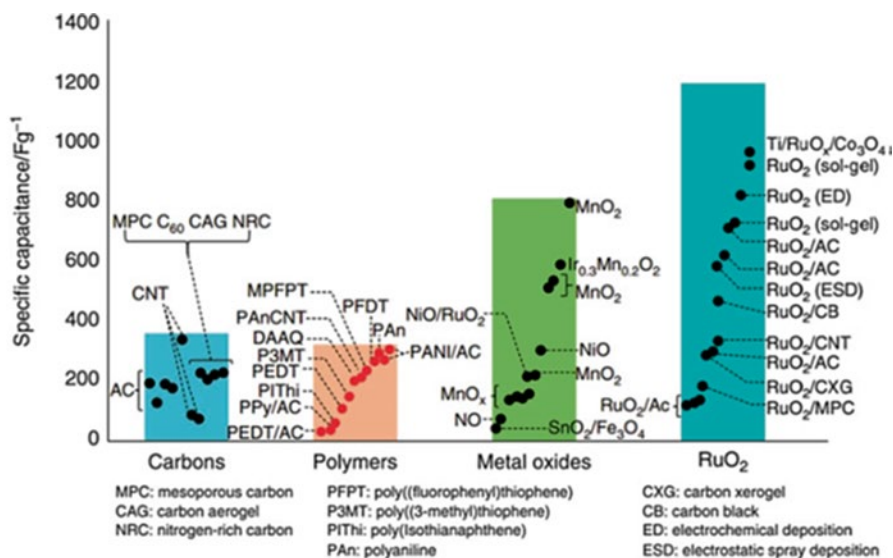
Fig. 21.5 Capacitive performance of various electrode materials reported in the literature [159] (reproduced with permission of The Electrochemical Society)

21.4.1 ECP-Based Textile Supercapacitors

Electrically conducting polymers (ECPs) were discovered in 1976 by Heeger, MacDiarmid, and Shirakawa, for which they were awarded the Nobel Prize in chemistry in 2000 [160]. ECPs belong to the class of polymers which have π conjugation along the polymer backbone such as polyaniline (PANI), polypyrrole (PPY), and polythiophene (PTH). One of the unique characteristics of ECPs is their ability to undergo oxidation–reduction reactions by gaining or losing electrons from the surrounding environment. This feature enables the application of ECPs in different areas such as in smart self-healing coatings for corrosion protection [78], chromatic display devices [58, 59], electrochemical mechanical actuators, electrochemical batteries [161, 162], and electrochemical supercapacitors [142]. As ECPs can be doped and dedoped rapidly to high charge density, they can be applied as active materials for pseudocapacitors. The most commonly used conducting polymers for supercapacitor applications include polyaniline (PANI), polypyrrole (PPY), poly[3,4-ethylenedioxythiophene] (PEDOT), and their derivatives [163]. High charge densities can be achieved as the charge–discharge process occurs through the volume of the ECP and not on the external surface area (Fig. 21.6). ECP-based pseudocapacitors with advantages such as high-redox active capacitance, high conductivity, and, essentially, high intrinsic flexibility have promised the most for high-performance portable, planar, and flexible supercapacitor applications [158].

One of the attractive features for utilizing ECP-based textiles for supercapacitor applications is the simple and diverse approaches for their preparation and
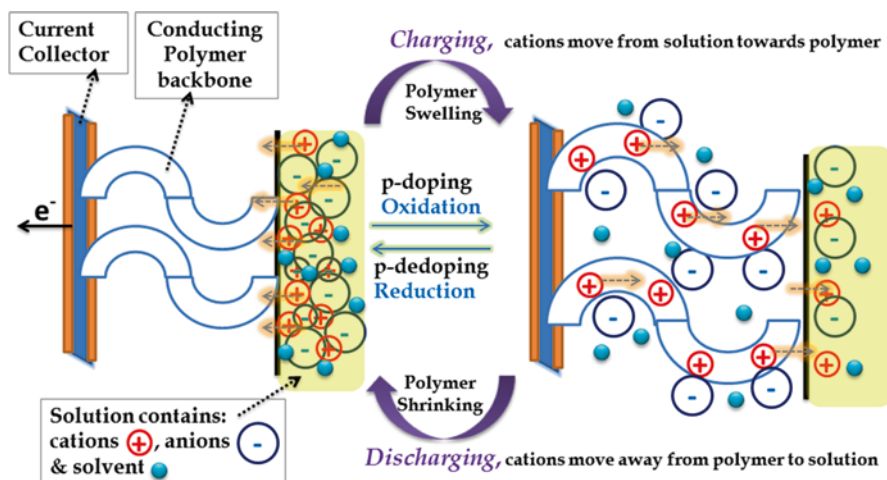
Fig. 21.6 Schematic illustration for charging–discharging of ECP-based pseudocapacitor through the doping/dedoping process

incorporation in the flexible textile devices, with an ability to control their nano-structured morphology. The following section discusses briefly the preparation of pseudocapacitor textiles based on pure ECPs.

21.4.1.1 Polyaniline-Based Textile Supercapacitors

Among the ECPs, PANI has attracted much interest due to its low cost, good mechanical and environmental stability, and adjustable conductivity. PANI can be synthesized chemically by oxidative polymerization or electrochemically by employing a cyclic voltammetry technique. PANI can be represented in three different convertible forms: the oxidized form (leucoemeraldine), the reduced form (pernigraniline), and the emeraldine base (EB). The most useful structure is the nonconducting EB which can be converted into the conducting emeraldine salt (ES) by acid treatment through a process known as "doping." The associated ionic materials/electrolytes are called "dopants." Although the protonated form of polyaniline (ES) is reported to have poor conductivity, PANI is one of the most studied ECPs for EC applications due its environmental stability and the high doping level of 0.5 (i.e., two monomer units per dopant). Theoretically, PANI has a maximum specific capacitance of up to 2000 (F g^{-1}) [164]. However, the reported specific capacitance in literature varies significantly according to parameters such as the nanostructured morphology, polymerization process, dopant type, dopant concentration, and the ionic diffusion length of the electroactive material. The essential requirements for achieving high capacitance using PANI-based

Table 21.1 Typical morphologies of pure PANI and their capacitance performance [77]

PANI morphologies	Capacitance [F g^{-1}]	Electrolytes	Configuration	Energy densities [Wh kg^{-1}]
Film [166]	150	Et$_4$NBF$_4$-actonitrile	Two-electrode	3.50^a
Microsphere [167]	421	H$_2$SO$_4$ aqueous	Three-electrode	N/A
Micro-tube [168]	522	HCl aqueous	Three-electrode	N/A
Particle [169]	408	H$_2$SO$_4$ aqueous	Two-electrode	6.35^a
Coral-like [170]	776	H$_2$SO$_4$ aqueous	Three-electrode	64
Nanowire networks [171]	742	H$_2$SO$_4$ aqueous	Three-electrode	110
Nanowire arrays [172]	950	HClO$_4$ aqueous	Three-electrode	130

^{a}The energy is calculated based on the total weight of two electrodes. The others are only based on the weight of a single electrode

pseudocapacitive electrodes are high surface area, controlled nanostructured morphology, and optimized type as well as concentration of the doping electrolyte [77, 165]. Table 21.1 shows the effect of various PANI morphologies on the obtained specific capacitance. The capacitance of polyaniline nanowire arrays is much larger than both compact film and disordered nanowire networks as electrodes for supercapacitors which is attributed to both a reduced path for ion diffusion and a lower ion diffusion resistance [77].

Kim et al. [173] fabricated a highly stable flexible supercapacitor electrode by coating PANI nanofibers on gold-coated polyvinylidene fluoride-co-hexafluoropropylene (PVDF-co-HFP) membranes. PANI nanofibers were prepared by rapid mixing of aniline monomer and APS initiator, with a 4:1 ratio, in 1 M sulfuric acid solution. A symmetric capacitor cell was prepared by sandwiching the two identical PVDF electrodes between Nafion membrane soaked with 0.5 M sulfuric acid. The assembled cell showed the performance of a practical flexible pseudocapacitor of the composite planar and bent electrode.

21.4.1.2   Polypyrrole-Based Textile Supercapacitors

Polypyrrole (PPY) is one of the most promising ECPs for pseudocapacitor applications due to its distinctive features such as high conductivity, fast charge–discharge mechanism, good thermal stability, low cost, and high energy density [81, 174–176]. Similar to PANI, PPY nanostructured morphology affects the performance of the fabricated supercapacitor. Compared with the specific capacitance obtained from PPY with nanobelt (296 F g^{-1}) and nanobrick (357 F g^{-1}) morphologies, PPY with a nanosheet morphology provided the highest specific capacitance (586 F g^{-1}) for a PPY-coated stainless steel pseudocapacitor [81]. The high capacitance of PPY nanosheets was attributed to the porous structure and high BET surface area of the

nanosheets being 37.1 m^2 g^{-1} as compared with nanobricks and nanobelts with BET surface areas of 26.4 m^2 g^{-1} and 22.6 m^2 g^{-1}, respectively.

Yuan et al. [177] have fabricated PPY-coated paper through a simple "soak and polymerization" methodology. The PPY-coated paper flexible electrodes showed a capacitance of 0.42 F cm^{-2} with high energy density of 1 mW h cm^{-3} at a power density of 0.27 W cm^{-3}. The conductance of the PPY-coated paper remained almost constant after 100 cycles of bending. This approach provides a practical and low-cost method for large-scale production of conductive paper-based electrodes for energy storage devices and flexible electronics.

Yue et al. [39] prepared a stretchable electrode for supercapacitor application by coating nylon lycra fabric with polypyrrole ECP. PPY was coated on the fabric by a simple oxidative polymerization employing ammonium persulfate (APS) as a redox initiator and naphthalene-2, 6-disulfonic acid disodium salt (Na$_2$NDS), at 4 °C for 2 h. The surface resistance of the PPY-coated fabric was 149 Ω/Sq. The electrical resistance decreased during stretching of the fabric and increased during fabric relaxation. This behavior was attributed to the better surface–surface contact within the yarns upon stretching, which improved the conductivity by penetration of the polymer into the fabric yarns. The electrochemical properties of the electrode were evaluated by cyclic voltammetry (CV) and electrochemical impedance spectroscopy (EIS) employing 1.0 M NaCl as the electrolyte solution. At scan rate of 10 mV s^{-1}, the PPY-coated electrode exhibited a nearly rectangular CV behavior which indicated that the charge–discharge responses of the electric double layer were highly reversible and kinetically facile. However, the rectangular CV shape became distorted when applying scan rates of ≥25 mV s^{-1}. This was attributed to the slow diffusion of the counter ions during the insertion/ejection process compared to the faster electron transfer process at high scan rates. Using the three-electrode system, the specific capacitance (C_{sp}) of the PPY-coated nylon lycra fabric was calculated using the following equation:

$$C_{sp} = \frac{A/2}{f \mathrm{x} v \mathrm{x} m} \tag{21.6}$$

where C_{sp} is the specific capacitance, A is the integral area of the cyclic voltammogram loop, f is the scan rate, v is the voltage window, and m is the mass of electroactive material (PPY). The delivered specific capacitance was found to be 123.3, 100.7, 69.7, and 39.4 F g^{-1} at a scan rate of 10, 25, 50, and 100 mV s^{-1}, respectively. When the two-electrode system was used, the discharge capacitance (C_m) was calculated using the following equation:

$$C_m = \frac{2Q}{\Delta V \times m} = \frac{2I \times t}{\Delta V \times m} \tag{21.7}$$

where C_m, I, t, ΔV, and m are the discharge capacitance per electrode, the current of charge–discharge, time of discharge, charge/discharge potential windows, and the

amount of active materials on one electrode, respectively. The specific capacitance obtained from PPY-coated fabric without strain applied was 108.5 F g^{-1}, with an energy density of 6.7 Wh kg^{-1} and power density of 753.4 W kg^{-1}. The capacitance increased to 117.6, 119.6, and 125.1 F g^{-1} with an elongation of 20 %, 40 %, and 60 %, respectively. It was found that the PPY-coated nylon lycra preserved its electrochemical properties with less than 10 % specific capacitance loss after being stretched to 100 % for 1000 times.

In a later study, Yue et al. [178] reported the fabrication of a PPY-coated fabric electrode for a supercapacitor application through the electrochemical polymerization method. PPY was polymerized electrochemically on the conductive gold-coated fabric substrate. Acetonitrile was employed as the polymerization solvent, and *p*-toluenesulfonic (*p*-TS) acid was used as the organic acid dopant. The conductive textile electrode sustained up to 140 % strain without electric failure. Using 1.0 M NaCl as the electrolyte, the flexible electrode delivered a high specific capacitance of 254.9 F g^{-1} at a scan rate of 10 mV s^{-1} and maintained this almost unchanged up to 50 % applied strain, accompanied with improved cycling stability.

Recently, super-high-rate stretchable polypyrrole-based supercapacitors with excellent cycling stability were reported [179]. The pseudocapacitor device was fabricated using electrochemical polymerization of purified pyrrole monomers on smartly tailored stretchable stainless steel meshes (Fig. 21.7). The capacitance of the fabricated supercapacitors increased from the initial 170 F g^{-1} at a
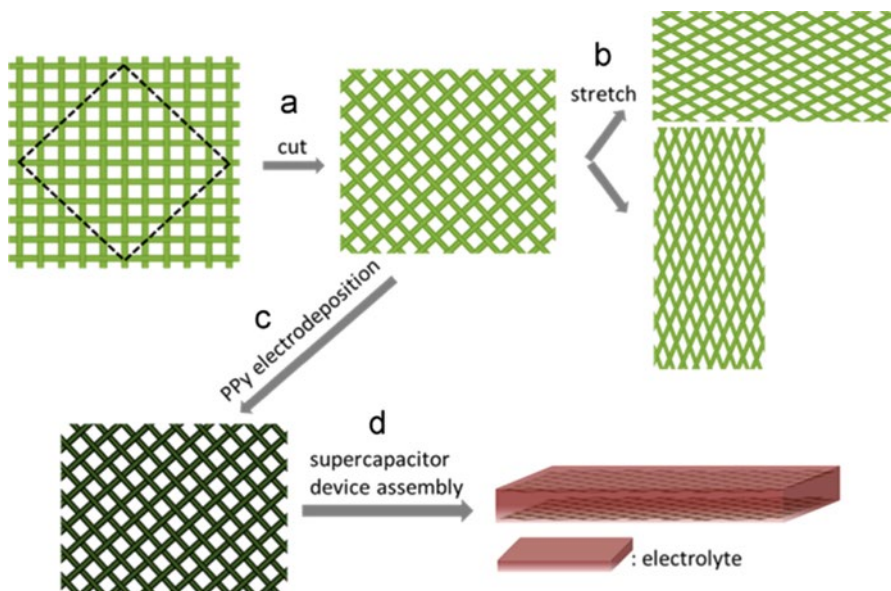
Fig. 21.7 Schematic illustration: (**a**) preparation of a stretchable steel mesh by cutting along the *dashed black lines*; (**b**) stretch the mesh biaxially; (**c**) PPY electrode position on the stretchable steel mesh; (**d**) supercapacitor device assembly by coating the H$_3$PO$_4$/PVA electrolyte [179] (reproduced with permission, copyright 2015, Elsevier)

relaxed state to 214 F g^{-1} at a 20 % strain at a specific current of 0.5 A g^{-1}. Surprisingly, it was found that the solid-state supercapacitors can be operated at super high rates of up to 10 Vs^{-1}, being 1–2 orders of magnitude higher than most scan rates for PPY electrodes measured, even in aqueous electrolytes. The fabricated PPY pseudocapacitors achieved capacitance retention of 98 % under 0 % strain and 87 % under a strain of 20 % applied after 10,000 cycles at a very high specific current of 10 A g^{-1}.

Babu et al. [180] investigated the capacitance of different PPY-coated textiles including cotton, viscose, linen, and polyester fabrics. A unit cell was fabricated to investigate the capacitive behavior by assembling two symmetric textile electrodes separated by a solid polymer electrolyte membrane (PVA/1 M H$_2$SO$_4$ gel). The textile electrodes prepared with PPY-cotton and PPY-viscose exhibited the highest specific capacitance values of 268 F g^{-1} and 244 F g^{-1}, respectively, at a scan rate of 5 mV s^{-1}. This was attributed to the strong ionic cross-linking through hydrogen bonding in case of PPY coating with cellulosic fabrics, providing uniform adsorption of pyrrole monomers and homogeneous polymer coating for the entire fabric.

21.4.1.3 Polythiophene-Based Textile Supercapacitors

Unlike PANI and PPY, which are p-type ECPs, polythiophene (PTH) and its derivatives can be both p-type and n-type ECPs. Compared with PANI and PPY, polythiophene exhibits much lower electrical conductivities and lower capacitance. However, the p-doped PTHs have advantages such as higher stability in air and humidified environments as well as their electrodes can be operated in a comparatively higher potential window ($\approx$1.2 V), which enables the fabrication of asymmetric supercapacitors with one ECP-based electrode. Among all PTH derivatives, poly (3, 4-ethylenedioxythiophene) (PEDOT), with high environmental stability, has been investigated thoroughly for supercapacitor and pseudocapacitor applications [181–184].

Laforgue reported the fabrication of an all-textile flexible supercapacitor using electrospun PEDOT nanofibers [38]. The nanofiber mats with diameters around 350 nm demonstrated good electrochemical properties due to their ultraporous structure and very high electrical conductivity (60 ± 10 S cm^{-1}). The mats were incorporated into an all-textile flexible supercapacitor, by using carbon cloths as current collectors and the electrospun PAN nanofibrous membranes as a separator. The supercapacitor device was fabricated by stacking and embedding the textile layers in a solid electrolyte containing an ionic liquid and PVDF-co-HFP as the host polymer. The pseudocapacitor showed a specific capacitance of 20 F g^{-1}, with limited cycling stability. This was attributed to the increased cell resistance caused by the turning of the identical electrodes into its nonconductive (undoped) state when the cell is at its maximum voltage. This drawback of using ECP-based electrodes can be circumvented by designing composite supercapacitor

electrodes using another type of active materials such as carbon nanotubes, carbon nanofibers, graphene nanosheets, and metal oxides.

21.4.2 Hybrid Textile Supercapacitors

The main shortcomings for utilizing pure ECPs in supercapacitors are discussed as follows: (1) The obtained practical specific capacitance is lower than theoretical prediction because the inner layer of the thick electrode cannot be fully used. (2) ECPs usually possess poor cyclic stability in long-term charge–discharge processes. The poor cyclic stability of conducting polymer electrodes could be attributed to the following three reasons [77]: (a) Poor mechanical stability due to reversible swelling/shrinkage caused by volumetric changes during the doping–dedoping process as a result of repeated insertion/de-insertion of ions during charging and discharging (Fig. 21.6) (b) Loss of the active material as a result of conducting polymers peeling off from the current collector or dissolving into the electrolyte (c) Over-oxidative degradation due to the limited working potential range

The above challenges of using pure ECP pseudocapacitive materials can be mitigated by fabrication of hybrid composite electrodes containing other types of materials with different capacitive performances and mechanisms. The following section highlights the recent progress in the fabrication of composite supercapacitor textiles using ECPs with carbon nanotubes, carbon cloths, graphene, and metal oxides.

21.4.2.1 Textile Supercapacitors Based on ECPs/CC Composites

Compared to textiles and fibers based on CNTs and GNSs, CC offers an alternative material as a current collector for supercapacitor devices due to their lower cost, porous 3D structure, high surface area, chemical oxidative stability, good electrical conductivity, and flexibility. Hence, a combination of CC as a conductive porous current collector with pseudocapacitive ECPs is expected to provide a supercapacitor with superior performance compared to a device with either CC or ECP alone.

Horng et al. [79] prepared a flexible supercapacitor based on conductive carbon cloth (CC)/PANI nanowires (PANI-NWs) composite electrodes. PANI-NWs were deposited on the CC by electrochemical polymerization using HCl as dopant ion. A symmetric supercapacitor device was fabricated by sandwiching two CC/PANI-NWs composite electrodes between a cellulose film separator and 1 M H_2SO_4 as the electrolyte. The textile supercapacitor demonstrated high flexibility, with only 0.05 % capacitance loss during the bending test. At 1.73 A g^{-1} discharge current, the gravimetric capacitance of 1079 F g^{-1} was obtained at a specific energy of 100.9 W kg^{-1} and a specific power of 12.1 kW kg^{-1}. The cycling performance of the PANI-NWs/CC electrode was studied at a current density of 8.65 A g^{-1} in 1 M H_2SO_4 aqueous electrolyte. After 2100 cycles, the initial gravimetric capacitance was

reduced by a factor of 14 %, which indicated the long-life electrochemical stability of the PANI-NWs/CC composite electrode.

Cheng et al. [80] investigated an electro-etched carbon fiber cloth coated with PANI-NWs as an alternative material for supercapacitor electrodes. It was found that the surface of carbon fibers becomes more hydrophilic after the etching process, which provided a more uniform and thin polyaniline coating around the carbon fibers, allowing them to be more accessible while also facilitating electrolyte transport among PANI-NWs and through various carbon fibers. The obtained mass-normalized specific capacitance was 1026.8 and 265.9 F g^{-1} at the PANI coating density of 1.8 and 9 mg cm^{-2}, respectively. The reduction in capacitance at a higher PANI coating density was attributed to the fact that only the PANI on or near the surface could participate to the redox reactions. Hence, it was concluded that some of the PANI was not utilized when the PANI coating layer was thick. Achieving both high mass-normalized capacitance and area-normalized capacitance for electrodes is crucial for practical applications. At the optimized conditions of 30 min coating time and 5.4 mg cm^{-2} PANI coating density, the mass-normalized specific capacitance and area-normalized specific capacitance were 673 F g^{-1} and 3.5 F cm^{-2}, respectively.

21.4.2.2 Textile Supercapacitors Based on ECPs/Graphene Composites

Graphene is a 2D single-atom-thick carbon allotrope tightly arranged in honeycomb lattices and has inspired an enormous amount of research [185, 186]. Due to its unique structure, graphene possesses ultrahigh theoretical specific surface area (SSA $\approx$ 2630 m^2 g^{-1}) and extraordinary electronic, mechanical, thermal, and optical properties. Hence, graphene is proposed as novel future material with great promise for potential applications in high-performance supercapacitors [142, 146, 187]. However, the serious aggregation and restacking of graphene is considered to be one of the major obstacles significantly inhibiting the commercial application of graphene in supercapacitors [142]. This problem can be overcome by incorporating pseudocapacitive materials such as ECPs into graphene as spacers to form composites, which can effectively prevent graphene agglomeration [142]. When ECPs are used as spacers, they can provide effective suppression for the irreversible restacking and, hence, maintain the intrinsic high SSA and provide more active sites to form EDLs. In addition, the use of ECPs/graphene composite electrodes provides accessibility for the pseudocapacitance mechanism (Faradic reactions) which may contribute to the overall specific capacitance. More importantly, the presence of highly conductive graphene with high SSA increases the contact between the deposited pseudocapacitive ECP material and the electrolyte, which alleviates the cycling stability drawback of the ECP-based electrodes. Yan et al. [188] synthesized a graphene/PANI composite using in situ polymerization which provided a maximum specific capacitance of 1046 F g^{-1} compared to 115 F g^{-1} for pure PANI. The large improvement of specific capacitance was attributed to the synergetic scenario between PANI

and graphene nanosheets. PANI nanoparticles prevented the agglomeration of graphene nanosheets as well as reduced the ion diffusion path during charge/discharge processes. The cycling stability was enhanced remarkably by the addition of 1 % CNTs into the graphene/PANI composite which provided 94 % retention after 1000 cycles, compared with 48 % for graphene/PANI composite due to the improved mechanical properties and presence of a highly conductive path during the doping/dedoping processes [189].

Xu et al. [190] employed a screen printing methodology for the fabrication of a screen-printable thin film supercapacitor device utilizing graphene/PANI ink. Flexible conductive carbon fabrics were used as substrates for screen printing which can function as electrodes for direct assembly of the supercapacitor. After 1000 cycles, the flexible textile supercapacitor provided a maximum specific capacitance ratio of 352 F g^{-1} at discharge rate of 1 A g^{-1}. The improved electrochemical stability was attributed to the combination of high graphene conductivity along with PANI reversible redox properties which is regarded as necessary to achieve supercapacitors with long cycle life. In a later study, Xu et al. [107] reported the utilization of graphene/PANI ink for preparation supercapacitors through an inkjet printing methodology. Electrochemical measurements with a 1 M H_2SO_4 electrolyte yielded a maximum specific capacitance of 82 F g^{-1}, power density of 124 kW kg^{-1}, and energy density of 2.4 Wh kg^{-1} when a scan rate of 20 mV s^{-1} was applied. The fabricated supercapacitors were flexible and showed a long cycle life over 1000 cycles.

Fan et al. [191] reported the use of self-assembling sulfonated graphene (SG)/PANI nanocomposite paper for high-performance supercapacitors. Sulfonated graphene was found to act as a dopant for PANI. The SG/PANI nanocomposite papers had thin, lightweight, and flexible characteristics, and its supercapacitor devices showed excellent electrochemical performance with a ratio capacitance of 478 F g^{-1} at a discharge rate of 0.5 A g^{-1} and its capacitance retention rate maintained 88 % of its original capacitance after 2000 cycles.

21.4.2.3 Textile Supercapacitors Based on ECP/CNT Composites

Pan et al. [192] prepared a flexible and transparent wearable supercapacitor device based on aligned CNT fiber textiles and polyaniline (CNTFT/PANI) (Fig. 21.8). PANI was deposited on the CNTFT using an electrochemical polymerization method. The weight percentage of PANI was determined by the electron transfer numbers and controlled by the electrodepositing time during synthesis.

The deposited PANI filled the voids among aligned CNTs with the critical weight of 50 %, above which the PANI started to aggregate into bulk particle material. The CNTFT/PANI composite was coated with PVA-H_3PO_4 gel electrolyte and two textile electrodes were stacked into a supercapacitor. It was found that the threshold weight percentage of PANI that provided the maximum capacitance is 50 % with observation of capacitance reduction above this value due to the pseudocapacitance property of PANI at high loads. The specific capacitance of the bare CNTFT was 7.7 F g^{-1}, whereas the specific capacitances of the CNTFT/
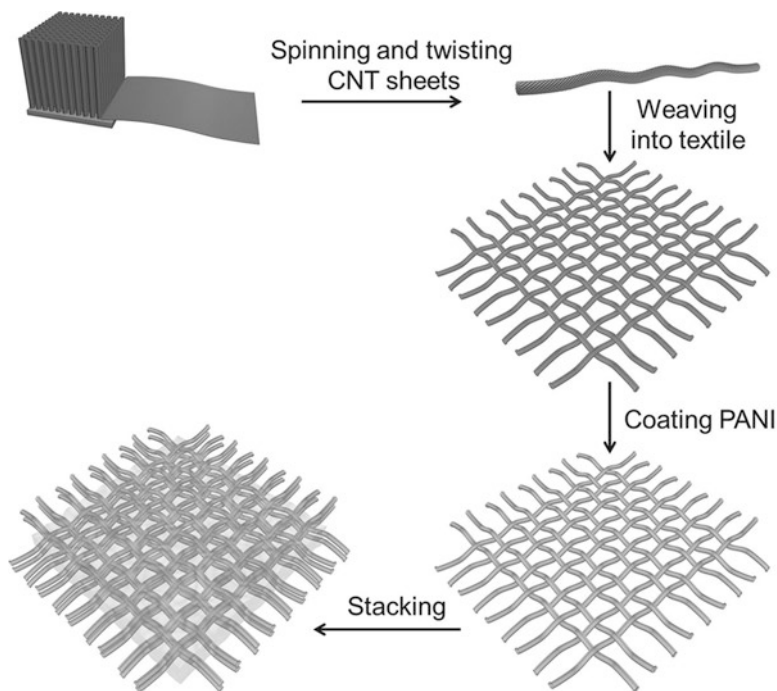
Fig. 21.8 Schematic illustration of the fabrication of a supercapacitor textile based on CNT/PANI composite fiber. Reproduced with permission from [192]

PANI composites were 108.5, 152.8, and 201.8–272.7 F g⁻¹ corresponding to 15 %, 30 %, 40 %, and 50 % PANI in the composite, respectively. When the PANI weight percentage reaches 60 %, the specific capacitance was slightly reduced to 240.6 F g⁻¹. The increased specific capacitance below 60 % was ascribed to the pseudocapacitive nature of PANI. However, beyond the critical point (60 %), PANI aggregates into particles which decrease the contact with aligned CNTs and, consequently, a reduction in charge transport. There was no obvious reduction in the capacitance of supercapacitor textiles when the current densities were increased, and hence, the supercapacitor can effectively work at a wide range of current density. The supercapacitor provided over 90 % retention of its capacity after 2000 charge/discharge cycles, which was attributed to the remarkable mechanical and electronic properties from aligned CNTs.

Furthermore, the supercapacitor textile was integrated to create a new energy textile that can convert solar energy to electrical energy instead of storing it, and a high entire photoelectric conversion and storage efficiency of 2.1 % was achieved. A combination of both photoelectric conversion (PC) and electrochemical storage was utilized for the fabrication of a wearable energy textile by stacking the PC part with the supercapacitor textile as illustrated in Fig. 21.9.
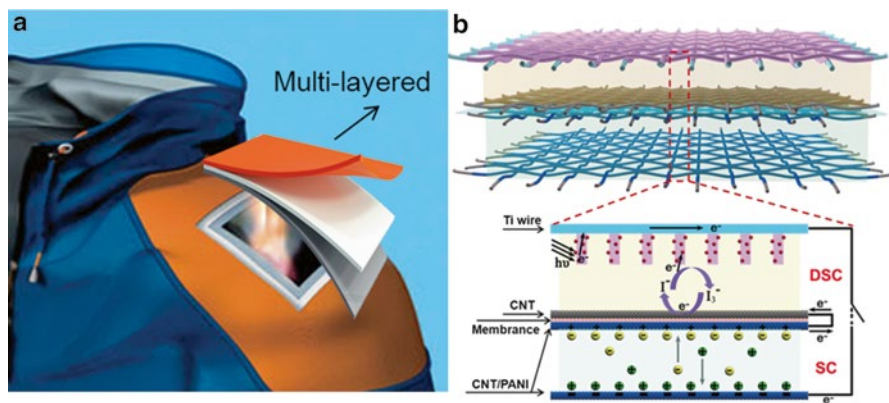
Fig. 21.9 (**a**) Photograph of multilayered clothes; (**b**) schematic illustration of the integrated energy textile. The enlarged view shows the working mechanism. Reproduced with permission from [192]

21.4.3 Supercapacitor Textiles from Supercapacitor Fibers

Supercapacitors can be fabricated using fiber-shaped devices or textile devices. Compared to fiber-shaped devices, textiles provide the feasibility of making planar devices such as planar flexible supercapacitor textiles. Planar textile devices can provide specific mass capacitance of $\approx$3000 F g^{-1}, while the fiber-shaped counterpart achieves $\approx$300 F g^{-1}, 10 times lower than planar textile device [193]. For practical applications, planar textile supercapacitor devices provide enhanced performance in terms of stability, durability, and lifetime [193]. For example, a uniform layer of gel electrolyte is critical for fiber-shaped ECs. If the layer is too thick or not uniform, the two electrodes will make contact with each other, and hence, the fiber-shaped device cannot be operated normally. Regardless, as mentioned previously (Sect. 21.2), conductive textiles can be made by weaving or knitting supercapacitor fibers.

Wang et al. [194] reported the fabrication of high-performance two-ply yarn supercapacitor based on a CNT/PANI-NW array [194]. A CNT yarn was coated with PANI-NWs by dilute polymerization, which was followed by coating it with PVA gel electrolyte. In the last step, two CNT@PANI@PVA yarns were twisted together to form a two-ply yarn, the final threadlike supercapacitor. The two-ply yarn is a solid-state supercapacitor that retains the characteristics of pure CNT yarn for conventional textile processing, such as weaving and knitting. As shown in Fig. 21.10a, a plain weave model fabric was manually constructed from six two-ply yarn supercapacitors. Figure 21.10b shows the co-woven two-ply yarn supercapacitor with conventional textile yarns. The model fabric is composed of four conventional two-ply cotton yarns and four two-ply CNT@PANI@PVA yarn supercapacitors. The performance of the composite flexible supercapacitor was
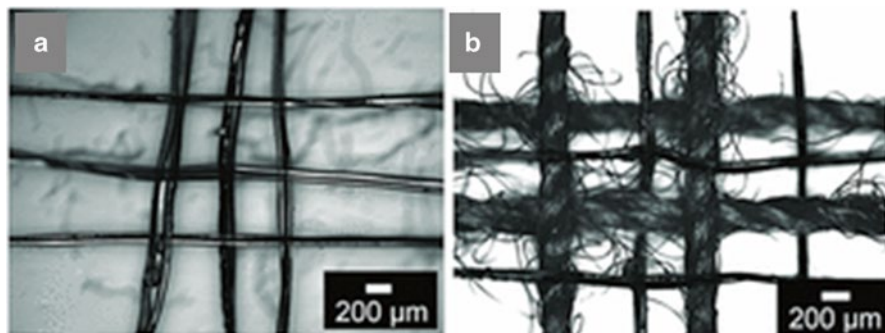
Fig. 21.10 Optical microphotographs: (**a**) a model woven energy storage device consisting of six two-ply yarn supercapacitors (reflection mode); (**b**) yarn supercapacitors are co-woven with conventional cotton yarns to form a flexible electronic fabric with self-sufficient power source. Reproduced with permission [194]

almost constant at different bending cycles. At the current density of 0.01 mA cm^{-2}, the CNT@PANI yarn-based supercapacitor showed a capacitance of 38 mF cm^{-2}, while the areal capacitance of the pure CNT yarn-based supercapacitor was only ≈2.3 mF cm^{-2}. Due to improved capacitance, flexibility, and feasibility of integration with textiles, the two-ply yarn supercapacitor might be used for power storage in electronic textiles for applications that require conventional fabric-like breathability and durability.

ECPs have been proposed for electrochromic applications due to its properties such as low operational voltage, ease in the fabrication of large area, the use of flexible substrates, high quality, optically transparent thin films, and excellent coloration contrast with matching rapid coloration rates [195]. Among the stated advantages, the possibility of using ECPs for the preparation of flexible electrochemical devices is very attractive for applications such as display devices and, particularly, flexible textile display devices [196].

Kelly et al. [58] reported the employment of PANI as solid-state electrochromic material in the application of flexible textile display. Nonwoven PET and viscose textiles were coated with PANI by in situ oxidative chemical polymerization using p-dodecylbenzenesulfonate as a doping agent. The electrochromic flexible display device was constructed by using four-layered sandwiched structure without the need for extra liquid electrolyte layers. The use of a solid electrochromic material offers a practical solution by preventing the leakage of liquid-phase electrochromic materials that require sufficient sealing for the fabricated device.

Recently, Chen et al. [197] reported the fabrication of a flexible electrochromic fiber-shaped supercapacitor. The fabrication process is illustrated in Fig. 21.11. Initially, the CNT sheet was wound onto an elastic rubber fiber. After that, PANI was electrochemically deposited onto the CNT sheet. The maximum specific capacitance based on the weight of CNTs and PANI was obtained at 70 % weight PANI (255 F g^{-1} at charge/discharge rate of 1 A g^{-1}). At higher weight percentage of PANI
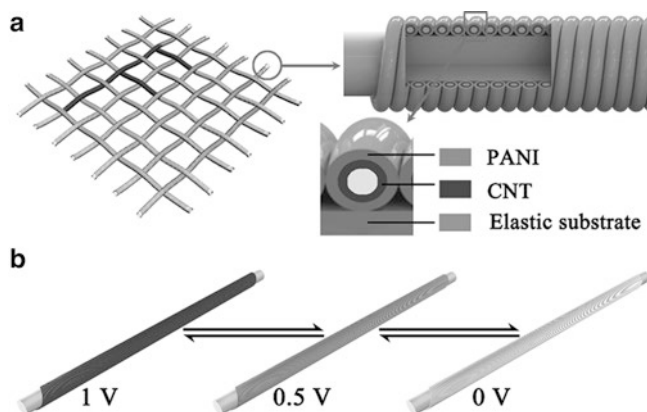
Fig. 21.11 Schematic illustration of the structure and display function of the electrochromic, wearable fiber-shaped supercapacitor. Reproduced with permission from [197]
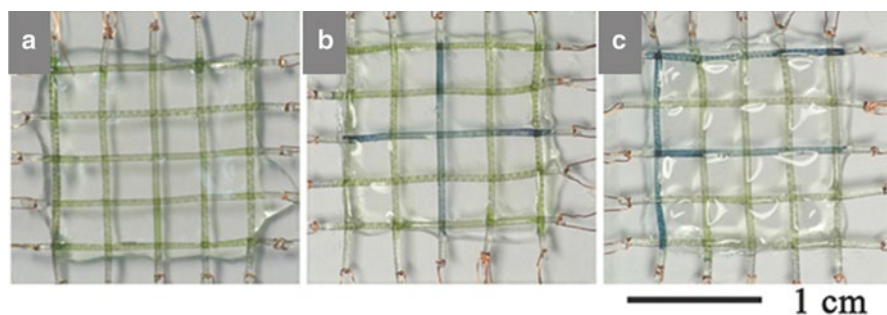
Fig. 21.12 Chromatic transitions during the charge–discharge process. (**a**) An energy storage textile woven from electrochromic fiber-shaped supercapacitors during the charge–discharge process; (**b** and **c**) electrochromic fiber-shaped supercapacitors that have been designed and woven to display the signs "+" and "F," respectively. Reproduced with permission from [197]

(e.g., 90 %), the excess PANI was found coated on the outer surface of the CNT/PANI composite fiber electrode and could not effectively make contact with the aligned CNTs, which eventually led to slower and less effective ion diffusion. Figure 21.12 shows the utilization of the wire-shaped electrochromic supercapacitors for the fabrication of a woven textile that can act as displayer.

Lee et al. [40] reported the utilization of a biscrolling technique for the fabrication of PEDOT/CNT composite supercapacitors for textiles and microdevice applications. The fabricated PEDOT/CNT redox supercapacitor yarn electrodes were made by a process called biscrolling (Sect. 21.2.3.4), which involves inserting a twist in a host sheet that is overlaid with the guest (Fig. 21.13). The biscrolled yarns were prepared by twist insertion in hundred-nanometer-thick ECP infiltrated
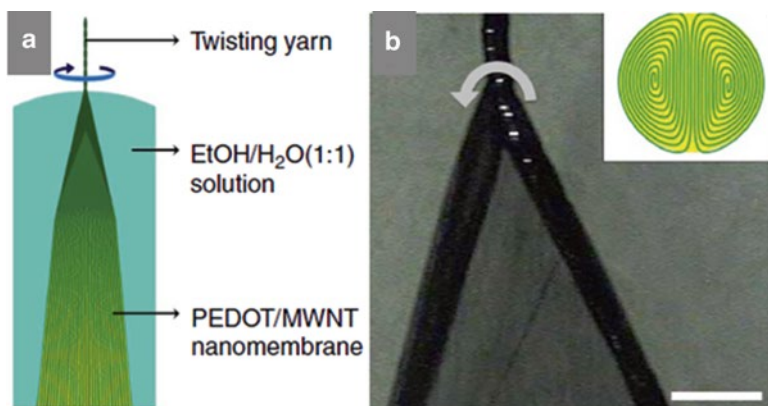
Fig. 21.13 (**a**) Schematic illustration showing the fabrication of a biscrolled PEDOT/MWNT yarn. (**b**) Optical microscope image of the spinning wedge, which shows the wedge edges being twisted to form a dual-Archimedean scroll yarn, which is schematically illustrated in the inset. Scale bar, 200 mm [40]. Copyright 2013, Nature Publishing Group

Fig. 21.14 Cyclic life and stability of solid-electrolyte biscrolled yarn supercapacitors when weaved into a glove (the yarn supercapacitor was 5 cm long). Reprinted with permission from [40]. Copyright 2013, Nature Publishing Group
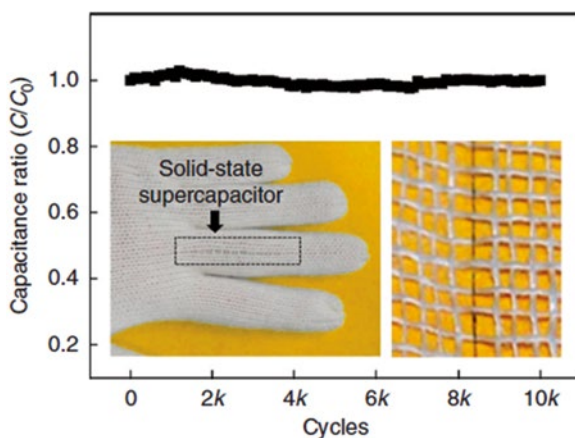
MWNT sheets. The ECP yarn guest was deposited on MWNT sheets by vapor phase polymerization (VPP), which is a well-known technique for providing uniform coatings of highly ECP layers on substrates. The volumetric capacitance of the plied biscrolled yarn/Pt wire device was up to 179 F cm^{-3}. The complete supercapacitor could be wound or sewn for 10,000 cycles with over 90 % performance retention rate (Fig. 21.14).

Recently, Huang et al. [198] reported a novel method for the fabrication of large wearable energy storage textiles from industrially weavable and knittable highly conductive yarns. The highly conductive yarns were made from 316 L stainless steel

thin fibers by the twist-bundle drawing technique (Fig. 21.15a). Stainless steel 316 L was selected due to its anticorrosion capability and thermal stability and flexibility of its micrometer-sized fibers compared to other types of stainless steel such as the brittle 304 stainless steel microfibers. The twisted long yarns have a small diameter of 180–250 μm and were found to be very soft and flexible as well, comparable to those conventional cotton yarns with higher tensile strength (>700 MPa), which facilitated the weaving and knitting process. The main advantage behind using metal-based conductive textiles is the ability of metal-based wires/yarns to provide effective long-distance electron transport [199]. As illustrated in Fig. 21.15b, the highly conductive yarns were prepared through a three-stage fabrication process. Initially, reduced graphene oxide (rGO) was introduced, which was followed by the electrodeposition of pseudocapacitive MnO_2 and PPY conductive layers in the subsequent steps, respectively. The PPY layer is expected to serve as a stress buffer during the various deformations that are usually faced by textiles [179]. A freestanding all solid-state yarn supercapacitor was made from two such parallel yarn electrodes using a PVA/H_3PO_4 gel electrolyte that exhibited a long cycle life (>92 % device capacitance retention over 4950 cycles). The possibility of the practical use of the hierarchically structured conductive yarns for preparation of energy storage textiles through weaving (Fig. 21.15c) and knitting (Fig. 21.15d) processes was successfully demonstrated.

21.5   Conclusion

Among the different approaches for the preparation of smart conductive textiles, ECPs have been proposed as a promising material for the preparation of conductive textiles without affecting their original properties such as flexibility, stretchability, and tensile strength. ECP-based textiles can be utilized for different applications (Fig. 21.1) including flexible textile electrodes for supercapacitors and energy storage applications. In the case of ECP-based textile supercapacitors, the energy storage is provided by a pseudocapacitive mechanism through reversible Faradic redox reactions during fast doping–dedoping processes (Fig. 21.6). In general, ECP-based textiles can be prepared directly by a simple coating onto various shaped textile substrates or indirectly by knitting or weaving ECP-based composite fibers. In the latter case, the limiting factors for fabrication of conductive textile are the tensile strength and flexibility of the conductive composite fibers that reflect the ability of fibers to withstand during the knitting/weaving process without being broken apart.

Like other material, the use of ECPs for textile supercapacitors has both advantages and challenges. The main characteristics of ECP-based textile supercapacitors are (1) their inherent flexibility, (2) ease of coating into various types and shapes of textiles, (3) diverse methods for polymerization and embedding into various conductive/nonconductive textile substrates, (4) possibility of controlling their nanostructured morphology with nanoscale dimensions, (5) possibility of use without
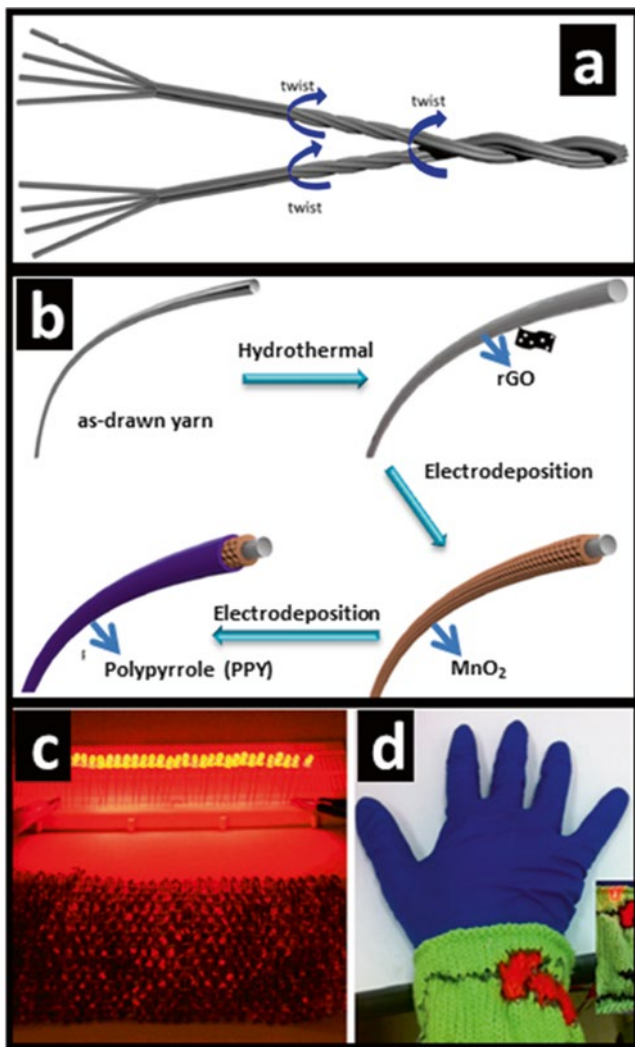
Fig. 21.15 (**a**) Schematics of yarn fabrication; (**b**) illustration of the three-stage fabrication process of the hierarchically structured conductive yarn; (**c** and **d**) photographs of the energy storage textiles made of yarns (the 15 cm × 10 cm woven clothes can light 30 LEDs) (**c**), and a wristband knitted with a pattern (inset shows the pattern powering a LED) (**d**). Reproduced with permission from [198]

electrolyte, (6) high theoretical specific capacitance, (7) relatively low cost for industrial scale-up process, (8) possibility for a wide range of working potential window based on the employed electrolyte, (9) possibility for integration into high-performance composite/asymmetric hybrid supercapacitors, and (10) the possibility of use in flexible textile display devices.

The main challenges for utilization of ECP-based textile supercapacitors are (1) their limited cycling stability due to the swelling/shrinkage during charging/discharging process (Fig. 21.6), (2) lower conductivity when compared to metals and metal nanoparticle, and (3) lower capacitance when employed with gel electrolytes compared to liquid electrolytes.

21.6 Future Outlook

The above limitations of using ECP-based textile supercapacitors can be resolved by: (1) Increasing the specific capacitance of pure ECP-based textile supercapacitors by designing nanostructured polymer coatings with controlled nanoscale dimensions, porous structure, and high surface area for achieving both reduced path for ion diffusion and lower ion diffusion resistance. (2) Improving the limited cycling stability by using composite materials such as ECP/CC, ECP/graphene, ECP/CNTs, and ECP/metal oxides. (3) Preparation of ECP-based textile supercapacitors indirectly from ECP-coated fibers. This approach is expected to provide conductive fibers without affecting their flexibility and tensile properties, and hence, it offers an alternative choice for preparation of textile supercapacitors through weaving and knitting process. Various fibers can be explored including natural and synthetic fibers, metal fibers, and carbon-based fibers. (4) Preparation of ECP-based textile supercapacitors through different technologies such as inkjet/screen printing or preparation of ECP-based conductive fibers through fiber welding and biscrolling methodologies. The latter two approaches allow for incorporation of ECPs with a wide range of guest materials for enhancing conductivity, redox properties, or other essential properties that might enhance the performance of the target textile supercapacitor.

References

1. Stoppa M, Chiolerio A (2014) Wearable electronics and smart textiles: a critical review. Sensors 14(7):11957–11992
2. http://www.textileworld.com/Articles/2015/February/The_Rupp_Report-Successful_Technical_Textiles_Part_II (Last Accessed Dec 10, 2015)
3. Jinlian H et al (2012) A review of stimuli-responsive polymers for smart textile applications. Smart Mater Struct 21(5):053001
4. Stuart MAC et al (2010) Emerging applications of stimuli-responsive polymer materials. Nat Mater 9(2):101–113
5. Li Z et al (2014) Ag nanoparticle–ZnO nanowire hybrid nanostructures as enhanced and robust antimicrobial textiles via a green chemical approach. Nanotechnology 25(14):145702
6. Kowal K et al (2014) Biocidal effect and durability of nano-TiO_2 coated textiles to combat hospital acquired infections. RSC Adv 4(38):19945–19952
7. Li Y-C et al (2010) Flame retardant behavior of polyelectrolyte–clay thin film assemblies on cotton fabric. ACS Nano 4(6):3325–3337

8. Horrocks AR (2011) Flame retardant challenges for textiles and fibres: new chemistry versus innovatory solutions. Polym Degrad Stab 96(3):377–392
9. Cain AA et al (2014) Intumescent nanocoating extinguishes flame on fabric using aqueous polyelectrolyte complex deposited in single step. Macromol Mater Eng 299(10):1180–1187
10. Carosio F et al (2014) Flame retardancy of polyester and polyester–cotton blends treated with caseins. Indus Eng Chem Res 53(10):3917–3923
11. Hu J (2007) Chapter 10 – Shape memory textiles. In: Hu J (ed) Shape memory polymers and textiles. Woodhead Publishing, Cambridge, pp 305–337
12. Mattila H (2015) Chapter 15 – Yarn to fabric: intelligent textiles. In: Sinclair R (ed) Textiles and fashion. Woodhead Publishing, Cambridge, pp 355–376
13. Hu J (2013) Chapter 10 – Shape memory finishing treatments for smart textiles. In: Hu J (ed) Advances in shape memory polymers. Woodhead Publishing, Cambridge, pp 259–280
14. Gugliuzza A, Drioli E (2013) A review on membrane engineering for innovation in wearable fabrics and protective textiles. J Membr Sci 446:350–375
15. Hsu P-C et al (2015) Personal thermal management by metallic nanowire-coated textile. Nano Lett 15(1):365–371
16. Wang X et al (2014) Smart hydrogel-functionalized textile system with moisture management property for skin application. Smart Mater Struct 23(12):125027
17. Yu D et al (2014) Modifying surface resistivity and liquid moisture management property of keratin fibers through thiol-ene click reactions. ACS Appl Mater Interfaces 6(2):1236–1242
18. Wang X et al (2015) Effect of surface modifications on the thermal and moisture behavior of wool fabric. Appl Surf Sci 342:101–105
19. Qi K et al (2006) Self-cleaning cotton. J Mater Chem 16(47):4567–4574
20. Qi K et al (2007) Facile preparation of anatase/SiO_2 spherical nanocomposites and their application in self-cleaning textiles. J Mater Chem 17(33):3504–3508
21. Bedford N, Steckl A (2010) Photocatalytic self cleaning textile fibers by coaxial electrospinning. ACS Appl Mater Interfaces 2(8):2448–2455
22. Afzal S, Daoud WA, Langford SJ (2014) Superhydrophobic and photocatalytic self-cleaning cotton. J Mater Chem A 2(42):18005–18011
23. Lina MC, Alison BF (2014) Smart fabric sensors and e-textile technologies: a review. Smart Mater Struct 23(5):053001
24. Hang Q, Oleg S, Maksim S (2015) Flexible fiber batteries for applications in smart textiles. Smart Mater Struct 24(2):025012
25. Saeed SE-S et al (2014) Novel chitosan-ZnO based nanocomposites as luminescent tags for cellulosic materials. Carbohydr Polym 99:817–824
26. Zhang P et al (2015) Luminescent golden silk and fabric through in situ chemically coating pristine-silk with gold nanoclusters. Biomaterials 36:26–32
27. Yang H, Lightner CR, Dong L (2011) Light-emitting coaxial nanofibers. ACS Nano 6(1):622–628
28. Lv Z et al (2012) Highly efficient and completely flexible fiber-shaped dye-sensitized solar cell based on TiO2 nanotube array. Nanoscale 4(4):1248–1253
29. Yun MJ et al (2014) Highly flexible dye-sensitized solar cells produced by sewing textile electrodes on cloth. Sci Rep 4:5322
30. Liu Z et al (2015) Flexible electronics based on inorganic nanowires. Chem Soc Rev 44(1):161–192
31. Singh MK (2011) Flexible photovoltaic textiles for smart applications. INTECH Open Access, Rijeka, Croatia
32. Hu L et al (2011) Lithium-ion textile batteries with large areal mass loading. Adv Energy Mater 1(6):1012–1017
33. Liu B et al (2012) Hierarchical three-dimensional ZnCo2O4 nanowire arrays/carbon cloth anodes for a novel class of high-performance flexible lithium-ion batteries. Nano Lett 12(6):3005–3011

34. Liu Y et al (2012) Flexible, solid electrolyte-based lithium battery composed of LiFePO4 cathode and Li4Ti5O12 anode for applications in smart textiles. J Electrochem Soc 159(4):A349–A356

35. Luo Y et al (2012) Seed-assisted synthesis of highly ordered TiO 2@ α-Fe 2 O 3 core/shell arrays on carbon textiles for lithium-ion battery applications. Energy Environ Sci 5(4):6559–6566

36. Cheng Q et al (2013) Folding paper-based lithium-ion batteries for higher areal energy densities. Nano Lett 13(10):4969–4974

37. Zhou X et al (2014) Cotton-templated fabrication of hierarchical SnO$_2$ mesoporous microtubes as the anode material of lithium ion battery. Mater Lett 120:279–282

38. Laforgue A (2011) All-textile flexible supercapacitors using electrospun poly (3, 4-ethylenedioxythiophene) nanofibers. J Power Sources 196(1):559–564

39. Yue B et al (2012) Polypyrrole coated nylon lycra fabric as stretchable electrode for supercapacitor applications. Electrochim Acta 68:18–24

40. Lee JA et al (2013) Ultrafast charge and discharge biscrolled yarn supercapacitors for textiles and microdevices. Nature Commun 4:1970–1977

41. Meng Y et al (2013) All-graphene core-sheath microfibers for all-solid-state, stretchable fibriform supercapacitors and wearable electronic textiles. Adv Mater 25(16):2326–2331

42. Ma TY et al (2014) Phosphorus-doped graphitic carbon nitrides grown in situ on carbon-fiber paper: flexible and reversible oxygen electrodes. Angew Chem 54(15):4646–4650

43. Yang P et al (2014) Worm-like amorphous MnO$_2$ nanowires grown on textiles for high-performance flexible supercapacitors. J Mater Chem A 2(3):595–599

44. Zhang D et al (2014) Core spun carbon nanotube yarn supercapacitors for wearable electronic textiles. ACS Nano 8(5):4571-4579

45. Wu Q et al (2010) Supercapacitors based on flexible graphene/polyaniline nanofiber composite films. ACS Nano 4(4):1963–1970

46. Bonfiglio A et al (2005) Organic field effect transistors for textile applications. IEEE Trans Inf Technol Biomed 9(3):319–324

47. Hamedi M, Forchheimer R, Inganas O (2007) Towards woven logic from organic electronic fibres. Nat Mater 6(5):357–362

48. Hamedi M et al (2009) Fiber-embedded electrolyte-gated field-effect transistors for e-textiles. Adv Mater 21(5):573–577

49. Bubnova O, Berggren M, Crispin X (2012) Tuning the thermoelectric properties of conducting polymers in an electrochemical transistor. J Am Chem Soc 134(40):16456–16459

50. Collins GE, Buckley L (1996) Conductive polymer-coated fabrics for chemical sensing. Synth Met 78(2):93–101

51. Babel A et al (2005) Electrospun nanofibers of blends of conjugated polymers: morphology, optical properties, and field-effect transistors. Macromolecules 38(11):4705–4711

52. Jung YS et al (2008) Nanowire conductive polymer gas sensor patterned using self-assembled block copolymer lithography. Nano Lett 8(11):3776–3780

53. Castano LM, Flatau AB (2014) Smart fabric sensors and e-textile technologies: a review. Smart Mater Struct 23(5):053001

54. Forzani ES et al (2004) A conducting polymer nanojunction sensor for glucose detection. Nano Lett 4(9):1785–1788

55. Shim BS et al (2008) Smart electronic yarns and wearable fabrics for human biomonitoring made by carbon nanotube coating with polyelectrolytes. Nano Lett 8(12):4151–4157

56. Shyamkumar P et al (2014) Wearable wireless cardiovascular monitoring using textile-based nanosensor and nanomaterial systems. Electronics 3(3):504–520

57. Cochrane C et al (2011) Flexible displays for smart clothing: Part I-Overview. Indian J Fibre Textile Res 36(4):422

58. Kelly FM et al (2013) Polyaniline: application as solid state electrochromic in a flexible textile display. Displays 34(1):1–7

59. Wang P-C et al (2013) Transparent electrodes based on conducting polymers for display applications. Displays 34(4):301–314

60. Abu-Thabit N, Basheer R (2014) Nanostructured conductive composite filter electrodes for water sterealization by application of low electrical current. In: Proceedings of the 1st international electronic conference on materials, 26 May–10 June 2014. Sciforum Electronic Conference Series, vol 1, b015. doi:10.3390/ecm-1-b015

61. Abu-Thabit NY, Basheer RA (2014) Synthesis of highly conductive cotton fiber/nanostructured silver/polyaniline composite membranes for water sterilization application. Mater Res Express 1(3):035010

62. Basheer R, Abu-Thabit N (2012) High-speed water sterilization using conducting polymer-metal nanoparticles composite. Abstracts of papers of the American Chemical Society, Washington, DC

63. Liu C et al (2013) Conducting nanosponge electroporation for affordable and high-efficiency disinfection of bacteria and viruses in water. Nano Lett 13(9):4288–4293

64. Liu C et al (2014) Static electricity powered copper oxide nanowire microbicidal electroporation for water disinfection. Nano Lett 14(10):5603–5608

65. Schoen DT et al (2010) High speed water sterilization using one-dimensional nanostructures. Nano Lett 10(9):3628–3632

66. Wang F et al (2010) A review of technology of personal heating garments. Int J Occup Saf Ergonom 16(3):387–404

67. Hsu P-C et al (2014) Personal thermal management by metallic nanowire-coated textile. Nano Lett 15(1):365-371

68. Matsunaga T et al (1992) Disinfection of drinking water by using a novel electrochemical reactor employing carbon-cloth electrodes. Appl Environ Microbiol 58(2):686–689

69. Carrott P et al (2001) Preparation of activated carbon fibres from acrylic textile fibres. Carbon 39(10):1543–1555

70. Ren Y, Lam DCC (2008) Properties and microstructures of low-temperature-processable ultralow-dielectric porous polyimide films. J Electron Mater 37(7):955–961

71. Mark JE (2009) Polymer data handbook, vol 27. Oxford University Press, New York, NY

72. Zeng W et al (2014) Fiber-based wearable electronics: a review of materials, fabrication, devices, and applications. Adv Mater 26(31):5310–5336

73. Hu L, Cui Y (2012) Energy and environmental nanotechnology in conductive paper and textiles. Energy Environ Sci 5(4):6423–6435

74. Wei Q (2009) Surface modification of textiles.Woodhead Publishing Limited, Cambridge, UK

75. Jur J et al (2011) Atomic layer deposition of conductive coatings on cotton, paper, and synthetic fibers: conductivity analysis and functional chemical sensing using "all-fiber" capacitors. Adv Funct Mater 21(11):1993–2002

76. Marichy C, Bechelany M, Pinna N (2012) Atomic layer deposition of nanostructured materials for energy and environmental applications. Adv Mater 24(8):1017–1032

77. Wang K et al (2014) Conducting polymer nanowire arrays for high performance supercapacitors. Small 10(1):14–31

78. Abu-Thabit NY, Makhlouf ASH (2014) Chapter 17 – Recent advances in polyaniline (PANI)-based organic coatings for corrosion protection. In: Makhlouf ASH (ed) Handbook of smart coatings for materials protection. Woodhead Publishing, Cambridge, pp 459–486

79. Horng Y-Y et al (2010) Flexible supercapacitor based on polyaniline nanowires/carbon cloth with both high gravimetric and area-normalized capacitance. J Power Sources 195(13):4418–4422

80. Cheng Q et al (2011) Polyaniline-coated electro-etched carbon fiber cloth electrodes for supercapacitors. J Phys Chem C 115(47):23584–23590

81. Dubal DP et al (2012) Porous polypyrrole clusters prepared by electropolymerization for a high performance supercapacitor. J Mater Chem 22(7):3044–3052

82. Kuila BK et al (2009) Vertically oriented arrays of polyaniline nanorods and their super electrochemical properties. Chem Commun 38:5749–5751

83. Stejskal J, Sapurina I, Trchova M (2010) Polyaniline nanostructures and the role of aniline oligomers in their formation. Prog Polym Sci 35:1420–1481

84. Agarwal M, Lvov Y, Varahramyan K (2006) Conductive wood microfibres for smart paper through layer-by-layer nanocoating. Nanotechnology 17(21):5319

85. Jeon J-W, Kwon SR, Lutkenhaus JL (2015) Polyaniline nanofiber/electrochemically reduced graphene oxide layer-by-layer electrodes for electrochemical energy storage. J Mater Chem A 3(7):3757–3767

86. Guan H et al (2010) Polyaniline nanofibers obtained by interfacial polymerization for high-rate supercapacitors. Electrochim Acta 56(2):964–968

87. Hao Q et al (2011) Morphology-controlled fabrication of sulfonated graphene/polyaniline nanocomposites by liquid/liquid interfacial polymerization and investigation of their electrochemical properties. Nano Res 4(4):323–333

88. Zhang X et al (2004) Nanofibers of polyaniline synthesized by interfacial polymerization. Synth Met 145(1):23–29

89. Wu C-G, Bein T (1994) Conducting polyaniline filaments in a mesoporous channel host. Science 264(5166):1757–1759

90. Menon VP, Lei J, Martin CR (1996) Investigation of molecular and supermolecular structure in template-synthesized polypyrrole tubules and fibrils. Chem Mater 8(9):2382–2390

91. Choi SJ, Park SM (2000) Electrochemical growth of nanosized conducting polymer wires on gold using molecular templates. Adv Mater 12(20):1547–1549

92. Zhong W et al (2005) Synthesis of large-area three-dimensional polyaniline nanowire networks using a "soft template". Macromol Rapid Commun 26(5):395–400

93. Pillalamarri SK et al (2005) Radiolytic synthesis of polyaniline nanofibers: a new template-less pathway. Chem Mater 17(2):227–229

94. Zhang X, Goux WJ, Manohar SK (2004) Synthesis of polyaniline nanofibers by "nanofiber seeding". J Am Chem Soc 126(14):4502–4503

95. Li W, Wang H-L (2004) Oligomer-assisted synthesis of chiral polyaniline nanofibers. J Am Chem Soc 126(8):2278–2279

96. Chiou NR, Epstein AJ (2005) Polyaniline nanofibers prepared by dilute polymerization. Adv Mater 17(13):1679–1683

97. Zhang X et al (2006) Fibrillar growth in polyaniline. Adv Funct Mater 16(9):1145–1152

98. Zhang X, Manohar SK (2004) Polyaniline nanofibers: chemical synthesis using surfactants. Chem Commun 20:2360–2361

99. Li G, Jiang L, Peng H (2007) One-dimensional polyaniline nanostructures with controllable surfaces and diameters using vanadic acid as the oxidant. Macromolecules 40(22):7890–7894

100. Winther-Jensen B, West K (2004) Vapor-phase polymerization of 3, 4-ethylenedioxythiophene: a route to highly conducting polymer surface layers. Macromolecules 37(12):4538–4543

101. Najar SS, Kaynak A, Foitzik RC (2007) Conductive wool yarns by continuous vapour phase polymerization of pyrrole. Synth Met 157(1):1–4

102. Dall'Acqua L et al (2006) Vapour phase polymerisation of pyrrole on cellulose-based textile substrates. Synth Met 156(5):379–386

103. Lee H-H, Chou K-S, Huang K-C (2005) Inkjet printing of nanosized silver colloids. Nanotechnology 16(10):2436

104. Perelaer J et al (2009) One-step inkjet printing of conductive silver tracks on polymer substrates. Nanotechnology 20(16):165303

105. Jang J, Ha J, Cho J (2007) Fabrication of water-dispersible polyaniline-poly (4-styrenesulfonate) nanoparticles for inkjet-printed chemical-sensor applications. Adv Mater 19(13):1772–1775

106. Chiolerio A, Bocchini S, Porro S (2014) Inkjet printed negative supercapacitors: synthesis of polyaniline-based inks, doping agent effect, and advanced electronic devices applications. Adv Funct Mater 24(22):3375–3383

107. Xu Y et al (2014) Inkjet-printed energy storage device using graphene/polyaniline inks. J Power Sources 248:483–488

108. Kaempgen M et al (2009) Printable thin film supercapacitors using single-walled carbon nanotubes. Nano Lett 9(5):1872–1876
109. Chen P et al (2010) Inkjet printing of single-walled carbon nanotube/RuO2 nanowire supercapacitors on cloth fabrics and flexible substrates. Nano Res 3(8):594–603
110. Tortorich RP, Choi J-W (2013) Inkjet printing of carbon nanotubes. Nanomaterials 3(3):453–468
111. Huang L et al (2011) Graphene-based conducting inks for direct inkjet printing of flexible conductive patterns and their applications in electric circuits and chemical sensors. Nano Res 4(7):675–684
112. Kong D et al (2012) Temperature-dependent electrical properties of graphene inkjet-printed on flexible materials. Langmuir 28(37):13467–13472
113. Li J et al (2013) Efficient inkjet printing of graphene. Adv Mater 25(29):3985–3992
114. Le LT et al (2011) Graphene supercapacitor electrodes fabricated by inkjet printing and thermal reduction of graphene oxide. Electrochem Commun 13(4):355–358
115. Cummins G, Desmulliez MP (2012) Inkjet printing of conductive materials: a review. Circuit World 38(4):193–213
116. Walker SB, Lewis JA (2012) Reactive silver inks for patterning high-conductivity features at mild temperatures. J Am Chem Soc 134(3):1419–1421
117. Li D et al (2009) Conductive copper and nickel lines via reactive inkjet printing. J Mater Chem 19(22):3719–3724
118. Meoli D, May-Plumlee T (2002) Interactive electronic textile development: a review of technologies. J Textile Apparel Technol Manage 2(2):1–12
119. Kazani I et al (2012) Electrical conductive textiles obtained by screen printing. Fibres Textiles East Eur 90(1):57–63
120. Behabtu N et al (2013) Strong, light, multifunctional fibers of carbon nanotubes with ultra-high conductivity. Science 339(6116):182–186
121. Dalton AB et al (2003) Super-tough carbon-nanotube fibres. Nature 423(6941):703
122. Zhang M, Atkinson KR, Baughman RH (2004) Multifunctional carbon nanotube yarns by downsizing an ancient technology. Science 306(5700):1358–1361
123. Cong H-P et al (2012) Wet-spinning assembly of continuous, neat, and macroscopic graphene fibers. Sci Rep 2, 613
124. Dong Z et al (2012) Facile fabrication of light, flexible and multifunctional graphene fibers. Adv Mater 24(14):1856–1861
125. Xu Z et al (2013) Ultrastrong fibers assembled from giant graphene oxide sheets. Adv Mater 25(2):188–193
126. Cheng H et al (2013) Textile electrodes woven by carbon nanotube–graphene hybrid fibers for flexible electrochemical capacitors. Nanoscale 5(8):3428–3434
127. Sun H et al (2014) Novel graphene/carbon nanotube composite fibers for efficient wire-shaped miniature energy devices. Adv Mater 26(18):2868–2873
128. Xu Z et al (2013) Highly electrically conductive ag-doped graphene fibers as stretchable conductors. Adv Mater 25(23):3249–3253
129. Peng H (2015) Electrically conducting fiber. In: Fiber-shaped energy harvesting and storage devices. Springer, Berlin, pp 7–38
130. Bowman D, Mattes B (2005) Conductive fibre prepared from ultra-high molecular weight polyaniline for smart fabric and interactive textile applications. Synth Met 154(1):29–32
131. Pomfret SJ et al (2000) Electrical and mechanical properties of polyaniline fibres produced by a one-step wet spinning process. Polymer 41(6):2265–2269
132. Pomfret SJ et al (1998) Inherently electrically conductive fibers wet spun from a sulfonic acid–doped polyaniline solution. Adv Mater 10(16):1351–1353
133. Mottaghitalab V, Spinks GM, Wallace GG (2005) The influence of carbon nanotubes on mechanical and electrical properties of polyaniline fibers. Synth Met 152(1):77–80
134. Okuzaki H, Ishihara M (2003) Spinning and characterization of conducting microfibers. Macromol Rapid Commun 24(3):261–264

135. Okuzaki H, Harashina Y, Yan H (2009) Highly conductive PEDOT/PSS microfibers fabricated by wet-spinning and dip-treatment in ethylene glycol. Eur Polym J 45(1):256–261
136. Jalili R et al (2011) One-step wet-spinning process of poly(3,4-ethylenedioxythiophene):poly(styrenesulfonate) fibers and the origin of higher electrical conductivity. Adv Funct Mater 21(17):3363–3370
137. Lima MD et al (2011) Biscrolling nanotube sheets and functional guests into yarns. Science 331(6013):51–55
138. Fang S et al (2012) Fabrication of biscrolled fiber using carbon nanotube sheet. US Patent No 8,968,756. Washington, DC: U.S. Patent and Trademark Office
139. Jost K et al (2014) Natural fiber welded electrode yarns for knittable textile supercapacitors. Adv Energy Mater 5(4):1–8
140. Haverhals LM et al (2010) Natural fiber welding. Macromol Mater Eng 295(5):425–430
141. Simon P, Gogotsi Y (2008) Materials for electrochemical capacitors. Nat Mater 7(11):845–854
142. Yan J et al (2014) Recent advances in design and fabrication of electrochemical supercapacitors with high energy densities. Adv Energy Mater 4(4):1-43
143. Yu G et al (2013) Hybrid nanostructured materials for high-performance electrochemical capacitors. Nano Energy 2(2):213–234
144. Zhang LL, Zhao X (2009) Carbon-based materials as supercapacitor electrodes. Chem Soc Rev 38(9):2520–2531
145. Frackowiak E, Beguin F (2001) Carbon materials for the electrochemical storage of energy in capacitors. Carbon 39(6):937–950
146. Zhu Y et al (2011) Carbon-based supercapacitors produced by activation of graphene. Science 332(6037):1537–1541
147. Cottineau T et al (2006) Nanostructured transition metal oxides for aqueous hybrid electrochemical supercapacitors. Appl Phys A 82(4):599–606
148. Deng W et al (2011) Electrochemical capacitors utilising transition metal oxides: an update of recent developments. RSC Adv 1(7):1171–1178
149. Lang X et al (2011) Nanoporous metal/oxide hybrid electrodes for electrochemical supercapacitors. Nat Nanotechnol 6(4):232–236
150. Dubal D et al (2015) Hybrid energy storage: the merging of battery and supercapacitor chemistries. Chem Soc Rev 44(7):1777–1790
151. Qu Q et al (2012) Core–shell structure of polypyrrole grown on V_2O_5 nanoribbon as high performance anode material for supercapacitors. Adv Energy Mater 2(8):950–955
152. Zhang K et al (2015) Flexible and all-solid-state supercapacitors with long-time stability constructed on PET/Au/polyaniline hybrid electrodes. J Mater Chem A 3(2):617–623
153. Hu L et al (2010) Stretchable, porous, and conductive energy textiles. Nano Lett 10(2):708–714
154. Huang Y et al (2015) High-performance flexible supercapacitors based on mesoporous carbon nanofibers/Co_3O_4/MnO_2 hybrid electrodes. RSC Adv 5(24):18952–18959
155. Jiang Y et al (2015) Flexible of multiwalled carbon nanotubes/manganese dioxide nanoflake textiles for high-performance electrochemical capacitors. Electrochim Acta 153:246–253
156. Zhang Z et al (2015) Superelastic supercapacitors with high performances during stretching. Adv Mater 27(2):356–362
157. Dong L et al (2015) High-performance compressible supercapacitors based on functionally synergic multiscale carbon composite textiles. J Mater Chem A 3(8):4729–4737
158. Shown I et al (2015) Conducting polymer-based flexible supercapacitor. Energy Sci Eng 3(1):2–26
159. Naoi K, Simon P (2008) New materials and new configurations for advanced electrochemical capacitors. J Electrochem Soc 17(1):34–37
160. Shirakawa H, McDiarmid A, Heeger A (2003) Twenty-five years of conducting polymers. Chem Commun 2003(1):1–4

161. Novák P et al (1997) Electrochemically active polymers for rechargeable batteries. Chem Rev 97(1):207–282
162. Li FS et al (2015) A mechanically robust and highly ion-conductive polymer-blend coating for high-power and long-life lithium-ion battery anodes. Adv Mater 27(1):130–137
163. Peng C et al (2008) Carbon nanotube and conducting polymer composites for supercapacitors. Prog Nat Sci 18(7):777–788
164. Li H et al (2009) Theoretical and experimental specific capacitance of polyaniline in sulfuric acid. J Power Sources 190(2):578–586
165. Chen W, Rakhi RB, Alshareef HN (2013) Facile synthesis of polyaniline nanotubes using reactive oxide templates for high energy density pseudocapacitors. J Mater Chem A 1(10):3315–3324
166. Fusalba F et al (2001) Electrochemical characterization of polyaniline in nonaqueous electrolyte and its evaluation as electrode material for electrochemical supercapacitors. J Electrochem Soc 148(1):A1–A6
167. Tan YT et al (2013) Synthesis and electrochemical properties of hollow polyaniline microspheres by a sulfonated polystyrene template. J Appl Polym Sci 127(3):1544–1549
168. Lu YF et al (2007) Direct electrochemistry and bioelectrocatalysis of myoglobin at a carbon nanotube-modified electrode. Acta Phys Chim Sin 23(1):5–11
169. Yang H-S, Zhou X, Zhang Q (2005) Electrochemical performances of supercapacitor with polyaniline particles with hierarchy as active electrode material. Acta Phys Chim Sin 21(04):414–418
170. Xiong SX et al (2012) Covalently bonded polyaniline/fullerene hybrids with coral-like morphology for high-performance supercapacitor. Electrochim Acta 85:235–242
171. Gupta V, Miura N (2005) Electrochemically deposited polyaniline nanowire's network – a high-performance electrode material for redox supercapacitor. Electrochem Solid State Lett 8(12):A630–A632
172. Wang K, Huang JY, Wei ZX (2010) Conducting polyaniline nanowire arrays for high performance supercapacitors. J Phys Chem C 114(17):8062–8067
173. Kim BC et al (2010) Preparation and enhanced stability of flexible supercapacitor prepared from Nafion/polyaniline nanofiber. Synth Met 160(1–2):94–98
174. Sharma R, Rastogi A, Desu S (2008) Pulse polymerized polypyrrole electrodes for high energy density electrochemical supercapacitor. Electrochem Commun 10(2):268–272
175. Zhang D et al (2011) Enhanced capacitance and rate capability of graphene/polypyrrole composite as electrode material for supercapacitors. J Power Sources 196(14):5990–5996
176. Ingram MD, Staesche H, Ryder KS (2004) 'Activated' polypyrrole electrodes for high-power supercapacitor applications. Solid State Ion 169(1):51–57
177. Yuan L et al (2013) Polypyrrole-coated paper for flexible solid-state energy storage. Energy Environ Sci 6(2):470–476
178. Yue B et al (2013) Electrochemically synthesized stretchable polypyrrole/fabric electrodes for supercapacitor. Electrochim Acta 113:17–22
179. Huang Y et al (2015) Super-high rate stretchable polypyrrole-based supercapacitors with excellent cycling stability. Nano Energy 11:518–525
180. Firoz Babu K, Siva Subramanian SP, Anbu Kulandainathan M (2013) Functionalisation of fabrics with conducting polymer for tuning capacitance and fabrication of supercapacitor. Carbohydr Polym 94(1):487–495
181. Carlberg J, Inganäs O (1997) Poly (3, 4-ethylenedioxythiophene) as electrode material in electrochemical capacitors. J Electrochem Soc 144(4):L61–L64
182. Ryu KS et al (2004) Poly (ethylenedioxythiophene)(PEDOT) as polymer electrode in redox supercapacitor. Electrochim Acta 50(2):843–847
183. Stenger-Smith JD et al (2002) Poly (3, 4-alkylenedioxythiophene)-based supercapacitors using ionic liquids as supporting electrolytes. J Electrochem Soc 149(8):A973–A977
184. Alvi F et al (2011) Graphene–polyethylenedioxythiophene conducting polymer nanocomposite based supercapacitor. Electrochim Acta 56(25):9406–9412

185. Zhu Y et al (2010) Graphene and graphene oxide: synthesis, properties, and applications. Adv Mater 22(35):3906–3924
186. Geim AK (2009) Graphene: status and prospects. Science 324(5934):1530–1534
187. Liu C et al (2010) Graphene-based supercapacitor with an ultrahigh energy density. Nano Lett 10(12):4863–4868
188. Yan J et al (2010) Preparation of a graphene nanosheet/polyaniline composite with high specific capacitance. Carbon 48(2):487–493
189. Yan J et al (2010) Preparation of graphene nanosheet/carbon nanotube/polyaniline composite as electrode material for supercapacitors. J Power Sources 195(9):3041–3045
190. Xu Y et al (2013) Screen-printable thin film supercapacitor device utilizing graphene/polyaniline inks. Adv Energy Mater 3(8):1035–1040
191. Fan T et al (2015) Self-assembling sulfonated graphene/polyaniline nanocomposite paper for high performance supercapacitor. Synth Met 199:79–86
192. Pan S et al (2014) Novel wearable energy devices based on aligned carbon nanotube fiber textiles. Adv Energy Mater 5(4):1–8
193. Peng H (2015) Fiber-shaped energy harvesting and storage devices. Springer, Berlin
194. Wang K et al (2013) High-performance two-ply yarn supercapacitors based on carbon nanotubes and polyaniline nanowire arrays. Adv Mater 25(10):1494–1498
195. Lu W et al (2002) Use of ionic liquids for π-conjugated polymer electrochemical devices. Science 297(5583):983–987
196. Meunier L et al (2011) Flexible displays for smart clothing: Part II-Electrochromic displays. Indian J Fibre Textile Res 36(4):429
197. Chen X et al (2014) Electrochromic fiber-shaped supercapacitors. Adv Mater 26(48):8126–8132
198. Huang Y et al (2015) From industrially weavable and knittable highly conductive yarns to large wearable energy storage textiles. ACS Nano. doi:10.1021/acsnano.5b00860
199. Lee MR et al (2009) Solar power wires based on organic photovoltaic materials. Science 324(5924):232–235

Chapter 22
Self-Healing Coatings for Corrosion Protection of Steel

Liana Maria Muresan

Abstract Self-healing coatings belong to a new generation of smart coatings for corrosion control, which have both passive characteristics (from matrix material) and active behavior towards the local environment (through incorporated or surface-mounted compounds acting as inhibitors). The coatings provide a rapid release of a repairing material (e.g., a corrosion inhibitor) after changes in coating integrity by mechanical/chemical damage of the coating or by local pH changes occurring near the metallic surface. Within all classes of materials, the one with the largest self-repair potential belongs to polymers since they display more useful properties than any other material. However, besides these materials, inorganic (including mainly silica, titania, zirconia, etc.), organic, or hybrid layers have been successfully used as matrices for self-repairing coatings. On the other hand, the self-healing agents embedded in the matrices belong to different classes varying from natural compounds (tung oil, spar varnish, camphor, linseed oil, etc.) to synthetic ones (isodecyl diphenyl phosphate, 2-mercaptobenzothiazole, alkyl ammonium salts, etc.). In this context, recent advances in preparation and characterization of different self-healing coatings on steel will be reviewed. The main techniques for obtaining self-healing coatings and the challenges for future research will be also briefly discussed.

Keywords Corrosion • Self-healing • Protective coatings • Steel • Corrosion inhibitors

22.1 Introduction

Self-healing coatings belong to a new generation of "smart" coatings for anticorrosion protection of metals, which are inspired from biological systems where damage triggers an autonomic healing response.

L.M. Muresan (✉)
Faculty of Chemistry and Chemical Engineering, Babes-Bolyai University,
Cluj-Napoca 400028, Romania
e-mail: limur@chem.ubbcluj.ro

Most of the materials currently used in industry are protected against corrosion by passive layers with barrier properties that could be irreversibly attacked by external factors. Initiation of cracks and other types of damage on a microscopic level has been shown to dramatically change the properties of the "classical" protective coatings and eventually leads to the whole-scale failure of the material. This is why efforts have been made in the direction of finding new and efficient protective coatings on metals. Most of them are passive coatings, acting only as physical barriers against corrosion, but some exert an active repairing action when the coatings are damaged.

The self-healing concept relies on an active repair based on the rapid release of a repairing agent after changes in the integrity of a coating as a consequence of mechanical/chemical damage or of factors originating from the surrounding environment (heat, UV radiation, humidity, etc.). Self-healing coatings are in fact stimuli-responsive systems. Ideal smart self-repairing coatings should not only replace any passive protection layers, but should be able to continuously control and monitor the integrity and functionality of the materials through sensing elements incorporated in their structure [1]. By prolonging the material's service life, self-healing contributes to saving natural resources and brings economic benefits to society. This is why, nowadays, considerable efforts are oriented towards the development of self-repairing anticorrosion coatings.

Steel is an important material that is widely used for construction, especially in heavy industries (mining, oil and gas industries, aircraft and automotive industries, etc.), and its corrosion represents a serious problem that can be prevented or minimized by applying protective coatings on its surface. Among these coatings, those possessing self-healing functionalities are preferred more and more.

In this context, recent advances in the preparation and characterization of self-healing coatings on steel are reviewed with an emphasis on their main components: matrices and healing agents. The challenges for future research are also briefly discussed.

22.2 Background of Self-Healing Coatings

22.2.1 Self-Healing Concept

For a material to be strictly defined as self-healing, it is necessary that the repairing process occurs automatically, without intervention of a human being. In other words, self-healing materials have the built-in capacity to recover after damage either autonomously or after application of a specific stimulus (heat, UV light, pH change, electric or magnetic field, etc.). Healing is due either to the formation of layers of corrosion products which act as a barrier against corrosion (passive protection) or to certain protective species generated in the presence of inhibitors (active protection) [2].

The active agents that ensure self-healing (e.g., corrosion inhibitors) can be embedded into the different passive components of the coating: pretreated surface layer, primer and/or topcoat. They can be introduced in the coating directly or by loading them into vascular networks or nanoreservoirs embedded into the passive matrix [3].

22.2.2 Matrices Used for Self-Healing Coatings

A wide range of materials can be used as matrices for self-healing coatings. Frequently, passive layers alternate with active layers in order to ensure the best stability and corrosion resistance of the coatings.

Polymers have the largest self-repairing potential, but there are many other materials that can be used as matrices for self-repairing coatings. Some of these materials belonging to different categories are reviewed below.

22.2.2.1 Inorganic Coatings

Self-healing metals and alloys do not count for a large number of representatives. Among them, zinc, Al–Cu–Mg, and Ti–Bi alloys are the most used [4]. However, it should be mentioned that the healing takes place only in the case of small defects.

In the case of zinc, the coatings deposited on steel exhibit self-healing properties due to chemical reactions that take place in the presence of oxygen and water (i.e., Zn dissolution in parallel with oxygen reduction) during the corrosion process:

$$Zn^{2+} + H_2O \rightarrow ZnOH^+ + H^+$$

$$ZnOH^+ + H_2O \rightarrow Zn(OH)_{2(aq)} + H^+$$
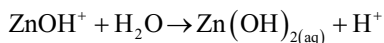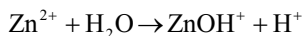
Zn (OH)$_2$ has a very low solubility product and precipitates in the scratches of the surface, filling, or refilling the cavities of damaged materials. A strategy to enhance the protective properties of zinc coatings would be the incorporation of other elements (i.e., nanoparticles) which improve their self-healing properties [5] or to use different treatments in order to generate conversion coatings on zinc surface.

Chromate conversion coatings used for corrosion protection of galvanized steel have recognized self-healing properties. Moreover, they are cheap and easy to prepare. However, due to the high toxicity of Cr (VI) salts, these conversion coatings are nowadays banished and efforts have been made to replace them with other effective, but less toxic, protective coatings [6].

Phosphate conversion coatings on zinc containing hydrated cerium (III) oxide were reported to also exhibit self-healing properties [7], but these properties are even more limited.

Thin, compact, and mesoporous silica coatings prepared by the sol–gel method can replace the traditional chromates conversion coatings and pretreatments on Zn [8]. The incorporation of certain corrosion inhibitors into the pores of these layers may offer a promising alternative to classical conversion coatings with self-healing abilities.

Silicate conversion coatings, which are also potential candidates for replacing chromate conversion coatings, exhibit self-healing abilities as well under certain experimental conditions [9]. This behavior is due to silicate anions migrating to the damaged area, forming new conversion coatings composed of Zn, O, and Si.

22.2.2.2   Organic Coatings

Organic coatings account for the largest number of representatives and are used in all sectors of industry. Organic-coated steel is certainly one of the products best able to respond to restrictive environmental regulations, and its use entails no danger for the consumer. Due to the fact that a wide range of organic compounds are used for the protection of steel, only some of them were selected and are shortly presented below.

Polymers

Within all classes of materials, the self-repair potential of polymers is probably the largest, since they display more useful properties than any other material [1]. Through self-healing after damage, the main properties of the polymeric material (tensile strength, smoothness, plasticity, etc.) are recovered and preserved.

Various self-repairing polymer matrices were proposed, including thermoplastic polymers such as polymethyl methacrylate (PMMA) and PMMA-poly (methoxyethylacrylate) [10], poly(ethylene-co-methacrylic acid)-based copolymers [11], polydimethylsiloxane elastomers [12], UV-cure polyester acrylate [13] and many others. The healing mechanism in the case of polymers relies upon molecular interdiffusion, reversible bond formation, chain rearrangement, swelling or the recombination of chain ends which can be triggered by temperature increase or can be photoinduced [14]. The protection effectiveness of the polymeric coating is related mainly to the quality of the deposited coating and on experimental parameters (coating thickness, homogeneity, surface preparation, etc.).

The polymeric matrices are ideal for hosting chemicals such as microencapsulated healing agents and dispersed catalysts which when reacted together, heal the material and prevent further crack growth.

Epoxy-Based Coatings

Epoxy resins, also known as poly-epoxides, are a class of reactive polymers which contain epoxide groups. Among the most used epoxy compounds are the epoxy phenol novolacs (EPN), epoxy cresol novolacs (ECN), glycidyl epoxy resins, cyclo-aliphatic epoxides and glycidylamine epoxy resins.

In order to improve the mechanical, chemical, and heat resistance properties of epoxy resins, linear resins are cross-linked with suitable compounds such as polyfunctional amines, acids (and acid anhydrides), phenols, alcohols and thiols [15] to form three-dimensional cross-linked structures.

Epoxy resins are currently used as strong adhesive materials for sticking different surfaces together and as primers to improve the adhesion of paints, especially on metal surfaces where corrosion (rusting) resistance is important.

The ease of incorporating different healing agents (e.g., microcapsules filled with inhibitors) in an epoxy matrix is one of the main advantages of these primers. Good adhesion between the microcapsules and the epoxy matrix can be reached by using epoxy-amine microcapsules, prepared, for instance, by an interfacial reaction in an inverse emulsion [16].

Hybrid Coatings

Hybrid organic–inorganic coatings allow for the combination of advantages of both organic and inorganic components. The organic component is mainly responsible for the system's flexibility and compatibility with subsequent polymeric coatings, while the inorganic component provides good adhesion to the metallic surface [17].

Hybrid coatings can also be realized from hybrid molecules. Organosilanes are an example of such molecules possessing both inorganic and organic functionalities which allow them to establish stable covalent bonds with both the native oxide film formed on the metallic surface and the subsequent painted layers [18]. At the same time, silane coatings act as a physical barrier against corrosion, blocking access of the electrolyte to the metallic substrate. The organic functionalities of silanes can be varied in a convenient manner in order to achieve the best stability and efficiency of the hybrid coating.

Hybrid silica coatings containing Ce (III) and Ce (IV) prepared by the sol–gel method were reported as being efficient in the corrosion protection of stainless steel [19]. Ce (III) ions enhance the corrosion resistance of the substrates through a barrier effect. The self-healing properties of the coatings are due to Ce $(OH)_3$ formation on the surface and to the complex reaction between Cr and Ce ions.

Similar enhancement in corrosion resistance is reported in the case of mesoporous silica-based hybrid coatings deposited on steel. The self-healing properties of the silane–zirconia hybrid coating were improved when silica nanocontainers filled with 2-mercaptobenzothiazole were embedded in the coating [20].

Paints

Paints are polymeric coating systems consisting of a binder (resin and plasticizers), fillers (pigments), and other substances such as driers, thickeners, etc. [21]. The quality and the protective properties of the paint strongly depend on the binder–filler, substrate–coating and coating–environment compatibility.

Various paint formulations can be used for metal protection, including polyurethane-based paints, acrylic primers, enamels, etc. They are convenient matrices to host capsules filled with corrosion inhibitors or other elements which enhance the corrosion resistance of the coatings.

Generally, the paint is applied as a layered system. For anticorrosion purposes, an efficient paint has three layers: a conversion coating of about 100 nm, a primer (i.e., an epoxy layer of 20–25 μm) and a topcoat (i.e., polyurethane of 50–100 μm thickness).

22.2.3   Healing Agents

In order to perform properly, a smart system must incorporate (embedded or surface mounted) a smart structure to counteract damage, thus introducing the possibility of self-healing properties. The healing agents can be incorporated directly in the matrix or can be included in capsules or microvascular systems [22]. The release of the healing agent can be induced by abrasion, shell degradation, mechanical stress, pH changes in the environment, exposure to UV light, etc.

This healing mechanism can be intrinsic or extrinsic [23]. Intrinsic healing occurs continuously and does not require the presence of an additional external healing compound, while extrinsic healing takes place in the presence of a catalyst or cross-linker which should be present in the surrounding environment or in the matrix.

Some of the most used healing agents, belonging to different classes of substances, are presented below.

22.2.3.1   Pigments

Sacrificial metal pigments (Zn, Mg, Al) can be introduced into sol–gel coatings in order to obtain inorganic metal-rich layers with protective properties on ferrous and steel substrates [24]. The size and shape of metal pigments, as well as their concentration, play an important role in the protective properties of the coatings. It was established that these pigments are involved in the cathodic protection of steel, and they determine the general corrosion resistance of the coatings, relying upon the barrier characteristics of the sol–gel coatings.

Ceramic pigments consisting of Ce (III) and Ca (II) exchanged bentonites have been reported as efficient corrosion inhibitors for organic-coated galvanized steel [25]. They were dispersed in polyester-resin-based primer paint and were efficient in preventing corrosion-driven coating delamination. Anionic inhibitors such as 2-benzothiazolylthio-succinic acid were included in anionic clays, such as layered double hydroxides [26]. Aggressive chloride ions trigger the release of these inhibitors and determine the self-healing capability of the coating.

Ca (II) and Zn (II) exchanged pigments based on cross-linked sulfonated polystyrene can also be used to protect galvanized steel surfaces [27].

22.2.3.2   Nanoparticles

Nanoparticles are effective as self-healing materials and can be successfully applied to anticorrosion protective coatings. Thus, composite Zn coatings on steel incorporating Ti and Ce oxide nanopowders, separately or in mixture, exhibited increased corrosion resistance as compared to pure Zn coatings [28]. Al_2O_3 nanoparticles co-electrodeposited with Ni and Zn were successfully used to obtain corrosion resistant Zn–Ni composite coatings on steel [29].
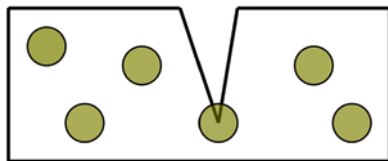
Fig. 22.1 Crack healing using nanocapsules filled with a repairing agent

CeO_2 nanoparticles were used as fillers for hybrid silane coatings applied on galvanized steel substrates [30]. Due to the corrosion-inhibiting effect of ceria nanoparticles activated with Ce (III) ions, the modified coatings demonstrate an enhanced passive domain for zinc and improved the barrier properties.

SiO_2 particles embedded in bis-functional silanes were also reported to improve the corrosion resistance of hot-dipped galvanized steel [31].

22.2.3.3 Nanocontainers with Inhibitors

The self-repairing concept based on the use of healing agents (e.g., film-forming compounds, inhibitors) stored in containers dispersed through a coating matrix and becoming active after breakage of the capsule is one of the most popular methodologies. The core constituents of the containers are released when the capsules are ruptured by damage and heal the defects induced by scratching (Fig. 22.1).

The nanocontainers can be manufactured from mesoporous silica [20], urea-formaldehyde [32, 33], latex [34], ceramic materials [17], epoxy-amine [16], etc.

On the other hand, the healing agents belong to very different classes of compounds, varying from natural compounds such as linseed oil [35, 36] and camphor [37] to synthetic substances, such as dicyclopentadiene [38], dodecylamine [39], 2 mercaptobenzothiazole [17], triethanolamine [34] as well as many others. They play the role of film formation agents and/or of corrosion inhibitors. To obtain an efficient self-healing effect, single [40] or multicomponent [37] repair compounds can be used.

The fabrication of the nanocontainers can be performed by sequential emulsion polymerization [34], interfacial reaction in an inverse emulsion [16], coacervation [41], in situ polymerization [33], extrusion or the sol–gel method [42].

Microencapsulation is advantageous because it can be used to encapsulate a large variety of materials (corrosion indicators and inhibitors, self-healing agents, etc.) in both solid and liquid phase. For example, water-core microcapsules encapsulating water-soluble inhibitors such as cerium nitrate, sodium benzoate, sodium molybdate, and others were produced then embedded in zinc primers in order to enhance the corrosion resistance of the steel substrates [43]. Another example is based on the electrostatic adsorption of polyelectrolytes on oil phase drops containing a corrosion inhibitor (a thiazole derivative) [44].

In all cases, the capsules have been embedded in a protective (e.g., epoxy based) coating. The compatibility between the shell material of the capsules and the matrix material plays an important role.

Fig. 22.2 Microvascular
system of hollow channels
that can be filled with a
healing agent
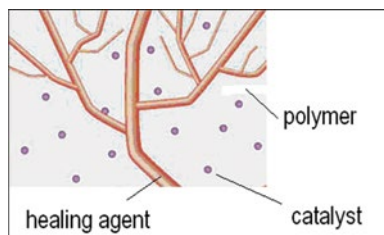
22.2.3.4 Microvascular Systems

Self-healing coatings containing microencapsulated healing agents exhibit good repairing properties but are limited to local autonomic repair. On the contrary, bio-inspired vascular networks containing healing agents are embedded in coatings; the coating-substrate design delivers healing agent to cracks via a three-dimensional network at any place it is needed, repairing the damage autonomously and repeatedly [45].

Microvascular networks consisting of channels filled with a specific healing agent (Fig. 22.2) mimic the architecture of the human vascular system and can be formed inside a polymeric coating, which can be used as an alternative to other self-repairing systems. The healing agent (e.g., a monomer) is transported through capillarity inside the channels mimicking those from living bodies. The monomer flows towards the scratch where it encounters a catalyst or a cross-linker previously embedded in the matrix that starts polymerization and repairs the crack.

3D scaffolds can be fabricated, for example, with a fugitive organic ink containing petroleum jelly and microcrystalline wax in a layer-wise scheme deposited on a substrate [46]. After deposition, the ink scaffold is infiltrated with an uncured epoxy resin, cured, cut to size, and polished. The fugitive ink is then removed by heating the substrate under vacuum. This results in a vascular system of hollow channels that can be filled with a healing agent.

22.3 Techniques for Obtaining Self-Healing Coatings

Several combinations between matrices and healing agents reported in literature for steel substrates are presented in Table 22.1.

As it can be observed, there are many techniques to obtain self-healing coatings. The most important are discussed below.

22.3.1 Layer-by-Layer Deposition

Layer-by-layer (LbL) deposition of multilayers can sometimes improve the corrosion resistance of the metallic substrate even in the absence of corrosion inhibitors; however multilayers containing inhibitors are much more effective. The inhibitors

Table 22.1 Self-healing coatings for steel

No.	Substrate	Coating matrix	Healing agent	Coating method	Ref.
1	AISI 304 stainless steel	Silica	Ce (IV) salts	Sol–gel	[19]
2	9Cr-1Mo ferritic steel	Hybrid silane–zirconia-based coating	Mesoporous silica nanocontainers filled with 2-mercaptobenzothiazole	Sol–hydrothermal method	[20]
3	Hot-dipped galvanized Q235 steel (carbon steel)	Silicate conversion coatings	–	Immersion in sodium silicate solutions of various SiO_2:Na_2O molar ratios	[47]
4	Mild steel	Zirconia-based hybrid coating	Propargyl alcohol	Sol–gel	[48]
5	Mild steel	Epoxy resin	Urea-formaldehyde microcapsules filled with linseed oil	Brush painting	[32]
6	Cold-rolled steel	Polyurethane resin with curing agent and wetting agent	Latex nanoreservoirs filled with triethanolamine	Bar coating	[34]
7	Stainless steel 304	Hybrid silica–zirconia	Nanocomposites (cloisite 15A, MWCNTs, $CeCl_3$)	Sol–gel dip coating	[49]
8	Carbon steel	Polyester acrylate	Polyaniline doped with phosphoric acid and CeO_2 nanoparticles	Spin coating	[13]
9	Hot-dipped galvanized steel	Weldable epoxy-based primer	Halloysites/2-mercaptobenzothiazole	Coating	[2]
			Vanadium oxide		
			TiO_2/2-mercaptobenzothiazole		
			TiO_2/8-hydroxyquinoline		
10	Hot-dipped galvanized steel	Polyvinyl butyral	Ca (II) and Zn (II) exchanged pigments based on cross-linked polystyrene	Bar casting	[27]
11	Cold-rolled steel	Epoxy resin	Urea-formaldehyde microencapsulated epoxy resin	Coating with doctor blade	[50]
12	Q steel	Epoxy primer + polyurethane topcoat	Inhibitor containing microcapsules	Brush application	[51]
13	Hot-dipped galvanized steel	Epoxy resin	Ceramic nanocontainers loaded with 2-mercaptobenzothiazole	Dip coating	[17]
14	Carbon steel AISI 1020	Paint	Nanocontainers with dodecylamine	Brush coating	[39]

Table 22.1 (continued)

No.	Substrate	Coating matrix	Healing agent	Coating method	Ref.
15	C steel	Epoxy resin	Micro/nanocapsules with urea-formaldehyde as a shell and drying linseed oil as a core	Film applicator	[35]
16	Hot-dipped galvanized steel	Bis-[triethoxysilylpropyl] tetrasulfide + silane	$Ce(NO_3)_3$	Immersion in the silane solution and curing	[52]
17	Hot-dipped galvanized steel	Bis-functional silanes	Microparticles of SiO_2	Immersion in the silane solution and curing	[31]
18	Galvanized steel	Polyester resin	Ca^{2+} and Ce^{3+}-loaded bentonites	Draw down method using gauge wire wound coating bars	[25]
19	Carbon steel	Epoxy resin	Mg–Al layered double hydroxides intercalated with 2-benzothiazolylthio-succinic acid	Spin coating	[26]
20	Steel	Epoxy-based paints	Urea-formaldehyde and gelatin shell microcapsules containing inhibitors (tung oil, spar varnish, isodecyl diphenyl phosphate, camphor, alkylammonium salt in xylene)	Brush coating	[37]
21	C steel	Epoxy resin	Encapsulated tung oil in urea-formaldehyde shell	Film applicator	[53]
22.	Mild steel	Epoxy resin	Urea-formaldehyde shell microcapsules containing linseed oil	Brush coating	[36, 54]
23	Low-carbon steel	Epoxy-amine paint	Epoxy-amine microcapsules containing $MgSO_4$ solution	Filmograph application	[16]
24	Cold-rolled steel sheet	Epoxy resin	Urea-formaldehyde shell microcapsules containing epoxy resin	Coating with a micrometer-controlled doctor blade	[33]
25	Steel	Polyelectrolyte multilayers	Polyethylenimine-sodium polystyrene sulfonate-8-hydroxyquinoline nanostructures	LbL coating	[46]
26	Galvanized steel	Silane coatings	CeO_2 nanoparticles	Immersion followed by thermal treatment	[30]
27	Galvanized steel	Bis-[triethoxysilylpropyl] tetrasulfide silane (BTESPT)	Cerium nitrate	Immersion followed by thermal treatment	[18]

can be either incorporated between layers or adsorbed in the layers [46] and can be released under the action of an external stimulus. The morphology and the characteristics of LbL coatings can be controlled by the number of deposition cycles, the chemical nature of the polyelectrolyte and the experimental conditions.

On the other hand, the LbL technique can be used to obtain nanocontainers hosting corrosion inhibitors that can be subsequently introduced in anticorrosive matrices. The formation of a nanocontainer shell is possible by the LbL deposition of a charged species (e.g., polyelectrolyte, biomaterial, etc.) on the surface of nanoparticles and can be used further for the storage of a corrosion inhibitor [3, 46, 55]. For example, mesoporous SiO_2 nanoparticles covered with polyelectrolyte layers loaded with inhibitor (2-(benzothiazol-2-ylsulfanyl)-succinic acid) were introduced into a hybrid ZrO_2–SiO_2 sol–gel film [55]. The release of the 2-(benzo-thiazol-2-ylsulfanyl)-succinic acid from containers with a polyelectrolyte shell is triggered at a pH of 10.

Polyelectrolytes (i.e., poly(ethyleneimine), poly(styrenesulfonate), etc.) possess self-repairing properties mainly due to their pH buffering activity. They are polycations, polyanions, or both, and their dissociation degree is pH sensitive. The deposition of polyelectrolytes can be done by spray drying, spin coating, or dip coating and can be repeated several times in order to obtain multilayers. The thickest film is obtained by spray drying [56]. LbL coatings used as corrosion-inhibiting coatings are advantageous as they provide the controlled release of inhibitor, pH buffering, self-healing, and sealing of surface defects and barrier properties.

The corrosion of stainless steel under anodic conditions in salt solutions was strongly suppressed by an ultrathin layer of polyelectrolyte complex, obtained by using the LbL deposition method [57].

Polyelectrolytes such as polyethyleneimine (PEI) and polystyrene sulfonate (PSS) layers, together with an inhibitor (dodecylamine), were alternatively deposited on the surface of SiO_2 nanoparticles, resulting in a final supramolecular structure of SiO_2/PEI/PSS/dodecylamine/PSS/dodecylamine [58]. Carbon steel coated with primer doped with 10 wt% of nanocontainers containing dodecylamine showed good self-healing ability through the release of the encapsulated inhibitor.

22.3.2   Incorporation in Sol–Gel Coatings

The sol–gel process is a convenient method for preparing different protective coatings on the surface of metals, including galvanized steel substrates, and consists of the formation of an oxide network by the condensation of precursors in a liquid medium [59]. The main advantages of the sol–gel method are (1) the possibility of preparation of materials with versatile composition that is not possible by solid-state fusion, (2) the availability to cast coatings in complex shapes, and (3) the use of low processing temperature [60].

Silica-based protective coatings are the most widely used for metal protection and can be successfully prepared by the sol–gel method, using alkoxysilanes as precursors. Due to the fact that the reaction is quite gentle and that dopants, such as

small amounts of nanoparticles (e.g., CeO_2, ZrO_2, etc.) with beneficial effects on the corrosion resistance, can be easily introduced in the silica layers [61], this approach is extensively used in corrosion protection. These silica layers, especially when doped or containing embedded nanoparticles, could significantly improve the barrier properties of the coatings and consequently their corrosion behavior.

Besides SiO_2, a wide range of sol–gel coatings, such as ZrO_2, TiO_2-SiO_2, and Al_2O_3-SiO_2, can be deposited on the surface of steel [60]. Thus, thin coatings of ZrO_2, SiO_2, $70SiO_2$-$30TiO_2$, and $88SiO_2$-$12Al_2O_3$ sol–gels have been prepared from sonicated sols and deposited by the dip-coating technique on stainless steel [62].

Mesoporous sol–gel coatings and nanoparticles are suitable as inhibitor carriers for self-healing corrosion resistant systems. Films formed with bis-[triethoxysilylpropyl] tetrasulfide doped with cerium nitrate applied on hot-dipped galvanized steel exhibited improved corrosion protection when compared to the coatings without cerium salt [52]. A sol–gel film for carbon steel was prepared by the copolymerization of epoxy resin and a hardener while varying the composition of TiO_2-SiO_2-ZnO-CeO_3 pigments [63]. The hybrid pigments conferred good adhesion on substrate surface and improved corrosion resistance of the coatings.

22.3.3 Other Methods for Self-Healing Coatings Preparation

Other methods to prepare self-healing coatings are:

- Painting by brush coating [32] or filmograph application [16]
- Immersion followed by thermal treatment [18, 30, 52]
- Self-assembling (e.g., a self-assembled monolayer (SAM) on steel can be obtained by using of hexadecanoate ion $C_{15}H_{31}CO_2^-$) [64]
- Electrodeposition (e.g., electrodeposition of cerium-based oxide layers on carbon steel from cerium nitrate) [65]
- Impregnation of sol–gel films with inhibitor-loaded polyelectrolyte multilayers. The polyelectrolyte contains polycations, polyanions, or both. Active species deposited into the polyelectrolyte film are able to be released on demand producing self-repairing [55].

All these methods offer wide possibilities for the design of application oriented self-healing material systems.

22.4 Conclusion

Self-healing coatings are promising alternatives to classical methods aimed at the protection of metallic substrates against corrosion. Thus, self-healing increases the durability and reliability of metallic devices while reducing maintenance costs. Although a large number of self-repairing systems were reported in the literature,

there are many others for different systems that, though not discussed, are not any less important. The development of new systems to protect metallic substrates against corrosion is a challenge of great importance for many industrial applications. The understanding of the systems' complexity and of the healing mechanisms will certainly lead to new discoveries in this field, which has a great future. Further developments should be oriented towards the production of novel self-repairing composites, new healing agents, a broader range of healing mechanisms, and the improvement of preparation technologies.

References

1. Fischer H (2010) Nat Sci 2(8):873
2. Taryba M, Lamaka SV, Snihirova D, Ferreira MGS, Montemor MF, Wijting WK, Toews S, Grundmeier G (2011) Electrochim Acta 56:4475
3. Shchukin DG, Möhwald H (2007) Small 6:926
4. Hager MD, Greil P, Leyens C, van der Zwaag S, Schubert US (2010) Adv Mater 22:5424
5. Thébault F, Vuillemin B, Oltra R, Ogle K, Allely C (2008) Electrochim Acta 53:5226
6. Dalbin S, Maurin G, Nogueira RP, Persello J, Pommier N (2005) Surf Coat Technol 194:363
7. Aramaki K (2003) Corros Sci 45:451
8. Albert E, Cotolan N, Nagy N, Sáfrán G, Szabó G, Muresan LM, Hórvölgyi Z (2015) Microporous Mesoporous Mater 206:102
9. Yuan M-R, Lu J-T, Kong G, Che C-S (2011) Surf Coat Technol 205:4507
10. Jud K, Kausch HH (1979) Polym Bull 1:697
11. Kalista SJ Jr, Ward TC, Oyetunji Z (2007) Mech Adv Mater Struct 14:391
12. Keller MW, Hampton K, McLaury B (2013) Wear 307:218
13. Sababi M, Pan J, Augustsson P-E, Sundell P-E, Claesson PM (2014) Corros Sci 84:189
14. Wu DY, Meure S, Solomon D (2008) Prog Polym Sci 33:479
15. http://en.wikipedia.org/wiki/Epoxy. Accessed 5 May 2015
16. Sauvant-Moynot V, Gonzales S, Kittel J (2008) Prog Org Coat 63:307
17. Kartsonakis IA, Balaskas AC, Koumoulos EP, Charitidis CA, Kordas GC (2012) Corros Sci 57:30
18. Trabelsi W, Cecilio P, Ferreira MGS, Montemor MF (2005) Prog Org Coat 54:276
19. Pepe A, Aparicio M, Duran A, Cere S (2006) J Sol-Gel Sci Technol 39:131
20. Chenan A, Ramya S, Gorge RP, Kamachi Mudali U (2014) Corrosion 70(5):496
21. Garcia SJ, Fisher HR, van der Zwaag S (2011) Prog Org Coat 72:211
22. Zvonkina IJ, Hilt M (2014) Strategies for developing multi-functional, self-healing coatings for corrosion prevention and other functions. In: Abdel Salam Hamdy Makhlouf (ed) Handbook of smart coatings for materials protection. Woodhead publishing series in metals and surface engineering, no 64, p 105
23. Garcia SJ, Fischer HR (2014) Self-healing polymer systems: properties, synthesis and applications. In: Aguilar De Armas MR, Román JS (eds) Smart polymers and their applications. Woodhead Publishing Ltd, p 271
24. Wang D, Bierwagen GP (2009) Prog Org Coat 64:327
25. Bohm S, McMurray HN, Powell SM, Worsley DA (2001) Mater Corros 52:896
26. Hang TTX, Truc TA, Duong NT, Pebère N, Olivier M-G (2012) Prog Org Coat 74:343
27. Williams G, Geary S, McMurray HN (2012) Corros Sci 57:139
28. Nemes PI, Zaharescu M, Muresan LM (2013) J Solid State Electrochem 17(2):511
29. Blejan D, Muresan LM (2013) Mater Corros 64(5):433
30. Montemor MF, Pinto R, Ferreira MGS (2009) Electrochim Acta 54:5179
31. Montemor MF, Cabral AM, Zheludkevich ML, Ferreira MGS (2006) Surf Coat Technol 200:2875

32. Selvakumar N, Jeyasubramanian K, Sharmila R (2012) Prog Org Coat 74:461
33. Zhang W, Liao LP, Zhao Y (2014) Handbook of smart coatings for materials protection. Woodhead Publishing, Cambridge, p 287
34. Choi H, Song YK, Kim KY, Park JM (2012) Surf Coat Technol 206:2354
35. Kouhi M, Mohebbi A, Mirzaei M, Peikari M (2013) Prog Org Coat 76:1006
36. Behzadnasaba M, Esfandeha M, Mirabedinia SM, Zohuriaan-Mehra MJ, Farnood RR (2014) Colloids and Surf A Physicochem Eng Aspects 457:16
37. Kumar A, Stephenson LD, Muray JN (2006) Prog Org Coat 55:244
38. Blaiszik BJ, Sottos NR, White SR (2008) Compos Sci Technol 68:978
39. Falcon JM, Batista FF, Aoki IV (2014) Electrochim Acta 124:109
40. Toncelli C, De Reus D, Broekhuis AA, Picchioni F (2012) In: Amendola V, Meneghetti M (eds) Self-healing at the nanoscale: mechanisms and key concepts of natural and artificial systems. CRC Press/Taylor & Francis Group, Boca Raton, FL, p 208
41. Lii CY, Liaw SC, Lai VMF, Tomasik P (2002) Eur Polym J 38:1377
42. Cao Z, Dong L, Li L, Shang Y, Qi D, Lv Q, Shan G, Ziener U, Landfester K (2012) Langmuir 28(17):7023
43. Calle LM, Li W (2014) Microencapsulated indicators and inhibitors for corrosion detection and control. In: Handbook of smart coatings for materials protection. Woodhead Publishing, Cambridge, p 370
44. Kopeć M, Szczepanowicz K, Mordarski G, Podgórna K, Socha RP, Nowak P, Warszyński P, Hack T (2015) Prog Org Coat 84:97
45. Toohey KS, Sottos NR, Lewis JA, Moore JS, White SR (2007) Nat Mater 6:581. http://www.nature.com/nmat/journal/v6/n8/abs/nmat1934.html (Last Accessed: May 2015)
46. Andreeva DV, Skorb EV (2014) Handbook of smart coatings for materials protection. Woodhead Publishing, Cambridge, p 307
47. Yuan MR, Lu JT, Kong G (2010) Effect of SiO_2. Surf Coat Technol 204:1229
48. Hosseini SMA, Jafari AH, Jamalizadeh E (2009) Electrochim Acta 54:7207
49. Jeeva Jothi K, Palanivelu K (2013) Ceram Int 39:7619
50. Yang Z, Wei Z, Le-ping L, Si-jie W, Wu-jun L (2012) Appl Surf Sci 258:1915
51. Mehta NK, Bogere MN (2009) Prog Org Coat 64:419
52. Cabral AM, Trabelsi W, Serra R, Montemor MF, Zheludkevic ML, Ferreira MGS (2006) Corros Sci 48:3740
53. Samadzadeh M, Hatami Boura S, Pekari M, Ashrafi A, Kasiriha M (2011) Prog Org Coat 70:383
54. Suryanarayana C, Chowdoji Rao K, Kumar D (2008) Prog Org Coat 63:72
55. Andreeva DV, Schukin DG (2008) Mater Today 11(10):24
56. Andreeva DV, Skorb EV, Schukin DG (2010) Appl Mater Interfaces 2:1954
57. Farhat TR, Schlenoff JB (2002) Electrochem Solid-State Lett 5(4):B13
58. Falcón JM, Batista FF, Aoki IV (2014) Electrochim Acta 124:109
59. Brinker CJ, Scherer GW (1990) Sol-gel science: the physics and chemistry of sol-gel processing. Harcourt Brace Jovanovich/Academic Press, Boston, MA, p 2
60. Barry Carter C, Grant Norton M (2007) Ceramic materials, science and engineering. Springer, New York, NY, p 400
61. Montemor MF, Trabelsi W, Lamaka SV, Yasakauc KA, Zheludkevich ML, Bastos AC, Ferreira MGS (2008) Electrochim Acta 53:5913
62. De Lima Neto P, Atik M, Avaca LA, Aegerter MA (1994) J Sol-Gel Sci Technol 2:529
63. Norzita N, Haziq M, Zurina M (2012) Int J Chem Environ Eng 3(4):267
64. Aramaki K, Shimura T (2003) Corros Sci 45(11):2639
65. Hamlaoui Y, Tifouti L, Remazeilles C, Pedraza F (2010) Mater Chem Phys 120:172

Chapter 23
Overview of Silane-Based Polymer Coatings and Their Applications

Katsuhiko Sano, Hideyuki Kanematsu, and Toshihiro Tanaka

Abstract Silane resin coatings, their structure, characteristics, and applications are reviewed. Generally, silane compounds are classified into two types, silicone and silicates, and make up organic paints and coating agents that are easy to handle and inexpensive and have high designing capability. However, they are vulnerable to ultraviolet light and heat due to the carbon–carbon bonds which also accounts for their lack of durability. Therefore, the authors herein have developed and investigated the applicability of alkoxysilane compounds for coatings and painting films. Conventionally, the mechanical strength and adhesion force to the substrate have not been good for silane polymer resins. However, the newly investigated and developed alkoxysilane compound films could solve these conventional problems. The concepts of the novel silane compound films and the rational for the research and development will be described. Further, the application possibilities in many industrial fields will be introduced in this chapter, with concrete examples mentioned.

Keywords Alkoxysilane compounds • Weathering • Corrosion resistance • Sealing agents • Antifouling properties

K. Sano (✉)
R&D Section, 7870-20, Sakura, Yokkaichi, Mie 512-1211, Japan
e-mail: sano@ddcorp.co.jp

H. Kanematsu (✉)
Department of Materials Science and Engineering, Suzuka, Mie 510-0294, Japan
e-mail: kanemats@mse.suzuka-ct.ac.jp

T. Tanaka (✉)
Department of Materials Science and Engineering, 2-1, Yamadaoka, Suita,
Osaka 565-0871, Japan
e-mail: tanaka@mat.eng.osaka-u.ac.jp

23.1   Introduction

In our modern civilization, we are surrounded by lots of construction, facilities, machines, and instruments on a daily basis. We can see soon the surfaces of them are coated by paintings; their applications are generally very versatile, ranging from just a decoration such as a coloring agent to electromagnetic or other optical functions for material surfaces. Paints are one of the most useful and flexible surface-coating methods among these many processes.

Since recorded history, there have been many materials used as paints and coating agents [1]. In days gone by, natural materials such as glue derived from animal bones and skins, plant sap, and lacquer have all been used as binders. However in modern days, various organic polymers have been devised with the advancement of engineering and technology, establishing mainstream paints, coatings, and binders.

As representative organic polymers for coating, paints, and binders, the following examples can be mentioned: alkyd resin, urethane resin, acrylate resin, epoxy resin, and polyester resin. These organic polymers have a basic structure composed of carbon–carbon bonds and various unique characteristics can be expressed depending on the combined species when monomers bind to form polymers. Basically, organic polymers for painting and coating have characteristics that they could improve workability by dilution or addition of chemicals as additives and also extend the application. Due to their high flexibility, these paint films could follow the deformation of substrate (i.e., shrinkage) as well as high resistance against cracking and spalling.

Even though paints and coatings composed of organic polymers might seem to be good in all aspects, they inevitably have some weak points. To name a few, there are phenomena that affect their applicability that occur on a daily basis. When a person lounges against a wall, their clothing may be contaminated with a white powder. This is called chalking where the main backbone of organic compounds is composed of carbon–carbon bonds that are collapsed by ultraviolet light, causing the paint film to be deteriorated and resulting in shabby-looking surfaces. Also, since the paint films could be composed of nearly all organic compounds, they do not have high heat resistance, potentially causing a fire to spread. This could be controlled by the addition of a fire-retarding material. However, decomposition at approximately 200°C could form toxic gas or cause the painted substrate materials heavy damage. When steel is used as substrate, rust might form at the site of spalling, since it would be exposed to a high-temperature atmosphere directly. Therefore, heat resistance is often required for applications.

Silane polymers are often used to compensate for such a weak point in the application. It has a main backbone composed of Si–O–Si. This is called a siloxane bond, and the technical term corresponds to an all-inclusive expression for organo-polysiloxane possessing various organic groups as a side chain. In the broad sense, quite a few compounds synthesized in various ways belong to the category at present. The common characteristics for compounds in this category are high heat resistance, cold hardness, insulating, repellency, and a weathering, all of these properties deriving from the siloxane bond itself. These merits have led the compounds to be used in

versatile applications such as lubrication, caulking materials (filling chinks in walls), cooking devices, etc. In the painting and coating fields, silicone and silicate are typically used. However, these materials are difficult to use from both stability and handling perspective. Therefore, the frequency of their use has not been very high at this point. In this chapter, the technology for the production of silane polymers as painting materials, their characteristics, and their applications will all be described.

23.2   History of Development

The silane compound has a relatively short history. Organic silicon composed of silicon with organic groups was synthesized by Friedel and Crafts for the first time in 1863 [2]. After that, Kipping proposed a new synthesis processes [3] and since then various processes for the production of organic silicon have been investigated. Finally, a direct process was realized for the production of organo-silicone polymers in 1941 [4]. In the 1940s, commercial exploitation of the compounds began due to their high thermal stability and electric resistance, extending the range of their applications to insulating coating, sealing materials for architectures and machines, etc. Recently, they are used for medical materials and implants, since they generally have high biocompatibility. Due to their high heat resistance and low staining properties, application as cooking appliances has already begun as well [5, 6].

23.3   Challenges with Silane-Based Polymer Coatings

Silane polymers have various excellent properties. However, they still have some problems when they are applied to painting and coating materials, realistically resulting in narrow field of application.

Generally, silane polymers are classified into two main classes, silicone and silicate. Silicone has methyl groups as a side chain, where the bond between the main chain and side one can be expressed as Si–C. On the other hand, silicate has a siloxane structure as the main chain (Si–O–Si) with methoxy groups as a side chain. The bond between the main and side chains is Si–O. Silicone has a relatively low surface tension as a liquid and a low surface free energy (20 mJ/m^2) as solid when compared with those of epoxy resin (about 40 mJ/m^2), urethane resin (about 50 mJ/m^2), and acrylic resin (about 40 mJ/m^2) [7]. Therefore, they tend to detach from the substrates as a solid film, even though they might be easy to get wet and stretch out on substrates as a liquid. It means the material is not appropriate for long-term service. When silicone polymers are applied to insulation coatings for electronic industry materials, they could be coated to avoid spalling, as they might wrap the objective electronic materials. The deterioration of mechanical strength would not be an issue, as the parts would not touch with others often. However, these basic weak points cannot be solved; therefore they are coated in different ways.

There are some methods to solve the weak attachment forces. Usually, silicone materials such as silicone oil have polysiloxane structures, straight-chain organic compounds with organic functional groups such (e.g., methyl group) as a side chain. If the straight chain is partly cross-bridged, the compounds would change to become flexible and elastic, such as in silicone gum. The bridging materials and additives used at that point could increase the adhesive property. However, even in such a case, the viscosity of silicone before cross bridging would still be generally high, and it must be diluted by an appropriate solvents. When they are applied to paints, volatile organic compounds (VOC) would be emitted, leading to environmental concerns.

Silicate may partly solve some of the problems, particularly the low attachment force that silicone materials have had, since their free surface energies are generally higher than those of silicone. Silicate also has the same polysiloxane structure as does silicone with an alkoxy group (i.e., –OR, with R being a hydrocarbon). Condensation polymerization occurs by de-alcoholization via hydrolysis, absorbing moisture in air. Theoretically, all alkoxy groups react to become silicon dioxides. Due to the restrictions of molecular movement, some parts of the alkoxy groups remain as unreacted solid polymeric substances. At this point, the decrease of volume for silicate becomes a problem, since the alcohol contents are released by de-alcoholization. This leads to the accumulation of inner stresses and tends to form cracks easily without the mitigation of the inner stresses, since the polymeric substance is generally rigid and adamant. As for the painted materials, the inner stress becomes larger than the cohesion force, forming cracks while developing spalling and detachment. Therefore, tone must be cautious about the application of paints and coating. Since the inner stress in coated films increases with thickness, a film thinner than several micrometers generally has a more difficult time forming cracks. However, the tendency and danger of crack formation increase with a thickness greater than several micrometers. Therefore, the usage of silicate instead of silicone would lead to spalling and detaching, even though the adhesion force to the substrate might increase, particularly when the thickness is not homogenous.

In addition to that, insufficient mechanical strength and low resistance against physical impacts would lead to the inappropriate selection of paint and coating materials, which could be attributed to the low cohesive force due to the chemical structure of polysiloxane. The chemical instability against alkali and acid chemicals would also narrow the possible applicability of silicone [6]. In conclusion, silicate would be difficult to use for paint and coating films.

On the other hand, silicone is still very attractive for paint and coating films. Their high weathering, heat resistance, cold resistance, and insulation properties are very attractive as paint and coating materials. Particularly, their weathering is very important for outdoor applications. Every day, infrared, visible, and ultraviolet lights are shining down on Earth as sunlight. Among all of them, ultraviolet light has the shortest wavelength, able to decompose organic compounds thus deteriorating industrial products composed of them. Generally, the ultraviolet light is classified into UV-A (315–400 nm), UV-B (280–315 nm), and UV-C (lower than 280 nm) due to their wavelength ranges. Almost 99 % of the ultraviolet reaching the Earth's surface actually is UV-A. UV-C does not reach the Earth's surface, since it is absorbed

Fig. 23.1 Three types of ultraviolet light
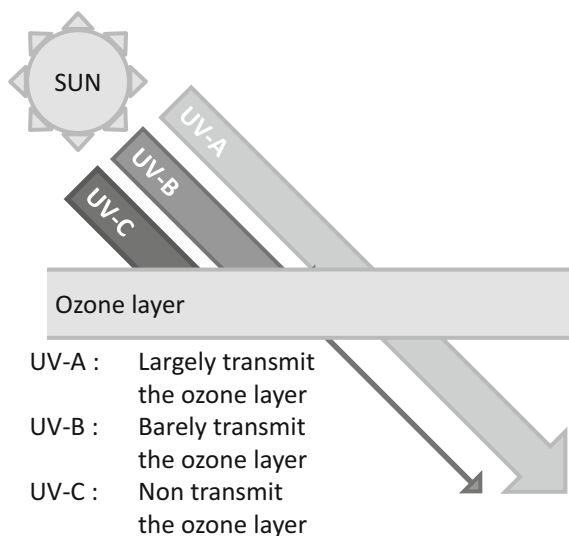
by the ozone layer (Fig. 23.1) [8]. The deterioration of organic compounds by ultraviolet light could be attributed to that of the polymer's main backbone which is composed of C–C bonds. Since the binding energy is 356 kJ/mol, the ultraviolet light, with its wavelength lower than 340 nm, could break the bond easily. The same decomposition by ultraviolet could occur for a C–O bond that has a binding energy of 329 kJ/mol, since the energy of UV-A could decompose it easily enough. Particularly, an epoxy resin composed mainly of C–C bonds and C–O bonds is very weak against ultraviolet light [9–11]. On the other hand, the binding energy of Si–O bonds, the main backbone of silicone, is relatively high (444 kJ/mol) and would require exposure to UV-C in order to break the bonds. However, since UV-C is absorbed by ozone layer, as described above, it can be stated that silicone has higher resistance against the ultraviolet light.

By strengthening the weak points (i.e., relatively low mechanical properties, adhesion force) by enhancing weathering, the application to paints and coating has been extended.

23.4 Properties of the Newly Developed Coating Material and Its Applications

The problems that could not be solved by conventional silicone resin nor silicate could be solved by an alkyl-alkoxysilane compound, a newly developed silane compound. The compound replaces some parts of the functional groups of alkoxysilane with alkyl groups such as a methyl or phenyl group. Even if alkoxy groups might detach through hydrolysis reactions, alkyl groups could remain in the compound.

Therefore, it does not accumulate inner stresses as much when compared to silicate and can also control crack initiation. As for surface free energy, alkyl-alkoxysilane compound is larger than that of silicone, with the adhesion force to substrate being higher than that of silicone. These properties depend on the content ratio between alkoxy and alkyl groups. Some examples of this are mentioned herein.

When the ratio of alkoxy groups is higher, shrinkage would become remarkable, since lots of alkoxy groups would detach from the compounds through a hydrolysis reaction. As a result, the silicate-like properties would become dominant. It would lead to a high adhesion force and high probability of crack initiation. On the other hand, when the ratio of alkyl groups is higher, there would be few alkoxy groups detaching from the compound through a hydrolysis reaction. As a result, the silicone-like properties would be dominant. Flexibility of the coating film would be high, even though the adhesion force to the substrate would be relatively low. In addition, the species of alkoxy and alkyl groups would affect the physical properties of coating films. The alkoxy group would affect the rate of hydrolysis reaction and the extent of shrinkage. On the other hand, the alkyl group would mainly affect the flexibility of coating films. For example, methyl groups could increase the hardness of the film and phenyl groups could increase its flexibility.

In addition to these main groups, cure agents, pigments, and other additives could increase various chemical and physical properties of coating films. The importance of cure agents follows for alkoxysilane. Those cure agents available for such purposes are classified into two types, phosphate compounds and organic metals. As for the metal components of organic metals, aluminum, titanium, zirconium, tin, and silicon can be mentioned. These metals can be used separately or together, depending on the case [12]. There are also many chemical structures of organic metals, (i.e., alkoxy groups such as methoxy group chemicals with chelates, plural ligands, or a combination). The complicated combinations of those metals and organic groups could control the reaction behaviors and reaction rates. Unfortunately, conventional silicone and siloxane could not control the reaction progress due to their high reactivity. Therefore, the products often contain two types of agents, a base resin and a cure agent. This type often has problems from the viewpoint of workability. In addition to that, stability might become problematic. However, a compound composed of alkoxysilane could contain cure agents from the start which could solve the problems of conventional agents.

As for the other characteristics of alkoxysilane, a broad range of viscosity can be mentioned. When an alkoxysilane compound with lower viscosity is to be used, paint and coating material of low viscosity could be produced without any organic solvent needed for the dilution; this is particularly the case for liquid alkoxysilane, with a structure close to that of silicone. Therefore, the surface tension is generally low and the wettability is high. The combination of low viscosity and surface tension would make the coating film that could follow the change of substrate's surface profile, thus penetrating the very tiny pores on the substrate's surface.

As for the reaction of the silane compounds with gas phases in air, it has a type of filter function. For example, carbon dioxide cannot penetrate through a film composed of said compound. However, water molecules can penetrate through it.

This filter function could release alcohol components as by-product into the air, and the alcohol does not remain in the silane compound's resin [6].

All of these unique properties have made many further applications available [6]. In the following sections, it will be described and explained how the silane compound could be applied to many industrial cases that have been investigated so far.

23.4.1 Spray Coating and Its Sealing

23.4.1.1 Metal Spray Coating

Originally, research and development of the silane compound began with the application as a sealing agent for spray coating. The meal spray coating has been applied to many anticorrosive materials. One of the representative materials is steel for high corrosion resistance. For the concrete application of spray coating to corrosion-resistant steels, the sandblast process has often been used as a pretreatment to remove corrosion products such as rust, oil contaminants, and painted films. Usually in this process, hard small mineral balls called grid are sprayed onto the material surface with compressed air. This process also increases the roughness of the specimen's surface to some extent, so that the following film formation process would be favorable. After that, spray coating should be completed. The choice of coating films is usually done from the viewpoint of the electrochemical properties and the differences between the film and the steel substrate. Usually, zinc, aluminum, and magnesium are used as spray coating materials. Each of these metals or a combination of metal powders is melted or semi-melted through the flame, arc, or plasma spray coating processes and sprayed onto steel surfaces by compressed air or high-velocity flaming gas. The spray coating process can be classified into many types and the best one is chosen, depending on the spray coating material and target substrates. The spray-coated metal is then coated and stacked on steel substrates to form corrosion-resistant films [13].

Metal spray coating films are used not only for corrosion resistance, but also for other various purposes in order to give different functions to the steel surface. Even though the application might be very interesting and useful as a surface treatment technology, this chapter cannot cover all of them. Readers can refer to many other sources found in literature relating to spray coating. Figure 23.2 shows an example of a spray coating apparatus, specifically an arc spray coating apparatus where zinc and aluminum wire are used to form a zinc–aluminum alloy film on steel surfaces.

23.4.1.2 Other Spray Coating Processes

Basically, any materials can be used as a spray coating material, if they can be melted somehow. For example, ceramics, cement, and resins are examples of spray coating materials. The choice of material depends on the end use. For example,
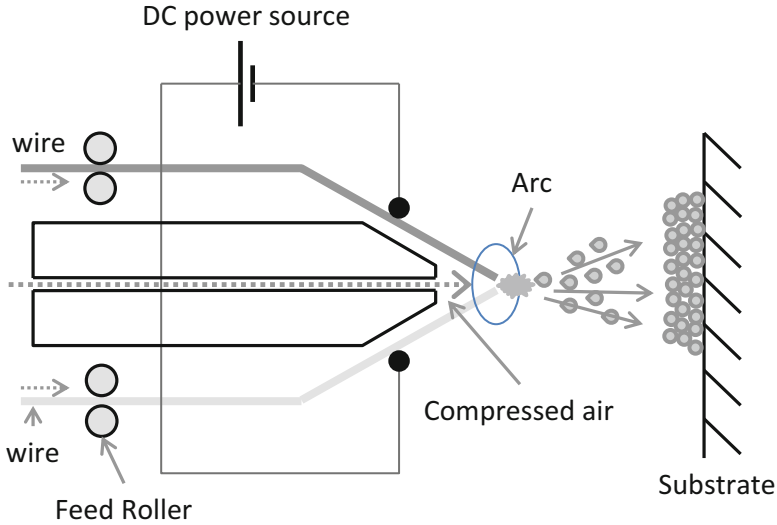
Fig. 23.2 Schematic illustration for a spray coating apparatus

ceramic coatings are used for electronics to improve the insulation properties and heat resistance. Resin coatings are often used to improve the corrosion resistance of specimens. Particularly, a resin coating does not require any full-scale large apparatuses and can even form thick films for any substrate shape. These merits have widened their availability for many different applications.

23.4.1.3 Sealing Agents for Spray Coating

Generally there are many pores, cracks, and other surface variations on substrates after they have been spray coated. Basically, it is very hard to decrease these surface defects completely. From the viewpoint of corrosion protection, the surface defects would allow an aqueous solution to penetrate through them and to reach the substrate surface, which might cause corrosion. In such a case, the spray coating for corrosion protection would not achieve its intended purpose. And for electronic parts, the spray coating would fail to satisfy not only the corrosion resistance but also other heat resistance and insulation properties. Therefore, surface defects such as crevices and pores should be minimized as much as possible.

Sealing agents are the chemicals used to fill the surface defects. Organic chemicals such as epoxy resins, phenol resins, silicone resins, as well as inorganic chemicals such as sodium silicate and silicate are used for this purpose. As for organic sealing agents, their solid content is usually adjusted to 10–15 wt% by organic solvents. The dilution is carried out to decrease viscosity and surface tension, so that the sealing agent can effectively penetrate into the surface defects. Without the dilution, the penetration would be not enough to fill the surface defects.

However, even if the defects are filled with the diluted sealing agents, the evaporation of organic solvent would decrease the solid content remaining in those defects. Therefore, the coating process should be repeated several times. However, evaporation may lead to environmental problems, since the released organic component might be often hazardous or toxic. In addition to these demerits, the additional painting process after sealing process might be needed from a design viewpoint, such as in the case of outdoor structural steel components. This would lead to the increase of the processes required and the total cost. In fact, so far it has affected spray coating process and completion time. To solve all of these problems, a one-component silane sealing agent based on alkoxysilane compound was proposed and then developed.

A key property required for sealing agents is that the agent should pierce deep into the heart of defects without leaving unfilled gaps. The viscosity should be kept low so as to penetrate into narrower pores as much as possible. However, too low of a viscosity might lead to some problems for workability (i.e., dripping) when the objective surfaces are set vertically or are inverted. From this viewpoint, the viscosity should be set appropriately. Impregnation starts soon after the sealing agent has made contact with the spray-coated film. On the other hand, if the viscosity of silane sealing agent is too high, the impregnation rate would be too slow to pierce deep enough into the heart of defects. The agent can react with moisture in the air and prematurely initiate the hardening process. The problem with the sealing agent hardening too much before impregnation might also occur in the case of low-viscosity sealing agents. In this case, the ratio of hardening agent to silane resin can increase the hardening rate drastically, causing rapid hardening to occur. Therefore, the control of hardening rate is very important from various viewpoints. For the purpose of corrosion protection, the thickness of spray coating film should be approximately 100 μm with the time for the sealing agent to reach the heart of surface defects being small. Therefore, the hardening time can be estimated as a maximum of 24 h in most cases. However, roughly 40 h may be needed in some cases, when the thickness of spray coating film is several hundred micrometers. This type of silane resin as sealing agent would also be available for dense spray-coated films that would have few pores and crevices. After hardening, the impregnated silane resin would work as an anchor to attach the substrate firmly. In such a case, the spray-coated film could be not detached from the substrate without being broken apart.

The silane sealing agent is usually applied to spray-coated films in one of the following two ways. In the first case, it is applied to the spray-coated films, and then it is removed from the surface before hardening completely, the agent remaining only in the surface defects. In the second case, the painted film on the substrate surface remains without being removed, so that the film displays a certain color tone with added pigments. If the silane resin film has very high weathering and corrosion resistance, inorganic pigments (e.g., burned pigments) are often used to prolong the service life.

When a colored sealing agent is made with silane resin and is applied to spray-coated films, fine pores work as filters, and the silane resin component preferentially

Outdoor exposure test (Miyako-isl. Okinawa)

Legend:
■ Silane based polymer coating
♦ fluoropolymer coatings
▲ acrylic silicone coating
● acrylic urethane resin coating

(Y-axis: Gloss Retention %; X-axis: Exposure Time (Months))
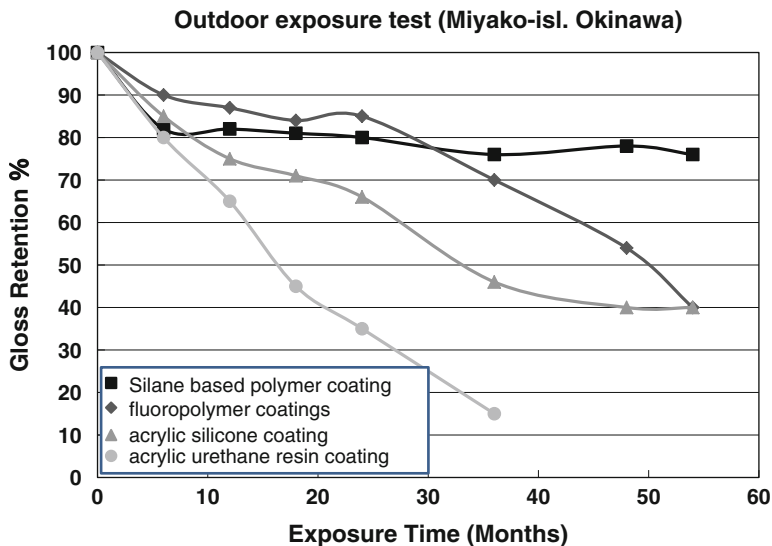
Fig. 23.3 Weathering for various organic paints exposed in practical environments

impregnates them. And as a result, only pigments remain at the surface of film. Therefore, the concentration of pigments would be high at the surface. Figure 23.3 shows the stability of sealing agents in a long service life, when no change in color or chalking would occur in the formation of the spray-coated films, thus allowing them to realize their high weathering.

23.4.2 Application for Hot-Dip Galvanized Steel

Under the similar concept with that of spray coating, the alkoxysilane resin could be applied to hot-dip galvanized steel in order to enhance the weathering of the steel. When steel is immersed into a melted zinc bath at around 450 °C for a very short time (typically several seconds to minutes), the iron reacts with the zinc to form thick zinc films (thickness ranges from several micrometers to several hundred micrometers) on its surface. At the interface between the steel and zinc layer, an intermetallic phase between the iron and zinc forms, usually increasing the adhesion force of the film. The steel with zinc film produced in this manner is called hot-dipped galvanized steel. Generally, zinc films protect the steel substrate by the sacrificial anode effect. When a film has defects on the surface (e.g., pores, crevices, etc.), environmental moisture or solutions could make contact with substrate steels. However, the upper zinc layer would dissolve preferentially, due to the potential difference between zinc and iron. As a result, the steel substrate would be protected against corrosion, so long as zinc layers exist.

However, painted coating applied to the zinc layer actually improves corrosion resistance of surface layers much more and also increases the color tones at the same time. Usually, zinc-rich paint coatings have been used for this specific purpose [14]. However, the applicability of alkoxysilane resin painted onto hot-dipped galvanized steel as substitute for zinc-rich paint was investigated, and the availability was confirmed.

Generally, organic paints on hot-dipped galvanized steel are easily broken down by ultraviolet light gradually, thus causing chalking. The painted film also can become thinner and thinner from exposure to the weather. On the other hand, painted films composed of silane resin have high resistance against ultraviolet light. Therefore, the service life can be prolonged in the case of silane resin. Usually, the painting process for hot-dipped galvanized steel is composed of multiple layers being applied to the surface. At a minimum, there is a priming coat and a top coat. When the top coat is applied to a prime coat composed of zinc-dispersed or aluminum-dispersed paint, the silane resin could fill in the defects of the prime coat. The top coat could also protect the substrate. Even if the top coat deteriorated for any reason, the prime coat would continue to work as an anticorrosion paint. All of these characteristics would work collaboratively to make the corrosion protection for steel last over a long period of time. Silane compounds could be applied not only to steels but also to other nonferrous materials as corrosion protection paint. By adjusting the composition of the silane compounds, the application will spread much more.

23.4.3   Sealing Agents for Anodic Oxidation Film

Generally, some metals can form protection films on their surface by electrolysis, where the metal itself is used as an anode in an electrolyte. It is called anodic oxidation [15]. Particularly, aluminum is very well known for the process [16]. However, titanium [17–22], magnesium [23, 24], and others are also available for the process.

Fig. 23.4 Schematic illustration for the structure of an anodic oxidation film
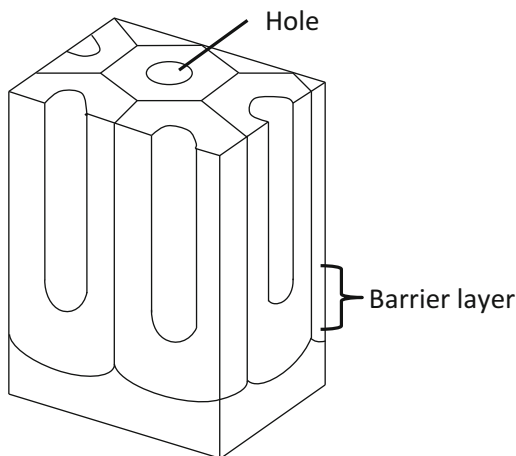
As sealing agent, the silane compound could be applied not only to the spray coating, but also to the anodic oxidation film containing microscopic pores. However, the pores of an anodic oxidation film belong in the nano-order (several tens to several hundreds of nanometers), much smaller than that of metal spray coatings (Fig. 23.4). In addition, the shape of the pores for an anodic oxidation film is usually different from that of metal spray coatings. The former is a rod-like pore where one end is completely stopped up, while the latter is spread in the form of a net. In the case of spray coating pores, a silane resin of low surface tension impregnates along the wall of the pore where the center part has room for the penetration of agents. In the case of pores for anodic oxidation films, it is hard for sealing agents to impregnate along the wall as well as in the center. Therefore, air can often remain at the bottom of the pore, since the pore of an anodic oxidation film is almost one dimensional. The situation is very different from the pore of a spray coating film, where the pore can lead to some exterior surface where the entrapped air could escape. The remaining air could be minimized through the usage of a silane resin whose surface tension or viscosity could be reduced by adjusting its components.

One of the unique characteristics for anodic oxidation films is their hardness after sealing. Particularly for aluminum's anodic oxidation, the film initiates cracks since the solidified silane resin can be too hard. Usually, the unfilled pore could mitigate the inner stress caused by the difference between the thermal coefficients of substrate aluminum and aluminum oxide as a film. However, a pore filled with hard silane resin would decrease the stress relaxation function for microscopic pores. To solve this problem and control the initiation of cracks, the silane resin could be applied after the hardening process completed. As described above, silane resins still have promising properties that can be used to seal the pores of anodic oxidation films. The application opportunities will increase with that of the anodic oxidation films themselves.

23.4.4   Protection of Concrete and Rocks

23.4.4.1   Deterioration of Concrete and Its Protection

Concrete has been used widely in construction since it can be produced at low cost and its synthesis is quite easy. It is composed of cement mixed with aggregates (e.g., sand and gravel) and solidifies into its final form when mixed with water. Its characteristics are determined by the mix ratio of components, the additives, and their amounts. Basically, the concrete has high resistance against compression, while it is weak when exposed to tension. Therefore, the concrete itself is easy to break when the structure bends. To increase its resistance to tension, steel is inserted in various shapes to form reinforced concrete. Usually, bar-type steel is used and is called rebar. However, there are many types of shapes available for reinforced steel. The reason why steel is used for reinforcement could be attributed to the fact that the thermal coefficient of concrete is almost the same as that of steels. Even if the

steel rebar reinforced concrete deformed at elevated temperatures, fractures would not easily occur [25].

Since concrete is free from the threat of oxidation and rust, it seems to be stable at a glance. However, it can deteriorate due to environmental exposure. To name a few, the surface of concrete can be damaged by the solidification of water that penetrates into its subsurface. Wear by wind and rain, automobiles, water waves and flows as physical phenomena, chemical deterioration by chloride ions and exposure to carbon dioxide in the air, and so on are but a few examples. Most of these attacks from the environment can be controlled by maintenance and repair with mortar. Or the concrete itself could be strengthened by adjusting its components and production conditions. However, some problems cannot be solved by such a countermeasure. One of them is the freezing of water inside concrete, a phenomenon that is often observed in cold areas. When water penetrates into concrete and freezes, the volume increases inside of the concrete, thus generating inner stress. When the inner stress increases and exceeds a threshold value, concrete begins to collapse locally. When the process is repeated, the steel rebar begins to make contact with the environment directly. As the severe corrosion of steel rebar occurs, this leads to the overall deterioration of concrete structures [26]. The phenomenon has been difficult to solve by just increasing the covering depth of concrete or by preventing water penetration with conventional paintings. In such a situation, it has been confirmed that alkoxysilane compounds could work well to protect the concrete from freezing water. When the alkoxysilane is adsorbed at the surface of the microscopic walls, the water-repellent characteristics of alkoxysilane resin push the inner water up through the pore of concrete to the outside area. It could protect any external material from penetrating into the interior of the concrete since alkoxysilane is a monomer and can impregnate to a depth of 4–7 mm. The penetration depth of alkoxysilane resin and the water-repellent characteristics are dependent on the pore itself.

As for chemical deterioration, it is a problem that is always critical for concrete structures. Chloride ions can come from seawater or deicing agents. It penetrates into the heart of the concrete and reaches the steel rebar where the corrosion of steel begins. Since the corrosion products increase the volume of rebar, inner stress occurs leading to cracks and spalling [27]. The coating of the concrete could solve the corrosion problem due to the penetration of chloride ions. However, conventional organic paints do not have an adequately high adhesion force, since they are typically attached to the concrete's substrate. In addition, they are vulnerable to ultraviolet light. Therefore, the coating film often breaks away in the service environment. On the other hand, silane resin could completely block out chloride ions. When applied to the concrete coatings, the corrosion protection of the steel rebar would be much more effective. The silane resin could penetrate into the pores of concrete deeply to develop the anchor effect in order to increase the adhesion force of the coating film.

Deterioration induced by carbon dioxide is a type of concrete chemical damage called carbonation [28]. Concrete's environment is strongly alkaline. Since iron is very stable in an alkaline environment, it does not typically corrode. However, there are some exceptions. Chloride ions are one of those, as described above.

Carbon dioxide is another. Concrete absorbs carbon dioxide in the air and neutralizes calcium hydrate within itself, an important factor for the internal alkaline environment. Therefore, the pH of concrete generally decreases with the progress of the carbonation process. The phenomenon occurs at the interface between the concrete and the atmosphere. The layer where carbonation occurs then moves into the inner part of concrete gradually. When it reaches steel rebar, the corrosion of steel begins since it is not when exposed to acidic conditions. In this case, the corrosion product induces the inner stress and breaks away from the concrete itself. Fortunately, silane resin could block out carbon dioxide just like chloride ions. This can be accomplished by two ways: through hardening on the surface and hardening after pore penetration.

23.4.4.2   Deterioration of Rock and Conservation

In our modern time, rocks are still used for constructions and many other objects. Even though rocks may be durable, they usually change their appearances and deteriorate due to external causes over tens or hundreds of years. Therefore, rocks often need conservation treatments. For example, marble used in ceilings and walls show improved brightness after polishing and when the surface is free from contamination. However, they actually have surface pores where contaminants can penetrate causing blemishes and stains. When the micro-pores on surfaces of rocks are filled with silane resin, any contaminants could no longer penetrate into the pores, thus solving the contamination problem.

For some stone materials made of rocks, "burner finishing," or roughening the surface of a rock by gas burners, is often carried out as a nonskid treatment. The surface would then be roughened too much, losing its original color tone. To adjust them from and atheistic viewpoint, silane resin could be applied to the surface as a coating. Concretely, the silane resin paint could change the roughened surface back to the original color tone of the polished rock.

In addition, the penetration of water into stone materials through their micropores can lead to deterioration due to the freezing, similar to the problem seen in concrete structures. The application of silane resin would solve this problem as well. Recently, the compound's characteristics have been be utilized in aiding in the protection of cultural assets made of rocks and stones [29].

23.4.5   Antibiofouling

23.4.5.1   Biofouling

Biofouling occurs around us on daily basis. In bathrooms and kitchens, viscous substances typically form on products and commodities stored within. Outdoors, one can see slimy matter at the inner wall of pipes. Along seacoasts, one could observe barnacles and other marine organisms attaching themselves to ships, structures, and piers.

From this viewpoint, biofouling can be seen everywhere. Biofouling is classified into two main categories: microfouling and macrofouling. The former is mainly caused by bacteria, leading to the formation of slimy matter and often brings about corrosion. The latter is caused by larger marine organisms such as barnacles and oysters as described above. These two categories are never independent of each other. Rather, they are related and actually microfouling is in most cases the previous step for the occurrence of macrofouling. Therefore, the control of biofilms, the main factor of microfouling, is very important. However, it is often very difficult to control biofilms, since many complicated factors are involved in its formation and growth [30].

One of the countermeasures is the use of antibacterial materials. Biofilms are caused by the attachment of bacteria to a material's surface. If the surface had antibacterial properties, the bacteria would avoid attaching to its surface. Even though bacteria could attach to the surface, the antibacterial surface would inhibit its growth remarkably. Therefore, silver, copper, titanium oxide, and others have been applied to the surface coating of materials, so that an antibacterial coating could be achieved. Those three materials have been well known for their practical antibacterial effects [31]. Among all of these matters, titanium oxide shows its antibacterial effects through photocatalytic properties. However, the other metallic elements such as silver and copper do not have any photocatalytic properties. Those metals form ions in aqueous environments and the formed ions could control bacterial growth to bind with proteins on bacteria surfaces. Those metallic ions could easily react with the proteins on bacterial membranes to inhibit their enzymatic functions in various ways. From this viewpoint, the appearances of antibacterial effects need to form ions of silver, copper, etc. as a premise. It means corrosion and deterioration occur simultaneously on the material's surface where these metals would be applied to the coating directly.

To solve this problem, the dissolution of antibacterial metals as ions on the material's surfaces could be controlled to some extent. For this purpose, silane resin can also be applied and utilized. In a trial, silver, copper, and other metals, or organic compounds are dispersed into alkoxysilane resin. They can then be coated onto many kinds of materials resulting in the silane resin coating controlling the biofouling on the substrate materials such as steel [32, 33].

23.5 Conclusion

Silane resin could be applied in many practical situations, and this possibility is expected to extend over the future. The most promising characteristic of silane resin is its weathering. These characteristics will be increasingly used as for infrastructures such as those in building structures and other construction application. As for natural rocks and stone materials, countermeasures against their deterioration of cultural assets will need to be developed more. Many engineers and researchers are accelerating their investigations into these materials. The characteristics of silane resins have and will be further applied to many more advanced fields in the near future.

References

1. Welsh L, Welsh P (2009) Rock-art of the Southwest. Wilderness Press, Berkeley, CA
2. Friedel C, Crafts JM (1863) Ueber einige neue organische Verbindungen des Siliciums und das Atomgewicht dieses Elementes. Ann Chem 127:28–32
3. Kipping FS (1904) Organic derivative of silicon. Preparation of alkylsilicon chlorides. Proc Chem Soc 20:15–16
4. Hyde JF, Delong RC (1941) Condensation products of the organo-silane diols. J Am Chem Soc 63:1194–1196
5. Colas A, Curtis J (2004) In: Ratner B, Hoffman A, Schoen F, Lemons J (eds) Biomaterials science. An introduction to materials in medicine, 2nd edn. Elsevier, Boston, MA, pp 80–86
6. Rochow EG (1987) Silicon and silicones. Springer, Heidelberg
7. Barquins M, Cognard J (1986) Adhesion characteristics of gold surfaces. Gold Bull 19:82–86
8. Emad Y, Raghad H (2013) Photodegradation and photostabilization of polymers, especially polystyrene. SpringerPlus 2:398–430
9. Kerr JB, Fioletov VE (2008) Surface ultraviolet radiation, ATMOSPHERE-OCEAN 46:159–184
10. Bhavesh GK, Raman PS, Nakamura T (2002) Degradation of carbon fiber-reinforced epoxy composites by ultraviolet radiation and condensation. J Compos Mater 36:2713–2733
11. Huheey JE (1983) Inorganic chemistry - principles of structure and reactivity. Inorganic chemistry, 3rd edn. Harper & Row, New York, NY
12. Gerald LW (1993) A silane primer: chemistry and applications of alkoxy silanes. J Coat Technol 65:57–60
13. Kuroda S, Kawakita J, Watanabe M, Katanoda H (2008) Warm spraying - A novel coating process based on high-velocity impact of solid particles. Sci Technol Adv Mater 9:1–17
14. Azizul HBS (2014) Corrosion protection of zinc rich paint coating on steels. Doctoral dissertation, Shibaura Institute of Technology, Graduate School of Engineering and Science
15. Sheasby PG, Pinner R (2001) The surface treatment and finishing of aluminum and its alloys 2, 6th edn. ASM International & Finishing Publications, Ohio
16. Zemanov M, Chovacovà M, Fellner P, Prekopp K (1998) Corrosion resistance and quality of sealed porous alumina coatings. Chem Papers 52:152–155
17. Emsley J (2001) Titanium. Nature's building blocks: an A-Z guide to the elements. Oxford University Press, New York, NY
18. Gils SV, Mast P, Stijns E, Terryn H (2004) Color properties of barrier anodic oxide films on aluminum and titanium studied with total reflectance and spectroscopic ellipsometry. Surf Coat Technol 185:303–310
19. Zuojia L, Xiaohui L, Uyime D, George ET, Peter S (2014) Corrosion behavior of the anodic oxide film on commercially pure titanium in NaCl environment. Int J Electrochem Sci 9:3558–3573
20. Liang W, Jianhua L, Mei Y, Songmei L, Hongxing L, Mengqi Z (2014) Effect of anodization time on morphology and electrochemical impedance of andic oxide films on titanium alloy in tartrate solution. Int J Electrochem Sci 9:5012–5024
21. Puippe JC (2003) Surface treatments of titanium implants. Eur Cells Mater 5:32–33
22. Jian HL, Liang W, Mei Y, Song ML, Guo LW, Zongjin L (2011) Effects of sealing process on corrosion resistance and roughness of anodic films of titanium alloy Ti-10V-2Fe-3Al. J Cent South Univ Technol 18:1795–1800
23. Hara M, Matsuda K, Yamauchi W, Sakaguchi M, Yoshikata T, Takigawa Y, Higashi K (2006) Optimization of environmentally friendly anodic oxide film for magnesium alloys. Mater Trans 47:1013–1019
24. Fanya J, Paul KC, Guidong X, Jun Z, Deli T, Honghui T (2006) Structure and mechanical properties of magnesium alloy treated by micro-arc discharge oxidation using direct current and high-frequency bipolar pulsing modes. Materials Science and Engineering A 435–436:123–126

25. Mörsch E (1909) Concrete-steel construction: (Der Eisenbetonbau). The Engineering News Publishing Company, New York, NY, pp 204–210
26. Huai SS, Ting HY (2013) Freeze-thaw durability of air-entrained concrete. Scientific World J 1–6
27. Kejin W, Nelsena DE, Nixon WA (2006) "Damaging effects of deicing chemicals on concrete materials. Cement Concrete Compos 28:173–188
28. Parrott LJ (1990) Damage caused by carbonation of reinforced concrete. Mater Struct 23:230–234
29. Doehne E, Price CA (2010) Stone conservation: an overview of current research, 2nd edn. The Getty Conservation Institute, Los Angeles, CA
30. Kanematsu H, Barry DM (eds) (2015) Biofilm and materials science. Springer, New York, NY
31. Kanematsu H, Ikegai H, Yoshitake M (2013) Patents for antibacterial metallic coating and its future trend in japan. Res Inventy Int J Eng Sci 3:47–55
32. Ogawa A, Noda M, Kanematsu H, Sano K (2015) Application of bacterial 16S rRNA gene analysis to a comparison of the degree of biofilm formation on the surface of metal coated glasses. Mater Technol 30:61–65
33. Kanematsu H, Sasaki S, Miura Y, Kogo T, Sano K, Wada N, Yoshitake M, Tanaka T (2015) Composite coating to control biofilm formation and effect of alternate electro-magnetic field. Mater Technol 30:21–26

Chapter 24
Smart Self-Healing Polymer Coatings: Mechanical Damage Repair and Corrosion Prevention

Pooneh Kardar, Hossein Yari, Mohammad Mahdavian, and Bahram Ramezanzadeh

Abstract Self-healing polymers are special category of smart materials where its properties change in response to an environmental stimulus. These materials have the capability to repair themselves when they are damaged without the need for any external intervention. In the first part, the principles and fundamentals of various types of smart coatings, materials, design, and processing methods are described. In the second part, various strategies to heal the mechanical damage have been targeted. Employing intrinsic self-healing materials with inherent bonding reversibility of the polymer matrix is the most important strategy which has been reviewed in this section. In the third part, the microencapsulation approaches to self-healing polymer development will be reviewed. This section will characterize polymer coatings that are classified as self-healing, based upon self-healing agents that are microencapsulated, active inhibitors loaded into nanoparticles, as well as nanocontainers and polymers that are constructed by the layer-by-layer (LbL) method. Finally, corrosion inhibitors that rely upon controlling micro- and nanoreservoirs release for the intercalation or encapsulation will be also reviewed. In this regard, application of layered double hydroxides (LDHs), porous nanoparticles, hollow spheres, zeolites, bentonite, and montmorillonite with active corrosion inhibitors are to be explained as well.

Keywords Self-healing polymer coatings • Mechanical damages • Reversible cross-links • Corrosion inhibition • Nanoreservoirs

P. Kardar • H. Yari • M. Mahdavian • B. Ramezanzadeh (✉)
Department of Surface Coatings and Corrosion, Institute for Color Science and Technology, Tehran, Iran
e-mail: kardar@icrc.ac.ir; yari-ho@icrc.ac.ir; mahdavian-m@icrc.ac.ir; ramezanzadeh-bh@icrc.ac.ir; ramezanzadeh@aut.ac.ir

24.1   Introduction

In the recent years, the need to have longer maintainability and reduced energy cost has driven researchers to design new materials. One of the most important challenges is to fabricate materials that can react to external changes (e.g., mechanical damage) automatically and respond without any interference. Thus, these receptive systems could inhibit terrible failure and improve the lifetime of the materials. A new breed of smart polymer that is capable of repairing damage inflicted upon them, on demand, without the need for external intervention, has been dubbed self-healing polymers.

24.1.1   Definition of Self-Healing

Materials that are classified as self-healing can automatically repair damage they have received [1, 2]. This ability has also been termed as self-repairing, self-healing, and self-recovery in various studies. More often than not, synthetic materials with self-healing properties cannot capitalize on this feature unless exposed to an external trigger. Therefore, self-healing materials are categorized into two types: autonomic (without any intervention) and non-autonomic (needs human intervention/external triggering) [3–7]. The scientific community currently only recognizes self-healing materials as those that can recover mechanical strength via crack healing. However, studies have put forth examples of both cracks and small pinholes that have been filled and healed, each displaying improved performance afterward. Herein, this chapter will discuss various types of properties that can be healed.

24.1.2   Design of Self-Healing Materials

Various products like plastics, paints, and even coatings have different healing mechanisms. Different approaches to self-healing methods will be investigated with the sections that follow.

24.1.2.1   Release of Healing Agents

Different materials like monomers, dyes, catalysts, corrosion inhibitors, and hardeners are enclosed into microcapsules, hollow fibers, or channels. During polymer or coating manufacturing, these reservoirs can be introduced into the systems, and in the case of a crack, they are broken. Then, the healing agent releases into the cracks, solidifies, and heals it by capillary force. The following sections review different strategies used to employ these types of self-healing materials.

Microcapsule Embedment

The methodology behind the micron-sized solid, liquid, or gas groups enclosed within shells that are inert is called microencapsulation and provides protection from the external environment [8–11]. The final outcome of this effort is the microcapsule creation. Comprised of two parts, a core and a shell, microcapsules can vary in both size (i.e., micro, nano) and shape (i.e., spherical, irregular).

Hollow Fiber Embedment

The drawback of the use of microcapsules is the possibility of not fully healing the damaged area as the healing agent is in a limited supply and the point where complete consumption is reached cannot be known. If additional healing agent is available in the system, better healing is possible. Therefore, hollow fibers or vascular systems are inserted into the composites so as to carry a larger amount of liquid healing agent, thus achieving multiple healing capabilities [12–17]. The production of synthetic materials comprised of such networks is both complex and difficult for practical applications. This design is advantageous, allowing for increased availability of healing agent designated for repairing damage, ability to use various resins, visibility of the damaged area for later inspection, and easy customization with conventional fibers for reinforcement.

24.1.2.2   Reversible Cross-Links

Polymeric cross-linking, while irreversible, provides superior mechanical properties to the material like a greater modulus, resisting solvents, and improved fracture strength. Disadvantages of these highly cross-linked materials include brittleness and a predisposition for cracking. Improved handling of cross-linked polymers can be achieved through the introduction of reversible cross-links within the polymer's network. While reversible cross-links can be re-fabricated and show self-healing properties, the system as a whole does not display such ability. These systems require an outside stimulus (e.g., thermal, photo, or chemical stimuli) to realize reversibility, triggering self-healing. The two groups of reversible cross-links (i.e., covalent, non-covalent) which imbue self-healing properties will be investigated in the following sections.

Covalent Reversible Cross-Links

When considering covalent reversible repairing polymers, the Diels–Alder (DA) reaction and its retro-Diels–Alder (RDA) reaction show potential, mainly due to their thermal reversibility [18, 19]. Typically, the monomer that has the desirable functional groups (e.g., furan, maleimide) systematically creates two carbon–carbon

bonds, and polymer formation is accomplished through the DA reaction. When heated, polymeric degradation begins, reducing it to its basic monomeric units via RDA reaction; cooling reforms the polymer along with any other return to the state of its initial conditions. Different systems were investigated and include dicyclopentadiene, maleimide/furan, and hetero-DA. Another covalent approach is a sulfur-based chemistry relying upon sulfur bonds' redox reactions, either light induced or exposure to oxidants/reducers [20]. It is frequently utilized in the formation of disulfide bonds in thiol–disulfide reactions in its oxidized form.

Non-covalent Reversible Cross-Links

Physical cross-linking is referred to the non-covalent interactions between polymeric chains which are not permanent with the ability to be alternatively formed and broken by external stimuli usually heat cycles. This cross-linking is usually considered as thermo-reversible cross-linking. The most important associations of a non-covalent nature include ionomeric, multi-hydrogen bondage, metal-ligand, and π-π stacking interactions [21, 22].

Supramolecular polymers are a unique category of novel polymeric materials. These recently developed materials include designed complex architectures with non-covalent interactions that behave like macromolecules [23]. A large subcategory of supramolecular polymers consists of those systems which are designed based on multiple hydrogen bonding. Hydrogen triple and quadruple bonding networks like urea, carbamate, and amide groups can enhance the physical linkages between polymeric chains.

Hydrogen bonding in coating systems provides a highly favorable type of interaction. In comparison with bulky polymeric materials, polymeric coating systems should have two main capabilities in order to strongly adhere to the substrate over which they are applied. The coating systems are usually formulated in such a way to be easily leveled on the substrate with the lowest amount of solvent usage and also have a high level of donating or accepting interfacial interactions between the coating and substrate to achieve a high degree of adhesion. Implementing hydrogen-bonding principles into coatings is highly desirable because it can enhance both applicability and adhesive properties of the coating. Hydrogen-bonded supramolecular self-healing coatings are usually low molecular weight oligomer chains which have been designed with alternating H-donor–H-acceptor polar architecture. While low molecular weight promotes the applicability, polar architecture enhances the adhesive properties of the system. The lack of need for external material for healing (e.g., catalyst, initiator, capsule, etc., which can spoil other coating properties) is another advantage of utilizing H-bonding-based moieties when developing self-healing coating systems.

Ionomeric polymers contain between 1 and 20 % of ionic repeating units and have organic or inorganic main chains [24, 25]. Therefore, ionomers are known as a system that resides between neutral polymers and polyelectrolytes. Ionomers with an organic structure have been proposed for self-healing although inorganic

ionomers are rarely used. In the case of deformation, the ionic groups rearrange and recover the damage by elastic recovery. These processes perform on different time scales and help the recovery of the damaged area, repairing mechanical properties by the creation of non-covalent bonds. Synthesis of ionomers is achievable by commercially available materials, possesses impressive properties (physical/mechanical), and has proven indispensable in both ballistic and various other applications. The combinations of these two advantages (i.e., physical properties and easy processing) as well as the ionic bonds' reversibility make them ideal candidates in the modeling of novel polymeric system with self-healing properties.

24.1.2.3 Miscellaneous Technologies

Electrohydrodynamics

This approach consists of two walls of a metallic cylinder, double layered, surrounding a colloidal particle suspension [26]. The inside wall is covered by a conductive coating, and the outer one is coated with a ceramic insulating layer with an electric field applied by a metal wire. When the insulating layer experiences a crack, the damaged area experiences an increase in current density, and the damaged area heals via colloidal particle agglomeration.

Conductivity

By introducing conductivity so as to insulate the polymers, they may become appropriate for self-healing systems [27]. When the system experiences cracking, the electron penetration value in the system decreases and the electrical resistance increases. As the conductivity of the system drops, it can increase the applied electric field, and this voltage bias produces extra heat in the damaged area. The system's original form, reduced resistance with a large current situation, can be achieved via the generated heat. Generally *N*-heterocyclic carbons are used for these self-healing applications.

Shape Memory Effect

Polymers that can be deformed to a temporary shape until later stimulation restores its original shape when triggered by external heating or other means are said to have the shape memory effect [28–30]. In order to push the crack surfaces closer together, two different methods can be employed: shape memory alloy (SMA) wires and shape memory polymer (SMP) fibers (Fig. 24.1). For a more effective application, localized positioning of either of the component's perpendicular to the crack is a prerequisite to success.

As it is well understood, the coatings are usually applied on a substrate to enhance the appearance of the structure (aesthetic function) and/or protect it from aggressive
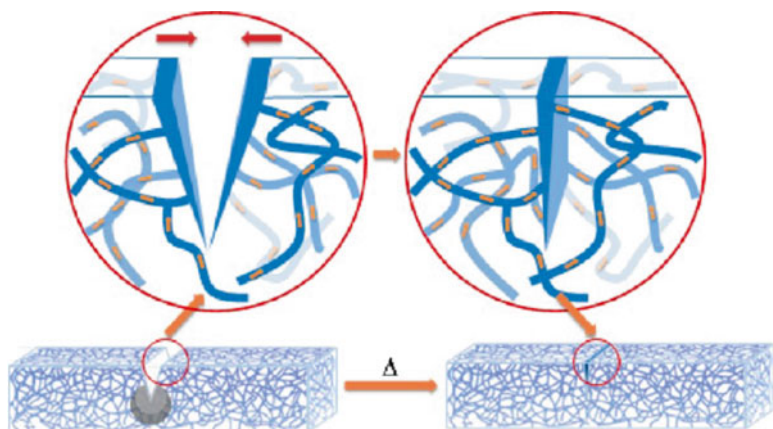
Fig. 24.1 Schematic illustration of the shape memory self-healing concept (reprinted with permission from [28], copyright American Chemical Society)

environmental degradation like corrosion (barrier function) [31]. When a coating is mechanically damaged, the coating partially or completely loses its aesthetic and barrier functions at that area, leading to a weak point which can catastrophically jeopardize the long-term properties of the coating and reduce the service life [32]. In the introduction, it was attempted to briefly review different approaches that can be implemented in coating formulation to autonomously or non-autonomously recover some functions of a coating which have been lost during a damaging process. In the following part, the focus is placed on the studies that aim to heal a mechanical damage and restore the damaged area to its original state via intrinsic or extrinsic self-healing mechanisms. The barrier properties and corrosion aspect of self-healing materials are not discussed in this part and will be considered in the next sections.

24.2 Healing of Mechanical Damage

The pioneering developmental studies in regard to self-healing polymeric composites using encapsulated therapeutics are specifically in reference to a letter published in Nature in 2001 [6]. In this paper, embedded microcapsules containing reactive components can be torn when they are subjected to a propagating crack tip. The reactive capsule ingredients are released into the crack and the previously embedded catalyst triggers the local polymerization, filling and bonding the crack faces. Various reactive healing agents like dicyclopentadiene/Grubbs' catalyst [6], polydimethylsiloxane/ tungsten [33–35], and isocyanates [36, 37] have been used for this purpose. In such a multicomponent complicated structure, there are several design parameters which should be controlled to achieve efficient healing. The most critical parameters such as thickness and relative stiffness of capsule shell as well as

interfacial strength at microcapsule/ matrix interface should be optimized [38]. Evaporation of the capsules' ingredients and thermal stability of the capsule wall are also vital parameters if they are to be incorporated into matrices that will be subjected to high temperatures during processing like epoxy systems. Therefore, the thermal stability should be improved. It has been revealed that combining urea/ formaldehyde with urethane chemistry to form a distinct double-walled capsule can enhance the thermal stability of the capsule as well as provide excellent interfacial bonding with epoxy matrices [39].

The principles of self-healing that rely upon reversible DA/RDA reactions were presented earlier. In self-healing thermosetting systems, heat is the stimulus for both curing of the network and cleavage of reversible cross-linked network; the curing temperature and healing efficiency can be a critical issue. In the coatings which the DA/RDA part has been grafted on a monomer or on the reactant oligomer, healing efficiency is highly connected to the temperature at which the curing reactions occur. Bai and coworkers [40] investigated different curing conditions of a healable epoxy system so as to determine the optimal curing setting for epoxy–amine reaction, while preventing the pre-scission of the DA adducts. The researchers produced a cross-linking diamine that possessed two adducts of DA [41]. Utilization of diglycidyl ether of bisphenol A (DGEBA) in the curing of this cross-linker at various curing regimes creates a healable epoxy system based on DA/RDA chemistry. Curing of thermosetting systems is usually performed at temperatures above 120 °C. The higher temperatures lead to higher levels of cross-linking. But, on the other hand, such temperatures are high enough to activate RDA reactions, leading to DA cleavage and formation of furan and maleimide moieties. The maleimide can react with an amine cross-linker as a side reaction which can result in lowered healing efficiency. It was found that curing at low temperatures around 60 °C for a long time can provide a high level of conversion and can also protect the DA moieties from undesired side reactions. In addition, these healing experiments revealed a high level of healing at 110 °C for a short time. Figure 24.2 depicts the scratches after exposing to thermal healing treatments for various short times.

As seen in Fig. 24.2, a microscale scratch on such a healable epoxy system was fully recovered at 110 °C after less than 5 min. It was concluded that this time can be even shorter provided that the temperature increases (0.16 min at 130 °C).

Luo and coworkers [28] have developed a new coating system which is highly healable, thanks to the shape memory characteristics of both thermosetting epoxy matrix and incorporated thermoplastic PCL fibers [28]. They randomly deposited the electro-spun PCL fibers on a surface and finally applied the epoxy onto the fibers via spin coating technique. The epoxy matrix was based on DGEBA/neopentyl glycol diglycidyl ether (NGDE) cured with poly(propylene glycol)bis(2-amino-propyl) ether. Upon heating to a temperature which is high enough to soften the matrix and melt the fiber, both the matrix and the fibers try to close and rebound the crack edges through their shape memory character. The matrix recovery causes the stored strain energy at the plastic zone to be released so as to close the crack. On the other hand, the PCL thermoplastic is locally melted and flows and, therefore, leads to crack rebounding. This system could successfully heal plastic scratches and completely close the cracks when the damaged areas were subjected to 80 °C for 10 min.
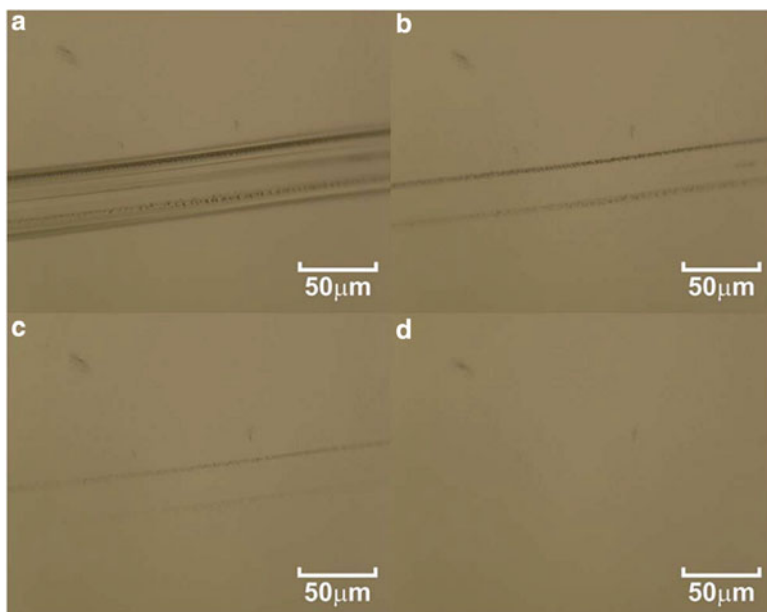
Fig. 24.2 Images of healed scratches exposed to 110 °C for various times (**a**) 0, (**b**) 0.16, (**c**) 1.66, and (**d**) 4.45 min (reprinted with permission from [40], copyright Royal Society of Chemistry)

Kashif and Chang [42] have recently developed a novel healable supramolecular elastomer based on cross-linking of maleated polyethylene-octene elastomer (mPOE) with 3-amino-1,2,4-triazole (ATA) [42]. They further blended this polymeric system with Nylon 12 and obtained a system which was synergistically enriched with ionic and hydrogen-bonding interactions. It was demonstrated that this resultant system had a high capability to repair scratches.

Meijer and his colleagues were the pioneering team in inventing and developing such polymeric systems. They introduced self-complementary 2-ureido-4-pyrimidone (UPy) motifs, with special conditions allowing self-association [22, 43]. UPy-grafted linear low molecular weight oligomers assemble into long polymeric chains and behave like high molecular weight polymers in dilute solutions. Such a polymeric structure is reversible and can be returned into its monomeric (not assembled) state at high temperatures or in polar solutions. Multiple hydrogen bonding has association energies between the strength of a single hydrogen bond and a covalent linkage. The association and disassociation constant of UPys is critical in controlling mechanical strength and self-healing efficiency. Since hydrogen bonding contributes to mechanical properties at low temperatures, therefore, a high level of hydrogen bonding will increase the mechanical properties [44, 45]. But, on the other hand, increased hydrogen bonding may slow down the disassociation rate of interactions, leading to slow healing. According to these facts, an optimized balance between self-healing properties and mechanical strength is the main challenge in designing self-healing polymers.

In classic polymers, the mechanical strength and modulus are attained mainly by chain entanglements (usually for thermoplastics) or covalent cross-linking (usually for thermosets). Both entanglements and covalent cross-linking are undesirable from a healing point of view [44]. Therefore, most self-healing systems developed so far suffer from poor mechanical properties. Because of this, most of self-healing systems have not found practical applications and been limited to laboratorial attempts. There have been numerous attempts to simultaneously enhance the self-healing and mechanical properties [46]. Sijbesma and coworkers [45] presented a chemically cross-linked system in which parts of the permanent covalent cross-links were substituted by reversible non-covalent cross-links [45]. Different polyester-urethane precursors were synthesized and then partially end capped with UPy units. Their findings revealed such modification which led to an increase in healing characteristics and a favorable balance of hardness versus ductility.

Electronic interactions between different components in a molecular compound can also be utilized to form supramolecular polymers. Complementary electronic π-π stacking interactions between a π-electron lacking group and a unit teeming with π-electrons can provide reversible bonding between two components to self-assemble into a physical polymeric network. It has been demonstrated that increasing the number of sites interacting via π-π stacking on one molecule can be an effective strategy in the enhancement of mechanical properties as well as yielding a tough, robust polymeric structure. For example, Hayes [47] has shown that poly(ethylene glycol)-based polymers end capped with three pyrenyl end groups (an electron-rich component) had higher tensile modulus, toughness, elasticity, and yield point compared to the same polymer having two pyrenyl end groups when they were self-assembled into a diimide–ether copolymer (an electron-deficient component).

A group of German researchers have recently combined the supramolecular chemistry with fluorine-based low surface energy components, thus creating a surface coating with superhydrophobic properties which can heal damage with a thermal treatment in a short time period [48]. They grafted perfluorinated compounds into a low molecular weight gelator based on urea. Such molecules, via hydrogen bonding of amide unit, can self-assemble into a long fiber-like polymeric structure. These fibrous scaffolds create a fluorine-enriched surface with nanometric roughness that resembles superhydrophobic lotus leaves. Beside self-cleaning characteristics, such coatings have self-reparative capabilities. The supramolecular coating's scratch healing abilities were also studied. Two scratches with different widths (226 and 40 μm, respectively, higher than and comparable to coating thickness) were created, and the coating was subjected to 900 W microwave treatment for 20 min.

Results showed that the wide scratch has been partially recovered. The partial recovery was mainly due to the low ratio of coating thickness to scratch width. Therefore, there are no sufficient supramolecules at the scratched area to completely fill the scratch. But, for the smaller scratch, it has completely disappeared after thermal treatment. It was also further revealed that the superhydrophobicity of the coating after scratch healing remained unchanged. Such a self-healing/cleaning coating was a preliminary attempt and there is still a room left for optimization.

24.3 Nano-/Microcontainers Loaded with Corrosion Inhibitors

A live protection effect on the metal substrate can be attained incorporating corrosion inhibitors alongside the organic coating. The easiest method for inclusion of the additive is through simple mixing. However, direct incorporation of inhibitors can raise many problems. Very low inhibitor solubility lowers the amount of active species at the substrate/coating interface, and high solubility leads to corrosion protection for a relatively short period. Incorporation of high inhibitor loadings is needed for this case in order to reach long-term protection performance goals. However, this will disturb the coating curing behavior, and the water can easily diffuse into the coating, leading to coating delamination and blistering. In addition, the inhibitor's interaction with the coating matrix will result in the deactivation of the corrosion inhibition effect. Also, it causes very fast polymer film detachment from the substrate. Self-healing coatings have been fabricated to overcome the aforementioned problems by synthesizing nano-/microscale containers filled with active inhibiting agents. In this way the active corrosion inhibiting species can be encapsulated and remains in a "trapped state" as long as the coating is undamaged. However, the mechanical impact or a change in the local environment forces the containers to release the active materials at the position needed.

24.3.1 Synthesis Procedure Micro-/Nanocapsules

Micro-/nanocapsules are small particles (3–800 μm) with a core made of liquid material covered by a coating layer. The most important methods used to produce the microcapsules are coacervation [49], interfacial polymerization [50], in situ polymerization [51], extrusion, and sol–gel methods. Of these, interfacial polymerization has been mostly used to encapsulate inhibitors in polymeric shells. The interfacial polymerization occurs at the interface between two liquid phases which are immiscible. For this purpose, the reactive monomer should be first dissolved in solvent 1. Then, a stable emulsion of this solution in solvent 2 can be obtained by using a surfactant. The second step of the polymerization reaction is adding another active monomer to the polymerization phase. Micro-/nanocapsules can be produced through the polymerization reaction between two monomers on the surface of emulsion droplets. Emulsions with different characteristics can be used for this purpose. Oil-in-water emulsions are used most commonly for the interfacial polymerization [52–57]. However, other proposals include the emulsions via inverse water-in-oil [58–60] and oil-in-oil [61–64]. Polymers that are both linear and cross-linked can be exploited in the creation of capsules' shells where the choice of polymer dictates the capsules' following properties: mechanical strength, elasticity, chemical inertness, and permeability. Capsules of different sizes can be obtained through stirring the reactants at different speeds during the emulsification step. Increasing the stirring speed reduces the capsules' average diameter. The relationship between the stirring speed and the capsule size can be studied by SEM analysis [51]. Generally,

the size, shape, morphology, and microcapsules' shell thickness can be altered by control over the stirring speed, chemical structure of the emulsifier, emulsifier concentration, pH of the reactants, thermal reaction conditions, and the length of time for the encapsulation reaction to occur [51, 65–67].

24.3.1.1   Mechanism of Smart Self-Healing

The on-demand corrosion inhibitor release from smart micro-/nanocapsules incorporated into the organic coatings yields self-healing coatings. The corrosion inhibitors' release from the capsules can occur as a result of mechanical triggering, pH, or temperature-controlled stimulation. The extent of healing depends on the capsules' material type as well as the capsules' shell sensitivity to pH. Mechanical impact or the change of local environment (i.e., pH) forces the capsules to release the corrosion inhibitors at the specified sites. The defect on the coating opens a pathway for chloride ion permeation toward the metal substrate. As a result, the corrosion processes start on the metal substrate. Hydroxyl ion (OH^-) creation during the cathodic reactions results in localized increases in pH at the metal surface's cathodic sites. The increase of pH causes the inhibitor release from the capsules into the defect due to polyelectrolyte shell destruction, leading to its permeability enhancement. The released corrosion inhibitor heals the damage while hindering corrosion. The capsule's shell is not pH sensitive; the mechanical triggering of the coating leads to the capsule shell tearing and the release of corrosion inhibitors.

24.3.1.2   Healing Agents Used in the Microcapsules

Capsules Filled with Water-Repelling Agents

Incorporation of water-repelling agents with long hydrophobic tails is one approach to passively heal the damaged part. Organofunctional silanes are potential candidates for encapsulation as the water-repelling materials needed for incorporation into self-healing protective coatings. The coating-containing microcontainers filled with an alkoxysilane and its self-healing properties are studied [68].

The mechanical triggering of the coating causes capsule damage leading to the release of encapsulated materials reaching the bare metal surface (uncovered). The reaction of water with alkoxysilanes forms a passive, hydrophobic film upon the surface of the metal, resulting in corrosion protection at the damaged area on the metals' surface.

Capsules Filled with Oil

Linseed oil has been used as the most important oil-based healing agent because of its oxidation drying mechanism used in film formation [69–74]. The drying process needs cobalt, calcium, lead, and zirconium as driers. Suryanarayana et al. [70] studied microcapsules, (urea–formaldehyde shell drying oil core, epoxy coated) and

self-healing properties. It was found that the microcapsules could successfully heal the damaged area. The ruptured microcapsules can release linseed oil which forms a protective film over the crack. As the released oil is exposed to oxygen, a film is formed through oxidative polymerization. The film formation prevents moisture and oxygen contact with metal surface and thus prevents corrosion.

Corrosion Inhibitors

Reinforcing organic/inorganic corrosion inhibitors into the organic polymer coating matrix is another approach used to produce micro-/nanocapsules for the self-healing coatings. Koh et al. [75] investigated polyurethane (PU)-based microcapsules filled with isosorbide derivative and their self-healing performance. They synthesized the microcapsules by combining a prepolymer of DE–TDI along with 1,4-butanediol in interfacial polymerization. It was found that the microcapsules loaded with corrosion inhibitor at concentration range of 25–200 ppm resulted in promising corrosion resistance and low rusting degree (0–0.47 %) (Fig. 24.3).

Studies performed by Kopec et al. [76] investigated the self-healing capabilities of epoxy water-based coatings reinforced by corrosion inhibitor-loaded nanocapsules including 2-methylbenzothiazole (BT) and 2-mercaptobenzothiazole (MBT). They showed that by embedding liquid core nanocapsules loaded with an organic corrosion inhibitor into the coating matrix showed the appropriate self-healing
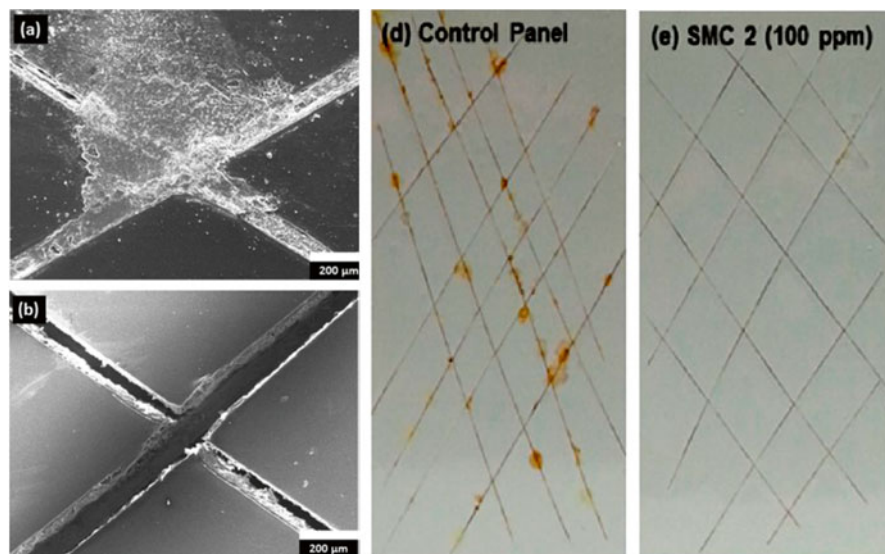
Fig. 24.3 SEM images of (**a**) the scratched region of the control panel and (**b**) the self-healing anticorrosion coating after healing, (**d**) visual performance of the control panel, and (**e**) the coating containing nanocapsules filled with inhibitor (reprinted with permission from [75], copyright American Chemical Society)
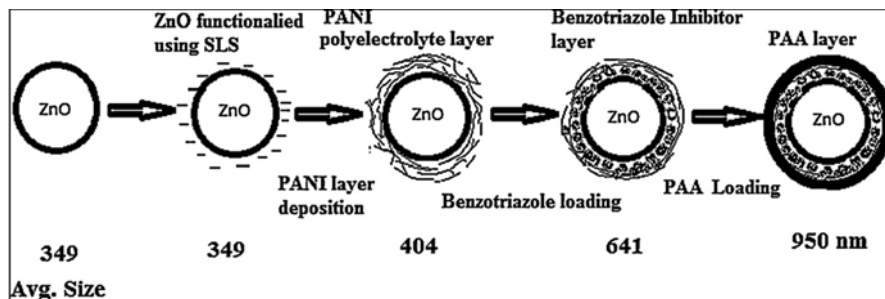
Fig. 24.4 Schematic illustration of the procedure for benzotriazole loading on ZnO nanoparticulate containers (reprinted with permission from [79], copyright Elsevier)

properties. Raps et al. [77] studied the healing mechanism for the epoxy primer doped with polyurea microcapsules. The active corrosion protection was seen for this system by releasing the inhibitor solution and formation of a passive film inside micro-cracks on the coating surface.

24.3.2 Layer-by-Layer (LbL) Assembled Nanocontainers

Corrosion inhibitors can be also encapsulated through the layer-by-layer method. In this method, the liquid active agent is encapsulated into the layer of oppositely charged polyelectrolyte layers. The nanocontainers produced by this method have excellent compatibility with the organic coating and provide good barrier properties for corrosion protection [78]. Metal oxide surface adsorption of oppositely charged species (i.e., polyelectrolytes) results in preparation of nanocontainers with the smart capability of releasing corrosion inhibitors on demand. Sonawane et al. [79] studied the self-healing properties of ZnO particles when benzotriazole was assembled on the surface by the LbL method (Fig. 24.4). They performed an in situ emulsion polymerization at first to assemble the polyaniline (PANI) layer on the ZnO surface. Benzotriazole (anticorrosion agent) was then adsorbed on the PANI-coated particles. So as to enhance the nanocontainers' compatibility in polymeric resin, PANI-ZnO nanoparticles were coated with a polyelectrolyte layer (polyacrylic acid). The nanocontainers produced showed good self-healing behavior at the materialized pH.

LBL halloysite nanocontainers were introduced for their long-term release behavior and reliable healing properties. In a work done by Shchukin et al. [78], the inhibitor was encapsulated by the inorganic halloysite (diameter of 25 nm). Halloysite tubules are inserted via the layer-by-layer (LbL) method due to the strong surface charge on the surface. The halloysite tubes have a layer of positive charge on the outside and negative charge at the inside surface (at pH 8). Therefore, the inhibitor can be released to a corrosive environment on demand. Shchukin et al. [78] loaded inner voids of halloysite nanotubes with inhibitor. In addition, they modified via layer-by-layer polyelectrolyte by means of the hybrid sol–gel methodology of the

outer surface. The synthesis procedure of halloysite/polyelectrolyte nanocontainers loaded with 2-mercaptobenzothiazole was studied. Bhanvase et al. [80] investigated the corrosion inhibition of cerium zinc molybdate nanocontainers produced through the LbL procedure. They estimated the imidazole corrosion inhibitor's release rate from the CZM nanocontainer at different pHs. Also, they attempted to find kinetic models for the release of corrosion inhibitor from the LbL nanocontainers. They showed that alkyd resin coatings containing this kind of nanocontainer exhibited good corrosion protection properties on a surface of mild steel (MS).

24.3.3 Layered or Porous Inorganic Materials

Layered or porous inorganic materials could serve as an organic or inorganic corrosion inhibitor holding cell or reservoir. Bentonite/montmorillonite, zeolites, layered double hydroxides (LDHs), halloysite, and porous nanoparticles are the most widely used containers. Modification of the reservoirs with corrosion inhibitors and subsequent on-demand release action of the corrosion inhibitors occurs mainly through an ion-exchange mechanism; however, physical entrapment in and release from the pores and lumen can also be important as illustrated in the example of halloysite, porous nanoparticles. and hollow spheres. The corrosion inhibitor's doping and release profile is dependent on the intrinsic ion-exchange capacity [i.e., cation-exchange capacity (CEC), anion-exchange capacity(AEC)] of the container, which itself depends on the positive or negative charge density in the inorganic scaffold, as well as the space available between the layers or in the pores. However in some cases, desorption of the adsorbed corrosion inhibitors and partial dissolution of inorganic structure could also play a role on inhibitor release and subsequent corrosion inhibition. In case of a partial dissolution of inorganic scaffold, the dissolved species may show synergistic corrosion inhibition with the corrosion inhibitors released from the container. In addition, it should be noted that not only the extent of release but also the release rate is important for corrosion inhibition. A retarded release of corrosion inhibitors may not provide sufficient concentration of material to the damaged area which may not lead to self-healing activity. In contrast, too fast of a release would lead to a rapid depletion of the container/coating from the corrosion inhibitor, thus causing an acceleration in corrosion after the initial protective stage. That is why, for different inhibitors and containers, a controlled release is preferred to provide sufficient protection over a reasonable period of time.

Controlled release of corrosion inhibitors by inorganic containers is frequently reported in some literature. However, surface modification of these inorganic containers with pH-sensitive polyelectrolytes or polymers could also be used to improve controlled release [81]. Application of modified hydrophilic inorganic containers with corrosion inhibitors in the polymer coatings may need surface modification to impart compatibility to the hydrophobic organic matrix. Therefore, the inorganic containers are sometimes double-modified: the first modification to impart active corrosion inhibition and the second modification to enhance controlled release of inhibitors or compatibility with the organic coating.

Besides inorganic materials, organic materials such as ion-exchange resins and organic traps could also be used to reserve the corrosion inhibitors, releasing only during corrosive attacks. Here, a brief review of each substance application as an on-demand release agent for corrosion protective coatings and, more specifically, for self-healing protective coatings is provided.

24.3.3.1 Bentonite and Montmorillonite

A permanent negative charge exists in the aluminosilicate layers of montmorillonite (MMT) and bentonite owing to the Al^{3+} for Si^{4+} isomorphous substitution in the tetrahedral layer and Mg^{2+} for Al^{3+} in the octahedral layer [82]. The composition of these minerals is $(Na,Ca)_{0.33}(Al,Mg)_2(Si_4O_{10})(OH)_2 \cdot nH_2O$ [83]. The interlayer space of the mineral scaffold holding the sodium and calcium cations could be exchanged with organic or inorganic corrosion inhibitive cations for smart release protective coating application.

The cation-exchanged Na-bentonite pigments with Zn^{+2} and group II cations (i.e., Mg^{+2}, Ca^{+2}, Ba^{+2}, and Sr^{+2}) were prepared to evaluate the smart release corrosion inhibition in galvanized steel coated with polyvinyl butyral [84]. It was showed that group II cation-exchanged bentonites moderately inhibited the cathodic disbonding when compared to the unpigmented coating. In contrast, the Zn^{2+} cation-exchanged bentonite pigment showed a more effective inhibition [84].

The Ce^{+3}-exchanged MMT was studied for its Ce^{+3} release behavior in different electrolytes [85]. It was found that the release kinetic was fast and considerable release of doped cerium ions occurred within 10 min of contact. Also it was reported that cerium release from interlayer space (doped cerium) started at an ionic strength for NaCl of approximately 0.25 M, and for $ZnCl_2$, it was approximately 0.1 M [84]. Galvanized steel coated with silane (composed of Ce-MMT and Na-MMT) displayed a high frequency time constant caused by the silane film being continuously doped, whereas the middle frequency time constant can be attributed to the zinc oxide layer developing for the Ce-MMT coating. This phenomenon was connected to the release of Ce^{+3} during the diffusion of electrolyte in the coating leading to the oxide layer reinforcement [85].

Hang et al. [86] employed an organic corrosion inhibitor, indole-3 butyric acid (IBA), in order to synthesize IBA-MMT [87]. An acid solution was used to protonate IBA so as to facilitate the cation-exchange mechanism with the Na^+ in the MMT interlayer space. It was shown that the release of IBA is favored for higher pH values. Therefore, a localized increase in pH at corrosion sites can facilitate the release of IBA. The decrease of impedance at the scratched area was observed in those epoxy coatings that contained IBA-MMT, indicating the self-healing effect of the coating.

Ghazi et al. [88] evaluated the corrosion inhibition of MMT doped with benzimidazole (BIA), MMT doped with Zn^{2+}, and their mixture in an epoxy ester coating. Surface analysis of the defect site of the coating during its early stages revealed that although both the Zn^{2+} and BIA leached out the coating, only Zn^{2+} tended to be adsorbed onto the mild steel surface, while BIA tended to leave. However, at

prolonged immersion periods, accumulation of BIA and Zn^{2+} cations in the scratched area was observed, meaning that the adsorbed zinc cations at the first stage facilitated the adsorption of BIA. Using a mixture of BIA-MMT and Zn-MMT, synergistic corrosion inhibition and self-healing behavior at defect site were obtained.

24.3.3.2 Zeolites

Zeolites are typically notated by the formula of $M^{n+}_{x/n}[(AlO_2)_x(SiO_2)_{2-x}]^{x-}\cdot mH_2O$, where M^{n+} represents the cation in the supercage and the sodalite cage is typically Na^+, K^+, or Ca^{2+} [89]. There is a constant negative structural charge on the framework due to the isomorphous substitution of SiO_4 group by the AlO_4 group [90]. The M^{n+} cations in the zeolites can be exchanged with corrosion inhibitive cations to provide the controlled release of inhibitor during corrosion.

Ahmed et al. [87] compared the corrosion protection performance of alkyd paints pigmented by Na-zeolites exchanged by Zn^{2+}, Ca^{2+}, and Mg^{2+} cations. The results showed that the Zn-zeolites outperform others, while Mg-zeolites provided the least amount of protection among the cation-exchanged zeolites, yet it was still superior when compared to Na-zeolites.

Williams et al. [91] studied the cation-exchange properties of zeolite compared to bentonite. They found that a zeolite pigment's exchange capacity in solution is three times greater than that of bentonite. However, in coating (polyvinyl butyral), they found that the Zn^{2+} cation-exchanged bentonite outperformed the Zn^{2+} cation-exchanged zeolite when the cathodic delamination area of the coatings was compared. It was proposed that the inhibition efficiency not only depended on the exchange medium's CEC but also on the Zn^{2+} cations' release rate at the disbondment front which was a more influential parameter. Exfoliation of the clay matrix in the aqueous media increased the ease of cation exchange compared to zeolite, where the zeolite particles' microporous structure provided a convoluted cation exchange, slowing down the exchange process.

La^{+3} cation-exchange properties of zeolite have been compared to that of bentonite [92]. Similar to the previous work on Zn^{+2} cations, superior cation-exchange capacity for zeolite (10.90 mg of La^{+3}/g mineral) compared to bentonite (5.70 mg/g mineral) was observed. No significant difference was reported for epoxy coatings containing La-zeolite and La-bentonite [93].

Ferrer et al. [93] prepared a sol–gel coating containing a double-doped zeolite with cerium and diethyldithiocarbamate (DEDTC). It was also shown that cerium cation ion exchange improved the adsorption of the DEDTC anion. They found that the large hydrated cerium cations can only access the supercages and cannot undergo ion exchange with sodium in the small sodalite cages. Immediate and sustained corrosion protection for the aluminum alloy with this double-doped zeolite was attributed to combined effect [i.e., slow release of cerium cation, fast release of diethyldithiocarbamate (DEDTC)].

24.3.3.3   LDHs

The general formula of LDHs is $[M^{2+}_{1-x}M^{3+}_x(OH)_2]^{x+} A^{n-}_{x/n} \cdot mH_2O$, where M^{2+} represents a divalent metal cation, M^{3+} a trivalent metal cation, and A^{n-} an interlayer anion, respectively [94]. There is a constant structural positive charge on the basal surface of LDHs from the isomorphous substitution of a divalent cation via a trivalent cation. Therefore, LDHs undergo anion-exchange reaction in contrast to the bentonite/montmorillonite and zeolites. As such, they are defined as anionic clays.

Various anions have been studied for corrosion inhibition. Two methods have been introduced for the doping of anions in LDH interlayer space. First, the ion-exchange reaction of the target corrosion inhibitive anion with the anion is intercalated in the scaffold during synthesis. This is followed by the direct inclusion of the target anion in the LDH interlayer space. Although direct synthesis is easier as it deals with one-step synthesis, in some cases this may not be a good choice due to the undesirable changes in the LDH scaffold.

Zheludkevich et al. [95] used Zn-Al and Mg-Al LDHs ion exchanged with vanadate anions for corrosion inhibition of an aluminum alloy. Considering the fact that the vanadate release was higher for vanadate-Mg-Al LDH than vanadate-Zn-Al LDH, vanadate-Zn-Al LDH revealed improved corrosion inhibition, which was attributed to the synergistic corrosion inhibition of Zn^{+2} cation released due to the partial dissolution and vanadate released due to the anion-exchange reaction. Doped Zn-Al and Mg-Al LDHs with quinaldate (QA) or 2-mercaptobenzothiazole (MBT) were prepared through the ion-exchange method [96]. Data gathered from the study indicated that MBT-loaded LDHs outperformed those loaded with QA. Similar to the previous findings, better inhibition was observed with Zn-Al LDH than Mg-Al LDH.

Li et al. [97] directly synthesized tungstate-Mg-Al through the coprecipitation method. It was found that due to the release of tungstate anion from LDH, corrosion at defect site was inhibited, resulting in self-healing behavior. Another example of the direct synthesis of inhibitor LDH was studied by Hang et al., where Zn-Al and Mg-Al LDHs doped with 2-benzothiazolylthio-succinic acid (BTSA) were synthesized for carbon steel's corrosion inhibition [98, 99]. It was shown that BTSA release occurs due to the anion-exchange reaction and slow dissolution of both LDHs. This was akin to Zheludkevich et al.'s observations [98], although the higher release of BTSA was observed for the Mg-Al LDHs and higher corrosion inhibition was obtained with Zn-Al LDH [98, 99].

24.3.3.4   Halloysite

The general formula of a halloysite is $Al_2Si_2O_4(OH)_6$ [100]. The chemical structure of halloysite is akin to that of kaolinite, but the diameter of its rolled tubes is 50 nm with a length of ca. 1000 nm [101]. Furthermore in respect to cationic and anionic species, it has displayed a greater adsorption capacity due to a negative outer SiO_2 surface and positive inner Al_2O_3 lumen surface [102, 103].

It was reported that doping a halloysite with benzotriazole (BTA) resulted in the slow release of BTA compared to its release from microcrystals. It was found that the release of BTA occurred in two stages, an initial burst within 10 min, followed by a prolonged release during 8–10 h [103]. It was shown that using only 0.01 % of the doped halloysite not only does not decrease the barrier effect of the ZrO_x-SiO_x sol–gel coating on aluminum but also imparts a self-healing effect to the coating [103].

Although they do not need exfoliation in the coating matrix, a surface modification to make the surface chemistry compatible with coating's chemistry may be required [103]. In addition, halloysite's release behavior is pH dependent. However, their pH sensitivity can be improved using a pH-sensitive polyelectrolyte shell [104]. It was shown that with a polyelectrolyte shell, the spontaneous release of BTA in neutral water decreased from 10 % to zero, while at a pH 10, BTA release was triggered [104]. But, it should be noted that the release of BTA caused irreversible distortion of polyelectrolyte shell, as 100 % reloading of the halloysite was shown not to be possible [105].

Abdullayev et al. [106] employed some organic corrosion inhibitors [i.e., BTA, 2-mercaptobenzimidazole (MBI) and 2-mercaptobenzothiazole (MBT)] as dopant for halloysite clay nanotubes to prepare self-healing composite coatings of acrylic and polyurethane for Cu. The release behavior of the doped halloysites showed that BTA and MBT release occurred in two stages (fast and slow), whereas the release of MBI was completed in a single stage. During the first (fast) stage, release of BTA and MBT was attributed to the dissolution of adsorbed inhibitors of the halloysite tubes' outer surface layer. The second (slow) stage was connected to the diffusion of the corrosion inhibitors from the tube lumen. MBI held the largest lumen loading value, while BTA had the lowest loading. For the coatings with artificial 5 mm scratches, MBT and MBI showed the highest self-healing effects.

As the lumen could be filled with various materials, fabrication of coatings with multiple active properties (e.g., self-healing and antistatic) was suggested by the simultaneous application of various halloysites filled with different active agents all while in a coating [107].

24.3.3.5   Porous Nanoparticles and Hollow Spheres

Absorption of the corrosion inhibitors by porous nanoparticles and hollow spheres is reported to be effective in providing prolonged release and therefore self-healing ability.

Zheludkevich et al. synthesized in situ the Ce^{+3}-doped zirconia nanoparticles in a hybrid sol–gel coating on an aluminum alloy [108]. The prolonged protection obtained for the Ce^{+3}-doped zirconia nanoparticles was due to the cerium ion's retarded release profile. Similar self-healing ability was reported for in situ synthesis of the Ce^{3+}-doped bohemite nanoparticles in a hybrid sol–gel coating on an Al alloy [109]. Skorb et al. prepared mesoporous silica nanoparticles, then doped the nanocontainer with 2-(benzothiazol-2-ylsulfanyl)-succinic acid, and, in order to

stop the spontaneous corrosion inhibitor release, fabricated an LbL polyelectrolyte shell [110]. The ZrO_x-SiO_x sol–gel coating containing the doped nanocontainers revealed a great level of self-healing protection from corrosion over an extended period of time [110]. Saremi et al. [111] used mesoporous silica nanoparticles doped with molybdate anions in a polypyrrole coating. They showed that molybdate release increases at higher pH values due to the more negative zeta potential and consequently larger electrostatic repulsion forces on molybdate anion.

Montemor et al. [112] used cerium molybdate hollow spheres doped with MBT (MBT-CeMo) and MBT doped LDH (MBT-LDH) in epoxy primer for self-healing activity for galvanized steel. It was shown that the delayed action of MBT-CeMo containers displayed effective corrosion inhibition when compared to the MBT-LDH ones. They suggested an interesting approach to prepare self-healing coating utilizing different kinetics of inhibition (i.e., the use of mixture of MBT-CeMo and MBT-LDH). It was shown that a mixture of MBT-CeMo and MBT-LDH, as expected, provided synergistic self-healing behavior by corrosion inhibition at both the early stages and prolonged exposure time [112].

Li et al. [113] synthesized silica/polymethylmetacrylate (PMMA) double-walled nanotubes for application in stimuli-responsive nanocontainers in self-healing coatings. It is showed that nanocontainers doped with BTA provide self-healing behavior in a hybrid sol–gel coating based on ZrO_x-SiO_x.

24.3.3.6   Other Containers

Besides the previously mentioned reservoirs for corrosion inhibitors, organic ion-exchanged pigments and organic encapsulations have been introduced for the on-demand release of corrosion inhibitors.

Application of a cation-exchange resin loaded with the desired corrosion inhibitive cations was first proposed for inhibiting scale formation and corrosion well penetrating into a subterranean formation [114]. It was shown that by using cation-exchange resins, the corrosion inhibitor was released slowly at an effective concentration into the fluids produced by the well, inhibiting scale formation and corrosion. However, the application of pigments based on cation-exchange resins as smart release pigments was reported by Williams et al. [91]. They suggested novel Ca^{2+} and Zn^{2+}-exchanged pigments built upon a cross-linked sulfonated polystyrene (CSP) base which could be applied in the reduction of cathodic disbondment on galvanized steel. It was shown that CSP has a higher CEC than zeolite and bentonite [91].

Physical organic traps can encapsulate the corrosion inhibitors in order to decrease the release rate. Cyclodextrins could be considered as a truncated cone-shaped structure with a hydrophilic exo-surface and a hydrophobic interior [115]. Physical entrapment of the organic corrosion inhibitors (e.g., MBT, MBI, mercaptobenzimidazole sulfonate (MBISA), and thiosalicylic acid (TSA) by β-cyclodextrin) was reported to be effective in decreasing the release rate, providing prolonged protection at the defect sites in sol–gel-derived hybrid coatings [115, 116].

24.4   Conclusion

This chapter has provided a review on the self-healing polymer coatings from a mechanism, processing, and application viewpoint. The two main functions of the coatings, mechanical integrity and corrosion protection, were considered. It was revealed that embedded capsulated healing agents in the coating matrix and molecular-scale modification of coating structure with covalent and non-covalent reversible cross-links were the most effective approaches in healing mechanical damage, thus restoring the coating integrity. Encapsulation and trapping active corrosion inhibitors using micro-/nanoreservoirs (i.e., LbLs, LDHs, porous nanoparticles, hollow spheres, zeolites, bentonite, and montmorillonite) were introduced as effective strategies in obtaining the on-demand release corrosion inhibitive coatings.

Most of the approaches mentioned in this chapter used to achieve polymeric coating systems, self-repairing in nature, that are in the preliminary developmental stage and have not been widely commercialized. This is mainly because of complicated processing procedures, limited time and dimensional ranges for their healing ability, and the undesirable consequences of the healing agents on the coating's additional properties. Therefore, current and future trends in the field of self-healing coatings are focused on optimizing the procedures so as to resolve the problems.

References

1. Ghosh SK (2009) Self-healing materials: fundamentals, design strategies, and applications. Wiley, Weinheim. ISBN 98-3-527-31829-2
2. Kessler MR (2007) Self-healing: a new paradigm in materials design. Proc Inst Mech Eng G J Aerosp Eng 221:479–495
3. Youngblood JP, Sottos NR (2008) Bioinspired materials for self-cleaning and self-healing. MRS Bull 33:732–741
4. White SR, Caruso MM, Moore JS (2008) Autonomic healing of polymers. MRS Bull 33:766–769
5. Wu DY, Meure S, Solomon D (2008) Self-healing polymeric materials: a review of recent developments. Prog Polym Sci 33:479–522
6. White SR, Sottos NR, Geubelle PH, Moore JS, Kessler MR, Sriram SR, Brown EN, Viswanathan S (2001) Autonomic healing of polymer composites. Nature 409:794–797
7. Caruso MM, Delafuente DA, Ho V, Sottos NR, Moore JS, White SR (2007) Solvent-promoted self-healing epoxy materials. Macromolecules 40:8830–8832
8. Thie C (2004) microencapsulation, Encyclopedia of polymer science and technology. Wiley, New York
9. Benita S (2005) Microencapsulation: methods and industrial applications. CRC Press, Boca Raton, FL. ISBN 10-0-8247-2317-1
10. Arshady R (1999) Microspheres, microcapsules and liposomes: general concepts and criteria. MML Ser 1:11
11. Dry C (1996) Procedures developed for self-repair of polymer matrix composite materials. Compos Struct 35:263–269
12. Hucker M, Bond I, Foreman A, Hudd J (1999) Optimisation of hollow glass fibres and their composites. Adv Compos Lett 8:181–189

13. Trask RS, Bond IP (2006) Biomimetic self-healing of advanced composite structures using hollow glass fibres. Smart Mater Struct 15:704

14. Pang JWC, Bond IP (2005) Bleeding composites—damage detection and self-repair using a biomimetic approach. Compos A Appl Sci Manuf 36:183–188

15. Pang JWC, Bond IP (2005) A hollow fibre reinforced polymer composite encompassing self-healing and enhanced damage visibility. Compos Sci Technol 65:1791–1799

16. Williams HR, Trask RS, Bond IP (2006) Vascular self-healing composite sandwich structures. In: Fifteenth United States national congress of theoretical and applied mechanics, 25–31 June

17. Williams G, Trask R, Bond I (2007) A self-healing carbon fibre reinforced polymer for aerospace applications. Compos A Appl Sci Manuf 38:1525–1532

18. Chen X, Dam MA, Ono K, Mal A, Shen H, Nutt SR, Sheran K, Wudl F (2002) A thermally remendable cross-linked polymeric material. Science 295:1698–1702

19. Chen X, Wudl F, Mal AK, Shen H, Nutt SR (2003) New thermally remendable highly cross-linked polymeric materials. Macromolecules 36:1802–1807

20. Chujo Y, Sada K, Naka A, Nomura R, Saegusa T (1993) Synthesis and redox gelation of disulfide-modified polyoxazoline. Macromolecules 26:883–887

21. Burattini S, Greenland BW, Merino DH, Weng W, Seppala J, Colquhoun HM, Hayes W, Mackay ME, Hamley IW, Rowan SJ (2010) A healable supramolecular polymer blend based on aromatic pi-pi stacking and hydrogen-bonding interactions. J Am Chem Soc 132:12051–12058

22. Lange RFM, Meijer EW (1996) Supramolecular polymer interactions using melamine. Macromol Symp 102:301–308

23. Brunsveld L, Folmer BJB, Meijer EW, Sijbesma RP (2001) Supramolecular polymers. Chem Rev 101:4071–4098

24. Eisenberg A, Kim J-S (1998) Introduction to ionomers. Wiley, New York

25. Eisenberg A (2012) Ion-containing polymers: physical properties and structure, vol 2. Elsevier

26. Plaisted TA, Amirkhizi AV, Arbelaez D, Nemat-Nasser SC (2003) Self-healing structural composites with electromagnetic functionality. In: Proc. SPIE 5054, Smart structures and materials 2003: Industrial and commercial applications of smart structures technologies, 372 (August 12, 2003); doi:10.1117/12.483894

27. Williams KA, Boydston AJ, Bielawski CW (2007) Towards electrically conductive, self-healing materials. J R Soc Interface 4:359–362

28. Luo X, Mather PT (2013) Shape memory assisted self-healing coating. ACS Macro Lett 2:152–156

29. Kirkby EL, Michaud VJ, Månson J-A, Sottos NR, White SR (2009) Performance of self-healing epoxy with microencapsulated healing agent and shape memory alloy wires. Polymer (Guildf) 50:5533–5538

30. Neuser S, Michaud V, White SR (2012) Improving solvent-based self-healing materials through shape memory alloys. Polymer (Guildf) 53:370–378

31. Yari H, Mohseni M, Ramezanzadeh B (2009) Comparisons of weathering performance of two automotive refinish coatings: a case study. J Appl Polym Sci 111:2946–2956

32. Ramezanzadeh B, Mohseni M, Yari H, Sabbaghian S (2009) An evaluation of an automotive clear coat performance exposed to bird droppings under different testing approaches. Prog Org Coat 66:149–160

33. Keller MW, White SR, Sottos NR (2007) A self-healing poly(dimethyl siloxane) elastomer. Adv Funct Mater 17:2399–2404

34. Cho SH, Andersson HM, White SR, Sottos NR, Braun PV (2006) Polydimethylsiloxane-based self-healing materials. Adv Mater 18:997–1000

35. Beiermann BAA, Keller MWW, Sottos NRR (2009) Self-healing flexible laminates for resealing of puncture damage. Smart Mater Struct 18:85001

36. Wang W, Xu L, Li X, Lin Z, Yang Y, An E (2014) Self-healing mechanisms of water triggered smart coating in seawater. J Mater Chem A 2:1914–1921

37. Yang J, Keller MW, Moore JS, White SR, Sottos NR (2008) Microencapsulation of isocyanates for self-healing polymers. Macromolecules 41:9650–9655

38. Kim H, Park S (2007) Preparation and properties of microcapsule with EVA core-PU shell structure. J Appl Polym Sci 103:893–902

39. Caruso MM, Blaiszik BJ, Jin H, Schelkopf SR, Stradley DS, Sottos NR, White SR, Moore JS (2010) Robust, double-walled microcapsules for self-healing polymeric materials. ACS Appl Mater Interfaces 2:1195–1199

40. Bai N, Simon GP, Saito K (2013) Investigation of the thermal self-healing mechanism in a cross-linked epoxy system. RSC Adv 3:20699

41. Bai N, Saito K, Simon GP (2013) Synthesis of a diamine cross-linker containing Diels–Alder adducts to produce self-healing thermosetting epoxy polymer from a widely used epoxy monomer. Polym Chem 4:724–730

42. Kashif M, Chang Y-W (2015) Supramolecular thermoplastic elastomer with thermally scratch repairable effect from 3-amino-1,2,4-triazole crosslinked maleated polyethylene-octene elastomer/nylon 12 blends. J Appl Polym Sci 132

43. Bosman AW, Sijbesma RP, Meijer EW (2004) Supramolecular polymers at work. Mater Today 7:34–39

44. Yari H, Mohseni M, Messori M, Ranjbar Z (2014) Tribological properties and scratch healing of a typical automotive nano clearcoat modified by a polyhedral oligomeric silsesquioxane compound. Eur Polym J 60:79–91

45. Dimopoulos A, Wietor J-L, Wübbenhorst M, Napolitano S, van Benthem RATM, de With G, Sijbesma RP (2010) Enhanced mechanical relaxation below the glass transition temperature in partially supramolecular networks. Macromolecules 43:8664–8669

46. Neal J, Mozhdehi D, Guan Z (2015) Enhancing mechanical performance of a covalent self-healing material by sacrificial non-covalent bonds. J Am Chem Soc 137(14):4846–4850

47. Hart LR, Hunter JH, Nguyen NA, Harries JL, Greenland BW, Mackay ME, Colquhoun HM, Hayes W (2014) Multivalency in healable supramolecular polymers: the effect of supramolecular cross-link density on the mechanical properties and healing of non-covalent polymer networks. Polym Chem 5:3680–3688

48. Wei Q, Schlaich C, Prévost S, Schulz A, Böttcher C, Gradzielski M, Qi Z, Haag R, Schalley CA (2014) Supramolecular polymers as surface coatings: rapid fabrication of healable super-hydrophobic and slippery surfaces. Adv Mater 26:7358–7364

49. Lii C-Y, Liaw SC, Lai VM-F, Tomasik P (2002) Xanthan gum–gelatin complexes. Eur Polym J 38:1377–1381

50. Shulkin A, Stover HD (2002) Polymer microcapsules by interfacial polyaddition between styrene–maleic anhydride copolymers and amines. J Membr Sci 209:421–432

51. Brown EN, Kessler MR, Sottos NR, White SR (2003) In situ poly(urea-formaldehyde) microencapsulation of dicyclopentadiene. J Microencapsul 20:719–730

52. Alexandridou CKFMAFS, Kiparissides C, Mange F, Foissy A (2008) Surface characterization of oil-containing polyterephthalamide microcapsules prepared by Interfacial polymerization. J Microencapsul 18(6):767–781

53. Toubeli A, Kiparissides C (1998) Synthesis and characterization of polyterephthalamide membranes for encapsulation use: effect of the amine type and composition on the membrane permeability. J Membr Sci 146:15–29

54. Frere W, Danicher L, Gramain P (1998) Preparation of polyurethane microcapsules by interfacial polycondensation. Eur Polym J 34:193–199

55. Hong K, Park S (1999) Preparation of polyurethane microcapsules with different soft segments and their characteristics. React Funct Polym 42:193–200

56. Kim IH, Seo JB, Kim YJ (2002) Preparation and characterization of polyurethane microcapsules containing functional oil. Polymer (Korea) 26:400–409

57. Kwon J-Y, Kim H-D (2006) Preparation and application of polyurethane-urea microcapsules containing phase change materials. Fibers Polym 7:12–19

58. Hong K, Park S (2000) Characterization of ovalbumin-containing polyurethane microcapsules with different structures. Polym Test 19:975–984

59. Crespy D, Stark M, Hoffmann-Richter C, Ziener U, Landfester K (2007) Polymeric nanoreactors for hydrophilic reagents synthesized by interfacial polycondensation on miniemulsion droplets. Macromolecules 40:3122–3135

60. Hernandez-Barajas J, Hunkeler D (1997) Heterophase water-in-oil polymerization of acrylamide by a hybrid inverse-emulsion/inverse-microemulsion process. Polymer (Guildf) 38:5623–5641

61. Müller K, Klapper M, Müllen K (2007) Preparation of high molecular weight polyurethane particles by nonaqueous emulsion polyaddition. Colloid Polym Sci 285:1157–1161

62. Klapper M, Nenov S, Haschick R, Müller K, Müllen K (2008) Oil-in-oil emulsions: a unique tool for the formation of polymer nanoparticles. Acc Chem Res 41:1190–1201

63. Kobaslija M, McQuade DT (2006) Polyurea microcapsules from oil-in-oil emulsions via interfacial polymerization. Macromolecules 39:6371–6375

64. Shukla PG, Kalidhass B, Shah A, Palaskar DV (2002) Preparation and characterization of microcapsules of water-soluble pesticide monocrotophos using polyurethane as carrier material. J Microencapsul 19(3):293–304

65. Hatami Boura S, Peikari M, Ashrafi A, Samadzadeh M (2012) Self-healing ability and adhesion strength of capsule embedded coatings—micro and nano sized capsules containing linseed oil. Prog Org Coat 75:292–300

66. Kouhi M, Mohebbi A, Mirzaei M, Peikari M (2013) Optimization of smart self-healing coatings based on micro/nanocapsules in heavy metals emission inhibition. Prog Org Coat 76:1006–1015

67. Wang R, Li H, Hu H, He X, Liu W (2009) Preparation and characterization of self-healing microcapsules with poly(urea-formaldehyde) grafted epoxy functional group shell. J Appl Polym Sci 113:1501–1506

68. Latnikova A (2012) Polymeric capsules for self-healing anticorrosion coatings. Universität Potsdam, den 10

69. Nesterova T, Dam-Johansen K, Pedersen LT, Kiil S (2012) Microcapsule-based self-healing anticorrosive coatings: capsule size, coating formulation, and exposure testing. Prog Org Coat 75:309–318

70. Suryanarayana C, Rao KC, Kumar D (2008) Preparation and characterization of microcapsules containing linseed oil and its use in self-healing coatings. Prog Org Coat 63:72–78

71. Jadhav RS, Mane V, Bagle AV, Hundiwale DG, Mahulikar PP, Waghoo G (2013) Synthesis of multicore phenol formaldehyde microcapsules and their application in polyurethane paint formulation for self-healing anticorrosive coating. Int J Ind Chem 4:31

72. Jadhav RS, Hundiwale DG, Mahulikar PP (2011) Synthesis and characterization of phenol-formaldehyde microcapsules containing linseed oil and its use in epoxy for self-healing and anticorrosive coating. J Appl Polym Sci 119:2911–2916

73. Mirabedini SM, Dutil I, Farnood RR (2012) Preparation and characterization of ethyl cellulose-based core–shell microcapsules containing plant oils. Colloids Surfaces A Physicochem Eng Asp 394:74–84

74. Nesterova T, Dam-Johansen K, Kiil S (2011) Synthesis of durable microcapsules for self-healing anticorrosive coatings: a comparison of selected methods. Prog Org Coat 70:342–352

75. Koh E, Lee S, Shin J, Kim Y-W (2013) Renewable polyurethane microcapsules with isosorbide derivatives for self-healing anticorrosion coatings. Ind Eng Chem Res 52: 15541–15548

76. Kopec M, Szczepanowicz K, Mordarski G, Podgorna K, Socha RP, Nowak P, Warszyński P, Hack T (2015) Self-healing epoxy coatings loaded with inhibitor-containing polyelectrolyte nanocapsules. Prog Org Coat 84:97–106

77. Raps D, Hack T, Kolb M, Zheludkevich ML, Nuyken O (2010) Development of corrosion protection coatings for AA2024-T3 using micro-encapsulated inhibitors. ACS Symp Ser 1050:165–189

78. Shchukin DG, Zheludkevich M, Yasakau K, Lamaka S, Ferreira MGS, Moehwald H (2006) Layer-by-layer assembled nanocontainers for self-healing corrosion protection. Adv Mater 18:1672–1678

79. Sonawane SH, Bhanvase BA, Jamali AA, Dubey SK, Kale SS, Pinjari DV et al (2012) Improved active anticorrosion coatings using layer-by-layer assembled ZnO nanocontainers with benzotriazole. Chem Eng J 189:464–472

80. Bhanvase BA, Patel MA, Sonawane SH (2014) Corros Sci 88:170–177

81. Shchukin DG (2013) Kinetic properties of layer-by-layer assembled cerium zinc molybdate nanocontainers during corrosion inhibition. Polym Chem 4:4871–4877

82. Ma J, Cui B, Dai J, Li D (2011) Mechanism of adsorption of anionic dye from aqueous solutions onto organobentonite. J Hazard Mater 186:1758–1765

83. Shi X, Nguyen TA, Suo Z, Liu Y, Avci R (2009) Effect of nanoparticles on the anticorrosion and mechanical properties of epoxy coating. Surf Coat Technol 204:237–245

84. Williams G, McMurray HN, Loveridge MJ (2010) Inhibition of corrosion-driven organic coating disbondment on galvanised steel by smart release group II and Zn(II)-exchanged bentonite pigments. Electrochim Acta 55:1740–1748

85. Motte C, Poelman M, Roobroeck A, Fedel M, Deflorian F, Olivier MG (2012) Improvement of corrosion protection offered to galvanized steel by incorporation of lanthanide modified nanoclays in silane layer. Prog Org Coat 74:326–333

86. Hang TTX, Truc TA, Olivier MG, Vandermiers C, Guérin N, Pébre N (2010) Corrosion protection mechanisms of carbon steel by an epoxy resin containing indole-3 butyric acid modified clay. Prog Org Coat 69:410–416

87. Ahmed NM, Emira HS, Selim MM (2011) Anticorrosive performance of ion-exchange zeolites in alkyd-based paints. Pigment Resin Technol 40:91–99

88. Ghazi A, Ghasemi E, Mahdavian M, Ramezanzadeh B, Rostami M (2015) The application of benzimidazole and zinc cations intercalated sodium montmorillonite as smart ion exchange inhibiting pigments in the epoxy ester coating. Corros Sci 94:207–217

89. Weller M, Overton T, Rourke J, Armstrong F (2014) Inorganic chemistry, 6th edn. Oxford University Press, Oxford

90. Deka RC, Tajima N, Hirao K (2001) Influence of isomorphous substitution on acidity of zeolites: ab initio and density functional studies. J Mol Struct 535:31–38

91. Williams G, Geary S, McMurray HN (2012) Smart release corrosion inhibitor pigments based on organic ion-exchange resins. Corros Sci 57:139–147

92. Roselli S, Bellotti N, Deyá C, Revuelta M, del Amo B, Romagnoli R (2014) Lanthanum-exchanged zeolite and clay as anticorrosive pigments for galvanized stee. J Rare Earths 32:352–359

93. Ferrer EL, Rollon AP, Mendoza HD, Lafont U, Garcia SJ (2014) Double-doped zeolites for corrosion protection of aluminium alloys. Microporous Mesoporous Mater 188:8–15

94. Cho MS, Shin B, Choi SD, Lee Y, Song KG (2004) Gel polymer electrolyte nanocomposites PEGDA with Mg-Al layered double hydroxides. Electrochim Acta 50:331–334

95. Zheludkevich MLL, Poznyak SKK, Rodrigues LMM, Raps D, Hack T, Dick LFF, Nunes T, Ferreira MGSGS (2010) Active protection coatings with layered double hydroxide nanocontainers of corrosion inhibitor. Corros Sci 52:602–611

96. Poznyak SK, Tedim J, Rodrigues LM, Salak AN, Zheludkevich ML, Dick LFP, Ferreira MGS (2009) Novel inorganic host layered double hydroxides intercalated with guest organic inhibitors for anticorrosion applications. ACS Appl Mater Interfaces 1:2353–2362

97. Li D, Wang F, Yu X, Wang J, Liu Q, Yang P, He Y, Wang Y, Zhang M (2011) Anticorrosion organic coating with layered double hydroxide loaded with corrosion inhibitor of tungstate. Prog Org Coat 71:302–309

98. Hang TTX, Truc TA, Duong NT, Vu PG, Hoang T (2012) Preparation and characterization of nanocontainers of corrosion inhibitor based on layered double hydroxides. Appl Clay Sci 67–68:18–25

99. Hang TTX, Truc TA, Duong NT, Pébre N, Olivier MG (2012) Layered double hydroxides as containers of inhibitors in organic coatings for corrosion protection of carbon steel. Prog Org Coat 74:343–348

100. Armstrong JA, Dann SE (2000) Investigation of zeolite scales formed in the Bayer process. Microporous Mesoporous Mater 41:89–97
101. Dong Y, Lisco B, Wu H, Koo JH, Krifa M (2015) Flame retardancy and mechanical properties of ferrum ammonium phosphate–halloysite/epoxy polymer nanocomposites. J Appl Polym Sci 132(13). doi:10.1002/APP.41681
102. Zhao Y, Abdullayev E, Vasiliev A, Lvov Y (2013) Halloysite nanotubule clay for efficient water purification. J Colloid Interface Sci 406:121–129
103. Lvov YM, Shchukin DG, Mo H, Price RR (2008) Halloysite clay nanotubes for controlled release of protective agents. ACS Nano 2:814–820
104. Andreeva DV, Shchukin DG (2008) Smart self-repairing protective coatings. Mater Today 11:24–30
105. Shchukin DG, Möhwald H (2007) Surface-engineered nanocontainers for entrapment of corrosion inhibitors. Adv Funct Mater 17:1451–1458
106. Abdullayev E, Abbasov V, Tursunbayeva A, Portnov V, Ibrahimov H, Mukhtarova G, Lvov Y (2013) Self-healing coatings based on halloysite clay polymer composites for protection of copper alloys. Appl Mater Interfaces 5:4464–4471
107. Shchukin DG, Lamaka SV, Yasakau KA, Zheludkevich ML, Ferreira MGS, Möhwald H (2008) Active anticorrosion coatings with halloysite nanocontainers. J Phys Chem C 112:958–964
108. Zheludkevich ML, Serra R, Montemor MF, Ferreira MGS (2005) Oxide nanoparticle reservoirs for storage and prolonged release of the corrosion inhibitors. Electrochem Commun 7:836–840
109. Tavandashti NP, Sanjabi S (2010) Corrosion study of hybrid sol-gel coatings containing boehmite nanoparticles loaded with cerium nitrate corrosion inhibitor. Prog Org Coat 69:384–391
110. Skorb EV, Fix D, Andreeva DV, Möhwald H, Shchukin DG (2009) Surface-modified mesoporous SiO_2 containers for corrosion protection. Adv Funct Mater 19:2373–2379
111. Saremi M, Yeganeh M (2014) Application of mesoporous silica nanocontainers as smart host of corrosion inhibitor in polypyrrole coatings. Corros Sci 86:159–170
112. Montemor MFF, Snihirova DVV, Taryba MGG, Lamaka SVV, Kartsonakis IAA, Balaskas ACC, Kordas GCC, Tedim J, Kuznetsova A, Zheludkevich MLL, Ferreira MGSGS (2012) Evaluation of self-healing ability in protective coatings modified with combinations of layered double hydroxides and cerium molibdate nanocontainers filled with corrosion inhibitors. Electrochim Acta 60:31–40
113. Li GL, Zheng Z, Möhwald H, Shchukin DG (2013) Silica/polymer double-walled hybrid nanotubes: synthesis and application as stimuli-responsive nanocontainers in self-healing coatings. ACS Nano 7:2470–2478
114. Snavely J, Earl S (1988) Method for scale and corrosion inhibition in a well penetrating a subterranean formation. US Patent 4779679
115. Khramov AN, Voevodin NN, Balbyshev VN, Donley MS (2004) Hybrid organo-ceramic corrosion protection coatings with encapsulated organic corrosion inhibitors. Thin Solid Films 447–448:549–557
116. Khramov AN, Voevodin NN, Balbyshev VN, Mantz RA (2005) Sol-gel-derived corrosion-protective coatings with controllable release of incorporated organic corrosion inhibitors. Thin Solid Films 483:191–196

Chapter 25
Optical Sensor Coating Development for Industrial Applications

Larissa Brentano Capeletti and João Henrique Zimnoch dos Santos

Abstract Optical sensors are important for in situ and ex situ monitoring in industrial processes and environmental control. The development of these tools involves the immobilization of a sensitive element within a matrix. Therefore, the sol-gel process represents a powerful strategy for developing and improving optical sensors, especially those for coating applications. This approach allows the use of several strategies in terms of different synthetic routes and the production of hybrid matrices, which can help to produce highly specific sensors and solve problems such as receptor element leaching. Controlling the textural characteristics allows for tuning of the matrix permeability of analytes to the receptor element without leaching from the network or affecting the receptor identity or functionality. The introduction of organic moieties appears to be a good alternative for providing systems with differentiated characteristics (i.e., performance). Here, recent results describing sol-gel hybrid optical coating sensors are reviewed to demonstrate their state-of-the-art industrial applications for gases, pH, solvents, and ionic species monitoring.

Keywords Optical sensors • Sol-gel • Silica • Industrial application

25.1 Introduction

Sol-gel technology is a powerful tool for optical sensor development due to its versatility and simplicity, which can result in materials with singular characteristics. This approach has been widely used for environmental, clinical, and industrial applications due to low cost, good sensibility, fast response, and amenability to reuse, miniaturization, and remote monitoring of the resulting materials. Optical sensors are commonly prepared by the incorporation of different chemical and biochemical compounds as receptor elements in porous thin films. Using the sol-gel method, these materials can be prepared at room temperature, resulting in a device

L.B. Capeletti • J.H.Z. dos Santos (✉)
Instituto de Química, UFRGS, Av. Bento Gonçalves, 9500 Porto Alegre, Brazil
e-mail: capeletti@gmail.com; jhzds@iq.ufrgs.br

with mechanical and thermal stability associated with good optical properties [1]. This chapter aims to provide an overview of the potential strategies for producing these functional materials for industrial application.

25.1.1 Basic Concepts for Sensors

According to IUPAC, a chemical sensor is a dispositive that transforms chemical information into a measurable analytical signal, depending on a sample-specific component concentration that is related to the total composition [2]. This chemical information can originate from a chemical reaction or from a physical property of the investigated system [2]. More generally, sensors can be divided into two broad classes as follows: physical sensors that can measure distances, mass, radiation, temperature, or pressure and chemical sensors that can detect and quantify substances using a chemical receptor element (i.e., a chemoreceptor). The latter class includes the subclass of biological sensors, which can identify substances using a biological receptor element (i.e., bioreceptor). Chemical (and biological) sensors selectively respond to a specific compound (analyte) through a chemical reaction at the sensor-sample interface. These sensors can be employed to qualitatively and preferentially detect and/or quantify analytes within the original (target) matrix [3, 4].

Both chemical and biosensors need to contain a receptor element that can be connected to a transducer, which will generate a signal that can be recorded. The receptor element is the key component of any sensor because it is responsible for the selective reaction to a specific analyte or groups of analytes without interference from other substances. The transducers are the components that can transform the energy carrying the chemical information about the sample in a measurable analytical signal. Transducers can be classified as follows: (1) optical (absorbance, reflectance, luminescence, fluorescence, refraction index); (2) electrochemical (voltammetric, potentiometric); and (3) electric (metallic oxides semiconductors, organic semiconductors, electrolytic conductivity). Also, transducers can be (4) mass sensitive (piezoelectric, surface acoustic waves); (5) magnetic (paramagnetic properties change); (6) thermometric (heat absorption or release due to the chemical reaction); and (7) another physical properties (e.g., radiation) [2]. The key components of a sensor are shown in Fig. 25.1.
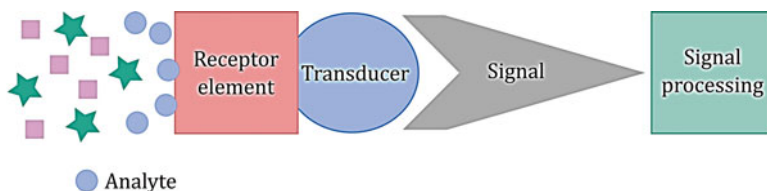
Fig. 25.1 Key components of a sensor

To produce a sensor, the receptor element should be able to selectively respond to the analyte and exhibit advantageous characteristics such as robustness, reproducibility, and chemical and physical stability. One strategy to achieve these characteristics involves a combination of the specificity of a chemical reaction with the rigidity of a solid matrix. This kind of device can be manufactured by the incorporation of reagents (receptor elements) in a suitable organic or inorganic matrix, which will not affect the reactions. In general, the design of a new sensor should consist of the following performance features:

– Selectivity: ability to differentiate between different substances
– Detection limit: the minimum amount of analyte needed to activate the detection sensor system
– Accuracy: how closely the measurement matches the actual quantity being measured
– Suitability under measurement conditions: how the sensor tolerates the measurement environment (pH, temperature, and ionic strength should be considered)
– Response time: time the sensor takes to exhibit a response after contact with the analyte
– Recovery time: time the sensor needs to be ready for another measurement
– Lifetime: time the sensor can stay active, which depends on its stability in the measurement environment

The most common applications for chemical sensors are in health-care settings (clinical analysis of blood, gases, metabolites in urine), industrial processes (pH monitoring, measuring the presence and concentration of gases such as CO, CO_2, NH_3, O_2), and environmental analysis (testing for soil elements and pesticides).

In this chapter, the focus will be on optical sensors due to their ease of use for technical applications because their response is evaluated primarily via visual perception.

25.1.2 Optical Chemical Sensors

Optical sensors are based on light measurements [5] (i.e., they employ electromagnetic radiation to produce an analytical signal from a receptor element) [6]. As previously mentioned, this type of sensor can work according to different principles as follows: absorbance, reflectance, luminescence, and fluorescence covering different regions of the electromagnetic spectrum, such as the ultraviolet, visible, infrared, and near-infrared regions. This behavior enables measurements based on not only light intensity but also other related properties, such as refraction index, scattering, diffraction, and polarization [6].

An effective strategy for preparing these sensors involves the immobilization of a colored reagent, such as a dye, that will change color when it comes in contact with an analyte. Ideally, this change should be proportional to the analyte concentration [4]. These sensors have some advantages: no reference electrode is necessary

(as compared to electrochemical sensors), the calibration is stable, and multiple receptor elements can be employed to detect multiple analytes. The disadvantages include: miniaturization is difficult, there may be problems associated with long-term stability due to incident light, and slow response times due to the necessary time for the mass transfer of the analyte to the reagent phase [3]. The development of a new device is focused on even more sensitive and selective systems for in situ analysis, automation, and miniaturization [7]. The use of sol-gel technology, which is based on receptor element immobilization within a solid matrix, is an interesting approach for achieving these goals. This approach is very interesting for the development of a new device because it is very flexible and works under mild synthesis reaction conditions. In addition, the matrix properties such as optical transparence and mechanical and chemical stability are very interesting for this type of application. Furthermore, the process flexibility enables the deposition of the synthesized material in several formats, such as coating deposition to provide special properties to a surface.

25.1.3 Sol-Gel Process

The sol-gel method is a process that involves a synthetic route in which a transition from a sol system to a gel system occurs (e.g., the growing and aggregation of colloidal particles result in a gel). The process typically involves the use of metal alkoxides, which undergo hydrolysis and condensation polymerization reactions to yield these gels. The term *sol* is employed to define a stable suspension of colloidal particles in a fluid (dimensions between 1 and 1000 nm), and a *gel* is defined as a system formed by the rigid structure of colloidal particles (colloidal gel) or polymeric chains (polymeric gel). In addition, this process is simple, is relatively inexpensive, and proceeds at a low temperature [8]. Inorganic and organic interconnected networks that produce so-called hybrid materials that may combine the rigidity of the inorganic counterpart with the functionality of the organic one can be prepared [9]. This method is very versatile, and various parameters, such as precursor type, water/alkoxide ratio, catalyst type, solvent type, temperature, pH, and composition of the precursor mixture, will affect the characteristics of the final material [10].

25.2 Optical Sensors Prepared Using the Sol-Gel Method

The production of optical sensors using the sol-gel method is typically based on the encapsulation of the receptor elements within a silica matrix, and the receptor changes color when in contact with the analyte. Recent studies have reported many different optical sensors involving different silica matrices. Table 25.1 depicts some recently developed sensors.

Table 25.1 Examples of sensors prepared by immobilization or encapsulation of a receptor element in silica matrices prepared using the sol-gel method.

Matrix	Receptor element	Analyte	Reference
Silica nanoparticles with aminopropyl and urease	ETH 5294 dye	Urea	[11]
Mesoporous silica obtained with Gemini 2-12-2	Bromothymol blue	H^+	[12]
Hybrid silica with methyl, phenyl, and octyl groups	36 different indicators	NH_3 and SO_2	[13]
Silica obtained by acid and basic routes	1,5-Diphenylcarbazone	Zinc traces	[14]
Core/shell silica obtained by Stöber method	Texas red and fluorescein isocyanate	Intracellular H^+	[15]
Silica in carbon paste electrode	Horseradish peroxidase	2-Aminophenol	[16]
Silica containing an organic group functionalized with Ru^{2+}	Ru^{2+}	Oxygen	[17]
Sol-gel silica and polyvinylic alcohol hydrogel	Prussian blue	Glucose	[18]
Ionic liquid modified silica	1-Propyl-3-methylimidazolium ionic liquid	NADH, dopamine and uric acid	[19]
Hybrid silica with a polyelectrolyte with Eu^{3+}	Eu^{3+}	Tetracycline	[20]

The diversity of sensors and the different analytes that can be detected are shown in Table 25.1. These sensors allow for pH, gas, or trace analysis measurements. The developed matrices also differ in terms of their compositions, which include bare silica, chemically modified silica (hybrid silica), and composites (silica and organic reticulated polymers). The majority of the receptor elements listed in Table 25.1 are pH indicators. In the context of optical sensors, the possibility of incorporating a molecule capable of changing color based on pH is very appealing. In particular, for the solid (encapsulated) sensor, this strategy is successful due to the two important properties of sol-gel materials (i.e., optical transparence and ion and gas permeability) [4].

25.2.1   Strategies for Compound Incorporation

As previously mentioned, the sol-gel process is an important tool for preparing solid sensors through the immobilization/encapsulation of receptor elements. To produce a sensitive material, the indicator must be robust in the synthesis conditions (i.e., primarily to the pH employed in the sol-gel synthesis; most of the reactions are conducted under mild temperature conditions). In addition, its interaction with the matrix must be sufficiently strong to avoid receptor element leaching but sufficiently weak to allow it to react with the target analyte. The use of organosilanes,

which are commercially available or relatively easily synthesized, may help to tune the textural and structural characteristics that can affect sensor performance.

The matrices manufactured using this approach are classified as hybrid materials. The hybrid material terminology is broad and may be employed to describe several different kinds of materials. Of such materials highly ordered crystalline coordination polymers, amorphous compounds prepared using the sol-gel method, and materials with or without chemical interactions between the organic and inorganic units can be mentioned [21]. Kichelbick defines a hybrid material as one that includes two materials mixed at a molecular level [22]. In general, one compound is an inorganic one, and the other compound is an organic one.

The different methods for the immobilization of these compounds include impregnation, covalent bonding, and chemical doping [23, 24]. In this context, impregnation refers to the physical or chemical adsorption of the compound in a previously prepared material. Chemical doping involves incorporation of the compound into the matrix during the sol-gel reaction by entrapment or encapsulation. The covalent bonding of the dye to the matrix is considered to be a more efficient method of immobilization because there is no significant leaching of the immobilized compound [23]. The chemical doping approach has received much interest due to the simplicity of the preparation [24]. Covalent grafting requires the presence of very specific functional groups in the compounds, and there are therefore fewer reports of this type of incorporation.

25.2.2 Sol-Gel Process Parameters

To optimize the process for this type of material, their performance in terms of the response time, sensitivity, stability durability, and suitable selected detection range should be addressed. Various strategies are employed, involving different synthetic routes, pH values, precursors, temperatures, solvent amount, and aging times, to prepare the best system for the desired application.

One key factor in the development of an encapsulated sensor is leaching resistance. For continuous monitoring, fine-tuning of the material is essential to avoid leaching of the sensitive element [4]. It is difficult to establish a standard protocol to address this problem because the sol-gel process is quite flexible and sensitive to the reaction conditions. Due to the numerous variables involved, reproducibility control may be a serious drawback of such routes. A compromise between low leaching and encapsulated molecule activity maintenance is required to allow the analyte to reach the receptor element without leaching [4]. Several characteristics, such as surface area (including pore volume and pore diameter) and the presence of organic groups in the matrix network, can affect this relationship, as shown in Fig. 25.2. If the immobilized compound is interacting too strongly with the silica network, the compound cannot react with the analyte (Fig. 25.2a). However, if the added organic groups hinder analyte permeation, the detection will also be hindered (Fig. 25.2b). The characteristics that affect the active site availability and analyte permeation can
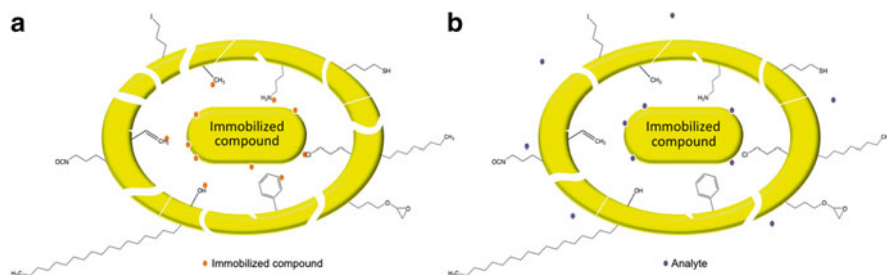
Fig. 25.2 Representation of the compromise between low leaching and encapsulated molecule activity maintenance. (**a**) Immobilized compound is interacting too strongly with the silica network. (**b**) Organic groups hinder analyte permeation
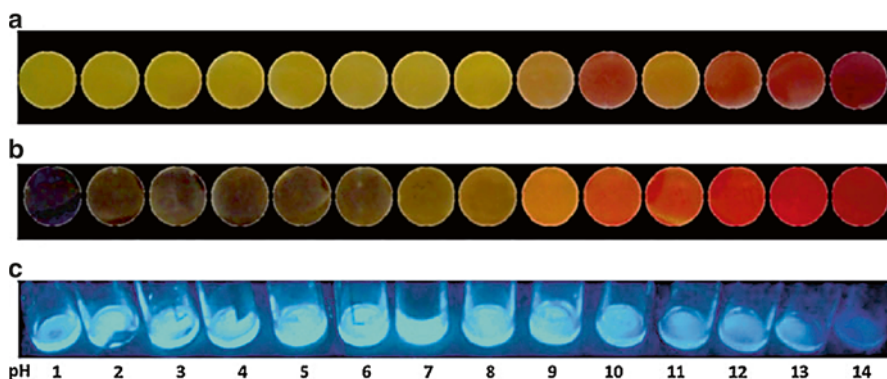
Fig. 25.3 Response of sensors prepared by encapsulation of (**a**) alizarin red, (**b**) brilliant yellow, and (**c**) acridine in aqueous solutions with a pH ranging from 1 to 14. Reprinted with permission from [25]

be controlled by some synthesis parameters (i.e., time of the receptor element addition in the sol-gel process, alkoxide precursors, alkoxide/water ratio, and catalyst amount and type).

Some studies have evaluated the effect of the synthetic route on the performance of sensors prepared using pH indicators encapsulated in silica [25, 26]. For example, different pH indicators with different color-change ranges prepared using different sol-gel routes, including an acid-catalyzed hydrolytic route, a basic catalyzed hydrolytic route, and a non-hydrolytic route, were analyzed. Figure 25.3 shows the behavior of the sensors prepared in this study by the acid-catalyzed hydrolytic route in aqueous solutions with a pH ranging from 1 to 14. Furthermore, Fig. 25.3 shows the behavior of alizarin red, brilliant yellow, and acridine encapsulated in silica. The observed transitions occurred at higher pH values compared to those reported for the bare indicator for alizarin red and brilliant yellow. The acridine indicator loses its ability to change color with the pH after encapsulation, and only a decrease in the luminescence was observed at high pH values [25].
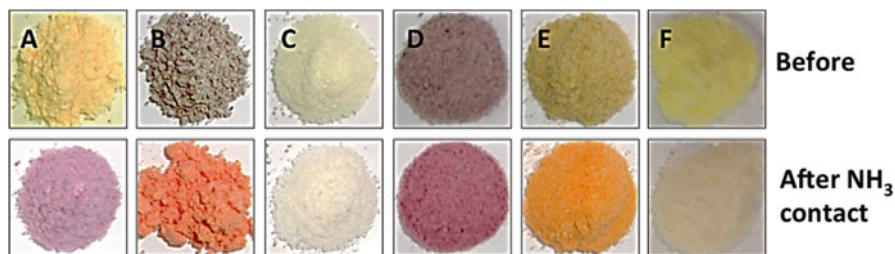
Fig. 25.4 Sensor behavior before and after contact with ammonia gas. (**a**), (**b**), and (**c**) are the sensors prepared using the acid route with alizarin red, brilliant yellow, and acridine, respectively, as receptor elements, and (**d**), (**e**), and (**f**) are the sensors prepared using the non-hydrolytic route with the same receptor elements

The use of a set of complementary techniques and performance evaluation (i.e., response time and colorimetry) allowed the identification of the acid route as the most suitable. Based on a detailed analysis of the data collected by 50 participants during the color-change process, shorter response times were observed for the material prepared using this route. Figure 25.4 shows the sensor behavior before and after contact with ammonia gas for the materials prepared by the acid and non-hydrolytic route. These sensors were in powder form, but they can also be deposited as a film on a surface. The results of the study also indicated that when the color change from one condition to another is more dramatic, the change can be detected more quickly. In addition, shorter response times may be due to higher encapsulated indicator content and higher surface areas.

This study demonstrated the possibility of tuning of the encapsulation route to achieve a high-performance sensor material. In addition, as previously discussed, the introduction of organic groups may be useful for achieving improvements in the performance. The literature indicates that the use of organic groups covalently bonded to the inorganic network favors the compatibility of the encapsulated organic molecules. Kowada et al. reported that the leaching problem in pH sensors decreased upon addition of methyl groups to the silica network [27].

Based on this type of approach, another extensive study was performed to evaluate the effects of a series of different functional groups on the performance of ammonia gas colorimetric sensors [28]. Eleven different organosilanes bearing different organic substituent volume and types of functional groups were employed (Fig. 25.5) to produce hybrid silica matrices encapsulating alizarin red (pH indicator) as a receptor element. Groups containing nitrogen atoms appeared to be ideal to increase the amount of the encapsulated receptor and shorten the response time. The surface area typically decreased when organosilanes were added. Therefore, higher surface areas for these hybrid materials were obtained with smaller groups, such as methyl and vinyl. In addition, when the difference in the color changes was more significant, the change that improved the sensor performance was more easily identified. This parameter primarily depends on the receptor element content in the matrix and on the shade or color of the sensor before and after contact with the analyte.
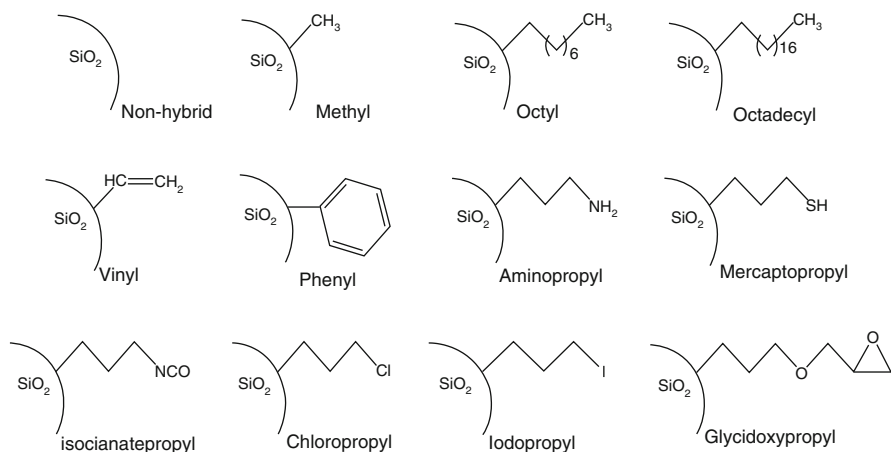
Fig. 25.5 Different hybrid silica-based matrices employed to evaluate the potential for tuning the sensor performance as a function of the organic substituent groups [28]

In general, the employed group volume influenced the response of material. This behavior was more pronounced for the cases where hydrophobicity was introduced to the material due to the voluminous aliphatic chains of the organic groups, which determined the sensor performance. Among the characteristics evaluated by a series of complementary techniques, the indicator content and surface area primarily affected the sensor response time.

In some situations, organosilane was the determinant for the success of a material success, which was demonstrated for cases where the indicator-matrix interaction was strong. When the interaction was stronger, the encapsulated indicator amount was higher. Nevertheless, strong interactions with the matrix may hinder the receptor reactivity to the analytes, preventing its ultimate performance (e.g., the aminopropyl group). This group exhibited the highest indicator-encapsulated content, but the interaction with the matrix was too strong and hindered the reaction with the analyte. Another important factor for sensor activity regulation was textural modification of the silica matrix due to organosilane addition. This modification can render a more exposed or more buried receptor within the silica matrix. In addition, if the organic groups introduced to the silica network were compatible with the medium, the access of analytes or external stimuli to the encapsulated receptor element favors improved response time and sensor performance [28].

25.2.3 Recent Advances

The sol-gel process can be designed to produce a variety of geometric configurations, such as monoliths, powders, thin films, fibers, arrays, or other structures, providing flexibility to the sensor design [29, 30]. These configurations can also be easily

Table 25.2 Different optical sensors fabricated with sensitive coatings encapsulating different receptor elements using sol-gel technology

Matrix	Receptor element	Analyte	Reference
Silica with methyl groups and polydimethylsiloxane	Rose natural dye	Formaldehyde	[31]
Highly porous silica	Bromocresol purple and cresol red	NH_3 and NO_2 gases	[32]
Silica prepared by hydrolytic acid route	Methylene blue	Humidity	[33]
Silica prepared by hydrolytic acid route	2,4,6-tri(2-pyridyl)-s-triazine	Fe (II)	[34]
Silica prepared at low temperature and microwave assisted	Fluorophore	Pb^{2+}	[35]
Porous silica prepared with triton X-100	Purple cabbage pigment	pH	[36]
Silica with methyl groups	Neutral red	pH	[37]
Silica with phenyl groups	Quantum dots, fuchsin, and Congo red	pH	[38]
Silica with methyl, ethyl, phenyl, or glycidoxypropyl groups	Bromocresol green	pH	[39]
Nanostructured silica film	Phenol red	pH	[40]
Silica with octyl groups	Platinum tetrakis pentafluorophenyl porphine	Temperature and oxygen	[41, 42]
Silica with phenyl groups	Phthalocyanines and porphyrins	Volatile organic compounds	[43]

miniaturized or attached to other materials [5], which can result in a series of different materials and configurations that can be adapted depending on the device use and application. Table 25.2 illustrates some recent developments in sol-gel films employed as optical sensors for the detection of species that are of industrial interest.

Meng et al. reported the synthesis of a novel ORMOSIL (organic modified silicate) sensing coating for the optical detection of formaldehyde using a natural dye extracted from roses. This dye is based on anthocyanins that were employed in the flavylium form (absorbance at 506 nm) under acidic conditions and the hemiketal form (pale yellow) under basic conditions. The material was prepared from methyltriethoxysilane and polydimethylsiloxane and deposited as a coating, which possessed a surface morphology consisting of rill-like folds. The absorbance at 506 nm was determined to have a linear relationship with the formaldehyde concentration, which indicated the potential of this low-cost disposable coating for colorimetric test strip manufacturing [31].

For the detection of gases such as ammonia and nitrogen dioxide, Tyszkiewicz and collaborators [32] employed several silica films with thin porosity as sensitive coating with bromocresol purple and cresol red. This type of sensor is based on pH indicators, and the spectral shift is determined by indicator protonation (Fig. 25.6). The results indicated that only the bromocresol purple could identify both analytes
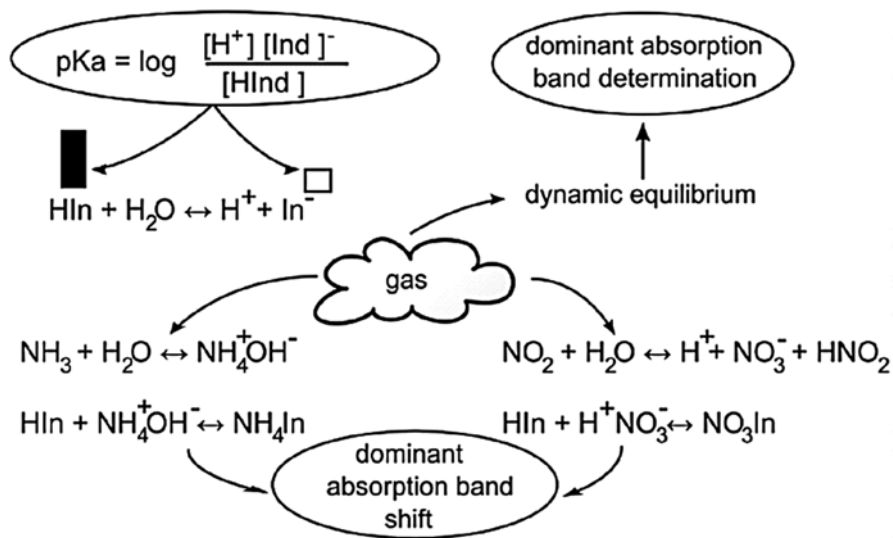
Fig. 25.6 Sensing mechanism leading to changes in the absorption of a pH indicator-based sensitive film. Reprinted with permission from [32]
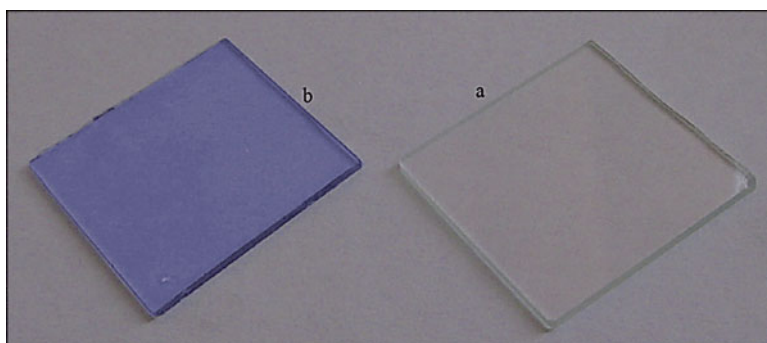
Fig. 25.7 Color changes of a glass slide before (**a**) and after reaction with Fe (II) (**b**). Reprinted with permission from [14]

(i.e., NH_3 and NO_2), and cresol red was sensitive to only NO_2. In addition, the absorbance bands generated by the two analytes were sufficiently separated to permit detection by two diodes operating at different wavelengths [32].

The detection of ions is also important for a series of industrial processes. For example, the detection of iron in water was investigated using a sol-gel coating prepared with 2,4,6-tri(2-pyridyl)-s-triazine as the sensing element. This sensor changed color from transparent to blue (Fig. 25.7) and exhibited excellent performance. This sensor was able to detect zinc ions in the range of 5–115 ng mL^{-1} with a lower detection limit of 1.68 ng mL^{-1} [34]. In another study, the selective detection of lead by a new fluorophore demonstrated the possibility of its use in optical fiber sensing applications [35].

As previously mentioned, an important area of application for sol-gel based sensors prepared by receptor element encapsulation is pH monitoring. This type of sensing is very important for industrial applications, and the use of smart sensor coatings can facilitate and accelerate the measurements. Chen et al. [36] described the use of a natural dye extracted from purple cabbage for the preparation of a pH-sensitive film. The device exhibited a 1–2 min response time in a pH range of 2–11 with linear calibration. The refraction index and thickness did not change even though the extinction coefficient changed regularly with pH [36]. However, the organic pH indicators are the most employed compounds for receptor elements. Neutral red, fucshine, Congo red, bromocresol green, and phenol red have all recently been reported as used for this purpose [37–40]. The latter was incorporated into a nanostructured film of silica (mesoporous material) obtained using cetyltrimethylammonium and exhibited a fast response time (less than 1 s). The pH range of detection was 5–12, and the sensor could be reused up to 15–18 times [40]. For the sensor developed with bromocresol green as the sensitive element, different organic modifications in the silica network via the addition of methyltriethoxysilane, ethyltriethoxysilane, phenyltrimethoxysilane, or glycidoxypropyltrimethoxysilane were also investigated. The device was designed to be integrated with a mobile wireless smart tag sensing system. The modifications with the different organosilanes changed the pK_{app} values of the immobilized bromocresol green pH indicator as well as the wettability of the films, which had a significant effect on the pH response time of these sensing films. The glycidoxy groups were the most suitable, and the results indicated that with careful design and rational selection of the sol-gel matrix materials and their composition, it is possible to tailor sol-gels with very specific and tunable surfaces and pH-sensing properties [39].

Another interesting approach involves a double layer film in which the first layer has two incorporated quantum dots (emission peaks at 525 and 605 nm) and the second has two different immobilized pH indicators. Using these two pH indicators with different pKa values, a sensor with a reproducible linear pH range from 4 to 10 was designed. The changes were observed by a ratiometric fluorescence emission as a function of pH. In addition, high durability was reported under continuous light exposure under severe acidic conditions and storage stability over a period of 6 months. This device demonstrates the ability to overcome the stability issues of common fluorescent optodes while maintaining the advantages of ratiometric fluorescent signal processing [38].

Volatile organic compounds (VOCs) can also be determined by sol-gel-based sensors. Mensing et al. [43] reported an inkjet-printed coating for the detection VOCs. The coatings were based on hybrid silica films embedded with different metal porphyrins and phtalocyanines (i.e., magnesium/manganese(III) chloride/zinc 5,10,15,20-tetraphenyl-21H,23H-porphyrin, magnesium 2,3,7,8,12,13,17,18-octaethyl-21H,23H-porphine, and zinc 2,9,16,23-tetratertbutyl-29H,31H-phthalocyanine). The different printed sensing layers could also be used to discriminate the VOCs. In addition, these materials undergo selective spectral changes upon exposure to oxidizing and reducing gases [43].

Table 25.3 Examples of patents claiming different optical sensors based on sensitive coatings encapsulating different receptor elements using sol-gel technology

Matrix	Receptor element	Analyte	Reference
Silica with methyl, ethyl, phenyl, and/or octyl groups	[Ru^{II}-tris(4,7-diphenyl-1,10-phenanthroline)]Cl$_2$ and pH indicator	O$_2$ and CO$_2$	[44]
Silica membrane with methyl groups deposited on a glass	Coumarin 1	Organophosphates	[45]
Silica coating on an optic fiber	pH	Bromophenol blue, cresol red, and chlorophenol red	[46]
Si and Zr oxide-based matrix	pH	Nile blue	[47]
Hybrid silica with groups like methyl, ethyl, phenyl, octyl, and vinyl embedded in a polymer	Amino, amide, oxygen-reducing compounds and/or vapors	Copper (I), sulfur, ascorbic acid, and citric acid	[48]

Another interesting approach for smart coatings is the capacity for analyte multidetection (i.e., sensors with the ability to detect more than one type of stimulus). For example, Chu et al. [41, 42] reported the development and optimization of a sensor for oxygen and temperature using the same dispositive. The sol-gel film was based on the encapsulation of an oxygen-sensing dye (i.e., platinum tetrakis pentafluorophenyl porphine in combination with 7-amino-4-trifluoromethyl coumarin [42] or 5(6)-carboxyfluorescein) [41]. This device can be employed as a portable optical dual sensor that is a cost-effective alternative to traditional electrochemical-based temperature and oxygen sensors.

Patent literature for chemical optical sensors includes reports on the use of sol-gel technology, as shown in Table 25.3. Macvoy et al. [44] described a sensor prepared by doping a sol-gel layer with a luminophore and pH indicator to detect gases such as O$_2$ and CO$_2$. The use of [Ru^{II}-tris (4,7-diphenyl-1,10-phenanthroline)]Cl$_2$ and pH indicators such as hydroxypyrene trisulfonate, fluorescein, and rhodamine B has been reported. In addition, the described sol-gel coatings can be applied to different substrates, such as polymeric materials, metals, flexible substrate materials including acetate and flexible polymers, paper, optical fiber, or glass/plastic caps [44].

Korent and Lobnik [45] developed an optical sensor based on a hybrid silica membrane prepared with a methyl group as the organic group and deposited on glass. Coumarin 1 was employed as the receptor element embedded in the matrix and exhibits a fluorescence intensity response proportional to the analyte concentration. The device can be employed to detect organophosphates that are widely used as pesticides, such as phosphamidon, dicrotophos, methamidophos, chlorpyrifos, diazinon, and malathion [45].

Fig. 25.8 Example of sensors prepared by Capeletti et al. [48] before and after contact with ammonia gas

Before   After NH₃ contact
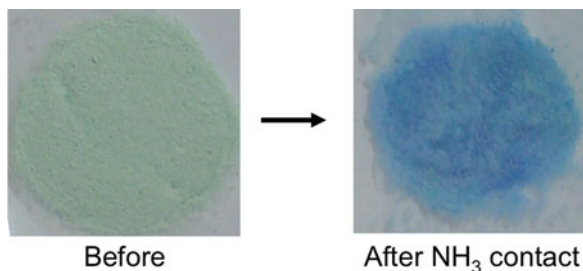
pH monitoring is also important in industrial applications. Dong and Cheng [46] reported a facile method for the preparation of an optical fiber with a sol-gel coating with immobilized pH indicators, such as bromophenol blue, cresol red, and chlorophenol red. Dong and Cheng [46] describe the invention as simple and reliable for remote and real-time pH monitoring. In addition, this sensor is small, lightweight, and flexible with anti-electromagnetic interference and good adaptability to the environment, which results in a measurement that does not require contact and is not destructive. A similar device was described by Moore et al. [47], who synthesized a sol-gel coating with a matrix network formed by silicon and zirconium oxides. This matrix was used to immobilize a pH indicator (Nile blue) and deposited on an optic fiber for use at high pH values (greater than 9) in chemical manufacturing processes and photographic developer solutions [47].

Intelligent and active optical sensors have been combined within the same device. Capeletti et al. [48] reported a hybrid silica-based additive that can be embedded in polymers and used in the food industry. This sensor and additive is based on the encapsulation of different compounds including copper (I), sulfur, ascorbic acid, and citric acid in hybrid silica matrix. The aforementioned sensor and additive were prepared with different organosilanes, such as tetraethylorthosilicate, ethyltriethoxysilane, methyltriethoxysilane, phenyltriethoxysilane, methyltrimethoxysilane, n-octylethoxysilane, n-butylethoxysilane, and vinyltrimethoxysilane. These materials were employed to change color (Fig. 25.8) when in contact with food degradation products, such as amino compounds, amides, oxygen-reducing compounds, and/or vapors. In addition, the active sensor can reduce the microbial activity of packed raw food. This gadget could increase the time that the product can be stored and consumed without health risks [48].

25.3   Conclusion

The sol-gel process has demonstrated its enormous potential for use in the rational design and optimization of optical sensors by immobilizing receptor elements within silica matrices. In addition, with careful selection of sol-gel process parameters and matrix composition, sol-gel materials can be tailored to have very specific surface areas and sensing properties. A balance of forces is necessary in terms of

receptor element leaching because the interaction between the receptor element and the organic groups cannot be so intense that this interaction could lock the active site and prevent the reaction with the analyte. In addition to the sensitive element content, the surface area and hydrophobicity can affect the analyte permeation and sensor response. Several studies have described the search for materials with robustness, good reproducibility, and chemical and physical stability.

The sol-gel approach is a very flexible and rich process. Therefore, more research to identify better materials remains important. In addition, some companies are specializing in this type of material elaboration because the miniaturization of dispositives allied to electronic interfaces requires more development and study. In general, multicomponent detection and discrimination in the same dispositive and long-term stability of these materials remain a challenge.

References

1. Lobnik A, Wolfbeis OS (2001) J Sol-Gel Sci Technol 20(3):303–311
2. Hulanicki A, Glab S, Ingman F (1991) Pure Appl Chem 63(9):1247–1250
3. Eggins BR (2002) Chemical sensors and biosensors. Wiley, Chinchester
4. Wolfbeis OS, Reisfeld R, Oehme I (1996) Sol-gels and chemical sensors, vol 85. Springer, Berlin
5. Wolfbeis OS (1991) Fiber optic chemical sensors and biosensors. CRC Press, Boca Raton, FL
6. Jeronimo PCA, Araujo AN, Montenegro M (2007) Talanta 72(1):13–27
7. Gründler P (2007) Chemical sensors – an introduction for scientists and engineers. Springer, Berlin
8. Brinker CJ, Scherer GW (1990) Sol-gel science – the physics and chemistry of sol-gel processing. Academic Press, San Diego, CA
9. Vioux A, Mutin PH (2004) Handbook of sol-gel science and technology, vol I. Kluwer, New York, NY
10. Schubert U, Hüsing N (2005) Synthesis of inorganic materials. Wiley, Weinheim
11. Alqasaimeh M, Heng LY, Ahmad M, Raj ASS, Ling TL (2014) Sensors 14(7):13186–13209
12. El-Nahhal IM, Zourab SM, Kodeh FS, Abdelsalam FH (2014) J Sol-Gel Sci Technol 71(1):16–23
13. LaGasse MK, Rankin JM, Askim JR, Suslick KS (2014) Sens Actuator B Chem 197:116–122
14. Samadi-Maybodi A, Rezaei V (2014) Sens Actuator B Chem 199:418–423
15. Korzeniowska B, Woolley R, DeCourcey J, Wencel D, Loscher CE, McDonagh C (2014) J Biomed Nanotechnol 10(7):1336–1345
16. Reddaiah K, Reddy TM (2014) J Mol Liq 196:77–85
17. Zhang HR, Lei BF, Liu YL, Liu XT, Zheng MT, Dong HW, Xiao Y, Zhang JY (2014) J Nanosci Nanotechnol 14(6):4615–4621
18. Albanese D, Sannini A, Malvano F, Pilloton R, Di Matteo M (2014) Food Anal Methods 7(5):1002–1008
19. Maroneze CM, Rahim A, Fattori N, da Costa LP, Sigoli FA, Mazali IO, Custodio R, Gushikem Y (2014) Electrochim Acta 123:435–440
20. Motorina A, Tananaiko O, Kozytska I, Raks V, Badia R, Diaz-Garcia ME, Zaitsev VN (2014) Sens Actuator B Chem 200:198–205
21. Sanchez C, Shea KJ, Kitagawa S (2011) Chem Soc Rev 40(2):471–472
22. Kickelbick G (2007) Hybrid materials synthesis, characterization and applications. Wiley, Weinheim

23. Wolfbeis OS (2004) Anal Chem 76(12):3269–3283
24. Lee K, Asher SA (2000) J Am Chem Soc 122(39):9534–9537
25. Capeletti L, Dos Santos J, Moncada E (2012) J Sol-Gel Sci Technol 64:209–218
26. Capeletti LB, Bertotto FL, Dos Santos JHZ, Moncada E, Cardoso MB (2010) Sens Actuators B 151(1):169–176
27. Kowada Y, Ozeki T, Minami T (2005) J Sol-Gel Sci Technol 33(2):175–185
28. Capeletti LB (2014) Federal University of Rio Grande do Sul, Porto Alegre, Brasil
29. Monton MRN, Forsberg EM, Brennan JD (2012) Chem Mater 24(5):796–811
30. Walcarius A, Collinson M (2009) Annu Rev Anal Chem 2:121–143
31. Meng Q, Han T, Wang G, Zheng N, Cao C, Xie S (2014) Sens Actuator B Chem 196:238–244
32. Tyszkiewicz C, Karasinski P, Rogoziski R (2012) Acta Phys Pol A 122(5):908–914
33. Zhao Z, Duan Y (2011) Sens Actuator B Chem 160(1):1340–1345
34. Samadi-Maybodi A, Rezaei V, Rastegarzadeh S (2015) Spectrochim Acta A 136:832–837
35. Guillemain H, Rajarajan M, Lin YC, Chen CT, Sun T, Grattan KTV (2013) Measurement 46(8):2971–2977
36. Chen X, Gu Z (2013) Sens Actuator B Chem 178:207–211
37. Jeon D, Yoo W, Seo J, Shin S, Han K-T, Kim S, Park J-Y, Lee B (2013) Opt Rev 20(2):209–213
38. Hiruta Y, Yoshizawa N, Citterio D, Suzuki K (2012) Anal Chem 84(24):10650–10656
39. Kassal P, Šurina R, Vrsaljko D, Steinberg I (2014) J Sol-Gel Sci Technol 69(3):586–595
40. Chauhan SS, Jasra RV, Sharma AL (2012) Ind Eng Chem Res 51(31):10381–10389
41. Chu C-S, Lin C-A (2014) Sens Actuator B Chem 195:259–265
42. Chu C-S, Lin T-H (2014) Sens Actuator B Chem 202:508–515
43. Mensing JP, Wisitsoraat A, Tuantranont A, Kerdcharoen T (2013) Sens Actuator B Chem 176:428–436
44. Mcevoy A, Maccraith B, Mcdonagh C, Von Bultzingslowen C, Von Bultzingslowen O (2006) US 20060257094
45. Korent US, Lobnik A (2012) WO2012071019-A1
46. Dong S, Cheng W (2006) CN1908633-A
47. Moore CP, Robert J, Blue RG, Stewart G, Robert JC (1997) EP793091-A1
48. Capeletti LB, Dos Santos JHZ, Moncada E (2013) EP2617764

Chapter 26
Sensory Polymers for Detecting Explosives and Chemical Warfare Agents

José M. García, Jesús L. Pablos, Félix C. García, and Felipe Serna

Abstract The detection of explosives (EXs) and chemical warfare agents (CWA) is challenging and a topic of current interest. It is driven by societal concerns about the widespread use of explosives in the mining industry and military endeavors and specifically in terrorist attacks and of CWA in the latter. The detection and quantification of these chemicals is twofold, through vapor and in solution detection. Sensory polymers are suitable materials for this purpose because they can be transformed or prepared as intelligent films, coatings, and fibers in sensory materials for transducing devices, as smart strips or tags that can be easily handled, or even as smart coatings for commercial fabrics as well as paint for all kinds of surfaces. The detection is based on any variation of a measurable property arisen from the target species/polymer interaction such as mass uptake, conductivity or resistivity changes, chemo-mechanical and electrochemical behavior variations, and chromogenic and fluorescence behavior modifications.

Keywords Explosives • Chemical warfare agents • Nerve agents • Polymers • Sensors

J.M. García (✉) • F.C. García • F. Serna
Departamento de Química, Facultad de Ciencias, Universidad de Burgos,
Plaza de Misael Bañuelos s/n, 09001 Burgos, Spain
e-mail: jmiguel@ubu.es; fegarcia@ubu.es; fserna@ubu.es

J.L. Pablos
Departamento de Química, Facultad de Ciencias, Universidad de Burgos,
Plaza de Misael Bañuelos s/n, 09001 Burgos, Spain

Polymer Photochemistry Group, Instituto de Ciencia y Tecnología de Polímeros, C.S.I.C.,
Juan de la Cierva 3, Madrid 28006, Spain
e-mail: jlpablos@ictp.csic.es

26.1   Introduction

The multiple-point release of sarin nerve gas in the Tokyo subway system (3/20/1995), the bombing of four Madrid trains (3/11/2004) and the London subway system (7/7/2005), and specifically the attack on the World Trade Center in New York (9/11/2001) showed the preparedness of developed countries in facing terrorist attacks and had suddenly turned into a global threat.

Among a number of challenges regarding civil security in our fast-moving globally interconnected world, both chemical warfare agents (CWAs) and explosives (EXs) are major societal concerns. Accordingly, their in situ and real-time detection is a challenge that is being tackled from an instrumental and chemical viewpoint.

CWAs are chemicals designed and prepared to be harassing, incapacitating, or lethal [1]. The discussion in this chapter will be focused on nerve agents (NAs), a specific family of CWAs somewhat derived from pesticide research. They are the most dangerous and lethal chemical warfare species; developed in the 1930s and 1950s, G and V type, respectively, have the sole purpose to be used as weapons. The sensing of CWAs is primarily directed toward the detection of vapors for attack prevention, though forensic analysis is also relevant after a terrorist act and for control of these chemicals according to the Chemical Weapon Convention, which entered into force in 1997.

Contrary to CWAs, commercial EXs are broadly used for different purposes and applications in civil engineering beyond their militarily use. The detection of EXs is mainly twofold focused: on forensic and criminal investigations of terrorist attacks and on homeland and civil security, the latter including humanitarian efforts in demining and specifically the prevention of terrorist attacks. From these viewpoints the main goal is directed toward trace explosive vapor detection, although detection in solution is also important for some fields related with forensic science as well as for environmental control and remediation. Three families of widely used commercial explosives are covered in this chapter, namely, nitroaromatics, nitrate esters, and nitramines. Peroxide explosives are also covered, though they are noncommercial explosives, because of their accredited use in terrorist attacks due to their easy preparation from widely available chemicals.

Sensory polymers are macromolecules that have in their structure both binding sites (or receptor motifs) for guest (or target) molecules and signaling units. They have lots of advantages over discrete or low molecular mass chemosensors which are discussed in the following examples [2]. First, these polymers can be prepared or transformed into films, coatings, or finished sensory materials with different shapes and exhibit collective properties sensitive to minor perturbations. Their distinct polymer geometries are affordable (linear, spherical, and tridimensional cross-linked network) and can be easily designed to work in hydrophobic or hydrophilic environments. Finally, while their sensory and signaling moieties cannot migrate, they can be used to sense both vapors and liquids [2].

26.2 Chemical Warfare Agents

CWAs can be classified as riot-control agents, incapacitating agents, blood agents, vesicants, chocking or respiratory agents, nerve agents, or binary and nontraditional agents [1]. As it has been pointed out in the introduction, NAs are covered in this chapter (Scheme 26.1 and Table 26.1) [3, 4]. Some of the G-agents, developed in Germany in the 1930s, and V-agents, British-developed chemicals around 1950, are shown in Scheme 26.1. The former agents are usually nonpersistent (i.e., volatile chemicals that are rapidly hydrolyzed), whereas the latter are usually persistent (i.e., not highly volatile chemicals that can persist in an area for a relatively long period of time) (Table 26.2) [5]. They have an organophosphoric acid ester or
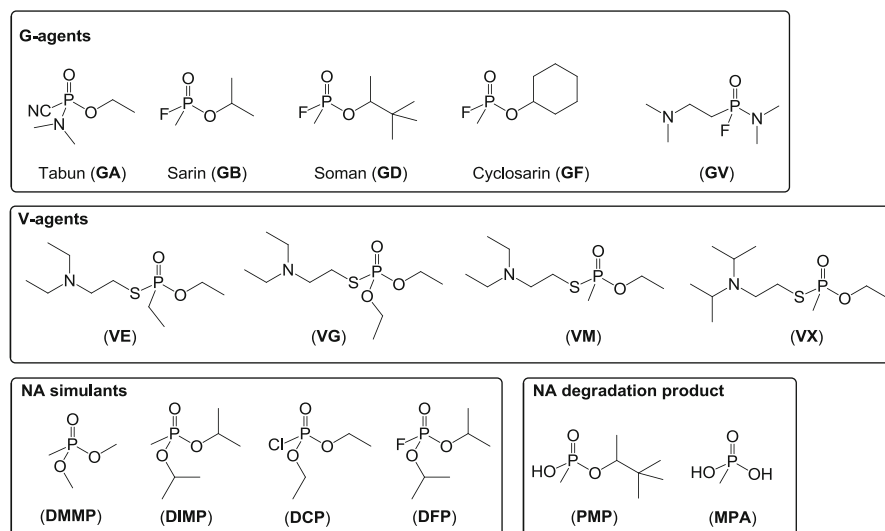
Scheme 26.1 Chemical structures, names, and codes of some NAs and NA simulants and degradation products. The structures do not provide stereochemistry information regarding some of the phosphorous atoms (also not for the asymmetric carbon in GD and PMP)

Table 26.1 Toxicity to man of some important CWAs (data from [4])

Agent type	Agent	LCt_{50} Inhalation (mg min/m^3)	LD_{50} Skin (mg/individual)
Nerve agent	Tabun (GA)	200	4,000
	Sarin (GB)	100	1,700
	Soman (GD)	100	300
	V-agents	50	10
Chocking agent	Chlorine	10,000	293
Blood agent	Hydrogen cyanide	5,000	200,000
Vesicant	Mustard (sulfur)	1,500	10,000

LD_{50}, dose at which 50 % of the exposed population will die; LCt_{50}, used for inhalation, is defined as the product of the concentration (C) and the length of exposure (t). L represents lethal and 50 stands for 50 % effect

Table 26.2 Selected data of some NAs (sorted from highest to lowest vapor pressure) (data from [5])

Nerve agent	Persistent (p)/nonpersistent (np)	Boiling point (°C)	Vapor pressure at 25 °C (atm)	ppb$_v$
GB	np	147	3.82×10^{-3}	3,820,000
GD	np	198	5.26×10^{-4}	526,000
GV	np	226	6.44×10^{-5}	64,400
GF	np	239	5.79×10^{-5}	57,900
GA	np	248	$4.86 \times 10^{-5 \, b}$	48,600
VM	p	~293	2.63×10^{-6}	2,630
VX	p	298[a]	9.21×10^{-7}	921
VE	p	311	7.26×10^{-7}	726
VG	p	315	7.11×10^{-7}	711

[a]Calculated

[b]Vapor pressure at 20 °C

organophosphorus structure, related to that of pesticides, which inhibit acetylcholinesterase (AChE) by irreversible binding to its active site and are considered the most infamous of synthetic chemical derivatives [6]. Their dangerousness, along with their ease of synthesis, odorless and colorless, underscores the need of their detection. At a bench scale, laboratories that are not conditioned to use NAs usually carry out research and development in this field using mimicking compounds (Scheme 26.1). Examples of these compounds are dimethyl methylphosphonate (DMMP), diisopropyl methylphosphonate (DIMP), diisopropyl fluorophosphate (DFP), and diethyl chlorophosphate (DCP). These mimicking compounds are not valid NAs because they are poorly persistent (readily hydrolyzed) or even hydrolyzed products, also known as degradation products, such as pinacolyl methylphosphonate (PMP) or methylphosphonic acid (MPA) [3].

To date, different detection techniques and methodologies have been used to achieve the goal of detection of CWAs in a real-time manner, while also meeting the affordability and portability criteria. For instance, remote or standoff monitoring has been carried out by infrared and Raman spectroscopy and on-the-spot detection by colorimetric, ion mobility spectrometry, surface acoustic wave sensors, flame photometry, photoionization and electrochemical detection, and carbon nanotube gas ionization sensors [1]. Some of these techniques are partially based on, or use, conjugated or conductive polymers (CPs), molecularly imprinted polymers (MIP), an array of sensors based on a set of polymers, or miscellaneous polymers comprising, for instance, dendritic or hyperbranch macromolecules, polymer chemosensors or chemodosimeters, and polymer-coated paper strips.

26.2.1 Conjugated or Conductive Polymers

A CP, also known as synthetic metal, is a macromolecule with a main chain comprised of alternating single and multiple bonds, which provide the material with a bandgap that endow it with semiconductive to insulating characteristics and can be

Table 26.3 Conjugated polymers used in the detection of nerve agent simulants and degradation products

NA simulant	Degradation products	Polymer	Other characteristics	Response	Cite	LOD or detection level
DMMP vapors		PANi		Resistive	[10, 11]	28 ppm
DMMP vapors		PANi		Conductivity	[13]	
DMMP vapors		PPy		Resistive	[10, 11]	28 ppm
DMMP vapors		PPy	Hybrid ppy/iron oxyhydroxide nanoparticles	Resistive	[15]	0.1 ppb
DMMP vapors		PEDOT	Nanonodule and nanorod structures		[16]	10 ppt
DMMP vapors		PPy		Chemochromic	[12]	26 ppm
DMMP vapors		PT		Resistive	[17]	0.05 ppm
DCP solutions		Poly(fluorene-co-quinoxaline)	Coated paper strips	Fluorescence	[14]	1.49×10^{-5} M
	PMP solution	PT	MIP	Frequency variation of a quartz crystal resonator	[18]	60 μM
	Degradation products of VE, VX, VG	PPy		Amperometric	[19]	3–4.5 μM

turned conductive by doping. Depending on the constitution, CPs may exhibit strong luminescence associated with the delocalization and polarization of the structures. These properties, along with the collective properties that CPs exhibits making them sensitive to minor perturbations, allow these polymers to be useful as sensitive materials for a number of detection technologies [2, 7–9]. Some of the CPs used in the detection of NAs, NA simulants, and degradation products are commented below and summarized in Table 26.3.

Conductive polyaniline (PANi) and polypyrrole (PPy) polymers coated onto woven poly(ethylene terephthalate) (PET) or nylon fabric were used as chemiresistive sensors for detecting a number of vapors, including DMMP [10, 11]. Moreover, the sensitivity of materials was increased by deposition of copper salts onto the coated sensory fibers. Doped PPy with 1,5-naphthalene, disulphonic acid, anthraquinone-2-sulphonic acid, and hydrochloric acid were also used as chromogenic material for the detection of DMMP. Thus, the coating of an optic fiber allowed for a chemochromic transducer with a sensitivity of 26 ppm [12, 13].

The fluorescence detection of DCP in solution was achieved with sensory paper strips prepared by simple immersion of filter paper in a poly(fluorene-co-quinoxaline) copolymer. The presence of the NA simulant quenched the emission of the paper-based strip, an emission that was restored after treatment with basic aqueous solution [14].

Hybrid nanomaterials such as PPy nanoparticles vertically decorated with iron oxyhydroxide metal oxide (FeOOH) nanoneedles were also used as chemoresistive materials for the detection of DMMP vapors at the sub-ppm level [15]. An even lower limit of detection (LOD) was achieved with hydroxylated poly(3,4-ethylenedioxythiophene) (PEDOT) nanotubes with nanonodule and nanorod structures, which were grown on a surface by vapor deposition polymerization (VDP). The integration of the sensory material on flexible PET substrates yielded a LOD of 10 ppt [16]. Carbon nanotube/polythiophene (PT) chemoresistive sensors gave rise to a conductance change of 1 % in an atmosphere containing 0.05 ppm of DMMP [17].

PT was also used for the detection in solution of PMP, the hydrolysis product of GD. The polymer was used to prepare a MIP that was electropolymerized in a quart crystal microbalance (QCM) [18, 19].

26.2.2   Molecularly Imprinted Polymers

MIPs are polymer networks with binding cavities for target molecules. The cavities are usually created by polymerization of different comonomers in the presence of these targets, which behave as templates and after their removal creates the cavity especially suited for a specific target chemical species [2].

Lanthanide complexes prepared from 4-vinylbenzoic acid and Eu^{3+}, along with a matrix of styrene and divinylbenzene (DVB) with the targets VX and G-type (GB and GD), were used to prepare an optic fiber MIP coating for the fluorescent recognition and quantification of target NAs in solution [20].

A DCP simulant was determined using a MIP membrane integrated with a potentiometric transducer. The membrane was comprised by 2-hydroxyethyl methacrylate (HEMA), a cross-linking monomer ethylene glycol dimethacrylate (EGDMA), and 4-vinylaniline (VA) as sensory motif and the template (DCP), which anchored covalently to VA and was finally leached by washing the membrane with acidic methanol [21]. Following a similar approach, methyl 3,5-divinylbenzoate/Eu^{3+} complexes allowed for the preparation of a MIP sensory material for the luminescent detection of the NA degradation product PMP [22]. β-Diketone/Eu^{3+}/PMP complexes were also described as potential imprinting compounds for the preparation of selective MIPs for PMP [23]. Regarding this point, a β-diketone/Eu^{3+}/PMP complex was designed as a reversible addition fragmentation chain transfer (RAFT) monomer to prepare fluorescent polymers end-capped with the β-diketone/Eu^{3+} motifs [24].

MPA, as one of the degradation product of G and V type NAs, was potentiometrically detected in solution with a MIP prepared from methacrylic acid (MAA) and *N*-vinylpyrrolidone (VP) as comonomers and EGDMA as a cross-linker, using MPA as template [25].

Table 26.4 Commercial polymers used for nerve agent detection and quantification based on sensor array

Acrylic-like polymers	Polysiloxanes
• Poly(vinyl acetate) (PVAc) • Poly(9-vinylcarbazole) (PVK) • Polyvinylpyrrolidone (PVP) • Poly(4-vinylphenol) (PVPH) • Poly(ethylene-co-vinyl acetate) (EVA)	• Polydimethylsiloxane (PDMS) • Poly(methyloctadecylsiloxane) (PMODS) • Poly((3-cyanopropyl)methylsiloxane) (PCPMS) • Poly((3-aminopropyl)propylsiloxane) (PAPPS) • Poly(trifluoropropylmethylsiloxane-co-dimethylsiloxane) (PMFTPMS) • Polysiloxanes with pendant 1-hydroxyhexa-fluoropropyl moieties (SXFA)
Rubber-like polymers	Miscellanea
• Polyisobutylene (PIB) • Polybutadiene (PBD) • Polyisoprene (PIP) • Poly(butadiene-co-styrene) (PBS)	• Polysulfone (PSU) • Polyethylenimin (PEI) • Polyethylene glycol (PEG) • Polyepichlorhydrin (PECH) • Polycaprolactone (PCL)

26.2.3   Sensor Array Based on a Set of Polymers

The lack of selectivity is a challenge that has to be tackled in sensor technology. One of the ways of addressing this challenge is by using an array of sensors or electronic nose (e-nose). The multiple cross-transduced signals collected from the array are statistically treated with pattern recognition algorithms, such as principal component analysis (PCA), as a straightforward way of reducing the dimensionality of the data [26].

A set of polymers is usually used and the transduction is typically based on variations of conductive properties of the polymers, resistivity changes, or frequency variation of acoustic waves such as QCMs, devices based on Rayleigh waves [e.g., surface acoustic wave sensors (SAWs)], transverse surface waves, and Love waves.

Polymers used are usually commercially available, both organic and inorganic, or even hybrid (chemical names and acronyms are depicted in Table 26.4).

SAW-based sensor array prepared by deposition of different polymers on a quartz substrate by dip and spray coating technique, discriminated DMMP and DCP vapors from other gases using PCA analysis [27], achieved sub-ppm sensitivity [28]. More sophisticated deposition techniques, such as laser-induced forward transfer (LIFT), were used to sense GB vapors with a sensitivity of 9 ppb with PECH coating and to differentiate from the simulant DMMP and a number of solvents [29, 30]. SAW-based e-nose with PECH and two polysiloxanes coatings led to (>95 %) identification performance of DMMP, DCP, and a binary mixture using an optimized artificial neural network (ANN) and PCA-ANN [31, 32].

Thus, chips consisting of ten parallel plates with polymers as dielectric materials were used to measure the dielectric constant upon exposure to atmospheres containing GA, GB, and GD vapors [33].

Nonconjugated polymers were used to build chemiresistive arrays by preparing carbon black/organic polymer composites. The sensory system behaved as DMMP and DIMP vapor detectors giving a LOD between 0.047–0.24 mg/m³, the lower limit obtained with the polymers EVA and PCL for the simulants DMMP and DIMP, respectively [34]. PCA analysis allowed for the differentiation of DMMP from SIMP and from a number of analytes, including diesel fuel and other solvents.

26.2.4 Miscellaneous

Dendritic and hyperbranched polyamidoamine (PAMAM) and polyurea-based sphere-like polymers were functionalized with dansyl and nitrobenzofurazan fluorophores. The materials responded to polarity changes of solutions with variation in the fluorescence intensity, which was used to differentiate between DMMP and a number of NA simulants [35].

The coating of paper with polynorbornene with pendant 8-hydroxyquinoline motifs gave rise to sensory paper strips for the detection of DCP vapors achieving a LOD of 25 ppb [36]. A hybrid methacrylamide monomer with pendant terpyridine/lanthanide³⁺ complexes allowed for the preparation of fluorescence copolymer chemosensors for detection in solution of DFP at the (ppb) level (LOD = 6 ppb) [37]. Hybrid polymer comprised of 2,2-bis(3-allyl-4-hydroxyphenyl) hexafluoropropane and oligosiloxane moieties was tested gravimetrically as a sorbent for DMMP [38]. Similar polymer structures were used as selective absorbing materials of DMMP in polymer-coated QCM [39].

26.3 Explosives

EXs can be broadly classified as secondary and primary explosives. Among the manageable secondary EXs, Scheme 26.2 depicts three families of commercially relevant EXs, namely, nitroaromatics, nitrate esters, and nitramines such as 2,4,6-trinitrotoluene (TNT), pentaerythritol tetranitrate (PETN), nitroglycerin (NG), 1,3,5-trinitro-1,3,5-triazacyclohexane (RDX), 1,3,5,7-tetranitro-1,3,5,7-tetrazocine (HMX), and 2,4,6-trinitrophenyl-methylnitramine (tetryl). 2,4- and 2,6-dinitrotoluene (DNT) and picric acid (PA) are broadly used as TNT mimics in detection studies due to their availability. From a civil security viewpoint though without commercial use, it is also relevant to mention the peroxide family, represented by triacetone triperoxide (TATP) and hexamethylene triperoxide diamine (HMTD).

Vapor detection of explosives is especially interesting for civil security. However, it is a challenging task due to the particularly low vapor pressures of commercialized and most widely used secondary explosives, such as HMX, RDX, PETN, and TNT (Table 26.5) [40]. Detection of explosive vapor traces has been carried out using a number of techniques (e.g., high performance liquid chromatography, gas
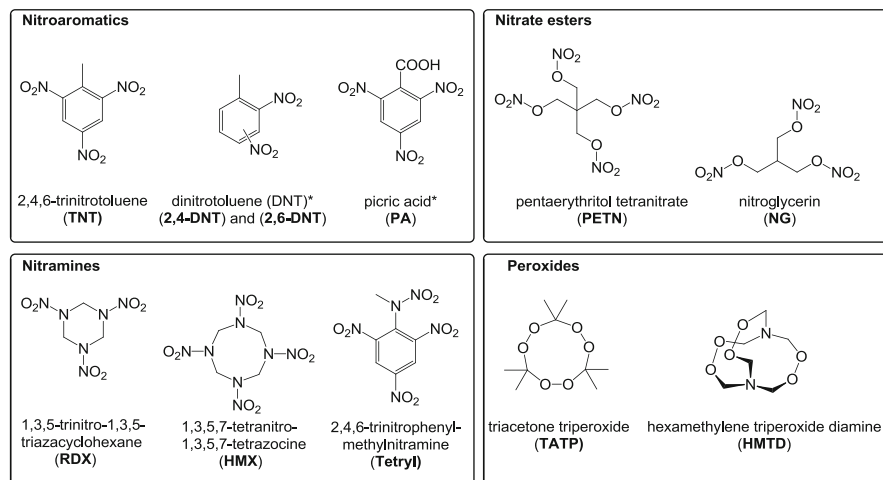
Scheme 26.2 Chemical structures and acronyms of some EXs (*PA is an explosive widely used as a TNT mimic in-lab studies due to its availability and inertness as wet chemical; DNTs are explosives widely used as a TNT mimic due to their availability)

Table 26.5 Vapor pressure at 25 °C of some explosives (sorted from lowest to highest) (data from [40])

Explosive	Vapor pressure (atm)	ppb$_v$
HMX	2.37×10^{-17}	0.0000000237
RDX	4.85×10^{-12}	0.00485
PETN	1.07×10^{-11}	0.0107
TNT	9.15×10^{-9}	9.15
2,4-DNT	4.11×10^{-7}	411
NG	6.45×10^{-7}	645
2,6-DNT	8.93×10^{-7}	893
TATP	6.31×10^{-5}	63,100

chromatography, and ion mobility spectroscopy). From a polymer viewpoint, the sensitivity and selectivity challenges have been tackled, for instance, using amplifying fluorescent conjugated polymers, array sensing, and SAW.

The scientific literature is much broader than that related to CWAs, and the reader is referred to the extensive number of specific reviews covering different aspects of the topic cited below.

26.3.1   Conjugated or Conductive Polymers

CPs can be grouped in different families according to the polymer backbone, such as poly(*p*-phenyleneethynylene)s (PPEs) (**P1**), poly(*p*-phenylenevinylene)s (PPVs) (**P2**), polyacetylenes (**P3**), polysilanes and related polymetallocenes (**P4**), and polyphenylene-like polymers (**P5**) (Scheme 26.3). Fluorescent CPs are the most
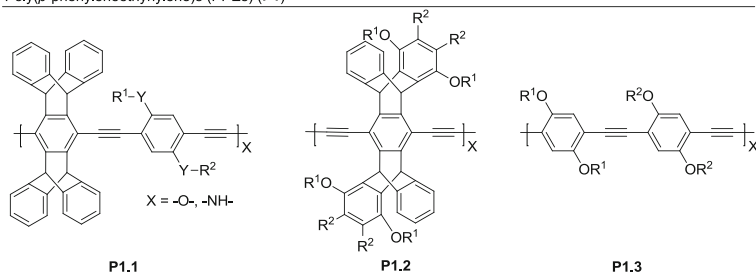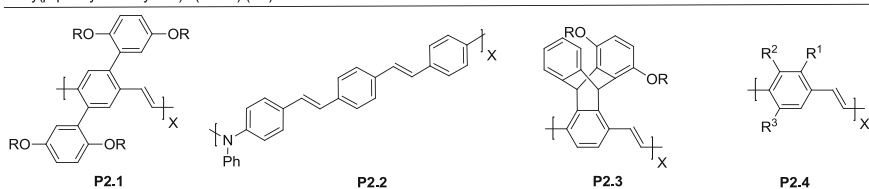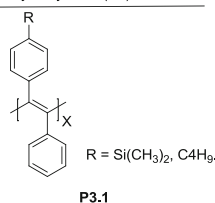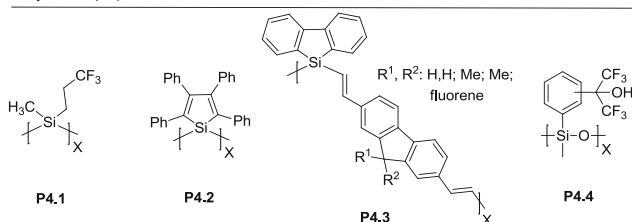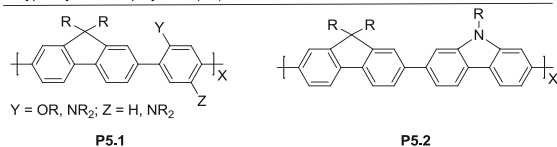
Scheme 26.3 CP chemosensors

sensitive to EX vapors due to the collective properties of these polymers and to the sensitivity of the fluorescence technique [2, 41–46]. For example, a commercial explosives trace detector, which is based on **P1.1**, has a sensitivity comparable to trained explosive detection canines (Fig. 26.1) [47]. Avoiding aggregation and self-quenching is a milestone in efficient fluorescence CP chemosensors in the solid state (e.g., films), and this is a key point of the rigid and bulky pentiptycene group of **P1.1**. The sensitivity of the systems is improved by increasing fluorescence lifetime by properly designing the alkyl R_1 and R_2 groups [48–53] and by including fused polycyclic aromatics that usually have a weakly allowed or forbidden transition, such as main chain triphenylene or dibenzochrysene residues [54, 55]. Pentiptycene-containing polymers were used to develop an e-nose based on an array of sensory materials attached to the distal tips of an optical fiber bundle for the

Fig. 26.1 Scheme of a sensory working device: (*1*) blue LED (light emitting diode), (*2*) lens, (*3*) interference filter, (*4*) glass substrate, (*5*) polymeric fluorophore thin film, (*6*) analyte, (*7*) interference filter, and (*8*) photomultiplier (reprinted with permission from [41], Copyright 2014 Springer)
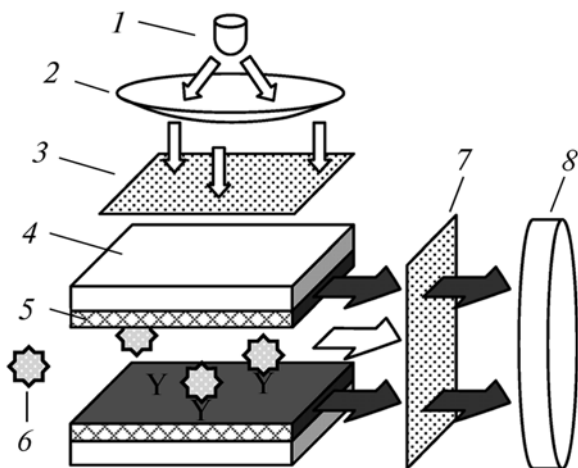
detection of DNT [56]. Higher sensitivity toward nitroaromatics was also achieved by the lasing action. For instance, PPV **P2.1** showed outstanding quantum yield in the solid state ($\Phi = 0.8$) as well as exceptional stability to photobleaching [57]. A good fluorescence quenching response toward RDX vapors was also observed in PPV networks [58]. The polymer **P2.2** showed a lasing emission that was 20 times more sensitive to TNT vapors than spontaneous emission, with a LOD of 10 ppb [59]. The bulkiness, the donating groups, and the extension of the conjugative system allowed for the tuning of the fluorescence and sensor capabilities rendering materials that showed quenching upon exposure to DNT and TNT vapors at the (ppm) level [60]. The increment of the electron richness of the even bulkier iptycene structures rendered polymers that exhibited static quenching, and the materials recovered their fluorescence much slower than **P1.1** after exposure to TNT vapors. The formation of complexes between TNT and **P1.2** was ascribed to the electron enrichment of the iptycenes due to the presence of substituted alkoxy groups [61]. Multiphoton excitation was also used to advantageously detect TNT at millimolar level [62]. The less bulky PPV **P2.3** also showed a similar response, although it was less sensitive to TNT. The influence of the iptycenes in the exciton transport and TNT sensitivity was demonstrated with chiral **P1.1** structures and chiral PPEs structures lacking in this group (**P1.3**), the latter exhibiting much lower fluorescence intensity in solution due to aggregation [51, 63]. Pyrene-containing polymers showed to have an enhanced selectivity toward TNT in water in relation to DNT and other explosive simulants [64]. In relation with the sensing performance of the CPs regarding TNT vapor detection, it can be improved also by physical means, for instance, by increasing the surface area by lyophilization from the proper solvent, as depicted for PPE [65].

PPVs with pendant-branched oligoethylene groups allowed for the detection of TNT in the solid state [66] and were also used to prepare composite materials with silica sensitive to traces of TNT vapors [67].

Polysilanes show unusual electronic and optical properties because of the delocalizable and polarizable σ-electrons along the Si-Si backbone. Fluoroalkylated polysilane polymer solid films (**P4.1**) have also been described as an excellent fluorescence chemosensor for nitroaromatic EXs in water, based on the fluorescence quenching in the near-UV region, with ppm sensitivity [68]. Related polysiloles prepared by 1,1 coupling, such as poly(2,3,4,5-tetraphenyl-1-silacyclopenta-2,4-diene) $(C_4Ph_4Si)_x$ **P4.2**, exhibit similar behavior. The fluoresce quenching permitted the evaluation of the presence of TNT down to 1 and 50 ppb in air and seawater, respectively, and also its visual detection on surfaces [69, 70]. Other polymetallole films (e.g., polygermole and its derivatives) were also used for the visual fluorescence detection of solid explosive traces [71, 72]. **P4.2** was used with the chemical 2,3-diaminonaphthalene in a tandem fluorescence off/on methodology for the selective solid-state detection of traces of the broad family of nitroaromatic, nitramine, and nitrate ester explosives [73]. Poly(tetraphenylsilole-vinylene), poly(tetraphenylsilole-silafluorene-vinylene), and poly(silafluorene-vinylene) showed fluorescence quenching to solid particulates of TNT, DNT, PA, RDX, HMX, tetryl, PETN, and NG [74]. Luminescent oligo(tetraphenyl)silole NPs were also used as chemical sensors for aqueous TNT [75]. Polymer with silafluorene and fluorene moieties **P4.3** presented fluorescence quenching response toward nitroaromatic explosives. The sensitivity of this kind of polymer chemosensors, poly(silafluorenyldiethynylspirobifluorene), and poly(tetrasiloledis ethynylspirobifluorene), to solid explosives was increased by chemically anchoring the polymers to a silica gel thin layer chromatography support [76, 77]. In water, the detection of TNT and RDX with this kind of material was achieved by suspensions of polymer/silica NPs, PPEs-grafted silica NPs, and amine-functionalized mesoporous silica NPs containing PPV [78–80].

The rigid structure of diphenyl substituted polyacetylenes (**P3.1**) provided a low level of aggregation and high free volume valid for the fluorescence detection of nitroaromatic chemical vapors [81].

Thin films of polythiophenes with pendant 1,2,3-triazole groups showed reversible fluorescence quenching upon exposure to DNT and TNT vapors [82]. A hybrid nanosensor of PEDOT nanojunction covered with a thin layer of ionic liquid was used to detect TNT [83].

Polymers with a main chain containing *o*-hydroxyphenyl groups into the 2- and 5-positions of oxadiazole gave rise to excited-state intramolecular proton transfer (ESIPT). Fluorescence was quenched by PA and DNT in organic solution [84–86].

Nanofibrous polypeptide doped PANi deposited on an electrode was used for the trace detection of TNT in solution by adsorptive stripping voltammetry [87]. Oligopeptides have also been used as nitroaromatic receptors in solution experiments using a QCM sensing platform [88, 89].

The detection of taggants [e.g., 2,3-dimethyl-2,3-dinitrobutane (DMNB)] was also accomplished studying the reversible binding of DMNB to **P5.1** in the solid state, the binding causing the fluorescence quenching. Other less effective CPs such as **P1.1** and **P5.2** were also analyzed [90]. Related with **P5.2**, films of polycarbazole with bulky pendant motifs (i.e., 4-[tris-(4-octyloxyphenyl) methyl] phenyl) were

used to sense TNT and DNT [91, 92]. Porous films and coated fibers prepared with polymers with similar structures having pendant cholesterol motifs were also described [93].

26.3.2 Molecularly Imprinted Polymers

The research concerning MIPs for detecting EXs emerged in this century and exploded in the last decade, with currently commercialized or ready to commercialized MIP-based sensory systems [94]. MIPs have been used for preparing electrochemical, acoustic wave, and optical sensors. Extended reports on this field were prepared by Kutner, D'Souza, et al. [95] and recently by Xue, Meng et al. [94], with representative examples provided below.

MIPs prepared from methacrylic acid were labeled with amine-functionalized quantum dots for the detection of DNT and TNT in solution, explosives that were used as templates and caused the fluorescence quenching [96].

Polymer beads and films obtained by direct surface polymerization on QCM were used to detect TNT and DNT by the mass uptake. Best results were obtained using acrylamide and EGDMA as monomer and cross-linker, respectively, with chloroform as the polymerization solvent, showing a TNT vapor uptake of about 150 pg/μg MIP per hour [97, 98]. Spherical polymer beads prepared with methacrylic acid and using PEG as porogen uptook TNT vapors with capacities ranging 0.2–0.3 ng/mg of MIP [99].

The selectivity of PPVs was also improved by preparing MIPs as micrometer-sized spheres for TNT using 2,4,6-triisopropyltoluene as non-quenching template. The exposure to TNT and DNT vapors gave rise to significant fluorescence quenching, and selectivity toward DNT was partially observed by tuning the bulkiness of the pendant substitutions of the main chain rings [100].

A sensor based on surface-enhanced Raman scattering (SERS) for TNT in solution was reported. The polysiloxane-based MIP, prepared with 3-aminopropyltriethoxysilane, 3-mercaptopropyltrimethoxysilane, and methyltriethoxysilane, was deposited on a SERS-active surface as the sensing layer, and the LOD was 3 μM [101]. The former monomer was previously used for molecular imprinting on the walls of silica nanotubes for the recognition of TNT [102].

A selective voltammetric TNT sensor in water and soil samples was reported. The MIP, based on methacrylic acid and incorporated in a carbon paste electrode, functioned both as a selectively recognition element and pre-concentrator agent for the explosive [103].

TATP in solution was sensed by differential pulse voltammetry in presence of other explosives such as PETN, RDX, HMX, and TNT. The sensor was prepared by electropolymerization of pyrrole on a carbon electrode using TATP as template [104].

TNT vapors were detected at the (ppb$_v$) using planar integrated optical waveguide (IOW) attenuated total reflection spectrometry, where MIPs deposited on the

waveguide surface acted as the sensing layer. The MIPs were prepared with silane monomers alongside carbamate groups with DNT motifs, which acted as templates and were chemically removed from the net [105].

The potentiodynamic electropolymerization on the Au-coated quartz crystal resonators (Au-QCRs) of complexes of 4-(di([2,2′-bithiophen]-5-yl)methyl)aniline and different nitroaromatic explosives was used to prepare sensors for the simultaneous chronoamperometry (CA) and piezoelectric microgravimetry (PM) determination of TNT, DNT, and PA [106].

A LOD of 12 fM for RDX in solution was achieved using imprinted composite of bisaniline-cross-linked AuNPs. Changes in the dielectric properties of the AuNP composite arisen from the interaction with RDX resulted in an amplified shift in the surface plasmon resonance (SPR) spectra [107, 108]. The combination of surface molecular assembly with nanostructures (nanowires/nanotubes) in the imprinting technique created effective recognition sites for TNT in a more effective way than the traditional use of porogens. The MIP nanostructures were prepared with acrylamide and EGDMA and porous alumina membranes [109].

26.3.3   Sensor Array Based on a Set of Polymers

Arrays of carbon black-polymer (PVAc, PMMA) composites were used to prepare a series of sensors that respond to vapors with a change in resistance. Thin composite films were deposited across two metallic leads; the films showing swelling-induced resistance changes upon exposure to vapors. TNT, DNT, and DNB were detected in air and discriminated from each other [110, 111].

An array of three luminescent sensory solid organic and hybrid polymer membranes were used to selectively detect and discriminate nitro explosive vapors. The sensory materials were based on dicoumarol hybrid complex monomers containing Tb (III) and Sm (III). PCA of the fluorescence data allows for both discrimination between TNT, PETN, and RDX vapors and a number of mimics [112].

Five commercial PPVs (**P2.4**) and fluorene-containing polymers were coated onto glass beads and used as a sensory array for nitroaromatics. PCA and LDA analysis of the data allowed for the discrimination of TNT, tetryl, and a number of explosive simulants and nonaromatic nitro-explosives [113].

26.3.4   Miscellaneous

A series of chemoselective polymers were evaluated as thin sorbent coatings on SAW devices for their vapor sorption and selectivity of TNT, DNT, and other nitroaromatics. Among different polymeric materials tested, siloxane polymers functionalized with acidic pendant groups showed the best results and among them **P4.2** with LOD at the ppt concentration range for 2,4-DNT [114]. A PEG polymer

coating was used to prepare a complete module of 150 MHz SAW for the detection 2,4-DNT vapors [115]. Vinyl functionalized cyclodextrins were also chemically incorporated into polysiloxane films and chemically anchored to the transducer surface as in SAW devices for DNT vapor with sensitivities at the ppb level. The cyclodextrins had electron-rich aromatic rings for enhancing the binding toward nitroaromatics [116].

Explosive fingerprint residues (i.e., trace amounts of explosives) were visually detected by using a specific color reaction between cyclopentadienylmanganesetricarbonyl (cymantrene) and explosives after a short period of low-power UV irradiation. The reaction was performed within thin polymer films (e.g., divinylbenzene/styrene copolymer) with embedded cymantrene, which were used as tactile sensors; upon gentle contact with a DNT contaminated fingertip, they retained trace amounts of EXs and EXs simulants as clear imprints [117].

Sensory polymeric materials for the visual sensing of TNT vapors and in aqueous media were developed using a straightforward strategy. Polymer chemosensory films and coated fabrics were prepared by bulk radical polymerization of hydrophilic commercial monomers, such as 2-hydroxyethyl acrylate with EGDMA as the cross-linker. In addition to this, small quantities of sensory monomer consisting of an amine-containing acrylic monomer (2-(dimethylamino)ethyl methacrylate, 4-{N-(2-(methylamino)-ethyl)aminomethyl}styrene, and 4-(aminomethyl)styrene) were also utilized. TNT gave rise to a highly colored complex with the amine groups of the polymers, giving rise to the transduction phenomenon. The quantification was achieved by processing the digital color definition (RGB parameters) of a picture taken of the materials [118, 119].

The fluorescence quenching of main chain coumarin-containing polymers was also observed in presence of DNT and TNT. The quenching of the coumarin fluorophore motifs was achieved in organic solution and in the sensing of vapors by polymer films [120]. Pyrene-doped polyethersulfone polymers also gave rise to fluorescence quenching upon entering into contact with a number of nitroaromatic explosive vapors, especially with DNT and TNT [121].

Hyperbranched conjugated poly(2,5-silole)s and poly(silylenephenylene)s responded to 1 ppm of PA in solution with a fluorescence quencher, where the fluorescence and the amplification was increased by aggregation-enhanced emissions [122–124]. The amplification of an aggregation-enhanced emission in solution was also observed in linear 2,5-tetraphenylsilole-vinylene-type polymers and in linear and hyperbranched poly(aryleneethynylenesilole)s for the detection of PA, DNT, and TNT [125, 126]. This type of amplification was also described for polymers with structural units having triazole and tetraphenylethene groups, which were not fluorescent in THF solution and turned highly fluorescent upon adding water. A further addition of PA turned the fluorescence off [127–129]. In a step forward in polytriazole polymers exhibiting aggregation-induced emission, hyperbranched structures with spring-like architectures were described. They exhibited this behavior due to the high compressibility of polymer spheres from solution to aggregates, thus permitting the detection of PA and TNT explosives with the superamplification effect [130].

The sensitivity of sensory materials depends also on physical aspects. Thus, solution-dispersed porous hyperbranched conjugated polymer NPs showed enhanced fluorescence sensitivity toward TNT, both as dispersion and in a solid state. The porous conjugated polymer network structure, prepared by Pd-catalyzed Suzuki cross-coupling polymerization of tris{4-(4,4,5,5-tetramethyl-[1,3,2]dioxa-borolane)phenyl}amine and 1,3,5-tribromobenzene in organic-in-water emulsion, played an important role in facilitating the diffusion of the target explosive [131].

Trace detection of peroxide vapors was carried out with a microcantilever sensor. A self-assembled monomer monolayer gave rise to chain polymerization in the presence of hydrogen peroxide radicals, causing a deflection of the cantilever [132]. Hydrogen peroxide (H_2O_2) is a peroxide explosive simulant, also present in home-made TATP and HMTD as it is employed in its synthesis, and is simultaneously a degradation product of explosives [133]. The bleaching capability of H_2O_2 was exploited as a color test in which the dye lissamine green was encapsulated with PVA; bleaching was observed with H_2O_2 vapor and also with other strong volatile oxidants, such as ozone and chlorine [134]. Filter papers coated with poly[3′,6′-bis(1,3,2-dioxaborinane)fluoran] gave rise to fluorescein upon entering into contact with H_2O_2 vapors, turning on the fluorescence of the strips [135]. A H_2O_2 sensor based on poly(vinyl alcohol)-multiwalled carbon nanotubes-platinum NPs hybrids modified glassy carbon electrode was also reported [136]. AgNPs decorated with poly(*m*-phenylenediamine) microparticles had a significant boost in catalytic performance toward the reduction of hydrogen peroxide H_2O_2. The sensor prepared with such composites showed a fast amperometric response time of less than 5 s with a LOD of <4 μM at the signal-to-noise ratio of 3 [137, 138]. The colorimetric detection of H_2O_2 in solution was tackled by a stimuli-triggered charge-generation polymer with AuNPs. The presence of H_2O_2 triggered the transformation of the neutral polymer to a cationic polyelectrolyte via the deprotection of carbamate-based amine protecting moieties. The cationic polyelectrolyte caused the aggregation of negatively charged AuNPs with the concomitant red shift of the surface plasmon resonance band [139].

26.4   Conclusion and Future Outlook

The detection and quantification of chemical species are key objectives of chemistry. For these purposes, a number of methodologies based on potent analytical techniques have been developed, such as gas chromatography-mass spectroscopy (GC-MS) or ion mobility spectrometry. These techniques have pros and cons, the former related with their selectiveness and sensitiveness and the latter with their high price, bulkiness, environment and maintenance requirements, as well as the requirement of highly trained personnel. The growth of the chemosensing field, associated with the sensing of a target chemical species by a receptor, the sensing relying on easily measurable transductions (even on a visible signal), is bringing

about a new era in the development of cheap, portable sensory devices, able to be used without training.

However, the discrete and low molecular mass receptor molecules exhibit significant drawbacks related with light and thermal instability, the migration in supported materials, the lack of solubility in water that hampers their use in this media, and as overall the absence of behavior as materials. On the other hand, polymer chemosensors can be directly prepared, transformed, and used as sensory materials (e.g., films, coatings, and labels). Moreover, the sensory motifs chemically anchored to the polymer backbone do not migrate, and the polymer structure provides higher thermal and mechanical resistance. Additionally, the materials can be used for sensing vapor species or species in water or organic solution by simply adjusting the chemical composition of the polymer to fit the affinity (e.g., hydrophilicity or hydrophobicity) toward the measuring media. Additionally, polymers exhibit cooperative properties that give rise to signal amplification with concomitant increase in sensitivity.

Among the target molecules, explosives and chemical warfare agents are of special interest and require a sensitive but selective way of detecting these chemicals for homeland and civil security applications, as well as for environmental and humanitarian endeavors (e.g., soil remediation and demining), and health and safety at work. The aforementioned attributes make polymer chemosensors the best choice when designing and developing chemosensory materials for explosive sensing. The field is open to further developments, such as naked eye sensing using smart labels and fibers, higher sensitivity, and selectivity sensing using conjugated and nonconjugated polymers. Other novel applications include sensory arrays coupled with statistical data treatment, coupling sensing materials with the availability, portability, and power of data analysis using mobile phones and tablets.

References

1. Pacsial-Ong EJ, Aguilar ZP (2013) Chemical warfare agent detection: a review of current trends and future perspective. Front Biosci (Schol Ed) S5:516–543
2. García JM, García FC, Serna F, de la Peña JL (2011) Fluorogenic and chromogenic polymer chemosensors. Polym Rev 51:341–390
3. Royo S, Martínez-Máñez R, Sancenón F, Costero AM, Parra M, Gil S (2007) Chromogenic and fluorogenic reagents for chemical warfare nerve agents detection. Chem Commun 4839–4847
4. Sadik OA, Land WH Jr, Wang J (2003) Targeting chemical and biological warfare agents at the molecular level. Electroanalysis 15:1149–1159
5. Hoenig SL (2007) Compendium of chemical warfare agents. Springer, New York, NY
6. Kim K, Tsay OG, Atwood DA, Churchill DG (2011) Destruction and detection of chemical warfare agents. Chem Rev 111:5345–5403

7. Rochat S, Swager TM (2013) Conjugated amplifying polymers for optical sensing applications. ACS Appl Mater Interfaces 5:4488–4502
8. Skotheim TA, Reynolds JR (eds) (2007) Handbook of conducting polymers. Conjugated polymers, theory, synthesis, properties and characterization. CRC Press, Boca Raton, FL
9. McQuade DT, Pullen AE, Swager TM (2000) Conjugated polymer-based chemical sensors. Chem Rev 100:2537–2574
10. Collins GE, Buckley LJ (1996) Conductive polymer-coated fabrics for chemical sensing. Synth Met 78:93–101
11. Collins GE, Buckley LJ (1997) Conductive polymer coated fabrics for chemical sensing. US Patent 5,674,752
12. Bansal L, El-Sherif M (2005) Intrinsic optical-fiber sensor for nerve agent sensing. IEEE Sens J 5:648–655
13. Hosseini SH, Ansari R, Noor P (2013) Application of polyaniline film as a sensor for stimulant nerve agents. Phosphorus Sulfur Silicon Relat Elem 188:1394–1401
14. Jo S, Kim D, Son S-H, Kim Y, Lee TS (2014) Conjugated poly(fluorene-quinoxaline) for fluorescence imaging and chemical detection of nerve agents with its paper-based strip. ACS Appl Mater Interfaces 6:1330–1336
15. Lee JS, Shin DH, Jun J, Jang J (2013) Multidimensional polypyrrole/iron oxyhydroxide hybrid nanoparticles for chemical nerve gas agent sensing application. ACS Nano 7:10139–10147
16. Kwon OS, Park SJ, Lee JS, Park E, Kim T, Park H-W, You SA, Yoon H, Jang J (2012) Multidimensional conducting polymer nanotubes for ultrasensitive chemical nerve agent sensing. Nano Lett 12:2797–2802
17. Wang F, Gu H, Swager TM (2008) Carbon nanotube/polythiophene chemiresistive sensors for chemical warfare agents. J Am Chem Soc 130:5392–5393
18. Vergara AV, Pernites RB, Pascua S, Binag CA, Advincula RC (2012) QCM sensing of a chemical nerve agent analog via electro polymerized molecularly imprinted polythiophene films. J Polym Sci A Polym Chem 50:675–685
19. Shulga OV, Palmer C (2006) Detection of V-type nerve agent degradation products at electrodes modified by PPy/PQQ using CaCl as supporting electrolyte. Anal Bioanal Chem 385:1116–1123
20. Jenkins AL, Bae SY (2005) Molecularly imprinted polymers for chemical agent detection in multiple water matrices. Anal Chim Acta 542:32–37
21. Prathish KP, Vishnuvardhan V, Prasada Rao T (2009) Rational design of in situ monolithic imprinted polymer membranes for the potentiometric sensing of diethyl chlorophosphate–a chemical warfare agent simulant. Electroanalysis 21(9):1048–1056
22. Jenkins AL, Uy OM, Murray GM (1999) Polymer-based lanthanide luminescent sensor for detection of the hydrolysis product of the nerve agent Soman in water. Anal Chem 71:373–378
23. Boyd JW, Cobb GP, Southard GE, Murray GM (2004) Development of molecularly imprinted polymer sensors for chemical warfare agents. Johns Hopkins APL Tech Dig 25:44–49
24. Southard GE, Van Houten KA, Ott EW Jr, Murray GM (2007) Luminescent sensing of organophosphates using europium(III) containing imprinted polymers prepared by RAFT polymerization. Anal Chim Acta 581:202–207
25. Prathish KP, Prasad K, Rao TP, Suryanarayana MVS (2007) Molecularly imprinted polymer-based potentiometric sensor for degradation product of chemical warfare agents Part I. Methylphosphonic acid. Talanta 71:1976–1980
26. Diehl KL, Anslyn EV (2013) Array sensing using optical methods for detection of chemical and biological hazards. Chem Soc Rev 42:8596–8611
27. Joo B-S, Huh J-S, Lee D-D (2007) Fabrication of polymer SAW sensor array to classify chemical warfare agents. Sens Actuators B 121:47–53
28. Matatagui D, Martí J, Fernández MJ, Fontecha JL, Gutiérrez J, Gràcia I, Cané C, Horrillo MC (2011) Chemical warfare agents simulants detection with an optimized SAW sensor array. Sens Actuators B 154:199–205

29. Di Pietrantonio F, Benetti M, Cannata D, Verona E, Palla-Papavlu A, Dinca V, Dinescu M, Mattle T, Lippert T (2012) Volatile toxic compound detection by surface acoustic wave sensor array coated with chemoselective polymers deposited by laser induced forward transfer: application to sarin. Sens Actuators B 174:158–167

30. Cannatà D, Benetti M, Di Pietrantonio F, Verona E, Palla-Papavlu A, Dinca V, Dinescu M, Lippert T (2012) Nerve agent simulant detection by solidly mounted resonators (SMRs) polymer coated using laser induced forward transfer (LIFT) technique. Sens Actuators B 173:32–39

31. Alizadeh T, Zeynali S (2008) Electronic nose based on the polymer coated SAW sensors array for the warfare agent simulants classification. Sens Actuators B 129:412–423

32. Matatagui D, Fernández MJ, Fontecha J, Santos JP, Gràciab I, Cané C, Horrillo MC (2012) Love-wave sensor array to detect, discriminate and classify chemical warfare agent simulants. Sens Actuators B 175:173–178

33. Mlsna TE, Cemalovic S, Warburton M, Hobson ST, Mlsna DA, Patel SV (2006) Chemicapacitive microsensors for chemical warfare agent and toxic industrial chemical detection. Sens Actuators B 116:192–201

34. Hopkins AR, Lewis NS (2001) Detection and classification characteristics of arrays of carbon black/organic polymer composite chemiresistive vapor detectors for the nerve agent simulants dimethylmethylphosphonate and diisopropylmethylphosonate. Anal Chem 73:884–892

35. Hartmann-Thompson C, Keeley DL, Rousseau JR, Dvornic PR (2009) Fluorescent dendritic polymers and nanostructured coatings for the detection of chemical warfare agents and other analytes. J Polym Sci A Polym Chem 47:5101–5115

36. Sarkar S, Shunmugam R (2014) Polynorbornene derived 8-hydroxyquinoline paper strips for ultrasensitive chemical nerve agent surrogate sensing. Chem Commun 50:8511–8513

37. Shunmugam R, Tew GN (2008) Terpyridine–lanthanide complexes respond to fluorophosphate containing nerve gas G-agent surrogates. Chem Eur J 14:5409–5412

38. Bhadury PS, Dubey V, Singh S, Saxena C (2005) 2,2-Bis(3-allyl-4-hydroxyphenyl) hexafluoropropane and fluorosiloxane as coating materials for nerve agent sensors. J Fluorine Chem 126:1252–1256

39. Maji S, Asrey R, Kumar S, Saxena C, Kumar N, Vyas KD, Banerjee S (2010) Polymer-coated piezoelectric quartz crystal sensor for sensing the nerve agent simulant dimethyl methylphosphonate vapor. J Appl Polym Sci 116:3708–3717

40. Ewing RW, Waltman MJ, Atkinson DA, Grate JW, Hotchkiss PJ (2013) The vapor pressures of explosives. Trend Anal Chem 42:35–48

41. Buryakov A, Buryakov TI, Matsaev VT (2014) Optical chemical sensors for the detection of explosives and associated substances. J Anal Chem 69:616–631

42. Thomas SW III, Joly GD, Swager TM (2007) Chemical sensors based on amplifying fluorescent conjugated polymers. Chem Rev 107:1339–1386

43. Toal SJ, Trogler WC (2006) Polymer sensors for nitroaromatic explosives detection. J Mater Chem 16:2871–2883

44. Hissler M, Dyer PW, Réau R (2003) Linear organic π -conjugated systems featuring the heavy group 14 and 15 elements. Coord Chem Rev 244:1–44

45. Salinas Y, Martínez-Máñez R, Marcos MD, Sancenón F, Costero A, Parra M, Gil S (2012) Optical chemosensors and reagents to detect explosives. Chem Soc Rev 41:1261–1296

46. Germain ME, Knapp MJ (2009) Optical explosives detection: from color changes to fluorescence turn-on. Chem Soc Rev 38:2543–2555

47. Cumming CJ, Aker C, Fisher M, Fox M, la Grone MJ, Reust D, Rockley MG, Swager TM, Towers E, Williams V (2001) Using novel fluorescent polymers as sensory materials for above-ground sensing of chemical signature compounds emanating from buried landmines. IEEE Trans Geosci Remote Sensing 39:1119–1128

48. Yang J-S, Swager TM (1998) Fluorescent porous polymer films as TNT chemosensors: electronic and structural effects. J Am Chem Soc 120:11864–11873

49. Yang J-S, Swager TM (1998) Porous shape persistent fluorescent polymer films: an approach to TNT sensory materials. J Am Chem Soc 120:5321–5322

50. Levitsky IA, Kim J, Swager TM (1999) Energy migration in a poly(phenylene ethynylene): determination of interpolymer transport in anisotropic Langmuir-Blodgett films. J Am Chem Soc 121:1466–1472

51. Zahn S, Swager TM (2002) Three-dimensional electronic delocalization in chiral conjugated polymers. Angew Chem Int Ed 41:4225–4230

52. Amara JP, Swager TM (2005) Synthesis and properties of poly(phenylene ethynylene)s with pendant hexafluoro-2-propanol groups. Macromolecules 38:9091–9094

53. Thomas SW III, Swager TM (2006) Trace hydrazine detection with fluorescent conjugated polymers: a turn-on sensory mechanism. Adv Mater 18:1047–1050

54. Rose A, Lugmair CG, Swager TM (2001) Excited-state lifetime modulation in triphenylene-based conjugated polymers. J Am Chem Soc 123:11298–11299

55. Yamaguchi S, Swager TM (2001) Oxidative cyclization of bis(biaryl)acetylenes: synthesis and photophysics of dibenzo[g,p]chrysene-based fluorescent polymers. J Am Chem Soc 123:12087–12088

56. Albert KJ, Myrick ML, Brown SB, James DL, Milanovich FP, Walt DR (2001) Field-deployable sniffer for 2, 4-dinitrotoluene detection. Environ Sci Technol 35:3193–3200

57. Rose A, Zhu Z, Madigan CF, Swager TM, Bulovic V (2005) Sensitivity gains in chemosensing by lasing action in organic polymers. Nature 434:876–879

58. Gopalakrishnan D, Dichtel WR (2013) Direct detection of RDX vapor using a conjugated polymer network. J Am Chem Soc 135:8357–8362

59. Deng C, He Q, He C, Shi L, Cheng J, Lin T (2010) Conjugated polymer–titania nanoparticle hybrid films: random lasing action and ultrasensitive detection of explosive vapors. J Phys Chem B 114:4725–4730

60. Chang C, Chao C, Huang JH, Li A, Hsu C, Lin M, Hsieh B, Su A (2004) Fluorescent conjugated polymer films as TNT chemosensors. Synth Met 144:297–301

61. Zhou D, Swager TM (2005) Sensory responses in solution vs solid state: a fluorescence quenching study of poly(iptycenebutadiynylene)s. Macromolecules 38:9377–9384

62. Narayanan A, Varnavski PP, Swager TM, Goodson T (2008) Multiphoton fluorescence quenching of conjugated polymers for TNT detection. J Phys Chem C 112:881–884

63. Chen S, Zhang Q, Zhang J, Gu J, Zhang L (2010) Synthesis of two conjugated polymers as TNT chemosensor materials. Sens Actuators B 149:155–160

64. He G, Yan N, Yang J, Wang H, Ding L, Yin S, Fang Y (2011) Pyrene-containing conjugated polymer-based fluorescent films for highly sensitive and selective sensing of TNT in aqueous medium. Macromolecules 44:4759–4766

65. Novotney JL, Dichtel WR (2013) Conjugated porous polymers for TNT vapor detection. ACS Macro Lett 2:423–426

66. Saxena K, Kumar P, Jain VK (2010) Fluorescence quenching studies of conjugated polymer poly[2-methoxy-5-(3′,7′-dimethyloctyloxy)-1,4-phenylenevinylene] in the presence of TNT. J Lumin 130:2260–2264

67. Levitsky IA, Euler WB, Tokranova N, Rose A (2007) Fluorescent polymer-porous silicon microcavity devices for explosive detection. Appl Phys Lett 90:041904

68. Saxena A, Fujiki M, Rai R, Kwak G (2005) Fluoroalkylated polysilane film as a chemosensor for explosive nitroaromatic compounds. Chem Mater 17:2181–2185

69. Sohn H, Calhoun RM, Sailor MJ, Trogler WC (2001) Detection of TNT and picric acid on surfaces and in seawater using photoluminescent polysiloles. Angew Chem Int Ed 40:2104–2105

70. Sohn H, Sailor MJ, Magde D, Trogler WC (2003) Detection of nitroaromatic explosives based on photoluminescent polymers containing metalloles. J Am Chem Soc 125:3821–3830

71. Toal SJ, Sanchez J, Dugan RE, Trogler WC (2007) Visual detection of trace nitroaromatic explosive residue using photoluminescent metallole containing polymers. J Forensic Sci 52:79–83

72. Sanchez J, Urbas SA, Toal SJ, Trogler WC (2008) Catalytic hydrosilylation routes to divinylbenzene bridged silole and silafluorene polymers. Applications to surface imaging of explosive particulates. Macromolecules 41:1237–1245

73. Sanchez JC, Toal SJ, Wang Z, Dugan RE, Trogler WC (2007) Selective detection of trace nitroaromatic, nitramine, and nitrate ester explosive residues using a three-step fluorimetric sensing process: a tandem turn-off, turn-on sensor. J Forensic Sci 52:1308–1313

74. Sanchez JC, DiPasquale AG, Rheingold AL, Trogler WC (2007) Synthesis, luminescence properties and explosives sensing with 1,1-tetraphenylsilol- and 1,1-silafluorene-vinylene polymers. Chem Mater 19:6459–6470

75. Toal SJ, Magde D, Trogler WC (2005) Luminescent oligo(tetraphenyl)silole nanoparticles as chemical sensors for aqueous TNT. Chem Commun 43:5465–5467

76. Sanchez JC, Trogler WC (2008) Efficient blue-emitting silafluorene–fluorene-conjugated copolymers: selective turn-off/turn-on detection of explosives. J Mater Chem 18:3143–3156

77. Martinez HP, Grant CD, Reynolds JG, Trogler WC (2012) Silica anchored fluorescent organosilicon polymers for explosives separation and detection. J Mater Chem 22:2908–2914

78. Yang J, Aschemeyer S, Martinez HP, Trogler WC (2010) Hollow silica nanospheres containing a silafluorene–fluorene conjugated polymer for aqueous TNT and RDX detection. Chem Commun 46:6804–6806

79. Feng J, Li Y, Yang M (2010) Conjugated polymer-grafted silica nanoparticles for the sensitive detection of TNT. Sens Actuators B 145:438–443

80. Feng L, Li H, Qu Y, Lü C (2012) Detection of TNT based on conjugated polymer encapsulated in mesoporous silica nanoparticles through FRET. Chem Commun 48:4633–4635

81. Liu Y, Mills R, Boncella J, Schanze K (2001) Fluorescent polyacetylene thin film sensor for nitroaromatics. Langmuir 17:7452–7455

82. Nagarjuna G, Kumar A, Kokil A, Jadhav KG, Yurt S, Kumar J, Venkataraman D (2011) Enhancing sensing of nitroaromatic vapours by thiophene-based polymer films. J Mater Chem 21:16597–16602

83. Aguilar AD, Forzani ES, Leright M, Tsow F, Cagan A, Iglesias RA, Nagahara LA, Amlani I, Tsui R, Tao NJ (2010) A hybrid nanosensor for TNT vapor detection. Nano Lett 10:380–384

84. Zhang X, Jenekhe SA (2000) Electroluminescence of multicomponent conjugated polymers. 1. Roles of polymer/polymer interfaces in emission enhancement and voltage-tunable multicolor emission in semiconducting polymer/polymer heterojunctions. Macromolecules 33:2069–2082

85. Hou S, Ding M, Gao L (2003) Synthesis and properties of polyquinolines and polyanthrazolines containing pyrrole units in the main chain. Macromolecules 36:3826–3832

86. Kin TH, Kim HJ, Kwak CG, Park WH, Lee TS (2006) Aromatic oxadiazole-based conjugated polymers with excited-state intramolecular proton transfer: their synthesis and sensing ability for explosive nitroaromatic compounds. J Polym Sci A Polym Chem 44:2059–2068

87. Wang F, Wang W, Liu B, Wang Z, Zhang Z (2009) Copolypeptide-doped polyaniline nanofibers for electrochemical detection of ultratrace trinitrotoluene. Talanta 79:376–382

88. Cerruti M, Jaworski J, Raorane D, Zueger C, Varadarajan J, Carraro C, Lee S-W, Maboudian R, Majumdar A (2009) Polymer-oligopeptide composite coating for selective detection of explosives in water. Anal Chem 81:4192–4199

89. Kim TH, Lee BY, Jaworski J, Yokoyama K, Chung W-J, Wang E, Hong S, Majumdar A, Lee S-W (2011) Selective and sensitive TNT sensors using biomimetic polydiacetylene-coated CNT-FETs. ACS Nano 5:2824–2830

90. Thomas SW III, Amara JP, Bjork RE, Swager TM (2005) Amplifying fluorescent polymer sensors for the explosives taggant 2,3-dimethyl-2,3-dinitrobutane (DMNB). Chem Commun 36:4572–4574

91. Nie H, Zhao Y, Zhang M, Ma Y, Baumgarten M, Müllen K (2011) Detection of TNT explosives with a new fluorescent conjugated polycarbazole polymer. Chem Commun 47:1234–1236

92. Nie H, Sun G, Zhang M, Baumgarten M, Müllen K (2012) Fluorescent conjugated polycarbazoles for explosives detection: Side chain effects on TNT sensor sensitivity. J Mater Chem 22:2129–2132

93. Nguyen HH, Li X, Wang N, Wang ZY, Ma J, Bock WJ, Ma D (2009) Fiber optic detection of explosives using readily available fluorescent polymers. Macromolecules 42:921–926

94. Lu W, Xue M, Xu Z, Dong X, Xue F, Wang F, Wang Q, Meng Z (2015) Molecularly imprinted polymers for the sensing of explosives and chemical warfare agents. Curr Org Chem 19:62–71

95. Sharma PS, Kutner W, D'Souza F (2012) Molecular imprinting for selective sensing of explosives, warfare agents, and toxins. In: Nikolelis DP (ed) Portable chemical sensors: weapons against bioterrorism, NATO science for peace and security series A: chemistry and biology. Springer, Dordrecht

96. Stringer RC, Gangopadhyay S, Grant SA (2010) Detection of nitroaromatic explosives using a fluorescent-labeled imprinted polymer. Anal Chem 82:4015–4019

97. Bunte G, Hürttlen J, Pontius H, Hartlieb K, Krause H (2007) Gas phase detection of explosives such as 2,4,6-trinitrotoluene by molecularly imprinted polymers. Anal Chim Acta 591:49–56

98. Bunte G, Heil M, Ruseling D, Hurttlen J, Pontius H, Krause H (2009) Trace detection of explosives vapours by molecularly imprinted polymers for security measures. Propellants Explos Pyrotech 34:245–251

99. Roeseling D, Tuercke T, Krause H, Loebbecke S (2009) Microreactor-based synthesis of molecularly imprinted polymer beads used for explosive detection. Org Process Res Dev 13:1007–1013

100. Lin J, Kending CE, Nesterov EE (2007) Chemosensory performance of molecularly imprinted fluorescent conjugated polymer materials. J Am Chem Soc 129:15911–15918

101. Holthoff EL, Stratis-Cullum DN, Hankus ME (2011) A nanosensor for TNT detection based on molecularly imprinted polymers and surface enhanced Raman scattering. Sensors 11:2700–2714

102. Xie C, Liu B, Wang Z, Gao D, Guan G, Zhang Z (2008) Molecular imprinting at walls of silica nanotubes for TNT recognition. Anal Chem 80:437–443

103. Alizadeh T, Zare M, Ganjali MR, Norouzi P, Tavana B (2010) A new molecularly imprinted polymer (MIP)-based electrochemical sensor for monitoring 2,4,6-trinitrotoluene (TNT) un natural waters and soil samples. Biosens Bioelectron 25:1166–1172

104. Mamo SK, Gonzalez-Rodriguez J (2014) Development of a molecularly imprinted polymer-based sensor for the electrochemical determination of triacetone triperoxide (TATP). Sensors 14:23269–23282

105. Walker NR, Linman MJ, Timmers MM, Dean SL, Burkett CM, Lloyd JA, Keelor JD, Baughman BM, Edmiston PL (2007) Selective detection of gas-phase TNT by integrated optical waveguide spectrometry using molecularly imprinted sol–gel sensing films. Anal Chim Acta 593:82–91

106. Huynh T-P, Sosnowska M, Sobczak JW, KC CB, Nesterov VN, D'Souza F, Kutner W (2013) Simultaneous chronoamperometry and piezoelectric microgravimetry determination of nitroaromatic explosives using molecularly imprinted thiophene polymers. Anal Chem 85:8361–8368

107. Riskin M, Tel-Vered R, Willner I (2010) Imprinted Au-nanoparticle composites for the ultra-sensitive surface plasmon resonance detection of hexahydro-1,3,5-trinitro-1,3,5-triazine/RDX). Adv Mater 22:1387–1391

108. Riskin M, Tel-Vered R, Bourenko T, Granot E, Willner I (2008) Imprinting of molecular recognition sites through electropolymerization of functionalized Au nanoparticles: development of an electrochemical TNT sensor based on π-donor−acceptor interactions. J Am Chem Soc 130:9726–9733

109. Xie C, Zhang Z, Wang D, Guan G, Gao D, Liu J (2006) Surface molecular self-assembly strategy for TNT imprinting of polymer nanowire/nanotube arrays. Anal Chem 78:8339–8346

110. Matzger AJ, Vaid TP, Lewis NS (1999) Vapor sensing with arrays of carbon black-polymer composites. Proc SPIE Int Soc Opt Eng 3710:315–320

111. Briglin SM, Burl MC, Freund MS, Lewis NS, Matzger AJ, Ortiz DN, Tokumaru P (2000) Progress in use of carbon-black-polymer composite vapor detector arrays for land mine detection. Proc SPIE Int Soc Opt Eng 4038:530–538

112. Pablos JL, Sarabia LA, Ortiz MC, Mendia A, Muñoz A, Serna F, García FC, García JM (2015) Selective detection and discrimination of nitro explosive vapors using an array of three luminescent sensory solid organic and hybrid polymer membranes. Sens Actuators B 212:18–27

113. Woodka MD, Schnee VP, Polcha MP (2010) Fluorescent polymer sensor array for detection and discrimination of explosives in water. Anal Chem 82:9917–9924

114. McGill RA, Mlsna TE, Chung R, Nguyen VK, Stepnowski J (2000) The design of functionalized silicone polymers for chemical sensor detection of nitroaromatic compounds. Sens Actuators B 65:5–9

115. Kannan GK, Nimal AT, Mittal U, Yadava RDS, Kapoor JC (2004) Adsorption studies of carbowax coated surface acoustic wave (SAW) sensor for 2,4-dinitro toluene (DNT) vapour detection. Sens Actuators B 101:328–334

116. Yang X, Du XX, Shi J, Swanson B (2001) Molecular recognition and self-assembled polymer films for vapour phase detection of explosives. Talanta 54:439–445

117. Dorozhkin LM, Nefedov VA, Sabelnikov AG, Sevastjanov VG (2004) Detection of trace amounts of explosives and/or explosive related compounds on various surfaces by a new sensing technique/material. Sens Actuators B 99:568–570

118. Pablos JL, Trigo-Lopez M, Serna F, García FC, García JM (2014) Solid polymer substrates and smart fibres for the selective visual detection of TNT both in vapour and in aqueous media. RSC Adv 4:25562–25568

119. Pablos JL, Trigo-Lopez M, Serna F, García FC, García JM (2014) Water-soluble polymers, solid polymer membranes, and coated fibres as smart sensory materials for the naked eye detection and quantification of TNT in aqueous media. Chem Commun 50:2484–2487

120. Kumar A, Pandey MK, Anandakathir R, Mosurkal R, Parmar VS, Watterson AC, Kumar J (2010) Sensory response of pegylated and siloxanated 4,8-dimethylcoumarins: a fluorescence quenching study by nitro aromatics. Sens Actuators B 147:105–110

121. Demirel GB, Daglarac B, Bayindir M (2013) Extremely fast and highly selective detection of nitroaromatic explosive vapours using fluorescent polymer thin films. Chem Commun 49:6140–6142

122. Liu J, Zhong Y, Lam JWY, Lu P, Hong Y, Yu Y, Yue Y, Faisal M, Sung HHY, Williams ID, Wong KS, Tang BZ (2010) Hyperbranched conjugated polysiloles: synthesis, structure, aggregation-enhanced emission, multicolor fluorescent photopatterning, and superamplified detection of explosives. Macromolecules 43:4921–4936

123. Liu J, Zhong Y, Lu P, Hong Y, Lam JWY, Faisal M, Yu Y, Wong KS, Tang BZ (2010) A superamplification effect in the detection of explosives by a fluorescent hyperbranched poly(silylenephenylene) with aggregation-enhanced emission characteristics. Polym Chem 1:426–429

124. Hong Y, Lam JWY, Tang BZ (2009) Aggregation-induced emission: phenomenon, mechanism and applications. Chem Commun 4332–4353

125. Shu W, Guan C, Guo W, Wang C, Shen Y (2012) Conjugated poly(aryleneethynylenesiloles) and their application in detecting explosives. J Mater Chem 22:3075–3081

126. Zhang L-H, Jiang T, Wu L-B, Wan J-H, Chen C-H, Pei Y-B, Lu H, Deng Y, Bian G-F, Qiu H-Y, Lai G-Q (2012) 2,3,4,5-Tetraphenylsilole-based conjugated polymers: synthesis, optical properties, and as sensors for explosive compounds. Chem Asian J 7:1583–1593

127. Qin A, Lam JWY, Tang L, Jim CKW, Zhao H, Sun J, Tang BZ (2009) Polytriazoles with aggregation-induced emission characteristics: synthesis by click polymerization and application as explosive chemosensors. Macromolecules 42:1421–1424

128. Hu R, Lam JWY, Liu J, Sung HHY, Williams ID, Yue Z, Wong KS, Yuend MMF, Tang BZ (2012) Hyperbranched conjugated poly(tetraphenylethene): synthesis, aggregation-induced emission, fluorescent photopatterning, optical limiting and explosive detection. Polym Chem 3:1481–1489

129. Li J, Liu J, Lama JWY, Tang BZ (2013) Poly(arylene ynonylene) with an aggregation-enhanced emission characteristic: a fluorescent sensor for both hydrazine and explosive detection. RSC Adv 3:8193–8196

130. Wang J, Mei J, Yuan W, Lu P, Qin A, Sun J, Mac Y, Tang BZ (2011) Hyperbranched polytriazoles with high molecular compressibility: aggregation-induced emission and superamplified explosive detection. J Mater Chem 21:4056–4059

131. Wu JX, Li H, Xu B, Tong H, Wang L (2014) Solution-dispersed porous hyperbranched conjugated polymer nanoparticles for fluorescent sensing of TNT with enhanced sensitivity. Polym Chem 5:4521–4525

132. Lock JP, Geraghty E, Kagumba LC, Mahmud KK (2009) Trace detection of peroxides using a microcantilever detector. Thin Solid Films 517:3584–3587

133. Burks M, Hage DS (2009) Current trends in the detection of peroxide-based explosives. Anal Bioanal Chem 395:301–313

134. Mills A, Grosshans P, Snadden E (2009) Hydrogen peroxide vapour indicator. Sens Actuators B 136:458–463

135. Sanchez JC, Trogler WC (2008) Polymerization of a boronate-functionalized fluorophore by double transesterification: applications to fluorescence detection of hydrogen peroxide vapor. J Mater Chem 18:5134–5141

136. Fang Y, Zhang D, Qina X, Miaoa Z, Takahashib S, Anzaib J-I, Chen Q (2012) A non-enzymatic hydrogen peroxide sensor based on poly(vinyl alcohol)–multiwalled carbon nanotubes–platinum nanoparticles hybrids modified glassy carbon electrode. Electrochim Acta 70:266–271

137. Tian J, Li H, Lu W, Luo Y, Wanga L, Sun X (2011) Preparation of Ag nanoparticle-decorated poly(m-phenylenediamine) microparticles and their application for hydrogen peroxide detection. Analyst 136:1806–1809

138. Wu Z, Yang S, Chen Z, Zhang T, Guo T, Wang Z, Liao F (2013) Synthesis of Ag nanoparticles-decorated poly(m-phenylenediamine) hollow spheres and the application for hydrogen peroxide detection. Electrochim Acta 98:104–108

139. Li C, Hu J, Liu T, Liu S (2011) Stimuli-triggered off/on switchable complexation between a novel type of charge-generation polymer (CGP) and gold nanoparticles for the sensitive colorimetric detection of hydrogen peroxide and glucose. Macromolecules 44:429–431

Chapter 27
Smart Polymeric-Based Microencapsulation: A Promising Synergic Combination

Felisa Reyes-Ortega and Majid Hosseini

Abstract Microencapsulation technology can be used to provide protection, control the release of the loaded material, negate compatibility issues, and avoid toxicity of the encapsulated materials. Microencapsulation provides the possibility of combining different types of smart polymers, thus achieving specific properties that are difficult to get using other techniques. This chapter describes the combination of microencapsulation technology using smart polymers for industrial applications, such as coatings and paints (encapsulation of self-healing agents), construction (encapsulation of phase-change materials), textile industry (encapsulation of thermal or moisture-sensitive polymers and light-responsive polymers), food and beverage industry (encapsulation of a vitamin, flavor, or aromatic substance), pharmaceutical formulations (encapsulation of a drug for its protection or controlled drug delivery), biomedical applications (encapsulation of a specific anticancer drug for target therapy, cell-based systems, and DNA or RNA encapsulation), and aerospace and automobiles applications (encapsulation of self-healing materials, flame retardant, plasticizers, and catalysts).

Keywords Stimuli-responsive polymer • Microencapsulation • Smart microcapsules • Controlled release • Self-healing

F. Reyes-Ortega
Tecnologías Avanzadas Inspiralia, S.L., Parque Científico de Madrid,
C/ Faraday 7, Cantoblanco 28049, Madrid, Spain

M. Hosseini (✉)
Manufacturing and Industrial Engineering Department, College of Engineering and Computer Science, The University of Texas – Rio Grande Valley,
Edinburg, TX, USA
e-mail: majid.hosseini01@utrgv.edu

27.1 Introduction

Smart materials are generally defined as those that are able to alter, in a controllable manner, a central characteristic upon introduction of an external stimulus. This external stimulus can be temperature, voltage, magnetic field, light, pH of the media, or a combination thereof. One of the most dynamic classes of polymers is those that are called "smart polymers". A smart polymer undergoes an abrupt physical alteration as a reaction to variations occurring in its environment [1]. The major identifier that allows a polymer to be called "smart" is their aptitude for sensing minute and localized environmental changes and responding to such changes accordingly. Such systems are also called "intelligent polymers" because small changes occur in response to an external trigger until a critical point is reached, returning to their former structure after the trigger is removed. The key ability of these materials is not just being able to respond to external cues, but they can also revert back to their original form once the stimulus has been removed [2]. The use of smart polymers is increasing noticeably for many applications, due to their sophisticated characteristics. Besides, these kinds of polymers can be potentially interesting when they are used as microencapsulation systems. Over the last few decades, researchers have delved deeper into the field of smart polymers. These soluble/insoluble stimuli/ environmentally sensitive systems have been utilized in biotechnology, biomedical, and various engineering fields [3].

Microspheres/capsules (i.e., with diameters of one to hundreds of micrometers) surround the desired compound, thus encapsulating it and defining microencapsulation technology. By utilizing a multitude of polymeric and non-polymeric compounds (e.g., poly(ethylene glycol)s [4] (PEGs), poly(methacrylate)s [5], poly(styrene)s [6] (PSts), cellulose [7], polyurethanes (PU) [8], poly(lactide)s (PLAs), poly(lactide-co-glycolide)s [9], gelatin [10], and acacia), the encapsulation process has proven successful for various active materials (e.g., drugs, enzymes, vitamins, pesticides, flavors, and catalysts). These systems will release their contents via various mechanisms which are highly dependent upon the payloads' end use. Implemented in many fields, such as food, agricultural, textile, and pharmaceutical, this methodology has even been used in the defense sector where self-healing composite materials were first conceptualized as along with chemical decontaminating fabrics [8]. The active compound is trapped via the formation of microparticles within the polymeric matrix. The delivery of the compound is dependent upon the type of microparticle employed within the system, either microspheres or microcapsules. Microspheres are homogeneous blends of those active compounds and raw materials; microcapsules, on the other hand, have a core [where the compound (solid, liquid, or gas) is loaded] that is typically delimited by the raw material [11].

The production of both categories of microparticles varies greatly in both raw materials (i.e., synthetic and natural) and in synthesizing methodology, thus yielding various microparticles differing in particle distribution and size, makeup, surface chemistry, topography, and morphology. The following features high-
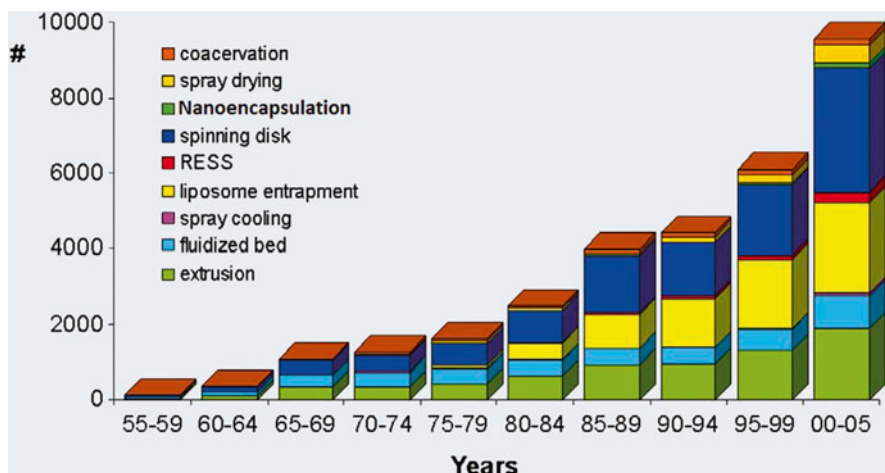
Fig. 27.1 Trends in microencapsulation technologies (Adapted with permission from [17], copyright Elsevier)

light the properties of microparticles that enable them as viable candidates for the microencapsulation process [11]: encapsulated materials' controlled release, supply of protection to the inner material from harsh reactions in the external environment, ability to mask organoleptic properties of the active compound, and easy handling of the finished product. Monocored, polycored, and matrix types are the three main categories of microcapsules. Monocored microcapsules consist of a singular hollow cavity, while polycore indicates multiple cavities of various shapes and sizes within the shell. The matrix type incorporates the active components into the shell's matrix.

Various methods can be employed to synthesize these systems, such as the solvent evaporation method, organic phase separation, interfacial polymerization, multiple emulsion technique, nanoprecipitation, and spray drying [12], to name a few. These techniques are briefly discussed in this chapter. The most common methodologies used to prepare external sensitive-responsive polymers are related to the typical polymer synthesis reactions that yield a well-defined and controlled structure. For the preparation of polymeric microparticles, it is necessary to synthesize amphiphilic (both hydrophilic and hydrophobic) polymer structures that are able to form core–shell microparticles. There are many factors to consider for the development of nanoparticle systems [13], but the most important are the kind of material [14], the amount of active agent to be incorporated [15], particle stability [16], release pharmacokinetics [5], and toxicity. Figure 27.1 shows the trends in different microencapsulation technologies reported over 50 years [17].

27.2   Microencapsulation Techniques: A General Overview

Microencapsulation methodologies are comprised of two general classes: chemical and physical/mechanical. Examples of chemical processes, where the microsphere creation is via a chemical reaction, are free-radical emulsion polymerization, interfacial polycondensation, dispersion, and suspension polymerization [18]. Furthermore, when utilizing the interfacial polycondensation method, shell morphology is dictated by the monomers' reactivity and reaction kinetics. The microcapsules' sizes are obtained by the temperature of the reaction, stir rate, and agitator blade choice [19]. The formation of the capsules also relies upon the presence of surface active agents. The second category consists of those methods in which the starting materials are polymers. Hence, in these methods no chemical reactions are involved, and only shape fabrication takes place. Of the physical/mechanical methods, solvent evaporation/extraction, coacervation/phase separation, precipitation, spinning disk, supercritical fluid expansion, melt solidification, co-extrusion, and LBL depositions can be mentioned [18–20]. Generally, the microencapsulation method chosen is dictated by the characteristics of the materials (e.g., polymers, monomers) used. Microencapsulated products can have a variety of compositional as well as morphological characteristics, all of which are determined by the combination of materials and methodologies.

Herein, commonly used microencapsulation techniques including emulsion polymerization, interfacial polycondensation, suspension cross-linking, solvent evaporation/solvent extraction, coacervation/phase separation, spray drying, fluidized bed coating, polymer precipitation, co-extrusion process, layer-by-layer deposition, supercritical fluid, and spinning disk are briefly discussed.

In the emulsion polymerization method [12], dropwise addition of the monomer (alkyl acrylates) to a stirred aqueous polymerization medium with the component to be encapsulated (core material), along with a suitable emulsifier, is completed. Once polymerization starts, the polymer initially synthesized precipitates into the aqueous medium, forming primary nuclei. As the process progresses, gradual nuclei growth coincides with entrapment of the active material, thus creating the microcapsules. This method is typically employed for lipophilic material encapsulation.

Interfacial polycondensation consists of a pair of complementary monomers polycondensing at the two-phase system's interface [21]. To synthesize microcapsules, the two-phase system is mixed while maintaining carefully controlled conditions to create small drops of the dispersed phase in the continuous suspension/phase medium [21, 22]. The active component that is going to be encapsulated is deliberately chosen so as to be dissolved/dispersed in the drops [22]. Also, in order to avoid the coalescence of the drops or the aggregation of particles, a tiny portion of stabilizer is added during the process and ensuing capsule creation [22]. Implementation of interfacial polycondensation can create monocore- or matrix-type microcapsules, determined by the polycondensates in the droplet phase. Should the matrix be soluble in the droplets, matrix-type microcapsules are formed, if insoluble monocore-type microcapsules are achieved via precipitation.

The suspension cross-linking technique realizes its potential when used to encapsulate proteins and polysaccharides [18]. This method disperses small drops of an aqueous polymeric solution of core materials into an immiscible organic solvent, alongside the presence of a stabilizer in the suspending medium in order to segregate the droplets/microcapsules [18, 23]. Covalent cross-linking stiffens the drops, thus converting them into microcapsules. Suspension cross-linking is another robust method that can encapsulate soluble, insoluble, liquid, or solid materials at both the micro- and nanoscale.

While similarities can be found between the creation of microcapsules via solvent evaporation/solvent extraction and suspension cross-linking, the former typically uses polyester which is hydrophobic [21]. The polymer and active component are dissolved and/or dispersed in a volatile organic solvent (e.g., chloroform and dichloromethane) immiscible or partly miscible in water [21]. The solution is added via a drop-by-drop addition to a stirred aqueous solution along with a stabilizer [i.e., poly (vinyl alcohol) or poly (vinyl-pyrrolidone)] and creates small droplets of polymer that encase the active component [24]. After solvent removal, the droplets are hardened and yield polymer microcapsules. Solvent removal takes place by either evaporation (i.e., heat, vacuum) or by extraction (introduction of a polymer precipitant, water and solvent miscible) [24]. Microcapsules formed by extraction were found to have greater porosity than those by evaporation [24]. A schematic illustration of the use of the solvent evaporation/solvent extraction technique in microsphere preparation showing the four principal process steps (i.e., incorporation of the bioactive compound, droplet formation, solvent removal, and microsphere harvest and drying) is presented in Fig. 27.2 [12]. Different morphologies of poly (D,L-lactide) [PDLLA] microspheres prepared by the solvent evaporation and solvent extraction are also shown in the photomicrographs of Fig. 27.3 [25].

Coacervation/phase separation, often used for gelatin and gelatin–acacia microcapsules along with cellulose and synthetic-based products, is another method presented [26]. These phase separation processes can be categorized as either simple or complex [26, 27]. Simple coacervation deals with a singular polymer (i.e., gelatin, ethyl cellulose) in either an aqueous or organic medium. The complex method includes a pair of polymers that are charged differently (e.g., gelatin and acacia) but are both soluble in the aqueous medium employed in the process. In either of these situations, coacervation takes place in a 40–50 °C prepared aqueous polymer solution where dispersion of the active material has already been completed. In order to avoid coagulation of the resulting microcapsules, a stabilizer may be added as well. Furthermore, a de-solvating/coacervating agent is slowly added, creating somewhat de-solvated polymeric molecules, precipitating on the core particles' surface [26, 27].

Spray drying is most often utilized in fragrance, oil, and flavor encapsulation [28]. For this method, preparation of the emulsion is done so through core material dispersion (i.e., immiscible material like oil with water) in a concentrated wall component solution [28]. The slurry is pumped into a revolving disk and is then transported to a spray drier where the produced emulsion is atomized into a mist. At this stage, evaporation of the emulsion's water content is completed, leaving the dry,
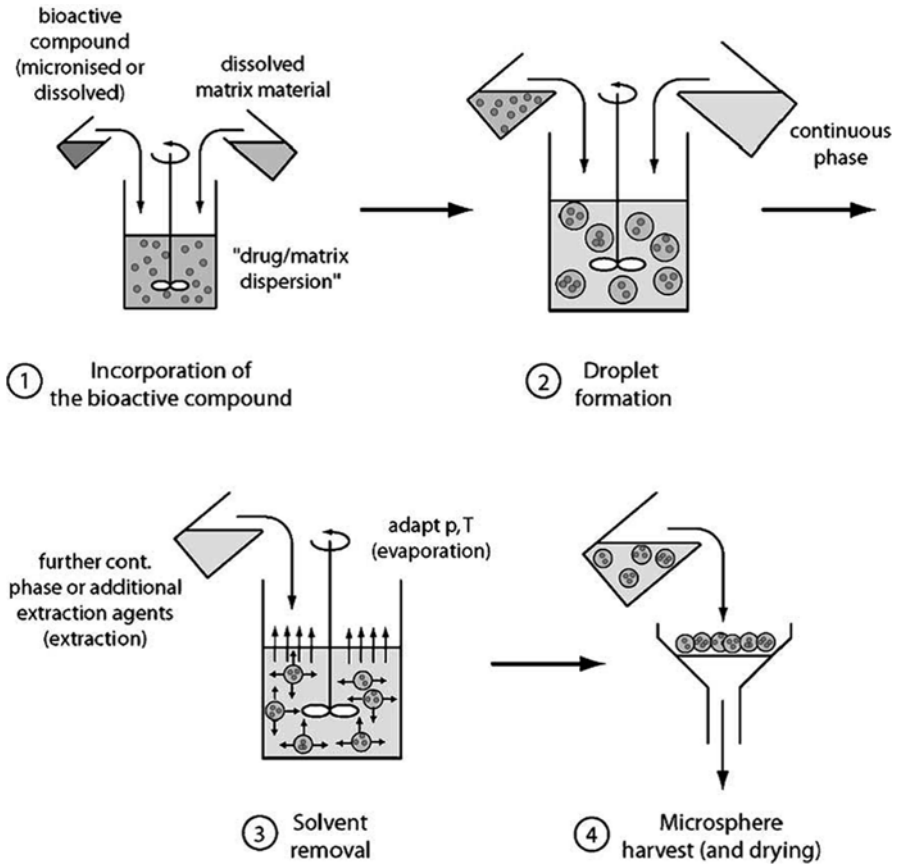
Fig. 27.2 The four principal process steps in microsphere preparation by solvent extraction/evaporation (Reprinted with permission from [12], copyright Elsevier)
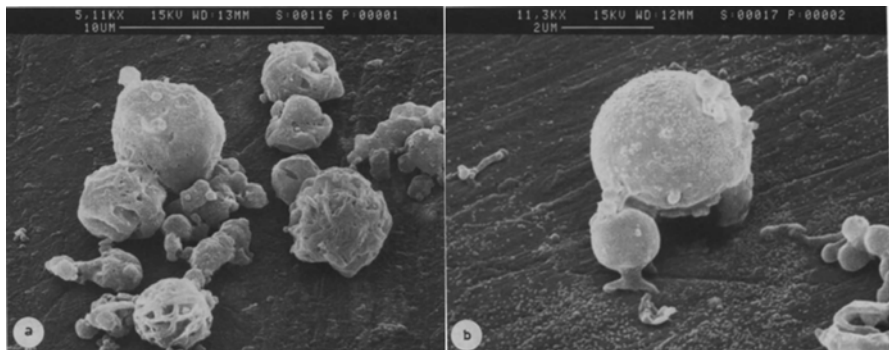
Fig. 27.3 Photomicrographs of PDLLA microspheres prepared by (**a**) solvent evaporation; (**b**) solvent extraction (Reprinted with permission from [25], copyright Elsevier)
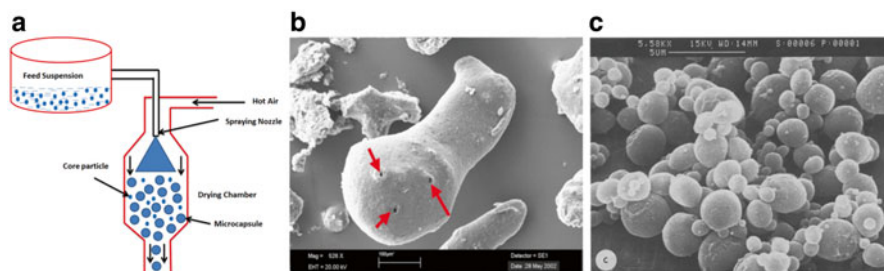
Fig. 27.4 (**a**) Schematic of spray-drying technique for microencapsulation process (Adapted with permission from [27], copyright Wiley-VCH Verlag GmbH & Co. KGaA.). (**b**) A "spray cooled particle, the *red arrows* point to active ingredient crystals sticking out of the fat matrix" (Reprinted with permission from [17], copyright Elsevier). (**c**) "Photomicrographs of PDLLA microspheres" prepared by spray drying (Reprinted with permission from [25], copyright Elsevier)

core encapsulations behind. Figure 27.4a shows a schematic of the spray-drying technique for the microencapsulation process [27]. Figure 27.4b shows a spray cooled particle [17], where the active ingredient crystals sticking out of the fat matrix are shown by the red arrows. Figure 27.4c represents the photomicrographs of PDLLA microspheres which were prepared by spray drying [25].

The fluidized bed coating method is frequently used when solid core agents along with saturated porous materials require encapsulation; more often than not, this methodology is used for therapeutics. Once suspended in an air stream, the solid agents are then sprayed with the fluidized coating material [29]. Shell solidification takes place in a controlled environment either by cooling or solvent vaporization. In order to obtain the desired shell thickness, this process can be repeated.

Using the polymer precipitation method, solidifying molten polymer drops or precipitating polymers can yield microcapsules that are biodegradable. Stirred with silicone oil, a drug dispersion added into molten polymer will create tiny polymer drug mixture droplets. After cooling, the hardened microcapsules are withdrawn from the oil. In other words, during the process of polymer precipitation, the aqueous polymeric solution and the drug are added dropwise into a stirred precipitating solution medium [30]. Precipitation takes place immediately to form the microcapsules which are now loaded with the drug.

In the co-extrusion process, two liquid streams of core and shell materials are pumped through concentric tubes, while being vibrated, thus forming drops [31]. Chemical cross-linking, cooling, or solvent evaporation is then preformed to harden the shell walls.

A layer-by-layer deposition technique is often utilized to create polyelectrolyte multilayers through the cyclic manner of sequential substrate immersion into oppositely charged polyelectrolyte solutions [32]. With cores of colloidal particles acting as a template for multilayer fabrication, core–shell particles can be created with the desired sizes and properties. Upon dissolving the core, hybrid particles, organic or inorganic, that are hollow can be acquired [33]. Utilizing this easy yet dynamic method, the properties can be tailored to any application by controlling the thickness of the multilayer film by varying the amount of total layers deposited.

In the supercritical fluid technique, the material which have the properties of liquids and gases, are highly compressed gases. Some of the supercritical fluids include CO_2, nitrous oxide (N_2O), and alkanes (C_2 to C_4). With a low critical temperature, low cost, availability, purity, nontoxicity, and nonflammable properties, supercritical CO_2 is used in many applications including polymer encapsulation of active agents [18]. By utilizing this technique, the following core materials have been encapsulated: vitamins, pharmaceutical ingredients, pesticides, flavors, dyes, and pigments [27].

For the spinning disk technique, a rotating disk is used to encapsulate core materials that have been suspended. A core particle and liquid shell suspension are loaded into a rotating disk, and via the spinning action [27], the liquid shell coats the core particles and is then cast to the disk's edge by centrifugal force, with shell solidification completed externally (typically via cooling). This process is considered as a quick, cheap, easy, and an efficient process.

27.3   Preparation of Smart Polymers

As previously mentioned, to prepare polymeric microparticles, amphiphilic (both hydrophilic and hydrophobic) polymer structures that are able to form core–shell microparticles should be synthesized. Herein, the most frequently used polymer synthesis reactions to obtain this amphiphilic structure are discussed.

Among the most popular of methods, emulsion polymerization can be used to create external stimuli polymers, specifically microgel and microparticle systems [34]. Latexes with tight particle size ranges can be obtained via radical chain polymerization. A combination of water, water-soluble initiator, monomer(s), and surfactant (emulsifier) is typically required for emulsion polymerization to be completed [35]. The stabilizing mechanisms exhibited by colloidal stabilizers can be electrostatic, steric, or electrosteric in nature [35, 36]. At phase separation, solid particle formation can occur either during pre- or post-termination [36].

Mini-emulsion polymerization is a variation on this standard, where low molecular mass compounds act as a co-stabilizer and a high-shear device (e.g., ultrasound) is used [36, 37]. Such emulsions are defined by the following characteristics: possess an interfacial tension substantially larger than zero, are critically stabilized, and need high shearing in order to reach steady state [34, 35, 37].

Katharina Landfester [38] described the preparation of well-structured polymeric nanoparticles for the encapsulation of solid or liquid, hydrophobic or hydrophilic materials via the mini-emulsion process. Functionalized nanoparticles were easily obtained using this technique and can be considered environmentally friendly.

Controlled radical polymerization (CRP) techniques enable control over the polymer architecture, which includes molecular weight distribution (polydispersity), molecular weight, functionality, and composition [39]. The occurrence of premature termination is minimized, and molecular weight proceeds linearly with

time until all of the monomer is consumed or intentionally terminated. CRP has branched into three fundamental techniques which are briefly described below.

Atom transfer radical polymerization (ATRP) is commonly known as an excellent synthetic polymer process that yields predetermined and tight molecular weight bands along with a great amount of chain-end functionalities [40, 41]. As a robust controlled/living radical polymerization methodology, ATRP can provide control to many vinyl and acrylic monomer polymerization reactions in mild environments [42–44]. An alkyl halide acting as an initiator alongside a lower oxidation state transition metal (e.g., Cu) is the basis for the ATRP initiating system [42, 45]. The unprecedented control over molecular architecture afforded by ATRP enables preparation of systematic polymer libraries.

Microparticle preparation requires amphiphilic polymer systems in order to form a core–shell material for encapsulation [46]. These amphiphilic polymer structures can be easily achieved by synthesizing block copolymers via ATRP. For example, self-assembling block copolymers with hydrophilic and hydrophobic segments, both in the solid state and in solution, can be prepared by ATRP to generate a variety of nanoscale structures. Recent studies on block copolymer self-assembly demonstrated that nanoscale morphology is highly dependent on block chain length, chain length ratios, polydispersity index, and block composition [39]. Therefore, it is essential to precisely control the degree of polymerization of each segment in the block copolymer and achieve a narrow molecular weight distribution [47]. ATRP is a convenient technique for the preparation of block copolymers because the growing polymer chain contains a stable halogen terminated ω-end that can act as an initiator for chain extension.

Satturwar et al. [48] found that PEG and *t*-butyl methacrylate, iso-butyl acrylate, *n*-butyl acrylate, or propyl methacrylate can be used to form block copolymers via ATRP [48]. Hydrolysis of the *t*-butyl groups yielded micelles that were responsive to changes in pH. This ATRP-synthesized block copolymer created high candesartan cilexetil (CDN) loadable micelles with pH-responsive drug release capabilities.

Reversible addition/fragmentation chain transfer (RAFT) polymerization is a versatile means to impart living characteristics upon radical polymerization [49]. Combining the benefits of living and free-radical polymerization methods, living free-radical/controlled radical polymerization can produce well-defined macromolecules [50]. Some of the benefits of RAFT polymerization reported in literature are as follows [51–53]: (I) polymerization control of most polymerizable monomers via radical polymerization, (II) the polymerization can be completed in an aqueous or protic medium while still being able to tolerate unprotected monomer/solvent functionality, (III) compatible with the reaction environment, and (IV) simplistic execution and low cost compared to other technologies.

Ideally, when the reaction begins, initiation takes place for all chains with growth occurring at a steady rate until the living polymerization is completed; irreversible chain transfer and termination do not occur [54]. Should initiation surpass propagation, the molecular weight distribution will be tight, and monomer additions will extend the chain. Chains are not all active simultaneously in radical polymerization [51].

RAFT best presents such attributes when mingling with reagents that cause propagating radicals to undergo reversible deactivation, where most living chains become dormant with the reaction conditions maintaining an active versus dormant chain rapid equilibrium [51, 55, 56]. In this environment, a linear trend of molecular weights and conversion can be observed, where there is a narrow molecular weight distribution and dormant chains prevail [56].

RAFT polymerization along with the careful selection of reagents and polymerization conditions can create well-defined homo-gradient [57], diblock [5], triblock, and star polymers [58], in addition to complex architectures such as microgels and brushes [59]. Applications utilizing the RAFT methodology entail drug carriers, coatings, adhesive biomaterials, novel surfactants, membranes, electro-active components, dispersants, and many more nanotech devices [51, 56].

With protein modded customizable bioactivity via a RAFT agent, the ambient polymerization of a smart polymer–protein conjugates in an aqueous media yielded poly(N-isopropylacrylamide) conjugates and a model protein, as described by Priyadarsi et al. [60]. The result was a novel RAFT agent immobilized polymer–protein conjugation via the "R-group" methodology [60]. The isolation of the conjugate was due in part by the immobilized polymer's responsive properties and the bioactive environmental modulation.

Nitroxide-mediated polymerization (NMP) stands out due to its simplicity: the polymerization is thermally initiated in the absence of an external radical source or a metal catalyst. NMP involves a combination of radical initiator, monomer, and nitroxide radical for trapping intermediate radical species [61]. For instance, the thermally promoted homolysis of benzoyl peroxide produces radicals that are capable of initiating the polymerization of styrene monomers. Propagation proceeds to produce polymer chains, while reversible termination occurs, involving reactions with nitroxide radicals to afford thermally labile alkoxyamines, mediating the availability of the reactive radical species and, thereby, providing control over the polymerization [61]. It is important to note that the stable nitroxide radicals are capable of reversible termination reactions but do not initiate polymerizations.

Alkoxyamine's isolation proved to be an essential advancement with NMP, finally realizing that it could become a unimolecular agent, supplying the reactive, radical initiation, as well as the stable, mediating nitroxide radical [61]. Initially, nitroxides were employed as additives to reversibly terminate polymer chains initiated by a separate radical source. By using 2,2,6,6-tetramethyl-1-piperidinyloxy (TEMPO) to trap a styrenyl radical initiated by benzoyl peroxide, Hawker [62] demonstrated an ability to tune the molecular weight, define end groups, and extend block copolymers, all while maintaining narrow molecular weight distributions [62]. He later developed a universal initiator, which has had broad applications in laboratories around the world.

The synthesis of PEG-based block copolymers via the initiating monohydroxy-terminated PEG reaction with sodium hydride, proceeded by the chloromethyl-substituted alkoxyamine, was conducted [62]. Styrene's nitroxide-mediated radical polymerization uses this PEG-based macro-initiator, yielding an amphiphilic block copolymer.

The term "click chemistry" is often used to describe a dynamic, modular technique used to combine two reactive components via a simple, fast, selective, predictable, and large yield reaction in mild conditions [63, 64]. This technique is becoming more frequently utilized in covalently cross-linking molecules, applied to many fields such as nanomaterial chemistry, chemical biology, drug delivery, and medicinal chemistry [65, 66]. By these characteristics, click chemistry is considered a "green chemistry" reaction. Recently popularized, copper catalyzed alkyne–azide cycloaddition (CuAAC) can be completed in many solvents like water, ethanol, or tert-butyl alcohol [64, 67, 68]. This advantage is due to its efficiency when exposed to a physiological environment, chemo-selectivity, and allows for functional bimolecular labeling such as peptides, proteins, nucleic acids, and polysaccharides [64, 69].

The high reliability of the CuAAC reaction provides a useful means of designing multifunctional nanocarriers, thus providing a schematic for therapeutic inventions [64, 68]. By testing this reaction in various environments, it has the potential to be implemented in synthetic architectures, where the components with various biological functions are localized. Click chemistry is also used to create multifunctional smart nanocarriers [68] built upon dendrimers and miktoarm polymers [70]. Benefiting from combined properties, these macromolecules can be led to certain cell organelles (i.e., mitochondria and lipid droplets). "Hyperbranched (dendrimers) architectures" and "branched (miktoarm stars)" are thought to be crucial in both medical and biological research, with click chemistry playing a key role in design implementation of multivalent and multifunctional nanocarriers [64].

27.4 Applications

Smart polymers are unique as the activation of their nonlinear response can be completed via a minute stimulus causing noticeable macroscopic changes in its architecture [71]. In the following sections, microencapsulated healing agents that respond to different external stimuli (i.e., mechanical, thermal, electrical, electromagnetic, or light stimuli), microencapsulation of phase-change materials, and microencapsulation of biologically responsive materials (i.e., drug, protein, enzymes, polysaccharides, cells, etc.) will be briefly discussed. The most common stimuli-responsive polymers which have found applications in microencapsulation are also briefly described.

27.4.1 Microencapsulated Self-Healing Agents

Fast and effective execution is paramount to reparative methodologies, essentially eliminating localized removal of a part for mending [72]. Smart materials can heal either intrinsically or extrinsically, via reversible bonds present within the matrix or

by a pre-added agent that responds to external stimulus, respectively [73]. Smart polymer microparticles (SPM) provide a stable reservoir that can encapsulate a healing agent and achieve a highly efficient repair system. SPM can be prepared using different synthesis methods, previously described, in order to get one or more external stimuli, such as mechanical, temperature, light, electrical, or magnetic field. The most typical responsive stimuli are described below.

Delicate and brittle polymer matrices can be strengthened by lightweight polymeric microcapsules. Offering room to load a reparative substance, polymeric microcapsules can be synthesized by the mini-emulsion polymerization technique, which deals with submicron oil-in-water dispersions of the polymeric components [72].

Most of the self-repairing composite systems that have undergone investigation consist of a urea–formaldehyde polymer that surrounds the liquid agent (i.e., dicyclopentadiene), thus creating a microcapsule [72, 74]. The reaction between urea and formaldehyde in the water phase during the in situ polymerization process creates a low molecular weight prepolymer [72, 73]. As the prepolymer's weight increases, it settles at the dicyclopentadiene–water interface, forming the microcapsule's densely cross-linked shell [75]. When this shell is broken, the healing agent is released and the reparative process begins.

The rigidity of the microcapsule in comparison to its surrounding environment will dictate how the healing agent will be distributed [76]. The shell's thickness is a critical design parameter that must be carefully considered. Should the shell's thickness be too thick, rupture will never occur and vice versa, if too thin, premature release could occur in production or could leach out/diffuse over time. Overall system performance is determined by the capsule's size, composite toughness, and amount of content filled within it. While some studies detailed that smaller systems displayed maximized strength at lower concentrations, others proved the converse, quite possibly due to the greater amount of available reparative matter [77].

On top of this, the healing agent's properties must also be studied. The healing kinetics, mechanical crack growth, and the relation between the two are of vital importance [78, 73]. Accelerated crack propagation that outpaces the repairing polymerization process will result in partial or no healing. Conversely, fast curing of the agent when the dissolution of catalyst is delayed will isolate repairs near the catalyst particles, lowering the efficiency of the healing process.

Healable thermal stimuli-responsive material can be prepared via Diels–Alder addition reaction. In order to impart the desired functionality, two carbon bonds from a cyclohexene ring, created via conjugation of a diene with a dienophile, can be manipulated. It should be noted that this cycloaddition reaction is completely thermally reversible.

Furan and cyclopentadiene are two types of cyclic dienes. If the polymer backbone has a dicyclopentadiene group incorporated into it, the resulting cross-linking creates a thermo-reversible polymeric system [79]. Researchers have also employed furan and maleimide groups as pendant diene and dienophile groups into the polymer, thus synthesizing gels that possess thermally reversible properties [73, 80].

Another example of a "thermally triggered self-healing material" has been described by Luo [81] who prepared a thermo-responsive self-repairing system by combining a high-heat epoxy resin with a thermoplastic polymer (poly([varepsilon]-

caprolactone) (PCL)). At first, the system is miscible, but as the epoxy cures, polymerization-induced phase separation (PIPS) takes place, creating morphologies that are compositionally dependent [81]. The behavior of heat-induced "bleeding" was described as the spontaneous molten PCL wetting of all free surfaces [82]. Perhaps this is due to PCL's volumetric thermal expansion beyond its melting point while in excess of epoxy brick expansion, which is also called "differential expansive bleeding (DEB)" [81, 82]. DEB could potentially be used to repair crack damage [82].

Stress that is applied in a continuous and/or cyclic manner creates and propagates micro-cracks, causing mechanical component fatigue and electronic systems failure [83]. As such, researchers have begun to focus their efforts on the design of self-healing electro-sensitive materials.

When electrical stimulation is applied, a polymeric matrix that has been combined with these components will undergo resistive heating, which is very useful for self-healing systems [83]. These electrical response polymers act as self-healing systems when a constant electric field is applied and heat is generated locally, only where the repair is needed. Initiation of the crack repair comes from the introduction of heat, returning the mechanical and electrical properties in the system previously possessed.

Many different and beneficial features can be gained by materials being incorporated with conductive properties. Case in point, the structural integrity of a material could be determined in real time via electronic feedback mechanisms. Such technology could provide a means for the excruciating task of micro-crack detection and quantification, leading to materials that can store records of stress and loading [84].

Future potential applications include the utilization of electric fields/currents for healing functionality (e.g., an "electrically driven self-healing" process) [83]. The obvious advantage being in new consumer electronics and the self-healing and conductive properties of these materials could also act as substitutes for sophisticated backup systems utilized in high-risk scenarios (e.g., deep-sea, space travel).

The incorporation of magnetic materials into systems can be beneficial, offering an option to use the electrical contacts of conductive materials by remote heating via electromagnetic induction [85]. Most frequently utilized in biomedical components, this heating technique requires the use of magnetic nanoparticles that heat upon the introduction of a high-frequency magnetic field after they were injected into the desired location (i.e., solid tumor) [86]. Because of the nanoparticle magnetic moment's vibration, the temperature of the cells increases; heat dissipation occurs by full magnetic particle rotation while in a fluid, or the magnetic moment rotates within the core [86].

Besides biomedical applications, magnetic and electric stimuli-responsive systems are desirable due to the ease of their control and potential for industrial growth. Suspensions of either of these particles are known as "electrorheological (ER)" or "magnetorheological (MR) fluids" [87]. ER fluids typically contain a dispersion of dielectric polarizable particles in an insulating medium [87], where MR fluids are generally a dispersion of magnetizable particles in a carrier medium. Other sought after properties of these systems include precise control and fast response time, making them ideal for application in a wide range of fields like medical therapies, micro-fluidic control, actuators, and seismic vibration dampers [87], to name a few.

The ionic interaction will also achieve reversible cross-linking in polymeric systems. Ionomers consist of polymers made up of 15% ionic content and have been studied for their restorative cross-linking healing, thus recovering its mechanical strength [73]. Polymers of elevated ion content ultimately boost the system's tensile strength and fracture resistance [88], supposedly from the internal ionic cluster formation that allows for increasingly effective ionic cross-links.

Cycloaddition reactions can also be photoinitiated when irradiated, where either cyclization or cleavage occurs [73]. Often utilized in organic synthesis, photochemical reactions have proven to be cheap, easily initiated, and an eco-friendly alternative to harsh reagents so as to begin chemical transformation [73]. When irradiated, a [2+2] cycloaddition reaction of olefin compounds creates cyclobutane that when exposed to a short wavelength of light, the new covalent bonds are reversibly cleaved, yielding the original olefins. Reversible cross-linking is accomplished photolytically when a polymeric matrix has been combined with these photosensitive groups. Some examples of the components employed in photoreactions are butadiene derivatives, maleimide, and coumarin [73].

The constant replacement of metal parts with polymer matrix composites is ongoing in the aerospace industry due to the many benefits they impart over their precursors. Unfortunately, detection of composite damage is extremely hard as sub-laminate locations are formed, which cannot been seen without visual aid [89]. In response to this, 20 years of study have yielded the creation of self-healing polymeric microparticles [90]. The most typical self-healing microparticles used in aerospace applications are poly(urea/formaldehyde) [74], polyurethane [89], and silica gel [91].

Lee et al. [92] was the first to propose polymeric nanoparticles with self-healing capabilities with integrated computer simulations with micromechanics to show that multilayer composites that were incorporated with nanoparticles would net a self-healing product. These responsive composites actively repair damage and have the potential to do so multiple times as long as there are available nanoparticles within the matrix. This behavior is due to the stretching and compression of the polymer chains near the nanoparticles [93], led by the desire to reduce nanoparticle–polymer interactions via nanoparticles segregated from the crack and pre-crack areas [94]. The study's findings reflect the effectiveness of the nanoparticles when compared to their larger brethren as they diffuse more quickly [92]. Nanoparticles with a functionalized surface (i.e., ligands) are a prerequisite in creating self-healing system, as put forth by Glogowski et al. [95]. Figure 27.5 is a schematic illustrating the movement of nanoparticles during crack growth in thermoplastics [94].

27.4.2 Microencapsulation of Phase-Change Materials

By exploiting latent heat, phase-change materials (PCM) are able to store or release energy over a tight thermal range [96–99]. These materials can alter their state in this temperature range. Upon heating (i.e., where phase change occurs), PCMs can
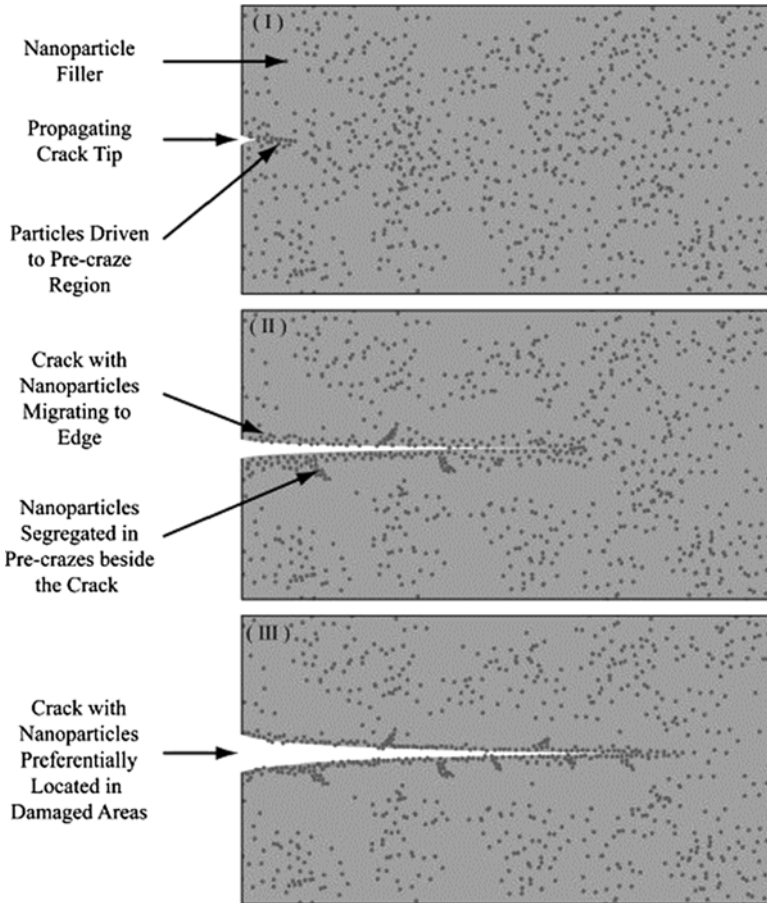
Fig. 27.5 Schematic diagram of nanoparticle movement during crack growth in thermoplastics (Reprinted with permission from [94], copyright Elsevier)

absorb energy and then release it to the environment during a cooling process (i.e., reversal of the phase) [98, 99].

PCMs also have an insulation effect that is dictated by both temperature and time, occurring solely during phase change (i.e., restricted thermal ranges), and ends upon completion of all PCM phase changes. As such, this results in temporary thermal insulation and is termed as dynamic thermal insulation [98]. Studies in heat transfer are currently evaluating the applicability of many potential applications that could benefit from melting phase, changing materials in enclosures.

PCM microencapsulation boasts an increased heat transfer area, reduced PCM's reactivity to external environmental conditions, as well as volume control and melted PCM leak prevention, while undergoing a phase change [100, 101].

Fibers, foams, or fabric coatings are a few of the materials that could benefit from the incorporation of PCM microcapsules [100]. In addition, they have higher chemical, thermal, and mechanical properties [101].

For example, in the textile industry, the encapsulation of PCM has become noteworthy in the last few years. Micro-PCMs, microcapsules incorporated with a tiny portion of PCM, were shown to substantially enhance cold climate clothing's thermally insulating properties [102]. Immediately localized, thermal response capabilities were displayed in fabrics containing phase-change components, specifically changes in temperature in the body [102]. Energy is absorbed and stored in the liquid phase-change components by the PCM microcapsules responding to a thermal event [102, 103]. As the temperature returns to normal levels, the stored energy is released by the microcapsules as they revert back to a solid state [102]. Figure 27.6 shows the formation of the micro-PCMs based on a *n*-octadecane core and resorcinol-modified melamine–formaldehyde shell through in situ polymerization [104]. PCM microcapsules coated on the surface of a fabric and embedded within the fiber are also shown in Fig. 27.7 [105].
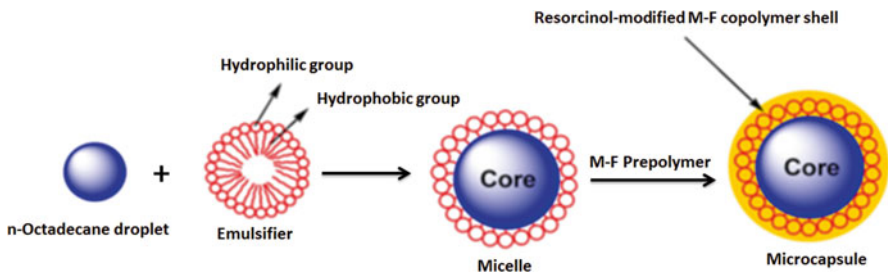
Fig. 27.6 Formation of the micro-PCMs based on *n*-octadecane core and resorcinol-modified melamine–formaldehyde shell through in situ polymerization (Reprinted with permission from [104], copyright, Elsevier)
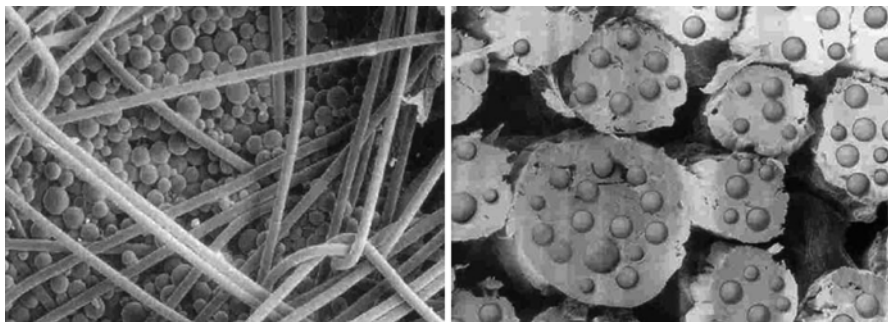
Fig. 27.7 PCM microcapsules coated on the surface of fabric (**a**) and embedded within fiber (**b**) (Reprinted with permission from [105], copyright Elsevier)

27.4.3 Microencapsulation of Biologically Responsive Materials

Pharmaceutical and biological therapeutics are often limited by their short half-lives, poor bioavailability, as well as their erratic physical and chemical behavior [71]. Physical instability more often than not deals with a highly ordered protein structure that is altered which then causes denaturation, aggregation precipitation, or other unwanted changes [71]. The controlled deliveries of drugs that maintain stability and retain their biologically active structure are the hallmarks of stimuli-responsive smart/intelligent polymers [106]. Through the years, awareness of stimuli-responsive smart/intelligent polymers has proliferated, and many studies aim to create environmentally sensitive macromolecules that can be fashioned into new smart polymers [107].

Drug carriers that have a smart polymer foundation provide reduced frequency of dosing, simple preparation, increased therapeutic concentration allowing for single dosing, prolonged release of the incorporated drug, reduced side effects, and improved stability [108]. Responses of a smart polymeric solution can be of various types. Responsiveness of a polymeric solution initiated by physical or chemical stimuli is limited to the destruction and formation of various secondary forces including Van der Waals forces, hydrophobic forces, hydrogen bonding, and electrostatic interaction [3, 106]. Chemical events include simple reactions such as oxidation, acid–base reaction, and reduction and hydrolysis of moieties attached to the polymer chain. In some cases, a dramatic conformational change in the polymeric structure occurs, such as the degradation of the polymeric structure due to irreversible bond breakage in response to an external stimulus.

Biologically responsive polymer microparticles are increasingly important in various biomedical applications. Bio-responsive polymers are classified into antigen-responsive, glucose-sensitive, and enzyme-responsive polymers [2]. The most typical bio-responsive polymer is the glucose-sensitive system.

Glucose-responsive polymers have the ability to mimic normal endogenous insulin secretion which minimizes diabetic complications and can release the bioactive compound in a controlled manner [109]. These are sugar sensitive and show variability in response to the presence of glucose. Such systems have piqued the interest of researchers due to the wealth of possibilities they hold including glucose sensing and insulin delivery applications [107].

The encapsulation of cells into polymeric microspheres or microcapsules has been shown to be effective in the encapsulation of cells, allowing for cell transplant in patients (human and animal) sans immunosuppressants [110, 111]. In order to provide the sustained release of drug (e.g., insulin), these cell-based therapies utilize donor cells and exhibit great disease-treating potential [112]. The microencapsulation of cells, or immuno-isolation, is an exciting new topic within the field, with alginate, a naturally occurring polymer in seaweed, receiving preferential treatment due to its gelling ability [111, 113]. While various natural polymers have the tendency to gel in physiological conditions, obstacles such as non-repeatable batch
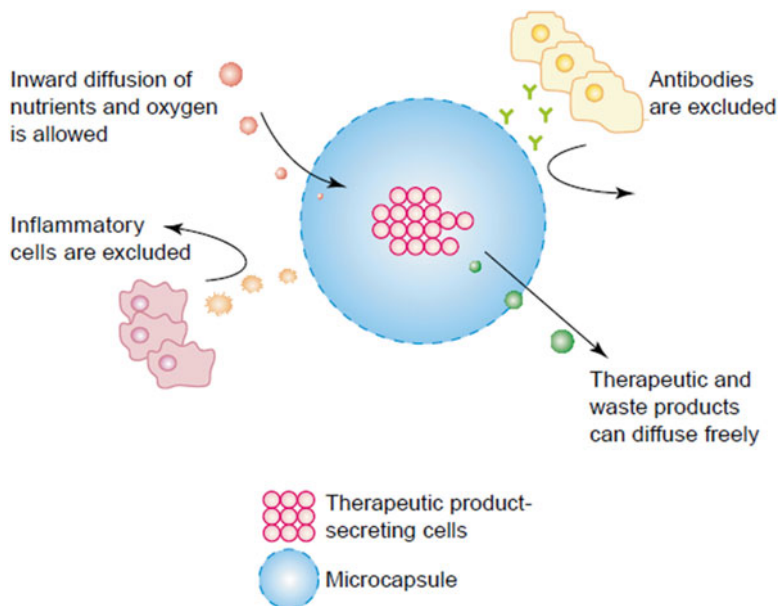
Fig. 27.8 A schematic representation of cell microencapsulation concept. "This technique consists of enclosing the biologically active material within a polymeric matrix surrounded by a semipermeable membrane that is designed to circumvent immune rejection. The capsule membrane allows the bi-directional diffusion of nutrients, oxygen and waste, and the secretion of the therapeutic product, but prevents immune cells and antibodies, which might destroy the enclosed cells, from entering the capsule" (Reprinted with permission from [114], copyright Elsevier)

formation and undesirable residual components can prompt an immune response once implanted [111]. Although synthetic materials sidestep these problems, their toxic polymerization methods are undesirable in living tissue [111]. As this field expands, researchers may well discover new techniques in the microencapsulation of cells into synthetic polymeric systems. Microencapsulation of cells is generally preferred for cell transplantation, while it can also be utilized in organ replacement and controlled drug delivery. Figure 27.8 is a schematic that represents cell microencapsulation technique [114].

Thermo-sensitive polymers undergo abrupt changes in their solubility in response to a small change in temperature [71, 115]. Controlled drug release rate while maintaining biological activity and physicochemical stability can be achieved via an aqueous, polymer solution that is thermally responsive to physiological conditions and displays reversible sol–gel transitions [71, 106]. This phenomenon is generally governed by the hydrophilic to lipophilic group ratio on the chain dictating said behavior and depends upon the free energy of mixing or the enthalpy or entropy of the system [106, 116]. Common features of temperature response polymers include the presence of a hydrophobic group. Of such groups, propyl, ethyl, and methyl can be mentioned [117]. These polymers possess two additional critical parameters: upper and lower critical solution temperatures (i.e., UCST and LCST, respectively). LCST is the temperature above which the polymeric monophasic system becomes hydrophobic

and insoluble, leading to phase separation, whereas below the LCST, the polymers are soluble. In contrast to UCST systems, an LCST system is preferred for most drug delivery circumstances due to the need for high temperatures in UCST systems, which are unfavorable for heat-labile drugs and biomolecules [118]. Poly(*N*-isopropyl acrylamide), poly(*N*,*N*-diethylacrylamide), poly(*N*-vinylalkylamide), poly(*N*-vinylcaprolactam), phosphazene derivatives, pluronics, tetronics, polysaccharide derivatives, chitosan, and PLGA–PEG–PLGA triblock copolymers are among the most frequently employed thermally sensitive polymers with a desirable LCST [118]. Poly (*N*-isopropyl acrylamide) is a thermo-sensitive polymer that exhibits a sharp LCST (32 °C) that can be shifted to body temperature through formulation with surfactants or additives [115, 119]. These polymers exhibit unique characteristics with respect to the sharpness of their almost discontinuous transition [115].

Polymers that react to environmental pH changes by accepting or releasing protons from their pendant moieties (acidic or basic in nature) are commonly known as pH-sensitive polymers. Polyelectrolytes are polymers that consist of a great amount of ionizable moieties. Polyelectrolytes are classified into two types: weak polyacids and weak polybases. At lower pH values, the weak polyacids typically accept protons, while at higher and neutral pH values, they release protons [120, 121]. Poly(acrylic acid) (PAAc) and poly(methacrylic acid) (PMAAc) are examples of pH-responsive polyacids that have been commonly utilized [122]. The pendant acidic group undergoes ionization at a specific pH value known as the pK_a upon changes in the environmental pH [123]. This quick change in net charge of the attached group causes an alteration in the molecular structure of the polymeric chain. pH-sensitive polymers containing a sulfonamide group are another example of polyacid polymers. These polymers have pK_a values in the range of 3–11, and the hydrogen atom of the amide nitrogen is readily ionized to form polyacids [124]. Narrow pH range and good sensitivity are the major advantages of these polymers over carboxylic acid-based polymers.

Polybases bearing an attached amino group are the most representative polybasic group. Poly(*N*,*N*-diethylaminoethyl methacrylate) (PDEAEMA) and poly(*N*,*N*-dimethylaminoethylmethacrylate) (PDMAEMA) are examples of widely used pH-responsive polymeric bases [39]. At higher pH values, the amino group is typically protonated and positively neutralized, while in lower pH environments, it is ionized. PDEAEMA has a hypercoiled conformation due to the existence of longer hydrophobic groups (i.e., ethyl groups) that cause interactions that are strongly hydrophobic which then act as an aggregation force [39, 125]. The introduction of a stronger hydrophobic group provides a tighter conformation as well as a greater discontinuous phase [125]. Chitosan is a polycationic biopolymer soluble in acidic solutions and undergoes phase separation at a pH range close to neutral through the deprotonation of the primary amino group by inorganic ions. Preparation of nanoparticles via ionic complex formation occurs through the electrostatic attraction between the ammonium group of the chitosan and an inorganic ion of the desired drug; as such, these systems can and are frequently used as drug carriers in biomedical applications [126].

In other words, the critical parameter of the pH must be taken into consideration when designing for biomedical applications as the human body consists of many

localized pH regions and gradients. When experiencing a change in pH, protons can be released or gained via the ionizable moieties found in pH-sensitive polymeric systems. The formerly coiled chains will violently extend when the generated charges' (anions or cations) electrostatic repulsions become ionized. The supplemental adjacent ionized groups' electrostatic repulsion is partially to blame for ionizing the polyelectrolytes' pendant acidic or basic moieties [124]. When polymeric systems containing weak acidic moieties experience an elevation in their environment's pH, their swelling index has been shown to increase, the converse being true for systems with weak basic moieties [124].

Upon the introduction of light, the response of a light-sensitive polymer is to complete a phase transition. The major advantages of light-sensitive polymers are that they are water-soluble, biocompatible, and biodegradable [71]. This includes their capacity for instantaneous delivery of payload via stimulus, making light-responsive polymers important for various engineering and biomedical applications [127, 128]. Polymers which respond to light are tempting to researchers who wish to trigger drug release due to the control they would have over the release mechanism, both spatially and temporally [129, 130]. Therefore, the release or activation of an encapsulated drug can be activated after irradiation via external light source. Factors that slow the widespread implementation of light-sensitive polymers are their non-repeatable response caused by noncovalently bonded chromophores that leach during structural flexing (i.e., swelling) as well as their slow response toward the stimulus [71].

The phase transition of these systems can be triggered by either UV or visible light; in effect, it is determined by the light's wavelength. More often than not, visible light-sensitive polymers are chosen due to their availability, safety, and simplicity. Bis (4-dimethylamino) phenylmethyl leucocyanide, a leuco derivative that is found within polymeric gels, undergoes phase transition when exposed to UV light [71, 131]. Triphenylmethane–leuco derivatives dissociate into ion pairs such as that of triphenylmethyl cations upon UV irradiation. The discontinuous swelling of the hydrogels at steady thermal conditions was caused by osmotic pressure increasing as a reactionary measure to UV irradiation but contracted upon the removal of the stimulus [128, 132]. Internal gel increases of osmotic pressure were caused by the presence of cyanide ions created by UV irradiation [132, 133]. Encapsulation of proteins and other macromolecules can be achieved using the network structure of the hydrogel matrices. The relationship between the diffusion coefficients of proteins and their sizes using photo-responsive hydrogels (with adjustable mesh size via light) [134] and the release of hydrophobic drugs using cyclodextrin (CD) modified dextran (Dex) hydrogels [135, 136] have been studied and reported.

As far as the encapsulation of small molecular substances is concerned, researchers have proposed using controllable alteration/modification techniques (e.g., "UV-stimulated shell cross-linking" for decreasing the mesh size of the capsule's shell) [130].

It was also reported that "intrinsically hydrophobic multilayers" with shells having smaller and less pores were favored for microencapsulation of small molecules [137]. Taking this into consideration, two types of the "diazoresin" (DAR) capsule systems have been proposed and reported (Fig. 27.9) [137].
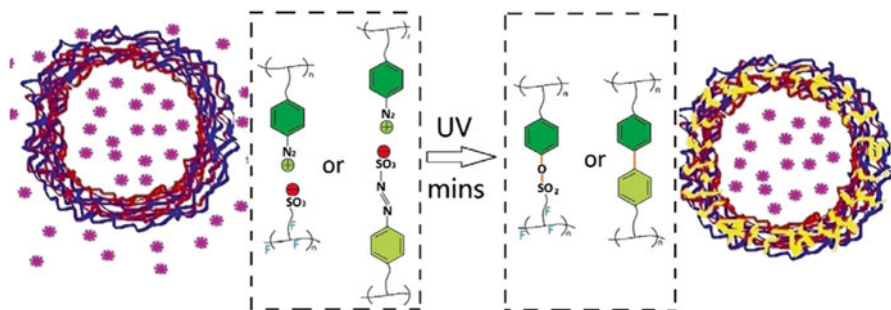
Fig. 27.9 Photolysis-induced small-molecule encapsulation in (**a**) Nafion/DAR and (**b**) DAR single-component multilayer capsules (Reprinted with permission from [137] with permission from the American Chemical Society)

When a polymer is able to physically alter its properties upon electric current stimulation, it is said to be electric field sensitive [71]. Along with also being pH-sensitive, these systems consist of a backbone with ionizable groups in great concentration, allowing them to convert electricity to mechanical energy, thus affording them a vast array of potential applications. These applications include controlled drug delivery [138], artificial muscle actuations, energy transductions, and sound dampening [139]. Their pH sensitivity comes from the electric current causing localized pH fluctuations, leading to hydrogen bonding disruption between the chains, thus allowing the drug to be released as the chain bends or degrades. Naturally occurring polymers including alginate, chitosan, and hyaluronic acid are commonly utilized when preparing electroresponsive materials [140]. Major synthetic polymers that have been used include allylamine, vinyl alcohol, acrylonitrile, methacrylic acid, and vinyl acrylic acid [141, 142]. A blend of both natural and synthetic polymers has been utilized in some scenarios. When exposed to an electric field, polymeric networks that exhibit anisotropic swelling or contraction (i.e., when charged ions navigate to the cathode or anode) are said to display electro-sensitive behavior and are classified as polyelectrolytes [106, 107]. The anode and adjoining areas experience a large amount of stress, while the cathode and its surrounding area see small gains in the stress load [106]. This gradient plays a role in the deforming of the anisotropic gel when subjected to an electric field. Electro-sensitive behavior in polymers that are neutral is predicated on the existence of a polarizable component that can react to an electric field [106].

27.5 Conclusion

A considerable amount of progress in the design of smart polymeric microparticles has been achieved. The field of stimuli-responsive materials has allowed an improvement in the materials' properties and therefore in different industrial applications. Microparticles have distinguished themselves as a significant piece of technology, finding novel applications along with a multitude of advantages like product quality

and stability. In order to be fully utilized in current and future applications, microparticles need increasingly more sophisticated components so as to ensure their success. With further advances in the synthesis of smart polymers, the creation of highly refined microparticles that exhibit enhanced performance capabilities will be possible. Autonomic delivery of active compounds (e.g., self-healing, vitamins, flavors, bioactive, catalyst, etc.) using stimuli-responsive microcapsules would provide a great advancement in manufacturing processes. Currently, many obstacles remain in the creation of smart polymer microparticles, thus making this field both highly exciting and rewarding.

References

1. Aguilar MR, Roman J (2014) Smart polymers and their applications. Elsevier
2. Kumar A et al (2007) Smart polymers: physical forms and bioengineering applications. Prog Polym Sci 32(10):1205–1237
3. Aguilar MR, San Román J (2014) 1 – Introduction to smart polymers and their applications. In: Aguilar MR, Román JS (eds) Smart polymers and their applications. Woodhead Publishing, Cambridge, pp 1–11
4. Cheng J et al (2007) Formulation of functionalized PLGA–PEG nanoparticles for in vivo targeted drug delivery. Biomaterials 28(5):869–876
5. Reyes-Ortega F et al (2013) Encapsulation of low molecular weight heparin (bemiparin) into polymeric nanoparticles obtained from cationic block copolymers: properties and cell activity. J Mater Chem B 1(6):850–860
6. Che Man SH et al (2013) Synthesis of polystyrene nanoparticles "armoured" with nanodimensional graphene oxide sheets by miniemulsion polymerization. J Polym Sci A Polym Chem 51(1):47–58
7. Jianguo Zhang TJE, Yunqiao P, Ragauskas AJ (2007) Facile synthesis of spherical cellulose nanoparticles. Carbohydr Polym 69:607–611
8. Yang J et al (2008) Microencapsulation of isocyanates for self-healing polymers. Macromolecules 41(24):9650–9655
9. Dinarvand R, Sepehri N, Manoochehri S, Rouhani H, Atyabi F (2011) Polylactide-co-glycolide nanoparticles for controlled delivery of anticancer agents. Int J Nanomedicine 6:877–895
10. Lee EJ, Khan SA, Lim KH (2011) Gelatin nanoparticle preparation by nanoprecipitation. J Biomater Sci Polym Ed 22(4–6):753–771
11. Campos E et al (2013) Designing polymeric microparticles for biomedical and industrial applications. Eur Polym J 49(8):2005–2021
12. Freitas S, Merkle HP, Gander B (2005) Microencapsulation by solvent extraction/evaporation: reviewing the state of the art of microsphere preparation process technology. J Control Release 102(2):313–332
13. Almouazen E et al (2012) Development of a nanoparticle-based system for the delivery of retinoic acid into macrophages. Int J Pharm 430(1–2):207–215
14. Borden MA et al (2005) Influence of lipid shell physicochemical properties on ultrasound-induced microbubble destruction. IEEE Trans Ultrason Ferroelectr Freq Control 52(11):1992–2002
15. Rickey ME, Ramstack JM, Lewis DH (2000) Preparation of biodegradable, biocompatible microparticles containing a biologically active agent. Google Patents
16. de Moraes SL, de Lima JRB, Neto JBF (2013) Influence of dispersants on the rheological and colloidal properties of iron ore ultrafine particles and their effect on the pelletizing process—a review. J Mater Res Technol 2(4):386–391

17. Gouin S (2004) Microencapsulation: industrial appraisal of existing technologies and trends. Trends Food Sci Technol 15(7):330–347
18. Dubey R (2009) Microencapsulation technology and applications. Def Sci J 59(1):82–95
19. Jyothi NVN et al (2010) Microencapsulation techniques, factors influencing encapsulation efficiency. J Microencapsul 27(3):187–197
20. Gutcho MH (1976) Microcapsules and microencapsulation techniques. Noyes Data Corporation, Park Ridge, NJ
21. Arshady R (1990) Review: biodegradable microcapsular drug delivery systems: manufacturing methodology, release control and targeting prospects. J Bioact Compat Polym 5(3):315–342
22. Morgan PW (2002) Interfacial polymerization. In: Matyjaszewski K (ed) Encyclopedia of polymer science and technology. Wiley, New York
23. Hunter RA, Turner PD, Rimmer S (2001) Suspension cross-linking of poly(aryl ether ketone)s containing carboxylic acid functionality. J Mater Chem 11(3):736–740
24. Jain RA (2000) The manufacturing techniques of various drug loaded biodegradable poly(lactide-co-glycolide) (PLGA) devices. Biomaterials 21(23):2475–2490
25. Pavanetto F et al (1992) Solvent evaporation, solvent extraction and spray drying for polylactide microsphere preparation. Int J Pharm 84(2):151–159
26. Ye A (2008) Complexation between milk proteins and polysaccharides via electrostatic interaction: principles and applications–a review. Int J Food Sci Technol 43(3):406–415
27. Ghosh S (2006) In: Ghosh SK (ed) Functional coatings and microencapsulation: A general perspective. Wiley-VCH Verlag GmbH & Co. KGaA, Weinheim, FRG. doi:10.1002/3527608478.ch1
28. Fuchs M et al (2006) Encapsulation of oil in powder using spray drying and fluidised bed agglomeration. J Food Eng 75(1):27–35
29. Teunou E, Poncelet D (2002) Batch and continuous fluid bed coating–review and state of the art. J Food Eng 53(4):325–340
30. Bilati U, Allémann E, Doelker E (2005) Development of a nanoprecipitation method intended for the entrapment of hydrophilic drugs into nanoparticles. Eur J Pharm Sci 24(1):67–75
31. Breitenbach J (2002) Melt extrusion: from process to drug delivery technology. Eur J Pharm Biopharm 54(2):107–117
32. Liu A et al (2006) Multilayered mesoporous titanate nanocomposite film: Fabrication by layer-by-layer self-assembly and its electrochemical properties with H+ intercalation. Electrochem Commun 8(2):206–210
33. Wang Y, Angelatos AS, Caruso F (2007) Template synthesis of nanostructured materials via layer-by-layer assembly. Chem Mater 20(3):848–858
34. Gong Y et al (2015) Magnetic, fluorescent, and thermo-responsive poly (MMA-NIPAM-Tb (AA) 3Phen)/Fe3O4 multifunctional nanospheres prepared by emulsifier-free emulsion polymerization. J Biomater Appl: p. 0885328215575761
35. Dai S, Ravi P, Tam KC (2008) pH-Responsive polymers: synthesis, properties and applications. Soft Matter 4(3):435–449
36. Rao JP, Geckeler KE (2011) Polymer nanoparticles: preparation techniques and size-control parameters. Prog Polym Sci 36(7):887–913
37. Ethirajan A (2008) Polymeric nanoparticles synthesized via miniemulsion process as templates for biomimetic mineralization. 2008, Ulm, Univ., Diss.
38. Landfester K (2009) Miniemulsion polymerization and the structure of polymer and hybrid nanoparticles. Angew Chem Int Ed 48(25):4488–4507
39. Reyes-Ortega F et al (2013) Smart heparin-based bioconjugates synthesized by a combination of ATRP and click chemistry. Polym Chem 4(9):2800–2814
40. Shahabuddin S, Mohamad S, Sarih NM (2015) Synthesis of well-defined three-arm star-branched polystyrene through arm-first coupling approach by atom transfer radical polymerization. Int J Polym Sci 2015 (ID 961914)
41. Baruah PK, Khan S (2013) Self-complementary quadruple hydrogen bonding motifs: From design to function. RSC Adv 3(44):21202–21217

42. Matyjaszewski K (2012) Atom transfer radical polymerization (ATRP): current status and future perspectives. Macromolecules 45(10):4015–4039

43. Tsarevsky NV, Matyjaszewski K (2007) \"Green\" atom transfer radical polymerization: from process design to preparation of well-defined environmentally friendly polymeric materials. Chem Rev 107(6):2270–2299

44. Matyjaszewski K, Xia J (2001) Atom transfer radical polymerization. Chem Rev 101(9):2921–2990

45. di Lena F, Matyjaszewski K (2010) Transition metal catalysts for controlled radical polymerization. Prog Polym Sci 35(8):959–1021

46. Zhao S et al (2014) Coaxial electrospray of liquid core–hydrogel shell microcapsules for encapsulation and miniaturized 3D culture of pluripotent stem cells. Integr Biol 6(9):874–884

47. Carreira A et al (2010) Temperature and pH responsive polymers based on chitosan: applications and new graft copolymerization strategies based on living radical polymerization. Carbohydr Polym 80(3):618–630

48. Satturwar P et al (2007) pH-responsive polymeric micelles of poly (ethylene glycol)-b-poly (alkyl (meth) acrylate-co-methacrylic acid): influence of the copolymer composition on self-assembling properties and release of candesartan cilexetil. Eur J Pharm Biopharm 65(3):379–387

49. Stenzel MH (2008) RAFT polymerization: an avenue to functional polymeric micelles for drug delivery. Chem Commun 30:3486–3503

50. Chiefari J et al (1998) Living free-radical polymerization by reversible addition-fragmentation chain transfer: the RAFT process. Macromolecules 31(16):5559–5562

51. Moad G, Rizzardo E, Thang SH (2005) Living radical polymerization by the RAFT process. Aust J Chem 58(6):379–410

52. Moad G, Rizzardo E, Thang SH (2009) Living radical polymerization by the RAFT process– a second update. Aust J Chem 62(11):1402–1472

53. Pietrzak M, Jędrzejewska B, Pączkowski J (2009) Unusually highly efficient, singlet state, visible light photoinitiators based on styrylbenzimidazolium phenyltributylborate photoredox pairs for vinyl monomers free radical polymerization. J Polym Sci A Polym Chem 47(16):4119–4129

54. Tsang EMW, Holdcroft S (2012) Alternative proton exchange membranes by chain-growth polymerization. In: Möller KM (ed) Polymer science: a comprehensive reference. Elsevier, Amsterdam, pp 651–689.

55. Averick S et al (2015) Well-defined biohybrids using reversible-deactivation radical polymerization procedures. J Control Release 205:45–57

56. Moad G, Rizzardo E, Thang SH (2008) Toward living radical polymerization. Acc Chem Res 41(9):1133–1142

57. Li Q et al (2014) A facile one pot strategy for the synthesis of well-defined polyacrylates from acrylic acid via RAFT polymerization. Chem Commun 50(25):3331–3334

58. Wei X et al (2014) Synthesis of cleavable multi-functional mikto-arm star polymer by RAFT polymerization: example of an anti-cancer drug 7-ethyl-10-hydroxycamptothecin (SN-38) as functional moiety. Sci China Chem 57(7):995–1001

59. Zheng Z, Ling J, Müller AH (2014) Revival of the R-group approach: a "CTA-shuttled" grafting from approach for well-defined cylindrical polymer brushes via RAFT polymerization. Macromol Rapid Commun 35(2):234–241

60. De Priyadarsi et al (2008) Temperature-regulated activity of responsive polymer–protein conjugates prepared by grafting-from via RAFT polymerization. J Am Chem Soc 130(34):11288–11289

61. Otsuka H (2013) Reorganization of polymer structures based on dynamic covalent chemistry: polymer reactions by dynamic covalent exchanges of alkoxyamine units. Polym J 45(9):879–891

62. Hawker CJ, Bosman AW, Harth E (2001) New polymer synthesis by nitroxide mediated living radical polymerizations. Chem Rev 101(12):3661–3688

63. Delaittre G, Guimard NK, Barner-Kowollik C (2015) Cycloadditions in modern polymer chemistry. Acc Chem Res 48(5):1296–307
64. Avti PK, Maysinger D, Kakkar A (2013) Alkyne-azide "click" chemistry in designing nano-carriers for applications in biology. Molecules 18(8):9531–9549
65. Kurra Y et al (2014) Two rapid catalyst-free click reactions for in vivo protein labeling of genetically encoded strained alkene/alkyne functionalities. Bioconjug Chem 25(9):1730–1738
66. Cai Z et al (2014) 64Cu-labeled somatostatin analogues conjugated with cross-bridged phosphonate-based chelators via strain-promoted click chemistry for PET imaging: in silico through in vivo studies. J Med Chem 57(14):6019–6029
67. Amblard F, Cho JH, Schinazi RF (2009) Cu (I)-catalyzed Huisgen azide– alkyne 1, 3-dipolar cycloaddition reaction in nucleoside, nucleotide, and oligonucleotide chemistry. Chem Rev 109(9):4207–4220
68. Johnson JA et al (2008) Construction of linear polymers, dendrimers, networks, and other polymeric architectures by copper-catalyzed azide-alkyne cycloaddition "click" chemistry. Macromol Rapid Commun 29(12-13):1052–1072
69. Hänni KD, Leigh DA (2010) The application of CuAAC 'click' chemistry to catenane and rotaxane synthesis. Chem Soc Rev 39(4):1240–1251
70. Rao J et al (2008) Facile preparation of well-defined AB2 Y-shaped miktoarm star polypeptide copolymer via the combination of ring-opening polymerization and click chemistry. Biomacromolecules 9(10):2586–2593
71. Oak M, Mandke R, Singh J (2012) Smart polymers for peptide and protein parenteral sustained delivery. Drug Discov Today Technol 9(2):e131–e140
72. Aïssa B et al (2012) Self-healing materials systems: overview of major approaches and recent developed technologies. Adv Mater Sci Eng 2012:17, Article ID 854203. doi:10.1155/2012/854203
73. Murphy EB, Wudl F (2010) The world of smart healable materials. Prog Polym Sci 35(1):223–251
74. Brown EN et al (2003) In situ poly (urea-formaldehyde) microencapsulation of dicyclopentadiene. J Microencapsul 20(6):719–730
75. Tong X-M et al (2010) Preparation and characterization of novel melamine modified poly (urea–formaldehyde) self-repairing microcapsules. Colloids Surf A Physicochem Eng Asp 371(1):91–97
76. Brown EN, White SR, Sottos NR (2004) Microcapsule induced toughening in a self-healing polymer composite. J Mater Sci 39(5):1703–1710
77. Rule JD, Sottos NR, White SR (2007) Effect of microcapsule size on the performance of self-healing polymers. Polymer 48(12):3520–3529
78. Böttger B et al (2013) Relationship between solidification microstructure and hot cracking susceptibility for continuous casting of low-carbon and high-strength low-alloyed steels: a phase-field study. Metall Mater Trans A 44(8):3765–3777
79. Tasdelen MA (2011) Diels–Alder "click" reactions: recent applications in polymer and material science. Polym Chem 2(10):2133–2145
80. Guimard NK et al (2012) Current trends in the field of self-healing materials. Macromol Chem Phys 213(2):131–143
81. Luo Xiaofan (2010) Thermally responsive polymer systems for self-healing, reversible adhesion and shape memory applications. Biomedical and Chemical Engineering–Dissertations, Paper 56. Syracuse University. http://surface.syr.edu/bce_etd/56 (Last Accessed: May 2015)
82. Luo X et al (2009) A thermoplastic/thermoset blend exhibiting thermal mending and reversible adhesion. ACS Appl Mater Interfaces 1(3):612–620
83. Williams KA, Boydston AJ, Bielawski CW (2007) Towards electrically conductive, self-healing materials. J R Soc Interface 4(13):359–362
84. Baugher M et al (2004) The secure real-time transport protocol (SRTP). RFC 3711, March
85. Chen Y, Bose A, Bothun GD (2010) Controlled release from bilayer-decorated magnetoliposomes via electromagnetic heating. ACS Nano 4(6):3215–3221

86. Pankhurst Q et al (2009) Progress in applications of magnetic nanoparticles in biomedicine. J Phys D Appl Phys 42(22):224001
87. Zhang WL, Choi HJ (2014) Stimuli-responsive polymers and colloids under electric and magnetic fields. Polymers 6(11):2803–2818
88. Garcia SJ (2014) Effect of polymer architecture on the intrinsic self-healing character of polymers. Eur Polym J 53:118–125
89. Périchaud A et al (2012) Auto-reparation of polyimide film coatings for aerospace applications challenges and perspectives. INTECH Open Access Publisher
90. Yang Z et al (2011) A self-healing cementitious composite using oil core/silica gel shell microcapsules. Cem Concr Compos 33(4):506–512
91. Rahmanian S et al (2015) Growth of carbon nanotubes on silica microparticles and their effects on mechanical properties of polypropylene nanocomposites. Mater Des 69:181–189
92. Lee JY, Buxton GA, Balazs AC (2004) Using nanoparticles to create self-healing composites. J Chem Phys 121(11):5531–5540
93. Lee J-Y et al (2006) Nanoparticle alignment and repulsion during failure of glassy polymer nanocomposites. Macromolecules 39(21):7392–7396
94. Wu DY, Meure S, Solomon D (2008) Self-healing polymeric materials: a review of recent developments. Prog Polym Sci 33(5):479–522
95. Glogowski E et al (2006) Functionalization of nanoparticles for dispersion in polymers and assembly in fluids. J Polym Sci A Polym Chem 44(17):5076–5086
96. Alkan C et al (2009) Preparation, characterization, and thermal properties of microencapsulated phase change material for thermal energy storage. Sol Energy Mater Sol Cells 93(1):143–147
97. Sanchez-Silva L et al (2010) Synthesis and characterization of paraffin wax microcapsules with acrylic-based polymer shells. Ind Eng Chem Res 49(23):12204–12211
98. Khudhair AM, Farid MM (2004) A review on energy conservation in building applications with thermal storage by latent heat using phase change materials. Energy Convers Manag 45(2):263–275
99. Singha K (2012) A review on coating and lamination in textiles: processes and applications. Am J Polym Sci 2(3):39–49
100. Zuckerman JL et al (2003) Fabric coating containing energy absorbing phase change material and method of manufacturing same. Google Patents
101. Farid MM et al (2004) A review on phase change energy storage: materials and applications. Energy Convers Manag 45(9):1597–1615
102. Mondal S (2008) Phase change materials for smart textiles–an overview. Appl Therm Eng 28(11):1536–1550
103. Pause B (1995) Development of heat and cold insulating membrane structures with phase change material. J Ind Text 25(1):59–68
104. Zhang H, Wang X (2009) Fabrication and performances of microencapsulated phase change materials based on n-octadecane core and resorcinol-modified melamine–formaldehyde shell. Colloids Surf A Physicochem Eng Asp 332(2):129–138
105. Nelson G (2002) Application of microencapsulation in textiles. Int J Pharm 242(1):55–62
106. Ravichandran R et al (2012) Advances in polymeric systems for tissue engineering and biomedical applications. Macromol Biosci 12(3):286–311
107. Roy D, Cambre JN, Sumerlin BS (2010) Future perspectives and recent advances in stimuli-responsive materials. Prog Polym Sci 35(1):278–301
108. Chi A et al (2013) Intelligent drug-delivery devices based on micro-and nano-technologies. Ther Deliv 4(1):77–94
109. Sharma G et al (2011) Recent trends in pulsatile drug delivery systems–a review. Int J Drug Delivery 2(3):200–212. doi:10.5138/ijdd.2010.0975.0215.02030
110. Kode JA et al (2009) Mesenchymal stem cells: immunobiology and role in immunomodulation and tissue regeneration. Cytotherapy 11(4):377–391
111. Olabisi RM (2015) Cell microencapsulation with synthetic polymers. J Biomed Mater Res A 103(2):846–859

112. Orive G et al (2003) Cell encapsulation: promise and progress. Nat Med 9(1):104–107
113. Lanza RP, WM Kuhtreiber, WL Chick (2000) Microcapsules and composite microreactors for immunoisolation of cells. Google Patents
114. Orive G et al (2003) Cell microencapsulation technology for biomedical purposes: novel insights and challenges. Trends Pharmacol Sci 24(5):207–210
115. Hatefi A, Amsden B (2002) Biodegradable injectable in situ forming drug delivery systems. J Control Release 80(1):9–28
116. Weber C, Hoogenboom R, Schubert US (2012) Temperature responsive bio-compatible polymers based on poly (ethylene oxide) and poly (2-oxazoline)s. Prog Polym Sci 37(5):686–714
117. Chu C (2003) Biodegradable hydrogels as drug controlled release vehicles. In: Yaszemski MJ et al. (eds) Biomaterials handbook–advanced applications of basic sciences, and bioengineering. Chapter 19 Tissue engineering and novel delivery systems. CRC Press, pp 871–909.
118. Yu L, Ding J (2008) Injectable hydrogels as unique biomedical materials. Chem Soc Rev 37(8):1473–1481
119. Ganta S et al (2008) A review of stimuli-responsive nanocarriers for drug and gene delivery. J Control Release 126(3):187–204
120. Reyes-Ortega F (2014) 3 – pH-responsive polymers: properties, synthesis and applications. In: Aguilar MR, Román JS (eds) Smart polymers and their applications. Woodhead Publishing, Cambridge, pp 45–92
121. Xue C, Li Q (2013) Stimuli-responsive smart organic hybrid metal nanoparticles. In: Li Q (ed) Intelligent stimuli-responsive materials: from well-defined nanostructures to applications. Wiley, Hoboken, NJ, pp 293–333 ISBN: 9781118680469
122. Mori H, Müller AH (2003) New polymeric architectures with (meth) acrylic acid segments. Prog Polym Sci 28(10):1403–1439
123. Tao H, Parthiban A (2014) Stimuli-responsive copolymers and their applications. In: Parthiban A (ed) Synthesis and applications of copolymers. Wiley, Hoboken, NJ, pp 274–306
124. Gil ES, Hudson SM (2004) Stimuli-responsive polymers and their bioconjugates. Prog Polym Sci 29(12):1173–1222
125. Chen J-K, Chang C-J (2014) Fabrications and applications of stimulus-responsive polymer films and patterns on surfaces: a review. Materials 7(2):805–875
126. Foglio MA et al (2013) Pharmaceutical compositions comprising arrabidaea chica extract in controlled release systems, production process and use thereof. Google Patents
127. Yasin MN et al (2014) Implants for drug delivery to the posterior segment of the eye: a focus on stimuli-responsive and tunable release systems. J Control Release 196:208–221
128. Bawa P et al (2009) Stimuli-responsive polymers and their applications in drug delivery. Biomed Mater 4(2):022001
129. Huang S et al (2014) Optimization and characterization of the photosensitive N-succinyl-N'-4-(2-nitrobenzyloxy)-succinyl-chitosan micelles. In: Twelfth International Conference on Photonics and Imaging in Biology and Medicine (PIBM 2014). International Society for Optics and Photonics
130. Yi Q, Sukhorukov GB (2014) UV light stimulated encapsulation and release by polyelectrolyte microcapsules. Adv Colloid Interf Sci 207:280–289
131. Ramteke K, Chavanke M, Chavanke P (2012) Stimuli sensitive hydrogels in drug delivery systems. Int J Pharm Sci Res 3(12):4604–4616
132. Qiu Y, Park K (2012) Environment-sensitive hydrogels for drug delivery. Adv Drug Deliv Rev 64:49–60
133. Tomatsu I, Peng K, Kros A (2011) Photoresponsive hydrogels for biomedical applications. Adv Drug Deliv Rev 63(14):1257–1266
134. Andreopoulos FM, Beckman EJ, Russell AJ (1998) Light-induced tailoring of PEG-hydrogel properties. Biomaterials 19(15):1343–1352
135. Peng K et al (2009) Cyclodextrin–dextran based in situ hydrogel formation: a carrier for hydrophobic drugs. Soft Matter 6(1):85–87

136. Peng K et al (2010) Cyclodextrin/dextran based drug carriers for a controlled release of hydrophobic drugs in zebrafish embryos. Soft Matter 6(16):3778–3783
137. Yi Q, Sukhorukov GB (2013) Photolysis triggered sealing of multilayer capsules to entrap small molecules. ACS Appl Mater Interfaces 5(14):6723–6731
138. Medeiros S et al (2011) Stimuli-responsive magnetic particles for biomedical applications. Int J Pharm 403(1):139–161
139. Maffli L (2014) Fluidically-coupled dielectric elastomer actuator structures for tunable optics and microfluidics. ÉCOLE Polytechnique Fédérale De Lausanne
140. Hong C, Sung J, Choi H (2009) Effects of medium oil on electroresponsive characteristics of chitosan suspensions. Colloid Polym Sci 287(5):583–589
141. Zhang K, Zhang WL, Choi HJ (2013) Facile fabrication of self-assembled PMMA/graphene oxide composite particles and their electroresponsive properties. Colloid Polym Sci 291(4):955–962
142. Yun J et al (2010) pH and electro-responsive release behavior of MWCNT/PVA/PAAc composite microcapsules. Colloids Surf A Physicochem Eng Asp 368(1):23–30

Chapter 28
Adhesion of Polymer Coatings: Principles and Evaluation

Irina J. Zvonkina

Abstract Adhesion of polymer coatings to a metal, polymer, or glass substrate is one of the main characteristics that affect the protective, decorative, and other properties of coatings. In different fields of applications, the challenges of protecting devices and constructions, while providing special functions, promote a growing interest in investigation and evaluation of coating adhesion. This leads to the development of new approaches for its enhancement. Different mechanisms of adhesion, including chemical bonding and physical adsorption, mechanical interlocking, and others, are considered in this chapter. Adhesion is influenced by the nature of the polymer material and the substrate surface properties, film thickness, internal stress, as well as by the conditions of the coating application and service. The approaches to enhancement of adhesion of polymer coatings to a substrate are demonstrated in this chapter. For coatings with different functions, including novel intelligent coatings, a reliable evaluation of adhesion is one of the key factors that affect the strategies for its improvement and the coating's overall performance. The chapter provides an overview of the approaches to the destructive and nondestructive characterization of adhesion, from the traditional methods that are common in research and industry to less common intelligent techniques. The main challenges, strengths, and weaknesses, related to evaluation of adhesion, are communicated in this chapter.

Keywords Adhesion • Polymer coatings • Nondestructive testing • Surface modification • Interface

28.1 Introduction

Adhesion of polymer coatings to a metal, polymer, or glass substrates is a relevant characteristic that influences the protective, decorative, and other properties of coatings. Adhesion is usually referred to as the interaction between atoms and molecules at the interface of two surfaces [1]. Adhesion can be also determined as a "…state

I.J. Zvonkina (✉)
University of Akron, 302 East Buchtel Avenue, Akron, OH 44325, USA
e-mail: irina.zvonkina@gmail.com

in which two surfaces are held together by interfacial forces…" [2]. The bonds that are responsible for the coating adhesion can be various in type, such as covalent, dipole-dipole, van der Waals, hydrogen bonds, or others, and can be characterized by a variety of the bonding energies [3]. The approximate ranges of the bonding energies for different types of the intermolecular interactions have been reported in the literature [3, 4].

In different fields of coating applications, the motivation of protecting devices and constructions, while providing special functions by the coatings, promotes a growing interest in investigation and evaluation of adhesion. De-adhesion results in coating defects that can lead to the damage of coatings, coated devices, automotive parts, and others. For instance, corrosion failure or fouling degradation due to a weakened coating adhesion can destroy a large number of goods and can result in a significant economic loss [5]. The possibility to measure and to predict adhesion of functional coatings determines a longer life performance of coated materials and devices, leading to saving energy and natural resources, and contributing to sustainability. This inspiration results in development of new approaches to the adhesion enhancement and promotes interest in creating new techniques for its evaluation. This chapter provides a concise overview of the main mechanisms of adhesion and factors affecting adhesion and shows strategies for its enhancement, as well as it demonstrates the techniques and approaches for the adhesion characterization. The discussed methods for adhesion characterization are relevant for coatings with different functions, from the anticorrosion primers to smart responsive coatings, in research and their industrial applications of coatings.

28.2   Mechanisms of Adhesion of Polymer Coatings

Several mechanisms of adhesion have been identified in the literature [3, 6–8]. The mechanisms can be related to the mechanical interlocking between the two adhering surfaces, chemical bonding at the interface, physical adsorption, electrostatic interaction, and others. The mechanism based on the mechanical interlocking takes into account the surface profile/roughness at the interface in the explanation of the adhesion phenomenon (Fig. 28.1). According to this mechanism, the surfaces are connected as a "hook and eye" [9]. Due to this, the higher the roughness, a better adhesion would be expected. Additionally, a higher roughness provides a larger surface area at the interface that affects stronger chemical and physical interactions between the two surfaces.

In many coating systems, an adhesion contact takes place due to adsorption and formation of the chemical or physical bonds at the interface between the coating and the substrate. According to these mechanisms, creation of the adhesion forces between the coating and the substrate is explained by the presence of the chemical or physical bonds, such as covalent, ionic, metallic, van der Waals, hydrogen, or other bonds. These interactions are affected by the functional groups on the sub-
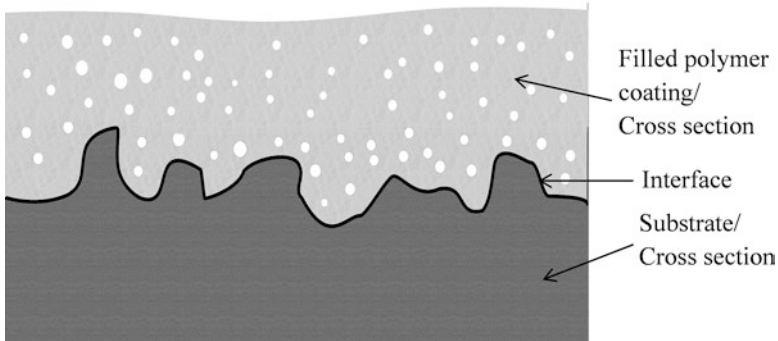
Fig. 28.1 Schematic demonstration of the mechanical interlocking mechanism of the adhesion contact
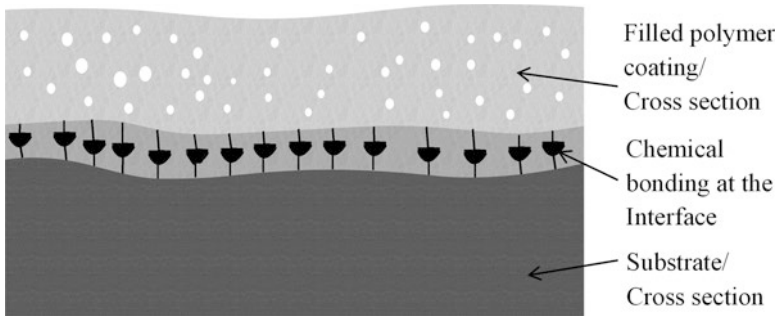
Fig. 28.2 Schematic demonstration of the chemical bonding at the interface between the coating and the substrate, leading to the adhesion contact

strate surface and within the coating material [8]. The mechanism of the adhesion contact based on the chemical bonding is schematically demonstrated in Fig. 28.2.

From the point of view of thermodynamics of an adhesion contact, the theoretical work of adhesion that holds two surfaces in an adhesion contact can be determined according to the equation as follows [10, 11]:

$$W_{Am} = \gamma_{1m} + \gamma_{2m} + \gamma_{12} \tag{28.1}$$

where W_{Am} is the thermodynamic work of adhesion in the medium m; γ_{1m} and γ_{2m} are the specific surface free energies in the medium m of the coating (1) and the substrate (2), respectively; and γ_{12} is the specific free energy at the coating-substrate interface.

The static and dynamic interface layers that can be formed between two interacting surfaces, related to the adhesion contacts on the molecular level, are considered in other documented sources [12–14].

28.3   Factors Influencing Adhesion of Coatings

To succeed in solving the challenges of improving and evaluating adhesion of polymer coatings to different substrates, it is of relevance to consider the driving forces and the factors that affect the adhesion strength. Main factors that influence adhesion are related to the chemical structure and composition of the polymer coatings, the substrate surface properties, coating thickness, mechanical properties and internal stresses, as well as temperature, humidity, and other environmental conditions during the application and service of the coatings.

The nature of a polymer coating material and the chemical structure of the substrate are responsible for the interfacial energy that affects the adhesion contact between the coating and the substrate surfaces. The structures of the coating and of the substrate materials determine the potential for the buildup of chemical and/or physical bonds at the interface, as well as the type and strength of such bonds that influence the adhesion forces. In terms of thermodynamics, as it follows from the equation above [Eq. (28.1)], the thermodynamic work of adhesion depends on the surface free energy of the coating and the substrate in a particular medium.

The chemical composition of the bulk polymer material of the coating, as well as that of the substrate, determine the cohesive forces inside the coating and the substrate materials [14]. The surface properties at the interface between the two interacting surfaces affect the adhesion forces [14–16]. Interplay between the cohesive and adhesive forces affects the adhesion strength. The quality of an adhesion interaction between two surfaces is both a battle and a compromise between the cohesive forces inside the coating polymer material, as well as inside the substrate, and the adhesion forces that attract the two surfaces to each other.

The intermolecular forces, identified as dispersive, polar, or hydrogen bond based, affect the surface energy of the material. These forces can be estimated based on the solubility parameters using several known techniques. The most common methods include evaluation of the refraction constants, dipole moments, and others [17]. The analysis of the adhesion bonds in two-layer polymer coating systems considering the acid-base interactions between the layers has been shown [12]. The authors demonstrate the effect of the polymer chain interactions at the transition interface layer, taking into account the steric structural effect and the interactions between the acid and the base functionalities of the polymer chains. Packham has demonstrated the effect of the surface energy and the surface roughness on wetting and on the joint strength [15]. Due to an increased roughness and redistribution of stress, a higher surface area and a higher energy of selected atoms within the surface asperities are considered. The factors that are discussed in this study contribute to the mechanical interlocking, chemical bonding, and physical adsorption mechanisms of adhesion. They affect thermodynamics at the interface and influence the selection of the routes for enhancement of adhesion of a polymer coating to a substrate [15].

The thickness of a polymer coating is a characteristic that contributes to the ratio between the cohesion and the adhesion forces at the coating-substrate interface, the

mechanical properties, and other factors, also affecting adhesion of said coatings. With increasing thickness of the coating at a certain range, the impact of the bulk polymer properties becomes stronger than the impact of the surface characteristics at the interface between the coating and the substrate, which determines the adhesion forces. The effect of thickness on the adhesion strength has been previously demonstrated [18, 19].

The internal stresses that can be enhanced during coating formation or service can decrease the adhesive forces. During the coating formation, the volume of the coating decreases as solvent evaporates and/or changes in the chemical composition alongside the structure take place. The area at the interface with the substrate, however, remains constant. This causes development of internal stresses at the plane of the coating-substrate interface. If the internal stress exceeds some certain value, it becomes sufficient enough to overcome the work of adhesion at the interface between the coating and the substrate to cause a failure of adhesion of the coating [19]. A correlation between the mechanical properties, particularly the elasticity and the storage modulus, of a polymer coating that are affected by the coating composition and the adhesion strength of the coating is discussed in several works [20–22]. Most of the studies report an improvement of the adhesion strength of polymer coatings with increasing elasticity of the coatings. An approach to tune adhesion of coatings considering the effect of the content and the functionality of the reactive diluents in UV-curable coating compositions on the coating adhesion was demonstrated in the study [21a]. The discussions on the relationships between adhesion, the rheological behavior, the glass transition temperature of the UV-curable materials and the polymer coatings, and the mechanical properties of the coatings can be found in this work [21].

During application and use of polymer coatings, one should consider the effect of the environmental conditions on adhesion. With raising temperature, the adhesive forces usually grow due to increasing mobility of the polymer chains. The effect of the relative humidity on the adhesion strength of polymer coatings to various substrates is demonstrated in several publications [23–25]. Quon et al. [25] studied hydrophobic n-octadecanethiol or hydrophilic 1-hydroxylunicosanethiol self-assembling monolayers applied on rough surfaces of mica or gold film. The reported results indicate an enhancement of adhesion in humid environmental conditions, referring to the capillary forces, taking into account the wettability of the surfaces.

28.4   Strategies for Enhancement of Adhesion of Polymer Coatings

Considering the relevance of adhesion for the performance of functional polymer coatings, a number of efforts have been undertaken in order to enhance the adhesion interaction between the coatings and the substrates. Taking into account different mechanisms of the coating adhesion, methods for enhancement of adhesion are

based mainly on modification of the chemical composition of the coating materials and of the substrate surface properties, including alterations of the surface profile and of the chemical composition at the surface.

The strategies related to alterations of the chemical composition and the structure of the coating material or changes in the properties of the substrate surface are mostly aimed in increasing the amount of functional groups. This creates stronger chemical and physical bonds between the coating and the substrate at the interface or would or results in decreasing the surface tension at the interface. Enhancement of the functionality can be achieved by incorporation of special additives, known as adhesion promoters, in the coating composition [26], or by a treatment of the substrate surface [27]. Depending on the nature of the coating material and the substrate, different adhesion promoters can be applied. The most common additives serving for improvement of adhesion are organosilanes, silicones, siloxanes, amide and amine, organophosphorus compounds, or other coupling agents [26, 28–32]. Adhesion of UV-curable coatings based on polyurethane oligomers, as well as the coating mechanical properties, can be modified by altering the composition of the acrylic reactive diluents [21]. This approach demonstrates a possibility to tune the properties of the coatings without changing the chemical structure of the oligomers, thus maintaining its advantages and functions.

Several other techniques for improving adhesion are known in the literature [27]. The substrate surface can be modified chemically, using plasma treatment, flame, fluorinated gas, and corona discharge, with application of laser or using other techniques in order to enhance adhesion [33–38]. Most of the existing methods for the surface modification of metal, polymer, or glass substrates have been applied in industry. Additionally, the surface treatment may implement application of the cathodic post-curing current to the coatings, as an alternative approach [39]. The motivation for bio-inspired approaches imitating the adhesion of gecko or of spider silk has resulted in several studies and development of intelligent surfaces with controlled adhesion properties [40–42].

28.5 Techniques for Characterization of the Coating Adhesion

A number of techniques for the evaluation of adhesion from the traditional destructive adhesion tests up to smart nondestructive methods have been developed. The existing techniques based on different principles of approaching adhesion evaluation are discussed below. An adhesion test is expected to provide a reliable and reproducible quantitative result, relevant for a specific field of applications, easy to carry out and to interpret, as well as, ideally, being nondestructive. Considering the requirements for an adhesion test, development of such method that would satisfy all the expectations still remains a challenge.

28.5.1   Destructive Methods for the Evaluation of the Coating Adhesion

One of the most common methods for the adhesion evaluation that is widely applied in industry and research is the crosshatch adhesion test [43–45]. It consists of the preparation of a series of parallel cuts at the coating surface crossing each other, attaching a pressure-sensitive adhesive tape of a certain type and pulling it off with a constant force. The adhesion is evaluated afterward by the area of the coating left attached to the substrate. The standard crosshatch characterization is currently performed according to the existing ASTM standard [46]. One should note, however, that the accuracy of the results of this test may depend on the peel angle and peel rate and on the contribution of the applied energy to the coating deformation rather than to the coating fracture [43, 44]. Besides its limitations, mainly related to its semiquantitative approach since it usually does not take into account a measured characteristic, this test is fast and easy to perform and it is commonly used in applications of coatings [43]. A modification of the traditional peel test implementing a thin elastomeric membrane led to the development of a novel axisymmetric test [47]. A method for an automatic characterization of adhesion based on the blister test [48, 49] has been reported [50]. The authors point out several advantages of the test, such as a relatively small angle and low separation rates that do not affect the deformation of the sample. The engineering evaluation of the test conditions that enhances the accuracy of the test is provided by the authors [50].

The pull-off test is based on the measurement of the normal force necessary to separate a metal stub of a constant weight and specific geometry glued to the surface (Fig. 28.3). The pull-off test has its advantages due to its potential to provide a quantitative characteristic of the separating force [9]. However, it requires the application of an adhesive material to the coating surface that may affect the measured adhesion value due to possible diffusion of the adhesive material through the coating. Potential
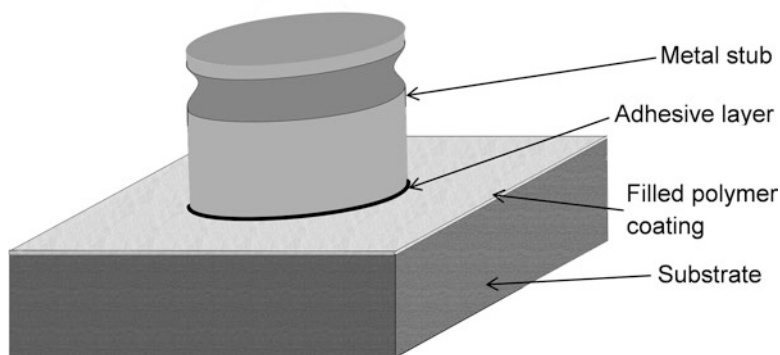
Fig. 28.3 A scheme of the pull-off test for the evaluation of adhesion of coatings

variations in the adhesion strength at the interface between the coating and the metal stub surfaces may appear as well when applying this technique.

For the evaluation of adhesion of thin films, scratch tests are commonly used. Bull and Berasetegui provide an overview of the techniques related to the scratch testing [51]. These methods are considered as semiquantitative, and they are affected by several factors that decrease the accuracy of the tests. The scratch testing however has been useful in the tasks of the development of hard thin coatings and in the coating quality control [48]. The application of atomic force microscopy (AFM) in the scratching tests for the determination of the adhesion strength has been fruitful in several applications [52]. For the evaluation of adhesion of the protective polymer coatings, an alternative method based on electrical impedance spectroscopy (EIS) was developed. This technique has been applied for the evaluation of the adhesion defects that would potentially lead to a corrosion failure [24, 53–55].

So far, a number of destructive methods for the adhesion evaluation have been developed. They involve the measurement of the force per unit area necessary to detach the coating from the substrate, evaluation of the coated surface after detaching the coating with a constant force, and characterization of the forces between the coating and substrate surfaces at the interface.

28.5.2 Nondestructive Methods of the Characterization of Adhesion

The nondestructive techniques for the evaluation of adhesion are beneficial for their potential in assessing and predicting adhesion during the service of the coatings, without degrading the coating material. The commonly used destructive methods for the evaluation of adhesion are relatively fast, easy to perform, and serve well in the tasks of development of new materials for coatings. However, a possibility to measure and predict adhesion without destroying the coating material in vivo during coating use is of high value. A capability to "look through" a coating to the interface with the substrate, in order to detect adhesion defects, creates a significant number of benefits in industrial applications of coatings, as well as it helps solving the challenges of the applied research. It can prolong the coating's service life, improve the protection of the coated surfaces, and contribute to the overall sustainability, while also taking into account the value of saving natural resources.

The existing techniques for the evaluation of adhesion of coatings include the application of ultrasonic microscopy analysis, infrared (IR) spectroscopy and thermal imaging methods, X-ray radiography, shearography, and several methods for characterization of adhesion on micro- and nanoscales. The existing approaches vary in accuracy, effectiveness, complexity of performing the measurements, duration of the measurements, and overall cost, while also considering the cost of the equipment [56, 57]. Several current approaches to nondestructive evaluation of adhesion are related to application of acoustic wave microscopy and ultrasonic analysis [55]. The

ultrasonic analysis approach is based on a difference in the ultrasonic signal intensity in different media and has been used in a range of tasks and materials in nondestructive material testing [58–62]. The principle scheme of this technique is demonstrated in Fig. 28.4. The measurements can be performed in several modes. In the contact mode, a sensor is attached directly to the analyzed surface. The noncontact methods implemented used to obtain the necessary measurements are performed with air coupling, immersion in water (water coupling), or in other media, applying a flow of water at the surface without immersing the analyzed sample or using a laser-stimulated technique [63]. The emitter applied for the analysis can serve simultaneously as the sensor or both the emitter and the sensor can be implemented separately [63]. Although ultrasonic evaluation has been applied in a number of tasks for qualitative characterization, the weak point of the method is its difficulty in performing the quantitative analysis of adhesion defects.

Czarnecki and coauthors [64] have demonstrated the application of ultrasonic analysis for the evaluation of the adhesion of polymer composite coatings applied on a concrete surface [64]. The results obtained by the developed technique were compared to the data measured by the traditional pull-off adhesion test and demonstrated a good correlation [64]. The application of the scanning acoustic microscopy (SAM) technique for the investigation of the coating adhesion, the phenomena related to the growth of blisters, propagation of the defects inside the polymer coatings, and disbonding at the polymer coating-metal substrate interface were demonstrated [65–67]. An alternative noncontact method for the measurement of adhesion was also proposed [68].

The techniques based on the infrared spectroscopy, including general thermal imaging methods [69], vibro-thermography [70], eddy current thermography [71], and thermal systems [72], have been widely used in the noncontact analysis of the composite materials in different industrial technologies, such as civil engineering, transportation, wind power, and electronics, as well as for materials used in the aviation industry [73–76]. An application of the transient active thermography for the nondestructive evaluation of the adhesion defects, as a part of the nondestructive material defect characterization, applied in manufacturing of wind turbine blades,
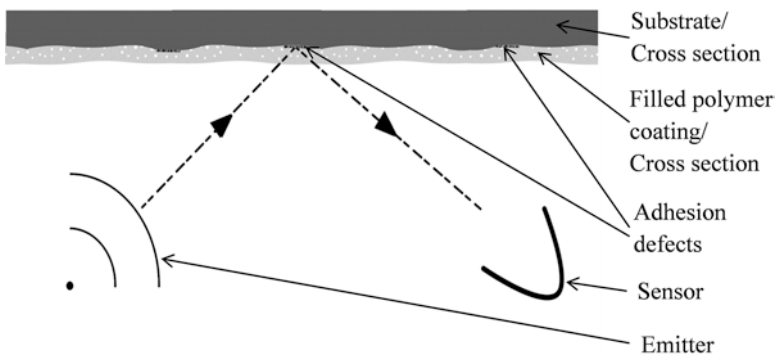
Fig. 28.4 A principle scheme of the nondestructive ultrasonic testing of the coating adhesion

has been demonstrated [77]. The authors point out several advantages of application of thermography as a tool for the industrial noninvasive analysis. It is easy to perform; the technique can be applied for the evaluation of large areas in a relatively short time [77]. When applying this method, however, one should take into account its limitations, such as difficulty to analyze the dimensions and the nature of the defects, as well as the presence of a heat flow distortion inside the analyzed material.

Other techniques, such as X-ray radiography and shearography, have been applied in the nondestructive evaluation of the adhesive contacts [63]. X-ray radiography evaluation is based on the difference in absorption of X-rays in media with different densities. This technique is capable of a relatively fine determination of the adhesive defects. However, its drawbacks are associated with high costs of the measurements mainly due to the implementation of expensive devices and long test duration. In contrast to the X-ray radiography, shearography analysis can be performed in a short time period [78]. It can be easily automated and applied to large analyzed areas [63, 79]. It is less applicable, however, in the detection of smaller defects [63]. Both the X-ray radiography and the shearography analyses of adhesive contacts are commonly applied in the aviation industry, especially for the adhesion evaluation of polymer adhesives at metal and composite joints. The results of comparison of the ultrasonic, X-ray, thermography, and shearography nondestructive techniques applied in the analysis of the delamination defects of the materials used for wind turbine blades have been demonstrated [80]. The applications of acoustic wave microscopy and spallation microscopy for the nondestructive characterization of the coating adhesion have been reported as well [81–83]. An approach and a device for the nondestructive evaluation of the adhesion of polymer coatings on nano- and microscales based on the Johnson-Kendall-Roberts (JKR) theory of the contact mechanics have been demonstrated in several publications [84–87]. This intelligent technique has been especially fruitful in the tasks of the direct determination of the work of adhesion, as well as of the surface free energy.

28.6   Conclusion

Adhesion is an essential characteristic of polymer coatings that affects their overall performance. Several adhesion mechanisms, such as chemical or physical bonding, mechanical interlocking, as well as thermodynamics at the interface, are summarized in this chapter. The factors that affect adhesion include the chemical composition of the substrate, coating thickness, mechanical properties, as well as coating service conditions, are discussed. The evaluation of adhesion is one of the key factors for improving the performance of the polymer coatings. Due to a growing interest in the creation of novel smart coatings, serving as intelligent protection and providing other special functions, as well as a capability to act "on demand," enhanced control of the coating adhesion is highly relevant. The growing functions and fields of applications of polymer coatings have motivated development of a

number of destructive and nondestructive techniques for adhesion testing. An overview of the existing methods for adhesion evaluation is provided in this chapter. Despite the variety of the destructive tests and their benefits in being relatively fast to perform and generally less expensive, development of new intelligent techniques that allow for the evaluation of coatings during their service life is highly welcome in research and industrial applications of coatings. These nondestructive techniques bring advantages in the adhesion characterization providing a possibility for the control of the coating performance in vivo. In addition to the existing methods, development of new sophisticated techniques for the evaluation of adhesion of various polymer coatings is of interest in materials science and technology and in industrial applications of the materials and coatings.

References

 1. Poisson C, Hervais V, Lacrampe MF, Krawczak P (2006) J Appl Polym Sci 101(1):118–27
 2. ASTM (2012) D907-12a, standard terminology of adhesives. ASTM International, West Conshohocken, PA
 3. Boiziau C, Lecayon G (1988) Surf Interface Anal 12:475–485
 4. Good RJ (1967) In: Patrick RL (ed) Treatise on adhesion and adhesives, vol 1. Marcel Dekker, New York, pp 9–68, Chap. 2
 5. Kreysa G, Schuetze M (eds) (2004) Corrosion handbook set: corrosive agents and their interaction with materials. Wiley, New York
 6. Chen J, Bull SJ (2011) J Phys D Appl Phys 44:1–20
 7. Moore DR (2001) Surf Coat Int J Part B Coat Trans 84:243–336
 8. Awaja F, Gilbert M, Kelly G, Fox B, Pigram PJ (2009) Prog Polym Sci 34:948–968
 9. Allen KW (2005) In: Packham DE (ed) Handbook of adhesion. Wiley, Chichester
10. Dupre A (1869) Theorie Mechanique de la Chaleur. Gauthier-Villars, Paris, p 36W
11. Schrader ME (1995) Young- Dupre revisited. Langmuir 11:3585–3589
12. Kviklys A, Lukosiute I (2004) Mech Compos Mater 40(3):253–258
13. Berlin AA, Basin VE (1974) Fundamentals of adhesion of polymers. Khimiya, Moscow
14. Lipatov YS (1980) Interphase phenomena in polymers. Naukova Dumka, Kiev
15. Packham DE (2003) Int J Adhes Adhes 23:437–448
16. Hoła J, Sadowski L, Reiner J, Stach S (2015) Constr Build Mater 84:111–120
17. van Krevelen DW (1972) Properties of polymers. Correlation with chemical structure. Elsevier, Amsterdam
18. Morris BA (2007) Understanding why adhesion in extrusion coating decreases with diminishing coating thickness. Part III: Analysis of peel test. 2007 TAPPI PLACE Conference
19. S.G. Croll, in: K.L. Mittal (Ed.). Adhesion and internal strain in polymer coatings. Adhesion aspects of polymeric coatings. Springer Science & Business Media, 2012.
20. Huang YH, Wang J (2013) Int J Adhes Adhes 40:49–55
21. Zvonkina IJ, Hilt M (2014) Tuning the mechanical performance and adhesion of UV-curable polyurethane coatings by modifying composition of the reactive diluents. European technical coatings congress (ETCC-2014). Cologne, Germany
22. Schwalm R (2006) UV coatings: basics, recent developments and new applications. Elsevier
23. Funke W (1985) J Oil Colour Chem Assoc 68:229
24. Miszczyk A, Szalinska H (1995) Prog Org Coat 25:357–363
25. Quon RA, Ulman A, Vanderlick TK (2000) Langmuir 16:8912–8916
26. Sathyanarayana MN, Yaseen M (1995) Prog Org Coat 26:275–313

27. Mittal KL (ed) (2009) Polymer surface modification: relevance to adhesion, vol 5. Koninklijke Brill NV, Leiden
28. Plueddemann EP (1983) Prog Org Coat V11(3):297–308
29. Munger CG (1984) Corrosion protection by protective coatings. National Association of Corrosion Engineers, Houston, TX, pp 206–212
30. Zucchi F, Frignani A, Grassi V, Balbo A, Trabanelli G (2008) J Mater Chem Phys 110:263–268
31. Garcia-Heras M, Jimenez-Morales A, Casal B, Galvan JC, Radzki S, Ville-gas MA (2004) J Alloys Compd 380:219–224
32. Puig M, Cabedo L, Gracenea JJ, Jiménez-Morales A, Gámez-Pérez J, Suay JJ (2014) Prog Org Coat 77:1309–1315
33. Hatefi A, Mohagheghi S, Kianvash A (2013) 743–747. J Coat Technol Res 10(5):743–747
34. Chan CM, Ko TM, Hiraoka H (1996) Polymer surface modification by plasmas and photons. Surf Sci Rep 24:3–54
35. Wolf RA (2007) Which surface activation system should I use for optimising adhesion to polymers? Annual Technical conference proceedings – Society of Vacuum Coaters, pp 704–708
36. Wolf RA (2010) Plastic surface modification. Surface treatment, decoration, and adhesion. Carl Hanser, Berlin
37. Gururaj T, Subasri R, Soma Raju KRC, Padmanabham G (2011) Effect of plasma pretreatment on adhesion and mechanical properties of UV-curable coatings on plastics. Appl Surf Sci 257:4360–4364
38. Lipatov Y (1995) Polymer reinforcement. ChemTec Publishing, Toronto
39. Fragni R, Zurlini C, Montanari A, Kiroplastis V, Penalba F (2006) Prog Org Coat 55:254–261
40. Yu J, Chary S, Das S, Tamelier J, Turner KL, Israelachvili JN (2012) Langmuir 28(31):11527–11534
41. Badge I, Stark AY, Paoloni EL, Niewiarowski PH, Dhinojwala A (2014) The role of surface chemistry in adhesion and wetting of gecko toe pads. Scientific Reports, vol 10
42. Stark AY, McClung B, Niewiarowski PH, Dhinojwala A (2014) Integr Comp Biol
43. Rickerby DS (1998) Surf Coat Technol 36:541–557
44. Napolitano MJ, Chudnovsky A, Moet A (1988) J Adhes Sci Technol 2:311–323
45. Chu YZ, Durning CJ (1992) J Appl Polym Sci 45:1151–1164
46. ASTM (2009) D3359-09e2, Standard test methods for measuring adhesion by tape test. ASTM International, West Conshohocken, PA
47. DeNolf GC, Haack L, Holubkam J, Straccia AJ, Blohowiak K, Broadbent C, Shull KR (2012) Axisymmetric peel test for adhesion measurement of polymer coatings. J Polym Sci Polym Phys 50:1706–1712
48. Dannenberg H (1961) J Appl Polym Sci 5:125–34
49. Dillard DA, Bao Y (1991) J Adhes 33:253–271
50. Taheri N, Mohammadi N, Shahidi N (2000) Polym Test 19:959–966
51. Bull SJ, Berasetegui EG (2006) Tribol Int 39:99–114
52. Adhikari S, Frankel GS, Bammel BD, Zimmerman J (2012) J Adhes Sci Technol 26:1591–1609
53. Deflorian F, Fedrizzi L (1999) J Adhes Sci Technol 13(5):629–645
54. Oliver MG, Poelman M (2012) In: Razavi RS (ed) Recent researches in corrosion evaluation and protection. InTech Publishing
55. Greenen FM, De Wit JHW (1990) Prog Org Coat 18:299
56. Amenabar I, Mendikute A, Lopez-Arraiza A, Lizaranzu M, Aurrekoetxea J (2011) Compos Part B 42:1298–1305
57. Garnier C, Pastor ML, Eyma F, Lorrain B (2011) Compos Struct 93:1328–1336
58. Veidt UM, Liew CK (2013) In: Karbhari VM (ed) Non-destructive evaluation (NDE) of polymer matrix composites. Woodhead Publishing

59. Myrdycz A, Callens D, Kot K, Monchau F, Radziszewski E, Lefebvre A, Hildebrand HF (2002) Biomol Eng 19:219–225
60. Achenbach JD (2002) Ultrasonics 40:1–10
61. Thomsen C, Maris HJ, Tauc J (1987) Thin Solid Films 154:217–223
62. Cawley P (1994) Composites 25(5):351–357
63. Ehrhart B, Valeske B (2013) In: Karbhari VM (ed) Non-destructive evaluation (NDE) of polymer matrix composites. Woodhead Publishing
64. Czarnecki L, Garbacz A, Krystosiak M (2006) Cem Concr Compos 28:360–369
65. Oehler H, Alig I, Lellinger D, Bargmann M (2012) Prog Org Coat 74:719–725
66. Alig I, Tadjbach S, Krueger P, Oehler H, Lellinger D (2009) Prog Org Coat 64:112–119
67. Bi H, Sykes J (2011) Corros Sci 53:3416–3425
68. Murthy Peri MD, Cetinkaya C (2005) J Colloid Interface Sci 288:432–443
69. Jorge Aldave I, Venegas Bosom P, Vega González L, López de Santiago I, Vollheim B, Krausz L, Georges M (2013) Infrared Phys Technol 61:167–175
70. Renshaw J, Chen JC, Holland SD, Thompson RB (2011) The sources of heat generation in vibrothermography. NDT E Int 44(8):736–739
71. Biju N, Ganesan N, Krishnamurthy CV, Balasubramaniam K (2009) Frequency optimization for eddy current thermography. NDT E Int 42(5):415–420
72. Giorleo G, Meola C (2002) Comparison between pulsed and modulated thermography in glass–epoxy laminates. NDT E Int 35:287–292
73. Avdelidis NP, Almond DP, Dobbinson A, Hawtin BC, Ibarra-Castanedo C, Maldague X (2004) Aircraft composites assessment by means of transient thermal NDT. Prog Aerosp Sci 40:143–162
74. Moropoulou A, Avdelidis NP, Koui M, Kakaras K (2001) An application of thermography for detection of delaminations in airport pavements. NDT E Int 34(5):329–335
75. Bates D, Smith G, Lu D, Hewitt J (2000) Compos Part B 31:175–185
76. Meola C, Di Maio R, Roberti N, Carlomagno GM (2005) Eng Fail Anal 12(6):875–892
77. Lario MA, Chiminelli A, Amenabar I (2015) Infrared Phys Technol 71:113–120
78. Hung YY, Ho HP (2005) Mater Sci Eng R 49:61–87
79. Liu Z, Gao J, Xie H, Wallace P (2011) Opt Lasers Eng 49:1462–1469
80. Michaloudaki M, Lehmann E, Kosteas D (2005) Int J Adhes Adhes 25:257–267
81. Du J, Tittmann BR, Ju HS (2010) Thin Solid Films 518:5786–5795
82. Guo Z, Achenbach JD, Madan A, Martin K, Graham ME (2001) Thin Sold Films 394:189–201
83. Kandula SSV, Hartfield CD, Geubelle PH, Sottos NR (2008) Thin Solid Films 516:7627–7635
84. Johnson KL, Kendall K, Roberts AD (1971) Surface energy and the contact of elastic solids. Proc R Soc A Math Phys Eng Science 324:301–313
85. Hui CY, Baney JM, Lin YY (2001) Adhes Meas Films Coat 2:299–328
86. Olah A, Vancso GJ (2005) Eur Polym J 41:2803–2823
87. Lin YY, Chang CF, Lee WT (2008) Int J Solids Struct 45(7–8):2220–2232

Chapter 29
Smart Polymer Nanoparticles for High-Performance Water-Based Coatings

José Paulo S. Farinha, Susana Piçarra, Carlos Baleizão, and J.M.G. Martinho

Abstract The increasing pressure to reduce the use of volatile organic compounds (VOCs) within the coatings industry has led to the development of waterborne systems. Water-dispersed polymer nanoparticles (i.e., latex) have been successfully used to this end, but the resulting films usually present less strength, hardness, and resistance to chemicals than solvent-borne coatings. A method to enhance the properties of these films is through chemical polymer chain cross-linking when the film is formed. This approach requires a careful balance of the cross-linking reaction rate and the polymer diffusion rate across the initial nanoparticle boundaries, and it has been extensively studied and used in industrial coatings. Herein, waterborne coatings based on reactive polymer nanoparticles and the first attempts to use "smart" polymer nanoparticles where the cross-linking is triggered by a stimulus which occurs after the desired extent of interdiffusion are reviewed. Different types of cross-linking that have the potential to be used in smart waterborne coatings, involving functional groups such as alkoxysilanes, carboxylic acids, carbodiimide, aziridine, isocyanates, and polyols, where the trigger can be a change in pH, temperature, or water content, are also discussed.

Keywords Waterborne coatings • Reactive latex • Smart nanoparticles • Polymer dispersions

J.P.S. Farinha (✉) • C. Baleizão • J.M.G. Martinho
Centro de Química-Física Molecular, IN-Institute of Nanoscience and Nanotechnology, Instituto Superior Técnico, University of Lisbon, 1049-001 Lisboa, Portugal
e-mail: farinha@tecnico.ulisboa.pt

S. Piçarra
Escola Superior de Tecnologia de Setúbal, Instituto Politécnico de Setúbal, 2910-761 Setúbal, Portugal

29.1 Introduction

Driven by environmental concerns, the coatings industry has moved from solvent-borne coatings toward waterborne coatings, in order to reduce volatile organic compound (VOC) releases, as forced by environmental concerns. Coatings based on aqueous dispersions of polymer nanoparticles (latex coatings) were found to be a good alternative to solvent-borne coatings, although generally with inferior performance essentially due to subpar properties such as strength, hardness, and solvent resisting capabilities. Nevertheless, polymer films with good properties can be obtained from latex dispersions containing large polymer chains, when the length over which the chains diffuse is comparable to their radius of gyration, resulting in interfacial healing between adjacent polymeric nanoparticles [1, 2]. However, the diffusion of large polymer chains is slow, requiring the use of VOCs to achieve reasonable film formation times. Alternatively, interparticle healing can be achieved by incorporating reactive groups in the nanoparticles, so that upon contact between the nanoparticles, the reactive groups form cross-links across adjacent particles. This approach has been used to improve the performance of zero VOC coatings in thermoset latex coatings.

The different stages involved in the formation of a polymer film from a water dispersion of polymer nanoparticles (latex) are depicted in Fig. 29.1 [3, 4]. After water evaporation, film drying leads to a densely close-packed arrangement of the polymer particles (stage I). This is followed by particle deformation via capillary, osmotic, and surface forces, which occurs if the film is above the "minimum film formation temperature"

Fig. 29.1 Film formation from a water dispersion of polymer nanoparticles
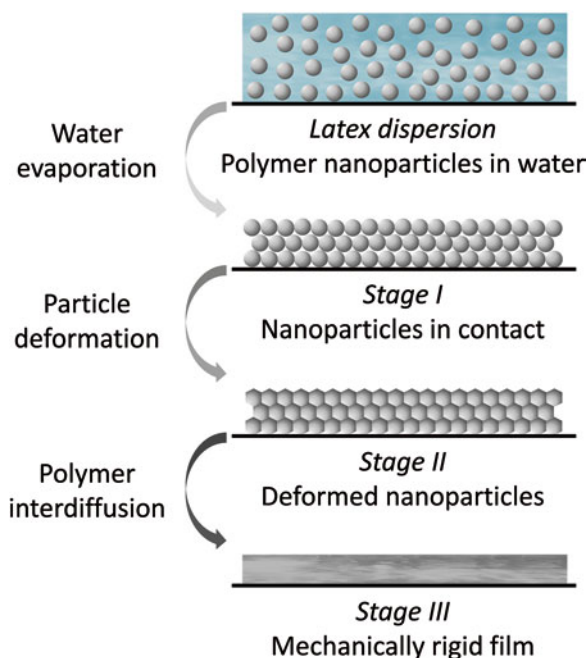
(near the polymer's glass transition temperature, T_g, in the presence of water), to yield a nascent film constituted by space-filling polyhedral in close contact (stage II). These transparent void-free films still have weak interfaces between the particles, which are strengthened by polymer chain diffusion among adjacent particles. Diffusion occurs at temperatures above the T_g of the polymer, until complete healing of the interface by interdiffusion of the polymer chains and formation of entanglements across the interfaces between particles, to form a mechanically rigid film (stage III). The degree of entanglements formed between particles determines how strong the interface is.

Thermoplastic latex films without chemical cross-links usually show poor performance since the interfaces generated during healing are relatively sharp due to the slow diffusion of polymer chains with molecular weight above the entanglement molecular weight. This has driven many efforts to develop high-performance thermoset latex films by cross-linking the polymer chains during the healing of the interfaces. This process must be fully controlled since cross-linking retards and even stops polymer diffusion. Thus, a fine balance between polymer interdiffusion and the rate of cross-linking is required to optimize the film's mechanical properties [5]. In addition, the cross-linking reaction must not occur during storage of the dispersion, should not produce VOCs, and the final film must have a performance comparable to that of organic solvent-based coatings.

29.1.1   Theory of Polymer Diffusion and Cross-Linking

The mechanical strength and toughness of a latex film (its ability to store and dissipate energy during deformation) is strongly influenced by the formation of entanglements across the interface during healing. However, it was shown that these properties can be further improved if the chains are anchored at opposite sides of the initial interface by cross-links created during polymer interdiffusion [6].

A theoretical model for diffusion and cross-linking within polymer films was developed by de Gennes [7, 8] to explain the coupling between diffusion and reaction, as well as the influence of long-chain branches and cross-linking on the properties of thermoset latex films. The model defines three main regimes [7]. In the first regime, the cross-linking reactions are much slower than polymer interdiffusion, leading to complete interfacial healing prior to significant gel development, with the properties of the resulting film being similar to those of the bulk material. The second regime is defined by comparable rates of reaction and interdiffusion, yielding a nonequilibrium interface in which a considerable amount of cross-links are developed during polymer diffusion and the mean chain length between cross-links spans the interface. The third and final regime corresponds to the case where the reaction outpaces diffusion, so that the polymer chains are trapped inside their original particles and there is no interface healing. In this last case, adhesion is entirely caused by the dangling polymer chain ends that diffuse upon completion of the reaction, a situation akin to that of films created from pre-cross-linked latex nanoparticles that show very poor mechanical properties [7].

The model considers a linear monodispersed statistical copolymer composed of two blocks, A and A^*, with a total number of monomers, N, higher than the critical number of monomers for entanglements, N_e. Each polymer chain contains one of its A^* sites functionalized with a small group X that can react upon encountering any of the A^* sites of another polymer chain to form a cross-link, with each chain forming a single cross-link (considered enough to stop the diffusion and immobilize the involved chains). A nondimensional parameter α is defined as the ratio of two characteristic times: the diffusion time, T_{diff}, and the reaction time, T_{reac}:

$$\alpha = \frac{T_{diff}}{T_{reac}} \qquad (29.1)$$

The diffusion time, T_{diff}, is considered in the context of the de Gennes theory of reputation [9, 10] as the time needed for a chain to diffuse out of its original confining tube:

$$T_{diff} = T_{rep} = \tau_0 \frac{N^3}{N_e} \qquad (29.2)$$

where τ_0 is the relaxation time of one monomer.

The reaction time, T_{reac}, is defined as the time for one cross-link to form in each chain and can be expressed in terms of the rate constant of the cross-linking reaction, k, the number of monomers between cross-links, N_c, and the number of A^* sites not bearing the functional group, A_0^*:

$$T_{reac} \cong \frac{N_c}{N} \frac{1}{kA_0^*} \qquad (29.3)$$

When the cross-linking density is low, $N_c \cong N$, and α is given by

$$\alpha = kA_0^* T_{rep} \qquad (29.4)$$

This means that α is the number of cross-links that a given chain forms in each displacement from the confining tube. This is a virtual number because the model assumes that each chain can only make a single cross-linking. The parameter α can also be understood as the number of cross-links that a given chain would form, if it were able to react an infinite number of times.

Values of $\alpha \gg 1$ define the fast-reaction regime in which reaction is much faster than interdiffusion, and hence all chains are fixed by cross-links before diffusing across the interface. In this case, no cross-links bridge the interface, and adhesion is due entirely to pullout of the dangling chain ends that cross the interface. A crossover occurs at $\alpha = 1$, from the fast to the slow regime. In the slow regime ($\alpha \ll 1$), the cross-linking reaction is much slower than interdiffusion, and consequently the interface heals before significant cross-links are formed, thus becoming similar to the bulk network.

The adhesion energy of a polymer film depends mainly on the polymer chain length, all other parameters being fixed. For short chains (fast diffusion), the system is in the slow-reaction regime ($\alpha \ll 1$), and the adhesion energy is independent of chain length, presenting its highest value. In this regime the chains bridge the interface, and fracture can only occur by scission of the chain. With the increase of chain length, the crossover ($\alpha = 1$) is reached, and within the fast-reaction regime ($\alpha \gg 1$), the adhesion energy decreases, first with a smaller slope up to $\alpha_2 = \left(N / N_c \right)^2$ and then faster, toward zero adhesion energy. These two sub-regimes are characterized by a minute amount of chain interfacial spanning. In the first sub-regime, the portion of the chain crossing the interface is still large enough to ensure that fracture can only occur by chain scission. In the second sub-regime, only the chain ends cross the interface, and fracture occurs mainly by pullout of the chain ends. As the energy to break a bond is around two orders of magnitude higher than the energy to extract a chain end from the network, the slopes change accordingly. The most interesting regime for waterborne latex films is the slow-reaction regime where adhesion attains its highest value.

29.1.2 Measuring Polymer Diffusion During Film Formation

Small angle neutron scattering (SANS) and Förster resonance energy transfer (FRET) are ubiquitous techniques for the characterization of polymer diffusion in latex films. Hahn [11, 12] was a pioneer in carrying out SANS experiments to investigate the relationship between polymer interdiffusion and film tensile strength [13, 14], by using deuterated polymer particles to achieve neutron scattering contrast. In the case of FRET, it is only needed that the polymer particles are labeled with a minute portion (<1 % mol) of fluorescent dyes (an energy donor and an acceptor). The methodology was established by Morawetz [15–17] and further developed and used by Winnik for latex film formation investigations [18–20]. The dyes necessary for FRET measurements are usually incorporated into the nanoparticles by copolymerizing the corresponding comonomer derivatives containing groups such as acrylate, methacrylate, or vinyl.

Since its humble beginnings, the use of FRET has been developed in order to be used in progressively more complex geometries [21–23] and dye distributions [24–26], allowing the experimental evaluation of complex nanostructured materials [27]. Specific cases in which the use of FRET has been implemented include the study of the effect of temperature [28], composition [29], moisture [30], coalescing aids [24, 31–33], polar groups at the particle surface [34, 35], and the presence of filler particles [36–39] on latex film formation.

FRET occurs from the electronically excited donor dye to an acceptor dye, when the emission spectrum of the first overlaps the absorption of the second and the dyes are in close proximity (typically a few nanometers), altering both the fluorescence emission spectra and the fluorescence decay of the dyes. The typical length scale of FRET matches the size of interparticle domains in latex films and is small enough to avoid the interference by capillary waves at the interface.

In FRET experiments, the films are prepared from a blend of donor and acceptor-labeled latex particles, where the dyes are chosen so that the fluorescence spectrum of the donor overlaps the absorption spectrum of the acceptor [27, 41]. Due to their extremely low molar fractions, the dyes act merely as tracers for the polymer location, so that the distribution of the dyes mimes the distribution of the polymer chains in the material. These experiments can thus provide detailed information on the distribution of the labeled polymer components and the morphology of the nanostructure [27]. If donor and acceptor dyes are located in different particles, FRET measurements can be used to evaluate the extent of mixing during the formation of the polymer film. In the nascent film, the dyes are confined in separate particles and the efficiency of FRET is limited (it occurs only between dyes located across the interface between adjacent particles). Subsequent curing of the film leads to polymer diffusion across the interface between particles, thus mixing donor- and acceptor-labeled polymer chains, and consequently increasing the efficiency of energy transfer.

To quantify the extent of polymer diffusion during the film formation process, one usually measures the donor fluorescence decay curve, $I_{DA}(t)$ [41]. At this point, one of two different strategies can be used to analyze the experimental results. If a thorough characterization of the film morphology is desired, the donor fluorescence decay curve should be analyzed using a detailed FRET model [27]. If only a comparative approach is needed, a simpler strategy utilizing the quantum efficiency of energy transfer $\Phi_{ET}(t_{diff})$ can be used to estimate the evolution of interdiffusion during film formation:

$$\Phi_{ET}\left(t_{diff}\right) = 1 - \frac{\int\limits_{0}^{\infty} I_{DA}\left(t\right)dt}{\int\limits_{0}^{\infty} I_{D}\left(t\right)dt} \tag{29.5}$$

where the integrals correspond to the areas beneath the donor decay curve for a latex film cast from a mixture of donor- and acceptor-labeled particles, $I_{DA}(t)$, and of a film cast from only donor-labeled particles, $I_{D}(t)$. Such a technique avoids multiple drawbacks found when determining FRET efficiencies via fluorescence spectra [41]. Indeed, by measuring the decay curves, it is not required that only the donors absorb the excitation light, because the donor decay is invariant to the presence or absence of excited acceptors. Furthermore, since only the decay shape is used in the analysis (and not the intensity), the films with only donors or mixtures of donors and acceptors do not need to have exactly the same optical density. Additionally, geometric effects that are important in steady-state fluorescence measurements do not affect the decay curves, and light scattering can be easily accounted for.

The evolution of the extent of mixing in the annealing process of latex films can be approximated by the increasing quantum efficiency of energy transfer, normalized against measurements obtained for pre-annealed ($t_{diff}=0$) and fully mixed films ($t_{diff}=\infty$) [24, 25]:

$$f_m\left(t_{diff}\right) \approx \frac{\Phi_{ET}\left(t_{diff}\right) - \Phi_{ET}\left(0\right)}{\Phi_{ET}\left(\infty\right) - \Phi_{ET}\left(0\right)} \tag{29.6}$$

Determination of a fully mixed film's quantum efficiency of energy transfer (corresponding to $t_{diff} = \infty$) is done through film casting from a suitable solvent for the said system. In cases where the particles are partially cross-linked and complete mixing is not experimentally accessible, it is necessary to estimate this value [39].

The result of Eq. (29.6) provides a decent approximation of the realistic extent of mixing in latex films ranging up to 70 % mixing [24]. Increasingly complex methodologies must be undertaken if a more precise extent of mixing estimation is desired, by taking into account the morphology of the evolving interparticle boundary during film formation [24, 25].

29.2   Reactive Cross-Linking Strategies

High-performance coatings usually rely on cross-linking to achieve strength and solvent resistance. Solvent-borne coatings have a particular prominence in the area of high-performance coatings. In these systems, usually constituted by low molecular weight polymers, the films develop their properties through the formation of cross-links in the dry film. However, waterborne polymeric systems can also be tailored so as to impart specific properties that are required in high-performance coatings, via the introduction of functional moieties in the polymer nanoparticle, which can create cross-linking in the dry film. These systems include functional latex nanoparticles containing, for example, epoxy groups, *N*-methylolamide groups, *N*-isobutoxymethylamide, acetoacetyl groups, and others. Some functional moieties, such as epoxies or alkoxymethylamines, will react with themselves when the appropriate conditions are met, whereas others require the incorporation of a multifunctional reactant (external cross-linker) [43] or that two reactive groups are confined in different nanoparticles and react during chain interdiffusion [42].

As noted in the previous section, in the design of effective reactive waterborne coating systems, the cross-linking agents have to be carefully chosen to avoid a large retardation (or even suppression) of chain interdiffusion, in which case only superficial cross-links would be formed, unable to endow good mechanical characteristics to the final film. While the polymer diffusion rate for linear chains mostly depends on the temperature and chain length, cross-links introduce branches in the polymer chains which decrease their diffusion rate exponentially and create networks that ultimately cease polymer diffusion [43]. Therefore, in order to obtain films with good mechanical performance and chemical resistance, the cross-linking reactions have to occur in a large extent, but only after substantial polymer mixing across the nanoparticle boundaries [40].

Three main strategies are used to adjust the relative rates of diffusion and reaction: change the type and concentration of catalyst (if one is used), which affects the

reaction rate; change the polymer chain length, which affects the rate at which it diffuses; or modify the temperature, which usually has a greater influence on the rate of polymer diffusion than on the rate of the cross-linking reaction.

As for the development of reactive dispersions, one can introduce reactive groups into polymer nanoparticles for waterborne coating formulations through one of two ways. The first is by copolymerization of reactive functionalities into the nanoparticles during emulsion polymerization and introduction of an external cross-linker immediately before application. The second is by the introduction of different reactive groups confined within separate nanoparticles that can only cross-link after chain diffusion between adjacent nanoparticles (reactive blends) [40, 45]. Some specific examples of these strategies implemented using different cross-linking chemistries will now be discussed.

29.2.1   Acetoacetoxy Cross-Linking

An example of the use of an external cross-linker that reacts with functional groups in the polymer nanoparticles was presented by Winnik and German [44], who studied the effect of polymer diffusion and cross-linking in low T_g methacrylate-based polymer nanoparticles bearing acetoacetoxy groups, cured with 1,6-hexanediamine cross-linker. The presence of diamine leads to the formation of enamines that induced the controlled flocculation of the dispersion, improving its rheological properties. The diamine and acetoacetoxy moieties' cross-linking reaction happens rapidly, even when dispersed, thus preceding polymer diffusion. Nevertheless, the films showed excellent solvent resistance, possibly due to the reversibility of the reaction between amine and acetoacetoxy allowing polymer diffusion to evolve even after significant gel content was achieved.

29.2.2   Melamine-Formaldehyde Cross-Linking

This chemistry has long been used in high-performance waterborne coatings. The functionality can either be introduced using an additive to the dispersion or by incorporating a reactive monomer directly in the polymer nanoparticles.

Aqueous dispersions of an acrylic latex containing –OH or –COOH groups react with melamine derivatives, for example, hexamethoxymethyl melamine (HMMM), upon heating (Fig. 29.2). This cross-linking technology has been extensively used in industrial coatings and presents a good balance of desirable traits like resistance to chemicals, flexibility, and strength.

By measuring the relative rates of cross-linking (from the film gel content) and interparticle polymer diffusion (from the FRET efficiency, by using dye-labeled polymer nanoparticles), it was possible to evaluate the role of temperature and nanoparticle morphology on the film properties and the location of the melamine-
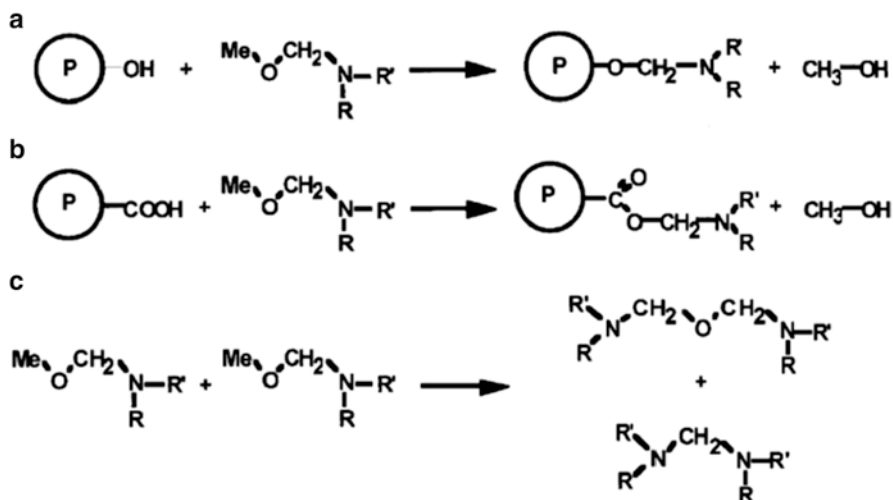
Fig. 29.2 Alkoxymethylene melamine derivatives can react with –OH groups in the polymer via acid-catalyzed alkoxy exchange (**a**), with the carboxylic acid groups of the MAA comonomer (**b**), or they self-condense (**c**). Reprinted with permission from [48]; Copyright 1999 Springer

formaldehyde resin in the dry film before the onset of cross-linking [48]. In films prepared from copolymer nanoparticles of poly(butyl methacrylate) (PBMA), hydroxyethyl methacrylate (HEMA), and methacrylic acid (MAA) containing HMMM, this acted as a plasticizer, enhancing the polymer diffusion rate by increasing the system's free volume, before acting as a cross-linker [48]. On the other hand, in films prepared from core-shell nanoparticles in which the core was PBMA and the shell was a copolymer containing HEMA and MAA, HMMM was confined to the polar polymer shell and could not act as a plasticizer for the PBMA, yielding films with poor mechanical properties. Cross-linking by HMMM is fast even at low temperatures (100 °C), catalyzed by –COOH groups within the polymer and with no need for externally added acid catalyst.

These systems allow some degree of control over the ratio between diffusion and reaction because the chain length and temperature dictate the polymer diffusion rate, while the temperature determines the melamine reaction rate along with the available acid (catalyst or –COOH groups) and the local concentration of cross-linkable functionality on the polymer. For all temperatures examined by the authors, the cross-linking reaction was outpaced by polymer diffusion, with diffusion and formation of entanglements occurring prior to the lockdown of the polymer network.

In the reactive monomer approach, acrylamide derivatives such as *N*-methylolacrylamide (NMA) or alkylether-containing monomers such as *N*-(isobutoxymethyl) acrylamide (IBMA) are introduced during the latex synthesis. Mild acidic environments will cause the condensation of the methylol groups with hydroxyl, carboxyl, or amide moieties (Fig. 29.3) and can also self-condense under acid or basic conditions.

Crosslinking Reaction Between Crosslinker and Polymer

Self-Condensation Reaction

$$2 \, {>}N\text{-}CH_2OR \longrightarrow {>}N\text{-}CH_2\text{-}O\text{-}CH_2\text{-}N{<} + ROH\uparrow$$

$$R = H, \, CH_3, \, CH_2CH_2CH_2CH_3$$
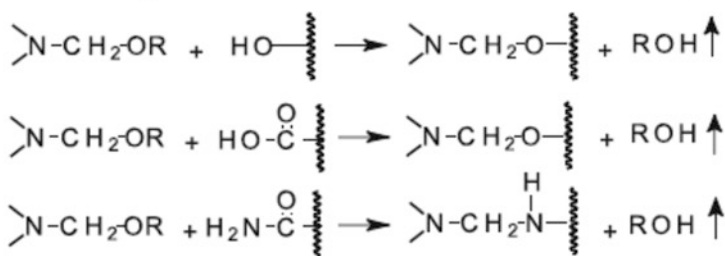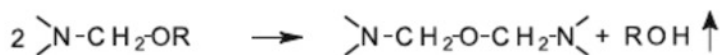
Fig. 29.3 Possible cross-linking (and self-condensation) reactions in polymers containing alkyl-ether functions. Reprinted with permission from [19]; Copyright 2004 Springer

In one example, nanoparticles of IBMA, butyl acrylate (BA), and methyl methacrylate (MMA) were used to cast films in which cross-linking by the IBMA comonomer (Fig. 29.4) formed long-chain branches that slowed the rate of polymer interdiffusion in the film [46]. In order to obtain films in which a larger extent of polymer interdiffusion preceded full gelation, the authors tried to boost the polymer interdiffusion rate relative to the cross-linking rate by decreasing the amount of acid catalyst or by using a weaker acid. On the other hand, increasing the thermal conditions impacts both rates, but has a larger influence on the rate of polymer diffusion. While there was no gel detected in films prepared without acid (with up to 3 h of curing at 80 °C), the rate of gel formation in films containing phosphoric acid was much slower than that obtained for the reaction catalyzed by *p*-toluenesulfonic acid (PTSA).

To evaluate the relative polymer diffusion and cross-linking rates, the authors used a latex film containing ca. 1 mol% of IBMA in a copolymer of BA-MMA. Polymer diffusion was monitored by FRET for films prepared from mixtures of nanoparticles labeled with either phenanthrene (donor) or anthracene (acceptor) [27]. In a film cured at 80 °C in the presence of 0.5 wt% PTSA, diffusion was retarded relative to the acid-free film, with the onset of polymer diffusion preceding extensive gel formation, but ceasing completely when the gel content reached ca. 40 %. Using a weaker acid (0.2 wt% phosphoric acid), the rate of cross-link formation was slowed down, and polymer diffusion occurred before full cross-linking [46].

N-methylolacrylamide (NMA) has also been proposed as a reactive comonomer to obtain homogeneous cross-linking in coatings. However, its higher water solubility is thought to lead to NMA selective enrichment of the nanoparticle shell region, favoring interfacial curing [50]. The massive yields of gel found within the films strongly limit the extent to which polymer diffusion and interfacial healing can take place.
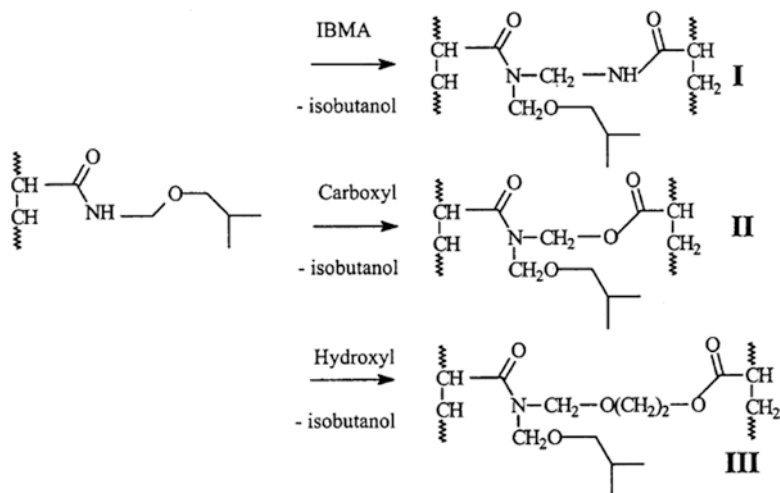
Fig. 29.4 Several reactions typical of IBMA cross-linking: reaction between two IBMA groups to form a methylene bis(acrylamide) linkage (I), exchange reaction with a polymer-bound carboxyl group (II), and exchange reaction with a polymer-bound hydroxyl group (III). Reprinted with permission from [46]; Copyright 2001 American Chemical Society

29.2.3 Acetal Cross-Linking

While stable in basic conditions, the acetal functional group can deprotonate in low pH environments, forming an intermediate that undergoes acid-catalyzed self-condensation and can be used to incorporate cross-links in polymers under ambient conditions (without the formation of toxic side products, such as formaldehyde, resulting from *N*-methylolacrylamide cross-linking). By introducing *N*-(4,4-diethoxybutyl) methacrylamide (MABEA, Fig. 29.5) into polymer nanoparticles produced via emulsion copolymerization with 2-ethylhexyl methacrylate (EHMA), it is possible to obtain cross-linked films by acidification of the nanoparticle dispersion before film formation [51].

In a low pH environment, hydrolysis of the acetal moieties yields functional groups (typically aldehyde) that are able to react at ambient conditions with diols or amines. Cross-linking reactions in polymer films can be triggered by the resulting aldehyde, occurring either by self-condensation (such as aldol condensation) or by reaction with an additional cross-linker. The hydrolysis kinetics of the acetal moieties happened faster than the following self-condensation reaction. This allows for diffusion of the lowest molecular weight polymer chains, which eventually reacted to become incorporated in the polymer network [51]. Cross-link formation kinetics was improved after lowering the latex dispersion's pH and raising the acetal functional content. Since the hydrolysis of the acetal groups is fast and efficient, practically all of these groups became available for cross-linking reactions. Furthermore, all films displayed good organic solvent resistance in addition to acceptable mechanical characteristic, as shown in the increases in tensile strength [51].

Fig. 29.5 Chemical
structure of *N*-(4,4-
diethoxybutyl)
methacrylamide (MABEA)
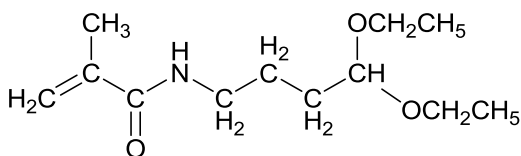
29.2.4 Epoxy Cross-Linking

Epoxy groups (oxiranes) react with carboxylic acids, their ammonium salts, and
with amines (Fig. 29.6). Epoxy groups have been incorporated into carboxylic acid-
containing nanoparticles using the glycidyl methacrylate (GMA) comonomer.
While the epoxy reacts slowly with the carboxylic acid moieties of the polymer at
ambient temperature, only a relatively small fraction is needed to start gel forma-
tion, which retards polymer diffusion, resulting in a weak film. Another approach
consists of separating the two reactants into different nanoparticles by blending
GMA-containing polymer nanoparticles with acid- or amine-containing polymer
nanoparticles, so that the cross-linking reaction only occurs after polymer interdif-
fusion. This approach, however, is strongly hindered by the hydrolysis of epoxy to
diols with time, which reduces the dispersion's shelf life. Furthermore, MMA-BA-
GMA copolymer nanoparticles showed rapid and spontaneous gel formation in
aqueous dispersion, which limited interparticle polymer diffusion in the films cast
from the dispersions [47, 49]. A variation of this strategy has been recently pre-
sented, in which GMA functionalized nanoparticles were introduced in a melamine-
formaldehyde resin or urea-formaldehyde resin [53].

29.2.5 Isocyanate Cross-Linking

Isocyanate-containing polymer nanoparticles have been prepared, for example, by
incorporating a comonomer of 1-(3′isopropenylphenyl)-1-methyl-ethylisocyanate
(TMI). El-Aasser examined the incorporation of the –N=C=O moiety into polymer
nanoparticles of poly(styrene-*co*-butyl acrylate) and the stability of this group toward
hydrolysis in the dispersion [52]. The films were cured by adding α,ω-diamino-
poly(isobutylene) to the dispersion. Films with surprisingly good mechanical proper-
ties were obtained in spite of the strong immiscibility of poly (isobutylene) and poly
(styrene-co-butyl acrylate). This was explained by the reaction between the groups of
the two polymers, which created an interphase between the nanoparticles.

29.2.6 Ionic Cross-Linking

Zinc cross-linking was one of the first successful waterborne non-formaldehyde
chemistries, with the addition of zinc salts to cross-link carboxylic acid-containing
waterborne dispersions being practiced within the industry. The strong coulombic

Fig. 29.6 Reactions of an epoxy group used for polymer cross-linking. Adapted with permission from [19]; Copyright 2004 Springer
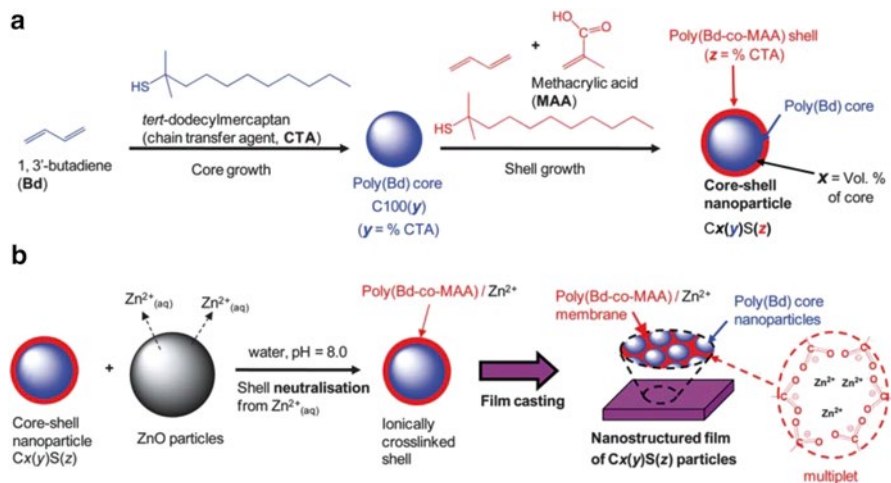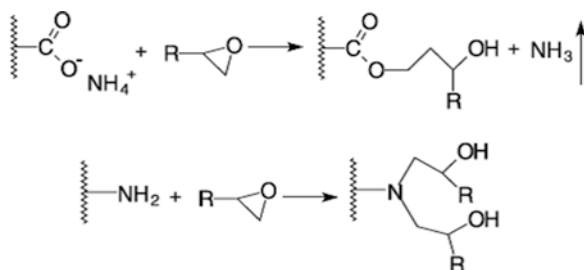
Fig. 29.7 Method used to prepare (**a**) core-shell nanoparticles with variably cross-linked cores and shells and (**b**) nanostructured ionomer films. The membranes of nanoparticle shell phases in the films are believed to contain multiplets (depicted). The symbols *x*, *y*, and *z* are the volume % of core in the C*x*(*y*)S(*z*) core-shell nanoparticles, wt% of CTA used to prepare the core, and wt% CTA used to prepare the shell, respectively. Adapted with permission from [54]; Copyright 2012 RSC

interaction between the zinc cations and carboxylate anions leads to tight ion pairs that tend to associate in ionomer-like interactions. The advantage of this technology is that it provides a one-pack stable system that produces ambient curable films with excellent hardness and water resistance, albeit with poor resistance to products containing competing anions, such as ammonia from cleaners [19]. More recently, the use of this cross-linking chemistry in waterborne coatings was revisited using core-shell nanoparticles with a rubbery 1,3-butadiene core and an ionomer copolymer shell of 1,3-butadiene and methacrylic acid (MAA) [54]. The system could be ionically cross-linked using zinc ions and cast to form nanostructured ionomer films (Fig. 29.7) [56]. The stress/strain results indicated the nanostructured films' modulus, and strain at break values could be tuned by changing the chain transfer agent concentration, which controls the extent of covalent cross-linking.

29.2.7   Carbodiimide Cross-Linking

This chemistry has been used to prepare "two pack in one pot" systems, consisting of a pair of components with high intrinsic reactivity toward each other but present in separate polymer nanoparticles, which can therefore be stored together for long periods of time. This approach can be implemented by using mixed dispersion of two different types of polymer nanoparticles, each with a different functionality. In one example, nanoparticles containing carbodiimide (–N=C=N–) groups were mixed with nanoparticles containing carboxylic acid moieties [45, 57]. In this blend, the freshly formed film's reactive moieties are confined to their separate nanoparticles, one composed of *t*-butyl-carbodiimidoethyl methacrylate (tBCEMA) and 2-ethylhexyl methacrylate (EHMA) and the other of MAA and EHMA. When the functional groups come into contact during film formation, they react to form an *N*-acylurea and in the process create a covalent bond between the two polymers. While some of these groups can react at the interface between nanoparticles, extensive reaction can only occur if the polymers containing the two types of reactive groups diffuse to neighbor nanoparticles. However, while polymer diffusion is necessary to bring the reactive groups together, once the chemical reaction occurs, it introduces chain branches which retard the rate of diffusion. As described before, if diffusion is much slower than the reaction, a tight cross-linked membrane at the interface between adjacent nanoparticles will be created, suppressing further diffusion across that boundary and eventually limiting the film performance.

One issue with this system is that the carbodiimide moiety stability is dictated by the polymer's hydrophobicity, the –N=C=N– group's steric protection, medium's pH, and the thermal conditions present. However, in a dispersion of copolymer nanoparticles of *t*BCEMA and EHMA, more than 90 % of the carbodiimide groups survived after a 1-year storage period at 23 °C [45].

Another issue (one that is common in polymer blends) is that although the polymer composition is similar in the two types of nanoparticles (both based in EHMA), the different comonomers (*t*BCEMA and MMA) reduce polymer mixability, thus limiting diffusion across the interparticle boundary and consequently decreasing cross-linking [42]. To evaluate this effect, the authors compared the mixing in the film, as measured by FRET efficiency, with the extent of carbodiimide reaction, monitored by the decrease in the FTIR intensity at 2128 cm^{-1}. The clearest indication of limited miscibility between the two dispersion components is observed in solvent-cast films prepared from freeze-dried blends of different dispersions. Annealing of the films at 60 °C initially led to polymer de-mixing (measured by the decrease in FRET efficiency for nanoparticles labeled with donor and acceptor dyes, Fig. 29.8). However, as the *t*BCEMA and MMA react (limiting the evolution of the de-mixing process), polymer diffusion begins to dominate, with the extent of carbodiimide reaction increasing to approximately 60 %. Model experiments suggest that the increased miscibility is partially due to the higher compatibility of –COOH and dialkyl urea groups, but is also contributed by graft copolymer formation [42].
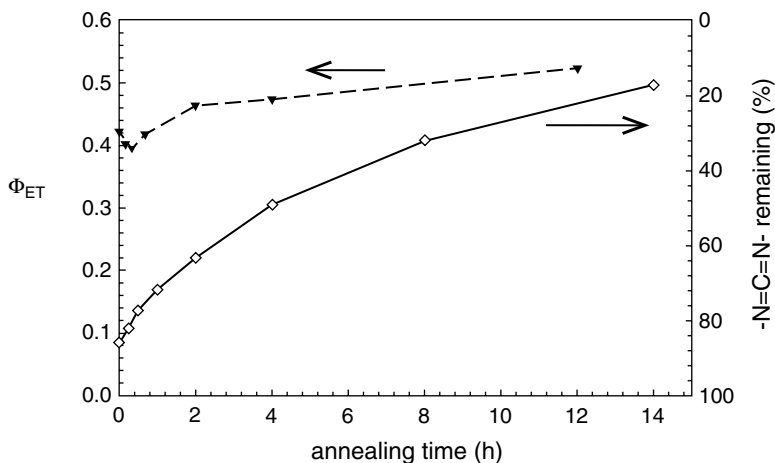
Fig. 29.8 Plots of ET and percentage of –N=C=N– remaining vs. time for THF-cast films prepared from the D-MAA-11/A-*t*BCEMA-5 blend and annealed at 60 °C in films formed at 22 °C. Reprinted with permission from [42]; Copyright 2000 American Chemical Society

In this system, the different functionalities present in the nanoparticles are not only responsible for the cross-linking reactions associated with good film mechanical properties but also play an important role in avoiding the segregation of the different polymers in the film, thus promoting the formation of the blend film. This multifunctional characteristic can be seen as a precursor to the "smart" systems discussed in the next section.

29.3   Smart Polymer Nanoparticles

In recent years a novel generation of smart polymer water-based coatings with improved properties has been emerging. These use polymer nanoparticles with specific functionalities that either respond to particular changes in the environment, or alternatively, to external applied stimuli. Some of the possible stimuli are temperature, light, pH, or water content.

The concept of *equilibrium dynamics* involving the water content of the drying film was used to develop a new class of smart nanoparticles that protect latent functional groups until they are needed to cross-link the film [58]. Smart acrylate particles were produced by the introduction of the functional monomer 4-hydroxyethylsulfonylstyrene (HESS), during the emulsion polymerization of BMA and BA. At neutral pH, the not-cross-linkable HESS groups are in dynamic equilibrium (by loss of water molecules) with vinyl sulfones, which are capable of reacting with OH nucleophile groups in the chains and form cross-links (Fig. 29.9). During storage, when excess water is present, any reactive species formed recombine to regenerate the latent HESS group, hence preventing
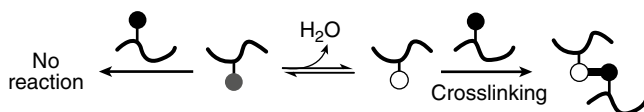
Fig. 29.9 Representation of the dynamic equilibrium and cross-linking of latent reactive chains, with spheres representing functional groups on polymer chains: (*gray*) latent hydroxyethylsulfone group, HEMA; (*white*) reactive derivative; and (*black*) hydroxyl group. Reprinted with permission from [58]; Copyright 2005 Royal Society of Chemistry

cross-linking reactions. However, during film formation, water loss promotes the formation of the reactive vinyl sulfone that leads to irreversible cross-linking. The dispersions are stable during very long periods of time (negligible gel fractions were observed for storage periods of at least 6 months) and the resulting films present good mechanical properties.

Another example of cross-linking triggered by water loss was developed by Chen et al. [55]. In this case, the dispersions were prepared by blending nanoparticles functionalized with chloromethylstyrene and with a tertiary amine in water, forming very stable self-curable latex films at room temperature. When cast and dried, these dispersions produce cross-linked continuous polymer films through the Menschutkin reaction concerning the reactive chlorides and tertiary amino moieties (Fig. 29.10). These blends are unreactive in aqueous media and stable for long periods of storage (at least 4 years, according to the authors). In solid state they cross-link to a large extent and form films with high gel content. The mechanical properties of the films strongly depend on the cross-linking density and can be tuned by controlling the reactive chloride and tertiary amino group ratio within the two copolymers.

Since the cross-linking reaction is reversible at high temperatures, with de-cross-linking occurring through the retro-Menschutkin mechanism [59, 61, 62], the films are self-curable, with thermo-compression at 215 °C yielding good flowability under shear. After cooling, continuous transparent films were obtained, with smooth surfaces and gel content similar to the original films. Due to their positive charges, the films also demonstrated catalytic activity, suitable for use as sealants and adhesives and for membrane applications [60].

Despite the advantages of the dispersions in the previous two examples, both present the drawback of still requiring surfactants for the synthesis of the nanoparticles, which can be detrimental for film performance. Indeed, residual emulsifier can migrate to the interface during film formation, inhibiting diffusion. In one example, this was solved by using a polymerizable surfactant (ammonium allyloxtmethylate nonylphenol ethoxylates sulfate) and a self-cross-linker (*N*-methylolacrylamide) as functional monomers in the emulsion polymerization of MMA and BA with the fluoroacrylate monomer dodecafluoroheptyl methacrylate (DFMA) [63]. In the polymerization, DFMA was incorporated into the acrylate polymer chains, creating nanoparticles with fluorinated shells. During film formation, the fluorinated polymer side chains migrate to the polymer-air interface, forming a fluorinated layer that contributed to the hydrophobicity and thermal resistance of the film surface. The smart
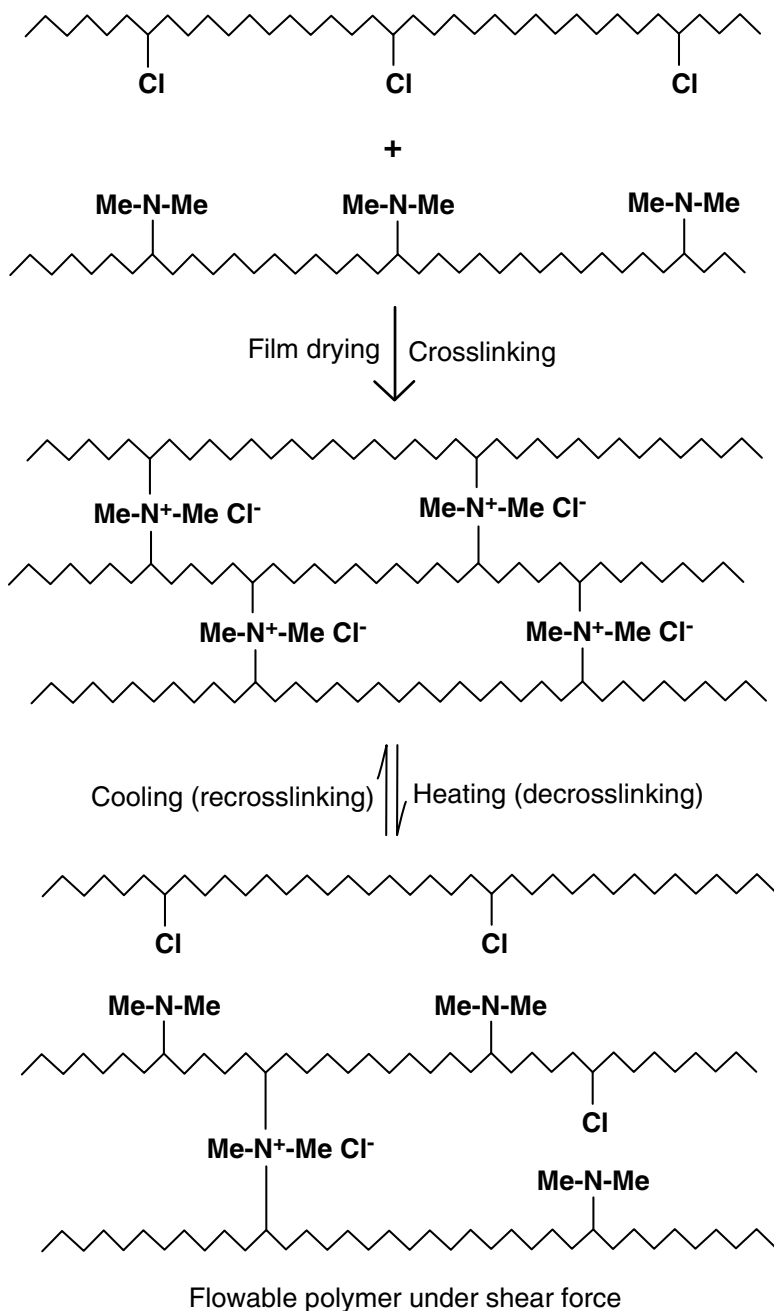
Fig. 29.10 Reversible cross-linking triggered by water loss in nanoparticles functionalized with chloromethylstyrene and tertiary amine groups, through the Menschutkin reaction. Reprinted with permission from [55]; Copyright 2005 Wiley

behavior of the nanoparticles resulted from the self-cross-linker functional monomer (also incorporated into the chains during emulsion polymerization), which remained unreactive in the dispersion but, once triggered by water loss, reacted to form cross-links in the film (Fig. 29.11). Cross-linking enhances the final films' mechanical properties and, restricting the fluoroalkyl groups from migrating into the interior of the film, improves the hydrophobic characteristics of the surfaces [63, 65, 77].

Reactive fillers, which can act as both latex fillers and cross-linkers, can also be used to obtain smart dispersions [66]. Peroxidized monodisperse polystyrene particles are suitable reactive fillers for acrylic and styrene–butadiene latexes. They can be produced by the emulsion polymerization of styrene alongside a polyperoxide initiator-surfactant, which becomes covalently grafted onto the surface of the particles during polymerization (Fig. 29.12). The polyperoxide functionalized latex particles are negatively charged and form very stable dispersions. However, when triggered by water loss, these reactive fillers can cross-link acrylic and styrene–butadiene latexes. Although the properties of these coatings depend both on the reaction
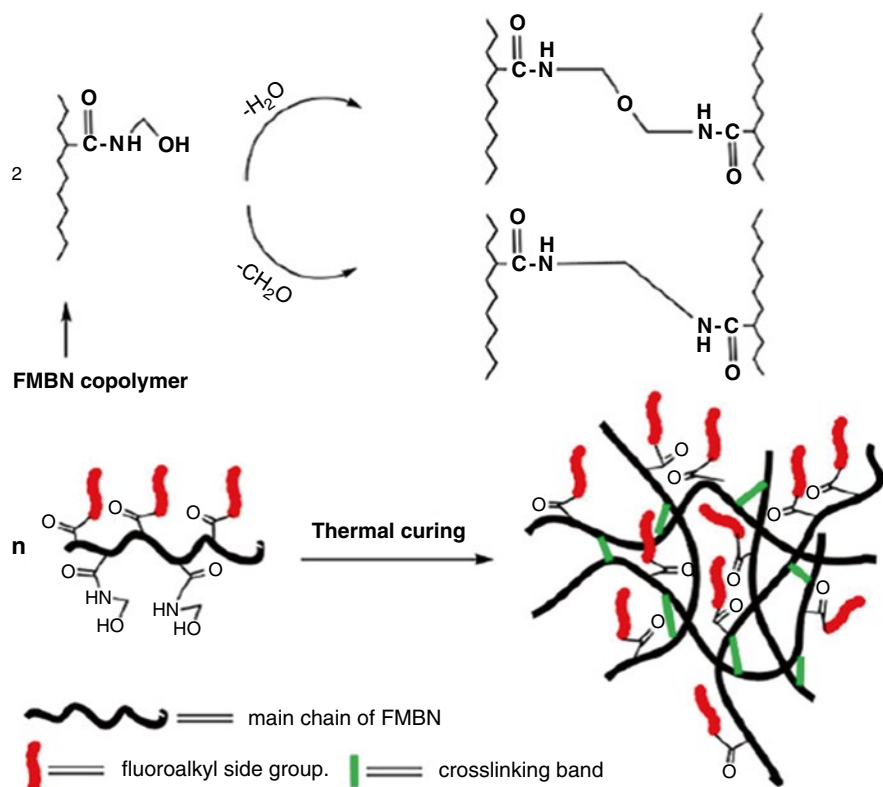
Fig. 29.11 Self-cross-linking of fluorinated polyacrylate chains during thermal cure, in particles containing a polymerizable surfactant (ammonium allyloxtmethylate nonylphenol ethoxylates sulfate) and a self-cross-linker (*N*-methylolacrylamide). Adapted with permission from [63]; Copyright 2013 Springer
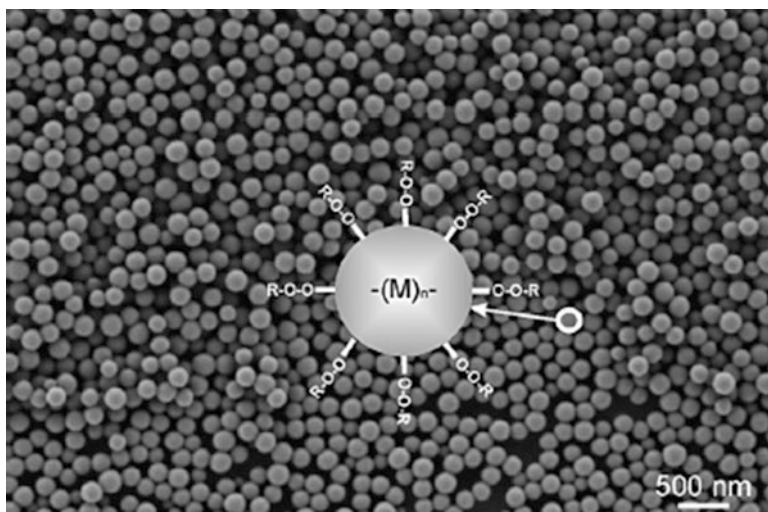
Fig. 29.12 SEM image of a surface-functionalized polystyrene latex particle, synthesized using a polyperoxide initiator-surfactant. Reprinted with permission from [66]; Copyright 2014 Elsevier

temperature and on the amount of the reactive filler, they show better hardness and solvent resistance when compared to coatings produced without the fillers.

Smart water dispersions were also produced using acrylic fatty acid copolymers (AcFAs) [64]. These play a double role as reactive coalescing aids (during film formation) and cross-linkers (upon H_2O evaporation and atmospheric O_2 exposure). AcFAs can be produced by conjugated fatty acids and ethylene glycol esterification, followed by esterification with acryloyl chloride [68]. When incorporated in acrylic latex, AcFAs had a plasticizer effect, lowering the minimum film formation temperature by 18 °C and thus dismissing the need for other plasticizers. Exposure to oxygen in the dried film promotes self-cross-linking of the polymer chains through the AcFAs, resulting in films with comparatively higher solvent resistance.

In a different approach, an alkoxysilane (silica precursor) was encapsulated in polymer nanoparticles [69], so that it remained unreactive in water dispersion, but acted both as plasticizers and cross-linkers after water evaporation during film formation. The optimum balance between chain interdiffusion and cross-link formation was achieved by tuning the temperature, to produce films with enhanced mechanical properties and chemical resistance, with no need for VOCs. The particles are composed of a copolymer of BMA and MAA (1 %) and labeled with FRET donors/acceptors and have encapsulated tetraethyl orthosilicate (TEOS) molecules (Fig. 29.13), forming stable dispersions in water during very long times at neutral pH.

FRET studies revealed that chain interdiffusion was significantly increased in the presence of TEOS, when cured at 80 °C (Fig. 29.14). Infrared DRIFT spectra showed that TEOS undergoes hydrolysis and condensation reactions during the annealing of the films, yielding silica (SiO_2) domains grafted to the polymer chains through the MAA groups and eventually forming bridges between distinct polymer
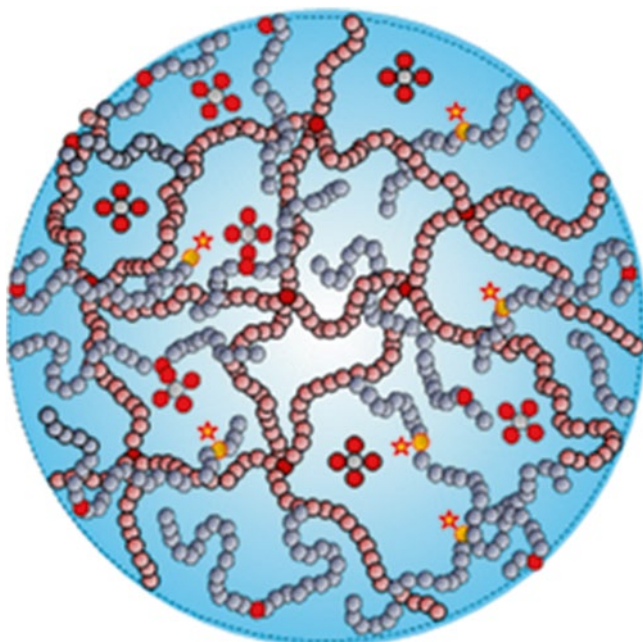
Fig. 29.13 Scheme of the smart polymer nanoparticles formed by p(BMA-co-MAA) chains encapsulating TEOS (✤), fluorescence donor-/acceptor-labeled comonomers (✺), and MAA comonomer (●). Adapted with permission from [69]; Copyright 2014 American Chemical Society

Fig. 29.14 Apparent fraction of mixture (f_m) determined by FRET as a function of curing time of films produced from (*a*) the smart nanoparticles containing TEOS and (*b*) of films produced from similar nanoparticles with TEOS. Reprinted with permission from [69]; Copyright 2014 American Chemical Society
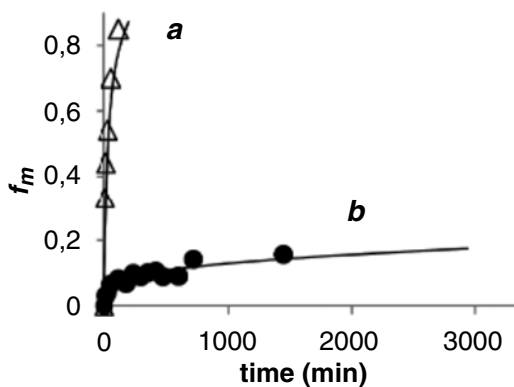
chains. The extent of cross-linking increased with the curing temperature, due to the increase in the mobility of water molecules inside the film that promoted the hydrolysis and condensation of TEOS. The film with the best healing properties was obtained at a temperature where chain interdiffusion occurred to a significant extent before cross-link formation through sol–gel reactions. After drying the film, the

water mobility inside the particles increased with temperature, increasing TEOS reactivity. This triggers its role as a cross-linker, increasing the film gel content.

This novel strategy allows the tuning of the diffusion/cross-linking balance in the formation of hybrid latex films. Not only is the coalescing aid (TEOS) not released from the film, but it is used as a cross-linker to improve the film's mechanical properties. This is an extremely attractive approach to produce waterborne, high-performance, environmentally friendly coatings with residual VOC content along with very good mechanical properties and chemical resistance.

Another novel class of intelligent polymer nanoparticles uses pH as a trigger to increase the film's *open time* (the period during which a newly applied paint film can be corrected *sans* brush indentations) [67]. These smart nanoparticles were produced from BA-MMA high molecular weight copolymer chains, loaded with low molecular weight chains (oligomers) of styrene, MAA, MMA, and BA. The oligomers are miscible with the high molecular weight polymer at acid pH (yielding uniform polymer blend nanoparticles), but immiscible at basic pH, yielding particles with a core of high molecular weight BA-MMA and an oligomer-rich shell (Fig. 29.15). The evolution of films cast from these particles was followed by FRET in a system where the high molecular weight polymer is labeled with a FRET acceptor and the oligomers with a FRET donor. The FRET efficiency changed from $\Phi_{ET} = 0.51$ at pH = 3 (which reflects the significant mixing between the two components in the blend nanoparticles) to $\Phi_{ET} = 0.22$ at pH = 11 (indicative of the microphase separation of the core-shell structures). Furthermore, the changes in Φ_{ET} (corresponding to changes in film morphology) were fully reversible with pH (Fig. 29.15). Films produced from alkaline solutions of these nanoparticles, with ammonia as a counter ion, showed delays of 30–40 min in the coalescence between particles when compared to films produced form particles without oligomers. The formation of hydrophilic membranes around the particles, through the $COO^-NH_4^+$ rich oligomer shells, retarded the final stages of drying, delaying chain interdiffu-
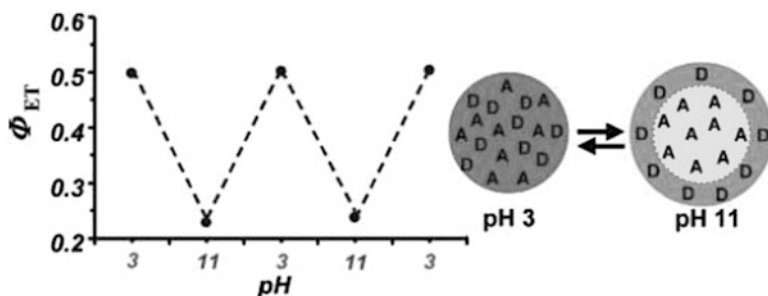
Fig. 29.15 Scheme of the particle morphology at acidic and alkaline conditions (*right*) and variation of the quantum efficiency of energy transfer, Φ_{ET}, with pH, when changing back and forth between acidic and alkaline conditions (*left*). Adapted with permission from [67]; Copyright 2011 American Chemical Society

sion across the particles boundaries. However, during drying, NH$_3$ evaporates and the carboxylic acid groups of the oligomers become protonated and thus soluble in the high molecular weight polymer of the core, acting as plasticizers to boost chain interdiffusion. The fraction of mixing between chains from different particles was thus strongly increased, compared to films produced from particles without oligomers.

These smart nanoparticles created coatings that simultaneously exhibit enhanced *open time* as a result of the particle's core-shell morphology at alkaline pH and do not need coalescing aids because the change in pH triggered by ammonia evaporation neutralizes the oligomers that act as plasticizers.

The recent development of smart polymer nanoparticles capable of triggering cross-linking reactions during film formation, in response to a stimuli following sufficient polymer diffusion, opens new possibilities for the development of high-performance water-based coatings. In the next session, other promising approaches for new smart polymer nanoparticles are discussed.

29.4 Future Outlook: Potential Smart Cross-Linking Reactions

The different strategies employed in water-based coatings and the multitude of reactions described above for cross-linking give a clear indication of the strategic relevance of this field. However, there is always a space for innovation, especially if one takes advantage of the environmental changes occurring during film formation in water-based coatings. In these systems, film formation is accompanied by a decrease in water content, so that cross-linking reactions whose kinetics are influenced by the decrease in water content, or the accompanying concentration increase of a specific component, are of particular interest to achieve triggering of the cross-linking reaction only after a chosen extent of diffusion.

The imine formation reaction from the condensation of an aldehyde and a primary amine (i.e., Schiff bases) releasing a water molecule is an alternative to conventional cross-linking reactions. This reaction is well known in the organic chemistry community since the nineteenth century, but its reversibility in the presence of water has been an obstacle in obtaining imines in aqueous reaction media. Typically, to obtain high conversions, water has to be removed from the system in order to avoid the reverse reaction and hydrolysis of the imine. Recently, this reversibility has been used as an advantage in fields like dynamic combinatorial chemistry [72] or reticular chemistry, for the design of new materials like metal organic frameworks (MOF) [73] and covalent organic frameworks (COF) [70]. In the present case, the commercial availability of polymerizable monomers containing primary amine groups to produce polymeric particles rich in amine groups and the handiness of water miscible dialdehydes (e.g., glutaraldehyde) strongly points to the viability

of this strategy. Due to the reversibility of the reaction in the presence of water, the dialdehydes (external cross-linker) can be present in the water dispersion. During film formation, the rate of imine formation increases as water evaporates, with the reverse reaction becoming negligible. This reaction does not need a catalyst and produces only water as a by-product. In the previous section, another example following the same strategy (preferably cross-linking after water evaporation) was already given with excellent film performance results [55].

An alternative to this strategy is to use aldehyde groups in some polymer nanoparticles while other particles feature primary amine groups. The aldehyde-bearing particles can be obtained from nanoparticles with primary hydroxyl groups, which can be oxidized to aldehydes, for example, using the Dess–Martin periodinane method.

A recent trend in polymer and materials science has been the use of "click" reactions. These, by definition, must have a broad scope, produce extremely large yields, create harmless and simple to remove by-products, use mild reaction conditions with easily procurable materials, and allow for simple product isolation [71]. It is curious that one of these "click" reaction families, the nucleophilic opening of highly strained rings such as epoxides or aziridines, has been widely used in cross-linking reactions in water-based coatings (highlighted in the previous sections) long before the widespread use of "click" chemistry.

Other types of "click" reactions used in polymers and materials are the Diels–Alder cycloaddition [74], the thiol-Michael addition [75], and the azide–alkyne cycloaddition [76]. Due to the specific constrains of water-based coatings, especially the presence of water and oxygen, the thiol-Michael addition is hard to implement in a cross-linking reaction for coatings. On the other hand, the cycloaddition reactions (Diels–Alder and the azide–alkyne) have already been used in polymers, and their application in water-based coating cross-linking is foreseeable. The Diels–Alder reaction involves a straightforward [4 + 2] cycloaddition between an electron-rich diene and an electron-poor dienophile, yielding stable cyclohexene adducts, without by-products. The reaction doesn't need catalysts, the kinetic is temperature dependent, and in some cases reversibility occurs at higher temperatures, which can be used to increase polymer diffusion or heal the material. One example is the reaction between furan and maleimide, which occurs between 25 °C and 100 °C and is reversible at temperatures higher than 120 °C [74]. Acrylate monomers with furan moieties are commercially available. The azide–alkyne reaction (or Huisgen cycloaddition) involves a 1,3-dipolar cycloaddition between an azide and an alkyne yielding a 1,2,3-triazole. The use of this reaction to modify polymers is widespread [76] and there are several alkyne-acrylate monomers commercially available, while the azide group can be easily introduced through substitution from tosyl groups or haloalkanes. The first examples were catalyzed by copper, which depending on the end use of the polymers could raise some concerns. Recently, copper-free azide–alkyne cycloadditions have been developed using cyclooctyne [76].

29.5   Conclusion

The quest for high-performance environmentally friendly polymer coatings is centered in two topics: the elimination of VOCs from the polymer nanoparticle dispersions and the development of highly mechanically and chemically resistant films. While conventional approaches have been centered on the use of reactive polymer dispersions, novel smart coatings are being proposed that rely on stimuli-responsive cross-linking reactions, able to auto-modulate the ratio of polymer diffusion and cross-linking kinetics to achieve maximum film performance.

References

1. Mohammadi N, Klein A, Sperling LH (1993) Polymer chain rupture and the fracture behavior of glassy polystyrene. Macromolecules 26:1019–1026
2. Kim KD, Sperling LH, Klein A, Hammouda B (1994) Reptation time, temperature, and cosurfactant effects on the molecular interdiffusion rate during polystyrene latex film formation. Macromolecules 27:6841–6850
3. Eckersley ST, Rudin A (1990) Mechanism of film formation from polymer latexes. J Coat Technol 62:89–100
4. Steward PA, Hearn J, Wilkinson MC (2000) An overview of polymer latex film formation and properties. Adv Colloid Interface Sci 86:195–267
5. Berrisford DJ, Lovell PA, Suliman NA, Whitting A (2005) Latent reactive groups unveiled through equilibrium dynamics and exemplified in crosslinking during film formation from aqueous polymer colloids. Chem Commun 47:5904–5906
6. Bufkin BG, Grawe JR (1978) Survey of applications, properties, and technology of crosslinking emulsions. J Coat Technol 50:41–55
7. Aradian A, Raphaël E, de Gennes P-G (2002) A scaling theory of the competition between interdiffusion and cross-linking at polymer interfaces. Macromolecules 35:4036–4043
8. Aradian A, Raphäel E, de Gennes P-G (2000) Strengthening of a polymer interface: interdiffusion and cross-linking. Macromolecules 33:9444–9451
9. de Gennes P-G (1971) Reptation of a polymer chain in the presence of fixed obstacles. J Chem Phys 55:572–579
10. Doi M, Edwards SF (1986) The theory of polymer dynamics, 1st edn. Clarendon, Oxford
11. Hahn K, Ley G, Oberthur R (1988) On particle coalescence in latex films (II). Colloid Polym Sci 266:631–639
12. Hahn K, Ley G, Schuller H, Oberthur R (1986) On particle coalescence in latex films. Colloid Polym Sci 264:1092–1096
13. Yoo JN, Sperling LH, Glinka CJ, Klein A (1990) Characterization of film formation from polystyrene latex particles via SANS. 1. Moderate molecular weight. Macromolecules 23:3962–3967
14. Yoo JN, Sperling LH, Glinka CJ, Klein A (1991) Characterization of film formation from polystyrene latex particles via SANS. 2. High molecular weight. Macromolecules 24:2868–2876
15. Morawetz H (1979) Some applications of fluorimetry to synthetic polymer studies. Science 203:405–410
16. Morawetz H (1988) Studies of synthetic polymers by nonradiative energy transfer. Science 240:172–176
17. Morawetz H (1999) On the versatility of fluorescence techniques in polymer research. J Polym Sci A Polym Chem 37:1725–1735

18. Winnik MA (1997) Latex film formation. Curr Opin Colloid Interface Sci 2:192–199
19. Taylor JW, Winnik MA (2004) Functional latex and thermoset latex films. JCT Res 1:163–190
20. Wang YC, Zhao CL, Winnik MA (1991) Molecular diffusion and latex film formation: an analysis of direct nonradiative energy transfer experiments. J Chem Phys 95:2143–2153
21. Baumann J, Fayer MD (1986) Excitation transfer in disordered two-dimensional and anisotropic three-dimensional systems: effects of spatial geometry on time-resolved observables. J Chem Phys 85:4087–4107
22. Klafter J, Blumen A (1984) Fractal behavior in trapping and reaction. J Chem Phys 80:875–877
23. Drake JM, Klafter J, Levitz P (1991) Chemical and biological microstructures as probed by dynamic processes. Science 251:1574–1579
24. Farinha JPS, Martinho JMG, Kawaguchi SK, Yekta A, Winnik MA (1996) Latex film formation probed by nonradiative energy transfer: effect of grafted and free poly(ethylene oxide) on a poly(n-butyl methacrylate) latex. J Phys Chem 100:12552–12558
25. Farinha JPS, Martinho JMG, Yekta A, Winnik MA (1995) Direct nonradiative energy transfer in polymer interphases: fluorescence decay functions from concentration profiles generated by fickian diffusion. Macromolecules 28:6084–6088
26. Yekta A, Duhamel J, Winnik MA (1995) Dipole-dipole electronic energy transfer. Fluorescence decay functions for arbitrary distributions of donors and acceptors: systems with planar geometry. Chem Phys Lett 235:119–125
27. Farinha JPS, Martinho JMG (2008) Resonance energy transfer in polymer nanodomains. J Phys Chem C 112:10591–10601
28. Ye X, Farinha JPS, Oh JK, Winnik MA, Wu C (2003) Polymer diffusion in PBMA latex films using a polymerizable benzophenone derivative as an energy transfer acceptor. Macromolecules 36:8749–8760
29. Wang Y, Winnik MA (1993) Polymer diffusion across interfaces in latex films. J Phys Chem 97:2507–2515
30. Feng J, Winnik MA (1997) Effect of water on polymer diffusion in latex films. Macromolecules 30:4324–4331
31. Kawaguchi S, Odrobina E, Winnik MA (1995) Nonionic surfactant effects on polymer diffusion in poly(butyl methacrylate) latex films. Macromol Rapid Commun 16:861–868
32. Winnik MA, Wang YC, Haley F (1992) Latex film formation at the molecular-level—the effect of coalescing aids on polymer diffusion. J Coat Technol 64:51–61
33. Juhué D, Wang YC, Winnik MA (1993) Influence of a coalescing aid on polymer diffusion in poly(butyl methacrylate) latex films. Makromol Chem Rapid Commun 14:345–349
34. Kim HB, Winnik MA (1994) Effect of surface acid group neutralization on interdiffusion rates in latex films. Macromolecules 27:1007–1012
35. Kim HB, Winnik MA (1995) Factors affecting interdiffusion rates in films prepared from latex particles with a surface rich in acid groups and their salts. Macromolecules 28:2033–2041
36. Tsutomu M, Koji A, Masatoshi M, Yoshiharu K (2006) Application of silica-containing nanocomposite emulsion to wall paint: a new environmentally safe paint of high performance. Prog Org Coat 55:276–283
37. Kobayashi M, Rharbi Y, Brauge L, Cao L, Winnik MA (2002) Effect of silica as fillers on polymer interdiffusion in poly(butyl methacrylate) latex films. Macromolecules 35:7387–7399
38. Mitsuru W, Toshiyuki T (2006) Acrylic polymer/silica organic–inorganic hybrid emulsions for coating materials: role of the silane coupling agent. J Polym Sci A Polym Chem 44:4736–4742
39. Ribeiro T, Fedorov A, Baleizão C, Farinha JPS (2013) Formation of hybrid films from perylenediimide-labeled core–shell silica–polymer nanoparticles. J Colloid Interface Sci 401:14–22
40. Zosel A, Ley G (1993) Influence of crosslinking on structure, mechanical properties, and strength of latex films. Macromolecules 32:2222–2227

41. Martinho JMG, Farinha JPS (2013) Fluorescence decay methods in the characterization of latex film formation. JCT Coat Technol 10:46–53
42. Pham HH, Farinha JPS, Winnik MA (2000) Cross-linking, miscibility, and interface structure in blends of poly(2-ethylhexyl methacrylate) copolymers: an energy transfer study. Macromolecules 33:5850–5862
43. Winnik MA (2002) Interdiffusion and crosslinking in thermoset latex films. J Coat Technol 74:49–63
44. Feng J, Pham HH, Macdonald P, Winnik MA, Geurts JM, Zirkzee H, van Es S, German AL (1998) Formation and crosslinking of latex films through the reaction of acetoacetoxy groups with diamines under ambient conditions. J Coat Technol 70:57–68
45. Pham HH, Winnik MA (2000) Synthesis, characterization, and stability of carbodiimide groups in carbodiimide-functionalized latex dispersions and films. J Polym Sci A Polym Chem 38:855–869
46. Liu R, Winnik MA, Di Stefano F, Venkatesan J (2001) Interdiffusion vs. Cross-linking rates in isobutoxyacrylamide-containing latex coatings. Macromolecules 34:7306–7314
47. Tronc F, Liu R, Winnik MA, Eckersley ST, Rose GD, Weishun JM, Meunier DM (2002) Epoxy-functionalized, low glass-transition temperature latex. I. Synthesis, characterizations, and polymer interdiffusion. J Polym Sci A Polym Chem 40:2609–2625
48. Winnik MA, Pinenq P, Krüger C, Zhang J, Yaneff PV (1999) Crosslinking vs. interdiffusion rates in melamine-formaldehyde cured latex coatings: A model for waterborne automotive basecoat. J Coat Technol 71:47–60
49. Tronc F, Chen W, Winnik MA, Eckersley ST, Rose GD, Weishun JM, Meunier DM (2002) Epoxy-Functionalized, Low-Glass-Transition-Temperature Latex. II. Interdiffusion versus Crosslinking in the Presence of a Diamine. J Polym Sci A Polym Chem 40:4098–4116
50. Krishnan S, Klein A, El-Aasser MS, Sudol ED (2003) Influence of chain transfer agent on the cross-linking of poly(n-butyl methacrylate-co-nmethylol acrylamide) latex particles and films. Macromolecules 36:3511–3518
51. Mazuel F, Bui C, Charleux B, Cabet-Deliry E, Winnik MA (2004) Interdiffusion and self-cross-linking in acetal-functionalized latex films. Macromolecules 37:6141–6152
52. Mohammed S, Daniels ES, Sperling LH, Klein A, El-Aasser MS (1997) Isocyanate-functionalized latexes: film formation and tensile properties. J Appl Polym Sci 66:1869–1884
53. Liu X, Fan X-D, Tang M-F, Nie Y (2008) Synthesis and characterization of core-shell acrylate based latex and study of its reactive blends. Int J Mol Sci 9:342–354
54. Tungchaiwattana S, Groves R, Lovell PA, Pinprayoonac O, Saunders BR (2012) Tuning the mechanical properties of nanostructured ionomer films by controlling the extents of covalent crosslinking in core-shell nanoparticles. J Mater Chem 22:5840–5847
55. Chen X, Pelton R, Ruckenstein E (2005) Long term stability of an ambient self-curable latex based on colloid dispersions in water of two reactive polymers. J Polym Sci A Polym Chem 43:2598–2605
56. Pinprayoon O, Groves R, Lovell PA, Tungchaiwattana S, Saunders BR (2011) Polymer films prepared using ionically-crosslinked soft core-shell nanoparticles: a new class of nanostructured ionomers. Soft Matter 7:247–257
57. Pham HH, Winnik MA (2006) Polymer interdiffusion vs cross-linking in carboxylic acid-carbodiimide latex films: Effect of annealing temperature, reactive group concentration, and carbodiimide substituent. Macromolecules 39:1425–1435
58. Berrisford DJ, Lovell PA, Suliman NR, Whiting A (2005) Latent reactive groups unveiled through equilibrium dynamics and exemplified in crosslinking during film formation from aqueous polymer colloids. Chem Commun 21(47):5904–5906
59. Chen XN, Ruckenstein E (2000) Emulsion procedures for thermally reversible covalent cross-linking of polymers. J Polym Sci Polym Chem 38:4373–4384
60. Wei Y, Huang RYM (1995) Pervaporation with latex membranes: a study on membrane and pervaporation effects. Sep Sci Technol 30:697–717

61. Ruckenstein E, Chen XN (2001) An ambient self-curable latex based on colloidal dispersions in water of two functionalized polymers and the thermally reversible crosslinked films generated. J Polym Sci A Polym Chem 39:389–397

62. Ruckenstein E, Chen XN (2000) Covalent cross-linking of polymers through ionene formation and their thermal de-cross-linking. Macromolecules 33:8992–9001

63. Hao L, An Q, Xu W, Zhang D, Zhang M (2013) Effect of polymerizable emulsifier and fluorine monomer on properties of self-crosslinking fluorinated polyacrylate soap-free latexes. J Polym Res 20:174

64. Barbosa JV, Moniz J, Mendes A, Magalhães FD, Bastos MMSM (2014) Incorporation of an acrylic fatty acid derivative as comonomer for oxidative cure in acrylic latex. J Coat Technol Res 11:765–773

65. Xiong PT, Lu DP, Chen PZ, Huang HZ, Guan R (2007) Preparation and surface properties of latexes with fluorine enriched in the shell by silicon monomer crosslinking. Eur Polym J 43:2117–2126

66. Popadyuk A, Tarnavchyk I, Popadyuk N, Kohut A, Samaryk V, Voronov S, Voronov A (2014) Reinforcing latex coatings with reactive latex particles. Prog Org Coat 77:2123–2132

67. Soleimani M, Haley JC, Majonis D, Guerin G, Lau W, Winnik MA (2011) Smart polymer nanoparticles designed for environmentally compliant coatings. J Am Chem Soc 133:11299–11307

68. Fu SY, Feng XQ, Lauke B, Mai YW (2008) Effects of particle size, particle/matrix interface adhesion and particle loading on mechanical properties of particulate-polymer composites. Compos Part B 39:933–961

69. Piçarra S, Fidalgo A, Fedorov A, Martinho JMG, Farinha JPS (2014) Smart polymer nanoparticles for high-performance water-borne coatings. Langmuir 30:12345–12353

70. Feng X, Ding X, Jiang D (2012) Covalent organic frameworks. Chem Soc Rev 41:6010–6022

71. Kolb HC, Finn MG, Sharpless KB (2001) Click chemistry: diverse chemical function from a few good reactions. Angew Chem Int Ed 40:2004–2021

72. Meyer CD, Joiner CS, Fraser Stoddart J (2007) Template-directed synthesis employing reversible imine bond formation. Chem Soc Rev 36:1705–1723

73. Yaghi OM, O'Keeffe M, Ockwig NW, Chae HK, Eddaoudi M, Kim J (2003) Reticular synthesis and the design of new materials. Nature 423:705–714

74. Tasdelen MA (2011) Diels–Alder "click" reactions: recent applications in polymer and material science. Polym Chem 2:2133–2145

75. Nair DP, Podgórski M, Chatani S, Gong T, Xi W, Fenoli CR, Bowman CN (2014) The Thiol-Michael addition click reaction: a powerful and widely used tool in materials chemistry. Chem Mater 26:724–744

76. Sumerlin BS, Vogt AP (2010) Macromolecular engineering through click chemistry and other efficient transformations. Macromolecules 43:1–13

77. Chen LJ, Wu FQ (2012) Preparation and characterization of novel self cross-linking fluorinated acrylic latex. J Appl Polym Sci 123:1997–2002

Chapter 30
Radiation-Curable Smart Coatings

Saeed Bastani and Pooneh Kardar

Abstract A quickly expanding process within the paint and coatings industry is the implementation of ultraviolet (UV) to cure or dry coating on various products (i.e., wood, metal, or plastic). Increasingly used in place of replacing conventional high-heat processing techniques, UV-cured coating produces materials with improved properties, lowers the operational costs (e.g., natural gas costs for bake curing), and reduces the overall environmental impact. This chapter describes this new class of smart UV-curable coatings. In the first part, UV-curable and smart coatings are introduced. In the following sections, smart coating properties such as self-cleaning, self-healing, antifog, and antibacterial are described separately and synthesize routes for smart coatings. Finally, this chapter will highlight different types of smart UV-curable coatings for various engineering applications.

Keywords UV-curable smart coating • Self-cleaning coatings • Self-healing coatings • Antifog coatings • Antibacterial coatings

30.1 Introduction

The interests in using UV-curable coatings have shown exponential growth in recent years [1, 2]. The VOC (volatile organic compounds) content of this type of coating is very low (almost zero), and it consumes a relatively low amount of energy during the curing process. Therefore, this coating system is considered as one of the cleanest and most environmentally friendly coating systems [3–5]. Radiation curing of coatings,

S. Bastani (✉)
Surface Coating and Corrosion Department, Institute for Color Science and Technology, Tehran, Iran

Center of Excellence for Color Science and Technology, Tehran, Iran
e-mail: bastani@icrc.ac.ir

P. Kardar
Surface Coating and Corrosion Department, Institute for Color Science and Technology, Tehran, Iran
e-mail: kardar@icrc.ac.ir

inks, adhesives, and sealants is known as a rapid process. In a radiation cure process, monomers and oligomers can be instantaneously polymerized and/or cross-linked. This process usually results in an effectively complete conversion of the liquid into a solid (i.e., radiation-cured coatings are essentially 100 % solid in nature) [6, 7].

On the other hand, the domain of coatings with smart property has been inundated with new advances and components [8, 9]. Literature provides several means to define a smart coating. "Materials that are capable of adapting their properties dynamically to an external stimulus are called responsive, or smart. The term 'smart coating' refers to the concept of coatings being able to sense the environment and make an appropriate response to that stimulus" [10].

New materials for UV-curable smart coatings are under investigation, some of which are discussed in the next section.

30.1.1 UV-Curable Self-Cleaning Coatings

Possessing the potential to reduce cleaning labor costs, a great deal of focus has been placed upon self-cleaning coatings and their application in commercial products including windows, cement, fabrics, and paints [11–13]. These coatings are typically segmented into two distinct categories: hydrophobic or hydrophilic coatings. Tensiometers are used to determine a coating's wettability and hydrophilic and hydrophobic properties. Coatings of both classes are self-cleaning when exposed to water.

An example of this is demonstrated in nature and is defined as the "lotus effect"; the leaf's hydrophobic properties repel water upon its surface, causing droplets to form. The contact angle (θ) was first defined by Thomas Young in 1805 through the investigation of the forces acting upon a still bead of liquid on a firm surface which was encompassed by a gas [14]:

$$\gamma_{SG} = \gamma_{SL} + \gamma_{LG} \cos\theta \qquad (30.1)$$

In Eq. 30.1, **γSG** stands for the solid/gas interfacial tension; **γSL** is the interfacial tension between the two liquid/solid phases; and **γLG** represents the interfacial tension between the gas phase and the liquid phase. The θ is measurable through the use of a contact angle goniometer.

Wenzel summarized that upon intimate contact between a fluid and a microstructured surface, θ undergoes modification to become θ_{w^*}:

$$\cos\theta_{w^*} = r\cos\theta \qquad (30.2)$$

In this equation the ratio of the actual area/projected area is given [15]. Wenzel's equation revealed that the surface's natural state could be amplified via surface microstructuring. When microstructured, an already hydrophobic surface ($\theta > 90°$) increased in hydrophobicity, its new value of θ exceeding the initial. Further, a hydrophilic surface ($\theta < 90°$) increases in hydrophilicity when microstructured, with its new θ

Fig. 30.1 Water droplets carrying dirt away from a hydrophobic surface
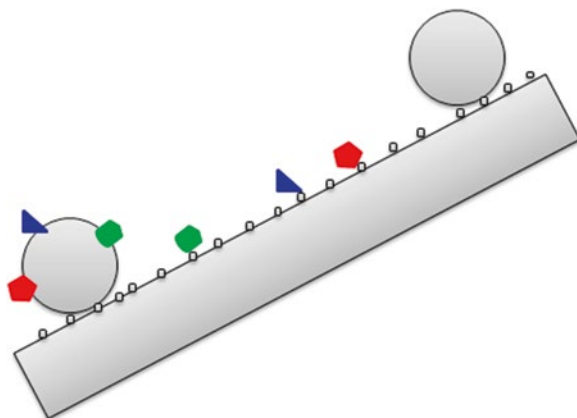
much smaller than the initial value [16]. As reported by Cassie and Baxter [17], if the fluid suspension occurs on top of the microstructures, the θ value transforms to θ_{CB^*} :

$$\cos\theta_{CB^*} = \varphi\left(\cos\theta + 1\right) \tag{30.3}$$

where φ is the solid's area fraction that makes contact with the fluid [17]. A fluid in the Wenzel state is far less prone to movement than that in the Cassie–Baxter state.

Utilizing both equations, the calculation of the new contact angle should predict the existence of either a Wenzel or Cassie–Baxter state. The calculation which has a new θ that is smaller has a greater probability of existence when the free energy argument is minimized. The inequality shown below is required to be correct in order for the Cassie–Baxter state to exist [18]:

$$\cos\theta < \left(\varphi - 1\right)/\left(r - \varphi\right) \tag{30.4}$$

Hydrophobic coatings possess water contact angles in excess of 90° [19, 20]. When the water θ value exceeds 150°, these self-cleaning coatings are described as superhydrophobic; extremely water repellent with formation of water droplets carrying dirt off the surface as they roll away (Fig. 30.1). The surface's chemical and topographical characteristics aid in the determination of the contact angle. In order to procure a superhydrophobic surface, the existing hydrophobic surface must first be exfoliated on the micro- and nanometer scales. It can then be stated that the surface's roughness and chemical makeup along with the dirt particle affinity to water adhesion will determine the overall efficiency of the self-cleaning coating.

"Photocatalysis" is the basis on which hydrophilic self-cleaning coatings function, meaning that upon exposure to light, impurities can then be broken down [12, 21]. Currently, windows are commercially available with this self-cleaning coating and function in two specific manners. *"Photocatalysis"* breaks down any organic matter that accumulated on the window, later washed away by water via the low contact angles. With desirable physical and chemical properties, hydrophilic self-
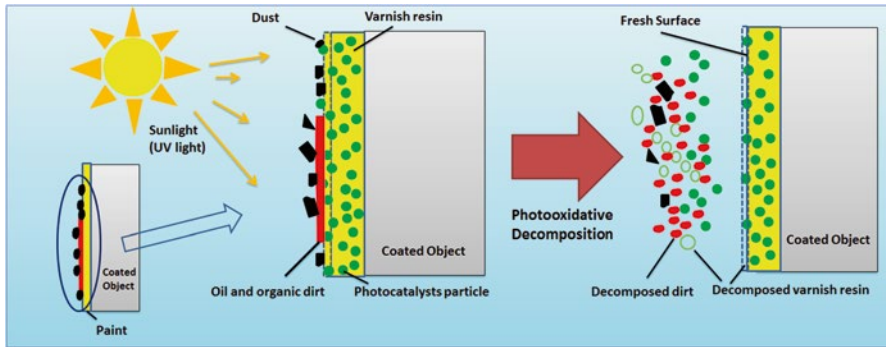
Fig. 30.2 Photocatalytic process of titanium dioxide [21]

cleaning materials are known to utilize titanium dioxide (TiO_2) coatings (Fig. 30.2). TiO_2 is nontoxic, inert when devoid of light, cheap, and manageable and is established in consumers' homes (makeup and paint pigmentations). TiO_2's superior oxidative properties and superhydrophilic characteristics enable it to be utilized in self-cleaning coatings, especially in outdoor applications.

However, there are few studies in literature about UV-curable self-cleaning coatings. For example, one study prepared different formulations of UV-curable coatings based on hybrid urethane acrylate oligomers, and the resulting UV-cured films intended for application were characterized as easy-to-clean coatings [22]. The effects of reactive monomer functionality and the oligomer structure on the reaction rate and extent of UV curing were investigated as well as the cured films' properties. The study began with the synthesis of two different hybrid urethane acrylate oligomers, and their chemical structures were characterized by NMR and FTIR. Six formulations of UV-curable coating were prepared by varying the type of urethane acrylate oligomers in addition to the type of reactive monomers, using the photoinitiator 2,2-dimethoxy-2-phenylacetophenone, methacrylic acid as a reactive diluent, and 3-aminopropyltrimethoxysilane as a coupling agent. The UV curing process of such coatings was monitored by FTIR, and the C=C bond conversion was expressed. Finally, the weight loss, water contact angle, crosscut adhesion, and tensile characteristics of the coatings that underwent UV curing were also investigated.

Literature also puts forth an inorganic/organic hybrid coating, cured at low temperature with UV exposure while maintaining impressive photoactive properties that are highly desirable in many applications (i.e., covers for solar cell, rearview mirrors for vehicles, electronic devices) [23]. The aqueous sol–gel technique and utilization of titanyl sulfate yielded a nano-titania sol–gel (19 nm particle size) that was incredibly photoactive by crystallization via microwave treatment; this is significant in hybrid film synthesis where typical heat curing is unfeasible. Optimizing the quantity of the silane moiety allowed for the titania particle to be semi-coated with silica. A solar cell cover glass was first coated with a multifunctional monomer which was followed by a photoactive titania particle dip coating and then later UV cured for 6 h. The properties of the final coated substrate included efficient photocatalytic behavior, good transparency (>90 %), and a water θ value (>90°) [24].

Atomic force microscopy (AFM) displayed the uniform surface distribution of tita-nia particles on the coating with the coating being approximately 2.5 mm thick. Substrate adhesion is dependent on the organic silanes/acrylates ratio, while the self-cleaning efficiency was found to be influenced by the hybrid silica/titania mix-ture by stopping surface contamination from atmospheric exposure; these multi-functional coatings are well suited as solar cell covers and could provide an efficiency increase of 15–25 % to the panel.

30.1.2   UV-Curable Antifog Coatings

Water vapor can condense on a solid surface at a certain temperature or humidity, with water on the surface forming little droplets if the solid surface has a very high surface energy. Therefore, the light that is refracted and scattered by water droplets causes the transparent materials to turn hazy, which can trigger fogging problems. Many optical devices suffer from fogging problems, such as eyeglasses, mirrors, windshields, and many other devices in specialized fields. There are two efficient ways to solve the problem. One is a heating device to make water vapor noncon-densing, and the other is to provide a solid surface with wetting characteristics such as hydrophilicity or even super hydrophilicity. Although the former method is effi-cient, energy costs limit its widespread application. Hydrophilic surfaces that have water θ value (<40°) are often utilized in antifog research [25–27]. The main reason is that condensing water droplets on this type of surface can rapidly spread into a well-distributed and non-light-scattering water coating. In this case, visibility through surface is good even though condensation is not prevented.

A UV-curable antifog coating is an extremely cross-linked polymer coating that possesses both hydrophobic and hydrophilic sections (Fig. 30.3). Surfaces treated with such materials are able to simultaneously spread and absorb water, thus granting antifogging properties to a plethora of optical substrates. These materials are durable and long lasting, all the while maintaining excellent antifogging and mechanical char-acteristics. Increased productivity, lower energy costs, and decreased capital invest-ments needed in curing facilities are benefits when using UV-curable coatings.
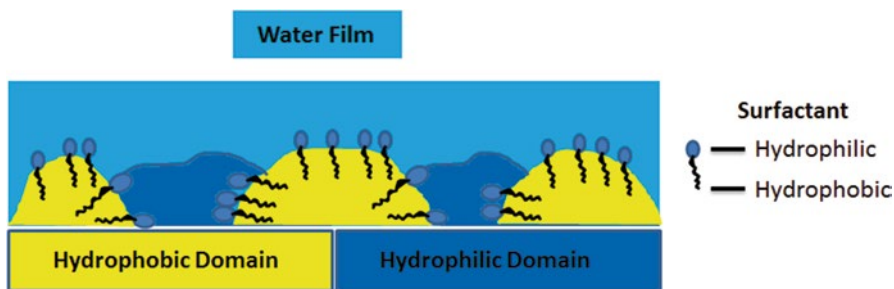
Fig. 30.3   Designs for antifog coatings

Grafting and block copolymerization methods were utilized by Jacubes et al. to synthesize a novel polyurethane acrylate oligomer that when optimally formulated yields superior optical characteristics while maintaining post-UV curing toughness [28]. In order to produce such oligomers, selection of raw materials of varying properties, such as of hydrophilicity, hydrophobicity, conductivity, elasticity, mechanical, and/or formulation compatibility, was arduous. These oligomers are specifically thought to be used for antifog applications, glass adhesion, and soft touch applications. Polycarbonate (PC) substrates coated with this antifogging material are quite desirable in real-world scenarios, with a few formulations comparable to readily available commercial products. Specifically, multifunctional UV-curable polyurethane acrylate oligomers were converted from branched or dendrimeric raw materials through the reaction of their hydroxyl groups with hetero-functional isocyanates.

In another study, development of an antifog transparent coating based on polyurethane-PEG-acrylate copolymers was reported [29]. Both thermal and UV curing was pursued. In order to obtain a polymer with hydrophilic properties, a poly (ethylene glycol) (PEG) chain is utilized as the polyol portion of the polyurethane. The molecular weight of PEG chain was either 1000 or 400 (g/mol) (PEG1000 and PEG400). An aliphatic diisocyanate, namely, isophorone diisocyanate (IPDI), was used in order to prevent yellowing. A PEG-IPDI polymer was produced in the first step. Because IPDI was used in excess, the polymer had isocyanate end groups. In the second step, these were reacted with 2-hydroxyethyl acrylate (HEA). Dibutyltin dilaurate (DBTL) was employed as the catalyst for the formation of the urethane bond. Cross-linking occurred via free radical polymerization of the acrylate groups. Films with wet thicknesses of 30, 60, 90, and 120 μm were produced on glass and polycarbonate surfaces. The performance parameters such as fog resistance in hot humid atmosphere, tackiness, scratch resistance, and adhesion were determined as a function of preparation parameters such as time of thermal curing, IPDI/PEG ratio, irradiation time, and content of wetting agent. A variety of techniques, including microscopy, confocal laser scanning microscopy, AFM, differential scanning calorimetry, hardness testing, and dynamic light scattering, were employed for characterization. While antifog activity was obtained via a wide variety of recipes, optimization of other properties (i.e., hardness, scratch resistance) turned out to be in conflict with the antifog activity. Antifog activity requires the carefully timed uptake of water. Hard films, on the other hand, have limited swelling capability. In order to avoid or at least diminish this problem, antifog coatings containing nano-sized inorganic fillers were developed. Various types of fillers were tested. Dry silica powder such as *"Aerosil R972"* is economical and widely used in the industry. However, it has proved to be impossible to disperse the aggregates without causing light scattering in the product, and as a result, the final films were hazy. An aqueous dispersion of silica (*"Köstrosol 2040"*) proved to be impractical because the PU was dissolved in acetone and phase transfer from water to acetone could not be achieved. Clay particles (*"Laponite RD"*) were aggregated inside the film and also resulted in slightly turbid films. These problems could be solved with self-prepared silica particles. As it so happens, the Stöber synthesis that typically carries out water could also be completed in mixtures of water and acetone. A water/acetone ratio

could be chosen so as to avoid precipitation of polymer when adding the dispersion of silica particles to the polymer. Silane coupling agents improved the optical properties of the resultant coating. This technique provides for a novel route to create scratch-resistant antifog coatings. The antifog activity will be optimized in further work. With regard to the hardness, the use of an organic/inorganic nanocomposite proved to be a decisive advantage.

In another study, a series of UV-curable hydrophilic acrylate polymers containing sulfonic acid groups was prepared via free radical copolymerization using "2-acrylamido-2-methylpropane sulfonic acid (AMPS)" as a monomer with hydrophilic properties that were later used as prepolymers for antifog coatings [30]. The expected structures were confirmed by FTIR, 1H NMR, and gel permeation chromatography (GPC). These UV-curable acrylate polymers were then mixed with reactive diluents and photoinitiators to form coating formulas. Various substrates were coated with these formulas and cured under UV exposure to obtain transparent coatings with good adhesion and hardness. The antifog properties of UV-cured coating were measured by contact angle testing and antifog analysis. The results showed that the AMPS content in the prepolymer was incredibly influential on the antifogging capabilities of the UV-cured coating. The formula was optimized and the corresponding UV-cured antifog coating was manufactured. The test results indicated the good mechanical properties, great optical transparency, and excellent antifog performance of coating.

Moreover, another type of UV-cured coating with antifog and antibacterial properties was investigated [31]. The study created and utilized a quaternary ammonium salt that was used as the monomer. FTIR and NMR analyses were used to determine its chemical structure. X-ray photoelectron spectroscopy was employed so as to observe nitrogen atoms upon the coating's surface. The polymer film's surface wettability was investigated via contact angle analysis, confirming the coating's hydrophilicity with a low water θ value of approximately 25°. Alternative conditions were used to measure the antifogging properties. Coatings containing 14 QAS obtained 99.9 % against *Staphylococcus aureus* and *Escherichia coli* when determining the antibacterial characteristics.

30.1.3 UV-Curable Self-Healing Coatings

Different coating layers or coating films are applied to the surfaces of electronic devices such as mobile phones, electronic material parts, home appliances, exterior or interior parts for vehicles, and plastic molded products for the purpose of protecting the products from damage caused by mechanical, physical, or chemical influences from the outside. As scratches occurring on the surface of the product coatings or cracks resulting from external impacts may lead to deterioration of external appearance and main performance of the products and shorten their lifetime, considerable research has been conducted to protect the surface of the product and thus maintain long-term quality.

Incorporation of self-healing properties in polymeric materials is classified in two categories: autonomic (sans intervention) and non-autonomic (requires a trigger) [32–35]. The two most commonly employed design approaches for self-healing materials are healing agent release and cross-links that are reversible.

In the case of healing agent release, while being produced, the active liquid agents such as monomers, dyes, catalysts, corrosion inhibitors, and hardeners along with microcapsules, hollow fibers, or channels are inserted into the polymer's network [32]. When they encounter a crack, these structures are broken and deliver the reactive agent into the crack thus healing the damage through solidification.

Self-repairing capability was not exhibited by a reversible cross-linked system without external intervention (e.g., thermal, photo, or chemical). Various methodologies considered in inducing cross-linked polymeric network's reversibility are ionomers, supramolecular, and the Diels–Alder reaction.

Recently, vigorous studies are underway for coating materials with self-healing capabilities since such materials require no additional coatings or repairs when damaged on the surface and have substantial advantages in maintaining their external appearance and performance. Actually, such studies have reported a UV-curable composition using an oligomer demonstrating self-healing capabilities and a composition including inorganic particles or fluorine compounds added so as to enhance scratch resistance and stain resistance [36, 37]. However, coating materials obtained from the mentioned compositions have drawbacks as they can have neither a high level of surface hardness nor show sufficient self-healing capabilities.

Moreover researchers claimed that using nanoparticles can improve the self-healing properties of coatings [38]. It is shown that due to the force of polymer chains on nanoparticles, the particles can migrate to the surface. As the scratches create two surfaces, the nanoparticles can travel to these two surfaces to fill the scratches and decrease the visibility of scratches. For instance, Kardar et al. presented that scratch visibility was reduced as nanoparticles were used [39]. The data obtained revealed that the sample containing nanoparticles had a higher scratch recovery. The samples with nanoparticles had a scratch depth of 50 % while samples without had 71 %. The samples' scratch width recoveries, again without and with nanoparticles, were 56 % and 61 %, respectively. These results prove the decrease of the scratch appearance for the sample containing nanoparticles. Nanoparticles appear to impart improved self-healing properties to the coatings.

30.1.4 UV-Curable Antibacterial Coatings

An antimicrobial surface inhibits or impedes the ability of microorganism growth on a material's surface through the use of an antimicrobial agent (Fig. 30.4). These materials have the potential to be used in a wide range of areas including clinical, industrial, and residential settings. Furthermore, linens and fabrics can house many types of bacteria, fungi, and viruses and, upon contact with skin, can be transmitted quite easily.

Fig. 30.4 Antibacterial
surface mechanism
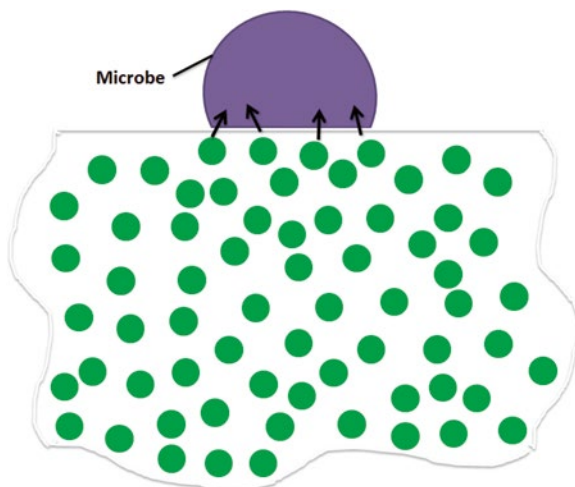
The typical way to imbue surfaces with antimicrobial capabilities is through co-antimicrobial coating agents such as antibiotics, Ag, Cu, and peptides [40, 41]. The antibacterial property is relying upon the gradual leaching release mechanism that delivers biocides into the surrounding areas. Antibacterial component loss, surface inactivation, and toxic biocide release into the environment are all disadvantages incurred when using this antibacterial mechanism. On the other hand, various studies have been completed so as to give antimicrobial properties to the surfaces via the chemical tethering of bactericidal functionalities or biocides with a multitude of methods [42].

Among the reported straightforward modification methods, other advantages of UV curing include those that are environmental and cost saving. Multiple films prepared with a contact-killing antibacterial mechanism were cured with UV light. Motlagh et al. reported the synergistic effect of nano-titanium dioxide (10 and 30 nm) and nano-silver (10 nm) as antibacterial agents on UV-curable clear coatings [43]. Antibacterial and physical–mechanical properties of the coating were optimized using response surface methodology experimental design. Twenty different samples of nano-Ag and nano-TiO$_2$ were prepared in this method. Antibacterial properties on Gram-negative bacteria (*E. coli*) were investigated. The results revealed that using equal amounts of two sizes of nano-TiO$_2$ promotes the antibacterial activity of nano-Ag. Therefore, the coating showed strong activity against *E. coli*. Physical–mechanical characteristics like surface hardness, abrasion resistance, scratch resistance, and gloss of the coating gloss were also evaluated. The results depicted appropriate physical–mechanical properties. Also, scanning electron microscope (SEM), AFM, and FTIR were used to investigate the nanoparticles' effect upon the coating properties.

Liu et al. investigated a method in order to synthesize a contact-killing, self-concentration antibacterial coating [44]. Production of "a quaternary ammonium compound (QAC) with a long aliphatic chain and a terminal methacrylate" [44],

acting as an antibacterial agent and a photo-curable monomer, was completed in a single-step process. While the presence of QAC weakened the coatings' most basic properties, it continued to exhibit decent properties including high glossiness, excellent hardness, and acceptable adhesion to a cherry wood base. Coatings containing QAC displayed superhydrophilicity along with good antifogging capability, extending the coatings' range of application. Fluorescence and XPS analyses confirmed QAC's self-concentration properties on the cured surface of the film, which is beneficial in preserving the bulk materials' physical characteristics while improving antibacterial activity on the surface.

30.2 Conclusion

In this chapter, a review on UV-curable smart polymer coatings from the mechanism, processing, and application viewpoint was prepared. It was revealed that in place of replacing conventional high-heat processing techniques, UV-cured coating produces materials with improved properties, lowers the operational costs (e.g., natural gas costs for bake curing), and reduces the overall environmental impact. A new class of smart UV-curable coatings is described in multiple sections. This chapter highlighted different types of smart UV-curable coatings for various engineering applications. However, most of the approaches pointed out in this chapter are in the initial stage of development and have not been broadly commercialized, mainly because of complicated processing procedures. Therefore, the current and future trends in UV-curable smart coatings have been dedicated on enhancing the procedures to resolve the problems.

References

1. Ciprian RM, Christophe B, Guy A, Bruno M (2012) J Therm Anal Calorim 110:287–294
2. Koleske V (2002) Radiation curing of coatings. ASTM International, Conshohocken, PA
3. Uhl FM, Webster DC, Davuluri SP, Wong SC (2006) Eur Polym J 42:2596–2605
4. Decker C, Nguyen T, Decker D, Weber-Koehl E (2001) Polymer 42:5531–5541
5. Decker C, Zahouily K, Decker D, Nguyen T, Viet T (2001) Polymer 42:7551–7560
6. Macarie L, Ilia G, Iliescu S, Popa A, Plesu N, Pascariu A (2008) Plast Rubber Compos 37:258–262
7. Steeman PAM, Dias AA, Wienke D, Zwartkruis T (2004) Macromolecules 37:7001–7007
8. Makhlouf ASH (2014) Handbook of smart coatings for materials protection. Woodhead Publishing, Cambridge
9. Li W, Hintze P, Calle LM, Buhrow J, Curran J (2009) Smart coating for corrosion indication and prevention: recent progress, Nace International
10. Clingerman M (2014) PCI magazine. http://www.pcimag.com/articles/98925-smart-coatings (Last accessed: May 2015)
11. Guldin S, Kohn P, Stefik M, Song J, Divitini G, Ecarla F, Ducati C, Wiesner U, Steiner U (2013) Nano Lett 13:5329–5335
12. Latthe SS, Liu S, Terashima C, Nakata K, Fujishima A (2014) Coatings 4:497–507

13. Verma G, Swain S, Khanna AS (2013) Int J Sci Eng Technol 2:192–200
14. Young T (1805) Philos Trans R Soc Lond 95:65–87
15. Wenzel RN (1936) Ind Eng Chem 28:988–994
16. Gennes D, Gilles P (2004) Capillarity and wetting phenomena. ISBN 0-387-00592-7
17. Cassie ABD, Baxter S (1944) Trans Faraday Soc 40:546–551
18. Quere D (2005) Rep Prog Phys 68:2495–2532
19. Soroushnia SH, Bastani S, Bozorgi MM, Rostami M (2015) Prog Org Coat 85:31–37
20. Lai Y, Tang Y, Gong J, Gong D, Chi L, Linc C, Chen Z (2012) J Mater Chem 22:7420–7426
21. http://www.hirecpaint.com/photocatalyst_selfcleaning_mechanism.html (Last accessed: May 2015)
22. Kaewpirom S, Kunwong D (2012) J Polym Res 19:9995–10007
23. Smitha VS, Jaimy KB, Shajesh P, Jeena JK, Warrier KG (2013) J Mater Chem A 1:12641–12649
24. Introzzi L, Fuentes-Alventosa JM, Cozzolino CA, Trabattoni S, Tavazzi S, Bianchi CL, Schiraldi A, Piergiovanni L, Farris S (2012) Appl Mater Interfaces 4:3692–3700
25. Howarter JA, Jeffrey P (2008) Macromol Rapid Commun 29:455–466
26. Chevallier P, Turgeon S, Sarra-Bournet C, Turcotte R, Laroche G (2011) Appl Mater Interfaces 3:750–758
27. Chang CC, Huang FH, Chang HH, Don TM, Chen CC, Cheng LP (2012) Langmuir 28:17193–17201
28. Jacubes D, Lechwar A, Bogdanova A, Longo R http://www.pcoatingsintl.com/wp-content/uploads/2014/04/Multifunctional-UVEB-Curable-Oligomers-for-Optical-Coatings-WP-Jacobs-Du.pdf (Last accessed: May 2015)
29. Zoromba MST (2009) Preparation and characterization of new nano-structured organic/inorganic composite coatings for anti-fog applications. Doctoral thesis. Faculty of Natural and Material Sciences, Clausthal University of Technology, El Manzala, Egypt
30. Yuan Y, Liu R, Wang C, Luo J, Liu X (2014) Prog Org Coat 77:785–789
31. Tang R, Muhammad A, Yang J, Nie J (2014) Polym Adv Technol 25:651–656
32. White SR, Caruso MM, Moore JS (2008) MRS Bull 33:766–769
33. White SR, Sottos NR, Geubelle PH, Moore JS, Kessler MR, Sriram SR, Brown EN, Viswanathan S (2001) Nature 409:794–797
34. Wu DY, Meure S, Solomon D (2008) Prog Polym Sci 33:479–522
35. Yin T, Rong MZ, Zhang MQ, Yang GC (2007) Compos Sci Technol 67:201–212
36. Clingerman M (2014) PCI Magazine
37. Kim HM, Chang YR, Kim H (2013) UV-curable coating composition having self-healing capabilities, coating film and method for preparing coating film. EP2644668 A2
38. Lee JY, Zhang Q, Emrick T, Crosby AJ (2006) Macromolecules 39:7392–7396
39. Kardar P, Ebrahimi M, Bastani S (2008) Prog Org Coat 62:321–325
40. Guarda A, Rubilar JF, Miltz J, Galotto MJ (2011) Int J Food Microbiol 146:144–150
41. DeVasConCellos P, Bose S, Beyenal H, Bandyopadhyay A, Zirkle LG (2012) Mater Sci Eng C 32:1112–1120
42. Chen Z, Chisholm B, Stafslien S, He J, Patel S (2010) J Biomed Mater Res A 95:486–494
43. Motlagh AL, Bastani S (2014) Prog Org Coat 77:502–511
44. Liu R, Zheng J, Li Z, Liu J, Liu X. RSC Adv. doi:10.1039/C5RA03881B

Chapter 31
New Functional Composite Silane-Zeolite Coatings for Adsorption Heat Pump Applications

Edoardo Proverbio, Luigi Calabrese, Lucio Bonaccorsi, Angela Caprì, and Angelo Freni

Abstract The adsorption heat pumps represent an innovative technology to increase the efficiency of thermal energy. To date, this technology requires in-depth analysis in order to increase the overall performance of the equipment. In this context, it is necessary to increase the overall performance of the equipment. The development of multifunctional adsorbent coatings is an important design solution to improve engineering and technology of adsorption heat pumps. Thanks to the use of adsorbent coatings, the heat exchangers and heat pumps can operate more efficiently. These coatings must not only be effective in terms of energy efficiency (thermodynamic and kinetic adsorption properties) but also in terms of mechanical and electrochemical stability. This chapter shows how this problem could be managed through the use of innovative multifunctional composite silane-zeolite coatings. The method proposed in this chapter is based on the deposition, using a hybrid silane binder, of the adsorbent material based on aluminum zeolite. The chemical-physical-mechanical characterization of the composite materials with the purpose to evaluate its industrial applicability is discussed. In particular, adhesion, hydrophobicity, and durability tests were performed. This chapter also highlights how different types of matrices can affect the performance of the coating. The results obtained showed that the performances of the coating were closely related to the interaction between zeolite filler and silane matrix. Furthermore, the type of matrix was an important variable in order to optimize the properties of the composite coating up to its use in the commercial field.

Keywords Silane • Zeolite • Coating • Adsorption • Heat pump

E. Proverbio • L. Calabrese (✉) • L. Bonaccorsi • A. Caprì
Department of Electronic Engineering, Industrial Chemistry and Engineering,
University of Messina, Contrada di Dio Sant'Agata, 98166 Messina, Italy
e-mail: lcalabrese@unime.it

A. Freni
CNR ITAE, Salita Santa Lucia Sopra Contesse 5, 98126, Messina, Italy

31.1 Introduction

Adsorption heat pumps are considered a promising technology used to increase the efficiency of thermal energy [1]. However, in order to consider them a mature technology for use in an industrial environment, it is necessary to increase the overall performance of the equipment. In this context, the development of multifunctional adsorbent coatings is an important design solution that improves both engineering and technology for adsorption heat pumps.

Thanks to the use of adsorbent coatings, the heat exchangers and heat pumps can operate more efficiently. Furthermore, these coatings must not only be effective in terms of energy efficiency (thermodynamic and kinetic adsorption properties) but also in terms of mechanical (adhesion) and electrochemical stability (corrosion protection properties and self-healing).

This chapter shows how this problem could be managed through the use of innovative multifunctional composite silane-zeolite coatings.

The method proposed in this chapter is based on the deposition, using a hybrid silane binder, of the adsorbent material based on aluminum zeolite. The main focus will be placed on the chemical-physical-mechanical characterization of the composite materials with the purpose to evaluate its industrial applicability. In particular, adhesion (peel-through and pull-off tests), hydrophobicity, as well as durability tests will be performed. It also will highlight how different types of matrices can affect the performance of the coating.

The results show that the performances of the coating are closely related to the interaction between zeolite filler and silane matrix. Furthermore, the type of matrix is an important variable in order to optimize the properties of the composite coating up to its use in the commercial field.

31.2 New Challenges on Adsorption Heat Pumps

31.2.1 Thermally Driven Adsorption Machines: An Introduction

Nowadays, adsorption heat pumps represent an attractive alternative to conventional electrically driven systems for a wide range of applications such as automotive air conditioning, solar air conditioning, waste heat recovery, and domestic heat pumping. The thermodynamic cycle of these adsorption machines is similar to compression heat pumps that are electrically driven. The main difference is that an eco-friendly thermal adsorption cycle, or "thermal compressor," is used in lieu of a traditional mechanical compressor. The use of these machines over their counterparts comes with a barrage of benefits such as load reduction during peak consumption, global warming potential mitigation, and primary energy saving, specifically when renewable heat sources (i.e., waste heat, solar energy) are utilized as primary energy. In this case, only the supplemental systems (e.g., recirculating external heat transfer fluid pump) require electrical consumption. Therefore, high electrical COPs (coefficient of performances)
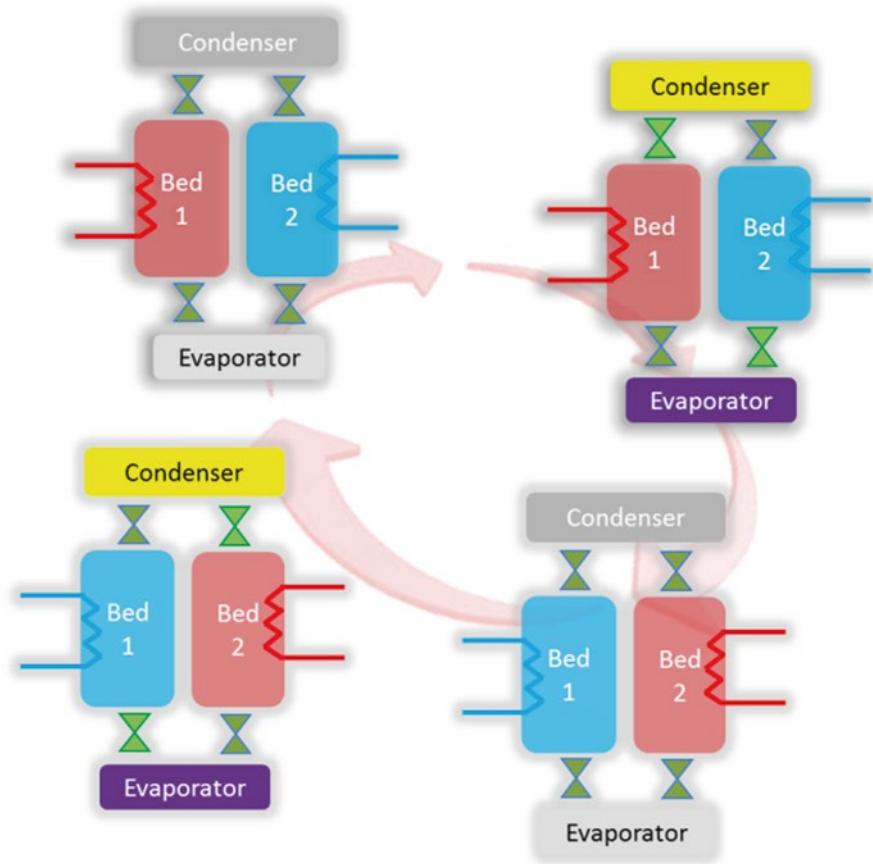
Fig. 31.1 Operating principle of a thermally driven adsorption machine

can be obtained, while primary energy consumption is reduced greatly. A "thermal compressor" also provides many other advantages such as running in silence, which is very desirable in certain applications (residential, theater, museums, etc).

In adsorption cycles, a solid, porous adsorption medium adsorbs the refrigerant in a reversible manner. The following combinations are those that are most frequently used: zeolite/H_2O, silica gel/H_2O, activated carbon/NH_3, and activated carbon/CH_3OH. Three temperature ranges are needed to operate a thermally driven adsorption heat pump/chiller: high temperature drives operation, medium temperature rejects process heat, and at low temperature is where there is a collection of heat energy. During this cycle, the rejected heat acts as a pumping mechanism, while cold produced at low temperature is useful when operating in a chilling capacity [1].

The basic configuration of the adsorption machine consists of four main components (Fig. 31.1): two adsorbent reactors, where the solid adsorbent is heated and cooled to enable the refrigerant adsorption/desorption process; the condenser, where the desorbed refrigerant vapor is condensed into liquid; and the evaporator, which feeds refrigerant to the adsorbent reactors and where the useful effect is produced in

cooling mode [1]. In order to maintain a continuous useful effect, the two reactors work in counter-phase operation and cycle between desorption heating and adsorption cooling modes. There is much more data available for liquid absorption heat pumps/chillers than those that are driven thermally, providing a unique opportunity for development, optimization, increased performance, and reduction of manufacturing costs. Various adsorption chiller or heat pump prototypes have been developed during the past several years, thus demonstrating the feasibility of this technology. In the 1980s, Nishiyodo and Mycom (Japan) were the first industries to sell silica gel/water adsorption chillers. Such chillers, still available on the market, can be efficiently driven by controlled via hot water (60–90 °C); these systems possess various cooling capacities (30–470 kW), ensure a COP of up to 0.6, and are still commercially available. Recently, some German companies started production of small-size adsorption machines for cooling or heat pumping purposes.

However, the current market for adsorption heat pumps and chiller is very small [1]. Indeed, adsorption machines are still too big, heavy, and expensive to compete with conventional heat pump systems. As a further detriment to the density of power, liquid sorption systems remain superior as adsorption systems typically display a lower thermal efficiency. In order to make headway in the market, further studies, development, and trials need to be completed. The research required must encompass an investigation into the system's foundation materials, design and engineering of the unit, advancement of processing technology, and finally a proof of concept piece that can be field tested.

31.2.2 Thermally Driven Adsorption Machines: Current R&D Advancement and Future Challenges

Research and development activity is being carried out worldwide covering all levels of technological development, from novel materials development to compact components design and finally to system integration.

Regarding the materials' portion, major research challenges concerning the selection of the optimal adsorption working pair (dependent on the final application) and the development of novel adsorbent materials capable of very high refrigerant uptake (leading to improved heat pump efficiency) need to be addressed [1]. Moreover, adsorption materials must be stable over several thousand working cycles. Among the most common adsorbents of water, classical aluminum-silicon zeolites (e.g., 4A, 13X, Y) are widely diffused, but they require very high temperature for regeneration (about 200 °C), due to the very high affinity for water molecules. Some years ago, UOP developed a novel zeolite "DDZ70," which is high silica content Y-zeolite exchanged with cerium to reduce its hydrophilicity [2]. Some studies demonstrated that utilization of DDZ70 can be advantageous for adsorptive cooling, due to the lower regeneration temperature (<150 °C) and lower water adsorption heat [3]. However, as far as the authors know, DDZ70 is no longer available on the market. Another common water adsorbent is microporous silica

gel, which can be efficiently regenerated when the heat for desorption is available at a temperature lower than 90 °C but that cannot guarantee adequate performance when the condensation and adsorption heat rejection temperature is higher than 30 °C. Nowadays, (silico)aluminophosphates (SAPOs, AlPOs), metallic organic frameworks (MOFs), and composites ("salt in porous matrix") can be considered the most promising classes of sorbents in terms of high water adsorption capacity and low regeneration temperature. A number of studies were carried out on different types of (silico)aluminophosphates (ALPO5, ALPO18, SAPO34, etc.) [4,5], confirming the interesting properties of such materials for adsorption cycles. The novel synthetic functionalized materials "AQSOA," belonging to the calls of aluminophosphates, evidenced effective absorption properties [6]. Experimental testing of the adsorbent AQSOA FAM-Z02 showed that this material can provide attractive performance traits in the typical operating conditions of adsorption chillers [7]. Furthermore, composites ("salt in porous matrix") are two-component materials based on a porous host matrix with a salt inside its pores [8]. The choice of the matrix and pore-filling solution allows for a wide variation of sorbent properties to fit the requirements of various applications. Recently, the composite sorbent SWS-8L sorbent proved to be attractive for utilization in adsorption chillers driven by low-grade heat [9]. Possible issues that must be further investigated for practical utilization are the risk of leakage of the corrosive salt and long-term hydrothermal stability. In addition, evaluation of super-molecular metal-organic frameworks (MOFs) for application in adsorption chiller is a major focal point for researchers in this field. MOFs first attracted attention due to their open crystalline structure and very high surface area. Some studies revealed a large capacity for water adsorption under practically useful operating conditions [10]. Possible obstacles for practical use are a significant ad-/desorption hysteresis and insufficient stability.

Figure 31.2 shows the water adsorption isobar ($p_{H_2O} = 11 \text{mbar}$) measured at CNR ITAE for different adsorbents by a thermogravimetric technique. The equilibrium curve comparison demonstrates that the adsorbents Y-zeolite DDZ70 from UOP and SAPO zeolite AQSOA FAM-Z02 from MPI allow a variation in water uptake that is much higher than a standard adsorbent, like zeolite 13X and microporous silica gel, under the typical conditions of the adsorption stage of an adsorptive cooling cycle ($p_{H_2O} = 11 \text{mbar}$, $T_{ads} = 65°C$, $T_{ads_{fin}} = 40°C$).

Research and development priorities in the area of components for adsorption machines are the heat and mass transfer intensification through the adsorbent heat exchanger (AdHex) unit, the design of compact, lightweight, high surface area heat exchangers, and the development of efficient evaporator and condenser concepts for low-pressure evaporating fluids such as water vapor. One of the main problems of adsorption machines that employ common packed adsorbent beds is the low heat transfer efficiency between the loose adsorbent grains contacting the heat exchanger and the heat transfer fluid [11]. To overcome this problem, early studies proposed the realization of thick consolidated beds with enhanced thermal conductivity [12]. Nowadays, research is focused on the development of heat exchangers coated with a thin layer of adsorbent material [13]. The most promising coating methods are in
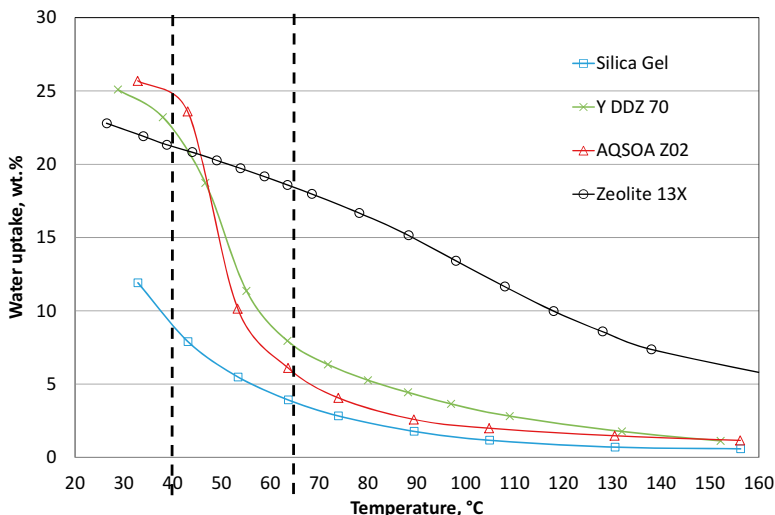
Fig. 31.2 Water adsorption isobar ($p_{H_2O} = 11$ mbar) measured at equilibrium for different adsorbents by thermogravimetric technique

situ zeolite crystallization [14] and dip (or spray)-coating processes [15]. Zeolite direct crystallization offers the clear advantage of high coating stability and perfect thermal contact between zeolitic crystals and metal surface. However, the process can be complex and expensive as the synthesis conditions can be rather drastic (e.g., 20 bars and 200 °C in autoclave for SAPOs zeolite). Moreover, a thinner coating is normally achieved (50–100 μm) which may represent a limit for the practical industrialization of this technique. Dip-coating methods offer the potential benefit of mild reaction conditions, easily variable coating thickness (up to 0.5 mm), and, in general, easier implementation in serial production lines. Per methodologies found in literature, a solution of active powders and organic/inorganic (resin vs. clay) binders is made for which the metal substrate is then submerged into. In order to obtain a tight adsorbent film, excess solvent must be removed via thermal treatment. This procedure can be easily applied to coat complex heat exchanger geometries with an adsorbent layer while maintaining a uniform thickness. Possible issues are the poor mechanical strength, adsorbent pore occlusion by the binder, production of volatile compounds from organic binders, and increased mass transfer resistance through the adsorbent layer. Sale-up of coating techniques for the adsorbent reactor and production cost optimization are important additional challenges. Figure 31.3 qualitatively resumes the previously described situation of adsorbers' development (granular, coated, and direct synthesized systems).

Finally, concerning the whole adsorption system, studies are aimed at defining the optimal control strategy and thermal management to guarantee high performance in terms of primary energy consumption per kWh cooling/heating power
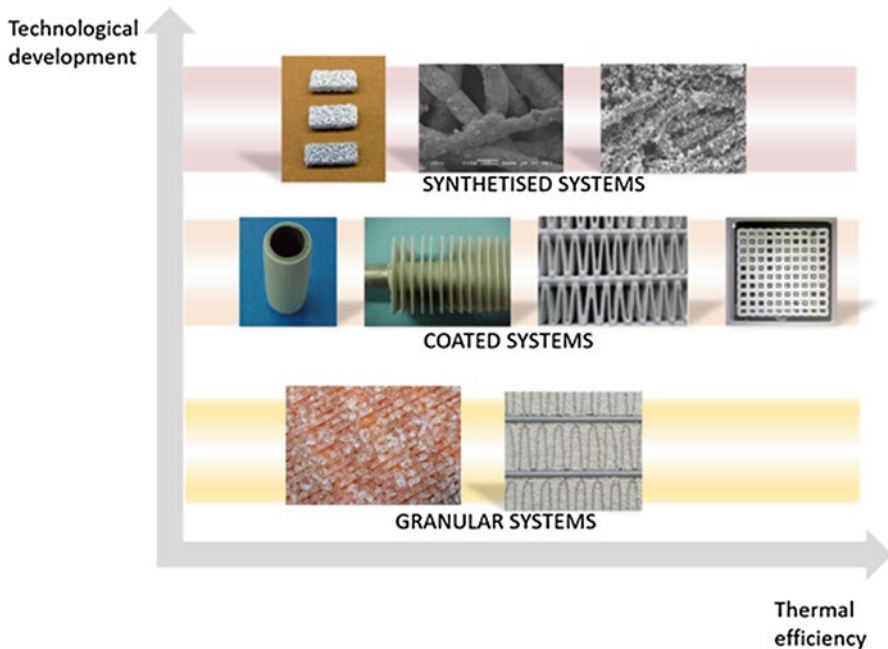
Fig. 31.3 Summary of different adsorber technologies employed in solar-assisted heat pumps

and an optimal system integration ensuring high primary energy saving. Special focus has been given to the research of advanced sorption cycle, trying to overcome two critical issues of the basic cycle: the discontinuity in the production of useful effect and the need to use a significant amount of heat for the desorption phase. The main advanced cycles that have been proposed are described below. The heat recovery cycle represents the first historical attempt to improve the COP of an adsorption machine. This is achieved with two beds working in counter phase so that the thermal energy needed during the isosteric phase of the bed undergoing heating is not provided by the heat source but instead from the thermal flux of the bed being cooled. Such thermal recovery is possible until the temperatures of the two beds are almost equal, so theoretically, even during part of the desorption phase. Thermal wave cycles are based on the division of adsorption chambers into several modular units [16], so that the fluid in the exchangers follows a multistep path which maximizes the difference between inlet and outlet temperatures. In this way, the thermal flux is used efficiently, and the recovery of up to 80 % of desorption heat is possible. Variants were proposed [17] where inert gases are used for the regeneration of beds. However, a complicated system layout and low efficiency in thermal exchange between the various units have limited the practical use of thermal wave cycles. Flow reversal cycles, such as the thermal wave, require inert gases to be introduced in the adsorption bed chambers to create a high-temperature differential. In particular, the flow of hot gases is periodically switched in the two

sides of the beds to allow a thermal recovery not only between adsorber and desorber but also in the adsorber itself. It has been noted that the main effect of such a cycle is to improve the power density. Multistage cycles have been proposed in order to reduce the temperature of the heat source needed [18] and consist of dividing the pressure drop between condenser and evaporator in more stages; up to eight beds are employed, thus complicating the layout of the system. Finally, a reallocation of adsorption/desorption phases is possible; usually adsorption and desorption phases are set to an equal cycle time. Nevertheless, it has been demonstrated that the kinetic of the desorption process is faster than the one of adsorption, the amount depending partly on the granulometry of the adsorbent material used [19]. It is then possible to close the connection between the hotbed and the heat source while the cold bed is still adsorbing. Consequently, qualitative criteria might be defined in order to maximize both the COP and SCP of heat pumps by simply fractionizing the adsorption cycle in a different way (reallocation is possible by using multiple bed machines).

Figure 31.4 demonstrates the remarkable influence of the cycle time and of the relative duration of the adsorption and desorption phases on the performance of a laboratory scale single bed water/zeolite adsorption chiller tested at ITAE [7]. Other research and development priorities to be addressed at a system level concern the optimization of the system control strategies, taking into account the fluctuating external operating conditions and user requirements, the development of efficient heat rejection units, and the reduction of parasitic energy consumption of auxiliaries.
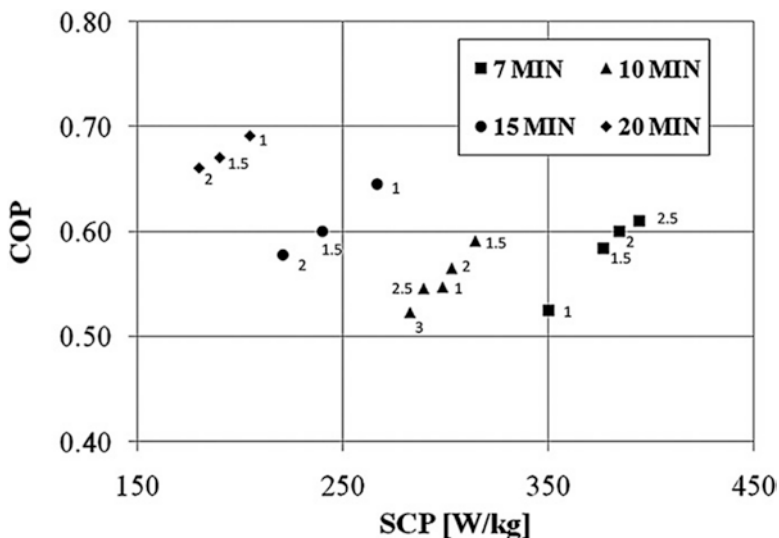
Fig. 31.4 Performance's map (cooling COP vs. specific cooling power) for different cycle times (7, 10, 15, 20 min) and ad-/desorption duration ratio ((R =1, 1.5, 2, 2.5, 3) at $T_{des}=90$ °C, $T_{ads}=T_{cond}=35$ °C, $T_{ev}=15$ °C) (with permission from [7])

31.3   Functional Composite Silane-Zeolite Coatings

Nowadays, adsorption heat pumps are an attractive alternative to conventional, electrically driven systems for a range of applications such as automotive air conditioning, solar air conditioning, waste heat recovery, and domestic heat pumping.

Various small-size closed-cycle adsorption prototypes have been developed in the past, thereby, demonstrating the feasibility of this technology [20].

One of the main problems of closed-cycle adsorption systems is the low heat transfer efficiency between the solid adsorbent material contacting the heat exchanger and the heat transfer fluid. Heat transfer efficiency can be improved using large surface area heat exchangers coated with adsorbent material rather than packed adsorbent beds. The most promising coating methods are in situ zeolite crystallization [21] and the dip-coating processes [22].

Dip-coating methods offer the potential benefits of mild reaction conditions, easily tunable coating thickness (up to 0.5 mm) and generally easier implementation in serial production lines. Furthermore, this procedure can be easily applied to coat an adsorbent layer with complex geometries, maintaining a uniform thickness. Possible issues are the poor mechanical strength, adsorbent pore occlusion by the binder, production of volatile compounds from organic binders, and increased mass transfer resistance through the adsorbent layer.

Zeolite-based coatings display a great potential in this field of study. Created by the formation of alternating silica and alumina tetrahedra linked together and composed in 3D structures, zeolites are crystalline nanoporous aluminosilicates with architectures consisting of channels and cavities with well-defined size.

Industry has begun to utilize zeolites to a large degree because of their ability to molecularly separate gas and liquid with their porous architecture (AKA "molecular sieves"), their ion exchange capability in solution, and their amazing catalytic characteristics imparted on them from their high surface area. Furthermore, zeolites' high thermal and chemical resistance grants them the ability to be utilized in many severe environments and operating conditions.

Due to their silica-aluminate structure, the relatively high chemical reactivity of zeolites comes mainly from their surface silanol groups. Based upon this fact, reaction with various agents, including silanes, can take place by means of a superficial interaction [23].

The silane matrix operates in surface engineering as a coupling agent and mainly offers an interlayer with good adhesion and homogeneity, able to provide further protective barrier action [24].

The realization of a zeolite-based composite coating would maintain the adsorbent properties of the zeolite materials (thereby ensure the industrialization potential for the adsorption heat pumps) but at the same time create a coating with the typical mechanical resistance and durability characteristics typical of silane coatings.

Per previous studies, particle component addition to the silane matrix, such as zeolite crystals, is an affordable approach to obtain effective multifunctional adsorption coatings with good mechanical properties [25] and effective durability in aggressive environmental conditions [26].

A better understanding of the relationship between structure and performances of the coating constituents would be extremely useful in coating technology design.

It has been claimed that the silane coupling agents lead to a significant improvement of filler dispersion, reducing the clumping of particles and improving the wettability by polymers [27].

The properties of the alkyl chain in the silane compounds play a relevant role in the performances of the protective coating. Frignani et al. [28] found that the presence of long aliphatic chain in the silane molecule vastly increased the protective action of the silane layers. In particular, a more evident effect was observed for longer alkyl chains. Van der Waals interactions between the aliphatic chains will favor the formation of an oriented multilayered system [29], which causes a noticeable hindrance to corrosion phenomena. Calabrese et al. [30] confirmed that good hydrophobic behavior of composite silanes with long alkyl chains could be associated with a regular and orderly arrangement of the long carbon chains linked to the generation of induced dipoles along the same plane.

Furthermore, the hydrophobic properties of the coating can be enhanced through a post-curing stage to increase the silane network reticulation [31,32]. A further cross-linking step may lead to the formation of Si–O–Si siloxane bonds which can increase the protective action of these coatings [28,33].

Hatefi et al. [34] found that the drying temperature is a factor that influences the adhesion of the coating with the substrate and also its performance in corrosive environments [35].

31.4 Application, Measurements, and Results

31.4.1 Materials and Testing

Three types of silane (*n*-propyl-trimethoxy silane, octyltriethoxysilane, and (3-aminopropyl) triethoxysilane) were combined with a SAPO 34 filler (filler 80 wt%) to obtain a protective composite coating by the sol-gel process.

In order to avoid that the comparison between the different formulations is made blurred by effects due to incomplete curing of the samples, all samples were subjected to a longtime curing treatment (80 °C for 48 h). This allowed the assertion that all batches had a comparable full curing condition. Consequently, the differences that may be discriminated in the experimental tests can be attributed mainly to the silane-zeolite interaction.

The equilibrium of water vapor adsorption on different adsorbent coatings was studied by a thermogravimetric method based on the use of a CAHN 2000 thermobalance (resolution: 0.1 mg, reproducibility, ±0.2 (mg), accuracy ±0.1 %). Initially, the sample (about 20 mg) was slowly heated up to 150 °C (heating rate 1 °C/min) under vacuum (1e-4 kPa), in order to degas the sample and determine its dry weight. Duration of the evacuation process was 8 h. Afterward, the measuring cell was

Table 31.1 Tables summarizing coating types

Code	Silane matrix	Pretreatment	Zeolite [%]	Thickness ([μm])
S3	*N*-Propyl-trimethoxy silane	S3	–	
S8	Octyltriethoxysilane	S8	–	
S2S3	S3 + dimethyl-dimethoxy silane	S2S3	–	
ZS3	SAPO-34 + S3	S3	80	14 ± 2
ZS8	SAPO-34 + S8	S3	80	17 ± 2
ZS2S3	SAPO-34 + S2S3	S3	80	13 ± 3

connected with an evaporator thermostated at fixed temperature T_{ev}, in order to maintain a static water vapor pressure $p_{H_2O}(T_{ev})$ over the sample, and the adsorption process was started. The water uptake was calculated as

$$w = m \frac{\left(p_{H_2O}, T\right)}{m_0} \tag{31.1}$$

where m_0 is the dry weight of the sample. After reaching the first equilibrium point, a stepwise variation of temperature over the sample (5–10 K) was applied, in order to measure the second equilibrium point and so on, until the full adsorption isobar was determined.

Wettability and adhesion studies were performed in order to evaluate the hydrophobic properties of the coating and chemical interaction between the substrate and the silane-zeolite composite coating. Furthermore, the electrochemical behavior of the coated and bare aluminum samples was evaluated by electrochemical impedance spectroscopy (EIS) tests performed in 3.5 % by weight NaCl solutions (pH 6.5).

The details of the coating types are given in Table 31.1. The thickness of the composite coatings was approximately 10 μm for all batches.

31.5 Results

31.5.1 Morphology

Figure 31.5 shows the SEM micrographs at ×500 magnification for all types of investigated coatings. The samples showed that the aluminum substrate was covered with a compact and homogeneous layer of composite coating. The zeolite grains are interconnected and well packed in the structure.

Moreover, the absence of surface cracks confirms the optimal interaction of the silane matrices with zeolite filler, thus displaying good mechanical stability of the coating even after the cross-linking process.

However, the surface of the specimens is slightly rough. Indeed occasionally "valleys" and "hills" may be identified, mainly on the sample with the bifunctional
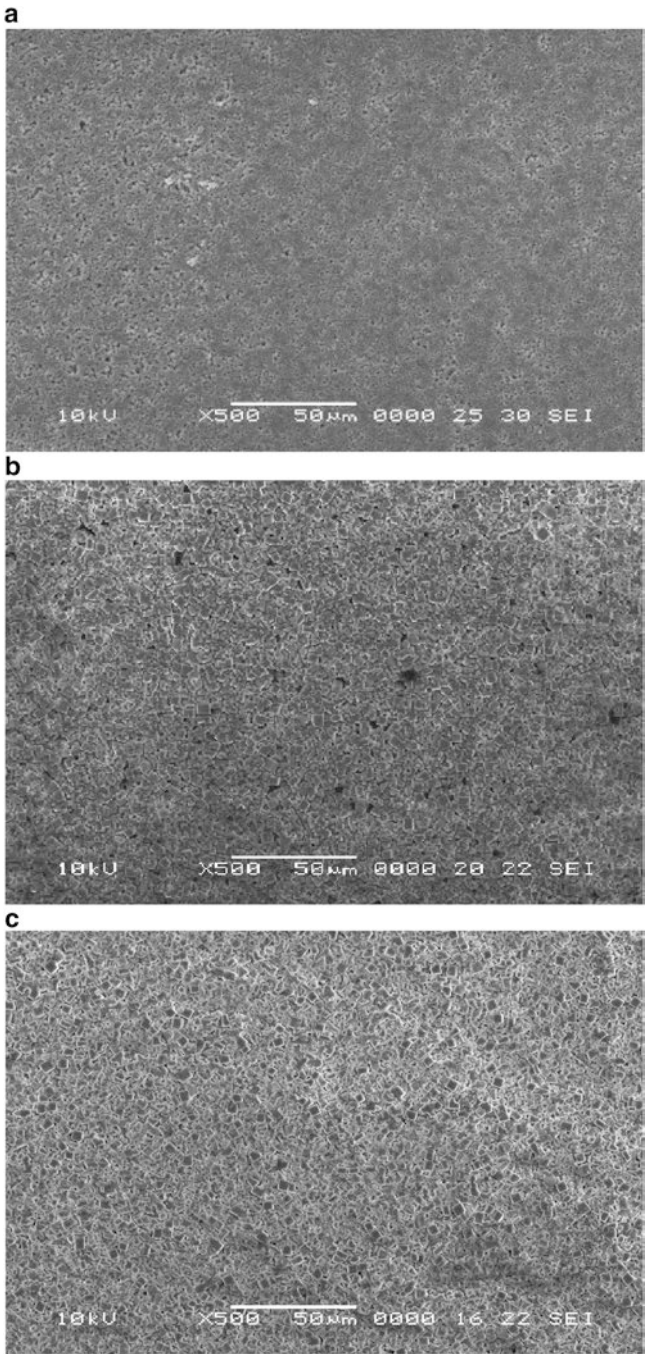
Fig. 31.5 SEM images at ×500 magnifications of (a) ZS3, (b) ZS2S3, (c) ZS8
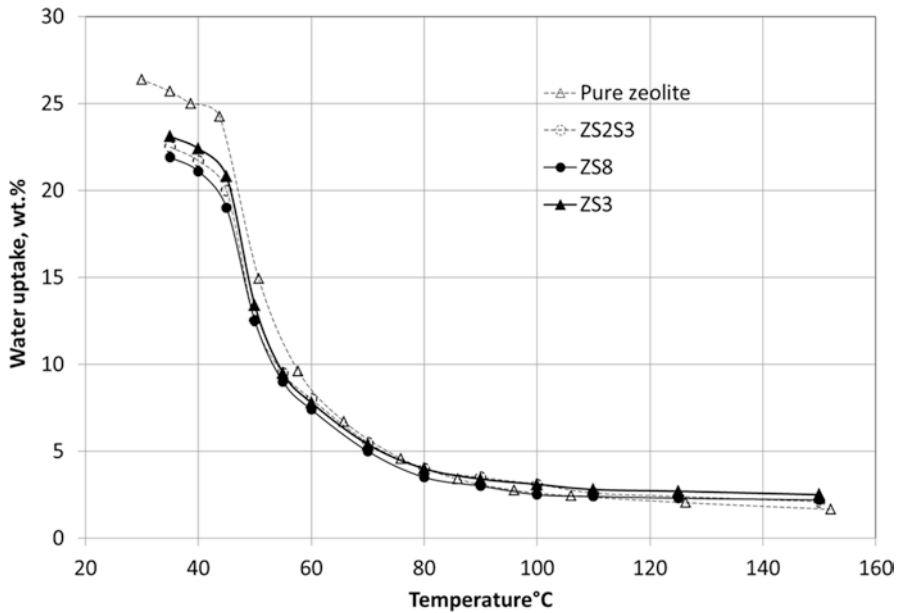
Fig. 31.6 Water adsorption isobars measured at 11 mbar for different coating formulations (ZS2S3, ZS8, ZS3) and for the pure zeolite

silane compound (ZS2S3 sample), as a result of a nonoptimal stratification of local zeolite domains for this sample.

Caused by localized surface voids, the ZS3 and ZS2S3 coatings' surfaces were slightly heterogeneous despite the ZS8 coating, indicated by the darker area on the micrographs. However, the depth of the cavities was not substantial enough to make contact with the underlying aluminum substrate, not considering the application of the coating itself.

31.5.1.1 Adsorption Tests

Figure 31.6 shows the isobars measured in the temperature range of 30–150 °C and at p_{H_2O} of 11 mbar for the coating formulations ZS2S3, ZS8, and ZS3. A water pressure of 11 mbar was specifically selected as it corresponds to evaporation temperature T_{ev} of 7 °C, which represents the typical temperature level for adsorption cooling applications. For comparison purpose, the isobar measured for the pure SAPO-34 powder at the same pressure level was presented. The obtained results demonstrated that all the adsorbent coatings under investigation presented the S-shaped adsorption curve within a narrow temperature window, which is typical of SAPO-34 silica-alumino-phosphates. Comparison among ZS2S3, ZS8, and ZS3 adsorption curves did not show any relevant difference within the error limits depending on the coating

Table 31.2 Wettability angle for distilled water on bare and coated aluminum samples

Contact angle (°)	Al	S3	ZS3	S8	ZS8	S2S3	ZS2S3
Average	60.8	102.3	130.8	108.2	140.4	112.4	145.0
St. dev.	2.3	3.4	4.5	2.8	3.9	3.8	4.3

formulation. The adsorption ability of the various adsorbent coatings is slightly lower than that of the pure SAPO-34 sample. This result was expected as the adsorbent coating formulations consist of 80 wt% of active material (the zeolite itself) and 20 % of binder solution, which can be considered as an inert mass. However, the maximum adsorption capacity of adsorbent coating samples is about 22 wt%, which is still attractive for application in adsorption machines.

31.5.2 Wettability Tests

Table 31.2 shows average contact angles measured on hybrid coatings of SAPO-34 zeolite. In order to better clarify the effect that the zeolite addiction had on the composite coating's hydrophobic behavior, each contact angle was compared with that which was observed on the film of the respective pure silane film.

The samples coated with an unfilled silane layer showed a contact angle greater than that of bare aluminum. In particular, there is an increase in contact angle of almost 100 % for all the samples. Higher values were observed for S2S3 coating (this is shown via silane film deposition onto an aluminum substrate that enhances the metal surface's hydrophobicity). However, samples that were zeolite filler coated displayed a significant increase in the contact angle. However, it is possible to observe as the addition of the zeolite can also induce further increases to the contact angle (20–30°) with respect to the unfilled silane film. In particular, the ZS2S3 and ZS8 samples showed a wettability behavior close to that of super-hydrophobic coatings (contact angle above 150°). High contact angles promote better and easy sliding of the solution along the zeolite coated surface, reducing the residence time below that of untreated surfaces.

The hydrophobic behavior of these composite coatings based on zeolite filler is due to the synergistic action of several factors. The surface morphology of this class of coatings plays an important role. As evidenced by the SEM images, the coating surface has a very bumpy morphology. When considering the surface roughness of the coating, a deposited droplet interfaces with the air entrapped in the pores of the surface, creating small air pockets underneath it. According to the Cassie-Baxter regime, a rough substrate with the air trapped under the droplet induces an improvement in the apparent contact angle [36]. All samples evidenced similar morphology; however, the increase of the contact angle induced by the roughness cannot be deemed responsible for the different hydrophobic behavior of the composite coatings.

Cross-linking density can be increased by incorporating zeolite filler into the silane matrix [34] resulting in a reduction in the surface coating's wettability [37].

The zeolite (having several hydroxyl groups on its surface) interacts with silanol groups of the silane molecules, acquiring external hydrophobic organic chains. The newly formed silane-zeolite micelles present in the peripheral regions are mainly composed of alkyl chains. The resulting composite structure exhibits a preferential orientation of hydrophobic chains, with the tendency to increase the coating surface's hydrophobicity [25].

More relevant is the evidence that the silane matrix has a relevant effect on the interaction of the water-surface interface. The nature and the steric hindrance of the organic chains for different silane compounds could influence the hydrophobic behavior of the coating. Longer alkyl groups of S8 silane shield the polar areas in the metal substrate inducing increases in the contact angle, when compared with the ZS3 sample. At the same time, the addition of bifunctional components in the trifunctional silane matrix (ZS2S3 sample) induces an increase in the contact angle compared with the unmodified one (ZS3 sample). This behavior could be explained by assuming that the presence of the bifunctional group significantly influences the flexibility of the molecular network chains.

The ZS2S3 sample displayed a greater degree of cross-linking than the composite film (due to a greater flexibility of the chains during the siloxane cross-linking step) and, due to the steric hindrance of the methyl groups that can act as a shield for the metal substrate, favors high hydrophobic behavior.

Regarding the samples ZS2S3, an increase in contact angle with respect to the ZS3 sample was observed. This behavior can be attributed to several factors. The reduction of the number of free hydroxyl groups associated with silane (due to a higher amount of covalent bonds in Si–O–Si) also reduces the number of hydrophilic sites, promoting hydrogen bonding with the solvent. Furthermore, as proposed by Fadeev and McCarthy [38], the contact angle of silane compounds with alkyl chains can be influenced by interactions with the methyl group ($-CH_3$) which presents more hydrophobic properties of the methylene groups ($-CH_2$). The use of the silane compound S2 increases the content of methyl groups in the structure, favoring contact angles greater than the ZS3 system.

31.5.3 Adhesion Tests

Figure 31.7 shows the results obtained by means of the ASTM D 3359 B adhesion test of the zeolite coating produced with different silane matrices. The red dotted line refers to a reference threshold of 4B index which, according to the D3359 standard (5 % of detached area), identifies acceptable coating performances [39]. The percentage of the detached area is heavily influenced by the silane compound used as the matrix in the composite coating. In particular, despite ZS2S3 and ZS8 batches, the ZS3 sample was not able to obtain affordable adhesion properties. For this sample, a detached area of about 10 % was obtained (3B according to D3359 standard). The best results were achieved by using the S8 silane matrix. For the ZS8 sample, a detached area of about 4 % (4B according to D3359 standard) was observed. All
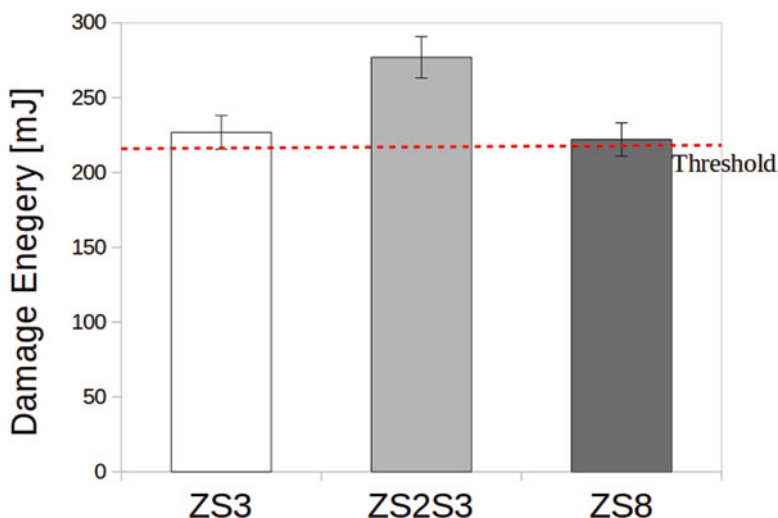
Fig. 31.7 Damage energy of composite coatings varying silane matrix

samples are characterized by their homogeneous morphology, confirming good zeolite-silane interlocking. The factor that distinguished each sample was the differences in the silane used as matrix. Therefore, the coatings' aluminum and silanol functional group bonding are crucial in promoting the interfacial interaction, which greatly influences the various composite coating's adhesion behavior [25].

31.5.4 Impact Test

Figure 31.8 shows failure impact energy of the composite coating at varying silane matrix. The dotted line refers to a reference threshold of 220 (mJ), identifying an acceptable coating performance [39]. The energy values for when the critical compressive collapse of the coating occurred were set as the failure impact energy. Good impact performances were observed for ZS2S3 samples with critical damage energy over to 270 mJ. The worst results were observed for the ZS3 and ZS8 samples with an impact resistance 20 % lower than the ZS2S3 samples.

31.5.5 Electrochemical Performances

In order to better understand the data analysis, low-frequency impedance (Z_{lf}, identified at 0.1 Hz) was employed, as shown in Fig. 31.9, so as to directly evaluate the corrosion performance of the coated samples [40].
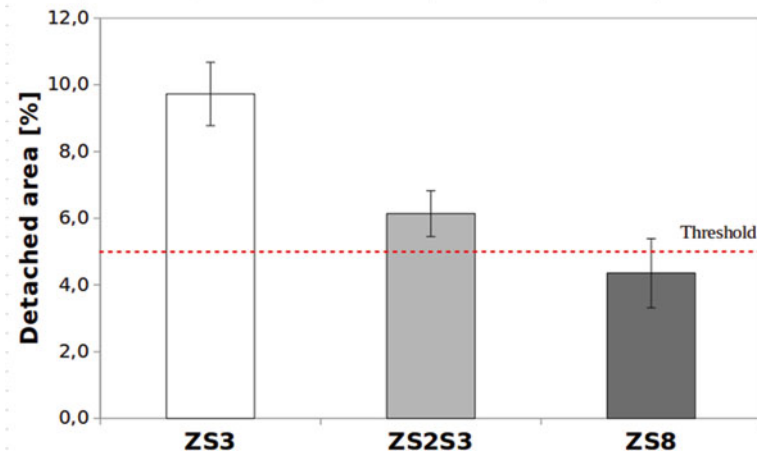
Fig. 31.8 Damage energy of composite coatings varying silane matrix
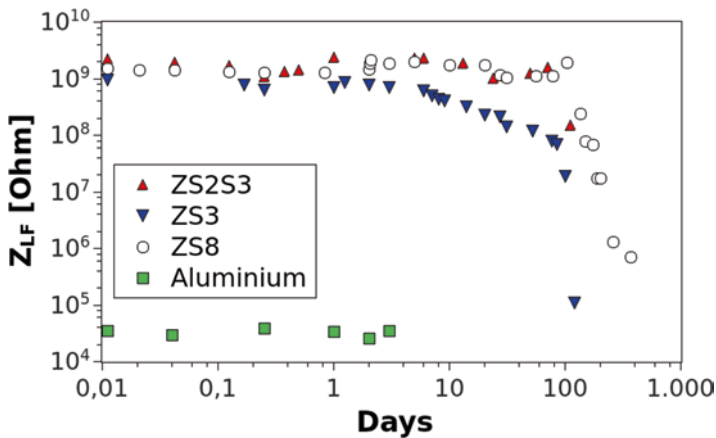
Fig. 31.9 Low-frequency impedance evolutions at increasing aging time for coated and uncoated samples

The results confirmed that better performance was obtained for the ZS2S3 coating. In any case, although the ZS3 sample had lower impedance resistance, it also displayed higher protective performance despite being uncoated and aged for a year. In-depth analysis of the impedance evolution during immersion over a period of time in three regions can be completed.

At first, for low immersion times, all samples exhibited very effective protective behavior on the aluminum substrate due to the significant barrier action offered by the silane-zeolite composite coating. The anticorrosion performance of the coating was stable, and the Z_{lf} magnitude was about 1×10^9 (Hz). This effect was not so

blatantly evidenced for the bare aluminum substrate. This stabilization phase is quite long for ZS8 and ZS2S3 samples where high impedance values are observed for approximately 100 days. This behavior could be related to water diffusion on the coating and the subsequent formation and passivation of conductive pathways.

By increasing aging time, a progressive reduction in the impedance values was observed. This reduction is related to the diffusion of water across the coating, favoring the activation of dissolution phenomena at the coating-substrate interface. In the ZS3 coating, this phenomenon is observed from days 10 to 70. The degradation phenomena are the activated. Afterward, as aging time increased, the performance of the ZS3 coating drastically reduced, and impedance values of 1×10^5 (Ω) were observed. Instead for ZS8 and ZS2S3, coating a gradual transition from high to low impedance values was not observed. An abrupt reduction of Z_{lf} was observed at approximately 140 days for ZS8 samples and 120 days for ZS2S3 coatings. After 1 year, the final impedance values of ZS8 and ZS2S3 coatings (Z_{lf} is $1 \times 10^6 \Omega$) were found to be 1–2 orders of magnitude higher than the uncoated aluminum sample.

The improved durability of ZS8 ZS2S3 coatings is attributable in part to the behavior of the composite coating surface. High surface hydrophobicity allows for reduced interaction between the coating and the electrolyte shortening the time required for the diffusion of water across the coating to the metal substrate. Finally, the strong hydrophobic behavior of the coating implied that there were greater protective properties at very long immersion times.

31.6   Zeolite-Coated Heat Exchanger

The above described coating technique was used to prepare a full-scale adsorber consisting of a SAPO-34 zeolite coating over a finned flat-tube aluminum HEX [metal mass, 0.565 (kg) and overall volume, 1.15 (dm³)]. As shown in Fig. 31.10, the original aluminum HEX was uniformly coated by the SAPO-34 zeolite layer [adsorbent mass, 0.125 kg and coating thickness, 0.4 (mm)], producing a coated AdHEX with a metal/adsorbent mass ratio of 4.09.

The so realized coated adsorber was tested by a laboratory scale adsorption chiller, which simply consists of a single bed adsorption unit [maximum power of 1 (kW)] connected to a test bench for simulating the external heat sources/sinks. More details about the testing facility features and the experimental procedure are reported elsewhere [7]. Tests were aimed at measuring the adsorber performance in terms of COP and the cooling power delivered. Results were achieved under typical cooling conditions ($T_{ev} = 15$ °C, $T_{con} = T_{ads} = 35$ °C, $T_{des} = 90$ °C, cycle time = 5 min) and are summarized in Table 31.3. The experimental error was less than 10 %.

The coated adsorber delivered very high mass-specific cooling power (MSCP) (1200 W/kg$_{ads}$) which is a clear advancement over currently available technology. The granular bed delivered higher volumetric cooling power, but the amount of SAPO-34 grains was much higher, increasing the capital costs.
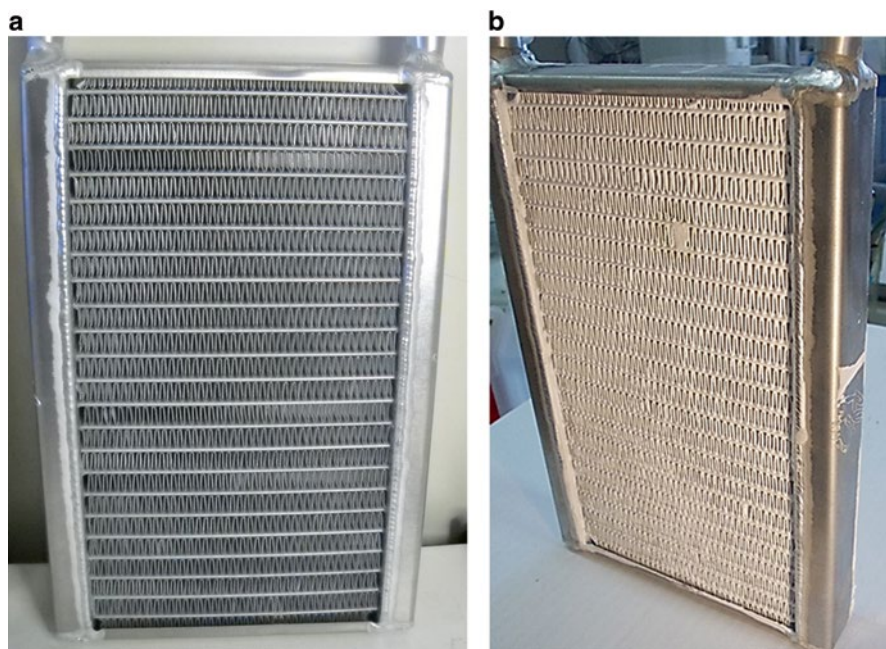
Fig. 31.10 Overall view of the blank (**a**) and dip coated (**b**) full-scale coated adsorber

Table 31.3 Performance measured for the full-scale coated and granular adsorber ($T_{ev} = 15$ °C, $T_{con} = T_{ads} = 35$ °C, $T_{des} = 90$ °C, cycle time = 5 min)

	Cooling COP	Differential water loading, wt.%	Mass-specific cooling power, W/kg$_{ads}$	Volumetric specific cooling power, W/dm^3
Innovative coated adsorber	0.5	10	1200	300
Traditional granular adsorber	0.48	8	400	500

31.7   Conclusion

In the present chapter, the comparison of adsorption, adhesion, and anticorrosive properties of various types of zeolite-based coatings, with different silane matrices on AA6061 aluminum substrates, was reported. This class of coatings, obtained by the sol-gel technique, showed good homogeneity and high levels of adhesion to the substrate metal. Electrochemical tests, performed in a 3.5 % (w/w) NaCl solution, displayed that electrochemical behavior is slightly influenced by the functional groups of the silane matrix, although all composite coatings exhibited high stability while at high potential in the chloride solution.

31.8   Future Outlook

The search for efficient adsorbent materials having moderate hydrophilicity [i.e., regenerable at low temperatures (80–150 °C)] and high water adsorption capacity] is the main goal for the development of a low-temperature adsorption heat pump. Zeolites belonging to the alumino-silicon-phosphor family, like SAPO-34, show adsorption properties at low equilibrium temperatures and pressures that are particularly appropriate to the range of operating conditions for such pumps [5]. In order to optimize the adsorption pump performances, a new approach could be to modify the surface properties of the zeolite filler (e.g., pretreatment with hydrophilic/hydrophobic compounds) [41]. In this way, it could be possible to influence the zeolite/water vapor interaction so that the thermodynamic cycle governing the machine efficiency can be better managed. However, the low thermal conductivity of zeolites has a negative impact on the heat transfer efficiency of the entire heat exchanger. Therefore, there is a need for new engineered materials that combine sorbent and heat transfer properties. In this respect, the use of zeolite-graphite composites represents a valid strategy for the ideal combination of low density, low heat capacity, and high thermal conductivity shown by the graphite substrates. In the past, some authors proposed a composite made by compressing graphite grains with hygroscopic salts or zeolites [42] to improve the thermal conductivity of the adsorbent bed. Such a combination, however, despite leading to a better thermal conductivity, resulted in an excessive rise in resistance to the water vapor's mass transfer [43]. An alternative solution was proposed by the direct synthesis of SAPO-34 on porous carbon supports, like graphite foams [44], in order to combine the needed vapor diffusivity with the thermal properties of carbon materials. A new stimulating approach is to use composite materials based on the deposition of SAPO-34 on high density graphite plates [45] (which can be easily machined to provide optimal configurations for the design of an advanced heat exchanger for solar cooling or automotive applications) giving promising results in order to optimize the process performance.

References

1. Strategic Research Priorities for Cross-Cutting Technology (Secretariat of the RHC-Platform, Brussels)
2. Dunne SR (1993) US5667560 A
3. Dawoud B, Vedder U, Amer EH, Dunne S (2007) Non-isothermal adsorption kinetics of water vapour into a consolidated zeolite layer. Int J Heat Mass Transf 50:2190
4. van Heyden H, Munz G, Schnabel L, Schmidt F, Mintova S, Bein T (2009) Appl Therm Eng 29:1514
5. Henninger SK, Schmidt FP, Henning H-M (2010) Appl Therm Eng 30:1692
6. Kakiuchi H, Shimooka S, Iwade M, Oshima K, Yamazaki M, Terada S, Watanabe H, Takewaki T (2005) KAGAKU KOGAKU RONBUNSHU 31:273
7. Sapienza A, Santamaria S, Frazzica A, Freni A (2011) Energy 36:5532

8. Aristov YI, Restuccia G, Cacciola G, Parmon VN (2002) Appl Therm Eng 22:191
9. Freni A, Sapienza A, Glaznev IS, Aristov YI, Restuccia G (2012) Int J Refrig 35:518
10. Henninger SK, Jeremias F, Kummer H, Janiak C (2012) Eur J Inorg Chem 2012:2625, http://onlinelibrary.wiley.com/doi/10.1002/ejic.201101056/abstract (Last Accessed: May 2015)
11. Mugnier D, Jakob U (2015) Wiley Interdiscip Rev Energy Environ 4:229
12. Pino L, Aristov Y, Cacciola G, Restuccia G (1997) Adsorption 3:33
13. Dawoud B (2013) Appl Therm Eng 50:1645–1651
14. Bonaccorsi L, Calabrese L, Freni A, Proverbio E, Restuccia G (2013) Appl Therm Eng 50:1590–1595
15. Freni A, Russo F, Vasta S, Tokarev M, Aristov YI, Restuccia G (2007) Appl Therm Eng 27:2200
16. Pons M, Poyelle F (1999) Int J Refrig 22:27
17. Critoph RE (1999) Int J Refrig 22:38
18. Alam KCA, Khan MZI, Uyun AS, Hamamoto Y, Akisawa A, Kashiwagi T (2007) Appl Therm Eng 27:1686
19. Glaznev IS, Aristov YI (2010) Int J Heat Mass Transf 53:1893
20. Critoph RE (2012) Int J Refrig 35:490
21. Bauer J, Herrmann R, Mittelbach W, Schwieger W (2009) Int J Energy Res 33:1233
22. Okamoto K, Teduka M, Nakano T, Kubokawa S, Kakiuchi H (2010) In: *IMPRES Conference* (Research Publishing Services), pp 27–32
23. Kawai T, Tsutsumi K (1998) Colloid Polym Sci 276:992
24. van Ooij WJ, Zhu D, Stacy M, Seth A, Mugada T, Gandhi J, Puomi P (2005) Tsinghua Sci Technol 10:639
25. Calabrese L, Bonaccorsi L, Caprì A, Proverbio E (2014) Prog Org Coat 77:1341
26. Calabrese L, Bonaccorsi L, Caprì A, Proverbio E, Coatings J (2014) Technol Res 11:883
27. Zaferani SH, Zaarei D, Danaee I, Mehrabian N (2014) J Adhes Sci Technol 28:151
28. Frignani A, Zucchi F, Trabanelli G, Grassi V (2006) Corros Sci 48:2258
29. Wang D, Ni Y, Huo Q, Tallman DE (2005) Thin Solid Films 471:177
30. Calabrese L, Bonaccorsi L, Capri A, Proverbio E (2014) Metall Ital 106:35
31. van Ooij WJ, Zhu D (2001) Corrosion 57:413
32. Franquet A, Le Pen C, Terryn H, Vereecken J (2003) Electrochim Acta 48:1245
33. Zhu D, van Ooij WJ (2003) Corros Sci 45:2177
34. Palanivel V, Zhu D, van Ooij WJ (2003) Prog Org Coat 47:384
35. Hatefi A, Mohagheghi S, Kianvash A, Coatings J (2013) Technol Res 10:743
36. Whyman G, Bormashenko E, Stein T (2008) Chem Phys Lett 450:355
37. Almanza-Workman AM, Raghavan S, Deymier P, Monk DJ, Roop R (2002) J Electrochem Soc 149:H6
38. Fadeev AY, McCarthy TJ (2000) Langmuir 16:7268
39. Freni A, Frazzica A, Dawoud B, Chmielewski S, Calabrese L, Bonaccorsi L (2013) Appl Therm Eng 50:1658
40. Zheludkevich ML, Yasakau KA, Bastos AC, Karavai OV, Ferreira MGS (2007) Electrochem Commun 9:2622
41. Lee JY, Lee SH, Kim SW (2000) Mater Chem Phys 63:251
42. Wang SG, Wang RZ, Li XR (2005) Renew Energy 30:1425
43. Meunier F (1998) Appl Therm Eng 18:715
44. Bonaccorsi L, Bruzzaniti P, Calabrese L, Freni A, Proverbio E, Restuccia G (2013) Appl Therm Eng 61:848
45. Vasta S, Giacoppo G, Barbera O, Calabrese L, Bonaccorsi L, Freni A (2014) Innovative zeolite coatings on graphite plates for advanced adsorbers. Appl Therm Eng 72(2):153–159

Chapter 32
Intercalation of Poly[oligo(ethylene glycol)-oxalate] into Lithium Hectorite

Iskandar Saada, Rabin Bissessur, Douglas C. Dahn, Matthieu Hughes, and Victoria Trenton

Abstract Intercalation of poly[oligo(ethylene glycol)-oxalate] (POEGO) into lithium hectorite was conducted. A series of nanocomposite materials were prepared by varying the molar ratio of the polymer to the lithium hectorite. The nanocomposites were characterized using powder X-ray diffraction (XRD), thermogravimetric analysis (TGA), differential scanning calorimetry (DSC), and attenuated total reflectance (ATR) spectroscopy. AC impedance spectroscopy was used to measure the ionic resistance of the nanocomposites when complexed with lithium triflate.

Keywords Lithium hectorite • Poly[oligo(ethylene glycol)-oxalate] • Nanocomposites • Solid electrolytes

32.1 Introduction

Lithium-ion batteries have become a prominent source of energy storage for small- and large-scale applications in the past two decades. Many academic and industrial battery material research labs are currently focused on improving the safety of lithium-ion batteries by searching for viable solid-state electrolyte materials. Solid-state electrolyte materials allow for the development of lithium-ion batteries that exhibit enhanced safety, flexible cell designs, and lower cost due to their simplified components. One such class of materials is solid polymer electrolytes (SPEs); SPEs are generating interest due to their ease of packaging and enhanced safety. However, SPEs tend to exhibit low dimensional stability at ambient temperatures, ultimately

I. Saada • R. Bissessur (✉)
Department of Chemistry, University of Prince Edward Island,
Charlottetown, PE, Canada, C1A 4P3
e-mail: rabissessur@upei.ca

D.C. Dahn • M. Hughes • V. Trenton
Department of Physics, University of Prince Edward Island,
Charlottetown, PE, Canada, C1A 4P3

681

Fig. 32.1 Structure of poly[oligo(ethylene glycol)-oxalate] (POEGO)
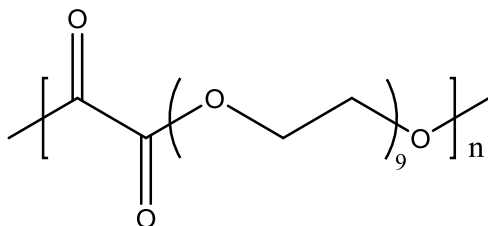
causing them to flow once assembled in batteries [1, 2]. To this end, enhancement of SPEs' dimensional stability is proposed via intercalating them into two-dimensional layered structures such as hectorite, specifically, lithium hectorite.

Clay–polymer nanocomposites have been the subject of much research since the early 1960s [3]. Interest in these nanocomposites stems from their optical transparency, biodegradability, tensile and mechanical strength, gas barrier properties, and ionic conductivity [4]. Specifically, ionically conductive clay–polymer nanocomposites are ideal candidates as electrolytes in solid-state lithium-ion batteries due to their ionically conductive and physical properties [5]. When an ionically conductive polymer is intercalated into a two-dimensional layered structure, the material could exhibit enhanced mechanical and thermal stability compared to the pristine polymer while retaining the ionic conductivity of the polymer [6].

The following approach uses a PEG-based polymer known as poly[oligo(ethylene glycol)-oxalate] (POEGO), displayed in Fig. 32.1, as a candidate. Pure POEGO is an insulator. However, the polymer is environmentally sensitive to the presence of small amounts of salts and becomes ionically conductive [7]. For instance, the polymer has been reported to yield ionic conductivity when complexed with small amounts of lithium triflate. In particular, the room temperature ionic conductivity of $(POEGO)_{16} LiCF_3SO_3$ can be as high as 5.9×10^{-5} (S cm^{-1}), depending on the number of oxyethylene in the oligo(ethylene glycol) units (shown as 9 in Fig. 32.1) [7]. The high ionic conductivity of the polymer has been ascribed to its low glass transition temperature resulting in significant segmental motion of the polymer, assisting the movement of ions within the polymer matrix [7]. Due to the large property change of the polymer from insulating to ion conducting when subjected to small amounts of salts (the external stimuli) and its characteristic low glass transition temperature, the polymer clearly fits within the definition of "intelligent/smart polymers" [8]. Rapid conductivity changes as a function of temperature also occur in some of these polymer/salt complexes [7] and could in principle be used in smart polymer applications where the external stimulus is temperature.

POEGO can potentially be used in lithium-ion battery applications. However, POEGO has low dimensional stability at ambient temperatures and would ultimately leak after cell assembly. In order to overcome this challenge, POEGO has been intercalated into two-dimensional layered structures such as tin disulfide [9], graphite oxide [10], and sodium hectorite with varying degrees of success [2].

Hectorite is a mineral that arises from volcanic ash and belongs to the family of smectite clays. Smectites are commonly used in many applications such as pharmaceuticals [11], cosmetics [12], and automobile components [13] and could
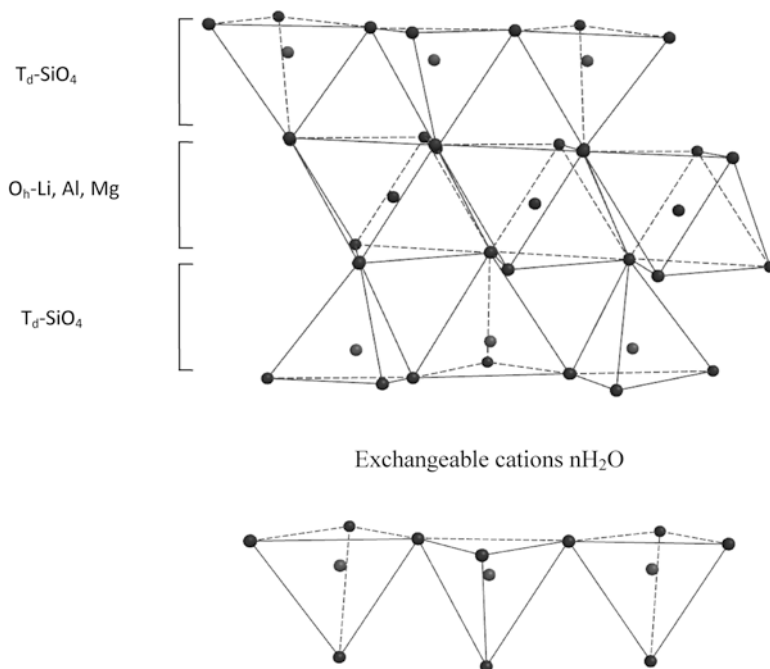
Fig. 32.2 Structure of hectorite

potentially be used as solid electrolytes in lithium-ion batteries [6, 14, 15]. Smectite clays are generally composed of 2:1 layers formed by two tetrahedral silicate sheets encompassing an octahedral sheet, as shown in Fig. 32.2 [16].

Hectorite is appealing as a layered host due to its high thermal stability, high surface area, exfoliation/restacking ability, and high cation exchange capacity [17]. Researchers have reported the intercalation of various materials such as polyethylene oxide [2], polystyrene/poly(ethyl methacrylate) blends [18], phthalocyanines [17], and ruthenium tris(bipyridine) [19] into sodium hectorite. However, in this article the intercalation of poly[oligo(ethylene glycol)-oxalate] (POEGO) into lithium hectorite is reported, rather than sodium hectorite. The lithiation process of sodium hectorite was conducted by exploiting the cation exchange capability of hectorite and displacing the naturally lying sodium ions with lithium ions [20].

A further goal of this research is to compare the characteristics of the produced nanocomposites to those of the pristine POEGO. In order to accomplish this goal, a series of nanocomposites were prepared by varying the molar ratio of POEGO to Li-hectorite. This comprehensive study was performed in order to monitor changes in thermal and ionic conductivity properties. The nanocomposites were characterized using powder X-ray diffraction, thermogravimetric analysis, differential scanning calorimetry, and attenuated total reflectance spectroscopy. Furthermore, AC impedance spectroscopy was used to determine the ionic resistance of the nanocomposites complexed with lithium triflate.

32.2 Experimental

32.2.1 Purification and Lithiation of Hectorite

Sodium hectorite (SHCa-1) was purchased from Source Clays Repository. Since the fine powder has calcium carbonate and other impurities within it, a purification process was performed as previously reported in the literature [2]. Once the purification process was complete, a cation exchange process was employed using a previously reported methodology in order to remove the sodium ions and replace them with lithium ions [20]. The cation exchange process began with the addition of a LiCl solution (0.75 M) to the purified sodium hectorite. This mixture was left to stir for one day and then centrifuged. The supernatant was discarded and the process was repeated twice. When the final LiCl exchange was complete, the white translucent gel was washed and centrifuged three times with deionized water. The resulting gel mixture was then dried in an oven at 100 °C for a minimum of 3 days. The solid clay was then rinsed three times with methanol in order to remove any excess LiCl and NaCl. Finally, the Li-hectorite was dried in an oven at 70 °C for at least 1 day. The lithiation process was carried out twice to ensure maximum substitution of lithium ions. Elemental analysis was used to monitor the sodium ion and lithium-ion content at the Guelph Chemical Laboratories Ltd. in Ontario, Canada. The data indicated an increase in lithium-ion proportion from $Li_{0.5} Na_{0.8} Si_1$ (sodium hectorite) to $Li_3 Na_{0.4} Si_1$ (lithium hectorite).

32.2.2 Synthesis of Polymers and Polymer–Salt Complexes

The synthesis of POEGO was performed by following procedures reported in the literature. The polymer-to-lithium triflate ($LiCF_3SO_3$) ratio, $(POEGO)_{16} LiCF_3SO_3$, was chosen based on previously reported literature in order to obtain the most ionically conductive polymer–salt complex [7]. The synthesized polymer was stored in a vacuum desiccator, and the polymer–salt complexes were intercalated as soon as they were prepared in order to minimize humidity absorption. Hereafter, the uncomplexed polymer will be referred to as POEGO, while the salt-complexed polymer will be referred to as Li-POEGO.

32.2.3 Preparation of Nanocomposites

A general procedure was employed for the intercalation of POEGO into Li-hectorite. Li-hectorite (0.100 g, 2.60×10^{-4} mol) was suspended in deionized water and left to stir until fully suspended (typically 30 min). During the suspension period, polymer with molar ratios 0.5, 1, 2, or 4 with respect to the Li-hectorite was dissolved in 5 mL of deionized water. A pipette was used to transfer the polymer solution to the

Li-hectorite suspension at a rate of one drop per second. The progress of the reactions was monitored via XRD, while the final products were isolated via freeze-drying and stored in a vacuum desiccator.

32.3 Instrumentation

32.3.1 Powder X-ray Diffraction

X-ray diffraction (XRD) was conducted on a Bruker AXS D8 Advance diffractometer. The equipment consists of a variable divergence slit, variable anti-scatter slit, and a scintillation detector. The monochromator is made of graphite, and Cu (kα) radiation ($\lambda = 1.542$ Å) was used. The data was collected at room temperature on glass substrates.

32.3.2 Thermogravimetric Analysis

Thermogravimetric analysis (TGA) was performed on a TA Q500 using a heating rate of 10 °C/min, with the use of platinum pans under dry compressed air. Samples were freeze-dried prior to TGA analyses in order to minimize their moisture content.

32.3.3 Differential Scanning Calorimetry

Differential scanning calorimetry (DSC) was performed on a TA Q100 using heat/ cool/heat cycle under nitrogen flow at a rate of 50 mL/min.

32.3.4 Attenuated Total Reflectance Spectroscopy

Attenuated total reflectance (ATR) spectroscopy data was collected using a Bruker Alpha A-T (resolution 0.9, 128 scans).

32.3.5 AC Impedance Spectroscopy

Impedance spectroscopy (IS) was used to measure the ionic conductivity of the nanocomposites and the polymer–salt complex [21]. Most of the IS samples were cast films formed on rectangular glass substrates with two stainless steel electrodes on the opposite ends of the substrates. During IS measurements, current flows

between the electrodes, along the film parallel to the substrate. Samples from reaction mixtures were cast onto the substrates after 3 days to ensure complete intercalation. One sample was a pressed pellet in the shape of a disk. For the pellet sample, IS measurements were made with the sample sandwiched between two stainless steel electrodes, with current flowing perpendicular to the plane of the disk.

In order to remove moisture, the samples were placed in a vacuum chamber for at least 24 h at room temperature prior to the data collection. During IS measurements, the temperature of the samples was controlled using a Cryodyne 350 CP refrigerator and a Lakeshore 321 temperature controller. The data collection was performed using a Solartron 1250 frequency response analyzer and a homebuilt accessory circuit for high-impedance samples. The voltage across the samples was 50 mV rms. The conductivity was then determined by fitting the IS data to an equivalent circuit model using a program named LEVMW [22] that carries out a complex nonlinear least-squares fit using the Levenberg–Marquardt algorithm.

32.4 Results and Discussion

32.4.1 POEGO/Lithium Hectorite

32.4.1.1 Powder X-ray Diffraction

Powder X-ray diffraction was used to confirm whether POEGO was successfully intercalated into lithium hectorite (Li-hectorite). The XRD data was used to compare the basal spacing (i.e., d-spacing) of the intercalated polymer nanocomposites to that of the pristine Li-hectorite and determine the effect that the various polymer molar ratios have on the basal spacing of the layered structure. Figure 32.3 compares the POEGO–Li-hectorite nanocomposite (1:1) to the control (Li-hectorite treated with H_2O) and illustrates the increase in basal spacing of the layered structure.

Throughout this research project, the polymeric molar ratio of POEGO was systematically increased with respect to Li-hectorite (0.5, 1, 2, and 4), and the basal spacing of the resulting nanocomposites was determined by using XRD. The net interlayer expansion is obtained by taking the difference between the basal spacing of the nanocomposites and dry Li-hectorite, heated to 650 °C (d-spacing = 9.5 Å). For example, a 1:1 POEGO–Li-hectorite nanocomposite has a basal spacing of 18.9 Å, which implies a net interlayer expansion of 9.4 Å. The XRD data of the nanocomposites are summarized in Table 32.1.

As illustrated in Table 32.1, increasing the POEGO–Li-hectorite molar ratio leads to an increase in the amount of intercalated POEGO. This enhancement in basal spacing is observed when the molar ratio of POEGO to Li-hectorite increases from 0.5 to 2. Increasing the molar ratio to 4 results in an amorphous material as shown by the XRD diffractogram, which also shows the characteristics of an exfoliated nanocomposite. From the X-ray patterns, the average crystallite size of the nanocomposites was determined by using the Scherrer formula and the results are
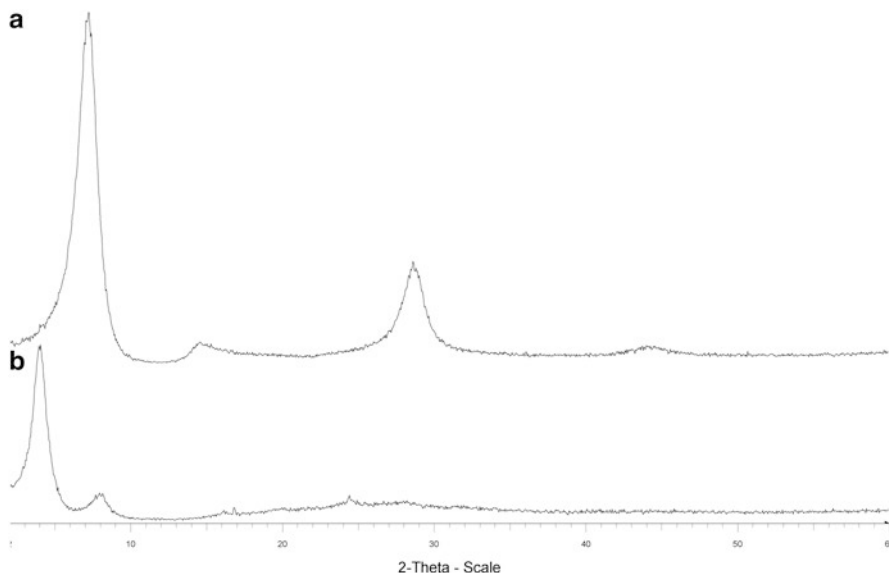
Fig. 32.3 XRD of (a) Li-hectorite–H$_2$O (control) and (b) POEGO–Li-hectorite (1:1) nanocomposite

Table 32.1 Summary of XRD data

Material	POEGO–Li-hectorite (Mol)	Basal spacing (Å)	Net expansion (Å)	Average crystallite size (Å)
POEGO	0.5:1	17.4	7.9	88
	1:1	18.9	9.4	88
	2:1	22.0	12.5	67
	4:1	–	–	–
Na-hectored	–	10.0	–	140
Li-hectorite–H$_2$O	–	12.1	–	60
Dry Li-hectorite	–	9.50	–	182

presented in Table 32.1 [23]. According to the overall trend, the average crystallite size appears to decrease upon increasing the amount of POEGO, indicating that the excess amorphous polymer significantly contributes to the reduction of the crystallite size of the nanocomposite.

The cross-sectional dimensions of POEGO from the top carbonyl oxygen to the bottom carbonyl oxygen were calculated using Spartan '08 and indicate that the largest possible dimension, assuming the polymer is linear, is approximately 3.5 Å [24]. This information suggests a bilayer arrangement of POEGO in the 1:1 nanocomposite, which has a net interlayer expansion of 9.4 Å. Although a bilayer arrangement is assigned to the 1:1 nanocomposite, it is important to note the polymer is likely not oriented in a linear fashion within the layers of hectorite and could be randomly
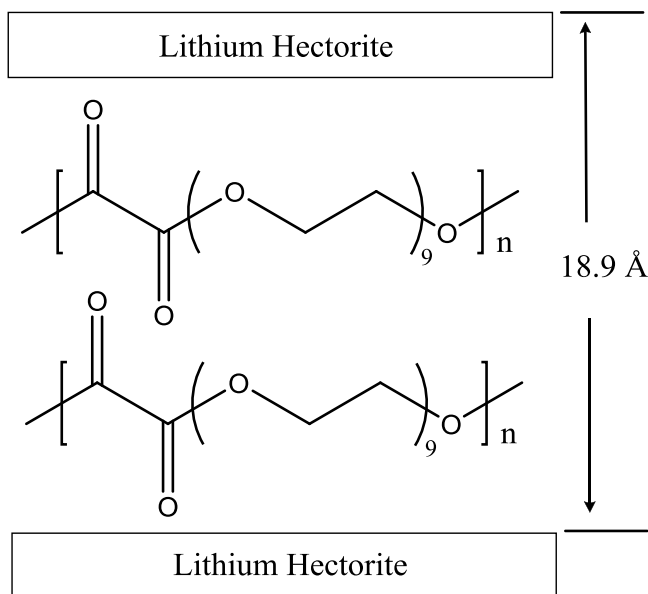
Fig. 32.4 Schematic of POEGO layers in lithium hectorite (1:1)

oriented between the layers due to its chain flexibility. A schematic diagram showing the bilayer arrangement of POEGO in Li-hectorite is illustrated in Fig. 32.4.

32.4.1.2 Thermogravimetric Analysis

Thermogravimetric analysis (TGA) was used to investigate the thermal stability of the pristine materials and nanocomposites. TGA was also used to calculate the stoichiometry of the nanocomposites. Figure 32.5 illustrates the thermal decomposition data of pristine POEGO, pristine POEGO–Li-hectorite nanocomposite (1:1), Li-POEGO, and Li-POEGO–Li-hectorite nanocomposite (1:1).

The thermograms of the nanocomposites (Fig. 32.5a, b) conducted in air display three distinguishable decomposition steps. The first step corresponds to the loss of co-intercalated water and occurs around 100 °C, while the second decomposition step is ascribed to the loss of externally bound polymer. The third and final step is the decomposition of the intercalated POEGO from the layers of hectorite. The thermal stability of the nanocomposites is displayed in Table 32.2.

As shown in Fig. 32.5 and summarized in Table 32.2, the 1:1 POEGO–Li-hectorite nanocomposite (thermogram (b)) has a higher onset decomposition temperature than the pristine POEGO (thermogram (d)). For pristine POEGO (thermogram (d)), full decomposition of the polymer is observed at approximately 400 °C. On the other hand, the decomposition of the intercalated POEGO begins at 408 °C in the
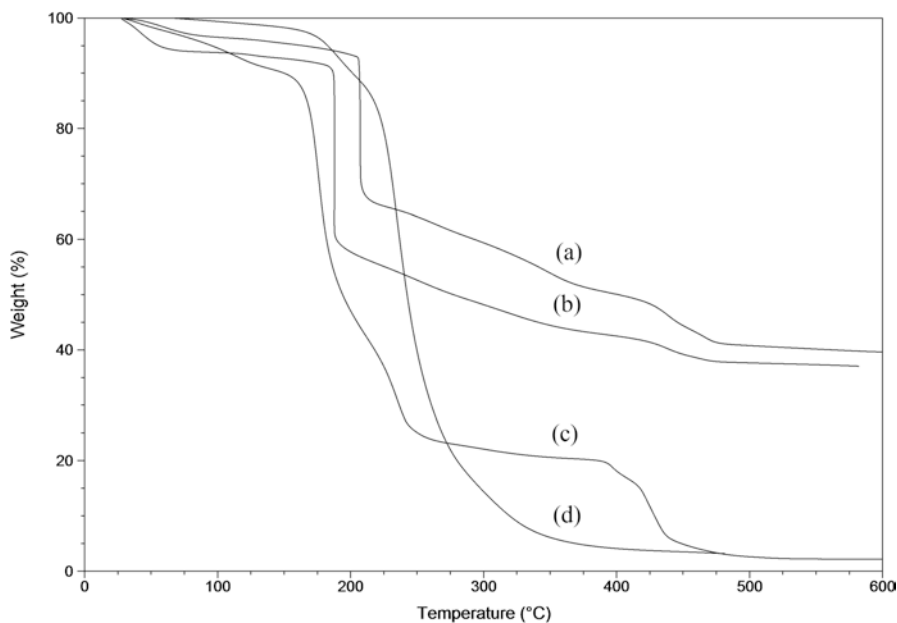
Fig. 32.5 TGA data of (a) Li-POEGO–Li-hectorite(1:1), (b) POEGO–Li-hectorite (1:1), (c) Li-POEGO, and (d) POEGO

Table 32.2 Summary of TGA data

Polymer	POEGO–Li-hectorite (Mol)	T_a (°C)	T_b (°C)	ΔT_c (°C)
POEGO	N/A	170	N/A	N/A
	0.5:1	182	402	232
	1:1	182	408	238
	2:1	186	420	250
	4:1	180	423	253

a = Onset decomposition temperature of externally lying POEGO or POEGO
b = Onset decomposition temperature of intercalated POEGO
c = Difference in decomposition temperature of intercalated polymer and pristine polymer

1:1 nanocomposite, thus indicating an increase in the onset decomposition temperature of 238 °C compared to the polymer (170 °C).

When the thermogram of the Li-POEGO–Li-hectorite nanocomposite (1:1) (thermogram (a)) is compared to the Li-POEGO (thermogram (c)), it is found that the decomposition of the Li-POEGO is slightly compromised due to the decomposition of the lithium triflate ($LiCF_3SO_3$) salt near 400 °C; the lithium triflate salt decomposes over the same region as the intercalated polymer. Due to this decomposition overlap near the 400 °C region, the thermograms of the salt-complexed nanocomposites were not used for the stoichiometry calculations. The stoichiometry of the POEGO–Li-hectorite nanocomposites was determined from their corresponding thermograms, and the results are summarized in Table 32.3.

Table 32.3 Stoichiometry of POEGO–Li-hectorite nanocomposites

POEGO–Li-hectorite (Mol)	Stoichiometry
0.5:1	$(H_2O)_{0.78}$ $(POEGO_{Ext})_{0.39}$ $(POEGO_{In})_{0.040}$ (Li-hectorite)
1:1	$(H_2O)_{3.7}$ $(POEGO_{Ext})_{1.1}$ $(POEGO_{In})_{0.11}$ (Li-hectorite)
2:1	$(H_2O)_{2.7}$ $(POEGO_{Ext})_{1.9}$ $(POEGO_{In})_{0.20}$ (Li-hectorite)
4:1	$(H_2O)_{5.0}$ $(POEGO_{Ext})_{4.0}$ $(POEGO_{In})_{0.43}$ (Li-hectorite)

Table 32.4 Summary of DSC data

Polymer	POEGO–Li-hectorite (Mol)	Glass transition temperature (T_g)
POEGO	N/A	−53
Li-POEGO	N/A	−57
	0.5:1	−55
	1:1	−59
	2:1	−62
	4:1	−62

From the data presented in Table 32.3, higher amounts of intercalated POEGO are observed with increasing molar ratios of POEGO to Li-hectorite, and this trend is in agreement with the XRD data. Furthermore, the amount of externally lying polymer present also increases with increasing polymer ratios. This is displayed as $POEGO_{Ext}$ in the stoichiometry data.

32.4.1.3 Differential Scanning Calorimetry

Differential scanning calorimetry was used to monitor the glass transition temperature (T_g) of the polymer upon intercalation into Li-hectorite. The T_g was determined for the pristine POEGO, pristine POEGO–Li-hectorite nanocomposite (1:1), Li-POEGO, and Li-POEGO–Li-hectorite nanocomposite (1:1).

The pristine polymer exhibits a glass transition temperature at −53 °C, which is in good agreement with the literature (−55 °C) [7]. Furthermore, the glass transition temperature of the polymer does not shift upon intercalation and slightly decreases when the polymer molar ratio is increased with respect to the layered structure. This indicates that polymer molecules in the nanocomposites are still flexible and theoretically should not affect the ionic conductivity of the material based on the theory of segmental motion [25]. This is in contrast to what has been previously reported in the literature, where intercalation of polymers into layered structures leads to an increase in the glass transition temperature of the polymers due to the rigid nature of the nanocomposites [6]. The T_g data for the POEGO–Li-hectorite nanocomposites is presented in Table 32.4.
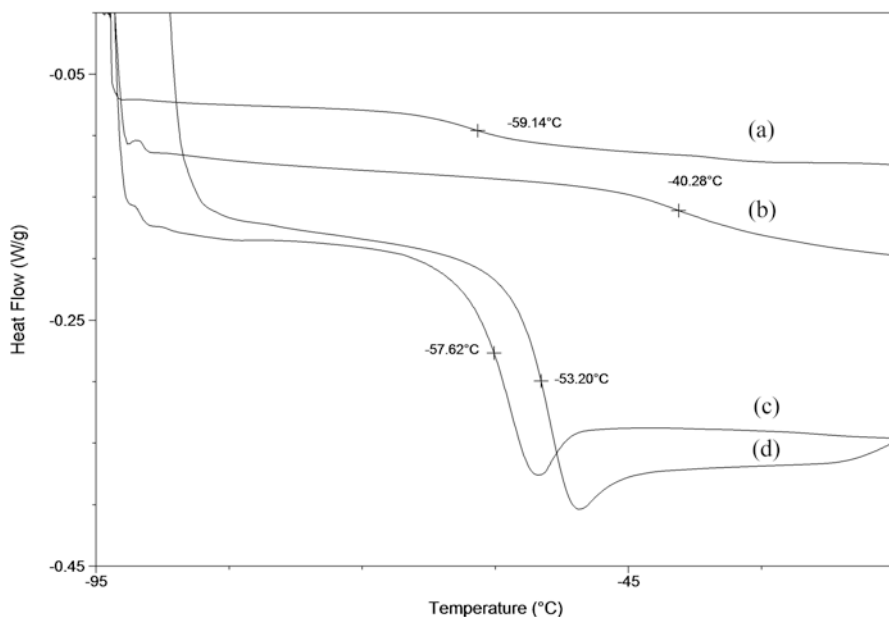
Fig. 32.6 DSC data for (a) POEGO–Li-hectorite (1:1), (b) Li-POEGO–Li-hectorite (1:1), (c) Li-POEGO, and (d) POEGO

While the POEGO–Li-hectorite nanocomposites do not exhibit a shift in glass transition temperatures, the Li-POEGO–Li-hectorite nanocomposite (Fig. 32.6b) behaves differently. The T_g observed in (Fig. 32.6b) shows a significant shift in its T_g to −40 °C, indicating a 13 °C increase in glass transition temperature. The increase in T_g of the salt-complexed nanocomposites is most likely due to the crystalline nature of the lithium triflate salt. Although the glass transition temperature increased, it is well below the optimal operation temperatures for lithium-ion batteries.

32.4.1.4   Attenuated Total Reflectance

Attenuated total reflectance was used to monitor the vibrations of pristine POEGO, pristine POEGO–Li-hectorite nanocomposites, Li-POEGO, and Li-POEGO–Li-hectorite nanocomposites. The IR spectra are presented in Fig. 32.7.

The IR spectra of pristine POEGO and POEGO–Li-hectorite nanocomposite (1:1) are depicted in Fig. 32.7a, c. Upon intercalation, the position of the carbonyl vibrations in the polymer remains unchanged (1744 cm^{-1}); however, the ester C–O vibrations shift to lower wave numbers (from 1180 to 1057 cm^{-1} and 1094 to 988 cm^{-1}). These shifts indicate enhanced interaction between the polymer and Li-hectorite. A similar trend is observed for the Li-POEGO (Fig. 32.7b) and Li-POEGO–Li-hectorite
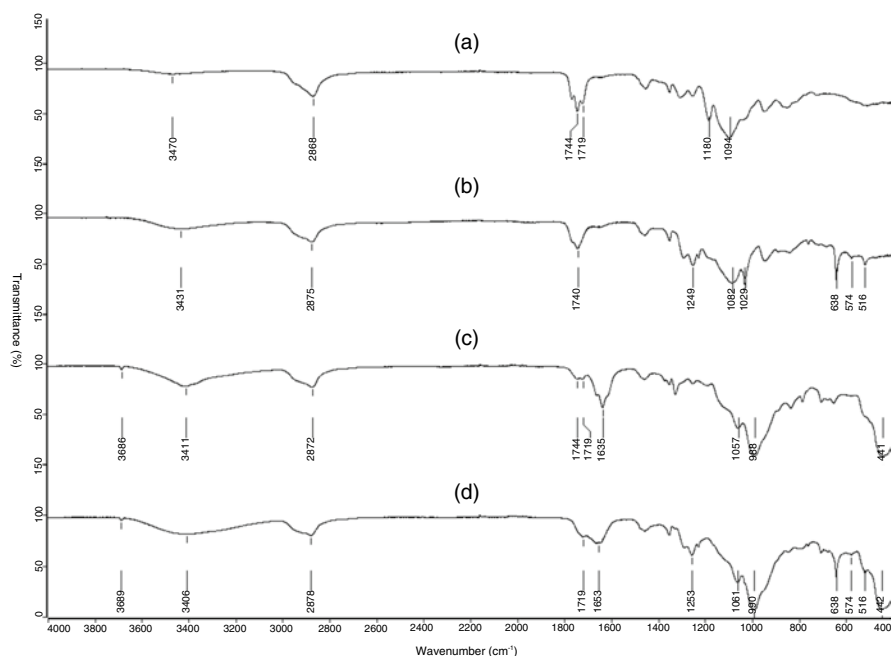
Fig. 32.7 IR spectra of (a) POEGO, (b) Li-POEGO, (c) POEGO–Li-hectorite (1:1), and (d) Li-POEGO–Li-hectorite (1:1)

Table 32.5 Summary of IR data

Major vibrations (cm⁻¹)	POEGO	Li-POEGO	POEGO– Li-hectorite (1:1)	Li-POEGO– Li-hectorite (1:1)
Li-hectorite HOH stretch	N/A	N/A	3689	3689
Hydroxyl	3470	3431	3411	3406
Sp³ C–H stretch	2868	2875	2872	2878
C=O Carboxylic acid	1719	–	1719	1719
C=O Ester	1744	1740	1740	–
Li-hectorite HOH bend	N/A	N/A	1635	1653
C–O ester/ether/alcohol	1180/1094	1082/1029	1057/988	1061/980
CF₃	N/A	1249	N/A	1253
C–F deformation	N/A	638	N/A	638
SO₃ asymmetric bend	N/A	573	N/A	573
SO₃ symmetric bend	N/A	518	N/A	518

–, Peak not found in spectrum

nanocomposites (1:1) (Fig. 32.7d), which indicates that the presence of the lithium triflate has little effect on the vibrations of the materials. This further solidifies the theory that the lithium salt is merely acting as a free lithium-ion source and not compromising the vibrations in the nanocomposites. The IR data are summarized in Table 32.5.
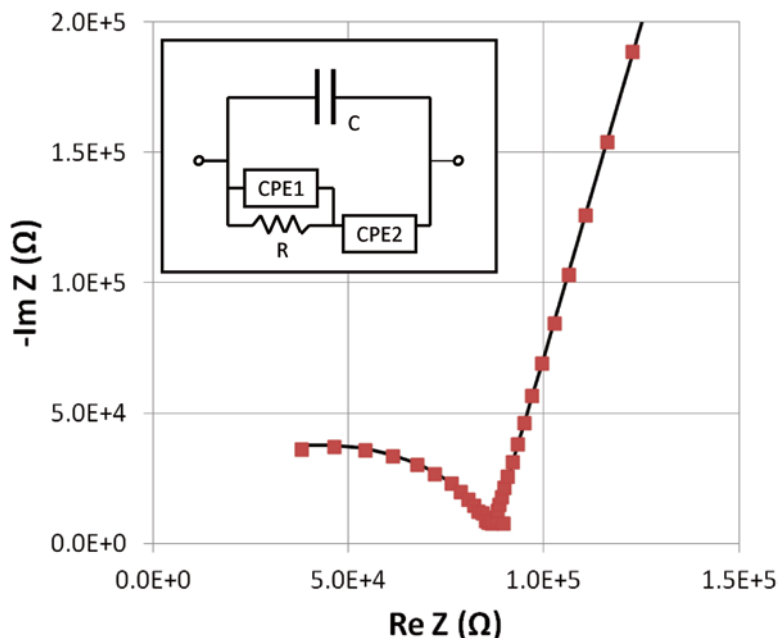
Fig. 32.8 Complex impedance of Li-POEGO–Li-hectorite (1:1) nanocomposite pellet at 300 K. The line is a fit to the equivalent circuit model shown in the inset

32.4.1.5   AC Impedance Spectroscopy

AC impedance spectroscopy was used to determine the conductivity of the Li-POEGO and Li-POEGO–Li-hectorite nanocomposites as a function of temperature. Figure 32.8 is a complex plane plot of the impedance data of a Li-POEGO–Li-hectorite (1:1) nanocomposite pellet over a frequency range from 5 kHz on the left end of the plot to 2 Hz on the top right. The temperature was 300 K. The curve has characteristics typical of an ionic conductor between blocking electrodes, an arc at high frequency and a diagonal spur at low frequency. The value of Re (Z) at which Im (Z) goes through a minimum is approximately the resistance (R) of the sample. The value of R and the dimensions of the polymer film can be used to calculate the ionic conductivity of the sample. In order to obtain more accurate values of R from the data obtained, a complex nonlinear least-squares fit was done to an equivalent circuit model using the program LEVMW [22]. A four-component equivalent circuit was used and is displayed in the inset in Fig. 32.8. The resistor R and constant-phase element CPE1 together represent ionic conduction through the bulk of the sample. CPE2 models the interface with the blocking electrodes, and capacitor C represents the bulk capacitance of the sample, as well as cable capacitance. The fit gives $R = (8.62 \pm .04) \times 10^4 \, \Omega$, and combining this with the dimensions of the sample (diameter $1.28 \pm .01$ cm and thickness 0.036 ± 0.001 cm) gives an ionic conductivity of $(3.2 \pm 0.1) \times 10^{-7}$ S cm^{-1}.
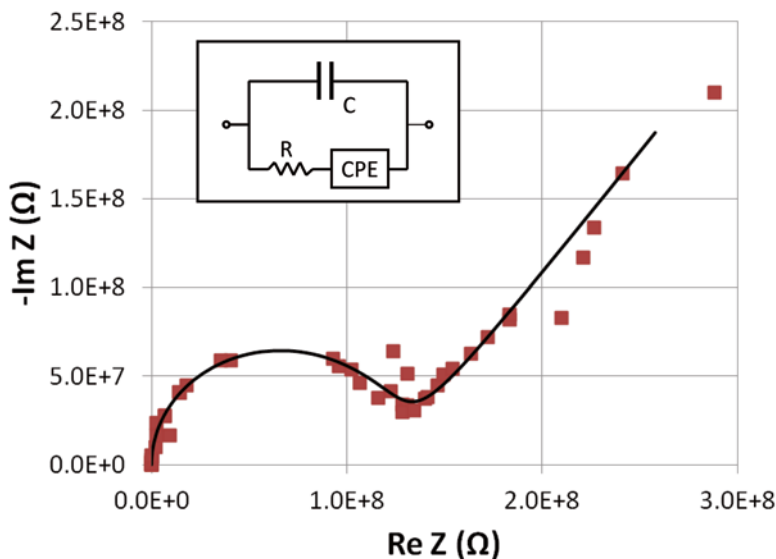
Fig. 32.9 Complex impedance of Li-POEGO–Li-hectorite (1:2) nanocomposite cast film at 300 K. The line is a fit to the equivalent circuit model shown in the inset

It was not possible to form pellets of Li-POEGO and some of the nanocomposites, so IS measurements were made on cast films. Figure 32.9 shows typical data for a cast film sample, in this case a 2:1 Li-POEGO–Li-hectorite nanocomposite at 300 K. The distance between electrodes in the direction of current flow was 0.79 ± 0.04 (cm), and the film was 0.87 ± 0.01 (cm) wide and $(2.5 \pm 1.0) \times 10^{-3}$ (cm) thick. A fit to the equivalent circuit model shown in the figure gives $R = (1.25 \pm 0.03) \times 10^8$ (Ω) and an ionic conductivity of $(3 \pm 1) \times 10^{-6}$ (S cm^{-1}). Conductivities measured on cast film samples have relatively high uncertainties, since the sample dimensions were measured with a micrometer, making it difficult to determine the thickness accurately. The thickness is also nonuniform. The uncertainty in sample thickness is the main source of error in the conductivity values. The very high resistance value is a consequence of the sample dimensions and the fact that the current flows along the plane of the thin film rather than through it from one side to the other. The high resistance implies very small current through the sample in response to the 50 mV rms excitation used, and the small signals result in a relatively poor signal-to-noise ratio, as can be seen in Fig. 32.9. In spite of this, thin film IS samples have the advantage that they are very easy to prepare, even for materials that are soft and difficult to form into pellets, and the IS data can be fit with a simple equivalent circuit.

The ionic conductivity is shown as a function of temperature in Fig. 32.10, for Li-POEGO and different ratios of Li-POEGO–Li-hectorite nanocomposites. Data for the Li-POEGO–Li-hectorite (1:1) pellet was fit to the Vogel–Tammann–Fulcher (VTF) equation [26]:
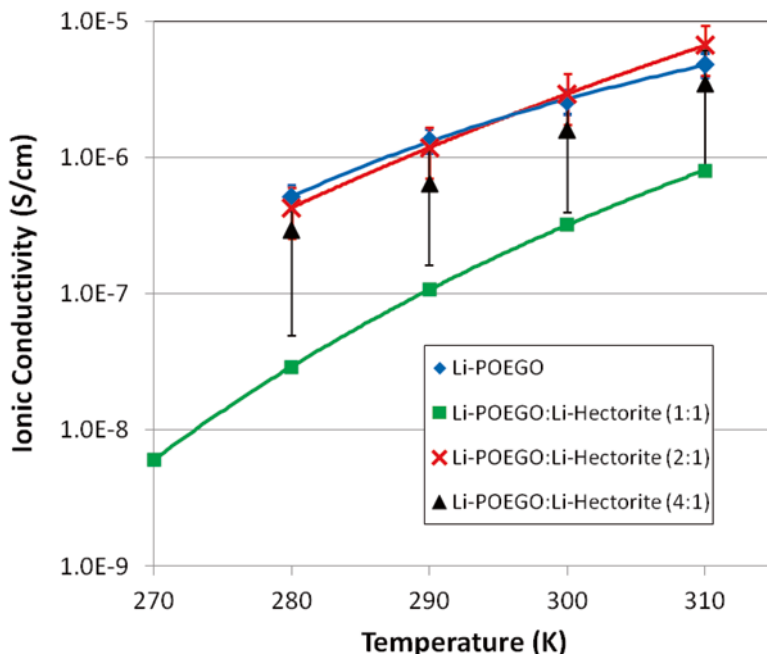
Fig. 32.10 Ionic conductivity of Li-POEGO–Li-hectorite nanocomposites and Li-POEGO. Lines are fits to the VTF equation

$$\sigma = \sigma_0 e^{-\beta/R(T-T_0)} \qquad\qquad (32.1)$$

The fit curve is shown in Fig. 32.10. Parameters determined from the fit are $\sigma_0 = (0.09 \pm 0.02)$ S cm^{-1}, $\beta/R = (1562 \pm 48)$ K, and $T_0 = (175 \pm 2)$ K. The conductivity for Li-POEGO and Li-POEGO–Li-hectorite (2:1) cast films also could be fit to the VTF equation (Fig. 32.10); however, because of the large error bars on the data, the fit parameters have little significance. Attempts to fit the Li-POEGO–Li-hectorite (4:1) data to the VTF equation failed, presumably because of noise in the data.

An upward trend in the ionic conductivity of the nanocomposites is observed when the molar ratio of Li-POEGO is increased with respect to Li-hectorite. This can be seen in Fig. 32.10 and in Table 32.6, which lists the conductivity for all the samples at 300 K. The 1:1 Li-POEGO–Li-hectorite nanocomposite has a conductivity significantly lower than Li-POEGO. The 2:1 and 4:1 nanocomposites have ionic conductivities of about the same magnitude as Li-POEGO. In fact, the conductivity of the 2:1 appears to be even higher than Li-POEGO; however, because of the large uncertainties, the difference is not significant.

The ionic conductivity measured for Li-POEGO without hectorite is lower than the maximum reported in the literature for (POEGO)$_{16}$ LiCF$_3$SO$_3$, i.e., 5.9×10^{-5} (S cm^{-1}) [7]. However, conductivity depends on the length of the oxyethylene chains (shown

Table 32.6 Ionic conductivity of Li-POEGO–Li-hectorite nanocomposites and Li-POEGO

Li-POEGO–Li-hectorite (Mol)	Ionic conductivity (Ω^{-1} cm^{-1}) at 300 K
1:1	$(3.2 \pm 0.1) \times 10^{-7}$
2:1	$(3 \pm 1) \times 10^{-6}$
4:1	$(1.5 \pm 1.2) \times 10^{-6}$
Li-POEGO	$(2.3 \pm 0.5) \times 10^{-6}$

as 9 in Fig. 32.1), reaching a maximum when the length is 23. The conductivity measured here for Li-POEGO [$(2.3 \pm 0.5) \times 10^{-6}$ (S cm^{-1})] is consistent with data in reference [7] for an oxyethylene chain length in the range of 5–9.

32.5 Conclusion

Varying amounts of poly[oligo(ethylene glycol)-oxalate] (POEGO) have been successfully intercalated into Li-hectorite as evidenced by the XRD data. The nanocomposites have also been characterized by TGA, DSC, ATR, and AC impedance spectroscopy. TGA data confirmed that an increase in the molar ratio of POEGO (0.5, 1, 2, 4) to the layered host results in a larger amount of the intercalated polymer. TGA data also indicates that the thermal stability of the POEGO–Li-hectorite (1:1) nanocomposites is enhanced by approximately 238 K when compared to pristine POEGO. Further characterization using AC impedance spectroscopy confirms that the Li-POEGO–Li-hectorite nanocomposites are ionically conductive. DSC confirms that the glass transition temperature of the nanocomposites remains relatively the same upon intercalation, indicating the polymer chains are still flexible at low temperatures, which are well below lithium-ion cell operation temperatures. ATR spectroscopy confirms that the polymer chains remain relatively flexible upon intercalation and do not affect the rigidity of the nanocomposites. In conclusion, the data obtained for the newly synthesized nanocomposites indicates that they exhibit enhanced physical and mechanical integrity compared to the pristine polymer while retaining the ionic conductivity of the pristine polymer. Li-POEGO–Li-hectorite nanocomposites can therefore be used in lithium-ion battery applications. The enhanced thermal stability of these materials over the pure polymer suggests that batteries designed from these materials will be able function over a wide range of temperatures from as low as the glass transition temperature, ca −55 °C, to as high as ca 220 °C, the thermal stability as observed from TGA. The materials can also be prepared as thin films and can be easily deposited via solution casting onto anode materials of different sizes and shapes. Our research shows that the conductivity of the nanocomposites can be controlled by synthetically tailoring the amount of polymer, triflate salt, and hectorite. The fact that the nanocomposites are ionically conductive over a wide range of temperatures further corroborates that batteries fabricated from these materials will function over a wide range of temperatures.

References

1. Panero S, Settimi L, Croce F, Scrosati B (2006) New types of rechargeable lithium and lithium-ion polymer batteries. ECS Trans 1:1
2. Scully SF, Bissessur R (2010) Encapsulation of polymer eectrolytes into hectorite. Appl Clay Sci 47:444
3. Blumstein A (1965) Polymerization of adsorbed monolayers. I. Preparation of the clay-polymer complex. J Polym Sci A 3:2653
4. Sinha Ray S, Okamoto M (2003) Polymer/layered silicate nanocomposites: a review from preparation to processing. Prog Polym Sci 28:1539
5. Kurian M, Galvin ME, Trapa PE, Sadoway DR (2005) Single-ion conducting polymer-silicate nanocomposite electrolytes for lithium battery applications. Electrochim Acta 50:2125
6. Scully SF, Bissessur R, MacLean KW, Dahn DC (2009) Inclusion of poly [bis(methoxyethoxyethoxy)phosphazene] into layered graphite oxide. Solid State Ionics 180:216
7. Xu W, Belieres J-P, Angell CA (2001) Ionic conductivity and electrochemical stability of poly[oligo(ethylene glycol)oxalate]−lithium salt complexes. Chem Mater 13:575
8. Hoffman AS (1995) "Intelligent" polymers in medicine and biotechnology. Macromol Symp 98:645. doi:10.1002/masy.19950980156
9. Bissessur R, Schipper D (2008) Exfoliation and reconstruction of SnS_2 layers: A synthetic route for the preparation polymer-SnS_2nanomaterials. Mater Lett 62:1638
10. Bissessur R, Scully SF (2007) Intercalation of solid polymer electrolytes into graphite oxide. Solid State Ionics 178:877
11. Carretero MI, Pozo M (2009) Clay and non-clay minerals in the pharmaceutical industry: Part I. Excipients and medical applications. Appl Clay Sci 46:73
12. Zhang D, Zhou C-H, Lin C-X, Tong D-S, Yu W-H (2010) Synthesis of clay minerals. Appl Clay Sci 50:1
13. Okada A, Usuki A (1995) The chemistry of polymer-clay hybrids. Mater Sci Eng C 3:109
14. Sandí G, Carrado KA, Joachin H, Lu W, Prakash J (2003) Polymer nanocomposites for lithium battery applications. J Power Sources 119–121:492
15. Riley M, Fedkiw PS, Khan SA (2002) Transport properties of lithium hectorite-based composite elctrolytes. J Electrom Soc 149:A667
16. Madejová J, Bujdák J, Janek M, Komadel P (1998) Comparative FT-IR study of structural modifications during acid treatment of dioctahedral smectites and hectorite. Spectrochim Acta Part A 54:1397
17. Carrado KA, Forman JE, Botto RE, Winans RE (1993) Incorporation of phthalocyanines by cationic and anionic clays via ion exchange and direct synthesis. Chem Mater 5:472
18. Voulgaris D, Petridis D (2002) Emulsifying effect of dimethyldioctadecylammonium-hectorite in polystyrene/poly(ethyl methacrylate) blends. Polymer 43:2213
19. Kuykendall VG, Thomas JK (1990) Photophysical and photochemical studies of ruthenium (tris(bipyridine) on hectorite. J Phys Chem 94:4224
20. Singhal RG, Capracotta MD, Martin JD, Khan SA, Fedkiw PS (2004) Transport properties of hectorite based nanocomposite single ion conductors. J Power Sources 128:247
21. Barsoukov E, Macondald JR (2005) Impedance spectroscopy: theory, experiment, and applications (2nd edn). Wiley, Hoboken, NJ

22. Macdonald JR (2015) jrossmacdonald.com/levmw, accessed 25 June 2015
23. Monshi A, Foroughi MR, Monshi MR (2012) Modified Scherrer equation to estimate more accurately nano-crystalline size using XRD. World J Nano Sci Eng 2:154
24. Spartan '08, Wavefunction Inc., Irvine, CA, 2008
25. Meyer WH (1998) Polymer electrolytes for lithium-ion batteries. Adv Mater 10:439
26. Ratner MA, Shriver DF (1988) Ion transport in solvent-free polymers. Chem Rev 88:109

Index